RILEM Bookseries

Francesco Canestrari
Manfred N. Partl *Editors*

# 8th RILEM International Symposium on Testing and Characterization of Sustainable and Innovative Bituminous Materials


Springer

# 8th RILEM International Symposium on Testing and Characterization of Sustainable and Innovative Bituminous Materials

**RILEM BOOKSERIES**

Volume 11

RILEM, The International Union of Laboratories and Experts in Construction Materials, Systems and Structures, founded in 1947, is a non-governmental scientific association whose goal is to contribute to progress in the construction sciences, techniques and industries, essentially by means of the communication it fosters between research and practice. RILEM's focus is on construction materials and their use in building and civil engineering structures, covering all phases of the building process from manufacture to use and recycling of materials. More information on RILEM and its previous publications can be found on www.RILEM.net.


More information about this series at http://www.springer.com/series/8781

Francesco Canestrari · Manfred N. Partl
Editors

# 8th RILEM International Symposium on Testing and Characterization of Sustainable and Innovative Bituminous Materials

Springer

*Editors*
Francesco Canestrari
Università Politecnica delle Marche
Ancona
Italy

Manfred N. Partl
Road Engineering/Sealing Components
EMPA—Swiss Federal Laboratories
for Materials Science and Technology
Dübendorf
Switzerland

ISSN 2211-0844 ISSN 2211-0852 (electronic)
RILEM Bookseries
ISBN 978-94-017-7341-6 ISBN 978-94-017-7342-3 (eBook)
DOI 10.1007/978-94-017-7342-3

Library of Congress Control Number: 2015946092

Springer Dordrecht Heidelberg New York London


Printed on acid-free paper

Springer Science+Business Media B.V. Dordrecht is part of Springer Science+Business Media (www.springer.com)

# Preface

RILEM (*International Union of Laboratories and Experts in Construction Materials, Systems and Structures*) is a volunteer organization grouping academics, researchers, testing laboratories, suppliers, and contractors with the aim to promote scientific cooperation in the area of construction materials and structures.

In the field of bituminous materials, since late 1960s, RILEM activities are organized through Technical Committees (TC) that delivered outstanding products such as guides to good practice, recommendations and prestandards, proceedings of symposia and workshops, state-of-the-art reports with extensive data basis, and papers in international journals.

The *8th RILEM International Symposium on Testing and Characterization of Sustainable and Innovative Bituminous Materials* belongs to a series of RILEM Symposia started in 1968 (Dresden) and follows up the last organized in Rhodes six years ago.

Nowadays, the increasing mobility demand and traffic loads call for using innovative high-performance materials and techniques for asphalt pavements and, at the same time, for taking care of environmental concerns in search of more sustainable infrastructures.

For the above-mentioned reasons, the main goal of the symposium is to enhance knowledge on sustainable and innovative bituminous materials as basis for their appropriate and reliable application within the pavement network. Achieving such objectives requires developing and implementing performance-oriented test methods through promotion of international networking and synergies.

In accordance with these objectives, over 80 papers from 26 countries were accepted after a rigorous peer review addressing the following topics:

- Characterization of binder–aggregate interaction;
- Innovative testing of bituminous binders, additives, and modifiers;
- Durability and aging of asphalt pavements;
- Mixture design and compaction analysis;
- Advanced characterization of interlayer systems;
- Modeling of road materials and pavement performance prediction;

- Environmentally sustainable materials and technologies;
- Advances in laboratory characterization of bituminous materials;
- Field measurement and in situ characterization;
- Recycling and reuse in road pavements;
- Cracking and damage characterization of asphalt pavements.

As it can be seen, the content of these proceedings appeals not only to researchers and students at university level but also to practitioners and decision makers providing an update on latest environment-related developments and performance-based evaluations in the field of testing and characterization of sustainable and innovative bituminous pavement materials and technologies.

We trust that the rigorous experimental approach and theoretical background adopted by the authors of the accepted papers will contribute to a further leap toward sustainable applications of bituminous road materials.

Moreover, we hope that the pavement engineering research community will understand this symposium as an opportunity to strengthen its efforts in fostering the environmentally friendly use of asphalt products for the sake of future generations.

For this reason, the editors would like to thank the RILEM Steering Committee of this symposium for supporting the main strategic decisions and all authors and reviewers for contributing to the excellent quality of the accepted papers. Their effort is highly appreciated.

Finally, we would also like to acknowledge the invaluable contributions from the Local Organizing Committee with its enthusiastic members, who have tirelessly dedicated time to the success of the symposium.

Ancona
October 2015

Francesco Canestrari
Manfred N. Partl

# Contents

# RILEM Publications

The following list is presenting the global offer of RILEM Publications, sorted by series. Each publication is available in printed version and/or in online version.

**RILEM Proceedings (PRO)**

**PRO 1**: Durability of High Performance Concrete (ISBN: 2-912143-03-9); *Ed. H. Sommer*
**PRO 2**: Chloride Penetration into Concrete (ISBN: 2-912143-00-04); *Eds. L.-O. Nilsson and J.-P. Ollivier*
**PRO 3**: Evaluation and Strengthening of Existing Masonry Structures (ISBN: 2-912143-02-0); *Eds. L. Binda and C. Modena*
**PRO 4**: Concrete: From Material to Structure (ISBN: 2-912143-04-7); *Eds. J.-P. Bournazel and Y. Malier*
**PRO 5**: The Role of Admixtures in High Performance Concrete (ISBN: 2-912143-05-5); *Eds. J. G. Cabrera and R. Rivera-Villarreal*
**PRO 6**: High Performance Fiber Reinforced Cement Composites—HPFRCC 3 (ISBN: 2-912143-06-3); *Eds. H. W. Reinhardt and A. E. Naaman*
**PRO 7**: 1st International RILEM Symposium on Self-Compacting Concrete (ISBN: 2-912143-09-8); *Eds. Å. Skarendahl and Ö. Petersson*
**PRO 8**: International RILEM Symposium on Timber Engineering (ISBN: 2-912143-10-1); *Ed. L. Boström*
**PRO 9**: 2nd International RILEM Symposium on Adhesion between Polymers and Concrete ISAP '99 (ISBN: 2-912143-11-X); *Eds. Y. Ohama and M. Puterman*
**PRO 10**: 3rd International RILEM Symposium on Durability of Building and Construction Sealants (ISBN: 2-912143-13-6); *Eds. A. T. Wolf*
**PRO 11**: 4th International RILEM Conference on Reflective Cracking in Pavements (ISBN: 2-912143-14-4); *Eds. A. O. Abd El Halim, D. A. Taylor and El H. H. Mohamed*
**PRO 12**: International RILEM Workshop on Historic Mortars: Characteristics and Tests (ISBN: 2-912143-15-2); *Eds. P. Bartos, C. Groot and J. J. Hughes*

**PRO 13**: 2nd International RILEM Symposium on Hydration and Setting (ISBN: 2-912143-16-0); *Ed. A. Nonat*
**PRO 14**: Integrated Life-Cycle Design of Materials and Structures—ILCDES 2000 (ISBN: 951-758-408-3); (ISSN: 0356-9403); *Ed. S. Sarja*
**PRO 15**: Fifth RILEM Symposium on Fibre-Reinforced Concretes (FRC)—BEFIB'2000 (ISBN: 2-912143-18-7); *Eds. P. Rossi and G. Chanvillard*
**PRO 16**: Life Prediction and Management of Concrete Structures (ISBN: 2-912143-19-5); *Ed. D. Naus*
**PRO 17**: Shrinkage of Concrete – Shrinkage 2000 (ISBN: 2-912143-20-9); *Eds. V. Baroghel-Bouny and P.-C. Aïtcin*
**PRO 18**: Measurement and Interpretation of the On-Site Corrosion Rate (ISBN: 2-912143-21-7); *Eds. C. Andrade, C. Alonso, J. Fullea, J. Polimon and J. Rodriguez*
**PRO 19**: Testing and Modelling the Chloride Ingress into Concrete (ISBN: 2-912143-22-5); *Eds. C. Andrade and J. Kropp*
**PRO 20**: 1st International RILEM Workshop on Microbial Impacts on Building Materials (CD 02) (e-ISBN 978-2-35158-013-4); *Ed. M. Ribas Silva*
**PRO 21**: International RILEM Symposium on Connections between Steel and Concrete (ISBN: 2-912143-25-X); *Ed. R. Eligehausen*
**PRO 22**: International RILEM Symposium on Joints in Timber Structures (ISBN: 2-912143-28-4); *Eds. S. Aicher and H.-W. Reinhardt*
**PRO 23**: International RILEM Conference on Early Age Cracking in Cementitious Systems (ISBN: 2-912143-29-2); *Eds. K. Kovler and A. Bentur*
**PRO 24**: 2nd International RILEM Workshop on Frost Resistance of Concrete (ISBN: 2-912143-30-6); *Eds. M. J. Setzer, R. Auberg and H.-J. Keck*
**PRO 25**: International RILEM Workshop on Frost Damage in Concrete (ISBN: 2-912143-31-4); *Eds. D. J. Janssen, M. J. Setzer and M. B. Snyder*
**PRO 26**: International RILEM Workshop on On-Site Control and Evaluation of Masonry Structures (ISBN: 2-912143-34-9); *Eds. L. Binda and R. C. de Vekey*
**PRO 27**: International RILEM Symposium on Building Joint Sealants (CD03); *Ed. A. T. Wolf*
**PRO 28**: 6th International RILEM Symposium on Performance Testing and Evaluation of Bituminous Materials—PTEBM'03 (ISBN: 2-912143-35-7; e-ISBN: 978-2-912143-77-8); *Ed. M. N. Partl*
**PRO 29**: 2nd International RILEM Workshop on Life Prediction and Ageing Management of Concrete Structures (ISBN: 2-912143-36-5); *Ed. D. J. Naus*
**PRO 30**: 4th International RILEM Workshop on High Performance Fiber Reinforced Cement Composites—HPFRCC 4 (ISBN: 2-912143-37-3); *Eds. A. E. Naaman and H. W. Reinhardt*
**PRO 31**: International RILEM Workshop on Test and Design Methods for Steel Fibre Reinforced Concrete: Background and Experiences (ISBN: 2-912143-38-1); *Eds. B. Schnütgen and L. Vandewalle*
**PRO 32**: International Conference on Advances in Concrete and Structures 2 vol. (ISBN (set): 2-912143-41-1); *Eds. Ying-shu Yuan, Surendra P. Shah and Heng-lin Lü*

**PRO 33**: 3rd International Symposium on Self-Compacting Concrete (ISBN: 2-912143-42-X); *Eds. Ó. Wallevik and I. Níelsson*
**PRO 34**: International RILEM Conference on Microbial Impact on Building Materials (ISBN: 2-912143-43-8); *Ed. M. Ribas Silva*
**PRO 35**: International RILEM TC 186-ISA on Internal Sulfate Attack and Delayed Ettringite Formation (ISBN: 2-912143-44-6); *Eds. K. Scrivener and J. Skalny*
**PRO 36**: International RILEM Symposium on Concrete Science and Engineering – A Tribute to Arnon Bentur (ISBN: 2-912143-46-2); *Eds. K. Kovler, J. Marchand, S. Mindess and J. Weiss*
**PRO 37**: 5th International RILEM Conference on Cracking in Pavements – Mitigation, Risk Assessment and Prevention (ISBN: 2-912143-47-0); *Eds. C. Petit, I. Al-Qadi and A. Millien*
**PRO 38**: 3rd International RILEM Workshop on Testing and Modelling the Chloride Ingress into Concrete (ISBN: 2-912143-48-9); *Eds. C. Andrade and J. Kropp*
**PRO 39**: 6th International RILEM Symposium on Fibre-Reinforced Concretes—BEFIB 2004 (ISBN: 2-912143-51-9); *Eds. M. Di Prisco, R. Felicetti and G. A. Plizzari*
**PRO 40**: International RILEM Conference on the Use of Recycled Materials in Buildings and Structures (ISBN: 2-912143-52-7); *Eds. E. Vázquez, Ch. F. Hendriks and G. M. T. Janssen*
**PRO 41**: RILEM International Symposium on Environment-Conscious Materials and Systems for Sustainable Development (ISBN: 2-912143-55-1); *Eds. N. Kashino and Y. Ohama*
**PRO 42**: SCC'2005—China: 1st International Symposium on Design, Performance and Use of Self-Consolidating Concrete (ISBN: 2-912143-61-6); *Eds. Zhiwu Yu, Caijun Shi, Kamal Henri Khayat and Youjun Xie*
**PRO 43**: International RILEM Workshop on Bonded Concrete Overlays (e-ISBN: 2-912143-83-7); *Eds. J. L. Granju and J. Silfwerbrand*
**PRO 44**: 2nd International RILEM Workshop on Microbial Impacts on Building Materials (CD11) (e-ISBN: 2-912143-84-5); *Ed. M. Ribas Silva*
**PRO 45**: 2nd International Symposium on Nanotechnology in Construction, Bilbao (ISBN: 2-912143-87-X); *Eds. Peter J. M. Bartos, Yolanda de Miguel and Antonio Porro*
**PRO 46**: ConcreteLife'06—International RILEM-JCI Seminar on Concrete Durability and Service Life Planning: Curing, Crack Control, Performance in Harsh Environments (ISBN: 2-912143-89-6); *Ed. K. Kovler*
**PRO 47**: International RILEM Workshop on Performance Based Evaluation and Indicators for Concrete Durability (ISBN: 978-2-912143-95-2); *Eds. V. Baroghel-Bouny, C. Andrade, R. Torrent and K. Scrivener*
**PRO 48**: 1st International RILEM Symposium on Advances in Concrete through Science and Engineering (e-ISBN: 2-912143-92-6); *Eds. J. Weiss, K. Kovler, J. Marchand, and S. Mindess*

**PRO 49**: International RILEM Workshop on High Performance Fiber Reinforced Cementitious Composites in Structural Applications (ISBN: 2-912143-93-4); *Eds. G. Fischer and V.C. Li*

**PRO 50**: 1st International RILEM Symposium on Textile Reinforced Concrete (ISBN: 2-912143-97-7); *Eds. Josef Hegger, Wolfgang Brameshuber and Norbert Will*

**PRO 51**: 2nd International Symposium on Advances in Concrete through Science and Engineering (ISBN: 2-35158-003-6; e-ISBN: 2-35158-002-8); *Eds. J. Marchand, B. Bissonnette, R. Gagné, M. Jolin and F. Paradis*

**PRO 52**: Volume Changes of Hardening Concrete: Testing and Mitigation (ISBN: 2-35158-004-4; e-ISBN: 2-35158-005-2); *Eds. O. M. Jensen, P. Lura and K. Kovler*

**PRO 53**: High Performance Fiber Reinforced Cement Composites—HPFRCC5 (ISBN: 978-2-35158-046-2); *Eds. H. W. Reinhardt and A. E. Naaman*

**PRO 54**: 5th International RILEM Symposium on Self-Compacting Concrete (ISBN: 978-2-35158-047-9); *Eds. G. De Schutter and V. Boel*

**PRO 55**: International RILEM Symposium Photocatalysis, Environment and Construction Materials (ISBN: 978-2-35158-056-1); *Eds. P. Baglioni and L. Cassar*

**PRO 56**: International RILEM Workshop on Integral Service Life Modelling of Concrete Structures (ISBN 978-2-35158-058-5); *Eds. R. M. Ferreira, J. Gulikers and C. Andrade*

**PRO 57**: RILEM Workshop on Performance of cement-based materials in aggressive aqueous environments (e-ISBN: 978-2-35158-059-2); *Ed. N. De Belie*

**PRO 58**: International RILEM Symposium on Concrete Modelling—CONMOD'08 (ISBN: 978-2-35158-060-8); *Eds. E. Schlangen and G. De Schutter*

**PRO 59**: International RILEM Conference on On Site Assessment of Concrete, Masonry and Timber Structures—SACoMaTiS 2008 (ISBN set: 978-2-35158-061-5); *Eds. L. Binda, M. di Prisco and R. Felicetti*

**PRO 60**: Seventh RILEM International Symposium on Fibre Reinforced Concrete: Design and Applications—BEFIB 2008 (ISBN: 978-2-35158-064-6); *Ed. R. Gettu*

**PRO 61**: 1st International Conference on Microstructure Related Durability of Cementitious Composites 2 vol., (ISBN: 978-2-35158-065-3); *Eds. W. Sun, K. van Breugel, C. Miao, G. Ye and H. Chen*

**PRO 62**: NSF/ RILEM Workshop: In-situ Evaluation of Historic Wood and Masonry Structures (e-ISBN: 978-2-35158-068-4); *Eds. B. Kasal, R. Anthony and M. Drdácký*

**PRO 63**: Concrete in Aggressive Aqueous Environments: Performance, Testing and Modelling, 2 vol., (ISBN: 978-2-35158-071-4); *Eds. M. G. Alexander and A. Bertron*

**PRO 64**: Long Term Performance of Cementitious Barriers and Reinforced Concrete in Nuclear Power Plants and Waste Management—NUCPERF 2009 (ISBN: 978-2-35158-072-1); *Eds. V. L'Hostis, R. Gens, C. Gallé*

**PRO 65**: Design Performance and Use of Self-consolidating Concrete—SCC'2009 (ISBN: 978-2-35158-073-8); *Eds. C. Shi, Z. Yu, K. H. Khayat and P. Yan*

**PRO 66**: 2nd International RILEM Workshop on Concrete Durability and Service Life Planning—ConcreteLife'09 (ISBN: 978-2-35158-074-5); *Ed. K. Kovler*
**PRO 67**: Repairs Mortars for Historic Masonry (e-ISBN: 978-2-35158-083-7); *Ed. C. Groot*
**PRO 68**: Proceedings of the 3rd International RILEM Symposium on 'Rheology of Cement Suspensions such as Fresh Concrete (ISBN 978-2-35158-091-2); *Eds. O. H. Wallevik, S. Kubens and S. Oesterheld*
**PRO 69**: 3rd International PhD Student Workshop on 'Modelling the Durability of Reinforced Concrete (ISBN: 978-2-35158-095-0); *Eds. R. M. Ferreira, J. Gulikers and C. Andrade*
**PRO 70**: 2nd International Conference on 'Service Life Design for Infrastructure' (ISBN set: 978-2-35158-096-7, e-ISBN: 978-2-35158-097-4); *Ed. K. van Breugel, G. Ye and Y. Yuan*
**PRO 71**: Advances in Civil Engineering Materials—The 50-year Teaching Anniversary of Prof. Sun Wei' (ISBN: 978-2-35158-098-1; e-ISBN: 978-2-35158-099-8); *Eds. C. Miao, G. Ye, and H. Chen*
**PRO 72**: First International Conference on 'Advances in Chemically-Activated Materials—CAM'2010' (2010), 264 pp., ISBN: 978-2-35158-101-8; e-ISBN: 978-2-35158-115-5, *Eds. Caijun Shi and Xiaodong Shen*
**PRO 73**: 2nd International Conference on 'Waste Engineering and Management—ICWEM 2010' (2010), 894 pp., ISBN: 978-2-35158-102-5; e-ISBN: 978-2-35158-103-2, *Eds. J. Zh. Xiao, Y. Zhang, M. S. Cheung and R. Chu*
**PRO 74**: International RILEM Conference on 'Use of Superabsorsorbent Polymers and Other New Addditives in Concrete' (2010) 374 pp., ISBN: 978-2-35158-104-9; e-ISBN: 978-2-35158-105-6; *Eds. O.M. Jensen, M.T. Hasholt, and S. Laustsen*
**PRO 75**: International Conference on 'Material Science—2nd ICTRC—Textile Reinforced Concrete—Theme 1' (2010) 436 pp., ISBN: 978-2-35158-106-3; e-ISBN: 978-2-35158-107-0; *Ed. W. Brameshuber*
**PRO 76**: International Conference on 'Material Science—HetMat—Modelling of Heterogeneous Materials—Theme 2' (2010) 255 pp., ISBN: 978-2-35158-108-7; e-ISBN: 978-2-35158-109-4; *Ed. W. Brameshuber*
**PRO 77**: International Conference on 'Material Science—AdIPoC—Additions Improving Properties of Concrete—Theme 3' (2010) 459 pp., ISBN: 978-2-35158-110-0; e-ISBN: 978-2-35158-111-7; *Ed. W. Brameshuber*
**PRO 78**: 2nd Historic Mortars Conference and RILEM TC 203-RHM Final Workshop—HMC2010 (2010) 1416 pp., e-ISBN: 978-2-35158-112-4; *Eds J. Válek, C. Groot, and J. J. Hughes*
**PRO 79**: International RILEM Conference on Advances in Construction Materials Through Science and Engineering (2011) 213 pp., e-ISBN: 978-2-35158-117-9; *Eds Christopher Leung and K.T. Wan*
**PRO 80**: 2nd International RILEM Conference on Concrete Spalling due to Fire Exposure (2011) 453 pp., ISBN: 978-2-35158-118-6, e-ISBN: 978-2-35158-119-3; *Eds E.A.B. Koenders and F. Dehn*
**PRO 81**: 2nd International RILEM Conference on Strain Hardening Cementitious Composites (SHCC2-Rio) (2011) 451 pp., ISBN: 978-2-35158-120-9, e-ISBN:

978-2-35158-121-6; *Eds R.D. Toledo Filho, F.A. Silva, E.A.B. Koenders and E.M. R. Fairbairn*

**PRO 82**: 2nd International RILEM Conference on Progress of Recycling in the Built Environment (2011) 507 pp., e-ISBN: 978-2-35158-122-3; *Eds V.M. John, E. Vazquez, S.C. Angulo and C. Ulsen*

**PRO 83**: 2nd International Conference on Microstructural-related Durability of Cementitious Composites (2012) 250 pp., ISBN: 978-2-35158-129-2; e-ISBN: 978-2-35158-123-0; *Eds G. Ye, K. van Breugel, W. Sun and C. Miao*

**PRO 85**: RILEM-JCI International Workshop on Crack Control of Mass Concrete and Related issues concerning Early-Age of Concrete Structures—ConCrack 3—Control of Cracking in Concrete Structures 3 (2012) 237 pp., ISBN: 978-2-35158-125-4; e-ISBN: 978-2-35158-126-1; *Eds F. Toutlemonde and J.-M. Torrenti*

**PRO 86**: International Symposium on Life Cycle Assessment and Construction (2012) 414 pp., ISBN: 978-2-35158-127-8, e-ISBN: 978-2-35158-128-5; *Eds A. Ventura and C. de la Roche*

**PRO 87**: UHPFRC 2013—RILEM-fib-AFGC International Symposium on Ultra-High Performance Fibre-Reinforced Concrete (2013), ISBN: 978-2-35158-130-8, e-ISBN: 978-2-35158-131-5; *Eds F. Toutlemonde*

**PRO 88**: 8th RILEM International Symposium on Fibre Reinforced Concrete (2012) 344 pp., ISBN: 978-2-35158-132-2, e-ISBN: 978-2-35158-133-9; *Eds Joaquim A.O. Barros*

**PRO 89**: RILEM International workshop on performance-based specification and control of concrete durability (2014) 678 pp, ISBN: 978-2-35158-135-3, e-ISBN: 978-2-35158-136-0; *Eds. D. Bjegović, H. Beushausen and M. Serdar*

**PRO 90**: 7th RILEM International Conference on Self-Compacting Concrete and of the 1st RILEM International Conference on Rheology and Processing of Construction Materials (2013) 396 pp, ISBN: 978-2-35158-137-7, e-ISBN: 978-2-35158-138-4, *Eds. Nicolas Roussel and Hela Bessaies-Bey*

**PRO 91 draft**: CONMOD 2014—RILEM International Symposium on Concrete Modelling (2014), ISBN: 978-2-35158-139-1; e-ISBN: 978-2-35158-140-7

**PRO 92**: CAM 2014—2nd International Conference on advances in chemically-activated materials (2014) 392 pp., ISBN: 978-2-35158-141-4; e-ISBN: 978-2-35158-142-1, *Eds. Caijun Shi and Xiadong Shen*

**PRO 93**: SCC 2014—3rd International Symposium on Design, Performance and Use of Self-Consolidating Concrete (2014) 438 pp., ISBN: 978-2-35158-143-8; e-ISBN: 978-2-35158-144-5, *Eds. Caijun Shi, Zhihua Ou, Kamal H. Khayat*

**PRO 94 (online version)**: HPFRCC-7—7th RILEM conference on High performance fiber reinforced cement composites, e-ISBN: 978-2-35158-146-9, *Eds. H.W. Reinhardt, G.J. Parra-Montesinos, H. Garrecht*

**PRO 95**: International RILEM Conference on Application of superabsorbent polymers and other new admixtures in concrete construction, ISBN: 978-2-35158-147-6; e-ISBN: 978-2-35158-148-3, *Eds. Viktor Mechtcherine, Christof Schroefl*

**PRO 96 (online version)**: XIII DBMC: XIII International Conference on Durability of Building Materials and Components, e-ISBN: 978-2-35158-149-0, *Eds. M. Quattrone, V.M. John*
**PRO 97**: SHCC3—3rd International RILEM Conference on Strain Hardening Cementitious Composites, ISBN: 978-2-35158-150-6; e-ISBN: 978-2-35158-151-3, *Eds. E. Schlangen, M.G. Sierra Beltran, M. Lukovic, G. Ye*
**PRO 98**: FERRO-11—11th International Symposium on Ferrocement and 3rd ICTRC—International Conference on Textile Reinforced Concrete, ISBN: 978-2-35158-152-0; e-ISBN: 978-2-35158-153-7, *Ed. W. Brameshuber*
**PRO 99 (online version)**: ICBBM 2015—1st International Conference on Bio-Based Building Materials, e-ISBN: 978-2-35158-154-4, *Eds. S. Amaziane, M. Sonebi*
**PRO 100**: SCC16—RILEM Self-Consolidating Concrete Conference, ISBN: 978-2-35158-156-8; e-ISBN: 978-2-35158-157-5
**PRO 101 (online version)**: III Progress of Recycling in the Built Environment, e-ISBN: 978-2-35158-158-2, *Eds. M. Quattrone, V.M. John*

**RILEM Reports (REP)**

**Report 19**: Considerations for Use in Managing the Aging of Nuclear Power Plant Concrete Structures (ISBN: 2-912143-07-1); *Ed. D. J. Naus*
**Report 20**: Engineering and Transport Properties of the Interfacial Transition Zone in Cementitious Composites (ISBN: 2-912143-08-X); *Eds. M. G. Alexander, G. Arliguie, G. Ballivy, A. Bentur and J. Marchand*
**Report 21**: Durability of Building Sealants (ISBN: 2-912143-12-8); *Ed. A. T. Wolf*
**Report 22**: Sustainable Raw Materials—Construction and Demolition Waste (ISBN: 2-912143-17-9); *Eds. C. F. Hendriks and H. S. Pietersen*
**Report 23**: Self-Compacting Concrete state-of-the-art report (ISBN: 2-912143-23-3); *Eds. Å. Skarendahl and Ö. Petersson*
**Report 24**: Workability and Rheology of Fresh Concrete: Compendium of Tests (ISBN: 2-912143-32-2); *Eds. P. J. M. Bartos, M. Sonebi and A. K. Tamimi*
**Report 25**: Early Age Cracking in Cementitious Systems (ISBN: 2-912143-33-0); *Ed. A. Bentur*
**Report 26**: Towards Sustainable Roofing (Joint Committee CIB/RILEM) (CD 07) (e-ISBN 978-2-912143-65-5); *Eds. Thomas W. Hutchinson and Keith Roberts*
**Report 27**: Condition Assessment of Roofs (Joint Committee CIB/RILEM) (CD 08) (e-ISBN 978-2-912143-66-2); *Ed. CIB W 83/RILEM TC166-RMS*
**Report 28**: Final report of RILEM TC 167-COM 'Characterisation of Old Mortars with Respect to Their Repair (ISBN: 978-2-912143-56-3); *Eds. C. Groot, G. Ashall and J. Hughes*
**Report 29**: Pavement Performance Prediction and Evaluation (PPPE): Interlaboratory Tests(e-ISBN: 2-912143-68-3); *Eds. M. Partl and H. Piber*
**Report 30**: Final Report of RILEM TC 198-URM 'Use of Recycled Materials' (ISBN: 2-912143-82-9; e-ISBN: 2-912143-69-1); *Eds. Ch. F. Hendriks, G. M. T. Janssen and E. Vázquez*

**Report 31**: Final Report of RILEM TC 185-ATC 'Advanced testing of cement-based materials during setting and hardening' (ISBN: 2-912143-81-0; e-ISBN: 2-912143-70-5); *Eds. H. W. Reinhardt and C. U. Grosse*
**Report 32**: Probabilistic Assessment of Existing Structures. A JCSS publication (ISBN 2-912143-24-1); *Ed. D. Diamantidis*
**Report 33**: State-of-the-Art Report of RILEM Technical Committee TC 184-IFE 'Industrial Floors' (ISBN 2-35158-006-0); *Ed. P. Seidler*
**Report 34**: Report of RILEM Technical Committee TC 147-FMB 'Fracture mechanics applications to anchorage and bond' Tension of Reinforced Concrete Prisms – Round Robin Analysis and Tests on Bond (e-ISBN 2-912143-91-8); *Eds. L. Elfgren and K. Noghabai*
**Report 35**: Final Report of RILEM Technical Committee TC 188-CSC 'Casting of Self Compacting Concrete' (ISBN 2-35158-001-X; e-ISBN: 2-912143-98-5); *Eds. Å. Skarendahl and P. Billberg*
**Report 36**: State-of-the-Art Report of RILEM Technical Committee TC 201-TRC 'Textile Rein-forced Concrete' (ISBN 2-912143-99-3); *Ed. W. Brameshuber*
**Report 37**: State-of-the-Art Report of RILEM Technical Committee TC 192-ECM 'Environment-conscious construction materials and systems' (ISBN: 978-2-35158-053-0); *Eds. N. Kashino, D. Van Gemert and K. Imamoto*
**Report 38**: State-of-the-Art Report of RILEM Technical Committee TC 205-DSC 'Durability of Self-Compacting Concrete' (ISBN: 978-2-35158-048-6); *Eds. G. De Schutter and K. Audenaert*
**Report 39**: Final Report of RILEM Technical Committee TC 187-SOC 'Experimental determination of the stress-crack opening curve for concrete in tension' (ISBN 978-2-35158-049-3); *Ed. J. Planas*
**Report 40**: State-of-the-Art Report of RILEM Technical Committee TC 189-NEC 'Non-Destructive Evaluation of the Penetrability and Thickness of the Concrete Cover' (ISBN 978-2-35158-054-7); *Eds. R. Torrent and L. Fernández Luco*
**Report 41**: State-of-the-Art Report of RILEM Technical Committee TC 196-ICC 'Internal Curing of Concrete' (ISBN 978-2-35158-009-7); *Eds. K. Kovler and O. M. Jensen*
**Report 42**: 'Acoustic Emission and Related Non-destructive Evaluation Techniques for Crack Detection and Damage Evaluation in Concrete'—Final Report of RILEM Technical Committee 212-ACD (e-ISBN: 978-2-35158-100-1); *Ed. M. Ohtsu*

# Part I
# Characterization of Binder-Aggregate Interaction

# Development of Failure Master Curve for Asphalt Mastics Characterization

**Pouya Teymourpour and Hussain U. Bahia**

**Abstract** Low temperature performance grading currently relies solely on Bending Beam Rheometer (BBR) for determining low temperature creep stiffness (S) and rate of modulus relaxation (m-value) at 60 s, both determined at low stress-strain levels, in the pre-failure zones. This aspect raises questions with regard to applicability of properties derived from the linear viscoelastic range for prediction of asphalt binder thermal cracking behavior. Furthermore, many researchers have reported a discrepancy between field cracking severity and predictions based on asphalt binder properties since the asphalt binder-aggregate interaction is non-existent in asphalt binder testing. Therefore evaluation of asphalt mastics properties which could save a considerable amount of time and equipment in comparison to mixture testing should be prioritized. These challenges indicate that considering fracture properties of asphalt mastics could be a better approach for prediction of thermal cracking in asphalt pavements. It is believed that development of failure master curves for the damage characterization of asphalt mastics at different temperatures and loading rates would be beneficial for better characterization of resistance to thermal cracking. Therefore, this study presents framework and preliminary results on the development of such asphalt mastic failure master curves using the new BBR-SENB test for damage resistance characterization. The complexity of the visco-elastic behavior of asphalt mastics in terms of time and temperature dependency is also recognized by the sensitivity of the failure properties to changes in loading time and temperature.

**Keywords** Asphalt mastic failure master curves · Strain at failure · Single edge notch-bending (SENB) · Rheology · Visco-elastic behaviour

P. Teymourpour (✉)
Department of Civil and Environmental Engineering, University of Wisconsin—Madison, 3346 Engineering Hall, 1415 Engineering Dr., Madison, WI 53706, USA
e-mail: teymourpour@wisc.edu

H.U. Bahia
Department of Civil and Environmental Engineering, University of Wisconsin—Madison, 3350 Engineering Hall, 1415 Engineering Dr., Madison, WI 53706, USA
e-mail: bahia@engr.wisc.edu



F. Canestrari and M.N. Partl (eds.), *8th RILEM International Symposium on Testing and Characterization of Sustainable and Innovative Bituminous Materials*, RILEM Bookseries 11, DOI 10.1007/978-94-017-7342-3_1

## 1 Introduction and Background

Since early 1900s the importance of the material selection for performance of asphalt mixtures has been realized and studied. Superpave, as the final product of the SHRP asphalt program is a performance related asphalt binder and mixture specification currently used in North America. Current Superpave asphalt binder specifications are based on linear viscoelastic properties and were primarily developed for unmodified asphalt binders. However, research has demonstrated the importance of damage resistance characterization of asphalt binders with respect to pavement distresses (Bahia et al. 2001). Given the increased complexity of mixes currently being produced, including WMA, mixes with high recycled components content, etc. and the fact that mixes accepted under the current specification framework exhibit varying levels of distress while in-service, it is essentially important to incorporate the damage characterization of asphalt materials.

Low temperature cracking is one of the major distresses in asphalt pavement which is a source of pavement deterioration and structural failure. Thermal cracks in asphalt pavement form as a result of high cooling rates and/or low pavement temperature drops due to climatic events. Asphalt research community has investigated thermal cracking extensively in the past two decades and yet it remains one of the most challenging pavement distresses to be evaluated and predicted. Significant progresses have been made in understanding the mechanisms and factors affecting this distress. However current low temperature specification relies on the rheological performance indicators as well as the time-temperature superposition principles under linear viscoelastic small stress-strain conditions. Low temperature performance grading currently relies solely on Bending Beam Rheometer (BBR) for determining low temperature creep stiffness (S) and rate of modulus relaxation (m-value) at 60 s, both determined at low stress-strain levels, in the pre-failure zones. This aspect raises questions with regard to applicability of properties derived from the linear viscoelastic range for prediction of asphalt binder failure properties, especially for modified asphalt binders.

Polymers and polymer-based composite materials usually exhibit time-dependent behavior. Relationship between time and temperature has been significantly important in investigating these types of materials. The time-temperature superposition is one of the most efficient methods for predicting the long-term behavior of polymers. This principle in which time is equivalent to temperature for viscoelastic materials was first proposed by Lenderman in 1943 (Starkova and Aniskevich 2009; Cheng and Yang 2005). Williams, Landel and Ferry subsequently proposed a semi empirical formula based on the concept of free volume to describe the principle quantitatively known as Williams-Landel-Ferry equation (Williams et al. 1955; Cheng and Yang 2005). The TTS principle has also been shown that can be applicable to asphalt materials and these types of materials can have thermo-rheologically simple behavior in small strain deformations. This implies that properties of the material at different set of conditions can be predicted by a limited set of stress-strain measurements under a given set of temperature and

loading rates/frequencies (Andriescu and Hesp 2009). Theoretical 'master curves' were then developed in order to express the effect of time and temperature on viscoelastic properties of material considering the effect of each factor to be equivalent. Master curves are determined by transiting the graphs of the viscoelastic functions (determined at different temperatures) along the log time or frequency axis at one reference temperature until they form a continuous curve. Christensen and Anderson have shown that the temperature dependence of asphalt binder can be expressed using the WLF equation and the shift factors determined from rheological data may be used to generate failure master curves (Anderson et al. 1994).

During the development of the Strategic Highway Research Program (SHRP) the time-temperature superposition principle was used to develop the low temperature specification of asphalt binders (Anderson et al. 1994; Anderson and Kennedy 1993). Significant progress has been made in understanding the rheology of bitumen under small stress-strain conditions. Traditionally, master curves for rheological properties such as complex modulus (G*) and phase angle (δ) have been used to predict the response of bitumen under different loading time and temperature conditions. Time-temperature superposition combines the rheological property data obtained at different temperatures to generate the master curves by shifting the data obtained at different temperatures horizontally with respect to time until they merge into a single smooth curve (Anderson and Kennedy 1993). This has to be done in order to effectively model the behavior of asphalt binders and predicts the stress-strain relationships over a wide range of temperatures and loading times.

The linear viscoelastic behavior of the asphalt binders determined from rheological master curves can be a good tool to predict the low temperature behavior of asphalt binders. Recently there have been some efforts in verifying the application of TTS during the presence of cracks in asphalt materials. In one of these studies the validity of TTS was evaluated when cracks initiated and propagated in asphalt mixtures using the four point bending beam. They have reported that by applying same shift factors driven from complex modulus of asphalt mixture, the smooth master curve can be captured crack propagation in asphalt mixtures (Nguyen et al. 2013). However, little work has been reported on the development of failure master curves for the non-linear and damage characterization of asphalt binder and asphalt mastics for different temperatures and loading rates, which might be necessary for the specification purposes and for a more realistic materials characterization. This study presents preliminary results on the development of such failure master curves for both asphalt binder and asphalt mastics. Failure characterization of bitumen and mastics is performed by using the Single Edge Notched Bending (BBR-SENB) test at different loading rates and testing temperatures. Stress and strain at failure ($\sigma_f$ and $\varepsilon_f$) are used as the properties to be shifted in the generation of the failure master curves.

The main objectives of this study are to determine the effects of asphalt binder-mineral filler interaction on thermal cracking behavior of asphalt mixtures through developing asphalt mastic failure master curves and cover shortcomings in the knowledge of asphalt mastics brittle and ductile fracture behavior.

# 2 Materials and Test Methods

## 2.1 Materials

An experiment was designed in order to characterize the failure properties of asphalt binder and asphalt mastics in addition to study the applicability of time-temperature superposition principle to construct a failure master curve. An unmodified PG 64-22 asphalt binder and six different asphalt mastics were selected for this study. There are several filler and asphalt binder properties that demonstrate some influence on asphalt mastic low temperature properties and thus a selected set of properties are controlled in this study. Mineral fillers used in the asphalt industry are predominantly natural materials that are commonly used in hot mix asphalts. Filler sources were controlled in this study with considering three parameters of Rigden Voids and surface area and specific gravity. Three different fillers including Granite, Basalt and Hydrated Lime, were selected and their corresponding Rigden Voids (RV), surface area (BET), and specific gravity (SG) values are summarized in Table 1. The fillers listed were selected in a way that spanned a wide range for the surface area and Rigden. The Cisler granite was acquired from a quarry located in central Wisconsin. The hydrated lime was acquired from Western Lime a subsidiary of Graymont.

The asphalt mastics used in the investigation were created using the mineral filler passing the #200 (75 μm) sieve and the asphalt binder previously mentioned. The amount of filler added corresponded with a volume fraction of filler expressed as a percentage of the total volume of the composite material. The asphalt binder and the mineral filler contents of asphalt mastic samples were determined based on the volume fraction chosen for the asphalt mastics as shown in the following equations. Therefore for each specimen with 20 % volume fraction, 120 g of asphalt binder and 80 g of mineral filler were prepared and mixed together while for the 35 % volume fraction specimens, the weight of asphalt binder and fillers were measured to be 83.6 and 116.4 g, respectively.

$$M_f = \frac{\varphi S_f}{S_b(1-\varphi) + \varphi S_f} M_m \tag{1}$$

$$M_b = M_m - M_f \tag{2}$$

**Table 1** Physical characterization of mineral fillers used in current study

| Mineral filler | Code | RV (%) | BET ($m^2/g$) | SG ($g/cm^3$) |
|---|---|---|---|---|
| Basal vesicular | BV1 | 37.80 | 10.21 | 2.79 |
| Cisler granite | CSG | 32.75 | 2.17 | 2.66 |
| Hydrated lime | HL | 52.80 | 21.31 | 2.46 |

where,
$M_m$ Asphalt mastic weight (i.e. 200 g)
$M_f$ Mineral filler weight (g)
$M_b$ Asphalt binder weight (g)
$S_b$ Asphalt specific gravity (i.e. 1.03)
$S_f$ Mineral filler specific gravity
φ Volume fraction

To blend the asphalt mastics different volume fractions were calculated in terms of their corresponding masses in grams for each component of asphalt and filler. The mastic specimens were prepared following the improved Superpave binder testing specimen procedure. For each specimen, the binder and filler were prepared and heated at mixing temperature (155 °C) in separate cans for 30 min. Then, the filler was slowly added to the asphalt binder in the oven. A mechanical mixer was used to blend the materials at mixing temperature. The mixing process was carefully followed to make sure that filler was homogeneously dispersed in the asphalt binder.

The mastic was continuously stirred as it cooled to prevent settling and once the asphalt mastic was completely blended it was placed in a vacuum oven at 155 °C for 1 h to remove any air entrapped in the asphalt mastic through the blending process. The mastics were stirred and then poured into the BBR-SENB molds. The specimens were allowed to cool down to room temperature for two hours and then de-molded.

## *2.2 Test Method*

The BBR-SENB system was developed for measuring asphalt binder, asphalt mastic, and mortar cracking resistance at low service temperatures (Velasquez et al. 2011, 2012). The test uses a modified Bending Beam Rheometer (BBR), with the addition of a loading motor that controls the displacement rate during testing, a load cell with a higher capacity than the regular BBR, and modified beam placement fixtures which further information about preparation and characteristics of specimen and test configuration can be found elsewhere (Velasquez et al. 2011). Tests were run at three displacement rate of 0.0025, 0.01 and 0.04 mm/s in this study. These three values were selected in a way to result in widest range of strain rate in one temperature with maintaining desirable repeatability. In the BBR-SENB analysis, an important fracture index obtained is the deflection at maximum load. Historically, maximum deflection at fracture has been found to correlate very well with field performance and it has been used as a parameter that indicates the ductile to brittle transition of asphalt binders (Marasteanu et al. 2012). Both asphalt binder and asphalt mastics were short term aged according to the Rolling Thin-Film Oven Test (RTFOT) procedure (AASHTO T240-09-UL) prior to specimen preparations. Table 2 provides a summary of the controlled variables and levels in the experimental plan.

**Table 2** Experimental plan for failure master curve study

| Factor | Asphalt binder | Filler type | Volume fraction | Temperature (°C) |
|---|---|---|---|---|
| Level | 1 | 3 | 2 | 5 |
| Description | PG 64-22 | Granite<br>Basalt<br>Hydrated lime | −6, −9, −12, −18, −24 | 0.0025<br>0.01<br>0.04 |

## 3 Discussion of Results

Nominal stress was computed by dividing the measured tensile force by the original cross-sectional ligament area (specimen cross section are with the exclusion of notch area). The displacement at failure, $u_f$, was calculated as the amount of displacement in motor ram of the BBR-SENB. Nominal strain was then computed using the three points flexural test. Equations used for measuring stress and strain are shown in the following:

$$\varepsilon_f = \frac{6u_f d}{L^2} \tag{2}$$

$$\sigma_f = \frac{3PL}{2bd^2} \tag{3}$$

where
$\varepsilon_f$ Strain at failure
$\sigma_f$ Stress at failure (kPa)
L Support span (mm)
P Load at failure (kN)
$u_f$ Displacement at failure (mm)
d Depth of tested beam (mm)
b Width of tested beam (mm)

The stress-strain curves are derived for each tested material and Fig. 1 shows the typical stress strain curves at a fixed temperature (i.e. −9 °C) at different deformation rates for the neat asphalt binder as well as one of the asphalt mastics (20 % HL).

It can be seen that both asphalt binder and asphalt mastic are strain rate sensitive materials. It can also be observed from Fig. 1 that the overall strain level experienced by specimen before failure increases with decreasing deformation (strain) rate; however the effect of strain rate on failure stress is relatively small for the three deformation rates investigated. In addition, for the same materials Fig. 2 shows the BBR-SENB test results at different temperatures with deformation rate of 0.01 mm/s.

These curves show higher tensile strength for asphalt mastic compared to that of asphalt binders which can be attributed to the presence of the filler in asphalt mastic.

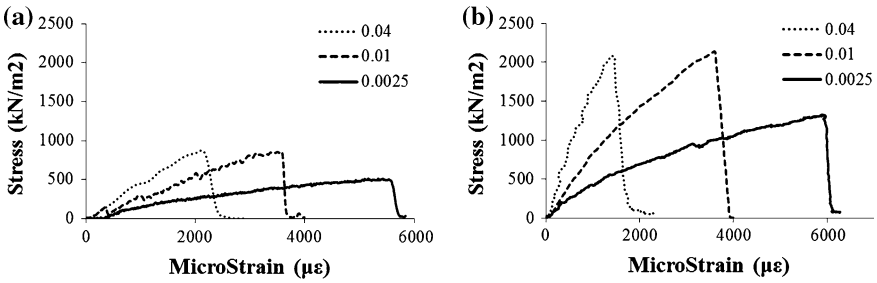


**Fig. 1** Effect of deformation rate on stress-strain curves for **a** neat asphalt binder **b** 20 % HL asphalt mastic

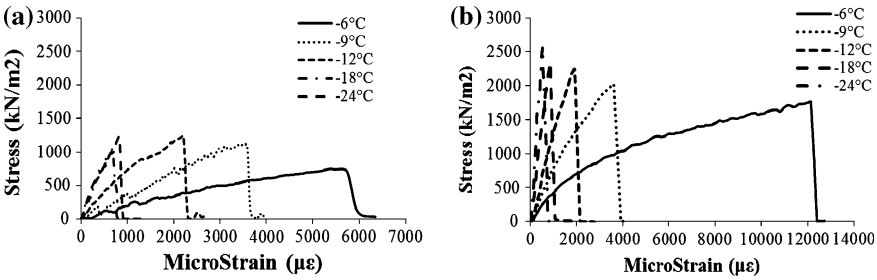


**Fig. 2** Effect of temperature on stress-strain curves for **a** neat asphalt binder **b** 20 % HL asphalt mastic

Fillers can delay fracture by their crack pinning effect as well as by increasing the crack path length. Figure 2 shows how decreasing the temperature at the same deformation rate (i.e. 0.01 mm/s) decreases the failure deflection, while the failure stress seems to increase up to a point, after which the failure stress does not significantly increase as temperature decreases.

The applicability of time-temperature superposition principle to low temperature properties of asphalt mastics has been studied in the current research and Fig. 3 show the dependence of the strain at failure on applied displacement rate for the bitumen and the mastics produced with 20 % volume fraction of different fillers.

What it can be seen from the figure is that the different mineralogy of fillers result in similar failure behavior at different temperatures. It can also be inferred that failure strain is less strain rate independent at lower temperatures. It indicates the presence of a low level of strain at failure for each material where changing the strain rate does not affect significantly the failure thermal strain. This low limit may be different for different base asphalt binders. The data presented suggest that failure strain can be combined to construct master curves. Previous studies have shown that failure strain for a given material is a universal function of a reduced strain rate although this might not be valid for very short loading times or high strain rate (Anderson et al. 1994). Although fillers are behaving as elastic materials

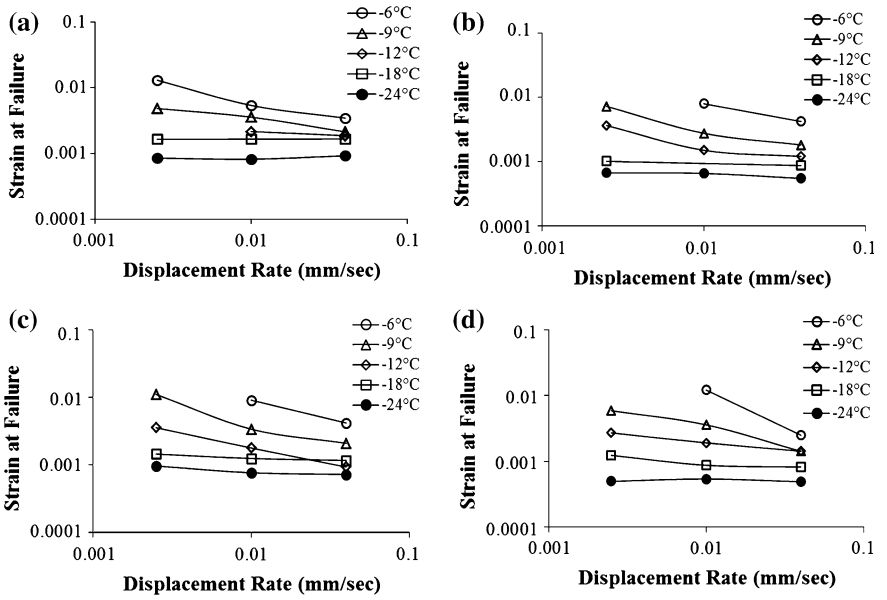


**Fig. 3** Failure strain versus real deformation rate for **a** neat asphalt binder **b** 20 % BV1 asphalt mastic **c** 20 % CSG asphalt mastic and **d** 20 % HL asphalt mastic

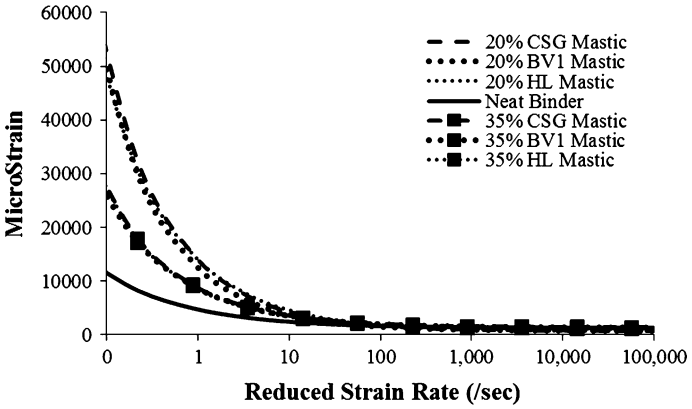


**Fig. 4** Failure strain master curves for neat asphalt binder and asphalt mastics with 20 and 35 % filler

in the asphalt mastic composites, the data presented in Fig. 3 suggests the probability of constructing master curves for asphalt mastics as well. Therefore failure master curves can be constructed for asphalt mastics in order to predict the behavior of the materials at high strain rates. Figure 4 shows failure strain master curves for bitumen and the six mastics investigated.

It was found that failure strain is related to reduced strain rate at a reference temperature of −12 °C by:

$$F(f) = \varepsilon_{min} + (\varepsilon_{max} - \varepsilon_{min})\left[1 + \left(f_c/a_{Tf}\right)^k\right]^{-m/k} \tag{3}$$

where

$$\log a_T = -c_1(T - T_0)/[c_2 + (T - T_0)] \tag{4}$$

The data presented earlier for each asphalt mastic at different temperatures (i.e. T) and strain rates (i.e. f) were fit to this function without any conditions by varying the parameters $\varepsilon_{min}$, $\varepsilon_{max}$, $f_c$, $m$, $k$, $c_1$ and $c_2$ to minimize the summation of squared errors using least square regression method. It is shown in Fig. 4 that although the mineralogy of the fillers have effect on the failure properties of asphalt mastics, the main factor governing the trend of the master curves is the volume fraction of filler in the asphalt mastic. Once again the results depicted that at very high strain rates all the asphalt mastics behave similarly showing their minimum strength toward failure.

In addition to strain master curves, stress at failure at different strain rates and temperatures should be considered for failure study of asphalt binders and asphalt mastics since determining the failure strengths of asphaltic materials by testing at a given temperature and at one selected strain rate is potentially inadequate for determining the behavior of the materials when they are subjected to a broad range of strain rates and temperatures. The same idea was applied to shift the stress at failures resulted from BBR-SENB at different temperatures horizontally to construct failure stress master curves. The measured stresses at different strain levels were fitted to a curve using the following equation:

$$F(f) = \sigma_{min} + (\sigma_{max} - \sigma_{min})\left[1 + \left(f_c/a_{Tf}\right)^k\right]^{-m/k} \tag{5}$$

where

$$\log a_T = \left(\frac{c_1}{2.302c_2}\right) * \left(\frac{1}{T} - \frac{1}{T_0}\right) \tag{6}$$

In this case as it was mentioned earlier the stresses at failure were divided by the initial cross-sectional area and then were shifted laterally to construct the master curve of failure stress versus strain rate. It should be also noted that the shift factors derived from the two formulas were almost identical for both strain and stress master curves. The results are presented in Fig. 5.

Results presented above show that for most of the materials at lower strain rates which corresponds to lower pavement cooling rates, the failure stress remains almost constant. Also stress at failures of asphalt mastics with different mineral

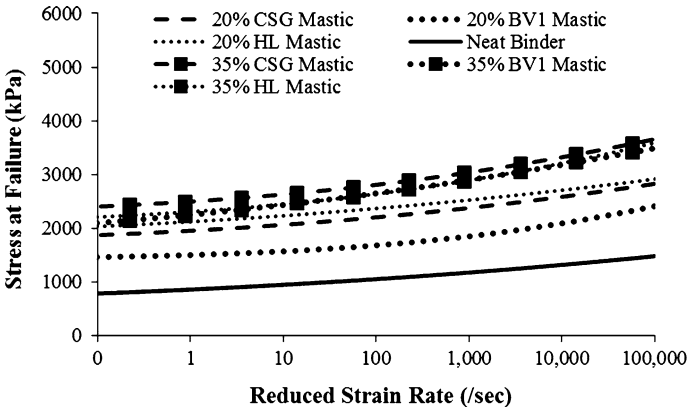


**Fig. 5** Failure stress master curves for neat asphalt binder and asphalt mastics with 20 % filler

fillers and concentrations showed to be not sensitive to strain rates especially at lower values of reduced strain rates. The different types and contents of fillers show a low and similar strain rate dependence, however they result in a different stress at failure values over of strain rates. Proper strain rate selection for an asphalt binder or asphalt mastic failure test such as the BBR-SENB used in current study is one of the most important factors for characterizing the behavior of viscoelastic materials. Furthermore, it is of significant importance to be able to use relevant conditions representing that of the expected pavement service conditions. In a recent study, Tabatabaee and Bahia (2014) investigated the relationship between pavement cooling rates and the resulting strain rate in asphalt binder and asphalt mastic phases. They measured thermal strain buildup during different cooling events and found the rate of increase in thermal strain of asphalt binder or asphalt mastic at that specific cooling rate is constant (Tabatabaee and Bahia 2014). Thermal cracking is happening as the result of shrinkage of a pavement when it is cooling down and the strain rate is dependent on the cooling rate. Therefore the applied strain rate tries to simulate the cooling phenomenon happening in the actual field and thus it is significantly beneficial to use a strain rate representing pavement service condition.

One of the advantages of constructing master curves is the capability to predict failure strain at different strain rates without actually testing them in all conditions and therefore with the proper selection of strain rate as explained, relevant failure properties of asphalt mastics in the actual pavements can be estimated.

## 4 Concluding Remarks

This study investigated the role of mineral fillers in the low temperature laboratory responses of asphalt mixtures by means of development of asphalt mastic fracture master curves. BBR-SENB testing was performed to evaluate the effect of mineral

fillers on fracture properties of asphalt mastics and also to construct the fracture master curves. The following points summarize the important findings:

- The results presented in this study show that time temperature superposition principles can be applied to asphalt mastics that are considered as composite materials including both elastic and viscoelastic materials.
- The results show that asphalt mastics have significantly different fracture behavior than asphalt binders and thus it is better to test asphalt mastics to predict mixture cracking.
- In the small number of samples tested, it is clear that filler volume fraction is very important but this needs to be further verified with a larger set of fillers and asphalt binders.
- The results show clearly that strain at failure is the most sensitive parameter to cooling rate while stress at failure is not very sensitive. Therefore in areas where cooling rates vary significantly, more emphasize on failure strain should be placed.
- At lower cooling rates and resulting lower asphalt mastic strain rates which are correspondent to field properties, the strain at failure showed to be the controlling factor since the failure stresses are almost constant.
- The constructed asphalt mastic failure master curves can be used to find the failure strain at different pavement cooling rates. This failure parameter can be used in estimation of strain failure at which asphalt mixture will crack at the specified cooling rate.

## References

Anderson, D. A. & Kennedy, T., 1993. Developement of SHRP binder specification. *Proceedings of Association of Asphalt Pavement Technologists,* Volume 62, pp. 481-507.

Anderson, D. A. et al., 1994. *binder characterization and evaluation (SHRP A-369), Vol. 3, Physical characterization,* Washington, D.C.: National research Council.

Andriescu, A. & Hesp, A. M., 2009. Time-temperatrue superposition in rheology and ductile failure of asphalt binders. *International Journal of Pavement Engineering,* 10(4), pp. 229-240.

Bahia, H. et al., 2001. *Characterization of Modified Asphalt Binders in Superpave Mix Design,* Washington D.C.: National Academy Press.

Cheng, R. & Yang, H., 2005. Application of time-temperature superposition principle to polymer transition kinetics. *Journal of Applied Polymer Science,* 99(4), pp. 1767-1772.

Marasteanu, M., Buttlar, W., Bahia, H. U. & Williams, C., 2012. *Investigation of Low Temperature Cracking in Asphalt Pavements,* s.l.: National Pooled Fund Study-Phase II.

Nguyen, M. L., Sauzeat, C., Di Benedetto, H. & Tapsoba, N., 2013. Validation of the Time-Temperature Superposition Principle for Crack Propagation in Bituminous Mixtures. *Materials and Structures,* Volume 46, pp. 1075-1087.

Starkova, O. & Aniskevich, A., 2009. Application of time-temperature superposition to energy limit of linear viscoelastic behavior. *Journal of Applied Polymer Science,* 114(1), pp. 341-347.

Tabatabaee, H. A. & Bahia, H. U., 2014. Establishing use of asphalt binder cracking test for prevention of pavement cracking. *Journal of Association of Asphalt Paving Technologists,* Volume 83.

Velasquez, R., Tabatabaee, H. & Bahia, H., 2011. Low temperature cracking characterization of asphalt binders by means of the Single Edge Notched Bending (SENB) test. *Journal of Association of Asphalt paving Technologists,* Volume 80, pp. 583-614.

Velasquez, R., Tabatabaee, H., Puchalski, S. & Bahia, H., 2012. *The role of asphalt binder fracture properties in thermal cracking performance of mixtures and pavements.* Vancouver, Canadian Technical Asphalt Association (CTAA).

Williams, M. L., Landel, R. F. & Ferry, J. D., 1955. The Tempratur Dependence of Relaxation Mechanisms in Amorphous Polymers and other Glass-Forming Liquids. *Journal of American Chemistry Society,* Volume 77, pp. 3701-3707.

# Semi-automatic Evaluation of the Degree of Bitumen Coverage on Bitumen-Coated Aggregates

**Riccardo Lamperti, Claudio Lantieri, Cesare Sangiorgi, Gabriele Bitelli and Andrea Simone**

**Abstract** EN 12697-11 is the standard providing test methods for evaluating affinity between aggregate and bitumen and its influence on the susceptibility of the mixture to stripping. Among the methods, the rolling bottle test has a number of advantages in terms of rapidity, low costs, and suitability for routine testing. However, since affinity is assessed by visual registration of two independent operators, results may be altered by a large amount being inevitably subjective. The authors suggest a semi-automatic procedure to overcome potential limits and shortcomings of the method and obtain accurate results. Different mixtures were analyzed and compared, using common natural and recycled aggregates and a 70/100 pen bitumen. The procedure was successfully validated with a manual pixel inspection and confusion matrixes were created. The results showed that the procedure lead to a more reliable registration compared to the standard method and it is suitable, with different accuracies, for both light and dark aggregates.

**Keywords** Rolling bottle test · Adhesion · Bitumen · Confusion matrix

## 1 Introduction

Asphalt mixture is a complex and heterogeneous material that includes aggregates, asphalt binder and air voids. Its overall mechanical response is primarily governed by the asphalt binder and by the stone-on-stone contacts between aggregates (Dondi et al. 2012; Vignali et al. 2014). Loss of adhesion between bitumen and aggregates and loss of cohesion within the mixture, in the presence of water, are referred to as moisture damage and represent one of the main causes of distress in asphalt pavements. The adhesion quality (i.e. affinity) between binder and aggregate is

R. Lamperti (✉) · C. Lantieri · C. Sangiorgi · G. Bitelli · A. Simone
Department of Civil, Chemical, Environmental, and Materials Engineering—DICAM, University of Bologna, Bologna, Italy
e-mail: riccardo.lamperti2@unibo.it



F. Canestrari and M.N. Partl (eds.), *8th RILEM International Symposium on Testing and Characterization of Sustainable and Innovative Bituminous Materials*, RILEM Bookseries 11, DOI 10.1007/978-94-017-7342-3_2

essential for the stability, quality and endurance of the road under climate and traffic. Although not all damage is caused directly by moisture, its presence increases the extent and severity of already existing distresses like cracking, potholes, and rutting (Miller et al. 2003). The presence of moisture results in a degradation of the mechanical properties of the asphalt mixture, i.e. loss of stiffness and mechanical strength, which ultimately leads to the failure of the road structure (Grenfell et al. 2014). Many researchers have recognized that the replacement of bitumen film from the aggregate surface by water, referred to as stripping, is linked to interfacial tension relations of these materials (Hefer 2004; Bhasin 2006).

The standardized approach to quantify the affinity between aggregate and bitumen is the rolling bottle test (EN 12697-11). It consists in placing a mix of bitumen and aggregates in a bottle filled with de-ionized water and then placing it in a rolling machine in order to subject the material to a mechanical stirring action in the presence of water. After defined time steps, normally 6 and 24 h, two independent operators visually estimate the residual degree of bitumen coverage of the particles. Despite being a rapid, simple and low costs test, results may be altered by a large amount being the determination of the bitumen coverage degree inevitably subjective. The main factors that may influence the estimation are linked to the skills of the operators, the light conditions and the color of the aggregates. Dark or grey aggregates like basalt or blast furnace slag may be confused with bitumen. Different attempts were made in order to improve the determination of the degree of bitumen coverage of aggregates after the rolling bottle test is performed. Mulsow (2012), based on the observation that the micro-roughness of the surface of the aggregate is significantly higher than bitumen, studied the adhesion with a multi-directional reflectance measurement. Grönninger et al. (2010) and Källén et al. (2012) used supervised classification and advanced segmentation methods of RGB images respectively. Despite these efforts, a standard and validated procedure has not been found yet.

## 2 Experimental Work

The aim of this paper is to propose an alternative assessment method in order to overcome the potential limits of the visual estimation procedure of the rolling bottle test. A series of rolling bottle tests was performed. Three independent skilled operators made visual observation of the samples after 6 and 24 h. Furthermore, at each time step, digital pictures of the samples were taken and processed with a software to obtain a second estimation. This estimation is based on RGB images that are subjected through a series of filters, first deleting the background, and then isolating the only bitumen pixels. The affinity estimation of blends is made by computing the areas of the bitumen and of the aggregates on the images.

Results of both estimations and a comparison between them is presented. The procedure was validated by checking the accuracy of the software measurements on a 51 × 51 grid of points on the images, for each different adopted aggregates. This lead to create confusion matrices to interpret the accuracy of the software estimation.

## 2.1 Materials and Equipment

Four different aggregates were tested: porphyry, limestone, basalt and blast furnace slag (Fig. 1). They were selected in order to cover a broad range of colors. All aggregates were sieved and washed to obtain a 8–11 mm fraction, according to standard. The adopted base bitumen was a 70/100 pen. Three bottles were tested for each mix for a total of 24 observations.

The materials were heated at 160 °C. All the procedures described in EN 12697-11 for mixing and testing were followed. Rolling speed was 60 rpm and the tests were performed at a temperature of 20 ± 1 °C. Visual observation were made after 6 and 24 h and digital images were taken accordingly.

## 2.2 Research Approach

The use of a computer aided analysis technique is suggested and is based on digital picturing of the bitumen-aggregate sample after the rolling phase and on the classification of characteristic color areas by means of a commercial software (Grönniger et al. 2010). In this regard a specific photographic set was developed (Fig. 1a). The tested blends were put into a plate filled with de-ionized water. The plate had a green background and was irradiated with 2 lamps with an angle of incidence of the light beam of 45° in order to avoid reflections. Picture were taken vertically with a 10 MP camera, with ISO 100, from a distance of 30 cm. Pictures were further processed with a public domain Java-based imaging program. Among the different color spaces available, the YUV was chosen. The YUV color space separate RGB into luminance and chrominance information (Ford et al. 1998) in terms of one luma (Y) and two chrominance (UV) components. Luma stands for brightness, or lightness, while U and V provide color information and are "color difference" signals of blue minus luma (B-Y) and red minus luma (R-Y). YUV was

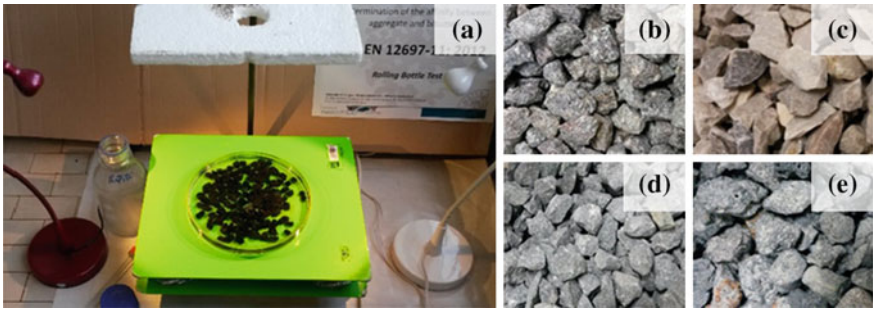


**Fig. 1** **a** Set for digital picturing of tested samples; **b** Porphyry; **c** Limestone; **d** Basalt; **e** Blast furnace slag samples


**Fig. 2** Image filtering process. **a** Original image; **b** Non-classified image; **c** Classified image

chosen because of its ability to decouple the luminance and color information where the image can be processed with no effect on the other color components (Ibraheem et al. 2012).

This peculiarity was confirmed after testing the other available color spaces (i.e. HSB, RGB and CIE Lab) which gave worse results in terms of quality of the image classifications.

The adopted software allows defining a specific threshold for each of the Y, U & V component that compose the image. Therefore, acting on these ranges the image was filtered, leaving out the background. Once the image contained only aggregates and bitumen pixels, referred to as *non-classified image* (Fig. 2b), the Y, U & V components ranges were further reduced in order to get only the bitumen pixels as shown in the *classified image* of Fig. 2c. At each step, the program allowed measuring the selection areas, i.e. the sum of pixels within the specified YUV ranges. The bitumen plus aggregates and the only bitumen areas were automatically computed, enabling the calculation of the percentage of the bitumen coverage of the aggregates with Eq. (1):

$$Bitumen\ coverage = \frac{A_{bitumen}}{A_{bitumen+aggregates}} \times 100\ [\%]. \tag{1}$$

## 3 Results

Table 1 shows the YUV ranges found for the image identification of the studied bituminous materials. Y, U & V can vary from 0 to 255. Lower or upper limits vary with different exposure conditions, i.e. with natural light, artificial light only or both. In order to reproduce the analysis of the same materials, an operator could apply these YUV sets and easily obtain the non-classified and the classified images. For example, for the identification of U parameter of the Limestone in the classified image, the lower limit is chosen between 80 and 100 and the upper limit is 255.

**Table 1** YUV ranges for materials' recognition

| | | Limestone (L) | Porphyry (P) | Basalt (B) | Blast furnace slag (S) |
|---|---|---|---|---|---|
| Non - classified image | Y | 0–195 | 0–165 | 0–165 | 0–195 |
| | U | (80 ÷ 100) − 55 | (80 ÷ 90) − 255 | (90 ÷ 110) − 255 | 100–255 |
| | V | (110 ÷ 120) − 255 | (115 ÷ 120) − 255 | (105 ÷ 120) − 255 | 120–255 |
| Classified image | Y | 0 − (55 ÷ 85) | 0 − (25 ÷ 35) | 0 − (25 ÷ 45) | 120–255 |
| | U | (80 ÷ 100) − 255 | (80 ÷ 90) − 255 | (90 ÷ 110) − 255 | 100–255 |
| | V | (110 ÷ 120) − 255 | (110 ÷ 120) − 130 | (105 ÷ 120) − 255 | 120–128 |

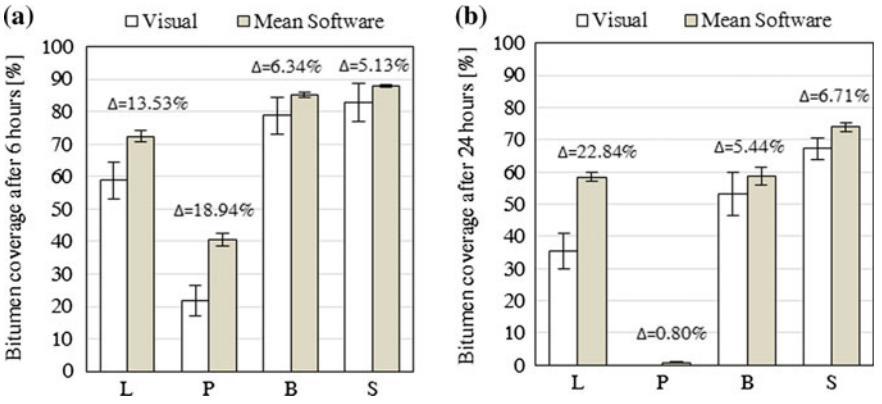


**Fig. 3** Results of rolling bottle tests after 6 h (**a**) and 24 h testing (**b**)

Figure 3 shows the results of the tests. The white columns represent the visual estimation carried out by three independent skilled operators, while the dark columns represent the software semi-automatic classification. Results are shown in terms of mean (%) and standard deviation of all the observations, i.e. three for the software and nine for the visual estimations (three bottles and three operators).

Considering the software recognition, the limestone exhibited a percentage of coverage at 6 h of 72.4 ± 1.6 and of 58.4 ± 1.4 after 24 h. The porphyry was the more prone to stripping (40.6 ± 2.0 after 6 h and 0.8 ± 0.2 after 24 h). The basalt showed a higher bitumen coverage after 6 h 85.2 ± 0.8 and reached a coverage comparable to that of limestone after 24 h (58.8 ± 2.6). The blast furnace slag gave the best performance compared to the other aggregates (87.91 ± 0.49 after 6 h and 73.93 ± 1.48 after 24 h).

Furthermore Fig. 3 allows for a comparison between the software and the visual registrations. Regardless of the accuracy, light colored aggregates (L & P) exhibited the higher gap between the visual estimation and the software recognition, with a maximum difference of 22.84 % for the limestone after 24 h. On the other hand, differences of recognition for dark aggregates like basalt and blast furnace slag

amounted to 5–6 %. Standard deviations of the results of the software measurements were smaller compared to those of the visual estimations. As a result, the proposed procedure would give reliable results with less tested bottles, reducing the material needed as well as test and processing time.

## 4 Procedure Validation

The proposed procedure was also validated in order to obtain its degree of accuracy. Pixels colors of samples images were manually checked to understand whether the imaging software classified them correctly (i.e. background, bitumen or aggregate) or not.

For this purpose a specific Java-based code was written, in order to superimpose a 51 × 51 grid of equidistant points on both the non-classified and the classified image and extract their RGB values and $x$, $y$ coordinates (Fig. 4).

The selected pixels of both images were grouped in three different classes (aggregate, bitumen and background) based on their RGB values. According to the described procedure of recognition, the passage from the non-classified to the classified image was analyzed: if the estimation of the software were correct the bitumen classified pixels would be still classified as bitumen, while the aggregate pixels would be re-classified as background. The superimposed grid helped in identifying whether the software classification was made correctly or not.

Figure 5 shows a detail of the pixels' color inspection. Circles represent the correctly classified pixels, (1) is background, (2) is bitumen and (3) is aggregate. The square (4) is an example of misclassification; in fact this pixel was classified as

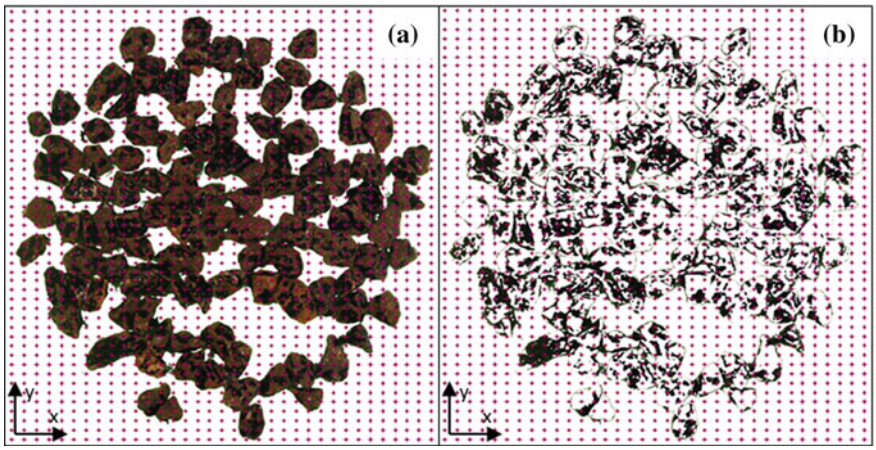


**Fig. 4** Validation of the technique: pixels' color inspection for the non-classified (**a**) and classified (**b**) images

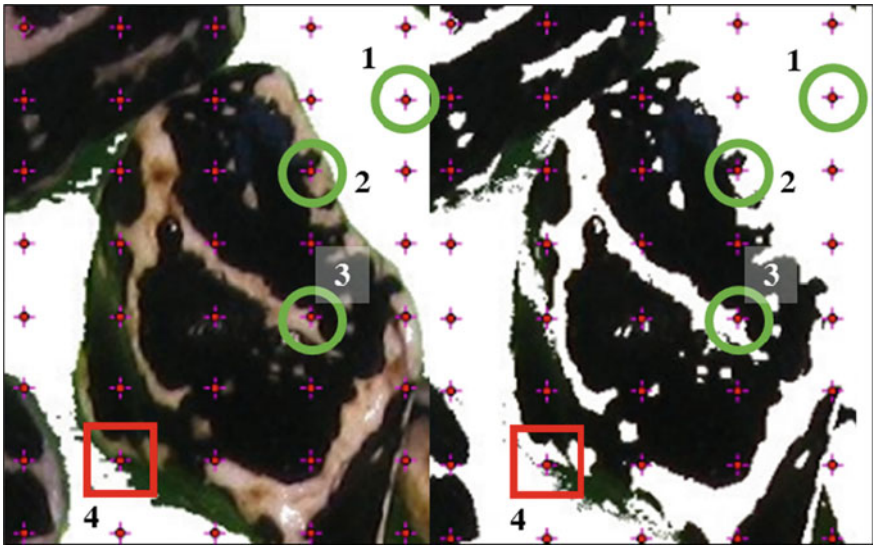


**Fig. 5** Detail of pixels' color inspection: correct and incorrect classifications

bitumen while it was actually a shadow pertaining to the background. However, almost all shadows were classified correctly and represented far less than 1 % of all the background pixels.

The adopted procedure validation allowed the generation of confusion matrices that could be used in a series of descriptive and analytical techniques, such as those based on accuracy indices.

In the search for the fundamental characteristics of a generalized confusion matrix for classifications, it is suggested that the matrix should fulfill two characteristics in order to identify a perfect matching case:

- Diagonalization. The matrix should be diagonal if, and only if, the assessed data match perfectly the reference data;
- Marginal sums. Marginal sums should match the total grades from the reference and assessed data.

Four different accuracy indexes were computed for each matrix (Table 2).

Where *Pkj* is the element in row *k* and column *j* and *Pkk* is the element in row *k* and column *k*. An overestimation of the reference pixel membership by the assessed pixel membership leads to errors of commission type (linked to the User accuracy). These commission errors appear in the off-diagonal cells along the row of the class. Conversely, an underestimation of the reference value by the assessed value leads to errors of omission type (linked to the Producer accuracy). These omission errors appear in the off-diagonal cells along the column of the class (Silván-Cárdenas et al. 2008). Tables 3, 4, 5, and 6 show the confusion matrices of the tested aggregates and their accuracy indexes. "*bkGD*" stands for background,

**Table 2** Accuracy indexes for a matrix with k classes

| Overall accuracy (OA) | Bitumen-aggregate accuracy (BAA) | kth user accuracy (UA) (k) | kth producer accuracy (PA) (k) |
|---|---|---|---|
| $\frac{\sum_k Pkk}{\sum_{kj} Pkj}$ | $\frac{\sum_{k=1}^{2} P_{kk}}{\sum_{k,j=1}^{2} P_{kj}}$ | $\frac{P_{kk}}{\sum_j P_{kj}}$ | $\frac{P_{kk}}{\sum_j P_{jk}}$ |

**Table 3** Confusion matrix and accuracy indexes for Limestone

| | Class | Reference data | | | Sum | User's accuracy (%) |
|---|---|---|---|---|---|---|
| | | L | Bit. | bkGD | | |
| Classified image | L | 204 | 17 | 2 | 223 | 91.5 |
| | Bit. | 5 | 529 | 8 | 542 | 97.6 |
| | bkGD | 0 | 0 | 1836 | 1836 | 100.0 |
| Sum | | 209 | 546 | 1846 | 2601 | |
| Producer's accuracy (%) | | 97.6 | 96.9 | 99.5 | | |

**Table 4** Confusion matrix and accuracy indexes for Porphyry

| | Class | Reference data | | | Sum | User's accuracy (%) |
|---|---|---|---|---|---|---|
| | | P | Bit. | bkGD | | |
| Classified image | P | 421 | 10 | 0 | 431 | 97.7 |
| | Bit. | 15 | 316 | 17 | 348 | 90.8 |
| | bkGD | 0 | 0 | 1822 | 1822 | 100.0 |
| Sum | | 436 | 326 | 1839 | 2601 | |
| Producer's accuracy (%) | | 96.6 | 96.9 | 99.1 | | |

**Table 5** Confusion matrix and accuracy indexes for Basalt

| | Class | Reference data | | | Sum | User's accuracy (%) |
|---|---|---|---|---|---|---|
| | | B | Bit. | bkGD | | |
| Classified image | B | 133 | 16 | 1 | 150 | 88.7 |
| | Bit. | 20 | 568 | 11 | 599 | 94.8 |
| | bkGD | 0 | 0 | 1852 | 1852 | 100.0 |
| Sum | | 153 | 584 | 1864 | 2601 | |
| Producer's accuracy (%) | | 86.9 | 97.3 | 99.4 | | |

while "*Bit.*" refers to the bitumen. Results show that the software easily drops out the background, with a producer's accuracy of 100 %. The example of Table 3 shows that 5 out of the 208 total pixels of Limestone were classified as bitumen while 17 out of the 222 pixels classified by the software as Limestone actually belongs to bitumen.

**Table 6** Confusion matrix and accuracy indexes for Blast furnace slag

| | Class | Reference data | | | Sum | User's accuracy (%) |
|---|---|---|---|---|---|---|
| | | S | Bit. | bkGD | | |
| Classified image | S | 127 | 37 | 0 | 164 | 77.4 |
| | Bit. | 13 | 397 | 10 | 420 | 94.5 |
| | bkGD | 0 | 0 | 2017 | 2017 | 100.0 |
| Sum | | 140 | 434 | 2027 | 2601 | |
| Producer's accuracy (%) | | 90.7 | 91.5 | 99.5 | | |

**Table 7** OA and BAA indexes for the tested aggregates

| Aggregate | L | P | B | S |
|---|---|---|---|---|
| OA (%) | 98.8 | 98.4 | 98.1 | 97.7 |
| BAA (%) | 97.1 | 96.7 | 95.1 | 91.3 |

The software well classified pixels belonging to L and P having a Producer's accuracy of respectively 97.6 and 96.6 %. As expected B and S, due to their dark grey color, were by far the most confound with the bitumen. Producer's accuracies were respectively 86.9 and 90.7 %. In the example in Table 6, 37 out of the total 164 pixels classified as blast furnace slag by the software, actually belonged to bitumen. Table 7 shows a summary of the Overall Accuracy (OA) and the Bitumen—Aggregate Accuracy (BAA) indexes for all the adopted aggregates.

The OA index shows that the software is highly accurate. The BAA index indicates that the accuracy in recognizing the difference between the bitumen and the aggregate is greater than 95 % for L, P and B and greater than 90 % for S.

It is concluded that the lighter the color of the aggregates, the higher the BAA.

These results confirmed the validity of the procedure compared to the visual estimation, with a consistent reduction of the errors and of the time for the test execution.

## 5 Conclusions

Based on the experiments and on the image analyses, the following can be summarized and concluded:

- the software estimation is, by far, more accurate compared to visual estimation;
- the standard deviation of the software results between each observation is smaller, demonstrating a low dispersion of the data;
- more discrepancy between visual and software recognition were observed with lighter aggregates. This variability can affect the comparison between different aggregates;

- all the tested aggregates were effectively recognized by the software, although light and middle dark rock types gave more accurate results due to the contrast between the aggregate and the bitumen;
- being the equipment quite simple and the software open source, this procedure is very cost-effective and may substitute or support the standard visual registration;
- as standard deviations of the results obtained by the software are smaller compared to those of the visual estimations, the proposed procedure requires less bottles to be tested, thus reducing the tested material as well as test and processing time.

## References

Bhasin A (2006) Development of methods to quantify bitumen-aggregate adhesion and loss of adhesion due to water. Diss. Texas A&M University. http://repository.tamu.edu/bitstream/handle/1969.1/5934/etd-tamu-2006A-CVEN-Bhasin.pdf?sequence=1. Accessed 21 Nov 2014

Dondi G, Simone A, Vignali V, Manganelli G (2012) Numerical and experimental study of granular mixes for asphalts. Powder Technology 232: 31–40. doi: 10.1016/j.powtec.2012.07.057

EN 12697-11 Bituminous mixtures – Test methods for hot mix asphalt – Part 11: Determination of the affinity between aggregate and bitumen

Ford A, Roberts A (1998) Colour space conversions. Westminster University, London, 1-31

Grönniger J, Wistuba MP, Renken P (2010) Adhesion in bitumen-aggregate-systems: New technique for automated interpretation of rolling bottle tests. Road Materials and Pavement Design 11(4): 881-898. doi: 10.3166/RMPD.11.881-898

Grenfell J, Ahmad N, Liu Y, Apeagyei A, Large D, Airey G (2014) Assessing asphalt mixture moisture susceptibility through intrinsic adhesion, bitumen stripping and mechanical damage. Road Materials and Pavement Design 15(1): 131-152. doi: 10.1080/14680629.2013.863162

Hefer AW (2004) Adhesion in bitumen-aggregate systems and quantification of the effects of water on the adhesive bond. Diss. Texas A&M University. http://repository.tamu.edu/bitstream/handle/1969.1/1457/etd-tamu-2004C-CVEN-Hefer.pdf?sequence=1. Accessed 21 Nov 2014

Kallen H, Heyden A, Astrom K, Lindh P (2012) Measurement of bitumen coverage of stones for road building, based on digital image analysis. Paper presented at IEEE Workshop on the Applications of Computer Vision, WACV 2012, Breckenridge, 9 January 2012

Ibraheem NA, Hasan MM, Khan RZ, Mishra PK (2012) Understanding Color Models: A Review. ARPN Journal of Science and Technology 2(3): 265-275. ISSN 2225-7217

Miller JS, Bellinger WY (2003) Distress Identification Manual for the Long-Term Pavement Performance Program. Publication FHWA-RD-03-031. FHWA, Virginia

Mulsow C (2012) Determination of the degree of gravel aggregate-bitumen coverage by multi-directional reflectance measurements. Paper presented at the XXII ISPRS Congress, Melbourne, 25 August – 01 September 2012

Silván-Cárdenas JL, Wang L (2008) Sub-pixel confusion–uncertainty matrix for assessing soft classifications. Remote Sensing of Environment 112(3):1081-1095. doi: 10.1016/j.rse.2007.07.017

Vignali V, Mazzotta F, Sangiorgi C, Simone A, Lantieri C, Dondi G (2014) Rheological and 3D DEM characterization of potential rutting of cold bituminous mastics. Construction and Building Materials 73: 339-349. doi: 10.1016/j.conbuildmat.2014.09.051

# An Advanced Low Temperature Rheological and Fracture Test Method for Bitumen Purchase Specifications and Pavement Performance Prediction: 4-mm DSR/ABCD

**Michael J. Farrar, Sang-Soo Kim, Troy Pauli and Jean Pascal Planche**

**Abstract** This paper proposes an advanced low temperature rheological test method which could be used to supplement and improve current purchase specifications for grading bitumens, and at the same time provide pavement low temperature thermal crack prediction for the Mechanistic Empirical Pavement Design Guide (MEPDG). The method is referred to as 4-mm DSR/ABCD i.e. 4-mm diameter parallel plate dynamic shear rheometry combined with the Asphalt Binder Cracking Device (ABCD) test. In addition to traditional low temperature binder purchase specifications such as m-value, creep stiffness and binder cracking temperature, the 4-mm DSR/ABCD method allows calculation of the thermal cracking temperature in the asphalt mix from a cooling event. The application of 4-mm DSR is an alternative to the mix indirect tensile (IDT) creep test. The fracture stress of the binder from the ABCD is an alternative to the mix IDT strength test. Mix IDT creep compliance and strength are the two primary inputs to the low-temperature, thermal cracking module in the MEPDG.

**Keywords** Thermal cracking · Thermal stress · Fracture stress · ABCD · 4-mm DSR · Bitumen · Asphalt

M.J. Farrar (✉) · T. Pauli · J.P. Planche
Western Research Institute, Laramie, USA
e-mail: mfarrar@uwyo.edu

T. Pauli
e-mail: tpauli@uwyo.edu

J.P. Planche
e-mail: jplanche@uwyo.edu

S.-S. Kim
Ohio University, Athens, USA
e-mail: kim@ohio.edu



F. Canestrari and M.N. Partl (eds.), *8th RILEM International Symposium on Testing and Characterization of Sustainable and Innovative Bituminous Materials*, RILEM Bookseries 11, DOI 10.1007/978-94-017-7342-3_3

## 1 Introduction

Low-temperature cracking occurs predominately in cold weather regions subject to sudden temperature drops. This type of failure is the result of tensile stress development from rapid cooling of the pavement and the resultant cracking when the pavement reaches a critical stress. It is often referred to as single-event thermal cracking.

The focus of this paper is to propose a low-temperature single-event thermal cracking method that is an adaptation and extension of methods proposed by Christensen and Bonaquist (2004), and by Bouldin et al. (2000).

The proposed method is a synergistic combination of 4-mm DSR, and the Asphalt Binder Cracking Device (ABCD), and is referred to as simply 4-mm DSR/ABCD.

4-mm DSR is defined as the application of dynamic shear rheometry using 4 mm diameter parallel plate geometry. In the 4-mm DSR test, oscillatory shear is performed at several low temperatures generating frequency sweeps that can be used to determine traditional US Superpave low temperature binder purchase specification parameters such as m-value and creep stiffness (Sui et al. 2011; Farrar et al. 2015), as well as the thermal stress build-up in the pavement by application of Boltzmann's Hereditary Integral (Farrar et al. 2013). Other researchers have made a similar calculation using Bending Beam Rheometer data rather than DSR (Christensen and Bonaquist 2004; Bouldin et al. 2000).

Olard et al. (2005) have made a similar calculation where the complex modulus of the asphalt mixture was obtained from the bitumen complex modulus using the method proposed by Di Benedetto et al. (2004) and Olard and Di Benedetto (2003).

Low temperature DSR was not used until recently because of issues with instrument compliance. However the compliance issue has been resolved (Sui et al. 2010). Details of the test method can be found in (Farrar et al. 2015).

In the ABCD test, a bitumen sample is restrained while the temperature is lowered causing thermal contraction and stress build-up until fracture occurs. The temperature at fracture is referred to as the critical cracking temperature (Tcr). The Tcr is a proposed binder purchase specification parameter in AASHTO TP 92-11. In addition to Tcr, the ABCD test captures the binder fracture strength.

When 4-mm DSR and ABCD are combined, the key inputs to the Mechanistic Empirical Pavement Design Guide (MEPDG) can be estimated for the thermal cracking module. The key inputs are the mix creep compliance and strength. 4-mm DSR is an alternative to the mix indirect tensile (IDT) creep test and the ABCD is an alternative to the IDT mix strength test.

Finally, this method can also be used with the global aging system (GAS) which is an integral part of the MEPDG. The GAS was developed by Mirza and Witczak (1995), and consists of a series of regression models that attempt to predict the change in binder viscosity in hot-mix asphalt (HMA) pavement with in-service time and pavement depth. In situ binder viscosity is a critical input for the determination of mix dynamic modulus, E*, which, after interconversion to E(t), is the primary

material property of interest in the thermal stress build-up calculation using the Boltzmann hereditary integral.

The GAS is not applied in the MEPDG to the thermal cracking prediction model since the input to the model is based on a mix test, which does not contain a binder component. However, the 4-mm DSR/ABCD method resolves this dilemma since the GAS can be applied to the 4-mm DSR data to calculate an E* and ultimately thermal stress determination that takes into account oxidative aging.

## 2 Experimental

The low and intermediate temperature rheological properties of the binders were measured using an ARES dynamic shear rheometer fitted with 4 mm diameter parallel plates and an environmental chamber equipped with a liquid nitrogen system for cooling. High temperature rheological properties, typically measured with 25 mm diameter parallel plate geometry, were not measured in this study.

The 4-mm DSR test method is described elsewhere by Sui et al. (2010) and Farrar et al. (2015). The method corrects for machine compliance and allows testing to temperatures as low as −40 °C. Frequency sweeps were typically performed at 15 °C intervals over a temperature range of −30 to 15 °C and an angular frequency range of 0.1–50 rad/s. A strain sweep was performed before each frequency sweep to insure the frequency sweep was in the linear regime.

The ABCD test was performed in general accordance with AASHTO TP 92-11. The ABCD measures the temperature and strain of a restrained asphalt binder ring subjected to a constant rate of cooling.

As shown Fig. 1a, asphalt binder sample is poured outside of ABCD ring. As temperature decreases at 20 °C/h in an environmental chamber, the binder sample contracts and the ring provides restraint, leading to eventual fracture. An electrical

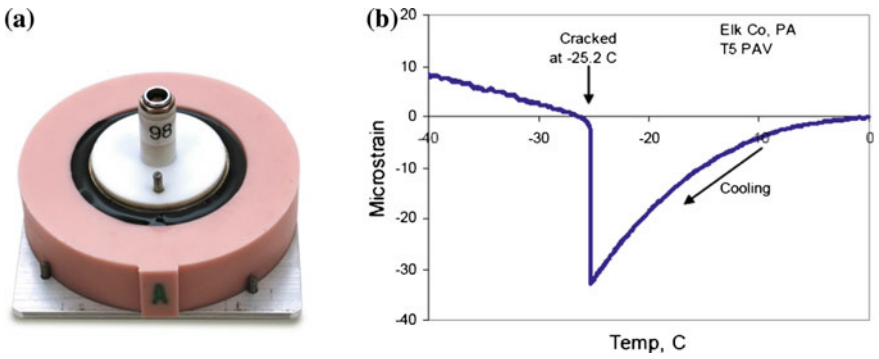


**Fig. 1** Asphalt binder cracking device (ABCD): **a** ring and sample in a silicone mold; **b** a typical test results

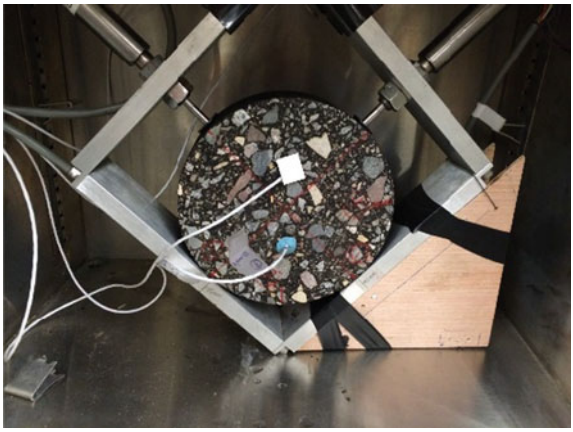

**Fig. 2** CTE measuring device

strain gauge instrumented inside of the ring detects this fracture. A typical ABCD test result is shown in Fig. 1b.

A new device, shown in Fig. 2, was used to measure the coefficient of thermal expansion CTE of the asphalt mixes prepared using the binders for this study. The square frame CTE set-up was calibrated and validated with two known metals; 6061 aluminium and 316 stainless steel. Thermal contraction of the test specimen was measured by two LVDT's arranged orthogonally while the chamber temperature was lowered from 20 °C to −40 °C at 20 °C/h rate. During the test, temperatures of chamber, CTE frame, the surface and interior of specimen were continuously recorded.

## 3 Materials

Two RTFO/PAV aged binders were used in this study: a PG 64-28 and a PG 70-22. The PG 64-28 was a polyphosphoric acid (PPA) modified binder typically used for intermediate pavement courses in Ohio. The PG 70-22 was an SBS modified binder typically used for surface course in Ohio.

Mixes for CTE analysis were prepared using a limestone aggregate. The mix properties are shown in Table 1. The particular aggregate used in this study had a CTE = 4.2 με/°C. The specimens were compacted using a gyratory compactor (65 gyrations). Two compacted mixes were prepared for each binder. Each compacted mix was cut in half to produce an approximate 50 mm thick by 150 mm diameter

**Table 1** Asphalt mixture properties

| 1/2" | 3/8" | #4 | #8 | #16 | #30 | #50 | #100 | #200 | Opt AC (%) | Air (%) |
|---|---|---|---|---|---|---|---|---|---|---|
| 100.0 | 95.6 | 54.6 | 33.9 | 22.3 | 12.8 | 6.6 | 3.5 | 2.2 | 5.7 | 4.0 |

disc-shape specimen for the CTE test. For 28 measurements of mix CTE covering mixtures with 5 binders and 2 aggregate types, the pooled standard deviation of CTE at −20 °C is 0.46 με/°C.

# 4 Results and Discussion

## *4.1 Standard Binder Purchase Specifications from the 4-mm DSR and ABCD Test Results*

The binder continuous grade temperatures used in this study, based on standard AASHTO criteria, are shown in Table 2. These temperatures were derived from 4-mm DSR data not Bending Beam Rheometry (BBR). The method used to convert 4-mm DSR data to BBR m-value and creep stiffness is covered by Sui et al. (2011) and Farrar et al. (2015).

The 4-mm DSR results for both the PG -28 and -22 are reasonable based on their project grades, however the PG -28 sample continuous grade temperature was, slightly warm, by 1.6 °C, to qualify as a PG -28. Both binders were highly m-controlled.

The standard ABCD results reported in accordance with AASHTO TP 92-11 are shown in Table 3. The cracking temperatures follow the same trend as the m-value continuous grade temperatures, i.e. the PG -22 is about 2 °C warmer than the PG -28, however there is about a six degree difference in temperature between the continuous temperature grades (based on m-value) and the critical cracking temperature based on ABCD. The approximate six degree difference in continuous temperature is probably attributable to the presence of the modifiers in the two

**Table 2** Binder m-value and creep stiffness continuous grade temperatures from 4-mm DSR

| Sample description | Binder 4-mm DSR | |
|---|---|---|
| | Binder continuous grade temperatures | |
| | $M_v$(60 s) = −0.300 (°C) | S(60 s) = 300 MPa (°C) |
| PG 64-28 | −26.4 | −34.5 |
| PG 70-22 | −24.5 | −33.3 |

**Table 3** ABCD test results

| Sample description | ABCD | | | | |
|---|---|---|---|---|---|
| | Avg. crack temp. (°C) | Avg. crack temp. Std Dev | Avg. strain jump (με) | Avg. strain jump Std Dev | Avg. fracture stress ($\sigma_{AC}$) (MPa) |
| PG 64-28 | −32.4 | 1.2 | 27.0 | 5.76 | 4.25 |
| PG 70-22 | −30.3 | 0.7 | 33.5 | 6.47 | 5.27 |

binders. Also, the average fracture stress is significantly greater for the PG -22 almost certainly due to differences in the effects of SBS versus PPA modification.

## 4.2 Mix Coefficient of Thermal Expansion (CTE)

The mix CTE is an important input in the mix thermal stress build-up calculation. The strain in the Boltzmann integral (see Eq. 3) can be replaced by the thermal strain ($\alpha\Delta T$) where $\alpha$ is the mix CTE and $\Delta T$ is the change in temperature.

The CTE of an asphalt mixture is different for regimes above and below the glass transition temperature. Unfortunately, the glass transition temperature is not a simple point on the temperature scale, but instead it is rather broad (several tens of degrees). Above the glass transition temperature the asphalt behaves in a ductile fashion, and below it approaches the glassy state. A model proposed by Bahia and Anderson (1993) was used to describe this phenomenon and it very nicely fits the data in this study as shown in Fig. 3. The Bahia and Anderson equation is of the following form:

$$\varepsilon = C + \alpha_g\left(T - T_g\right) + \ln\left(1 + \exp\left(\left(T - T_g\right)/R\right)\right)^{R(\alpha l - \alpha g)} \quad (1)$$

where $\varepsilon$ is thermal strain, C is constant, $\alpha_l$ is the slope of the liquid state asymptote, $\alpha_g$ is the slope of the glassy state asymptote, $T_g$ is the glass transition temperature, and R is the parameter determining the width of the glass transition.

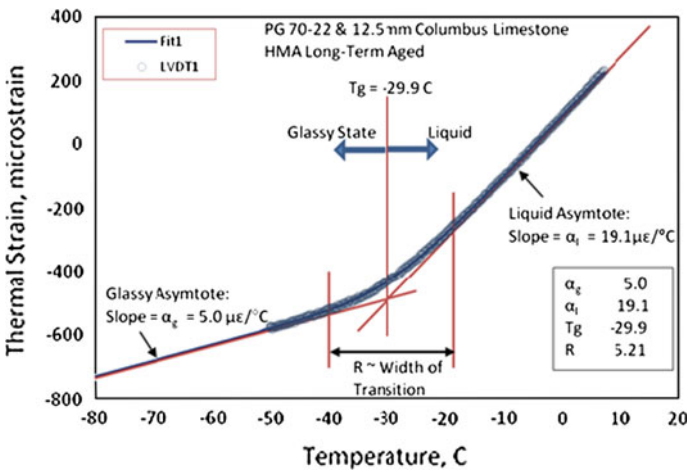


**Fig. 3** Comparison of the Bahia and Anderson equation fit versus the data for the PG 72-22 binder, limestone aggregate mix

**Table 4** CTE parameters

| Temp (°C) | Coefficient of thermal expansion (CTE) (με/°C) | | | |
|---|---|---|---|---|
| | PG 64-28 | | PG 70-22 | |
| | Rep 1 (1A) | Rep 2 (2A) | Rep 1 (1B) | Rep 2 (2B) |
| 0 | 20.8 | 20.4 | 20.6 | 19.9 |
| −10 | 20.5 | 20.2 | 20.3 | 19.8 |
| −20 | 19.5 | 19.5 | 19 | 19 |
| −25 | 18.3 | 18.4 | 17.4 | 17.7 |
| −30 | 16.5 | 16.2 | 14.7 | 15.3 |
| Bahia-Anderson model best-fit parameters | | | | |
| cv | −862 | −664.5 | −669.3 | −578.4 |
| $\alpha_g$ | 0 | 0 | 0 | 2.5 |
| $\alpha_1$ | 20.9 | 20.4 | 20.7 | 20 |
| $T_g$ | −40.5 | −38 | −36.1 | −35.7 |
| R | 7.8 | 5.9 | 6.7 | 5.6 |

CTE is the first derivative of the thermal strain with respect to temperature.

$$\text{CTE or } \alpha = d\varepsilon/dT = \alpha_g + (\alpha l - \alpha g)\exp\left((T - T_g)/R\right)/\left(1 + \exp\left((T - T_g)/R\right)\right) \quad (2)$$

where α is the coefficient of linear thermal contraction.

For single value application, it is suggested the CTE value at −20 °C should be used. For more accurate application, Eq. 2 can be used with parameters given in Table 4. For this study the single value at −20 °C for each binder was used.

## 4.3 Using 4-mm DSR Data to Calculate the Thermal Stress Variation in the Pavement

AASHTO T 322-03 was selected during NCHRP Project 1-37 A to characterize mix properties related to low temperature cracking in HMA for the MEPDG. T 322 has undergone modification since 2003 based primarily on the findings of the NCHRP 530 project (Christensen and Bonaquist 2004). The latest AASHTO version is T 322-07.

The creep compliance and tensile strength of HMA material, measured in accordance with AASHTO T 322, are required for the thermal cracking analysis in the MEPDG. The important feature of MEPDG thermal cracking module is that it considers both the rheology and fracture properties of the asphalt mix at low service temperatures to predict thermal cracking in the pavement.

One of the conclusions from NCHRP 530 was that additional research was warranted to evaluate the accuracy of the mix creep compliance and tensile strength determined by using the Hirsch model (Christensen et al. 2003) to estimate creep compliance values and empirical methods for determining approximate tensile

strength. It was suggested that such a procedure would have application for general mixture selection, mixture design guidance, quality control applications, and as a possible replacement for the current Level 2 and 3 thermal cracking data input for the MEPDG (Christensen and Bonaquist 2004).

A few years earlier, Bouldin et al. (2000) proposed a semi-empirical model to determine the critical cracking temperature, $T_{CR}$ in asphalt pavements. The model used the creep compliance data from the BBR to predict the thermal stress in the binder from a single cooling event. The thermal stress in the pavement is approximated by using a damage transfer function referred to as the Pavement Constant (PC). The PC was determined by statistically comparing the binder cracking temperatures with cracking temperatures observed in the field (Anderson et al. 2001).

The method is theoretically sound, but to the extent that it uses a PC, it is empirical. In a study by Roy and Hesp (2001) it was found the pavement constant could vary between 3.4 and 16.7 based on comparing the stress buildup in a restrained cooling test to the estimated stress build-up using the pavement constant. Also, the Bouldin et al. method uses the Direct Tension test (DTT) to estimate fracture stress and while the device is well engineered it has not been widely adopted in the last ten years since it underwent considerable modification to improve reliability of the test.

In the Bouldin et al. method, TCR is determined by comparing the estimated thermal stress development in the pavement to the binder tensile strength measured using the DTT. The method was adopted by AASHTO as PP 42-02 (2005). The equivalent ASTM specification is D6816-11.

Both the Christensen and Bonaquist, and the Bouldin et al. approaches are similar. In both cases the BBR data are interconvered from creep compliance to relaxation modulus and the relaxation modulus along with other input, such as the CTE is used to compute thermal stress build-up.

However, the Christensen and Bonaquist approach is more fundamental in that the mix relaxation modulus, E(t) is determined using the Hirsch model and the thermal stresses in the pavement determined using the Boltzmann hereditary integral, where the thermal stress response $\sigma(t)$ to an arbitrary thermal strain history can be derived at any time, $t$, by applying the integral shown in Eq. 3.

$$\sigma(t) = \int_0^t E(t-\tau)\frac{\partial \varepsilon(\tau)}{\partial \tau}\partial\tau \tag{3}$$

where $E(t)$ is the thermal relaxation modulus at time $t$, and $\varepsilon(t)$ is the thermal strain at time $t$. The Bouldin et al. method also uses the Boltzmann hereditary integral, but calculates the thermal stress development in the bitumen.

The Bouldin et al. method further diverges from the method proposed by Christensen and Bonaquist in that the goal was to determine a critical cracking temperature, $T_{CR}$, for binder purchase specifications and not provide input to the MEPDG.

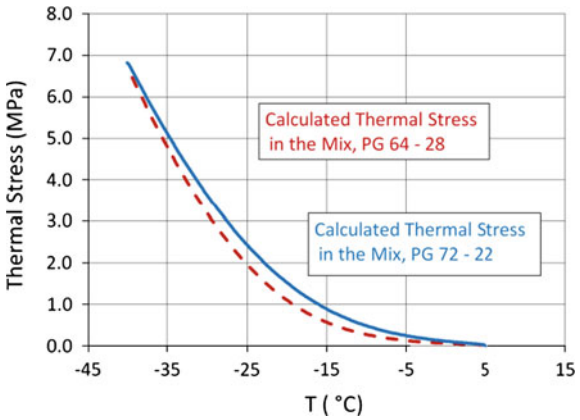


**Fig. 4** Thermal stress build-up from a cooling event (2 °C/h) starting at 5 °C

The 4-mm DSR/ABCD method provides estimation of the necessary input for the MEPDG thermal cracking model, i.e. the mix thermal stress development from the 4-mm DSR test and mix tensile strength estimated from the ABCD test. Both tests are relatively simple and rapid, which is an important consideration given that the asphalt mixture testing in accordance with AASHTO 322-07 is expensive and time-consuming.

The FHWA Binder Expert Task Group is conducting ruggedness testing and round-robin testing on 4-mm DSR, which will lead to eventual adoption by AASHTO and ASTM. The round-robin testing will lead to a formal repeatability statement. Currently, the test method is in use in about a dozen research laboratories, primarily in the U.S. In general the test has been found satisfactory in terms of repeatability.

The ABCD test method has been adopted as an AASHTO provisional standard: TP 92-11. Single operator and multilaboratory precision estimates are included in TP 92-(11).

The calculation of mix thermal stress build-up from a cooling event without resorting to an empirical Pavement Constant and by applying data from 4-mm DSR has been demonstrated by Farrar et al. (2013). Using the Farrar method the calculated thermal stresses for the two bitumens used in this study are shown in Fig. 4.

## *4.4 Using the Calculated Thermal Stress Build-up in the Mix from 4-mm DSR and the Measured Fracture Stress from the ABCD to Calculate a Mix Critical Cracking Temperature*

The corrected strain output from the ABCD device, where the strain has been corrected based on an open ring calibration, can be converted to thermal stress in the bitumen using the following equation (Kim and Kovach 2006):

$$\sigma_{AC} = \varepsilon_{corr} E_{ABCD} A_{ABCD} / A_{AC} \quad (4)$$

where $\sigma_{AC}$ is the thermal stress in the binder, $\varepsilon_{corr}$ is the corrected strain of the ABCD ring, $E_{ABCD}$ is Young's modulus of the ABCD ring ($E_{invar}$ = 141 GPa), and $A_{ABCD}$, $A_{AC}$ are cross-sectional areas of ABCD ring and binder, respectively.

However, Eq. 4 is not entirely suitable for studying the thermal stress development within the binder itself because it does not take into account: (1) the strain relief by contraction of the ABCD ring, and (2) the specimen elongation relative to where the protrusion is located.

Both will reduce the measured stress (or strain jump), but the magnitude will be very small. Typical the CTE for a binder is about 200 microstrain per °C and the strain relief by the ring is 1 microstrain per °C or smaller. The span of the protrusion on the ABCD ring is 6.35 mm over 159.51 mm circumference (4 % of circumference containing 60 % volume filled with binder, resulting in more mechanical strain or elongation due to higher stress.

The hole in the bitumen ring generates a stress concentration factor of about 2.02. The fracture stress equation with the stress concentration factor estimates the actual strength of the binder at the cracking temperature

$$\sigma_f = (K)\varepsilon E_{ABCD} A_{ABCD} / A_{binder} \quad (5)$$

where $\sigma_f$ is the thermal fracture stress taking into consideration stress concentration, and (K) is the Stress concentration factor, ε is the strain jump, $E_{ABCD}$ is Young's modulus of the ABCD ring ($E_{invar}$ = 141 GPa), and $A_{ABCD}$, $A_{AC}$ are cross-sectional areas of ABCD ring and binder, respectively.

Figure 5 demonstrates the results of combining the thermal stress build-up calculation with the ABCD measured fracture stress.

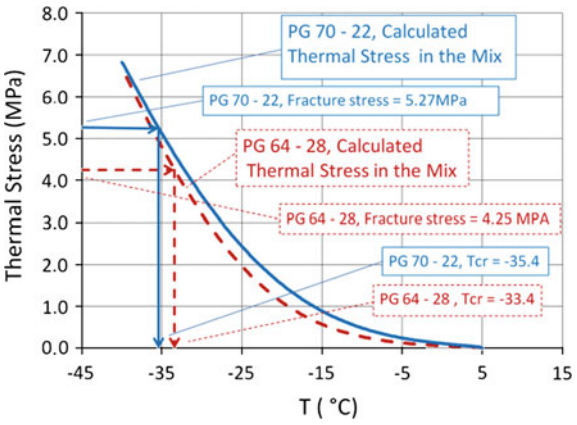


**Fig. 5** The thermal stress buildup in the mix from a 2 °C/h cooling event combined with the thermal fracture stress of the binder based on the ABCD

## 5 Conclusions

This study aimed to develop an advanced low temperature rheological and fracture test method referred to as 4-mm DSR/ABCD.

In terms of 4-mm DSR, the proposed method provides current US Superpave specification parameters such as m-value and creep stiffness. The ABCD provides additional low temperature purchase specification parameters such as the binder critical cracking temperature. The 4-mm DSR/ABCD provides the pavement critical cracking temperature, and also the key input to the MEPDG thermal cracking module where 4-mm DSR is an alternative to the mix indirect tensile (IDT) creep test, and the ABCD is an alternative to the mix IDT strength test.

We strongly recommend consideration be given to adopting 4-mm DSR/ABCD in place of current low temperature purchase specifications and as an alternative to the mix IDT creep and strength test for the MEPDG low temperature cracking module.

**Acknowledgements/Disclaimer** The authors gratefully acknowledge the Federal Highway Administration, U.S. Department of Transportation, for financial support of this project under contract nos. DTFH61-07-D-00005 and DTFH61-07-H-00009. Also, the RHEA™ software package, developed by Abatech Consulting Engineers, was used extensively during the data analysis phase of this study. This document is disseminated under the sponsorship of the Department of Transportation in the interest of information exchange. The United States Government assumes no liability for its contents or use thereof. The contents of this report reflect the views of the Western Research Institute and the accuracy of the data presented herein. The contents do not necessarily reflect the official views of the policy of the United States Department of Transportation. Mention of specific brand names of equipment does not imply endorsement by the United States Department of Transportation, or the Western Research Institute.

## References

AASHTO TP 92-11 *Determining the Cracking Temperature of Asphalt Binder using the Asphalt Binder Cracking Device, ABCD*

AASTHO PP 42-02 *Standard Practice for Determination of Low-Temperature Performance Grade (PG) of Asphalt Binders*

AASHTO T 322-07 *Standard Method of Test for Determining the Creep Compliance and Strength of Hot-Mix Asphalt (HMA) Using the Indirect Tensile Test Device*

Anderson DA, Lapalu L, Marasteanu MO, Le Hir YM, Planche JP, Martin D (2001) Low-temperature Thermal Cracking of Asphalt Binders as Ranked by Strength and Fracture Properties. TRR, Journal of the TRB, Volume 1766/2001, Asphalt Binders 2001, 1-6

Bahia HU, Anderson DA (1993) Glass Transition behaviour and Physical Hardening of Asphalt Binders. Asphalt Paving Technology, 62: 93-129

Bouldin MG, Dongre RN, Rowe GM, Sharrock MJ, Anderson DA (2000) Predicting Thermal Cracking of Pavements from Binder Properties: Theoretical Basis and Field Validation. Proceedings of the Association of Asphalt Paving Technologists, 69: 455-496

Christensen DW, Bonaquist RF (2004) Evaluation of Indirect Tensile Test (IDT) Procedures for Low-Temperature Performance of Hot Mix Asphalt. NCHRP 530, Advanced Asphalt Technologies, LLC, Sterling, VA

Christensen DW, Pellinen T, Bonaquist RF (2003) Hirsch Model for Estimating the Modulus of Asphalt Concrete. Journal of the Association of Asphalt Paving Technologists, 72: 97-121

Di Benedetto H, Olard F, Sauzeat C, Delaporte B (2004) Linear viscoelastic behaviour of bituminous materials: From binders to mixes. Road Materials and Pavement Design, Vol. 5, Special Issue, 163-202

Farrar M, Sui C, Salmans S, Qin Q (2015) Determining the Low Temperature Rheological Properties of Asphalt Binder Using a Dynamic Shear Rheometer (DSR). Technical White Paper FP08 prepared by Western Research Institute for the Federal Highway Administration, Contract No. DTFH61-07-D-00005, March 2015.

Farrar MJ, Hajj EY, Planche J-P, Alavi MZ (2013) A method to estimate the thermal stress build-up in an asphalt mixture from a single cooling event. Road Materials and Pavement Design, 14, sup1: 201-211

Kim S, Kovach J (2006) Determination of low temperature thermal cracking of asphalt binder by ABCD. In TRR, Journal of the TRB, No. 1962

Mirza MW, Witczak MW (1995) Development of a Global Aging System for Short and Long Term Aging of Asphalt Cements. Journal of Association of Asphalt Paving Technologists, 64: 393-431

Olard F, Di Benedetto H (2003) General 2S2P1D model and relation between the linear viscoelastic behavior of bituminous binders and mixes. Road Materials and Pavement Design, 4: 1-40

Olard F, Vaniscote J-C, Loup F (2005) Prediction of thermal cracking resistance of some SBS modified binder and mixes. Proceedings of the Seventh International Conference on the Bearing Capacity of Roads, Railways and Airfields, NTNU, Trondheim, Norway, 27–29 June 2005, pp. 1-10

Roy SD, Hesp SAM (2001) Fracture Energy and Critical Crack Tip Opening Displacement: Fracture Mechanics-Based Failure Criteria for Low-Temperature Grading of Asphalt Binders. Proceedings of the Canadian Technical Asphalt Association, 2001, 185-212

Sui C, Farrar MJ, Harnsberger PM, Tuminello WH, Turner TF (2011) New Low-Temperature Performance-Grading Method Using 4-mm Parallel Plates on a Dynamic Shear Rheometer. In TRR: Journal of the TRB, No. 2207, 43-48

Sui C, Farrar MJ, Tuminello WH, Turner TF (2010) New Technique for Measuring Low-Temperature Properties of Asphalt Binders with Small Amounts of Material. In Transportation Research Record, Journal of the Transportation Research Board, No.2179, 23-28

# Microstructure-Based Visco-Elastoplastic Continuum Model of Asphalt Concrete

**Mohammad Hosein Zahabi, Mohammad M. Karimi and Nader Tabatabaee**

**Abstract** Asphalt concrete is a heterogeneous and multi-phase material that consists of aggregates, asphalt binder, and pores. These components create a complex microstructure. There is no consensus on how to quantify the microstructure and the required parameters from two-dimensional images. The load transfer can be managed by aggregate-aggregate or aggregate-mastic interactions that depend on the gradation, aggregate internal structure, and asphalt binder viscoelastic properties. The most important internal structure indices affecting the behavior of HMA are aggregate orientation, contact orientation, contact length, and number of contact points. In this paper, the influence of aggregate structure and binder viscoelastic properties on viscoelastic and visco-elastoplastic response of asphalt concrete is investigated for mixtures with different aggregate gradations and types of asphalt binders. Two factors were defined that describe the mechanical properties of the mixture to its microstructure; aggregate structure factor (ASF) and binder irrecoverable strain factor (ISF). ASF as a function of the aggregate internal structure relates the aggregate geometry and stresses to the stiffness of the asphalt mixture. Binder ISF describes the role of the aggregate structure in the accumulation of permanent strain in asphalt mixtures.

**Keywords** Aggregate structure · Anisotropy · Continuum model · Image processing

M.H. Zahabi · M.M. Karimi (✉) · N. Tabatabaee
Department of Civil Engineering, Sharif University of Technology, Tehran, Iran
e-mail: mohammadkarimi@mehr.sharif.edu

M.H. Zahabi
e-mail: ehsanzahabi@mehr.sharif.edu

N. Tabatabaee
e-mail: nader@sharif.edu



F. Canestrari and M.N. Partl (eds.), *8th RILEM International Symposium on Testing and Characterization of Sustainable and Innovative Bituminous Materials*, RILEM Bookseries 11, DOI 10.1007/978-94-017-7342-3_4

## 1 Introduction

Conventional procedures for the design of asphalt mixes (such as Marshal, Hveem and Superpave) require a specific level of air voids or a target density; however, mixes with same density can provide significantly different mechanical performances (Roohi 2011; Bahia et al. 2013). This indicates the need to introduce parameters that can describe mixture performance properties more accurately. It is believed that the commonly overlooked microstructural properties of asphalt mixes can play an important role in better describing mixture performance. Microstructural properties can be evaluated using digital visualization (i.e., image processing). Two-dimensional (2D) digital images can now be analyzed efficiently by various commercially-available software packages; however, there is no consensus on which image parameters are needed to quantitatively describe aggregate structure. This paper provides a macroscopic model to explain the microscopic interaction of asphalt concrete using the 2D image processing software iPas2 (Coenen et al. 2012) and predicts the visco-elastoplastic response using microstructure parameters and bitumen properties.

## 2 Background

In the past, asphalt concrete was considered to be an isotropic material (Wagoner and Braham 2008). This assumption allowed for laboratory test specimens fabricated by different methods (Superpave gyratory compactor, field cores, slabs, etc.) to be compared directly. Previous studies have revealed that asphalt mixtures are anisotropic (Masad et al. 2002); they are directionally dependent on microstructural properties. Aggregate microstructure is related to the macroscopic behavior of an asphalt mixture. Several studies have quantified aggregate microstructure through analysis of 2D images (Tashman et al. 2001; Roohi 2011; Coenen et al. 2012).

Anisotropy of asphalt mixtures is attributed to the orientation of the coarse and fine aggregates. Moreover, the influence of aggregate depends on their size, spatial distribution, and orientation and all three parameters must be considered when quantifying anisotropy. Vector magnitude was introduced by Curray in 1956 to quantify the directional distribution of aggregate orientation as shown in "Eq. 1" (Henderson et al. 2011):

$$\Delta = \frac{1}{M}\sqrt{\left(\sum_{i=1}^{M}\sin 2\alpha_i\right)^2 + \left(\sum_{i=1}^{M}\cos 2\alpha_i\right)^2} \tag{1}$$

where $\alpha_i$ is the inclination angle of the $i$th particle; and $M$ is the total number of aggregates. Coarse aggregate parameter $\alpha_i$ is obtained from 2D images or cross-sectional images from X-ray CT scanners. Figure 1 shows the aggregate

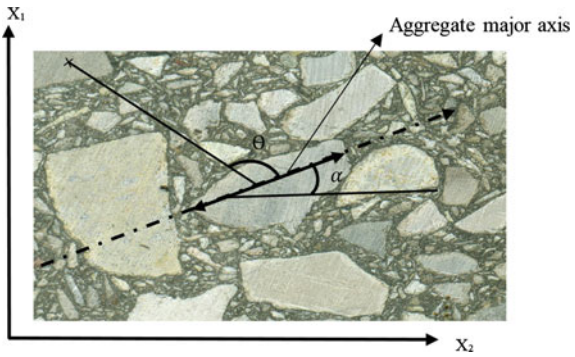


**Fig. 1** Aggregate orientation in vertical section of asphalt mixture

orientation of an asphalt mixture. The value of Δ ranges from zero to unity. A zero value denotes complete random distribution of aggregates, which is analogous to an isotropic material, and unity denotes aggregates oriented in only one direction and is analogous to an anisotropic material.

The mechanical response of asphalt mixtures and microstructure measurements is linked to develop a valid continuum model (Tashman et al. 2007). The most common theory for continuum modeling is strain-rate based in which the strain rate is decomposed into an elastic and a viscoplastic component (Dessouky et al. 2006; Saadeh et al. 2007; Yu et al. 2014). Elastic strain rate is defined using Hook's law and viscoplastic strain rate is typically defined using flow rule theory.

Many studies have modeled the performance of asphalt mixtures. Masad et al. (2002) presented a viscoplastic model to describe the three major phenomena that occur during permanent deformation; viscoplastic deformation associated with the asphalt binder, evolution of the microstructure, and crack initiation and propagation. Parameter Δ was determined from the analysis of 2D images. Strength and creep tests were used to determine model parameters. For model validation, a visual basic program was written for the creep test. The results indicated that by increasing parameter Δ, anisotropy plays a role in increasing the confining pressure and material strength.

Dessouky (2005) proposed an elasto-viscoplasic model with a Drucker-Prager yield surface to predict asphalt mixture response and relate microstructure parameters to rutting. The model considered several factors which have been determined to influence asphalt mixture permanent deformation, such as aggregate structure friction and dilation, confining pressure, strain rate, stress path dependency, and microstructure characteristics that reflect anisotropy and damage. Saadeh et al. (2007) presented a nonlinear visco-elastoplastic model to evaluate the influence of anisotropic aggregate distribution on asphalt mixture response. They measured aggregate physical characteristics using the aggregate imaging system (AIMS), which employs the wavelet method to measure texture on grey images of aggregate surfaces and the gradient method to measure angularity on black and white images of aggregate projections.

# 3 Methodology

## 3.1 Specimen Preparation

Two types of aggregates with two gradations and two types of asphalt binders were used. Specimens were compacted with a Superpave gyratory compactor (SGC) for a 3–10 million ESAL design life. The asphalt binder content corresponds to the 4 % target air void (Table 1). To avoid complications in binder testing, gap-graded mixtures were prepared without fiber. The asphalt specimens obtained from the SGC had a diameter of 150 mm and a height of 140 mm. Specimens with a diameter of 92 mm were obtained by coring the compacted asphalt mixtures (Fig. 2).

## 3.2 Uniaxial Compression Test

Uniaxial compression testing was used to determine the uniaxial compression strength of an asphalt mix. "Equation 2" is based on Hook's law and demonstrates the general form of the linear elastic behavior (Zhang et al. 2011):

**Table 1** Types of asphalt mixtures used

| Specimen | DL64 | DS64 | DL58 | GL64 |
|---|---|---|---|---|
| Gradation | Dense | Dense | Dense | Gap |
| Nominal max. size (mm) | 19 | 19 | 19 | 19 |
| Aggregate type | Limestone | Silica | Limestone | Limestone |
| Binder type | PG64-22 | PG64-22 | PG58-22 | PG64-22 |
| Pb (%) | 4.2 | 4.2 | 4.1 | 6.1 |

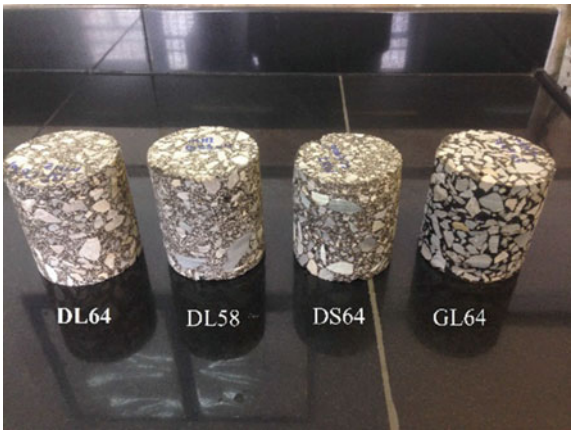


**Fig. 2** Specimens prepared for this study

$$\varepsilon = S\sigma \tag{2}$$

For uniaxial loading, and under non-aging isothermal conditions, the linear viscoelastic stress-strain relationships are represented by the Boltzmann convolution integral shown in "Eqs. 3 and 4":

$$\sigma(t) = \int_0^t E(t-\tau)\frac{\partial \varepsilon}{\partial \tau}d\tau \tag{3}$$

$$\varepsilon^{ve}(t) = \int_0^t D(t-\tau)\frac{\partial \sigma}{\partial \tau}d\tau \tag{4}$$

where $E(t)$, $D(t)$, and $\tau$ denote the relaxation modulus, creep compliance, and integration variable, respectively. Applying the convolution theorem for the Laplace transform to "Eqs. 3 and 4" produces "Eqs. 5 and 6":

$$\sigma(s) = sE(s)\varepsilon(s) \tag{5}$$

$$\varepsilon(s) = sD(s)\sigma(s) \tag{6}$$

Based on these two equations, "Eq. 7" demonstrates the relation between the relaxation modulus and creep compliance in the Laplace domain:

$$E(s)D(s) = \frac{1}{s^2} \tag{7}$$

Subsequently, using the creep compliance series obtained from the creep test, the relaxation modulus series can be calculated (Kim 2009). "Equation 8" shows the Prony series, which models creep compliance. Substituting this into "Eq. 4" yields "Eq. 9":

$$D(t) = D_0 + \sum_{i=1}^{N} D_i\left(1 - \mathrm{e}^{\left(-\frac{t}{T_i}\right)}\right) \tag{8}$$

$$\varepsilon^{ve}(t) = \int_0^t \left(D_0 + \sum_{i=1}^{N} D_i\left(1 - \mathrm{e}^{\left(-\frac{t-\tau}{T_i}\right)}\right)\right)\frac{\partial \sigma}{\partial \tau}d\tau \tag{9}$$

where $D_0$ and $D_i$ are the constants of the Prony series, and $T_i$ is the retardation time.

Figure 3 shows the type of loading used in this study. The specimens were loaded using a 100 kN universal testing machine at 25 °C. The data from the unloading stage was used to compute the viscoelastic parameters (Table 2).

The $D_i$ parameters were used to determine creep compliance as described by the Prony series in "Eq. 8". The viscoplastic strain $(\varepsilon^{vp})$ can then be determined by

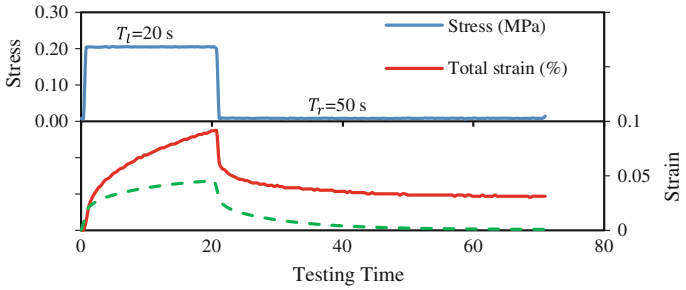


**Fig. 3** Loading of specimens

**Table 2** Parameters for viscoelastic equation (1/MPa)

| | $D_0$ | $D_1$ | $D_2$ | $D_3$ | $D_4$ | $D_5$ | $D_6$ | $D_7$ |
|---|---|---|---|---|---|---|---|---|
| DL64 | 0.00179 | 0.00007 | 0.000148 | 0.00030 | 0.00044 | 0.00133 | 0.00019 | 0.00056 |
| DS64 | 0.00196 | 0.00027 | 0.000088 | 0.00016 | 0.00040 | 0.00077 | 0.00025 | 0.00011 |
| DL58 | 0.00245 | 0.00016 | 0.000092 | 0.00011 | 0.00078 | 0.00096 | 0.00028 | 0.00322 |
| GL64 | 0.00471 | 0.00019 | 0.000202 | 0.00012 | 0.00065 | 0.00120 | 0.00028 | 0.00010 |
| Ti (s) | | 0.001 | 0.01 | 0.1 | 1.0 | 10 | 100 | 1000 |

**Table 3** Parameters of viscoplastic model

| Specimens | Γ (s-1) | α | $k_0$ (MPa) | $k_1$ (MPa) | $k_2$ | N |
|---|---|---|---|---|---|---|
| DL64 | 0.2328 | 0.2328 | 0.1830 | 0.002024 | 10,560 | 1 |
| DS64 | 0.0531 | 0.2320 | 0.1838 | 0.000600 | 14,240 | 1 |
| DL58 | 0.0399 | 0.1884 | 0.1821 | 0.005078 | 13,955 | 1 |
| GL64 | 0.0765 | 0.1951 | 0.1833 | 0.003697 | 7969 | 1 |

subtracting the viscoelastic strain $\varepsilon^{ve}$ from the total strain $\varepsilon^{t}$ at any time during loading. The Perzyna model with a Drucker-Prager yield surface was used to model the rate of viscoplastic strain, as observed in "Eq. 10":

$$\dot{\varepsilon}_{vp} = \Gamma\left[\frac{\sigma_1 - \alpha\frac{\sigma_1}{3} - \left(k_0 + k_1\left(1 - \exp\left(-k_2\varepsilon_{vp}\right)\right)\right)}{\sigma_y^0}\right]^N \tag{10}$$

where $\dot{\varepsilon}_{vp}$ is the rate of viscoplastic strain, Γ is the fluidity parameter, $\sigma_1$ is the applied stress, and $k_0, k_1$, and $k_2$ are the coefficients of the hardening equation. $\sigma_y^0$ is used to normalize the yield function and is assumed to be unity. Table 3 shows the computed values for the parameters of viscoplastic model.

### 3.3 Aggregate Structure Parameters

iPas 2 software was used to process and quantify the aggregate microstructure. The specimens were divided into four slices; six 2D images were taken of the cross-sections (Fig. 4). Table 4 shows the computed parameters of the aggregates microstructure. The minimum aggregate size of 2.36 mm was used for image analysis. The following five parameters were used to quantify the structure of the aggregates:

- Number of aggregates $(N_a)$
- Number of contacts $(N_c)$
- Total of aggregates perimeter $(P_a)$
- Total contact length $(L_c)$
- Vector magnitude $(\Delta_r)$: The calculation of this parameter is like that in "Eq. 1", except that the radial angle of the aggregates $(\theta)$ is used instead of the angle of aggregates relative to the horizontal direction (Fig. 1).

### 3.4 Constitutive Model of Asphalt Binder

Rheological testing was carried out using a dynamic shear rheometer (DSR) to characterize the asphalt binders using ASTM D7175-08 protocol. The dynamic shear modulus $(G^*)$ and phase angle $(\delta)$ were computed. The multiple stress creep recovery (MSCR) test was developed in accordance with ASTM D7405-10 to investigate the rutting characteristics of binders. Rutting potential is related to the

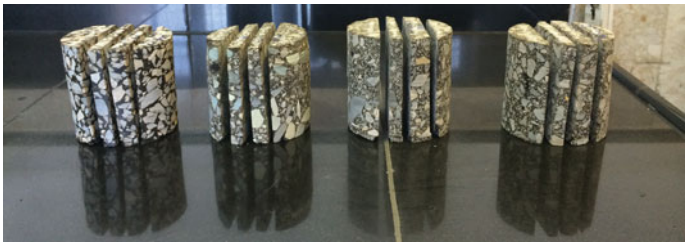

**Fig. 4** Specimens cut into four slices

**Table 4** Parameters of aggregate microstructure

| Specimens | $N_a$ | $N_c$ | $P_a$ (mm) | $L_c$ (mm) | $\Delta_r$ |
|---|---|---|---|---|---|
| DL64 | 189 | 149 | 2333 | 510 | 0.108 |
| DS64 | 195 | 191 | 2585 | 515 | 0.107 |
| DL58 | 227 | 207 | 2715 | 522 | 0.133 |
| GL64 | 165 | 146 | 2682 | 426 | 0.079 |

**Table 5** Parameters of fitted model for PG64-22 and PG58-22 asphalt binders (MPa)

| | $E_0$ | $E_1$ | $E_2$ | $E_3$ | $E_4$ | $E_5$ |
|---|---|---|---|---|---|---|
| PG64-22 | 0.0969 | 24.4800 | 13.8100 | 2.1790 | 0.6093 | 0.0229 |
| PG58-22 | 0.0002 | 50.0800 | 7.4650 | 1.6600 | 0.3497 | 0.0988 |
| Ti (s) | | 0.01 | 0.1 | 1.0 | 10 | 100 |

**Table 6** Non-recovered compliance ($J_{nr}$) for 3.2 kPa creep stress (1/MPa)

| Temp (°C) | 52 | 58 | 64 |
|---|---|---|---|
| PG64-22 | 0.522 | 1.516 | 4.042 |
| PG58-22 | 0.845 | 2.315 | 6.178 |

non-recoverable creep compliance ($J_{nr}$), the ratio of average non-recovered strain for 10 creep and recovery cycles and the applied stress for those cycles.

DSR tests were carried out on two types of RTFO aged bitumen (PG64-22 and PG58-22) at 20, 25, and 30 °C. $G^*$ was then obtained using the principle of time-temperature superposition for a reference temperature of 25 °C. "Equation 11" converts the values for $G^*$ to those of complex modulus $E^*$.

$$G^* = \frac{E^*}{2(1+\vartheta)} \tag{11}$$

where $\vartheta$ is The Poisson's ratio and was assumed to be 0.4. The Prony series was used in the frequency domain in "Eq. 12" to model the behavior of the bitumen. In this equation, $\omega$ is the frequency and $T_i$ is the relaxation time model coefficients, as shown in Table 5.

$$E^*(\omega) = E_0 + \sum_{i=1}^{N} \frac{E_i T_i^2 \omega^2}{1 + T_i^2 \omega^2} + \frac{E_i T_i \omega}{1 + T_i^2 \omega^2} i \tag{12}$$

Table 6 shows the MSCR results and Fig. 5 shows the logarithmic relationship between the $J_{nr}$ data. The binder irrecoverable strain factor (ISF) at 25 °C can be well-approximated using "Eq. 13". In this equation, $b$ is a constant the value as shown in Fig. 5.

$$\log(ISF) = \log(J_{nr}(T_{binder})) - b\left(T_{binder} - T_{testing}\right) \tag{13}$$

## 4 Data Analysis

A new parameter was needed to relate the aggregate structure to the mechanically attainable properties of asphalt mixture and binder. The ratio of stiffness moduli of asphalt mixture and binder was selected as an indicator of mechanical property of

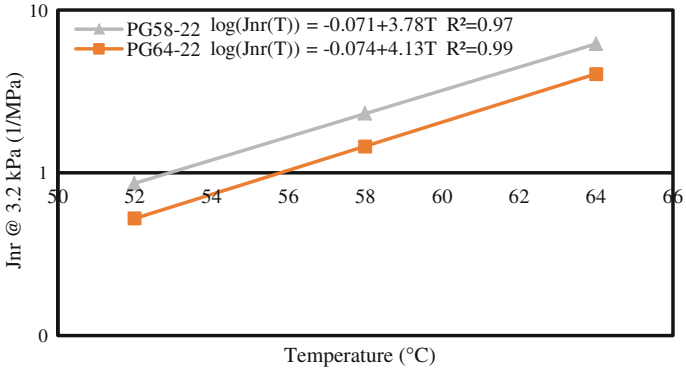


**Fig. 5** Results of MSCR test and fitted model for two asphalt binders

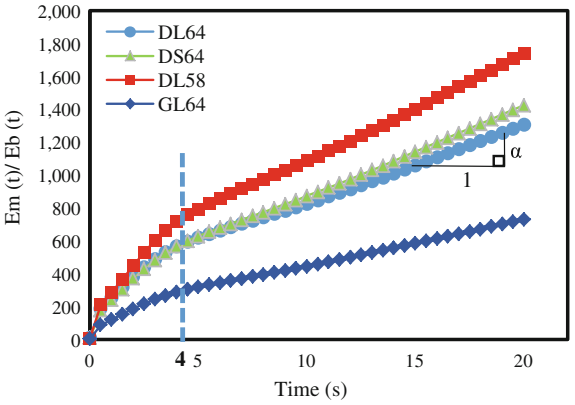


**Fig. 6** Ratio of stiffness modulus of asphalt mixture to bitumen

aggregate structure. The aggregate structure factor (ASF) composed of aggregate geometric properties, contact points and lengths, as shown in "Eq. 14", was introduced to describe the aggregate microstructure. Figure 6 shows that two linear segments exist in the plot of stiffness ratios with time. "Equation 15" describes this relationship.

$$\mathrm{ASF} = \frac{L_c}{P_a} * \frac{N_c}{N_a} * \Delta_r \tag{14}$$

$$\alpha = \frac{d}{dt}\left(\frac{E_m(t)}{E_b(t)}\right) = F(ASF) \tag{15}$$

Figures 7 and 8 show the relationship between ASF and $\alpha$ for each linear region. The results show good correlation between these two parameters. A binomial exponential equation was fitted to the viscoplastic strain rate data during loading for

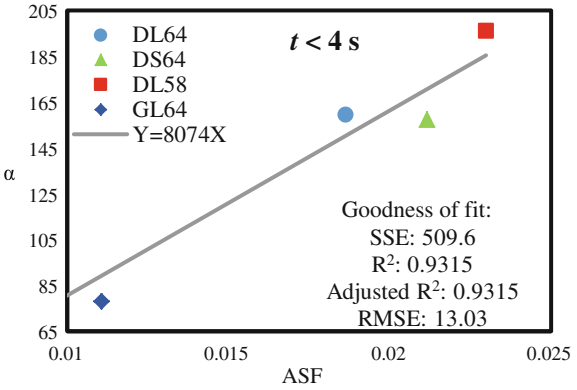


**Fig. 7** Relationship between ASF and $\alpha$ where $t < 4$ s

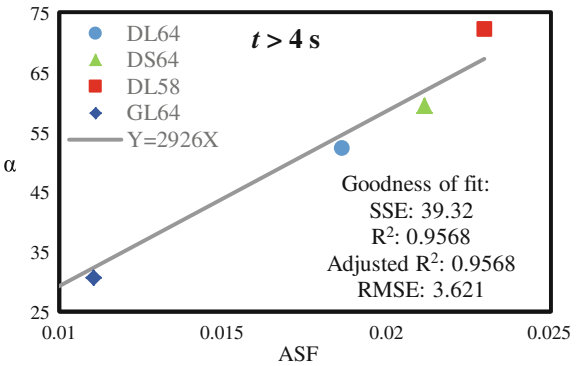


**Fig. 8** Relationship between ASF and $\alpha$ where $t > 4$ s

the different asphalt mixtures ("Eq. 16"). Comparison of the equations revealed that $\beta$ varied noticeably, while $A$, $B$ and $C$ remained nearly constant. "Equation 17" shows the values obtained for these coefficients.

$$\frac{\dot{\varepsilon}_{vp}}{\sigma_1} = \beta \exp(A * t) + B * \exp(C * t) \tag{16}$$

$$\frac{\dot{\varepsilon}_{vp}}{\sigma_1} = \beta \exp(-0.55t) + 6 * 10^{-5} \exp(-0.02t) \tag{17}$$

Various models were examined to describe $\beta$ as a function of ISF and ASF. "Equation 18" was found to fit the experimental data best. Figure 9 shows the good correlation between the parameters.

$$\beta = F\left(\frac{ISF}{ASF^2}\right) \tag{18}$$

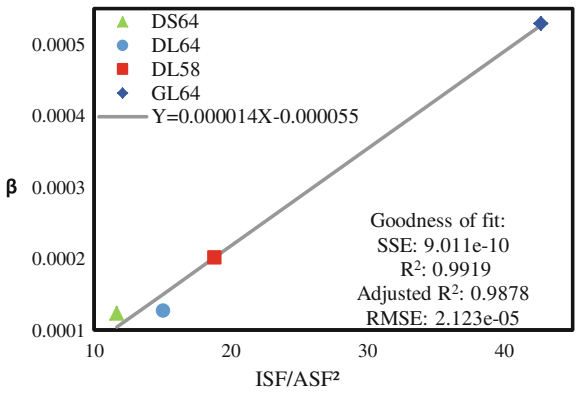


**Fig. 9** Relationship between $\beta$ and ISF/ASF$^2$

## 5 Conclusions

The study examined asphalt specimens with different aggregate gradations and asphalt binder types. An ASF microstructure-based indicator was proposed and its relationship with the viscoelastic and viscoplastic behavior of asphalt mixtures was investigated. In the viscoelastic range, the stiffness modulus ratio of asphalt mixture to binder was described as a function of ASF. The viscoplastic strain rate in the viscoplastic range was found to be a function of ASF and ISF. The results revealed that knowing the characteristics of the aggregate structure and binder properties allows prediction of the viscoelastic and viscoplastic behavior of asphalt mixtures.

## References

Bahia HU, Coenen A, Tabatabaee N (2013) Mixture design and compaction. In: Partl MN, Bahia HU, Canestrari F, Roche C, Di Benedetto H, Piber H, Sybilski D (Eds.) Advances in interlaboratory testing and evaluation of bituminous materials. State-of-the-art report of the RILEM Technical Committee 206-ATB, Dordrecht; Springer, New York, p 85-142

Coenen A, Kutay ME, Roohi Sefidmazgi N, Bahia HU (2012) Aggregate structure characterization of asphalt mixtures using 2-dimensional image analysis. J Road Materials and Pavement Design 13(3):433-454. doi:10.1080/14680629.2012.711923

Dessouky S. (2005) Multiscale approach for modeling hot mix asphalt. Ph.D. Dissertation, Texas A&M University

Dessouky S, Masad E, Little D, Zabib H (2006) Finite-element analysis of hot mix asphalt microstructure using effective local material properties and strain gradient elasticity. J Engineering Mechanics 132(2):158-171. doi: 10.1061/(ASCE)0733-9399

Henderson R, Herrington P, Patrick J, Kathirgamanathan P, Cook S (2011) Analysis of particle orientation in compacted unbound aggregate. J Road Materials and Pavement Design 12 (1):115-127. doi:10.1080/14680629.2011.9690355

Kim R (2009) Modeling of asphalt concrete. McGraw Hills Companies

Masad E, Tashman L, Little D (2002) Micromechanics-based analysis of stiffness anisotropy in asphalt mixtures. J Materials in Civil Engineering 14(5):374-383. doi: 10.1061/(ASCE)0899-1561

Roohi Sefidmazgi N (2011) Defining effective aggregate skeleton in asphalt mixture using digital imaging," Master of Science Thesis, University of Wisconsin-Madison, Madison, Wisconsin.

Saadeh S, Masad E, Little D (2007) Characterization of asphalt mix response under repeated loading using anisotropic nonlinear viscoelastic-viscoplastic model. J Materials in Civil Engineering 19(10):912-924. doi: 10.1061/(ASCE)0899-1561

Tashman L, Masad E, Peterson B, Saleh H (2001) Internal structure analysis of asphalt mixes to improve the simulation of Superpave gyratory compaction to field conditions. J Association of Asphalt Paving Technologists 70: 48-57

Tashman L, Wang LB, Thyagarajan S (2007) Microstructure characterization for modeling HMA behavior using imaging technology. J Road Materials and Pavement Design 8(2):207-238

Wagoner MP, Braham AF (2008) Anisotropic behavior of hot mix asphalt at low temperatures. J Transportation Research Board, No. 2057, p 83-88

Yu H, Muhunthan B, Shen S (2014) An anisotropic nonlinear elasto-viscoplastic model for rutting of asphalt mixtures. J Engineering Mechanics 140(2):242–249. doi: 10.1061/(ASCE)EM.1943-7889.0000655

Zhang Y, Luo R, and Lytton R (2011) Microstructure-based inherent anisotropy of asphalt mixtures. J Materials in Civil Engineering 23(10):1473-1482. doi: 10.1061/(ASCE)MT.1943-5533.0000325

# Estimation of Appropriate Filler Quantity in Asphalt Mix from Microscopic Studies

**Ambika Kuity and Animesh Das**

**Abstract** The type and quantity of filler influences the property of the asphalt mix. The filler quantity, similar to fine and coarser aggregates, is typically specified in proportions of weight. If the specific gravity of the filler is significantly different than the rest of the aggregates (for example, alternative fillers derived from industrial and domestic wastes), weight proportioning may lead to undesirably low or high quantity of filler in the mix. To investigate this issue further, in the present work filler concentration (in terms of percentage area occupancy) is studied at the microscopic level with the help of a scanning electron microscope. Three different types of fillers are chosen and are separately added to asphalt mix in varying proportions. The indirect tensile strength values and the corresponding filler concentration levels of these samples are noted. From limited data gathered in the present study, it appears that the average filler concentration values corresponding to the maximum indirect tensile strength levels for the mixes are statistically same. That means, even though optimum filler quantities (by weight) are different for these three mixes, the filler concentration values are almost the same. Subsequently, design chart is suggested to estimate the optimum quantity (by weight) of filler for asphalt mix for any given type of filler.

**Keywords** Asphalt mix · Filler · SEM · Statistical analysis

A. Kuity · A. Das (✉)
Department of Civil Engineering, Indian Institute of Technology Kanpur, Kanpur 208016, India
e-mail: adas@iitk.ac.in

A. Kuity
e-mail: ambika@iitk.ac.in



F. Canestrari and M.N. Partl (eds.), *8th RILEM International Symposium on Testing and Characterization of Sustainable and Innovative Bituminous Materials*, RILEM Bookseries 11, DOI 10.1007/978-94-017-7342-3_5

## 1 Introduction

Asphalt mix is composed of varied size of aggregates and asphalt binder. Finer fractions, typically smaller than 75 μ, are known as fillers (Kavussi and Hicks 1997; Little and Petersen 2005; NCHRP 673 2011; Sharma et al. 2010). Fillers remain suspended in asphalt binder. Presence of fillers improves workability, stiffness, moisture sensitivity, rutting resistance of the asphalt mix and so on (Anderson 1991; Al-Suhaibani et al. 1992; Hislop and Coree 2000; Kavussi and Hicks 1997; NCHRP 673 2011; Wang et al. 2011).

The aggregates (coarse, fines and fillers) of different sizes are generally mixed following certain pre-specified weight proportions to prepare an asphalt mix (Chen et al. 2011; Yiqiu et al. 2012). Thus, the mix specifications are typically expressed as upper and lower limits of the aggregate gradation (that is, a recommended range of cumulative percentage weight passing against various sieve sizes). One may further vary the material quantity (say, filler quantity in the present case) within the specified gradation range to 'fine tune' the proportion of the materials needed (Al-Suhaibani et al. 1992).

In recent times, many waste materials (for example, fly ash, incinerated municipal waste, rice husk ash, waste cement, brick powder, marble dust, waste ceramic, recycled aggregate dust etc.) are being utilized as alternative to conventional fillers (Sharma et al. 2010; Das and Swamy 2014; Huang et al. 2009; Karasahin and Terzi 2007; Kuity et al. 2014; Mills-Beale and You 2010; Sargin et al. 2013; Taha et al. 2002; Xue et al. 2009). Given that the specific gravity values of some of these alternative fillers may significantly be different than the conventional ones, use of weight proportioning may result in application of undesirably low or high quantity of filler in the mix.

An alternative approach to handle this issue can be the use of volume proportioning. Limited literature is available which identifies the above issue and proposes use of volume proportioning while estimating the filler quantity in the asphalt mix (Kuity et al. 2014; Zulkati et al. 2012). However, measure of volume is affected by the level of compaction applied. Thus, the actual 'quantity' of filler which is optimally needed for a mix, may not be appropriately known. This has motivated the present authors to investigate the issue of 'quantity' of filler which would be appropriate for a given asphalt mix.

Thus, it is proposed that the concentration of the fillers in the asphalt mix may be studied microscopically (refer Fig. 1). Hence, the scope of the present work can be identified as,

- Study on variation of strength of asphalt mix strength with the variation of filler content.
- Study on optimal filler concentration for different mixes prepared with different types of fillers (while the other constituents and proportions are held fixed).
- Estimation of appropriate filler quantity for any given filler.

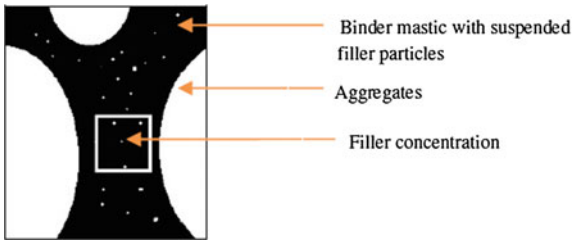


**Fig. 1** A 2-D conceptualization of filler concentration

## 2 Experimental Study

In the present study, three different fillers are taken namely stone dust, fly ash and brick dust. The aggregates and fillers are collected locally. The fillers are sieved through 75 μ sieve. The physical properties of fillers and asphalt binder are presented in the Tables 1 and 2 respectively. The impact test (IS 2386, Part-IV) and Los Angeles abrasive test (IS 2386, Part-IV) of aggregate are observed to be 13.06 and 15.35 % respectively (Kuity et al. 2014). Bituminous concrete (BC) grade II as per Indian specification is adopted as aggregate gradation (MORT&H 2013). The gradation is shown in Table 3. The particle size distributions of the fillers are found out by using hydrometer analysis (ASTM D422-63) and the results are presented in Table 4.

Three types of asphalt mix samples are prepared (as per ASTM D6926) by using the three types of fillers chosen in the present study. Asphalt binder content is kept fixed at 5.5 % with respect to the weight of mix, that is, 5.91 % by weight of the aggregates excluding fillers. The compositions of the mixes are kept the same except the quantity of the filler is varied from 6 to 12 % (by weight of the aggregates excluding the weight of filler) for each type of mixes. A larger range of filler quantity is chosen (than typically specified in the guidelines) so as to capture exhaustively possible variation of mix property with respect to variation of filler quantity. Two types of tests are conducted in the present study, (i) indirect tensile strength test (IDT) as an estimator of strength for asphalt mix, and (ii) scanning electron microscope (SEM) imaging to study the filler occupancy level. These are discussed in the following paragraphs.

### *2.1 Indirect Tensile Test*

The Indirect Tensile Strength (IDT) tests are performed following ASTM D 6931. The results are plotted in Fig. 2 including the fitted curves. As expected, the IDT value is observed to increase first and then decrease with the increase of the filler content. This indicates that the filler content corresponding to the peak IDT value

**Table 1** Physical properties of filler

| Properties | Standard/method | Stone dust | Fly ash | Brick dust |
|---|---|---|---|---|
| Specific gravity[a] | ASTM C128 | 2.62 | 2.41 | 2.68 |
| Compacted bulk density (kg/m$^3$)[a] | ASTM C29 | 1184 | 1000 | 1208 |
| Specific surface area (m$^2$/kg)[a] | IS 4031 (Part-II) 1999 | 278.96 | 304.61 | 256.06 |
| Rigden Air-void (%)[a] | MOT, Ontario | 16.97 | 15.49 | 17.32 |
| Particle shape and surface texture | SEM[b] imaging | 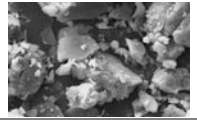 | 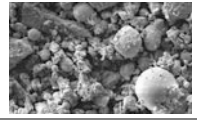 | 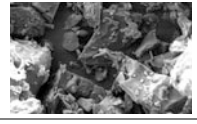 |

[a]Average of three samples
[b]Scanning electron microscope

**Table 2** Physical properties of the asphalt binder

| Properties | Value | Standard/method |
|---|---|---|
| Penetration | 92 | IS 1203 |
| Ductility | 78 cm | IS 1208 |
| Softening point | 49 °C | IS 1205 |
| Flash point | 272 °C | IS 1209 |

**Table 3** Aggregate gradation adopted in the present study

| Sieve size (mm) | 19.0 | 13.2 | 9.5 | 4.75 | 2.36 | 1.18 | 0.6 | 0.3 | 0.15 | 0.075 |
|---|---|---|---|---|---|---|---|---|---|---|
| passing adopted (%) | 100 | 95.0 | 79.0 | 62.0 | 50.0 | 41.0 | 32.0 | 23.0 | 16.0 | Variable (6–12) |

**Table 4** Particle size distribution of fillers obtained by hydrometer analysis

| Diameter of particles (μ) | Percentage by weight | | |
|---|---|---|---|
| | Stone dust | Fly ash | Brick dust |
| 75P-45R | 18 | 12 | 9 |
| 45P-37R | 6 | 4 | 3 |
| 37P-25R | 19 | 22 | 16 |
| 25P-lower | 57 | 62 | 72 |

can possibly be taken as optimum filler content for a given type of filler. From Fig. 2, it can be seen that the optimum filler content is the least for fly ash, followed by stone dust and then brick dust. These values can be read as 8.0, 9.0 and 9.5 %, respectively (by weight of the mix excluding the weight of the filler). It is interesting to note that the specific gravity, specific surface area and the Rigden air void values (refer Table 1) also follow the similar order.

## *2.2 Scanning Electron Microscope (SEM) Study*

Studies are conducted using SEM on the exposed surface of asphalt mix samples to estimate the filler concentration. Typically middle portion of mastic is chosen for such study (refer Fig. 1). SEM study primarily involves three stages, namely sample preparation, imaging and image analysis. These are discussed in the following.

Samples for SEM testing are prepared by making small pieces from the original Marshall samples. The steps involved are cutting, grinding and polishing. The final dimension of the sample becomes about 1.5 cm × 1 cm × 0.5 cm (refer Fig. 3). As asphalt mix is nonconductive, a thin layer of gold coating is done before placing the sample under SEM electron beam. The images are captured in backscattered

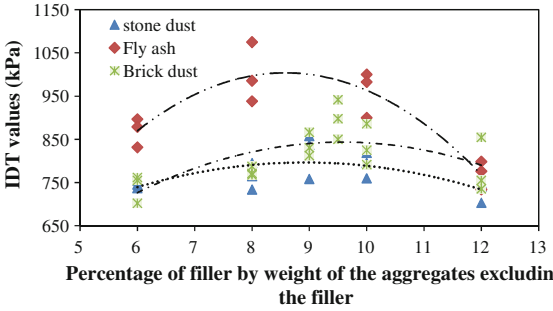


**Fig. 2** Variation of IDT with varying percentage of filler (by weight of the aggregates excluding the filler) for stone dust, fly ash and brick dust

**Fig. 3** Sample prepared for SEM study

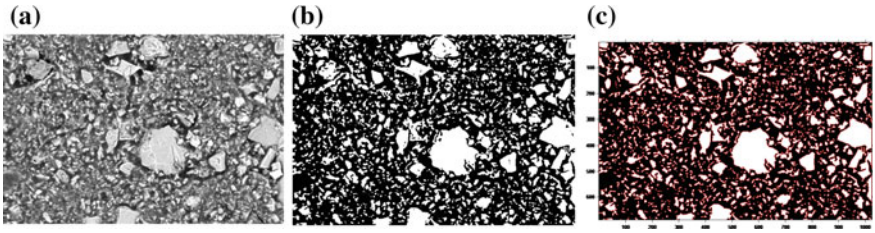


**Fig. 4** Image analysis on **a** original SEM image, **b** after thresholding, **c** after identifying fillers

electron mode. Twenty images are taken for each filler content and for each type of filler.

Figure 4 shows the steps involved in the image processing and analysis. Figure 5 shows a pictorial example (for brick dust filler) of how the filler occupancy level changes with the increase in filler quantity.

Figure 6 shows images at respective optimum filler contents. To evaluate the filler occupancy level, a parameter namely filler concentration ($F_c$) is proposed. $F_c$ may be defined as area occupied by filler particles divided by the total area of the sample space. The average $F_c$ values obtained from analyzing the images are

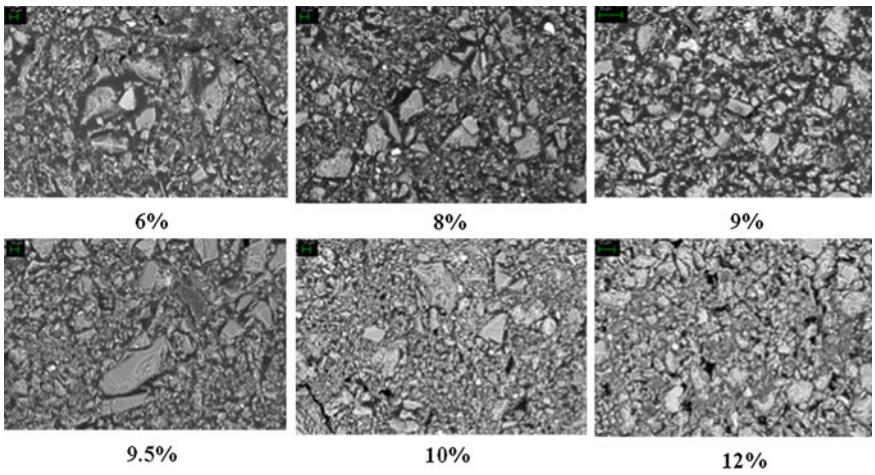


**Fig. 5** Images at different percentages of filler content (by weight of the aggregates excluding the filler) for brick dust as filler

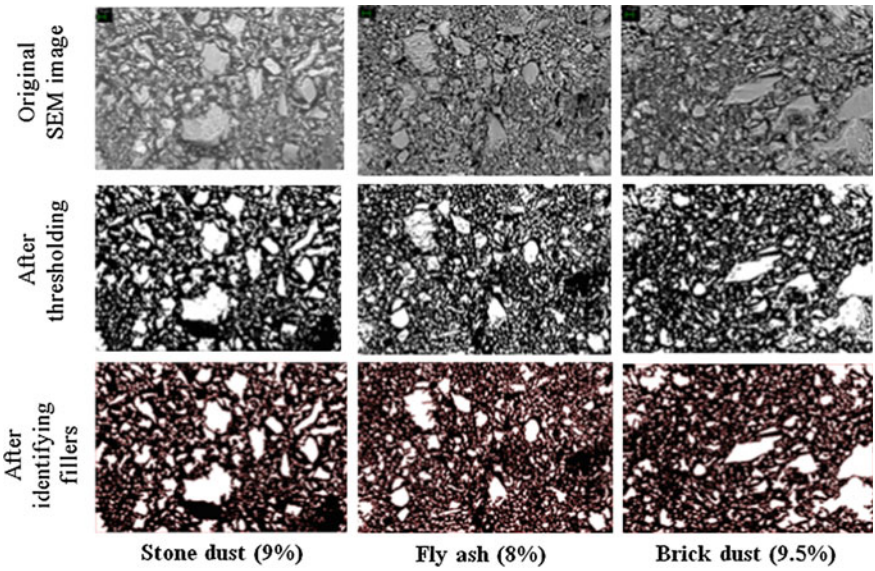


**Fig. 6** Images at optimum filler contents for stone dust, fly ash and brick dust

mentioned in Table 5. It is interesting to see that the $F_c$ values appear to be comparable to each other, even though the weight proportions at maximum IDT values are different (refer Fig. 7).

To investigate this further, the following null hypothesis is proposed:

**Table 5** Average filler concentration values at maximum IDT

| Type of fillers | Stone dust | Fly ash | Brick dust |
|---|---|---|---|
| Number of images studied | 20 | 20 | 20 |
| Weight proportion (%)[a] | 9.0 | 8.0 | 9.5 |
| Average filler concentration ($F_c$) | 38.82 | 36.20 | 37.00 |
| Standard deviation of $F_c$ | 6.38 | 5.40 | 3.89 |

[a]With respect to the total weight of aggregates excluding filler

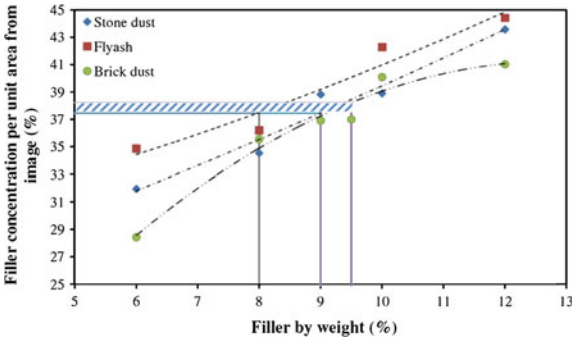


**Fig. 7** Variation of $F_c$ with filler content by weight

The average $F_c$ values for each pair of fillers, corresponding to their respective maximum IDT values are statistically same.

Since the sample size for images of each asphalt mix composition is less than 30, *t*-distribution is considered for statistical analysis (Walpole et al. 2011). Table 6 shows the results of hypothesis testing. The t-values for each pair are observed to be less than critical t-value of 1.686 for 95 % confidence interval. Thus the null hypothesis is not rejected and therefore, average $F_c$ values for each pair of filler types can be considered to be same. The argument can be extended further saying that the filler concentration ($F_c$) at optimum filler content is statistically same across three different fillers used in the present study.

Although based on limited data, this hypothesis provides an insight to the optimal filler quantity in asphalt mix. This concept can be used for deciding appropriate filler quantity for a given asphalt mix, especially with alternative fillers, having specific gravity values different than the conventional ones. However, given the fact that SEM study may not always be feasible at the mix design state, a chart can be developed to help a mix designer to decide the optimal filler content. Figure 8 shows such a chart based on current results obtained from the three fillers studied. This, however, needs to be further validated with more number of fillers and asphalt mixes.

It may be noted that bulk density (at a given compaction level) is influenced by the specific gravity, gradation, form and texture of the filler particles, hence, effects of these parameters are automatically included in the measurement of bulk density. Further research is ongoing to understand the correspondence between bulk density,

**Table 6** *t*-distribution test results at 95 % confidence interval

| Comparison between | *t*-distribution test statistic | Remarks |
|---|---|---|
| 9 % stone dust and 8 % fly ash | 1.400 | Null hypothesis is not rejected |
| 8 % fly ash and 9.5 % brick dust | 0.537 | |
| 9.5 % brick dust and 9 % stone dust | 1.089 | |

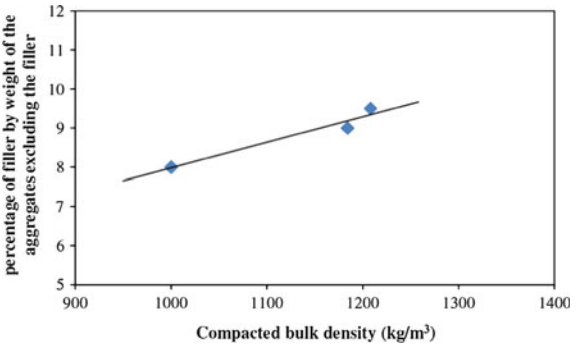


**Fig. 8** Suggested chart to decide the optimal filler quantity for any given filler

filler concentration at microscopic level and the physical and shape properties of filler particles.

## 3 Conclusions

The issues involved in estimation of appropriate filler quantity in asphalt mix have been identified. The microscopic observations on limited number of samples, using three different types of fillers, suggest that the filler concentration at the respective optimal levels (corresponding to maximum IDT) tend to assume the same value. Using this as a basis, recommendation is suggested to choose optimum filler quantity for any given filler. However, further studies are needed on more number of samples and across different types of fillers and asphalt mixes to finalize such recommendation.

**Acknowledgments** Laboratory tests have been conducted at various laboratories of IIT Kanpur. The authors like to thank all staff members in various laboratories for their help and support during preparation of samples and testing.

## References

Al-suhaibani A, Al-Mudaiheem J and Al-Fozan F (1992) Effect of filler type and content on properties of asphalt concrete mixes. In: Meininger RC (ed) Effects of aggregate and mineral fillers on asphalt mixtures performance, ASTM STP 1147, Philadelphia, p 107–130.

Anderson DA, Dongre R, Christensen DW and Dukatz EL (1991) Effects of minus no. 200 sized aggregate on fracture behavior of dense-graded hot mix asphalt. In: Meininger RC (ed) Effects of Aggregates and Mineral Fillers on Asphalt Mixture Performance, ASTM STP 1147, Philadelphia, p 1541–1576.

ASTM C29 (2007) Standard test method for bulk density (unit weight) and voids in aggregate. ASTM, West Conshohocken.

ASTM C128 (2012) Standard test method for density, relative density (specific gravity), and absorption of fine aggregate. ASTM, West Conshohocken.

ASTM D422-63 (2007) Standard test method for particle-size analysis of soils. ASTM, west Conshohocken.

ASTM D6926 (2010) Standard practice for preparation of bituminous specimens using Marshall apparatus. ASTM, West Conshohocken.

ASTM D6931 (2012) Standard test method for indirect tensile (IDT) strength of bituminous mixtures. ASTM, West Conshohocken.

Chen M, Lin J and Wu S (2011) Potential of recycled fine aggregates powder as filler in asphalt mixture. Constr Build Mater 25:3909–3914.

Das A and Krishna Swamy A (2014) Reclaimed waste materials in sustainable pavement construction. In: Gopalakrishnan K, Steyn WJ and Harvey J (ed) Climate Change, Sustainability, Energy, and Pavements, Chapter 15, Springer-Verlag, Berlin, 419-438.

Hislop WP and Coree BJ (2000) VMA as design parameter in hot-mix asphalt. Proceedings of Mid-continent Transportation Symposium 2000, p 24–29. Available via http://www.ctre.iastate.edu/pubs/midcon/Hislop.pdf . Accessed 27 Mar 2015.

Huang B, Dong Q and Burdette EG (2009) Laboratory evaluation of incorporating waste ceramic materials into Portland cement and asphaltic concrete. Constr Build Mater 23(12):3451–3456.

IS 1203 (2004) Determination of penetration. Bureau of Indian Standard, Bureau of Indian Standard, New Delhi.

IS 1205 (2004) Determination of softening point. Bureau of Indian Standard, Bureau of Indian Standard, New Delhi.

IS 1208 (2004) Determination of ductility. Bureau of Indian Standard, Bureau of Indian Standard, New Delhi.

IS 1209 (2004) Determination of flash point. Bureau of Indian Standard, Bureau of Indian Standard, New Delhi.

IS 2386 (Part IV) (2002) Methods of test for aggregates for concrete. Bureau of Indian Standard, New Delhi.

IS 4031 (Part II) (1999) Determination of fineness by specific surface by Blaine air permeability method. Bureau of Indian Standard, New Delhi.

Karasahin M and Terzi S (2007) Evaluation of marble waste dust in the mixture of asphaltic concrete. Constr Build Mater 21:617–620.

Kavussi A and Hicks RG (1997) Properties of bituminous mixtures containing different fillers. Proceedings, Association of Asphalt Paving Technologists 66:153–186.

Kuity A, Jayaprakashan S and Das A (2014) Laboratory investigation on volume proportioning scheme of mineral fillers in asphalt mix. Constr Build Mater 68:637-643.

Little DN and Petersen C (2005) Unique effects of hydrated lime filler on the performance related properties of asphalt cements: Physical and chemical interactions revisited. Journal of Materials in Civil Engineering, 17(2):207-218.

Mills-Beale J and You Z (2010) The mechanical properties of asphalt mixtures with recycled concrete aggregates. Constr Build Mater 24:230-235.

Ministry of transportation Ontario (2001) Method of test for volume of voids (Rigden voids) in compacted filler or fines. Laboratory test manual, test method LS-628, rev no. 23:1-7. Available via applications.roadauthority.com/Standareds/Home/FileDownload?standard Field = 1131e8f5-2c1a-490a-9f2a-740df9081c8c. Accessed 27 Mar 2015.

MORT&H (2013) Specifications for road and bridge works. Indian Roads Congress, New Delhi.

Muniandy R, Aburkaba E and Taha R (2013) Effect of mineral filler type and particle size on the engineering properties of stone mastic asphalt pavements. TJER, 10(2):13-32.

NCHRP 673 (2011) A manual for design of hot mix asphalt with commentary, National cooperative highway research program, Report no: 673, Advanced Asphalt Technologies, LLC, Sterling, VA. Available via http://onlinepubs.trb.org/onlinepubs/nchrp/nchrp_rpt_673.pdf. Accessed 27 March 2015.

Sargin S, Saltan M, Morova N, Serin S and Terzi S (2013) Evaluation of rice husk ash as filler in hot mix asphalt concrete. Constr Build Mater 48:390-397.

Sharma V, Chandra S and Choudhary R (2010) Characterization of fly ash bituminous concrete mixes. Journal of Materials in Civil Engineering 22(12): 1209-1216.

Taha R, Al-Rawas A, Al-Harthy A and Qatan A (2002) Use of cement bypass dust as filler in asphalt concrete mixtures. Journal of Materials in Civil Engineering 14(4):338-343.

Walpole R E, Myers RH, Myers SL and Ye K (2011) Probability & Statistics for Engineering & Scientists, Ninth edition, Prentice Hall.

Wang H, Al-Qadi IL, Faheem AF, Bahia HU, Yang SH and Reinke GH (2011) Effect of mineral filler characteristics on asphalt Mastic and mixture rutting potential. Journal of the Transportation Research Board, 2208: 33–39.

Xue Y, Hou H, Zhu S and Zha J (2009) Utilization of municipal solid waste incineration ash in stone mastic asphalt mixture: Pavement performance and environmental impact. Constr Build Mater 23:989-996.

Yiqiu T, Xiaolin Li and Jiantao W (2012) Internal influence Factors of asphalt- aggregate filler interactions based on rheological characteristics. Journal of materials in civil engineering, 24:1520-1528.

Zulkati A, Diew WY and Delai DS (2012) Effects of fillers on properties of asphalt –concrete mixture. Journal of transportation engineering, 138(7): 902-910.

# A Mineralogical Approach of the Interactions Between Bitumen, Clay and Water in Hot Mix Asphalt (HMA)

**Chi-Wei Chen, Vincent Gaudefroy, Myriam Duc, Yannick Descantes, Ferhat Hammoum and Jean-Pierre Magnan**

**Abstract** Clay fines are known to reduce the water resistance of bitumen-aggregates binding and cause stripping in Asphalt Concrete (AC) mixtures. To address this phenomenon, a better understanding of the mineralogical composition of aggregates is needed as well as an assessment of the bitumen-clay-water interactions. This paper contributes to reach this goal from a mineralogical perspective. The most common clays in natural aggregates, kaolinite, illite and montmorillonite, were used to prepare thin clay films and artificial clay-rich aggregates. The bitumen-clay interaction was studied using the sessile drop and the Oliensis spot tests on those thin clay films, whereas Duriez tests allowed measuring the stripping potential of AC mixtures containing the clay-rich aggregates. The results show that the water-bitumen-clay interaction and water resistance of the AC mixture are specific to the clay mineralogy. Furthermore, they show that the bitumen-clay interaction may be captured upon determining the surface energy of bitumen, the chemical composition and pH value of the clay and the bitumen-clay compatibility. Hence, predicting the water resistance of clay rich AC mixtures from mineralogical properties of the bitumen-clay interaction seems feasible.

**Keywords** Clay · Mineralogical analysis · Chemistry of bitumen · Water-bitumen-clay interaction · Work of adhesion · Water susceptibility · Duriez test · HMA · Aggregates

C.-W. Chen (✉) · M. Duc · J.-P. Magnan
IFSTTAR, University of Paris-Est, 14-20 Boulevard Newton, Champs sur Marne, Marne la Vallée, Cedex 2, France
e-mail: chi-wei.chen@ifsttar.fr

V. Gaudefroy · Y. Descantes · F. Hammoum
IFSTTAR, LUNAM Université, MAST, Route de Bouaye, 44341 Bouguenais, France



F. Canestrari and M.N. Partl (eds.), *8th RILEM International Symposium on Testing and Characterization of Sustainable and Innovative Bituminous Materials*, RILEM Bookseries 11, DOI 10.1007/978-94-017-7342-3_6

## 1 Introduction

The presence of clay in fine aggregates is known to increase the moisture susceptibility of Asphalt Concrete (AC) mixtures. Therefore, Huet (1991), Tarrer and Wagh (1991) suggested the removal of fines (particles passing the 0.063 mm sieve) by washing or their treatment with lime (Lesueur et al. 2013) prior to incorporating fine aggregates into AC mixtures. Meanwhile, several studies have investigated the moisture susceptibility of AC mixtures and reported adhesive failure phenomena at the bitumen-aggregate interface, also called stripping (Curtis et al. 1993), which occur more easily when the clay content of aggregates increases. These results call for additional investigation at the bitumen-aggregate interface.

Kaolinite, montmorillonite, and illite are three types of clay minerals commonly present in aggregate quarries (Nesse 2000). Their crystallographic layer charge and exchangeable cations affect the interlayer spacing and swelling properties of the clay mineral, which can be represented by its cation exchange capacity (CEC) and its specific surface area (SSA) (Pentrák et al. 2012). For instance, a swelling clay mineral (e.g. montmorillonite) exhibits higher CEC than non-swelling clay minerals (e.g. kaolinite) due to a higher amount of exchangeable cations present in the interlayer surface (internal specific surface, Maurice 2009). Moreover, this swelling clay mineral highly expands by attracting a high amount of molecules into the interlayer, such as water molecules (Carter et al. 1986). On the other hand, non-swelling and low-swelling phyllosilicates such as kaolinite and illite have mainly external surfaces and negligible internal surface to attract water molecule.

Bitumen consists of four groups of components which are Saturates, Aromatics, Resins and Asphaltenes (SARA). Resins and Asphaltenes, which are the dark sticky semisolid liquids of bitumen, contain O, N, and S in the form of anhydrides, carboxylic acids, sulfoxides, etc.… These polar components of bitumen have a high affinity with water molecules, whereas the Saturates are light colored and non-polar (dispersive) components (Sjöblom 2001). Generally, the proportion of each chemical compound in bitumen is adapted to desired AC pavement properties. Given the French temperate climate, hard AC pavements require high contents of Resins and Asphaltenes.

From the chemical point of view, the acidic components from bitumen resin and asphaltene compounds easily bind with clay exchangeable cations by losing hydrogen atoms from the −COOH components, sulfoxide, 2-quinolone. Unfortunately, these bonds may easily be broken by water molecules (Hefer and Little 2005). As a consequence, a high proportion of exchangeable cations on clay surface may severely weaken the bitumen-clay binding due to weak electrostatic bonds (Kanitpong and Bahia 2003), which contribute to the high affinity to water molecules (Plancher et al. 1977; Curtis et al. 1993; Bagampadde et al. 2004).

The present paper deals with a preliminary research to address stripping phenomena through bitumen-clay interaction from the clay mineralogy perspective.

Section 2 describes the preparation of test specimens as well as the tests used to assess the bitumen-clay water interaction at mineralogical scale. Section 3 presents and discusses the test results, then interprets them in light of AC mixtures behavior at macro-scale.

## 2 Materials and Test Procedures

### 2.1 Aggregates

Kaolinitic, illitic and montmorillonitic rocks were respectively supplied from the quarries Société Kaolinière Armoricaine (SOKA company, France), Argile du Velay (ARVEL company, France), and Argiles du Bassin Méditerranée (ABM company, France). The raw clay fractions were extracted from these rocks in the laboratory by wet sieving through the 0.063 mm sieve, then dried at room temperature, and finally ground until the particle size was less than 0.063 mm. The fine aggregate fraction was prepared by washing the St. Colomban sand (France) and keeping the aggregate fraction retained on the 0.063 mm sieve. Each material was further tested to identify its mineral phases and several physical-chemical properties summarized in Table 1.

### 2.2 Preparation of Clay-Rich AC Mixtures

The grading curve of a 0/6 mm gap-graded AC mixture was adopted for this study (BBTM6A according to Delorme et al. 2007 and NF EN 13108-1 2007) with the maximum clay content set to the maximum permitted fines content (Table 2). Each

**Table 1** Mineralogical and physical-chemical properties of tested materials

| Mat. | Particle size (mm) | Mineralogical phases | | SSA ($m^2$/g) | | CEC (meq/100 g) | MB (g/kg) |
|---|---|---|---|---|---|---|---|
| | | Major | Minor | Ext. | Int. | | |
| K | <0.063 | Kaolinite > 76 % | Quartz; illite | 15 | 0 | 1.3 ± 0.2 | 9.7 ± 0.4 |
| I | | Illite > 84 | Quartz; kaolinite; calcite | 25 | 5 | 23.3 ± 0.1 | 42.6 ± 0.9 |
| M | | Montm. > 85 % | Illite | 50 | 750 | 103.6 ± 2.5 | 236.1 ± 8.5 |
| Sand | >0.063 | Quartz | Amorphous silica; feldspars | 0.1[a] | n/a | 0.1 ± 0.01 | 0.4 ± 0.1 |

*K*, *I* and *M* are kaolinite, illite and montmorillonite respectively. *Int* or *ext SSA* Internal or external specific surface area [typical values from Morel (1996), Olphen and Fripiat (1979)], *CEC* cation exchange capacity, *MB* methylen blue value (The standard deviation was assessed from 3 measurements)

[a]Calculated from sample particle size distribution

**Table 2** Experimental design of gap-graded BBTM6A AC mixtures

| Design | Binder | Coarse aggregates | Fine aggregates | | Filler |
|---|---|---|---|---|---|
| Aggregates fraction | – | Coarse fraction | Sand fraction | Clay fraction | – |
| Material | Bitumen $_{35/50}$ | Diorite | Washed sand | K. or I. or M. | Limestone |
| Particle size (mm) | N/A | $D_{4/6}$ | $D_{0.063/2}$ | $D_{0/0.063}$ | $D_{0/0.063}$ |
| Content | Richness 3.6 | 75 % | 16 % | 9 % | 9 %[a] |

[a]Limestone filler is substituted for clay in the reference sample of AC mixture

clay-rich fine aggregate fraction (0/2 mm) was prepared by mixing the clay fines with the pre-soaked sand fraction until well coated (Leroux and Unikowski 1980), then used to prepare the corresponding AC mixture for water resistance tests (NF P 98-251-1 2002; NF EN 13108-1 2007; NF EN 12697-35+A1 2007).

## 2.3 Test Procedures

The surface energy of clays and the work of adhesion ($W_{ad}$) at bitumen-clay interface were measured by sessile drop tests. The test portion preparation protocol consists in gently dropping 1.5 ml of a 0.4 % extracted clay suspension on a clean and dry microscope glass slide (2.5 cm × 2.5 cm), and then drying the glass slide at room temperature over a week to form a clay film less than 10 µm thick. The sessile drop test was performed using a Drop Shape Analyser DSA100 from Kruss GmbH and four liquids, water, glycerol, ethylene glycol and diiodo-methane. The surface energy of clay was calculated from liquid-clay contact angle measurements. The work of adhesion at bitumen-clay interface was calculated from corresponding contact angle measured in a climate chamber at a constant temperature of 140 °C. The temperature reduction from 160 °C (common AC temperature) to 140 °C was applied to increase the viscosity of bitumen in order to stabilize the volume of each bitumen drop.

The Oliensis spot test was used to assess the bitumen-clay contact compatibility (ASTM D1370 2012). A drop of molten bitumen (6.0 µl ± 1.1) was placed on a thin clay film at a constant temperature of 140 °C, and kept for 4 h. The Oliensis result was calculated as the ratio of the thickness of the oil ring surrounding the drop to the spot radius (oil ring + drop).

The water resistance of AC mixtures was checked according to the Duriez test protocol (NF EN 12697-12 2008). Stripping resistance was evaluated on specimens compacted by direct axial compression and then stored at a temperature of 18 °C in water and in air (50 % relative humidity) (Huet 1991). Direct compressive strengths of these specimens and the r/R ratio of resistances are measured. r/R = 1 means that stripping resistance and coating quality are maximum.

# 3 Results and Discussion

## 3.1 Surface Energy

The polar forces $(\gamma_S{}^P)$, the dispersive forces $(\gamma_S{}^D)$, and the surface energy $(\gamma_S = \gamma_S{}^P + \gamma_S{}^D)$ of each clay and the glass substrate were determined from the measured contact angles between four liquids and the clay (Ziyani 2013), upon applying a linear fit and identifying the terms of the Owens-Wendt model (Eq. 1):

$$\frac{\gamma_L(cos\theta + 1)}{2(\gamma_L{}^D)^{1/2}} = (\gamma_S{}^P)^{1/2}\frac{(\gamma_L{}^P)^{1/2}}{(\gamma_L{}^D)^{1/2}} + (\gamma_S{}^D)^{1/2} \quad (1)$$

where

$\gamma_L{}^P$ and $\gamma_L{}^D$ are the polar forces and the dispersive forces of liquid,
$\gamma_S{}^P$ and $\gamma_S{}^D$ are the polar forces and the dispersive forces of solid, and
$\theta$ is the contact angle between solid and liquid.

Table 3 shows more or less the same polar and dispersive forces for the glass slide, kaolinite and montmorillonite, whereas illite is prone to higher dispersive forces.

The consistency of these values was checked in light of previous works. Chassin et al. (1986) stated that the dispersive forces originate from the surface oxygen groups of the silica tetrahedral, whereas polar forces derive from the exchangeable cations. The high polar forces of glass slide result from its non-regular $SiO_2$ structure and the $Na^+/Al^{3+}$ addition, which was used for increasing the toughness and the photosensitivity (Trukhin et al. 2009). Montmorillonite is assumed to be characterized by high polar forces which result from its high amount of exchangeable cations (CEC = 103.6 meq/100 g). However, such clay has approximately the same polar and dispersive forces according to our measurements.

**Table 3** The surface energy of liquids, bitumen and clays

| Material | Type | Polar forces ($mJ/m^2$) | Dispersive forces ($mJ/m^2$) | Surface energy ($mJ/m^2$) | References |
|---|---|---|---|---|---|
| Liquids | Water | 51.0 | 21.8 | 72.8 | Strom (1987) Rosenholm (2007) |
| | Ethylene glycol | 16.8 | 30.9 | 47.7 | |
| | Glycerol | 26.4 | 37 | 63.4 | |
| | Diiodo-Methane | 0.0 | 50.8 | 50.8 | |
| Bitumen | 35/50 at 140 °C | 5.0 | 23.0 | 28.0 | Somé (2012) |
| Materials | Kao | 5.6 ± 0.6 | 5.4 ± 0.5 | 11.0 | N/A |
| | Illite | 5.3 ± 0.5 | 6.4 ± 0.4 | 11.7 | |
| | Montm. | 5.7 ± 0.4 | 5.6 ± 0.3 | 11.3 | |
| | Glass slide | 5.9 ± 0.3 | 5.1 ± 0.3 | 11.0 | |

It is caused by the presence of hydrated exchangeable cations in interlayer spaces that keep their water molecules even after the drying of clay suspension at room temperature. Moreover, hydrates such as $X.yH_2O$ probably precipitate on montmorillonite surface during drying, thus contributing to polar forces mitigation by decreasing the amount of hydrogen bonds (Prost 1975). Illite not only has a lower surface charge and less exchangeable cations than montmorillonite, hence lower polar forces, but it also has calcite ($CaCO_3$) in its mineral phases, hence higher dispersive forces originating from the oxygen groups on silica tetrahedral sheet and calcite. Even though kaolinite is a charge-free and an exchangeable-ion-free mineral, its polar and dispersive forces appear more or less the same. It may be caused by the dissolution of the silica tetrahedrons caused by the low pH value of the suspension (pH = 4.5 for kaolinite solution, whereas pH = 9.5 and 8.3 for illite and montmorillonite suspensions respectively). During the subsequent kaolinite drying process, this dissolution is followed by the precipitation of superficial acidic aluminum residue, which provides the hydrogen responsible for polar forces increase.

## 3.2 *Bitumen-Clay Interaction (Work of Adhesion)*

The clay-bitumen work of adhesion $W_{ad}$ can be derived either from the measured contact angle θ, or from the calculation of the interaction force. Both results will indeed be compared in this study. $W_{ad}$ from contact angle measurement is calculated upon introducing the Young expression of the tension at bitumen-clay interface into the Dupré equation (Eq. 2, Dupré and Dupré 1869). $W_{ad}$ from tension at bitumen-clay interface is calculated upon combining the Young's formula with the Owens-Wendt equation (Owens and Wendt 1969) to determine first the interfacial tension $\gamma_{ad}$ (Eq. 3), then introducing the resulting expression into the Dupré equation (Eq. 4):

$$W_{ad} = \gamma_L(1 + \cos\theta) \tag{2}$$

$$\gamma_{ad} = \gamma_S + \gamma_L - 2(\sqrt{\gamma_S{}^P \gamma_L{}^P} + \sqrt{\gamma_S{}^D \gamma_L{}^D}) \tag{3}$$

$$W_{ad} = 2(\sqrt{\gamma_S{}^P \gamma_L{}^P} + \sqrt{\gamma_S{}^D \gamma_L{}^D}) \tag{4}$$

Figure 1a depicts the bitumen-clay and water-clay work of adhesion calculated from Eqs. 2 and 4, as well as corresponding surface tensions calculated from Eq. 3. Upon fixing the liquid and calculation method, the interfacial tension is more or less the same whatever the clay. A similar conclusion may be drawn from work of adhesion results, except at the bitumen-illite interface for which Eq. 2 calculations yield a lower value than for bitumen-kaolinite and bitumen-montmorillonite interfaces. This study agrees with usual values of $W_{ad}$ from contact angle measurement (Eq. 2) but not with those from interfacial tension calculations (Eqs. 3 and 4). One reason is that the contact angle measurement method allows analyzing the

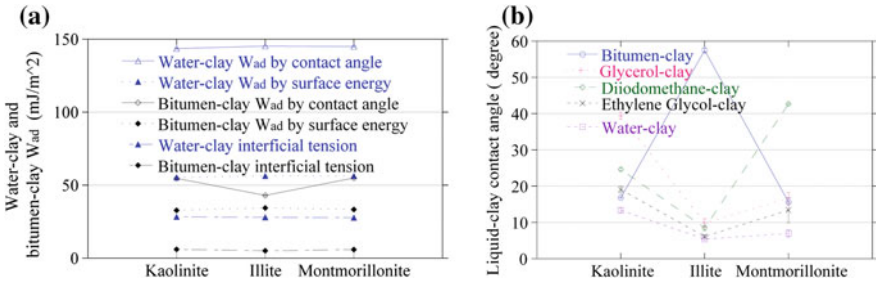


**Fig. 1** **a** Work of adhesion and surface tension at water-clay (*triangle symbol*) and bitumen-clay (*diamond symbol*) interfaces, resulting from contact angle measurements (*halo symbol* with *solid line*) and surface tension calculations (*full symbol* with *dotted line*). Water-clay (*solid triangle symbol*) and bitumen-clay (*solid diamond symbol*) interfacial tensions are depicted with long-short discontinued lines. **b** Contact angles between liquids (bitumen, water, diiodomethane, Ethylene glycol and Glycerol) and clays (kaolinite, illite, and montmorillonite)

surface properties of clays at their exact surface (van Oss 2002). Furthermore, values calculated from Eqs. 3 and 4 may be seriously impacted by the polar and dispersive parts of bitumen surface tension; the sensibility between four detecting liquids and clay surface properties.

According to the results from contact angle measurements depicted in Fig. 1a and the variations of contact angles as a function of liquids and clays in Fig. 1b, the higher $W_{ad}$ and the lower contact angle at water-clay interface than at bitumen-clay interface indicate higher susceptibility of clay to water molecule than to bitumen compounds. The lower $W_{ad}$ at bitumen-illite interface illustrates poor bitumen-illite affinity, which is consistent with the high value of its contact angle shown on Fig. 1b. Even though illite and bitumen consistently have higher dispersive forces and supposedly the highest $W_{ad}$ among clays, this contradictory result is caused by the shortage of electron donors and acceptors from illite surface caused by high pH environment and intermediate amount of exchangeable cations.

Figure 2 shows the results of Oliensis tests performed on each clays. Whereas an oil ring is visible around the central drop on kaolinite and montmorillonite spots, evidencing segregation between bitumen components, no such phenomenon is visible on bitumen-illite spots. Furthermore, this segregation of bitumen tends to be concomitant with the development of a much larger contact area at bitumen-kaolinite and bitumen-montmorillonite interfaces when compared to that at bitumen-illite interface.

Additional investigations have been carried out to explain bitumen segregation and bitumen-clay contact area differences evidenced on Fig. 2. The negligible segregation of bitumen and the small contact area at bitumen-illite surface reflects poor affinity between bitumen and illite, which is consistent with the lower value of the work of adhesion and the higher contact angle shown on Fig. 1a, b respectively.

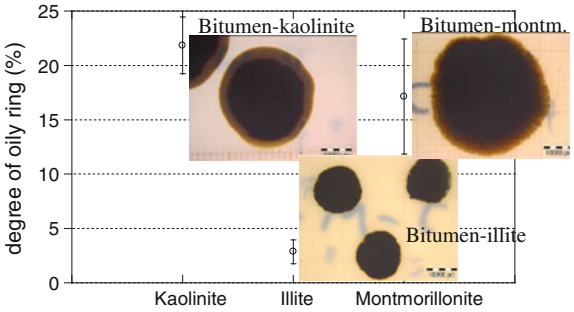


**Fig. 2** Screenshots of bitumen-clay spots and calculated degree of Oliensis (ratio of the oil ring to whole spot radii)

The straw color of clear oil ring formed around the bitumen-kaolinite drop was determined to belong to the Saturates group. Such a high degree of segregation is probably due to the residual vapor-phase reaction of tetrahydrothiophene from saturates group which was catalyzed by alumina from kaolinite surface, whereas the large contact area may result from the low molecular weight of Saturated group contributing to their high mobility in a low pH environment (protonation) (Masson and Collins 2008; Allsop et al. 1995).

The acidic components from Asphaltenes and Resins such as anhydride and carboxylic acid seem to be responsible of the wide bitumen-montmorillonite contact area. Indeed, these acidic components are prone to bind with exchangeable cations upon losing their hydrogen (Allsop et al. 1995; Bukka et al. 1994). Accordingly, the large black bitumen-montmorillonite contact area reflects the spreading of high molecular weight and high viscosity groups of bitumen, which are Asphaltenes and Resins over the montmorillonite surface. Simultaneously, the expandable interlayer of montmorillonite facilitates the diffusion of low molecular weight and low viscosity groups of bitumen, causing the segregation of Saturates from bitumen which explains the straw color around bitumen-montmorillonite spots.

## *3.3 Water Resistance of Clay-Rich AC Mixture*

Figure 3 depicts the Duriez results obtained with the various clay-rich and clay-free AC mixtures tested. According to French practice, Duriez values above 0.8 ($ITSR_{80}$, see Delorme et al. 2007) correspond to water-resistant AC mixtures (threshold value applicable to BBTM6A). Figure 3 shows that AC mixtures with filler in place of clay (clay-free AC mixtures taken as the reference) have a Duriez value of 1, meaning that these AC mixtures are water resistant (no stripping). By contrast, clay-rich AC mixtures have Duriez values below 0.8, meaning that clay decreased their water resistance. Given the location of clay at the aggregate-bitumen interface, stripping is responsible of the Duriez value decrease. Furthermore, for the

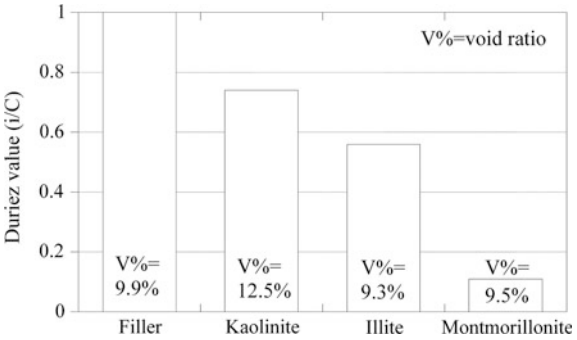


**Fig. 3** Water resistance (Duriez value) of AC mixtures with 9 % fines

same proportion of clay (9 %), the water resistance drop varies with clay mineralogy, and the kaolinite-rich AC mixtures being less affected than illite-rich and far less than montmorillonite-rich AC mixtures.

The Duriez values of clay-rich AC mixtures may be interpreted in light of water-bitumen-clay interaction. In fact, low water resistance values of clay-rich samples reflect higher water-clay affinity than bitumen-clay affinity in the sample, which is consistent with the previous results of $W_{ad}$ shown on Fig. 1a. In the case of montmorillonite, the bitumen-montmorillonite binding occurs between, on the bitumen side, acidic components from Resins and Asphaltenes and, on the montmorillonite side, exchangeable cations. It shall be noted that these bitumen compounds have a high affinity with water molecules. Given the high amount of exchangeable cations available in montmorillonite interlayer, weak electrostatic bonds with hydrophilic bitumen compounds may explain the intrusion of water at the bitumen-montmorillonite interface, yielding stripping and Duriez value drop.

In the case of kaolinite, bitumen Saturates contribute to the bitumen-kaolinite binding, hence this oily bitumen (non-polar group) has a waterproofing action on kaolinite. Moreover, kaolinite has a low water content (Wt = 0.6 %) and far less exchangeable cations (CEC = 1.3 meq/100 g), making it less attractive to water. As a consequence, kaolinite-rich AC mixtures are more water-resistant than the other clay-rich AC mixtures.

Eventually, illite-rich AC mixture shows an intermediate water resistance among the three clays. A first reason could be that illite has water content (2.7 %) and CEC (23.3 meq/100 g) values in between those of kaolinite and montmorillonite. A second reason could be the high binding energy of bitumen when in contact with surface oxygen groups of illite silica tetrahedral and calcite. Furthermore, even though bitumen-illite interface is less water-accessible due to the contribution of bitumen oil components to the binding, stripping is caused by poor coverage of bitumen on illite surface. As a result, bitumen-illite bonding is intermediate between those of bitumen-kaolinite and bitumen-montmorillonite due to a strong binding but high contact angle values. Together with fewer exchangeable cations available for water binding, this could explain the occurrence of less degradation on bitumen-illite interaction than observed on bitumen-montmorillonite interaction.

## 4 Conclusions and Outlook

This study investigates the water resistance drop of clay-rich AC mixtures prepared from clean fine aggregates mixed with three types of raw clays, a kaolinite, an illite and a montmorillonite. Whereas Duriez values evidence no decrease of water resistance with clay-free AC mixtures, various levels of water resistance drop caused by stripping occur in clay-rich AC mixtures. Those Duriez value drops may hence be attributed to water-bitumen-clay interaction. Consequently, for each type of clay tested, explanations have been brought to clarify the stripping mechanisms from water-bitumen-clay interaction: the most deleterious mechanism occurs in montmorillonite-rich AC mixtures, whose clay resulting from basic igneous rocks (fairly high pH conditions) incorporates a high amount of exchangeable cations interacting with bitumen high dispersive forces.

As a consequence, assessing the water-bitumen-clay interaction could be extremely useful to predict the water resistance of clay-rich AC mixtures. To do so, a set of information shall be collected.

- Clay fraction: a mineralogical analysis should be performed to identify the mineral phases, chemical composition (exchangeable cation included), pH value and cation exchange capacity. High pH environment and high cation exchange capacity of clay-rich aggregates tend to yield low water resistance of clay-rich AC mixtures when bitumen with preponderant polar forces is used;
- Bitumen binder: the surface energy of bitumen should be measured, in order to assess the chemical reaction with aggregates. Indeed, bitumen will probably show a good affinity with kaolinite-rich aggregate in low pH environment, since the mineral composition of kaolinite suits the Saturates group;
- Clay-bitumen compatibility: The water resistance of AC mixture will be weaker when Resins and Asphaltenes groups interact with clay.

Preserving clay properties from the quarry to the laboratory is also important, since small negligence may induce big changes of clay such as the surface energy (cation substitution), pH value, clay content and particle size distribution. Further work is needed on water-bitumen-clay interaction in order to predict the water resistance of clay-rich AC mixtures and improve it. In particular, the nature and proportions of exchangeable cations in various clays will be given more consideration.

**Acknowledgments** The authors gratefully acknowledge the support and generosity of Annick Lalloret, Olivier Burban and Olivier Garcin from IFSTTAR Nantes (France) for their contribution to the sample preparation and experiments, without whom the present study could not have been completed.

## References

Allsop R, Dussek I, Hayton B, Heimerikx G, Prince L, Rosa JD, Southern M, Vonk W, Whiteoak D, Woolf L, and Yin P (1995) The shell bitumen industrial handbook. Shell bitumen, p.86.

ASTM D1370 (2012) Standard test method for contact compatibility between asphaltic materials (Oliensis test).

Bagampadde U, Isacsson U, and Kiggundu BM (2004) Classical and contemporary aspects of stripping in bituminous mixture. Road material and pavement design 5:7-43.

Bukka K, Miller JD, Hanson FV, Misra M, and Oblad AG (1994) The influence of carboxylic acid content on bitumen viscosity. Fuel 73:257-268.

Carter DL, Mortland MM, and Kemper WD (1986) Specific surface Methods of soil analysis. In: Methods of Soil Analysis, Part I. Physical and Mineralogical Methods—Agronomy Monograph, 2nd Edn. American Society of Agronomy—Soil Science Society of America, USA, p. 413-423.

Chassin P, Jouany C, and Quiquampoix H (1986) Measurement of the surface free energy of calcium-montmorillonite. Clay Minerals 21:899-907.

Curtis CW, Ensley K, and Epps J (1993) Fundamental properties of asphalt-aggregate interactions. Including Adhesion and Adsorption, SHRP-A-341, National Research Council, Washington, DC.

Delorme JL, Wendling L (2007) LPC Bituminous mixtures design guide. The RST Working Group "Design of bituminous mixtures".

Dupre AM, Dupre P (1869) Théorie mécanique de la chaleur. Gauthier-Villars, Paris

Hefer A, Little D (2005) Adhesion in bitumen-aggregate systems and quantification of the effects of water on the adhesive bond. ICAR/505-1, Texas

Huet M (1991) Incidence de la variation de la valeur de bleu sur certaines caracteristiques des fines et des enrobes. LPC, 14, France

Kanitpong K, Bahia HU (2003) Role of adhesion and thin film tackiness of asphalt binders in moisture damage of HMA. AAPT 72:611-642.

Leroux A, Unikowski Z (1980) Mise en évidence de l'influence des fines argileuses dans les granulates a beton. Bull Liaison Pont Chauss, France, p 101-108.

Lesueur D, Petit J, Ritter H (2013) The mechanisms of hydrated lime modification of asphalt mixtures a state-of the art review. Road material and pavement design 14:1-16.

Masson JF, Collins P (2008) FTIR study of the reaction of polyphospheric acid and model bitumen sulfur compounds. NRCC-50828, Ottawa, Canada.

Maurice PA (2009) Environmental surfaces and interfaces from the nanoscale to the global scale. John Wiley & Sons, Inc., USA, p 441.

Morel R (1996) Constituants argileux. In: Tec et Doc/ Lavoisier (ed) Les sols cultivés, France, p 52-70.

Nesse WD (2000) Introduction to mineralogy. Oxford University Press, USA

NF EN 12697-12 (2008) Bituminous mixtures. Test methods for hot mix asphalt, Part 12: Determination of the water sensitivity of bituminous specimens.

NF EN 12697-35 + A1 (2007) Bituminous mixtures. Test methods for hot mix asphalt, Part 35: Laboratory mixing.

NF EN 13108-1 (2007) Material specification. Part1: Asphalt concrete.

NF P 98-251-1 (2002) Test relating to pavements- Static test on bituminous mixtures. Part 1: Duriez test on hot mix.

Olphen HV, Fripiat JJ (1979) Data handbook for clay materials and other non-metallic minerals. Pergamon Press.

Owens D, Wendt R (1969) Estimation of the surface free energy of polymers. Journal of Applied Polymer Science 13:1741-1747.

Pentrák M, Czímerová A, Madejová J, Komadel P (2012) Changes in layer charge of clay minerals upon acid treatment as obtained from their interactions with methylene blue. Applied Clay Science 55:100-107.

Plancher H, Dorrence SM, Petersen CJ (1977) Identification of chemical types in asphalts strongly adsorbed at the asphalt-aggregate interface and their relative displacement by water. The Association of Asphalt Paving Technologists 46:151.

Prost R (1975) Etude de l'hydratation des argiles : Interactions eau-minéral et mécanisme de la rdtention de l'eau. Université Pierre et Marie Curie, France.

Rosenholm JB (2007) The role of surface forces, part II: colloids and interface science. In: Tadros TF (ed) Colloid stability, vol. 2, Wiley-VCH Verlag Gmbh Co, Germany.

Sjöblom J (2001) Encyclopedic handbook of emulsion technology. CRC Press

Somé SC (2012) Comportement thermomécanique des enrobés tièdes et de l'interface bitume-granulat. École Polytechnique de l'Université de Nantes, France, p136-138.

Ström G, Fredriksson M, Stenius P (1987) Contact angles, work of adhesion, and interfacial tensions at a dissolving hydrocarbon surface. Journal of Colloid and Interface Science 119:352-361.

Tarrer AR, Wagh V (1991) The effect of the physical and chemical characteristics of the aggregate on bonding. Edward T.Harrigan, SHRP-A/UWP-91-510, p 1-23

Trukhin AN, Teteris J, Fedotov A, Griscom DL, and Buscarino G (2009) Photosensitivity of $SiO_2$–Al and $SiO_2$–Na glasses under ArF (193 nm) laser. Non-Crystalline Solids 355:1066-1074.

Van Oss CJ (2002) Use of the combined Lifshitz-van der Waals and Lewis acid-base approaches in determining the apolar contributions to surface and interfacial tensions and free energies. Journal of Adhesion Science Technology 16:669-677.

Ziyani L (2013) Etude des phénomènes physico-chimiques à l'interface émulsion de bitume/substrat minéral – Application à la formulation de Bétons Bitumineux à l'Emulsion (BBE). Ecole centrale de Nantes, France, p 59-139.

# Part II
# Innovative Testing of Bituminous Binders, Additives and Modifiers

# Storage Stability of Bituminous Binders Reinforced with Nano-Additives

**Ezio Santagata, Orazio Baglieri, Lucia Tsantilis and Giuseppe Chiappinelli**

**Abstract** The experimental investigation presented in this paper focused on storage stability of bituminous binders containing nano-sized additives. Several blends were prepared in the laboratory by combining three base bitumens with two different types of nanoclays and one type of carbon nanotubes at various dosages. A technique based on the combination of simple shear mixing and sonication was proposed to achieve adequate dispersion of nano-particles in bitumen. Capability of materials to withstand segregation phenomena was evaluated by means of viscosity measurements performed on samples derived from simulative laboratory storage tests. Results obtained in the study revealed that high-temperature stability of nano-reinforced binders is dependent upon physico-chemical properties of base components, thus highlighting the key role played in such a context by interaction mechanisms that take place between nano-additives and dispersing bituminous medium.

**Keywords** Nanoclays · Carbon nanotubes · Bituminous binders · Storage stability

E. Santagata (✉) · O. Baglieri · L. Tsantilis · G. Chiappinelli
Department of Environment, Land and Infrastructure Engineering, Politecnico di Torino, 24, Corso Duca degli Abruzzi 10129, Turin, Italy
e-mail: ezio.santagata@polito.it

O. Baglieri
e-mail: orazio.baglieri@polito.it

L. Tsantilis
e-mail: lucia.tsantilis@polito.it

G. Chiappinelli
e-mail: giuseppe.chiappinelli@polito.it



F. Canestrari and M.N. Partl (eds.), *8th RILEM International Symposium on Testing and Characterization of Sustainable and Innovative Bituminous Materials*, RILEM Bookseries 11, DOI 10.1007/978-94-017-7342-3_7

## 1 Introduction

Use of nano-sized additives in bituminous binders for road paving applications has aroused increasing interest among researchers worldwide (Gopalakrishnan et al. 2011). Investigations have not yet reached full scale implementation due to uncertainties over the actual cost-effectiveness of nano-reinforcement and as a result of several practical production issues which still need to be addressed. Nevertheless, according to studies documented in literature, the most promising products which have been considered for such applications are by far nanoclays and carbon nanotubes (Yang and Tighe 2013).

Nanoclays are layered silicate minerals that have the potential to establish a significant interaction with surrounding media as a result of clay sheet detachment. In order to change the character of clays from hydrophilic to hydrophobic, inorganic exchange cations which lie on the surfaces of the layers can be replaced by organic onium ions. Such a treatment provides the twofold advantage of changing the polarity of clay surfaces and expanding clay galleries. This facilitates the diffusion of organic molecules within gallery space, leading to intercalated and/or exfoliated morphologies of the composite material. Intercalation occurs when penetration of molecules produces an expansion of galleries, but silicate platelets still maintain their original crystallographic structure. On the other hand, exfoliation occurs when clay sheets no longer interact through surfactant chains, thus generating a random distribution within the dispersing medium (Le Baron et al. 1999).

Carbon nanotubes are one-dimensional carbon materials which are characterized by very high aspect ratios. They consist of rolled-up graphene sheets made of hexagonal networks of carbon atoms. At least one end of such cylindrical structures is capped with a half fullerene molecule, thus generating seamless hollow structures with nanometric diameters. Depending on their synthesis process, carbon nanotubes can assume either single-wall or multi-wall configurations. Even though the carbon atoms on tube walls are chemically stable as a result of the aromatic nature of bonds, non-negligible interactions typically arise between individual nanotubes. These are generated by intermolecular van der Waals forces and can lead to the formation of several hierarchical morphologies of bundles in composite materials (Dresselhaus et al. 2001; Ma et al. 2010; Brown et al. 2005).

One big challenge in developing nano-reinforced bituminous binders is the dispersion of nano-particles within the base matrix by means of a proper mixing technique (Santagata 2015a, b; Khattak et al. 2012; Merusi et al. 2012). Moreover, for end-use purposes, achieved dispersion should be maintained in time during high-temperature storage.

When considering mixing and stability issues, several studies have focused on the role played by nano-additives when included as third components in polymer-modified bitumens (Golestani et al. 2012; Zhang et al. 2009; Yu et al. 2007a; Galooyak et al. 2010). However, very few researchers have addressed the problem of segregation phenomena in binary nano-modified bituminous binders. Polacco et al. (2008) demonstrated that no phase separation occurs in

nanoclay-bitumen blends when bitumen is able to intercalate and partially exfoliate silicate layers. Yu et al. (2007b) and Abdelrahman et al. (2014) highlighted the importance of nanoclay concentration, which can be a key factor in controlling the morphology of nano-particle arrangement within the bituminous matrix.

Due to the scarcity of information which is currently available on this topic, the work presented in this paper focused on storage stability of bituminous binders containing nanoclays and carbon nanotubes. Stability of blends, which were subjected to simulative storage tests at high temperature, was assessed via viscosity measurements. Results obtained from the experimental investigation were analysed with the specific goal of highlighting the role played by the type and relative quantities of base components in ensuring adequate stability to nano-reinforced binders.

## 2 Experimental Investigation

### *2.1 Materials*

Three base bitumens and three nano-sized additives were considered in the experimental investigation.

In the attempt of highlighting the effects due to variations of binder composition and microstructure, base bitumens were taken from two different Italian refineries which operate on crudes of various origins according to different fractionation schemes. The first refinery provided a 70/100 penetration grade bitumen, marked in the experimental study as A1, while the second one supplied a 70/100 and a 50/70, marked as B1 and B2, respectively.

Base bitumens were subjected to preliminary characterization by determining their performance grade (PG) according to AASHTO M 320 (2010) and by measuring relative amounts of saturates, aromatics, resins and asphaltenes by means of Thin Layer Chromatographic (TLC) analysis. Corresponding results are shown in Table 1.

Nano-sized additives employed in the present study were commercially available products: two types of nanoclays (NCA and NCB) and one type of carbon nanotubes (CNT). The two nanoclays were natural montmorillonites which were made organophilic by means of different surfactant coatings. Carbon nanotubes were produced by means of the Catalyzed Chemical Vapour Deposition (CCVD) process

**Table 1** Preliminary characterization of base bitumens

| Base bitumen | PG (-) | Saturates (%) | Aromatics (%) | Resins (%) | Asphaltenes (%) |
|---|---|---|---|---|---|
| A1 | 58-22 | 5.5 | 38.1 | 42.0 | 14.4 |
| B1 | 58-22 | 3.0 | 65.3 | 16.0 | 15.8 |
| B2 | 64-22 | 2.4 | 63.4 | 17.5 | 16.7 |

**Table 2** Main properties of nanoclays

| Nanoclay | Organic modifier | Anion | Basal spacing (nm) | Cation Exchange Capacity (CEC) (meq/100 g) | Density ($g/cm^3$) |
|---|---|---|---|---|---|
| NCA | Dimethyl, dihydrogenatedtallow, quaternary ammonium | Chloride | 3.15 | 125 | 1.66 |
| NCB | Methyl, tallow, bis-2-hydroxyethyl, quaternary ammonium | Chloride | 1.85 | 90 | 1.98 |

**Table 3** Main properties of multiwall carbon nanotubes

| Carbon nanotubes | Average diameter (nm) | Average length (μm) | Surface area ($m^2/g$) | Carbon purity (%) | Metal oxide (%) |
|---|---|---|---|---|---|
| CNT | 9.5 | 1.5 | 250–300 | 90 | 10 |

in multi-wall structures. Main characteristics of the additives, based on manufacturers' technical specifications, are reported in Tables 2 and 3.

By combining bitumens and additives at different dosages, 18 nano-reinforced blends were prepared in the laboratory by following a protocol defined in previous studies (Santagata et al. 2015a, b) which is based on the combination of shear mixing and sonication.

The procedure begins with initial hand-mixing of the additive in bitumen preheated at 150 °C, followed by a second phase during which the blend is mixed with a mechanical stirrer operated at 1550 rpm for 90 min. A sonication phase of 60 min is then carried out by employing an ultrasonic homogenizer. During this third phase, a continuous ultrasonic wave, characterized by an amplitude of 157.5 μm and a frequency of 24 kHz, is transmitted throughout the binder by a titanium sonotrode of 7 mm diameter. During the entire sonication process, temperature is kept constant at 150 °C as in the previous two phases.

On the basis of previous investigations (Santagata et al. 2012, 2013, 2015a, b), adopted percentages of nano-additive (by weight of base bitumen) were equal to 3 and 6 % for the two nanoclays (NCA and NCB) and to 0.5 and 1 % for CNT. Such dosages allow a suitable modification of the rheological response of neat bitumen while limiting total costs of base materials.

## 2.2 Testing Program

Storage at high temperature under quiescent conditions which commonly take place in industrial plants was simulated in the laboratory according to EN 13399 (2010). Homogeneous samples of nano-reinforced bitumen were poured in aluminium foil tubes of standard dimensions and maintained in the vertical position at 180 °C for

72 h. In order to quantitatively assess the occurrence of segregation phenomena, samples retrieved from the upper and lower section of tubes (indicated as top and bottom, respectively) were subjected to tests for the determination of dynamic viscosity. Measurements were performed by means of a Brookfield rotational viscometer operated at 180 °C at three different shear rates (100, 150, and 200 $s^{-1}$).

At least two replicates were run for each test and average data were considered in the analysis.

## 3 Results and Discussion

### *3.1 Bitumen-Nanoclay Blends*

Results obtained for bitumen-NCA blends after high-temperature storage are presented in Figs. 1, 2 and 3, where viscosity values corresponding to top and bottom tube sections are compared. As discussed in detail in the following paragraphs, different considerations can be made by analysing blends prepared with the lower nanoclay dosage (3 %) and those prepared with the higher one (6 %).

When 3 % NCA was used, blends showed a satisfactory capability to withstand segregation phenomena, as proven by the negligible difference observed between the flow behaviour of materials sampled from the two tube sections. A discrepancy was only recorded in the case of the blend prepared with bitumen B1. Such a binder is similar to bitumen A1 in terms of rheological properties and to bitumen B2 in terms of chemical composition (Table 1). Thus, experimental data do not allow identification of the single factor that controls storage stability, which is affected by the combination of physico-chemical properties.

At 6 % dosage, all blends showed significant phase separation effects, regardless of the type of neat bitumen used. The relative differences found between top and

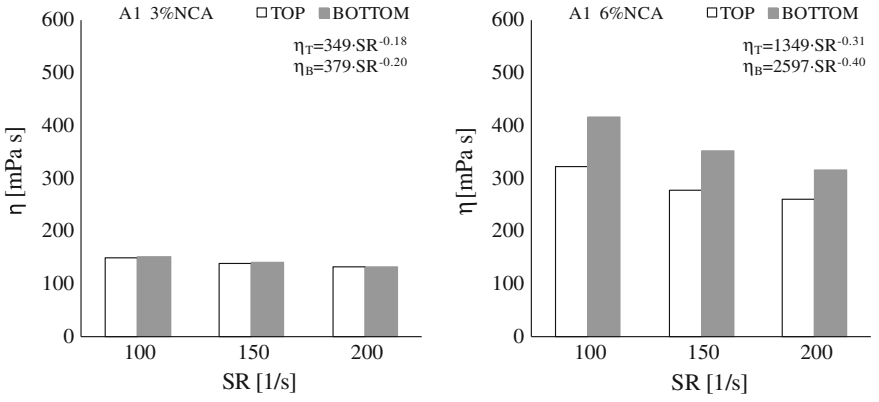


**Fig. 1** Viscosity (η) versus shear rate (SR) of A1-NCA blends

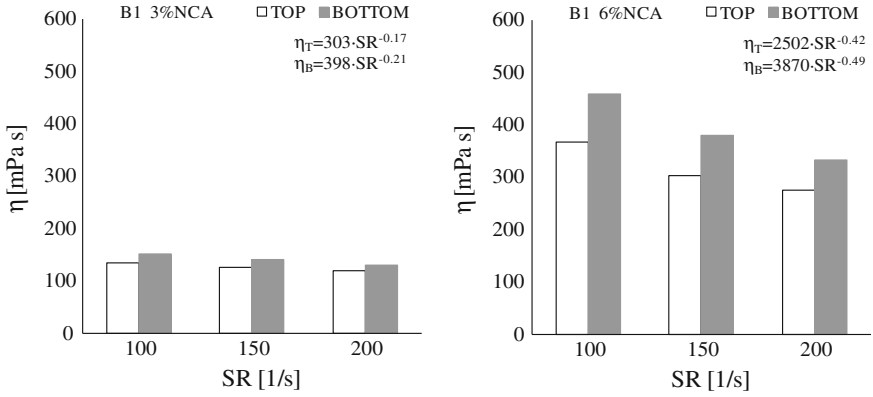


**Fig. 2** Viscosity (η) versus shear rate (SR) of B1-NCA blends

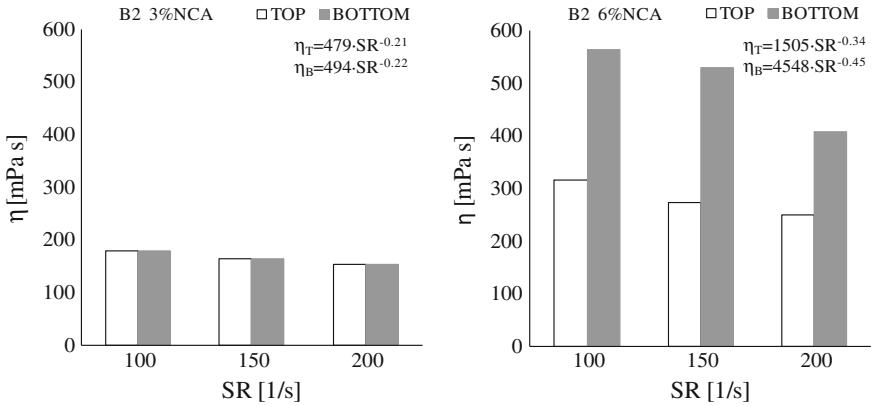


**Fig. 3** Viscosity (η) versus shear rate (SR) of B2-NCA blends

bottom viscosity values were around 20 % in the case of the softer base bitumens (A1 and B1, classified as PG58-22) and higher than 50 % in the case of the harder one (B2, classified as PG64-22).

Analysis of viscosity data can be supplemented by the evaluation of shear rate dependency of tested blends by considering the exponent of the power-law function fitted to experimental data (Figs. 1, 2 and 3). As expected, for the lower dosages, which did not lead to significant phase separation, shear rate dependency was found to be equivalent for all blends, with exponent values of the order of −0.2, showing only a slight increase when comparing the top and bottom sections. However, it is interesting to observe that for the higher dosage bitumen storage and consequent phase separation yielded not only an increase in viscosity but also a more pronounced shear rate dependency, indicative of a stronger non-Newtonian behaviour.

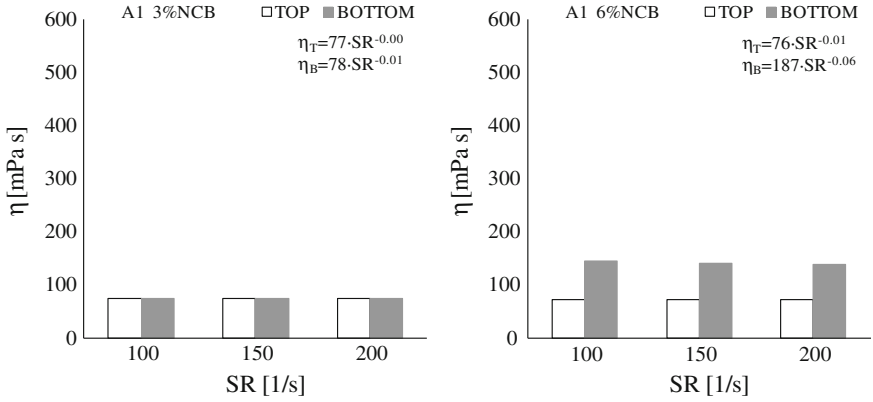


**Fig. 4** Viscosity (η) versus shear rate (SR) of A1-NCB blends

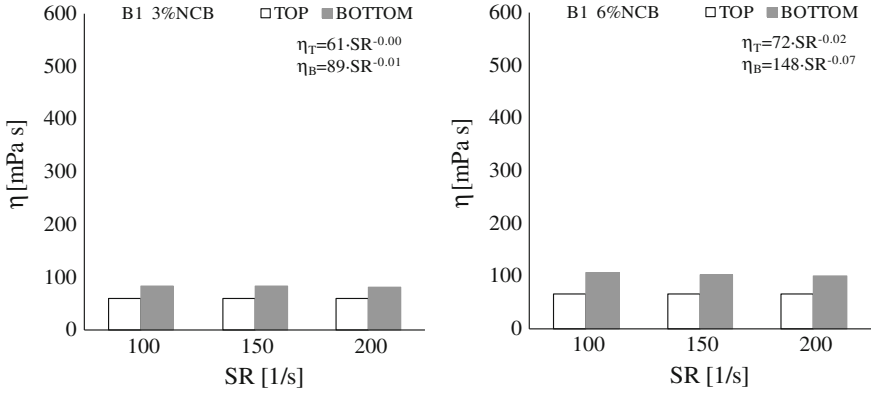


**Fig. 5** Viscosity (η) versus shear rate (SR) of B1-NCB blends

This is proven by the exponent values that ranged between −0.3 and −0.5, with relative differences between top and bottom sections of the order of 20 %.

Figures 4, 5 and 6 provide an overview of the storage stability of all blends containing nanoclay NCB. As discussed in the following paragraphs, different observations can be made depending upon the base bitumen employed for preparation.

In the case of blends obtained by nano-reinforcing bitumen A1 (provided by the first refinery), findings were fully coherent with those highlighted for NCA blends. Adoption of the lower additive dosage (3 %) gave satisfactory results in terms of binder homogeneity after high-temperature storage, while the use of the higher dosage (6 %) led to non-negligible segregation phenomena, as indicated by the difference found between top and bottom viscosity values (around 64 %). Such a scenario confirms the importance of selecting, for stability purposes, an appropriate additive dosage.

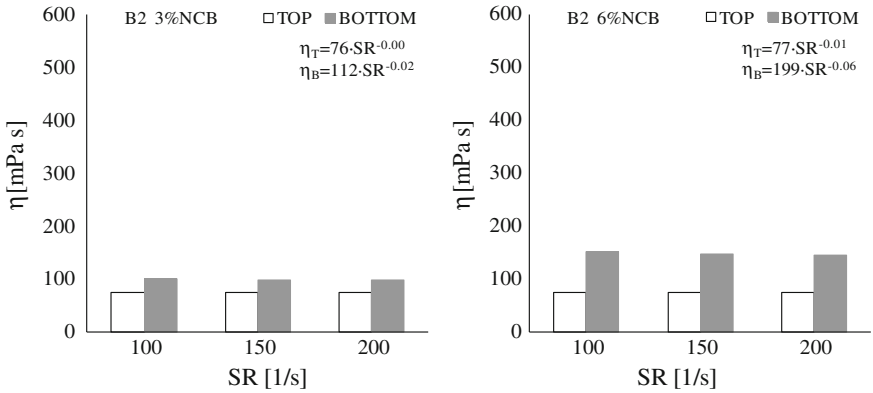


**Fig. 6** Viscosity (η) versus shear rate (SR) of B2-NCB blends

As shown in Figs. 5 and 6, completely different results were obtained in the case of blends prepared with base bitumens supplied by the second refinery (B1 and B2). In this case, phase separation always occurred, with a relative difference between top and bottom viscosity values of about 30 % for 3 % dosage and significantly higher for 6 % dosage (44 and 67 % for binders derived from bitumen B1 and B2, respectively).

Results reported above for bitumen-NCB blends suggest that, besides factors related to the amount of nano-particles, composition of base bitumen may also play a role in controlling storage stability. In particular, experimental data indicate that for this specific nanoclay, stability conditions are promoted by a higher percentage of polar fractions. Such a statement is supported by the data listed in Table 2, which indicate that the relative amount of resins and asphaltenes is equal to 56 % in the case of bitumen A1 and significantly lower in the case of bitumens B1 and B2 (equal to 32 and 34 %, respectively), which yielded unstable blends.

The importance of polar aromatics in the interfacial bonds which take place between bitumen and mineral particles has been demonstrated by numerous studies (Petersen and Plancher 1998; Acevedo et al. 1995; Pernyeszi et al. 1998). However, since the magnitude of surface activity is highly influenced by particle geometry, such effects can generally be neglected in the case of coarse aggregates (Craus et al. 1979), while they were found to be significant in the case of fine fractions (Pernyeszi et al. 1998).

Additional information on the abovementioned interactions can be gathered by comparing results obtained for blends prepared with the two different types of nanoclays (Figs. 1, 2 and 3 and 4, 5 and 6 for NCA and NCB, respectively). In fact, it was found that regardless of base bitumen, binders containing NCA always exhibited viscosity values which were considerably higher than those of NCB blends. Moreover, modification with NCA induced a clear non-Newtonian behaviour, not recorded in the case of NCB.

Results described above are extremely valuable since it is well known that viscosity measurements may yield information concerning the morphology of composite materials (Macosko 1994). When bitumen-nanoclay blends are considered, viscosity variations are mainly attributed to the organization of silica platelets. In fact, in the case of highly intercalated and/or exfoliated structures, dispersed platelets hinder bitumen flow as a consequence of the confinement of its molecular chains within galleries and/or of the geometrical constraints which result from their complex distribution within the dispersing matrix. In such conditions, an additional contribution to viscosity change is provided by the strength of molecular bonds which arise along bitumen-silicate interfaces. Moreover, enhancement of shear thinning behaviour can be associated with the orientation effect of randomly distributed two-dimensional particles (Liu 2011).

Based on test results and on consequent discussion, it can be inferred that nanoclay NCA has a greater aptitude to be intercalated and/or exfoliated by bitumen with respect to NCB, probably as a result of the higher values of basal spacing and cation exchange capacity (Table 2). The different packing configurations hypothesized for the two nanoclays during high-temperature storage also seem to support their different sensitivity to changes in chemical composition of the bituminous media. It can thus be concluded that the exfoliated/intercalated platelets of NCA can be maintained in a stable state within the bituminous medium due to interaction phenomena which occur at the nano-scale. By contrast, the compacted layers of NCB seem to be more prone to segregation if a sufficient peptizing action is not provided by the polar fractions of bitumen.

## *3.2 Bitumen-Nanotube Blends*

Experimental results obtained for bitumen-CNT blends after high-temperature storage are displayed in Figs. 7, 8 and 9.

In general terms it was observed that these binders exhibited a better storage stability than those prepared by using nanoclays. Relative differences between top and bottom viscosities were in most cases lower than 10 %, indicating the occurrence of a limited phase separation. The only exception was represented by the blend prepared with 0.5 % dosage by using A1 as a base, which showed relative variations between the two tube sections of more than 30 %.

At both CNT dosages it was found that blends prepared with base bitumens supplied by the second refinery (B1 and B2) were more stable than those derived from bitumen A1. This may be explained by considering that bitumens characterized by a high content of non-polar aromatics can generate a more efficient phase equilibrium due to the inert nature of non-functionalized carbon nanotubes (Ma et al. 2010). This assumption is consistent with the findings of investigations

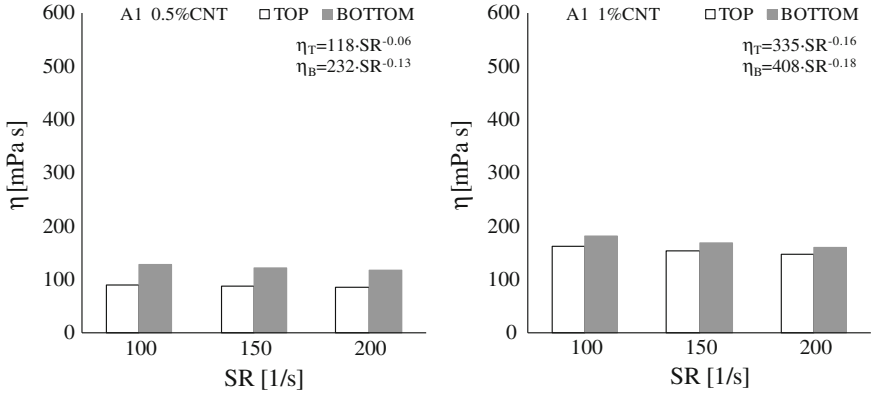


**Fig. 7** Viscosity (η) versus shear rate (SR) of A1-CNT blends

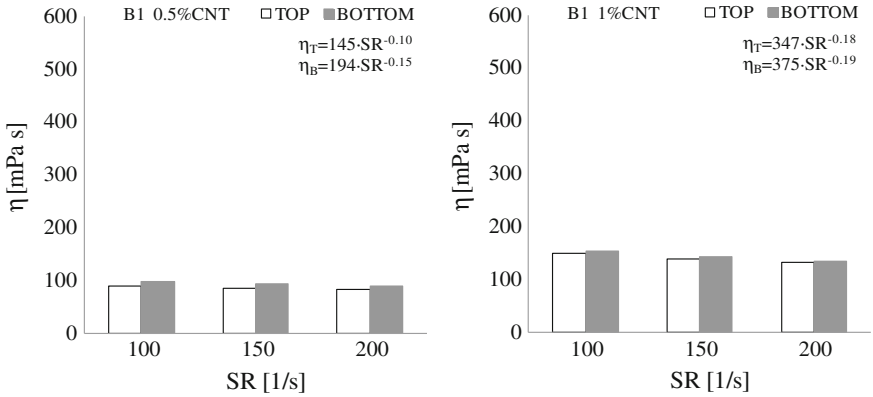


**Fig. 8** Viscosity (η) versus shear rate (SR) of B1-CNT blends

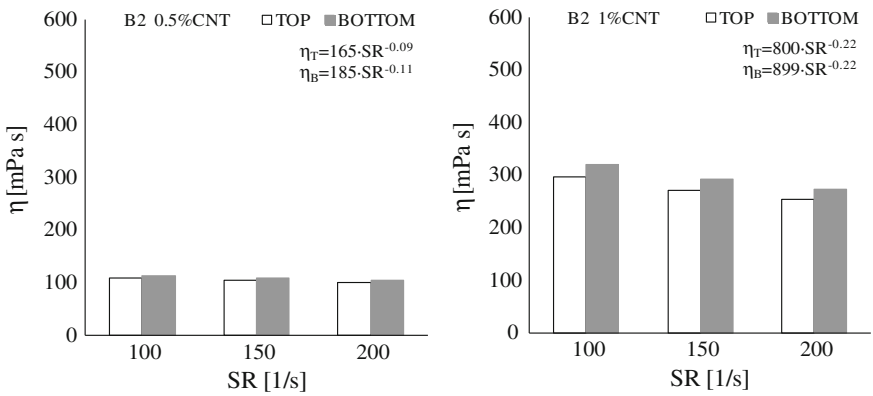


**Fig. 9** Viscosity (η) versus shear rate (SR) of B2-CNT blends

carried out by Chen et al. (2001), who demonstrated that strong interactions may arise between non-polar aromatic compounds and the sidewalls of carbon nanotubes via π-stacking mechanisms.

When considering the influence of CNT concentration on storage stability, experimental results showed that in the case of base bitumens B1 and B2 similar responses were obtained at both dosages (0.5 and 1 %), while for bitumen A1 more stable conditions were reached at 1 % CNT. This unexpected result may be explained by considering the well-known aptitude of CNT to self-assemble in the form of ropes, that, in the case of sufficiently high concentrations, may lead to the formation of network structures (Brown et al. 2005). As a result of the different chemical composition of the bitumens provided by the two refineries, it can thus be hypothesized that the less polar bitumens B1 and B2 reach a stable condition already at 0.5 % dosage, while a higher CNT concentration is required in the case of the more polar bitumen A1.

## 4 Conclusions

Based on the experimental results presented in this paper, it can be concluded that storage stability of bituminous binders containing nano-sized additives, such as montmorillonite nanoclays and multi-wall carbon nanotubes, depends upon physico-chemical properties of base components. Such a finding highlights the key role played by interaction mechanisms that take place between nano-additives and dispersing medium, that should be thoroughly considered for material selection and blend preparation.

In the case of bitumen-nanoclay blends, it was observed that their capability to withstand phase separation is highly influenced by the morphological configuration of nano-particles and by the peptizing power of bitumen. On the other hand, stability of blends prepared with carbon nanotubes was found to be mainly governed by their interaction with the non-polar aromatic fraction of bitumen.

Outcomes of this preliminary investigation should be validated by future research dedicated to a deeper understanding of the mechanisms which take place during storage at high temperatures. This should be done by extending the material matrix as well as by supporting viscosity measurements with direct morphology observations carried out at the nano-scale.

**Acknowledgments** The study reported in this paper is part of the FIRB research project on "Innovative nano-structured and polymer-modified bituminous materials" funded by the Italian Ministry of Education, University and Research (MIUR). Technical support provided by Nanocyl s.a. is gratefully acknowledged.

## References

Abdelrahman M, Katti DR, Ghavibazoo A, Upadhyay HB, Katti KS (2014) Engineering physical properties of asphalt binders through nanoclay-asphalt interactions. J Mater Civ Eng 26(12): 04014099.

Acevedo S, Ranaudo MA, Escobar G, Gutierrez L, Ortega P (1995) Adsorption of asphaltenes and resins on organic and inorganic substrates and their correlation with precipitation problems in production well tubing. Fuel 74(4):595-598.

Brown JM, Anderson DP, Justice RS, Lafdi K, Belfor M, Strong KL, Schefer DW (2005) Hierarchical morphology of carbon single-walled nanotubes during sonication in an aliphatic diamine. Polymer 46:10854-10865.

Chen RJ, Zhang Y, Wang D, Dai H (2001) Noncovalent sidewall functionalizationof single-walled carbon nanotubes for protein immobilization. J Am Chem Soc 123:3838-3839.

Craus J, Ishai I, Por N (1979) Selective sorption in filler-bitumen systems. J Mater Sci 14:2195-2204.

Dresselhaus MS, Dresselhaus G, Avouris Ph (2001) Carbon nanotubes: Synthesis, Structure, Properties, and Applications. Topics in Applied Physics 80, Springer; New York.

Galooyak SS, Dabir B, Nazarbeygi AE, Moeini A (2010) Rheological properties and storage stability of bitumen/SBS/montmorillonite composites. Construct Build Mater 24:300-307.

Golestani B, Nejad FM, Galooyak SS (2012) Performance evaluation of linear and nonlinear nanocomposites modified asphalts. Construct Build Mater 35:197-203.

Gopalakrishnan K, Birgisson B, Taylor P, Attoh-Okine N (2011) Nanotechnology in civil infrastructures: a paradigm shift. Springer, Berlin.

Khattak MJ, Khattab A, Rizvi HR, Zhang P (2012) The impact of carbon nano-fiber modification on asphalt binder rheology Construct Build Mater 30:257-264.

Le Baron PC, Wang Z, Pinnavaia TJ (1999). Polymer-layered silicate nanocomposites: an overview. Appl Clay Sci 15:11-29.

Liu G (2011) Characterization and identification of bituminous materials modified with montmorillonite nanoclay. Delft University of Technology, Delft, The Netherlands.

Ma PC, Siddiqui NA, Marom G, Kim JK (2010) Dispersion and functionalization of carbon nanotubes for polymer-based nanocomposites: a review. Composite: Part A 41:1345-1367.

Macosko CW (1994) Rheology: principles, measurements, and applications. Wiley-VCH, NY.

Merusi F, Giuliani F, Polacco G (2012) Linear viscoelastic behaviour of asphalt binders modified with polymer/clay nanocomposites. Procedia - Social and Behavioral Science. SIIV - 5$^{th}$ International Congress, 53:335-345.

Pernyeszi T, Patzkó A, Berkesi O, Dékány I (1998) Asphaltene adsorption on clays and crude oil reservoir rocks. Colloids and Surfaces A: Physicochem Eng Aspects 137:373-384.

Petersen JC, Plancher H (1998) Model studies and interpretative review of the competitive adsorption and water displacement of petroleum asphalt chemical functionalities on mineral aggregate surfaces. Petroleum Sci Technol 16:89-131.

Polacco G, Kríz P, Filippi S, Statstna J, Biondi D, Zanzotto L (2008) Rheological properties of asphalt/SBS/clay blends. European Polymer J 44:3512-3521.

Santagata E, Baglieri O, Tsantilis L, Dalmazzo D (2012) Rheological characterization of bituminous binders modified with carbon nanotubes. Procedia - Social and Behavioral Science. SIIV - 5th International Congress, 53, 546-555.

Santagata E, Baglieri O, Tsantilis L, Chiappinelli G (2013) Effects of Nano-sized Additives on the High-Temperature Properties of Bituminous Binders. International RILEM Symposium on Multi-Scale Modeling and Characterization of Infrastructure Materials 297-309.

Santagata E, Baglieri O, Tsantilis L, Chiappinelli G (2015a) Effect of sonication on the high temperature properties of bituminous binders reinforced with nano-additives. Construct Build Mater 75:395-403.

Santagata E, Baglieri O, Tsantilis L, Chiappinelli G (2015b) Fatigue properties of bituminous binders reinforced with carbon nanotubes. Int J Pave Eng 16(1):80-90.

Yang J, Tighe S (2013) A review of advances of nanotechnology in asphalt mixtures. Procedia - Social and Behavioral Science. CICTP - 13th COTA International Conference of Transportation Professionals, 96: 1269-1276.

Yu J, Wang L, Zeng X, Wu S, Li B (2007a) Effect of montmorillonite on properties of styrene-butadiene-stirene block copolymer modified bitumen. Polymer Eng Sci 47 (9):1289-1295.

Yu J, Zeng X, Wu S, Wang L, Liu G (2007b) Preparation and properties of montmorillonite modified asphalts. Mater Sci Eng A 447:233-238.

Zhang B, Xi M, Zhang D, Zhang H, Zhang B (2009) The effect of styrene–butadiene–rubber/montmorillonite modification on the characteristics and properties of asphalt. Construct Build Mater 23:3112-3117.

# Ageing Performances of Asphaltite Modified Bitumens; Comparisons with Equivalent Petroleum Bitumens

**Andrea Themeli, Emmanuel Chailleux, Fabienne Farcas, Cyrille Chazallon, Bernard Migault and Gilles Didelet**

**Abstract** This work focuses on the ageing behavior of asphaltite modified paving bitumens. The addition of asphaltites in soft petroleum bitumens gives harder binders which are suitable for the production of high modulus bituminous mixes used in pavements construction. Such techniques are already used in several projects. However it is not known how asphaltite modified binders behave during ageing. In general, bitumens get harder, more elastic and consequently more brittle during ageing. In order to evaluate the ageing incidence we have studied the evolution of several mechanical properties of asphaltite modified bitumens during ageing. The evolutions of asphaltite modified bitumens during aging are compared

A. Themeli (✉) · C. Chazallon · B. Migault
ICUBE (UMR 7357, CNRS, National Institute of Applied Sciences),
24, Boulevard de La Victoire, 67084, Strasbourg Cedex, France
e-mail: andrea.themeli@insa-strasbourg.fr; andrea.themeli@yahoo.com; andrea.themeli@ifsttar.fr

C. Chazallon
e-mail: cyrille.chazallon@insa-strasbourg.fr

B. Migault
e-mail: bernard.migault@insa-strasbourg.fr

A. Themeli · E. Chailleux (✉) · G. Didelet
LUNAM University, IFSTTAR, MAST, MIT, Route de Bouaye, BP 4129,
44341 Bouguenais, France
e-mail: emmanuel.chailleux@ifsttar.fr

G. Didelet
e-mail: gilles.didelet@ifsttar.fr

A. Themeli · F. Farcas
University Paris-Est, IFSTTAR, MAST, CMPD, 14-20 Boulevard Newton,
77447 Champs-Sur-Marne, Marne-La-Vallée, France
e-mail: fabienne.farcas@ifsttar.fr

A. Themeli
EPSILON Ingénierie, Parc de Ruissel, Avenue de Lossburg, 69480, Anse, France

A. Themeli · E. Chailleux
IFSTTAR-Nantes, Route de Bouaye, BP 4129, 44341 Bouguenais Cedex, France



F. Canestrari and M.N. Partl (eds.), *8th RILEM International Symposium on Testing and Characterization of Sustainable and Innovative Bituminous Materials*, RILEM Bookseries 11, DOI 10.1007/978-94-017-7342-3_8

with the evolutions of pure petroleum bitumens of equivalent grade. The petroleum bitumens of equivalent grade, used for comparison purposes, are produced in refinery in France by the same fabricant as the soft petroleum bitumen which has been selected to be modified by asphaltites. All the petroleum bitumens satisfy the European Norms and are used currently in France and elsewhere. The present study shows that the asphaltite modification gives hard paving binders which have better performances, regarding to the ageing evolution, compared to hard petroleum bitumens produced in refinery. The asphaltite appears to be an ageing inhibitor.

**Keywords** Asphaltite · Bitumen modification · Bitumen aging · Bitumen production

## 1 Introduction

Hard bitumens are of real interest in pavement engineering nowadays. They are used in the production of high modulus asphalt concretes (HMAC). HMAC allow the reduction of thickness of structural pavement layers and/or the prolongation of the pavement lifetime.

Hard bitumens are produced in petrol refineries by processing the residue of the vacuum distillation of petrol by means of different techniques as air blowing, oxidation, solvent deasphalting etc. (Asphalt Institute and Eurobitume 2011). Geographically, the industry allowing the application of these techniques is mainly located in industrialized countries. For this reason the access to hard bitumens is difficult for developing countries or countries which do not have the adequate technologies. Furthermore, hard bitumens are lacking also in industrialized countries and appeals are made to the careful use of this material (Lombardi 2012). For these reasons, several studies have been conducted or are in progress in order to develop alternatives for the production of hard bitumens from the soft petroleum ones.

These alternatives very often consist in the modification of soft petroleum bitumens by various modifiers like polymers, polyphosphoric acid, rubbers, recycled plastics, fibers of various types, natural bitumens and asphalts (Bardesi et al. 1999). Several researchers have studied the composition and mechanical properties of various modified bitumens (Huang and Shu 2009; Kök et al. 2011; Yildirim 2007; Aflaki and Tabatabaee 2009; Aflaki et al. 2014).

In the context of bitumen modification, asphaltites have a good potential. Asphaltites are very hard natural bitumens and are chemically similar to petroleum bitumens. Due to their chemical similitude, asphaltites and petroleum bitumens have a very good compatibility.

In this paper we will focus on the ageing behavior of asphaltite modified bitumens. The natural asphaltite used in this study is mined in Albania in the region of Selenizza. The asphaltite modification of soft petroleum bitumens gives hard

binders, suitable for the production of HMAC. However, we do not know how asphaltite modified bitumens behave during ageing. So, the scope of the work presented in this paper is to study the ageing performances of Selenizza asphaltite modified bitumens. All this is achieved by following the evolution of several mechanical properties of asphaltite modified bitumens during ageing. In addition to this, we have followed the evolutions of the same mechanical properties on pure petroleum bitumens of equivalent penetration grade. This will allow to make a relevant comparison and to draw clear conclusions. The comparison with pure petroleum bitumens of equivalent grades will answer to the question whether hard asphaltite modified binders are or not suitable to replace hard petroleum bitumens in the production of HMAC.

## 2 Approach to Quantify Ageing

The artificial ageing is carried out by the Roll Thin Film Oven Test (RTFOT) (EN 12607-1) and followed in the Pressure Ageing Vessel (PAV) (EN 14769).

The ageing of bitumens is manifested by hardening and by elasticity gain. The hardening is shown by the increase of the complex modulus norm (Fig. 1a), and the elasticity gain is shown by the decrease of the complex modulus phase angle (Fig. 1b). In addition to this other mechanical properties evolve during ageing. For example, the ring and ball softening temperature increases and the needle penetration decreases.

Since the evolution of these mechanical properties indicates the evolution of the bitumen during ageing, in the present study, the ageing will be quantified by applying the following expression:

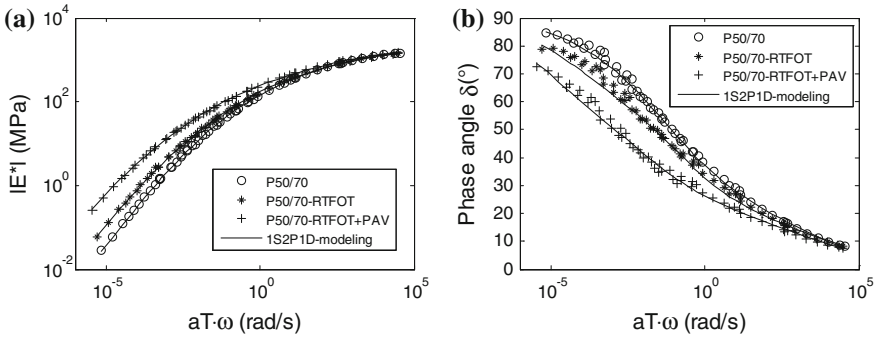


**Fig. 1** **a** Complex modulus norm and **b** complex modulus phase angle master curves at $T_{ref} = 0$ °C of a petroleum bitumen of grade 50/70 before and after artificial ageing procedures of RTFOT and PAV

$$EV_x = \frac{\left|x^{RTFOT+PAV} - x^{New}\right|}{x^{New}} \cdot 100 \quad (1)$$

where
$EV_x$—The evolution of the mechanical property $x$.
$x^{RTFOT+PAV}$—The mechanical property after RTFOT and PAV artificial ageing.
$x^{New}$—The mechanical property before ageing.

# 3 Experimental

## 3.1 Ageing Procedures

The materials of this study are subjected to the Rolling Thin Film Oven Test (RTFOT) (EN 12607-1) and then to the Pressure Aging Vessel (PAV) test (EN 14769). It is considered that the RTFOT simulates the aging of bitumens during the asphalt concrete production and the PAV test simulates the long term aging under service conditions.

## 3.2 Consistency Measurements

The consistency of the bitumens is characterized by the needle penetration test and by the ring and ball softening temperature determined according to Standards EN (1426) and EN (1427) respectively.

## 3.3 Rheological Measurements and Modelling

### 3.3.1 Rheological Measurements

Rheological properties of bitumens in terms of complex modulus in the linear domain are determined by oscillatory rheological tests carried out on a viscoanalyser METRAVIB. Annular shearing and traction—compression geometries were adopted for the high and the low temperature domains respectively. The complex shear modulus (G*), obtained by annular shearing is converted to complex traction—compression modulus (E*) by applying a Poisson's ratio of 0.5, thus considering the asphalt as an incompressible material above 20 °C. The complex moduli of pure, modified and aged asphalts are measured from −10 to 60 °C and from 1 to 80 Hz.

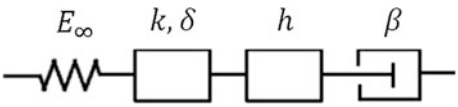


**Fig. 2** Analogical model to fit the experimental data on pure, modified and artificially aged bitumens

This temperature and frequency ranges allows to cover almost the entire viscoelastic domain $(phase\,angle \approx 0 - \pi/2)$ of most of our binders.

### 3.3.2 Rheological Modelling

In order to enable the calculation of the evolutions of linear viscoelastic properties of bitumens during ageing at any frequency and temperature, the experimental data are fitted by a rheological model. Fitting allows also the extrapolation of the rheological behavior in domains experimentally inaccessible (very high and very low frequencies).

The isotherms, determined experimentally, are shifted to master curves at a reference temperature $T_{ref}$ = 0 °C according to the LCPC method (Chailleux et al. 2006) and then the experimental measurements are modelled by 1S2P1D (1 Spring, 2 Parabolic elements and 1 Dashpot) analogical model (Such 1983). The model is presented in Fig. 2 and its mathematical form is given by Eq. 2. The adjustment of the model is carried out by an error minimization procedure applied simultaneously on the modulus norm and on the phase angle data. The fitting quality is very satisfactory. The minimal determination factors are $R^2$ = 0.9993 for the modulus norm and $R^2$ = 0.9932 for the phase angle.

$$E^*(i\omega\tau) = \frac{E_\infty}{1 + \delta(i\omega\tau)^{-k} + (i\omega\tau)^{-h} + (i\omega\beta\tau)^{-1}} \tag{2}$$

where $\omega$ is the radial frequency, $\tau$ is the relaxation time which is function of temperature, $E_\infty$ is the complex modulus when $\omega\tau \to \infty$, $\delta$, $k$, $h$ and $\beta$ are dimensionless parameters. $\tau$, $E_\infty$, $\delta$, $k$, $h$ and $\beta$ are the adjustable parameters of the model.

## 4 Materials

All the materials considered in this study are referenced and described in Table 1.

**Table 1** Materials considered in the study

| Reference | Description |
|---|---|
| AS | Organic phase of purified asphaltite extracted in deep layers of the mine |
| P50/70 | Petroleum bitumen of **50/70** grade |
| P35/50 | Petroleum bitumen of **35/50** grade |
| P20/30 | Petroleum bitumen of **20/30** grade |
| P10/20 | Petroleum bitumen of **10/20** grade |
| 5 % AS + 95 % P50/70 | **50/70** grade petroleum bitumen modified with **5** % of asphaltite |
| 10 % AS + 90 % P50/70 | **50/70** grade petroleum bitumen modified with **10** % of asphaltite |
| 15 % AS + 85 % P50/70 | **50/70** grade petroleum bitumen modified with **15** % of asphaltite |

## *4.1 The Asphaltite*

The asphaltite is mined in Albania in the region of Selenizza. In its natural state it contains 15–18 % of fine mineral material. The organic phase, which is used to modify the petroleum bitumens, is isolated by dissolution in tetrachloroethylene and filter-centrifugation. We have employed a purified asphaltite mined in deep layers of the mine. The composition and some basic properties of the asphaltite are given in Table 2 in comparison to a petroleum bitumen. The SARA fractions, the FTIR indices, the agglomerate contents and the glass transition temperatures are determined according to methods explained by Le Guern et al. (2010). As we can see in

**Table 2** Some characteristics of Selenizza asphaltite

| Test | | AS | P50/70 |
|---|---|---|---|
| c7—precipitation (NF T60-115) | Asphaltenes c7 (%) | 43.8 | 10.2 |
| | Maltenes (%) | 56.2 | 89.8 |
| SARA fractions | Saturates (%) | 1.7 ± 0.35 | 6.7 ± 0.65 |
| | Aromatics (%) | 24.8 ± 2.29 | 50.5 ± 1.81 |
| | Resins (%) | 35.1 ± 1.35 | 26.1 ± 1.64 |
| | Asphaltenes Iatrosc. (%) | 38.4 ± 1.88 | 16.7 ± 1.42 |
| Oxidation (FTIR[b] indexes) | Sulfoxyde | 6.36 | – |
| | Carbonyl | 3.99 | – |
| Agglomerate content (HS-SEC[a]) (%) | | 2.4 | 0.92 |
| Glass transition temperature (°C) | | −1.1 | −22.9 |
| Penetrability (0.1 mm) (EN 1427) | | 0 | 54 |
| R&B Temperature (°C) (EN 1426) | | 119 | 49 |
| $\lvert E^* \rvert$ (15 °C, 10 Hz) (Pa) | | $1.23 \times 10^9$ | $1.26 \times 10^8$ |

[a]High speed size exclusion chromatography
[b]Fourier transform infrared spectroscopy

the Table 2 the asphaltite is rich in resins and asphaltenes, compounds responsible for its elevated hardness (high R&BT, high $|E^*|$ and zero penetration).

## 4.2 The Petroleum Bitumens

The P50/70 is chosen to be modified by asphaltite (Table 1). The other petroleum bitumens, chosen for comparison, are of different (harder than P50/70) penetration grades. All the petroleum bitumens are produced in France by the same fabricant (Table 1). This choice is made in order to allow comparisons between hard bitumens issued form asphaltite modification and hard bitumens produced in refinery. All the petroleum bitumens satisfy the European Norms (EN 12591, EN 13924) and are currently used in pavement construction.

## 4.3 The Modified Bitumens

The modifying process consists in adding the fine grained asphaltite ($\Phi < 1$ mm) in the preheated soft petroleum bitumen P50/70. The blend is carried out by mixing both materials with a high shear mixer for 1 h at 180 °C. These mixing conditions assure a homogeneous blend of the two components. Modification rates of 5, 10 and 15 % are chosen (Table 1). The modified binders get harder with the modification rate. Starting from a soft bitumen of 50/70 grade, harder grades are obtained: 35/50, 20/30 and 10/20 with 5, 10 and 15 % of asphaltite respectively. These modification rates give binders comparable to the hard petroleum binders chosen for comparison (Fig. 3). All the modified bitumens satisfy the European Norms (EN 12591, EN 13924).

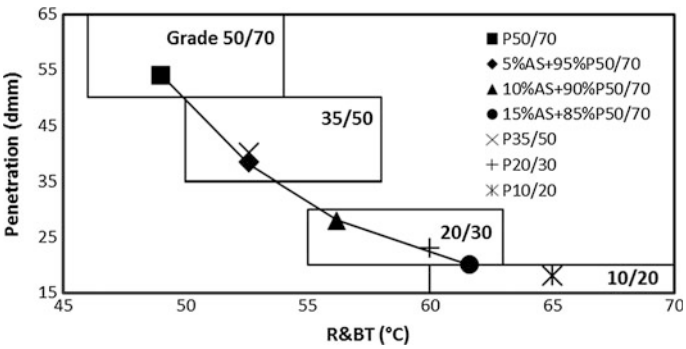


**Fig. 3** Properties of asphaltite modified bitumens

## 5 Calculation of Evolutions

In this paragraph we will calculate the evolutions of the penetration, of the ring and ball temperature and that of the viscoelastic properties with the artificial ageing RTFOT + PAV. This will be achieved by applying the Eq. 1 to the respective experimental measurements before and after the artificial ageing.

### *5.1 The Evolution of Penetration and R&BT During Ageing*

In Figs. 4 and 5 are shown the evolutions of the penetration and of R&BT respectively. Evolutions are calculated by the Eq. 1. We note that the modified binders show lower evolutions of penetration and of R&BT compared to the same evolutions of the starting petroleum bitumen P50/70 (Figs. 4 and 5). We observe that the higher the modification rate, the slower the evolutions during ageing. This indicates that the asphaltite behaves as an ageing inhibitor. In addition to this, comparing the evolutions of the modified binders with the evolutions of petroleum bitumens of the same penetration grade, we note that the asphaltite modified bitumens present a much better aging behavior. For example the petroleum bitumen of

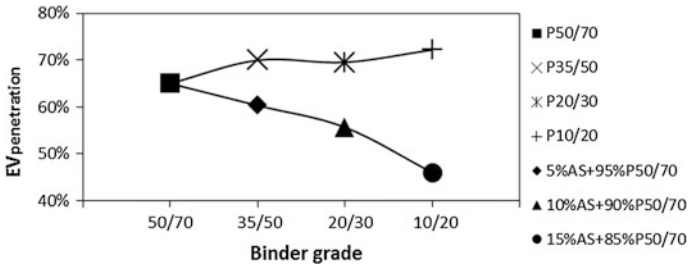


**Fig. 4** Evolution of penetration after artificial ageing RTFOT and PAV

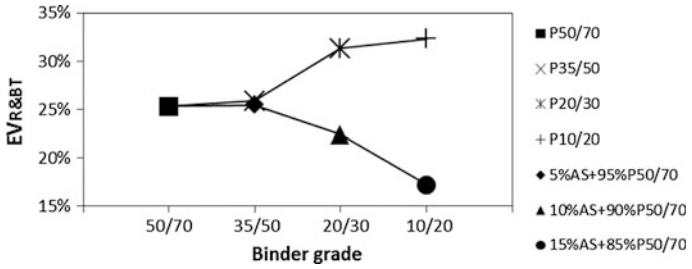


**Fig. 5** Evolution of R&BT after artificial ageing RTFOT and PAV

10/20 grade presents an evolution of penetration of 72 % while the penetration evolution of the modified binder at 15 % of asphaltite is only 46 %. Equivalent conclusions can be drawn if we consider R&BT evolutions presented in Fig. 5.

## 5.2 The Evolution of Linear Viscoelastic Properties During Ageing

The ageing evolution can be quantified by the evolution of the linear viscoelastic properties. For example, for a given loading frequency the aged bitumen is harder and more elastic than the fresh bitumen (Fig. 1). This evolution of the properties during ageing, for the given frequency, serves to quantify the aging evolution.

In the Figs. 6 and 7 we have presented the evolutions of the complex modulus norm and that of the complex modulus phase angle respectively under loading frequency $\omega = 10^{-4}$ rad/s and temperature $T_{ref} = 0$ °C. Other loading conditions give similar tendencies. The evolutions presented in Figs. 6 and 7 confirm the results of Figs. 4 and 5 and the same interpretations hold. As an example, the 10/20 penetration grade petroleum bitumen presents a phase angle evolution of 35.5 % while the phase angle evolution of the modified binder at 15 % of asphaltite is only 22.8 %.

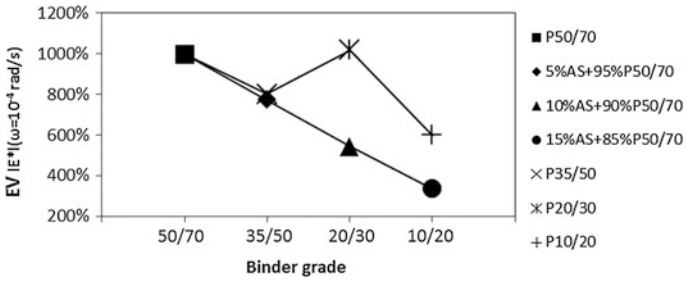


**Fig. 6** Evolution of complex modulus norm after artificial ageing RTFOT and PAV

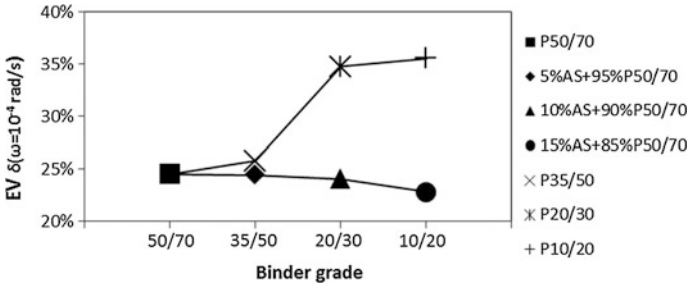


**Fig. 7** Evolution of complex modulus phase angle after artificial ageing RTFOT and PAV

## 5.3 The Evolution of Loading Conditions for Equivalent Viscoelastic States Before and After Ageing

As described in the experimental part we have measured the linear viscoelastic properties of our bitumens in terms of complex modulus. Two parameters are needed to fully describe the viscoelastic state of a material under given loading conditions; the real and the imaginary part of the complex modulus, the norm and the phase angle of the complex modulus, or any two other frequency-dependent properties. A proper combination of these two parameters would give a viscoelastic state function. The approximate relaxation spectrum calculated by the following expression (Marasteanu and Anderson 1999) is a proper function of the viscoelastic state:

$$H(\tau) \cong \frac{1}{\pi}[|G^*| \cdot \sin 2\delta]_{\omega=1/\tau} \tag{3}$$

with this function the viscoelastic state for a given relaxation time τ is expressed by the spectral value H(τ) depending on the complex modulus norm |G*| and the complex modulus phase angle δ. The aging of bitumens is manifested by a widening of the relaxation spectrum (Fig. 8).

One way to calculate the evolution during ageing could be to find the loading frequency evolution in order to have equivalent viscoelastic states of the material before and after ageing. For example, the frequency needed to obtain a certain modulus norm before ageing is higher than the frequency needed to obtain the same modulus norm after ageing (Fig. 1a). Similar considerations can be made based on the phase angle measurements (Fig. 1b). Since two parameters are needed to describe the viscoelastic state of a material we have used the approximate relaxation

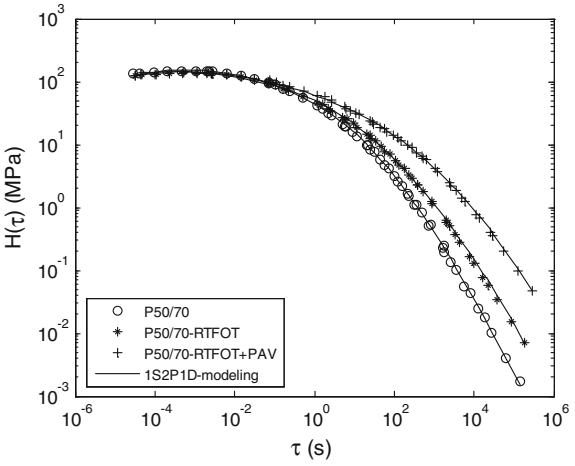


**Fig. 8** Approximate relaxation spectrum at T = 0 °C of a petroleum bitumen of grade 50/70 before and after artificial ageing procedures of RTFOT and PAV

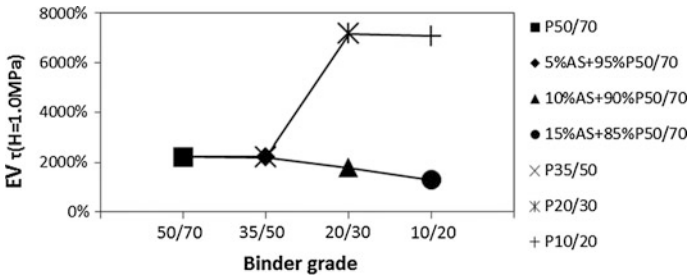


**Fig. 9** Evolution of the relaxation time after artificial ageing RTFOT and PAV

spectrum (Eq. 3) for our analysis. The evolution of the material during ageing is quantified by the widening of the relaxation spectrum.

In the Fig. 9 we have presented the evolution during ageing of the relaxation times for the spectral value of $H(\tau) = 1.0$ MPa at $T_{ref} = 0\,^{\circ}\text{C}$. Consideration of other spectral values gives similar tendencies. The determination of the relaxation time for the given spectral value is carried out by a half-interval search algorithm (dichotomy algorithm) applied on the approximate relaxation spectrum (Eq. 3) issued by the 1S2P1D model (Eq. 2). The evolutions presented in Fig. 9 confirm the previous results on the penetration, R&BT, complex modulus norm and phase angle. The same interpretations hold i.e. that the asphaltite is an ageing inhibitor and asphaltite modified bitumens present slower ageing evolution than the petroleum bitumens of the same grade. For example the petroleum bitumen of 10/20 grade presents an evolution of relaxation time for $H(\tau) = 1.0$ MPa at $T_{ref} = 0\,^{\circ}\text{C}$ of 7100 % while the relaxation time evolution of the modified binder at 15 % of asphaltite is 1300 %.

## 6 Conclusions

The scope of the present work was the study of the ageing performance of Selenizza asphaltite modified bitumens. The evolutions of various mechanical characteristics during artificial ageing determined on asphaltite modified bitumens are compared with the respective evolutions determined on pure petroleum bitumens of equivalent grade. For comparison purposes were chosen hard petroleum bitumens produced in France by the same fabricant as the soft petroleum bitumen selected to be modified. The experimental results show that the asphaltite behaves as an ageing inhibitor. The evolutions during ageing slow down with the modification rate. In addition to this, the comparison with the pure petroleum bitumens of the respective grade shows that the asphaltite modified binders present a much more advantageous ageing behavior. This indicates that the modification by Selenizza asphaltite gives hard paving binders which have better performance, regarding to the ageing, than

the bitumens produced in refineries. From the ageing point of view, asphaltite modified binders can successfully replace hard petroleum bitumens in the production of HMAC. The results hold for the blends realized in laboratory conditions, however similar tendencies should be obtained in field applications. In addition, the conclusions hold for the tests effectuated in this paper which are based on empiric and linear viscoelastic properties of the binders. It would be interesting to test the behavior and evolutions during ageing of modified bitumens in the non-linear domain.

**Acknowledgments** The authors express their gratitude to EPSILON Ingénierie Company and its president Mr. Jean-Louis Duchez for providing the materials and the financial support of this work.

## References

Aflaki S. and Tabatabaee N. (2009) Proposals for modification of Iranian bitumen to meet the climatic requirements of Iran. Construction and Building Materials, 23:2141–2150.

Aflaki S., Hajikarimi P., Fini E., and Zada B. (2014) Comparing effects of biobinder with other asphalt modifiers on low temperature characteristics of asphalt. J. Mater. Civ. Eng., 26(3), 429-439.

Asphalt Institute & Eurobitume (2011) The bitumen industry - A global perspective. Production, chemistry, use, specification and occupational exposure. Asphalt Institute Inc. & European Bitumen Association-Eurobitume.

Bardesi A., Brûlé B., and Corté J.-F. (1999) Use of modified bituminous binders, special bitumens and bitumens with additives in road pavements. Technical report, World Road Association PIARC.

Chailleux E., G. Ramond, Ch. Such, and Chantal de La Roche. (2006) A mathematical-based master-curve construction method applied to complex modulus of bituminous materials. Road Materials and Pavement Design; 7(sup1):75–92 .

EN 12607-1: Bitumen and bituminous binders - Determination of the resistance to hardening under the influence of heat and air - part 1: RTFOT method, 2007.

EN 1427: Bitumen and bituminous binders - Determination of softening point - ring and ball method, 2007.

EN 1426: Bitumen and bituminous binders - Determination of needle penetration, 2007.

EN 14769: Bitumen and bituminous binders - Accelerated long-term ageing conditioning by a pressure ageing vessel (PAV), 2013.

EN 13924: Bitumen and bituminous binders - Specifications for hard paving grade bitumens, 2006.

EN 12591: Bitumen and bituminous binders - Specifications for paving grade bitumens, 2009.

Huang B. and X. Shu (2009) Investigation into two procedures of applying gilsonite into hma mixtures. In Efficient Transportation and Pavement Systems.

Kök B. V., Yilmaz M., and Guler M. (2011) Evaluation of high temperature performance of SBS + gilsonite modified binder. Fuel, 90:3093–3099.

Le Guern M., Chailleux E., Farcas F., Dreessen S. & Mabille I. (2010) Physico-chemical analysis of five hard bitumens: Identification of chemical species and molecular organization before and after artificial aging. Fuel. 89(11):3330 – 9.

Lombardi B (2012) Les bitumes de grade dur et le 20/30. Bitume Info, August 2012.

Marasteanu M. O. and Anderson D. A. (1999) Booij and Thoone approximation and bitumen relaxation spectrum generation. In Eurobitume Workshop for Performance Related Properties for Bituminous Binders, number no. 134.

Such C. (1983) Analyse du comportement visqueux des bitumes. Bulletin de liaison des Laboratoires des Ponts et Chaussées, 127:25–35.

Yildirim Y. (2007) Polymer modified asphalt binders. Construction and Building Materials, 21:67–72.

# The Interaction of Polyphosphoric Acid with Bituminous Binders

**Hilde Soenen, Serge Heyrman, Xiaohu Lu, Per Redelius and John C. Edwards**

**Abstract** The purpose of this study is to evaluate how different binders react with polyphosphoric acid (PPA), and to contribute to a better understanding of this interaction. A number of bituminous binders were characterized before and after adding PPA, using rheological and chemical test methods, including FT-IR, uv-vis spectroscopy, NMR and gel permeation chromatography. The interaction with PPA is quantified as the change in softening point after adding a specific percentage of PPA. Most bitumen show an increase in R&B. Also in rheology, the stiffness increases, while the phase angle decreases when adding PPA. These observations are well-known and have been reported frequently by other authors. However, for one of the binders, small amounts of PPA lead to a decrease in R&B and to an increase in penetration. Rheological tests on this binder confirmed that the complex modulus decreases after adding PPA. These effects could be attributed to a precipitation, induced by PPA. This is very clear when investigating a drop of the bitumen-PPA blend in an optical microscope, and is also confirmed by storage stability tests. In conclusion, the findings suggest that PPA interacts with conjugated aromatic compounds, and this can in some cases lead to a precipitation.

**Keywords** Polyphosphoric acid · Aromaticity · Asphalthenes · Bitumen

H. Soenen (✉) · S. Heyrman
Nynas AB, Noorderlaan 18, 2030 Antwerp, Belgium
e-mail: hilde.soenen@nynas.com

S. Heyrman
e-mail: serge.heyrman@nynas.com

X. Lu · P. Redelius
Nynas AB, Oljeraffinaderiet, SE-14982 Nynäshamn, Sweden
e-mail: xiaohu.lu@nynas.com

P. Redelius
e-mail: per.redelius@nynas.com

J.C. Edwards
Process NMR Associates, Danbury, USA
e-mail: john@process-nmr.com



F. Canestrari and M.N. Partl (eds.), *8th RILEM International Symposium on Testing and Characterization of Sustainable and Innovative Bituminous Materials*, RILEM Bookseries 11, DOI 10.1007/978-94-017-7342-3_9

## 1 Introduction

Polyphosphoric acid (PPA) is used to modify bitumen, and a large number of publications have studied the effect of PPA. On the binder level, all studies report improvements in the high temperature rheological properties without affecting the low temperature rheological properties (De Filippis et al. 1995; Le Guern et al. 2010). When PPA is used in polymer modified binders, it will not only give the beneficial effects seen in unmodified binders, but literature reports that it also increases the efficiency of the polymer network. This in turn allows a reduction of the polymer content, leading to additional advantages like better storage stability of the PmB, improved handling conditions at high temperatures, and a lower production cost (Baumgardner 2010). Also in asphalt mixture tests, positive effects of PPA modification have been observed (Romagosa et al. 2010). Edwards et al. (2006) however, reported stiffening effects of PPA on the binder level at medium and higher temperatures, which could not be shown in dynamic creep tests on asphalt concrete mixtures.

Although a lot of beneficial properties of PPA modification have been reported, the reasons for this and possible reactions that may happen still remain fairly unknown. Orange et al. (2004) stated that PPA strongly interacts with the asphaltene fraction of bitumen as opposed to the maltene fraction. It has been suggested (Baumgardner et al. 2005) that PPA breaks up and disperses asphaltene agglomerates. The main support for this model is based on chromatography, where a reduction in the molecular weight of the agglomerated phase was observed after modification with PPA. Segregation of material on a micro scale level using AFM also supports this model but this type of segregation was not observed for all the investigated binders (Baumgardner et al. 2005).

Regarding the reaction mechanism, it has been proposed that PPA donates a hydrogen ion, which could act as the primary initiator for the interaction of PPA with bitumen (Fee et al. 2010). However, Masson (2008) pointed out that when adding PPA to bitumen, the PPA comes in a rather non-polar medium, and is not expected to dissociate in ions, unless enclaves of high dielectric constant would exist in bitumen. According to Masson, the existence of such areas is speculative, but not impossible. It has also been reported that after modification with PPA, no new chemical species, containing phosphorous compounds were formed in the bitumen-PPA mixture (Huang et al. 2008 and Miknis and Thomas 2008).

The main purpose of this study was to evaluate why different binders react differently with PPA, and to help understand how PPA interacts with bitumen.

## 2 Experimental

The selected binders and empirical properties are shown in Table 1. The PPA, used in this study contained 105 % $H_3PO_4$. Bitumen and PPA were mixed at 160–180 °C and were stirred with a blade mixer for 1 h.

**Table 1** Overview of the investigated samples, all binders are unmodified

| Samples | Pen, 25 °C (dmm) | R&B (°C) | PI |
|---|---|---|---|
| B1 | 10 | 69.5 | −0.44 |
| B2 | 20 | 60.4 | −0.81 |
| B3 | 24 | 58.9 | −0.76 |
| B4 | 26 | 61.2 | −0.19 |
| B5 | 27 | 67.1 | 0.91 |
| B6 | 30 | 62.4 | 0.32 |
| B7 | 53 | 52.4 | −0.47 |
| B8 | 58 | 49.5 | −1.00 |
| B9 | 67 | 49.5 | −0.63 |
| B10 | 71 | 47.9 | −0.91 |
| B11 | 83 | 45.2 | −1.28 |
| B12 | 84 | 44 | −1.62 |
| B13[a] | 442[b] | 27.8 | −4.72 |

samples from the same crude origin: B2, B3, B4, B12, B13
[a]B13 is the n-heptane soluble part of B12
[b]The penetration at 25 °C was calculated from G* tested at 25 °C and 0.4 Hz

Rheological tests were conducted with a Dynamic Shear Rheometer (DSR) from Anton Paar. Temperature-frequency sweeps were recorded in a frequency range from 0.01 up to 10 Hz, 8 mm plates were used from 0 to 50 °C, 25 mm plates were used from 40 to 90 °C. Strain levels were respectively 0.0005 for 8 mm plates and 0.01 for 25 mm plate tests.

Gel permeation chromatography (GPC) was conducted with an Alliance 2690 Separator with a differential refractometer (RI) detector and a Waters 996 photo diode array (PDA) detector. Both detectors were used in series. In the PDA detector, the concentration of absorbing substances in the eluent is monitored using UV-visible light absorption (UV-vis); with a wavelength variation from 200 to 610 nm. The reported uv-vis absorptions are areas; since the absorption was summated over all elution volumes at specific wavelengths. The GPC columns consisted of 3 Jordi columns with respective pore sizes of 100, 500, and 1000 Å. Calibration for molecular weight was performed with narrow polystyrene standards. The tests were conducted with THF as the eluent.

Fourier transform infrared spectroscopy, (FT-IR) with attenuated total reflection (ATR) was applied with a Nicolet IS 10 with a diamond cell (smart-orbit). In this case, samples can be investigated without using solvents. To obtain good contact between the sample and the ATR crystal a small sample press, delivered with the equipment was available.

Optical microscopy was performed with a Carl Zeiss Axioskop 40F1 equipped with a digital camera DP200a. Fluorescence microscopy in reflection and transmission microscopy were performed. A magnification of 200× was used.

Bitumen generic fractions were determined by Iatroscan (thin-layer chromatography with flame ionization detection, TLC-FID). A commercial equipment

Iatroscan MK-6 s was used. 2 % (w/v) solutions of bitumen were prepared in dichloromethane, and a 1 µl sample solution was spotted on chromarods. The separation of bitumen into four generic fractions was performed by a three-stage development using n-heptane, toluene/n-heptane (80/20 by volume), and dichloromethane/methanol (95/5 by volume), respectively. In fact that part of the sample that did not move with any of the solvents is referred to as the asphalthene fraction. This fraction is probably not equal to the insoluble fraction in n-heptane.

NMR analysis was performed by Process NMR Associates (USA). Liquid-State NMR was performed on a Varian Mercury MVX-300 NMR spectrometer equipped with a Varian 5 mm broad-band ATB-PFG probe, operating at a resonance frequency of 75.36 MHz for $^{13}C$ and 299.67 MHz for $^{1}H$. Samples were prepared by adding an accurately weighed amount of sample (around 150 mg) into approximately 0.75 ml of CDCl3 (deuterated chloroform)—CrAcAc (0.05 M). NMR experiments were obtained with a 45° tip angle pulse width, a 1 s relaxation delay, a 0.64 s acquisition time and were acquired with inverse gated high power proton decoupling to prevent NOE enhancements. DEPT-45 experiments were acquired with a relaxation delay of 1 s, acquisition time of 0.85 s. $^{1}H$ NMR experiments were performed by dissolving a 20 mg of sample in 99.98 % D CDCl3—a relaxation delay of 2 s and an acquisition time of 9 s were utilized along with a 45° tip angle. 32 transients were accumulated with an observed spectral width of 8 kHz. $^{1}H$ type calculations were performed that removed the signals of residual protons in the 99.9 %D CDCl3 from the aromatic spectral integrals. More detailed information is available in Andrews et al. (2011).

## 3 Results

### 3.1 Empirical and Mechanical Related Tests

In Fig. 1 the increase in softening point after adding 1.5 % PPA is shown. As the binders are ranked according to their penetration, it is clear that this increase is not related to the penetration level. There is also a slight interaction when adding PPA

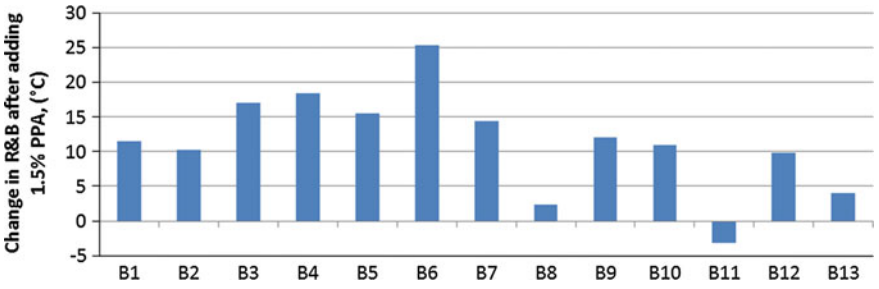


**Fig. 1** Change in R&B temperature after adding 1.5 % PPA

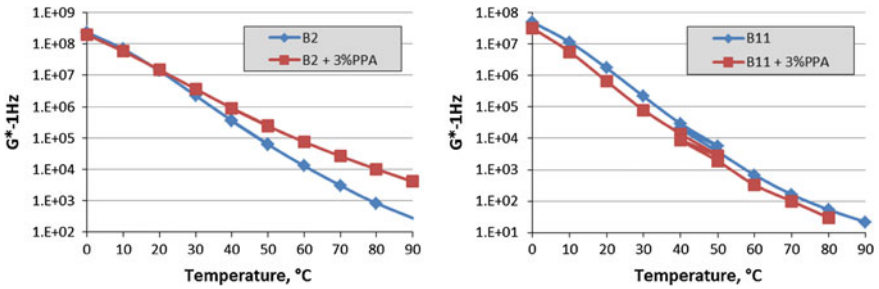


**Fig. 2** G* (at 1 Hz) versus temperature before and after adding PPA, B2 (*left*), B11 (*right*)

to the maltene fraction (B13). For one binder (B11) a decrease in R&B is observed. Examples of DSR tests, before and after adding PPA are shown in Fig. 2 for B2 and B11. For B2 the effect of PPA is as expected, an increase in modulus, which is more pronounced at higher temperatures, is observed. For B11 adding PPA results in a decrease in the modulus level. In Fig. 2, the modulus is presented logarithmically, the small difference in the graph refers to a difference of up to 60 % at stiffness levels in the temperature range 30–60 °C.

## 3.2 Chemical Test Methods

In Fig. 3a the measured weight average molecular weight (Mw) is shown as a function of PPA content for three binders. Bitumen, B2 and B4, having higher molecular weights show a clear decrease in Mw after adding PPA, while for the lower molecular weight binder, B11 there is no effect. The decrease at the higher molecular weights is larger compared to the precision of 10 %. In Fig. 3b changes in the uv-vis absorption areas after adding PPA are shown for binder B2. Upon adding PPA, absorption areas decrease, longer wavelengths decrease more compared to shorter ones. This was observed for all the binders, including B11.

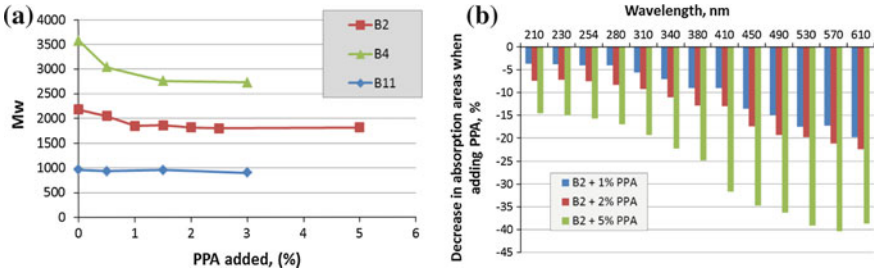


**Fig. 3** Changes in the GPC measurements after adding PPA **a** changes in Mw, **b** changes in the uv-vis absorption areas

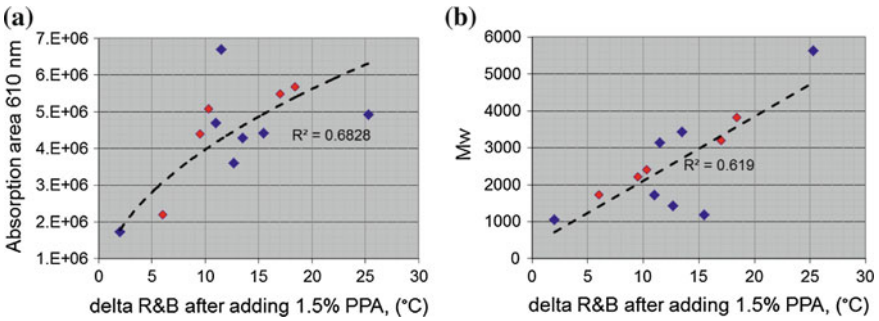


**Fig. 4** Relation between the interaction with PPA and chemical characteristics of the binders: **a** relation to the uv-vis absorption area at 610 nm, **b** relation to Mw (B11 is not included)

In GPC, binders are diluted in a solvent and injected on a porous column. This complicates the interpretation of the results; associations may form in or with the solvent, increasing the Mw, or on the other hand, components may adhere to the column material and decrease the detected Mw. It is also possible that not all components are soluble in the solvent and this insoluble material is removed from the data. In this study, uv-vis absorptions are integrated over all retention times, therefore one can assume that the effects of a possible adherence of substances to the column or of associations are limited. When evaluating Fig. 4, the observed decrease in the molecular weight and in the uv-vis absorption levels could be interpreted as if material is not recorded and is missing after adding PPA.

Trends were observed between the interaction with PPA and the uv-vis absorption areas measured before adding PPA. Only the absorption area at the longest wavelengths showed a trend. Similarly, a trend was observed between the measured Mw of the unmodified binders and the interaction with PPA. This is shown in Fig. 4. If only binders originating from the same crude are compared, illustrated by red symbols in Fig. 4, the relations are much better.

FT-IR spectroscopy was performed before and after adding PPA. The spectra showed the presence of PPA, but no other changes could be observed. The interaction of PPA with bitumen did not show trends with FT-IR absorption levels. The C = O signal around 1700 $cm^{-1}$ for example did not change after PPA addition, indicating that these groups do not react with PPA. But samples from the same crude source showed a good relation between the signal at 1600 $cm^{-1}$, related to aromatic carbons, and the interaction with PPA.

## 3.3 *Microscopy*

PPA modified binders were investigated by optical microscopy. In Fig. 5, examples are shown for binder B11 and B2 after adding 1.5 % PPA. For B11, an irregular structure of black particles was seen, in fluorescence as well as in transmission

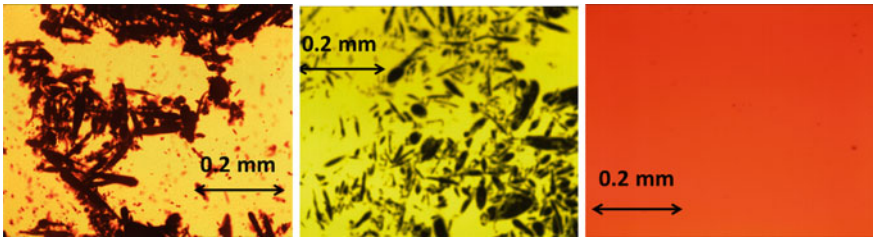


**Fig. 5** Microscopy images, B11 + 1.5 % PPA, optical microscopy (*left*) and fluorescence (*middle*), B2 + 1.5 % PPA optical microscopy (*left*) The magnification is 200× in all graphs

mode, indicating that something precipitates after adding PPA. None of the other binders showed this behaviour, as shown for B2. The decrease in R&B temperature and the decrease in G* could be attributed to this precipitation. Because of this precipitation, B11 was not included in the relations shown in Fig. 4.

## *3.4 Storage Stability and Investigations of Top and Bottom Parts*

For two binders, B2 and B11, storage stability tests were conducted after adding PPA. In this test the sample is stored 3 days at 180 °C, afterwards top and bottom part are investigated. For B2 + 3 % PPA, the values of top and bottom did not differ in R&B, FT-IR and rheology, indicating that this binder is storage stable. For B11 with PPA it was already clear visually that the bottom part had a different consistency compared to the top part, Fig. 6. Upon heating, the bottom part only softened and could not be poured. And for those tests where the sample needed to be dissolved in a solvent, the bottom part could not be dissolved fully, traces of a precipitate were observed in the solvent mixture. Therefore this analysis focuses on comparisons of top part and unmodified binder.

**Fig. 6** Photograph of the bottom (*left*) and top (*right*) part of the toothpaste tube, after the storage stability test, B11 + 3 % PPA

**Table 2** Investigation of B11, top, bottom and modified and unmodified binder

| Samples | R&B (°C) | FT-IR area 1600 $cm^{-1}$ | G*-70 °C -1 Hz (Pa) | S | A | R | A | GPC (Mw) |
|---|---|---|---|---|---|---|---|---|
| B11 | 45.2 | 1.049 | 163.4 | 7.3 | 53.2 | 20.3 | 19.2 | 968 |
| B11 + 3 % PPA | 44 | 1.069 | 100.1 | 6.9 | 48.7 | 23.4 | 21 | 904 |
| B11 + 3 % PPA Top | 35.6 | 0.779 | 32.7 | 8 | 54 | 24.8 | 13.2 | 998 |
| B11 + 3 % PPA Bot. | – | 1.535 | – | – | – | – | – | – |

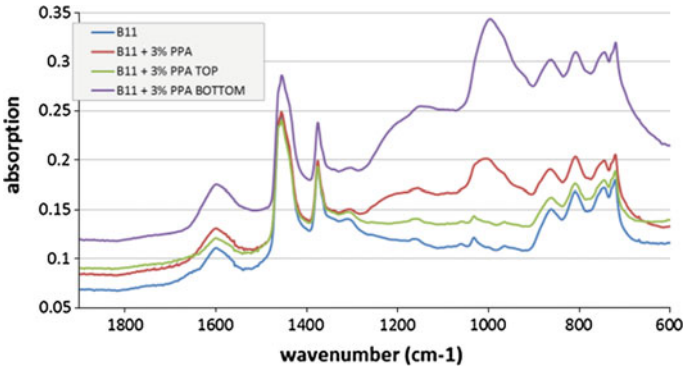


**Fig. 7** FT-IR spectra of several samples

Data are reported in Table 2. For R&B, the value for the top is lower compared to the unmodified sample. In FT-IR ATR, the bottom part could be measured and it contained a lot of PPA, the top part has no signs of PPA. FT-IR Spectra are illustrated in Fig. 7. In these spectra there is also a clear difference in aromatic content of the samples, signal at 1600 $cm^{-1}$. Peak integrations are included in Table 2. Rheological tests show that the top has a lower G* and viscosity compared to the original binder. As an indication, the G* level at 70 °C, 1 Hz is shown in Table 2. The asphaltene fraction of top and plain binder, determined by iatroscan also differs considerably. In GPC tests, differences in the uv-vis absorption area are shown in Fig. 8. The top part contains less larger aromats compared to the unmodified binder. There were also differences in Mw between top and unmodified binder.

$^{1}H$ and $^{13}C$ NMR were conducted on the unmodified binder and on the top part of B11. Results are shown in Tables 3 and 4 for $^{1}H$ and of $^{13}C$ NMR respectively. In $^{1}H$ NMR there was almost no difference in aromatic and aliphatic protons between top and original binder. In $^{13}C$ NMR, differences are more pronounced; there is a clear decrease in aromatic carbons in the top part, combined with a slight

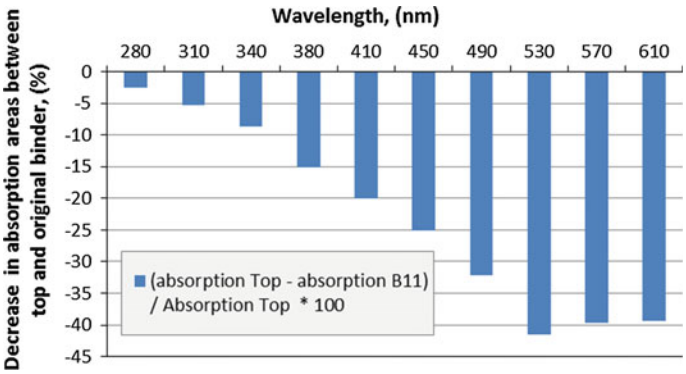


**Fig. 8** Change in uv-vis absorption areas for B11 between B11 and the top part of B11 + 3 %PPA

**Table 3** Results from $^{1}$H NMR on B11 and the top part of B11

| Proton type | Description | B11 | Top | Difference |
|---|---|---|---|---|
| Har | Aromatic protons | 7.8 | 7.4 | −0.4 |
| Hal | Aliphatic protons | 92.1 | 92.5 | 0.4 |
| Holefin | Olefin protons | 0.1 | 0.1 | 0.0 |
| H-2_alpha | Protons on carbons bridging two aromatic rings | 4.0 | 3.7 | −0.3 |
| Halpha | Protons on carbons adjacent to aromatic rings | 10.4 | 9.8 | −0.7 |
| H_CH2_CH | Methylene and methine aliphatic carbons | 38.0 | 36.8 | −1.2 |
| H_Long CH2 | Methylene carbons in long aliphatic chains | 21.8 | 23.9 | **2.1** |

**Table 4** Results from $^{13}$C NMR on B11 and the top part

| Description | B11 (%C) | Top (%C) | Difference |
|---|---|---|---|
| Carboxyl carbon (%) | 0.0 | 0.0 | 0.0 |
| Carbon aromaticity (%) | 38.3 | 34.1 | −4.2 |
| Carbon aliphaticity (%) | 67.0 | 71.2 | 4.2 |
| Phenolic aromatic C (%) | 0.4 | 0.3 | 0.0 |
| Substituted aromatic C (%) | 14.6 | 13.3 | −1.2 |
| Bridgehead aromatic C (%) | 17.4 | 14.9 | −2.5 |
| Protonated/hetero aromatic C (%) | 6.0 | 5.5 | −0.4 |
| Non-protonated aromatic C (%) | 32.3 | 28.6 | −3.7 |
| Methyl attached to aromatics | 5.3 | 5.3 | 0.0 |
| Methyl aliphatic C (%) | 12.4 | 12.8 | 0.3 |
| Methylene/methine C (%) | 49.3 | 53.1 | 3.8 |

increase in aliphatic carbons. The decrease is almost fully represented in the non-protonated aromatic carbons. Therefore, it can be we concluded that larger aromatic conjugated rings are depleted from the top part.

## 4 Discussion

The interaction of bitumen with PPA has been evaluated. In most cases PPA addition results in the expected effects, described extensively in literature. However for one of the binders PPA induces a precipitation. If this happens it is detrimental for the performance. A further characteristic of this binder is its lack of storage stability; this unstable binder allows isolating a non-interacting top phase, and an interacting phase in the bottom part. Comparisons of this non-interacting top and the original unmodified binder were conducted. NMR results indicate that mainly non-protonated aromatic carbons are depleted from the top part, with almost no decrease in aromatic protons and in substituted aromatic carbons. Iatroscan indicates that the asphaltene content of the top part is significantly lower compared to the original bitumen. The modulus and viscosity of the top part are also lower compared to those of the original binder.

It is not clear whether PPA reacts chemically or whether PPA is interacting without creating new bonds. In favour of a chemical reaction is the observation that the precipitate does not fully re-dissolve, even not in a good solvent. On the other hand, FT-IR spectra do not show any signs of a new chemical component. In literature, so far, the formation of a precipitate with PPA has not been reported. But, the formation of a precipitate after adding (ortho)phosphoric acid has been reported by De Filippis et al. (1996). These authors propose the addition of phosphoric acid, followed by an investigation of the sample under a microscope as a test to distinguish visbroken binders from other bitumen. In the sample set investigated in this paper, B11 was the only visbroken residue. Based on this information, it seems that visbroken residues are more prone to this precipitate formation. The reason for this must be related to the chemical structure. It has been reported that during the visbreaking process the molecular weight decreases by dealkylation, dehydrogenation and/or ring opening of naphthenic rings (Singh et al. 1993). Side chains and naphthenic rings attached to an aromatic cluster may cause a steric hindrance so that aromatic clusters cannot come close together or so that PPA cannot fully interact or react with these structures. Aliphatic side chains may also act as a compatibiliser, keeping the aromatic cluster in solution, also in n-heptane. Up to now, the number, length and branching of side chains on the aromatic structures is missing information.

Regarding relations between the chemical characteristics of bitumen and the interaction with PPA, good relations are only obtained when considering bitumen

from the same crude source, in this case 5 binders. Good relations were obtained between the interaction of PPA and Mw, aromaticity determined by the FT-IR signal at 1600 $cm^{-1}$ and by the uv-vis absorption area. The reason why bitumen from the same origin gives good relations may be related to the similarity of aromatic compounds in these binders. In FT-IR for example, the signal at 1600 $cm^{-1}$ is only an indication of the amount of aromatic bonds, since each molecular structure has its own extinction coefficient, and therefore its own effect on the absorption level. Bitumen consists of aromatic molecules with a distribution in aromatic sizes (the number of rings taking part in the conjugation). For each size, there are different possible ways of arranging the rings; linear or in a more compact shape. And all these molecules may have variations in the position and type of side groups. In principle, the FT-IR signal at 1600 $cm^{-1}$ can only be considered as an average if the distribution of the aromatic molecules over the different ring sizes, ring arrangements and side groups is the same in all the bitumen samples. And this assumption could apply to binders originating from the same crude. A similar reasoning can be used for the uv-vis absorption areas. In this case it is possible to distinguish according to the size of the conjugated aromatic structure.

A bitumen model based on mutual solubility of all bitumen components has been proposed and the importance of pi-pi interactions has been shown Redelius and Soenen (2014). If in such a model, PPA interacts with the polyaromatic carbons, this would increase the elasticity and viscosity of the system, and could explain the changes observed in mechanical properties.

To explain the observations of tests in which the sample is first dissolved in a solvent is more difficult; as mentioned before, a solvent may induce associations and influence existing interactions.

## 5 Conclusions

Conclusions can be summarized: The addition of PPA to bitumen binders can in some cases lead to a precipitation. The precipitation is seen in an optical microscope and in storage stability tests.

For binders that do not show a precipitate, it seems that trends between the interaction with PPA are observed with the uv-vis absorption area (long wavelengths) and with the molecular weight of the binders.

The binder showing a precipitation upon adding PPA allowed isolating fractions; a top part not interacting with PPA, and a bottom part interacting with PPA. An investigation of these fractions and the original binder showed that PPA interacts mainly with the non-protonated aromatic carbons, in this case the conjugated aromatic ring structures. Separating fractions could only be conducted for one of the binders, so it is not clear if these results can be considered as general.

## References

Andrews A B, Edwards J C, Pomerantz A E, Mullins O C, Nordlund D, Norinaga K (2011) Comparison of Coal-Derived and Petroleum Asphaltenes by 13C Nuclear Magnetic Resonance, DEPT, and XRS. Energy & Fuels 25(7):3068.

Baumgardner GL (2010) Why and how of polyphosphoric acid modification - An industry perspective. AAPT 79:663-678.

Baumgardner GL, Masson J-F, Hardee JR, Menapace AM, Williams AG (2005) Polyphosphoric Acid Modified Asphalt: Proposed Mechanisms. AAPT 74:284-308.

De Filippis P, Giavarini C., Scarsella M. (1995), Improving the ageing resistance of straight-run bitumens by addition of phosphorus compounds. Fuel 74(6):836-841.

De Filippis P, Giavarini C, Scarsella M (1996) Integrated process for stabilization and upgrading of residues and bitumens. Fuel Science and Technology International 14 (6):821-838.

Edwards Y, Tasdemir Y, Isacsson U (2006) Influence of commercial waxes and polyphosphoric acid on bitumen and asphalt concrete performance. Materials and Structures 39(291):725-737.

Fee D, Maldonado R, Reinke G, and Romagosa H (2010) Polyphosphoric Acid Modification of Asphalt. Transportation Research Record 2179:49-57.

Huang S-C, Turner TF, Miknis FP, Thomas KP (2008) Long-term aging characteristics of polyphosphoric acid-modified asphalts. Transportation Research Record 2051:1-7.

Le Guern M, Chailleux E, Farcas F, Dreessen S, Mabille I (2010) Physico-chemical analysis of five hard bitumens: Identification of chemical species and molecular organization before and after artificial aging. Fuel 98:3330-3339.

Miknis FP, Thomas KP (2008) NMR analysis of polyphosphoric acid-modified bitumens. Road Materials and Pavement Design 9(1):59-72.

Masson J-F (2008) Brief review of the chemistry of polyphosphoric acid (PPA) and bitumen. Energy and Fuels 22(4):2637-2640.

Orange G, Dupuis D, Marin J V, Farcas F, Such C, Marcant B (2004) Chemical Modification of Bitumen through Polyphosphoric Acid. 3rd E& E Congress Paper 334:733-745.

Romagosa EE, Maldonado R, Fee D, Dongré, R, Reinke G (2010) Polyphosphoric acid binder modification. AAPT 79:743-771.

Redelius P, Soenen H (2014) Relation between bitumen chemistry and performance. Fuel published online DOI: 10.1016/j.fuel.2014.09.044.

Singh D, Kothiyal V, Kapoor MP., Ramaswamyt V, Aloopwan MKS (1993) Structural changes during visbreaking of light Arabian mix short residue. Fuel 72(6):751-754.

# LIBS: An Innovative Laboratory Technique for the Characterisation of Bituminous Material

**Hélène Martin and Graziella Durand**

**Abstract** The principal use for bitumens is in road construction. Some of the properties of bitumens, for example their consistency, change throughout their life, from manufacture to the end of their service life. Analytical techniques can be used to ascertain their chemical structure but not fully, due to the complexity of their composition. For several years, variability in the quality of bitumen has been observed. The conventional laboratory tests performed on bituminous materials are unable to identify any difference between the binders in question. More detailed studies reveal that they differ in terms of their elemental composition, for example the metals they contain, which are also markers of the origin of the crude oil. Metal contents can be quantified by various analytical techniques such as Atomic Absorption Spectroscopy (AAS) and Inductively Coupled Plasma (ICP) which are unfortunately quite complex to perform. Recently, a laboratory technique for determining the elements present in materials has attracted the attention of the scientific community. This method, known as Laser Induced Breakdown Spectroscopy (LIBS), uses a laser coupled with an optical emission spectrometer. We have adapted the LIBS protocol to make it suitable for the characterization of bituminous materials, and it represents a highly innovative technique for bitumen testing. This method is compatible with the precepts of sustainable development because, amongst other things, it does not use any solvents and generates no waste. This paper explains the principle of the LIBS technique, the necessary equipment, the way it is set up and practical applications in the field of road construction.

**Keywords** LIBS · Innovative · Characterisation · Bituminous binder

H. Martin
Campus Scientifique et Technique Colas, Boulogne-Billancourt, France
e-mail: martin@campus.colas.fr

G. Durand (✉)
Road Chemistry Department, Campus Scientifique et Technique Colas, Boulogne-Billancourt, France
e-mail: durand@campus.colas.fr



F. Canestrari and M.N. Partl (eds.), *8th RILEM International Symposium on Testing and Characterization of Sustainable and Innovative Bituminous Materials*, RILEM Bookseries 11, DOI 10.1007/978-94-017-7342-3_10

## 1 Introduction

In today's context of global warming, it is necessary to find ways of limiting the environmental impact of every technical field and encourage more environmentally responsible approaches. The pervasive presence of roads requires the sector to set an example. The highways industry has been committed to this type of policy for many years, for example by recycling material from old pavements. This has allowed us to considerably lower consumption of new pavement materials, conserve natural resources and reduce stockpiles of waste materials. The industry is going even further in this direction by making use of methods that are more environmentally friendly, particularly in the case of the analysis techniques for characterizing the materials it uses. Bitumen, which is of fundamental importance for roads, is subjected to particularly detailed analyses because in recent years it has been observed to exhibit a degree of variability due to the difficulty of obtaining crude of sufficient quality.

For roads to be durable, the materials used in them must have long-lasting properties. It is therefore necessary to check the quality of bitumens. Conventional bitumen characterisation techniques provide an initial picture of their properties, but give us no certainty as to their intrinsic quality. The reason for this is that the intrinsic quality does not depend on the empirical characteristics of the bitumen, but on its chemical composition. However, the latter is complex as bitumen is made up of thousands of different highly complex molecules. The use of new analysis methods is therefore essential to improve our knowledge about the material.

The current issues we are experiencing with bitumens are due to the variability in their quality, the possible presence of contaminants and the origin of the crudes. In this connection, it has been found that the presence and concentration of certain metals affects the potential uses of bitumens (bitumen in emulsions for example).

A range of techniques are is available for determining the metal content, for example flame absorption spectroscopy and the plasma torch. These techniques are relatively complex to perform in the laboratory and are generally only used with appropriate justification (for example, in the case of an expert appraisal) and on a limited number of specimens. They are not appropriate for the systematic analysis of bitumens which limits the possibilities of creating a database, carrying out follow-up studies and taking preventive measures.

In recent years (Green News Techno 2009; Romero and De Saro 2010; Haider and Rony 2013) LIBS (Laser Induced Breakdown Spectroscopy) technology has come to be seen as an alternative to the analysis methods mentioned above. LIBS provides a way of analysing the elemental constituents of a material. It is compatible with our company's policy of environmentally responsible development as it is straightforward to perform, rapid (it only takes about ten minutes), contact-free, minimally destructive, and produces no effluent emissions. The results are obtained immediately, and as the technique does not require samples to be taken, management and traceability are much less problematic. The implementation costs are

**Fig. 1** LIBS: an innovative device for analysing bitumen

therefore very low. This technique is rapidly establishing itself and a range of equipment is currently available on the market.

We have therefore adapted the analysis protocol to the appraisal of bitumens thus developing an innovative analysis technique for their characterisation (Fig. 1). Its advantages compared to conventional techniques and its potential applications are outlined below.

## 2 General Description

### *2.1 Comparison Between LIBS and Other Techniques for the Determination of Metal Contents*

Three techniques (Diaz Rosadoa 2013) can be used to determine the Na, Ca, Mg, V and Ni contents of bitumen:

- Plasma torch (ICP-AES or ICP-OES) or Inductively Coupled Plasma Atomic Emission Spectroscopy or Inductively Coupled Plasma Optical Emission Spectroscopy
- Atomic Absorption Spectroscopy (AAS)
- Laser Induced Breakdown Spectroscopy (*LIBS*)

The first two techniques, which have been in common use for several years, have many drawbacks. At the outset, it is necessary to prepare specimens, which requires the use of relatively dangerous solvents such as nitric acid during mineralisation in the case of ICP or nitric acid and xylene in the case of AAE.

In addition, Atomic Absorption Spectrometry uses gases such as acetylene (which is inflammable and burns in the presence of air or any other oxidising agent, and which may also create explosive environments), or nitrous oxide ($NO_2$) whose

major danger as asphyxiation due to a lack of oxygen. In addition, it is classified as a pollutant in the Kyoto protocol as it is a greenhouse gas and the fourth most important contributor to global warming after water vapour ($H_2O$), carbon dioxide ($CO_2$) and methane ($CH_4$). Its global warming capacity is 310 times that of $CO_2$. ICP requires the use of considerable quantities of argon.

These analytical techniques are relatively complex and also have other disadvantages. Sampling creates a degree of uncertainty, the preparation and analysis processes are relatively long (between three hours and one day), and these techniques are destructive and therefore consume materials.

As it is so simple to perform, LIBS can be used to analyse the elements in a material without the need to prepare specimens, or use solvents or gases and only affects a very small piece of material that is a few tens of micrometres long and a few micrometres deep. Its advantages can be summed up in two words: speed and simplicity.

## 2.2 *The Principle of LIBS (Laser Induced Breakdown Spectroscopy)*

LIBS has existed for some time, the technique was developed 1963. It is based on the information that is emitted during the interaction between a laser beam and the material, a phenomenon observed by Maiman in 1960 shortly after the invention of the laser. The general principle is very simple and can be described in three stages (Fig. 2):

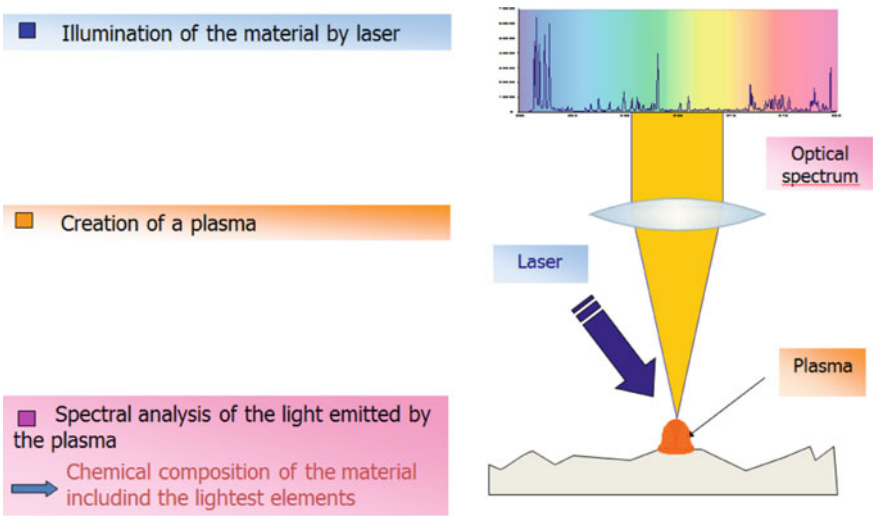


**Fig. 2** The general principle of LIBS

- illumination of the material by laser,
- creation of a plasma,
- spectral analysis of the light emitted by the plasma.

Nevertheless, the use of LIBS technology involves a considerable number of complex physical phenomena (Ismaël et al. 2009), which explains why devices for applying the technique has taken so long to appear on the market. It is necessary to concentrate the energy from a laser onto the material to be analysed in order to achieve a surface power density of the order of one GW/cm$^2$. This is done by focusing ultrafast laser pulses with a duration of a few nanoseconds (ns).

These conditions of intense radiation result in the immediate vaporisation of a few micrograms of material at the focal point, with the breakdown of the molecules and the creation of a plasma [4] (Fig. 3). This transfer is the result of ionisation of the vapour due to electron acceleration, and the outcome is a system consisting of atoms, irons and electrons whose composition is representative of the target under investigation.

The plasma cools as it expands into the surrounding gas (Fig. 4) emitting radiation which is characteristic of the atoms and ions in the plasma. Part of this light energy is analysed by a spectrometer which makes it possible to conduct an exhaustive determination of the elements present in the material, from light to heavy, as they are found in the periodic table.

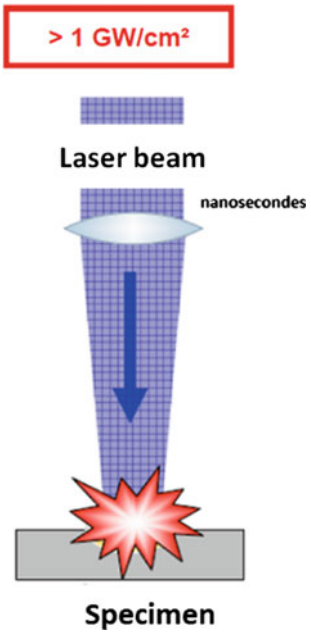


**Fig. 3** Creation of plasma

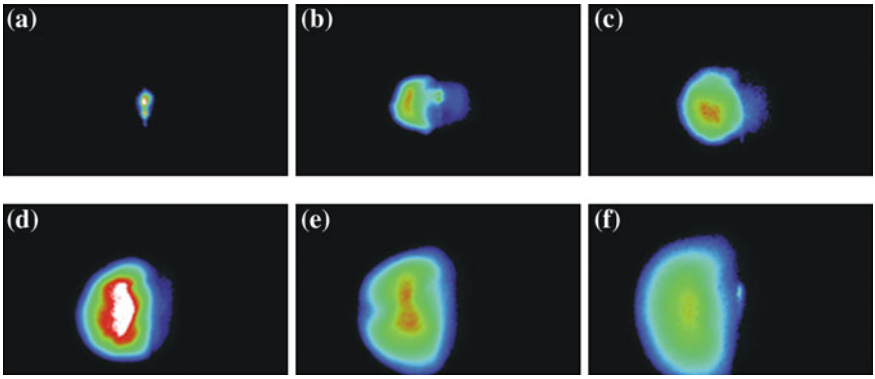


**Fig. 4** Expansion of plasma

LIBS is able to:

- carry out qualitative analysis based on the wavelengths of the characteristic emission peaks of the constituents of the specimen (Adam and Leone 2012),
- carry out quantitative analysis by measuring the intensity of the emission peaks, which is proportional to the number of atoms present in the measured volume of plasma (INERIS 2011).

### *2.3 Instrumentation*

The apparatus used to perform LIBS is able to analyse the elements present in all forms of material, solids, liquids or gases, quickly and without contact. A typical system is shown in Fig. 5. It consists of a pulsed laser, a system for focusing the beam on the specimen, a system to collect the light emitted by the plasma and a fibre optic cable to carry it to a spectrometer that is linked to a computer that controls the apparatus, acquires the data and processes the spectra.

## 3 LIBS and Bitumen

LIBS is used on bitumens in order, amongst other things, to determine their heavy metal content using calibration line techniques.

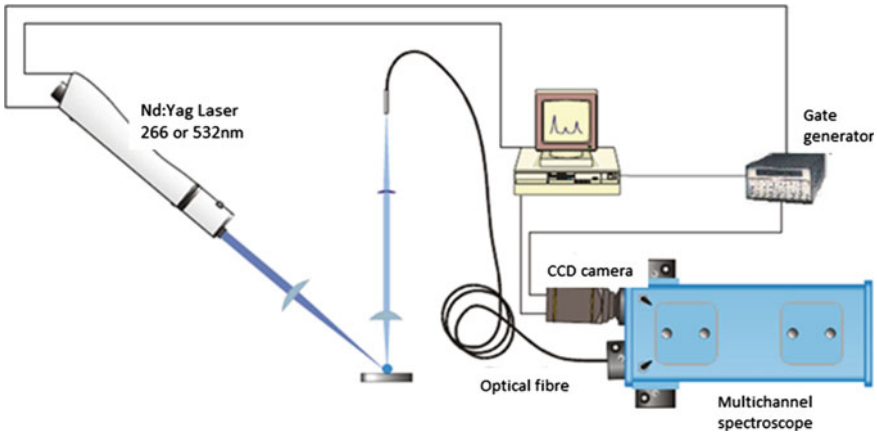


**Fig. 5** Instruments used in a LIBS system

## *3.1 Adapting LIBS for use on Bitumen*

The analysis of a specimen is subject to many types of bias, particularly when it interacts with its environment (the surrounding air, the supporting matrix,…). The calibration process therefore varies according to the materials and their state, which is why the standard addition method is used. Thus, bitumen specimens were prepared from bitumen and single-element standards in a non-volatile bitumen-compatible oil (Conostan® oil analysis standards also used in ICP or AA).

### 3.1.1 Calibration Lines

Initially, we used the bitumen standards to optimise the parameters of the apparatus, in particular the spectrometer, so as to obtain the highest signal-to-noise ratio. This stage was necessary to eliminate phenomena such as the generation of ghost peaks and self-absorption (due to signal saturation). The goal was to define analysis parameters that could be applied to all the elements while at the same time achieving the highest possible sensitivity (which corresponds to the gradient of the calibration line: the steeper the gradient, the higher the sensitivity). We thus plotted the calibration lines which are shown in Fig. 6. They allow us to determine the amount of metal in the analysed bitumen rapidly and with a high degree of precision. The high sensitivities for Na, Ca and Mg are striking, but the sensitivity is lower for V and even more so for Ni, suggesting limits with regard to the quantification of the latter.

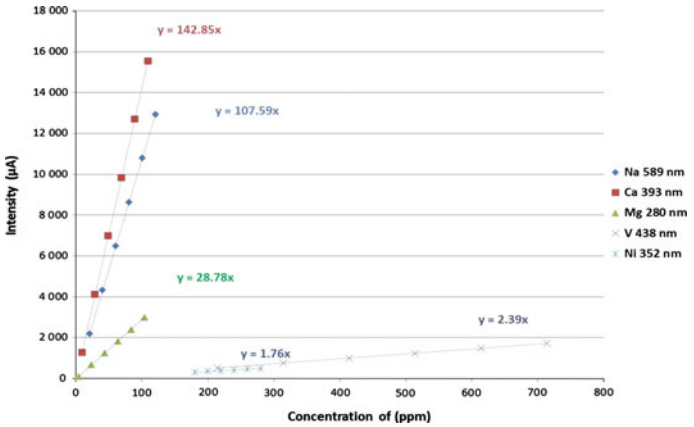


**Fig. 6** Calibration lines for the various elements

### 3.1.2 Precision, Lower Limit of Detection (LLD) and Repeatability

In order to conduct analyses with a high level of precision (i.e. with accurate and consistent measurements), it is necessary to make a large number of measurements to reduce the relative uncertainty. In our case, we made 25 measurements for each bitumen standard or specimen, and for each measurement, 200 shots are done.

Moreover, the lower limit of the detection (LLD, which is the minimum value of the measured quantity that can be detected) and the repeatability must both be known when analysing the results. The reason for this is that a result may not be reliable when the signal is only slightly above the background noise. The same applies for the repeatability of the analysis technique. Table 1 sets out these data for each of the control peaks for the analysed elements.

The LLDs we obtained were very low, and repeatability was satisfactory for the measurement ranges used for bitumen. However, these tests have shown that it is not possible to analyse Ni with this apparatus and these parameters as both the sensitivity and the LLD are low (below the usual concentration range of Ni).

**Table 1** Lower limit of detection for the different elements and repeatability

| | λ (nm) | LDD (ppm) | Usual concentration in bitumen (ppm) | Repeatability (%) |
|---|---|---|---|---|
| Na | 589.02 | ~1.5 | 10–100 | ±10 |
| Ca | 396.86 | ~0.7 | 0–20 | ±10 |
| Mg | 279.56 | ~1.0 | 0–20 | ±10 |
| V | 437.95 | ~44 | 200–800 | ±10 |
| Ni | 341.49 | ~72 | 10–70 | Not determined |

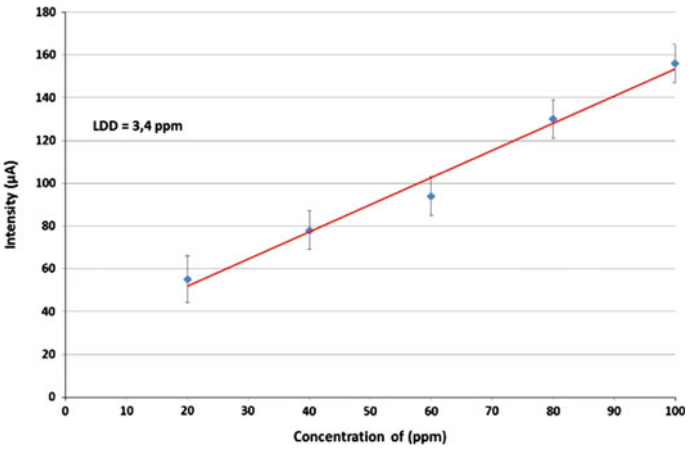


**Fig. 7** Calibration line for Ni with the monochromator

### 3.1.3 The Particular Case of Ni

It is difficult to determine Ni concentrations because its emission peaks have the same wavelength as those of some molecules present in bitumen. It is therefore very difficult to identify the presence of low concentrations. So, in spite of the use of specific parameters, the LLD with a multichannel spectrometer is less satisfactory than for the other elements. A different detection system with a monochromator coupled with a photomultiplier was therefore tested and gives the calibration line shown below (Fig. 7) once the parameters had been adjusted.

This gave us an LLD of 3.4 ppm, which was approximately 20 times lower than with the multichannel spectrometer (Note technique IVEA 2012).

The usefulness of the monochromator-photomultiplier system for the quantitative analysis of Ni has therefore been clearly demonstrated. This apparatus can also be used to analyse other elements which are difficult to determine with a multichannel spectrometer.

## *3.2 Studies on Bitumen*

### 3.2.1 An "Identity Card" for Bitumens

Due to our systematic analysis of the different bitumens we have built up a database and created "identity cards" for our bitumens. Figure 8 shows the metal contents for certain bitumens based on their origin. These parameters allow us to distinguish

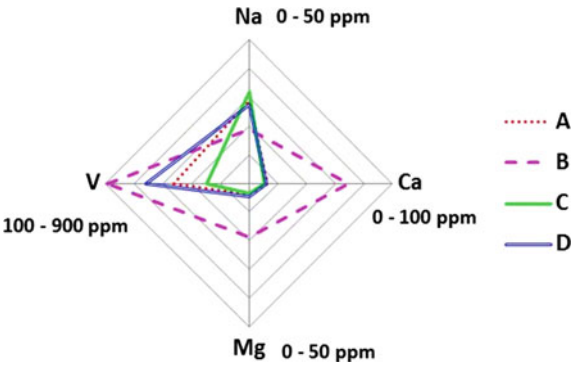


**Fig. 8** Identity card for different bitumens

between certain bitumens in a clear and statistically significant manner, as well as to establish with certainty when there is any variation in the metal content of our bitumens.

All the bitumens present the same physical and rheological properties (35/50 penetration grade); the main difference comes from their origin: naphthenic bitumen for B and various paraffinic bitumens for A, C and D.

### 3.2.2 Assessment of Bitumen

Below, we shall describe a LIBS analysis of a bitumen which was suspected of having caused problems on site and a commonly-used bitumen which will serve as a control.

The problem is as follows: difficulties appeared during emulsification tests on the suspect bitumen. While both bitumens produced mixes with satisfactory performance, their behaviour with regard to emulsification was markedly different: only the commonly-used bitumen could be used to manufacture emulsions with certainty, as the emulsion obtained with the suspect bitumen was so viscous that its characterisation was not possible.

The normal tests were performed and confirmed that both bitumens complied with the specifications laid down in the standard EN 12591.

The LIBS analysis (Fig. 9) showed that there were differences in the metallic salt contents of the two bitumens. More specifically, the two bitumens differed with regard to their Na and Ca contents (Table 2). Both these elements are recognised as causing problems when bitumens are used in certain applications. The metal contents identified in the suspect bitumen could on their own be sufficient to explain the observed emulsionability issues.

Other applications have enabled us to resolve other problems, both in the framework of expert appraisals and in a research and development setting.

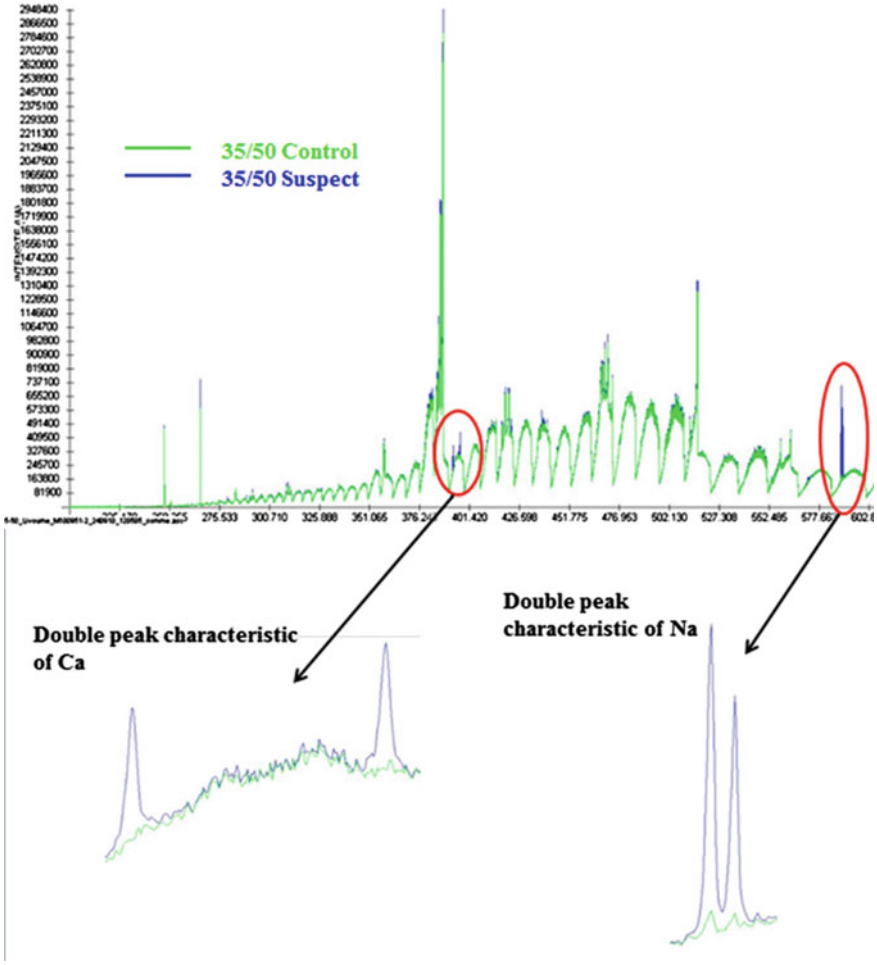


**Fig. 9** Spectra of the 2 bitumens

**Table 2** Metal contents

| Elements analysed (λ in nm) | 35/50 control content in ppm | 35/50 suspect content in ppm |
|---|---|---|
| Na (589 nm) | 26 | ~300[a] |
| Ca (393 nm) | 2 | 15 |

[a]The Na content is so high that this result is outside the calibration lines (maximum 100 ppm)

## 4 Conclusions and Outlook

LIBS is the combination of a laser ablation technique with optical emission spectroscopy. It is contact-free and can be used for the exhaustive determination of the elemental composition of a material, from light to heavy elements. It is precise, rapid (taking approximately 10 min) and minimally destructive. It is compatible with our company's policy of environmentally responsible development due to the fact that, as it does not use any solvents, it is more environmentally-friendly than the usual techniques for determining metal contents (ICP and AAE). Its innovative nature means this technology is still in the process of development, and its finalisation will depend on the ability to control all the parameters that are at play.

The calibration method has been validated and the first results show the technique's ability to analyse specimens with a high degree of precision, in terms of repeatability, lower limit of detectability and sensitivity. Some shortcomings of the apparatus, which were identified during experiments, have been resolved following the acquisition of a monochromator.

The availability of this analysis technique means that we are systematically able to monitor the metal content of the bitumens of different origins, which means we are able to:

- monitor how they change over time,
- recommend, or on the contrary, advise against the use of some bitumens for some applications in order to ensure that our products are of the highest possible quality.

Moreover, when we conduct expert appraisals, this technique is both less time-consuming and more effective than those used previously. This has an impact on the progress of the construction project in question and the implementation of any remedial measures. It also allows us to maintain the quality of the products we offer our clients, in spite of the marked variability that bitumens sometimes display.

Apart from the analysis of bitumens, there are many other potential applications, for example the detection of heavy metals in contaminated soils, or aggregate testing.

## References

Adam P., Leone N. (2012), La spectroscopie de plasma induit par laser (LIBS) pour le diagnostic chimique et biologique, Société des Experts Chimistes de France, Revue n°977 - 2e semestre 2012, p 17 - 26

Diaz Rosadoa J.C. (2013), Étude et développement de la spectroscopie d'émission optique sur plasma induit par laser pour la réalisation d'analyses de terrain : application à l'analyse en ligne de métaux dans les liquides. Available via DIALOG. http://hal.inria.fr/docs/00/81/89/09/PDF/VA_DIAZ-ROSADO_JOSE-CARLOS_07032013.pdf. Accessed 10 september 2014

Gondal M. A., Siddiqui M. N., Nasr M. M (2009), Detection of Trace Metals in Asphalttenes Using an Advanced Laser-Induced Breakdown Spectroscopy (LIBS) Technique, Energy & Fuels, 2010, 24, p 1099-1105

Green News Techno (2009), Analyse : le LIBS confirme son potentiel. Available via http://www.libs-france.com/ Accessed 15 september 2014

Haider A. F. M. Y., Rony M. A. (2013), Determination of the Ash Content of Coal without Ashing: A Simple Technique Using Laser-Induced Breakdown Spectroscopy, Energy & Fuels, 2013, 27, p 3725 - 3729

INERIS MAG (2011), Voir les « nanos » dans l'air, p 18 - 19

Ismaël A., Travaillé G., Bousquet B., Canioni L. (2009), Spectroscopie laser appliquée à l'analyse des sols pollués, RE 133 LAB-1, Editions T.I

Romero C. E., De Saro R. (2010), Laser-Induced Breakdown Spectroscopy for Coal Characterization and Assesing Slagging Propensity, Energy & Fuels, 2009, p 510 - 517

# Rheological Evaluation of Short- and Long-Term Performance for Warm Mix Asphalt (WMA) Binders

**Mohammed Sadeq, Eyad Masad, Hussain Al-Khalid, Okan Sirin and Dallas Little**

**Abstract** Warm-mix asphalt (WMA) additives are environmentally friendly and cost-effective products that lower the viscosity of bituminous binders to allow reduction of mixing and compaction temperatures in asphalt mix production. In this study, two WMA additives were used; Sasobit® and Advera®. Both were mixed in the lab with unmodified 60/70 Pen and modified PG 76-22 binders. Strain oscillation and viscosity measurement tests were performed to determine the rheological properties of the binder with and without WMA additives. Different ageing processes were performed in this study; half and full short-term ageing using the Rolling Thin Film Oven (RTFO) procedure, and long-term ageing using the Pressurized Ageing Vessel (PAV) procedure. Test results have shown that the addition of Sasobit® increased the stiffness of both binders and changed PG grade by one unit up (6 °C PG grade). Also, Sasobit® presented better rutting resistance in modified and unmodified binders than Advera®, while both WMA additives decreased the fatigue cracking resistance. Multiple Stress Creep Recovery (MSCR) test was also conducted on both unaged and RTFO aged binders. Modified binder

M. Sadeq (✉)
Centre for Engineering Sustainability, University of Liverpool, Liverpool, UK
e-mail: mohammed.sadeq@liverpool.ac.uk; mohammed.sadeq@qatar.tamu.edu

M. Sadeq · E. Masad
Mechanical Engineering Program, Texas A&M University at Qatar, Doha, Qatar
e-mail: eyad.masad@qatar.tamu.edu

H. Al-Khalid
Centre for Engineering Sustainability, School of Engineering, University of Liverpool, Liverpool, UK
e-mail: khalid@liverpool.ac.uk

O. Sirin
Department of Civil and Architectural Engineering, College of Engineering, Qatar University, Doha, Qatar
e-mail: okansirin@qu.edu.qa

D. Little
Zachry Department of Civil Engineering, Texas A&M University, College Station, TX, USA
e-mail: d-little@tamu.edu



F. Canestrari and M.N. Partl (eds.), *8th RILEM International Symposium on Testing and Characterization of Sustainable and Innovative Bituminous Materials*, RILEM Bookseries 11, DOI 10.1007/978-94-017-7342-3_11

with Sasobit® and Advera® exhibited the same performance of the original binder after complete short-term ageing. However, Sasobit® increased the potential of rutting resistance in the unmodified binder more than Advera® did. The viscosity measurements revealed that adding Sasobit® to modified or unmodified binders lowered the viscosity more than Advera® did. These measures were considered as preliminary data required for further studies on the effect of WMA additives on the resistance of bituminous binders to fatigue cracking.

**Keywords** WMA · Sasobit · Advera · DSR · Ageing · RTFO · PAV · RV

## 1 Introduction

Warm Mix Asphalt (WMA) technology was introduced by different European countries in 1995 and has since attracted the attention of practitioners and researchers. Numerous international organisations started producing WMA additives using different mechanisms. These additives were mixed with bituminous binders to reduce mixing and compaction temperatures of asphalt mixtures. Advantages of using WMA additives went further by lessening the fuel consumption and smoke emission during construction. These advantages made this technology an eco-friendly product and encouraged researchers to study the additives influence on pavement performance.

Warm mix asphalt (WMA) is a technology that allows a significant reduction in the mixing and compaction temperatures compared to the temperature used in hot-mix asphalt (HMA) production. Whilst this reduction should not jeopardise the performance characteristics of the asphalt, it should lower the plant's fuel consumption by 10–35 %. This reduction favourably impacts the economic appraisal of their adoption (Hurley and Prowell 2006). In addition, earlier research revealed that harmful vaporous emissions may also be decreased by 15–70 % when using WMA (D'Angelo et al. 2008). Reduction would help in attaining healthier and faster paving.

Different manufacturing approaches were adopted in the production of current WMA additives, such as an organic (wax), chemical and foaming varieties. Typically, WMA additives are introduced in the mixing phase, which alters the characteristic of the conventional HMA through binder viscosity reduction. This chemical alteration process promotes an adequate binder coating over the aggregates, thereby improving the mixture workability and compaction at lower temperatures. This study was conducted to evaluate the ageing effect on the rheological properties of bituminous binders mixed with WMA additives.

Using the technology of WMA additives with asphalt binders can be done in two ways. Additives can be mixed with the binder at the conventional temperature as

HMA, which would improve bitumen/aggregate coating and rutting resistance. Alternatively, mixing the additives with the binder at lower temperature, which will provide most of the WMA benefits by lowering the smoke emission and fuel consumption for a better paving practice. In addition, it will reduce the effect of ageing on the binder with using lower mixing temperature.

## 2 Objectives of the Study

The main objectives of this study are as follows:

- Evaluate the rheological properties of different WMA binders at high and intermediate temperatures.
- Assess the effect of different ageing processes on WMA rutting and fatigue behaviour.

The objectives are achieved by conducting rheological tests on binders mixed with WMA additives. Dynamic Shear Rheometer (DSR) and Rotational Viscometer (RV) were used to perform various tests on binders over a wide temperature range. Rolling Thin Film Oven (RTFO) and the Pressurized Ageing Vessel (PAV) procedures were used for simulating short and long-term aging of binders, respectively.

## 3 Testing Materials

### *3.1 Asphalt Binder*

Bitumen is imported to Qatar for asphalt pavements from Kingdom of Bahrain. Bitumen arrives as unmodified 60/70 Pen binder and then local companies modify it to produce mostly modified PG 76-22 asphalt which is distributed to contractors in Qatar for constructing of new roads. Unmodified 60/70 Pen binder still in use for construction of local roads and lower pavement layers.

### *3.2 Advera*

Advera® is aluminosilicate specialty zeolite free flowing white to grey powder (100 % passing the 0.075 mm (No. 200) sieve) produced by PQ Corporation in the US. As shown in Fig. 1a such particle size would advantage the uniform destitution of the particles within the asphalt mix. The manufacturer claims that adding Advera® by 0.25 % of the asphalt mix (4.8–5.0 % by weight of the binder) can lower

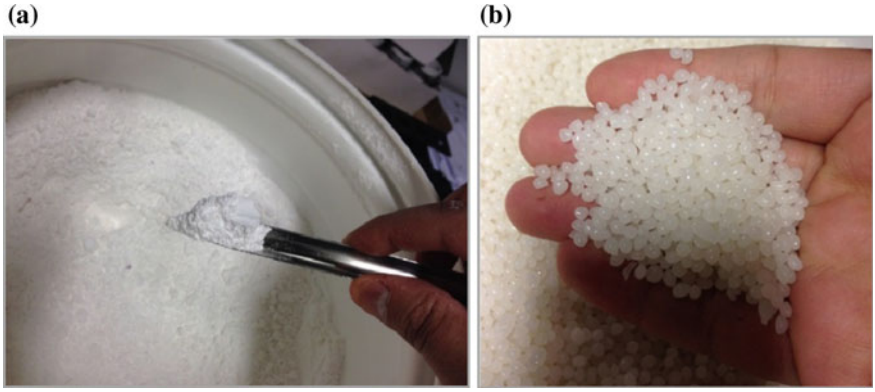


**Fig. 1** **a** Advera® WMA additive acquired from PQ Corporation. **b** Sasobit® WMA additive acquired from Sasol Company

the bitumen production temperature by 20–30 °C. Adding Advera® would never change the design of asphalt mix. Advera® contains about 21 % of entrapped water in particles crystalline structure which starts to emit at temperature over 100 °C. The emitted water causes a sustained, time-release foaming of the asphalt binder. The foaming process temporarily increases the workability and enhances aggregate coating. Advera® is an inorganic material that does not change the performance grade of the asphalt binder (PQ Corporation 2014).

## *3.3 Sasobit*

Sasobit® is a fine crystalline long chain aliphatic hydrocarbon manufactured by Sasol Wax in South Africa. It is manufactured from natural gas using the Fisher Tropsch process of polymerization. Sasobit® is available in three solid forms; a 5-mm diameter prill, 1-mm diameter prill, or 3-mm chips flaked form. Sasobit® is used to reduce the viscosity of the asphalt binder and improve the flow. The manufacturer claims that when Sasobit® is in a liquid form, the aggregate moves more freely in the binder, while when it cools down, it forms an uniform linked structure in the binder. Also, the manufacturer recommends the dosage rate of the Sasobit® to be between 0.8 % up to maximum 4.0 % of the binder weight. It can be introduced into the asphalt binder or directly to the asphalt mixture. Once blended, the manufacturer states that Sasobit lower the mixing and handling temperatures by 10–30 °C (Sasol Wax 2014). In this study, the 5-mm diameter prill, shown in Fig. 1b, is used at dosage rate of 2 % of the bitumen weight based on the recommendation of the supplier.

## 4 Experimental Work

In this study, bitumen samples with and without WMA additives were tested in the Dynamic Shear Rheometer (DSR) and rotational viscometer (RV). Samples were subjected to different ageing processes and tested only at low and intermediate temperatures. Three replicates were tested as per the experimental matrix shown in Fig. 2.

Short-term ageing was performed with two different ageing periods; 45 and 85 min. The temperature used with both periods was the standard conventional ageing temperature (163 °C). The conventional temperature was used to evaluate the effect of ageing time on the asphalt binder with different WMA technologies. On the other hand, long-term ageing process was performed by using the pressurized ageing vessel (PAV) system on RTFO-aged binders. This system is set on a pressure of 2.10 MPa inside the vessel for 20 h at 110 °C (AASHTO - T 240 2009).

Using Dynamic Shear Rheometer (from TA Instruments, model HR-1), two types of tests were conducted. The oscillation strain test measures the rheological properties of the asphalt binder. Then, the Multiple Stress Creep Recovery test (MSCR) measures the permanent deformation of asphalt binder under cyclically repeated shear loading. Both tests were prepared by following the AASHTO Standards T-315 and TP-70, respectively (AASHTO - T 315 2009; AASHTO - TP 70 2009). The oscillation strain test was performed using the strain controlled feature at 12 % strain for the unaged binder, 10 % strain for RTFO aged binder, and 1 % for PAV aged binder. The test was performed using two plates' sizes; 25-mm with 1-mm gap for unaged and RTFO aged binder, and 8-mm with 2-mm gap for the PAV aged binder (Zelelew et al. 2013). Three replicate samples were tested using different ageing processes. The bitumen was aged for 45 min with the RTFO ageing, aged for 85 min with the RTFO ageing, and aged for 20 h with PAV system. The test was conducted at PG grade temperatures to assess the performance grading of asphalt binders based on AASHTO M-320 (AASHTO - M 320 2009). Modified PG 76-22 binders were tested at 76 °C for rutting factor and at 31 °C for fatigue factor, while unmodified 60/70 pen binders were tested at 64 °C for rutting factor and at 25 °C for fatigue factor. The frequency used in the test was 1.59 Hz (10 rad/s).

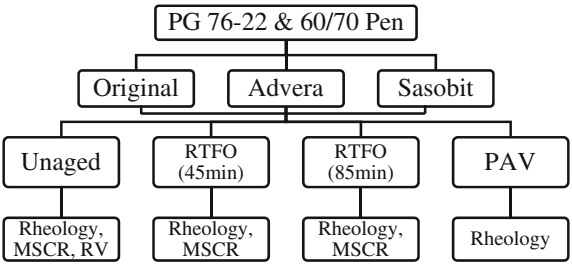


**Fig. 2** Experimental matrix for modified and unmodified binder mixed with WMA additives

MSCR test was performed using DSR at two different stress levels, 0.1 and 3.2 kPa. The stress was applied on the sample for 1.0 s and then released for 9.0 s for relaxation. AASHTO - TP 70 (2009) assigned the MSCR test for the RTFO residue. However, in this study, the test was executed on short-term aged and unaged samples to consider the effect of the ageing on the bitumen with different WMA Additives (Arega et al. 2013).

Viscosity measurements were made by using two methods. The first one was by applying different rotational speeds on the spindle at constant temperature, and then by applying the same rotational speed at different temperatures. The first analysis was conducted to check if adding WMA additives would affect the Newtonian behaviours of asphalt binder. The viscosity was measured at 20, 40, 60, 80, and 100 rpm at 135 °C. While the second measurement was performed to predict the mixing and compaction temperature for each binder type with different WMA additives (Kim et al. 2010).

## 5 Results and Discussion

### *5.1 Strain Oscillation Test Results*

The rutting factors (G*/sin(δ)) and fatigue factors (G* · sin(δ)) were calculated based on the Dynamic Shear Rheometer (DSR) measurements and the results are presented in Figs. 3 and 4.

It can be noticed from the results that the trends of both binder types are similar. Adding Sasobit® to both binders leads to higher complex modulus (G*) and lower phase angle (δ). The complex modulus (G*) increased with ageing but the phase angle (δ) did not. This increment led the binder to have a higher rutting factor (G*/sin(δ)). Rutting factor of the binder after adding Sasobit® increased at the test temperature (76 °C) which showed that the binder with Sasobit® can pass the performance grade specification of PG 82. Similarly with 60/70 Pen when adding Sasobit®, the binder can pass the performance grade specification of PG 70.

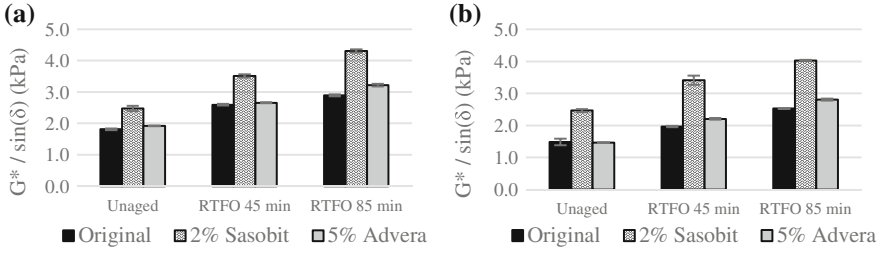


**Fig. 3** Rutting factor (G*/sin(δ)) for **a** modified PG 76-22 binder at 76 °C and **b** unmodified 60/70 Pen binder at 64 °C mixed with WMA additives at different ageing processes

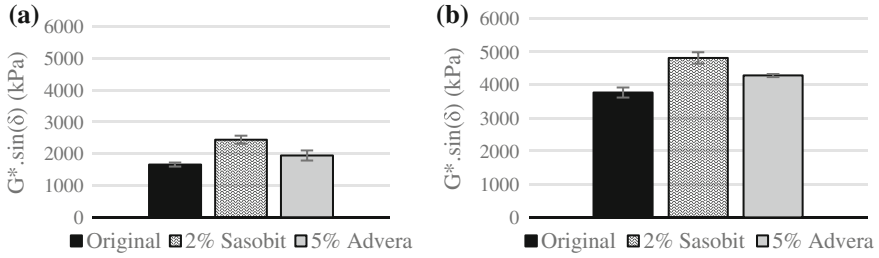


**Fig. 4** Fatigue Factor (G* · sin(δ)) for **a** modified PG 76-22 binder at 31 °C and **b** unmodified 60/70 Pen binder at 25 °C with different WMA additives and aged by PAV system for long-term ageing

The effect of adding Advera® to both asphalt binder types was insignificant. The complex modulus and phase angle values remained almost constant before and after adding 5 % of Advera®. Rutting factor remained the same at the early stages of the binder, but it showed a slight difference after full short-term ageing. It is also noticeable when testing the binder at lower temperature to check the fatigue factor while Advera® is slightly affecting the asphalt binder compared to Sasobit®.

## *5.2 Multiple Stress Creep Recovery (MSCR) Test Results*

The MSCR test was performed on RTFO aged binders in order to explore the rutting resistance of the asphalt binder at early stages. Using the MSCR test on an original binder was meant to show the effect of WMA additives on the binder performance before and after the construction. Figure 5 shows the percentage of recovery (R) and non-recoverable creep compliance ($J_{nr}$) at both stress levels and in different ageing processes for each modified bitumen.

It can be noticed from Fig. 5a that the difference in percentage of recovery at 0.1 kPa stress level changed slightly with different ageing and WMA additives. Comparison between binders at a low-stress level is insufficient. However, in the case of high-stress level (3.2 kPa), the percent of recovery is getting higher with more ageing. After complete short-term ageing, Advera® and Sasobit® showed roughly similar percentage of recovery to the unaged binder. Results showed that mixing WMA additives with asphalt binders would perform similarly against rutting after the binder fully aged. Equally, the non-recoverable creep compliance ($J_{nr}$) values were almost identical after the complete short-term ageing. Experiments on unmodified 60/70 Pen binder shown in Fig. 6 indicate that the effect of Sasobit® on percentage of recovery and non-recoverable creep compliance was more sufficient than the modified binder. Sasobit® provides the binder more percent recovery which was not presented in the case of original binder. The effect of Sasobit® on the percentage of recovery appears in both high and low-stress levels. On the other hand, adding Advera® to the 60/70 Pen did not improve the performance of the

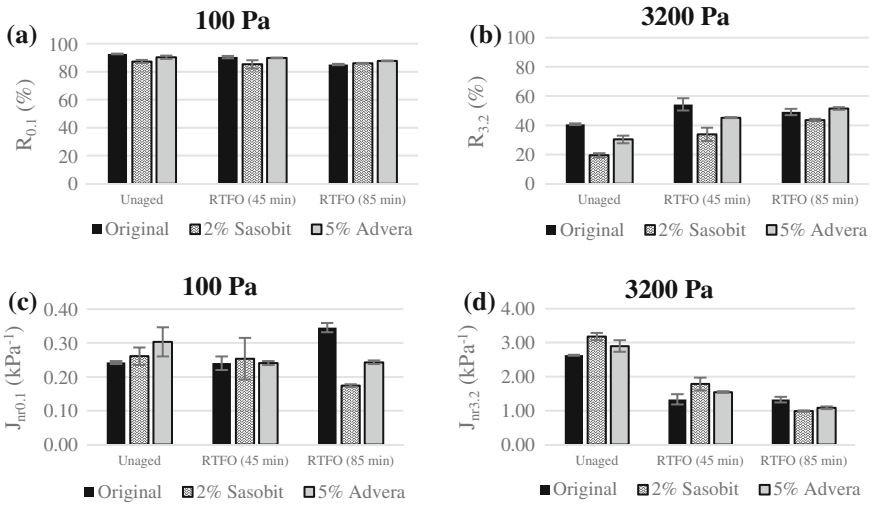


**Fig. 5** MSCR results for modified PG 76-22 binder mixed with WMA additives at different ageing processes: **a** $R_{0.1}$ (%); **b** $R_{3.2}$ (%); **c** $J_{nr0.1}$ (kPa$^{-1}$); **d** $J_{nr3.2}$(kPa$^{-1}$)

binder, inversely, it lowered the recovery over complete short-term ageing. In addition, adding Sasobit® significantly lowered the unrecovered creep compliance of asphalt binder 60/70 Pen over ageing at both stress levels, while Advera® effect was considered to be very little.

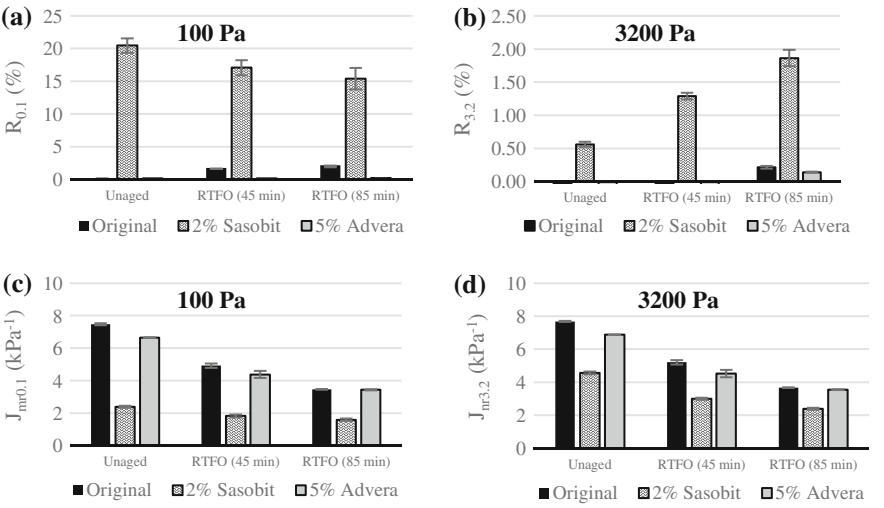


**Fig. 6** MSCR results for unmodified 60/70 Pen binder mixed with WMA additives at different ageing processes: **a** $R_{0.1}$ (%); **b** $R_{3.2}$ (%); **c** $J_{nr0.1}$ (kPa$^{-1}$); **d** $J_{nr3.2}$(kPa$^{-1}$)

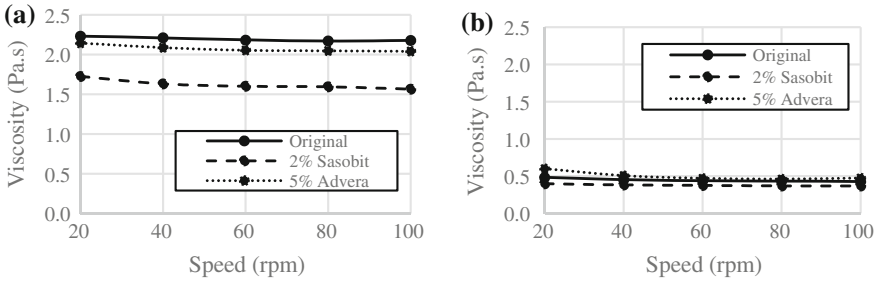


**Fig. 7** Viscosity measurement at different rotational speed for **a** modified PG 76-22 asphalt binder and **b** unmodified 60/70 Pen asphalt binder mixed with WMA additives

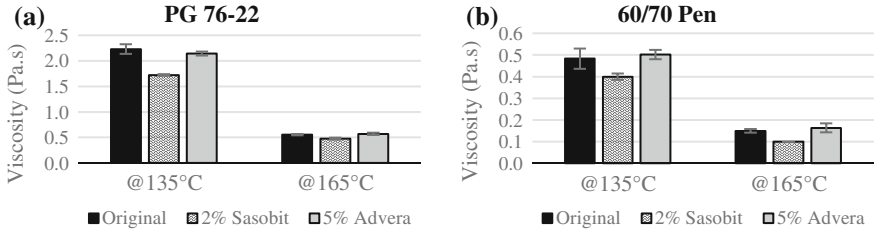


**Fig. 8** Viscosity measurements for **a** PG 76-22 **b** 60/70 Pen asphalt binders mixed with WMA additives

### *5.3 Viscosity Measurements*

Asphalt binders were tested using the Rotational Viscometer at 135 °C with different WMA additives using different rotational speeds (20, 40, 60, 80 and 100 rpm). As shown in Fig. 7, it can be noticed that asphalt binders kept the Newtonian behaviour with various WMA additives.

However, adding WMA additives had different effects on asphalt binders in terms of viscosity (Fig. 8). The addition of Sasobit® to modified PG 76-22 binder had higher effect than adding Advera®. Sasobit® lowered the viscosity of the asphalt binder at mixing and compaction temperatures. Contrariwise, Adding Advera® had minor reduction in viscosity in both temperatures (135 and 165 °C).

## 6 Summary of Findings

This study was conducted to evaluate the properties of asphalt binders incorporating warm-mix asphalt (WMA) additives under different ageing processes. These additives are used in order to reduce mixture preparation temperature and achieve

greener construction. Temperature reduction helps in lowering the fuel consumption in asphalt production plants' and reducing smoke emissions that increase the efficiency of the construction practice. Contractors in the State of Qatar are using unmodified 60/70 Pen binder in constructing the local roads and lower layers of asphalt pavements. Local companies in Qatar modify the asphalt binder with polymers in order to produce modified PG 76-22 binder. Modified binder is used in constructing the first layers in asphalt pavements in Qatar in order to offer resistance for rutting and fatigue cracking. In this study, PG 76-22 and 60/70 Pen binders were tested with two WMA additives: Sasobit® and Advera® to evaluate rheological properties of asphalt binders. Sasobit® increased the rutting factor and enhanced the PG grade of the binder by one unit (6 °C in PG grading) when added at 2 % of the weight of asphalt binder. This stiffness increment also affected the fatigue resistance factor, which increases the possibility of having fatigue cracking at low temperature. Sasobit® gained asphalt binder stiffness in all ageing processes. Also, the viscosity is reduced with using Sasobit® at the conventional mixing and compaction temperatures.

Advera®, mixed at dosage rate of 5 % of binder weight, has limited effect on asphalt binder. It had a minor influence on the performance of bitumen against rutting resistance. However, Advera increased the potential of fatigue cracking at low temperature.

Multiple Stress Creep Recovery (MSCR) test examined the viscoelastic behaviour of asphalt binder before and after adding WMA additives. Modified PG 76-22 asphalt binder mixed with Sasobit® performed similarly to original binder after full short-term ageing. Results indicate that Sasobit® would affect the fresh asphalt binder only in lowering the mixing and compaction temperatures, but would perform the same as original binder against rutting. However, when Sasobit® was mixed with unmodified 60/70 pen binder, it increased the potential of recovering the strain eight times higher than the original binder. Consequently, Sasobit® decreased the non-recoverable creep compliance which would lead to lower rutting of asphalt pavement. Advera® effect on permanent deformation of modified and unmodified asphalt binder was insignificant and ignorable.

Viscosity measurements showed that the valuable reduction in viscosity would occur while mixing Sasobit® with modified or unmodified asphalt binder while the effect of Advera® was negligible with both binders.

## 7 Future Work

This study will be continued to work on evaluating the fatigue cracking resistance of warm-mix asphalt. In addition, climate of Qatar will be simulated using the weathering machine to study the effect of ageing on WMA.

**Acknowledgments** This work was made possible by the NPRP award [NPRP 5-506-2-203] from the Qatar National Research Fund (a member of Qatar Foundation). The statements made herein are solely the responsibility of the authors.

## References

AASHTO - M 320, 2009. Performance-Graded Asphalt Binder. In American Association of State Highway and Transportation Officials.

AASHTO - T 240, 2009. Effect of Heat and Air on a Moving Film of Asphalt Binder (Rolling Thin-Film Oven Test). In American Association of State Highway and Transportation Officials.

AASHTO - T 315, 2009. Determining the Rheological Properties of Asphalt Binder Using a Dynamic Shear Rheometer (DSR). In American Association of State Highway and Transportation Officials.

AASHTO - TP 70, 2009. Multiple Stress Creep Recovery (MSCR) Test of Asphalt Binder Using a Dynamic Shear Rheometer (DSR). In American Association of State Highway and Transportation Officials.

Arega, Z. a. Z., Bhasin, A. & Kesel, T.D.T., 2013. Influence of extended aging on the properties of asphalt composites produced using hot and warm mix methods. *Construction and Building Materials*, 44, pp.168–174. Available at: http://www.sciencedirect.com/science/article/pii/S0950061813002432 [Accessed June 21, 2013].

D'Angelo, J., Harm, E. & Bartoszek, J., 2008. Warm-mix asphalt: European practice. Available at: http://trid.trb.org/view.aspx?id=859207 [Accessed October 22, 2013].

Hurley, G. & Prowell, B., 2006. Evaluation of potential processes for use in warm mix asphalt. *Journal of the Association of Asphalt Paving Technologists*. Available at: http://www.warmmix.net/submissions/10_20071127_Evaluation_of_Potential_Processes.pdf [Accessed September 12, 2013].

Kim, H., Lee, S.-J. & Amirkhanian, S.N., 2010. Effects of warm mix asphalt additives on performance properties of polymer modified asphalt binders. *Canadian Journal of Civil Engineering*, 37(1), pp.17–24. Available at: http://www.nrcresearchpress.com/doi/abs/10.1139/L09-118 [Accessed May 23, 2014].

PQ Corporation, 2014. Advera Warm mix asphalt. Available at: http://www.adverawma.com/wma.html [Accessed May 18, 2014].

Sasol Wax, 2014. Sasobit - Sasolwax US. Available at: http://www.sasolwax.us.com/ [Accessed May 18, 2014].

Zelelew, H. et al., 2013. Laboratory evaluation of the mechanical properties of plant-produced warm-mix asphalt mixtures. *Road Materials and Pavement Design*, 14(1), pp.49–70. Available at: http://www.tandfonline.com/doi/abs/10.1080/14680629.2012.735799 [Accessed April 28, 2014].

# Rheological Characterization of Asphalt Binders and Mixtures Modified with Carbon Nanotubes

**Haopeng Wang, Jun Yang and Minghui Gong**

**Abstract** Nanotechnology has the potential to create many new materials and devices with wide-ranging purposes. Carbon nanotubes (CNTs) have been used in numerous applications to improve the properties of various materials. The objective of this study was to investigate and evaluate the rheological characteristics of asphalt binders and mixtures containing carbon nanotubes. The experimental design for this study included three binder sources, base asphalt, styrene-butadiene-styrene (SBS) modified asphalt, and CNTs modified asphalt (1 % weight of the base asphalt). Various binder test including penetration, ductility, softening point, dynamic shear rheometer (DSR) and beam bending rheometer tests were utilized to determine rheological properties of three asphalt binders. Dynamic modulus test was also conducted to testify the results obtain from binders at mixture scale. The results indicate that the CNTs modified asphalt exhibit improved viscoelastic response and resistance to rutting. Moreover, the aging resistance of base binder has a substantial increase due to the addition of CNTs. However, the low-temperature performance of CNTs modified asphalt was not encouraging. The stiffing effect of CNTs is also verified in asphalt mixture in terms of dynamic modulus.

**Keywords** Asphalt · Carbon nanotubes · Rheology · Viscoelastic · Rutting · Fatigue

## 1 Introduction

The application of nanotechnology in various field is receiving widespread attention. Nanotechnology deals with the creation and use of functional materials, devices and systems with novel properties and functions that are achieved through the control of matter at the atomic and molecular level (Goldberg et al. 2007). Nano-structured materials hold the potential to redefine the field of traditional

H. Wang (✉) · J. Yang · M. Gong
School of Transportation, Southeast University, Nanjing 210096, People's Republic of China
e-mail: crazywhp@seu.edu.cn



F. Canestrari and M.N. Partl (eds.), *8th RILEM International Symposium on Testing and Characterization of Sustainable and Innovative Bituminous Materials*, RILEM Bookseries 11, DOI 10.1007/978-94-017-7342-3_12

materials in terms of both performance and potential applications (Kuchibhatla et al. 2007). Many researches have recently introduced nanomaterial in pavement engineering, especially in the field of asphalt modification (Buehler and Ackbarow 2007; Sobolev and Gutierrez 2005; Steyn 2009).

Carbon nanotubes (CNTs) are considered one of the most promising nano-reinforced materials (Kuchibhatla et al. 2007). CNTs can be structurally approximated to "rolled-up" sheets of graphite. The combination of high aspect ratio, small size, low density, and unique physical and chemical properties makes them perfect candidates for reinforcement in multifunctional and smart cement-based materials (Sanchez and Sobolev 2010). Researchers and engineers have been challenged to explore whether the optimum physical characteristics of CNTs can exhibit the best performance as an asphalt binder modifier. Santagata et al. (2012) indicated that when added in a sufficiently high dosage, CNTs could lead to a significant impact on the rheological properties of asphalt binders. Moreover, when compared with other nano-sized additives such as nanoclays, CNTs were found to provide higher anti-rutting resistance when added to asphalt binders (Santagata et al. 2013). The dispersion of CNTs in the base asphalt binders is a big challenge for developing nanocomposite. Ziari et al. (2012) investigated several mixing methods, including mechanical mixing, high shear mixing and ultrasonic mixing. The study recommended that the ultrasonic mixer could make a homogeneous mixture and separate nano particles from each other. In addition, Santagata et al. (2014) showed that the use of ultrasonic waves combined with shear mixing seemed to be necessary in order to reach a good dispersion of the nano particles in the asphalt matrix. In their research, encouraging results on the possible fatigue resistance enhancements, which may be provided by CNTs, used as additives in asphalt for road paving applications were also obtained. Most of the aforementioned studies have been limited to asphalt binders. However, the assessment of these innovative materials to the industrial scale, like its use in hot mix asphalt (HMA) mixtures and pavement construction, was not involved. In addition, the relationship and differences between the CNTs modified binders and mixtures have not yet been investigated. This has raised the need for more research utilizing CNTs to improve the rheological and engineering characteristics of asphalt binders and mixtures to develop some guidelines to help obtain an optimum balance in the use of these materials.

## 2 Objective

The objective of this study was to investigate the impact of CNTs modification on the rheological properties of both asphalt binders and mixtures. Specific objectives are as follows:

1. Experiments were carried out to evaluate properties of the binder such as penetration, ductility, softening point, complex modulus, phase angle and creep stiffness and m-value at low temperature.

2. The aging resistance of binders was also investigated by comparing the rheological properties of binders before and after aging.
3. Dynamic modulus test was conducted to evaluate the viscoelastic properties of different asphalt mixture.

# 3 Experimental Investigation

## *3.1 Materials and Sample Preparation*

Three types of asphalt binder, including conventional base binder namely 70# (PG 64-22), SBS modified binder (PG 76-22), and Carbon Nano-Tubes (CNTs) modified binder (70# base binder was taken as the virgin binder.) were investigated in this study.

There are two types of carbon nanotubes: single-walled nanotubes (SWNTs) and multi-walled nanotubes (MWNTs), respectively. SWNTs only have one wall that constitutes a tube, whereas MWNTs are made up of multiple walls that can slide against each other. The used CNTs were commercially available MWNTs produced with the catalyzed chemical vapor deposition technique, which are considered competent for modifying asphalt and cheaper than SWNTs. Main characteristics of CNTs are listed in Table 1. Due to their peculiar physical and chemical properties, their average cost is approximately 20–30 times than that of elastomeric polymers usually used for asphalt modification. According to previous researches and considering the cost effectiveness, the dosage of CNTs was 1 % by weight of the base binder.

A simple shear mixing technique was employed to incorporate CNTs into the base asphalt not only because it is very convenient in laboratory operations, but also because it has the potential of being easily transferred to the industrial scale in hot mix asphalt plants. Following preliminary attempts in which different mixing rates and times were considered, the final mixing protocol adopted in this study was mixing the asphalt-CNTs blends at a speed of 3000 rpm for a total time of 30 min at the constant temperature of 165 °C. Part of each asphalt binder were put into a rolling thin film oven (RTFO) for a short-term aging procedure (85 min and 163 °C) in accordance with AASHTO T240. The aged residues were used for further rheological tests.

Local basalt aggregates and limestone fillers were used in this study. Aggregate gradation AC-13 as shown in Table 2 was designed in accordance with Marshall Method. Its optimum asphalt content is 4.85 %, air void is 3.6 %, voids in mineral

**Table 1** Main characteristics of used CNTs

| Diameter (nm) | Length (μm) | Carbon purity (%) | Specific surface area ($m^2/g$) |
|---|---|---|---|
| >50 | 10–20 | >90 | >40 |

**Table 2** Aggregate gradation

| Gradation | Sieve size, mm (% passing) | | | | | | | | | |
|---|---|---|---|---|---|---|---|---|---|---|
| AC-13 | 16 | 13.2 | 9.5 | 4.75 | 2.36 | 1.18 | 0.6 | 0.3 | 0.15 | 0.075 |
| | 100 | 96.0 | 75.7 | 52.0 | 38.6 | 25.8 | 16.8 | 11.2 | 8.9 | 6.9 |

aggregates are 13.84 %, and voids filled with asphalt are 74 %. Each mix was preheated in an oven, and samples were compacted with a Superpave Gyratory Compactor into a 150-mm-diameter mold to approximately 160 mm in height. Test specimens for both dynamic modulus test and flow number test were then coring from the center of the gyratory compacted samples into 100 mm in diameter by 150 mm in height.

## *3.2 Test Program*

### 3.2.1 Asphalt Binder Test

Various routine binder tests, including penetration test, softening point test and ductility test, were conducted to evaluate the basic properties of binders.

Viscosity of binders was determined using the Brookfield rotational viscometer following AASHTO D4402 at 135 and 175 °C. About 10 ml of heated asphalt binder was poured into the cylinder. The spindle was lowered into the binder and the assembly was allowed to reach an equilibrium test temperature. The test was run at 20 rpm and the viscosity readings in Pa s were recorded at 60 s.

The high temperature rheological properties of each binder were measured using a dynamic shear rheometer (DSR) in accordance with AASHTO T315. The binder was sandwiched between lower fixed plate and an upper oscillation plate. The gap between the two plates is maintained at 1 mm for higher temperature testing (>46 °C). Testing was conducted at various temperatures and frequencies to determine the complex shear modulus ($G^*$) and phase angle ($\delta$).

The low temperature rheological properties of each binder were measured using a beam bending rheometer (BBR) in accordance with AASHTO T 313. This method was designed to determine the flexural creep stiffness ($S$) or compliance of asphalt binders at 60 s and the slope of the stiffness curve (the $m$-value).

### 3.2.2 Asphalt Mixture Test

The dynamic modulus test for asphalt mixtures was conducted in accordance with AASHTO TP 79-10 using the IPC Asphalt Mixture Performance Tester (AMPT), also called Simple Performance Tester. Testing was conducted at four temperatures (14, 30, 45, 55 °C) and nine frequencies (25, 20, 10, 5, 2, 1, 0.5, 0.2 and 0.1 Hz).

# 4 Results and Discussions

## 4.1 Basic Properties

The basic properties of three types of asphalt binder are given in Table 3. The penetration value of CNTs modified asphalt is lower than base asphalt, indicating CNTs make the binder stiffer. Due to the addition of CNTs, softening point of asphalt has a slight increase whereas the low-temperature ductility is just the opposite. SBS modified asphalt has both superior high and low temperature performance, and its elastic deformation restorability is favorable. Comparing to SBS modified asphalt binder, the basic properties of asphalt-CNTs blends seem to fall in between basic and SBS modified binders.

## 4.2 Rotational Viscosity (η)

Viscosity provides a measure of the flow characteristics of asphalt binders. Binders must be sufficiently fluid at high temperatures so that they can be easily pumped and handled during production, storage and laying of asphalt mixtures for paving applications. Figure 1 synthesizes the results obtained from viscosity tests carried out on unaged asphalt binders. As expected, viscosity values of all binders decrease as temperature increases from 135 to 175 °C. Moreover, both viscosities of CNTs

**Table 3** Properties of asphalt binder

| Properties | 70# | SBS | CNTs |
|---|---|---|---|
| Penetration (25 °C, 100 g, 5 s, 0.1 mm) | 68 | 54 | 58 |
| Ductility (5 cm/min, 5 °C, cm) | 8.6 | 31.3 | 7.9 |
| Softening point (R&B, °C) | 48 | 78 | 50 |
| Density (15 °C, g/cm$^3$) | 1.032 | 1.031 | – |

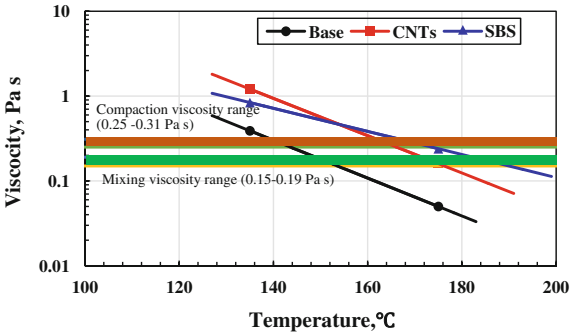


**Fig. 1** Viscosity-temperature curve of various asphalt binders

modified asphalt at 135 and 175 °C increase to three times as that of base asphalt. However, the viscosity of CNTs modified asphalt at 175 °C is lower than that of SBS modified asphalt. The viscosity-temperature curve indicates CNTs modified binder has a higher mixing and compaction temperatures than base binder, whereas lower than SBS modified binder. Nevertheless, the increase in viscosity maybe beneficial in improving resistance to permanent deformation. The reason might be that very high surface area of CNTs results in a strong interaction between asphalt binder and nanoparticles. It can be concluded from the slopes of different viscosity-temperature curves that the temperature susceptibility of CNT modified binders is similar to that of the base binder. However, SBS improves the temperature susceptibility.

## 4.3 Complex Modulus (G*) and Phase Angle (δ)

Performance grading (temperature sweep) tests for the three kinds of binders were carried out by dynamic shear rheometer at 10 rad/s to obtain complex modulus and phase angle at various temperatures, results are illustrated in Fig. 2. The figure shows a significant increase of rutting factor $G^*/\sin\delta$ for CNTs modified asphalt binder due to the addition of CNTs. It indicates that CNTs make base binder stiffer and improve the deformation resistance under shear loading. However, SBS modified asphalt is preferable in terms of $G^*/\sin\delta$. In addition, the phase angles of CNTs modified binder at various temperature slightly increase accompanied by an enhancement of elastic response, thus indicating a change in rheological behavior or the proportion of viscous and elastic component. These effects may be attributed to CNT reinforcement, which is believed to be produced by a network of nanotubes, formed within the binder matrix. As mentioned before, SBS modified binder has a superior elastic deformation restorability, which resulting in a significant change in the phase angle. It also implies SBS modified binder has a decent high and low temperature performance.

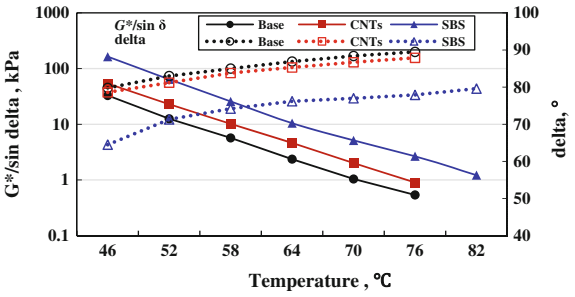


**Fig. 2** $G^*/\sin\delta$ and phase angle curves from DSR test

## 4.4 Effect of Short-Term Aging

The influences of TFOT aging on rheological properties of three binders are shown in Table 4. $G^*$, δ and $G^*/\sin\delta$ at 64 °C are selected to characterize the high temperature performance of asphalt, while *S* and *m-value* at −12 °C are employed to evaluate the low temperature performance of asphalt. It is considered that asphalt with high $G^*$ and low δ has high elasticity and low viscosity. Lower creep stiffness and higher m-value of asphalt binder indicates a better low-temperature thermal cracking performance of paving mixtures.

Table 4 demonstrates clearly that the addition of CNTs would increase the elasticity and decrease the viscosity of the binder, which indicates a better high temperature performance. However, the higher S and lower m of unaged CNTs modified asphalt raise the concern of its low flexibility at low temperature. What's more, aged CNTs modified asphalt performs better than aged base asphalt in both high and low temperature performance. Comparing to aged SBS modified asphalt, it is interesting to find that aged CNTs modified asphalt has worse high temperature performance and better low temperature performance.

In general, RTFO aging would increase $G^*$ and decrease δ for all asphalts. However, the influence of aging on low temperature performance for base and modified asphalts are distinctly different. In order to evaluate hardening effects, the following aging index was introduced:

$$AI = \frac{(P_i)_A}{(P_i)_U} \tag{1}$$

where $(P_i)_A$ and $(P_i)_U$ are rheological parameters respectively obtained in aged and unaged conditions; $P_i$ can be $G^*$, δ, $G^*/\sin\delta$, S, and m-value.

AI values of different asphalt binders are depicted in Fig. 3. It can be seen that aging would induce a drastic degradation of low temperature performance for base asphalt. However, S and m of both CNTs and SBS modified asphalt almost remain unchanged after aging. It is proved again that CNTs modified asphalt owns a better anti-aging performance because its aging indexes of all the parameters are closer to 1 (Virgin Line) than that of base asphalt.

**Table 4** Rheological properties of asphalt binders before and after aging

| Parameters | Base asphalt | | CNTs modified asphalt | | SBS modified asphalt | |
|---|---|---|---|---|---|---|
| | Unaged | Aged | Unaged | Aged | Unaged | Aged |
| $G^*$(64 °C, kPa) | 2.4 | 6.4 | 3.7 | 7.3 | 7.1 | 11.5 |
| δ(64 °C, degree) | 86.9 | 83.5 | 85.4 | 83.9 | 62.8 | 63.7 |
| $G^*/\sin\delta$(kPa) | 2.4 | 6.4 | 3.73 | 7.3 | 8.0 | 12.8 |
| *S*(−12 °C, MPa) | 82.6 | 146 | 112 | 118 | 137 | 175 |
| *m-value*(−12 °C) | 0.443 | 0.376 | 0.415 | 0.402 | 0.386 | 0.354 |

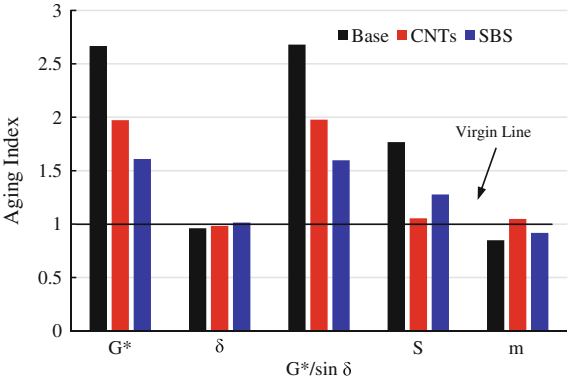


**Fig. 3** Aging indexes of different asphalt binders

## 4.5 *Dynamic Modulus (E*) Test*

Dynamic modulus ($E^*$) is one of the key elements of a mechanistic-empirical based flexible pavement design procedure. It is used to characterize the viscoelastic properties of asphalt mixture and determine the stress-strain response of a pavement at different loading conditions.

The properties of asphalt binder are directly related to mechanical performance of the mixture. Three different asphalt binders (base binder, CNTs modified, and SBS modified binder) were investigated in this study to evaluate the effect of binder type on $E^*$ master curve. According to the Time-Temperature Superposition (TTS) principle, high and low temperatures correspond to low and high frequencies, respectively.

As shown in Fig. 4, $E^*$ master curve of SBS modified asphalt mixture is higher compared to CNTs modified and base asphalt mixtures at higher temperatures. As expected, SBS modified asphalt binder with higher PG can increase the high temperature performance (rutting resistance) significantly due to its polymer components. It is also observed that CNTs modified asphalt mixture $E^*$ master curve is

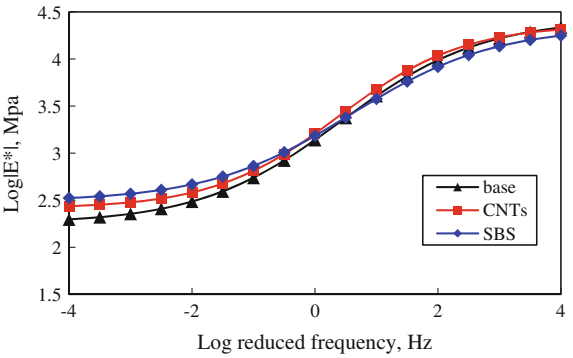


**Fig. 4** $|E^*|$ master curve of different asphalt mixtures

higher than both SBS modified and base binder at low temperatures. It is implied that CNTs may decrease the low temperature deformation flexibility, which is also confirmed from the BBR test result. Moreover, CNTs can benefit the high temperature performance compared to base asphalt, in spite of inferior to SBS. When temperature decreases continuously to lower, $E^*$ master curves are overlapped with no specific trend.

As shown in Fig. 4, asphalt type, especially the high-temperature performance has a significant influence on the dynamic modulus at high temperature and low frequency. However, the influence of the binder on the dynamic modulus at high $|E^*|$ level (low temperature and high frequency) is less prominent.

## 5 Conclusions and Recommendations

The experimental investigation described in this paper yielded encouraging results on the possible rheological properties enhancements that may be provided by CNTs used as additives in asphalt binder and mixture for road paving applications. The overall rheological properties of CNTs modified binder falls between in base binder and SBS modified binder, which are also testified by dynamic modulus test on asphalt mixtures. Based on the laboratory test results, the following specific important conclusions can be drawn:

1. The analysis of penetration, softening point, viscosity, complex modulus and phase angle shows that the added CNTs leads to a significant improvement in terms of stiffness and elasticity, thus providing beneficial effects on the potential rutting resistance.
2. Results from low-temperature ductility and BBR tests indicate negative influence on the low temperature thermal cracking resistance of unaged CNTs modified asphalt. However, aged CNTs modified asphalt exhibit different low temperature performance, which needs to be concerned in future study.
3. The anti-aging property of base binder increases significantly due to the addition of CNTs, which is also slightly superior to SBS modified binder.
4. The stiffing effect of CNTs is also verified in asphalt mixture in terms of dynamic modulus.

In conclusion, findings of this preliminary study indicate that modification of asphalt binders by means of multiwall carbon nanotubes (CNT) appears to be a very promising technique for the improvement of the field performance of bituminous mixtures for paving applications. Despite of the inspiring results from CNTs modified asphalt, several critical points need to be addressed for the use of such nano-structured binders in full-scale paving applications. First, the dispersion of CNTs in the base asphalt requires the development of a simple and reliable technique, which can produce homogeneous CNTs-asphalt blends and can also be applied at industrial scale with a safe, non-toxic process. The second point needs to be concerned is the low-temperature performance of CNTs modified asphalt.

Furthermore, the evaluation of cost-effectiveness should be subjected to analysis in order to gain extensive applications at the industrial scale. All mentioned above require an optimum design and balance of the properties of the used CNTs modified asphalt binder and mixture.

**Acknowledgement** The authors gratefully acknowledge the financial support of National Engineering Laboratory for Advanced Materials and the Specialized Research Fund for the Doctoral Program of Higher Education of China (Grant No. 20120092110053).

## References

Buehler, M. J., & Ackbarow, T. (2007). Fracture mechanics of protein materials. *Materials Today, 10*(9), 46-58

Goldberg, M., Langer, R., & Jia, X. Q. (2007). Nanostructured materials for applications in drug delivery and tissue engineering. *Journal of Biomaterials Science-Polymer Edition, 18*(3), 241-268. doi: Doi 10.1163/156856207779996931

Kuchibhatla, S. V. N. T., Karakoti, A. S., Bera, D., & Seal, S. (2007). One dimensional nanostructured materials. *Progress in Materials Science, 52*(5), 699-913

Sanchez, F., & Sobolev, K. (2010). Nanotechnology in concrete - A review. *Construction and Building Materials, 24*(11), 2060-2071

Santagata, E., Baglieri, O., Tsantilis, L., & Chiappinelli, G. (2013). Effects of Nano-sized Additives on the High-Temperature Properties of Bituminous Binders: A Comparative Study, 297-309. doi: 10.1007/978-94-007-6878-9_22

Santagata, E., Baglieri, O., Tsantilis, L., & Chiappinelli, G. (2014). Fatigue properties of bituminous binders reinforced with carbon nanotubes. *International Journal of Pavement Engineering, 16*(1), 80-90. doi: 10.1080/10298436.2014.923099

Santagata, E., Baglieri, O., Tsantilis, L., & Dalmazzo, D. (2012). Rheological Characterization of Bituminous Binders Modified with Carbon Nanotubes. *Procedia - Social and Behavioral Sciences, 53*, 546-555. doi: 10.1016/j.sbspro.2012.09.905

Sobolev, K., & Gutierrez, M. F. (2005). How nanotechnology can change the concrete world. *American Ceramic Society Bulletin, 84*(11), 16-19

Steyn, W. J. (2009). Potential Applications of Nanotechnology in Pavement Engineering. *Journal of Transportation Engineering-Asce, 135*(10), 764-772

Ziari, H., Rahimof, K., Fazilati, M., Goli, A., & Farahani, H. (2012). Evaluation of Different Conditions on the Mixing Bitumen and Carbon Nano-Tubes. *International Journal of Civil & Environmental Engineering, 12*, 53-59

# Part III
# Durability and Aging of Asphalt Pavements

# Bitumen/Aggregate Affinity—Rilem Round Robin Test on Rolling Bottle Test

**Laurent Porot, Jeroen Besamusca, Hilde Soenen, Alex Apeagyei, James Grenfell and Dariusz Sybilski**

**Abstract** Pavement durability is often linked with water damage either through raveling or loss of integrity, especially considering asphalt materials. A large number of tests exist to address the water sensitivity and affinity between aggregates and asphalt binder. In Rilem TC 237 SIB, TG1 looked at the common test methods used to evaluate the adhesion or affinity of asphalt binder to aggregate surfaces. One of the main purposes was to run a Round Robin Test to evaluate the reproducibility and repeatability of these test methods and to give recommendations for improvement. Three asphalt binders were selected, two unmodified and a polymer modified binder and four aggregate types with different mineralogy. This paper presents the first results obtained for the rolling bottle test. The influence of aggregate type is higher than that of the asphalt binder. While there are some potential trends after 24 h comparing the different combinations of aggregate and binder, there is still a lot of variability in the absolute results. The underlining reasons are not yet clearly identified.

L. Porot
Arizona Chemical, Garden City, USA
e-mail: laurent.porot@azchem.com

J. Besamusca
Kuwait Petroleum Research and Technology, Rozenburg, Netherlands
e-mail: j.besamusca@Q8.com

H. Soenen
Nynas NV, Stockholm, Sweden
e-mail: hilde.soenen@nynas.com

A. Apeagyei (✉) · J. Grenfell
University of Nottingham, Nottingham, UK
e-mail: alex.apeagyei@nottingham.ac.uk

J. Grenfell
e-mail: james.grenfell@nottingham.ac.uk

D. Sybilski
Road and Bridge Research Institute, Warsaw, Poland
e-mail: d.sybilski@ibdim.edu.pl



F. Canestrari and M.N. Partl (eds.), *8th RILEM International Symposium on Testing and Characterization of Sustainable and Innovative Bituminous Materials*, RILEM Bookseries 11, DOI 10.1007/978-94-017-7342-3_13

**Keywords** Asphalt · Affinity bitumen aggregate · Adhesion · Water sensitivity · Rolling bottle test

## 1 Introduction

One of the most important aspects of asphalt pavement deterioration is the ingress of water into the pavement which leads to loss of the material characteristics, even integrity with stripping loss. Thus the behavior of asphalt mixture under moisture conditions is one of the key parameters for specifications.

A large number of test methods are available to estimate the affinity between aggregates and asphalt binders. These test methods can be subdivided in different ways; a first distinction can be based on the presence or absence of water during the test procedure. If water is present, the evaluation is in fact referred to as a water sensitivity or moisture damage test. Another distinction can be based on the type of sample that is evaluated: the test sample can be an un-compacted, coated aggregate or a compacted asphalt core, or the individual components of asphalt binder and aggregate can be tested separately. Furthermore, test methods can also be based on the test results, whether a qualitative or a more quantitative evaluation is obtained.

The adhesion for road applications is a long search starting in the early 1900s and still continues to be widely investigated. The Riedel and Weber test (1933) was published in 1933 and used boiling water doped with increasing sodium carbonate concentration. An overview of different tests with pros and cons has been published by Mathews et al. (1965).

In the 1980s and 1990s during the Strategic Highway Research Program (SHRP) a huge amount of data was gathered, reviewed and published (Curtis 1990). Some reports combine molecular structures of bitumen components with aggregate components to identify possible adhesion and absorption (Jeon and Curtis 1992; Curtis et al. 1993; Lee et al. 1990; Tarrer and Wagh 1991). SHRP-A-398 (Hicks and Finn 1994) report showed proof of test methods with road experience. And several pieces of literature concluded that binder or aggregate alone was not valid for ranking, but that pairs are needed for ranking (Scholz et al. 1994; Terrel and Al-Swailmi 1994). Moisture sensitivity was identified as one of the most important parameters influencing the adhesion between aggregate and binder (Hicks 1991).

In the European committee on standardization, CEN, the technical committee on asphalt mixes TC227 and on binders TC336 combined their effort to identify the current test methods (Besamusca et al. 2012). They showed that most test methods are related to other aspects than adhesion resulting in a ranking of products not related to adhesion and the influence of aggregate is bigger than that of the bitumen source. Bagampadde (2006) also concluded that the influence of aggregate is more pronounced on adhesion properties than the influence of bitumen.

Considering the affinity between aggregates and asphalt binder, there are different test methods available. One of the most widely used tests in Europe is the rolling bottle test as described in the EN 12697-11 standard.

Jorgensen (2002) published round robin results of the Boiling water test and the Rolling bottle test. He showed that the Boiling water test was valid to identify bad combinations of binder and aggregate but the Rolling Bottle test could rank combinations. Several publications (Grönniger et al. 2010; Källén et al. 2013; Morgenstern et al. 2010; Renken et al. 2010; Grönniger 2008) showed that visual inspection is very subjective and is the main disadvantage of the method used.

In Rilem TC 237 SIB, TG1 the initial intention is to further understand the fundamental mechanism of water interaction, and to review the various test methods available, to identify which test is the most suitable. In these conditions, one main purpose is to evaluate the reproducibility and repeatability of common test methods used to evaluate the adhesion or affinity of asphalt binder to aggregate surfaces, and to give recommendations for improvement.

To support this evaluation a round robin test was conducted between 13 laboratories. Three asphalt binders have been selected, two unmodified binders from different sources and a polymer modified binder. Four aggregate types with different mineralogy have also been selected.

The test methods, considered in this study, included the rolling bottle test with 8 laboratories, the static test with 3 laboratories, and the boiling water stripping test with 5 laboratories and the bitumen bond strength test with 4 laboratories.

The main purpose of this paper is to present the results of a collaborative study that evaluated the reproducibility and repeatability of the rolling bottle test (EN 12697-11) by using an international round robin testing scheme composed of the eight laboratories located across Europe and the US.

The results of the other test methods will be subject of a later publication from the Rilem Task Group in order to supplement these outcomes.

## 2 Methodology

### *2.1 Materials*

The four aggregates (Basalt, Granite, Greywacke and Limestone) were all supplied by Aggregate Industries from different quarries located in the UK. These aggregate types were selected because of their different moisture sensitivity resulting from their diverse mineral compositions. The aggregate can be ranked according to their degree of stripping as slight (greywacke), slight to moderate (Limestone and Basalt) and severe (Granite) (Hicks 1991). Therefore, it was expected that a reliable laboratory test should be able to distinguish between the mixtures based on the selected aggregates. The aggregates were supplied as crushed with nominal aggregate size

**Table 1** Principal properties of the used asphalt binders

| | Unit | Standard | Bit 1 | Bit 2 | Bit 3 |
|---|---|---|---|---|---|
| Binder type | | | 50/70 | 50/70 | PmB 45/80-60 |
| Penetration value at 25 °C | 0.1 mm | EN 1426 | 43 | 47 | 42 |
| Softening point | °C | EN 1427 | 50.7 | 50.6 | 65.5 |

expected of 8/11 mm. Only material retained between the 8 and 11 mm sieve was used for conducting the rolling bottle tests.

A total of three asphalt binders from two different suppliers were used for coating the aggregates. Two unmodified 50/70 paving grade asphalt binders according to EN 12591 and one Polymer modified Bitumen graded as 45/80-60 according to the EN 14023. The properties of the three binders are reported in Table 1.

## *2.2 Test Method*

The rolling bottle test (RBT) was conducted in accordance with EN 12697-11 (bituminous mixtures—test methods for hot mix asphalt—part 11: determination of the affinity between aggregate and bitumen) with minor modifications based on each laboratory practice. It should be noted that the RBT is a subjective test in that affinity is expressed by visual estimation of the degree of bitumen coverage on un-compacted bitumen-coated mineral aggregate particles after the influence of mechanical stirring action in the presence of water.

To prepare samples for testing, dust-free aggregate samples weighing 510 g were dried in an oven at 110 ± 5 °C overnight to constant mass and then coated with about 17 g of hot bitumen (150 °C for the 50/70 pen and 180 °C for the 45/80 pen) binder in a mixing bowl. The aggregate–binder mixture was then cooled loose at room temperature. The mixed material was stored at ambient temperature between 12 h and 64 h before testing. Each of the test bottles was filled to about half their volume with cold (5 °C) deionized water, and about 150 g of the loose aggregate–mixture was placed in each bottle before topping the bottle with deionized water to the shoulder (about 2/3 full). The whole assembly was put in the bottle roller rotating at a speed of 60 rotations per minute for 6 h. The room temperature throughout the test has to be maintained between 15 and 25 °C. At the end of the 6 h period, the aggregate particles were emptied from the test bottle into a test bowl which was then filled with fresh, cold deionized water to a level just above the top of the surface of the particles. Subsequently, the test bowl was placed on a white surface. The purpose of adding fresh water was to allow for optimal visual determination of binder coverage on the aggregate particles. At least three replicates of each sample were tested.

At the end of the test, the degree of bitumen coverage of the aggregate particles was estimated by visual observation and recorded to the nearest 5 %. The degree of binder coverage was defined as the average proportion of the surface area of the aggregate particles that are covered with the binder, expressed as a percentage (= 100—the percentage of stripping). The degree of binder coverage on the aggregate particles was visually estimated by two experienced technicians independently. The procedure (i.e. rotation in the bottle roller and measuring of binder coverage) was repeated for three more cycles (24, 48 and 72 h) with the original fouled water replaced by fresh deionized water in the test bottle at the end of each cycle and the degree of binder coverage estimated as discussed earlier. For each rolling time (6, 24, 48 and 72 h), the mean value of each technician's recordings of the average degree of binder coverage obtained on the three part samples (three bottles) was calculated to the nearest 5 %, and the results were averaged to obtain the degree of binder coverage for a given mixture.

## 2.3 Participants

Within the whole Round Robin Test from TG 1, a total of 13 laboratories participated running different test methods addressing the affinity between aggregates and asphalt binder as listed in Table 2.

**Table 2** List of the laboratories participating in the RRT and their tests

| Institution | Country | Test method | Standard |
|---|---|---|---|
| IBDiM | Poland | Rolling bottle | EN 12697-11 (A) |
| Nynas | Belgium | Rolling bottle | EN 12697-11 (A) |
| Nottingham university | UK | Rolling bottle, static, boiling water stripping | EN 12697-11 (A, B, C) |
| | | Aggregate surface energy | DVS test |
| | | Wihelmy plate method | DCA test |
| | | Bitumen bond test | ASTM D 4541 |
| Repsol | Spain | Boiling water stripping | EN 12697-11 (C) |
| IFSTTAR | France | Rolling bottle | EN 12697-11 (A) |
| | | Bitumen bond test | ASTM D 4541 |
| | | Angle contact between rock and binder | Specific device drop method |
| Arizona chemical | The Netherlands | Rolling bottle | EN 12697-11 (A) |
| BRRC | Belgium | Boiling water stripping | EN 12697-11 (C) |
| University of Parma | Italy | Bitumen bond test | ASTM D 4541 |

(continued)

**Table 2** (continued)

| Institution | Country | Test method | Standard |
|---|---|---|---|
| University of Ancona | Italy | Bitumen bond test | ASTM D 4541 |
| Wisconsin University | US | Bitumen bond test | ASTM D 4541 |
| VTI | Sweden | Rolling bottle, static, boiling water stripping | EN 12697-11 (A, B, C) |
| TU Braunschweig | Germany | Rolling bottle | EN 12697-11 (A) |
| | | Contact angle measurement | German test method |
| University Roma La Sapienza | Italy | Rolling bottle, static, boiling water stripping | EN 12697-11 (A, B, C) |

# 3 Outcomes

A total of 8 laboratories conducted the rolling bottle test following the EN 12697-11 method A. The test was performed for 6 and 24 h, three laboratories have run the test to 48 and 72 h as well. For these conditions for the three different binders, four different aggregates and two time periods for eight laboratories and additional two time periods for three laboratories a total of 264 pieces of data were generated.

## *3.1 Test Conditions*

Each participant of this Round Robin Test used the same standard test method as described in EN 12697-11 method A. While the standard describes the different conditions to prepare the sample, to run the test and to interpret the results, there is still some freedom to conduct the test.

Aggregate size is either 6/10 or 8/11, most of laboratories used the 8/11 gradation, only one used the 6/10. In all cases, aggregates were washed before the test. One reported they removed the flat and elongated aggregates for Basalt.

As the aggregate density may be different due to the petrographic nature of the stone, the standard advises to adjust the quantity of binder with a density factor, however only 3 laboratories reported they did so.

The mixing temperature was in accordance with the one required by bitumen grade, 150 °C for the 50/70 pen grade bitumen and 180 °C for the PmB.

After mixing the coated aggregates have to be kept between 12 and 64 h at 20 °C, however the exact time was not specifically reported by the laboratories.

The speed of the rolling bottle is adjustable according to the grade of the binder; the softer the asphalt binder, the lower the speed. For the 50/70, only two laboratories used 40 rpm while the others used 60 rpm as recommended by the standard.

Finally the test temperature should be between 15 and 25 °C. As the test is done at room temperature, there was some variation between laboratories but the

temperature was reported between 17 and 23 °C with half of participants running the test at 21 °C.

## 4 Results

After each period of the test the aggregate coating was reported as the percentage of residual binder covering the aggregates, 100 % being fully coated and 0 % being not coated anymore. The graphs (Figs. 1 and 2) display the results after 6 h and 24 h for each aggregate and each asphalt binder. The error bars provide the variability of the results and are equal to minimum and maximum values from the eight laboratories.

After 6 h the scattering of the results between laboratories is high. Granite aggregates display the worst results with values between 25 and 75 %. Limestone aggregates display good results with limited variability, between 80 and 95 %. However it is not discriminant enough to clearly distinguish between Basalt and Greywacke with values between 50 and 100 %. When considering the different binders, the Polymer modified binder may display slightly better results, but it is still within the variability of the results between laboratories.

After 24 h the scattering of the results is still high but the outcomes become more discriminant between aggregates. The extreme results, bad results for Granite and good results for Limestone are more pronounced. Intermediate aggregates, Basalt and Greywacke have intermediate values with a high variation between 10 and 75 %. And again the Polymer modified binder may display better results but the variability overlaps that of the standard pen grade bitumen.

Other results after 48 and 72 h are also available but are mostly relevant for the aggregates which remained coated after the 24 h. However, as only 3 laboratories

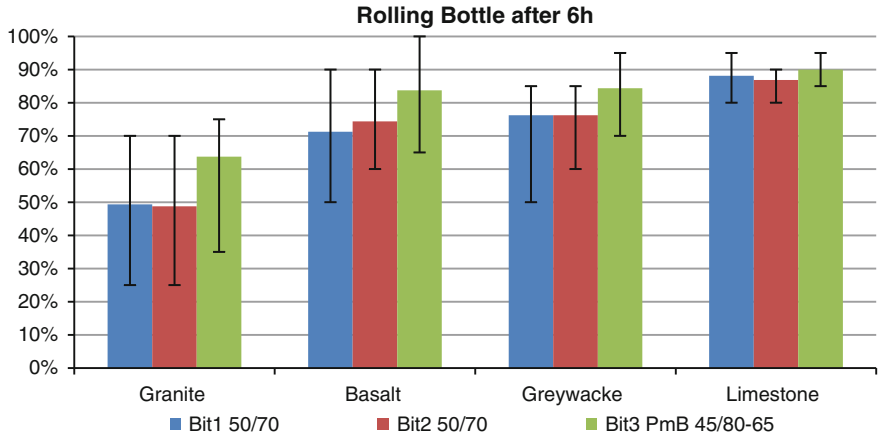


**Fig. 1** Results of the rolling bottle test after 6 h

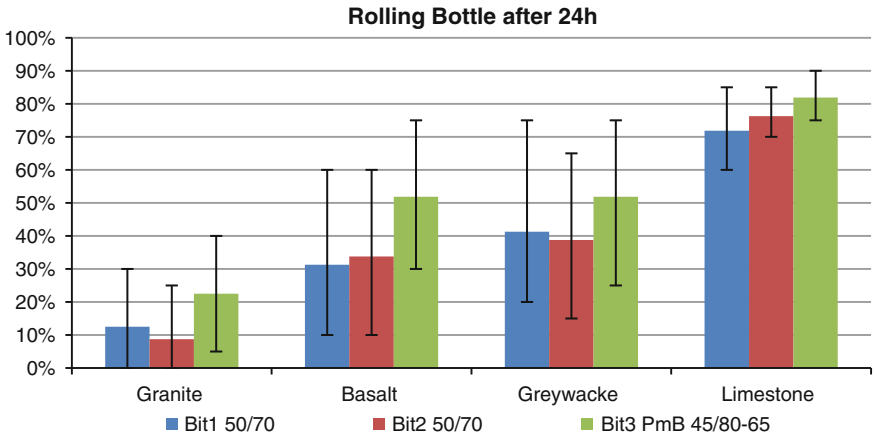


**Fig. 2** Results of the rolling bottle test after 24 h

conducted these extra time steps, the statistical analysis is not as relevant as for the standard duration.

## 5 Discussion

Based on the raw results, the first outcomes are:

- the results are more discriminant after 24 h compared to 6 h,
- the type of aggregates has a significant influence
- the type of asphalt binder has limited influence, with a slightly better results for the Polymer modified binder compared to the pen grade binders

However, the overall results of this test do not appear really accurate and a lot of variability is observed from the different laboratories. The highest variation being for Basalt and Greywacke aggregates which displayed intermediate values, regardless the asphalt binder. To some extent this is aligned with the precision statement of the EN 12697-11. A reproducibility of 30 % is given in the standard with the note: "The obtainable precision may depend on the level of the result as determinations close to 0 or 100 are easier visually to determine than 'mid-range' results between 25 and 75 %". Also *it* has to be noted that these aggregates were dark aggregates and to some extent it was difficult to qualify the remaining coating of asphalt binder.

Analyzing in detail the results, the first thought to explaining such a difference, was the visual interpretation of the coverage. The standard provides some reference scale to "quantify" the coating degree. The final value has to be an average of observation from at least two different technicians on three samples. Some laboratories provided the full observation. Mostly the variation between two observers

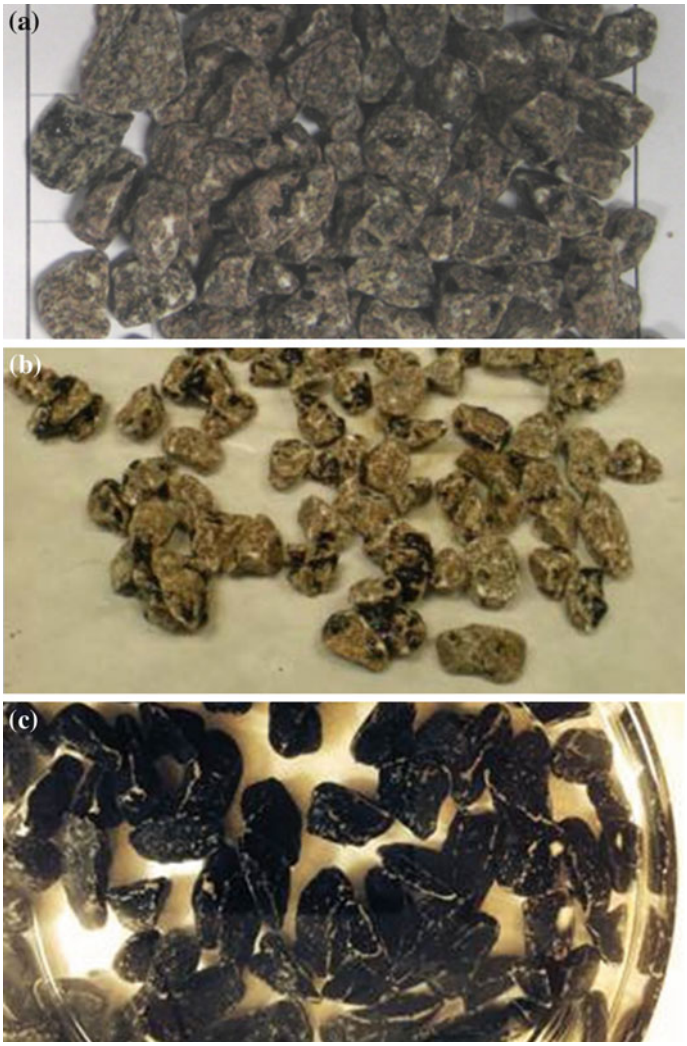


**Fig. 3** **a**. Pictures of granite aggregate with PmB after 24 h from lab 1 with 5 % coating. **b**. Pictures of granite aggregate with PmB after 24 h from lab 4 with 20 % coating. **c**. Pictures of granite aggregate with PmB after 24 h from lab 3 with 40 % coating

and samples was no more than 10 % coating. Some laboratories also provided pictures of samples. Examples are given in Fig. 3a–c, for the Granite aggregates with Polymer modified Bitumen after 24 h. As Granite is a light colored aggregate, the pictures are easier to interpret. One laboratory recorded only 5 % remaining coating another 20 % and the other 40 %. From the pictures the difference is still recordable.

Both assumptions, of the variation between technicians and the visual interpretation cannot alone explain the variability of the results.

Another point of interest was to compare the ranking of the different aggregates. Table 3 summarizes the results for pen grade bitumen and also a comparison with the boiling water test, with 1 being the highest remaining coating and 4 the lowest. For the Rolling Bottle Test, there is a clear trend that Granite displays the worst results and Limestone the best, but for Greywacke and Basalt the ranking is equally balanced between laboratories. However, comparing with the ranking from the boiling water stripping test, the Granite aggregates are still the worst, but the ranking changes with Basalt being the best, then Limestone and finally Greywacke.

So far the test results are not always consistent within the same test method. The reproducibility is very poor, and does not seem to come fully from the visual observation, maybe there are some underlining reasons. Another possible reason could come from the test conditions themselves. The EN standard still leaves some freedom for the test conditions such as the test temperature, if the bottles are already used or are brand new etc. This certainly needs more attention.

Another important topic is how to correlate these test conditions to field behavior. As asphalt binder viscosity is temperature dependent, it automatically affects the adhesion/cohesion properties of the binder. For example when considering Polymer modified Bitumen, it could be recommended to perform the test in more severe conditions and adapt the test temperature to target similar binder viscosity. There is still limited research at this point of time to understand how the temperature influences the affinity or adhesion. If lowering the temperature, will that reduce the adhesion, is there a linear relation or is there a temperature where the adhesion is worst? And finally this test is performed on fresh asphalt binder, while

**Table 3** Ranking between laboratories for the rolling bottle and boiling water stripping tests

| | Granite | Basalt | Greywacke | Limestone |
|---|---|---|---|---|
| Rolling bottle test | | | | |
| Lab 1 | 4 | 3 | 2 | 1 |
| Lab 2 | 4 | 3 | 2 | 1 |
| Lab 3 | 4 | 3 | 2 | 1 |
| Lab 4 | 4 | 3 | 2 | 1 |
| Lab 5 | 4 | 2 | 3 | 1 |
| Lab 6 | 4 | 2 | 3 | 1 |
| Lab 10 | 4 | 2 | 3 | 1 |
| Lab 13 | 4 | 2 | 3 | 1 |
| **Average** | **4** | **2.5** | **2.5** | **1** |
| Boiling water stripping test | | | | |
| Lab 6 | 4 | 1 | 3 | 2 |
| Lab 7 | 4 | 1 | 3 | 2 |
| Lab 11 | 4 | 1 | 3 | 2 |
| **Average** | **4** | **1** | **3** | **2** |

on the road the binder was already processed through the mix plant and is already aged. The behavior could be influenced by aging.

These are the next topics that the TG1 of the Rilem TC 237 SIB is looking to consider in the near future.

## 6 Conclusion

As water damage is one important part of asphalt pavement durability, in Rilem TC 237 SIB, Task Group 1, TG1, worked on the adhesion and affinity between aggregates and asphalt binder. A Round Robin Test was conducted with 13 laboratories and various test methods using four different aggregate types and three asphalt binders. The Rolling Bottle Test was one of the test methods used by eight laboratories.

The rolling bottle test consists of recording the remaining percentage of asphalt binder coating on aggregate after being rolled in a water bottle. While the test is run for 6, 24, 48 and 72 h, the outcomes start to be really discriminant after 24 h.

The analysis of these results shows that the reproducibility of the rolling bottle test is to date rather poor; one reason is related to the visual interpretation of the percentage of coating but this is certainly not the only reason. Other possible causes are discussed in the paper and the study needs to be pursued further.

When comparing rankings as obtained by each participant, the results are much more consistent. All participating laboratories have ranked the Limestone aggregate as the best one and Granite the worst; the intermediate Greywacke and Basalt are more difficult to distinguish. The ranking of the stone types is rather independent of the binder type. Regarding the binders, the Polymer modified binder ranks slightly better for all stone types, compared to the two straight run binders, which perform similarly.

In order to validate the rolling bottle test method to experience from field behavior; the effect of the variations in the field temperature and the effect of aged binder need to be taken into account.

## Bibliography

Bagampadde, U., Isacsson, I. and Kiggundu, B.M. (2006) Impact of bitumen and aggregate composition on stripping in bituminous mixtures, Materials and Structures, 39, 303-315

Besamusca, J., Rooijen van, R., Robertus, C. and Beuving, E. (2012) The search for simple test to assess the complex of adhesion and durability of adhesion, 5th Eurasphalt Eurobitume congress

Curtis, C.W., (1990), A literature review of liquid antistripping and tests for measuring stripping, SHRP-A/UIR-90-016

Curtis, C.W., Ensley.K and Epps. J. (1993) Fundamental properties of asphalt-aggregate interactions including adhesion and absorption, SHRP-A-341

Grönniger, J. (2008) Computergestuetzte Auswertung von Rolling-Bottle-Tests / Computer aided analysis of Rolling-Bottle-Tests. Strasse Und Autobahn, Volume 59, Issue 7, 415-9

Grönniger, J., Wistuba, M.P., Renken, P.(2010) Adhesion in bitumen-aggregate-systems: New technique for automated interpretation of rolling bottle tests, Road Materials and Pavement Design, 11 (4), pp. 881-898

Hicks G. (1991) NCHRP Moisture Damage in Asphalt Concrete, NCHRP Synthesis of Highway Practice 175

Hicks, R.G. and Finn, F.N. (1994), Stage 1 Validation of the relationship between asphalt properties and asphalt-aggregate mix performance, SHRP-A-398

Jeon, Y.W and Curtis, C.W (1992) A literature review of the adsorption of asphalt functionalities on aggregate surfaces, SHRP-A-313

Jorgensen, T. (2002) Testing adhesion between bitumen and aggregate with the rolling bottle test and the boiling test., 6th International Conference on the Bearing Capacity of Roads and Airfields Lisbon, Portugal, Volume 2 p. 889-97

Källén, H.a, Heyden, A.a, Lindh, P.b (2013) Measuring bitumen coverage of stones using a turntable and specular reflections, International Conference on Computer Vision Theory and Applications, 1, pp. 333-337.

Lee, D.L., Guinn, J.A., Khandhal, P.S. and Dunning, R.L. (1990) Absorption of asphalt into porous aggregates, SHRP-A/UIR-90-009

Mathews, D.H., Colwill, D.M. and Yüce, R. (1965) Adhesion tests for bituminous materials, J. Appl.Chem

Morgenstern, A; Sschulze, C; Marschke, L.(2010) Verbesserung der Praezision der Pruefung zur Bestimmung des Haftverhaltens zwischen groben Gesteinskoernungen und Bitumen / Improved test methods for the determination of the affinity between aggregate and bitumen. Strasse Und Autobahn, Volume 61, Issue 12, 879-84

Renken, P., Wistuba, M.P., Groenninger, J., Schindler, K. (2010) Adhesion von Bitumen am Gestein: Verfahren der quantitativen Bestimmung auf Grundlage der Europaeischen Normung. Forschung Strassenbau und Strassenverkehrstechnik, Issue 1043, 140S

Rieder, W. and Weber, H. (1933) Adhesion of Bituminous Binders to Stone, Asph.u.Teer, 37-41

Scholz, T.V., Terrel, R.L., Al-Joaib, A. and Bea, J. (1994) Water sensitivity: Binder validation, SHRP-A-402

Tarrer, A.R. and Wagh, V. (1991) The effect of the physical and chemical characterization of the aggregate on bonding, SHRP-A/UIR-91-507

Terrel, R.L. and Al-Swailmi, S. (1994) Water sensitivity of asphalt-aggregate mixes: Test sections, SHRP-A-403

# Study on the Ageing Behavior of South American Bitumen

**S.A. Mohan, J.L.M. Voskuilen and S.A. Firtoe**

**Abstract** In Suriname, located at the north east part of South America, only one type of bitumen is available for road construction. This bitumen, a pen grade bitumen 60/70 is produced by the Surinam refinery Staatsolie. The crude is always of the same origin. Based on the climatic conditions, it is presumed that ageing of bitumen is often the cause of premature damage in different types of roads, such as fatigue and alligator cracks, raveling and potholes. To obtain insight to which extent the ageing behavior of the bitumen provides an explanation for the premature failure, extensive research has been conducted on bitumen recovered from three premature damaged road sections. The degree of short term ageing was first examined by means of empirical bitumen test methods, rheological characterization, FTIR analysis and GPC measurements. After this an attempt was made to mimic the observed long term field ageing using the RCAT method. This paper reports on the research carried out on field aged and RCAT artificially aged bitumen and the relationship between field and artificially aged bitumen.

**Keywords** Bitumen · Ageing · RCAT · FTIR · GPC

## 1 Introduction

### *1.1 General*

Due to exposure of oxygen, UV and high temperatures bitumen undergoes changes during its service life which finally results in a decrease of its functionality. When

S.A. Mohan
Dura Vermeer Infrastructuur bv., Almere, The Netherlands

J.L.M. Voskuilen (✉)
Ministry of Infrastructure and the Environment, The Hague, The Netherlands
e-mail: jan.voskuilen@rws.nl

S.A. Firtoe
Anton de Kom University of Suriname, Paramaribo, Suriname



F. Canestrari and M.N. Partl (eds.), *8th RILEM International Symposium on Testing and Characterization of Sustainable and Innovative Bituminous Materials*, RILEM Bookseries 11, DOI 10.1007/978-94-017-7342-3_14

applied in asphalt mixtures, aged bitumen results in a loss of mixture properties which on its turn enhances the initiation and propagation of damage in asphalt pavements. It is widely reported and accepted in pavement engineering that a proper mixture design and material selection procedures are of paramount importance for obtaining the maximum performance in practice. Here maximum performance is described by the optimum between durable, sustainable and economic benefits. Especially for pavement engineers the challenge lies in assuming an technical lifetime expectancy for asphalt mixtures in e.g. maintenance schemes.

The latter requires accurate information about the long term field behavior of different asphalt mixtures. In the quest for predicting this long term field performance, numerous studies (van Oort 1954; Petersen et al. 1994; Hagos 2008; Das 2014) have been conducted during the past 65 years all over the world. Majority of these studies focusses on understanding the phenomena that occur and develop in bitumen during its service life. The authors believe that it is of little use to summarize concluding results from previous studies. Instead they believe that implementation of these findings in daily practice, identification of practical issues towards the implementation and development of practical decision tools provides a more solid base to assist pavement engineers towards making choices. Subsequently these practical "unknowns" can provide new insights when setting up an experimental plan for laboratory experiments which is what this paper focusses on.

## *1.2 Ageing of Bitumen in General*

Bitumen, sometimes referred to as the "left overs" of straight run distillation process, is an organic material from which the exact composition is not yet known (Read and Whiteoak 2003), because of its complexity. As a result, capturing all the compositional changes that occur due to ageing and relating these changes to physical properties are considered to be more spot measurements which help to understand but cannot be simply extrapolated to develop a general explanation.

Traditionally regarded as a colloidal system, bitumen consists of highly polar and high molecular weight asphaltene micelles which are hosted in a lower molecular weight oily medium, usually referred to as maltenes. Maltenes can be divided into saturates, resins and aromatics. The overall proportions in which the different molecules are present in the bitumen, determines its overall behavior (Read and Whiteoak 2003).

Being an organic substance the mechanical properties and the chemical structure of bitumen can deteriorate due to exposure to the environment which is also known as age hardening. This ageing of bitumen is considered to be mainly caused by the oxidation and ultraviolet (UV) radiation. In this process, temperature plays the role of a catalyst. Oxidative surface ageing is an irreversible chemical reaction between hydrocarbons of bitumen and available atmospheric oxygen. The UV radiation catalyzed reaction occurs rapidly, which takes place at the few top millimeters of the exposed bitumen surface (Hagos 2008; Petersen 2009). During both processes

several carbon groups are formed which increase the polarity of the host compounds and make them much more likely to associate with other polar compounds. As they form these associations, they create less soluble hydrocarbons which in turn increase the bitumen's viscosity (Lesueur 2009; Redelius 2009) and affect other physical properties.

The above mentioned chemical and/or compositional changes occur rapidly during the mixing and laying process of the asphalt mixture (short term ageing). On the road the ageing occurs at a much slower rate (long term ageing). Several studies (Petersen et al. 1994; Hagos 2008; Das 2014) have tried to capture these changes and develop laboratory ageing protocols to mimic the field ageing. Majority of these protocols are performed using laboratory ageing methods and to speed up the research time relative high temperatures are used, which doesn't occur in the actual pavements in practice. Further on in most situations, the initial mechanical and chemical properties of the bitumen used in the pavement was not measured, one type of bitumen produced from different crudes is used, actual loading on the pavement is not always monitored while in some situations, high temperature periods can heal damage which is initiated during winter periods. As a result, correlating observed damage in practice to changes in bitumen properties, consist of relative large uncertainties.

## *1.3 Objectives*

In Suriname, located on north east coast of South America, the bitumen used in road construction is supplied by the state-run company Staatsolie. Suriname's land area is part of the Guianas Shield that runs from Venezuela to French Guiana and could contain recoverable oil reserves over 13.6 billion barrels and gas reserves of 39 trillion ft3 (Argus 2014) estimated by the US Geological Survey. It is interesting to note that in road construction only one type of bitumen is used for the different asphalt layers (NEA 2010) while the crude is constant making it thus interesting and obviously less complex, to investigate variation of the bitumen properties in time and its effect on pavement performance. This is important, because Suriname has a tropical climate, the average high respectively low temperatures are 32 and 23 °C, the UV index is between 10 and 11.

Despite the above, little to no attention is paid to the engineering properties of the bitumen and it's possible variations on pavement performance in practice. The reasons behind this were captured in an EU funded project called "Institutional Strengthening of the Transport Sector" (ISTS) in Suriname which ran from 2009–2011 (NEA 2010). The results of the project motivated the quest to develop a practical framework for the Suriname Ministry of Public Works and local contractors in order to improve and optimize current maintenance strategies.

The main objective of this study was to characterize the bitumen from Suriname using test methods which are commonly adapted when studying the ageing of bitumen. The characterization was performed on virgin bitumen and artificially

aged bitumen and then compared with field obtained samples. Observations from the different phases are discussed, providing a useful starting point and criteria for road authorities and contractors towards the implementation of quality control indicators for bitumen deliveries in practice and the monitoring of long term field behavior of bitumen and thus pavement performance.

## 2 Experimental

### *2.1 Materials*

The bitumen used in this study is pen grade 60/70 bitumen produced by Staatsolie. The properties of the bitumen are summarized in Table 1.

Apart from investigating virgin bitumen, bitumen was recovered from field samples, cored in 2013 from three different locations (Fig. 1). Cores were taken from the surface layer and the binder layer, which failed prematurely. At all three locations, a dense asphalt concrete mixture was applied for both layers. For location C, bitumen was recovered only from the binder layer. Table 2 describes the different field samples.

The recovery of the bitumen from drilled field cores was performed on the total core itself. No distinction was made between the upper part and the bottom part of the asphalt layer. The reasons for this were some local practical constraints such as

**Table 1** Properties virgin pen grade 60/70 bitumen

| | |
|---|---|
| API gravity (–) | 8.8 |
| Penetration $10^{-1}$ mm (T = 25 °C) | 63 |
| Softening point R&B (°C) | 47.2 |

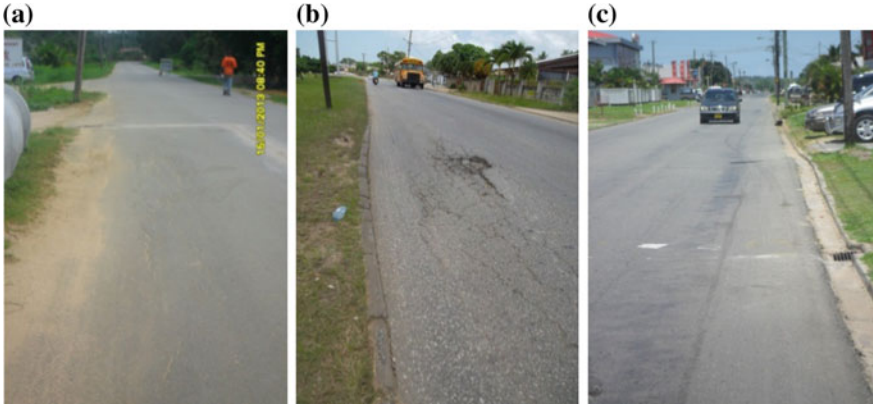


**Fig. 1** Observed damage: (*left*) location A, (*middle*) location B, (*right*) location C

**Table 2** Properties field samples

| Sample id | Location (layer) | Thickness (mm) | Age (years) |
|---|---|---|---|
| A1 | A (surface) | 33 | 5 |
| B1 | B (surface) | 45 | 11 |
| C2 | C (binder) | 50 | 4 |

too less available cores. Knowing that ageing in practice differs as function of asphalt layer thickness, in this study it was decided to continue with the recovered bitumens from the whole cores while at the same time highlighting the importance for proper preparation of test samples. Visual inspections at the different sites revealed that the observed failure was more local, structural failure which suggested that bitumen ageing and its impact on mixture performance might not have been the primary cause for the manifested damage. This observation stipulates the difficulty when developing models to predict long term pavement performance on the basis of ageing studies on bitumen level. Apart from defining a preferred asphalt mixture property which varies from country to country, the authors believe that it is equally important to characterize bitumen using test methods which correlate or can easily predict mixture performance.

## 2.2 Test Methods

All the studied bitumens were subjected to physical and chemical characterization. Empirically, the bitumens were subjected to softening point measurements according to the European standard EN 1427. Complex modulus and complex viscosity measurements were carried out using an Anton Paar MCR302 rheometer. Complex viscosity measurements were performed using the cone-plate (D = 25 mm) setup at an incremental shear rate from 0.1 to 300 (1/s) at two temperatures, 100 and 135 °C. Frequency sweeps were performed using the plate-plate setup in a temperature range from −10 to 50 °C and frequency range from 0.1 to 300 rad/s. To construct a mastercurve, the different isotherms were shifted using the William Landel Ferry equation (Christensen 1982), Eq. 1, while for quantitative comparison purposes, a model was fitted in the shifted test results. The model used was a modified Huet–Sayegh (Huet 1963), developed by Woldekidan (2011), Eq. 2.

$$\log(a_T) = \frac{-C_1(T - T_r)}{C_2 + (T - T_r)} \tag{1}$$

$$(G^*(\omega))^{-1} = \left(G_0 + \frac{G_\infty - G_0}{1 + \delta(j\omega\tau)^{-m_1} + (j\omega\tau)^{-m_2}}\right)^{-1} - \frac{j}{\eta_3\omega} \tag{2}$$

In Eq. 2, $G^*(\omega)$, $G_0$ and $G_\infty$ denote the complex shear modulus, rubbery shear modulus, here assumed to nil, and the instantaneous shear modulus value. The model parameters $\delta$, $m_1$ and $m_2$ are identical as the original Huet–Sayegh model while the terms $\tau$ and $\eta_3$ denote the time constant and the linear dashpot parameter.

The addition of a linear dashpot element in series with the original Huet–Sayegh model, makes the model attractive for modelling the permanent deformation of asphalt mixtures. In Suriname usually bitumen rich mixtures, such as dense asphalt concrete, are applied as surface layers. In these mixtures the contribution of the viscous deformation of the bitumen to the overall mixture deformation is significant. Since the bitumen type and crude are constant, the model parameters can serve as an excellent measure to optimize rutting properties of asphalt mixtures. Subsequently model parameters can also serve as quality control indicators.

To investigate the chemical changes due to environmental conditions and artificially ageing, Gel Permeation Chromatography (GPC) and Fourier Transform Infrared (FTIR) spectroscopy measurements were carried out.

Artificially long term ageing of the virgin binder in the laboratory was conducted using the Rotating Cylindrical Ageing Test (RCAT). Due to practical limitations, the short term ageing (RCAT 163) was not performed. The bitumen was subjected to a temperature of 90 °C with a constant flow of oxygen. Conditioning and oxygen rate were selected according to European standard EN 15323. Samples for further analysis were taken after the following time intervals: 4, 21, 48, 144 and 240 h.

## 3 Results and Discussion

### *3.1 Empirical*

Figure 2 presents the measured softening points of the different bitumens. All the field binders show an increased softening point. A difference of approximately 6 °C is observed between the virgin and field bitumens. For the C2 bitumen which was recovered from the binder layer, an increase of 2 °C was measured. Because the

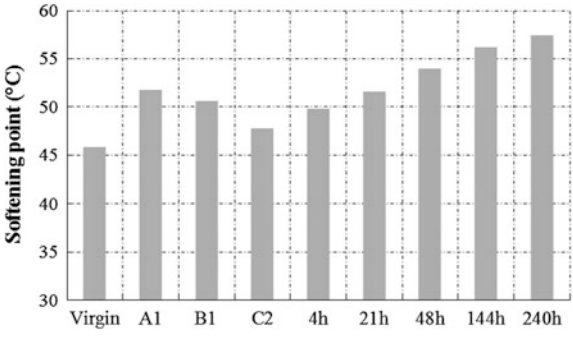


**Fig. 2** Softening point results of virgin, field and artificially (RCAT) aged bitumen

service life of B1 is 11 years, a higher softening point is expected than A1, which has a service life of 5 years. Possibly the short term ageing caused by production, transport and laying may differ, but this is unknown. The results suggest that to mimic 5–11 year field ageing of the bitumen of the top layer, it takes about 21 h artificial ageing with RCAT to obtain identical softening points while for the binder layer, it takes less than 4 h.

## 3.2 Rheological

Table 3 summarizes the obtained model parameters for the different bitumens. Using the model, the complex modulus was calculated at two different loading frequencies. The behavior of the different binders at these frequencies is compared in Fig. 3.

The obtained correlation coefficients the for the complex modulus and phase angle, in the last two columns of Table 3, indicate the accuracy of the model to

**Table 3** Obtained model parameters, $T_{reference}$ = 30 °C

| Par. | $C_1$ | $C_2$ | $m_1$ | $m_2$ | δ | τ (s) | $\eta_3$ (MPa.s) | $G_\infty$ (MPa) | $r^2$ G* | $r^2$ Phase |
|---|---|---|---|---|---|---|---|---|---|---|
| Virgin | 14.8 | 139.3 | 0.17 | 0.53 | 0.10 | 5.12E-02 | 0.05 | 930 | 0.999 | 0.999 |
| A1 | 14.4 | 144.9 | 0.21 | 0.57 | 5.02 | 1.63E-01 | 0.16 | 1000 | 0.998 | 0.996 |
| B1 | 15.0 | 148.0 | 0.30 | 0.69 | 4.93 | 1.28E-01 | 0.13 | 532 | 0.999 | 0.997 |
| C2 | 16.1 | 160.5 | 0.23 | 0.61 | 4.66 | 8.01E-02 | 0.08 | 1000 | 0.998 | 0.997 |
| 4 h | 11.9 | 115.8 | 0.18 | 0.56 | 2.88 | 8.02E-02 | 0.08 | 1000 | 0.994 | 0.996 |
| 21 h | 12.7 | 124.6 | 0.20 | 0.57 | 2.52 | 1.28E-01 | 0.13 | 710 | 0.998 | 0.996 |
| 48 h | 13.2 | 127.6 | 0.21 | 0.59 | 2.70 | 1.77E-01 | 0.18 | 719 | 0.988 | 0.996 |
| 144 h | 18.0 | 156.5 | 0.21 | 0.59 | 3.39 | 4.68E-01 | 0.47 | 927 | 0.999 | 0.998 |
| 240 h | 18.0 | 160.0 | 0.20 | 0.55 | 2.82 | 6.00E-01 | 0.60 | 772 | 0.999 | 0.997 |

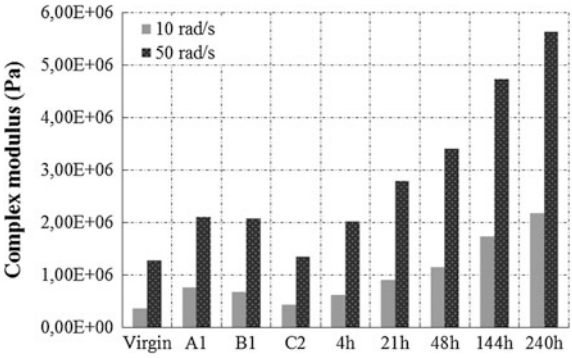


**Fig. 3** Comparison of complex modulus at an reference temperature of 30 °C

describe the measured data within the tested range. The found differences for the model parameters indicate that due to ageing, the response of the different bitumens at a given temperature changes. This is illustrated in Fig. 3.

This change in response is best illustrated in Fig. 4 where the results of the complex viscosity measurements are compared with each other. All samples were subjected to an incremental shear rate from 0.1 to 300 s-1. In Fig. 4 the resulting shear stresses in the sample are plotted against the calculated viscosity. All the test results follow the same trend while it can be observed further that the resulting shear stresses are the lowest for the virgin material and the highest for the A1 bitumen and the 240 h artificially aged bitumen.

In Fig. 5 the complex viscosities of the different bitumens are compared with each by means of an ageing index. The measured viscosities for all the samples were divided by the viscosity of the virgin bitumen. Comparisons are made for viscosity values at a shear stress of 50 Pa.

It can be seen in Fig. 5 that the required ageing time to mimic field measured viscosity values, ranges from approximately 21 to 240 h. Interestingly this required time differs from the required time to obtain identical softening points and complex modulus values while the observed trend between the different bitumens remains constant in the different test methods.

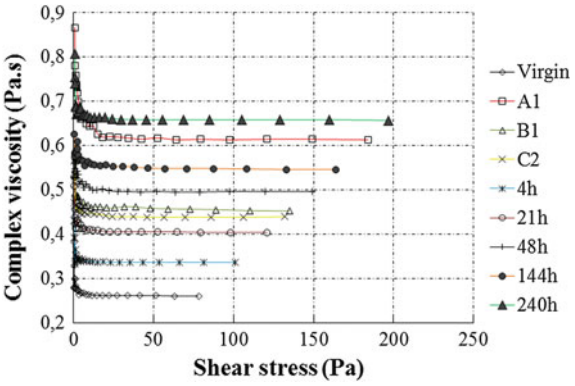


**Fig. 4** Test results complex viscosity measurements at test temperature of 135 °C

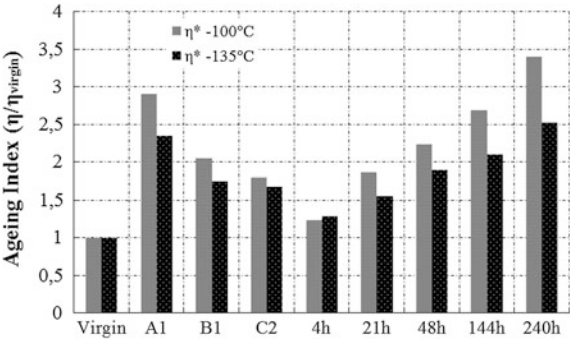


**Fig. 5** Comparison of test results complex viscosity measurements

### 3.3 Chemical

In Fig. 6 GPC results from the different bitumens are compared with each other by dividing the measured data into two groups:

- Molecules with a mass greater than 4500 Dalton
- Molecules with a mass smaller than 500 Dalton

It can be observed that ageing results in an increase of the larger molecules and subsequently a decrease in smaller molecules is observed. This confirms that maltenes during the ageing process transform party to asphaltenes. It is interesting to note that for dense asphalt mixtures, ageing usually occurs at surface of the layer and in this study the bitumen was recovered from the total core. Despite this, a clear change in molecular mass is observed even for bitumen C2, recovered from the binder layer.

In Fig. 7a comparison is made between the different bitumens by means of infrared measurements. The area under de peak at the intervals which indicate the formation of ageing components, was calculated by available software packages. Some scatter is observed for the artificially aged samples however a logical trend can be observed that the area under the peaks increases with ageing time. It is

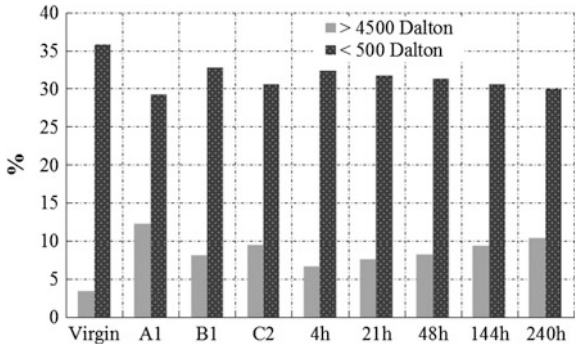


**Fig. 6** GPC test results

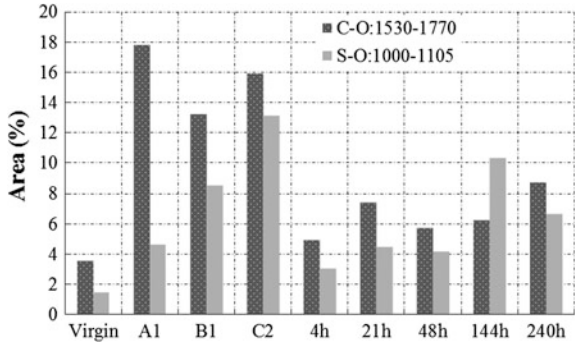


**Fig. 7** Computed area under peak at different wave length intervals

interesting to observe the relative large difference between the field samples and the artificially aged samples. Considering the facts that the field bitumens were recovered from the total core itself and that all these samples have experienced the production a processing phase in practice, the differences could possibly be explained by the absence of the short term ageing which was not performed in this study.

### *3.4 Discussion*

All the studied bitumens showed that ageing affects both the physical and chemical properties of the original bitumen. The difference in required ageing times to mimic field values stipulates the importance of selecting the correct initial values when one wants to calculate ageing indices. Here it was assumed that the tested virgin bitumen was identical for the field locations and storage and production conditions at the asphalt mix plant were constant hence the observed differences in required laboratory ageing time to mimic field values for the studied properties. Apart from this, bitumen was extracted from the total core itself. Nevertheless the results were discriminative enough to compare the different bitumens with each other which was also confirmed by the constant arrangement of the samples in the different test methods.

The methodology used in this study provides an excellent starting point to develop an understanding about long term pavement performance in practice. However to be able to accurately predict technical lifetime expectancies in practice on the basis of bitumen ageing rates, the authors believe it is mandatory to capture the properties of bitumen before production, after production and during its service life by means of periodically field sampling.

## 4 Conclusions and Recommendations

On the basis of all the obtained test results, the following conclusions and recommendations are summarized:

- To mimic long term field ageing under Surinam climate conditions, 4 to 24 h RCAT ageing is sufficient for top layers and less than 4 h is sufficient for binder layers.
- RCAT ageing mimics the field long term ageing, but the required time to mimic the field obtained properties differ from property to property and also differ for the recovered field bitumens.
- Recommended is to focus on the upper part of a core, when field ageing of top layers is the topic, this will give more discriminative results.

**Acknowledgments** The authors wish to acknowledge Dr. Wim van den Bergh (University of Antwerpen) and Dave van Vliet (TNO Delft) for accommodating some of the experiments. Special thanks go out to Eric van Oosterhout (InfraLinq) for performing all the rheological measurements.

## References

Argus (2014) Argus Asphalt Report. Available via ARGUS. http://www.argusmedia.com/~/media/Files/PDFs/Samples/Argus-Asphalt.pdf. Accessed 20 Oct 2014

Christensen, R.M (1982) Theory of viscoelasticity: An introduction, Second edition. Academic press, New York

Das P K (2014) Ageing of Asphalt Mixtures: Micro – scale and mixture morphology investigation. KTH Royal Institute of Technology

Hagos E T (2008) The Effect of Ageing on Binder Properties of Porous Asphalt Concrete. Delft University of Technology

Huet, C (1963) Etude par une méthode d'impédance du comportement visco-élastique des matériaux hydrocarbonés. Faculté des Sciences de Paris, Paris.

Lesueur D (2009) The colloidal structure of bitumen: Consequences on the rheology and on the mechanisms of bitumen modification. Adv. Colloid Interface Sci. 145: 42-82

NEA (2010) Quick scan: Faalmechanismen asfaltwegen in Suriname. Available via NEA Suriname. http://www.neasurinameists.org/?page_id=6. Accessed 1 Oct 2014

Oort van W P (1954) A study of the ageing of asphaltic bitumen. Delft University of Technology

Petersen et al. (1994) Binder Characterization and Evaluation, volume 1. Washington DC

Petersen J C (2009) A Review of the Fundamentals of Asphalt Oxidation. In: Transportation Research Circular. Available via TRB. http://onlinepubs.trb.org/onlinepubs/circulars/ec140.pdf. Accessed 1 Oct 2014

Read J, Whiteoak D (2003) The Shell Bitumen Handbook, Fifth edition. Thomas Telford, London

Redelius P (2009) Asphaltenes in Bitumen, What They Are and What They Are Not. Road Materials and Pavement Design, 10: sup1, 25-43. DOI: 10.1080/14680629.2009.9690234.

Woldekidan M F (2011) Response Modelling of Bitumen, Bituminous Mastic and Mortar. Delft University of Technology

# Asphalt Mixture Sensitivity to Water and Frost

**Maciej Maliszewski, Adam Zofka, Dominika Maliszewska and Dariusz Sybilski**

**Abstract** This paper presents recent study on the moisture susceptibility of asphalt mixtures under various water and frost conditioning. Moisture susceptibility of asphalt mixture is a very important property influencing significantly pavement durability. In particular, asphalt layers are subjected to a deterioration factor which is traffic independent—water and frost/thaw cycles. It is a common practice that during the mix design process qualitative experiments are conducted in order to assess the moisture resistance of trial mixes. Therefore there is a need for a suitable, validated and generally accepted method. This paper presents the results of the extensive research study conducted recently in Poland to compare several different testing protocols and associated requirements for the moisture sensitivity. Different aspects of the asphalt mixtures were investigated, in particular aggregate type, anti-stripping agent and bitumen type. Specimens for the moisture susceptibility were conditioned using four methods including an original method comprising the frost/thaw cycles as well as AASHTO T-283 protocol. In addition to the standard evaluation of the indirect tensile strength, there were several performance based tests conducted in the laboratory on the specimens before and after the conditioning procedures. The analysis shown in this paper lead to the development of the alternative specifications for the moisture susceptibility in Poland.

**Keywords** Water sensitivity · Frost/thaw weathering · Indirect tensile strength · Interlaboratory tests · Performance of asphalt mixes

M. Maliszewski (✉) · A. Zofka · D. Maliszewska · D. Sybilski
Road and Bridge Research Institute, Warsaw, Poland
e-mail: mmaliszewski@ibdim.edu.pl



F. Canestrari and M.N. Partl (eds.), *8th RILEM International Symposium on Testing and Characterization of Sustainable and Innovative Bituminous Materials*, RILEM Bookseries 11, DOI 10.1007/978-94-017-7342-3_15

## 1 Introduction

It is generally accepted that water damage to asphalt mixtures is one of the main deterioration factors in pavements (Majidzadeh and Brovold 1968; Kandhal 1992). This phenomenon is caused by two main factors: stripping susceptibility of binder/aggregate contact area and physical disintegration of compacted asphalt structure by water freeze/thaw cycles. Both phenomenon lead to the same, mediocre effect, the material premature destruction.

Water sensitivity of hot mix asphalt (HMA) was evaluated in many research efforts, starting with early stage tests (Lottman 1978; Kennedy et al. 1983), as well as in modern investigations (Kringos and Scarpas 2008; Azari 2010; Canestrari et al. 2010; Jaskuła 2004a, b). In terms of standard testing all there are at least four documents. These methods are based either on compacted mixtures using indirect tensile strength ratio or compressive strength or on evaluating the residue of bitumen separated from mixture after conditioning in water. The first group of tests, the strength tests, usually comprises the set of reference specimens and set of conditioned specimens. Reference specimens are usually kept dry on a flat surface. Wet specimens are conditioned under various combinations water, frost, pressure or vacuum cycles. Upon completion, specimens from both sets are subjected to strength tests, which lead to the assessment of strength change due to the conditioning.

Road and Bridge Research Institute (IBDiM) has recently finalized a research project focused to water sensitivity test procedure. This project was triggered by significant fluctuations in the test results obtained from different laboratories as well as problems with achieving required results level with some HMAs (Sybilski et al. 2013). Test procedure and requirement levels for the HMAs were proposed after implementing the European Standards in 2008.

This paper focuses on the conditioning procedure of the wet subset specimens, as well as presents some performance based tests which were meant to validate the water sensitivity results.

The presented stages differ by the presence of the short term oven ageing procedure (STOA), compaction energy with the use of the Marshall compactor, applied vacuum level while specimens submerged in water, following water temperature conditioning and finally the test temperature. One of the most well-known methods are AASHTO T-283 (later named as protocol 1) and EN 12697-12 (protocol 2). On basis of both methods IBDiM has worked out a procedure containing stages from American and European Standard procedures. The procedure was presented in Polish technical document WT-2 2010 (protocol 3). Evaluation prepared in scope of this research work led to preparation of current version of water sensitivity procedure (protocol 4), which has been adopted in revision of technical document WT-2 and published in 2014 (GDDKiA 2014).

**Table 1** Summary of conditioning procedures

| Protocol | STOA | Compaction energy | Vacuum | Water conditioning temp. °C | | | Test temperature (°C) |
|---|---|---|---|---|---|---|---|
| | | | | 40 | −18 | 60 | |
| 1 AASHTO T-283 | + | To reach 7 % air voids level | 34–88 kPa (water saturation 55–80 %) | − | + | + | 25 |
| 2 EN 12697-12 | + | 2 × 35 blows | 6.7 kPa | + | − | − | 25 |
| 3 WT-2 2010 | + | 2 × 35 blows | 6.7 kPa | + | + | + | 25 |
| 4 WT-2 2014 | + | 2 × 35 blows (min. 10 specimens) | 6.7 kPa (water saturation 55–80 %) | + | + | − | 25 |

Short evolution of conditioning procedure stages are shown in Table 1.

## 2 Experimental Program

This research paper shows the results of four studies:

- First study was intended to review whether the materials selection and mix composition affects the water sensitivity of HMA
  - results of ITSR (protocol 3, see Table 1) were evaluated to find if there appears a difference between result levels coming from use of particular asphalt constituent, its proportion or physical property of compacted mix (e.g. air void content, compaction level).
- The second study was to evaluate how conditioning procedure affected HMA properties on basis of TSRST, fatigue and stiffness test, in foreground of ITSR test results
  - one asphalt mixture, relatively weak to water and frost damage in TSRST test, was tested by means of generally called "performance tests"
  - the test specimens prepared for TSRT, fatigue and stiffness modulus tests were preconditioned with use of WT-2 2010 method (protocol 3, Table 1).
- The third study was to compare different testing protocols of water sensitivity
  - different testing protocols of HMA water sensitivity test (protocol 1–4, as described in Table 1) were conducted on same mixes
  - the goal was to evaluate "severity" of conditioning procedure, as final testing procedure was the same in all cases.
- The fourth study in this paper shows interlaboratory comparison of ITSR tests as well as some requirements considerations.

## 3 Materials

There were several different materials selected for the mix composition. Mixes were composed with the use of binders, aggregates and antistrip agents shown in Table 2. As it was proven in later analysis, properties of binders were not the main point of interest, but generally, they met requirements according to Polish National Appendix to the European Standard. Antistripping agents were chosen as the commercial products, "off the shelf". In terms of the selection of the aggregates, the complete palette of materials from Polish market were chosen. Detailed information is provided in report (Sybilski et al. 2013).

**Mixture types** There were ten asphalt mix formulas composed for the purpose of this project (Tables 3 and 4).

These mixes were combined with ITSR tests using different antistrip agents. For laboratory tests there were three SMA 11 wearing course and four asphalt concretes, AC 16 (binder course) and AC 22 (base course) designed. For interlaboratory comparison there were two mixtures designed, SMA 8 wearing course and HMAC 16 high modulus asphalt concrete. Mixes presented in Table 3 were

**Table 2** HMA factors and their designations

| Binder type | Aggregates type | Antistripping agent |
|---|---|---|
| 20/30 pen | Amphibolite (A) | Amine-based (A) |
| 35/50 pen | Basalt (B) | Hydrated lime (H) |
| 50/70 pen | Dolomite (D) | Alkylamidopoliamine (I) |
| PMB 45/80-65 | Gabbro (G) | Phosphoric acid (P) |
| PMB 45/80-55 | Granite (R) | Amine-based (T) |
| | Limestone (L) | Amidopolyamin of tall oil (W) |
| | Melaphyre (M) | |
| | Quartzite (Q) | |
| | Glacier gravel (V) | |

**Table 3** Material matrix for the laboratory testing

| No | Mix type | Bitumen type | Mix designation: | | | | | |
|---|---|---|---|---|---|---|---|---|
| | | | Aggregate type/Antistrip agent | | | | | |
| 1 | SMA 11 | 45/80-55 | B/W | B/T | B/A | B/I | B/P | B/H |
| 2 | SMA 11 | 45/80-55 | G/W | G/T | G/A | G/I | G/P | G/H |
| 3 | SMA 11 | 45/80-55 | R/W | R/T | R/A | R/I | R/P | R/H |
| 4 | AC 16 | 50/70 | D/W | D/T | D/A | D/I | D/P | D/H |
| 5 | AC 16 | 50/70 | A/W | A/T | A/A | A/I | A/P | A/H |
| 6 | AC 16 | 50/70 | Q/W | Q/T | Q/A | Q/I | Q/P | Q/H |
| 7 | AC 22 | 35/50 | L/W | L/T | L/A | L/I | L/P | L/H |
| 8 | AC 22 | 35/50 | M/W | M/T | M/A | M/I | M/P | M/H |

**Table 4** Materials used in the interlaboratory comparison

| No | Mix type | Bitumen type | Mix components | | | | | Added filler | Antistr. agent |
|---|---|---|---|---|---|---|---|---|---|
| | | | Aggregate size and type | | | | | | |
| 1 | HMAC 16 | 20/30 | 11/16 M | 8/16 L | 2/8 L | 0/4 V | 0/2 L | L | W |
| 2 | SMA 8 | 45/80-65 | 5/8 A | 2/5 A | 0/2 V | 0/2 L | Cellulose | L | W |

designed with use of 100 % of aggregate from specified source, e.g. B, means that mix was designed with use of basalt chippings and sands. Only the added filler was of the limestone origin.

**Samples** Laboratory tests were conducted on specimens prepared with use of Marshall compactor according to PN-EN 12697-30 (ITSR, air voids content) or slab compactor according to PN-EN 12697-33 and cutting operation by using saw to produce beam specimens suitable for testing (TSRST, rutting, fatigue and stiffness). Asphalt mixture for laboratory tests was prepared from constituent materials using laboratory mixer according to PN-EN 12697-35. Short temperature oven ageing test was preceding the compaction process. Mixtures for the interlaboratory comparison were prepared at the mixing plant, sampled and transported to the laboratory for compaction (i.e. it was reheated once, prior to the compaction without additional ageing process).

## 4 Testing Methods

Laboratory tests were performed according with Table 5.

**Table 5** Methods of laboratory tests

| Laboratory test | Standard | Method | Specimens |
|---|---|---|---|
| ITSR | EN 12697-12 | Method A | At least 4 specimens per each set |
| Fatigue tests | EN 12697-24 | Method 4 PB-PR, 10 °C, 10 Hz | 6 beams per mix |
| Stiffness tests | EN 12697-26 | Method 4 PB-PR, 10 °C, 10 Hz | 4 beams per mix |
| TSRST | EN 12697-46 | – | At least 3 beams per mix |
| Bulk density | EN 12697-6 | Geometrical | – |

# 5 Test Results

## 5.1 HMA Factors Under Single Method

In this section test protocol 3 (see Sect. 1) was used to describe the difference in test results taking into account different aggregate types, different antistripping agents and mix compositions. The criteria for evaluation were indirect tensile strength ratio ITSR (presented in Fig. 1) and fracture energy ratio from ITS test (Fig. 2). Fracture unit energy ratio was calculated on basis of ultimate strength normalized by the geometrical bulk density of specimen from wet and dry subset. To calculate the ratio, unit energies from wet and dry subset were divided.

In Fig. 1 it can be noticed that amphibolite, basalt and gabbro aggregates were in group of highest level of ITSR, with average result close to 100 %, while limestone, melaphyre, quartzite and granite were in lower zone, with mean value close to 80 %. Weakest aggregate of the test program was the dolomite, with average ITSR of 50 %. Unit fracture energy ratio results were in similar order as ITSR, but are of higher values. Also unit fracture energy ratios characterize themselves with higher data span, producing significantly higher confidence interval ranges. This method should be subjected to further analysis. Influence of binder type on ITSR value led to ambiguous results, confirmed by ANOVA (analysis of variance). None of binders had significant influence on water sensitivity values in this research.

From Figs. 1 and 2 also the effectiveness of particular antistrip agent could be concluded. Figure 3 helped to analyze information by introducing additional ratio.

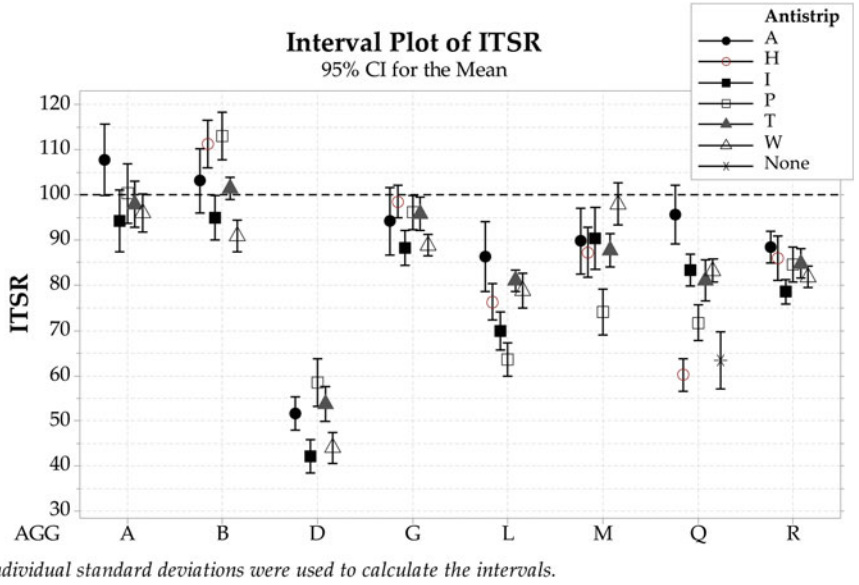


**Fig. 1** ITSR (%) results for different aggregate types (AGG) and antistrip agent (antistrip)

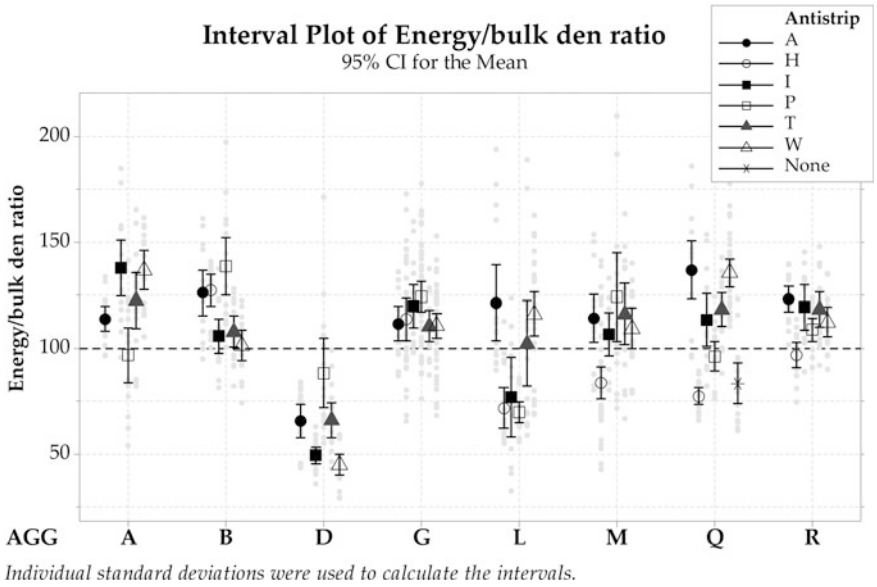


**Fig. 2** Unit energy ratio (%) for different aggregate types (AGG) and antistrip agent (antistrip)

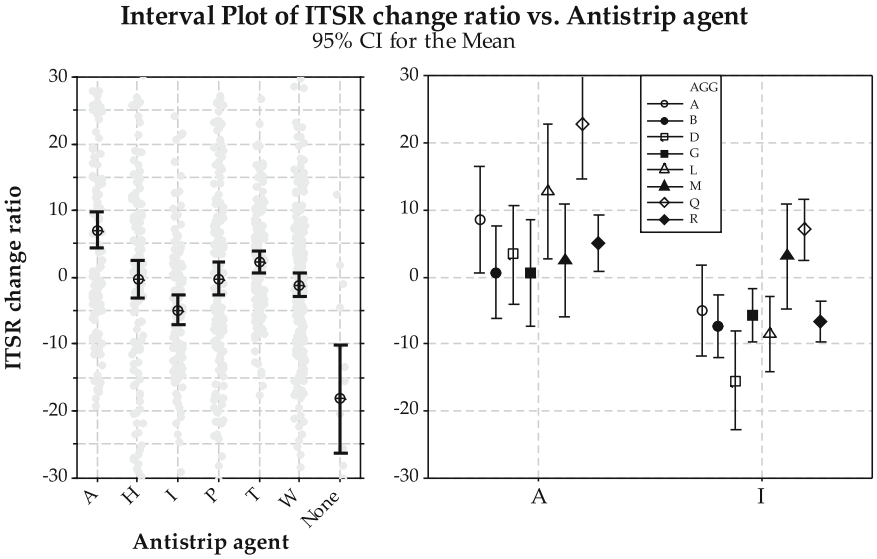


**Fig. 3** Relative difference in ITSR (%) values with the reference to the average value within each *aggregate* group presented by different *antistrip* agent

It was defined by difference between average and actual ITSR value compared to average value. The average value was calculated within every aggregate type separately.

It is obvious that different chemical composition of antistrip agent influences different aggregates, but it could be concluded, that adhesive type A would be the best choice, if we did not know the aggregate type (Fig. 3, left part). It achieved a ITSR increase of over 10 % amongst other adhesives in this research. Also positive ITSR increase was achieved with adhesive T. Adhesive H, P and W were not standing out amongst other. Adhesive I was below the average, forming the relatively negative influence on ITSR comparing to other adhesives. These conclusions are changing when analyzing particular adhesives (A and I), for different aggregates (Fig. 3, right part). Each type of aggregate defined its best adhesive agent influencing the ITSR.

## 5.2 *Four Methods on One Material*

Below described tests were completed on same asphalt mixes, using different test methods (protocols 1–4). Criterion for evaluation was the ITSR value. Results of this evaluation was shown in Fig. 4.

First observation to notice was that AASHTO test (protocol 1) produced relatively lower variation results in comparison to EN (protocol 2) and WT-2 2010 (protocol 3). In ¾ of test results EN (protocol 2) produced slightly higher ITSRs comparing to AASHTO (protocol 1) and WT-2 2010 (protocol 3). WT-2 2010 (protocol 3) was the most severe amongst other methods, producing significantly

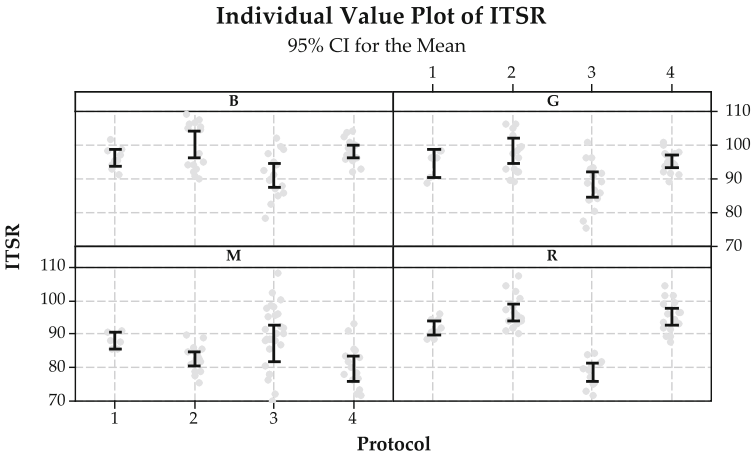


**Fig. 4** ITSR (%) values for one material from different conditioning protocols

lower values than protocol 1 and 2. It was one of the main reasons to design protocol 4, which did not eliminate freeze/thaw cycle, but in most cases produced better or similar results to protocol 3 and 1. Protocol 4, presented in WT-2 2014 (GDDKiA 2014) is meant as a compromise between requirements of EN standard and level of test results achieved with use of different methods on different asphalt mixes.

## *5.3 Performance Tests*

In this research project some of the mixes were chosen to perform performance based tests, evaluating the degree of specimen deterioration in terms of fatigue decrease ratio, complex modulus decrease ratio and low-temperature behavior decrease ratio. These ratios were calculated as typical ITSR on basis of results derived from wet subset divided by dry subset of specimens. The difference was that not cylindrical Marshall specimens but prismatic specimens prepared for performance tests were subjected to conditioning complying with method 3. These specimens formed a wet subset, and after tests they were compared to specimens from dry subset, tested in the same conditions but without requirements of method 3. For this research project four performance based test were chosen, forming following results:

- TSRST S—Thermal Stress Restrained Specimen Test, maximum stress, MPa,
- TSRST T—temperature at break point, °C,
- Modulus—4 point bending test on prismatic specimens (4 PB-PR), MPa,
- Fatigue—4 PB-PR, tested at 10 Hz constant strain amplitude of 380 μm/mm until 50 % decrease of modulus, expressed in cycles,
- ITS, indirect tensile strength test, MPa.

After finishing these tests, wet subset results are divided by dry subset results, forming ratios respectively. These results were shown in Fig. 5.

Summarizing the performance tests, it can be concluded, that conditioning procedure included in method 3 decreases properties of asphalt mixes. The most affected parameter was TSRST S. It presented a 30 % decrease of this parameter after conditioning. It meant that conditioning process highly affected low temperature strength of specimens. On the other hand the TSRST T, together with Modulus were the least affected parameters (decrease of ratio not exceeding 10 %), so it could be also concluded that low temperature breaking conditions did not change significantly, as well as specimen stiffness. About 20 % decrease was observed on ITSR and Fatigue ratio. One-Way ANOVA showed that ITSR results did not differ significantly from TSRST S and Fatigue, while was significantly lower than Modulus ratio and TSRST T ratio.

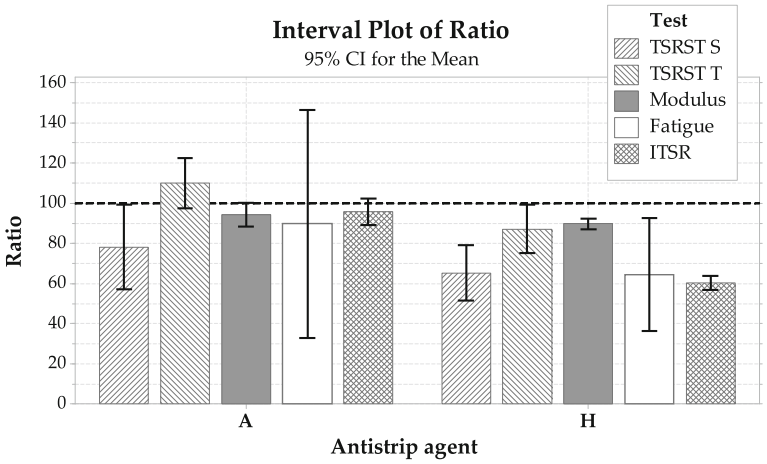


**Fig. 5** Parameter ratios (*wet/dry*) from two performance tests after single conditioning procedure

## 5.4 Interlaboratory Comparison

Interlaboratory comparisons were carried out in two stages. In the first stage, there were a total of 23 polish laboratories involved. Test were performed according to WT-2 2010 (procedure 3). Two types of bituminous mixtures were used: HMAC 16 and SMA 8. The assessment of the test results for each test parameter ($ITS_d$, $ITS_w$, ITSR) were made by the mean value, standard deviation, coefficient of variation and Z-score. In the case of HMAC, most laboratories met the Z-score criterion (one laboratory had questionable result, but still satisfactory). In the case of SMA two laboratories showed questionable ITSR results and one $ITS_w$ result. Coefficient of variation was approx. 10 % for each parameter in case of HMAC. SMA showed variation of $ITS_d$ and $ITS_w$ at approx. 11 %, the ITSR results showed only 6 % variation. It showed much smaller scatter of ITSR results for SMA 8 than HMAC 16.

In the second stage, 12 laboratories attended the tests. This time comparison was made according to procedure 4, on the same set of mixes. In case of HMAC, all laboratories met the Z-score criterion so the results were satisfactory. In case of SMA only one laboratory provided questionable results. Differentiation of the results was higher for the $ITS_w$ (approx. 14 %), then other parameters (approx. 10 %). In case of SMA, while the parameters $ITS_d$ and $ITS_w$ were similar to each other (at approx. 11–12 %), the ITSR value variation was 5 % only. To sum up the variability of test results has not changed significantly at interlaboratory level after introducing new procedure, but less questionable results were provided. Smaller scatter of test results could be observed for ITSR in case of SMA 8 than HMAC 16.

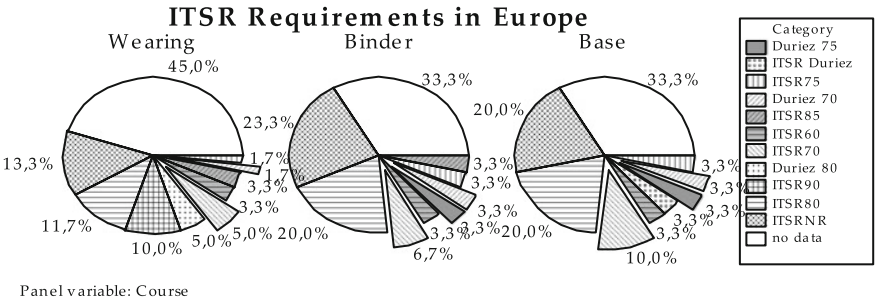


**Fig. 6** ITSR requirements across Europe

### *5.5 Requirements Level*

In scope of this research programme, there has been also prepared a survey about requirements level of ITSR across European countries. Fifteen respondents sent back filled out questionnaires. Figure 6 presents the requirements level received from poll.

It can be concluded that over 50 % of responding countries either did not set requirements or set ITSR NR (not required) category for asphalt layers in their countries. ITSR 80 % is the most common requirement for all pavement asphalt layers. Poland has relatively the most strict requirements for ITSR: 70, 80 and 90 % (base, binder and wearing course respectively). Over 80 % of respondents do not require freeze/thaw cycles for wet subset of specimens.

## 6 Summary and Conclusions

Sensitivity of asphalt mixtures to water and frost effect is a very important factor. Test results presented in this paper showed that mainly aggregate type is influencing the results. *Antistrip* agents had positive influence on the ITSR but should be selected carefully. Despite the laboratory tests showing that modified procedure had positive influence on the variation of the ITSR, the interlaboratory testing did not confirm this observation at expected level. A general suggestion is that variability of the test results should lead to the update of the evaluation of the test results by e.g. rounding results to the nearest 10 %. Performance tests after conditioning in water and frost showed a significant decrease of the fatigue life. The less affected parameters were the TSRST cracking temperature and 4 PB modulus. It is concluded that the performance tests should be continued in order to evaluate their influence on the deterioration of asphalt pavements.

## References

Azari, H., 2010. NCHRP Web-Only Document 166: Contractor's Final Task Report for NCHRP Project 9-26A., (September).

Canestrari, F. et al., 2010. Adhesive and Cohesive Properties of Asphalt-Aggregate Systems Subjected to Moisture Damage. Road Materials and Pavement Design, 11(sup1), pp.11–32. Available at: http://www.tandfonline.com/doi/abs/10.1080/14680629.2010.9690325 [Accessed November 15, 2014].

GDDKiA, 2014. Technical Specifications for asphalt mixes WT-2 2014., p.50. Available at: https://www.gddkia.gov.pl/userfiles/articles/z/zarzadzenia-generalnego-dyrektor_13901/zalacznikdozarz47.pdf.

Jaskuła, P., 2004a. Dissertation: Analysis of deteriorating effect of water and frost on asphalt mixes. Gdansk Technical University.

Jaskuła, P., 2004b. Niszczące oddziaływanie wody i mrozu na miszanki mineralno-asfaltowe - Przegląd literatury. Drogi i Mosty, 4, pp.5–44.

Kandhal, P., 1992. Moisture susceptibility of HMA mixes: identification of problem and recommended solutions.

Kennedy, T.W, Roberts, F. L., Lee, K.W., 1983. Evaluation of Moisture Effects on Asphalt Concrete Mixtures. Transportation Research Record, 911, pp.134–143.

Kringos, N. & Scarpas, A., 2008. Physical and mechanical moisture susceptibility of asphaltic mixtures. International Journal of Solids and Structures, 45(9), pp.2671–2685. Available at: http://linkinghub.elsevier.com/retrieve/pii/S002076830700515X [Accessed November 6, 2014].

Lottman, R.P., 1978. Predicting Moisture-Induced Damage to Asphaltic Concrete." NCHRP Report 192, Washington, DC.

Majidzadeh, K., Brovold, F., 1968. Effect of water on bitumen–aggregate mixtures.

Sybilski, D. et al., 2013. Research report: Verification and update of water sensitivity test method with freeze-thaw cycle, Warsaw. Available at: https://www.gddkia.gov.pl/userfiles/articles/p/prace-naukowo-badawcze-w-trakcie_3434/EtapIIISpr_TN255_2013_Wodoodpornosc_koncowedodruku.pdf.

# Using Highly Oxidant Gas for Simulating Long-Term Ageing of Asphalt Mix Specimens in the Lab

**Daniel Steiner, Bernhard Hofko, Markus Hospodka, Florian Handle, Lukas Eberhardsteiner, Josef Füssl, Hinrich Grothe and Ronald Blab**

**Abstract** Ageing of bitumen leads to increased stiffness and brittleness. Thus, bituminous bound pavements become more prone to failure by low-temperature and fatigue cracking. Therefore, the ageing behavior of bitumen has a crucial impact on durability, as well as recyclability of pavements. To assess ageing of bitumen, RTFOT and PAV are standardized methods for short-term and long-term ageing in the lab. For lab-ageing of hot mix asphalt (HMA), various methods have been developed in the last decades. This paper presents an optimized lab-aging procedure (Viennese Aging Procedure—VAPro) for compacted HMA specimens to assess mix performance of long-term lab-aged specimens. Thus, it is possible to optimize mix design not only for short-term performance but to take into account effects of oxidative aging during its in-service life. VAPro is based on a triaxial cell with forced flow of a gaseous oxidant agent through the specimen. The oxidant agent is enriched in ozone and nitric oxides to increase the rate of oxidation. It is shown by stiffness tests of unaged and lab-aged specimens, as well as by DSR tests of recovered binder from aged specimens that asphalt mixes can be long-term aged at moderate temperatures (+60 °C) and within 4 days and a flow rate of 1 l/min by applying VAPro. Thus, VAPro can simulate long-term ageing at conditions that are representative of conditions that occur in the field within an efficient amount of time.

**Keywords** Oxidative ageing · Ozone · Asphalt mix · Bitumen · Dynamic modulus · Dynamic shear modulus · Gaseous phase ageing

D. Steiner (✉) · B. Hofko · M. Hospodka · L. Eberhardsteiner · R. Blab
Institute of Transportation, Vienna University of Technology, Vienna, Austria
e-mail: daniel.steiner@tuwien.ac.at

F. Handle · H. Grothe
Institute of Materials' Chemistry, Vienna University of Technology, Vienna, Austria

J. Füssl
Institute for Mechanics of Materials and Structures, Vienna University of Technology, Vienna, Austria



F. Canestrari and M.N. Partl (eds.), *8th RILEM International Symposium on Testing and Characterization of Sustainable and Innovative Bituminous Materials*, RILEM Bookseries 11, DOI 10.1007/978-94-017-7342-3_16

## 1 Introduction and Background

Bitumen as an organic material is subject to changes in its behavior throughout its life by thermal and oxidative ageing. In pavement engineering, ageing of bitumen and bituminous bound pavements is divided into short-term ageing (STA) in the process of HMA production and compaction within a few hours and long-term ageing (LTA) of a pavement during its in-service life within years. STA is triggered by fast oxidation due to high temperatures and a high specific surface contacting with oxidant agents at mix production, as well as evaporation of remaining volatile components from the bitumen (thermal ageing) (Petersen et al. 1994; Baek et al. 2012). LTA is driven by slow oxidation especially of the upper pavement layers by atmospheric oxygen and other highly oxidant gases available in the field (e.g. ozone, nitric oxides) (Morian et al. 2011). Bitumen becomes stiffer and more brittle and thus, pavements are more prone to failure by low-temperature and fatigue cracking with increasing ageing of the binder (Teshale et al. 2011). Since bitumen ageing affects durability and recyclability of pavements crucially, it is important to assess ageing behavior and resistance to ageing of binders and mixes at the stage of mix design optimization to achieve cost and energy efficient pavements with low maintenance demands, a long service-life and high recycling potential.

To assess bitumen ageing in the lab within an efficient amount of time, the rolling thin film oven test (RTFOT) (ASTM 2012; CEN 2007a) and the pressure ageing vessel (PAV) (ASTM 2013; CEN 2012; Airey 2003; Mallick and Brown 2004) are standardized and widely accepted methods to transfer virgin binders into the state of STA (RTFOT) and LTA (RTFOT + PAV) (da Costa et al. 2010; Lu and Isacsson 1998; Airey 2003; Mallick and Brown 2004).

The mineral component and mix design of a pavement can have an impact on ageing of the mix. Thus, it seems important to have a standardized method for LTA of HMA in the lab as well. Therefore, HMA ageing procedures could assist in analyzing changes of HMA material behavior due to ageing from changes of binder behavior. More than 30 lab-ageing procedure of loose or compacted asphalt mix have been developed in the last decades (Steiner 2014; Bell et al. 1994; Çetinkaya 2011). Most of these methods have to be seen as critical due to the following reasons:

- For all methods that incorporate ageing of loose HMA before specimen compaction, it is questionable how binder ageing affects compatibility and quality of cohesion and adhesion of the compacted mix. Thus, it cannot be determined in the subsequent mechanical testing of these specimens whether difference in results between unaged and aged specimens are due to oxidative ageing or rather due to imperfect compaction.
- High temperatures (+100 °C and higher) that are used in ageing protocols for loose HMA exceed temperatures that usually occur in surface layers of pavements. Additional thermal effects (e.g. vaporization of further volatile binder components) could be activated that cannot occur in the field. In addition high temperature could lead to other chemical reactions than in the field, like

increased oligomerization and polymerization with less decomposition reactions.
- The duration of existing ageing protocols for compacted specimens is quite high for some methods (even up to several weeks). Thus, it is questionable whether these methods could be applied for routine testing in the future efficiently.
- To increase the oxidation rate, some protocols for compacted specimens apply high pressures (comparable to pressures in the PAV). Again, these conditions could lead to other chemical reactions than those occurring in the field.

Thus, the main objective of an on-going research project is to develop a new or optimize an existing procedure for ageing of compacted HMA specimens in the lab. To develop an efficient procedure that produces realistically lab-aged specimens for further mechanical testing, an emphasis was put on the following issues:

- Temperature and pressure should not exceed values that are regularly achieved within a surface layer to prevent chemical reactions in the lab that could not occur in the field.
- Increased oxidation should be achieved by using high concentrations of highly reactant gaseous agents that occur in the field in lower concentrations.
- To be applicable for future routine use in the practice, it is important that the procedure can be carried out within a reasonable amount of time.

The procedure presented within this paper can be seen as an extension of a method used within SHRP-A-383 (Bell et al. 1994). The paper contains

- the principles of the developed ageing procedure,
- an in-depth parameter study on impacts of temperature and duration of ageing on the viscoelastic behaviour of a typical surface layer mix, as well as of bitumen recovered from lab-aged specimens,
- a preliminary analysis of the repeatability of the method and
- a set of parameters for the procedure based on a benchmark of RTFOT + PAV aged bitumen samples.

## 2 Materials and Test Methods

### *2.1 Materials*

For the presented study, an asphalt concrete with a maximum nominal aggregate size of 11 mm (AC 11) was employed. The coarse aggregates used for the mix is a porphyrite, the filler is powdered limestone. As a binder an unmodified 70/100 pen (P 58-22) was used. The main characteristics of the binder are listed in Table 1.

The binder content was set to 5.2 % by mass with a target void content of 8.0 % by volume. The maximum density of the AC 11 70/100 was determined to be 2282 kg/m$^3$.

**Table 1** Main characteristics (mean values) of binders

| Parameter | 70/100 pen |
|---|---|
| Penetration (1/10 mm) | 91 |
| Softening point ring and ball (°C) | 46.8 |
| SHRP performance grade (°C) | 58–22 |

## 2.2 Specimen Preparation

The mix was prepared in a laboratory reverse-rotation compulsory mixer, according to EN 12697-35 (CEN 2007c), with a mixing temperature of +165 °C. HMA Slabs (50 × 26 × 4 cm) were compacted in a roller compactor according to EN 12697-33 (CEN 2007b). The compacter consists of a roller segment for compacting the slabs, which corresponds to the dimensions of a standard roller compactor used in the field. All slabs were compacted with one lift. From the slabs, eight specimens are cored out with a diameter of 100 mm. The air void content of the specimens range from 6.8 to 8.7 % by volume.

For bitumen testing, bitumen was extracted according to EN 12697-3 (CEN 2013) with tetrachloroethylene ($C_2Cl_4$) as a solvent. The solvent-bitumen solution was distilled according to EN 12697-3 (CEN 2013) to recover the binder samples.

## 2.3 Gaseous Phase Ageing (GPA)—Viennese Ageing Procedure (VAPro)

Figure 1 shows the setup and equipment which was used for VAPro. Compressed air at ambient temperature was supplied from the local laboratory system and passed a pressure regulator, which ensures a constant flow rate and gas pressure. The subsequent ozone generator, using a dielectric barrier discharge tube (Kogelschatz 2003), enriches the compressed air with ozone and nitrogen oxides. This enriched gas flows through a coiled Cu-Ni tubing with a flow rate of 1 l/min, where it is heated up to $T_{liq}$ = +70 °C. Therefore the coil is placed in a beaker glass, filled with vegetable oil and positioned on a heatable magnetic stirrer.

The HMA specimen is assembled within a triaxial cell between to filter stones and is covered by an elastic membrane. A slight overpressure of 80 kPa was applied in the triaxial cell to force the gas mixture to flow through the specimen instead of passing on the outside. The triaxial cell and setup for heating up the gas are located in a heating cabinet, where the temperature $T_{air}$ was varied for the first experimental run.

Due to the highly corrosive gases, all tubes and connections have to be resistant to corrosion. Thus, all tubes used within the device are made of polytetrafluoroethylene (PTFE).

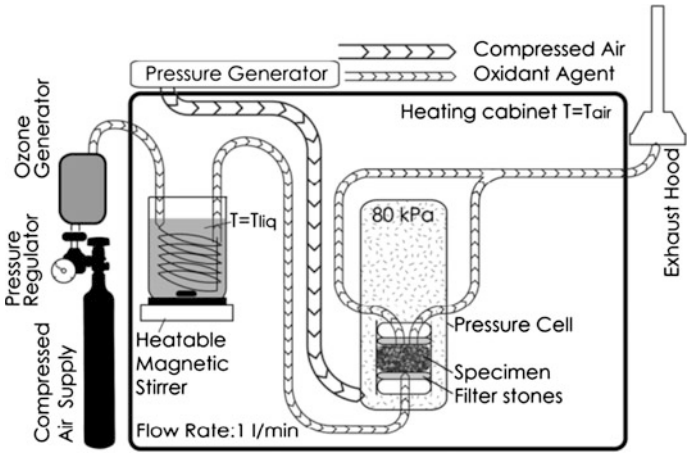


**Fig. 1** Aging setup for VAPro

## 2.4 Dynamic Modulus Testing of HMA

Cyclic indirect tensile tests (IT-CY) were carried out on all specimens before and after ageing at a temperature of +10 °C and frequencies ranging from 0.1 to 20 Hz by applying a sinusoidal load. From test data the dynamic modulus |E*| and the phase angle φ can be determined to describe the viscoelastic behavior of the specimen (Di Benedetto et al. 2001).

In a series of pretests, the upper stress level of the sinusoidal load (see Table 2) was determined so that the elastic horizontal strain amplitude of the specimen during testing is lower than $5 \times 10^{-5}$ m/m. It was shown that repeated tests on the same specimen are possible with these loading conditions (Steiner 2014). This is a necessary precondition since all specimens were tested twice, before and after lab ageing.

## 2.5 Dynamic Shear Modulus of Bitumen

Dynamic Shear Rheometer (DSR) tests were carried out on bitumen samples recovered from all lab-aged HMA specimens. The test conditions were chosen

**Table 2** Test conditions for IT-CY|+10 °C

| Frequency (Hz) | 0.1 | 1 | 5 | 10 | 20 |
|---|---|---|---|---|---|
| Lower stress level (kPa) | 35 | 35 | 35 | 35 | 35 |
| Upper stress level (kPa) | 210 | 240 | 300 | 360 | 390 |
| Number of load cycles (–) | 9 | 15 | 50 | 100 | 100 |

according to the SHRP procedure (Petersen et al. 1994) and EN 14770 (CEN 2005) with a temperature sweep from +46 to +82 °C using the large plate (diameter: 25 mm) and a 1 mm gap. A frequency of 1.6 Hz is employed. From test data the dynamic shear modulus |G*| and the phase angle φ against frequency are determined.

### *2.6 Thermal Ageing Effects in VAPro*

To validate the ageing procedure presented in this paper, it is necessary to analyse and differentiate the oxidative from the thermal impact on ageing. To investigate whether any thermal ageing occurs in VAPro, an HMA specimen was placed within the triaxial cell. Instead of the oxidant gas, the specimen as well as the triaxial cell was saturated with nitrogen to prevent any oxidation. The triaxial cell was placed in the heating cabinet for 4 days at +75 °C. Stiffness tests were carried out on the specimen before and after ageing, as well as DSR tests on the recovered binder from the aged specimen.

## 3 Experimental Program

Table 3 gives an overview of the test program on HMA specimens on the left and on recovered binder samples on the right. The first part of the study looked into the impact of temperature $T_{air}$ and ageing time. Therefore three different temperatures $T_{air}$ = +45 / +60 / +75 °C were combined with ageing times of 1, 2, 3 and 6 days. The results of this first phase should give an overview of the expected increase of dynamic modulus |E*| and dynamic shear modulus |G*|.

In the second part, the dynamic shear modulus |G*| of an RTFOT + PAV-aged binder was set as a benchmark to determine which conditions (ageing time, $T_{air}$) in VAPro match an RTFOT + PAV ageing of bitumen. This benchmark to set ageing conditions for VAPro will be replaced in the future by data from actually field-aged samples that will be taken from a test field in Vienna (Hofko et al. 2014). Furthermore, the repeatability of VAPro was examined by a replication of ageing on three specimens.

**Table 3** Test program for lab ageing of HMA specimen and IT-CY, DSR tests

| | | **IT-CY +10 °C 0.1–20 Hz** | | | | | **DSR SHRP 1.6 Hz 46–82 °C** | | |
|---|---|---|---|---|---|---|---|---|---|
| | | *Temperature* $T_{air}$ (°C) | | | | | *Temperature* $T_{air}$ (°C) | | |
| | | 45 | 60 | 75 | | | 45 | 60 | 75 |
| *Ageing time* (days) | 1 | B/A | B/A | B/A | **VAPro** | **Long-term aged** | x | x | x |
| | 2 | B/A | B/A | B/A | | | x | x | x |
| | 3 | B/A | B/A | B/A | | | x | x | x |
| | 4 | | | | | | | 3x | |
| | 6 | | B/A | B/A | | | | x | x |
| | 4 | | | B/A | **$N_2$ storage** | | | | x |
| B<br>A<br>C&R | –Tested before ageing<br>–Tested after ageing<br>–Compacted and recovered | | | | **RTFOT + PAV** | | x | | |
| | | | | | **Control specimen C&R** | **Short-term aged** | x | | |
| | | | | | **RTFOT** | | x | | |
| | | | | | | **Virgin** | x | | |

# 4 Discussion and Laboratory Test Results

## *4.1 Investigation into Thermal Ageing Effects*

### 4.1.1 Hot Mix Asphalt

To check VAPro for any non-oxidative, i.e. thermal ageing effects due to elevated temperatures, a specimen was stored in the triaxial cell under nitrogen atmosphere at +75 °C for 4 days. Stiffness tests were run on the specimen before and after the storage to analyse changes in the behavior due to nitrogen storage. Figure 2 shows the relative change in the dynamic modulus |E*| after nitrogen storage versus before storage for 3 frequencies in the left diagram. The right diagram shows the change in the phase lag. Both diagrams indicate that no significant change in the material behavior occurs due to thermal effects. The dynamic modulus is reduced by 5–10 %, the phase angle φ increases by 1.0°–2.2°. Thus, it can be stated that no effect of increasing HMA stiffness due to temperature can be found for VAPro.

### 4.1.2 Bitumen

A second check on potential effects from temperature was carried out. Bitumen was extracted and recovered from the nitrogen stored specimen, as well as from a control specimen that was just compacted without any further ageing. DSR tests were run on these samples.

The results are presented in Fig. 3. It shows the relative change in dynamic shear modulus |G* from recovered bitumen samples versus virgin bitumen. Both, the control specimen and the nitrogen stored specimen deliver very similar results that

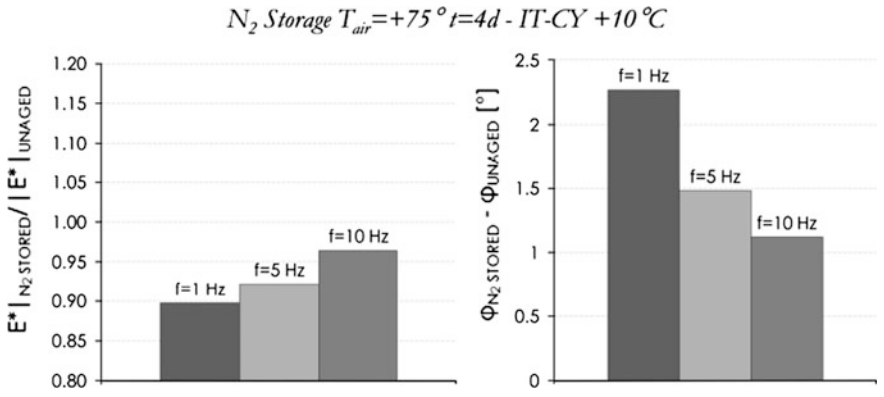


**Fig. 2** Change in dynamic modulus |E*| (*left*) and phase angle φ (*right*) of $N_2$ stored HMA specimen relative to unaged condition

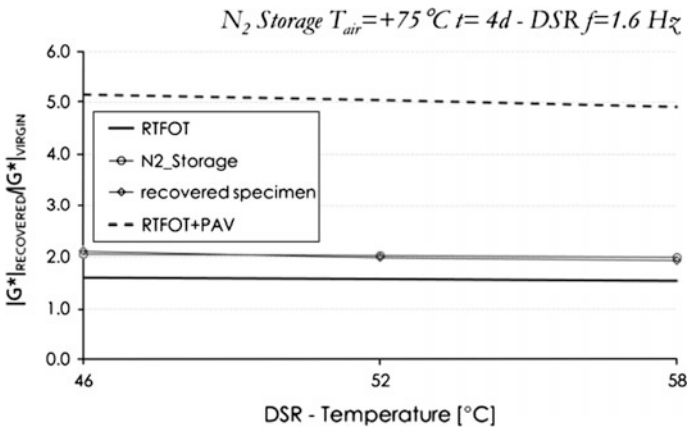


**Fig. 3** Change in dynamic shear modulus |G*| of bitumen recovered from $N_2$ stored HMA specimen to virgin bitumen sample

are close to the RTFOT-aged binder sample. Thus, no thermal effect can be found from the bitumen analysis either, which is consistent with other research carried out in this field (e.g. Ongel and Hugener 2014).

## *4.2 Impact of Temperature and Duration on Ageing*

### 4.2.1 Hot Mix Asphalt

HMA specimens were subjected to VAPro for 1, 2, 3 and 6 days at temperatures ranging from +45 to +75 °C at a constant flow rate of the oxidative gas of 1 l/min. The specimens were tested for their viscoelastic behavior (dynamic modulus |E*| and phase angle φ) in the IT-CY at +10 °C and frequencies ranging from 0.1 to 20.0 Hz. All specimens used for the study were tested before and after ageing to directly compare changes in its behavior due to VAPro. The results are shown in Fig. 4. The diagram shows the relative change in dynamic modulus |E*| of the aged specimen versus unaged specimen over the duration of ageing. Results for +45, +60 and +75 °C are depicted. The data shown in the diagram are mean values (MV) of the frequencies 1, 5 and 10 Hz.

At all temperatures a logarithmic increase of stiffness can be observed with increasing ageing time. At +45 °C ageing durations between 1 and 3 days show no significant changes in the stiffness of the aged specimens, since the data is within the repeatability of the test method. At +60 and +75 °C, changes in stiffness become significant after 2 days of ageing, though no difference between +60 and +75 °C can be seen between 1 and 3 days of ageing. After 6 days of ageing, results from ageing

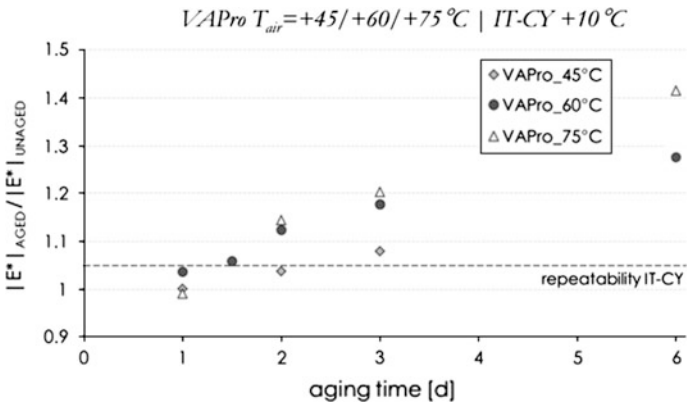


**Fig. 4** Change in dynamic modulus |E*| of lab-aged HMA specimen relative to unaged condition

at +60 and +75 °C show clear differences. While the specimens aged at +60 °C for 6 days come to an increase in stiffness of around 30 %, the increase in stiffness at +75 °C and 6 ageing days is over 40 %.

### 4.2.2 Bitumen

From all VAPro-aged HMA specimens, bitumen was extracted and recovered for analysis of changes of the viscoelastic behavior in the DSR. In addition, STA bitumen by RTFOT and LTA bitumen by RTFOT + PAV was tested as well to compare standardized bitumen ageing procedures to VAPro.

Results are presented in Fig. 5. Analogue to the test results shown for the HMA specimens in Fig. 4, the diagram in Fig. 5 shows the relative change in the dynamic

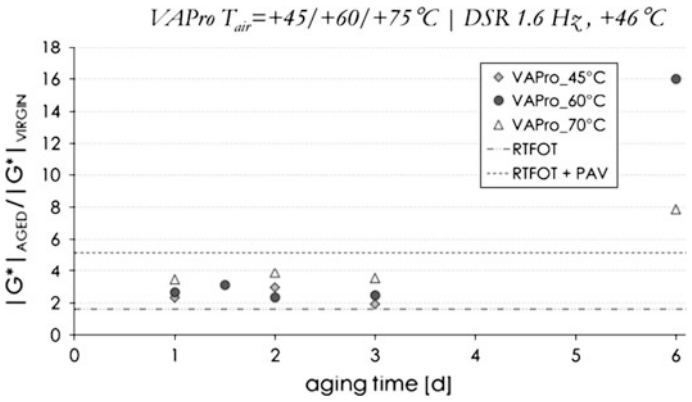


**Fig. 5** Change in dynamic shear modulus |G*| of bitumen recovered from lab-aged HMA specimen to virgin bitumen sample

shear modulus |G*| of bitumen extracted from VAPro-aged HMA specimens versus virgin bitumen over the duration of ageing. Data was obtained from SHRP DSR testing at 1.6 Hz and +46 °C. The dotted lines represent data from the RTFOT and RTFOT + PAV aged bitumen. Similar to the data from stiffness tests on HMA specimens, no significant changes in the binder seem to occur for 1–3 days of ageing. Independent from ageing temperature, all recovered bitumen samples show stiffness similar to RTFOT aged binder. After 6 days of VAPro at +60 °C, the extracted binder is 2 to 3 times stiffer than RTFOT + PAV aged binder. From the results of the +60 °C aged samples, it is obvious that different from the evolution of HMA stiffness with duration of ageing (Fig. 4), the stiffness of the extracted binder samples show a non-linear, exponential increase with increasing duration of ageing.

## 4.3 VAPro Repeatability

For a preliminary analysis of the repeatability of VAPro, three single HMA specimens were aged at +60 °C for 4 days and a flow rate of 1 l/min. The reason for this set of ageing parameters is that the preliminary test program showed, that the extracted binder should behave similarly to RTFOT + PAV aged bitumen at these conditions. The viscoelastic behavior of RTFOT + PAV aged bitumen is the temporary benchmark for the set of parameters of VAPro. It will be replaced by actual data from field-aged HMA samples taken from a test field that was constructed with the same mix design in summer 2012 (Hofko et al. 2014) as soon as data from these field-aged samples become available.

Subsequent to the HMA ageing, binder was extracted and recovered separately for each specimen and SHRP DSR tests were run at 1.6 Hz from +46 to +82 °C. Figure 6 shows the results in 2 diagrams. The left diagram contains the relative

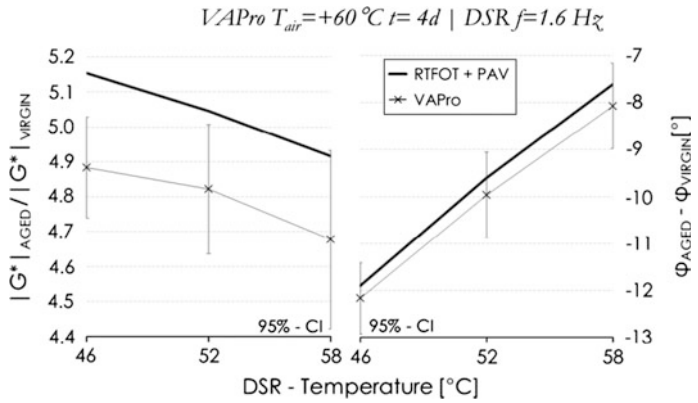


**Fig. 6** Change in dynamic shear modulus |G*| (*left*) and phase angle φ (*right*) of bitumen recovered from VAPro-aged HMA specimen to virgin bitumen sample

change in dynamic shear modulus |G*| over the test temperature from +46 to +58 °C. The right diagram shows the change in phase angle φ over the test temperature. The data from the extracted binder is a mean value from three samples together with the 95 % confidence interval. The bold line represents the results of an RTFOT + PAV aged binder. As it can be seen from both diagrams in Fig. 6, the chosen ageing conditions (+60 °C, 4 days) lead to binder that behaves similar to RTFOT + PAV aged samples. The VAPro binder is 4.7 to 4.9 times stiffer than the virgin bitumen, whereas the RTFOT + PAV sample is 5.05 to 4.9 times stiffer. In terms of change in phase angle φ, both, the VAPro and RTFOT + PAV aged samples show a decrease between 8° and 12°.

## 5 Conclusions and Future Research

The main drive for the research project presented within this paper is to develop an efficient lab-ageing method for compacted HMA specimens to assess long-term performance at the stage of mix design optimization in the future.

The presented ageing procedure, Viennese Ageing Procedure (VAPro), is an extension of a procedure used within SHRP-A-383 (Bell et al. 1994). It is based on a triaxial cell with forced flow of a highly oxidative gaseous agent through the specimen at elevated temperatures. In contrary to existing ageing methods for loose or compacted HMA, VAPro works at temperatures that regularly occur on surface layers in summer (+60 °C). It seems important to keep the temperatures as close to the field as possible in order not to enable any chemical reactions that cannot occur in the field. The oxidation rate is increased by using a compressed air that is enriched in highly oxidative ozone and nitric oxides. Both gases also occur in the field, just in smaller concentrations.

To investigate changes in the viscoelastic behavior of the HMA specimens, cyclic indirect tensile tests were run on the unaged and lab-aged samples. Changes in the dynamic modulus |E*| were compared. In addition bitumen was extracted and recovered from all lab-aged HMA specimens and DSR tests were run to analyse changes in the bitumen behavior and to compare the changes to virgin bitumen samples.

In a preliminary analysis, it was proven by using nitrogen instead of the oxidant gases that no thermal ageing occurs within VAPro, since nitrogen storage at +75 °C for 4 days did not result in significant changes of the viscoelastic behavior of HMA and bitumen.

VAPro was carried out on HMA specimens at +45, +60 and +75 °C with ageing time ranging from 1 to 6 days to investigate the impact of temperature and time on the ageing behavior of the mix. From the stiffness tests carried out on the HMA specimens, it was found that ageing times of 3 days and less lead to no significant ageing at +45 °C. At +60 and +75 °C significant ageing occurs after 2 days of ageing. Significant differences between the two temperatures are only visible after

6 days of ageing. In general, there is a linear trend between increase in stiffness and ageing time in VAPro.

From the extracted binder samples from VAPro-aged HMA samples, it becomes obvious that the stiffness in terms of dynamic shear modulus |G*| increases in a non-linear, exponential way with ageing time. For ageing times of 3 days and less, no significant impact can be found on the bitumen behavior for any of the three ageing temperatures applied. 4 days of ageing at +60 °C is similar to RTFOT + PAV ageing, 6 days of ageing leads to bitumen stiffness that is 2 to 3 times higher than RTFOT + PAV aged samples.

In a first repeatability study with 3 HMA specimens aged at +60 °C for 4 days, the repeatability was found to be satisfying.

Since the results presented within this paper are encouraging, research on VAPro will be continued:

- A detailed analysis of the oxidant gases with a residual gas analyser (RGA) will be carried out to optimize the gas mix in terms of flow rate and concentration of oxidizing gases.
- A test field with the same mix used as for this study, which has been constructed in summer 2012 (Hofko et al. 2014), will be sampled regularly to analyse field aged mixes. Therefore, mechanical and chemical investigation of HMA and recovered bitumen samples will be carried out and compared to data from the VAPro-aged samples to check the procedure for compliance with field ageing. The field-aged samples will also be used as a benchmark that is closer to the field than the RTFOT + PAV aged samples that are used as a benchmark at the present stage.
- The ageing device will be adapted for different specimen dimensions to be able to study the low-temperature and fatigue resistance of lab-aged mixes in a future test program.
- Impact of different mix design parameters, like the void and binder content or the mineral source on ageing behavior will be studied.
- Also, the impact of various HMA modifiers that should reduce ageing (e.g. Sustersic et al. 2013) can be studied in the lab thoroughly before being used in a large-scale test field.

## References

AIREY, G. D. 2003. State of the Art Report on Ageing Test Methods for Bituminous Pavement Materials. *International Journal of Pavement Engineering,* 4, 165-176.

ASTM 2012. ASTM D2872 - 12e1: Standard Test Method for Effect of Heat and Air on a Moving Film of Asphalt (Rolling Thin-Film Oven Test). West Conshohocken, PA.

ASTM 2013. ASTM D 6521-13: Standard Practice for Accelerated Aging of Asphalt Binder Using a Pressurized Aging Vessel (PAV). West Conshohocken, PA.

BAEK, C., UNDERWOOD, B. & KIM, Y. 2012. Effects of Oxidative Aging on Asphalt Mixture Properties. *Transportation Research Record: Journal of the Transportation Research Board,* 2296, 77-85.

BELL, C. A., ABWAHAB, Y., CRISTI M.E. & D., S. 1994. Selection of Laboratory Ageing Procedures for Asphalt Aggregate Mixtures (SHRP-A-383). *Strategic Highway Research Program.* Washington, DC: National Reserach Counil.

CEN 2005. EN 14770: Bitumen and bituminous binders - Determination of complex shear modulus and phase angle - Dynamic Shear Rheometer (DSR). Brussels.

CEN 2007a. EN 12607-1: Bitumen and bituminous binders - Determination of the resistance to hardening under the influence of heat and air - Part 1: RTFOT method. Brussels.

CEN 2007b. EN 12697-33: Bituminous mixtures - Test methods for hot mix asphalt - Part 33: Specimen prepared by roller compactor. Brussels.

CEN 2007c. EN 12697-35: Bituminous mixtures - Test methods for hot mix asphalt - Part 35: Laboratory mixing. Brussels.

CEN 2012. EN 14769: Bitumen and bituminous binders - Accelerated long-term ageing conditioning by a Pressure Ageing Vessel (PAV). Brussels.

CEN 2013. EN 12697-3: Bituminous mixtures - Test methods for hot mix asphalt - Part 3: Bitumen recovery: Rotary evaporator. Brussels.

ÇETINKAYA, R. 2011. *Bewertung der Einflussgrößen auf die thermisch-oxidative Alterung von Bitumen im Asphalt,* Bochum; Germany, Europ. Univ.-Verl.

DA COSTA, M. S., FARCAS, F., SANTOS, L., EUSEBIO, M. I. & DIOGO, A. C. 2010. Chemical and Thermal Characterization of Road Bitumen Ageing. *Advanced Materials Forum V, Pt 1 and 2,* 636-637, 273-279.

DI BENEDETTO, H., PARTL, M. N., FRANCKEN, L. & DE LA ROCHE SAINT ANDRE, C. 2001. Stiffness testing for bituminous mixtures. *Materials and Structures,* 34, 66-70.

HOFKO, B., HOSPODKA, M., BLAB, R., EBERHARDSTEINER, L., FUESSL, J., GROTHE, H. & HANDLE, F. Impact of Field Ageing on Low-Temperature Performance of Binder and Hot Mix Asphalt. Proceedings of the 12th ISAP Conference on Asphalt Pavements, 2014 Raleigh, NC.

KOGELSCHATZ, U. 2003. Dielectric-Barrier Discharges: Their History, Discharge Physics, and Industrial Applications. *Plasma Chemistry and Plasma Processing,* 23, 1-46.

LU, X. H. & ISACSSON, U. 1998. Chemical and rheological evaluation of ageing properties of SBS polymer modified bitumens. *Fuel,* 77, 961-972.

MALLICK, R. B. & BROWN, E. R. 2004. An Evaluation of Superpave Binder Aging Methods. *International Journal of Pavement Engineering,* 5, 9-18.

MORIAN, N., HAJJ, E. Y., GLOVER, C. J. & SEBAALY, P. E. 2011. Oxidative Aging of Asphalt Binders in Hot-Mix Asphalt Mixtures. *Transportation Research Record: Journal of the Transportation Research Board,* 2207, 107-116.

ONGEL, A. & HUGENER, M. 2014. Aging of bituminous mixes for rap simulation. *Construction and Building Materials,* 68, 49-54.

PETERSEN, J. C., ROBERTSON, T., BRANTHAVER, J. F., HARNSBERGER, P. M., DUVALL, J. J., KIM, S. S., ANDERSON, D. A., CHRISTIANSEN, D. W., BAHIA, H. U., DONGRE, R., C.E., A., SHARMA, M. G., BUTTON, J. W. & GLOVER, C. J. 1994. Binder Characterization and Evaluation Volume 4: Test Methods (SHRP-A-370). *Strategic Highway Research Program.* Washington, DC: National Reserach Counil.

STEINER, D. 2014. *Towards an optimized lab aging protocol for asphalt mix specimen to assess long-term aging.* MSc Master Thesis, Vienna University of Technology.

SUSTERSIC, E., TUSAR, M. & VALANT, A. Z. 2013. Rheological and mechanical characterization of waste PMMA/ATH modified bitumen. *Construction and Building Materials,* 38, 119-125.

TESHALE, E. Z., MOON, K.-H., TUROS, M. & MARASTEANU, M. 2011. Pressure Aging Vessel and Low-Temperature Properties of Asphalt Binders. *Transport Research Record: Journal of the Transport Research Board*, 117-124.

# Methods for Analyzing the Chemical Mechanisms of Bitumen Aging and Rejuvenation with FTIR Spectrometry

**Peter Mikhailenko, Alexandra Bertron and Erick Ringot**

**Abstract** The recycling of asphalt is a process where old pavement is broken up and used as reclaimed asphalt pavement (RAP) in new asphalt pavement, often with the aid of recycling agents. The goal of asphalt recycling agents is to reintroduce the properties lost in bitumen and asphalt during aging such as penetration, softening point, viscosity, ductility, cohesion and adhesion to aggregate, reducing the performance of asphalt and requiring its replacement. The purpose of this study is to observe the chemistry of bitumen aging and the effects of recycling agents may have in reversing it. Fourier transform infrared spectroscopy (FTIR)-attenuated total reflectance (ATR) was used to analyse the bitumen aging and regeneration in terms of the evolution of carbonyl, sulfoxide and other bands. FTIR-ATR microscopy was used to study the distribution of these bands between the aggregates in order to understand the remobilization of the old asphalt (RAP) by the recycling agents through observing their penetration into the RAP. A method for aging bitumen and mastic in a ventilated oven was developed. An increase in C=O and S=O indices was observed with aging, plateauing after 7d.

**Keywords** Bitumen aging · FTIR · RAP · Asphalt rejuvenating agent

## 1 Introduction

The service life of asphalt pavement can depend on many factors including the traffic loading, the environment, the drainage and the quality of construction. While regular maintenance cycles can mitigate the aging effects, the long-term aging effects on the bitumen will eventually lead to surface cracks that require the pavement to be rehabilitated or replaced (Smith and Edwards 2001). The initial

P. Mikhailenko (✉) · A. Bertron · E. Ringot
Laboratoire Matériaux et Durabilité des Constructions (LMDC), Université Paul Sabatier, Toulouse, France
e-mail: mikhaile@insa-toulouse.fr



F. Canestrari and M.N. Partl (eds.), *8th RILEM International Symposium on Testing and Characterization of Sustainable and Innovative Bituminous Materials*, RILEM Bookseries 11, DOI 10.1007/978-94-017-7342-3_17

hardening of the bitumen (short-term aging) is largely due to the evaporation of the lighter aromatics, naphthene aromatics during bitumen storage at hot temperature (160–180 °C), along with mixing (160 °C+) while the long-term aging effects are due to the oxidation over the in-service time (Chávez-Valencia et al. 2007; Siddiqui and Ali 1999). Another possible contributor to aging is ultraviolet (UV) radiation from exposure to the sun (Durrieu et al. 2007).

With the aging of asphalt pavement roads around the world, their need for replacement can create enormous waste disposal problems. While surface rejuvenation can extend the service life of a pavement, the mechanical changes from bitumen aging makes it inevitable that the asphalt will need to be replaced. When the price of oil (and bitumen) was relatively low, recycling asphalt was not considered economically necessary. Recently however, as this situation is changing, recycling asphalt is becoming more widespread (Brownridge 2010; Davidson et al. 1978). The recycling of asphalt is a process where old pavement is broken up and used as reclaimed asphalt pavement (RAP) in new asphalt pavement. RAP is defined as "asphalt reclaimed by milling of asphalt road layers, by crushing of slabs ripped up from asphalt pavements or lumps from asphalt slabs and asphalt from reject and surplus production" by EN 13108-8. Some RAP can be characterized as "black rock", that is, bitumen will not be able to act as a binder for asphalt with conventional mixing procedures, but most RAP is able to recover a part of its adhesive abilities (Chen et al. 2007).

In addition to the cost benefits of being able to produce new asphalt from old, there is also the advantage of reducing the carbon footprint of the construction significantly by reducing the transportation emissions and extraction of virgin aggregates. Additionally, this allows for the clean and relatively easy removal of a waste product in old asphalt. On the other hand, VOCs from bitumen volatilization have been found to increase with recycling rate (Jullien et al. 2006).

As RAP is derived from old asphalt, its performance characteristics are determined largely by the aging of the bitumen. The resulting characteristics include a decrease in penetration, increase in softening point, increase in viscosity, decrease in ductility, cohesion, and adhesion of aggregates and bitumen, along with a decrease in thermal resistance for asphalt (Al-Qadi et al. 2007). The capacity of the asphalt to heal itself is also decreased (Van den bergh and Van de Ven 2012). In addition to these negative effects, the rutting and fatigue resistance are sometimes increased due to the bitumen becoming harder, although this is not always the case, and the performance can also be equal or worse in these two parameters compared with asphalt without RAP addition. In the final analysis, the performance of the RAP asphalt will depend heavily on the quality of the RAP aggregates (Al-Qadi et al. 2007; Aravind and Das 2007).

Asphalt recycling agents or rejuvenators have been known since the 1950s. Without the recycling agents, the % RAP that can compose the new pavement is much more limited. It is important that the recycling agent be compatible with the given RAP that is, being able to contact and interact with the old bitumen (Chen et al. 2007).

The purpose of this paper is to study the chemical mechanisms of bitumen aging and rejuvenation with FTIR spectrometry techniques. The principal tasks of this study are to (i) adapt a method for the laboratory aging bitumen and mastic in a ventilated oven, (ii) analyse the nature of bitumen oxidation globally using FTIR-ATR and microscopically (locally) using FTIR-ATR microscopy and (iii) analyse the nature of the rejuvenating agents and their effect on bitumen by FTIR-ATR microscopy. The rejuvenating agent tested was a bio-sourced agent developed for this study.

## 2 Materials and Methods

The experimental program was a working compromise between the goals of the research and the facilities available to the researchers. In order to observe the aging and rejuvenation of bitumen, the techniques for aging and rejuvenation needed to be developed. The consisted of using methods adapted from those in studies with similar objectives.

### *2.1 Materials*

Several types of samples were prepared for this study, including bitumen, mastic and rejuvenating agents.

**Bitumen**: The bitumen was Total 35/50 as classified by NF EN 12591, indicating a penetration (ASTM D5-NF EN 1426) value of between 3.5 and 5.0 mm.

**Sand**: The sand was 0.315–1 mm Larronde—Ainhoa ($\rho V = 2.85$ g/cm$^3$) limestone. The sand was graded and washed in order to remove fines (<0.315 mm) that may interfere with the microscopic analysis as with El Béze et al. (2012).

**Mastic**: While the grain size of the RAP can be controlled through the crushing process, due to the diverse conditions of fabrication and for the original asphalt of RAP, its properties will have a high variability potential from one source to the next. In addition to this, one source of RAP may have a high variability within it depending on where the aggregates were positioned in the road (depth, near water sources, amount of sun exposure). The bitumen in the top few millimeters of the surface has a significant increase in viscosity (Smith and Edwards 2001). Thus, there exists a need for lab-manufactured RAP in order to provide a homogeneous material for testing (El Béze 2008; Navaro 2011). El Béze et al. (2012) and Van den bergh and Van de Ven (2012) fabricated RAP mastic (bitumen + sand).

For the preparation of the mastic, the bitumen (80 %) is pre-heated at 160 °C for 2h ± 15 min in a closed pot. The Ca sand (20 %) is heated to 160 °C for at least 6 h before the mixture. The sand is incorporated in the pot and mixed with a Heidolph RZR mixer (2–5 min) disposed on a Fisher Scientific Isotemp hot plate (160 °C, temperature control with thermocouple in the pot). The mastic is then

poured into a trapezoidal of silicone mold with dimensions 65–77 mm × 21–29 mm × 30 mm and consolidated with a spatula. The samples are cooled for 6 h at room temperature and are then stored at 4 °C in a refrigerator, so as to reduce sample melting, but not so cold as to induce damage to the bitumen from crystallization of the saturates that occurs below −7 °C (Fuentes-Audén et al. 2008; Garcia-Morales et al. 2006; McNally 2011).

**Rejuvenating agents**: There have been several types of recycling agents used with RAP. Some examples include lubricating and extender oils, which contain high proportions of maltenes [Terrel and Epps (1989) cited by Al-Qadi et al. (2007)]. The compatibility of the agent with bitumen can be an issue. Recycling agents with high aromatic and low saturate contents are usually more compatible with RAP bitumen [(Dunning and Mendenhall 1978; Wood 1978) cited by Al-Qadi et al. (2007)]. The development of bio-sourced agents is still relatively novel (Hajj et al. 2013; Kim 2014; Reinke et al. 2014; Zargar et al. 2012). Part of this study is the development of a bio-sourced and biodegradable rejuvenating agent, labelled (B1). The aged mastic sample is heated at 160 °C for 2 h in a closed pot, after which, the agent incorporated into the mastic at 7.5 %w, is placed with a spatula directly into the pot on a balance. It is mixed with a Heidolph RZR mixer (2–5 min) for homogenization. The mastic was left to cool to room temperature for 6 h before testing.

## 2.2 *Bitumen and Mastic Aging*

Due to the fact that the life cycle of asphalt is many years, several accelerated laboratory aging methods have been developed in order to simulate the effects of aging on bitumen for a shorter period of time. This can be separated into short-term and long-term aging. Short-term aging refers to the change in properties of asphalt during storage at the plant and conventional hot-mixing (both around 160 °C) and can performed by TFOT (EN 12607-1/ASTM D 1754) and RTFOT - EN 12607-2/ASTM D 2872). Long term aging is the bitumen oxidation the hot-mixing, during the service-life of the asphalt before it would need replacement, this can be performed by PAV (ASTM D 6521), which is intended to simulate the effects of oxidation for several years, although the precise date is still up for debate (Farcas 1996; Mouillet et al. 2008).

For this study, a ventilated oven was used for the long-term aging process of both bitumen and mastic. The oven needs to be well ventilated for the test to provide a consistent supply of oxygen to the sample, which should be made a thin as possible in order to provide more surface area for the oxidation. For asphalt aging, there are varied temperatures suggested such as 60 °C by Durrieu et al. (2007) or 60, 80 and 100 °C for 24, 36 and 48 days by Chávez-Valencia et al. (2007) finding that 24–36 days over oven aging at 100 °C can be correlated with approximately 1–2 year of aging in the field for certain properties but not others, such as viscosity, penetration and oxidation by FTIR. The asphalt in the field for

example, would not lose as many volatiles compounds as during high temperature oven aging (Tahirou 2009). This is because some of the volatiles for their in-field conditions would never achieve their volatility temperature. De la Roche et al. (2013) conducted the aging of asphalt in two stages; the first at 135 °C for 4 h and the second at 85 °C for 9 days, finding that plant and laboratory manufactured asphalt ages differently in terms of the same indicators.

The same aging time and temperature parameters were used in this study, only adapted for bitumen and mastic. The bitumen was aged by pouring a 2.5 ± 0.2 mm layer of bitumen (pre-heated in a closed pot at 160 °C for 2 h) on a silicone plate, as silicone has a very low adhesion to bitumen. The bitumen is placed in the oven at 135 °C for 4 h and the second at 85 °C for a period determined from correlating with the rheology of the aged bitumen. The bitumen is allowed to cool for at least 6 h before being tested. For mastic aging, the sample was preheated at 160 °C for 2 h, placed on a silicone plate for a thickness of 20 ± 10 mm. The mastic is agitated after 1 day and then every two days for the aging process, and the aging parameters were the same as for bitumen.

## *2.3 FTIR-ATR Analysis*

Fourier transform infrared spectroscopy (FTIR) has been used to obtain infrared spectrum of material, including bituminous material. The spectra correspond to vibrations of various chemical bonds, allowing for them to be characterized. The attenuated total reflectance (FTIR-ATR) mode allows for analyzing the bitumen sample directly on a crystal (Farcas et al. 2009).The change of key FTIR bands as a result of bitumen aging in the literature is summarized in Table 1.

The oxidation of hydrocarbons is associated, notably, with the increase of C=O (1700 $cm^{-1}$) and S=O (at 1030 $cm^{-1}$) bonds for laboratory aged asphalt (Mouillet et al. 2008; Siddiqui and Ali 1999). This has been confirmed with in situ aging on asphalt roads by Lamontagne et al. (2001a), Jung (2006) and Chávez-Valencia et al. (2007). More specifically, Mouillet et al. (2008) considers the S=O bands to represent the short term aging during asphalt manufacturing and the C=O bands to represent the long-term aging during the service life of the asphalt. Aromaticity (at 1600 $cm^{-1}$) is the measure with FTIR of the relative contents of aromatic C=C bonds, respectively. This could be an indication of volatile naphthene aromatics and heavier particles such as resins and asphaltenes as well. It was found by Lamontagne et al. (2001b) and Mouillet et al. (2008) that the aromaticity of bitumen tends to increase somewhat with aging in both lab and field environments as the heavier and less volatile chemicals in bitumen, notably resin and asphaltene, tend to be more aromatic. Tachon (2008) observed the SARA fractions with FTIR and found that the peak associated with polarity (around 3450 $cm^{-1}$) is present in only the heavier resin and asphaltene fractions; although this was not correlated with bitumen aging. The FTIR analyses of RTFOT aged bitumen appear to show some decrease in

**Table 1** FTIR bands with bitumen aging

| Chemical Group | Bond | Approximate wave number ($cm^{-1}$) | Change with aging | Intensity | Expression | References |
|---|---|---|---|---|---|---|
| Sulphoxide | S=O | 1030 | Increases in short-term | Weak | $\frac{A_{1030}}{A_{1460}+A_{1376}}$ | Lamontagne et al. (2001a), Lu and Isacsson (2002), Jung (2006), Chávez-Valencia et al. (2007), Durrieu et al. (2007), Mouillet et al. (2008), Vargas et al. (2008), Araújo et al. (2011), El Béze et al. (2012), Yao et al. (2013) |
| Carbonyl | C=O | 1700 | Increases in long-term | Weak to medium | $\frac{A_{1700}}{A_{1460}+A_{1376}}$ | |
| Aliphatics (asymmetric) | $C–CH_3$ | 1460, 1376 | Relatively constant to small decrease | Medium | $\frac{A_{1460}+A_{1376}}{\Sigma A^a}$ | |
| Aromatics | C=C | 1600 | Relatively constant to increase | Medium | $\frac{A_{1600}}{\Sigma A^a}$ | Lamontagne et al. (2001b), Mouillet et al. (2008), Tachon (2008)[b] |
| Aliphatics | $CH_2$, $CH_3$ | 2923, 2853 | Relatively constant to small decrease | Medium to strong | $\frac{A_{2923}+A_{2850}}{\Sigma A^a}$ | Tachon (2008)[b], Lins et al. (2008), Yao et al. (2013)[c] |
| Polarity | O–H | 3450 | Increases | Strong | $\frac{A_{3450}}{\Sigma A^a}$ | Tachon (2008)[b], Araújo et al. (2011) |

[a] $\Sigma A = A_{1700} + A_{1600} + A_{1460} + A_{1376} + A_{1030} + A_{864} + A_{814} + A_{743} + A_{724} + A_{(2953,2923,2862)}$ (Lamontagne et al. 2001a, b) or $\Sigma A = A_{2000} + A_{600}$ (Yao et al. 2013)

[b] Hypothesized from results of FTIR analysis of SARA fractions by Tachon (2008)

[c] Observed from results of FTIR analysis of SARA fractions by Yao et al. (2013)

aliphatics (2925 and 2853 $cm^{-1}$) peaks with aging (Araújo et al. 2011). The carbonyl index (%) and sulfoxide index (%) are defined in Table 1 for C=O and S=O, respectively, with a higher value indicating relatively more bonds. The bands around 1460 $cm^{-1}$ and 1376 $cm^{-1}$ are for the $CH_2$ and $CH_3$ groups, serve as baselines for the analysis as they change relatively little during aging (El Béze 2008).

The FTIR-ATR analysis was performed with a PerkinElmer Spotlight 400 and a Ge ATR crystal. The analysis was effectuated 16 times (per sample) with a 4 $cm^{-1}$ resolution and a band range of 4000–600 $cm^{-1}$ on a Germanium crystal, due to the compatibility of Ge with analyzing organic compounds. For the bitumen, around 0.5 g is placed with a spatula (at ambient temperature) on the crystal with a vertical pressure of 100 ± 10 N in order to reduce air between the sample and the crystal. The crystal is cleaned with ethanol before each test.

### 2.4 FTIR-ATR Microscope Imaging

FTIR-ATR microscopy allows for cartography of the distribution of the spectra in the asphalt, that is, in relation to the position of the bitumen and aggregates. El Béze (2008) used FTIR-ATR microscopy to observe the aging in laboratory made RAP mortar sample with an ATR germanium crystal for an analysis depth of 1–3 µm. The samples were polished beforehand in order to flatten their surface and reduce discrepancies in the contact between the crystal and bitumen, although the lack of surface flatness caused significant problems in this form of testing. Calcium aggregates were appropriate for this method as their signature (864 $cm^{-1}$) does not conflict with the principal indicators of bitumen oxidation at 1700 and 1000 $cm^{-1}$ for C=O and S=O, respectively, making them distinguishable from the bitumen relative to the asymmetric aliphatic peaks at 1460 and 1376 $cm^{-1}$. The oxidation indicators appeared to be higher close to the aggregate grain, although their distribution in the middle points of the bitumen was heterogeneous (El Béze et al. 2012).

The FTIR-ATR analyses were performed with a PerkinElmer Spotlight 400 couples with a PerkinElmer Frontier Imager and a ZnSe ATR crystal. The analyses were effectuated 4 times (per sample) with a 16 $cm^{-1}$ resolution, a band range of 4000–750 $cm^{-1}$, and a pixel size of 1.56 µm. The mastic samples were stored at 4 °C for a minimum of 6 h and then cut by a saw to ensure that they were relatively flat on both sides. The samples were then polished using 3 polishing discs (Presi-Tissediam) at 250 µm (for 2–3 min), 75 µm (1 min) and 40 µm at a rotational speed of around 200 rpm. The samples are kept in a cooler between each step of this process in order to reduce melting. The mastic is analyzed by applying the crystal to the surface of the samples, taking FTIR cartographies of 150 × 150 µm.

## 3 Results and Discussion

### 3.1 Bitumen Aging by FTIR-ATR

The bitumen samples were subjected to oven aging in order to determine an appropriated aging duration. Three series of aging were conducted with FTIR-ATR analysis for oven aging of up to 17d (3 samples) and 42d (1 sample), with two spectra for each sample. For the first series of aging, the change in mass of the 3 samples was measure by taking its mass with a balance precise to 0.01 g. The results for the change in mass, $I_{C=O}$ and $I_{S=O}$, $A_{1600}$, are shown in Figs. 1 and 2.

During the oven aging, the bitumen loses the majority of the volatiles (3 % of its total mass) during the first 24 h (Fig. 1). There is no further mass loss after 48 h, while there is a very small gain after 7 days, which could be either an increase in oxidation products in the bitumen or an error with the balance.

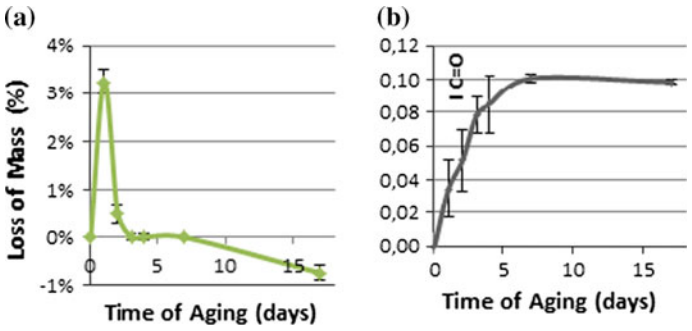


**Fig. 1** **a** Mass loss % from 0–17 days of bitumen aging. **b** Change in $I_{C=O}$ 0–17 days for bitumen oven aging (average of three samples)

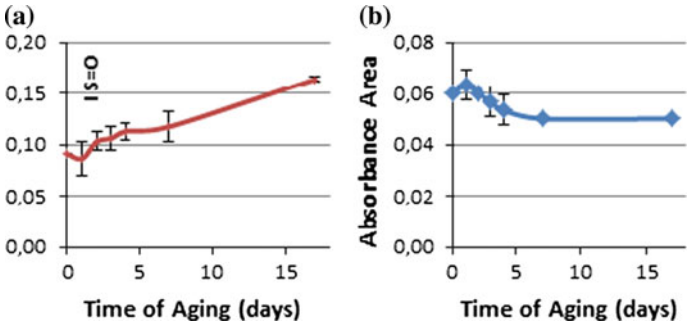


**Fig. 2** **a** Change in $I_{S=O}$ 0–17 days for bitumen oven aging. **b** Change in $A_{1600}$ for 0–17 days of bitumen aging (average of three samples)

For the first series of aging up to 17d, the C=O index increased for the first 7d of aging, after which, it plateaued (Fig. 1). The S=O continued showed a small increase from 7–18d (Fig. 2), and so a second series of aging was conducted up to 42d, for which the S=O appeared to plateau after 7d with some fluctuation. The C=O index, after an initial plateau after 7d, appeared to increase further after 21d of aging, and continues up to 42d (data not shown due to article length considerations). The nature of the $A_{1600}$ was inconclusive as it was stable in the first series (Fig. 2) of aging (data not shown), while having an increase in the second series after 2d and further up to 29d, descending thereafter. An increase was also found with Lamontagne et al. (2001b) and Mouillet et al. (2008). The 1600 $cm^{-1}$ can be an indicator with aging, but is much less reliable than the oxidation bands.

## 3.2 Mastic Aging and Regeneration by FTIR-ATR Microscope Imaging

In a parallel study, the oven-aging of bitumen showed a correlation with bitumen aged with RTFOT + PAV for bitumen at 11 days for penetration (EN 1426) and 18 days for dynamic viscosity (EN 14770). Based on these findings, the mastic was aged for 14 days in the oven. The images were extrapolated by taking the band ratios for oxidation from the spectra. While the C=O spectra were difficult to observe, the S=O appeared consistently, and thus the band ratio from Table 1 was used. The images for unaged mastic and mastic aged for 14 days in an oven are shown in Fig. 3, while the aged mastic with the rejuvenating agent is show in Fig. 4. A higher ratio indicates a higher degree of oxidation.

The S=O indices proved to be a clearer indication of oxidation than the C=O indices, which possible showed a need to increase the accuracy of the FTIR analysis by having more scans per analysis for example, or improving the surface polishing. The band ratio for $I_{S=O}$ allowed for the distinction of the bitumen zones from the aggregates. The mastic aged for 14 days indicated significantly higher oxidation than the unaged mastic, having zones exceeding 0.05 for the most part and a significant quantity of zones exceeding 0.1, while the unaged mastic was around 0.02–0.03 (Fig. 3). The bitumen showed higher oxidation around the sand, due to the oxidation that is induced by the hot aggregates on the bitumen during mixing (Atkins 2003; Chen et al. 2007). However, in general, the pattern of oxidation was not consistent, similar to the experience of El Béze (2008). The addition of the rejuvenating agent resulted in a decrease in the oxidation overall (Fig. 4), having a lower quantity of zones above 0.1, although it is not certain whether it is from a dilution effect or from chemical changes. The fact that the quantity of the agent was only 7.5 %w could indicate that this was not solely a dilution effect. The spots of

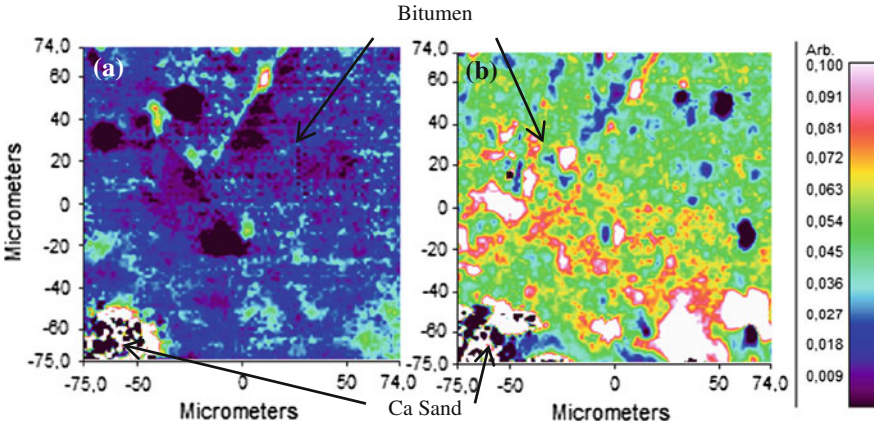


**Fig. 3** FTIR-ATR microscope 1030 $cm^{-1}$/(1460 + 1376 $cm^{-1}$) band ratio images for: **a** unaged mastic and **b** mastic aged for 14 days in oven (*right*)

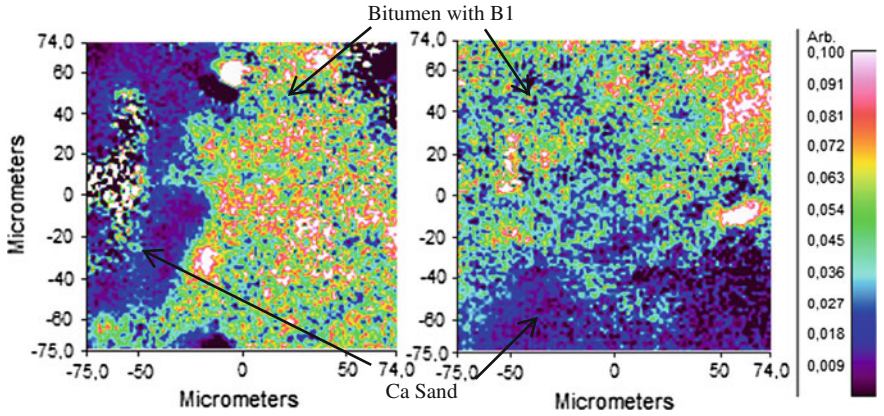


**Fig. 4** FTIR-ATR microscope 1030 $cm^{-1}$/(1460 + 1376 $cm^{-1}$) band ratio images for mastic aged for 14 days in oven 7.5 % B1 added

+0.1 absorbance also appear to be much less coagulated than for the aged bitumen. A parallel study confirmed the reduction in the dynamic viscosity (EN 14770) of the bitumen with 7.5 % of the agent, although not up to the rheology as for unaged 35/50 bitumen. The melting of the bitumen during the test was found to be a serious problem with FTIR microscopy in terms of getting a clear analysis.

## 4 Conclusions

The conclusions in the methods for analyzing the chemical mechanisms of bitumen aging and rejuvenation with FTIR spectrometry are as follows:

- The bitumen loses most of its volatiles during the first 24 h of oven aging;
- C=O are and S=O are consistent indicators of bitumen aging, increasing for up to 7d oven aging;
- Oven-aging of bitumen showed a correlation to bitumen aged with RTFOT + PAV for bitumen at 11 days for penetration (EN 1426) and 18 days for dynamic viscosity (EN 14770);
- Bitumen oxidation is identifiable through FTIR microscopy, occurring the most significantly around the aggregates; the addition of a rejuvenating agent has shown a capacity to reduce S=O in the bitumen.

## References


Al-Qadi, I.L., Elseifi, M., Carpenter, S.H., 2007. Reclaimed Asphalt Pavement–A Literature Review. Research Report FHWA-ICT-07-001, Illinois Center for Transportation, USA.

Araújo, M.F. a. S., Lins, V.F.C., Pasa, V.M.D., 2011. Effect of ageing on porosity of hot mix asphalt. Braz. J. Pet. Gas 5. doi:10.5419/bjpg.v5i1.145.

Aravind, K., Das, A., 2007. Pavement design with central plant hot-mix recycled asphalt mixes. Constr. Build. Mater. 21, 928–936. doi:10.1016/j.conbuildmat.2006.05.004.

Atkins, H.N., 2003. Highway materials, soils, and concretes. Prentice Hall, Upper Saddle River.

Brownridge, J., 2010. The role of an asphalt rejuvenator in pavement preservation: use and need for asphalt rejuvenation, in: First International Conference on Pavement Preservation.

Chávez-Valencia, L.E., Manzano-Ramírez, A., Alonso-Guzmán, E., Contreras-García, M.E., 2007. Modelling of the performance of asphalt pavement using response surface methodology —the kinetics of the aging. Build. Environ. 42, 933–939. doi:10.1016/j.buildenv.2005.10.013.

Chen, J.S., Huang, C.C., Chu, P.Y., Lin, K.Y., 2007. Engineering characterization of recycled asphalt concrete and aged bitumen mixed recycling agent. J. Mater. Sci. 42, 9867–9876. doi:10.1007/s10853-007-1713-8.

Davidson, D.D., Canessa, W., Escobar, S.J., 1978. Single additive recycling for asphalt pavements. Civ. Eng.-ASCE.

De la Roche, C., Van de Ven, M., Planche, J.-P., Van den Bergh, W., Grenfell, J., Gabet, T., Mouillet, V., Porot, L., Farcas, F., Ruot, C., 2013. Hot Recycling of Bituminous Mixtures, in: Advances in Interlaboratory Testing and Evaluation of Bituminous Materials. Springer, pp. 361–428.

Dunning, R., Mendenhall, R., 1978. Design of Recycled Asphalt Pavements and Selection of Modifiers, in: Recycling of Bituminous Pavements: A Symposium. ASTM International.

Durrieu, F., Farcas, F., Mouillet, V., 2007. The influence of UV aging of a Styrene/Butadiene/Styrene modified bitumen: Comparison between laboratory and on site aging. Fuel 86, 1446–1451. doi:10.1016/j.fuel.2006.11.024.

El Béze, L., 2008. Recyclage à chaud des agrégats d'enrobés bitumineux: Identification de traceurs d'homogénéité du mélange entre bitume vieilli et bitume neuf d'apport. Doctoral Thesis, Université Paul Cézanne Aix-Marseille III, Marseille.

El Béze, L.E., Rose, J., Mouillet, V., Farcas, F., Masion, A., Chaurand, P., Bottero, J.-Y., 2012. Location and evolution of the speciation of vanadium in bitumen and model of reclaimed bituminous mixes during ageing: Can vanadium serve as a tracer of the aged and fresh parts of the reclaimed asphalt pavement mixture? Fuel 102, 423–430. doi:10.1016/j.fuel.2012.06.080.

Farcas, F., 1996. Etude d'une methode de simulation du vieillissement sur route des bitumes. Doctoral Thesis, Universit de Paris VI, Paris.

Farcas, F., Mouillet, V., Besson, S., Battaglia, V., Petiteau, C., Le Cunff, F., 2009. Identification et dosage par spectrometrie infrarouge a transformee de Fourier des copolymeres SBS et EVA dans les liants bitumineux. ME 71, LCPC, Paris.

Fuentes-Audén, C., Sandoval, J.A., Jerez, A., Navarro, F.J., Martínez-Boza, F.J., Partal, P., Gallegos, C., 2008. Evaluation of thermal and mechanical properties of recycled polyethylene modified bitumen. Polym. Test. 27, 1005–1012. doi:10.1016/j.polymertesting.2008.09.006.

Garcia-Morales, M., Partal, P., Navarro, F.J., Gallegos, C., 2006. Effect of waste polymer addition on the rheology of modified bitumen. Fuel 85, 936–943.

Hajj, E.Y., Souliman, M.I., Alavi, M.Z., Loría Salazar, L.G., 2013. Influence of Hydrogreen Bioasphalt on Viscoelastic Properties of Reclaimed Asphalt Mixtures. Transp. Res. Rec. J. Transp. Res. Board 2371, 13–22.

Jullien, A., Monéron, P., Quaranta, G., Gaillard, D., 2006. Air emissions from pavement layers composed of varying rates of reclaimed asphalt. Resour. Conserv. Recycl. 47, 356–374. doi:10.1016/j.resconrec.2005.09.004.

Jung, S.H., 2006. The Effects of Asphalt Binder Oxidation on Hot Mix Asphalt Concrete Mixture Rheology and Fatigue Performance. Doctoral Thesis, Texas A&M University.

Kim, Y., 2014. Proceedings of 12th ISAP Conference on Asphalt Pavements in Raleigh, North Carolina, CRC Press, London.

Lamontagne, J., Dumas, P., Mouillet, V., Kister, J., 2001a. Comparison by Fourier transform infrared (FTIR) spectroscopy of different ageing techniques: application to road bitumens. Fuel 80, 483–488.

Lamontagne, J., Durrieu, F., Planche, J.P., Mouillet, V., Kister, J., 2001b. Direct and continuous methodological approach to study the ageing of fossil organic material by infrared microspectrometry imaging: application to polymer modified bitumen. Anal. Chim. Acta 444, 241–250.

Lins, V.F.C., Araújo, M.F.A.S., Yoshida, M.I., Ferraz, V.P., Andrada, D.M., Lameiras, F.S., 2008. Photodegradation of hot-mix asphalt. Fuel 87, 3254–3261. doi:10.1016/j.fuel.2008.04.039.

Lu, X., Isacsson, U., 2002. Effect of ageing on bitumen chemistry and rheology. Constr. Build. Mater. 16, 15–22. doi:10.1016/S0950-0618(01)00033-2.

McNally, T., 2011. Polymer Modified Bitumen: Properties and Characterisation. Elsevier.

Mouillet, V., Lamontagne, J., Durrieu, F., Planche, J.-P., Lapalu, L., 2008. Infrared microscopy investigation of oxidation and phase evolution in bitumen modified with polymers. Fuel 87, 1270–1280. doi:10.1016/j.fuel.2007.06.029.

Navaro, J.C., 2011. Cinétique de mélange des enrobés recyclés et influence sur les performances mécaniques. Doctoral Thesis, Arts et Métiers ParisTech, Paris.

Reinke, G., Glidden, S., Listberger, S., Stauduhar, S., 2014. Reduction of low temperature asphalt binder stiffness using a Renewable Additive, in: Asphalt Pavements. CRC Press, pp. 1707–1712.

Siddiqui, M.N., Ali, M.F., 1999. Studies on the aging behavior of the Arabian asphalts. Fuel 78, 1005–1015. doi:10.1016/S0016-2361(99)00018-6.

Smith, H.R., Edwards, A.C., 2001. Recycling of bituminous materials: final report. Project report pr/int/225/01, Department for International Development, UK.

Tachon, N., 2008. Nouveaux types de liants routiers a hautes performances, a teneur en bitume reduite par addition de produits organiques issus des agroressources. Doctoral Thesis, L'Institut National Polytechnique de Toulouse, Toulouse, France.

Tahirou, M., 2009. Influence of Bitumen Ageing on Asphalt Quality, Comparison Between Bitumen and Asphalt Ageing. Doctoral Thesis, Universiteit Gent Vrije Universiteit Brussel, Belgium.

Terrel, R.L., Epps, J.A., 1989. Using additives and modifiers in hot mix asphalt. National Asphalt Pavement Association, USA.

Van den bergh, W., Van de Ven, M.F.C., 2012. The Influence of Ageing on the Fatigue and Healing Properties of Bituminous Mortars. Procedia - Soc. Behav. Sci., SIIV-5th International Congress - Sustainability of Road Infrastructures 2012 53, 256–265. doi:10.1016/j.sbspro.2012.09.878.

Vargas, X.A., Afanasjeva, N., Álvarez, M., Marchal, P.H., Choplin, L., 2008. Asphalt rheology evolution through thermo-oxidation (aging) in a rheo-reactor. Fuel 87, 3018–3023. doi:10.1016/j.fuel.2008.04.026.

Wood, L.E., 1978. Recycling of Bituminous Pavements: A Symposium. ASTM International.

Yao, H., You, Z., Li, L., Goh, S.W., Lee, C.H., Yap, Y.K., Shi, X., 2013. Rheological properties and chemical analysis of nanoclay and carbon microfiber modified asphalt with Fourier transform infrared spectroscopy. Constr. Build. Mater. 38, 327–337. doi:10.1016/j.conbuildmat.2012.08.004.

Zargar, M., Ahmadinia, E., Asli, H., Karim, M.R., 2012. Investigation of the possibility of using waste cooking oil as a rejuvenating agent for aged bitumen. J. Hazard. Mater. 233, 254–258.

# LEAB-PA, A Half Warm Porous Asphalt Can Increase the Lifetime

**G. Gaarkeuken, M. Oosterveld, M.L.M. Sprenger and J.L.M. Voskuilen**

**Abstract** BAM Wegen constructed the first LEAB (in Dutch: Laag Energie AsfaltBeton; in English: Low Energy Asphalt Concrete) test sections in 2003 Compared to conventional hot produced asphalt mixes, the production temperature of LEAB reduced significantly using foamed bitumen. At first the LEAB concept was applied for asphalt concrete bind and base mixtures (AC bind and AC base mixtures). More recently also test sections with Porous Asphalt (PA) have been built with foamed bitumen. The mixture is called LEAB-PA. The slow lane average lifetime of PA16 in the Netherlands is approximately 11 to 12 years. The fast lane average lifetime is 16 years. The predominant damage of PA is ravelling, which is mainly caused by the ageing of the mortar in the PA mix by oxidation and UV light. The lower production temperature of the LEAB-PA procedure reduce the short term ageing of the mortar in the PA mix. Loss of mortar flexibility in the PA mix by ageing of the bitumen is the predominant factor for ravelling. It is expected that LEAB-PA will have a higher resistance to ravelling and a longer life span in comparison with hot produced PA mixes. Since 2010 different test sections with LEAB-PA are constructed combined with a section of conventional hot produced PA with the same mix composition as a reference. The shear moduli (mastercurve) of the mortar of the LEAB-PA and the conventional PA are monitored periodically using DSR tests. Also the penetration and softening point Ring & Ball of the bitumen are monitored. Additionally indirect tensile strength tests and CPX measurements for noise reduction have been executed. After 3 years of monitoring it is

G. Gaarkeuken (✉) · M. Oosterveld · M.L.M. Sprenger
BAM Wegen TMA, Bunnik, The Netherlands
e-mail: b.gaarkeuken@bamwegen.nl

M. Oosterveld
e-mail: m.oosterveld@bamwegen.nl

M.L.M. Sprenger
e-mail: m.sprenger@bamwegen.nl

J.L.M. Voskuilen
Rijkswaterstaat, Utrecht, The Netherlands
e-mail: jan.voskuilen@rws.nl



F. Canestrari and M.N. Partl (eds.), *8th RILEM International Symposium on Testing and Characterization of Sustainable and Innovative Bituminous Materials*, RILEM Bookseries 11, DOI 10.1007/978-94-017-7342-3_18

concluded that the difference in ageing between LEAB-PA and conventional PA is still significant. Lower production temperatures reduce short term ageing. Therefore we expect it will increase the lifetime of PA.

**Keywords** Foamed bitumen · Porous asphalt · Ageing · DSR · LEAB-PA · Mortar

## 1 Introduction

The Netherlands was one of the countries that signed the Kyoto protocol, that commits State Parties to reduce greenhouse gases emissions, based on the premise that (a) global warming exists and (b) man-made $CO_2$ emissions have caused it. The ministry of Infrastructure and the Environment wanted to give a good example and asked Rijkswaterstaat to inventorise, how $CO_2$ could be reduced in the whole infrastructure process. One of the ways was to produce asphalt mixtures at lower temperatures, so Rijkswaterstaat challenged the market to develop asphalt mixtures, which could be produced at lower temperatures. To stimulate the appliance of those mixtures, Rijkswaterstaat developed a so-called best value procurement, where a contractor receives a financial benefit as he offers an environmental friendly asphalt mixture. The contractor has to prove the suitability of these mixtures: this means that the functional properties and the durability must be at least the same as the standard asphalt mixture.

One of the products that is able to cope with the environmental challenges is Low Energy Asphalt Concrete (LEAB). BAM Wegen introduced the LEAB concept in 2003. Compared to conventional hot mixed asphalt the production temperature of a LEAB mix is reduced significantly using foamed bitumen. At first the LEAB concept is applied in asphalt concrete bind and base layers. From 2010 also test sections with Porous Asphalt (PA) are constructed with foamed bitumen. The mixture is called LEAB-PA. Compared with standard PA the production temperatures decreased from 165 °C to 110 °C.

During production of LEAB-PA, the $CO_2$ emission has been monitored several times. For the production of 1 ton hot mix PA 11.93 kg $CO_2$ is produced. The production of 1 ton LEAB-PA produces 9.26 kg $CO_2$. A reduction of 22 % by mass has been reached. With further improvements an energy reduction (and $CO_2$ reduction) of 25–30 % (compared to hot mix PA) should be reached in future.

More than 90 % of the Dutch highways have been provided with a hot mixed PA top layer (PA16). After approximately 20 years of experience with hot produced PA16, in 2003 the average lifetime of the slow lane had increased to 11–12 years (Verra 2003) and the fast lane to 16 years. Since 2007 the lifetime of PA16 is increased furthermore by the application of 1 % (m/m) more bitumen (Sule 2005) and a drainage inhibitor. This mixture is called PA16+. Table 1 gives an overview of the PA16 and PA16+ mix compositions.

**Table 1** Mix composition of PA16 and PA16+

| Sieve size (mm) | PA16 (% m/m passing) | PA16+ (% m/m passing) |
|---|---|---|
| C22.4 | 100 | 100 |
| C16 | 96.6 | 96.6 |
| C11.2 | 72.0 | 72.0 |
| C8 | 42.0 | 42.0 |
| 2 mm | 15.0 | 12.7 |
| 63 µm | 4.5 | 5.5 |
| Bitumen pen grade 70/100 (% m/m) | 4.2 | 5.1 |
| Void content (% V/V) | 20.0 | 20.1 |

Except environmental benefits, the half warm mixing process can also increase the lifetime of the PA mix. The predominant damage of PA16 is ravelling. It is generally excepted that ageing of the mortar and erosion of the mortar have a large influence on the ravelling process (Huurman 2008; Huurman et al. 2010, 2012). Lower production temperature decreases short term ageing substantially. As a result it is expected that the LEAB procedure can increase the lifetime of PA mixtures.

In cooperation with the Innovation Test Centre of Rijkswaterstaat BAM Wegen constructed test sections of LEAB-PA16+ on highway A18 (2013) and highway A4 (2014). Already in 2010 a test section of LEAB-PA16+ is constructed on the sub-urban road N314. As a reference adjacent to all of these test sections a standard (hot) PA16+ test section has been built (with the same mix composition). These three test locations are monitored. Especially the ageing development of the LEAB-PA16 + and the adjacent PA16+ are of interest. This paper discusses the degree of ageing of LEAB-PA16+ and PA16+ and the consequences on their behaviour and lifetime. Composition demands to prevent bitumen drainage are described.

## 2 Lifetime Optimization Tool

The Lifetime Optimization Tool (LOT) is developed by the Technical University Delft (Huurman 2008) as part of the IPG research project of Rijkswaterstaat. LOT is a mechanical design tool for PA mixtures.

The lifetime of PA16(+) is mainly dependent on ravelling. During the winters of 2008/2009 and 2009/2010 suddenly unexpected and more extensive ravelling occurred on parts of the Dutch highways. This triggered BAM Wegen, TU Delft and Rijkswaterstaat to analyse this winter damage with the help of the LOT tool. The tool is validated by measurements on different preselected road sections with unexpected good or bad behaviour (Huurman et al. 2012). The main conclusions:

1. The wintertime day and night temperature variation will result in a displacement controlled load in the PA mixture caused by restrained shrinkage and expansion. To prevent failure, flexibility of the mortar is required;

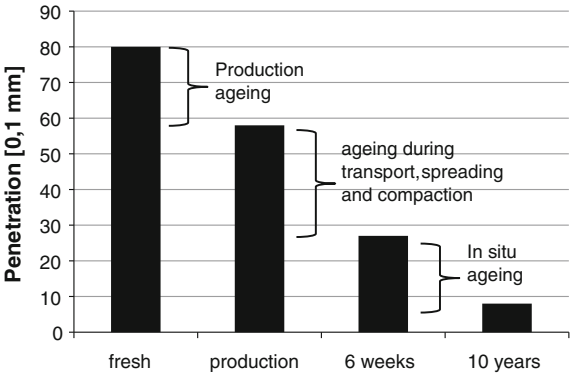


**Fig. 1** Penetration of the PA16 bitumen during lifetime (Besamusca 2012)

2. The shear modulus (G*) of the mortar in the frequency range of $1 \times 10^{-5}$ to 10 Hz is very important (NEN-EN 14770). In this frequency range the mortar needs to be flexible. The residual lifetime of the PA16 is highly dependent on the decreased flexibility of the mortar;
3. There is a strong relation between the ravelling resistance and the G* master-curve at −10 °C ($1 \times 10^{-5}$ to 10 Hz);
4. The preselected sections have unexpected good or bad behaviour. For these sections there is no strong correlation between the age of the PA16 and the ravelling resistance. There are old PA16 road sections with excellent ravelling resistance whereas recent sections have a lack of flexibility and vice versa.

In 2012 the penetration of fresh pengrade 70/100 bitumen and the extracted bitumen after PA16+ production are reported by Besamusca (Besamusca 2012). For the fresh bitumen, a penetration of 80 (0.1 mm) is found. Besamusca also visualized the penetration of the extracted bitumen 6 weeks and 10 years after PA16+ construction (Fig. 1). The penetration decline is dependent on the amount of ageing. A lot of ageing occurs during production in the asphalt mixing plant, transport to the construction site and in situ installation. The ageing during production, transport and installation is highly dependent on the production temperature. It is expected that lower production temperatures will increase the flexibility and the lifetime of the PA16(+) mixture. To achieve this, BAM Wegen has developed a PA16 mixture with a production temperature of approximately 100–110 °C using foamed bitumen.

## 3 LEAB-PA Test Sections

BAM Wegen has constructed test sections with LEAB-PA16+ on highways A4 and A18 (in association with Rijkswaterstaat) and on the suburban road N314. As a reference adjacent to the LEAB-PA16+ sections also a conventional hot produced PA16+ is constructed. During production and installation an extensive monitoring

**Table 2** Test program test section LEAB-PA16+ and conventional PA16+

| Production | Construction | After construction | Monitoring |
|---|---|---|---|
| Gas production[1] | Cooling curves | Air void content (NEN-EN 12697-8) | Density/degree of compaction (NEN-EN 12697-6) |
| $CO_2$ emission[1] | | Mix composition (NEN-EN 12697-1, 2) | Bitumen penetration |
| Ravelling resistance (Cantabro, ARTe) | | Density/degree of compaction (NEN-EN 12697-6) | Bitumen content (in wheel track) (NEN-EN 12697-1) |
| | | Mastercurve mortars (DSR) | Bitumen content (between wheel tracks) |
| Mastercurve (DSR) | | Bitumen drainage | |

[1]Not measured on all test sections

program is performed. Until the end of the service life the in situ quality of the LEAB-PA16+ and conventional PA16+ will be monitored. Only the relevant tests for this paper are listed in Table 2.

The test section on the A4 is in 2014 constructed. This paper is based on the results of the A18 (2013) and the N314 (2010).

## *3.1 Cooling Curves*

With the help of temperature sensors the in situ temperature of the asphalt mix is monitored (Fig. 2). During construction and compaction (approximately 1 h) there is a temperature difference between conventional PA16+ and LEAB-PA16+ of

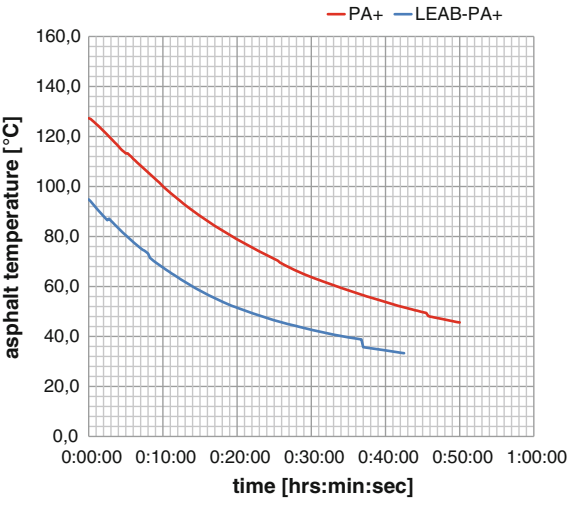


**Fig. 2** In situ temperature of the asphalt after laying

20–30 °C caused by lower production temperatures. Ageing of bitumen is mainly due to oxidation of the maltenes in the bitumen. The oxidation process is instigated by high temperatures and will result in a more stiff and less flexible bitumen. Based on the cooling curves, it is expected that the LEAB PA16+ mortar ageing is less extensive. Penetration tests on extracted bitumen or DSR tests on extracted mortar can confirm this statement. These tests will be discussed in the next paragraphs.

## 3.2 Bitumen Penetration

On the N314 test section the penetration of the extracted bitumen is monitored. Three years after construction the differences between LEAB-PA16+ and standard PA16+ are evident.

For LEAB-PA16+ a reduction of 7 (0.1 mm) over the last 2 years is measured. After 3 years there is a significant difference in bitumen penetration between PA16+ and LEAB-PA16+. It is concluded that there is a significant difference in ageing between LEAB-PA16+ and standard PA16+ bitumen. This conclusion is in line with the results of Gaudefroy (2008) and Olard (2011).

## 3.3 DSR Measurements

During construction of the A18 test section, loose mix was sampled. A few days after construction cores were taken. From the loose mix and the cores, the LEAB-PA16+ and PA16+ mortar was extracted and the shear modulus mastercurve was determined with the help of the DSR (NEN-EN 14770). For the extraction of the mortar from the loose mix and the core, the following procedure is used:

- Heat the material until 60 °C and crumble it;
- Extract the mortar with the help of a spatula;
- Sieve the extracted mortar over a 1 mm sieve (wet sieving) to get rid of pollution

The shear modulus mastercurve after production was identical to the results a few days after construction. Transport and installation of the asphalt have a marginal effect on the shear modulus G* of the mortar. Figure 3 presents the mastercurve results of LEAB-PA16+ and PA16+. Typical ageing phenomena are observed especially at low frequencies. At high frequencies both mastercurves approach the same glassy point. It is concluded that mixing temperatures have a substantial influence on the G* of the mortar in the low frequency range.

6 and 12 months after construction DSR tests were repeated on mortar extracted from cores from the emergency lane of highway A18. The influences of wheel loads and air pumping are thus excluded. The same extraction procedure is executed. Figure 4 presents the PA16+ and LEAB PA16+ G*-results after production (0), 6 months after construction (6 m) and 12 months after construction (12 m). 6 and

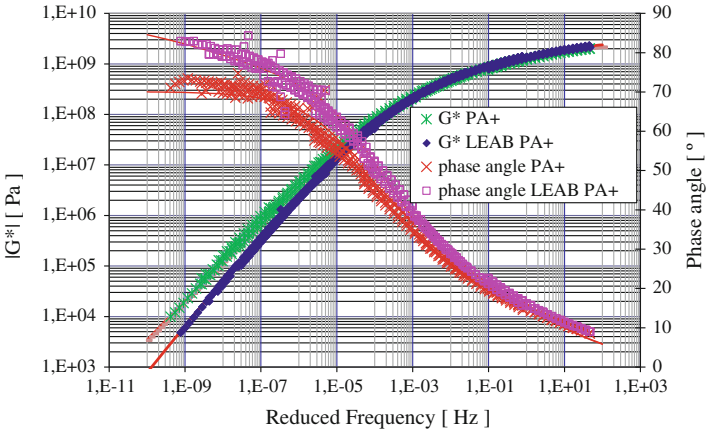


**Fig. 3** Shear modulus mastercurve at −10 °C of LEAB-PA16+ and standard PA16+ after production; highway A18 test section

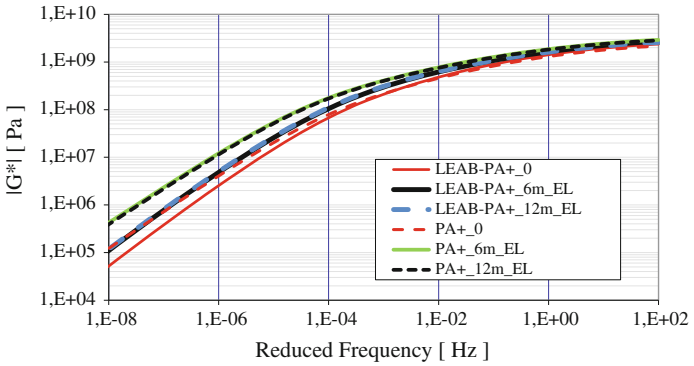


**Fig. 4** G* shear modulus mastercurve comparisons between fresh, 6 and 12 month old mortars from LEAB-PA16+ and standard PA16+ mix at $T_{ref}$ = −10 °C

12 months after construction differences in production ageing are still noticeable. Between 6 and 12 months after construction (autumn period), the effect of ageing on G* is negligible. The ageing is dependent on temperature and UV. The G* of 12 months old LEAB-PA16+ is comparable with the G* of PA16+ after production.

## *3.4 Indirect Tensile Strength (ITS)*

To monitor the strength of the PA, Indirect Tensile Strength tests (ITS) at 15 °C have been executed on the N314 test section (NEN-EN 12697-23). The ITS is

**Table 3** Indirect tensile strength at 15 °C (4 samples, mean value and standard deviation)

| Mixture | 0 year Loose mix from the asphalt plant (MPa) | 1 year cored between wheel tracks (MPa) | 3 years cored between wheel tracks (MPa) | 3 years cored in right wheel track (MPa) |
|---|---|---|---|---|
| PA16+ | 0.875(0.095) | – | 1.729(0.190) | 1.740(0.092) |
| LEAB PA16+ | 0.725(0.023) | 0.989(0.005) | 1.582(0.093) | 1.715(0.093) |

**Table 4** Bitumen penetration (25 °C) of LEAB-PA16+ and PA16+ on test section N314

| | LEAB PA16+ (0.1 mm) | Standard PA16+ (0.1 mm) |
|---|---|---|
| Fresh bitumen 70/100 | 73 | 73 |
| 1 year after construction | 39 | |
| 3 years after construction | 32 | 14 |

determined on gyratory compacted loose mix from the production plant and on cored cylinders. In Table 3 the results are presented. Within 3 years the ITS is doubled. This is attributed to the ageing of the mortar and to the stiffening effect of the mix.

Compared to gyratory compacted loose mix LEAB-PA16+ specimens, the strength of the corresponding loose mix PA16+ specimens is approximately 20 % higher. After 3 years the difference is reduced to less than 10 %. Although the penetration results 3 years after construction (Table 4) showed that the LEAB-PA16 + bitumen is more flexible, the strength of the LEAB-PA16+ is almost comparable with conventional PA16+.

## *3.5 Bitumen Content, Bitumen Drainage and Erosion*

To prevent the drainage of the mortar on the N314 test sections an drainage inhibitor is added in the PA16+ mixture. At LEAB-PA16+ production temperatures (100–110 °C) the addition of a pellet size drainage inhibitor was not possible. At these low mixing temperatures the pellets will not dissolve and will remain as small pellets in the asphalt mix. Because of lower temperatures of the LEAB-PA16+ mixture less bitumen drainage during transport and installation was expected.

On the N314 test sections the bitumen drainage is determined on drilled cores with a Nanotom CT-scanner. The cores were drilled a few days after construction. Analyses with the Nanotom resulted in a distribution of air voids, mastic and coarse material over the height of the core (see Fig. 5). Although no drainage inhibitor is added, the bitumen and mortar drainage of LEAB-PA16+ is very small and comparable with standard PA16+ (Table 5).

Three years after the N314 construction, the mix composition is determined on drilled cores. The PA16+ and LEAB-PA16+ cores were taken in the wheel track as

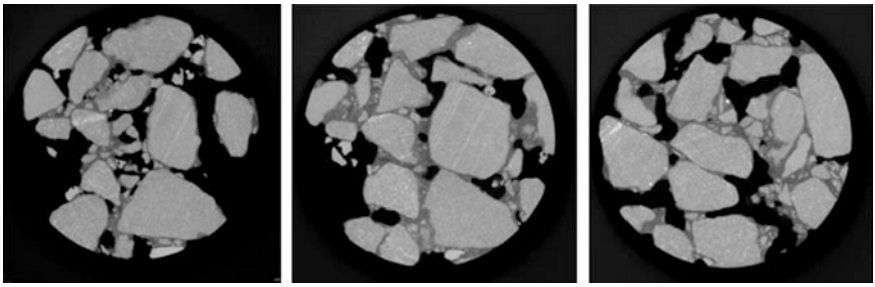

**Fig. 5** Example of CT-scans of LEAB-PA16+ after laying (3 different heights of the core)

**Table 5** Average CT scan results

| Mixture | Part of the cylinder | Air void content (% V/V) | Mortar content (% V/V) | Coarse aggregates content (% V/V) |
|---|---|---|---|---|
| PA16+ (3 cores) | 10–30 mm | 16.8 | 17.6 | 65.5 |
| | 30–50 mm | 15.8 | 18.3 | 65.9 |
| | **Difference** | **1.0** | **−0.7** | **−0.4** |
| LEAB PA16+ (3 cores) | 10–30 mm | 15.4 | 19.3 | 65.3 |
| | 30–50 mm | 17.1 | 19.1 | 63.7 |
| | **Difference** | **−1.7** | **0.2** | **1.6** |

well as between wheel tracks. The cores were horizontally cut in an upper and a lower half. In Tables 6 and 7 the composition is presented.

The combined average bitumen contents of the top and bottom half of the cores are comparable with construction control in 2010. After three years the amount of erosion caused by air and/or water pumping is negligible. The bitumen drainage however is severe. The bottom part of the LEAB-PA16+ right wheel track cores (RWTB) have a very high bitumen content and consequently a low void content. In addition to the bitumen, also drainage of the filler and sand is observed. The mortar drainage must have started after construction. The use of a drainage inhibitor is necessary. Because a pellet sized drainage inhibitor is not applicable, at half warm

**Table 6** In situ mix composition PA16+

| PA16+ | Construction control (2010) | RWTB[1] (2013) | RWTT[1] (2013) | BWTB[1] (2013) | BWTT[1] (2013) |
|---|---|---|---|---|---|
| Density (kg/m$^3$) | 2036 | 2090 | 2030 | 2065 | 1991 |
| Void content (% V/V) | 18.8 | 16.4 | 19.6 | 17.4 | 20.7 |
| Granular material < 2 mm (% m/m) | 15.6 | 15.4 | 15.3 | 16.0 | 15.8 |
| Bitumen content (% m/m) | 4.7 | 5.0 | 4.3 | 4.9 | 4.7 |

[1]*RWTB* Right Wheel Track Bottom, *RWTT* Right Wheel Track Top, *BWTB* Between Wheel Tracks Bottom, *BWTT* Between Wheel Tracks Top

**Table 7** In situ mix composition LEAB-PA16+

| LEAB PA16+ | Construction control (2010) | RWTB[1] (2013) | RWTT[1] (2013) | BWTB[1] (2013) | BWTT[1] (2013) |
|---|---|---|---|---|---|
| Density (kg/m$^3$) | 2033 | 2223 | 2067 | 2089 | 2017 |
| Void content (% V/V) | 18.8 | 10.3 | 18.1 | 16.4 | 19.9 |
| Granular material < 2 mm (% m/m) | 17.5 | 18.9 | 16.1 | 17.8 | 16.1 |
| Bitumen content (% m/m) | 4.7 | 5.7 | 4.4 | 5.1 | 4.5 |

[1]*RWTB* Right Wheel Track Bottom, *RWTT* Right Wheel Track Top, *BWTB* Between Wheel Tracks Bottom, *BWTT* Between Wheel Tracks Top

mixing temperatures a drainage inhibitor based on pure fibers is recommended. Bitumen and mortar drainage reduce the size of the adhesive bridges between the coarse aggregates at the surface of the LEAB-PA16+ and PA16+ mixtures. Stress controlled loads (for instance wheel loads) will induce higher stresses in the mortar and therefor ravelling will appear sooner. Loss of adhesion and/or bitumen drainage combined with bitumen ageing accelerate the ravelling process even more. LEAB-PA16+ mortar is less aged and will be less sensitive to ravelling.

## 3.6 Analyses

Delft University (Huurman et al. 2010, 2012) LOT analyses proved a strong relationship between mortar stiffness and ravelling lifetime for conventional PA+ mixtures. Especially in winter time the mortar is extensively loaded with displacement controlled temperature loads (frost thaw cycles) with low frequencies of approximately $1 \times 10^{-5}$ Hz (day/night frequency). Micro cracks in the mortar appear. In the end surface shear loads caused by heavy traffic will loosen the stones from the road surface. Flexibility is what the mortar needs. On the other hand, the mortar should provide enough strength to withstand the stress controlled wheel loads. Based on penetration and DSR-tests, it is proved that LEAB-PA16+ is less susceptible to strain controlled temperature loads. Attention should be given to the risk of bitumen drainage. Bitumen drainage can make LEAB PA16+ more susceptible for stress controlled wheel loads. Therefor additional laboratory ravelling tests have been executed on the N314 and A18 projects to examine the resistance to stress controlled wheel loads.

## 3.7 Laboratory Ravelling Tests

The ravelling resistance of standard PA16+ and LEAB-PA16+ is determined with Cantabro and Aachener Ravelling Tester (ARTe) tests. In a Cantabro test (NEN-EN

12697-17) laboratory prepared specimens are tested in a Los Angeles machine (300 rotations with 30–33 rotations per minute, 25 ± 1 °C). The tests are executed on fresh, unaged material. The loss of mass after testing is measured. In case of a hot PA16+ mixture the average loss of mass was equal to 28.0 % (m/m). For LEAB-PA16+ the loss of mass was equal to 21.4 % (m/m). LEAB-PA16+ performed better than hot PA16+.

Additionally ravelling tests using the ARTe (prTS 12697-50 Annex A) were executed on laboratory made slabs from standard PA16+ and LEAB-PA16+. In the ARTe slabs are loaded by a set of delivery van tires which rotate with a severe amount of slip (Fig. 6). For each slab 600 cycles were executed. After 300 cycles the slabs were rotated over 180°. Half of the slabs were aged by the Mandela method (van de Ven 2012). After testing the mass loss of the slabs was measured (Table 8). For unaged material, the ravelling resistance of LEAB-PA16+ was better than hot PA16+. However after ageing the ravelling of the LEAB-PA16+ is more severe.

For the A18 project the ARTe tests were repeated on laboratory made and aged slabs. Except the change of mass also the change of volume at the surface of the slab was measured using a 3D laser scan device (Table 9). Based on these results it is concluded that LEAB-PA16+ performed better than standard PA16+. It is likely that the huge differences between the N314 and A18 LEAB-PA16+ ARTe performances are caused by bitumen drainage (during slab fabrication and/or slab ageing). It has provided insight in the drainage sensitivity of the process.

**Fig. 6** BAM Wegen ARTe testing facility

**Table 8** ARTe test results N314 project

| Mixture | | Mass loss unaged (gr/m$^2$) | Mass loss aged (gr/m$^2$) |
|---|---|---|---|
| PA16+ | Slab 1 | 580 | 187 |
| | Slab 2 | 560 | 342 |
| LEAB PA16+ | Slab 1 | 83 | 825 |
| | Slab 2 | 340 | 1242 |

**Table 9** ARTe test results (A18 project)

| Mixture | Average mass loss aged (% m/m) | Average volume loss aged (% V/V) |
|---|---|---|
| PA16+ | 0.32 | 0.82 |
| LEAB PA16+ | 0.15 | 0.37 |

## 4 Conclusions and Recommendations

The conclusions are based on A18 and N314 LEAB-PA16+ test sections. The following conclusions are made:

- Compared with hot PA16+ the production temperatures decreased from 165 °C to 110 °C. As a result the $CO_2$ emissions (kg/ton) have reduced with 22 %.
- Based on penetration and DSR tests it is concluded that 3 years after construction the difference in production ageing between hot PA16+ and LEAB-PA16+ is still present. Based on the DSR test the G* of 12 months old LEAB-PA16+ is comparable with fresh produced PA16+ (Fig. 4).
- With LEAB-PA+ attention should be given to the risk of bitumen drainage. Although production temperatures have decreased significantly, an anti dripping agent is still necessary. Pure fibers instead of pellets are recommended.
- Three years after construction the erosion of mortar in the PA16+ and LEAB-PA16+ is negligible.

## References

Besamusca J., Volkers A., Van de Water J., Gaarkeuken G. (2012) Simulating Ageing of EN 12592 70/100 Bitumen at laboratory conditioning compared to PA. 5th Eurasphalt and Eurobitume Congress, Istanbul.

Gaudefroy V., Olard F., Le Quernec F., de la Roche, C. (2008) Laboratory investigation on the total organic compounds emissions of half-warm mix asphalt technology versus traditional hot mix asphalt, ISAP-2008.

Huurman M. (2008) Lifetime Optimisation Tool, LOT, Main Report. Rijkswaterstaat, Innovatie Programma Geluid, Report 7-07-170-1.

Huurman M., Jacobs M.M.J., Mohan S. (2012) LOT en de verklaring van winterschade, CROW Infradagen 2012.

Huurman M., Mo L.T., Woldekidan M.F. (2010) Mechanistic Design of Silent Asphalt Mixtures and its Validation. Asphalt Paving Technology 2010, Sacramento.

Olard F., Gaudefroy V. (2011) Laboratory assessment of mechanical performance and fume emissions of LEA® HWMA (90C) vs. traditional HMA (160C), 2nd International Conference on Warm-Mix Asphalt, St Louis.

Sule M., Voskuilen J. (2005) Evaluatie ZOAB 0/16 + , proefvakken en laboratoriumonderzoek. Rijkswaterstaat, Dienst Weg- en Waterbouwkunde, DWW-2005-079.

Van de Ven M.F.C, Voskuilen J.L.M. and Jacobs M.M.J.(2012),Practical laboratory ageing method for porous asphalt, 5th Eurasphalt and Eurobitume Congress, Istanbul.

Verra N, Van den Bol M, Gaarkeuken G (2003) De levensduur van ZOAB, gemiddelde levensduurbepaling op basis van MJPO-2003. Rijkswaterstaat, Dienst Weg- en Waterbouwkunde.

# Part IV
# Mixture Design and Compaction Analysis

# Production of Hot-Mix Asphalt with PMB: Compactability and Mechanical Behaviour Characterization

**Rui Micaelo, Ana Gameiro, Luís Quaresma and Luís Picado-Santos**

**Abstract** The traditional approach used to select production (mixing and compaction) temperatures for hot-mix asphalts (HMA) with polymer modified bitumens (PMB) often lead to extremely high temperatures, which increase energy consumption and may cause bitumen-polymer bond degradation. Moreover, field experience indicates that lower temperatures can be used without compromising aggregate coating with bitumen and on-site compaction. This paper presents a lab study aiming to assess the influence of production temperatures in the on-site paving operations and the in-service performance of asphalt pavements. An AC 14 Surf PMB 45/80-65 (EN 13108-1) was produced and compacted at three different mixing-compaction temperatures groups, based on the suppliers' recommendation and the temperatures determined with the traditional (Superpave) and the high-shear rate viscosity (HSRV-E) methods. The results showed an important effect of the production temperatures in the asphalt behaviour. Minimum compaction resistance value was obtained with the Superpave temperatures while HSRV-E produced the highest resistance. The water sensitivity test values and the rutting resistance values were very similar for the three temperatures groups. Independently of the test frequency, the stiffness modulus was always higher for the HMA produced at the suppliers' recommended temperatures. The resistance to fatigue is very similar for the Superpave and HSRV-E temperatures, and higher than with the suppliers' recommended temperatures. Fatigue resistance was not affected by the use of a higher mixing temperature, recommended by the Superpave method. The best performance was not obtained with any single temperatures group tested and the

R. Micaelo (✉) · A. Gameiro · L. Quaresma
Department of Civil Engineering, Universidade Nova de Lisboa, Caparica, Portugal
e-mail: ruilbm@fct.unl.pt

A. Gameiro
e-mail: gameiro_ana@hotmail.com

L. Quaresma
e-mail: lmtq@fct.unl.pt

L. Picado-Santos
Department of Civil Engineering/CESUR, Instituto Superior Técnico, Lisbon, Portugal
e-mail: luispicadosantos@tecnico.ulisboa.pt



F. Canestrari and M.N. Partl (eds.), *8th RILEM International Symposium on Testing and Characterization of Sustainable and Innovative Bituminous Materials*, RILEM Bookseries 11, DOI 10.1007/978-94-017-7342-3_19

results show that both mixing and compaction temperatures are very important for the HMA behaviour.

**Keywords** Temperature · Mixing · Compaction · Mechanical tests

## 1 Introduction

The construction process of bituminous layers has two main phases, mixing and compaction, which together determine asphalt end quality and pavement performance. The mixing and compaction processes are influenced by the bitumen viscosity which varies with the temperature and the type of bitumen. During mixing, the viscosity influences the coating of coarse aggregates by the bitumen (or the bituminous mastic) and, during compaction, the ability to form a dense, resistant, durable, and cohesive structure with designed air void content (Read and Whiteoak 2003; Yildirim et al. 2000).

The current method used for the selection of construction temperatures comprises two tasks: (i) the evaluation of viscosity variation of the bitumen with the temperature; (ii) the determination of the temperatures that correspond to the recommended viscosity levels for mixing and compaction operations (Bahia et al. 2006). This procedure is considered adequate and is accepted worldwide for the bituminous mixtures with neat bitumens. In contrast, modified bitumens have a very complex rheology, with non-Newtonian behaviour even at very high temperatures. Thus, the use of the current method results in very high temperatures which may compromise the durability of the bitumen. It brings also more energy consumption and air pollution during production. Field experience indicates that lower temperatures can be used without compromising the performance in-service.

During the last 20 years several research groups have studied the mixing and compaction operations of hot-mix asphalt with modified bitumens, and proposed different methodologies for the determination of mixing and compaction temperatures. Table 1 presents briefly the current method and four other methods proposed in literature. The Superpave method (AI 1997) is the traditional method and uses the same viscosity values recommended long ago by the Asphalt Institute. The High Shear Rate Viscosity (HSRV) (Yildirim et al. 2000, 2006; West et al. 2010) and Zero Shear Rate Viscosity (ZSRV) (Bahia et al. 2001; Stuart 2001) methods define a different test protocol for the characterization of the bitumen viscosity with the rotational viscometer (RV) and/or different viscosity values for mixing and compaction in comparison to the Superpave method. Both the Steady Shear Flow (SSF) and the Phase Angle (PA) methods (West et al. 2010) use the Dynamic Shear Rheometer (DSR) to characterize the bitumen behaviour.

Micaelo et al. (2012) determined the temperatures with the different versions of the HSRV and LSRV methods for several polymer (SBS) modified bitumens. The

**Table 1** Methodologies for the determination of mixing and compaction temperatures

| | Superpave | High shear rate viscosity | | Zero shear rate viscosity | | Steady shear flow test (SSF) | Phase angle (PA) |
|---|---|---|---|---|---|---|---|
| | | Original (HSRV-O) | Evolution (HSRV-E) | Original (ZSRV-O) | Simplification (ZSRV-S) | | |
| Testing | | | | | | | |
| Apparatus | RV | RV | | RV | | DSR | DSR |
| T [°C] | 135 & 165 | 135 & 165 | | 120, 135 & 165 | | 76, 82 & 88 | 50, 60, 70 & 80 |
| $\dot{\gamma}$ [$s^{-1}$] | 6.8 | Variable | | Variable | 6.8 | – | – |
| τ [Pa] | – | – | – | – | – | 500 | – |
| w [rad $s^{-1}$] | – | – | – | – | – | – | 0.001–100 |
| Recommended temperatures | | | | | | | |
| | | T@η($\dot{\gamma}$) | | T@η($\dot{\gamma}$) | | T@η(τ) | $T = f[W(\delta)]$ |
| | | $\dot{\gamma} = 500\ s^{-1}$ | $\dot{\gamma} = 500\ s^{-1}$ | $\dot{\gamma} = 0\ s^{-1}$ | $\dot{\gamma} = 6.8\ s^{-1}$ | $\tau = 500$ Pa | $\delta = 86^{\circ}$ |
| Mix | 0.17 ± 0.02 | 0.17 ± 0.020 | 0.275 ± 0.020 | 3.000 | 0.750 ± 0.050 | 0.170 ± 0.020 | $\left[\frac{325 \times w(\delta)^{-0.0135} - 32}{1.8}\right]$ |
| Comp | 0.28 ± 0.03 | 0.28 ± 0.030 | 0.55 ± 0.030 | 6.000 | 1.400 ± 0.100 or 1.100 ± 0.200 | 0.350 ± 0.030 | $\left[\frac{325 \times w(\delta)^{-0.0120} - 32}{1.8}\right]$ |

method that leaded to temperatures closer to the manufacturers' recommendations was the High Shear Rate Viscosity (evolution version) (HSRV-E).

In this study, the effect of the variation of production temperatures on the behaviour during paving operations (compactibility) and on the in-service performance is studied. An asphalt concrete mixture with a PMB binder was produced at several mixing-compaction (M–C) combination temperatures and the performance of the mixture was assessed with several mechanical tests.

## 2 Experimental Program

### *2.1 Materials*

An Asphalt Concrete type mixture with a PMB binder was selected for this study with the objective of comparing three methods for the selection of production temperatures. The PMB binder is a PMB45/80-65, classified according to the NP EN 14023:2013, with properties shown in Table 2. The selected bituminous mixture is an *AC 14 surf PMB45/80-65*, which was designed according to the Marshall method following the NP EN 13108-1:2011 and the Estradas de Portugal (EP 2009) specifications. In the mix design procedure the temperatures recommended by the binder manufacturer for mixing (170 °C) and compaction (160 °C) operations were used. The aggregate gradation is shown in Fig. 1 and the properties obtained in mix design are listed in Table 3.

In order to determine the production temperatures according to the Superpave and HSRV-E methodologies, the dynamic viscosity of the binder was measured using a rotating spindle apparatus at several temperatures, 130 to 190 °C with 5 °C interval, and at 3 to 5 different shear rate values for each temperature value. The viscosity and shear rate intervals of measurement are a function of the spindle used and the torque working ranging of the equipment. The Cross model curve was fitted to measurements at each temperature. Then, it was plotted the viscosity with the

**Table 2** Bitumen properties: PMB 45/80-65

| Property | Test method | Results |
|---|---|---|
| Penetration at 25 °C [0.1 mm] | NP EN 1426:2010 | 51 |
| Softening point [°C] | NP EN 1427:2010 | 70.4 |
| Durability | | |
| Retained penetration [%] | NP EN 12607-1:2010 | ≥60 |
| Increase in softening point [°C] | | ≤10 |
| Change of mass [%] | | ≤1 |
| Elastic recovery at 25 °C [%] | EN 13398:2010 | ≥70 |
| Frass point [°C] | EN 12593:2007 | ≤−15 |
| Flash point [°C] | EN ISSO 2592 | ≥235 |

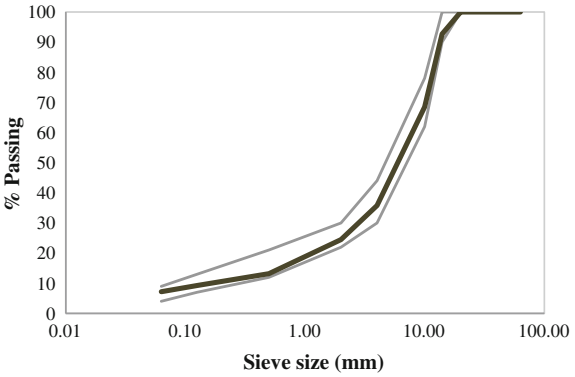


**Fig. 1** Grading curve of the aggregate—AC 14 Surf PMB 45/80-65

**Table 3** Asphalt mixtures design properties

| | | AC 14 Surf PMB 45/80-65 |
|---|---|---|
| Binder content | $\%_{Mass}$ | 4.6 |
| Bulk density | $kg/m^3$ | 2508 |
| Air voids | % | 4.7 |
| Voids in mineral aggregate | % | 15.9 |
| Voids filled with bitumen | % | 79.4 |
| Marshall stability | kN | 14.1 |
| Marshall flow | mm | 4.0 |

temperature at the shear rate defined in the methodology (Superpave and HSRV-E), and a linear model was fitted to results in the log (η)-temperature plot. Finally, the mixing and compaction temperatures were determined for the viscosity values defined in both methodologies. The temperatures recommended by the manufacturer and obtained with the two methodologies are presented in Table 4. The Superpave temperatures are very high, approximately 20 °C above the manufacturer's recommended temperatures. The HSRV-E methodology led to an increase of 10 °C and 2 °C for mixing and compaction, respectively, from the recommended temperatures. The obtained temperature differences are in agreement with the results of a previous study (Micaelo et al. 2012).

**Table 4** Mixing and compaction temperatures for PMB 45/80-65

| Method | Mixing (°C) | Compaction (°C) | Reference |
|---|---|---|---|
| Manufacturer recommendation | 170 | 160 | AC 170/160 |
| Superpave | 193 | 180 | AC 193/180 |
| High shear rate viscosity (HSRV-E) | 180 | 162 | AC 180/162 |

In the experimental program, the mixtures tested at each mixing-compaction temperatures combination are referred by "AC" followed by the two temperatures as shown in Table 4.

## 2.2 Performance Tests

In order to assess the effect of the mixing and compaction temperatures on the mixture behaviour during the construction phase and in-service, several tests were carried out. The compactibility of the mixture was measured with the impact method in accordance with EN 12697-1:2001/AC:2007. The adopted method comprises compacting a different specimen for each level of compaction energy, and recording the density of the specimen. The increase of the density with the compaction energy is modelled with

$$\rho(E_1) = \rho_\infty - (\rho_\infty - \rho_0) \cdot \exp(-E_1/C) \quad (1)$$

where, $\rho(E_1)$ is the bulk density of the specimen compacted at compaction energy (number of blows) $E_1$; $\rho_\infty$ is the maximum achievable bulk density; $\rho_0$ is the initial specimen bulk density; C is the compaction resistance. The model is fitted to the results with the least square method. The C value and $(\rho_\infty - \rho_0)/\rho_\infty$ are used to define the compactibility of the mixture.

The in-service performance of the mixture produced at different temperatures was assessed based on the water sensitivity, the resistance to permanent deformation, the stiffness modulus and the resistance to fatigue.

Stripping is considered an important distress mode in bituminous mixtures and is, traditionally, assessed comparing the mechanical behaviour of two groups of specimens conditioned in different environments (air and water). In the present study the water sensitivity test was carried out following the procedure of the EN 12697-12 standard. The mixture performance is assessed with the ratio (ITRS) between the average results of the indirect tensile strength (ITS) test (EN 12697-23) of the wet and dry groups of specimens.

The resistance to permanent deformation was evaluated with the wheel tracking test (WT), following the procedure of the EN 12697-22 standard. It was used the small size device and followed the procedure B. The test was carried out at 60 °C, with two specimens.

The stiffness modulus and the resistance to fatigue were determined with the four point bending test (4 PB), with displacement control, in accordance to the EN 12697-24 and -26 standards. The stiffness modulus and phase angle were measured for each beam before the fatigue test, with a small strain level (50 μm/m) imposed to the specimen for 100 cycles. This test was performed at five frequency levels in the 0.1–20 Hz interval. The fatigue tests were performed at three strain levels (200, 275 and 350 μm/m), which were previously determined in order to comply with the number of cycles to failure in the $1 \times 10^4$ to $2 \times 10^6$ interval. The conventional

criterion of failure (50 % initial modulus loss) was adopted. The fatigue tests were carried out at the single frequency of 10 Hz, with three specimens. Both tests were performed at the constant temperature of 20 °C.

The specimens used for the WT and 4 PB tests were cut from slabs fabricated in lab. The mixture was produced using a large lab mixer and compacted using a small size double steel-wheel roller. The pre-determined mass of mixture was spread within the steel frame mould and the roller made several passes till there was contact of the drum with the steel frame.

## 3 Results and Discussions

### *3.1 Compactibility*

Figure 2 plots average bulk density values with the compaction energy level used in the test for the mixture produced at the three mixing-compaction temperatures. Table 5 presents the resistance to compaction (C) and $(\rho_\infty - \rho_0)/\rho_\infty$ values, obtained from fitting the compaction model (Eq. 1) to the results. The groups with the lowest and highest mixing temperatures show similar compaction evolution while AC 180/162 has significantly smaller density values at all compaction energy levels. In this situation, the specimen did not attain the design density value even when 100 blows were applied in each side of the specimen. The compaction resistance is minimum (C = 22.5) for the highest M–C temperatures while the

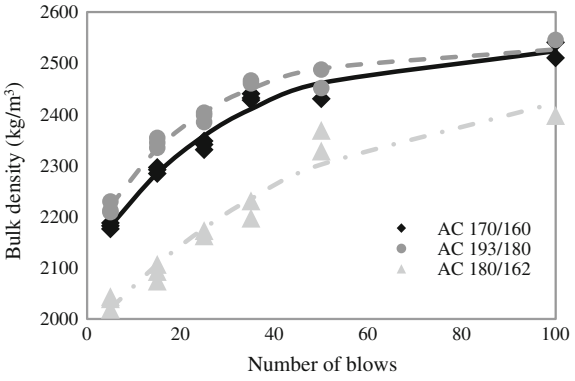


**Fig. 2** Evolution of the bulk density with the compaction energy (impact)

**Table 5** Compactibility test results

| Mixture | C | $(\rho_\infty - \rho_0)/\rho_\infty$ (%) |
|---|---|---|
| AC 170/160 | 29.2 | 16.6 |
| AC 193/180 | 22.5 | 15.3 |
| AC 180/162 | 49.3 | 20.9 |

maximum occurs for the AC 180/162 (C = 49.3). The $(\rho_\infty - \rho_0)/\rho_\infty$ ratio is also significantly high for AC 180/162, which proves the difficulty to attain compaction when the mixture is produced at those M–C temperatures.

These results may have been affected by the method used in the test (several specimens) and, also, the impact method is known for not reproducing well field compaction.

## 3.2 Mechanical Tests

The water sensitivity test results are shown in Table 6. The three mixtures show very good performance in this test, with ITRS values above 85 %. Also, the ITS values do not show significant variation among the groups. These results are in agreement with the conclusions of Gorkem and Sengoz (2009), which showed that the polymer (SBS and EVA) modification of bitumen increases the resistance of the bituminous mixtures to the damaging effect of water.

Figure 3 compares the evolution of the rut depth with the number of cycles, at 60 °C in the wheel tracking test, for the three bituminous mixtures. Table 7 shows the average values of the wheel tracking slope ($WTS_{air}$), the mean proportional rut depth ($PRD_{air}$) and the mean rut depth ($RD_{air}$). Although the air voids content are higher than determined in mix design, the mixture shows a good resistance for the three groups of production temperatures. The similarity in air voids content for the three mixtures is explained by the compaction method, where the end of the compaction process was defined by the slab height reduction (drum-mould frame contact) and not by the material's compaction limit as occurs in field. Thus, the very good results, despite the high test temperature, are most likely related with the use of the PMB binder.

Figure 4 shows the variation of the stiffness modulus and the phase angle with the frequency (0.1–20 Hz), at 20 °C, for the three mixtures. The three mixtures show similar trends of variation with the frequency for both mechanical parameters. Thus, AC 193/180 and AC 180/162 have very similar values at the various

**Table 6** Indirect tensile strength test results

| Mixture | Property | Wet group | Dry group |
|---|---|---|---|
| AC 170/160 | ITS (average) (kN) | 24.4 | 21.7 |
| | ITSR (%) | 88 | |
| AC 193/180 | ITS (average) (kN) | 27.3 | 25.7 |
| | ITSR (%) | 94 | |
| AC 180/162 | ITS (average) (kN) | 25.8 | 22.4 |
| | ITSR (%) | 87 | |

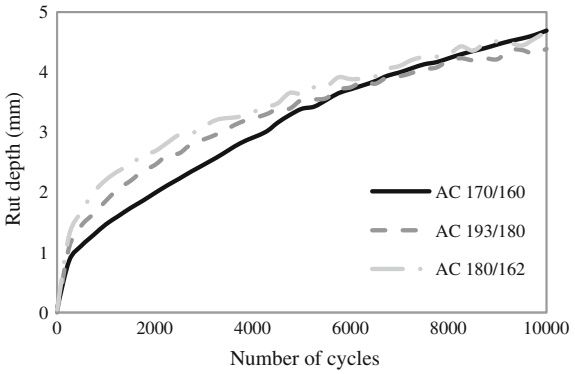


**Fig. 3** Evolution of permanent deformation in the wheel tracking test

**Table 7** Wheel tracking test results

| | | AC 170/160 | AC 193/180 | AC 180/162 |
|---|---|---|---|---|
| Air voids content | % | 5.4 | 5.7 | 6.0 |
| $WTS_{air}$ | mm/$10^3$ load cycles | 0.260 | 0.169 | 0.207 |
| $PRD_{air}$ | % | 7.7 | 7.2 | 7.7 |
| $RD_{air}$ | mm | 4.7 | 4.4 | 4.7 |

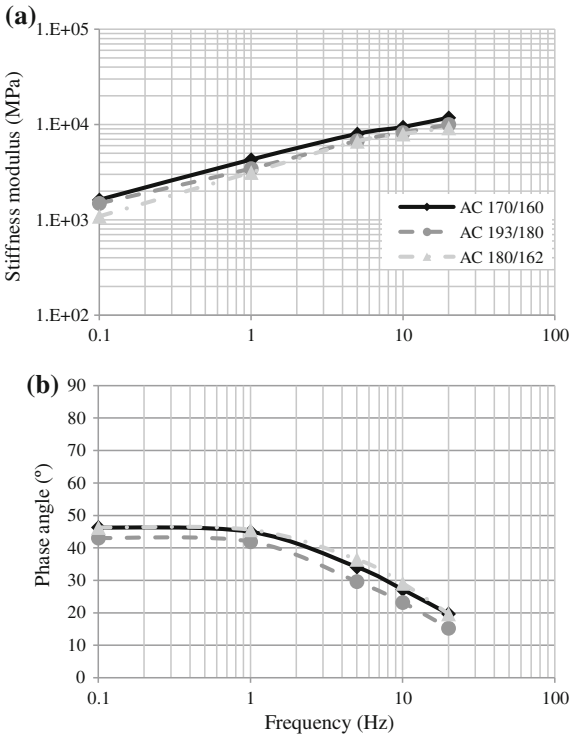


**Fig. 4** Stiffness modulus (a) and phase angle (b) results (4 PB)

frequency values. Surprisingly, AC 170/160 has the highest values of stiffness modulus and the lowest values of phase angle. It is common knowledge that the use of high production temperatures increases bitumen hardening, being one the pointed "problems" to the traditional method of determining the production temperatures for PMBs. However, the mechanical behaviour of the mixture is only partially dependent on the binder, being also important the packing structure of the aggregate. The phase angle does not increase at very low frequencies (0.1–1.0 Hz), which can be associated with the polymer modification.

The results of the fatigue test are presented in Fig. 5. For each mixture, the number of cycles to failure (N) at the three strain levels (ε) is fitted with the fatigue law

$$\log(N) = a + (1/b)\ \log(\varepsilon) \tag{2}$$

where, *a* and *b* are the constants of the model. Table 8 shows the constants for each mixture and, variables $\varepsilon_6$ and $N_{100}$, defined in EN 12697-24, for the fatigue cracking resistance assessment.

The fatigue resistance of AC 170/160 is visibly lower than that of the mixture produced at the other temperatures. It is known that when the fatigue test is carried out in displacement-controlled mode, the fatigue life decreases with the increase of

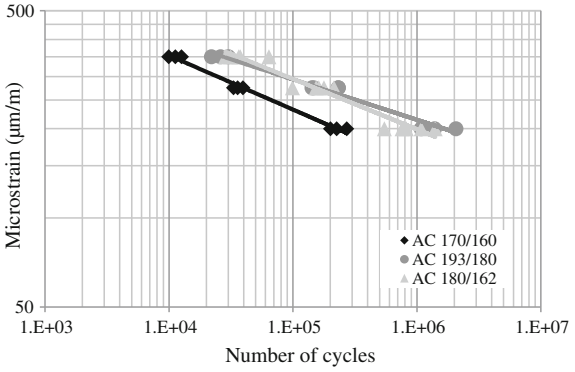


**Fig. 5** Four point bending fatigue test results

**Table 8** Fatigue test results

| Mixture | a | 1/b | $R^2$ | $N_{100}$ | $\varepsilon_6$ (μm/m) |
|---|---|---|---|---|---|
| AC 170/160 | 17.917 | −5.464 | 0.99 | 9.73E + 06 | 151.6 |
| AC 193/180 | 19.523 | −5.882 | 0.95 | 5.73E + 07 | 199.0 |
| AC 180/162 | 23.150 | −7.353 | 0.98 | 2.78E + 08 | 215.0 |

the stiffness modulus. However, the stiffness modulus of AC 180/162 is about 18 % lower of that of AC 170/160 while $N_{100}$ is 28 times higher. AC 193/180 and AC 180/162 show similar fatigue performance. Nevertheless, the fatigue resistance of the bituminous mixture is somewhat high because of the PMB binder.

## 4 Conclusions and Recommendations

The technical guides do not define a methodology for the determination of the mixing and compaction temperatures when modified bitumens are used, or it simply defines as the EN 12697-33 does "when using modified binder or hard grade bitumen binder or additives, the temperature may be adjusted". Besides the serious consequences to modified bitumens (oxidation, breakdown of long chain polymers, volatile loss, emissions, odor-causing compounds) there is the risk to compromise the behaviour of the asphalt during paving operations and the in-service performance.

This paper presented an experimental study with the objective of assessing the effect of the mixing and compaction temperatures on the compactibility and on the in-service performance of hot-mix asphalts with PMB binder. An AC 14 Surf PMB 45/80-65 (EN 13108-1) was produced and compacted at three different mixing-compaction temperatures groups.

The results showed that the mixture behaviour is influenced by the production temperatures. The compactibility of the mixture was similar for the two temperature groups with the highest (Superpave) and the lowest (manufacturer recommendation) temperatures. The compaction resistance is very high when the mixture is fabricated and compacted at the HSRV-E temperatures. The mixture showed no significant differences in the water sensitivity test and in the wheel tracking test, which is for certain related with the good compaction level of all specimens tested. On the other hand, despite the good compaction values of the test specimens there were significant differences in the stiffness modulus and the fatigue resistance of the mixture fabricated at the manufacturer's recommended temperatures (lowest).

Although, only one mixture and bitumen combination was analysed, the results showed that there is not a unique temperature that optimizes all performance variables. The mechanical performance of the material is better if a high level of compaction is achieved but there are also differences in the microstructure of the material, not captured by the air voids content, that affect the final performance. Thus, this subject is worth for future research, with other mixtures and bitumens.

**Acknowledgments** The authors would like to thank Probigalp for supplying the binder and allowing the use of the laboratory for most of the tests.

## References

AI (1997) Superpave Mix Design, Superpave Series No. 2 (SP-2), Asphalt Institute, Lexington, USA.

Bahia H-U, Hanson D-I, Zeng M, Zhau H, Khatr M-A, Anderson R-M (2001) Characterization of Modified Asphalt Binders in Superpave Mix Design, National Cooperative Highway Research Program (NCHRP), Report 459, Transportation Research Board, Washington, DC, USA.

Bahia H-U, Fahim A, Nam K (2006) Prediction of compaction temperatures using binder rheology. Transportation Research Circular E-C105, Transportation Research Board, Washington, DC, USA.

EP (2009) Construction Specifications Book (in Portuguese), in 15.03 - Paving. Estradas de Portugal, S.A., Portugal.

Gorkem C, Sengoz B (2009) Predicting stripping and moisture induced damage of asphalt concrete prepared with polymer modified bitumen and hydrated lime. Construction and Building Materials 23:2227–2236.

Micaelo R, Santos A, Duarte C (2012) Mixing and Compaction Temperatures of Asphalt Mixtures with Modified Bitumen. Paper presented at the 5th Congress Eurasphalt & Eurobitume. Istanbul, Turkey.

Read J, Whiteoak D (2003) The Shell Bitumen Handbook, 5th ed, Thomas Telford, London

Stuart K-D (2001) Methodology for Determining Compaction Temperatures for Modified Asphalt Binders, FHWA-RD-02-016, Federal Highway Administration, McLean, Virginia, USA.

West R-C, Watson D-E, Turner P-A, Casola J-R (2010) Mixing and Compaction Temperatures of Asphalt Binders in Hot-Mix Asphalt, National Cooperative Highway Research Program, NCHRP Report 648, Transportation Research Board, Washington, DC, USA.

Yildirim Y, Solaimanian M, Kennedy T-W (2000) Mixing and Compaction Temperatures for Hot Mix Asphalt Concrete, University of Texas, Austin.

Yildirim Y, Ideker J, Hazlett P-E (2006) Evaluation of Viscosity Values for Mixing and Compaction Temperatures. Journal of Materials in Civil Engineering 18:545–553.

# Compaction of Open-Graded HMAs Evaluated by a Fuzzy Clustering Technique

**Antonio Amadore, Gaetano Bosurgi, Orazio Pellegrino and Giuseppe Sollazzo**

**Abstract** The aim of this paper is the proposal of an expeditious procedure to be used during the execution of an asphalt layer for improving the compaction task. This procedure, based on a fuzzy clustering technique, starts from the knowledge of some information recorded by ordinary measuring instruments and provides an aid to the decision-maker on the number of roller passes needed to achieve a specific density at a certain temperature. This result can be deduced with great rapidity during the paving operations on site without waiting for the time spent in the core extraction and in the subsequent laboratory analysis. In this way it is possible to identify more precisely which aspects of the execution have to be corrected for performing the best compaction.

**Keywords** Compaction · Hot mix asphalt · Density · Fuzzy C-means

## 1 Introduction

The main purpose of the compaction is to reach a value of density at least equal to the minimum requirement specified in the design (Roberts et al. 1996) so that the pavement can have an optimum resistance to plastic deformation, fatigue, aging and cracks (Radziszewski 2007).

A. Amadore · G. Bosurgi (✉) · O. Pellegrino · G. Sollazzo
DICIEAMA Department, University of Messina, Messina, Italy
e-mail: gbosurgi@unime.it

A. Amadore
e-mail: aamadore@unime.it

O. Pellegrino
e-mail: opellegrino@unime.it

G. Sollazzo
e-mail: gsollazzo@unime.it



F. Canestrari and M.N. Partl (eds.), *8th RILEM International Symposium on Testing and Characterization of Sustainable and Innovative Bituminous Materials*, RILEM Bookseries 11, DOI 10.1007/978-94-017-7342-3_20

Recently, this topic has been addressed from a theoretical and experimental point of view. In both cases it was found that the solution is very complex by virtue of a very large number of variables related to the nature of the relationship among them. At this regard, for example, the numerous sensors today on the market (Kavussi and Hashemian 2011) can detect at very high frequencies the characteristics of the scenario, but they produce large databases difficult to manage (Manik et al. 2008).

However, the scientific literature (Airey et al. 2008) shares the opinion that the material temperature is the most important parameter for the achievement of a high density. Besides, below a certain threshold, said "temperature of cessation", any also remarkable effort in terms of energy transferred with the roller does not improve appreciably the density of the layer, but it is useful only for making more attractive the surface appearance (Attaelmanan et al. 2011; Sanchez-Alonso et al. 2011). Of course, this study has especially deepened the role of the temperature, the characteristics of the roll, its speed and the number of passes, assuming constant other important variables (such as gradation, bitumen content, aggregate shape, bitumen/filler ratio) that can influence the compaction.

The use of some clustering techniques, in front of a certain analytical simplicity, guarantee the processing of large amounts of data and the identification of preferential relationships, also not known a priori, among the variables. As a matter of fact, adopting numerous digital measuring instruments not only facilitates the operator during the surveys, but also it often produces a data set with an overly large number of variables that, in some particular cases, may be unnecessary and thus have to be eliminated (Bosurgi et al. 2010, 2011; Pellegrino 2011, 2012).

## *1.1 The Present Research*

The purpose of this research is to obtain an instrument of easy and immediate consultation during the execution of an asphalt pavement. Once some data concerning the characteristics of the material and the compacting machine have been acquired, it is sufficient to execute a small portion of the layer to have a data set of sufficient size. The processing of data with a fuzzy clustering technique (in this case the Fuzzy C-Means was applied) is used to respond in a very short time to questions regarding the needed roller passes, the cessation temperature, the target density of the HMA and so on.

This procedure could be applied to various cases and for this reason a test was performed on two different materials founding, as expected, different outcomes: the first one is a traditional open-graded HMA, while the second is the same material added with glass fibers and cellulose.

The deducted results may be used for the purpose of classification and decision support or may form the backbone of models of a certain complexity based on a first phase of learning (Bosurgi and Trifirò 2005a, b, 2006).

## 2 Method

To measure the density of the hot mix asphalt in real time, an electrical density gauge that introduces a weak current through the material, able to create an electrical sensing field was used. The impedance can be seen as the resistance to flow of an AC current at a determinate frequency. The dielectric constant represents the capability of a material to conserve electrostatic energy per unit of volume. Since the global dielectric constant of a composite material as an HMA depends on the volume of each component multiplied by its individual dielectric constant, it is possible to quantify the relative density of the material.

The output depends on the response of this electrical sensing field to changes in the pavement complex impedance that is then calibrated to the pavement density. Its accuracy (declared around 98 %) can be surely accepted if compared with the uncertain of ordinary laboratory tests. Of course, this threshold can be reached only executing the calibration procedure provided by the manufacturer, observed also in this case.

The following characteristics were almost constant during the experiment and did not processed numerically in the later stages of the analysis:

- Roller speed: 4 km/h.
- Roller weight: 2 t on the anterior drum and 2 t on the rear drum.
- Dynamic parameters: amplitude 0.37 mm, frequency 60 Hz.
- Load per cm of drum contact (in static): 14.6 kg/cm
- Drum width: 1.40 m
- Air temperature: between 26 and 28 °C

During the test, the main variables used in the following clustering procedure were recorded:

- Passes number.
- Material temperature in °C.
- Density of the compacted material in kg/m$^3$.

Regarding the asphalt pavement, two different open-graded materials were tested, defined by the characteristics reported in Fig. 1 and Table 1.

The second material was added with glass fibers and cellulose in percentage of 0.30 % by weight of the aggregates. The used fibers are cellulose and glass based, with a dosage of 0.30 % by aggregate weight. The main characteristics of the pellets are: average diameter 4–6 mm, average length 3–20 mm, brown to black, 0.34–0.55 density g/cm$^3$.

The material is officially termed to as a “semi-open graded fiber-reinforced” layer and represents a mix still under study. In this phase, it was tested also in order to understand his attitude to compaction.

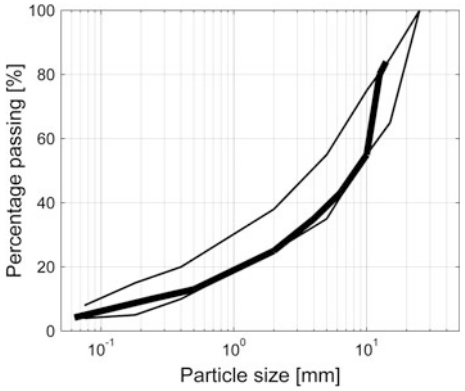


**Fig. 1** Grading curve of the tested material referred to a open-graded material

**Table 1** Common characteristic of the two materials

| | |
|---|---|
| Effective specific gravity (kg/m$^3$) | 2180 |
| Air voids (%) | 8 |
| Marshall stability (kN) | 11 |
| Marshall flow (mm) | 3 |
| Bitumen class (dmm) | 50/70 |
| Bitumen content (%) | 4.5 |

The contract specifications in force in Italy include the use of the Marshall test (performed on samples having a density of 2180 kg/m$^3$, air voids of 8 % asphalt content of 4.5 %) which produced the following results: stability (50 blows) 11 kN, flow 3 mm.

## *2.1 Brief Notes About Clustering*

The utilized data come from physical surveys of the variables of interest and each observation consists of n measured features, grouped into an n-dimensional vector:

$$x_k = [x_{k1}, x_{k2}, \ldots, x_{kn}]^T, \quad x_k \in R^n \tag{1}$$

Therefore, a set of N observations can be represented as a matrix N × n:

$$X = \begin{bmatrix} x_{11} & x_{12} & \cdots & x_{1n} \\ x_{21} & x_{22} & \cdots & x_{2n} \\ \vdots & \vdots & \ddots & \vdots \\ x_{N1} & x_{N2} & \cdots & x_{Nn} \end{bmatrix} \tag{2}$$

Some soft computer techniques (Jang 1993; Abonyi and Feil 2007), as fuzzy logic, admit that an object can belong to a number of clusters c simultaneously, with different membership degrees between 0 and 1. Naturally, the sum of the different membership degrees about the interested clusters must be equal to one. The structure of the partition matrix N × c, then, is the following:

$$U = \begin{bmatrix} \mu_{11} & \mu_{12} & \cdots & \mu_{1c} \\ \mu_{21} & \mu_{22} & \cdots & \mu_{2c} \\ \vdots & \vdots & \ddots & \vdots \\ \mu_{N1} & \mu_{N2} & \cdots & \mu_{Nc} \end{bmatrix} \tag{3}$$

where c is the number of fuzzy subsets or of clusters. This matrix $U = [\mu_{ik}]$ is subject to the following conditions:

$$\mu_{ik} \in [0,1], \quad 1 \le i \le c, \ 1 \le k \le N \tag{4}$$

$$\sum_{i=1}^{c} \mu_{ik} = 1, \quad 1 \le k \le N \tag{5}$$

$$0 < \sum_{k=1}^{N} \mu_{ik} < N, \quad 1 \le i \le c \tag{6}$$

With these premises, the fuzzy partitioning space for X is represented by the set:

$$M = \left\{ U \in R^{c \times N} \middle| \mu_{ik} \in [0,1], \ \forall i,k; \sum_{i=1}^{c} \mu_{ik} = 1, \ \forall k; \ 0 < \sum_{k=1}^{N} \mu_{ik} < N, \ \forall i \right\} \tag{7}$$

The i-th column of U contains the membership function values of the i-th fuzzy subset of X. With reference to Eq. (5), the sum of each column is 1 and thus the total membership of each $x_k$ in X equals one.

## 3 Results

The methodology described above was applied to a lay down of the two different material before illustrated in a rural road located near the town of Messina (Italy). The asphalt plant was near to the construction site and this allowed to the material to have temperatures high enough (between 165 and 172 °C) to ensure a reasonable useful period for compaction.

**Table 2** Open-graded HMA. Survey of the principal characteristics during the compaction

| Distance (m) | Passes | Temperature (°C) | Density (kg/m$^3$) |
|---|---|---|---|
| 0 | 0 | 128.4 | 1887 |
| 0 | 2 | 82.9 | 1933 |
| 0 | 4 | 73.4 | 1986 |
| 0 | 5 | 82.3 | 2013 |
| 0 | 6 | 74.4 | 2187 |
| … | … | … | … |

**Table 3** Open-graded HMA with fibers. Survey of the principal characteristics during the compaction

| Distance (m) | Passes | Temperature (°C) | Density (kg/m$^3$) |
|---|---|---|---|
| 0 | 0 | 139.9 | 1851 |
| 0 | 1 | 68.7 | 1977 |
| 0 | 2 | 57.4 | 2006 |
| 0 | 3 | 54.0 | 1998 |
| 0 | 4 | 65.1 | 2021 |
| … | … | … | … |

Paving occurred with a paver, for a width of m 3.00, with a nominal thickness of the layer of 4 cm and a speed of 0.11 m/s, followed by a roller with double metallic drum, the characteristics of which have been previously specified in the Method paragraph.

The measures were recorded in 7 sections placed at a distance of 10 m from one another and for 7 passes of the roller. The number of passes was not more increased, since the temperature would be lowered so as to render ineffective the action of the roller.

In this way, a database consisting of 49 rows (observations), with 4 columns (partial distance in m, number of pass, material temperature in °C and density of the HMA in kg/m$^3$) was obtained, partially shown in Tables 2 and 3, representing respectively the traditional open-graded HMA and the other one added with fibers.

As expected, the behavior of the two types of asphalt pavement is quite different. Tables 2 and 3 are, for this purpose, little explanatory and, for this reason, the most interesting relationships were reported in some graphics, avoiding trivial and intuitive representations such as, for example, the trend of the temperature with the number of passes (or time).

As already said, all the measures were recorded in 7 sections along the layer, placed at a distance of 10 m from one another.

The density was put in relation with the number of passes of the compacting machine (Fig. 2) and, although an increased trend could be predicted, the difference between the two materials is quite interesting.

In Fig. 3a, b there are the trends of the temperature and the density versus the distance. Since there are some peaks apparently incomprehensible, the tendency

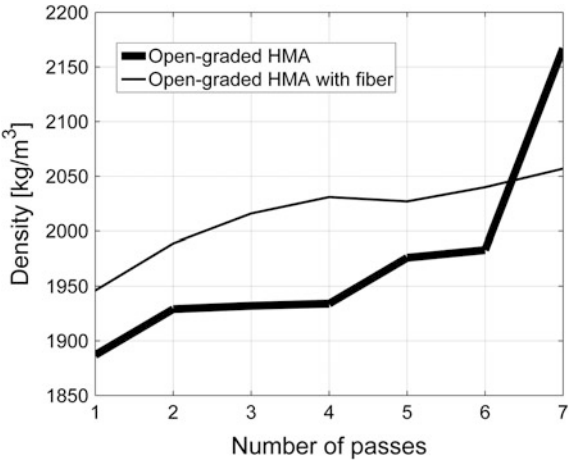


**Fig. 2** Relationship between the material density and the number of passes of the compacting machines at a distance of 30 m from the start

may not seem rational. However, it is interesting to note that both the temperature and the density follow the same rules.

Finally, Fig. 4 illustrates the relationship (almost linear) that occurred during the experiments between the density and the temperature. This correlation, illustrated only in sections placed at 30 m (but similar in other sections) away from the starting point, shows a good growth of the material density, even if the temperature dropped considerably.

In order to create a tool for decision support, authors used the two data sets reported in Tables 2 and 3 to which they applied the Fuzzy C-Means technique. The objective of this analysis was to identify the number of passes required to reach the desired density of that material at a specific temperature. For this reason, 7 clusters representative of 7 passes of the compacting machines were identified so that the operator can refer to one of these clusters a certain observation characterized by a value of density and temperature of the material.

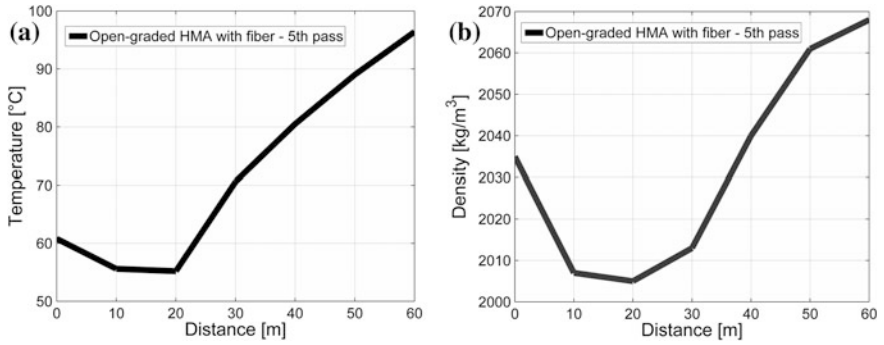


**Fig. 3** Similar trend of the material temperature (**a**) and density (**b**) along the strip during the fifth pass of the roll

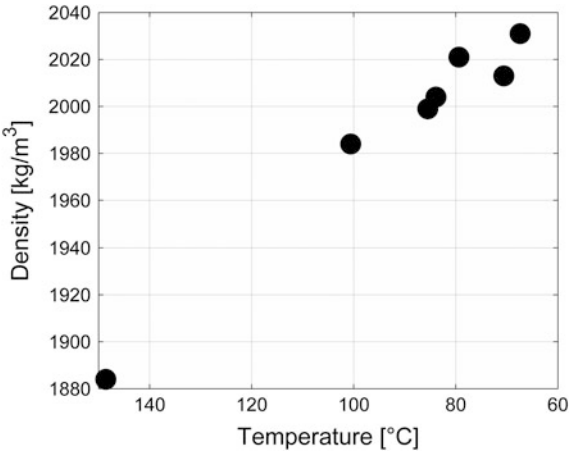


**Fig. 4** Trend of the material temperature along the strip during the fifth pass of the roll at a distance of 30 m from the starting point

**Table 4** Open-graded HMA. The distance matrix containing the square distances between the data points and the cluster centers, regarding only the first five observations

| N | c1 | c2 | c3 | c4 | c5 | c6 | c7 |
|---|---|---|---|---|---|---|---|
| 1 | 31.148 | 245.340 | 56.146 | 93.835 | 123.893 | 297.440 | 211.045 |
| 2 | 86.134 | 9.405 | 194.487 | 40.163 | 70.249 | 247.337 | 158.251 |
| 3 | 126.636 | 141.602 | 59.459 | 21.254 | 20.992 | 194.386 | 105.028 |
| 4 | 142.686 | 114.490 | 84.124 | 41.145 | 10.285 | 167.339 | 78.421 |
| 5 | 306.228 | 59.776 | 258.182 | 215.001 | 8.112 | 184.128 | 95.976 |
| | … | … | … | … | … | … | … |

In the following tables are reported only the case of the HMA without fibers. The application of the Fuzzy C-Means algorithm returned numerous results but only the distance matrix containing the square distances between the data points and the cluster centres were reported (Table 4).

Finally, the insertion of new observations (Table 5) has permitted to evaluate the membership to the clusters without knowing the value of the number of passes. This phase assured also to determine the partition matrix for the evaluated data set

**Table 5** Open-graded HMA. Insert of new observations without information about number of passes

| N′ | Temperature | Density |
|---|---|---|
| 1 | 90 | 2015 |
| 2 | 94 | 2001 |
| 3 | 93 | 2191 |
| 4 | 161 | 1888 |
| 5 | 98 | 1902 |
| 6 | 85 | 1951 |
| 7 | 73 | 1963 |
| 8 | 70 | 1998 |

**Table 6** Open-graded HMA with fibers. Distance matrix with the distances between the new observations and the cluster centers

| N′ | c1 | c2 | c3 | c4 | c5 | c6 | c7 |
|---|---|---|---|---|---|---|---|
| 1 | 140 | 113 | 85.6 | 42.4 | 12.7 | 166 | 77.6 |
| 2 | 126 | 127 | 71.7 | 28.8 | 9.33 | 180 | 92.2 |
| 3 | 306 | 64.9 | 262 | 218 | 188 | 17.7 | 102 |
| 4 | 5.1 | 253 | 80.8 | 111 | 138 | 304 | 221 |
| 5 | 61.6 | 226 | 28.2 | 71 | 102 | 279 | 191 |
| 6 | 94.2 | 177 | 22.6 | 22.1 | 52.2 | 229 | 140 |
| 7 | 111 | 165 | 38.2 | 19 | 42 | 217 | 128 |
| 8 | 138 | 130 | 71.9 | 32.2 | 16.1 | 183 | 93.1 |

U* (c × N′) and the distance matrix, representative of the distances between the evaluated data points and the cluster centres $D*_{ik}^{2}$ (c × N′), with N′ = 6 number of new observations (Table 6).

## 4 Discussion

Generally, handling very homogeneous data (even if not particularly numerous), the fuzzy clustering technique adopted here (Fuzzy C-Means) can produce good results. However, a proper data set is extremely difficult to achieve completely and, also in the experiments reported in this paper, some small discrepancies, that had to be clarified immediately, can be noted.

Figure 2, for example, shows a better performance of the asphalt pavement with fibers up to the fifth passes. With the sixth and seventh passes it was recorded an improvement of the traditional material in terms of density. The fibers always provided higher density (with other conditions being equal) respect to traditional HMA. However, experimentation has shown that the traditional material maintained a certain ability to thicken even for fairly low temperatures, on the contrary of the HMA with fibers. However, this feature is not very profitable because its utilization requires significant addition of the number of roller passes.

Figure 3a, b illustrate the density and the temperature values along the pavement at a certain number of passages of the roller. There is a good homogeneity between temperature and density, and it seems that they follow the same trend along the strip also because, obviously, a hotter material is easier to compact.

However, the trend of the temperature and, consequently, of the density along the layer is not always constant or descending as could be expected. Especially the change of the temperature, for the same material and for the same number of passes, could show a detection error of the measurements. Instead, the phenomenon is due to the particular machines used in the experiment. The truck, in fact, poured into the hopper of the floating screed the material more exposed to air and, therefore, more

cold. This detail caused that the first sections of the paving were characterized by considerably more cold temperature (even differences of 40 °C) with a greater difficulty of compaction.

Another interesting aspect relates to the so-called "temperature of cessation", below which it would no longer be possible to thicken the material, despite more roller passes occur. Figure 4, relating to the pavement with fibers, seem to disprove in part this hypothesis, because of a certain gain in terms of density even at lower temperatures (around 68 °C). This figure was obtained for the material added with fibers but the normal open-graded material showed a greater aptitude to be thickened with high numbers of steps and, consequently, with even lower temperatures.

About the fuzzy clustering procedure, interesting results were obtained, albeit with some limitations of which will deepen the meaning.

As already mentioned in the Method section, the purpose of this experiment was to identify the number of roller passes needed to obtain a certain density. The fuzzy clustering technique, by means of the survey, "learned" the relationships between the number of passes, the temperature and the density through the knowledge of 49 observations for the open-graded material and further 49 observations for the same material added with fibers.

The result of the analysis was the identification of 7 clusters: this association between a temperature and a density value with a suitable number of passes is strongly contextualized to that particular scenario. This means that a section of a similar pavement, but laid in different ways (temperature, compaction machines, etc.), requires the preparation of a new learning data set.

The last phase of the procedure permitted to associate some new observations to an appropriate cluster, that is the number of passes needed to reach a certain density with a definite temperature of the material. In order to test the method, therefore, eight new observations for the open-graded HMA (Table 5) and eight new observations for the material added with fibers were added. The results are reported in Table 6. As it is possible to note, a specific observation has not an unique cluster membership (the analysis, otherwise, would be of a hard type), but is assigned to all clusters, specifying a certain distance from them. The smaller this distance, the closer to that cluster the observation and, consequently, the easier the determination of the corresponding number of passes. Anyway, it may happen that the observation is close enough to more than one cluster. This is not a limit of the analysis, but rather a point of strength and this quantifies the uncertainty of the final result. For example, in Table 6, the observation 6 presents a distance with the clusters 3 and 4 substantially similar (22.6 and 22.1).

Yet it can be noted, for example, that the material without fibers, characterized by a temperature of 82.3 °C and a density of 2013 kg/m$^3$, requires 5 passes (Table 2). This is directly detectable by the minimum distance to the cluster 5 (8.112) of this observation with respect to the other clusters. Similarly, the observation 4 (temperature 82.9 °C and density of 1933 kg/m$^3$) requires a double pass of the compacting machine (9.405).

The analysis outcome for the second type of material (with fibers) is similar and, even if there is not any table, some examples can be described. The observation

no. 1, characterized by a temperature of 55 °C and a density of 1990 kg/m$^3$ requires 6 passes. Here, the algorithm recognizes a very low temperature and, therefore, this observation was positioned close to the cluster 6. The observation no. 5, characterized by a temperature of 152 °C and a density of 1910 kg/m$^3$ requires only one pass. As in the case of traditional material, the algorithm identifies a very high temperature and for this reason the density can be achieved with a single pass.

## 5 Conclusions

In this paper, the compaction problem was studied and, in particular, the choice of the most appropriate number of roller passes to suit a certain density, knowing the temperature of the material.

Some choices are extremely difficult because the scenario is changeable in time (for example, the air and the material temperature) and the number of the involved variables is very high. The use of traditional procedures, consisting in examining and testing core samples extracted from the pavement already layered, is not optimal. First of all, this is due to the long waiting times necessary to know the outcomes of the laboratory test and, secondly, because the value of the density could be deducted only at the last pass of the roller, without any information on the evolution of the density and the temperature during the execution. Only the knowledge of these relationships may allow the operator to prepare a prediction analysis or a tool for decision support.

The present proposal is based, instead, on a preliminary survey of all the involved variables that feed a database on which were applied a clustering technique. The purpose is to highlight also hidden relationships among the variables that it is not possible or convenient to represent in analytical forms. The links shown in Figs. 2–4 are, therefore, all content and considered by this procedure and the final result was appropriately influenced.

In this way it is possible to assist substantially the operator that, knowing the temperature of the material and having as objective a certain density, can set the number of required passes. The result, of course, suffers from a certain lack of precision but the fuzzy nature of the algorithm guarantees to quantify this inaccuracy.

Paradoxically, this extremely simple procedure exceeds the two approaches traditionally used and previously described: this method is very fast in the issuance of the results, it is not computationally expensive, requires a data set sufficiently short and provides the final results specifying their reliability.

In this study only two types of material have been tested because it would be too complicated to expand the investigation to a number of different types on roads that will be opened to traffic. However the authors intend to extend this research in the near future to a greater number of material, in order to highlight similarities that might lead to a standardization of the compacting procedure. From this point of view, the study proposed in this manuscript is preliminary to further study.

## References

Abonyi, J., Feil, B. (2007). Cluster Analysis for Data Mining and System Identification, Birkhäuser Basel.

Airey, G.D., Hunter, A.E., Collop A.C. (2008). The Effect of Asphalt Mixture Gradation and Compaction Energy on Aggregate Degradation, Construction and Building Materials 22 (2008) pp. 972–980.

Attaelmanan, M., Pei Feng, C., Al-Hadidy, AI. (2011). Laboratory evaluation of HMA with high density polyethylene as a modifier, Construction and Building Materials 25 (2011) pp. 2764–2770.

Bosurgi, G., D'Andrea, A., Pellegrino, O. (2010). Could drivers' visual behaviour influence road design? Advances in Transportation Studies 22 (2010) pp. 17-30.

Bosurgi, G., D'Andrea, A., Pellegrino, O. (2011). Context sensitive solutions using interval analysis, Transport 26(2) (2011) pp. 171-177.

Bosurgi, G., Trifirò, F. (2005a). A model based on artificial neural network and genetic algorithms for pavement maintenance management. International Journal Of Pavement Engineering 6 (2005) pp. 201 - 209.

Bosurgi, G., Trifirò, F. (2005b). A Hybrid Approach For Pavement Maintenance Management Of An Italian Motorway. International Conference On Computing In Civil Engineering, ASCE Cancun July, 12-15 2005.

Bosurgi, G., Trifirò, F. (2006). A genetic algorithm approach for pavement maintenance program optimization using safety evaluation data. International Journal Of Pavements 5 (2006) pp. 164 - 174.

Jang, J.S.R. (1993). ANFIS: Adaptive-Network-based Fuzzy Inference Systems, IEEE Trans. Systems, Man, and Cybernetics 23 (1993) pp. 665-685.

Kavussi, A. and Hashemian, L. (2011). Properties of WMA–foam mixes based on major mechanical tests. Journal of Civil Engineering and Management, 17(2) (2011) pp. 207-216.

Manik, A., Gopalakrishnan, K., Singh, A. and Yan, S. (2008). Neural networks surrogate models for simulating payment risk in pavement construction, Journal of Civil Engineering and Management 14 (4) (2008) pp. 235-240.

Pellegrino, O. (2011). Road context evaluated by means of fuzzy interval. Cognition, Technology and Work 13(1) (2011) pp. 67-79.

Pellegrino, O. (2012). The application of drivers' cognitive reliability using fuzzy techniques. Applied Artificial Intelligence 26(6) (2012) pp. 517-540.

Radziszewski, P. (2007). Modified asphalt mixtures resistance to permanent deformations. Journal of Civil Engineering and Management 13 (4) (2007) pp. 307-315.

Roberts, F.L., Kandhal, P.S., Brown, R.E., Lee, D.Y. and Kennedy, T.W., (1996). Hot Mix Asphalt Materials, Mixture Design, and Construction, Second Edition, NAPA Education Foundation, Lanham Maryland, 585 pgs.

Sanchez-Alonso, E., Vega-Zamanillo, A., Castro-Fresno, D., Del Rio-Prat, M. (2011). Evaluation of compactability and mechanical properties of bituminous mixes with warm additives, Construction and Building Materials 25 (2011) pp. 2304–2311.

# Effects of Anisotropy on Performance of HMA Specimens Due to Roller Compaction

**Bernhard Hofko and Ronald Blab**

**Abstract** The segmented roller compactor is a standardized method to produce HMA-slabs in the lab. Specimens are cored and cut from the slabs for further testing. The relation between the direction of compaction and testing in the laboratory is not always the same relation as it is between the direction of compaction and actual loading in the field. The paper presents research on the influence of the compaction direction on performance characteristics of roller compacted HMA specimens. Performance parameters of a base layer mix are obtained, including high-temperature, stiffness, fatigue and low-temperature tests. The relation between direction of compaction and testing is varied in all three dimensions to find relevant influences. It can be concluded from the results that all obtained performance parameters are sensitive to the material anisotropy due to compaction, especially for stiffness and fatigue performance. For the high temperature performance specimens from path- and force-controlled compaction were compared. The applied compaction work rather than the compaction method is linked to the difference in the regarding results. The uniformity of the compaction in terms of the variation of bulk density of the specimens reflects on the scattering of test results.

**Keywords** Performance based test methods · Compaction · Hot mix asphalt

## 1 Introduction

Achieving consistency in compaction, both in the laboratory and in the field is necessary to obtain reliable correlation between HMA laboratory performance and the observed in-service behavior. Different laboratory compaction methods may produce volumetrically identical specimens but with widely varying mechanical performance (Brown and Gibb 1999; Renken 2000; Iwama et al. 2007). Reason is

B. Hofko (✉) · R. Blab
Research Center of Road Engineering, Vienna University of Technology, Vienna, Austria
e-mail: bernhard.hofko@tuwien.ac.at



F. Canestrari and M.N. Partl (eds.), *8th RILEM International Symposium on Testing and Characterization of Sustainable and Innovative Bituminous Materials*, RILEM Bookseries 11, DOI 10.1007/978-94-017-7342-3_21

that the method of compaction has an influence on the aggregate orientation and therefore on the performance itself (Masad et al. 1999; Hunter et al. 2004). Airey et al. (2005) found that the roller compaction used to produce hot mix asphalt (HMA)-slabs in the lab provide the best correlation with field specimens in terms of internal aggregate structure and mechanical properties.

Still, for one specific compaction method, performance indicators show anisotropy. Masad et al. (2002) states that stiffness of asphalt specimens differ up to 30 % depending on the direction of testing.

In this paper the effect of the direction of compaction and the orientation of the specimens cored and cut from the compacted HMA-slab on performance parameters of the mix are investigated. Also the compaction method was varied to compare force- and path-controlled compaction. For the preparation of the HMA-slabs the roller compaction according to EN 12697-33:2007 was used. To fully describe the characteristics of the mix the research program included tests to assess performance in terms

- high-temperature (Triaxial Cyclic Compression Test (TCCT) acc. to EN 12697-25),
- stiffness and fatigue (Cyclic Indirect Tension Test (IT-CY) acc. to FGSV AL Sp-Asphalt 09 and EN 12697-24), and
- low-temperature (Temperature Stress Restrained Specimen Test (TSRST) and Uniaxial Tension Stress Test (UTST) acc. to prEN 12697-46)

## 2 Materials

The mix type used in this study was chosen to represent a base layer asphalt concrete (AC base) commonly used in Austria with a maximum aggregate size of 22 mm. It is known that effects of anisotropy tend to increase with increasing aggregate size in the mix. The base layer is specified as an AC 22 base 50/70 acc. to EN 13108-1:2006. Details are listed in Table 1.

**Table 1** Mix design

| | |
|---|---|
| Type | AC 22 base 50/70 |
| Binder | Pen 50/70, unmodified |
| Binder content (optimized acc. to Marshall) | 4.5 % (m/m) |
| Content of air voids | 3.5 % (v/v) |
| Maximum density | 2616 kg/m$^3$ |
| Bulk density | 2524 kg/m$^3$ |
| Aggregate type | Limestone |

## 3 Specimen Preparation and Test Program

For the preparation of the specimens the mix was produced in a reverse-rotation compulsory mixer acc. to EN 12697-35:2007. The HMA-slabs were compacted by two different roller compactors acc. to EN 12697-33:2007 to produce slabs with dimensions 500 × 260 mm for high-temperature and stiffness/fatigue tests and 320 × 260 mm for low-temperature tests. In general the compaction was path-controlled. The necessary mass of mix was derived from the aimed volume of the slab and the target density. The compaction was then carried out by a path-controlled precompaction phase and a path-controlled main phase to the target height of the slab. In the path-controlled compaction, the roller compacts the HMA-slab to a target height with a constant change in height per cycle (0.3 mm/cycle).

A smaller part of the slabs was produced by force-controlled compaction to compare these two methods. In the force-controlled compaction, the roller compacts the HMA-slabs with a constant increase in force per cycle for a specified number of cycles, followed by a constant decrease in force per cycle with the same rate. For force-controlled compaction, it is necessary to carry out pre-tests to derive the change in force per cycle and the number of cycles to make sure that the HMA-slab is compacted to the target density. In case of this study, the change in force per cycle was determined to by 1.3 kN/cycle for a number of 15 cycles. Table 2 shows the dimensions of the slabs produced for the study.

To analyze differences in the performance characteristics as a function of compaction direction, different patterns (i.e. orientation of specimen testing vs. orientation of compaction) were used when the specimens were cut and cored. Figure 1 shows the coordinate system set for compaction. The x-axis is orthogonal to the roller path and the compaction force. The y-axis runs along the roller path and z-axis represents the direction of the compaction force. Also depicted in Fig. 1 is a scheme of the specimens used for the different test types. In addition the direction of the loading is plot as well as the direction of the relevant reaction measured in the test.

Table 3 gives an overview of the test programme. For each test type it is shown which orientations were tested together with the name of the pattern used as an acronym for identification. For example the F-Z-Y indicates an IT-CY (fatigue test) with the orientation of test loading in z-direction and the orientation of the relevant

**Table 2** Slab dimensions

| Dimensions (l × w × h) (mm) | Compaction | Test type |
|---|---|---|
| 320 × 260 × 60 | Path-controlled | TSRST, UTST |
| 500 × 260 × 150 | Path-controlled | IT-CY |
| 500 × 260 × 140 | Path-controlled | TCCT |
| 500 × 260 × 220 | Path-controlled | TCCT |
| 500 × 260 × 220 | Force-controlled | TCCT |

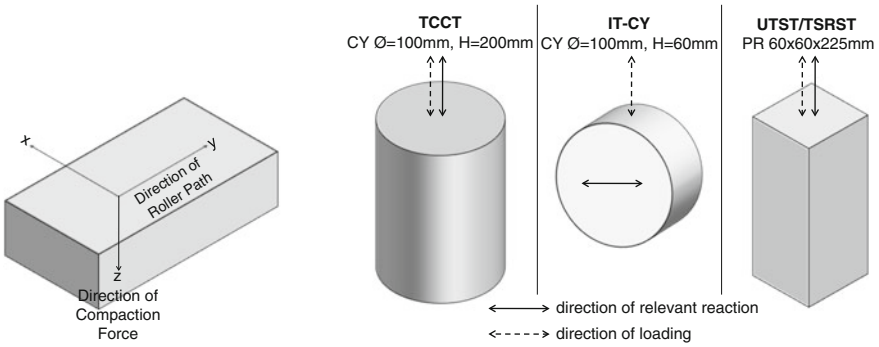


**Fig. 1** Coordinate system of compaction (*left*) and principal directions of testing (*right*)

reaction in y-direction. The orientation is taken from the coordinate system of compaction (Fig. 1). Thus, a link between the compaction and the orientation of testing is achieved. In Table 3 the loading-compaction configuration that matches the situation in a pavement under traffic is highlighted in bold letters for each test type. In theory for the UTST/TSRST three variations of the orientation are possible, as well as for the TCCT. For the IT-CY six variations could be tested. For the test programme those orientations were chosen that represent the situation in the road and the orientations that are commonly used in a lab to ensure an efficient and economic production of specimens.

## 4 Test Procedures and Results

To quantify the influence of the direction of compaction, the performance of the AC 22 mix was characterized by performance based tests at low (TSRST, UTST), intermediate (IT-CY) and high (TCCT) temperatures. The test procedures and results are presented in this chapter.

### *4.1 Low-Temperature Performance*

To assess the resistance to low-temperature cracking, two test types, the TSRST and UTST were carried out in accordance to prEN 12697-46. By combining the results of the UTST and TSRST at a certain temperature, the tensile strength reserve ($\Delta\beta_t$) can be obtained. It is the difference between the cryogenic stress from the TSRST and the tensile strength from the UTST at the same temperature. The difference between the two stresses is the theoretical strength reserve that a pavement can take in traffic load at a certain temperature before cracking.

**Table 3** Orientation of specimen and testing

| Test | Orientation of loading | Orientation of relevant reaction | Pattern | |
|---|---|---|---|---|
| | Direction of coordinate system of compaction | | | |
| **UTST/TSRST** | **X** | **X** | **L-X-X** | 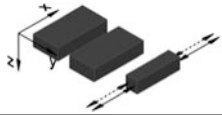 |
| **UTST/TSRST** | **Y** | **Y** | **L-Y-Y** | 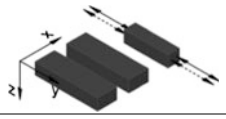 |
| IT-CY | X | Y | F-X-Y | 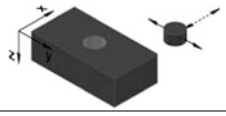 |
| **IT-CY** | **Z** | **Y** | **F-Z-Y** | 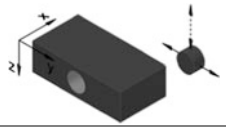 |
| **TCCT** | **Z** | **Z** | **H-Z-Z** | 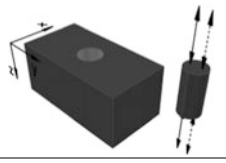 |
| TCCT | X | X | H-X-X | 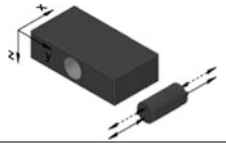 |
| TCCT | Y | Y | H-Y-Y | 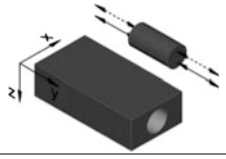 |

### 4.1.1 Results

Both tests were carried out at specimens with an L-X-X and an L-Y-Y orientation. Table 4 and Fig. 2 show relevant results. The L-X-X configuration results in a lower cracking temperature at lower cryogenic stresses in the TSRST. Also the cryogenic stresses at −20 °C are lower than for the L-Y-Y configuration. The tensile strength at −20 °C obtained from the UTST is again smaller for the L-X-X specimens. For both test types the variation of the results in terms of standard deviation (SD) is

**Table 4** Low-temperature results

| | L-X-X | | L-Y-Y | | $\Delta_{X\text{-}X/Y\text{-}Y}$ (%) | |
|---|---|---|---|---|---|---|
| | MV | SD | MV | SD | MV | SD |
| $T_{crack}$ (°C) (TSRST) | −28.5 | 2.9 | −26.7 | 0.8 | −6.3 | −72.4 |
| $\sigma_{cryo,crack}$ (N/mm$^2$) (TSRST) | 3.5 | 0.3 | 4.0 | 0.3 | 14.3 | 0.0 |
| $\sigma_{cryo}$ @ −20 °C (N/mm$^2$) (TSRST) | 1.1 | 0.6 | 1.9 | 0.2 | 72.7 | −66.7 |
| $\beta_t$ @ −20 °C (N/mm$^2$) (UTST) | 3.7 | 0.3 | 4.0 | 0.4 | 8.1 | 33.3 |
| $\Delta\beta_t$ @ −20 °C (N/mm$^2$) | 2.5 | 0.9 | 2.1 | 0.6 | −16.0 | −33.3 |

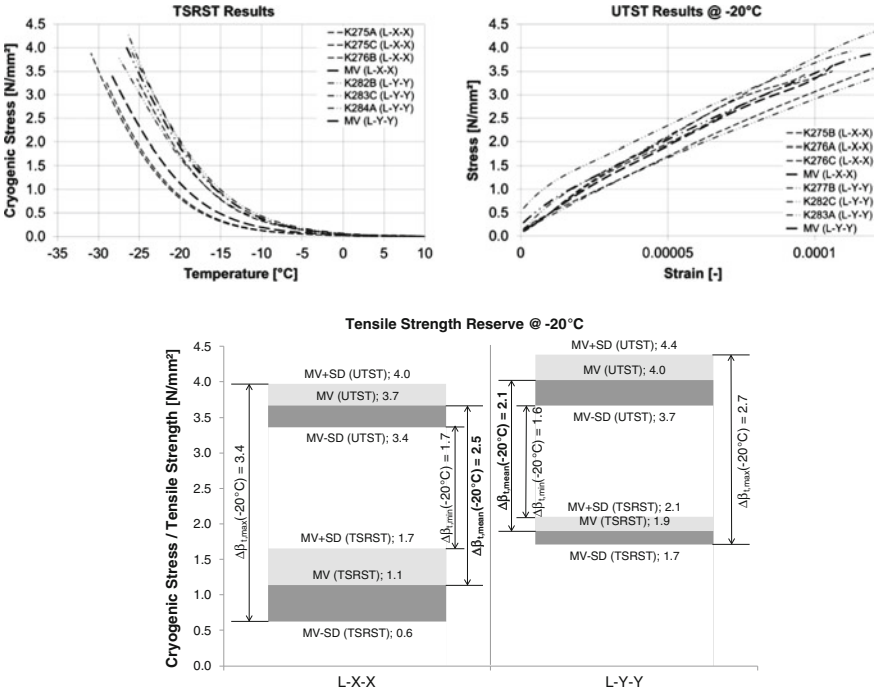


**Fig. 2** TSRST results (*upper left*), UTST results (*upper right*) and tensile strength reserve (*below*)

higher for the L-X-X configuration. The tensile strength reserve at −20 °C as the main result for the low-temperature behaviour is 2.5 N/mm$^2$ (mean value MV) for the L-X-X with a range from 1.7 to 3.4 N/mm$^2$ taking into account the SD. For the L-Y-Y configuration the MV of the reserve is 2.1 N/mm$^2$ ranging from 1.6 to 2.7 N/mm$^2$.

This shows that the low-temperature performance is sensitive to the anisotropy of the mix. In transverse orientation (L-X-X) the performance is better in terms of temperature induced stresses (TSRST) as well as of strength reserve although the tensile strength at low temperatures is smaller than in longitudinal direction (L-Y-Y).

## 4.2 Stiffness and Fatigue Performance

For the characterization of the stiffness and especially the fatigue performance the cyclic indirect tension test (CY-IT) was carried out. The test procedure is standardized by the German Road and Transportation Research Association (FGSV) in the AL Sp-Asphalt 09 on the basis of EN 12697-24:2007. A cylindrical specimen is located between two load plates in a way that a sinusoidal compressive stress is applied to the lateral surface of the specimen. This cyclic compression mainly leads to tensile stresses along the vertical axis which is responsible for fatigue deterioration and finally the failure of the specimen. Within one test procedure 9 specimens are tested (3 specimens at 3 different load levels) at 20 °C and a test frequency of 10 Hz. The test is force-controlled with a constant minimum stress of 35 kPa and three different maximum stresses to realize 3 load levels (in this case 100, 200 and 400 kPa). During the test the horizontal deformation is recorded by linear variable differential transformers (LVDTs). Due to increasing fatigue the specimen's stiffness decreases causing increasing horizontal strain as the stress level is held constant. After the test is finished the dynamic modulus $|E^*|$ is analyzed versus number of load cycles. The point of fatigue is achieved when the dynamic modulus has reached half the initial dynamic modulus which is obtained after the 100th load cycle. To characterize the fatigue performance a fatigue function (power function) combining the elastic strain amplitude after the 100th load cycle ($\varepsilon_{el,100}$) versus the number of load cycles until fatigue ($N_{fat}$) is derived (Fig. 3, left).

To characterize and compare the stiffness of specimens, the dynamic modulus after the 100th load cycle is used as a benchmark (Fig. 3, right).

### 4.2.1 Results

In the study, the fatigue performance was derived for the F-X-Y and the F-Z-Y orientation. The F-Z-Y configuration reflects the load situation in a road pavement. The direction of the traffic load is the same as the direction of the compaction force (Z). The traffic load leads to flexural stresses in the pavement with the largest

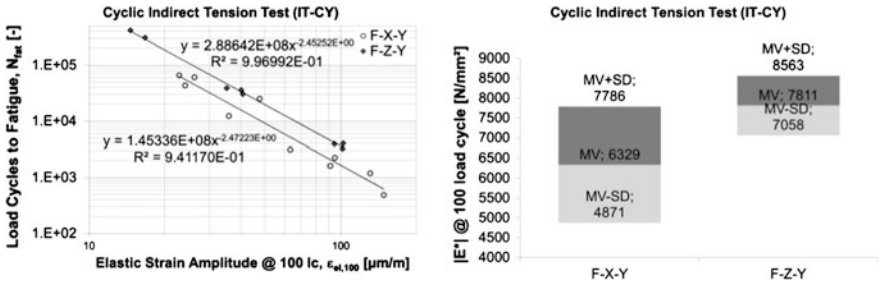


**Fig. 3** IT-CY results: fatigue function (*left*), and stiffness (*right*)

**Table 5** Fatigue and stiffness results

| | F-X-Y | | F-Z-Y | | $\Delta_{X\text{-}Y/Z\text{-}Y}$ (%) | |
|---|---|---|---|---|---|---|
| $\varepsilon_{el,100}$ @ $N_{fat}$ of 1.000 (µm/m) | 123 | | 168 | | 36.6 | |
| $\varepsilon_{el,100}$ @ $N_{fat}$ of 10.000 (µm/m) | 48 | | 66 | | 37.5 | |
| $\varepsilon_{el,100}$ @ $N_{fat}$ of 100.000 (µm/m) | 19 | | 26 | | 36.8 | |
| | MV | SD | MV | SD | MV | SD |
| $\lvert E^* \rvert$ (MPa) @ 20 °C, 10 Hz | 6329 | 1458 | 7811 | 752 | 23.4 | −48.4 |

stresses on the bottom of the bound layers in longitudinal direction (Y). Results can be taken from Fig. 3 and Table 5. The left diagram in Fig. 3 shows the fatigue function for the two tested orientations in log-log-scale. The F-Z-Y configurations results in a better fatigue performance with a higher number of load cycles until fatigue. Also the scattering of test results is significantly lower than for the F-X-Y direction. Table 5 shows that the fatigue performance in F-Z-Y orientation is about 37 % higher than in the other direction. Interestingly enough the two fatigue functions are parallel in the log-log-scale (similar exponents).

The right diagram in Fig. 3 provides information about the dynamic stiffness of the mix. Again the F-Z-Y leads to higher results and a smaller variation. In respect to the mean values of |E*|, F-Z-Y is about 23 % higher than F-X-Y.

It can be concluded, that the fatigue and stiffness performance is very sensitive to the anisotropy of the mix with higher fatigue resistance for the F-Z-Y orientation which reflects the loading situation in the road.

## *4.3 High Temperature Performance*

The high temperature performance as the resistance against permanent deformation can be obtained by the TCCT according to EN 12697-25:2006. The test was carried out at a test temperature of 50 °C and a frequency of 3 Hz. The axial load ranged from 150 to 750 kPa, the confining pressure was set to 150 kPa. For each test procedure 3 specimens were tested.

As a result a relationship between the number of load cycles and the permanent axial strain is derived. A power function is used to describe the loading-strain curve. To compare different mixes the creep rate ($f_c$) is obtained indicating the increase of permanent deformation in µm/m per load cycle. The creep rate represents the exponent of the power function. The smaller the absolute value of the creep rate the better is the high temperature performance.

For the high temperature performance not only different orientations of testing versus compaction were analyzed but also different methods of compaction (path- vs. force-controlled).

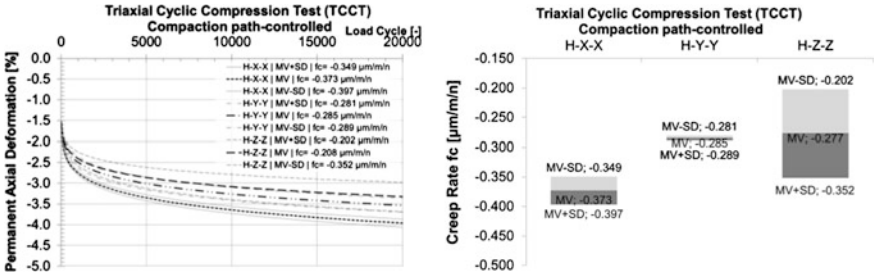


**Fig. 4** TCCT results for path-controlled compaction: creep curve (*left*), and creep rate (*right*)

### 4.3.1 Results—Path-Controlled Compaction

In this test the H-Z-Z orientation represents the load situation in a pavement structure. The traffic load and the main orientation of reaction (permanent deformation) occur in the direction of the compaction force (Z).

The results for path-controlled compaction are presented in Fig. 4. The H-Y-Y and H-Z-Z configuration show similar results with slightly higher resistance to permanent deformation for the H-Z-Z specimens (+3 %) and also a far larger scattering in results. The H-X-X orientation produces the highest creep rate and largest permanent deformations. The creep rate for the H-Z-Z is 26 % lower and for the H-Y-Y 24 % lower than for the H-X-X (Table 6).

As the TCCT is a test where the specimen is loaded similarly as during compaction, part of the difference in the performance might be connected to the compaction effort. Thus, Fig. 5 compares the bulk density [derived acc. EN 12697-6, saturated dry surface (SSD)] and its variation of the path-controlled compacted TCCT specimens. Comparing the creep rates (right diagram in Fig. 4) with the bulk density there is no interrelation between the MV of the bulk density and the creep rates. But another interesting trend is described. The larger the variation of the bulk density, the larger is the variation of the creep rates. Thus, the

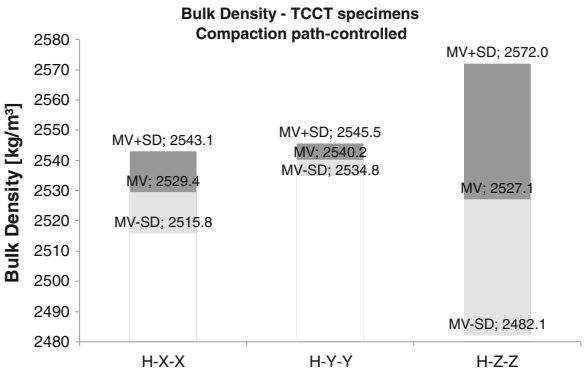


**Fig. 5** Bulk density of path-controlled compacted TCCT specimens

**Table 6** High temperature results—path-controlled compaction

| | H-X-X | | H-Y-Y | | H-Z-Z | | $\Delta_{X\text{-}X/Y\text{-}Y}$ (%) | | $\Delta_{Y\text{-}Y/Z\text{-}Z}$ (%) | | $\Delta_{X\text{-}X/Z\text{-}Z}$ (%) | |
|---|---|---|---|---|---|---|---|---|---|---|---|---|
| | MV | SD | MV | SD | MV | SD | MV | SD | MV | SD | MV | SD |
| $f_c$ (µm/m/n) | −0.373 | 0.024 | −0.285 | 0.004 | −0.277 | 0.075 | −23.6 | −83.3 | −2.8 | 1775 | −25.7 | 212.5 |

difference in the creep rate between the three test orientations seems to be connected to anisotropy of the material whereas the scattering of the test results within one test series is linked to variation of the compaction quality itself.

### 4.3.2 Results—Force-Controlled Compaction

Analogue to the results of the path-controlled compaction, the same trend can be derived when testing forced-controlled compaction (Fig. 6). H-X-X shows the poorest resistance to permanent deformation, followed by H-Y-Y (−35 %). H-Z-Z (−50 %) again produces the smallest creep rate. The variation in the results is similar for the H-X-X (SD: 0.038) and H-Y-Y (SD: 0.046) configuration and significantly lower for the H-Z-Z (SD: 0.012) orientation. This is a difference to path-controlled compaction.

Again the bulk density of the specimens is depicted in Fig. 7. Compared to the bulk density of the path-controlled compaction (Fig. 5) the variation of specimens from different slabs is quite smaller. This can be explained by the fact that the force-controlled compaction applies the same amount of compaction work into each slab. As the difference of the bulk density of different slabs is not significant the

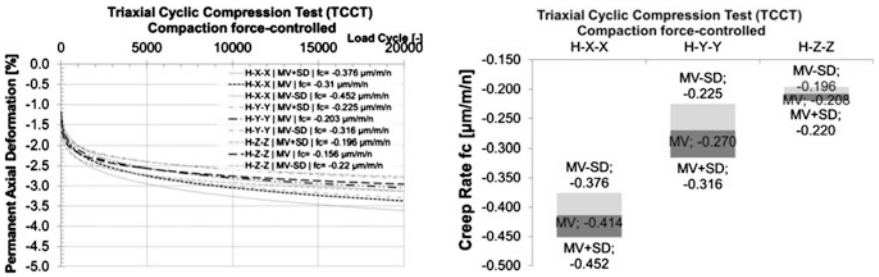


**Fig. 6** TCCT results for force-controlled compaction: creep curve (*left*), and creep rate (*right*)

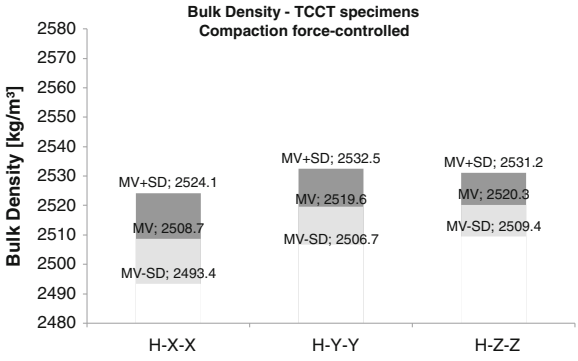


**Fig. 7** Bulk density of force-controlled compacted TCCT specimens

**Table 7** High temperature results—force-controlled compaction

| | H-X-X | | H-Y-Y | | H-Z-Z | | $\Delta_{X\text{-}X/Y\text{-}Y}$ (%) | | $\Delta_{Y\text{-}Y/Z\text{-}Z}$ (%) | | $\Delta_{X\text{-}X/Z\text{-}Z}$ (%) | |
|---|---|---|---|---|---|---|---|---|---|---|---|---|
| | MV | SD | MV | SD | MV | SD | MV | SD | MV | SD | MV | SD |
| $f_c$ (µm/m/n) | −0.414 | 0.038 | −0.270 | 0.046 | −0.208 | 0.012 | −34.8 | 21.1 | −23.0 | −73.9 | −49.8 | −68.4 |

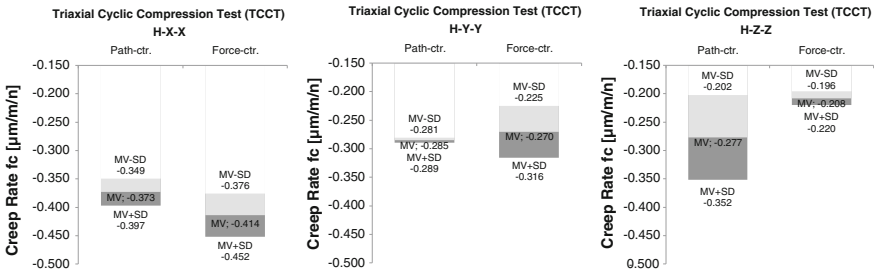


**Fig. 8** TCCT results—path- versus forced-controlled compaction: creep rates

difference of the calculated creep rate seems to be related to the anisotropy of the material due to compaction (Table 7).

### 4.3.3 Path- Versus Force-Controlled Compaction

Figure 8 compares the results of path- and force-controlled compaction. As the mix design of all produced slabs is the same, the difference between path- and force-controlled slabs should be linked to the compaction work applied to each slab. Thus, the specific compaction work for each slab was calculated. The compactor records the compaction force and path for each cycle. By integrating the compaction force (N) over the compaction path (mm) and dividing it first by the length of the compaction path (mm) and then by the height of the compacted slab (mm) a specific compaction work (N mm/mm$^2$) can be derived. This parameter is compared in Fig. 9.

Starting with H-Z-Z a higher compaction work produces a higher resistance to permanent deformation. The force-controlled compacted slab was produced with a 19 % higher compaction work leading to a 25 % lower creep rate.

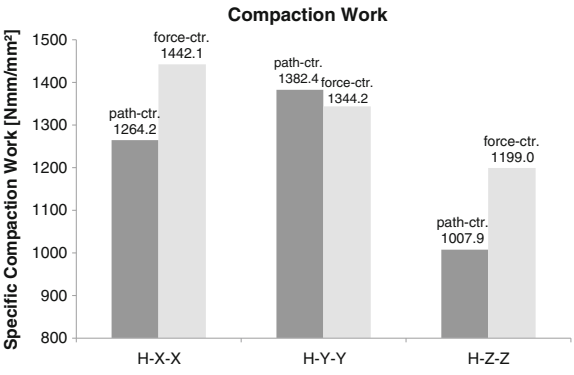


**Fig. 9** Compaction work of HMA-slabs used for TCCT specimens

For the H-X-X a higher compaction work leads to a higher creep rate. For the force-controlled compacted slab a 14 % higher input in compaction work is calculated and yet it shows a poorer resistance to permanent deformation with an 11 % higher creep rate. The H-Y-Y configuration shows only a slight sensitivity to the applied compaction work. The path-controlled compacted slab with a 3 % higher compaction work leads to a 5 % higher creep rate. Specimens tested in direction of the compaction force (Z) with a higher compaction work result in smaller creep rates. For specimens tested in x- and y-direction the situation is vice versa. Taking into account that a higher degree of compaction leads to a situation where more aggregates are oriented in the x-y plane it is assumed that when specimens are tested in x- or y-direction a higher compaction work is counterproductive since more aggregates can slide past each other rather than being resistant to deformation—especially at high temperature when the mastic has lost most of its capacity to transfer load. This thesis is based on limited data and needs to be verified by further testing.

## 5 Conclusions

Specimens were cut and cored out of the slabs in different patterns (i.e. orientation of specimen testing vs. orientation of compaction). For the high temperature performance, the compaction method was varied as well to compare path- and force-controlled compaction. Low temperature and fatigue and stiffness tests were carried out only on path-controlled compacted specimens. Summing up the results the following findings can be given:

- The low-temperature performance is moderately sensitive to the material anisotropy. Specimens tested in the x-direction (orthogonal to compactor path and compaction force) perform better than specimens tested in the y-direction (in direction of compactor path orthogonal to compaction force) with lower cracking temperatures in the TSRST and a higher tensile strength reserve.
- The stiffness and fatigue performance is highly sensitive to the material anisotropy. The tested F-Z-Y orientation reflecting the loading situation on the road was about 23 % stiffer than the F-X-Y direction (at 20 °C and 10 Hz) and resulted in a better fatigue performance (+36 %).
- The high temperature performance was assessed for all three orientations and for path- and force-controlled compaction. For both compaction methods an anisotropic performance was found. In this test part of the difference in performance might be connected to the compaction effort itself. Therefore the bulk density of the tested specimens was compared to the calculated creep rates. Interestingly enough the larger the variation of the bulk density, the larger the scattering in the creep rates is. The different creep rates in the three test directions seem to be connected to anisotropy of the material whereas the variation of the results is linked to the variation of the compaction quality itself. Best

performance was found for specimens tested in direction of the compaction force (Z) which reflects the loading situation on the road followed by y- and x-orientation.

- Comparing the results of path- and force-controlled compaction in terms of the high temperature performance, it seems that the applied compaction work rather than the compaction method is linked to the difference in path- and force-controlled compaction.
  For the z-direction a higher compaction work results in smaller creep rates. For the x- and y-direction a lower compaction work produces smaller creep rates. It is assumed that a higher degree of compaction leads to a situation where more aggregates are oriented in the x-y plane. Thus, when specimens are tested in x- and y-direction a higher compaction work does not lead to a decrease of the resulting creep rate since aggregates would slide past each other rather than being resistant to deformation. This is especially true at high temperatures when the mastic has lost most of its capacity to bear loads. This thesis is based on very limited data and needs to be verified by further testing.

From the results the following conclusions can be drawn:

- When specifying performance indicators of HMA by laboratory testing the specimen preparation and orientation of testing have a crucial influence on the results for the entire temperature range as the performance is sensitive to the material anisotropy due to compaction.
- Specimens in the lab are often cut and cored out of slabs in a way that is most economic and efficient in terms of material use and easy to handle specimen preparation. More care needs to be put on the fact that specimens should be tested in the same orientation as the pavement structure is stressed under traffic and climate loading if the performance indicators produced by sophisticated test procedures should reflect reality in the most reliable way. This is especially true for high-temperature and fatigue and stiffness testing.
- This fact is even more important when the material parameters determined by laboratory testing should be implemented into modelling and simulation (Hofko and Blab 2009). The anisotropic performance must be taken into account to obtain realistic simulation results.
- An influence of the compaction method (path- vs. force-controlled) on the performance indicators at least in the high-temperature range was not found by the study. Differences in results are rather linked to the compaction work applied during compaction of the slabs. A higher compaction work leads to better deformation resistance in the z-direction and a lower resistance in x- and y-direction. The uniformity of the compaction in terms of variation of bulk density of the specimens reflects on the scattering of test results.

## References

Airey, G. D., Collop, A. C. and Zoorob, S., 2005. *The Influence of Laboratory Compaction Methods on the Performance of Asphalt Mixtures.* Final Report, Engineering and Physical Science Research Council.

Brown, S. F. and Gibb, J. M., 1999. *Effects of compaction on mechanical properties of asphalt mixtures.* Proceedings of the 7th Conference on Asphalt Pavement for Southern Africa.

EN 12697-24, 2007. Bituminous mixtures - Test methods for hot mix asphalt - Part 24: Resistance to fatigue.

EN 12697-25, 2006. Bituminous mixtures - Test methods for hot mix asphalt - Part 25: Cyclic compression test.

EN 12697-33, 2007. Bituminous mixtures - Test methods for hot mix asphalt - Part 33: Specimen prepared by roller compactor.

EN 12697-35, 2007. Bituminous mixtures - Test methods for hot mix asphalt - Part 35: Laboratory mixing.

EN 13108-1, 2006. Bituminous mixtures –Material specifications – Part 1: Asphalt Concrete.

FGSV AL Sp-Asphalt 09, 2009. Arbeitsanleitung zur Bestimmung des Steifigkeits- und Ermüdungsverhaltens von Asphalten mit dem Spaltzug-Schwellversuch als Eingangsgröße in die Dimensionierung (in German).

Hofko, B., and Blab, R. 2009. *Performance Based Lab Tests to Predict Pavement Fatigue.* Proceedings of the Fifth International Conference on Construction in the 21st Century, Paper-Nr. 171, Istanbul, Turkey.

Hunter, E. A., Airey, G. D. and Collop, A. C., 2004. *Aggregate Orientation and Segregation in Laboratory-Compacted Asphalt Samples.* Journal of the Transportation Research Board, Volume 1891, pp. 8-15.

Iwama, M., Airey, G. D. and Hunter, A. E., 2007. *Influence of asphalt mixture compaction method and specimen size on internal structure and mechanical properties.* Proceedings of the International Conference on Advanced Characterisation of Pavement and Soil Engineering Materials, Athens, pp. 1063-1073.

Masad, E., Muhunthan, B., Shashidhar, N. and Harman, T., 1999. *Quantifying Laboratory Compaction Effects on the Internal Structure of Asphalt Concrete.* Journal of the Transportation Research Board, Volume 1681, pp. 179-185.

Masad, E., Tashman, L., Somedavan, N. and Dallas L., 2002. *Micromechanics-Based Analysis of Stiffness Anisotropy in Asphalt Mixtures.* Journal of Materials in Civil Engineering, Volume 14, Issue 5, pp. 374-383.

prEN 12697-46, 2009. Bituminous mixtures - Test methods for hot mix asphalt - Part 46: Low Temperature Cracking and Properties by Uniaxial Tension Tests.

Renken, P., 2000. *Influence of Specimen Preparation onto the Mechanical Behaviour of Asphalt Mixtures.* Proceedings of the 2nd Eurasphalt & Eurobitume Congress, Session 1: Performance Testing and Specifications for Binders and Mixtures, pp. 729-735, Barcelona, Spain.

# Reliance of Pavement Texture Characteristics on Mix-Design and Compaction Process

**Giuseppe Cantisani, Antonio D'Andrea, Paola Di Mascio and Giuseppe Loprencipe**

**Abstract** The surface texture in Hot Mix Asphalt (HMA) pavements has an important role respect to all functional performances: wet and dry friction, rolling noise generation, tire wear, and so on. The texture of a new pavement is a consequence of HMA composition (mix-design) and of construction techniques, especially considering the compaction process. While numerous studies have investigated the effect of mix design on texture, it is still unclear the effect of construction techniques. In this research, some experimental results coming from on-site investigations during the HMA construction, were processed, in order to determine the texture characteristics of pavement surfaces, in terms of mega, macro and micro-texture, using both volumetric and profilometric measures. Furthermore, the asphalt mix composition (grain size, void ratio, bulk density, percentage of bitumen, etc.) were assessed on pavement cores. Some statistical correlations between texture and asphalt mix composition were also carried out. The results confirm that the main influence on the pavement texture level is related to the aggregate maximum dimension, but also the void percentage has a significant influence. The compaction conditions, instead, seem to determine a lower effect, but nevertheless some observations can be deducted. More general, the presented

G. Cantisani · A. D'Andrea · P. Di Mascio · G. Loprencipe (✉)
Dipartimento di Ingegneria Civile, Edile e Ambientale, Sapienza Università di Roma, Rome, Italy
e-mail: giuseppe.loprencipe@unroma1.it

G. Cantisani
e-mail: giuseppe.cantisani@unirom1.it

A. D'Andrea
e-mail: antonio.dandrea@uniroma1.it

P. Di Mascio
e-mail: paola.dimascio@uniroma1.it



F. Canestrari and M.N. Partl (eds.), *8th RILEM International Symposium on Testing and Characterization of Sustainable and Innovative Bituminous Materials*, RILEM Bookseries 11, DOI 10.1007/978-94-017-7342-3_22

research proposes some considerations, useful to improve the design of mixtures and the compaction techniques of HMA, especially in order to obtain a reduction of rolling noise generation.

**Keywords** Mix design · Pavement texture · Compaction techniques · Rolling noise

## 1 Background

The safety and efficiency of road exercise are related with pavement surface characteristics. Texture is a geometric property related, in different way, to some conflicting performances of a pavement (Hibbs and Larson 1996; Baran and Henry 1983; D'Andrea et al. 2013); it is important, in fact, to have an high texture level in order to maximize some functions (friction, vehicle control, prevention of aqua-planing) (Flintsch et al. 2012; Hall et al. 2009), whereas considering other requirements (noise, tyres and fuel wearing, comfort), it is better to have a low texture level (Rasmussen et al. 2007).

A synthetic representation of the quali-quantitative effects of texture and unevenness on pavement performances, in terms of good or bad influence on them, also considering the different wavelengths, was proposed by PIARC and can be explained by means of the graph reproduced in Fig. 1.

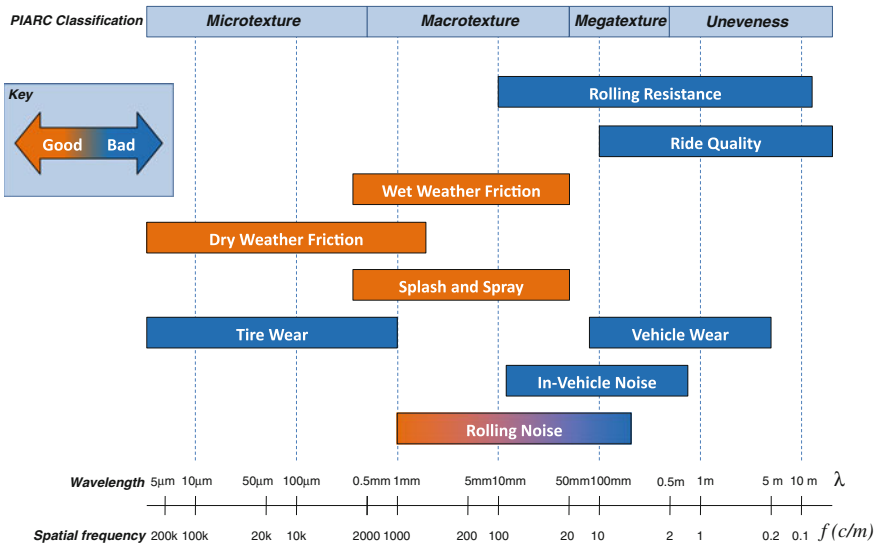


**Fig. 1** Pavement surface characteristic influence (Wambold and Henry 1994)

The texture of a new pavement is a consequence of HMA composition (mix-design) and of construction techniques, especially considering the compaction process (Boscaino et al. 2009).

In the last decades, many researches dealing with road-tyre rolling noise generation were performed. As a result, the best wavelength range of the surface texture of the pavement, needed to reduce the rolling noise, is now well-known (Sandberg and Descornet 1980).

Starting from these results and from other similar researches (Huschek 1996), a three year European research project (TINO) investigated the link between the road-tyre rolling noise total level and a new texture index depending on the pavement unevenness and macro and mega-texture (Domenichini et al. 1999). Moreover, the spectral shape of the texture has been correlated to some asphalt concrete mix characteristics, as the maximum aggregate size $D_{MAX}$ and fractal dimension of the grain grading (D'Andrea et al. 1999).

With the same approach, Atzeni et al. (2008) use a fractal model of the porous microstructure of earth-based materials.

Another interesting study relates the fractal dimension with the skid resistance of concrete pavement (Chen et al. 2013).

The approach with the technique of fractal geometry is not very recent (Canestrari 1993; Chaudhuri and Sarkar 1995; Lina et al. 2000) and it shows some prerogatives compared to traditional methods in the treatment of the texture. It is known that both the texture and the mix design have a strong stochastic component and, for this reason, the fractal approach seems to provide good results for the treatment of these data.

While numerous studies focused on the mix design and its effect on the texture, it is still unclear the role of construction techniques. Recently, various researches have been developed to predict the typical texture properties starting from mix design parameters and construction features (Vaiana et al. 2013).

During the above mentioned TINO research many data were collected, so, after the project end, a retrospective analysis started. This analysis clarified the reasons of the observed variability of the texture spectral shapes in the laboratory samples, even though they were composed with very similar mixtures. In addition, the construction of the prototype could be different from the common methods for roads' construction, because of both the equipment and the accuracy of the controls and, as a result, the texture of the paved surface could be uneven.

Therefore, some years later, another national research project (IASPIS) started, including an extensive test plan on some roads near Rome, where pavement works had been planned. The project studied the influence of construction equipment and their usage techniques on the texture of various pavement stretches, made with the same mix.

The IASPIS results were partially spread to the international research community (VV. AA 1998); then it appears worthwhile to reconsider them with an eye to the new developments coming in recent years.

## 2 Results of Tests on Experimental Roads

To investigate the effect of the construction process on the texture, a test plan was designed and realized considering certain roads under construction in the municipality of Rome.

In particular, the performed test plan had two objectives:

- definition of the relation between compaction level and texture spectral shape of pavements, composed of the same asphalt concrete mixture;
- study of the relation between texture variations and spatial vibration frequency of roadroller.

A total of 32 pavement stretches included in 6 worksites were tested. Table 1 lists the adopted rolling methods for all the surveyed pavements.

Two 20 × 50 cm slabs were taken from each stretch after the material was cold and before opening the road to the traffic. The following measurements were made on each of them:

- Grain grading.
- Bitumen percentage.
- Bulk density of the mixture.

These tests supplied the following data:

- $D_{MAX}$—maximum aggregate size (grain size of 10 % retained).
- %Vr—percentage of air void.
- Fractal dimension of the grain grading, using the method proposed by D'Andrea et al. (1999).

The maximum aggregate size and fractal dimension were similar in each worksite and quite close among the different worksites; instead, the air void contents were very different also among the sample slabs coming from the same worksite. Probably it depends on the worksite organization and the processing phases: roller passage far or close to the paver, asphalt concrete temperature in the machine and on the layer, etc.

The pavement texture was evaluated both with macro-texture traditional tests (sand patch) and with an automated laser profilometer.

The analytical treatment of the profiles, obtained by the Fourier transform (Domenichini et al. 1999; Loprencipe and Cantisani 2013), gives the representation of the pavement texture in the spatial frequency domain, in terms of texture levels in dB respect to the amplitude reference value of $10^{-6}$ mm, or directly in terms of amplitude texture (in μm).

Figure 2 shows the elaborations of the measurements carried out on the worksite n. 5. Similar forms were obtained for the other worksites. The representation of the texture measures is provided in terms of levels in dB for third octave bands of wavelength (from 250 to 0.615 mm), which correspond to the domain of spatial frequencies between 4 and 1625.5 cycles/m.

**Table 1** Adopted rolling methods for all the surveyed pavements

| Worksite stretches | Compaction method | Roller weight (kg) | Speed (m/s) | Vibration frequency (Hz) | Number of passages |
|---|---|---|---|---|---|
| Pav 1_1 | Static | 6530 | 0.8 | – | 1 |
| Pav 1_2 | Dynamic | 6530 | 1.3 | 40 | 1 |
| Pav 2_1 | Static | 6530 | 1.2 | – | 2 |
| Pav 2_2 | Static | 6530 | 1.5 | – | 4 |
| Pav 3_1 | Static | 6530 | 1.3 | – | 2 |
| Pav 3_2 | Static | 6530 | 1.5 | – | 2 |
| Pav 3_3 | Static | 6530 | 1.8 | – | 2 |
| Pav 3_4 | Dynamic | 6530 | 1.2 | 40 | 2 |
| Pav 3_5 | Dynamic | 6530 | 1.7 | 40 | 2 |
| Pav 3_6 | Dynamic | 6530 | 2.4 | 40 | 2 |
| Pav 3_7 | Static | 6530 | 1.2 | – | 2 |
| Pav 3_8 | Static | 6530 | 2.0 | – | 2 |
| Pav 3_9 | Static | 6530 | 2.5 | – | 2 |
| Pav 3_10 | Dynamic | 6530 | 1.5 | 40 | 2 |
| Pav 3_11 | Dynamic | 6530 | 1.8 | 40 | 2 |
| Pav 3_12 | Dynamic | 6530 | 2.7 | 40 | 2 |
| Pav 4_1 | Static | 7500 | 1.4 | – | 2 |
| Pav 4_2 | Static | 7500 | 1.5 | – | 3 |
| Pav 4_3 | Static | 7500 | 1.3 | – | 5 |
| Pav 4_4 | Static | 7500 | 1.7 | – | 5 |
| Pav 4_5 | Static | 7500 | 1.5 | – | 6 |
| Pav 5_1 | Static | 7500 | 1.3 | – | 2 |
| Pav 5_2 | Static | 7500 | 1.5 | – | 2 |
| Pav 5_3 | Static | 7500 | 2.3 | – | 2 |
| Pav 5_4 | Dynamic | 7500 | 1.0 | 40 | 2 |
| Pav 5_5 | Dynamic | 7500 | 2.4 | 40 | 2 |
| Pav 6_1 | Static | 7500 | 3.1 | – | 2 |
| Pav 6_2 | Static | 7500 | 7.2 | – | 2 |
| Pav 6_3 | Static | 7500 | 8.5 | – | 2 |
| Pav 6_4 | Dynamic | 7500 | 3.8 | 40 | 2 |
| Pav 6_5 | Dynamic | 7500 | 5.8 | 40 | 2 |
| Pav 6_6 | Dynamic | 7500 | 7.6 | 40 | 2 |

The values of the final compaction of the layers resulted enough variable, so the project was useful to analyze the influence of the compaction parameter on the surface texture.

The compaction level or the percentage of air void volume in the finished asphalt concrete layer are the indexes that allow to estimate the effectiveness of different

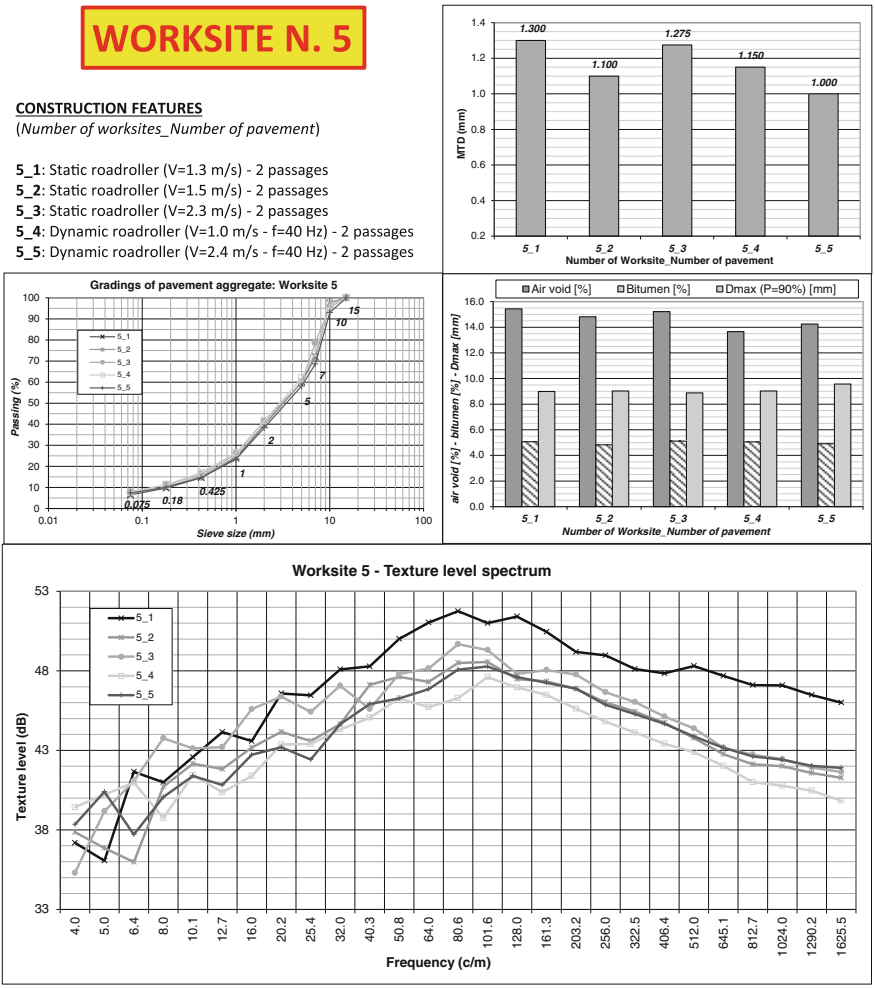


**Fig. 2** Elaboration of the measurements carried out on the worksite n. 5

procedures of compaction. For example, Fig. 3 shows the results found by Domenighetti (1970), varying the vibration frequency of a 8 t tandem roadroller.

Similar results were found by Boscaino et al. (2009) thus demonstrating the importance of construction techniques on the pavement characteristics surface in terms of texture.

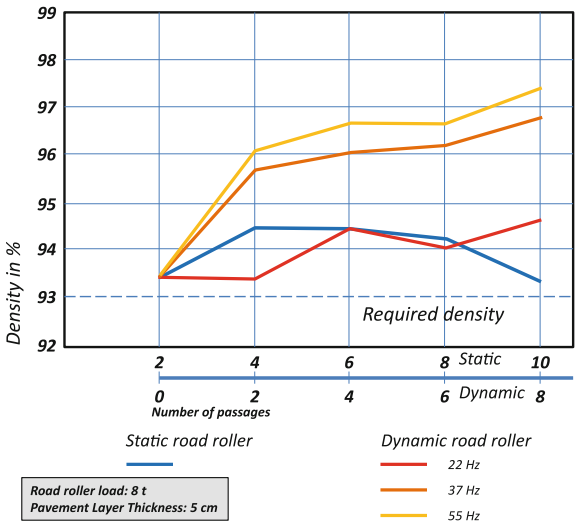


**Fig. 3** HMA density in function of vibration frequency of a 8 t tandem roadroller (Domenighetti 1970)

## 3 The Influence of the Rolling Procedure on Final Bulk Density and Texture

The texture level diagrams (as that in Fig. 2 for the worksite n. 5), coming from the laser profilometer surveys, typically present a very regular shape in the descending part of the curve, corresponding to the range between the maximum value of texture and the highest frequencies (minimum wavelengths). On the contrary, the curve has many picks when the frequencies are lower (corresponding to 2–20 cm wavelength range).

The analyses of data do not provide evidence as regard to a possible influence of the compaction modalities on the mega-texture, while the volume of the residual voids is clearly dependent from the compaction. As a matter of the fact, the results of pavements in the worksite 3, 5 and 6 show that the compaction roller with active vibration produces a layer with a lower average void content respect to the modality with inactive vibration, for a same number of passages. These results regard all the observed worksite (except the n. 6) and the measured decrease was 1–2 % (Fig. 4).

The influence of the dynamic compaction on the Macro Texture Depth (MTD) is much more evident: reductions of 0.1–0.2 mm have been measured (Fig. 5).

Finally, the analysis of the texture spectral shapes demonstrates that the right part of the texture level curves in Fig. 2, representing the shorter wavelengths, has always very homogenous and regular slope and it reaches its maximum at different levels for each compaction procedure, even if the asphalt concrete has the same grading and bitumen content. Figure 6 represents the maximum values of the texture levels versus the mixture air void contents.

Because the primary dependence of the texture maximum level from the maximum grain size $D_{MAX}$ is now certain, data referring to gradings with similar $D_{MAX}$,

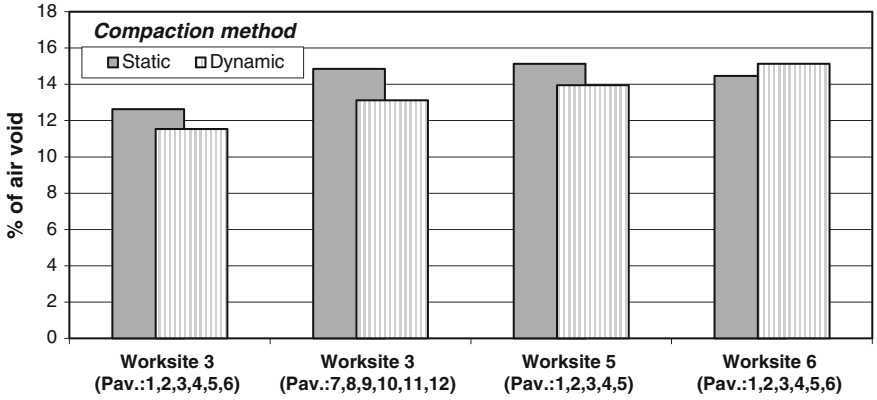


**Fig. 4** Comparison between pavement air void contents resulting from dynamic and static compaction

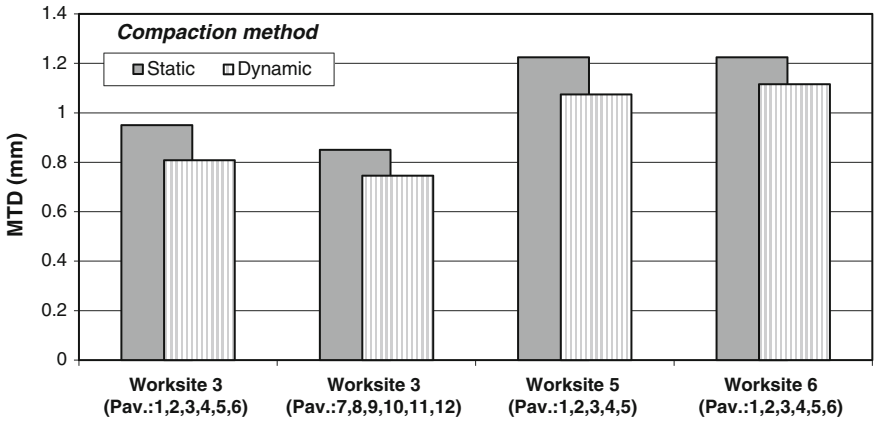


**Fig. 5** Comparison between MTD measured on pavement with dynamic and static compaction

has been associated. This is the case of the asphalt concrete in the worksites 3, 4 and 5 ($D_{MAX}$ = 9 mm), while that one in the worksite 6 has $D_{MAX}$ = 6 mm.

The correlations observed in these grouped data show that there is a secondary dependence of the maximum level of texture from the content of residual voids, with a high degree of statistical confidence.

This result suggests that it is possible to perform a linear multiple regression between the voids content and both maximum grain size and texture. The multiple regression analysis leads to the definition of a new characteristic index of the composition of the wearing course (ICC), defined by Eq. 1:

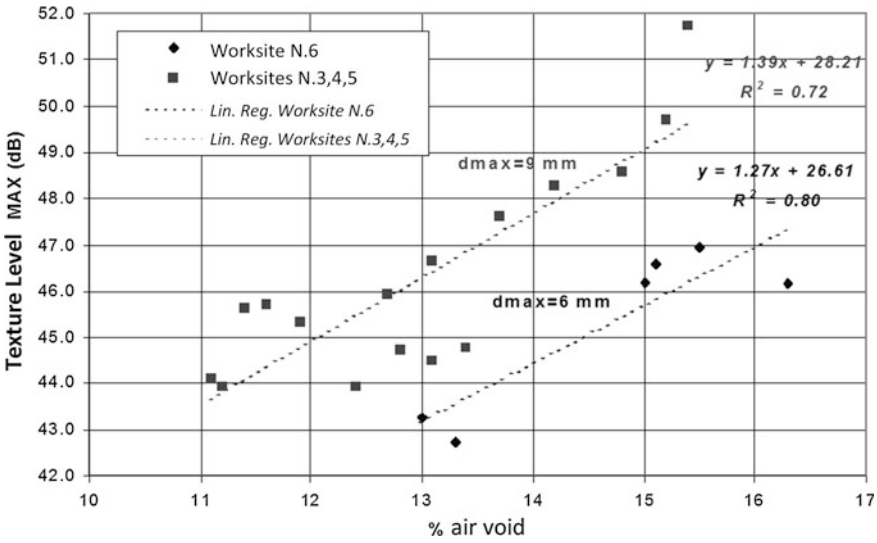


**Fig. 6** Maximum values of the texture levels versus mixture air void contents

$$ICC = 1.4 \cdot \%Vr + 0.9 \cdot D_{MAX} \quad (1)$$

This index is well correlated with both the maximum level of texture ($TL_{MAX}$) and the texture level of the wavelength equal to 10 cm ($TL_{10}$) with a $R^2 > 0.8$ in both cases. The latter correlation suggests also a strong dependence of the mega texture by the characteristics of the final compaction. These regressions are shown in an unique diagram in Fig. 7.

In this regard, D'Andrea et al. (1999) already demonstrated that the rolling noise is dependent on both the maximum texture level, expressed by the texture index, and the texture levels, in dB, corresponding to wavelengths of 10 cm approximatively.

Therefore, the present study confirms that the maximum grain size is essential to reduce the rolling noise on the wearing course but, in addition, it is also necessary to limit the asphalt concrete void content by mean of a good compaction during the laying.

Indeed, the insufficient compaction of low-noise rolling surface such as close asphalt concrete could considerably worsen the surface acoustic characteristics, in addition to the known reduction in resistance and impermeability.

Two pavements characterized by the same maximum grain size can have different ICC, due to different compaction and consequently different air void contents. The pavement with the higher ICC will be noisier than the other. In fact, the rolling traffic noise is directly related to the texture level. An efficient rolling noise reduction needs the control both of air voids and maximum grain size. The ICC index assigns the relative weights to these two factors.

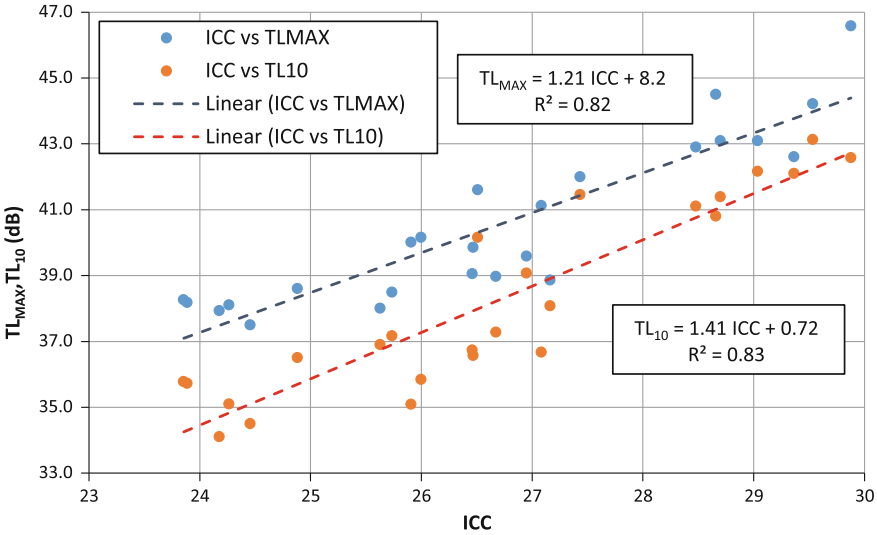


**Fig. 7** Regression between index of the composition of the wearing course and texture levels

## 4 Conclusion

The analysis of the spectral shape of road surfaces, in the whole domain of macro and mega texture, is an effective methodology for understanding the relationship between texture and rolling noise. This knowledge could be useful to improve the technological progress of the asphalt concrete composition, with the aim to set the parameters that mainly affect the texture of the finished layer.

Already previous researches showed that the maximum grain size is one of this parameter. It affects the texture wavelength corresponding to the maximum of the diagram of texture levels.

In addition, the fractal dimension of the grain size grading is related to the slope of the descending part of the texture level diagram, in the area of the shorter wavelengths.

This study has investigated the influence of compaction process on texture, by means of the elaboration of data coming from in situ tests, referred to pavements that have a very similar composition.

All the experimental results are quite uniquely interpretable and they prove that a higher void content does not change the shape of the curve of texture levels, but shifts it upwards. This means a worsening of the acoustic qualities of the wearing course, because the attitude to generate rolling noise increases. Also the insufficient compaction of the HMA layers could worsen the acoustic properties, in addition to the well-known reduction in resistance and impermeability.

The presented considerations can be useful to improve the design of mixtures and compaction techniques of HMA.

## References

Atzeni C, Pia G, Sanna U, Spanu N (2008) A fractal model of the porous microstructure of earth-based materials. Construction and Building Materials, 22(8), 1607-1613.

Baran R, Henry J (1983) Tire Noise and Its Relation to Pavement Friction. Transportation Research Record, No. 946, 00389581(HS-037 873), pp. 44-48.

Boscaino G, Celauro B, Celauro C, Amadore A (2009) Evaluation of the laboratory prediction of surface properties of bituminous mixtures. Construction and Building Materials, 23(2), 943-952.

Canestrari F (1993). La dimensione frattale applicata allo studio della rugosità superficiale nelle pavimentazioni stradali, Le Strade n. 1296, (in Italian).

Chaudhuri BA, Sarkar N (1995) Texture segmentation using fractal dimension. Pattern Analysis and Machine Intelligence, IEEE Transactions on, 17(1), 72-77.

Chen, Y, Wang, KJ., Zhou WF., (2013) Evaluation of surface textures and skid resistance of pervious concrete pavement Journal of Central South University, Central South University, 2013, 20, 520-527. doi: 10.1007/s11771-013-1514-y.

D'Andrea A, Di Mascio P, Domenichini L, Ranzo A (1999) TINO Prototype of a low noise asphalt. Roma, Italy, TINO First International Colloquium on Vehicle Tyre Road Interaction.

D'Andrea A, Tozzo C, Boschetto A, Bottini L (2013) Interface roughness parameters and shear strength. Modern Applied Science, 7(10), p1.

Domenichini L, Fracassa A, La Torre F, Loprencipe G, Ranzo A, Scalamandrè A (1999) Relationship between road surface characteristics and noise emission. Roma, Italy, TINO First International Colloquium on Vehicle Tyre Road Interaction.

Domenighetti D (1970) Tecnologia elementare dell'addensamento – Collana Opus Volume 1 – Seconda edizione.

Flintsch G, McGhee K, de León Izeppi E, Najafi S (2012) The Little Book of Tire Pavement Friction.

Hall JW, Smith KL, Titus-Glover L, Wambold JC, Yager TJ, Rado Z (2009) Guide for Pavement Friction, Washington D.C. USA.: National Cooperative Highway Research Program. http://onlinepubs.trb.org/onlinepubs/nchrp/nchrp_w108.pdf.

Hibbs B, Larson R (1996) Tire Pavement Noise and Safety Performance, Washington D.C., USA.: FHWA, U.S. Department of Transportation.

Huschek S (1996) Characterization of pavement surface texture and its influence on tire/road noise. Christchurch, New Zealand, s.n.

Lina A, Cohen P, Herve JY (2000) Pavement Roughness Estimation Using Path Tortuosity and 2-D Lacunarity Measure. 350-356.

Loprencipe G, Cantisani G (2013) Unified analysis of road pavement profiles for evaluation of surface characteristics. Modern Applied Science, 7(8), 1-14.

Rasmussen R, Bernhard R, Sandberg U, Mun E (2007) The Little Book of Quieter Pavements, Washington D.C., USA: USDOT, Federal Highway Administration.

Sandberg U, Descornet G (1980) Road Surface Influence on Tire/Road Noise- Part I. Miami, Florida, s.n., pp. 259-266.

Vaiana R, Praticò FG, Iuele T, Gallelli V, Minani V (2013) Effect of Asphalt Mix Properties on Surface Texture:an Experimental Study. Applied Mechanics and Materials 368-370:1056–1060. doi: 10.4028/www.scientific.net/AMM.368-370.1056.

VV. AA. (1998) IASPIS. Interazione ambiente-sicurezza nel progetto delle infrastrutture stradali. Final Report of MURST 1998 Project. ISBN: 88-8250-020-9. Pisa (Italy). (in Italian).

Wambold JC, Henry JJ (1994) International PIARC experiment to compare and harmonize texture and skid resistance measurement. Nordic Road and Transport Research.

# Coloured Asphalt Pavements: Mix Design and Laboratory Performance Testing

**Nathalie Piérard, Joëlle De Visscher, Stefan Vansteenkiste and Ann Vanelstraete**

**Abstract** Coloured asphalt pavements are increasingly used in large public areas and at dangerous intersections such as crossroads, roundabouts or pedestrian crossings. In the former application, the role of the coloured pavement is often to give the space a particular aesthetic character or to integrate it well in its surroundings; in the latter, its major role is to enhance the safety of users by improving visibility and road legibility. However, coloured pavements are also subjected to traffic and climate-induced stresses and must, therefore, exhibit a similar mechanical performance as their uncoloured counterparts. Desired colours are obtained by using specific materials such as coloured aggregates, pigments and clear binders. However, the application of latter constituents may affect the performance and durability of coloured asphalt mixtures. Therefore, in a first step, BRRC (Belgian Road Research Centre) determined the characteristics of these particular materials such as the rheological behaviour of clear binders both at high and low temperatures and the stiffening effect of pigments acting as filler. Subsequently, the impact of the material characteristics on volumetric mix design was investigated. In a next phase their effect on the mechanical performance of coloured mixtures was studied in the laboratory. The latter performance was evaluated by testing for water sensitivity, rutting resistance and low-temperature cracking. This contribution summarizes the major findings from the study.

**Keywords** Coloured asphalt · Mix design · Performance testing · Synthetic binder

N. Piérard (✉) · J. De Visscher · S. Vansteenkiste · A. Vanelstraete
Belgian Road Research Centre (BRRC), Woluwedal 42, 1200 Brussels, Belgium
e-mail: n.pierard@brrc.be



F. Canestrari and M.N. Partl (eds.), *8th RILEM International Symposium on Testing and Characterization of Sustainable and Innovative Bituminous Materials*, RILEM Bookseries 11, DOI 10.1007/978-94-017-7342-3_23

## 1 Introduction

Coloured asphalt mixtures are used more and more often in several road paving applications, especially in urban areas. At first, coloured asphalt mixtures were predominantly applied for cycling-tracks, but more recently coloured asphalt pavements partially replace conventional black pavements, in particular at dangerous intersections such as crossroads, roundabouts or pedestrian crossings. In latter cases, their primary role is to increase safety for the road users by enhancing visibility and legibility of the road. Recently, the application of clear pavements in tunnels in Italy, with the aim to reduce to power consumption for electric light and to improve safety conditions, have reported (Bocci and Bocci 2014). In some cases, coloured asphalt pavements also contribute to the aesthetic character of surroundings and therefore enhance liveability of public areas (St-Jacques and Brosseaud 2006; Brailly and Rennesson 1995). Consequently, coloured asphalt mixtures are increasingly subjected to traffic beside climate-induced stresses. Therefore, it is obvious that their mechanical performance plays a major role in guaranteeing their durability.

In order to obtain coloured asphalt pavements of a desired colour of optimal quality, one makes use of special constituents, such as coloured aggregates, pigments and clear or pigmentable binders (Sicard et al. 2007). Although little experience is currently available, it is generally accepted that the use of such specific components does affect significantly the performance of coloured asphalt mixtures. The lack of knowledge in this area is further substantiated by field observations of premature failures including ravelling or cracking. Therefore, issues directly related to durability such as: rheological as well as ageing behaviour of clear binders, the resistance of coloured pavements to temperature variations are of major importance (Pouget and Loup 2013).

To provide an answer to the above described needs and other topics such as the objective determination of colour and the durability of colour, BRRC (Belgian Road Research Centre) conducted a four year research project. In this paper, the major findings related to the mechanical performance and mix design are reported. Other important issues such as the objective determination of the colour or its durability are discussed at length elsewhere (Denolf et al. 2012; Destrée et al. 2015).

## 2 Characterization of Binders

In order to achieve asphalt pavements with an optimal colour effect, one has to make use of pigmentable or clear binders to replace the regular black bitumen. Clear binders may be categorized according to their origin in three families: pigmentable bituminous binders, clear synthetic binders (which may be polymer modified) and vegetal or bio-binders (Merusi and Giuliani 2012). In this study, both empirical as well as performance related characteristics of a series of clear binders were determined.

## 2.1 Empirical Characteristics

In a first step, the conventional empirical properties such as the needle penetration (EN1426) and softening point R&B (EN 1427) of a series of clear binders (B–F) were measured. A paving grade bitumen 50/70 was included as reference (A). The results are summarized in Table 1.

The following conclusions follow from this table:

- The clear binder of vegetal origin B is characterized by an extremely elevated penetration value and a low softening point.
- The polymer modified synthetic binder E is showing a remarkable high softening point which differs substantially from polymer modified binder F although penetration values are similar.
- Values observed for all other clear binders are comparable with a conventional paving grade bitumen 50/70 or 70/100.

## 2.2 Rheological Properties

In second step, the rheological behaviour of binders A–F at both high as well as low temperature was evaluated. Latter properties are related to the performance of the asphalt mixtures. In particular, the complex shear modulus G*, i.e. its norm |G*| and phase angle δ of binders were measured as a function of temperature (10–70 °C) and frequency (0.1 up to 10 Hz) while using Dynamic Shear Rheometer (DSR) according to EN 14770. Moreover, the flexural creep stiffness (critical temperatures at S (60 s) = 300 MPa and m = 0.300) was determined while using Bending Beam Rheometer (BBR) according to EN 14771.

Table 2 shows G* and δ values obtained by DSR measurements at 50 °C and 1.6 Hz and of critical BBR temperatures. Latter results are indicative for the rheological behaviour at high and low temperature and can be linked to the resistance to rutting or cracking of the corresponding asphalt mixtures (see Sect. 4.2 and 4.3) (Nicholls 2006).

The following conclusions can be drawn:

**Table 1** Overview of the empirical characteristics of clear binders

| Binder | Nature binder | Pen. (0.1 mm) | R&B (°C) |
|---|---|---|---|
| A | Paving grade bitumen 50/70 (reference) | 52 | 51.6 |
| B | Vegetal origin (bio-binder) | 148 | 42.2 |
| C | Pigmentable bituminous binder | 53 | 51.0 |
| D | Synthetic | 69 | 44.8 |
| E | Synthetic—polymer modified | 54 | 71.8 |
| F | Synthetic—polymer modified | 54 | 55.8 |

**Table 2** Overview of G* and δ values (@50 °C and 1.6 Hz) and of critical temperatures at S(60 s) = 300 MPa and m = 0.300 of clear binders

| Binder | G* (kPa) | δ (°) | T (°C) S(60 s) = 300 MPa | T(°C) m = 0.300 |
|---|---|---|---|---|
| A | 13.0 ± 1.5 | 81.9 ± 0.2 | −16.6 ± 0.2 | −20.2 ± 0.2 |
| B | 5.6 ± 3.1 | 79.6 ± 0.3 | −18.0 ± 0.5 | −22.7 ± 0.1 |
| C | 8.1 ± 0.4 | 88.1 ± 0.2 | −12.9 ± 0.1 | −16.3 ± 0.1 |
| D | 3.0 ± 0.2 | 88.5 ± 0.2 | −18.0 ± 0.2 | −21.3 ± 0.3 |
| E | 13.7 ± 1.2 | 62.2 ± 1.9 | −18.1 ± 0.1 | −21.0 ± 0.4 |
| F | 6.5 ± 0.3 | 67.5 ± 0.2 | −18.1 ± 0.1 | −20.3 ± 0.2 |

- All clear binders are characterized by a lower G* value as compared to the reference paving grade bitumen 50/70 except for polymer modified binder E. Latter phenomenon is consistent with the empirical properties (Table 1).
- The G* value of binder D can be considered as low and is similar to values of vegetal binders. This value is in line with both the elevated penetration value (69 dmm) as well as the low R&B temperature (44.8 °C).
- A large variability was observed with respect to phase angle δ. Both pigmentable bituminous binders C as well as unmodified synthetic binder D are characterized by high δ-value correlated to a predominant viscous behaviour as compared to paving grade bitumen. The δ-value of vegetal binder B although is similar to a paving grade bitumen. Both binders E and F show smaller δ-values correlated to a more elastic behaviour. The results are in line with conventional PmB's.
- All clear binders are characterized by critical temperatures comparable with the reference bitumen except for the pigmentable bituminous binder C. Latter binder shows a much higher critical temperature and is therefore to be considered as more susceptible to low temperature cracking.

## *2.3 Resistance to Oxidative Ageing*

In a last step, the oxidative ageing behaviour of clear binders was probed for. Therefore, binders were conditioned in order to simulate short-term ageing (STA) and long-term ageing (LTA). The Rotating Cylinder Ageing Test (RCAT) device was used both to simulate the short-term ageing according to EN 15323 Annex A (RCAT163) as well as the long-term ageing according to EN 15323 (RCAT90). In order to determine the impact of ageing, empirical characteristics (pen and R&B) and rheological characteristics (G* and δ) were determined before and after each stage of binder conditioning. The empirical characteristics are given in Table 3.

**Table 3** Impact of short-term and long-term ageing while using RCAT device on the empirical characteristics of clear binders

| Binder | Ageing regime | Δ pen (0.1 mm) | Δ TR&B (°C) | Retained pen (%) |
|---|---|---|---|---|
| C | STA | −13 | 2.6 | 78 |
| | STA + LTA | −35 | 8.8 | 42 |
| D | STA | −6 | 1.4 | 92 |
| | STA + LTA | −17 | 1.0 | 76 |
| E | STA | −3 | 1.2 | 94 |
| | STA + LTA | −8 | −6.8 | 84 |
| F | STA | −10 | −1.2 | 82 |
| | STA + LTA | −14 | −0.6 | 75 |

Clear binders do not necessarily behave in the same way as paving grade bitumen in which case generally a decrease in penetration and in phase angle, and an increase in stiffness modulus and softening temperature are observed:

- Pigmentable bituminous binder C behaves like paving grade bitumen, but its short-term ageing is milder. However its long-term ageing profile is similar. Typical values for retained penetration of a paving grade binder 50/70 are of the order of 71 % (STA) and 39 % (STA +LTA) (Verhasselt 2003).
- Clear synthetic binders (D, E and F) behave differently. Whether polymer modified (binder E and F) or not (binder D), their empirical characteristics are little affected by oxidative ageing. The combined impact of short and long-term ageing remains smaller than that of short-term ageing observed for paving grade bitumen.
- The rheological measurements (however not discussed in detail here) confirm these findings. An example is shown for the synthetic binder F in Fig. 1. The changes in G*-values after short- and long-term ageing are 60 % at maximum, whereas typical values for bituminous binders are of the order of 400–600 %. Latter figure also shows that the impact of ageing on stiffness can vary largely depending on temperature. Such effects can be related to the particular chemical structure of these binders. They can be very product dependent and are not the objective of this paper.

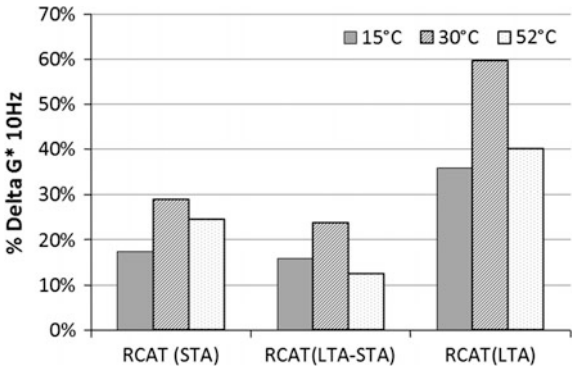


**Fig. 1** Impact of short- and long-term ageing on G* values (binder F)

# 3 Impact of Specific Materials on Volumetric Mix Design

## *3.1 Stiffening Power of Pigments*

Special attention shall be paid to the role of pigments and the impact on mix design. A pigment is added for colour, but it is also an additional component that affects the composition of the mixture and consequently its mechanical properties.

Table 4 shows the characteristics of three types of pigment. Grading, density and Rigden voids are needed as input parameters for volumetric mix design with the BRRC software PradoWin (Francken et al. 2003). Because of their grading, pigments are considered as part of the fine aggregate. This implies that pigments affect the mastic properties. The stiffness of the mastic has a substantial impact on various mix properties: the mastic has to be sufficiently stiff to provide a high resistance to permanent deformation, but if the mastic is too stiff, the workability of the mixture may suffer from it.

To investigate the stiffening effect of pigments when mixed with the binder, the delta R&B according to EN 13179-1was measured. This test determines the increase in softening point of a mixture of binder and filler aggregate with respect to the softening point of the neat binder, as a measure for the stiffening power of the filler aggregate. However, mixing the pigments with the binder in the proportion specified in the standard (37.5/62.5 v/v) was found to be unfeasible: the stiffening effect was so strong that it was impossible to obtain mastic of appropriate consistence. The test was, therefore, carried out with a mixture of only 10 volume parts of pigment. It is noted that the test procedure deviated from the standard not only by the ratio filler to binder but also by use of binder E instead of a bitumen 70/100. Table 4 shows the test results for the three pigments, compared to limestone filler. Considering the low pigment to binder ratio, it is clear that the stiffening power of the pigments is very important compared to the limestone filler. As observed in Table 4, this correlates very well with the high percentage of Rigden voids. Latter observation is in good agreement with literature data (Vansteenkiste and Vanelstraete 2008; Grabowski et al. 2009).

**Table 4** Characteristics of pigments with an impact on mix design

| Pigment | Passing 125 µm (w-%) | Passing 63 µm (w-%) | Density ($g/cm^3$) | Rigden voids (%) | $v_f/v_b$ (*) | ΔR&B (°C) |
|---|---|---|---|---|---|---|
| Yellow (α-FeOOH) | 100 | 100 | 4.09 | 78 | 10/90 | 13.8 |
| Red ($\alpha$-$Fe_2O_3$) | 100 | 100 | 5.16 | 62 | 10/90 | 10.1 |
| White ($TiO_2$ rutile) | 100 | 100 | 4.30 | 52 | 10/90 | 8.2 |
| Limestone filler | 100 | 93 | 2.74 | 35 | 35/65 | 13.6 |

(*) $v_f/v_b$: filler to binder volumetric ratio

### 3.2 Mix Design

Because of their high stiffening power, pigments cannot be added to an asphalt mixture without decreasing the quantity of filler aggregate. Decreasing the volume of filler aggregate by the same amount as the volume of pigment, so that the total volume of fine aggregate remains the same, is not a good option. Because of the high difference in stiffening effect between pigments and common filler, this would lead to a considerable increase in stiffness. An alternative approach is to decrease the mass of filler aggregate by the same amount as the mass of added pigment. As the density of pigments is high compared to the density of filler aggregate (see Table 4), this leads to a reduction of the total volume of fine aggregates, which may partly compensate for the stiffening effect of pigments. This approach of replacing by mass a part of the filler by pigment was further used in this project. The performance tests on the mixtures show that this approach leads to coloured mixtures with similar performance than their black counterparts.

The design of coloured asphalt mixtures which were used in this study was derived from a known formula of a conventional black AC6.3 mixture. Asphalt concrete with a small maximum aggregate size is a very common choice for coloured asphalt due to the fine texture, which enhances both colour as well as workability. Workability allows easier paving and results in a more homogeneous surface, even in confined spaces requiring a lot of manual work.

In the formula of the black asphalt mixture, the conventional bitumen was replaced by a clear binder and the filler aggregate was replaced by white limestone filler. If needed, also coarse and sand aggregates were replaced by coloured aggregates. Knowing the density and grading of the aggregates, the proportions were tuned to maintain the same volumetric composition as the black reference mixture. Finally, pigments were added while decreasing the limestone filler (6.5 m-% of dry mixture) by the same amount of mass. Following this procedure, two coloured mixtures were designed: a yellow mixture using the same type of aggregate (grey porphyry) as the reference mixture, and a red mixture using red porphyry. Table 5 shows the resulting grading of both mixtures compared to the black reference. The variations on the small size sieves are due to the pigments replacing part of the limestone filler (Table 6). The fraction passing the 63 µm sieve increases slightly in mass since 100 % of the pigment passes this sieve. In terms of volume, however, there is a decrease, as intended to limit mastic stiffness. The small variations in volumetric grading have no significant impact on the volumetric composition and voids content as shown by gyratory compaction tests. Only yellow variants and the black reference mixture were selected for the subsequent performance testing (see Sect. 4).

**Table 5** Grading of black (reference) and coloured asphalt mixtures (numbers expressed as v-% or w-% passing a given sieve

| Sieve size (mm) | | 10 | 6.3 | 4 | 2 | 0.5 | 0.25 | 0.063 |
|---|---|---|---|---|---|---|---|---|
| Black (reference) | v-% | 100 | 98 | 72.5 | 43.4 | 27.6 | 22.9 | 7.1 |
| | w-% | 100 | 98 | 72.5 | 43.3 | 27.7 | 23 | 7.3 |
| Yellow | v-% | 100 | 98 | 72.3 | 42.9 | 26.9 | 22.2 | 6.5 |
| | w-% | 100 | 98 | 72.5 | 43.3 | 27.6 | 23 | 7.5 |
| Red | v-% | 100 | 97 | 72.9 | 42.8 | 27.1 | 21.6 | 6.8 |
| | w-% | 100 | 97 | 73.2 | 43.4 | 27.7 | 22.2 | 7.5 |

# 4 Mechanical Performances of Coloured Asphalt Mixtures

In this part of the study the durability of coloured asphalt mixtures was evaluated by applying a series of performance related asphalt tests. The obtained test results were compared to standard specifications valid for an uncoloured counterpart. In particular, the performance of a series of yellow asphalt mixtures while varying the nature of the clear binder (see Sect. 3, Table 5) was investigated.

## *4.1 Water Sensitivity*

The water sensitivity was determined according to EN 12697-12 method A in combination with EN 12697-23. The measurement of the indirect tensile strength (ITS), before and after water conditioning at 40 °C during 3 days, was carried out at 15 °C. Test specimens were prepared by gyratory shear compaction according to EN 12697-31 (# 25 gyr). Air void content of test samples was determined by hydrostatic weighing according to EN 12697-6 part B. Table 7 shows the performance of the black type AC6.3 reference mixture with a paving grade binder 50/70, compared to the yellow mixture designed in Sect. 3.2. Moreover, latter yellow mixture was also prepared with various types of clear binders in order to investigate its impact on water sensitivity.

From the results summarized in Table 6, the following conclusions were drawn:

**Table 6** Composition of the added filler and pigments for coloured AC6.3 variants expressed as w-% of dry AC6.3 mixture

| AC6.3 variant | Limestone filler (w-%) | White pigment (w-%) | Red pigment (w-%) | Yellow pigment (w-%) |
|---|---|---|---|---|
| Yellow | 4 | 2 | – | 0.5 |
| Red | 3.5 | – | 1.5 | – |

**Table 7** Results of the water sensitivity tests—impact of binder

| Yellow AC6.3 variant | Before conditioning | | After conditioning | | |
|---|---|---|---|---|---|
| | ITS (MPa) | Voids (%) | ITS (MPa) | Voids (%) | ITS-ratio (%) |
| Binder A (reference) | 1.55 ± 0.04 | 7.7 ± 0.2 | 1.56 ± 0.08 | 7.6 ± 1.0 | 101 ± 3 |
| Binder B | 2.10 ± 0.09 | 7.5 ± 0.8 | 1.57 ± 0.07 | 7.3 ± 0.3 | 74 ± 3 |
| Binder C | 1.98 ± 0.28 | 8.7 ± 1.1 | 1.38 ± 0.14 | 8.5 ± 0.6 | 70 ± 7 |
| Binder D | 1.30 ± 0.01 | 7.7 ± 0.6 | 1.28 ± 0.03 | 7.6 ± 0.5 | 98 ± 1 |
| Binder E | 1.39 ± 0.02 | 7.3 ± 0.3 | 1.31 ± 0.03 | 7.1 ± 0.2 | 94 ± 1 |

- The reference mixture is characterized by the highest ITSR-value (101 ± 3 %).
- Coloured AC6.3 variants containing a synthetic clear binder (polymer modified or not) are performing significantly better as compared to mixtures containing either binder B (vegetal origin) or binder C (pigmentable bituminous binder).
- All AC6.3 variants satisfied the tender specifications prevailing in Belgium at the time of testing (ITSR-ratio ≥ 70 %). However, the future specifications will become more severe (ITSR-ratio ≥ 80 %) which means that the mixtures with binder B and binder C will not meet the future specifications.

## 4.2 Resistance to Rutting

Resistance to rutting was measured by the wheel tracking test using a large size device according to EN 12697-22. All tests were performed at 50 °C, the standard temperature for rutting tests in Belgium. Figure 2 shows the performance of the black AC6.3 reference mixture with a paving grade binder 50/70, compared to a series of yellow mixtures designed in Sect. 3.2. As can be seen from Fig. 2, coloured asphalt mixtures may perform better or worse as compared to a black asphalt mixture with a similar volumetric composition, depending on the type of clear binder used.

Figure 3 shows that the G*/sinδ ratio of the binder, measured at 0.1 Hz and 50 °C, is a fairly good indicator for rutting resistance (De Visscher et al. 2006).

## 4.3 Low Temperature Behaviour

The low temperature behaviour of a series of coloured asphalt mixtures was measured by the Thermal Stress Restrained Specimen Test (TSRST) according to EN12697-46. Test specimens were conditioned at 10 °C for 2 h before applying a cooling gradient of −10 °C/h. An overview of the test results in terms of failure temperature $T_{failure}$ (°C) and failure stress $\sigma_{cry,failure}$ (MPa) is given in Table 8.

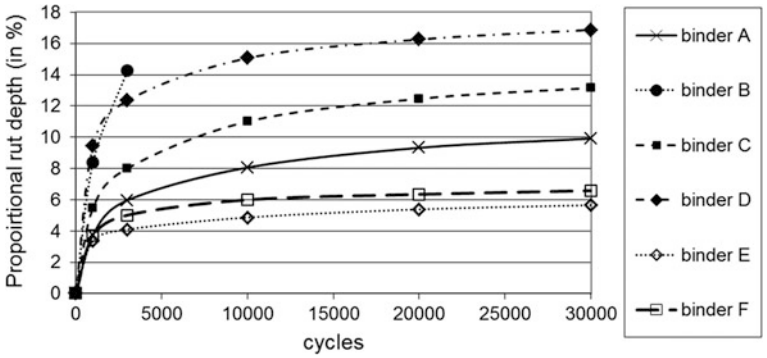


**Fig. 2** Overview of the wheel tracking test for a series of coloured AC6.3 mixtures

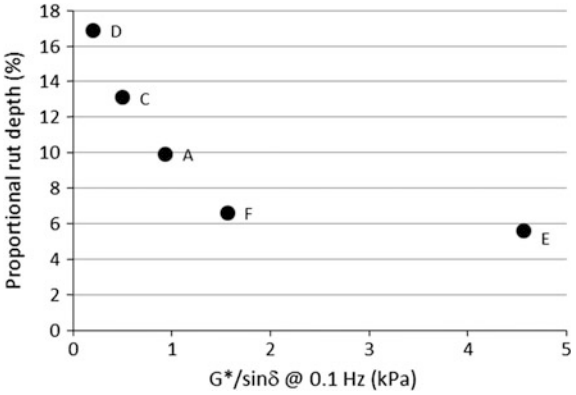


**Fig. 3** Relationship between G*/sinδ (kPa) at 0.1 Hz and 50 °C and proportional rut depth (%) at 30,000 cycles of a series of coloured AC6.3 mixtures (binders A–F)

**Table 8** Overview of low temperature characteristics of coloured asphalt mixtures

| Yellow AC6.3 variant | $T_{failure}$ (°C) | | $\sigma_{cry,failure}$ (MPa) | |
|---|---|---|---|---|
| | Mean | STD | Mean | STD |
| Binder A (reference) | −27.7 | 0.7 | 4.9 | 0.4 |
| Binder B | −25.7 | 0.5 | 4.7 | 0.2 |
| Binder C | −22.8 | 1.3 | 4.7 | 0.2 |
| Binder D | −25.5 | 1.0 | 4.5 | 0.5 |
| Binder E | −25.7 | 0.6 | 4.9 | 0.5 |
| Binder F | −27.6 | 0.6 | 6.5 | 0.6 |

No significant differences with respect to the reference mixture were observed for all AC6.3 coloured asphalt mixtures tested, except for the variant containing pigmentable bituminous binder C. In latter case, the failure temperature $T_{failure}$ is reduced by approximately 20 % in comparison with the reference. The brittleness of this variant can be explained by the higher critical temperatures at S(60 s) = 300 MPa and m = 0.300 of binder C, respectively −12.9 and −16.3 °C (see Table 2) as measured during BBR-testing.

## 5 Conclusions

In this study, European empirical as well as performance related test methods were applied to clear binders and coloured asphalt mixtures.

The impact of special materials on the mix design of coloured asphalt mixtures was demonstrated. In particular, the very elevated stiffening power of pigments affecting mastic stiffness was clearly of major importance and has to be taken into account during the mix formulation phase. Furthermore, the influence of the binder nature on asphalt mixture performance was shown through a series of performance related tests. Performance at both low as well as high temperature could be linked to rheological properties of clear binders.

Finally, results obtained in this study revealed that by an appropriate choice of special constituents and optimising the volumetric mix design, durable coloured AC6.3 mixtures characterized by equivalent mechanical performance as compared to uncoloured counterparts are achievable.

**Acknowledgements** We gratefully acknowledge the Belgian Bureau for Standardization (NBN) for financial support (convention CC-CCN PN/NBN-707-757-907) as well as the cooperation received from quarry operators, road administrations and the manufacturers/suppliers of binders, pigments. Finally, authors also like to thank the technical staff at BRRC.

## References

Bocci E and Bocci M (2014) Clear asphalt concrete for energy saving in road tunnels. Proceedings of the 12th International Conference on Asphalt Pavements (ISAP), Vol 2: 1817-1825, Raleigh 2014.

Brailly MC, Rennesson C (1995) Coloration des revêtements routiers et sécurité routière. RGRA N° 733: 47-49.

Denolf K, Piérard N, Vanelstraete A (2012) Development of an objective test method to determine the colour of coloured asphalts. Paper presented at 5th Eurasphalt & Eurobitume Congress, Istanbul, Turkey, 13-15th June 2012.

Destrée A., N.Piérard and A.Vanelstraete (2015) Development of a test method to determine the color durability of colored bituminous mixtures, submitted for EAPA 2015-conference, Stockholm, June 2015.

De Visscher J, Soenen H, Tanghe T, Vanelstraete A and Redelius P (2006) Binder performance indicators for rutting: evaluation of the experimental correlation with asphalt tests. Paper presented at the 10th International Conference on Asphalt Pavements (ISAP 2006), Québec, August 12 to 17, 2006.

Francken L, Vanelstraete A, Léonard D, Pilate O (2003) New developments in the PRADO volumetric mix design, Paper presented at 6th International RILEM Symposium on Performance testing and evaluation of bituminous materials PTEBM'03, Zurich 2003.

Grabowski W, Wilonowicz J, Sobol T (2009) Structural and functional properties of fillers modified with hydrated lime. Paper presented at MAIREPAV6, Torino, July 2009.

Merusi F and Giuliani F (2012) Chromatic and rheological characteristics of clear road binders. Transportation Research Record: J. of the Transportation Research Board, N°2293: 114-122.

Nicholls C (2006) BitVal - Analysis of Available Data for Validation of Bitumen Tests, Report on Phase 1 of the BitVal Project, Available via http://bitval.fehrl.org/fileadmin/bitval/BitVal_final_report.pdf

Pouget S and Loup F (2013) Thermo-mechanical behavior of mixtures containing bio-binders. Road Materials and Pavement Design 14 (N° S1): 212-226.

Saint-Jacques M, Brosseaud Y (2006) Coloured bituminous wearing courses in France – Overview of uses. Paper presented at 10th International Conference on Asphalt Pavements, Quebec City, Canada, 12-17 August 2006.

Sicard D, Bonvalot F, Bonnet G (2007) Le choix des revêtements colorés à base de bitume ou de résine pour la voirie urbaine - recommandations, Laboratoire régional de l'Ouest Parisien, Centre d'études sur les réseaux, les transports, l'urbanisme et les constructions publiques, 2007.

Vansteenkiste S, Vanelstraete A, (2008) Properties of fillers: Relationship with laboratory performance in hot mix asphalt, Paper presented at 83rd AAPT meeting, Philadelphia, 27-30 April 2008.

Verhasselt A.F (2003) Short- and long-term ageing of bituminous binders – Simulation with RCAT method, Paper presented at 6th International RILEM Symposium on Performance testing and evaluation of bituminous materials PTEBM'03, Zurich 2003.

# Evaluation of Air Voids in Reinstatement Materials for Footways

**Ignacio Artamendi, Bob Allen, Chris Allpress, Phil Sabin and Paul Phillips**

**Abstract** The specification for reinstatement of openings in highways in the UK prescribes the materials that may be used and sets out the fundamental requirements for compaction. The preferred mixture for the reinstatement of footways is AC 6 complying with EN 13108-1. Meeting in situ air voids requirements for this mixture is not always achievable in practice due to, among others, the variability of plant produced mixtures, compaction conditions, surcharge and test variability. In this work, two standard AC 6 mixtures, a coarse graded and a fine graded, have been evaluated along with an alternative AC 4 mixture designed to give low air voids with minimum compaction effort. The mixtures were compacted in the laboratory at different temperatures and compaction efforts. Air voids were determined using standard methods. X-ray computed tomography (CT) was also used for measuring the internal structure of the asphalt specimens. Results showed large differences in air voids between the two standard AC 6 mixtures. Considerably lower voids were obtained for the AC 4 mixture. CT scanning showed better compactability of the AC 4 mixture as seen by the air voids distribution with specimen thickness. Also, the AC 6 coarse mixture had a relatively small number of large air voids whereas the AC 6 fine mixture had a relative large number of small air voids. The AC 4 material, on the other hand, had the smallest air voids and their number was small compared to the AC 6 fine mixture but similar to that of the AC 6 coarse mixture.

**Keywords** Reinstatement materials · Air voids · Surcharge · Computed tomography

I. Artamendi (✉) · B. Allen · C. Allpress · P. Sabin · P. Phillips
Aggregate Industries, Coalville, UK
e-mail: ignacio.artamendi@aggregate.com



F. Canestrari and M.N. Partl (eds.), *8th RILEM International Symposium on Testing and Characterization of Sustainable and Innovative Bituminous Materials*, RILEM Bookseries 11, DOI 10.1007/978-94-017-7342-3_24

## 1 Introduction

Utility companies are responsible for maintaining the underground infrastructure, such as gas, electric, water and telecommunications and for all aspects of excavation and reinstatement of the highway in connection with these services. They are required to reinstate to national performance standards and to comply with minimum guarantee periods in accordance with the Specification for Reinstatement of Openings in Highways (SROH) (DfT 2010).

This Specification prescribes the materials and performance requirements to be complied with for the duration of the Guarantee Period. Compaction requirements are specified using air voids as a surrogate property for permeability (air and water), in order to safeguard the pavement structure, both within and adjacent to the reinstatement. Performance is measured on in situ air voids limits on cores taken after the completion of the reinstatement, permeability is not directly measured. Specified air voids limits however vary and depend on the type of asphalt mixture used in the reinstatement.

Asphalt mixtures permitted for the reinstatement of openings have to comply with the requirements given in the European standards. Specification limits for standard mixtures, such as Asphalt Concrete (AC), are very wide in terms of grading and binder content. Thus, differences in air voids would be expected for standard compliant mixtures but with different composition.

The SROH also provides guidance for compaction which includes numbers of passes of different compaction equipment and layer thickness. There is, however, evidence that following this guidance does not guarantee the required level of compaction measured by air voids (Steele and Burtwell 2005).

The majority of reinstatements are small rectangular-type openings and trenches and are carried out in restricted or confined areas, many of these on footways and footpaths (Burtwell and Spong 1999). They are typically hand laid rather than machine laid and small compaction plant equipment is typically employed in these works. Heat loss due to temperature, storage and weather conditions can in these cases have a large effect on the compaction achieved during placing. Current void content specifications are derived from machine laid mixtures, pre-compacted by a vibrating screed and rolled by highly efficient compaction equipment and may be, therefore, unrealistic for the installation methods and equipment used in reinstatements.

Another factor that has an effect on air voids is the surcharge applied during placing. The surcharge is the additional thickness of uncompacted material required to achieve the final compacted lift thickness. It is sometimes quoted as a percentage. For surfacing materials, the surcharge used is typically around 40 % of the finished lift thickness; however, selecting the correct surcharge for a particular material and lift thickness requires experience and practice (DfT 2006). Completed reinstatements ideally should be as flat and flush as possible with the surrounding adjacent surfaces. For surface layers, however, too much surcharge can result in excessive surface crowning whereas too little surcharge can lead to a surface depression.

The air voids of a core specimen are typically determined indirectly by calculating the maximum density of the mixture and the bulk density of the core. Uncertainties of measurements for these methods (repeatability and reproducibility) are given in the standards. Variability in these values can affect material compliance in terms of air voids (Zohrabi and Blackman 2005). But this variability is not reflected in the specification limits. Also, larger variability in air voids is found when the material is hand-laid due to segregation and when the cores are taken at various locations (near the edge/middle) of the reinstatement. Thickness of the specimen and surface roughness can also affect the accuracy of the air voids determinations.

Over the past decades, imaging methods for measuring the internal structure distribution of asphalt mixtures have been developed. These methods utilize imaging techniques to quantify the distribution of aggregates and air voids by analyzing two-dimensional and three dimensional images of the internal structure. X-ray computed tomography (CT) has been used to obtain 3D images of the internal structure of asphalt and to study air void distribution of laboratory specimens and field cores (Masad et al. 1999).

This work focuses on reinstatement asphalt mixtures for footways. In footways, the stresses applied to the material are low compared to those applied by the traffic in a road. For the reinstatement of footways, the preferred mixture is Asphalt Concrete (AC) with a 6 mm maximum aggregate size and medium to soft bitumen (100/150 pen or 160/220 pen). Compaction requirements for this mixture given in the specification established that in situ air void content shall be between 2 % (minimum) and 13 % (maximum). These air voids requirements, however, are not always achieved in practice. As explained before, some of the factors that affect compaction and, therefore, air voids are mixture variability during production, installation and compaction methods, size and accessibility of the opening, temperature and weather conditions during the works, surcharge and test variability.

In this work, two standard and compliant AC 6 surface course mixtures, coarse graded and fine graded, were evaluated. An alternative material, an AC 4 surface course mixture, was also designed and evaluated in the study. This mixture was designed to achieve minimum air voids with minimum compaction and with less sensitivity to temperature. The mixtures were compacted in the laboratory using an impact compactor. Different compaction effort and compaction temperatures were employed. Air voids were determined using standard methods. The effect that surcharge had on air voids and surface profile of the reinstatement was also examined. Computed tomography (CT) X-ray scanning was also used to determine air void content and air void size and number with specimen thickness.

## 2 Materials

Two standard AC 6 mixtures, a coarse graded and a fine graded, complying with PD 6691 (BSI 2010) and EN 13108-1 were designed using 2/6.3 mm and 0/4 mm granite aggregate and limestone filler. The binder used was a 160/220 pen. Typical target binder content for this type of mixture is 6.2 %. To account for plant tolerances i.e. ±0.5 %, binder contents employed were 5.7 % for the AC 6 coarse graded mixture and 6.7 % for the AC 6 fine graded mixtures to reflect the permissible extremes of the mixture specification. Table 1 presents the grading enveloped and tolerances for an AC 6 dense surf mixture (BSI 2010) and the actual gradings and binder contents for the AC 6 coarse and fine mixtures used in the study. It can be seen that both materials complied with the specification limits in terms of grading and binder content.

An alternative AC 4 mixture for footways was also designed in the laboratory. The main requirement for this mixture was that it had to be highly workable and it had to achieve the specified in situ air voids with minimum compaction effort. An AC 4 mixture with binder contents ranging from 7.5 to 10.2 % was evaluated using the gyratory compactor. The mixtures were produced with 0/4 mm granite aggregate and limestone filler. The binder used was a 160/220 pen. All the mixtures were mixed and compacted at the same temperature i.e. 130 °C. At each binder content three specimens were prepared.

Figure 1 shows the air voids with number of gyrations for AC 4 mixtures with various binder contents. It can be seen that for binder contents of 9.0 % and higher, the mixtures achieved air voids below the specified maximum (i.e. 13 %) just after 1 gyration. Thus, minimum compaction effort was required to achieve compliant mixtures in terms of air voids. Furthermore, the mixtures achieved full compaction (refusal density) after at a relatively small number of gyrations (15 gyrations). In comparison, the number of gyrations used in the design of mixtures for roads typically varies from 25 up to 200 depending on mixture type and layer thickness (Delorme et al. 2007).

**Table 1** Grading and binder content

| Sieve size (mm) | AC 6 (specs) % passing | AC 6 coarse % passing | AC 6 fine % passing | AC 4 % passing |
|---|---|---|---|---|
| 10 | 100 (−2/0) | 100 | 100 | 100 |
| 6.3 | 98 (−8/+5) | 96 | 98 | 100 |
| 2 | 42–56 (±6) | 42 | 56 | 67 |
| 1 | 24–46 (±4) | 26 | 35 | 44 |
| 0.25 | 11–19 (±4) | 11 | 17 | 22 |
| 0.063 | 4.0–8.0 (±2) | 4.4 | 8.0 | 12.0 |
| Binder cont. (%) | 6.2 (±0.5) | 5.7 | 6.7 | 9.0 |

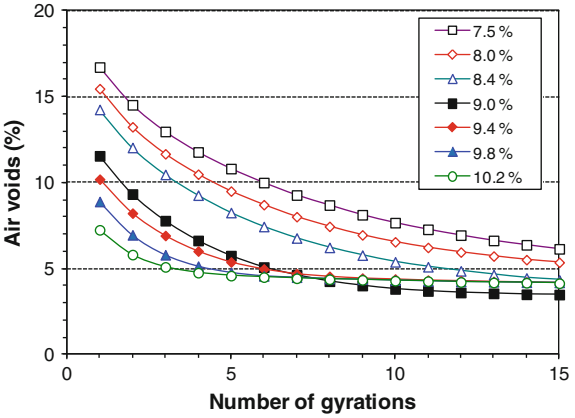


**Fig. 1** Air voids with number of gyrations for AC 4 mixtures with different binder contents

Based on the above the target binder content selected for the AC 4 mixture was 9.0 %. Thus, the designed binder content of the AC 4 mixture was higher than those of the AC 6 mixtures. Also, the grading of the AC 4 mixture was finer than those for the AC 6 mixtures (see Table 1).

## 3 Air Voids

### *3.1 Effect of Compaction Effort and Compaction Temperature*

Laboratory compaction was carried out by impact compaction (Marshall Hammer). It was believed that this type of compaction method was more representative to those used in trench reinstatements than the gyratory compactor. The mixtures were first mixed and then compacted at 130 °C. Compaction effort applied was 10, 30 and 50 blows on each side. Two specimens were compacted at 10 and 30 blows whereas 14 specimens were compacted at 50 blows. Maximum density, bulk density by dimensions and air voids of laboratory compacted specimen were then determined using EN standard test methods.

Figure 2 shows the air voids of the mixtures investigated. It can be seen that the AC 6 Coarse mixture had higher voids than the AC 6 Fine mixture and the AC 4 mixture had the lowest air voids. The figure also indicated that the workability of the AC 6 mixtures was poor. The AC 4 mixture was, on the other hand, very workable and easily compacted. Furthermore, a limited number of blows (i.e. 10 × 2 blows) were required to achieve acceptable air void levels.

The effect of compaction temperature on air voids was evaluated by compacting the mixtures for the same number of blows (50 × 2) at 80 and 130 °C (see Fig. 2). It can be seen that as the compaction temperature decreased the air void content

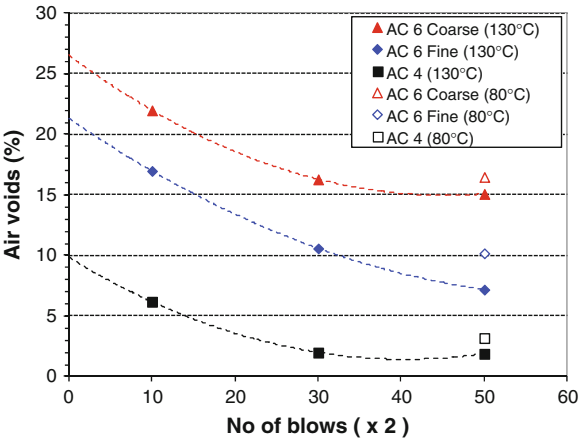


**Fig. 2** Effect of compaction effort and compaction temperature on air voids

increased for all specimens however even at the low compaction temperature the AC 4 mixture could achieve very low air voids (3.2 %). This suggested that this mixture was less susceptible to temperature variations and could therefore be installed and compacted over a wider temperature window reducing the risk of having in situ air voids above the specified value.

## *3.2 Test Variability*

The variability of the air voids test data was determined for specimens compacted at 130 °C and 50 × 2 blows. The number of specimens used per mixture was 14. Probability distributions are presented in Fig. 3. The 99 % confidence interval of the mean was calculated using the t-distribution with n − 1 = 13 degrees of freedom and a two-tailed distribution (t = 3.012). Thus, confidence intervals (99 % confidence)

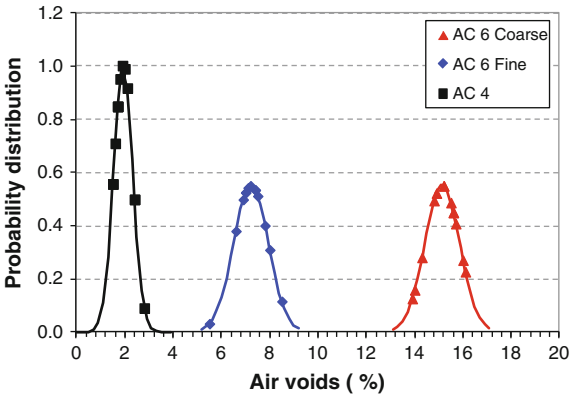


**Fig. 3** Air voids probability distributions for mixtures compacted at 50 × 2 blows and at 130 °C

determined were 15.1 ± 0.6 % for the AC 6 Coarse, 7.2 ± 0.6 % for the AC 6 Fine and 1.9 ± 0.3 % for the AC 4 mixture. Thus, less variability in the air void content was determined for the AC 4 mixture.

Lower variability in air voids for the AC 4 mixture might help to reduce the risk of non-conformities. It should be noted, however, that these are specimens manufactured in the laboratory and not cores taken in situ. For in situ cores larger variability in air voids would be expected. Nevertheless, this variability will be associated not only the material but also to the installation conditions.

## 4 Surcharge

The surcharge applied during placing an asphalt mixture on a reinstatement is the additional thickness of uncompacted material required to achieve the final compacted lift thickness. After compaction, reinstatements ideally should be flat and flush with the surrounding surface. Differences in surcharge can affect both the air voids achieved after compaction and the surface profile of the reinstatement. Too little surcharge can lead to high voids and/or surface depression whereas too much surcharge can result in excessive surface crowning (see Fig. 4).

The effect of surcharge thickness on air voids can be estimated theoretically using the following equation:

$$\text{Voids } (\%) = \left[1 - \frac{\frac{\rho_{\text{unc}} \times (h+s)}{h}}{\rho_{\max}}\right] \times 100 \tag{1}$$

where $\rho_{\text{unc}}$ is the uncompacted mixture density (Mg/m$^3$), $\rho_{\max}$ is the maximum mixture density (Mg/m$^3$), $h$ is the lift thickness (mm) and $s$ is the surcharge (mm). Maximum density values were calculated as 2.525 Mg/m$^3$ for AC 6 Coarse, 2.482 Mg/m$^3$ for AC 4 Fine and 2.402 Mg/m$^3$ for AC 4. The uncompacted densities, on the other hand, were estimated from regression analysis using the air voids of the uncompacted mixtures, i.e. at 0 blows, in Fig. 2. Uncompacted density values obtained were 1.856 Mg/m$^3$ for AC 6 Coarse, 1.953 Mg/m$^3$ for AC 4 Fine and 2.167 Mg/m$^3$ for AC 4.

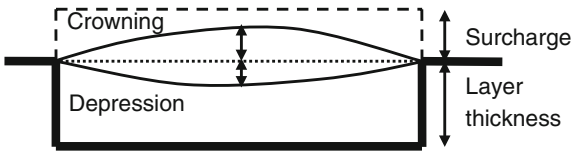


**Fig. 4** Surcharge

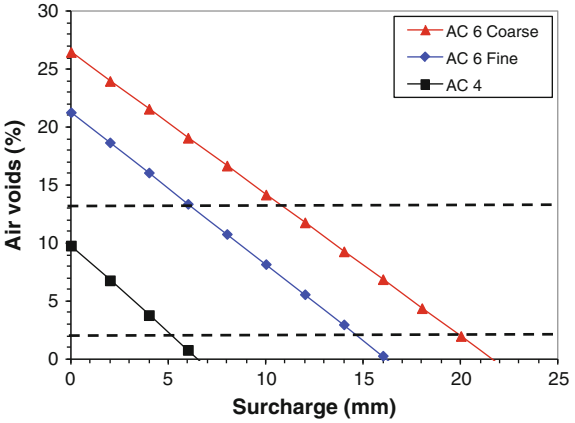


**Fig. 5** Effect of surcharge on air voids

For the reinstatements of flexible footways, the surface layer is typically 30 mm thick laid in one lift and is laid on top of 50 mm of a binder course layer (e.g. AC 20 bin 100/150). Alternatively, a single layer 60 mm thick also laid in one lift of AC 6 is laid on top of the sub-base.

Figure 5 shows the effect of surcharge on air voids for a square opening with a depth ($h$) of 60 mm assuming that the surface of the reinstatement after compaction is flush with the surrounding surface. It can be seen that a surcharge between 11 and 20 mm for the AC 6 Coarse mixture and between 6 and 15 mm for AC 6 Fine are required to achieve compliant air voids between 2 and 13 %. For the AC 4 mixture a surcharge from 0 (level) to 5 mm is needed to comply with the air voids requirements. It should be noted that in practice it would be very difficult to control the level of surcharge to say 16 ± 5 mm for the AC 6 coarse and 11 ± 5 mm for the AC 6 Fine to achieve compliant air voids. Better chances of achieving compliant air voids would be expected by using the AC 4 mixture and up to 5 mm surcharge. Also, the depth of an opening is not always constant but varies within the surface area covered. Thus, for a particular surcharge level, localized changes in thicknesses will affect the air voids distribution within that area where surcharge is constant.

The effect of surcharge on surface profile can also be estimated from Eq. 1 and is shown in Fig. 6. The figure shows the height above or below the surface level for different surcharge values when the material is compacted to 2–13 % air voids. These values correspond to a surface reinstatement 60 mm thick. Surface crowning and surface depression limits for reinstatements are given in the SROH. For reinstatements of up to 400 mm wide these limits are both 10 mm (DfT 2010).

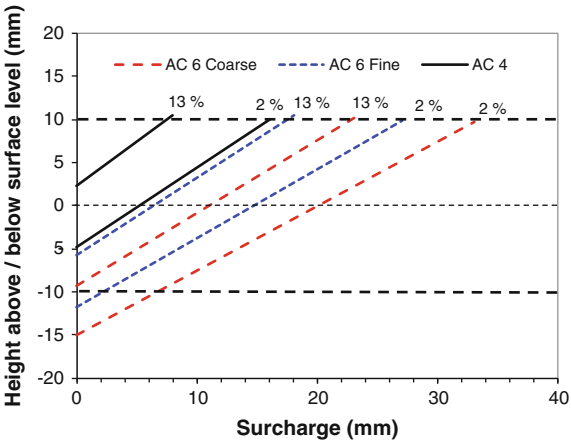


**Fig. 6** Effect of surcharge on surface profile

## 5 Computed Tomography

X-ray Computed Tomography (CT) scanning is a non destructive technique used for the visualization of internal features inside objects and for 3D imaging. The technique is based on the attenuation of X-ray radiation when it passes through the sample; the higher the attenuation the higher the density of the material.

Images of the internal structure of asphalt specimens (cores) were obtained using a 225 kV X-ray source. Core specimens were scanned every 0.5 mm interval Digital image processing was applied to remove noise and improve image quality. Post-processing was carried out in order to determine air void distribution, size and number of air voids. Typical CT scans at mid height of the core specimens for the AC 6 Coarse and the AC 4 mixtures are shown in Fig. 7. It can be seen that 2D air voids (in red) of the AC 6 mixture were markedly higher than that for the AC 4.

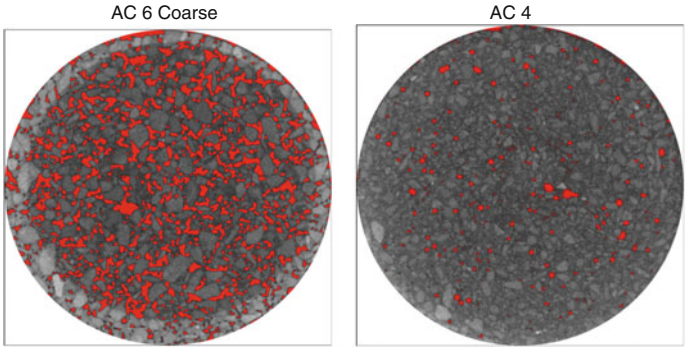


**Fig. 7** CT scans (mid height of the core—air voids in *red*)

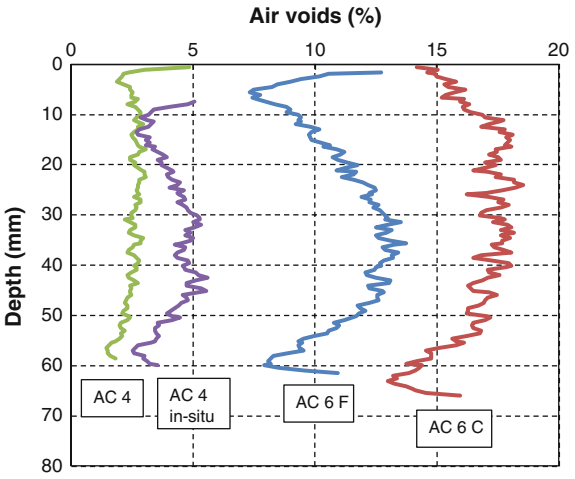


**Fig. 8** Air voids with core depth

The distribution of air voids with core thickness is presented in Fig. 8. It can be seen that for the laboratory prepared AC 6 mixtures, higher air voids are observed towards the mid height of the specimens compared to the top and bottom. This indicated that most of the compaction energy was spent on the compaction of the material at the top and bottom of the specimen. Thus, most of the compaction energy was not transmitted through the rest of the material but spend in the compaction of the upper and lower layers. Distribution of air voids with specimen thickness for the AC 4 mixture compacted in the laboratory (50 × 2 blows) is also presented in Fig. 9. It can be seen that, compared to the AC 6 mixtures, the air void content did not change appreciably with specimen thickness. Thus, the compaction energy applied was transmitted thoroughly over the total thickness of the specimen. This indicated that the AC 4 mixture was more compactable than the AC 6 mixtures. Furthermore, average air voids obtained from CT scanning were in good agreement with those obtained by standard test methods. The distribution of air voids for an AC 4 in situ specimen, on the other hand, showed lower voids at the top and bottom. Overall air voids, however, were low and just slightly higher than that for the lab prepared specimen.

Average air void size (air void diameter) with specimen thickness is presented in Fig. 9. It was found that the average size of the air voids of the AC 6 Coarse mixture was larger than those of the AC 6 Fine and AC 4 mixtures. The smallest air voids were found on the AC 4 mixture. Also, larger air voids were observed towards the middle section of the AC 6 specimens. For the AC 4 mixture, on the other hand, the air void size remained practically constant with specimen thickness. As regards the AC 4 in situ specimen, air void sizes were slightly higher than those obtained for the laboratory compacted specimen but still smaller than those for the AC 6 mixtures.

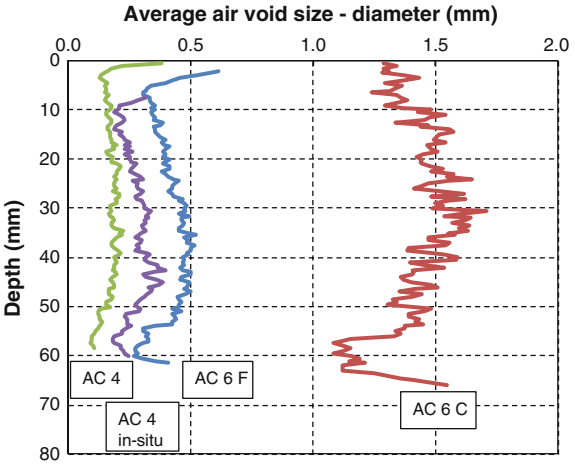


**Fig. 9** Air voids size with core depth

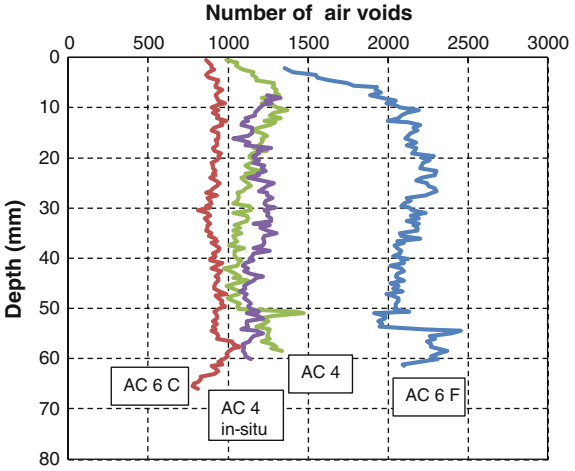


**Fig. 10** Air voids number with core depth

The variation of the number of air voids with specimen thickness is shown in Fig. 10. It can be seen that the number of air voids of the AC 6 Fine mixture was the highest whereas the AC 6 Coarse mixture was the lowest. Number of voids for both, laboratory prepared and in situ core of the AC 4 mixture, were just above those found for the AC Coarse mixture. It is believed that permeability is closely related not only to the overall air voids but more importantly to the distribution of voids within the layer thickness and the size and number of voids which affect the tortuosity, defined as the geometric complexity of a porous medium, and inter-connectivity between air voids.

## 6 Conclusions

Based on the laboratory work carried out to evaluate the air voids of reinstatement materials for footways, the following conclusions can be drawn:

- The differences in air voids between the two standard and compliant AC 6 mixtures were large and were attributed to aggregate grading and binder content.
- An alternative mixture (AC 4) was designed to achieve compliant air voids with minimum compaction effort.
- Under the same compaction conditions, much lower voids were obtained for the designed AC 4 mixture compared to the standard AC 6 mixtures.
- Less variability in air voids was determined for the AC 4 mixture compared to the standard AC 6 mixtures.
- Surcharge had a large effect on both air voids and surface profile. Surcharge levels for the AC 4 mixture should be easier to control in practice.
- CT scanning showed better compactability of the AC 4 mixture as seen by the distribution of air voids with specimen thickness.
- The AC 6 coarse mixture had a small number of large air voids whereas the AC 6 fine mixture had a large number of small air voids. Air voids of the AC 4 material were the smallest and their number was relatively small.

## References

British Standard Institution (2010) Published Document PD6691:2010, Guidance on the use of BS EN 13108 Bituminous Mixture – Material specifications

Burtwell MH, Spong (1999) The effectiveness of the utility reinstatement specification, TRL Report 324, TRL Limited

Delorme JL, de la Roche C, Wendling L (2007) LPC Bituminous Mixtures Design Guide. Laboratoire Central des Ponts et Chausses, Paris, France

Department for Transport (2006) Practical guide to street works, The Stationery Office, London, UK

Department for Transport (2010) Specification for the Reinstatement of Openings in Highways, Third Edition, New Roads and Street Works Act 1991, Code of Practice for England, The Stationery Office, London, UK

Masad EA, Muhunthan B, Shashidhar N, Harman T (1999) Quantifying Laboratory Compaction Effects on the Internal Structure of Asphalt Concrete, Transportation Research Record No. 1681, TRB, Washington, D.C., pp. 179-184

Steele DP, Burtwell MH (2005) Compliance testing of street works reinstatements, Unpublished Project Report UPR/ISS/26/05, TRL Limited

Zohrabi M, Blackman DI (2005) Validation testing of the performance of SROH 600-1000 kg/m single drum rollers, TRL Report 624, TRL Limited

# Part V
# Advanced Characterization of Interlayer Systems

# Inter-laboratory Shear Evaluation of Reinforced Bituminous Interfaces

**Gilda Ferrotti, Antonio D'Andrea, Maciej Maliszewski, Manfred N. Partl, Christiane Raab, Cesare Sangiorgi and Francesco Canestrari**

**Abstract** Over the last decades, the use of grids between asphalt layers has been gaining interest. Several test methods have been proposed in order to simulate the complex mechanical behavior of reinforced pavements and to assist practitioners in the selection of the appropriate reinforcement product. For this purpose, the Task Group 4 (*Pavement Multilayer System Testing*) of the RILEM technical committee TC 237-SIB (*Testing and Characterization of Sustainable Innovative Bituminous Materials and Systems*) organized an inter-laboratory experiment, constructing one trial test section to obtain double-layered asphalt pavement samples for the participating laboratories. The experiment placed two grid types (a glass fiber reinforced polymer grid and a carbon fiber/glass fiber pre-bituminised grid) between two asphalt layers, thereby creating two reinforced double-layered systems. As a control, an unreinforced interface was also realized. This paper presents the overall

G. Ferrotti (✉) · F. Canestrari
Università Politecnica delle Marche, Ancona, Italy
e-mail: g.ferrotti@univpm.it

F. Canestrari
e-mail: f.canestrari@univpm.it

A. D'Andrea
Sapienza, Università di Roma, Rome, Italy
e-mail: Antonio.dandrea@uniroma1.it

M. Maliszewski
IBDiM, Road and Bridge Research Institute, Warsaw, Poland
e-mail: mmaliszewski@ibdim.edu.pl

M.N. Partl · C. Raab
EMPA—Swiss Federal Laboratories for Materials Science and Technology, Dübendorf, Switzerland
e-mail: Manfred.partl@empa.ch

C. Raab
e-mail: christiane.raab@empa.ch

C. Sangiorgi
Università di Bologna, Bologna, Italy
e-mail: cesare.sangiorgi4@unibo.it



F. Canestrari and M.N. Partl (eds.), *8th RILEM International Symposium on Testing and Characterization of Sustainable and Innovative Bituminous Materials*, RILEM Bookseries 11, DOI 10.1007/978-94-017-7342-3_25

results of interlayer shear tests carried out by five participating laboratories using five different shear testing methodologies. The objective is to show the effect of two grid types on the shear behaviour of reinforced double-layered systems and to compare the findings which emerged from using different test devices and methods under different testing conditions (e.g. sample geometry, temperature, loading time, normal stress). Consistent and reliable results have been obtained through the various methodologies adopted. It has been observed that grid-reinforced samples provide lower interlayer shear strength compared with unreinforced samples. Glass-fiber grid system, which is of greater thickness and greater torsional stiffness, displayed less shear strength than carbon fiber/glass fiber-reinforced grid systems.

**Keywords** Asphalt concrete · Inter-laboratory test · Interface shear · Grid reinforcement

## 1 Introduction

Service life of asphalt pavements is affected by many factors, such as traffic loading, ageing, environmental and subgrade conditions. These factors accelerate degradation and could lead to premature failure of the pavement structure if they are not adequately considered during design and construction phases. Depending on the type of distress and its development, suitable rehabilitation and maintenance solutions become fundamental in order to restore (and, in some cases, to upgrade), the original mechanical and/or functional characteristics of asphalt pavements.

The use of reinforcement systems within bound layers is mainly addressed to prevent or delay reflective cracking and rutting and improve fatigue life (Austin and Gilchrist 1996; Brown et al. 2001; Montestruque et al. 2004; Nguyen et al. 2013; Prieto et al. 2007; Sobhan and Tandon 2008; Zielínski 2008). However, the presence of reinforcements at the interface can cause an interlayer de-bonding effect (Brown et al. 2001; Canestrari et al. 2012; Vanelstraete et al. 1997; Zamora-Barraza et al. 2010) that could affect the overall pavement behaviour. Both quasi-static (Canestrari et al. 2013) and dynamic (Brown et al. 2001) shear tests performed on double-layered specimens with or without the application of a constant normal stress showed that a general shear strength decrease is observed when a reinforcement is placed at the interface of asphalt concrete layers.

Although interface bonding conditions influence pavement response in terms of stress–strain distribution (Shukla and Yin 2004; Sobhan and Tandon 2008), de-bonding is not necessarily a negative aspect for pavement mechanical performance. In this sense, when geosynthetics are employed to improve load spreading ability, rutting resistance and fatigue resistance, reinforcements should guarantee high interlayer bonding between the lower and the upper layer (Lee 2008). However, this may result in a limited capability to prevent crack propagation from the underlying pavement layers, which is instead promoted by de-bonding.

The Task Group 4 (*Pavement Multilayer System Testing*) of the RILEM technical committee TC 237-SIB (*Testing and Characterization of Sustainable Innovative Bituminous Materials and Systems*), decided to investigate the effectiveness deriving from the installation of reinforcements between asphalt layers through the preparation of an experimental test section.

This paper presents the overall results of interlayer shear tests carried out by five different laboratories with the objective of studying the effects of two geogrid types on the shear behavior of reinforced double-layered systems and compare findings emerged with different devices and testing conditions (e.g. sample geometry, temperature, normal stress).

## 2 RILEM Project Description and Material Characteristics

This study is part of the research project "Advanced Interface Testing of Geogrids in Asphalt Pavements" promoted by Task Group 4 of RILEM Technical Committee 237-SIB.

In order to compare experimental procedures and devices for the mechanical characterization of geogrid reinforced interfaces in asphalt concrete pavements, a full-scale pavement test section, using real scale paving equipment and geogrid installation techniques, was constructed (Canestrari et al. 2013). This section consists of three double-layered asphalt concrete sub-sections, characterized by different interfaces: an unreinforced (UN) and two reinforced (CF and FP).

The two bituminous layers, having a thickness of 50-mm-each, were prepared with the same Asphalt Concrete (AC) mixture. It is a typical Italian dense graded mix with 12 mm maximum aggregate size (AC 12) and 70/100 penetration bitumen dosed at 5.5 % by aggregate weight. In both reinforced and unreinforced sub-sections, an SBS polymer-modified tack coat emulsion, classified as C 69 BP 3 (EN 13808), was applied on the surface of the lower layer with a rate of 0.25 kg/m$^2$ of residual binder. The residual binder of the modified emulsion is characterized by a penetration value at 25 °C of 55–65 dmm, a Ring and Ball Temperature of 65–75 °C, a viscosity value at 160 °C of 0.2–0.8 Pa s and a Fraass Breaking Point <−18 °C.

In the reinforced interfaces, two different geogrids were installed. The Carbon Fiber/Glass Fiber geogrid (CF) is pre-coated with bitumen and characterized by carbon fiber rovings in the transversal direction and glass fiber rovings in the longitudinal direction, with a 20 mm-square mesh. The product is sanded on the upper side, whereas a burn off film is applied on the lower side. The Glass Fiber Reinforced Polymer geogrid (FP) is obtained by weaving continuous alkaline-resistant pre-tensioned glass fibers, covered with a thermosetting epoxy resin (vinylester). The grid has a bi-directional square geometry with flat transversal strands woven into longitudinal twisted strands, with a 33 mm-square mesh and a thickness of about 3 mm. The main characteristics of CF and FP geogrids are shown in Table 1. Apart from the constituent material and mesh size, the main difference

**Table 1** Characteristics of CF and FP geogrids

| Geogrid | Direction | Material | Grid size (mm) | Tensile modulus ($N/mm^2$) | Elongation at rupture (%) | Tensile force mesh (kN/m) |
|---|---|---|---|---|---|---|
| CF | Longitudinal | Glass fiber | 20 | 73,000 | 3–4.5 | 111 |
| | Transversal | Carbon fiber | 20 | 240,000 | 1.5 | 249 |
| FP | Longitudinal | Glass fiber reinforced polymer | 33 | 23,000 | 3 | 211 |
| | Transversal | Glass fiber reinforced polymer | 33 | 23,000 | 3 | 211 |

among the two geogrids is their torsional rigidity, also called aperture rigidity (Kinney and Yuan 1995). In fact, the FP geogrid is extremely stiff as twisting and distorting its square mesh is very difficult, whereas the CF geogrid mesh is highly flexible and deformable.

From the full-scale pavement test section, slabs of different sizes (52 × 52 cm and 65 × 65 cm) were cut and sent to the participating laboratories. From these slabs, each laboratory obtained double-layered asphalt concrete specimens to be tested for the evaluation of the interlayer shear properties.

# 3 Shear Test Devices and Procedures

## *3.1 Pure Direct Shear Configuration*

### 3.1.1 Leutner Test

The Leutner test (Leutner 1979) consists in applying a constant shear displacement rate across the interface of a layered specimen while recording the resulting shear force and the applied displacement. The testing frame is installed into an ordinary Marshall testing machine and allows testing 100 or 150 mm-diameter specimens, taken either from a pavement structure or prepared in the laboratory. The standard shear displacement rate is 50.8 mm/min. The test output is a shear force-shear displacement curve, that allows the interlayer shear strength ($\tau_{peak}$) to be obtained, corresponding to the failure conditions.

### 3.1.2 Layer-Parallel Direct Shear (LPDS) Test

The Layer-Parallel Direct Shear (Raab and Partl 2009) is an EMPA modified version of equipment developed in Germany by Leutner, being more versatile in geometry and more defined in the clamping mechanism. It allows pure direct shear

testing of multi-layered cylindrical samples with a nominal diameter of 150 mm. One part of the pavement core is laid on a circular u-bearing and held with a well-defined pressure of 0.5 MPa by a pneumatic clamping system. The other part, the core head, remains unsuspended. Shear load is induced to the core head by a semicircular shear yoke with a displacement rate of 50 mm/min, thus producing fracture within the pre-defined shear plane (Partl and Raab 1999). The gap width between the shearing rings is 2.5 mm.

## *3.2 Direct Shear Configuration with Normal Stress*

### 3.2.1 Ancona Shear Testing Research and Analysis (ASTRA) Test

The ASTRA device, compliant with the European Standard prEN 12697-48 and the Italian Standard UNI/TS 11214, is a direct shear box. A double-layered specimen, with a nominal diameter of 100 mm, is installed in two half-boxes separated by an unconfined interlayer shear zone (Canestrari et al. 2013). During the test, a constant shear displacement rate of 2.5 mm/min (standard conditions) occurs while a constant vertical load, perpendicular to the interface plane, can be applied in order to generate a given normal stress ($\sigma_n$). This test returns a data-set where the interlayer shear stress ($\tau$), the horizontal ($\xi$) and the vertical ($\eta$) displacements are reported as a function of time, allowing the calculation of the interlayer shear strength ($\tau_{peak}$). The whole apparatus is located in a climatic chamber with temperature and relative humidity control.

### 3.2.2 Sapienza Direct Shear Test Machine (SDSTM)

The Sapienza Direct Shear Testing Machine (SDSTM) is able to test double-layered cylindrical specimens with a nominal diameter of 100 mm (Tozzo et al. 2014). In the working scheme, the specimen is held in two moulds with a gap between the two restraints of 10 mm. The specimen interface is placed in the middle, leaving 5 mm from the edge of each mould. A loading machine applies the shear load (T) on one half of the specimen while the other half is fixed, preventing movement. A normal load (N) can also be applied. The device is equipped with LVDT for the interface displacement measurement. In standard conditions, a constant shear displacement rate of 2.5 mm/min is applied. A shear force-shear displacement curve is obtained in order to determine the interlayer shear strength $\tau_{peak}$. The device can also evaluate the interface shear fatigue behavior under dynamic conditions. The maximum vertical capacity of the loading machine is 100 kN with load frequencies up to 5 Hz.

### 3.2.3 Shear Tester (ST)

The Shear Tester is a device that allows testing double-layered specimens in shear configuration, through a MTS servohydraulic 100 kN loading frame (Gajewski and Mirski 2012). The apparatus allows fixing the specimen and applying the shear load in correspondence with the interface plane, parallel to the basis of the specimen. Additionally, a normal load, perpendicular to the specimen interface, can be applied through a pneumatic standalone controller. Tests were performed on 150-mm-diameter specimens, applying a constant displacement rate of 50.8 mm/min. ST returns a shear force-shear displacement curve that can be used to determine the interlayer shear strength $\tau_{peak}$. The apparatus is placed in a climatic chamber in order to perform controlled temperature tests.

## 4 Laboratory Experimental Program

The laboratory experimental program focuses on the evaluation of interlayer shear characteristics of reinforced and unreinforced double-layered bituminous systems in order to compare their mechanical behavior. To achieve this aim, three different interface types (UN, CF and FP) were investigated according to the test program shown in Table 2.

**Table 2** Laboratory experimental program for each interface type (UN, CF, FP)

| Laboratory | Specimen diameter $D$ (mm) | Test speed $v$ (mm/min) | Test temperature $T$ (°C) | Normal stress $\sigma_n$ (MPa) | Number of repetitions for each $\sigma_n$ |
|---|---|---|---|---|---|
| EMPA | 150 | 50.8 | 10 | 0.00 | 7 |
| | | | 20 | | 7 |
| | | | 30 | | 7 |
| | | | 40 | | 6 |
| IBDiM | 150 | 50.8 | 10 | 0.00; 0.15 | 1 |
| | | | 20 | | 1 |
| | | | 30 | | 1 |
| UNIRM | 100 | 2.5 | 20 | 0.00; 0.20; 0.40 | 3 |
| UNIBO | 150 | 50.8 | 20 | 0.00 | 9 |
| UNIVPM | 100 | 2.5 | 10 | 0.00; 0.20; 0.40 | 4 |
| | | | 20 | | 4 |
| | | | 30 | | 4 |

The five laboratories, participating on a voluntary basis in this study are listed as follows:

- Swiss Federal Laboratories for Materials Science and Technology (EMPA), Dübendorf, Switzerland
- Road and Bridge Research Institute (IBDiM), Warsaw, Poland
- Sapienza, Università di Roma (UNIRM), Italy
- Alma Mater Studiorum, Università di Bologna (UNIBO), Italy
- Università Politecnica delle Marche, Ancona (UNIVPM), Italy

As it is shown in Table 2, each laboratory considered different test conditions in terms of specimen diameter, test speed, test temperature, normal stress applied to the interface and number of repetitions, depending on the characteristics of the adopted methodology.

The interlayer shear strength $\tau_{peak}$ and the corresponding displacement of each specimen were measured and the average values were considered. When different normal stress levels $\sigma_n$ were applied, a complete assessment of interface failure properties was obtained according to the following equation:

$$\tau_{peak} = c_0 + \sigma_n \cdot \tan \Phi_p \tag{1}$$

where $c_0$ is the pure shear strength and $\Phi_p$ is the peak friction angle.

## 5 Results and Analysis

In order to check the statistical significance of the interface type (UN, CF and FP) on the interlayer shear strength $\tau_{peak}$, a one-way analysis of variance (one-way ANOVA) at 95 % confidence level, was performed.

Results of ANOVA of each participating laboratory are summarized in Table 3, where the relevant p-value is shown for each test condition, in terms of normal stress $\sigma_n$ and test temperature $T$. For an easier interpretation of ANOVA results, the p-values that represent non-significant differences between two interface types are reported in bold in Table 3. As far as IBDiM laboratory is concerned, ANOVA was not performed due to the low number of repetitions.

The analysis of variance shows that there is no statistical difference between UN and CF results in all laboratories and for almost all of test conditions. This result suggests that the presence of CF geogrid does not significantly influence interlayer shear properties of double-layered systems. On the contrary, Table 3 clearly shows that FP geogrid has a significant influence on interlayer shear strength, highlighting statistical differences with both UN and CF interface types.

In order to investigate the influence of test temperature and define a possible ranking between the different interface types (UN,CF and FP), interlayer shear

**Table 3** ANOVA: influence of interface type (UN, CF, FP) on interlayer shear strength

| Lab | $\sigma_n$ (MPa) | T (°C) | p-value UN versus CF | p-value UN versus FP | p-value CF versus FP |
|---|---|---|---|---|---|
| EMPA | 0.00 | 10 | **0.688** | 2.6E-5 | 9.1E-6 |
| | | 20 | **0.256** | 4.1E-3 | 1.2E-3 |
| | | 30 | **0.634** | 1.4E-2 | 9.4E-3 |
| | | 40 | 2.3E-2 | **0.095** | **0.627** |
| UNIRM | 0.00 | 20 | **0.284** | 1.1E-3 | 4.8E-4 |
| | 0.20 | | **0.380** | 1.2E-3 | 1.6E-3 |
| | 0.40 | | **0.175** | 4.5E-3 | 5.9E-3 |
| UNIBO | 0.00 | 20 | **0.705** | 3.0E-6 | 6.0E-6 |
| UNIVPM | 0.00 | 10 | **0.076** | 2.8E-4 | 1.7E-4 |
| | | 20 | **0.258** | 1.6E-3 | 7.3E-4 |
| | | 30 | **0.394** | 2.9E-3 | 1.5E-2 |
| | 0.20 | 10 | **0.641** | 5.3E-5 | 1.2E-4 |
| | | 20 | **0.161** | 6.4E-4 | 1.4E-3 |
| | | 30 | 3.2E-2 | 2.3E-3 | 1.3E-2 |
| | 0.40 | 10 | **0.216** | 1.9E-4 | 3.3E-4 |
| | | 20 | **0.202** | 4.6E-2 | 2.3E-3 |
| | | 30 | **0.088** | **0.120** | **0.986** |

strength results were represented at a given normal stress $\sigma_n$, considering the laboratories that performed tests at different temperatures (Fig. 1). Interlayer shear strength decreases with increasing temperature for both reinforced and unreinforced interfaces, for all the investigated shear test devices and test conditions (normal stress and interface type).

Figure 1 shows that UN and CF interfaces provide very similar results, as it was already observed with the statistical analysis, even if it seems that UN interface guarantees, in general, a slightly higher interlayer shear strength with respect to CF interface. On the contrary, FP geogrid provides the lowest interlayer shear strength with respect to the other two interface types. This is probably due to the greater thickness and stiffness of the FP geogrid, which inhibit the achievement of an optimal compaction of the upper AC layer in the interface proximity, and reduces the interlocking between the two bituminous layers in contact (Santagata et al. 2008). Nevertheless, at higher temperatures the difference between the three interface types becomes almost negligible (Fig. 1). Here, higher temperatures lead to reduced differences between geogrids so that $\tau_{peak}$ appears mainly controlled by the characteristics of the asphalt concrete layers in contact.

The correlation between interlayer shear strength and temperature can also be represented in a semi-logarithmic plane and can be described with a relationship obtained in a previous RILEM research project on interlayer bonding of asphalt pavements (Canestrari et al. 2012):

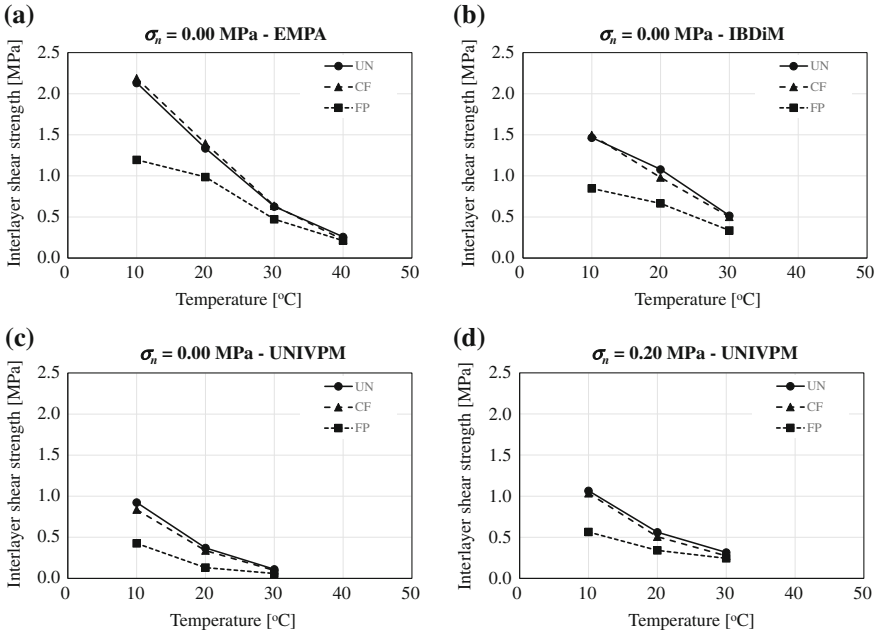


**Fig. 1** Correlation between interlayer shear strength and temperature for different laboratories and different test conditions

$$\log \tau_{peak} = a \times T + b \tag{2}$$

where the parameters $a$ and $b$ were determined in different test conditions. In particular, for unreinforced and polymer modified tack-coated interfaces, the parameters $a$ and $b$ were found $a = -0.026$, $b = 0.586$ when $D = 150$ mm and $v = 50.8$ mm/min. The comparison of these values with the parameters $a$ and $b$ determined in this investigation (Fig. 2) shows that EMPA and IBDiM results,

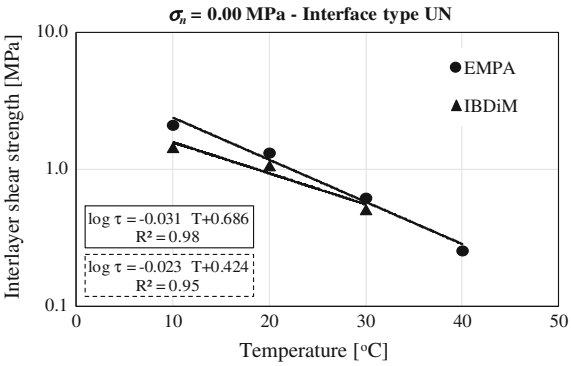


**Fig. 2** Correlation between interlayer shear strength and temperature for UN interface type, without normal stress

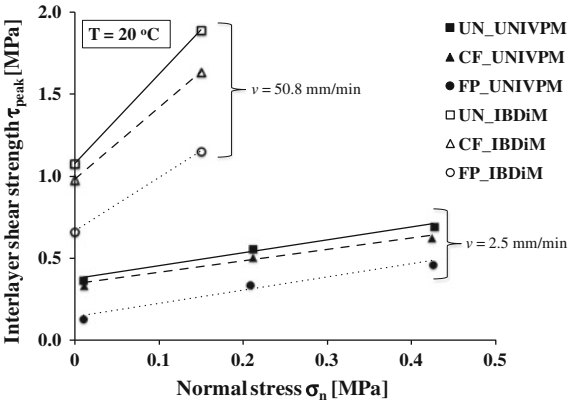


**Fig. 3** Peak envelopes of different interface types and for different laboratories

obtained with $D$ = 150 mm and $v$ = 50.8 mm/min, are in reasonable agreement with previous results (Canestrari et al. 2012).

The peak envelopes of the interlayer shear strength obtained for the three interface types and for the three laboratories that investigated different normal stresses are presented in Fig. 3. Contrarily to Fig. 1, where differences between UN and CF interfaces were not so evident, Fig. 3 clearly shows that geogrid-reinforced interfaces (CF and FP) provide lower interlayer shear strength compared to the unreinforced interface (UN), particularly in terms of pure shear strength ($c_0$). This is in accordance with previous investigations, carried out with various experimental devices (Brown et al. 2001; Canestrari et al. 2013; Zamora-Barraza et al. 2010; Zielínski 2008), where a similar interlayer de-bonding effect was measured after the installation of geogrid reinforcement. As already observed in Fig. 1, FP interface provides lower $\tau_{peak}$ values with respect to CF interface, due to the higher thickness and stiffness of FP geogrid.

Figure 3 clearly shows that in absolute terms, the two laboratories (UNIVPM and IBDiM) provide different $\tau_{peak}$ results, mainly due to the different displacement rates (50.8 and 2.5 mm/min).

The effects of the two geogrid types on the shear behavior of reinforced double-layered systems were also compared through the normalization of $\tau_{peak}$ of CF and FP interfaces with respect to $\tau_{peak}$ of UN interface, for all the investigated shear test devices, considering $T$ = 20 °C and $\sigma_n$ = 0.0 MPa. Results are shown in Fig. 4, where LPDS, Leutner and ST data are obtained with $D$ = 150 mm and $v$ = 50.8 mm/min, whereas SDSTM and ASTRA data are obtained with $D$ = 100 mm and $v$ = 2.5 mm/min. Figure 4 shows that different devices provide very similar normalized $\tau_{peak}$ values for CF interface whereas more scattered results were observed for FP interface. This is probably due to FP geogrid mesh dimension (33 mm-square), resulting in a different number of strands in the single specimen and thus influencing the corresponding interlayer shear strength.

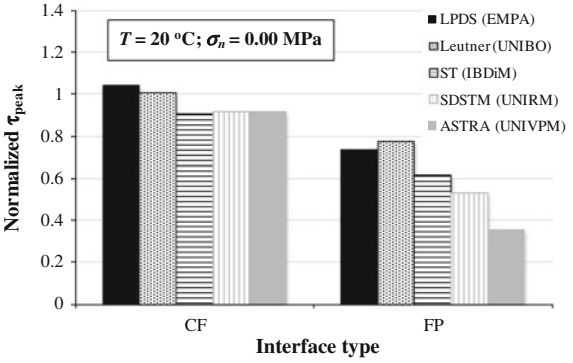


**Fig. 4** Comparison between CF and FP interfaces

As far as the interlayer shear strength of the two interface types is concerned, whatever the experimental device and test conditions are, it is confirmed that FP geogrid produces a significant de-bonding effect with respect to the unreinforced interface, whereas CF geogrid results are very similar to those of UN interface.

Starting from these results, it is expected that the FP geogrid provides in the field an improved reflective cracking resistance thanks to the de-bonding effect highlighted by shear tests. In a different way, a similar reflective cracking pattern should be observed for UN and CF reinforced pavements.

## 6 Conclusions

This paper focuses on the effects of geogrid reinforcement on the interlayer shear behavior of asphalt pavements. It is part of the RILEM research project "Advanced Interface Testing of Geogrids in Asphalt Pavements" promoted by Task Group 4 of the TC 237-SIB. Several laboratories participated in this interlaboratory investigation performing tests, with their own shear test device, on three interface types: unreinforced, reinforced with a carbon fiber/glass fiber pre-bituminised geogrid and reinforced with a fiber reinforced polymer geogrid.

Results showed that the studied grid-reinforced interfaces provide lower interlayer shear strength with respect to the unreinforced one even if the analysis of variance highlighted a difference not statistically significant between the unreinforced interface and the carbon fiber/glass fiber grid reinforcement. On the contrary, a significant de-bonding effect is evident with the fiber reinforced polymer geogrid characterized by greater thickness and torsional stiffness as compared to the carbon fiber/glass fiber geogrid.

As far as the temperature effect is concerned, it was observed that interlayer shear strength decreases with increasing temperature for both reinforced and unreinforced interfaces and for all the test conditions considered. However, higher temperatures lead to reduced differences between geogrids.

Finally, it was also observed that the correlation between interlayer shear strength and temperature for unreinforced interface is in good agreement with results obtained in a previous RILEM research project on interlayer bonding of asphalt pavements.

## References


Austin RA, Gilchrist AJT (1996) Enhanced performance of asphalt pavements using geocomposites. Geotext Geomembranes 14(3-4):175–186. doi: 10.1016/0266-1144(96)00007-6.

Brown SF, Thom NH, Sanders, PJ (2001) A study of grid reinforced asphalt to combat reflection cracking. J Assoc Asphalt Pav 70:543–569.

Canestrari F, Ferrotti G, Lu X, Millien A, Partl MN, Petit C, Phelipot-Mardelé A, Piber H, Raab C (2012) Mechanical Testing of Interlayer Bonding in Asphalt Pavements. In: Partl MN, Bahia HU, Canestrari F, de la Roche C, Di Benedetto H, Piber H, Sybilski D (ed) State-of-the-Art-Reports 9: Advances in Interlaboratory Testing and Evaluation of Bituminous Materials, 1st edn. Springer, Berlin, p 303–360. doi: 10.1007/978-94-007-5104-0_6.

Canestrari F, Belogi L, Ferrotti G, Graziani A (2013) Shear and flexural characterization of grid-reinforced asphalt pavements and relation with field distress evolution. Mater Struct. doi: 10.1617/s11527-013-0207-1.

Gajewski M, Mirski K (2012) Shear tests of two-layer asphalt specimens made in a proposed apparatus allowing side pressure application. Logistyka Journal, 3: 593-602.

Kinney TC, Yuan X (1995) Geogrid aperture rigidity by in-plane rotation. Paper presented at Geosynthetics '95, Nashville, 1995: 525-537.

Lee SJ (2008) Mechanical performance and crack retardation study of a fiberglass-grid-reinforced asphalt concrete system. Can J Civil Eng 35(10):1042–1049. doi: 10.1139/L08-049.

Leutner R (1979) Untersuchung des Schichtverbundes beim bituminösen Oberbau. Bitumen 3: 84-91.

Montestruque G, Rodrigues R, Nods M, Elsing A (2004) Stop of Reflective Crack Propagation with the Use of PET Geogrid as Asphalt Overlay Reinforcement. Paper presented at the 5th International RILEM Conference on Cracking in Pavements, Limoges, 5-8 May 2004.

Nguyen ML, Blanca J, Kerzréhoa JP, Hornych P (2013) Review of glass fibre grid use for pavement reinforcement and APT experiments at IFSTTAR. Road Mater Pavement. 14 (1): 287-308.

Partl MN, Raab C (1999). Shear Adhesion between Top Layers of Fresh Asphalt Pavements in Switzerland. Proceedings, 7th Conf. on Asphalt Pavements for Southern Africa, CAPSA '99, Victory Falls, Zimbabwe, 5.130-5.137.

Prieto JN, Gallego J, Perez I (2007) Application of the wheel reflective cracking test for assessing geosynthetics in anti-reflection pavement cracking systems. Geosynth Int 14(5):287-297. doi: 10.1680/gein.2007.14.5.287.

Raab C, Partl MN (2009) Interlayer bonding of binder, base and subbase layers of asphalt pavements: Long-term performance. Constr Build Mater 23: 2926-2931. doi:10.1016/j.conbuildmat.2009.02.025.

Santagata FA, Partl MN, Ferrotti G, Canestrari F, Flisch A (2008) Layer characteristics affecting interlayer shear resistance in flexible pavements. J Assoc Asphalt Paving 77:221–256.

Shukla SK, Yin JH (2004) Functions and installation of paving geosynthetics. Paper presented at the 3rd Asian Regional Conference on Geosynthetics, Seoul, 21-23 June 2004.

Sobhan K, Tandon V (2008) Mitigating reflection cracking in asphalt overlay using geosynthetic reinforcements. Road Mater Pavement 9(3):367–387. doi: 10.1080/14680629.2008.9690124.

Tozzo C, Fiore N, D'Andrea A (2014) Dynamic shear tests for the evaluation of the effect of the normal load on the interface fatigue resistance. Constr Build Mater 61: 200-205. doi: 10.1016/j.conbuildmat.2014.03.010.

Vanelstraete A, de Bondt AH, Courard L (1997) Characterization of overlay systems. In: Vanelstraete A. and Franken L (Ed) Prevention of Reflective Cracking in Pavements, RILEM Report 18, 1st edn. E & FN Spon, London, p 61-83.

Zamora-Barraza D, Calzada-Pérez MA, Castro-Fresno D, Vega-Zamanillo A (2010) New procedure for measuring adherence between a geosynthetic material and a bituminous mixture. Geotext Geomembranes 28(5):483-489. doi: 10.1016/j.geotexmem.2009.12.010.

Zielínski P (2008) Fatigue investigations of asphalt concrete beams reinforced with geosynthetics interlayer. Paper presented at the 6th RILEM International Conference on Cracking in Pavements, Chicago, 16-18 June 2008: 751-759. doi: 10.1201/9780203882191.ch73.

# Comparison of Interlayer Bond Behavior Due to Ageing

**Christiane Raab, James Grenfell, A.O. Abd El Halim and Manfred N. Partl**

**Abstract** The research focuses on the question of the influence of age on the interlayer bonding properties of two layered specimens. The evaluation compares and discusses the behavior of different datasets from laboratory and in situ pavements from Switzerland, United Kingdom and Italy using traditional data evaluation and Artificial Neural Network (ANN) analysis. The results show that it is possible to use ANN techniques to derive models from datasets and to predict interlayer bond strength. The findings demonstrate that age has a positive effect on the interlayer bond of asphalt pavements and that long term oven ageing can lead to similar results as in situ ageing. In addition it was found that the positive effect of ageing is greater when a tack coat is used. According to the results of the investigation a linear model from all data would predict that maximum strength may roughly increase by 1 % per month over a period of 10 years.

**Keywords** Bond test devices · Asphalt pavements · Tack coat · Ageing · Artificial neural network

C. Raab (✉) · M.N. Partl
EMPA—Swiss Federal Laboratories for Materials Science and Technology, Dübendorf, Switzerland
e-mail: christiane.raab@empa.ch

M.N. Partl
e-mail: manfred.partl@empa.ch

J. Grenfell
University of Nottingham, University Park, Nottingham, UK
e-mail: James.Grenfell@nottingham.ac.uk

A.O. Abd El Halim
Department of Civil and Environmental Engineering, Carleton University, Ottawa, Canada
e-mail: AbdEl.Halim@carleton.ca



F. Canestrari and M.N. Partl (eds.), *8th RILEM International Symposium on Testing and Characterization of Sustainable and Innovative Bituminous Materials*, RILEM Bookseries 11, DOI 10.1007/978-94-017-7342-3_26

## 1 Introduction

For many years different countries have established methods and equipment for testing interlayer bond of pavement layers for quality assurance of construction sites and for defining technical requirements (Raab et al. 2009). Generally, bonding properties are determined immediately after construction and evaluated with respect to requirements in national standards. In order to improve the bond between the different layers of a pavement, tack coats are widely used and their benefit is generally unquestioned (Uzan et al. 1978; Hachiya et al. 1997; Mohammad et al. 2002; Miro et al. 2003).

However, it is still disputed if the bonding properties should be tested directly after construction and how the tack coat properties are influenced by ageing. Given this situation, the question of how bonding properties develop over time is of special interest especially in cases where interlayer bonding requirements are not met. Some recent investigations on long term performance of bonding properties of tack coats have indicated that ageing can have a positive effect on the bonding properties (Canestrari et al. 2013; Raab and Partl 2008; Sutanto 2009).

In addition to traditional data evaluation, recent research (Raab et al. 2013) found Artificial Neural Networks (ANN) a suitable tool for the evaluation of interlayer bonding, supporting the above mentioned findings concerning ageing of tack coats. The aim of this paper was to investigate and compare the change of interlayer bonding properties over time for different datasets from research projects dealing with tack coats and pavements from Switzerland, United Kingdom and Italy. The investigation was conducted by combining traditional data evaluation and Artificial Neural Networks (ANN) for analysing long-term interlayer shear results. The paper is based on an investigation from Raab et al. (2014) giving more attention to the evaluation and interpretation of the comparison of the different datasets (Raab et al. 2014).

## 2 Shear Test Devices and Testing Procedures

For interlayer shear testing two different devices were used.

Shear testing on the Swiss and Italian pavements was conducted with the Swiss Layer-Parallel Direct Shear (CH-LPDS) test device, which is an EMPA modified version of the equipment originally developed in Germany by Leutner (1979). This device is more versatile in geometry and more defined in the clamping mechanism (Raab and Partl 2008) than the original Leutner device. It has a gap width of 2 mm between the shearing rings.

British pavements were investigated using the modified UK Leutner shear device with a gap width of 5 mm (Choi et al. 2005). Both test devices are depicted in Fig. 1. The deformation rate was 50 mm/min in both cases.

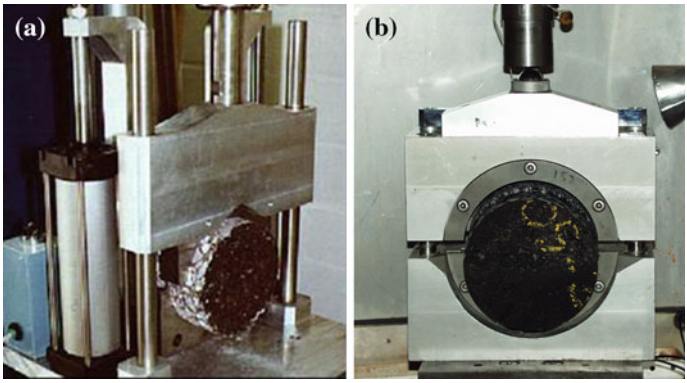


**Fig. 1** **a** CH-LPDS shear device, **b** modified UK Leutner shear device

Before testing, specimens were conditioned in a climate chamber for at least 4 h and the tests were conducted at 20 °C. From the shear test, the shear force F as a function of the vertical shear deformation w was obtained.

Nominal maximal shear stress, i.e. the average shear stress in the cross section, was calculated by dividing the maximum shear force by the cross sectional area of the cylindrical specimen.

## 3 Using Artificial Neural Networks for Data Evaluation

An artificial neural network is a biologically inspired computational model consisting of several single units, called artificial neurons, connected with weighting coefficients, (Ghaffari et al. 2006). This system is capable of recognising, capturing and mapping patterns in a data set with a high number of interconnections between neurons allowing the processing of information in parallel.

A basic network is composed by three or more layers of neurons. The first layer contains the input data, while the last layer contains the output data. One or more layers, known as hidden layers, are placed between the input and output layers. The arriving signals, called inputs, multiplied by the connection weights, are first summed and then passed through a transfer function to produce the output for that neuron. An activation function acts on the weighted sum of the neuron's inputs. The most commonly used functions are sigmoid and hyperbolic tangent functions. Most commonly a feed forward ANN is used. There are many different learning algorithms but the most common is the back propagation algorithm. For back propagation, two other parameters, the learning rate and the momentum coefficient, need to be defined. The learning rate is an adjustable factor that controls the speed of the learning process. The momentum coefficient determines the proportion of the last weight change that is added to the new weight change.

Information from input data is fed forward through the network to optimise the weights between neurons. Optimisation of the weights is made by backward propagation of the error during the training or learning phase. The ANN reads the input and output values in the training data set and changes the value of the weighted links to reduce the difference between the predicted and target (observed) values. The error in prediction is minimised across many training cycles until the network reaches a specified level of accuracy (Ghaffari et al. 2006).

## 4 Datasets

The datasets compared in this research come from different research projects and laboratory studies (Raab and Partl 2009; Sutanto 2009; Piber et al. 2009; Canestrari et al. 2013) on pavements from different countries, i.e. Switzerland, United Kingdom and Italy. Table 1 provides an overview on the different datasets.

The Swiss data "Lab Pavement CH" data was determined during a laboratory study in which a cationic tack coat was used between two layered specimens produced with a laboratory compactor to investigate the influence of tack coat on different parameters such as surface roughness and the influence of curing time on the bond between the layers (Raab and Partl 2009).

The British data "Lab Pavement UK" was taken from an investigation developing an interlayer bond database for UK materials and constructions (Sutanto 2009). Here, specimens with different tack coats and compacted with a roller in the laboratory have been investigated.

The dataset "RILEM pavement" was retrieved during the interlaboratory test program on interlayer shear testing initiated by the RILEM TC 206-ATB TG 4 (Piber et al. 2009; Canestrari et al. 2013), where cores from a two layered model pavement near Ancona, Italy, had been tested with the CH-LPDS device.

**Table 1** Overview on the datasets analysed by ANN

| | Database description | Type of data | Country |
|---|---|---|---|
| Lab pavement CH | Bond data from study using cationic tack coat to investigate the influence of parameters such as curing time | Lab compaction | CH |
| Lab pavement UK | Bond data from study of roller compacted specimens using different tack coats | Lab compaction | UK |
| RILEM pavement I/CH | Bond data from an interlaboratory study on interlayer testing using different tack coats | In field compaction | I/CH |

## 4.1 Swiss (CH) Laboratory Pavement Dataset

The specimens were produced with a laboratory roller compactor and the bonding properties of cores taken from the slabs were evaluated by means of CH-LPDS direct shear testing according to Swiss standards (Swiss Standard, SN 670461, 2000). The tack coat was an unmodified bituminous cationic emulsion with a residual bitumen content of 50 % according to the European standard, EN 13808 (European Standard EN 13808 2005). The total application rate was 200 g/m$^2$ residual bitumen. For comparison 10 cores (d = 150 mm) with tack coat were taken from one half of the slab and compared to 10 cores without tack coat.

In order to simulate the influence of time and age, one slab was constructed, but left for 2 months outdoors before cores were taken and testing was carried out. Since the whole experiment took place during the summer time (June to August), the temperature varied between 11 and 35 °C and occasionally heavy rain fall occurred.

## 4.2 United Kingdom (UK) Lab Pavement Dataset

In order to build up a comprehensive database of bond between the upper two interfaces for a wide range of UK material combinations and bonding conditions, typical surfacing and binder course materials were used. All materials were designed according to the relevant Standards (British Standards Institution 2005a, 2006a and b); details can be found in Sanders and Nunn (2005), Sutanto et al. (2006), Sutanto (2009). Slabs of 305 by 305 mm, each comprising two layers, were manufactured with a slab 'roller' compactor in accordance with BS EN 12697-33 (British Standards Institution 2003d).

At the interface of the two layers three different treatments were applied:

- Non-modified tack coat emulsion, with 200 g/m$^2$ of residual bitumen
- Polymer modified bond coat with 300 g/m$^2$ residual bitumen
- No tack (bond) coat.

From each slab, 150 mm diameter cores were taken for UK Leutner shear testing. Generally six identical tests were undertaken for each test condition to assess variability.

The investigation into the effect of ageing on interface bonding properties was carried out by performing a long-term oven ageing protocol called LINK (Brown and Scholz 2000) on a number of specimens prior to the interlayer bond testing. This long-term oven ageing procedure comprises of ageing a compacted specimen in a forced-draft oven at a temperature of 85 ± 1 °C for 120 ± 0.25 h. The oven is switched off at the end of the ageing period and the specimen is left in the oven to cool to room temperature. Next, the specimen is conditioned in a temperature controlled cabinet at a designated testing temperature prior to UK Leutner shear testing.

### 4.3 Italian/Swiss (I/CH) RILEM Pavement Dataset

This dataset was produced during the interlaboratory test program initiated in 2008 by RILEM TC 206-ATB TG 4 (Piber et al. 2009; Canestrari et al. 2013).

For this interlaboratory test, the Università Politecnica delle Marche in Ancona constructed a trial pavement of 3.50 by 21.0 m with two asphalt concrete layers. The whole pavement area was divided into 3 parts of 7.0 m. For each section a different interface treatment was applied:

- Pavement 1 without treatment (not hot on hot)
- Pavement 2 pre-coated with a polymer modified emulsion
- Pavement 3 pre-coated with a conventional cationic emulsion

After construction cores were taken from the pavement sections and sent out to different laboratories and organizations for testing at different temperatures and deformation rates. For every test condition 7 cores were provided.

In the course of that project, EMPA tested the three tack coat conditions at different temperatures and deformation rates. Additionally, pavement 2 was cored and tested again 1.5 years later, in order to evaluate the influence of ageing.

## 5 Modelling with Artificial Neural Network

For modelling Alyuda Neurointelligence (© 2001–2009 Neo Digital) software was used in this research. The applied software offers the possibility to analyse ANN results with so-called response graphs. The response graphs display the response of the model output by varying one of the variables, while keeping the other input variables constant. The constant value for each variable is the mean value of that variable in the dataset. For all data sets maximum shear force $F_{max}$ [kN] and the resulting maximum nominal shear stress $\tau_{max}$ [MPa] were chosen as output variables. The input variable selection for ANN modelling of the databases was conducted using a feature selection mode inbuilt in the applied ANN software.

### 5.1 Swiss (CH) Laboratory Pavement

The chosen input variables for the CH Laboratory Pavement dataset were type of tack coat, (categorical value), treatment (categorical value), age (months), air void content of layer 1 (vol.%) and air void content of layer 2 (vol.%).

ANN modelling using the query files for validating the determined network leads to a good prediction for the output variables with an $R^2$ value of 0.84. When taking the response graph for the CH Laboratory Pavement based on the input variable age, an increase in shear force of about 5 % over the period of 2 months can be found. Leading to the following equation:

$$F_{predicted} = 36.5 + 0.9 \cdot t \quad \text{t [months]},\ \text{F[kN]},\ 0 \leq \text{t} \geq 2 \tag{1}$$

The positive effect of ageing also corresponds to the above mentioned laboratory study by Raab and Partl (2009). In that investigation it could be shown that the positive effect of ageing depends on whether a tack coat was used or not. In the case of using a tack coat, the shear force increased by about 10 kN or appr. 26 %, while for uncoated specimens only a very small increase, with a mean value of 0.5 kN or appr. 1.5 % was found.

## 5.2 United Kingdom (UK) Laboratory Pavement

The following input variables for UK Laboratory Pavement dataset were chosen: Type of tack coat, tack coat (categorical value), age (un-aged, aged; 0–1), air void content of layer (vol.%) and air void content of layer 2 (vol.%).

For UK Lab Pavement ANN modelling can predict the output data although the prediction has only a comparatively lower $R^2$ value of 0.68 when using the query files for validating the determined network.

The results shown in the response graph (Fig. 2) demonstrate that this ageing process increases the interface shear strength. For the long-term oven ageing an increase of 48 % was found. In the traditional investigation this increase of shear strength was found to be between 16 and 41 % (Sutanto 2009).

## 5.3 Italian/Swiss (I/CH) RILEM Pavement

The chosen input variables for the I/CH RILEM Pavement dataset were type of tack coat, tack coat (categorical value), age (years), temperature (°C), deformation rate

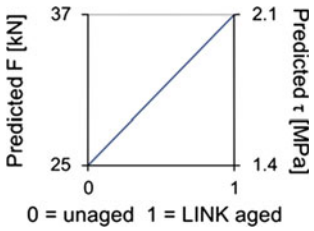


**Fig. 2** Response graph "Age", maximum shear force and shear stress as a function of age (long-term aged/non-aged)

(mm/min), air void content of layer 1 (vol.%) and air void content of layer 2, (vol. %). For this dataset ANN modelling using the query files for validating the determined network led to a very good prediction for the output variables with an $R^2$ value of 0.94. Form the response graph based on the input variable age, an increase in shear force of about 70 % after 1.5 years can be found. Leading to the following equation:

$$F_{predicted} = 15 + 0.583 \cdot t \quad \text{t[months]},\ \text{F[kN]},\ 0 \leq \text{t} \geq 18 \tag{2}$$

## 6 Discussion

Figure 3 shows the prediction of $F_{max}$ and $\tau_{max}$ for the combination of the 3 datasets with a prediction accuracy value $R^2$ of 0.86.

For all three datasets the ANN modelling shows an increase of maximum shear force and shear stress with age. The amount of increase clearly depends on the time, so in case of CH Laboratory Pavement when the ageing took only two months, an increase in shear force of appr. 2 kN or stress of 0.1 MPa was achieved while for the "RILEM Pavement", when the aged specimens were tested after 1.5 years, an increase of more than 10.5 kN or 0.6 MPa was found. For the UK dataset, when long-term ageing in the oven was conducted the increase in shear force was up to

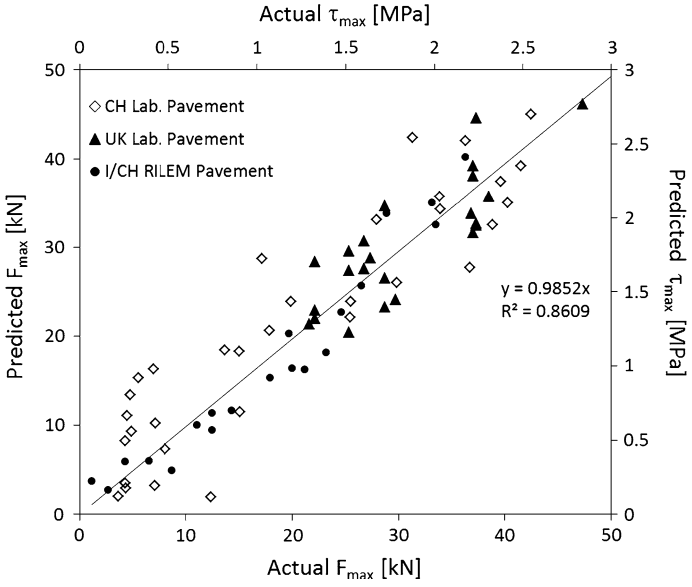


**Fig. 3** Prediction of $F_{max}$ and $\tau_{max}$ for the independent query test dataset


**Fig. 4** Response graph "Age", maximum shear force and shear stress as a function of age (time)

12 kN or shear stress of 0.7 MPa. This result is also comparable to long-term in situ ageing of 10 years as in an investigation by Raab et al. (2013), as depicted in Fig. 4 and in Eq. 3. In this figure it can be seen that the shear force increases by 22.5 kN or the shear stress by 1.3 MPa.

$$F_{predicted} = 16.5 + 0.1875 \cdot t \quad \text{t [months]}, \ \text{F[kN]}, \quad 0 \leq \text{t} \geq 120 \tag{3}$$

In Fig. 5 the trend lines (cut-out up to 10 months) for the increase of shear force over time for CH Lab Pavement, I/CH RILEM Pavement datasets and additionally for the CH LTPP Pavement dataset are given. The UK Pavement was not taken into consideration in this graph since the long-term oven ageing cannot be fitted into the time scale.

From Fig. 5 it is evident that LTPP Pavement and RILEM Pavement start from very similar initial interlayer bond values, while the initial value of the Lab Pavement due to its laboratory fabrication is significantly higher. While the rate of increase in interlayer bond (slope of the curve) is more or less similar for CH Lab and I/CH RILEM Pavement, it is noticeably slower for the CH LTPP Pavement. Regarding the LTPP Pavement it is important to note, that the considered time

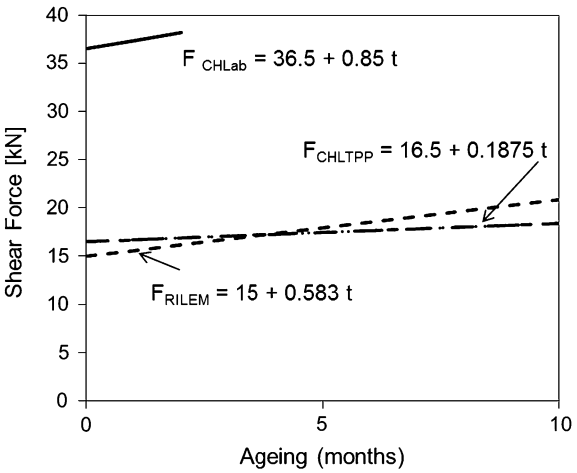


**Fig. 5** Trend lines (cut-out up to 10 months) for the increase of shear force over time for CH Lab Pavement, I/CH RILEM Pavement and the CH LTPP Pavement datasets

period for these pavements was at least 10 years and that the pavements during this time were trafficked and exposed to extreme climate conditions (very cold winters up to −10 °C and hot summers up to 30 °C). Furthermore, all pavements including pavements with traffic volume exceeding design limits and thus leading to noticeable deterioration had been included in the evaluation, a fact that may also contributes to the slower increase rate. For CH Lab Pavement and I/CH RILEM Pavement only one type of pavement (with different tack coats and treatments) was looked at while the LTPP Pavement dataset combined a great variety of pavement types and compositions. The ageing of I/CH RILEM Pavement happened in only 18 months in a noticeably warmer climate (Ancona, Italy) with hotter and longer summer periods and shorter and warmer winters, improving the bond between layers (gluing) and leading to higher increase in shear strength. For the CH Lab Pavement the effect of ageing is different since it was rather a curing process. That the improvement rate is so high may be attributed to the fact that the interlayer bond improvement in the first weeks after construction due to curing processes is rather important and should be considered for testing. When comparing the prediction of ageing for the different datasets from the response graphs and from classical evaluation—which is only possible for the investigated time range—one has to take into account the differences in considered database and input variables. Regarding long-term prediction of interlayer bond properties CH LTPP Pavement obviously represents the most realistic case and shows that for the prediction of the development of interlayer bond behaviour long-term data are needed.

Normalisation with respect to the initial values of the response graphs for all datasets leads to Fig. 6. When the values for all datasets are normalized with respect to the initial values as shown in Fig. 6, the increase for the UK Laboratory Pavement with the described long-term ageing would be about 48 %, corresponding roughly to an increase due to the influence of age of about 43 months, i.e. 3.5 years. Keep in mind that these specimens were tested after oven ageing at 85 °C for 120 h. The RILEM data is a bit higher than the regression line, i.e. its increase in ageing is 18 months compared to 2 months outdoor ageing in Switzerland. The linear model produced from all the data would predict that the maximum strength overall may increase by 1 % per month over a period of 10 years. However, for a statistically sound evaluation more data is needed. Furthermore, it is important to keep in mind

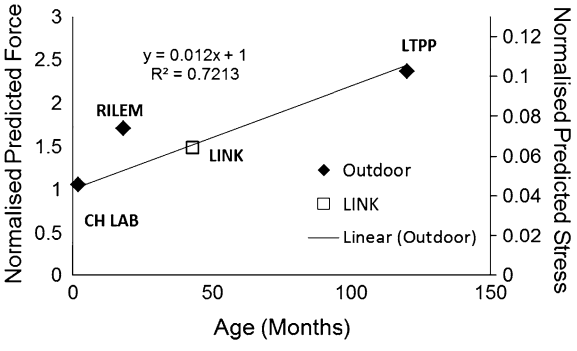


**Fig. 6** Normalised values with respect to the initial values for all datasets

that the development of interlayer bond properties may not be linear but will depend on all influencing factors.

## 7 Conclusions

The results presented in this paper show that ageing has a positive effect on the interlayer shear bond of asphalt pavements and that ANN techniques can be used to derive models from datasets to predict interlayer shear bond properties. It was further shown that ANN techniques and conventional evaluation lead to similar results. Using ANN techniques can help to evaluate and explain the differences in the ageing behavior of different datasets. In this context the high improvement rate in the first weeks after construction due to curing processes shows that short-term interlayer bond improvement as a result of curing is rather important and should be considered for quality control testing and requirements. Overall, bonding properties of aged specimens are better than those for un-aged specimens. As known from other studies, this is true as long as traffic volume and percentage of heavy traffic meet design limits. If traffic volume exceeds the design limits over a certain period of time, the pavements start to deteriorate, often leading to visible distress phenomena, such as cracking and rutting, which are measurable in a decrease of shear strength. Furthermore, it was observed that the increase of shear bond strength is even greater when a tack coat is used between the layers. The long-term oven ageing procedure (LINK), where the specimens are heated in the oven at a temperature of 85 ± 1 °C for 120 ± 0.25 h, leads to an increase in shear strength corresponding to an outdoor ageing of the order of 3.5 years. According to that result, which needs to be confirmed by additional data, the LINK test procedure provides a valuable method to predict outdoor short-term ageing. According to the results of this investigation a linear model from all data would predict that maximum strength may roughly increase by 1 % per month over a period of 10 years. However, as mentioned earlier for a statistically sound evaluation more data is needed as to improve the prediction accuracy of ANN modeling. For the prediction of long term development of interlayer bond long term data is needed and/or factors influencing the long-term behaviour have to be considered.

## References

Brown SF and Scholtz TV (2000) Development of Laboratory Protocols for the Ageing of Asphalt Mixtures.2nd Eurasphalt & Eurobitume Congress, Barcelona, Spain.

Canestrari F, Belogi L, Ferrotti G, Graziani A (2013) Shear and flexural characterization of grid-reinforced asphalt pavements and relation with field distress evolution. Mater Struct. doi: 10.1617/s11527-013-0207-1.

Choi Y, Sutanto M, Collop A and Airey G (2005) Bond between asphalt layers. Project Report to the UK Highways Acency, Scott Wilson Pavement Engineering Ltd.

Ghaffari A, Abdollahi H, Khoshayand MR, Soltani Bozchalooi Dadgar A and Rafiee-Therani M (2006) Performance comparison of neural network training algorithms in modelling of bimodal drug delivery. Science Direct. International Journal of Pharmaceutics 327, pp 126-138.

Hachiya T and Sato K (1997) Effect of tack coat on bonding characteristics at the interface between asphalt concrete layers. Proceeding of the 8thInternational Conference on Asphalt Pavements, Seattle, USA, pp.349-362.

Leutner R (1979) Untersuchung des Schichtverbundes beim bituminösen Oberbau. Bitumen 3: 84-91.

Mirò R, Pérez Jiménez F and Borras Gonzalez JM (2003) Evaluation of the effect of tack coats. LCB shear test. 6th RILEM Symposium PTEBM 03, Zurich, Switzerland, pp 550-556.

Mohammad LN, Raqib MA, Wu Z and Huang B (2002) Measurement of interlayer bond strength through shear tests. 3rd International Conference bituminous mixtures and pavements, Thessaloniki, Greece.

Piber H, Canestrari F, Ferrotti G, Lu X, Millien A, Partl MN, Petit C, Phelipot-Mardelle A and Raab C (2009) RILEM Interlaboratory Test on Interlayer Bonding of Asphalt Pavements, Proceedings of 7th International RILEM Symposium ATCBM09 on Advanced Testing and Characterization of Bituminous Materials, Volume 2, 27-29 May 2009 in Rhodes, Greece, pp1181-1189.

Raab C and Partl MN (2008) Investigation on Long-Term Interlayer Bonding of Asphalt Pavements. The Baltic Journal of Road and Bridge Engineering 3(2): 65–70. DOI: 10.3846/1822-427X.2008.3.65–70.

Raab C and Partl MN (2009) Laboratory Study on Interlayer Bonding Using Cationic Tack Coats Proceedings of 7th International RILEM Symposium ATCBM09 on Advanced Testing and Characterization of Bituminous Materials, Volume 1, 27-29 May 2009 in Rhodes, Greece, pp.3-12.

Raab C, Partl MN and Abd El Halim AO (2009) Evaluation of Interlayer Shear Bond Devices for Asphalt Pavements. Baltic Journal of Road and Bridge Engineering. Vol 4 No 4, pp 176-195.

Raab C, Abd El Halim AO and Partl MN (2013) Utilisation of Artificial Neural Network for the Analysis of Interlayer Shear Properties, Baltic Journal of Road and Bridge Engineering. BJRBE 8(2), pp107-116.

Raab C, Grenfell J, Abd El Halim AO and Partl MN (2014) The Influence of Age on Interlayer Shear Properties. Int. Journal of Pavement Engineering, 12 pages, DOI: 10.1080/10298436.2014.943212 published on line.

Sanders PJ and Nunn M (2005) The Application of Enrobé à Module Élevé in Flexible Pavements. TRL Report 636, TRL Ltd., Crowthorne, UK.

Sutanto M (2009) Assessment of Bond between Asphalt Layers. PhD Thesis, Nottingham University, Great Britain.

Sutanto M, Collop A, Airey G, Elliott R and Choi Y (2006) Laboratory measurement of bond between asphalt layers. International Journal of Pavement Engineering and Asphalt Technology, Liverpool, UK, Vol.7, Issue 1, pp.38-57.

Uzan J, Livneh M and Eshed Y (1978) Investigation of Adhesion Properties between Asphaltic Concrete Layers, Journal of the Association of Asphalt Paving Technologists 47: 495–521.

# Investigation of Dilatancy Effects on Asphalt Interface Shear Strength

**Cristina Tozzo, Nicola Fiore and Antonio D'Andrea**

**Abstract** Dilatancy is described as the shear-induced volume change in granular materials. An inclined shear test was used in this study to measure dilatancy on double layer asphalt specimens, where, due to the configuration of the device, dilatancy cannot be inhibited. Under monotonic loading conditions, three angles of 30°–45°–60° between the specimen axle and the horizontal were considered, so as to set different ratios between normal and shear force. A guillotine shear test was used to compare allowed and inhibited dilatancy at different levels of applied normal stress. The dilatancy angle $\psi$ and the dilatancy speed were introduced as useful parameters to characterize the phenomenon. The results proved that, by inhibiting dilatancy, the interface shear strength increases of a constant amount regardless of the applied normal pressure. Moreover, the comparison of the test outcomes between the two devices highlighted the non-contemporaneity between the dilatancy speed peak and the shear stress peak in the inclined shear test. It can be attributed to the fact that the volumetric expansion of the specimen is countered by the normal stress, which increases proportionally to the shear stress during the test.

**Keywords** Dilatancy · Interface · Shear strength · Asphalt layers

C. Tozzo (✉) · N. Fiore · A. D'Andrea
Sapienza University of Rome, Via Eudossiana 18, 00184 Rome, Italy
e-mail: cristina.tozzo@uniroma1.it

N. Fiore
e-mail: nicola.fiore@uniroma1.it

A. D'Andrea
e-mail: antonio.dandrea@uniroma1.it



F. Canestrari and M.N. Partl (eds.), *8th RILEM International Symposium on Testing and Characterization of Sustainable and Innovative Bituminous Materials*, RILEM Bookseries 11, DOI 10.1007/978-94-017-7342-3_27

## 1 Introduction

Dilatancy is defined as the change in volume associated with the overriding of granular aggregates as they are subjected to shear sliding. This occurs in dense soils and is strongly related to the compaction level. Dilatancy firstly described by Reynolds (1885), can be characterized by the dilatancy angle ψ. This angle controls the amount of plastic volumetric strain developed during plastic shearing and is assumed constant during plastic yielding. The value of ψ = 0 corresponds to the volume preserving deformation while in shear, as shown in Fig. 1a. On the other hand, when distortion and volumetric strain occur during shear, as in Fig. 1b, ψ is a function of plastic shear strain and plastic volumetric strain (Trivedi 2010).

According to Bolton (1986), the assumption of rigid blocks, that bound the straining zone and induce the shear, ensures that there is no extension in z direction. As Fig. 1b depicts, the dilatancy angle is then given by:

$$\tan \psi = \frac{dy}{dz} \tag{1}$$

Bolton also considers the fact that, in practice, many single failures can occur progressively, with different mobilizations of strength and dilatancy, along a developing slipping surface. The saw blades model of dilatancy is an idealization of this complex phenomenon (Fig. 2). According to this theory, overriding must occur unless particles crack. The formation of one rigid zone at the top, with inclined microfacets as saw blades, leads the sliding over the rigid zone beneath with an angle of Ψ. This angle matches the dilatancy angle measured during tests.

The angle of shearing Φ′ on the rupture surface is given by the following formula:

$$\phi' = \phi'_{crit} + \psi \tag{2}$$

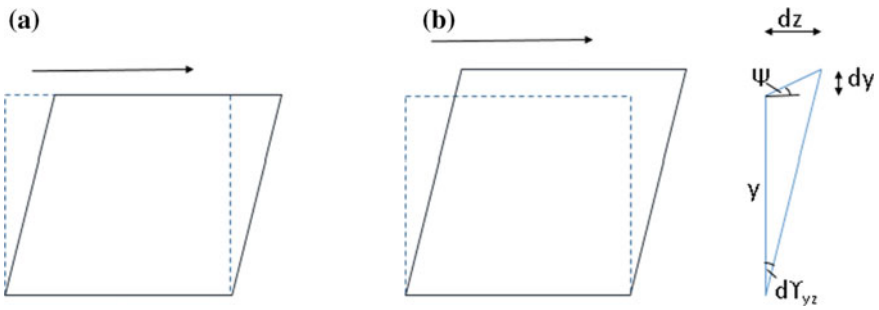


**Fig. 1** Schematization of the shear test in inhibited (**a**) and allowed dilatancy (**b**)

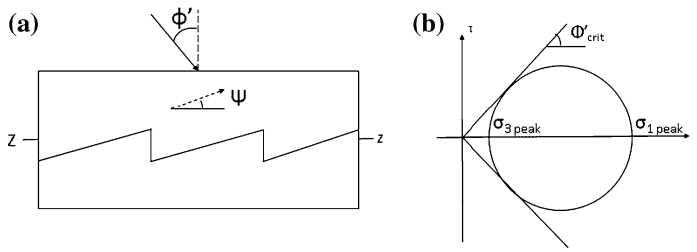


**Fig. 2** Bolton's saw blades model (**a**) and identification of $\Phi'_{crit}$ on the Mohr circle of stress (**b**)

where:

ψ is the dilatancy angle;

$\Phi'_{crit}$ is the angle of shearing observed in a simple shear test on loose soil, sufficient to constitute a critical state with no dilatancy. This is obtained by dropping a tangent from the origin to the Mohr circle of peak stresses (Fig. 2b).

A variety of more sophisticated theories have been put forward. As well several researchers have focused their attention on experimental analysis to investigate the dilatancy effects on shear behavior.

According to Collop et al. (2003), when shear tests are performed on double-layered systems reproducing the contact plane between pavement layers, the behaviour of granular materials is the same as for asphalt concretes. The frictional resistance, that in soils is directly proportional to frictional characteristics, is replaced in asphalt layers by the contact stiffness due to bond coat or adhesion.

Ozer et al. (2008) proposed a fracture-based friction method to predict dilatancy. The main features include the possibility to take into account surface roughness and the resulting volumetric deformation, because of surface irregularity, and the determination of the pressure dependence of the interface shear strength. Several numerical examples validated the model and proved its ability to reproduce the entire range of response from an initial elastic state to a fully debonded state.

From an experimental point of view, significant efforts were made to investigate dilatancy in direct shear tests (Canestrari et al. 2005; Canestrari and Santagata 2005). According to these studies, the interlayer shear resistance of multilayered system ($\tau_{peak}$) can be represented as the sum of the following contributions:

$$\tau_{peak} = \tau_{res} + \tau_d + \tau_{ic} + \tau_a \tag{3}$$

where:

$\tau_{res}$ is the residual friction
$\tau_d$ is the dilatancy contribution
$\tau_{ic}$ is the inner cohesion rate
$\tau_a$ is the adhesion given by tack coat

Recording vertical and horizontal movement of the ASTRA shear box during the tests a dilatancy parameter "d", i.e. the ratio between the vertical and the horizontal

displacements was introduced. It corresponds to the tangent of the dilatancy angle, according to the Bolton assumption. The relation between the estimated volume changes and the progressive shearing has been demonstrated. The two response curves achieve their peaks at the same time. Experimental results showed that the dilatancy phenomenon ends when the shear stress remains constant around the residual value due to residual friction. This behaviour is linked to the maximum aggregates' diameter; in fact, around the strength residual value, "d" is close to zero because the overriding finishes. The normal stress and the test temperature were also identified as important factors for dilatancy. If normal pressure increases, dilatancy decreases as the mutual overriding of the aggregates in contact is counteracted during shearing. On the other hand, when the test temperature decreases, dilatancy also decreases due to increasing stiffness and a related limitation to the local raveling at the interface.

In the scenery of shear test methods and devices for the determination of the bond strength between asphalt layers, the cited test devices represent only a test system. Several prototypes were developed worldwide, differing mainly in the selected loading and application mode, the specimen area as well as the test repeatability (Raab et al. 2009). Focusing on the dilatancy phenomenon, different working schemes lead to configurations where dilatancy could be fully or partially prevented. This is what happens in the case of direct shear tests when clamping or gluing methods keep the samples firm to avoid movements perpendicular to the shear load direction. Quantifying this effect in some cases is hard, because not all the devices are equipped with sensors for the dilatancy measurement. Also, if the phenomenon is prevented, the results of shear strength are expected to be higher than in the case of allowed dilatancy. Thus it is hard to compare the results of the various test devices.

## 2 Objective

This research aim is to investigate dilatancy effects on shear strength of double layer asphalt specimens. For this purpose, two different shear testing devices are considered. One device is characterized by an inclined test configuration. The assumption of allowed dilatancy is investigated through the introduction of useful parameters such as the dilatancy speed. The trend of the recorded volumetric expansion can be compared with the shear stress response curve. The second device, a guillotine shear test, permits to test the double layer specimens in either allowed or inhibited dilatancy and to measure the possible increase in shear strength.

The trends of the different devices in the graph shear stress versus normal stress can highlight the contribution of dilatancy to the shear strength. Moreover, the dilatancy angle will be computed in correspondence to the shear stress peak for each tested specimen.

## 3 Materials and Specimens' Preparation

Double-layered cylindrical specimens representing the first interface between binder and wearing course were manufactured in the lab. Two HMA mixes were designed, with the same binder (penetration 70/100), in compliance with the Italian standard. The specimens were prepared in moulds with an interior diameter of 101.6 mm for a total height of 120 mm (60 mm each layer). The Marshall compactor was used to compact each layer applying blows only on the upper side, according to previous studies by the same authors (D'Andrea et al. 2013b; D'Andrea and Tozzo 2012). The compaction level to be achieved was calculated using as target 98 % of the average bulk density of the same mixture compacted according to the Marshall standard UNI EN 12697-30 (2012). To improve the bond at the interface, a cationic emulsion was spread with an application rate of 0.46 kg/m$^2$ residual bitumen. Before performing tests, the specimens were left to cool at room temperature.

## 4 Equipments Used

The Sapienza Inclined Shear Testing Machine (SISTM), developed in the Road Materials Lab at Sapienza University, Rome, is a direct shear test similar to the device used by Romanoschi and Metcalf (2001). The most important SISTM modification in respect of the Romanoschi model is the change of the top attachment by a groove which engages the top half of the equipment at the loading machine, so to avoid that this upper part of the device could weigh the specimen.

As can be seen from a schematic drawing of the device (Fig. 3a), the specimen is angled thanks to two moulds, hinged at the bases, that allow testing in several inclinations, ranging the sample's axis from 0° to 65° on the horizontal plane.

The device can work both in monotonic and cyclic conditions (Tozzo et al. 2014b). Due to the inclined location of the specimen, the vertical load applied by

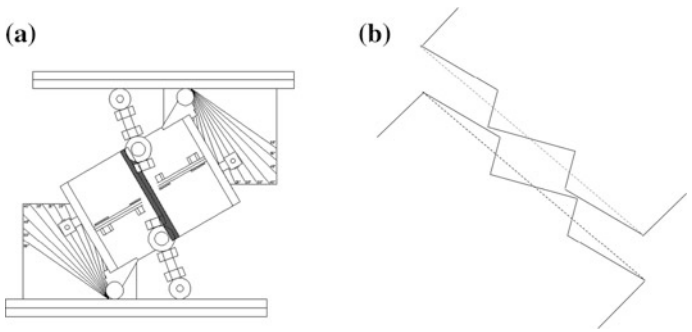


**Fig. 3** Schematic drawing of the SISTM (**a**) and representation of the dilatancy behavior (**b**)

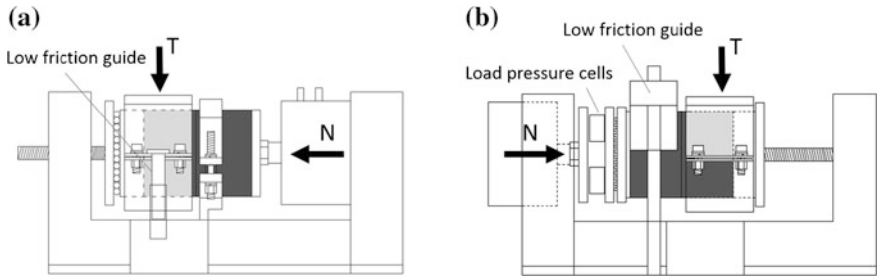


**Fig. 4** SDSTM in the two test configurations: inhibited (**a**) and allowed dilatancy (**b**)

the loading machine is decomposed in normal and shear loads at the interface. The ratio between the stress components is fixed by the inclination. The normal ($\sigma$) and shear ($\tau$) stress can be estimated by dividing the shear or normal component of the vertical load for the initial nominal area of the sample.

The proportionality between normal and shear stress was kept constant throughout the test. The lower part of the equipment can translate horizontally during the test, with a direct effect on the shear displacement. In fact, due to the device configuration, shear and normal stress, as well as shear and normal displacement, evolve in a fixed ratio. If the specimen needs dilatancy during shear, it involves higher shear displacement to allow this movement. This relationship is further discussed in the result's section.

Dilatancy was recorded by three linear variable differential transducers (LVDT) measuring the expansion displacements at three points of the lower layer side. Two more LVDTs were set to measure the shear displacements.

The Sapienza Direct Shear Testing Machine (SDSTM) is the latest device designed and developed at the Road Materials Lab at Sapienza University, Rome (D′Andrea et al. 2013a; Tozzo et al. 2014a).

For the purpose of this research, the same device was assembled in the two configurations of inhibited (a) and allowed (b) dilatancy. A schematic drawing of both the configuration is depicted in Fig. 4.

The shear stress $\tau$ is evaluated by dividing the shear load for the initial nominal area of the sample.

## 5 Testing Conditions

To investigate dilatancy and the effect of its inhibition/allowance, the same test conditions were selected for both devices. The specimens were tested under monotonic conditions with a displacement rate of the loading machine of 2.5 mm/min at a test temperature of 20 °C. The interface was placed 5 mm away from the edges of each mould.

For the SISTM, three inclinations of the specimens on the horizontal (30°, 45°, 60°) were chosen to investigate three possible ratios of shear and normal stress at the interface. These test conditions cover the cases of predominance of shear stress, predominance of compression stress and also the case of equal value of the two components in which the vertical load is decomposed. For each angle, tests were performed on five replicates.

For the guillotine SDSTM, in both configurations, five levels of nominal normal pressure (0.1, 0.2, 0.3, 0.4, 0.5 MPa) were applied by the pneumatic compressor and kept constant during the test. For each normal stress, tests were also performed on five replicates.

## 6 Analysis of the Results

The two devices used for the purpose of this study as stated earlier were configured differently and yield different kinematic behaviours. The response curves were quite different, too. In fact, in the inclined machine the two parts of the specimen can separate after the interface failure while, in the guillotine, the two parts remain in contact thanks to permanent normal pressure. Therefore, for the inclined SISTM the shear stress drops immediately after the peak.

The parameters selected to investigate dilatancy effects on interface shear strength were shear stress peaks for both devices.

For the inclined SISTM, the relation between shear and dilatancy displacement, depending on the device configuration, has already been described in Fig. 3b. This relation did not influence the correct evolution of dilatancy, as confirmed by the displacements recorded by the single LVDTs.

For inclinations of 30° and 45°, the interface breaks after the peak of the shear stress and eventually detaches. Contemporarily, dilatancy decreases and the re-approaching of the two layers is observed. Hence dilatancy behaviour after the peak is uncertain in this kind of device.

However, when the interface was tested at 60°, the specimen inclination leads to the predominance of the normal stress; in this condition the shear stress does not achieve a peak value, displaying an indefinite growth.

In Fig. 5 the maximum of the shear stress as well as the maximum dilatancy, estimated as the average of the three LVDTs, are drawn for the inclinations of 30° and 45°. Due to the fact that shear stress and dilatancy achieve their peaks contemporarily, the values are representative of the same instant in time. Dilatancy outcomes are largely scattered and it is not possible to identify any particular rule. This can be attributed to the nature of the phenomenon, directly related to the failure surface irregularity and to the number of asperities that are involved in the overriding mechanism.

The scattering of the dilatancy results is the same as identified for the SISTM interface shear displacements. This can be attributed to the device functioning, where the two displacements are linked by the inclination of the specimen. This

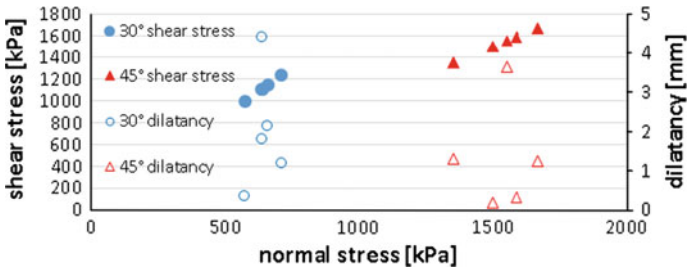


**Fig. 5** Summary of the SISTM data

relation makes it difficult to characterize the dilatancy behaviour through the dilatancy angle, especially where dilatancy and shear displacement are comparable.

The SISTM dilatancy investigation can also be supplemented by introducing the dilatancy speed $d_{speed}$. This parameter is a medium dilatancy rate computed in intervals of 2 s. A common trend is shown in Fig. 6a.

As it can be seen from the graph, the dilatancy speed achieves its peak early if compared with the trend of the shear stress, also if the peaks of the dilatancy and the shear stress are contemporary.

The explanation of this phenomenon can be found in the state of stress applied during the test. In fact, the dilatancy increase is very fast at the beginning, where the shear and normal stress are lower. As the test continues, the state of stress applied proportionally increases and the dilatancy speed reaches its maximum before compression is too high to allow further expansion. For this reason dilatancy advances more slowly up to the interface failure in correspondence to the maximum shear strength.

The guillotine SDSTM device was employed in two test configurations: inhibited and admitted dilatancy. In the second configuration, the SDSTM was equipped with 3 LVDTs for the dilatancy measurements.

The interface response in terms of shear stress after peak is characterized by a frictional behavior and decreases until it reaches a residual value. The specimen

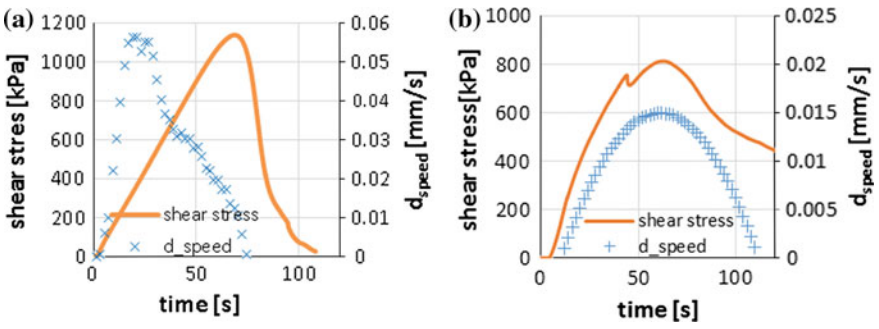


**Fig. 6** Dilatancy speed in the SISTM (**a**) and dilatancy speed in the SDSTM (**b**)

also records volumetric expansion and the trend over time shows that the dilatancy curve has an inflection in correspondence to the maximum shear stress. Figure 6b compares the shear stress with the dilatancy speed trend. As it can be seen from the graph, both curves achieve their maximum contemporarily when the normal load is constantly applied through the test. Moreover, $d_{speed}$ reaches zero when the shear achieves the residual value. This implies a residual strength even if the interface fails. In this condition, no volumetric expansion is required by the shear sliding, the two half specimens already being detached and the grains reoriented.

Experimental results show that the dilatancy phenomenon ends when the shear stress remains constant around the residual value. This confirms the theory of (Canestrari and Santagata 2005) whereby the correspondence between the achievement of the residual shear stress and the drop to zero value of the dilatancy parameter "d" is linked to the achievement of a final interface configuration where the overriding has already taken place. The dilatancy at the peak varies between less than 1 mm and about 2.5 as in the few cases with a normal pressure of 100 kPa.

For a better characterization of the dilatancy using the SDSTM, the relation between shear and dilatancy displacement can be enriched by the dilatancy angle ψ, estimated with the Bolton formulation. At the peak of the shear stress, all the specimens achieve a dilatancy angle between 11° and 19°. This variation in results is coherent with the assumption that the interface behaviour and dilatancy strongly depends on the interface roughness. This is because aggregate positioning at the interface that can affect the height of the peaks and thus the required dilatancy during the shear. On the other hand, the same composition of the specimen restricts the range of the dilatancy angle.

To quantify the other terms of the Bolton Eq. (1), a failure curve on the Mohr plane has to be defined to derive the Mohr circle for each level of normal pressure. The failure model selected in this research to better represent the asphalt interface behaviour is the Hoek-Brown criterion (Hoek and Brown 1980) as proposed by Ucar (1986). The suitability of this failure criterion to model the interface shear strength was investigated in Tozzo et al. (2015).

The failure curve for the soil has the following form:

$$\frac{\tau_\alpha}{\sigma_c} = A\left(\frac{\sigma_\alpha}{\sigma_c} - \frac{\sigma_t}{\sigma_c}\right)^B \tag{4}$$

where:

$\tau_\alpha$ and $\sigma_\alpha$ are the shear and normal stress at the failure plan
$\sigma_c$ is the uniaxial compressive strength
$\sigma_t$ is the tensile strength

A and B are constants dependent on the material properties

Using a computational software such as Wolfram Mathematica, the best fit of the experimental data ($R^2$ = 0.98) is achieved for the following values of the

parameters: A = 3.89; B = 0.815; and $\sigma_c$ = 3.73 kPa. $\sigma_t$ is equal to −300 kPa as the results of pull-off test.

The observed angle of shearing $\Phi'$ varies between 30° and 45°.

Bolton's equation gives $\Phi'_{crit}$ by subtracting the angle of dilatancy $\psi$ from the just computed angle of shearing $\Phi'$ in a simple shear test on loose soil. In the case of interface between asphalt layers, $\Phi'_{crit}$ could be tentatively associated with adhesion performance of the tack coat. This assumption is in accordance with the explanation proposed by Collop et al. (2003) regarding shear failure. The estimated values of these angles are reported in Fig. 7 in the order of decreasing $\varphi'$ and increasing normal pressure.

By increasing the applied normal stress the angle of dilatancy $\psi$ rises slightly. This can be attributed to lower shear displacements when normal stress is higher. In fact dilatancy displacements vary between 0.2 and 0.8 mm for the interface condition of this study. Further studies will be performed to confirm these achievements.

Finally to investigate dilatancy effects on the interface shear strength, tests using the SDSTM were replicated by inhibiting dilatancy. Shear strength and shear displacements are considered for the analysis. In Fig. 8 the comparison between the results obtained with both configurations is shown. The graph clearly highlights the increase in strength when the horizontal displacement is inhibited. The increase is constant at different levels of normal pressure. In the case of the kind of interface

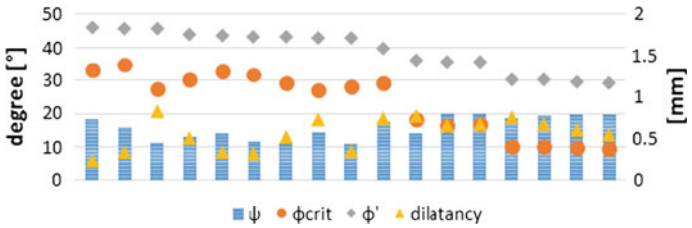


**Fig. 7** Dilatancy and shearing angles

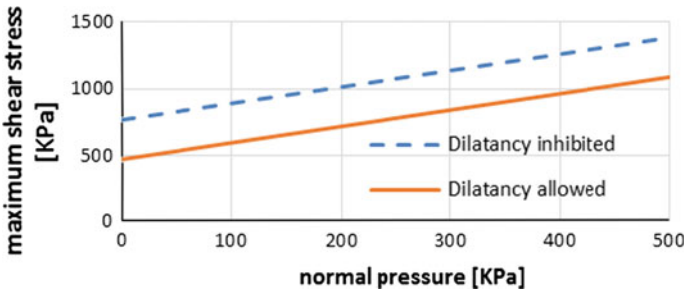


**Fig. 8** Comparison of the results in the conditions of allowed or inhibited dilatancy

investigated in this study, for the set test temperature, this corresponds to an increase of about 300 kPa.

On the other hand, for the shear displacement it is not possible to identify a clear trend between the test results. The outcomes are very scattered due to the natural variability of the interface roughness for the single specimen that strongly affects the shear displacements.

## 7 Conclusions

Dilatancy, defined as the shear-induced volume change in granular materials, was investigated analysing the results of two different shear test devices, the SISTM and the SDSTM. The parameters selected for the analysis were the dilatancy at the peak of the shear stress; the dilatancy angle, defined as the ratio between dilatancy and shear displacements, and the dilatancy speed.

It can be stated that:

- Dilatancy is scattered in both the test devices, due to the different roughness of each interface where aggregates distribution and protrusion can affect the volumetric expansion.
- In the SDSTM, dilatancy speed achieves the peak contemporarily with the shear stress. In the SISTM, the maximum of the dilatancy speed occurs before because the volumetric expansion of the specimen is countered by the normal stress, which increases proportionally to the shear stress during the test.
- By inhibiting dilatancy, the interface shear strength increases. The SDSTM results highlighted that this increment is equal to 300 kPa, regardless of the applied normal pressure.

With further research, different materials and interface treatments will be tested, as well as different test temperatures, to extend the quantification of dilatancy effects on shear strength to a range of test conditions.

## References

Bolton M (1986) The strength and dilatancy of sands Geotechnique 36:65-78.

Canestrari F, Ferrotti G, Partl MN, Santagata E (2005) Advanced testing and characterization of interlayer shear resistance Transportation Research Record: Journal of the Transportation Research Board 1929:69-78.

Canestrari F, Santagata E (2005) Temperature effects on the shear behaviour of tack coat emulsions used in flexible pavements International Journal of Pavement Engineering 6:39-46.

Collop A, Thom N, Sangiorgi C (2003) Assessment of bond condition using the Leutner shear test Proceedings of the ICE-Transport 156:211-217.

D'Andrea A, Russo S, Tozzo C (2013a) Interlayer shear testing under combined state of stress Advanced Materials Research 723:381-388.

D'Andrea A, Tozzo C, Boschetto A, Bottini L (2013b) Interface roughness parameters and shear strength Modern Applied Science 7:p1.
D'Andrea A, Tozzo C (2012) Interlayer Shear Failure Evolution with Different Test Equipments Procedia-Social and Behavioral Sciences 53:556-567.
Hoek E, Brown ET (1980) Empirical strength criterion for rock masses Journal of Geotechnical and Geoenvironmental Engineering 106.
Ozer H, Al-Qadi IL, Leng Z (2008) Fracture-based friction model for pavement interface characterization Transportation Research Record: Journal of the Transportation Research Board 2057:54-63.
Raab C, Partl MN, Halim A (2009) Evaluation of interlayer shear bond devices for asphalt pavements.
Reynolds O (1885) Lvii. on the dilatancy of media composed of rigid particles in contact. with experimental illustrations The London, Edinburgh, and Dublin Philosophical Magazine and Journal of Science 20:469-481.
Romanoschi SA, Metcalf JB (2001) Characterization of asphalt concrete layer interfaces Transportation Research Record: Journal of the Transportation Research Board 1778:132-139.
Tozzo C, D'Andrea A, Al-Qadi IL Prediction of fatigue failure at asphalt concrete layer interface from monotonic testing. In: Transportation Research Board 94th Annual Meeting, 2015. vol 15-3761.
Tozzo C, D'Andrea A, Cozzani D, Meo A (2014a) Fatigue investigation of the interface shear performance in asphalt pavement Modern Applied Science 8:p1.
Tozzo C, Fiore N, D'Andrea A (2014b) Dynamic shear tests for the evaluation of the effect of the normal load on the interface fatigue resistance Construction and Building Materials 61:200-205.
Trivedi A (2010) Strength and dilatancy of jointed rocks with granular fill Acta Geotechnica 5:15-31.
Ucar R (1986) Determination of shear failure envelope in rock masses Journal of geotechnical engineering 112:303-315.
UNI EN 12697-30 (2012) Bituminous mixtures. Test methods for hot mix asphalt. Specimen preparation by impact compactor ISBN 978 0 580 75767 9.

# Field Study to Investigate the Impact of Conditions of Application of Tack Coats on the Interlayer Bond Strength

**Alexandra Destrée, Joëlle De Visscher, Nathalie Piérard and Ann Vanelstraete**

**Abstract** The intrinsic characteristics of tack coats play an important role in the adhesion between layers, but the conditions of application of these coats are equally crucial. In this context, the Belgian Road Research Centre actively participates in a working group on tack coats with the objective to carry out a field study about interlayer bonding while evaluating the influence of different parameters– such as type and rate of spread of emulsion, nature and preparation of the underlayer, etc. With a view to this objective, a test site was constructed and the bond strengths were investigated by direct shear and direct tensile tests according to pre-standard prEN 12,697-48. This article describes the conditions of application, the measurements made on site and the results of the interlayer adhesion tests.

**Keywords** Tack coat · Interlayer bonding · Shear test · Direct tensile test

## 1 Introduction

Pavements are multi-layered structures and their overall bearing capacity and lifetime depend not only on the thickness and stiffness of each individual layer, but also on the bond between them. The purpose of a tack coat is to provide the necessary bond between layers. However, even if the intrinsic characteristics of tack coats (viscosity, breaking index, binder content and the characteristics of the residual binder) play an important role in the adhesion between layers, their conditions of application are equally crucial. In this context, the BRRC actively participates in a Belgian working group on tack coats initiated by the Walloon federation of road contractors and the Walloon public service. The objective of this joint working group is to carry out a field study on adhesion between layers while evaluating the influence of different parameters—such as tack coat type and

A. Destrée (✉) · J. De Visscher · N. Piérard · A. Vanelstraete
Belgian Road Research Centre (BRRC), Woluwedal 42, 1200 Brussels, Belgium
e-mail: a.destree@brrc.be



F. Canestrari and M.N. Partl (eds.), *8th RILEM International Symposium on Testing and Characterization of Sustainable and Innovative Bituminous Materials*, RILEM Bookseries 11, DOI 10.1007/978-94-017-7342-3_28

application rate, underlayer characteristics, curing time, etc.—using interlayer bonding tests described in the pre-standard (prEN 12697-48 2013). A suitable location was found on the regional road N3 at Fléron in Belgium, which is a road with one traffic lane and one cycle track in each direction and a central reserve lane in the middle. A stretch of 600 m length and 9 m width was divided into eleven sections of each 150 m length differing in type of tack coat, rate of spread of residual binder, curing time and type of underlayer (see Sect. 4).

## 2 Objective

The objective of this field study was to investigate the factors that influence the adhesive bond provided by the tack coat at the interface between pavement layers. These factors include:

- *Type of tack coat*: cationic anti-adhesive bituminous emulsions, C60B1 50/70 and C65B150/70
- *Rate of spread of emulsion:* various target residual binder quantities are considered, ranging between 150 and 350 g/m$^2$
- *Nature and preparation of the underlayer:* milled surfaces (milling speed: 5, 10 and 17 m/min) cleaned with a high-pressure suction sweeper, new asphalt concrete (AC 20) and new bitumen-bound graded aggregate (GB 20)
- *Curing time* of the emulsion before overlaying (AC 20, SMA 10): 1, 3 and one night.

The bond strengths were investigated by direct shear and direct tensile tests (see Sect. 3) according to pre-standard prEN 12697-48. These two interlayer bonding tests give complementary information on the mechanical performance of the interface. To collect a maximum of useful information for the interpretation of the aforesaid interlayer adhesion tests, several measurements were performed on site (see Sect. 6) and the two tack coats were evaluated for conventional properties (EN 13808, see References).

## 3 Interlayer Bonding Tests

### *3.1 Shear Bond Test (SBT)*

The specimens are cores with a diameter of (150 ± 2) mm, conditioned and tested at 20 °C, using a Leutner shear test device. The test is strain-controlled at a rate of (50 ± 2) mm/min. Shear strength is calculated as the average of three specimens. Switzerland (SN 640 430b 2008) and Germany (FGSV 2003) (Stöckert 2002) specify minimum average shear strength limits for tack coat in function of the tested interface (Table 1).

**Table 1** Leutner shear test specifications (on 150 mm diameter cores)

| Interface | Minimum average shear strength (MPa) | |
|---|---|---|
| Wearing course-binder course | 0.85 | 1.41 |
| Binder course-base layer | 0.68 | 1.13 |
| Reference | (SN 640 430b), (FGSV 2003) | (Stöckert 2002) |

### *3.2 Tensile Adhesion Test (TAT)*

The specimens are cores with an outer diameter of 150 mm. A concentric ring-shaped groove (100 ± 2) mm is drilled into the surface layer of the specimen, to a depth of 10 mm below the interface. The specimens are conditioned and tested at (10 ± 1) °C. The test is stress-controlled by applying a tensile force (200 N/s) until failure. Tensile bond strength is calculated as the average of three specimens. Austria specifies minimum tensile strength at 0 °C depending on the nature of the tack coat (Table 2).

For the two above-mentioned interlayer bonding tests, according to prEN 12697-48, after the specimens fail, they are visually inspected to determine what mode of failure has occurred: adhesion break (at the interface), cohesion break (within the pavement layer) or mixed break (partly at the interface and in the pavement layer).

## 4 Construction of the Test Sections

In August 2013, the following construction work was carried out on the eleven sections of this test site on the regional road N3 at Fléron (Fig. 1):

- On Sections 1–4: milling (speed = 10 m/min for Sections 1, 2a–4a and 17 m/min for Sections 2b–4b) and replacement of the wearing course by a 3.5 cm thick layer in SMA 10
- On Sections 5–8: milling (speed = 5 m/min) and replacement of the binder course and the wearing course by a 7 cm thick layer in AC 20 and a 3.5 cm thick layer in SMA 10
- On Sections 9–11: laying of a crushed stone base, followed by the successive application of 12 cm of new bitumen-bound graded aggregate (GB 20), 7 cm of AC 20 and 3.5 cm of SMA 10.

**Table 2** Tensile test specifications (RVS 08.16.01 2010)

| Tack coat type | Minimum average tensile strength at 0 °C (MPa) |
|---|---|
| Unmodified | 1.00 |
| Polymer-modified | 1.50 |

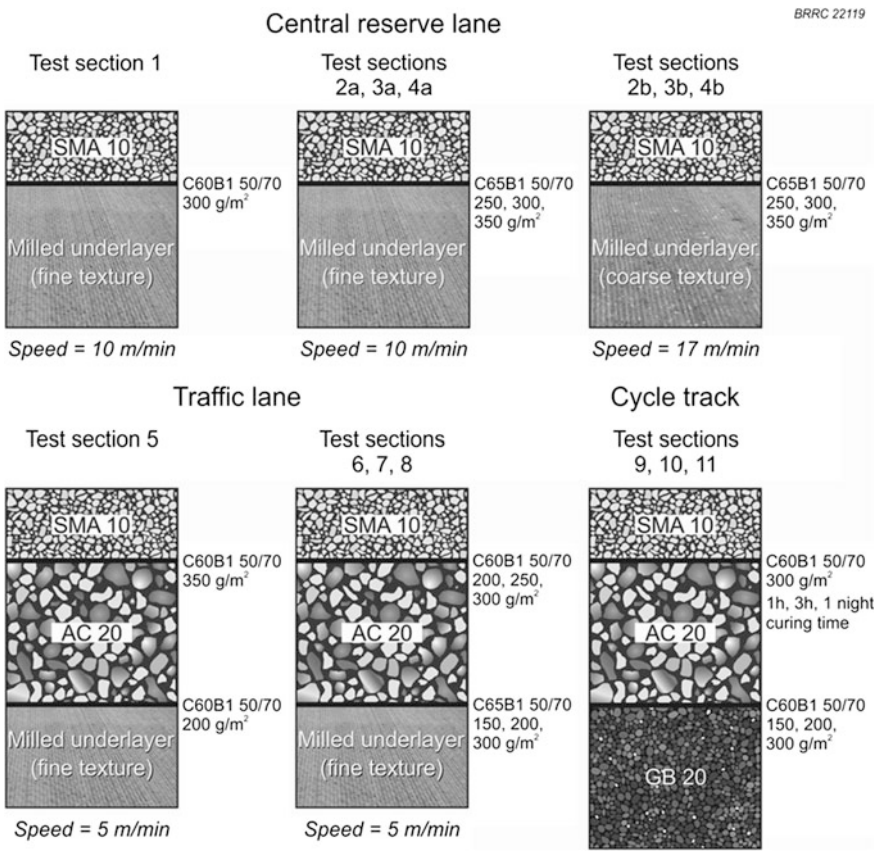


**Fig. 1** Broad outline of the construction layout of the eleven test sections (The rate of spread of emulsion is expressed in target residual binder quantities in g/m$^2$)

A tack coat (C60B1 50/70, C65B1 50/70) was applied to the underlayers of the eleven test sections (milled underlayers, AC 20, GB 20) at different target residual binder rates (ranging between 150 and 350 g/m$^2$) prior to the HMA overlay construction (AC 20, SMA 10).

## 5 Properties of Tack Coats

Two tack coats were used on the test site: the first, C60B1 50/70, has a residual binder content of 60 % and the second, C65B1 50/70, of 65 %. The tack coat with the highest bitumen content is expected to be more appropriate for milled underlayers (with much macrotexture), as it will flow less because of its higher viscosity —thereby avoiding the accumulation of emulsion in troughs and the absence of

**Table 3** Characteristics of tack coats and their residual binders

| Characteristics | C60B1 50/70 | C65B1 50/70 |
|---|---|---|
| pH | 2.1 | 1.9 |
| Binder content (%) | 60.3 | 65.1 |
| Breaking value (Sikaisol) | 40 | 49 |
| Efflux time 2 mm at 40 °C | 42 | 45 |
| Penetration at 25 °C (1/10 mm) | 45 | 48 |
| Softening point (°C) | 52.3 | 51.9 |

emulsion on peaks. These emulsions were tested with various standardized European tests (EN 13808 2013). The results presented in Table 3 indicate that the binder contents of the two emulsions are in agreement with their specifications and that the two tack coats and their residual binders have equivalent characteristics.

## 6 Measurements on Site

The various underlying layers in the eleven test sections were characterized in terms of texture (EN 13036-1 2010), compaction monitoring, temperature, humidity, cleanliness (Lavoie 2014) and tack coat application rates (EN 12272-1 2012). The analysis of these characteristics leads to the following findings:

- Macrotexture (characterised by mean texture depth-MTD) is significantly different between the four types of underlayer analysed (see Fig. 1) and can be ranked in ascending order, as follows:
  - Very smooth (MTD ≤ 0.50 mm): AC 20 (*Sections* 5–11)
  - Smooth (MTD > 0.70 mm): GB 20 (*Sections* 9–11)
  - Fine texture (1.60 mm ≤ MTD ≤ 2.00 mm): Milled underlayers (*Sections* 1, 2a–4a *and* 5–8)
  - Coarse texture (MTD ≥ 2.40 mm): Milled underlayers, milled at high speed (*Sections* 2b–4b)
- The AC 20 courses were all compacted by a total sequence involving eight roller passes or more, to ensure adequate and uniform compaction. The only exception was Section 11, which was far less compacted with only five roller passes.
- Before spraying of the tack coats, all underlayers were well above 15 °C, a moisture content lower than 2.5 % and they were free from ponding or runoff water.
- The cleanliness of the milled underlayers could generally be rated as excellent on the scale proposed by MTQ (Lavoie 2014).

- The two emulsions were spread at an average temperature of approximately 85 °C and all the measured application rates were relatively close to the target rates. For correctness these target rates will always be expressed in measured residual binder content throughout the chapter seven where the interlayer bonding results will be discussed. We will only specify the target residual binder contents when comparing test sections where these small deviations from target have no or very limited influence compared to impacts of other laying factors.

## 7 Results of Interlayer Bonding Tests and Discussion

An analysis of variance (ANOVA) was performed using Microsoft Excel statistical analysis. The ANOVA was conducted with level of significance, α of 0.05, in order to analyse and compare the maximum average tensile or shear bond strength in function of the four tested factors that may influenced the interlayer bonding (Sects. 7.1–7.4). For the sake of simplicity and concision this paper will not present the ANOVA analysis results of the interlayer bonding tests but they have been taken into account in our interpretations and our conclusions.

### *7.1 Influence of Tack Coat Type*

According to Fig. 2, there is no significant statistical difference in the mean shear and tensile strengths between the two emulsion types. These two tack coat types used for the milled underlayers (fine texture) give mean shear and tensile values that reach and even exceed in general the higher average requirements specified in

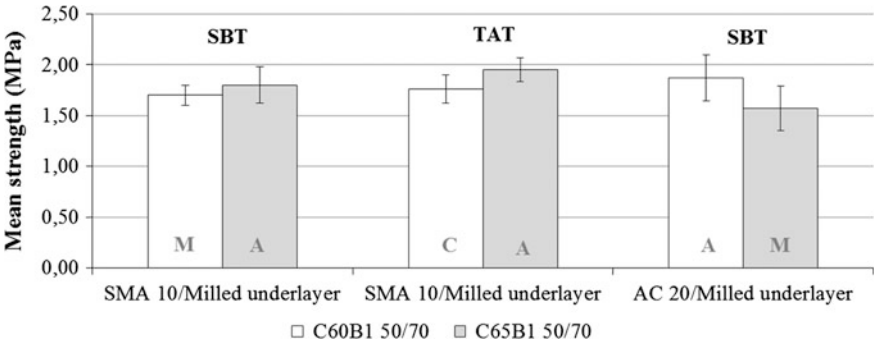


**Fig. 2** Results of interlayer bonding tests (SBT, TAT)-Impact of tack coat type on milled underlayers. Note that the failure modes are indicated in each bar (*A* adhesion, *C* cohesion, *M* mixed). The *error bars* represent the standard deviation

Tables 1 (1.41 MPa) and 2 (1.50 MPa), respectively. The application on a fine milled underlayer of a binder content tack coat of 65 % as opposed to a lower content one (60 %) does not seem to have a positive influence on the adhesion between the two tested upper layers (SMA 10 or AC 20). The results seem logical in view of the similar intrinsic characteristics of the two types of tack coat used and the small differences in binder content (see Sect. 5). Nevertheless, it can be seen that the average values for shear and tensile strength are systematically lower in mixed (*partly in the bottom layer, partly at the interface*) or cohesion (*in the bottom layer*) failure modes in comparison with adhesion failure (*at the interface)*. It is then logically hypothesized that interlayer bond strength probably decreases with poor compaction of the underlayers because this means lower inner cohesion. This finding indicates that the internal cohesion of the two layers present in the tested cores has a real impact on interlayer adhesion.

## 7.2 *Influence of Tack Coat Application Rate*

The analysis of the interlayer bonding results in the Figs. 3 and 4 leads to the following findings:

- *For the interface between the SMA 10 surface course and the milled underlayers* (Fig. 3), in general no significant statistical difference in shear strength is recorded between the various measured tack coat application rates. We note nevertheless that the higher tack coat application rate on AC 20 underlayer gives a slightly lower average shear strength value. This tendency can be explained by the nature of the underlayer itself; the AC 20 is new and therefore has a coat of mastic at the surface that may also play a role in interlayer adhesion. As a result, the total amount of binder at the interface may be too high and consequently

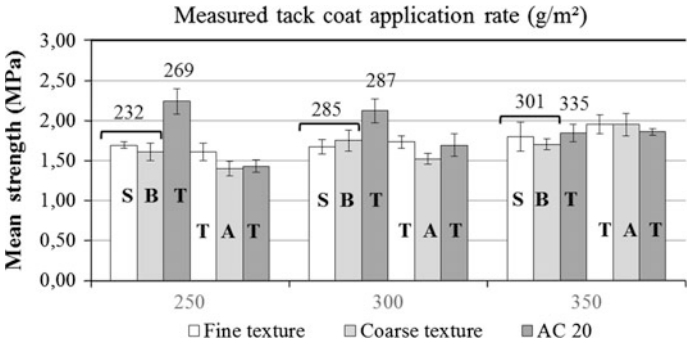


**Fig. 3** Results of interlayer bonding tests (SBS, TAT)-Impact of tack coat application rate and nature and preparation of the underlayer for the interface between SMA 10 and three underlayers. Note that the measured tack coat rates are indicated above each bar. The *error bars* represent the standard deviation

allow some displacement between layers, thereby slightly reducing shear strength. On the other hand, when analysing the results from direct tensile tests it appears that in comparison with the underlayer in AC 20, the milled underlayers (fine and coarse textures) are more sensitive to variations in tack coat application rate. The impact is small, but there is a trend for average tensile strength to increase with application rate. It is well known that when a tack coat is spread on milled underlying layers with a deep macrotexture, it may accumulate in the troughs and remain absent from the peaks if the rate of spread is not adapted to the macrotexture in place. This fact could, therefore, explain the increase in average strength with the tack coat application rate on the milled underlayer. We also note that all the tack coat application rates used for the underlayers give mean shear and tensile values that reach and even exceed in general the average requirements specified in Tables 1 (1.41 MPa) and 2 (1.50 MPa), respectively.

- *For the interface between the AC 20 and the milled underlayer-fine texture* (Fig. 4), we note that the higher tack coat application rate gives a slightly higher average shear strength value but the differences are not significant and all the measured tack coat application rates used give mean shear values that reach and even exceed the stricter requirement specified in Table 1 (1.13 MPa).
- *For the interface between the AC 20 and the GB 20* underlayer (Fig. 4), no significant statistical difference in shear strength is recorded between the two lower measured tack coat application rates but these values don't even reach the least requirement specified in Table 1 (0.68 MPa). We note also that the higher tack coat application rate on GB 20 underlayer gives a significantly higher average shear strength value that even exceeds the requirement specified in Table 1 (1.13 MPa). The low shear strengths could find their origin in the level of compaction of GB 20. Since the GB 20 is probably richer in voids than specified, the emulsion may have percolated into its underlayer rather than playing its role in providing adhesion to the binder course in AC 20. With a

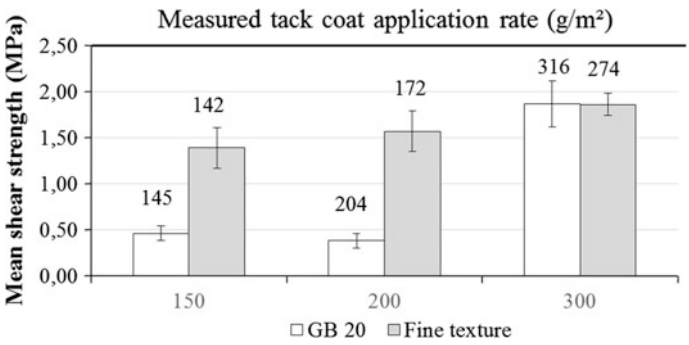


**Fig. 4** Results of shear bond test-Impact of tack coat application rate and nature and preparation of the underlayer for the interface between AC 20 and two underlayers. Note that the measured tack coat rates are indicated above each bar. The *error bars* represent the standard deviation

measured tack coat rate of 274 ± 39 g/m$^2$ the emulsion is able to play its role as a tack coat, in spite of possible percolation into the bitumen-bound graded aggregate. In this case equivalent strength values are observed as for other type of underlying surfaces with sufficient tack coat quantities (shown in Fig. 3).

## 7.3 *Influence of Nature and Preparation of the Underlayer*

Given that the results for the two emulsions are equivalent (see Sect. 5), for same target tack coat application rates, it can be concluded that:

- *For the interface between the SMA 10 surface course and the milled underlayers* (Fig. 3), no significant difference in average shear and tensile strengths are recorded and these values reach and even exceed the average specifications specified in Tables 1 (1.41 MPa) and 2 (1.50 MPa), respectively. It can be seen that the AC 20 underlayers exhibit higher average shear strength than the milled underlayers, except for the higher application rate where there is no significant difference. This trend observed between the two underlayer types can be explained by their nature. As a matter of fact, a milled underlayer is less "malleable" than an underlayer in AC 20; this characteristic may imply fewer contact points for the surface course to anchor itself in the rough surface of the milled underlayer, thus explaining the lower individual values for shear strength. This effect is probably more important for a surface course like SMA 10, due to its stony skeleton and relatively large stones. On the other hand, a slight difference in average tensile strength can be noted between the two textures of the milled underlayer, with the fine-textured underlayer almost systematically giving higher values than the coarse-textured underlayer. This difference can be explained by the fact that owing to its greater specific surface, an underlayer with a finer texture will offer more contact points for the overlying layer. When spread to an insufficient residual binder rate, the tack coat will be unable to cover the surface entirely if the relief of the underlayer is too strong (coarse texture), which will result in lower tensile strength. The higher residual binder rate seems ideal to make up for the fewer contact points in the coarse-textured underlayer, as the same tensile strengths are obtained as with the fine-textured underlayer.
- *For the interface between the AC 20 and the two underlayers* (Fig. 4), there is a significant difference in average shear strength between the underlayer in GB 20 and the milled underlayer, albeit only for the first two ranges of tack coat application rates. The GB 20 underlayer performs markedly lower for interlayer adhesion than the milled underlayer. The reasons were explained in Sect. 7.2.

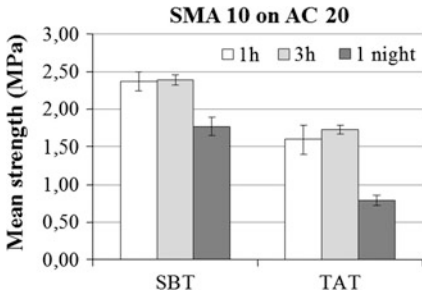


**Fig. 5** Results of interlayer bonding tests (SBS, TAT)-Impact of curing time. The *error bars* represent the standard deviation

### *7.4 Influence of Curing Time*

From Fig. 5, it can be concluded that there is no significant statistical difference in the mean shear and tensile strengths between 1 and 3 h but in case of one night, the mean strengths are clearly lower than the two other curing times:

- For curing times of 1 and 3 h, the mean shear and tensile values greatly exceed the average requirements in the Tables 1 (1.41 MPa) and 2 (1.50 MPa), respectively.
- For curing time of 1 night, the mean shear value however reaches the requirement (1.41 MPa) but the mean tensile value comes up to only 0.79 MPa.

After analysing the types of failure in the core samples taken from section with 1 night curing time, it appears that the poorer interlayer adhesion in this section could find its origin in the level of compaction of the AC 20 layer. In comparison with sections with 1 h and 3 h curing times, the AC 20 layer was, indeed, much less compacted (test Section 11, see Sect. 6), leading to a higher voids content that resulted in poorer internal cohesion. Additionally, part of the emulsion may have percolated into the less compacted and therefore, more porous underlying layer, thereby reducing its contribution to interlayer adhesion.

## 8 Conclusions

The construction work was carried out, in the eleven sections of the field study on the regional road N3 at Fléron in Belgium, with weather (hot, dry, windy and sunny) and site conditions (underlayer ≥ 15 °C, clean, dry and not too coarse-textured; emulsion spread to evenly cover the underlayer and at an adequate temperature) that were favourable. The following are the conclusions of this field study:

- *Interlayer bonding tests requirements*. For the most part, all the field conditions (tack coat type and application rate, surface roughness, curing time) lead to

average shear and tensile strengths that reached comfortably the German and Austrian requirements, respectively. Only in case of the GB 20 underlayer, the requirements are not always met.

- *Tack coat application rate.* There was a slight effect of the application rates on the interlayer bond strength. The optimum binder rate seems to depend strongly on the type and texture of the underlayer. In case of a milled layer or a porous underlayer such as GB 20, a high application rate is needed. In case of a new and dense underlayer such as AC 20, the residual rate should be within limits because an excessive amount of tack coat can cause potential slippage between layers (particularly in case of binder-rich layers).
- *Preparation of the underlayer*. The surface conditions of the underlayer including cleanliness, wetness and efficient compaction, are very important factors that influence the bond strength at the interface. It is recommended that tack coat be applied to a clean, dry and well-compacted underlayer.
- *Nature of underlayer*. It seems to turn out that milling and the type of milling has an influence on the strengths, in particular for low (insufficient) spread rates. Once the spread rate is high enough, there is no influence. The reason is that with an insufficient spread rate, the tack coat will be unable to cover the surface entirely if the relief of the underlayer is too strong (coarse texture).
- *Curing time.* The shortest two curing times (1 and 3 h) seem to have a similar impact on interface bonding performance. It could be not demonstrated that an extended curing time has a positive effect on the strengths. They were even lower than for the shorter curing times (1, 3 h). This could be explained by a poorly compacted underlayer.

The paper shows that many parameters influence adhesion in a significant way: tack coat application rate, curing time, nature and preparation of the underlayer (texture, cleaning, internal cohesion…). These parameters also interfere with each other. Understanding why in some cases parameters have an influence and why in some others the same parameters do not have an influence, is only possible if the whole picture is taken into account.

**Acknowledgments** The authors wish to thank ir. P.-P. Brichant for the choice of the different variants and the planning of the works and all logistic support. This research was only made possible by the contractor Gravaubel. The authors are grateful to them for their contribution. The authors also express their gratitude to the Belgian Bureau for Standardisation for the financial support for the development of the mechanical performance tests. In addition the authors wish to thank gratefully O. Moens, F. Kaddouri and P. Crabbé for their technical support.

## References

EN 12272-1 (2012) Surface dressing: test methods. Part 1 Rate of spread and accuracy of spread of binder and chippings.

EN 13036-1 (2010) Road and airfield surface characteristics. Test methods. Part 1 Measurement of pavement surface macrotexture depth using a volumetric patch technique.

EN 13808 (2013) Bitumen and bituminous binders. Framework for specifying cationic bituminous emulsions.

FGSV (2003) Forschungsgesellschaft für straβen und verkehrswesen. Arbeitsanleitungen zur prüfung von asphalt. ALP A-StB, Teil 9. Bestimmung der haftzugfestigkeit von dünnen schichten im heiβ und kalteinbau.

Lavoie M (2014) Formation sur la mise en œuvre des enrobés. Formation interne. Ministère des Transports du Québec (MTQ).

prEN 12697-48 (2013) Bituminous mixtures. Test methods for hot mix asphalt. Part 48 Interlayer Bonding.

RVS 08.16.01 (2010) Technical contract conditions. Bituminous base and wearing courses. Requirements for bituminous courses.

SN 640 430b (2008) Enrobés bitumineux compactés. Conception, exécution et exigences relatives aux couches en place. Chapitre G Exigences relatives aux couches et leurs contrôles. Partie 45 Liaison entre les couches, p 23.

Stöckert U. (2002) Ein Beitrag zur Festlegung von Grenzwerten für den Schichtenverbund im Asphaltstraßenbau. Dissertation. Technische Universität Darmstadt.

# The Use of Four-Point Bending Notched Beam Fatigue Tests to Rank Crack-Mitigating Interlayers

**Andrew D. Wargo, Shayan Safavizadeh and Richard Y. Kim**

**Abstract** The laboratory characterization of reflective crack-mitigating interlayer systems has been challenging due to the difficulty in establishing loading conditions that can simulate field behavior. Due to their widespread use in characterizing the fatigue resistance of single-layered asphalt concrete (AC) specimens, four-point beam fatigue tests are considered to be possible index tests for evaluating the behavior of various systems. However, the boundary conditions of the beam fatigue test and the criteria used to determine failure of the system with interlayers must be taken into account or else the results can be misleading. In this study, notched layered AC beams with various interlayer systems were subjected to four-point bending fatigue tests. The interlayer systems included three geosynthetics (two paving mats and one paving fabric), a chip seal layer, and a tack coat-only sample. Digital Image Correlation (DIC) was used to monitor deformation and crack propagation within these beams, and the results from the DIC analysis were compared with traditional beam fatigue failure criteria to evaluate their ability to rank the relative performance of the samples. This study found that commonly used beam fatigue failure criteria are inadequate measures of performance for layered beam tests, as they are incapable of quantifying all of the damage mechanisms that occur within layered samples, and that rankings obtained using these criteria can be misleading. Future research is needed to develop improved failure criteria and a better understanding of the correlation between the behavior of the interlayer systems tested in the four-point bending test and behavior in the field.

**Keywords** Reflective cracking · Beam fatigue · Fabric · Chip seal · Digital image correlation (DIC)

A.D. Wargo (✉) · S. Safavizadeh · R.Y. Kim
North Carolina State University, Raleigh, USA
e-mail: adwargo@ncsu.edu

S. Safavizadeh
e-mail: ssafavi@ncsu.edu

R.Y. Kim
e-mail: kim@ncsu.edu



F. Canestrari and M.N. Partl (eds.), *8th RILEM International Symposium on Testing and Characterization of Sustainable and Innovative Bituminous Materials*, RILEM Bookseries 11, DOI 10.1007/978-94-017-7342-3_29

## 1 Introduction

Over the last century, the world's paved roadway networks have developed gradually. Often, for maintenance and preservation, new pavement layers were simply added on top of existing roadways in order to take advantage of the structural capacity of the underlying pavement. Today, it is common practice to place a relatively thin layer on top of an existing pavement. Frequently, this practice comes in the form of a thin asphalt concrete (AC) overlay of existing flexible, rigid, or composite pavement. However, the practice of placing AC overlays onto existing cracked or jointed pavements presents unique challenges to highway agencies and roadway engineers. Specifically, the discontinuities in the existing pavement can cause stress concentrations in the new AC overlay (Kazimierowicz 2008; De Bondt 1999). These stress concentrations then cause rapid cracking in the new AC surface. Because the pattern of these cracks in the overlay resembles the cracks in the existing pavement, this phenomenon is known as reflective cracking.

Although reflective cracking has been recognized as a problematic pavement distress for many years, it has been difficult to mitigate. The main reasons for the difficulties in reflective crack mitigation are related to the complex nature of its causes and numerous contributing factors. Reflective cracking is driven mainly by traffic loading (shear and bending) and thermal effects in the pavement (tension and curling) (Lytton et al. 2010).

Over the years, many different types of interlayer systems have been designed to help mitigate reflective cracking (Caltrans 2001). These systems are placed between the AC layers in an attempt to reinforce the pavement structure or absorb the stress concentrations caused by the cracks in the existing pavement. Many trials and research projects have been conducted using these interlayer systems with varying degrees of success. Part of the reason for the mixed results is the inherent variability of field construction and environmental conditions. Therefore, it is desirable to have a small-scale test that can simulate the behavior of these systems in the laboratory. However, because of the complex nature of the reflective cracking phenomenon, the simulation of reflective cracking in the laboratory is difficult. No single test method is available that can accurately simulate all the modes of loading or environmental conditions in a manner consistent with actual field behavior. Even so, several test methods have been employed to simulate a single mode of loading or environmental condition. The overlay tester simulates thermal cracking (Zhou and Scullion 2005), vertical shear tests simulate the effects of traffic-induced shear (De Bondt 1999), and beam tests simulate the effects of traffic-induced bending. Also, scaled-down wheel load devices are available to simulate various traffic-related effects (Wargo et al. 2014). Each type of test has limitations, which should be considered carefully when attempting to correlate the test results with the field behavior of pavements subjected to reflective cracking.

One common test method, beam fatigue testing, has been undertaken by several researchers to help characterize reflective cracking (Jimenez and Meier 1985; Sulaiman and Stock 1995; Sousa et al. 2000; Zhengqi and Dengliang 2000; Bennert

and Maher 2008; Vismara et al. 2012). Although beam fatigue tests are limited by the boundary conditions of the test, useful information about the behavior of interlayer systems may still be obtained from them.

## 2 Objectives

The main objectives of this research are: (1) to investigate the reflective cracking performance of asphalt concrete reinforced with interlayer systems via four-point bending notched beam fatigue (NBF) tests and Digital Image Correlation (DIC) method and (2) to evaluate the validity of various failure criteria to rank the performance of interlayer materials.

In this research, two main sources of information were used to obtain data regarding the beam fatigue test samples. The first was DIC method, which allows the tracking of full-field strain and displacement contours of the surface of the specimen. This DIC information can be used to identify areas of cracking within the sample, to determine movement that occurs at the interface of the layer sample, and to visualize ways that such movement affects the overall behavior of the NBF test sample. The second source of information was provided by the load and displacement measurements obtained from a servo-hydraulic test machine. This data was then used in conjunction with existing beam fatigue failure criteria. It was hoped that these criteria might be linked to the behavior observed in the DIC analysis. In this way, laboratories that do not have access to DIC equipment could use the load and displacement failure criteria to rank interlayer systems empirically, even though these criteria were not developed originally to be used with layered samples or with samples that exhibit crack localization and propagation. Also, if clear correlations between the existing failure criteria and the mechanisms observed using DIC analysis were evident, then future researchers might be able to correlate the mechanisms present in beam fatigue testing with the actual field behavior of samples through the use of finite element modeling.

## 3 Materials and Methods

The procedure used for fabrication and testing of all NBF samples is as follows. First, using a roller compactor, a 50 mm × 305 mm × 400 mm slab of AC was compacted. After cooling, the selected interlayer system was applied to the surface of this layer. Next, a second AC layer was compacted to bring the height of the total sample to 100 mm. Three 64 mm wide beams were then sawn from the center of the slab in order to reduce the effects of high air voids near the edges of the mold. These beams were trimmed to the final dimensions (54 mm × 64 mm × 400 mm, with the interlayer located 18 mm from the bottom of the sample) and a 5 mm × 2.6 mm (L × W) notch was cut in the center across the full width of each beam. These

beams were then painted and speckled to provide contrast and improve the accuracy of the DIC system. Next, the samples were placed in a four-point bending beam fatigue test device inside an environmental chamber. The beams were then temperature-conditioned at 20 °C for 2 h. Displacement-controlled haversine loading was then applied using a servo-hydraulic loading machine until a crack was seen to penetrate the full depth of the specimen. The displacement amplitudes were selected to produce 900 μ strain at the bottom of the beam during maximum displacement and were applied at a frequency of 5 Hz. Load and displacement data were tracked using an 11.1 kN load cell and linear variable displacement transducers (LVDTs). Full-field strains, displacements, and crack propagations were monitored in the samples using the DIC technique. It should be noted that test temperature and loading frequency were selected to be reasonably consistent with typical rates found in literature and the strain level was selected in order to ensure failure could be seen in the geosynthetic samples within a reasonable time period.

In this study, three geosynthetics were used in the NBF tests: a paving mat consisting of fiberglass fibers coated in an elastomeric compound embedded between two polyester textiles (paving mat #1), a paving mat consisting of a nonwoven blend of fiberglass and polyester fibers (paving mat #2), and a nonwoven polypropylene paving fabric. Also, samples containing a chip seal interlayer consisting of 8.14 kg/m$^2$ of a 9.5 mm crushed granite aggregate (#78 m) embedded in a cationic, rapid setting emulsion (CRS-2) with a CRS-2 fog seal placed on top were fabricated. Lastly, tack coat-only samples consisting of CRS-2 emulsion were constructed to serve as control samples. Two replicates of each interlayer system were tested. Table 1 shows the binder application rates for each interlayer type, which were selected based on typical field application rates.

As expected, the construction of each interlayer system was slightly different. The three geosynthetic samples were constructed by placing a predetermined amount of binder on the surface and smoothing it using a heated spatula, and then placing the geosynthetic on top by hand. The chip seal system was constructed by pouring a predetermined amount of CRS-2 emulsion onto the surface and spreading it with a notched squeegee, covering the emulsion with 10.85 kg/m$^2$ aggregate, then placing a rubber sheet onto the aggregate and seating it using a steel wheel roller. After curing, the chip seal sample was swept to remove the loose aggregate. The loose aggregate was weighed in order to determine the final aggregate retention rate of 8.14 kg/m$^2$, and a fog seal was applied to the surface of the chip seal to help it bond with the overlay and help the interlayer behave more like a Stress Absorbing

**Table 1** Interlayer tack coat information

| Interlayer type | Paving mat #1 | Paving mat #2 | Paving fabric | Tack coat | Chip seal w/fog seal |
|---|---|---|---|---|---|
| Tack coat rate (l/m$^2$) | 0.77 | 0.91 | 1.13 | 0.32 | 1.84 (chip seal)/0.36 (fog seal) |
| Tack coat type | PG 64-22 | PG 64-22 | PG 64-22 | CRS-2 | CRS-2 |

Membrane Interlayer (SAMI). The control system was constructed by brushing a premeasured mass of CRS-2 emulsion onto the surface.

# 4 Results

## 4.1 Digital Image Correlation Data

Digital image correlation measurements were the most informative data gathered from the NBF tests. These results provided information about crack propagation in the beams as well as the interfacial behavior of the samples. Von Mises strain (Eq. 1) contour plots (Fig. 1) were used to identify areas of cracking and damage as well as to help determine the primary damage mechanisms.

$$\varepsilon^e = \frac{\sqrt{2}}{3}\left[(\varepsilon_1 - \varepsilon_2)^2 + (\varepsilon_3 - \varepsilon_2)^2 + (\varepsilon_3 - \varepsilon_1)^2\right]^{1/2} \quad (1)$$

where $\varepsilon_1$, $\varepsilon_2$, and $\varepsilon_3$ are the principal strains at an element, and $\varepsilon^e$ is the Von Mises strain.

Based on these results, the researchers observed differences in behavior among the various interlayer types. Three different general descriptions of damage evolution within the different sample types were developed:

- For the tack coat-only samples, cracking penetrated through the bottom AC layer with minimal interfacial movement; the crack spent little to no time 'trapped' at the interlayer, and rapidly propagated through the top layer.
- For the geosynthetic samples, cracks began to propagate in the bottom AC layer, and then interfacial movement started to occur. Once the vertical crack reached the interlayer, interfacial movement increased significantly. This interfacial movement helped to stall the crack at the interface for some time before cracking (both top-down and bottom-up) in the top layer caused a full-depth crack to develop.
- For the chip seal samples, crack initiation in the bottom AC layer occurred simultaneously with high interfacial movement. Also, stress concentrations due to the chip seal aggregate helped to initiate cracks in the top AC layer early on. Next, increased interfacial movement occurred once the crack penetrated all the way to the interface. Then, one or more top-down cracks formed in the top layer. Lastly, one pair of top-down and bottom-up cracks became dominant and eventually joined, creating a full-depth crack.

In addition to the Von Mises strains, component strain field (horizontal, vertical, and shear strains) contour plots were used to understand the mechanisms that caused the areas of high strain seen in the Von Mises contour plots. By viewing these figures for all samples tested, the researchers found that both separation and sliding occurred at the interface for all the samples. Both the magnitude and the

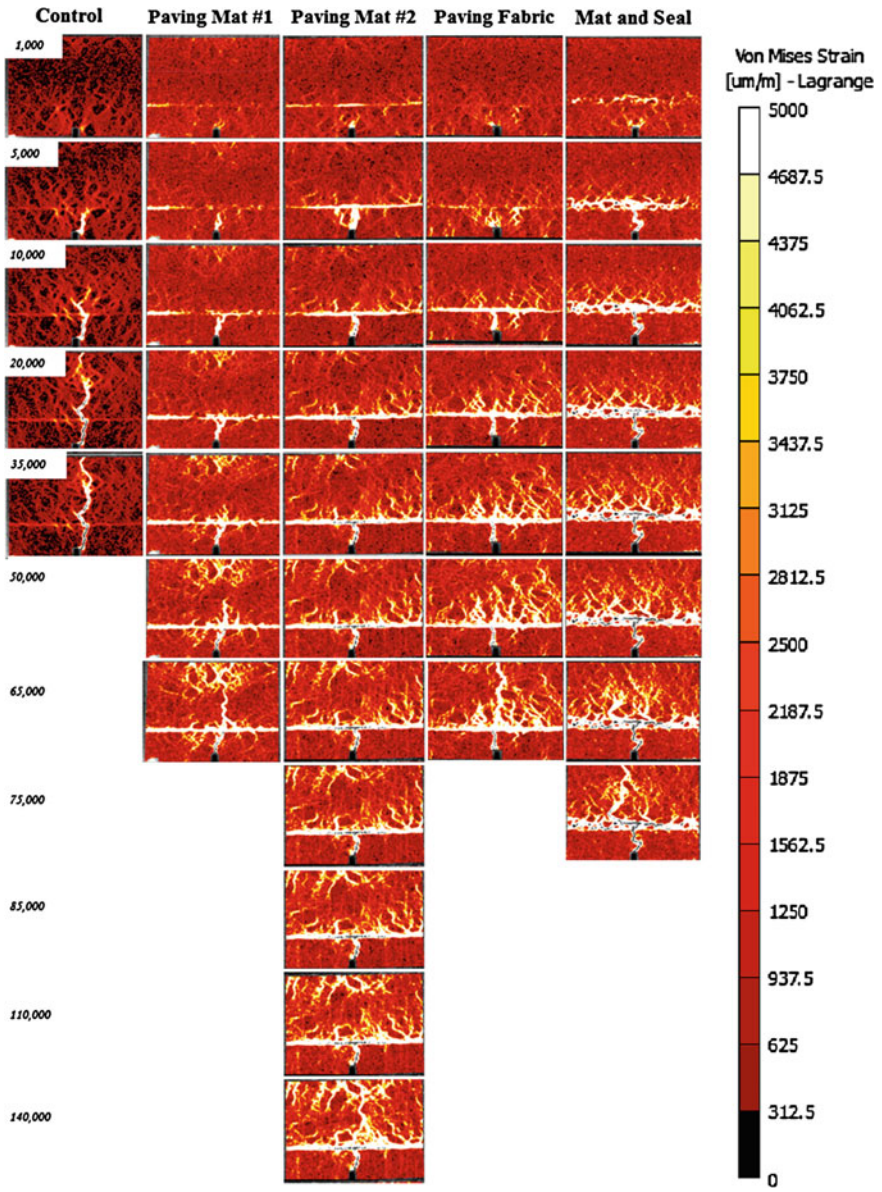


**Fig. 1** Crack propagation in the NBF test

timing of these interfacial movements depended on the type of interlayer used, with samples containing reflective crack mitigating interlayer systems exhibiting more substantial interfacial movements that occurred earlier in the test as compared with the control samples.

## 4.2 Stiffness Graphs

An independent set of data collected during each test included the load and displacement information obtained from the test machine. Using these data, several parameters could be determined and compared with the DIC results. First and foremost was the stiffness parameter. Stiffness was defined using the definition of stiffness in ASTM D 7460, which incorporates sample geometry, loading geometry, and displacement amplitude by using traditional beam theory to calculate the maximum stress and strain within the beam sample, and defining stiffness as the ratio of these two parameters. This stiffness value was used for several purposes. First, the stiffness value was simply plotted versus the number of cycles.

Because constant displacement amplitude was used, the stiffness value was at its highest initially and then continuously dropped throughout the test. Changes in the slope of this line tended to correspond to physical changes that occurred within the sample, as seen in the DIC contour plots. Figure 2a presents a representative curve and identifies the major regions and points. It should be noted that not all of the samples for all of the conditions tested exhibited all of these characteristics, but rather, this figure is meant to provide a summary of the potential mechanisms.

The first region of Fig. 2a is associated with interfacial movement and cracking in the bottom AC layer, as in many cases both of these phenomena occurred simultaneously at the beginning of the test. During this phase, as the crack approaches the interlayer, a significant drop in stiffness occurs. This drop corresponds to a significant increase in interfacial movement, as seen in the DIC results. However, because the DIC method can only measure cracking at the surface of the beam, it is expected that the crack actually reaches the interlayer at different times across the width of the beam. Therefore, point A is considered to be the point where the crack has reached the interlayer across the full width of the beam.

The second region of the graph is typically the longest and is characterized by a slow, steady decline in the stiffness curve. This stiffness decrease is due to micro- and macro-crack initiation and propagation within the top AC layer and further interfacial damage. The end of this region (point B) is often characterized by the initiation of one or more top-down cracks in the beam.

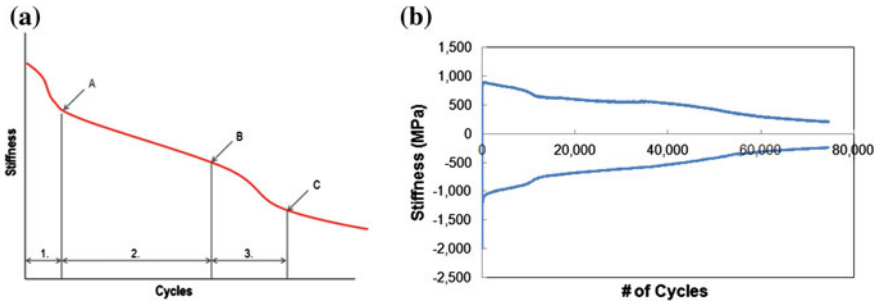


**Fig. 2** **a** General behavior of NBF stiffness. **b** Example of real stiffness data

The last region of the graph represents a nonlinear decrease in stiffness and is associated with the formation of 'dominant' cracks within the top AC layer and their propagation toward one another. The end of this region is marked by point C, where the cracks have reached the full depth of the sample. It should be noted, however, that point C often is not well defined, which is likely due to problems that are similar to those associated with point A.

Although it may appear that the failure of the sample is characterized well by the stiffness curve, stiffness curves derived from actual test data are generally harder to interpret, with regions that are less obvious. Often, it is the DIC information that allows the researcher to determine the points and regions of the graphs accurately, rather than simply using the stiffness curve itself to find these points. Additionally, even in cases where clearly defined regions are present, the accuracy of this type of analysis is dependent on the scale on which the graph is plotted and, therefore, is subjective (Fig. 2b). It should be noted that the negative stiffness in this graph is related to the peak displacement of the sample and positive stiffness is associated with the load required to pull the sample back to the zero position.

## *4.3 Failure Criteria*

In an attempt to find a more quantitative measure of failure due to the load response of the sample, several types of failure criteria were employed in this study. These failure criteria include stiffness-based criteria, an energy-based criterion similar to that found in ASTM D 7460, and the phase angle drop failure criterion. In order to determine which criteria are useful in describing the behavior of the beam samples, each was compared to several DIC-based criteria.

**Stiffness Criteria**. The stiffness criteria employed were typical stiffness threshold criteria. These failure criteria involve finding the initial stiffness value of the sample (typically the stiffness value at cycle #50 or cycle #200) and defining failure as the point at which the stiffness of the sample has degraded below a certain threshold value. Threshold values of 50 and 20 % of the initial stiffness values are found in the literature (Shen 2011).

**Energy-based Criterion**. The energy-based criterion involves multiplying the stiffness of the sample for any given cycle by the number of cycles and plotting this value versus the number of cycles. The peak value of this plot is taken as the failure point (ASTM 2010).

**Phase Angle Failure Criterion**. In the cyclic testing of bituminous materials, it is well known that the peak stress and peak strain in the material occur at different times. A material property known as phase angle can be obtained by relating this time lag to the loading frequency of the test. For samples experiencing damage, the phase angle changes throughout the test, eventually reaching a point where a sharp drop in phase angle occurs. This phase angle drop point is often used as an indication of the failure of the material (Zhang 2013).

**DIC-based Criteria**. DIC-based criteria include: the number of cycles before cracks reach the interlayer, the number of cycles before cracks reach the full depth of the sample (full-depth DIC), maximum layer separation, and maximum interfacial sliding.

**Comparison of Failure Criteria**. Using all of this information, a correlation coefficient table was created to help identify the level of correlation among all of these parameters. Several important observations were made from this analysis:

- The parameters that correlated well with the DIC full-depth criteria were the ASTM failure criterion, the phase angle criterion, the 20 % of cycle #200 criterion, and the 20 % of cycle #50 criterion.
- In general, both of the 50 % reduction in stiffness criteria correlated somewhat with the number of cycles needed to reach the interlayer and the amount of layer separation. These criteria did not correlate well with the DIC full-depth criteria.
- The magnitude of sliding between layers did not relate significantly to any other parameter.

Additionally, some correlations that the researchers had expected to find based on their engineering judgment were not as significant as hypothesized. Specifically, early research had indicated that layer separation correlated fairly well with the number of cycles to reach full depth. In order to investigate this finding further, these parameters were cross-plotted, as shown in Fig. 3a.

This plot shows that most of the samples fall along a narrow band, with the chip seal layers falling significantly outside of this area. The reason for this discrepancy is twofold. First is the fact that the top AC layers of the chip seal samples contained multiple areas of stress concentration due to the presence of the chip seal aggregate. Thus, crack initiation in the top layer was highly dependent on the number and location of these stress concentrations. Secondly, the chip seal aggregate physically took up more space than the thin geosynthetic layers; thus, cracks in the top layer had less distance to travel to reach the surface of the sample. In order to eliminate this variability, a second correlation coefficient matrix was created by eliminating the chip seal data and rerunning the analysis. These results indicated that the amount of layer separation does correlate with the number of cycles to full-depth

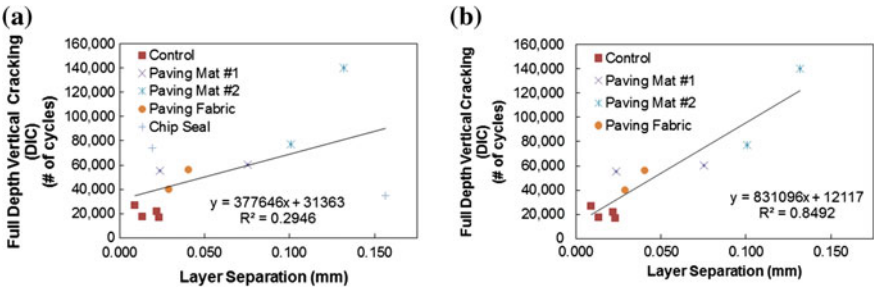


**Fig. 3** Correlation between layer separation and cycles to full depth cracking: **a** including chip seals and **b** geosynthetics and control samples only

cracking for all the control and geosynthetic samples. A cross-plot showing this improved correlation is presented in Fig. 3b.

## 5 Discussion

Because reflective cracking is associated primarily with full-depth cracks through the top AC layer, the full-depth DIC criterion was considered originally to be the best failure criterion for quantifying vertical crack growth. As such, all the other criteria were compared against it. The ASTM failure criterion was found to correlate well with the full-depth DIC criterion. The fact that the change in energy due to interfacial movement was small and occurred early on means that interfacial damage does not have a significant effect on the energy-based ASTM failure criterion peak value. Thus, the ASTM criterion value depends mostly on vertical crack growth in the AC layers, which is exactly what the full-depth DIC criterion measures.

The correlation between the ASTM criterion and the phase angle drop criterion also was not surprising. In reality, the phase angle drop is caused mainly by the method used to determine the phase angle. That is, once the sample has become severely damaged, the load response curve in a displacement-controlled test varies significantly from an actual sinusoidal function. This distortion is responsible for the drop in the phase angle. Because the energy dissipated within a cycle is highly dependent on the load shape, it is expected that an energy-based criterion, such as the ASTM criterion or the phase angle criterion, would be highly correlated.

The correlation of the 20 % of the initial stiffness criterion and the full-depth DIC criterion can be explained by the fact that the changes seen in the stiffness graphs were attributable mainly to vertical cracking within the samples. However, it was observed that, in some cases, the beams experienced full-depth cracking before the 20 % of cycle #200 failure threshold was ever reached, possibly due to the reinforcing effects of the geosynthetics. As such, the 20 % of cycle #50 criterion seems to be the better of the two 20 % stiffness-based criteria for ranking vertical crack growth in the sample, but it does not seem to provide any significant benefits over the phase angle or ASTM-based criteria in terms of simple ranking.

Good correlations were found between the layer separation and the full-depth DIC criteria if the chip seal cases were considered separately, as shown in Fig. 3b. This outcome was due mainly to the weaker interfacial bonds of the geosynthetic samples, which allowed more layer separation and energy dissipation within the beam. This separation caused the cracks to turn along the interlayer, increasing the time necessary to initiate new cracks in the top AC layer. However, this improvement was highly dependent on the boundary conditions of the NBF test, which does not capture the adverse effects of high levels of horizontal debonding. For this reason, the performance improvements seen from the NBF test results may not necessarily correlate with improved field performance. Furthermore, many studies, as well as general engineering experience, show that highly debonded layers lead to rapid failure in actual pavements (Baek 2010). Thus, the fatigue life that is based on

the number of cycles needed for the crack to reach the full depth of the beam (or any of the criteria that correlate with it) should not be used as a simple ranking criterion on its own. Rather, some balance must be found between the ability of an interlayer system to reduce vertical crack growth and resist shear and separation forces at the interface. Unfortunately, no load-based criteria or parameters that could accurately capture these effects using the NBF tests were identified in this study.

## 6 Conclusions

- The NBF test with the DIC technique can be used to investigate the vertical crack growth and horizontal debonding in asphalt concrete reinforced with interlayer systems under cyclic loading.
- The stiffness curves obtained from the NBF test results were able to provide useful information about the mechanisms of failure that occurred within the beams, but they could not fully characterize the behavior of all the test samples.
- The results of this study indicate that even though traditional beam fatigue failure criteria were not developed originally to be used with layered beams during crack localization, these criteria can still be useful in ranking the vertical crack propagation rate in NBF test samples.
- Interfacial movement that occurred in the NBF tests was substantial and significantly affected the vertical crack propagation rate for most of the interlayer systems tested. That is, substantial interfacial movement may cause significant delays in vertical crack growth.
- Shear testing, along with the numerical modeling of actual pavements, is needed in order to better correlate the horizontal debonding behavior seen in the NBF tests to the behavior of pavements in the field.
- In order for the NBF test to be used to rank interlayer systems for combined performance of vertical crack growth and horizontal debonding, better failure criteria would be needed to quantify the amount of horizontal debonding for a wide range of test conditions, ideally by correlating horizontal debonding to interfacial strength. Further development of DIC-based failure criteria might be useful for this purpose.

## References

ASTM D7460-10 (2010). Standard Test Method for Determining Fatigue Failure of Compacted Asphalt Concrete Subjected to Repeated Flexural Bending. American Society for Testing and Materials, West Conshohocken, PA.

Baek, J. (2010). Modeling Reflective Cracking Development in Hot-Mix Asphalt Overlays and Quantification of Control Techniques. Dissertation, University of Illinois at Urbana-Champaign.

Bennert, T. and A. Maher (2008). Field and Laboratory Evaluation of a Reflective Crack Interlayer in New Jersey. Transport Res. Rec., No. 2084, Washington, D.C., pp. 114-123.

Caltrans (2001). *Flexible Pavement Rehabilitation Manual*, California Department of Transportation.

De Bondt, A. H. (1999). Anti-Reflective Cracking Design of (Reinforced) Asphaltic Overlays. Dissertation, Delft University of Technology.

Jimenez, R. A. and W. R. Meier, Jr. (1985). Laboratory Evaluation of an Asphalt-Rubber SAL. Transport Res. Rec., No. 1034, Washington, D.C., pp. 86-96.

Kazimierowicz, K. (2008), Comparison of Stress and Strain States in Pavements With and Without Reflective Cracks. J. Transp. Eng., Vol. 134, pp.483-492.

Lytton, R. L. et al. (2010). Model for Predicting Reflection Cracking of Hot-Mix Asphalt Overlays. NCHRP Report 669, Washington, D.C.

Shen, S. and Z. Lu (2011). Energy Based Laboratory Fatigue Failure Criteria for Asphalt Materials. J. of Test. Eval., Vol. 39, No. 3. pp. 846-852.

Sousa, J. B. et al. (2000). Comparison of Laboratory Test Performance Between Asphalt-Rubber Hot Mix and Dense Graded Asphalt Concrete. Proceedings of the 4th International RILEM Conference, pp. 251-266.

Sulaiman, S. J. and A. F. Stock (1995). The Use of Fracture Mechanics for the Evaluation of Asphalt Mixes. J. of Assoc. of Asp. Pav. Tech., Vol. 64, pp. 500-533.

Vismara, S. A. et al. (2012). Characterizing the Effects of Geosynthetics in Asphalt Pavements. Proceedings of the 7th RILEM International Conference on Cracking in Pavements, Vol. 2, pp. 1199-1207.

Wargo, A. et al. (2014). The Reflective Cracking Tester: A Third-Scale Accelerated Pavement Tester for Reflective Cracking. Proceedings of the International Conference on Asphalt. Pavements, Raleigh, NC, pp. 1685-1693.

Zhang J. et al. (2013). Development of a Failure Criterion for Asphalt Mixtures under Fatigue Loading. Road Mater. Pavement, Vol. 14, Supplement 2, 2013, pp. 1-15.

Zhengqi, Z. and Z. Dengliang (2000). Evaluation of Geonet Reinforcement in Resisting Reflective Cracking of Asphalt Pavement. Proceedings of the 4th International RILEM Conference, pp. 455-462.

Zhou, F. and T. Scullion (2005). Overlay Tester: A Rapid Performance Related Crack Resistance Test. FHWA/TX-05/0-4467-2 Report, Texas Department of Transportation.

# Effects on Bonding of Anti-reflective Cracking Solutions at the Top Bituminous Interface of a Small Airport Pavement: A Laboratory and Modeling Study

**Piergiorgio Tataranni, Cesare Sangiorgi, Andrea Simone, Valeria Vignali, Pierpaolo Viola and Giulio Dondi**

**Abstract** The maintenance of bituminous airport pavements is of high concern when the limited available time for interventions and the performance effectiveness of the adopted materials are considered. In many cases, due to their former military vocation, small airport pavements have robust, sound and durable foundations that seldom require deep interventions of maintenance. Thus, it is more often needed to rehabilitate the pavement bituminous surface layers to restore the functional characteristics of the runaway and to protect the bottom layers from water leaching through the surface damages (e.g. cracks). This paper shows an example of airport pavement maintenance that was designed to rehabilitate the wearing course of a cracked bituminous structure that was proven to have sufficient bearing capacity. In order to prevent the reflection of cracks on the new layer, the effects of using both a geosynthetic net and a Stress Absorbing Membrane Interlayer (SAMI) were investigated at the old-new materials interface. The effects of debonding and the potential risk of slippage or delamination of the new wearing course were assessed by means of laboratory direct shear tests and multilayer elastic pavement system modeling.

**Keywords** Airport pavement · Bonding · Direct shear test · Bituminous interface

## 1 Bonding Between Bituminous Layers

In the recent years a number of research groups have studied the relevant aspect of the interface bonding of both roads and airports pavements (Collop et al. 2003; Raab and Partl 2004; Canestrari et al. 2005; Mohammad et al. 2012). In order to get

P. Tataranni · C. Sangiorgi (✉) · A. Simone · V. Vignali · P. Viola · G. Dondi
Department of Civil, Chemical, Environmental and Materials Engineering (DICAM), Alma Mater Studiorum, University of Bologna, Bologna, Italy
e-mail: cesare.sangiorgi4@unibo.it

P. Tataranni
e-mail: piergiorg.tataranni2@unibo.it



F. Canestrari and M.N. Partl (eds.), *8th RILEM International Symposium on Testing and Characterization of Sustainable and Innovative Bituminous Materials*, RILEM Bookseries 11, DOI 10.1007/978-94-017-7342-3_30

**Fig. 1** Nagoya airport debonding failure and high-speed taxi way slippage

the needed structural performance of the pavement, it is important that sufficient mechanical collaboration between the bituminous layers is guaranteed. A weak bonding leads to reduced bearing capacity of the pavement and to a reduction of its level of service; failures due to relative slippage between layers are possible and the detachment of surface layer portions can drastically reduce the functionality of the pavement as well as safety.

Delamination and debonding are very serious problems in airport pavements, because of the heavy loads from aircrafts and of the effects on airport management (Mejía et al. 2008); the issue is especially relevant where airplanes break or change in direction. The most critical conditions are given by the main landing gears of aircrafts that travel the pavement at full load and apply a sudden breaking. This may result in slippage between the wearing course and the bottom layer; in some critical cases it is possible that severe debonding occurs (Fig. 1).

A number of factors influence the shearing strength of the interface bonding and should be taken into account when pavement design and material selection is done: the layer thickness: a thicker layer reduces the interface shear stresses; the adhesion and cohesion of binders at the interface; the quantity and the adhesive and cohesive characteristics of the tack coats; the interlocking given by the reciprocal contacts of aggregates from the top and bottom layer at the interface; the presence of interlayer materials; the pavement temperature at the interface.

Today the methods for the assessment of bonding of bituminous interfaces can be non-destructive (PSPA, Hammer test, FWD, etc.), or simulating direct shear on double layer pavement portions in the laboratory (Leutner Test, ASTRA, Wedge test, etc.) (Mohammad et al. 2012). A recent interlaboratory research on different interlayer bonding properties of asphalt pavements was run by RILEM TC 237 SIB (TG4—Multilayer Systems Testing) where a set of testing procedures was performed on three interface conditions of real pavement (Canestrari et al. 2012).

This work aims at developing the interface design of a small Italian airport pavement under rehabilitation. The effects on interface bonding of three different solutions and the potential risk of slippage of the new wearing course are assessed by means of laboratory direct shear tests and multilayer elastic system modeling.

**Table 1** Design pavement structure and materials referred to a conventional temperature of 20 °C

| Layer | Material | Thickness (mm) | Modulus (MPa) | Poisson |
|---|---|---|---|---|
| 1 | Top hot mix asphalt | 50 | 2000 | 0.35 |
| 2 | Existing hot mix asphalt | 230 | 4716 | 0.35 |
| 3 | Existing granular mixed base | 240 | 1024 | 0.38 |
| 4 | Existing natural subgrade | – | 237 | 0.40 |

## 2 Runway Rehabilitation Project

The rehabilitation project of the runway of the considered airport consists in the replacement of the top bituminous layer (thickness 50 mm); in particular the existing pavement is made of a 280 mm thick bituminous layer and a 240 mm thick unbound granular foundation constructed over the natural subgrade. Falling Weight Deflectometer (FWD) testing showed a sufficient bearing capacity of the base and foundation layers and thus the designers focused the rehabilitation on the functionality of the top layer by replacing only the surface bituminous material. Table 1 shows the design pavement layers, their thickness and average elastic modulus of the existing layers estimated with FWD tests. A modulus of 2000 MPa is considered for the new polymer modified hot mix asphalt, in accordance with laboratory test results on similar materials.

## 3 Numerical Modeling

A Bisar-like software based on the multi-layered elastic system theory was used to model and design the airport pavement structure: in particular shearing forces at the first bituminous interface were considered relevant for this kind of rehabilitation intervention. For the verification of the design, results from modelling will be compared to data obtained from direct shear testing in the laboratory.

### *3.1 Loads Applied by Airplanes*

Based on traffic data and on information provided by the airport management, Airbus A330-300, as airplane with the largest weight, and Boeing B737-800, as airplane with the largest traffic frequency per year, have been chosen for the evaluation of the critical shear stress. Both airplanes have a tricycle landing gear. The tricycle arrangement has one nose gear in the front and two main gears under the wings. The two main gears are designed to take most of the airplane weight (around 95 %). Main gear includes 4 wheels in a double tandem configuration for the A330-300 and 2 wheels in a twin configuration for the B737-800 (Fig. 2).

**Fig. 2** Airbus A330-300 (*left*) and Boeing B737-800 (*right*)

**Table 2** Airbus A330-300 and Boeing B737-800 maximum weights

| Operations | A330-300 | B737-800 |
|---|---|---|
| Maximum taxi weight (kg) | 233,900 | 78,471 |
| Maximum takeoff weight (kg) | 230,000 | 78,245 |
| Maximum landing weight (kg) | 187,000 | 65,317 |

**Table 3** Main gear: force per single wheel, tire size and pressure

| Force (kN) | A330-300 | B737-800 |
|---|---|---|
| Vertical | 274 | 183 |
| Horizontal | 220 | 146 |
| Characteristic | | |
| Tire size | 1400 × 530 R23; 54 × 21-23 | H44.5 × 16.5–21 28 PR |
| Tire pressure | 14.5 bar (1450 kPa) | 14.4 bar (1440 kPa) |

Table 2 reports the maximum weights of both airplanes during the different operations. Data are taken from the technical specification of the airplane producers (A330 2011, B737 2010).

Assuming the weight is equally distributed on the wheels of the main gear, the vertical and horizontal forces on each wheel during the aircraft braking are shown in Table 3. The horizontal force is the maximum horizontal ground load declared by the producers. Tire type and pressure (Table 3) allow calculating the tire-pavement contact area through which the loads are distributed to the pavement.

## *3.2 Multilayered Elastic Models*

In the first analysis, the forces applied on the pavement are the vertical and horizontal loads of the airplane with the maximum weight: the Airbus A330-300; vertical loads are evenly distributed over an equivalent circular surface with a contact stress equal to the tire pressure, approx. 1450 kPa. The radius of the contact surface is 24.5 cm. Figure 3, shows the model with the load configuration.

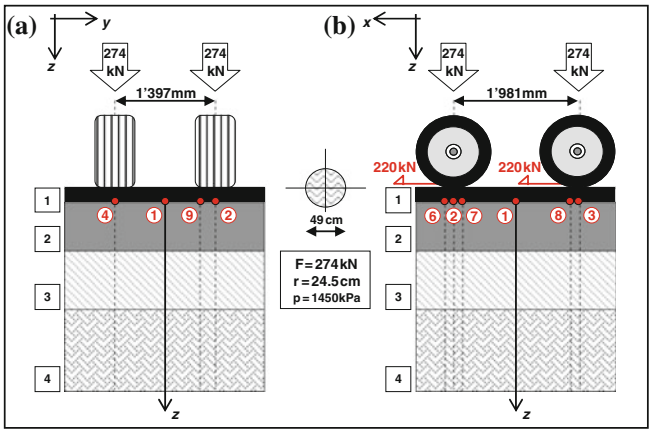


| Calculation points | | |
|---|---|---|
| pt. | x (m) | y (m) |
| 1 | 0.000 | 0.000 |
| 2 | 0.990 | 0.698 |
| 3 | -0.990 | 0.698 |
| 4 | 0.990 | -0.698 |
| 5 | -0.990 | -0.698 |
| 6 | 1.235 | 0.698 |
| 7 | 0.745 | 0.698 |
| 8 | -0.745 | 0.698 |
| 9 | 0.990 | 0.453 |

**Fig. 3** Pavement model with A330-300 loads: **a** x-z view, **b** y-z view and calculation points

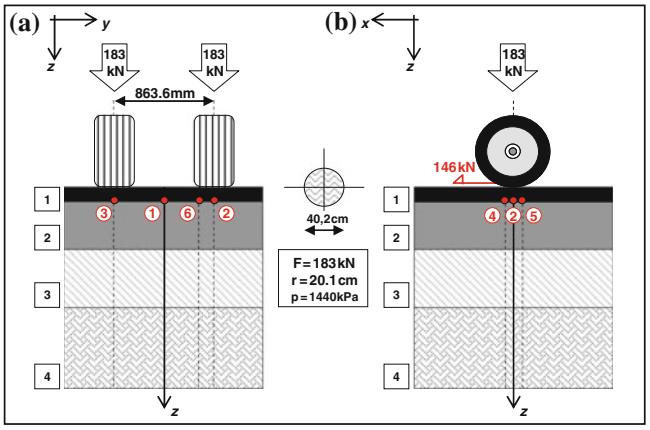


| Calculation points | | |
|---|---|---|
| pt. | x (m) | y (m) |
| 1 | 0.000 | 0.000 |
| 2 | 0.000 | 0.431 |
| 3 | 0.000 | -0.431 |
| 4 | 0.201 | 0.431 |
| 5 | -0.201 | 0.431 |
| 6 | 0.000 | 0.230 |

**Fig. 4** Pavement model with B737-800 loads: **a** y-z view, **b** x-z view and calculation points

Figure 3 shows the points at the interface between the new and the existing asphalt concrete layers where stresses, strains and displacements are calculated. The pavement analysis focused on the developed horizontal shear stresses $\tau_{xz}$.

Figure 4 shows the model adopted for the Boeing B737-800 analysis.

## 3.3 *Modeling Bonding with the Spring Compliance Modulus*

Particular attention should be paid to model a bond condition between pavement layers that differs from the perfect bonding. The Spring Compliance Modulus (*Ks*)

assumes that the shear stress at the interface produces a relative displacement between top and bottom layers which is proportional to the shear stress itself.

*Ks* is also defined as the inverse of the Horizontal Reaction Modulus (*K*), introduced by Goodman (Goodman et al. 1968) and adopted by Uzan (Uzan et al. 1978) to represents the bond condition of a multilayer flexible pavement: the bonding between two layers is similar to a thin film of material with shear modulus (*G*) and thickness (*t*) and the interface shear stress ($\tau$), due to the applied external load, produces a relative horizontal displacement ($\Delta u$):

$$\tau = (G/t) \cdot \Delta u \tag{1}$$

that can be written as,

$$\tau = K \cdot \Delta u \tag{2}$$

where ($\tau$) is in N/m$^2$, ($\Delta u$) in m and the Horizontal Reaction Modulus (*K*) at the interface is expressed in N/m$^3$. Equation (2) represents the Goodman's law that describes the behavior at the interface in an elastic multi-layer structure and the modulus (*K*) is assumed as constant.

## 4 Trial Field

In order to assess the shear strength at the interface between the new asphalt concrete layer and the existing pavement, direct shear tests have been performed on layered samples cored from a trial field constructed in proximity of the runway. The trial field aim was to investigate the effective bonding obtained adopting the materials and technologies potentially available for the runway rehabilitation. The trial field was made with three different interface technologies to be compared: a Polymer modified Bitumen (PmB) emulsion tack coat, a geosynthetic grid with bituminous bond coat and a bituminous Stress Absorbing Membrane Interlayer.

### *4.1 Trial Field Construction*

The trial field was built on an existing airport pavement adjacent to the runway. The existing bituminous pavement and its materials were considered equivalent.

The existing pavement was milled to a depth of 50 mm and cleaned. The surface was then divided into 3 sections as follows (Figs. 5 and 6):

- Section 1: PmB bituminous emulsion with 70 % of residual bitumen;
- Section 2: PmB emulsion and a fiberglass grid (25 × 25 mm) reinforcement geosynthetic with polymer coating;
- Section 3: SAMI with PmB emulsion and limestone aggregates.

The three sections were completed laying a 50 mm thick PmB wearing course.

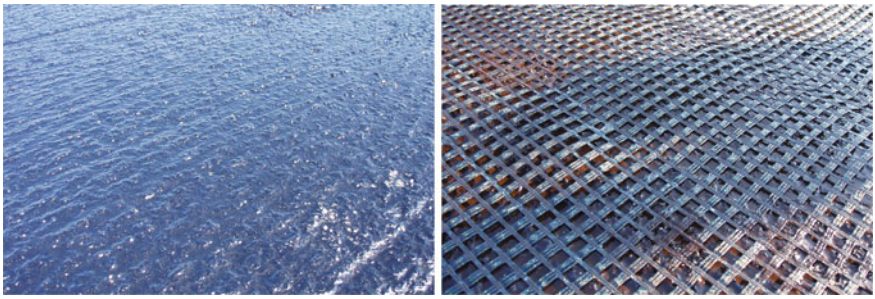

**Fig. 5** PmB emulsion section (*left*) and fiberglass grid section (*right*)

**Fig. 6** SAMI section (*left*) and trial field completion with PmB wearing course (*right*)

## *4.2 Cores and Direct Shear Testing*

After construction cores were taken from the trial field (Table 4).

Direct shear testing on each sample were performed by means of the Leutner device according to ALP A-Stb 2312 (1999) (Fig. 7). Testing conditions are: 20 °C and 50.8 mm/min constant speed. The test result are the load (shear)-displacement curve to failure and the peak values of force and displacement. It should be noted that standard Leutner testing does not apply a normal load to the specimen while shearing and no displacement is measured in that direction. In real pavements and in the described models a normal load is applied by wheels.

**Table 4** 150 mm diameter cores codes

| Sample | Trial site section | Cores code |
|---|---|---|
| S1 | Section 1 | 01EM, 02EM,03EM, 04EM |
| S2 | Section 2 | 11GR, 12GR, 13GR, 14GR |
| S3 | Section 3 | 06SA, 07SA, 08SA |

**Fig. 7** Leutner shear testing and a tested specimen

## 5 Comparison Between Laboratory Test Results and Models

Table 5 shows the Leutner testing results from the three groups of specimens.

Stresses are calculated assuming a constant shear circular surface. Peak loads and displacements describe the strength and the ductility of the bonding at the interface. Average values show that sample S1 is the strongest, while S3 is the weakest; S2 has slightly higher average strength than S3. Displacements are always lower than 2 mm.

It was then possible to compare the shear test results with the stress-strain output from the multilayered elastic modeling. A set of models output was recorded using different Spring Compliance Modulus at the shear interface, corresponding to different bonding conditions. The maximum shear stresses at the first bituminous interface and for different bonding conditions were considered for both aircrafts models. On the other hand, to allow the comparison, Spring Compliance Moduli

**Table 5** Leutner test results, peak values of force, displacements at peak

| Sample | Spec | Force (kN) | Avg (kN) | τ max (kPa) | Avg (kPa) | Displ (mm) | Avg (mm) |
|---|---|---|---|---|---|---|---|
| S1 | 01EM | 11.57 | 16.55 | 720.51 | 1030.40 | 2.04 | 1.79 |
| | 02EM | 20.84 | | 1297.54 | | 1.84 | |
| | 03EM | 12.85 | | 799.89 | | 1.50 | |
| | 04EM | 20.94 | | 1303.64 | | 1.76 | |
| S2 | 11GR | 10.49 | 11.42 | 653.35 | 711.36 | 2.00 | 1.70 |
| | 12GR | 14.76 | | 918.96 | | 1.80 | |
| | 13GR | 9.22 | | 573.97 | | 1.38 | |
| | 14GR | 11.23 | | 699.14 | | 1.62 | |
| S3 | 06SA | 8.73 | 9.74 | 543.44 | 606.54 | 1.64 | 1.62 |
| | 07SA | 9.81 | | 610.61 | | 2.02 | |
| | 08SA | 10.69 | | 665.56 | | 1.20 | |

**Table 6** Spring compliance moduli (*Ks*)

| Sample | Spec | *Ks* ($m^3$/N) | Avg ($m^3$/N) |
|---|---|---|---|
| S1 | 01EM | 2.83E−09 | 1.87E−09 |
| | 02EM | 1.42E−09 | |
| | 03EM | 1.88E−09 | |
| | 04EM | 1.35E−09 | |
| S2 | 11GR | 3.06E−09 | 2.44E−09 |
| | 12GR | 1.96E−09 | |
| | 13GR | 2.40E−09 | |
| | 14GR | 2.32E−09 | |
| S3 | 06SA | 3.02E−09 | 2.71E−09 |
| | 07SA | 3.31E−09 | |
| | 08SA | 1.80E−09 | |

were calculated from Leutner test curves at very small displacements (less than 0.1 mm). Failure curves are approximately linear before the peak and the shear stress-displacement slope at the very beginning of the test can be assumed as the Horizontal Reaction Modulus (*K*) at the interface. Briefly, the slope coefficient of the Leutner curves at small displacements can be considered a good estimate of the real Horizontal Reaction Modulus (*K*) (i.e. of the Spring Compliance Modulus) and of the actual bonding condition between the layers.

Table 6 summarizes the *Ks* values and the average results for the three samples. It should be noted how the *Ks* are always lower than 1.0E−08 that is generally assumed as the possible higher limit and representative of a debonded condition.

Nevertheless a consistent difference is visible between the three samples values as represented in Fig. 8.

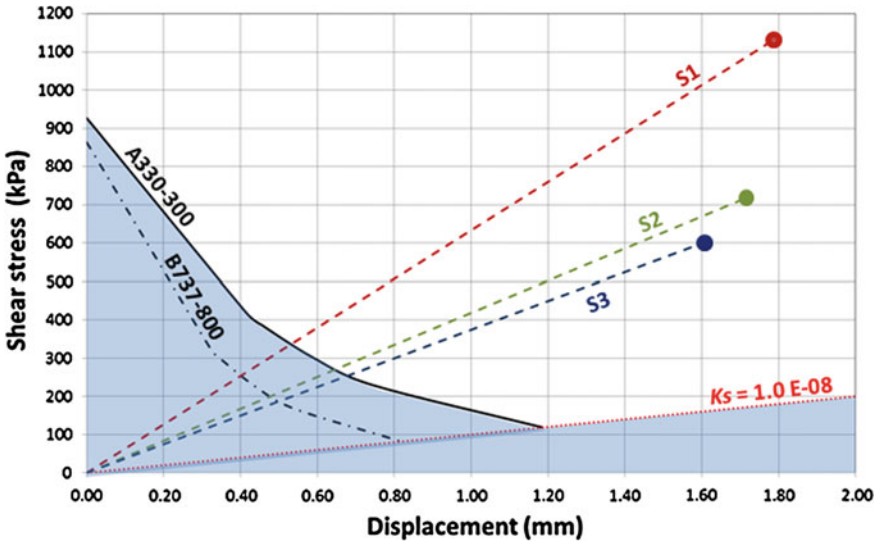


**Fig. 8** Stress-displacement graph: comparison between tests and models results

The strongest stresses at the bituminous interface are produced by the breaking of the Airbus A330-300. Hence, the average values from laboratory shear tests can be compared with the curve of maximum shear stress-displacement from the same aircraft obtained with the multilayered elastic models. This curve plots the limits of the stress-displacement pairs that correspond to potential bonding failures at the modeled interface when an A330-300 instantaneously breaks on the runway.

The three tested samples taken from the trial field real pavement exhibit values above these limits and show that all three sections have admissible bonding conditions with displacements at failure ranging between 1.6 and 1.8 mm. The *Ks* value for sample S1 is greater showing an higher stiffness of the bonding created with the sole use of PmB emulsion. The two anti-reflective cracking solutions, on the other hand, show similar but less stiff and resistant bonding as generally happens for these interlayer bituminous systems.

It can also be seen that at each real effective Spring Compliance Modulus, the interfaces could withstand single breaking conditions producing higher stress-displacement pairs; in particular, the available strength above the A330-300 curve is larger for the S1 interface.

Interface bonding fatigue due to repeated loading (breaking) and the simultaneous effects of other forms of distress are not considered in this analysis. Also, the effects of permanent reciprocal slippage at the interface on residual bonding and on pavement functionality are not taken into account.

## 6 Conclusions

This paper shows the verification of different solutions of rehabilitation at the interface between the new asphalt concrete layer and the existing bituminous pavement of a small airport runway. The analysis has considered the shear conditions caused at 20 °C by the breaking of both the heaviest and the most frequent aircrafts.

A trial field was constructed in order to assess the bonding characteristics at the interface created by three different construction technologies. Three sets of specimens were cored and tested for direct shear strength by means of the Leutner method.

Test results have been compared with the stress conditions calculated at the new interface by means of multilayered elastic models, where instantaneous breaking configurations from A330-300 and B737-800 are applied.

It can be inferred that the three rehabilitation solutions at the interface show different behaviors. In particular, the section with PmB emulsion exhibits the strongest bonding with shear strength values from 300 to 400 kPa higher than the other two sections. The SAMI records are the lowest.

According to the bonding conditions reached in the trial field and represented by the Spring Compliance Modulus measured in the laboratory, it can be inferred that all the proposed rehabilitation solutions satisfy the minimum bond stiffness.

Furthermore, from the shear test-modeling comparison it can be deduced that none of the three rehabilitation solutions has bonding conditions lower than those obtained by the instantaneous breaking models. The S1 section, though, shows the highest values of stiffness and strength.

Finally, it should be noted that the proposed analysis is referred to the actions generated by single breaking events and does not take into account the resilience of the bonding with reference to the breaking actions produced in the same point of the runway by other aircrafts. Also, other temperatures and simultaneous forms of distress that can reduce the new interface bonding conditions have not been investigated and may be object of further studies.

## References

Canestrari F, Ferrotti G, Partl MN, Santagata E (2005) Advanced testing and characterization of interlayer shear resistance. Transp. Res. Rec. 1929, 69e78.

Canestrari F, Ferrotti G, Lu X, Millien A, Partl MN, Petit C, Phelipot-Mardelé A, Piber H, Raab C (2012) Mechanical testing of interlayer bonding in asphalt pavements. Advances in Interlaboratory Testing and Evaluation of Bituminous Materials. State-of-the-Art Report of the RILEM Technical Committee 206-ATB. p. 303–60.

Collop AC, Thom NH, Sangiorgi C (2003) Assessment of bond condition using the Leutner shear test. Proceedings of the Institution of Civil Engineers. Transport, vol. 156, p. 211-217, ISSN: 0965-092X.

Goodman RE, Taylor RL, Brekke TL (1968) A Model for the Mechanics of Jointed Rock Journal of the Soil Mechanics and Foundations Division, Proceedings of the American Society of Civil Engineers, Vol.94, May, pp.637-658.

Mejía D, Celaya M, Iyer S, Rao C, Shokouhi P, Nazarian S (2008) A Work Plan toward Evaluation of Technologies to Assess Presence and Extent of Delamination of HMA Airfield Pavements. Research Project 06-04: Non-Destructive Testing to Identify Presence and Extent of Delamination of HMA Airfield Pavements.

Mohammad LN, Elseifi MA, Bae A, Patel N, Button J, Scherocman JA (2012) NCHRP Report 712, Optimization of Tack Coat for HMA Placement, Transportation Research Board, Washington D.C.

Raab C and Partl M (2004) Interlayer Shear Performance: Experience with Different Pavement Structures.3rd Eurasphalt and Eurobitume Congress, Vienna.

Uzan J, Livneh M, Eshed Y (1978) Investigation of adhesion properties between asphalt concrete layers. Proceedings AATP, Vol.47, 495-521.

ALP A-Stb 2312 Teil 4 (1999), Prüfung des Schichtenverbundes nach Leutner.

# Geocomposite-Reinforcement of Polymer-Modified Asphalt Systems

**Francesco Canestrari, Gilda Ferrotti, Musab Abuaddous and Emiliano Pasquini**

**Abstract** Geosynthetic reinforcement has proven to be an effective method to improve road pavement performance. In this regard, composite materials obtained combining bituminous membranes with reinforcing grids represent a promising option thanks to the waterproofing and stress-relieving effect produced by the membrane and the enhanced mechanical characteristics provided by the grid. This research had the objective of evaluating the effectiveness of pavement rehabilitation by means of an optimized composite material, consisting of an elastomeric bituminous membrane reinforced with a fiberglass grid, applied at the interface of a polymer-modified asphalt system. An unreinforced reference configuration was also investigated for comparison purpose. Interlayer shear tests and three-point bending tests were performed on double-layered specimens in order to evaluate bond strength at the interface and toughness (i.e. fracture resistance) of the pavement system, respectively. Shear tests showed that the reinforcement at the interface reduces the bonding between asphalt layers even if a residual cohesion contribution is provided after shear failure. As far as flexural properties are concerned, the real contribution of the reinforcement consists in the delay of crack propagation rather than in the inhibition of crack initiation.

**Keywords** Grid-reinforced membrane · Shear strength · Flexural behavior

F. Canestrari · G. Ferrotti (✉) · M. Abuaddous · E. Pasquini
Polytechnic University of Marche, Ancona, Italy
e-mail: g.ferrotti@univpm.it

F. Canestrari
e-mail: f.canestrari@univpm.it

M. Abuaddous
e-mail: m.abuaddous@univpm.it

E. Pasquini
e-mail: e.pasquini@univpm.it



F. Canestrari and M.N. Partl (eds.), *8th RILEM International Symposium on Testing and Characterization of Sustainable and Innovative Bituminous Materials*, RILEM Bookseries 11, DOI 10.1007/978-94-017-7342-3_31

## 1 Introduction

Damage occurring in asphalt pavements leads to a growing need of effective rehabilitation methodologies. In this sense, the only application of an overlay above the damaged pavement could be ineffective due to reflective phenomena from existing cracks. On the other hand, the reinforcement with geosynthetics can be considered as a valid alternative since such materials are able to improve the mechanical properties of pavements against cracking (Austin and Gilchrist 1996; Brown et al. 2001; Ferrotti et al. 2012; Prieto et al. 2007; Shukla and Yin 2004; Sobhan and Tandon 2008; Vanelstraete and De Visscher 2004; Zamora-Barraza et al. 2011).

In particular, geocomposites (i.e. combination of two or more geosynthetic types) obtained combining bituminous membranes and reinforcing grids represent a promising solution as they intend to join the improved tensile properties of the reinforcements with the stress absorbing and the waterproofing effects of the membranes.

However, the presence of a reinforcement at the interface inevitably causes also a reduction of the interlayer bonding (Brown et al. 2001; Ferrotti et al. 2011; Pasquini et al. 2013; Zamora-Barraza et al. 2010) that influences the pavement response in terms of stress-strain distribution (Perkins and Edens 2002).

This paper illustrates a part of an ongoing wider research project which aims at evaluating the effectiveness of asphalt pavement rehabilitation with grid-reinforced membranes. In this research, double-layered systems prepared with mixtures containing a SBS polymer modified bitumen and reinforced with an optimized geocomposite (Canestrari et al. 2012; Pasquini et al. 2014a) were investigated. To this aim, interlayer shear tests and three-point bending tests were performed on double-layered reinforced samples. An unreinforced reference system was also investigated for comparison purposes.

## 2 Materials

Double-layered slabs were prepared in the laboratory with a dense graded asphalt concrete classified as AC16 according to EN 13108. Such a mixture was prepared with limestone aggregates and styrene butadiene styrene (SBS) polymer modified bitumen dosed at 5.7 % by the weight of the mix.

A cationic SBS polymer modified emulsion, classified as C65BP4 according to EN 13808, was used as tack coat at the interface of the unreinforced double-layered slabs (UN). The bituminous emulsion was spread at a rate of 0.15 kg/m$^2$ of residual binder.

The geocomposite selected as reinforcement is obtained by combining an elastomeric bituminous membrane, modified with SBS synthetic copolymers, with a fiberglass grid having a mesh size of 12.5 × 12.5 mm$^2$. The upper side of the

geocomposite is coated with a fine sand whereas the lower side is characterized by an auto-thermo-adhesive SBS-modified bituminous film. According to the product datasheet, the geocomposite has a thickness of 2.5 mm and is characterized by a biaxial behavior with identical tensile strength of 40 kN/m and tensile elongation at rupture less than 4 % in both the longitudinal and transversal direction.

## 3 Test Methods and Protocols

### *3.1 Laboratory Specimen Preparation*

Double-layered square slabs (305 × 305 $mm^2$) were compacted in the laboratory using a steel roller compactor compliant with EN 12697-33.

The lower layer was compacted with a thickness of 30 mm assuming a target of 5 % air void content. Then, it was left 4 h at room temperature for cooling before adding the tack coat or the geocomposite on its surface. Subsequently, a 40 mm thick upper layer was compacted with the same target air void content of the lower layer. Finally, the compaction direction was marked on the surface in order to perform tests in the traffic flow direction.

Two specimen types were obtained from the slabs: cores for Ancona Shear Test Research and Analysis (ASTRA) tests and beams for three point bending (3PB) tests. From each slab, five 95 mm diameter cylindrical specimens for ASTRA tests or three 305 mm long, 90 mm wide and 70 mm thick specimens for 3PB tests were obtained.

### *3.2 ASTRA Test*

The ASTRA test allowed the evaluation of the influence of the geocomposite on the interlayer shear behavior of double-layered cylindrical specimens.

The ASTRA device (Fig. 1), compliant with the European Standard prEN 12697-48, is a direct shear box, similar to the device used in soil mechanics. The double-layered specimen is installed in two half-boxes separated by an unconfined interlayer shear zone (Canestrari et al. 2005). During the test, a constant horizontal displacement rate of 2.5 mm/min occurs while a constant vertical load, perpendicular to the interface plane, can be applied in order to generate a given normal stress ($\sigma_n$). The whole apparatus is located in a climatic chamber with temperature and relative humidity control.

This test returns a data-set where interlayer shear stress ($\tau$), horizontal ($\xi$) and vertical ($\eta$) displacement are reported, allowing the calculation, for each specimen,

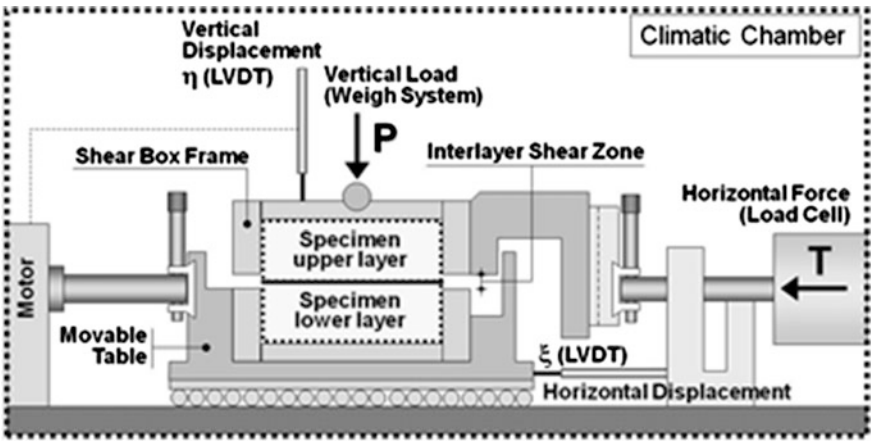


**Fig. 1** Working scheme of ASTRA equipment

of the interlayer shear strength ($\tau_{peak}$) that represents the maximum value assumed by $\tau$. Carrying out ASTRA tests at various stress levels $\sigma_n$, it is possible to obtain a complete assessment of failure and residual properties (post-peak) of interfaces (Canestrari et al. 2005) in terms of peak and friction envelopes obtained as linear regression of the representative shear data (Fig. 2). The envelope characteristic parameters are the pure shear resistance $c_0$, the peak friction angle $\Phi_{peak}$, the pure shear resistance after the failure $c_{res}$ and the residual friction angle $\Phi_{res}$.

## *3.3 Three-Point Bending Test*

Prismatic beam samples are subjected to a constant displacement rate, in bending configuration. Load and beam deflection at the mid-span of the specimen are measured by means of a load cell and a Linear Variable Displacement Transducer (LVDT), respectively.

The performance of double-layered reinforced systems can be evaluated through the maximum pre-cracking flexural load $P_{max}$ (flexural strength), the corresponding deflection $\delta$, the pre-cracking energy D, that is the area under the load-vertical deformation curve up to the $P_{max}$ value (Fig. 3a), and the fracture energy or toughness T, that is the area under the entire recorded load-vertical deformation curve (Fig. 3b). The pre-cracking energy D takes into account the crack initiation of the beam, whereas the toughness T provides an indication of the overall deformation energy and therefore can be used to evaluate the performance of the geocomposite reinforcement in the post-peak crack propagation phase (Lee 2008; Canestrari et al. 2012, 2013).

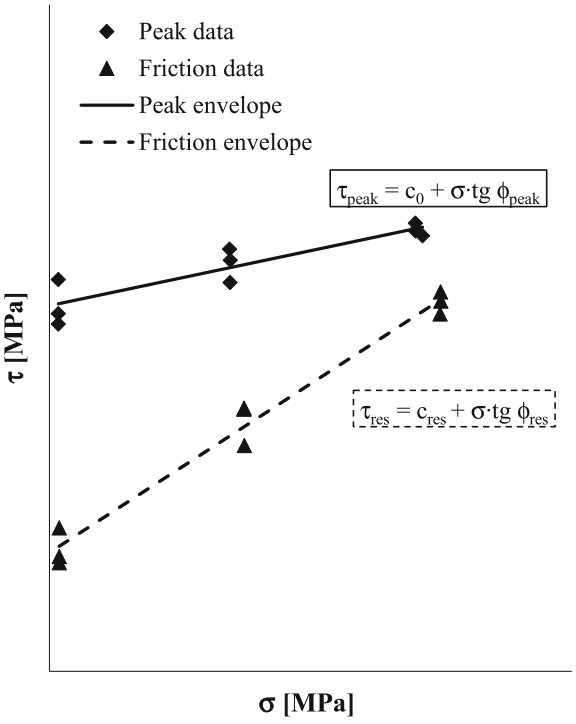


**Fig. 2** Peak and friction envelopes

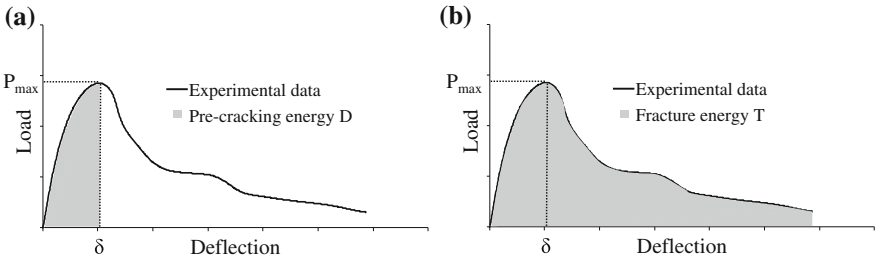


**Fig. 3** Analysis of 3PB test results: **a** pre-cracking energy D, **b** fracture energy T

## 4 Experimental Program

The influence of the selected geocomposite on the performance of double-layered polymer modified asphalt concrete specimens was evaluated in the laboratory by comparing the mechanical properties of the reinforced systems (GR) with those of a reference unreinforced configuration (UN).

**Table 1** Experimental program

| Configuration | ASTRA test repetitions (T = 20 °C) | | | 3PB test repetitions (T = 20 °C) | |
|---|---|---|---|---|---|
| | σ = 0.0 MPa | σ = 0.2 MPa | σ = 0.4 MPa | v = 5.0 mm/min | v = 50.8 mm/min |
| UN | 5 | 5 | 5 | 3 | 3 |
| GR | 5 | 5 | 5 | 3 | 3 |

The ASTRA tests were carried out at 20 °C under three normal stresses ($\sigma_n$ = 0.0, 0.2 and 0.4 MPa), performing five repetitions for each test configuration (Table 1). The quasi-static 3PB tests were carried out at a temperature of 20 °C in displacement-controlled mode, considering two test speeds: 5.0 and 50.8 mm/min. Three repetitions were performed for each test configuration (Table 1).

## 5 Result and Analysis

### *5.1 ASTRA Test Results*

The ASTRA test results are presented in Fig. 4, where the values of the envelope characteristic parameters are also shown.

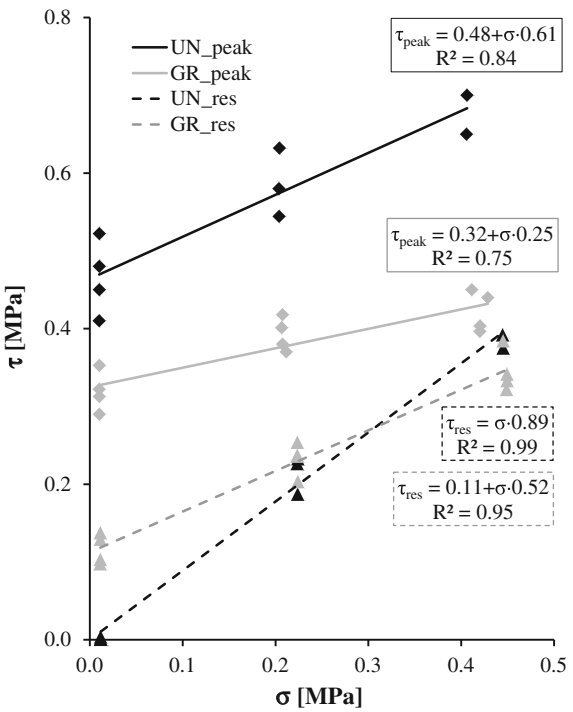


**Fig. 4** ASTRA test results: peak and friction envelopes

Experimental results show that the interlayer shear strength of the unreinforced system (UN) is sensibly higher than that of the reinforced one (GR), as the presence of the geocomposite at the interface inevitably leads to the reduction of interlayer bonding (Canestrari et al. 2013; Pasquini et al. 2014a; Graziani et al. 2014). However, after failure, the two layers of the reinforced specimens were still held together by the membrane showing that the failure is located within the membrane and not at the interface between the membrane and the asphalt layers. This fact leads to a residual cohesion ($c_{res} \neq 0$) of the double layered systems and could be due to the deformable bituminous film which caused the asphalt layers to shift each other without breaking (Canestrari et al. 2006; Pasquini et al. 2014a, b). Moreover, the reinforcing material causes a reduction of the peak friction angle $\Phi_{peak}$ with respect to the UN configuration, probably due to the fact that the thick reinforced bituminous membrane produces a "cohesive" interlayer which inhibits the shear stress contributions provided by friction and dilatancy (Pasquini et al. 2014a).

In order to evaluate possible differences in performance due to the application of the geocomposite at the interface of dense graded mixtures prepared with polymer modified binder or with plain bitumen, the comparison between the ASTRA test results achieved in this study and those obtained in a previous research (Pasquini et al. 2014a) was performed. This comparison can be reasonably carried out as Pasquini et al. (2014a) tested, with ASTRA equipment, both unreinforced (UN.ME) and reinforced (GB.00) double-layered asphalt concrete specimens prepared with plain bitumen and with the same geocomposite, in the same testing conditions. Experimental results for both mixtures (i.e. prepared with plain and modified bitumen) are reported in Table 2. It can be observed that, even if the value of the pure shear resistance $c_0$ of the unreinforced configuration of the mixture with plain bitumen (UN.ME) is higher than that of the modified one (UN), the reinforced interface with the modified mixture (GR) provides a slightly higher $c_0$ with respect to that of the mixture with plain bitumen (GB.00). Thus, the reduction (in percentage) of $c_0$ between the unreinforced and the reinforced configuration of the modified mixture (33.3 %) is lower than that of the mixture prepared with plain bitumen (55.2 %). These findings allow to remark that the studied geocomposite behaves better in systems containing modified bitumen with respect to those prepared with plain bitumen.

**Table 2** ASTRA test results: plain (Pasquini et al. 2014a) versus polymer-modified interfaces

| Bitumen type in the mixture | Configuration | $\tau_{peak} = c_0 + \sigma \text{ tg } \Phi_{peak}$ | | Reduction of $c_0$ (%) |
|---|---|---|---|---|
| | | $c_0$ (MPa) | $\Phi_{peak}$ (°) | |
| Modified | UN | 0.48 | 31 | – |
| | GR | 0.32 | 14 | 33.3 |
| Plain | UN.ME | 0.59 | 31 | – |
| | GB.00 | 0.27 | 18 | 54.2 |

Moreover, ASTRA test results obtained during the present study can be compared with those achieved in another research project (Pasquini et al. 2014b), where the same geocomposite was placed at the interface between a dense graded mixture and a porous asphalt mix (named GFG system). This comparison allows the assessment of the influence of the geocomposite placed between dense graded mixtures with respect to the use of such reinforcement underneath porous asphalt (PA) layers. It is worth noting that both mixtures were characterized by SBS polymer-modified bitumen.

Figure 5 shows that the cohesion $c_0$ achieved by the GR system (0.32 MPa) was noticeably higher than that obtained by GFG (0.20 MPa). This difference can be attributed to the higher percentage of voids of the porous material (systems GFG) which provides a lower number of contacts between the geocomposite and the upper layer compared to the dense graded material (system GR). This fact results in establishing a lower degree of adhesion between the reinforcement and the asphalt concrete as a lower number of points where the heat can be transmitted from the upper layer to the geocomposite exists.

On the other hand, the porous asphalt in the upper layer (system GFG) provided a higher peak friction angle $\Phi_{peak}$ compared to dense graded asphalt system (GR). According to Canestrari et al. (2006), this phenomenon is likely due to the larger amount of big-sized aggregates and voids in the upper porous layer, resulting in a

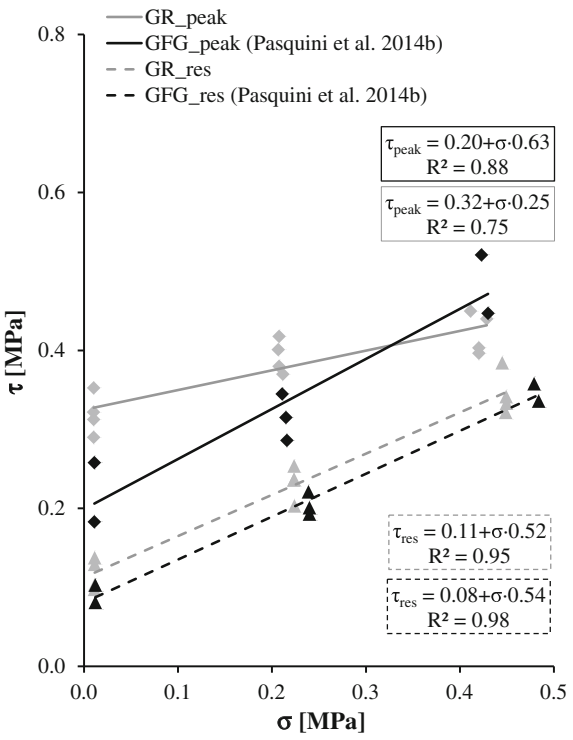


**Fig. 5** ASTRA envelopes: conventional (GR) versus porous (GFG) reinforced asphalt interfaces

noticeably higher level of texture at the interface, which can interlock better with the geocomposite. In terms of pure shear resistance after failure $c_{res}$ and residual friction angle $\Phi_{res}$, both systems provided similar results, proving that the residual phase does not depend on the asphalt material.

## 5.2 3PB Test Results

The results obtained from 3PB tests performed at 5.0 and 50.8 mm/min are synthesized, respectively, in the load-displacement curves of Fig. 6a, b, in which each curve depicts the average behavior of 3 repetitions of a tested configuration. The values of the basic parameters obtained from these curves, such as the strength properties before cracking ($P_{max}$, δ and D) and the toughness (T) are shown in Table 3. For both test speeds (5.0 and 50.8 mm/min), the GR configuration has a slightly lower pre-cracking flexural strength $P_{max}$ compared to the UN configuration but at a higher value of deflection δ. Such a result leads to a higher pre-cracking energy D of GR with respect to UN configurations. However, the real contribution of the reinforcement consists in the delay of crack propagation rather than in the inhibition of crack initiation, as shown by the noticeably higher toughness T experienced by the reinforced configurations (GR) with respect to the unreinforced ones (UN).

In this sense, Fig. 6a, b clearly represent the ductile characteristics of the double-layered bituminous systems reinforced with a geocomposite. In fact, no significant differences can be detected between the two systems (reinforced and unreinforced) up to the flexural strength point ($P_{max}$, δ) allowing to observe that the initial crack resistance mainly depends on the characteristics of the mixture respect to the reinforcement type. The slightly lower strength ($P_{max}$) of the reinforced beam is probably related to the de-bonding effect at the interface that causes some separation between the asphalt layers with respect to the unreinforced system which shows a behavior more similar to a single-layered system (Fig. 4). After the flexural

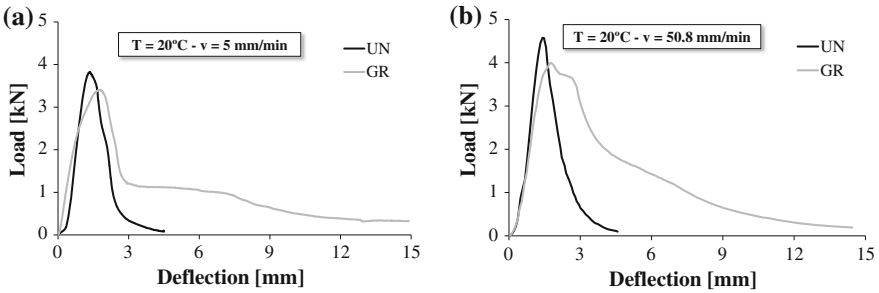


**Fig. 6** 3PB test results: **a** 5.0 mm/min; **b** 50.8 mm/min

strength point is reached, both reinforced and unreinforced systems show a decrease in load bearing capacity due to the crack propagation towards the interface. For the unreinforced system, this loss of resistance is rapid and the specimen steadily arrives at failure, whereas the reinforced system shows a post-peak deformation phase that brings to higher toughness values (about three times than the unreinforced configuration—Table 3). This is due to the fact that the reinforcement is able to absorb a portion of the applied flexural stress keeping a certain degree of flexural strength in the crack propagation phase. This reflects in a higher post-peak energy for the reinforced double-layered systems and thus in a certain inhibition of crack propagation, which means higher ductility. Results reported in Table 3 also show that almost all values provided by the basic parameters, related to both crack initiation and propagation, increase with the increasing of the test speed. However, for both test speeds, the reinforced system is able of ensuring almost the same performance enhancement in terms of toughness T with respect to the unreinforced one (172 % at 5.0 mm/min and 183 % at 50.8 mm/min).

Also in this case, results reported in Table 3 can be compared with those obtained in a previous research (Pasquini et al. 2014a) where analogous unreinforced (UN.ME) and reinforced (GB.00) systems, prepared with a HMA containing plain bitumen, were tested with 3PB equipment at 50.8 mm/min and 20 °C.

Table 4 shows that the systems prepared with the plain bitumen evidenced better performance than the modified one. This difference is due to the fact the two systems are characterized by two different thicknesses. In fact, the samples containing plain bitumen were 30 + 45 mm-thick (i.e. 30 mm thick lower layer and 45 mm thick upper layer) whereas those prepared with polymer modified bitumen had a thickness of 30 + 40 mm (i.e. 30 mm thick lower layer and 40 mm thick upper layer). Thus, it is not reliable to perform a direct comparison between the two systems but, for both materials, it is significant to compare the increase of the parameter T provided by the reinforced samples with respect to the unreinforced ones. In this sense, experimental data (Table 4) show that the increase of toughness due to the use of geocomposite is higher in the case of polymer modified asphalt mixes.

**Table 3** Summary of 3PB test results (standard deviation given within brackets)

| Configuration | Test speed (mm/min) | $P_{max}$ (kN) | δ (mm) | D (N × m) | T (N × m) | Increase of T (%) |
|---|---|---|---|---|---|---|
| UN | 5.0 | 3.82 | 1.34 | 2.23 (1.08) | 5.52 (2.13) | – |
| GR | | 3.40 | 1.75 | 3.82 (0.65) | 15.04 (2.84) | 172 |
| UN | 50.8 | 4.58 | 1.41 | 2.66 (0.27) | 6.68 (0.05) | – |
| GR | | 4.00 | 1.78 | 3.60 (1.29) | 18.94 (2.24) | 183 |

**Table 4** 3PB test results at 50.8 mm/min: plain (Pasquini et al. 2014a) versus polymer-modified asphalt systems (standard deviation given within brackets)

| Bitumen type in the mixture | Configuration | $P_{max}$ (kN) | δ (mm) | D (N × m) | T (N × m) | Increase of T (%) |
|---|---|---|---|---|---|---|
| Modified | UN | 4.58 | 1.41 | 2.66 (0.27) | 6.68 (0.05) | – |
| | GR | 4.00 | 1.78 | 3.60 (1.29) | 18.94 (2.24) | 183 |
| Plain | UN.ME | 5.31 | 2.01 | 6.36 (0.11) | 14.19 (1.37) | – |
| | GB.00 | 5.14 | 2.27 | 7.34 (0.56) | 26.83 (1.79) | 89 |

## 6 Conclusions

The research described in this paper has the objective of evaluating the effectiveness of pavement rehabilitation of modified asphalt concrete layers with reinforced geomembranes. In this respect, the experimental investigation involved interface shear tests and static flexural tests carried out on double-layered reinforced and unreinforced samples prepared in the laboratory.

On the basis of the results arisen from the experimental research, the following main conclusions can be drawn:

- the installation of reinforcements at the interface of asphalt concrete layers reduces interlayer shear strength;
- after failure, interfaces reinforced with geocomposites exhibit a "residual cohesion" provided by the deformable bituminous film of the membrane;
- the use of polymer modified bitumen in the mixture instead of traditional plain bitumen can enhance interlayer shear strength of geocomposite-reinforced interfaces;
- the real contribution of the reinforcement consists in the delay of crack propagation rather than in the inhibition of crack initiation;
- flexural performance enhancement guaranteed by the reinforcing geocomposite does not depend on 3PB test speed;
- the increase of the toughness provided by the reinforcement is higher in the case of polymer-modified asphalt mixture with respect to mixture with plain bitumen.

**Acknowledgments** This study was sponsored by INDEX Construction Systems and Products S.p.A. (Italy) that gave both financial and technical support for the research project. Test results and opinions are those of the authors and do not necessarily reflect those of the sponsoring company.

## References

Austin RA, Gilchrist AJT (1996) Enhanced performance of asphalt pavements using geocomposites. Geotext Geomembranes 14(3-4):175-186. doi: 10.1016/0266-1144(96)00007-6.

Brown SF, Thom NH, Sanders, PJ (2001) A study of grid reinforced asphalt to combat reflection cracking. J Assoc Asphalt Pav 70:543–569.

Canestrari F, Ferrotti G, Partl MN, Santagata E (2005) Advanced testing and characterization of interlayer shear resistance. Transp Res Record 1929:69–78. doi: 10.3141/1929-09.

Canestrari F, Grilli A, Santagata FA, Virgili A (2006) Interlayer shear effect of geosynthetic reinforcements. In: 10th International Conference on Asphalt Pavements, Quebec City, August 2006, vol I. Curran Associates Inc., Red Hook, Brooklin, p 811.

Canestrari F, Pasquini E, Belogi L (2012) Optimization of Geocomposites for Double-Layered Bituminous Systems. In: Scarpas T, Kringos N, Al-Qadi IL, Loizos A (eds) 7th RILEM International Conference on Cracking in Pavements, Delft, June 2012, vol 2. Springer, Dordrecht, p 1229.

Canestrari F, Belogi L, Ferrotti G, Graziani A (2013) Shear and flexural characterization of grid-reinforced asphalt pavements and relation with field distress evolution. Mater Struct. doi: 10.1617/s11527-013-0207-1.

Ferrotti G, Canestrari F, Virgili A, Grilli A (2011) A strategic laboratory approach for the performance investigation of geogrids in flexible pavements. Constr Build Mater 25(5):2343–2348. doi: 10.1016/j.conbuildmat.2010.11.032.

Ferrotti G, Canestrari F, Pasquini E & Virgili A (2012) Experimental evaluation of the influence of surface coating on fiberglass geogrid performance in asphalt pavements. Geotext Geomembranes 34:11–18. doi: 10.1016/j.geotexmem.2012.02.011.

Graziani A, Pasquini E, Ferrotti G, Virgili A, Canestrari F (2014) Structural response of grid-reinforced bituminous pavements. Mater Struct 47(8):1391-1408. doi: 10.1617/s11527-014-0255-1.

Lee SJ (2008) Mechanical performance and crack retardation study of a fiberglass-grid-reinforced asphalt concrete system. Can J Civil Eng 35(10):1042–1049. doi: 10.1139/L08-049.

Pasquini E, Bocci M, Ferrotti G, Canestrari F (2013) Laboratory characterisation and field validation of geogrid-reinforced asphalt pavements. Road Mater Pavement 14(1):17-35. doi: 10.1080/14680629.2012.735797.

Pasquini E, Bocci M, Canestrari F (2014a) Laboratory characterization of optimized geocomposites for asphalt pavement reinforcement. Geosynth Int 21(1):24-36. doi: 10.1680/gein.13.00032.

Pasquini E, Cardone F, Canestrari F (2014b) Moisture Sensitivity of Interlayers between Conventional and Porous Asphalt Mixes. In: Kim YR (ed) Asphalt pavements. Proceedings of the 12th International Conference on Asphalt Pavements ISAP 2014, Raleigh, June 2014, vol 2. CRC Press/Balkema, Leiden, p 1291.

Perkins SW, Edens MQ (2002) Finite element and distress models for geosynthetic-reinforced pavements. Int J Pavement Eng 3(4):239-250. doi: 10.1080/1029843021000083504.

Prieto JN, Gallego J, Perez I (2007) Application of the wheel reflective cracking test for assessing geosynthetics in anti-reflection pavement cracking systems. Geosynth Int 14(5):287-297. doi: 10.1680/gein.2007.14.5.287.

Shukla SK, Yin JH (2004) Functions and installation of paving geosynthetics. In: Shim JG, Yoo C, Jeon H-Y (eds) 3rd Asian Regional Conference on Geosynthetics, Seoul, 2004.

Sobhan K, Tandon V (2008) Mitigating reflection cracking in asphalt overlay using geosynthetic reinforcements. Road Mater Pavement 9(3):367–387. doi: 10.1080/14680629.2008.9690124.

Vanelstraete A, De Visscher J (2004) Long term performance on site of interface systems. In: Petit C, Al-Qadi IL, Millien A (eds) PRO37: cracking in pavements – mitigation, risk assessment and prevention. Proceedings of the 5th International RILEM conference on cracking in pavements, Limoges, May 2005. RILEM Publications SARL, Bagneux, p 699.

Zamora-Barraza D, Calzada-Pérez MA, Castro-Fresno D, Vega-Zamanillo A (2010) New procedure for measuring adherence between a geosynthetic material and a bituminous mixture. Geotext Geomembranes 28(5):483-489. doi: 10.1016/j.geotexmem.2009.12.010.

Zamora-Barraza D, Calzada-Pérez MA, Castro-Fresno D, Vega-Zamanillo A (2011) Evaluation of anti-reflective cracking systems using geosynthetics in the interlayer zone. Geotext Geomembranes 29(2):130–136. doi: 10.1016/j.geotexmem.2010.10.005.

# Part VI
# Modeling of Road Materials and Pavement Performance Prediction

# Prediction of the Mechanical Properties of Aged Asphalt Mixes from FTIR Measurements

**Miguel Perez-Martinez, Paul Marsac, Thomas Gabet and Emmanuel Chailleux**

**Abstract** Setting a method to evaluate the mechanical properties of an aged asphalt mix using a rapid chemical measurement from small samples, would be of high interest at different steps of a road structure life cycle: at the design step, to optimise the estimates of the service lifetime usually based on the properties of unaged materials; during the service life, to update the residual lifetime expectation of an existing structure according to the actual properties of the in situ aged materials; and at the end of the service life or for maintenance management, to evaluate the recyclability of the materials of the structure. This study was carried out aiming at comparing results from Fourier Transform InfraRed and Dynamic Shear Rheometer tests. Experimental data came from an international round robin test, organised by the RILEM TC ATB, designed to set an ageing protocol on loose bituminous mixtures. The evolutions of the carbonyl index ($IC_O$) calculated from the FTIR spectra are compared to the evolutions of the parameters of a modified Huet Rheological Model (1S2P1D) fitted on the experimental linear viscoelastic data measured on the recovered binder. A significant relationship is observed suggesting that chemical and rheological properties could be correlated. Based on this observation, a method is proposed for predicting the G* values of a binder aged at a given $\Delta IC_O$ level. Subsequently, this method could be used to predict the complex modulus E* of a given mix from the shear modulus G* of the binder using existing binder/mix transfer models.

**Keywords** Binder characterisation · Rheological model · FTIR spectra · Ageing process · Asphalt mix · Performance prediction

M. Perez-Martinez (✉) · P. Marsac · T. Gabet · E. Chailleux
LUNAM, IFSTTAR, Bouguenais Cedex, France
e-mail: miguel.perez-martinez@ifsttar.fr

P. Marsac
e-mail: paul.marsac@ifsttar.fr

T. Gabet
e-mail: thomas.gabet@ifsttar.fr

E. Chailleux
e-mail: emmanuel.chailleux@ifsttar.fr



F. Canestrari and M.N. Partl (eds.), *8th RILEM International Symposium on Testing and Characterization of Sustainable and Innovative Bituminous Materials*, RILEM Bookseries 11, DOI 10.1007/978-94-017-7342-3_32

## 1 Introduction

Road engineering evaluation and monitoring is highly dependent on the changes experienced by the mechanical properties of the infrastructure during service life. The changes associated to mechanical damage caused by traffic (fatigue and cracking) have been heavily studied and ended up with many test proposals for bituminous materials characterisation, however very few is known about the properties changes induced by on-site chemical ageing of these materials. Thus far, these changes could be very significant, and a detailed knowledge on their evolution may help to better evaluate the real service life expectancy of the new designed pavements or the residual state of the old ones (Lui et al. 1996; Petersen 2009).

The search for a method that can ascertain a relation between the chemical state of the pavement and its durability seems challenging. If it would be possible to get the needed information with a simple and rapid chemical measure on cored samples to be correlated with the mechanical properties of the road materials, the real state of the asphalt mixture would be easily known. Moreover, rehabilitation works could be optimised to extend the expected lifetime and the recyclability of the possible milled materials studied in advance.

In order to study this correlation, a research work was conducted at IFSTTAR as part of a PhD thesis funded by the European commission within the framework of the European Project SUP&R ITN. This research is based on Fourier Transform InfraRed (FTIR) and Dynamic Shear Rheometer (DSR) test results obtained during an international round robin test, organised by the RILEM TC ATB, to set up an ageing protocol on loose bituminous mixtures (de la Roche et al. 2013).

The objective of this paper is to assess a possible relationship between a chemical ageing index and the parameters of a rheological model simulating the mechanical properties of an aged material over the complete frequency and temperature range.

## 2 RILEM TC ATB Round Robin Test

An asphalt concrete mixture with aggregate gradation of 0/10 mm and 35/50 bitumen content of 5.4 % was aged at 6 different levels as loose mix in a ventilated oven in four different laboratories. With the aim of detecting a possible difference between the lab and plant produced materials, 2 batches were separated according to the mixing process: lab mixing (batch B1) and plant mixing (batch B3). The overall experimental design is summed up in Fig. 1. At each ageing step, FTIR and DSR measurements were made by the participating laboratories.

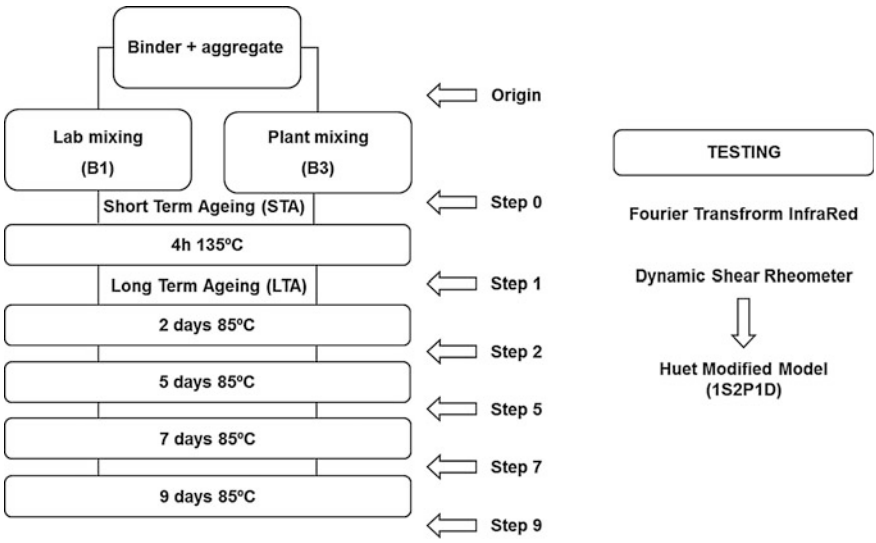


**Fig. 1** Resume of the experimental design

## *2.1 Fourier Transform InfraRed and Ageing Index*

In a material, the different types of molecular bonds are characterised by specific vibration and rotation modes. The energy associated to these modes is quantified and a higher level can only be reached if a quantity of energy exactly equal to the difference between two energy levels is transmitted to the molecule. As the energy of a photon is equal to the product of the frequency of the radiation and the Planck's constant, a given type of bond can only reach a higher activation level by absorbing a quantum corresponding exactly to a specific frequency. The Fourier Transform InfraRed test consists on exciting the material with Infra-Red light and then quantifying the different types of molecular bonds through characteristic absorption bands in the Infra-Red light spectrum.

Carbonyl groups (esters, ketones etc.) characterised by C=O double bond are among the major functional groups formed during oxidative ageing (Petersen 2009) and it was demonstrated that their formation changes the physical properties of the binder in a predictable way (Lui et al. 1996). For this reason, the carbonyl ageing index $IC_O$ was chosen to quantify the evolution of the binder with ageing. This carbonyl index was calculated from the raw FTIR spectra by a deconvolution method.

This method consist on fitting the spectrum with a series of 5 Lorenztian functions (1) centred on wavenumbers 1700, 1460, 1375, 1600 and 1340 $cm^{-1}$ and a parabolic function.

$$y = \frac{2A}{\pi} \cdot \left( \frac{w}{4(v - v_c)^2 + w^2} \right) \quad (1)$$

where A is the area of the function; w is the width at half the maximum height and $v_c$ is the location of the peak.

The combination of the parabolic function and the Lorentzian function centred at 1340 $cm^{-1}$ is intended to fit the base curve of the spectra while the other Lorentzian functions are used to fit the specific peaks. The parameters of $A_i$ and $w_i$ of the Lorentzian functions and the parameters of the parabolic function are determined using the square adjustment method.

The calculated carbonyl index by deconvolution is the peak amplitude of the Lorentzian function centred at 1700 $cm^{-1}$ divided by the sum of the peaks amplitudes of the Lorentzian functions centred at 1460 and 1375 $cm^{-1}$ (Marsac et al. 2014).

## 2.2 Dynamic Shear Rheometer

The Dynamic Shear Rheometer was employed to assess the rheological properties of the recovered bitumens from aged mixtures. This test is capable of quantifying the viscoelastic properties of bituminous binders in wide temperature and loading frequencies ranges.

The bitumen sample is placed between a fix bottom plate and a rotating top plate. Then, shear strain is applied to the bitumen through angularly oscillations of the top plate. For a given temperature and frequency couple, the bitumen is characterised by a complex shear modulus G* calculated as the ratio of the sinusoidal shear stress to the sinusoidal shear strain.

In each laboratory, the DSR measurements were carried out with 8 mm plates and a gap of 2 mm at 11 equally logarithmic spaced frequencies from 0.1 to 10 Hz and 7 temperatures from −5 to 55 °C, that is to say 88 values of the norm |G*| and the phase angle of the complex modulus for each sample and ageing step. To allow an efficient data mining, the first basic idea of this study was to concentrate the information represented by these 88 couples of values within a few number of parameters of a model describing the properties of the binder for all the temperature and frequency ranges.

## 2.3 Modelling the Bitumen

Several studies carried out in different countries demonstrate that the Huet Modified Model (1S2P1D) (Such 1982, 1983; Olard 2003; Yussof et al. 2010) is one of the most appropriate models to depict the rheological properties of a bitumen. It consists on a spring (instantaneous elastic modulus, noted as $G_\infty$), two parabolic

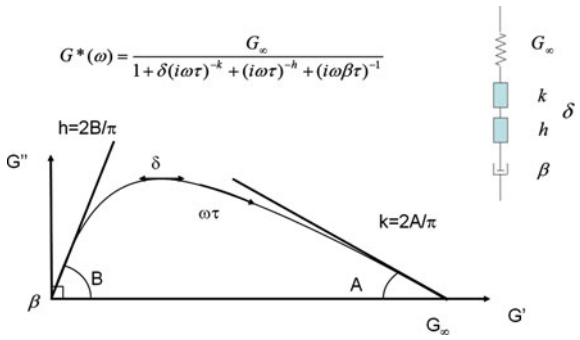


**Fig. 2** Huet modified model (1S2P1D), equation and representation of the Cole-Cole diagram

elements ($1 > h > k > 0$) regulated by a positive adimensional coefficient (δ), and a dashpot (β), all placed in series as shown in Fig. 2.

The IFSTTAR software Visco-analyse (Chailleux 2007) is used to fit the 1S2P1D model of the on the experimental data. This software uses the approximation of Booj and Thoone of the Kramers-Kroning relations for the construction of the master curve at 10 °C and then the model parameters are fitted using a trust region reflective algorithm.

## 3 Analysis of Results

This section presents the evolution of the chemical index represented by the carbonyl index $IC_O$, and the mechanical properties represented by the 6 parameters of the 1S2P1D model ($G_\infty$, h, k, δ, β, τ) according to each ageing step.

### *3.1 Evolution of the Chemical Index $IC_O$*

The values of $IC_O$ according to the ageing step are plotted in Fig. 3 (legend: LxBy for Lab x and Batch y). As can be appreciated, the evolution of the carbonyl index is not so far affected by laboratory effects neither by manufacturing processes effects, as the $IC_O$ increases throughout the ageing phases.

### *3.2 Evolution of the Mechanical Parameters*

#### $G_\infty$ parameter

The glassy modulus $G_\infty$ represents the value of G* at infinite frequency. This parameter remains almost constant for the four laboratories regardless the ageing

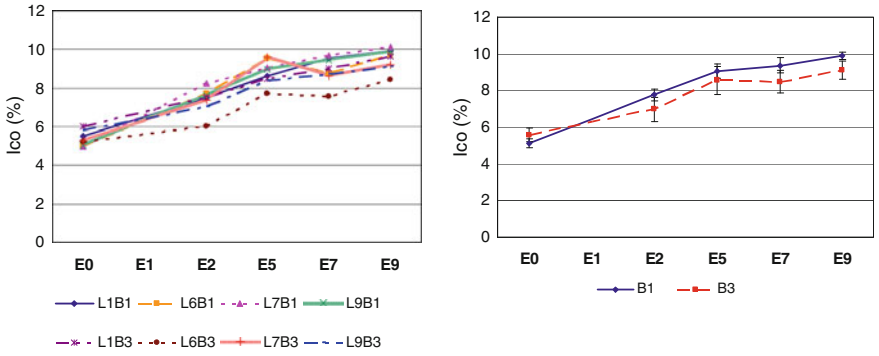


**Fig. 3** FTIR Index Carbonyl results

step and manufacturing procedure as Fig. 4a shows. On the other hand, a strong laboratory effect is detected with an average glassy modulus of ≈700 MPa obtained for Lab4 and Lab8 (which seems consistent with usual values for binders) while an average value of ≈400 MPa is obtained for the two other laboratories.

As a variation of the value of $G_\infty$ in the expression of G*, it represents a homothetic transformation of center 0 in the Cole-Cole diagram. This could indicate a constant relative difference for the |G*| measurements in the two groups of laboratories possibly related to different stiffness or calibration of the DSR devices. The other parameters, accounting for the shape of the model response in the Cole-Cole plan would not a priori be affected by this laboratory homothetic dependency.

### δ parameter

The δ parameter represents the balance between the two parabolic elements k and h at medium temperatures or frequencies. Figure 4b shows that the general trend of the value is to increase with ageing, reflecting a tendency towards k when ageing. Nevertheless, the amplitude of this variation seems to be affected by a laboratory effect, with the same two groups of laboratories noticed for the $G_\infty$ parameter. This suggests a slight interdependence between the δ and the $G_\infty$ parameters contrary to what was a priori assumed above.

### k parameter

The k parameter, first parabolic element, is proportional to the slope of the model in the Cole-Cole plan at low temperature and/or high frequency (proportional to the ratio $\Delta G''/\Delta G'$). As can be observed in Fig. 4c, an almost constant average value of ≈0.3 is obtained for all laboratories, mixing procedures and ageing steps. Thus, the ageing process shows no effect on this parameter.

### h parameter

The h parameter of the second parabolic element is proportional to the slope of the model in the Cole-Cole plan at high temperature and/or low frequency (proportional

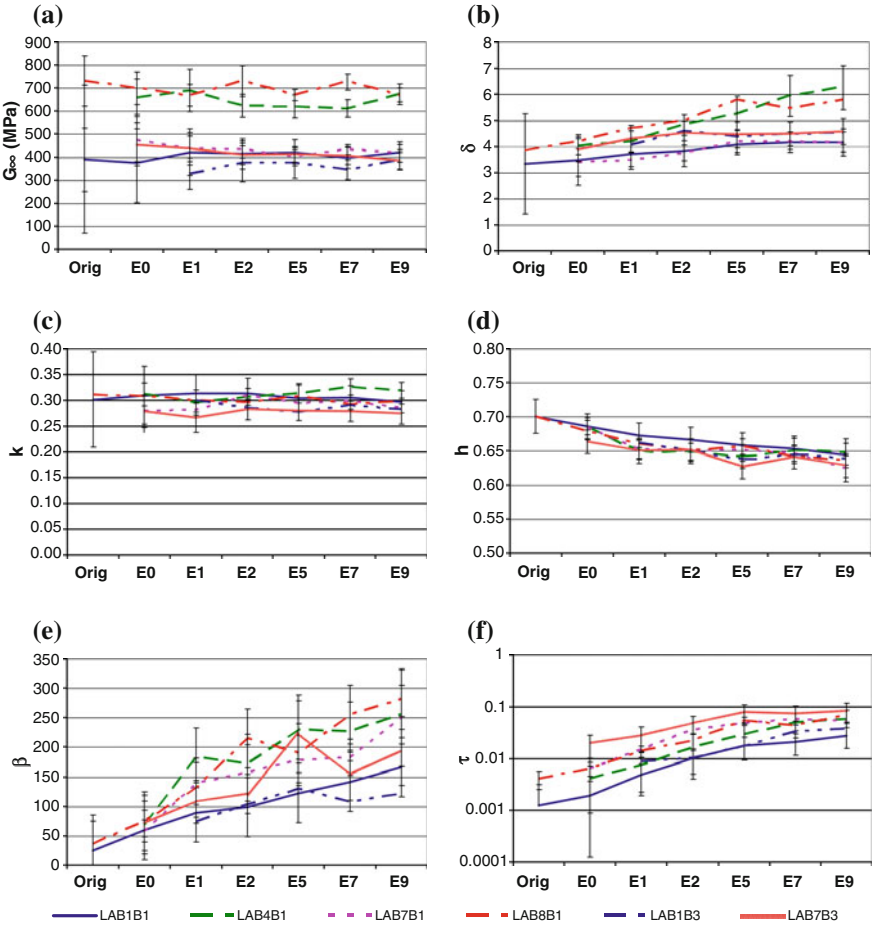


**Fig. 4** $G_\infty$, δ, k, h, β and τ laboratory and plant mixtures modelling results

to the ratio $\Delta G''/\Delta G'$). As can be seen, tendency for h value with ageing is consistent in all cases, decreasing from 0.70 to 0.63; this tendency can be appreciated in Fig. 4d.

### β parameter

The dashpot parameter β represents the viscosity of the model at very high temperatures or very low frequencies. The standardized tendency observed in Fig. 4e substantially increase with ageing, but there are laboratory differences within results, as well as possible plant/laboratory manufacturing effects. It can be noticed the random increase/decrease experienced by the plant mixture of LAB7B3 on the ageing step E5, which may indicate a possible error of measuring on the sample.

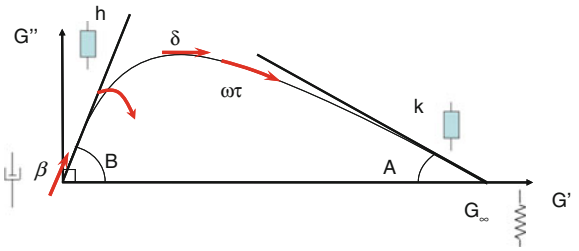


**Fig. 5** Cole-Cole diagram of parameters influence with ageing

**τ parameter**

Finally, the frequency multiplier τ at 10°C seems to exponentially increase for all laboratories when going through the ageing process, as it is shown in Fig. 4f. The disposition of this parameter to change through the ageing phases is marked, being the main parameter on affecting the value of |G*|.

From a mechanical point of view, the ageing process of the binder from the virgin step to E9 step is approximately equivalent to multiplying the angular frequency ω by a factor of 14.

### *3.3 Results Overview*

The values of the carbonyl index $IC_O$ experienced an increase during the ageing procedure, showing the importance of the index on the study and characterization of ageing.

In the case of DSR results, it can be said that almost the same trends have been experienced by all laboratories and mixture manufacturing procedures. Through the six ageing steps, three different behaviours have been noted:

- The values of the τ, β and δ parameters tend to increase;
- The value of the h parameter tends to decrease;
- The values of the parameters k and $G_\infty$ remain almost constant through the six ageing steps.

Figure 5 represents the Cole-Cole diagram under the effect of the case study parameters when an ageing procedure is developed.

## 4 Rheological Versus Chemical Relation

As observed in Sect. 3, the chemical index $IC_O$ shows significant evolution with ageing as well as the mechanical parameters h, δ, β and τ. The second basic idea of this study was seeing if a possible relationship could be established between the evolution of the chemical index and the evolution of the 4 mechanical parameters.

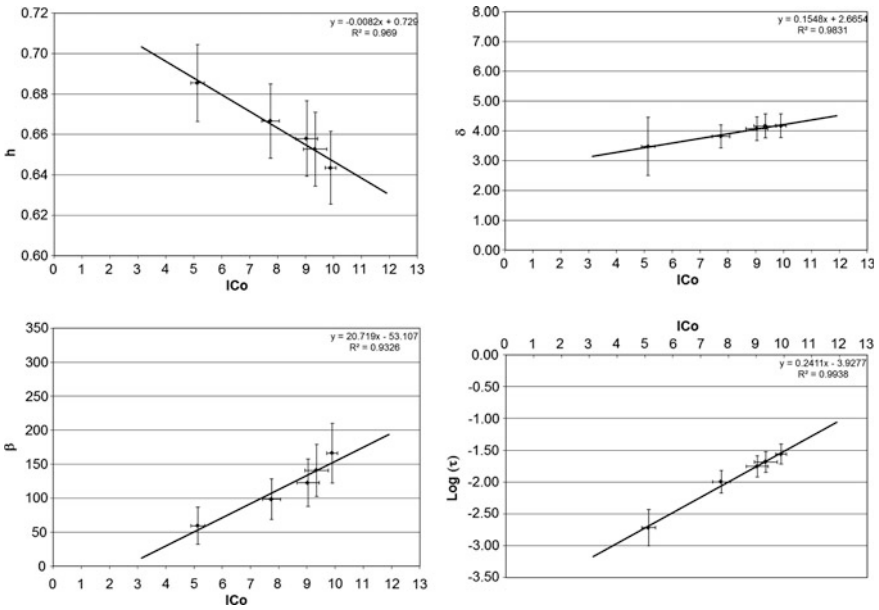


**Fig. 6** LAB01 and Batch 1 results

**Table 1** Parameters prediction according to laboratory results

| Parameter | $a_h$ | $a_\delta$ | $a_\beta$ | $a_\tau$ |
|---|---|---|---|---|
| LAB01 | 0.0082 | 0.15 | 20.72 | 0.24 |
| LAB04 | 0.0080 | 0.44 | 38.88 | 0.24 |
| LAB07 | 0.0100 | 0.18 | 34.96 | 0.20 |
| LAB08 | 0.0080 | 0.18 | 39.17 | 0.21 |
| Average | 0.0082 | 0.24 | 33.43 | 0.23 |

For each laboratory/batch combination, the values of the 4 mechanical parameters are plotted versus the average values of the chemical index. Figure 6 shows typical results obtained for the Lab1 Batch1.

Significant relationships are observed for all combinations: linear relationship for h, δ and β, and ponential relationship for τ. The slopes obtained for all combinations are summarised in the Table 1.

The general trend is the same for all combinations but the values of the slope can be significantly different from on laboratory to another. These differences could be probably partly explained by reproducibility errors of the DSR measurements.

## 5 Prediction of G* from $IC_O$

Taking into account the relationships obtained in Sect. 4, it seems then possible to predict the value of G* at a given ageing step from a simple $IC_O$ measurement by knowing the 1S2P1D parameters of the original binder. Using the expression of G* for the original binder (2), G* for an aged binder could be estimate by relation (3) allowing the access to the overall viscoelastic spectrum of the aged binder.

$$G_{orig} * (\omega) = \frac{G_\infty}{1 + \delta(i\omega\tau)^{-k} + (i\omega\tau)^{-h} + (i\omega\beta\tau)^{-1}} \tag{2}$$

$$G_{aged} * (\omega) \approx \frac{G_\infty}{1 + \delta_{aged}(i\omega\tau_{aged})^{-k} + (i\omega\tau_{aged})^{-h}_{aged} + (i\omega\beta_{aged}\tau_{aged})^{-1}}. \tag{3}$$

with:

$$\tau_{aged} \approx \tau \cdot 10^{a_\tau \cdot \Delta IC_o}$$

$$h_{aged} \approx h + a_h \cdot \Delta IC_o$$

$$\delta_{aged} \approx \delta + a_\delta \cdot \Delta IC_o$$

$$\beta_{aged} \approx \beta + a_\beta \cdot \Delta IC_o$$

Finally, the complex modulus E* of a bituminous mix at a given ageing level could be predicted from (2) using existing binder/mix transfer models.

These types of linear and potential relationships may be expected when studying other type of bitumens. In that case, the values awaited for $a_h$, $a_\delta$, $a_\beta$ and $a_\tau$ may be different. Future research steps could be linked with other types of bitumens and different processing conditions on the same bitumen in order to set similar relationships between FTIR measures and DSR parametrizations.

## 6 Conclusions and Recommendations

From this study, it appears that a prediction of the overall viscoelastic properties of aged asphalt mixes from FTIR measurements seems achievable knowing the parameters of a 1S2P1D model of the original binder and the evolution laws of these parameters according to the carbonyl ageing index.

However, the chemical/mechanical relationships used were obtained through a laboratory simulated ageing. To extend the prediction to real site materials, the validity of these relationships should be ascertain for on-site ageing.

**Acknowledgments** The research presented in this presentation was carried out as part of the Marie Curie Initial Training Network (ITN) action, FP7-PEOPLE-2013-ITN. This project has received funding from the European Union's Seventh Framework Programme for research, technological development and demonstration under grant agreement number 607524.

## References

Chailleux E (2007) Note d'utilisation de l'application logicielle Visco-analyse. IFSTTAR

De la Roche C, Van de Ven M, Planche JP, Van de Bergh W, Grenfell J, Gabet T, Mouillet V, Porot L, Farcas F, Ruot C (2013) Advances in Interlaboratory Testing and Evaluation of Bituminous Materials, RILEM State of the Art Report TC 206-ATB Chapter 7 Hot recycling of Bituminous Mixtures

Liu M, Lunsford KM, Davison RR, Glover CJ, Bullin JA (1996) The Kinetics of Carbonyl Formation in Asphalt, AIChE J 42-4:1069-1076

Marsac P, Piérard N, Porot L, Van den Bergh W, Grenfell J, Mouillet V, Pouget S, Besamusca J, Farcas F, Gabet T, Hugener M (2014) Potential and limits of FTIR methods for reclaimed asphalt characterisation. Mater Struct 44, 1273-1286.

Olard F (2003) Comportement thermomécanique des enrobés bitumineux à basse températures Ph D Thesis INSA Lyon

Petersen JC (2009) A Review of the Fundamentals of Asphalt Oxidation. Transportation Research Circular E-C140. Washington

Such C (1982) Etude de la structure du bitume – analyse du comportement visqueux. Rapport interne CHG01189, LCPC.

Such C (1983) Analyse du comportement visqueux des bitumes. Bulletin de liaison des laboratoires des ponts et chaussées 127.

Yusoff MD, Monieur D, Airey G (2010) The 2S2P1D: An excellent linear viscoelastic model. UNIMAS e-Journal of Civil Engineering

# Micromechanical Description of Bitumen Aging Behavior

**Lukas Eberhardsteiner, Josef Füssl, Bernhard Hofko, Florian Handle, Markus Hospodka, Ronald Blab and Hinrich Grothe**

**Abstract** For the design of durable pavement constructions, considering the change of material properties of hot mix asphalt over time is essential. Hardening and embrittlement of bitumen lead to a reduced resistance against cryogenic cracks and the premature formation of fatigue cracks in bituminous layers. This phenomenon called aging is induced by environmental impacts. Within this work, a micromechanical model extending an existing multiscale model for hot mix asphalt is proposed, which allows a prediction of the consequences of microstructural changes observed as a result of aging effects. On the basis of AFM and ESEM images, a microstructure of bitumen consisting of a contiguous matrix with an embedded micelle-like structure can be identified. Hence, a structural concept based on SARA fractions arranged in a representative volume element is suggested. Static shear creep tests on artificially composed bitumen with asphaltene contents varying between 0 and 30 wt% in aged and laboratory-aged (RTFOT+PAV) conditions were conducted to identify the properties of material phases as well as to validate the presented model assumptions. A very good accordance between model predictions and experimental results indicates that the model is able to reproduce as well as to describe significant microstructural effects related to aging.

**Keywords** Bitumen aging · Microstructure · SARA fractions · DSR

L. Eberhardsteiner (✉) · B. Hofko · M. Hospodka · R. Blab
Institute of Transportation, Vienna University of Technology, Vienna, Austria
e-mail: lukas.eberhardsteiner@tuwien.ac.at

J. Füssl
Institute for Mechanics of Materials and Structures, Vienna University of Technology, Vienna, Austria

F. Handle · H. Grothe
Institute of Materials' Chemistry, Vienna University of Technology, Vienna, Austria



F. Canestrari and M.N. Partl (eds.), *8th RILEM International Symposium on Testing and Characterization of Sustainable and Innovative Bituminous Materials*, RILEM Bookseries 11, DOI 10.1007/978-94-017-7342-3_33

## 1 Introduction

In times of a predictable shortage of crude oil, asphalt recycling and the use of reclaimed asphalt pavements (RAP) gain more and more importance. Furthermore, the development of more sustainable and renewable alternatives to bitumen seems to become an important challenge in the future. Obviously, the microstructure of bitumen and microstructural changes related to significant effects like aging are a key to understand in detail how bitumen works mechanically and, hence, important to create durable mixes used in high performance pavement constructions.

For a complex composite material like bitumen, examining the material's microstructure is a reliable way to a better understanding of the mechanical behavior and, moreover, a phenomenon like aging. Thereby, SARA fractionation separating bitumen into saturates, aromatics, resins and asphaltenes (Lesueur 2009; Corbett 1969) is the most common way to identify the constituents of bitumen. Imaging methods like Atomic Force Microscopy (AFM) or Environmental Scanning Electron Microscopy (ESEM) enable to visualize the (micro)structures built up by these constituents (Stangl et al. 2006; Jäger et al. 2004; Masson et al. 2006; Nahar et al. 2013a, b, 2014; Schmets et al. 2010; Pauli et al.2001; Forbes et al. 2001; Bearsley et al. 2004; Lesueur 2009; Espinat et al.1998; Bodan 1982) and, hence, allow for the development of models predicting the mechanical behavior.

In recent years, Lackner et al. introduced a multiscale model to predict the viscoelastic material behavior of HMA (Aigner et al. 2009; Lackner et al. 2004, 2005; Pichler and Lackner 2009). This model is able to describe the macroscopic behavior as a function of microstructural characteristics down to the so-called mastic-scale, consisting of bitumen and filler, where, however, bitumen is considered as homogenous phase. An extension of the existing model by taking the microstructure of bitumen into account was recently published in Eberhardsteiner et al. (2014a).

Before a structural RVE concept of bitumen aging can be derived within the framework of continuum micromechanics, the constituents of bitumen and their arrangement have to be identified in this work.

## 2 Identification of Bitumen Microstructure

A well-accepted concept to characterize the constituents of bitumen is SARA fractionation. Thereby, bitumen is separated by n-heptane into asphaltenes (non-soluble particles) and maltenes (soluble phase) (Richardson 1913). Based on differences regarding polarity, the maltene phase can be further split into saturates, aromatics and resins (Lesueur 2009; Rostler 1965) by column chromatography [according to ASTM Standard 4124 (ASTM 2001; Lesueur 2009; Corbett 1969)]. Saturates account for about 5–15 wt% and appear as a colorless or slightly colored oily liquid at room temperate (Lesueur 2009) (see Fig. 1). While resins form a black

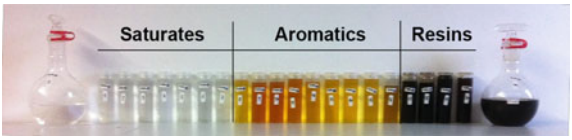


**Fig. 1** Maltene fractions (saturates, aromatics and resins) from chromatography according to modified ASTM standard 4124 (ASTM 2001)

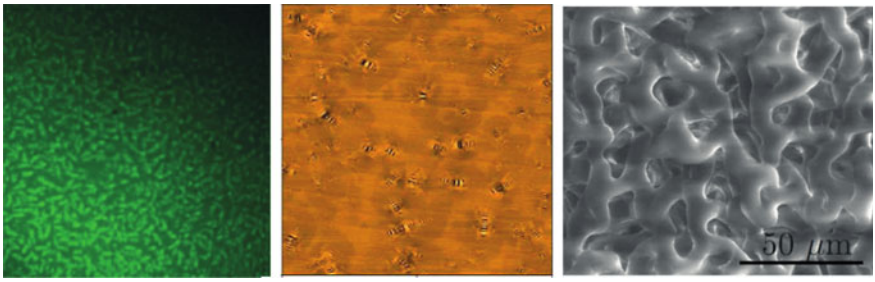


**Fig. 2** CLSM image (Handle 2013) (*left*), AFM topograhy scan (Jäger et al.) (*center*), and ESEM result (Stangl et al. 2006) (*right*)

solid, aromatics look like a yellow to red oily liquid and are mainly responsible for the viscous behavior of bitumen. Aromatics and resins contribute to approximately 30–45 wt% to bitumen each and act as an important stabilizer for the asphaltenes, which account for about 5–20 wt% of paving grade bitumen. As they form a black powder at room temperature, they are responsible for the black color of bitumen.

The arrangement of these constituents—in other words the microstructure—can be made visible by imaging methods, like Confocal Laser Scanning Microscopy (CLSM), Atomic Force Microscopy (AFM), or Environmental Scanning Electron Microscopy (ESEM). As these techniques investigate different properties and levels of observation within the material, the interpretation of the results is not a trivial task. CLSM images visualize fluorescent centers related to the aromatic phase (Handle 2013) (see Fig. 2). By using the AFM experimental setup, the surface of the sample is scanned and a contiguous matrix with embedded "bee"-like inclusions can be observed (Jäger et al. 2004). Since the top film of the matrix is removed by an electron beam, ESEM images give an insight into the material and suggest a string-link structure within a matrix (Stangl et al. 2006) showing spherical centers connected by the strings. As all these inclusions, fluorescent centers and spherical structures exhibit similar dimensions (size range between 1 and 10 µm), they are assumed to represent the same structures.

Recent studies on bitumen microstructure by means of AFM investigations link asphaltenes with these inclusions (Hofko et al. 2015). Additionally, experimental results from rheological (Creep-Recovery) tests conducted on artificially composed bitumen (defined asphaltene content, reduced saturate content) suggest asphaltenes

**Table 1** Main characteristics of paving grade bitumen pen 70/100

| | | |
|---|---|---|
| Penetration | (1/10 mm) | 91 |
| Softening point ring and ball | (°C) | 46.7 |
| SHRP PG | (°C) | 58–22 |

to be responsible for the stiffness of bitumen. According to a widely excepted (Lesueur 2009; Read and Whiteoak 2003; Solaimany Nazar and Rahimi 2009; Sheu 1996; Fawcett and McNally 2003) and recently confirmed concept (Handle 2013), aromatics and resins (fluorescent centers in CLSM image in Fig. 2) adhere to highly polar asphaltenes. Thereby, a solvation layer (mantle) is formed around the asphaltenes smoothing the difference in polarity between them and surrounding maltenes, and so leading to a micelle structure. Depending on the asphaltene content, these micelles—moreover, the mantles around the asphaltenes—interact with each other establishing a network-like structure (see Fig. 5a and Eberhardsteiner et al. 2014a for details).

To investigate the characteristics of these microstructure and the properties of the constituents Creep-Recovery tests and AFM investigations were conducted on artificially composed (precipitated) bitumen with varying asphaltene content (see Eberhardsteiner et al. 2014a and Hofko et al. 2015 for details). These artificial binders originate from an unmodified pen 70/100 paving grade bitumen with a natural asphaltene content of 8.73 wt% and the main characteristics according to Table 1.

Using n-heptane extraction according to ASTM 4124 (ASTM 2001), bitumen was separated into maltenes and asphaltenes. A dispersion of around 10 g of bitumen and 300 ml of n-heptane was assembled and heated to 90 °C for approximately 90 min. After cooling and sedimentation of particles, the dispersion was filtered trough a Büchner-funnel and the asphaltene phase was obtained by further extraction of the remaining particles using a Soxhlet extractor filled with around 700 ml of n-heptane for 72 h. The liquid phase of the Soxhlet extraction was combined with the filtrate of the n-heptane extraction and the solvent n-heptane was evaporated (160 °C, 10 mbar, 50 min) to obtain the maltene phase. Asphaltenes and maltenes were dissolved in toluene and mixed again with a defined asphaltene content. After evaporating the toluene, asphaltenes are "re-dispersed" in the maltenes.

In that way, artificially composed bitumen with an asphaltene content of 0, 5, 20 and 30 wt% could be produced, which were subjected by static shear creep tests—so called Creep-Recovery (CR) tests. These experiments were performed on the experimental setup of a dynamic shear rheometer (DSR) to obtain the mechanical (viscoelastic) behavior of the artificially composed binders. The rheological behavior in terms of linear viscoelasticity (LVE) of these precipitated binders is investigated by analyzing experimental results obtained in CR tests at −5, +5 and +15 °C (see Fig. 3). As these results are detailed in (Eberhardsteiner et al. 2014a) only the key findings are summarized as follows:

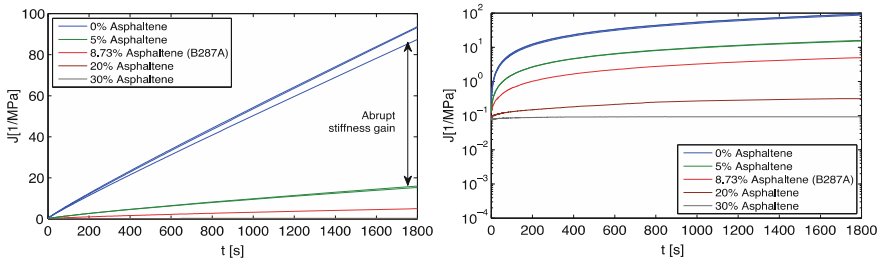


**Fig. 3** Creep response of original and artificially composed bitumen samples from CR tests at +5 °C (Hofko et al. 2015)

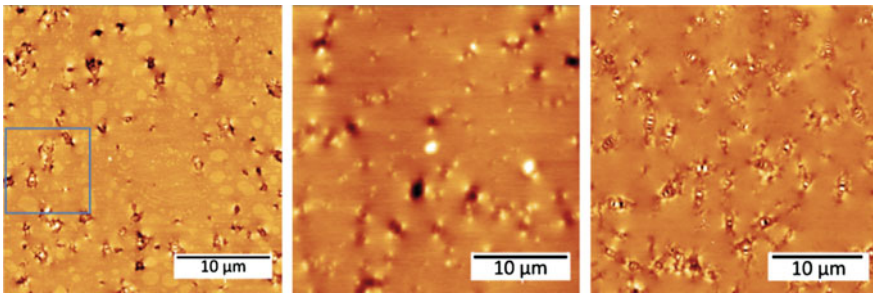


**Fig. 4** The original bitumen with an asphaltene content of 8.73 wt% (*left*, AFM topography scan of the maltene phase (*center*), and an artificially composed binder with an asphaltene content of 8.73 wt% (*right*) (Hofko et al. 2015)

- Adding only low amounts of asphaltenes (5 wt%) results in an increase in stiffness, which cannot be explained by only adding asphaltenes. This already suggests a structure within bitumen related to asphaltenes, which affects the overall mechanical behavior significantly and can be associated with the string-like structures seen in the ESEM images in Fig. 2.
- The original bitumen (8.73 wt% asphaltenes) shows a creep response in between the viscoelastic results of the 5 and 20 wt% precipitated samples (see Fig. 3) indicating the artificially composed binders to exhibit valid linear viscoelastic behavior.

To confirm these assumptions, precipitated binders are examined by AFM analysis. Thereby, the microstructural morphology of the original bitumen, its maltene phase and an artificially composed binder with 8.73 wt% asphaltenes is investigated (see Fig. 4 and Hofko et al. 2015).

The microstructure of the maltenes can be seen in Fig. 4b showing a contiguous matrix with dispersed spherical features. Typical "bee"-like inclusions (as can be seen in Fig. 2b, c) are missing indicating that these structures are n-heptane insoluble.

Four phases can be observed within the original bitumen (see Fig. 4a). "Bee"-like structures (or catana phase) appearing as ellipsoidal inclusions exhibiting

wrinkling along the long axis are dispersed over a contiguous matrix (perpetua phase). Both phases are often mentioned as typical characteristics for the bitumen microstructure (Stangl et al. 2006; Masson et al. 2006; Nahar et al. 2013a, b, 2014; Schmets et al. 2010; Pauli et al. 2001). While terraced patterns form a third phase adjacent to the catana phase, the spherical inclusions in the matrix (fourth phase) is not commonly observed within the bitumen microstructure indicating an incompatibility in interaction between different molecular classes, which suggests that the bitumen is a blend of petroleum products of different crude oil origins to exhibit a desired penetration index (Hofko et al. 2015).

Figure 4c shows the morphology of the artificially composed binder with the same asphaltene content as the original bitumen (8.73 wt%). In contrast to the maltene phase, the same "bee"-like structures embedded in a contiguous matrix as in the original bitumen can be observed. This comeback of the microstructure by "re-dispersing" asphaltenes in the maltene phase as described before can be seen as an evidence for the restoration of characteristic microstructural properties. Hence, artificial binders composed as described before not only react like bitumen in terms of linear viscoelastic behavior but also are valid bitumen-like materials from a microstructural point of view (Hofko et al. 2015).

## 3 Micromechanical Description of Viscoelastic Bitumen Behavior

In Eberhardsteiner et al. (2014a), a micromechanical approach to predict the homogenized behavior of bitumen on the basis of the identified material phases is presented (see Fig. 5b) considering the framework of continuum micromechanics (Hill 1963, 1965; Suquet 1997; Zaoui 2002, 1997; Scheiner and Hellmich 2009). Thereby, an RVE of bitumen is built up by a contiguous matrix of aromatics and resins (labelled by suffix "arom") enclosing spherical saturate inclusions (suffix "sat"). Asphaltenes ("aspha") are also described by spherical inclusions, while an interaction phase (labelled by "ip") represents the aforementioned network-like structure set up by the micelle mantles, which appear as needles oriented in all directions. According to Eq. 1, the relaxation tensor of bitumen follows

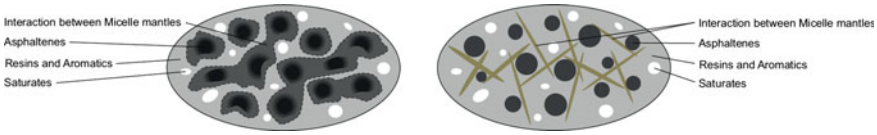


**Fig. 5** Microstructural concept of bitumen based on SARA fractions (*left*), and derived structural RVE concept for microstructural modeling (*right*) (Eberhardsteiner et al. 2014a)

$$
\begin{aligned}
\mathbf{R}^{*}_{bit}(p) = \Big\{ & \big(1 - f_{aspha} - f_{ip} - f_{sat}\big)\mathbf{r}^{*}_{arom}(p) \\
& + f_{aspha}\mathbf{r}^{*}_{aspha}(p) : \Big[\mathbf{I} + \mathbf{P}^{*,\mathrm{arom}}_{sph}(p) : \Big(\mathbf{r}^{*}_{aspha}(p) - \mathbf{r}^{*}_{arom}(p)\Big)\Big]^{-1} \\
& + f_{ip}\mathbf{r}^{*}_{ip}(p) : \int_{\varphi=0}^{2\pi}\int_{\vartheta=0}^{\pi} \Big[\mathbf{I} + \mathbf{P}^{*,\mathrm{arom}}_{cyl}(\vartheta,\varphi,p) : \Big(\mathbf{r}^{*}_{ip}(p) - \mathbf{r}^{*}_{arom}(p)\Big)\Big]^{-1} \frac{\sin\vartheta\, d\vartheta\, d\varphi}{4\pi} \\
& + f_{sat}\mathbf{r}^{*}_{sat}(p) : \Big[\mathbf{I} + \mathbf{P}^{*,\mathrm{arom}}_{sph}(p) : \big(\mathbf{r}^{*}_{sat}(p) - \mathbf{r}^{*}_{arom}(p)\big)\Big]^{-1} \Big\} \\
& : \Big\{ \big(1 - f_{aspha} - f_{ip} - f_{sat}\big)\mathbf{I} \\
& + f_{aspha}\Big[\mathbf{I} + \mathbf{P}^{*,\mathrm{arom}}_{sph}(p) : \Big(\mathbf{r}^{*}_{aspha}(p) - \mathbf{r}^{*}_{arom}(p)\Big)\Big]^{-1} \\
& + f_{ip}\int_{\varphi=0}^{2\pi}\int_{\vartheta=0}^{\pi} \Big[\mathbf{I} + \mathbf{P}^{*,\mathrm{arom}}_{cyl}(\vartheta,\varphi,p) : \Big(\mathbf{r}^{*}_{ip}(p) - \mathbf{r}^{*}_{arom}(p)\Big)\Big]^{-1} \frac{\sin\vartheta\, d\vartheta\, d\varphi}{4\pi} \\
& + f_{sat}\Big[\mathbf{I} + \mathbf{P}^{*,\mathrm{arom}}_{sph}(p) : \big(\mathbf{r}^{*}_{sat}(p) - \mathbf{r}^{*}_{arom}(p)\big)\Big]^{-1} \Big\}^{-1}
\end{aligned}
\tag{1}
$$

where $f_i$ and $\mathbf{r}_i^{*}(p)$ denote the volume fraction and LC-transformed relaxation tensor of phase $i$ with $i \in$ [aspha, ip, arom, sat]. $\mathbf{I}$ is the unity tensor and $\mathbf{P}^{*,\mathrm{arom}}_{\mathrm{sph}}(p)$ and $\mathbf{P}^{*,\mathrm{arom}}_{\mathrm{cyl}}(p)\mathbf{P}^{*,\mathrm{arom}}{}_{\mathrm{cyl}}(p)$ are the fourth-order Hill tensors representing the morphology of spherical and cylindrical inclusions (see Eberhardsteiner et al. 2014a for details). CLSM, AFM and ESEM images suggest the characteristic lengths of the inclusions to be significantly smaller than filler particles at the mastic scale. So, this approach is valid to extend the existing multiscale modeling for HMA described in Aigner et al. (2009), Lackner et al. (2004, 2005, 2009), by adding a bitumen scale.

As bitumen exhibits viscoelastic behavior, its constituents are also assumed to show viscoelastic characteristics. In contrast to the mechanical properties of the maltene phase (saturates, aromatics and resins) the viscoelastic behavior of the asphaltenes has not been identified in a first step but was back-calculated from CR tests conducted on artificially composed binders with defined asphaltene content. Asphaltenes and their mantles are assumed to show the same creep response but are distinguished in terms of morphology and volume content. The volume fraction of the interaction phase is also back-determined from identification experiments and seems to depend on the asphaltene content. Correlating these two results in an exponential relation for (realistic) asphaltene contents, not unlikely for a molecular agglomeration process in nature. Furthermore, saturate inclusions and aromatics-resin-matrix are assumed to exhibit the same viscoelastic behavior also identified in CR tests.

While the identification experiments were conducted at +5 °C on precipitated bitumen with varying asphaltene content, CR tests were performed at −5 and +15 °C to validate the presented model showing a remarkable accordance between experimental results and predicted creep response (see Fig. 6 and Eberhardsteiner et al. 2014a).

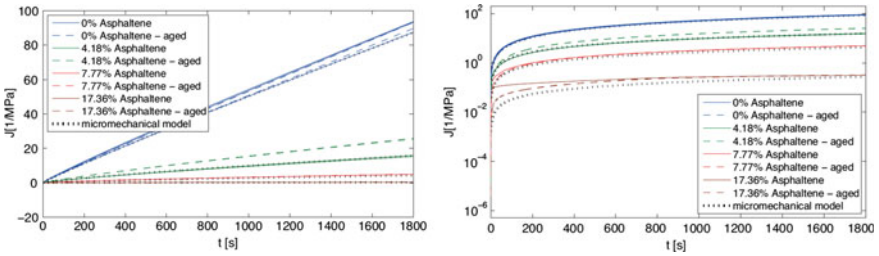


**Fig. 6** Comparison of experimental results and multiscale model predictions for aged artificial bitumen with asphaltene contents of 4.18, 7.77, 12.32 and 17.36 % at +5 °C. Creep compliance is shown on a linear scale (*left*) and on a logarithmic scale (*right*) for a better representation of creep curves with high asphaltene content

## 4 Modeling of Bitumen Aging Behavior

The potential of this approach is presented in Eberhardsteiner et al. (2014b), where the effects of aging on the microstructure are described. Experimental investigations conducted on laboratory-aged (RTFOT+PAV aging) samples of artificially composed binders show that the viscoelastic response of the constituents remain unaffected (see Fig. 6), while a remarkable increase in asphaltene content (7.79–13.36 vol%) can be observed.

While saturates can be considered as almost inert, asphaltenes only exhibit low reactivity at ambient conditions due to their solid state. Hence, the significant susceptibility of highly polar aromatics and resins to oxidative species makes the micelle mantles likely to be responsible for aging effects like decreasing elasticity and ductility. As the degree of associated state of the constituents—and thus the polarity—decreases with increasing distance to an asphaltene micelle center, oxidation occurs mainly at the surface of the micelle mantles (see blue line in Fig. 7). Due to the low mobility of molecules at ambient conditions, a highly polar layer is

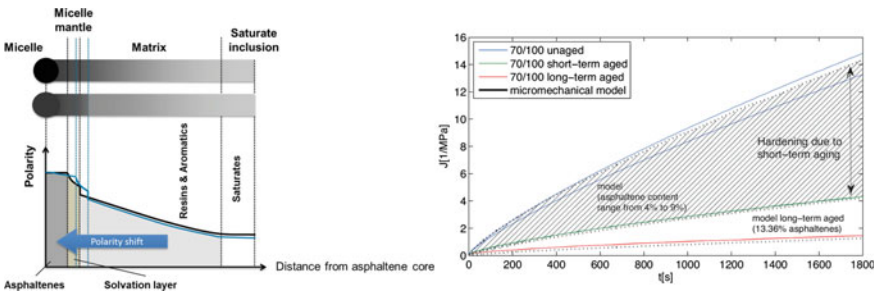


**Fig. 7** Model for the polarity distribution in material phases, for unaged (*black line*) and aged (*blue line*) bitumen (*left*), and comparison of experimental results and micromechanical model predictions for unaged, RTFOT− and RTFOT+PAV-aged natural bitumen pen 70/100 (*right*)

formed at the outside of the mantle increasing the "effective" volume content of the asphaltenes (Handle 2013). Thereby, the substances considered as material phases do not transform and, hence, their material characteristics do not change.

The presented micromechanical model is able to describe these effects by only varying the asphaltene content showing a very good accordance between predicted and experimental results from CR tests not only conducted on precipitated binders (see Fig. 6) but also performed on unaged, laboratory short-term aged (RTFOT aging) and laboratory long-term aged (RTFOT+PAV aging) samples of an unmodified bitumen pen 70/100 with known asphaltene contents. The results can be seen in Fig. 7 (*right*). While model predictions considering a realistic asphaltene content for unaged and short-term aged samples between 4 and 9 % cover experimental results very well, the experimentally obtained long-term aging behavior can be reproduced by model predictions—taking the determined asphaltene content into account—to a remarkable extend.

## 5 Conclusions

Complex processes within HMA like failure, fatigue damage or aging effects strongly depend on the performance of the binder. Hence, an existing multiscale model is extended by adding a micromechanical description of the bitumen level. Before a structural RVE concept, to predict the viscoelastic behavior of aging bitumen, could be introduced, the microstructure was identified by imaging techniques like Confocal Laser Scanning Microscopy (CLSM), Atomic Force Microscopy (AFM) and Environmental Scanning Electron Microscopy (ESEM). In addition, static shear creep tests on artificially composed bitumen with defined asphaltene content, which were confirmed to exhibit valid bitumen-like behavior, were conducted. Thereby, a remarkable accordance between experimental results and model predictions could be shown.

Additionally, aging effects were examined on artificially composed bitumens with varying asphaltene content in static shear creep tests in unaged condition as well as after laboratory long-term aging (RTFOT+PAV aging). A comparison between results from aged and unaged samples show that the material properties of the constituents remain unaffected and, hence, only the remarkable increase in asphaltene content observed (from 7.79 to 13.36 vol%) appears to be responsible for the aging-induced increase of stiffness and decrease of creep rate $\mathrm{d}J/\mathrm{d}t$ and ductility of the bituminous layers. As validation experiments conducted on unaged, laboratory short- term (RTFOT) and long-term aged (RTFOT+PAV) samples of a natural bitumen pen 70/100 show, the presented micromechanical model allows to reproduce these microstructural aging effects remarkably.

Due to the complex assembling of artificially composed binders, only the microstructure of one specific unmodified bitumen pen 70/100 was studied in the course of this work. Validating the findings by observing the composition of another pen 70/100 bitumen as well as identifying the microstructure of an unmodified and

modified bitumen (exhibiting another penetration index) shall be a topic of further research. Further micromechanical modeling of failure mechanisms and fatigue effects at the bitumen level appears as useful extension to the presented model.

**Acknowledgments** The authors gratefully acknowledge financial support from the Austrian Research Promotion Agency (FFG) and the sponsors Pittel+Brausewetter, Swietelsky and Nievelt through project "OEKOPHALT—Physical-chemical fundamentals on bitumen aging". They further appreciate the support of Daniel Großegger and Thomas Riedmayer with sample preparation and execution of Creep-Recovery tests.

## References

AIGNER, E., LACKNER, R. & PICHLER, C. 2009. Multiscale prediction of viscoelastic properties of asphalt concrete. *Journal of Materials in Civil Engineering,* 21, 771-780.

ASTM 2001. ASTM D 4124-01: Standard Test Methods for Separation of Asphalt into Four Fractions.

BEARSLEY, S., FORBES, A. & HAVERKAMP, R. G. 2004. Direct observation of the asphaltene structure in paving-grade bitumen using confocal laser-scanning microscopy. *Journal of Microscopy-Oxford,* 215, 149-155.

BODAN, A. N. 1982. Polyquasispherical Structure of Petroleum Asphalts. *Chemistry and Technology of Fuels and Oils,* 18, 614-618.

CORBETT, L. W. 1969. Composition of Asphalt Based on Generic Fractionation Using Solvent Deasphaltening Elution-Adsorption Chromatography and Densimetric Characterization. *Analytical Chemistry,* 41, 576-&.

EBERHARDSTEINER, L., FÜSSL, J., HOFKO, B., BLAB, R., GROTHE, H., HANDLE, F. & HOSPODKA, M. 2014a. Influence of asphaltene content on mechanical bitumen behavior - Experimental invesitgation and micromechanical modeling. *Materials and Structures,* 10.1617/s11527-014-0383-7.

EBERHARDSTEINER, L., FÜSSL, J., HOFKO, B., BLAB, R., GROTHE, H., HANDLE, F. & HOSPODKA, M. 2014b. Towards a microstructural model of bitumen aging behavior. *International Journal of Pavement Engineering,* DOI 10.1080/10298436.2014.993204.

ESPINAT, D., ROSENBERG, E., SCARSELLA, M., BARRE, L., FENISTEIN, D. & BROSETA, D. 1998. Colloidal structural evolution from stable to flocculated state of asphaltene solutions and heavy crudes. *Structures and Dynamics of Asphaltenes*, 145-201.

FAWCETT, A. & MCNALLY, T. 2003. Polystyrene and asphaltene micelles within blends with a bitumen of an SBS block copolymer and styrene and butadiene homopolymers. *Colloid and Polymer Science,* 281, 203-213.

FORBES, A., HAVERKAMP, R. G., ROBERTSON, T., BRYANT, J. & BEARSLEY, S. 2001. Studies of the microstructure of polymer-modified bitumen emulsions using confocal laser scanning microscopy. *Journal of Microscopy-Oxford,* 204, 252-257.

HANDLE, F. Bitumen Structure and Bitumen Ageing. Proceedings of the 15th Austrian Chemistry Days, 2013 Graz, Austria.

HILL, R. 1963. Elastic properties of reinforced solids: some theoretical principles. *Journal of the Mechanics and Physics of Solids,* 11, 357 - 362.

HILL, R. 1965. Continuum micro-mechanics of elastoplastic polycrystals. *Journal of Mechanics and Physics of Solids,* 13, 89 - 101.

HOFKO, B., EBERHARDSTEINER, L., FÜSSL, J., GROTHE, H., HANDLE, F., HOSPODKA, M., NAHAR, S., SCHMETS, A. & SCARPAS, A. 2015. Impact of Maltene and Asphaltene Phase on Mechanical Behavior and Microstructure of Bitumen. *Materials and Structures (accepted for publication).*

JÄGER, A., LACKNER, R., EISENMENGER-SITTNER, C. & BLAB, R. 2004. Identification of Microstructural Components of Bitumen by Means of Atomic Force Microscopy (AFM). *PAMM,* 4, 400-401.

LACKNER, R., BLAB, R., JAGER, A., SPIEGL, M., KAPPL, K., WISTUBA, M., GAGLIANO, B. & EBERHARDSTEINER, J. 2004. Multiscale modeling as the basis for reliable predictions of the behaviour of multi-composed materials. *Progress in Engineering Computational Technology,* 8, 153-187.

LACKNER, R., SPIEGL, M., BLAB, R. & EBERHARDSTEINER, J. 2005. Is low-temperature creep of asphalt mastic independent of filler shape and mineralogy? Arguments from multiscale analysis. *Journal of Materials in Civil Engineering,* 17, 485-491.

LESUEUR, D. 2009. The colloidal structure of bitumen: Consequences on the rheology and on the mechanisms of bitumen modification. *Advances in Colloid and Interface Science,* 145, 42-82.

MASSON, J. F., LEBLOND, V. & MARGESON, J. 2006. Bitumen morphologies by phase-detection atomic force microscopy. *Journal of Microscopy-Oxford,* 221, 17-29.

NAHAR, S. N., MOHAJERI, M., SCHMETS, A. J. M., SCARPAS, A., VAN DE VEN, M. F. C. & SCHITTER, G. 2013a. First Observation of Blending-Zone Morphology at Interface of Reclaimed Asphalt Binder and Virgin Bitumen. *Transportation Research Record,* Doi 10.3141/2370-01, 1-9.

NAHAR, S. N., QIU, J., SCHMETS, A. J. M., SCHLANGEN, E., SHIRAZI, M., VAN DE VEN, M. F. C., SCHITTER, G. & SCARPAS, A. 2014. Turning back time: Rheological and microstructural assessment of rejuvenated bitumen. *TRB 93rd Annual Meeting Compendium of Papers*, 1-17.

NAHAR, S. N., SCHMETS, A. J. M., SCARPAS, A. & SCHITTER, G. 2013b. Temperature and thermal history dependence of the microstructure in bituminous materials. *European Polymer Journal,* 49, 1964-1974.

PAULI, A. T., BRANTHAVER, J. F., EGGLESTON, C. M. & GRIMES, W. 2001. Atomic force microscopy investigation of SHRP asphalts. *Abstracts of Papers of the American Chemical Society,* 221, U220-U220.

PICHLER, C. & LACKNER, R. 2009. Upscaling of viscoelastic properties of highly-filled composites: Investigation of matrix-inclusion type morphologies with power-law viscoelastic material response. *Composite Science and Technology,* 69, 2410-2420.

READ, J. & WHITEOAK, D. 2003. *The Shell Bitumen Handbook,* London, Thomas Telford Ltd.

RICHARDSON, C. 1913. *The modern Asphalt Pavement,* New York, Wiley.

ROSTLER, F. S. 1965. *Fractional composition: Analytical and functional significance,* New York, Interscience Publishers.

SCHEINER, S. & HELLMICH, C. 2009. Continuum microviscoelasticity model for aging basic creep of early-age concrete. *Journal of Engineering Mechanics,* 135, 307 – 323.

SCHMETS, A., KRINGOS, N., PAULI, T., REDELIUS, P. & SCARPAS, T. 2010. On the existence of wax-induced phase separation in bitumen. *International Journal of Pavement Engineering,* 11, 555-563.

SHEU, E. Y. 1996. Physics of asphaltene micelles and microemulsions - theory and experiment. *Journal of Physics: Condensed Matter,* 1996, 17.

SOLAIMANY NAZAR, A. R. & RAHIMI, H. 2009. Investigation on Agglomeration-Fragmentation Processes in Colloidal Asphaltene Suspensions. *Energy & Fuels*, 8.

STANGL, K., JAGER, A. & LACKNER, R. 2006. Microstructure-based identification of bitumen performance. *Road Materials and Pavement Design,* 7, 111-142.

SUQUET, P. 1997. *Continuum micromechanics*, Springer, Wien - New York.

ZAOUI, A. Structural morphology and constitutive behavior of microheterogeneous materials. Continuum micromechanics, 1997. Springer, Wien - New York, 291 – 347.

ZAOUI, A. 2002. Continuum micromechanics: Survey. *Journal of Engineering Mechanics (ASCE),* 128, 808-816.

# Three Different Ways of Calibrating Burger's Contact Model for Viscoelastic Model of Asphalt Mixtures by Discrete Element Method

**Huan Feng, Matteo Pettinari and Henrik Stang**

**Abstract** In this paper the viscoelastic behavior of asphalt mixture was investigated by employing a three-dimensional discrete element method. Combined with Burger's model, three contact models were used for the construction of constitutive asphalt mixture model with viscoelastic properties in the commercial software $PFC^{3D}$, including the slip model, linear stiffness-contact model, and contact bond model. A macro-scale Burger's model was first established and the input parameters of Burger's contact model were calibrated by adjusting them so that the model fitted the experimental data for the complex modulus. Three different approaches have been used and compared for calibrating the Burger's contact model. Values of the dynamic modulus and phase angle of asphalt mixtures were predicted by conducting DE simulation under dynamic strain control loading. The excellent agreement between the predicted and the laboratory test values for the complex modulus shows that DEM can be used to reliably predict the viscoelastic properties of asphalt mixtures.

**Keywords** Asphalt mixtures · Viscoelastic · Discrete element method · Burger's model

## 1 Introduction

Asphalt is a composite of mastic, aggregate and air void, in which the mastic phase exhibits viscoelastic behavior in pavement service conditions. The mechanical performance of asphalt mixture is dependent on the material properties, the environmental and loading conditions. From the material properties point of view, asphalt mixture's individual components and the way they are interacting with each

H. Feng (✉) · M. Pettinari · H. Stang
Department of Civil Engineering, Technical University of Denmark,
Kongens Lyngby, Denmark
e-mail: hufe@byg.dtu.dk

H. Stang
e-mail: hs@byg.dtu.dk



F. Canestrari and M.N. Partl (eds.), *8th RILEM International Symposium on Testing and Characterization of Sustainable and Innovative Bituminous Materials*, RILEM Bookseries 11, DOI 10.1007/978-94-017-7342-3_34

other at micro scale level play a significant role in the asphalt mixtures performance. The complex modulus including both dynamic modulus and phase angle has been used widely as the reference parameter for asphalt mixtures in pavement structural design procedures. Experimental testing is the most straight forward method to obtain the complex modulus properties of a specific mixture over a wide range of temperature-frequency. While, numerical simulation based on fundamental material mechanics and theories has the advantage of being able to access the impact of individual material component on the performance of asphalt mixture, and is comparatively more convenient and economic to implement. Discrete element method is one type of numerical simulation method which allows the finite displacement and rotation of discrete particles. Especially after combined with Burger's model, DEM could be used as an excellent tool to capture the viscoelastic behavior of asphalt mixture.

Among recent DEM research studies, Dondi et al. (2014) investigated the DSR complex shear modulus of asphalt binder using 3D discrete element approach. The model has been proved to be able to predict complex modulus and the phase angle of the studied polymer modified bitumen over a wide range of temperatures and frequencies. Liu et al. (2009) developed a viscoelastic model for asphalt mixture, where the viscoelastic behavior of asphalt mastic (including fines, fine aggregates, and asphalt binder) was represented with Burger's model. The Burger's model parameters were calibrated by fitting the Laboratory test data for each frequency. The same approach of calibrating the Burger's model has been adopted by Yu and Shen (2013) and Jun et al. (2011, 2012). The irregular shape of aggregate particles was modeled using a clump of spheres. The nonlinear behavior of the complex modulus was captured. Cai et al. (2014) investigated the behavior of the asphalt mixture under constant strain rate uniaxial compression tests. By combining Burger's model with parallel bond, the time-dependent contact stiffness was obtained with the ability to transmit moment and torsion. Different design parameters have also been studied, such as Burger's model parameters, friction coefficient, and bond radius multiplier.

In summary, existing studies provided meaningful insights into understanding and simulating the viscoelastic behavior of asphalt mixture by adopting Burger's model. However, the same conventional approach of calibrating the Burger's model has been used by many different researchers. Based on previous research (Feng et al. 2015), three different ways of calibrating the Burger's model were further investigated in this paper.

## 2 Laboratory Tests

The mixture was a Stone Mastic Asphalt with a maximum aggregates dimension of 11 mm. The bitumen used was Polymer modified 45/80–65. The measurements were collected using a Frequency Sweep test in Direct Tension Compression configuration in a strain control condition. A sinusoidal strain with amplitude of

**Table 1** FST results from 1 to 20 Hz at 10 °C

| Frequency sweep test results at 10 °C | | |
|---|---|---|
| Red. frequency (Hz) | Complex modulus (MPa) | Phase angle (°) |
| 1.00 | 4115.00 | 27.30 |
| 2.00 | 4976.00 | 25.30 |
| 5.00 | 6281.00 | 22.60 |
| 10.00 | 7402.00 | 21.50 |
| 15.00 | 8019.00 | 19.60 |
| 20.00 | 8494.00 | 18.90 |

35με was applied to a cylindrical sample glued on two steel plates screwed to the loading rig. The tests were conducted in a range of frequencies between 0.1 and 40 Hz, at the temperatures of −15, −10, 0, 10 and 20 °C. In this paper, only the results collected at 10 °C from 1 to 20 Hz have been considered (Table 1).

The adopted range of frequency can be explained and justified through two different and fundamental ways. The first is because of the properties of the Burgers model itself. Nilsson et al. (2002) have shown that Burger's model is a simple one capable of characterizing the viscoelastic property of asphalt concrete, but it cannot be used for a wide range of frequencies or temperatures. They found that the Stiffness Modulus was adequately described by the Burger model between 0.5 and 40 Hz. Outside of this range the Modulus was underestimated. The corresponding phase angle values were only estimated correctly between 5 and 25 Hz. Considering both Stiffness Modulus and Phase angle, these authors demonstrated that Burgers model was able to describe these mechanical properties acceptably over a limited frequency range (in the order of 1–20 Hz).

The second is because of the need for investigation of asphalt mixture response at the natural frequency of a flexible pavement when subjected to traffic loading. As suggested by different authors, the natural frequency, which depends on type and speed of the vehicle as well as temperature and type of pavement structure, can range from 6 to 12 Hz (Uddin 2003; Darestani et al. 2006). It has been found also that truck loading frequency is about 4.6 Hz at a speed of 58 km/h and 6.5 Hz at 82 km/h (Gillespie 1993).

## 3 DEM Contact Model and Simulation Method

As one of the key components in defining DEM modeling, the contact model describes the constitutive behavior of a contact associated by two particles. In this paper, the asphalt mixture sample is modeled at meso-scale level without distinguishing irregular shape aggregate and asphalt binder, and the properties of the asphalt binder are determined based on the appropriate contact mechanisms. $PFC^{3D}$, the commercial DEM program used in this study, provides two standard

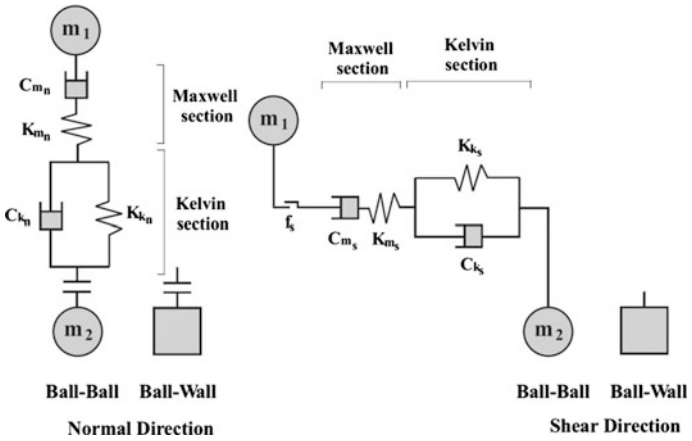


**Fig. 1** Mechanical entities comprising the Burger's model (Itasca 2008)

contact models (Linear and Hertz) and several alternative contact models including the Burger's model. The Burger's model simulates the creep properties using a combination of a Kelvin model and a Maxwell model connected in series in both the normal and shear directions. There are eight parameters to describe the contact relations between two microscopic particles. The microscale schematic plot of the Burger's model is shown in Fig. 1 (Itasca 2008). The Burger's contact model provides the considerations of the time dependent characteristic of asphalt mixture in a relative effective and simple way. This contact model is thus used in the DEM simulation for predicting the complex modulus of asphalt mixture.

## *3.1 Calibrations of Burger's Model*

There is no straight forward way for the calibration of model parameters related to the micromechanical properties of the material, and their values cannot be obtained directly from the experimental results. Therefore, a macroscale Burger's model will first be established to be correlated to the experimental dynamic modulus and phase angle. The parameters of the macroscopic Burger's model can then be converted into the microscopic model parameters. In this study, it was also chosen to equate the normal and shear direction parameters of Burger's contact model (Liu and You 2008; Adhikari and You 2010; Feng et al. 2015).

### 3.1.1 Constant Set of Burger's Contact Model

Total strain in the Burger's model may be written as:

$$\varepsilon = \varepsilon_{de} + \varepsilon_{ie} + \varepsilon_{cp} \tag{1}$$

Further, stress-strain relationship may be written as:

$$\sigma = E_1\varepsilon_{ie}, \quad \sigma = \eta_1\frac{\partial}{\partial t}\varepsilon_{cp}, \quad \sigma = E_2\varepsilon_{de} + \eta_2\frac{\partial}{\partial t}\varepsilon_{de} \tag{2}$$

Substituting Eq. (2) into Eq. (1) we can obtain:

$$\varepsilon = \frac{\sigma}{E_1} + \frac{\int \sigma dt + C_1}{\eta_1} + \mathrm{e}^{\int -\frac{E_2}{\eta_2 dt}}\left(\int \frac{\sigma}{\eta_2}\mathrm{e}^{\int \frac{E_2}{\eta_2 dt}dt} + C_2\right) \tag{3}$$

where $E_1$, $\eta_1$, $\eta_2$ and $E_2$ = Burger's model parameters as mentioned. $\sigma$ and $\varepsilon$ = stress and strain; $C_1$ and $C_2$ = constants determined by the Eq. (4) below when $t = 0$,

$$\frac{\int \sigma dt + C_1}{\eta_1} = 0 \quad \mathrm{e}^{\int -\frac{E_2}{\eta_2 dt}}\left(\int \frac{\sigma}{\eta_2}\mathrm{e}^{\int \frac{E_2}{\eta_2 dt}dt} + C_2\right) = 0 \tag{4}$$

When asphalt mixtures are subjected to dynamic stress $\sigma^* = \sigma_0\,\mathrm{e}^{i\omega t}$, the resulting dynamic strain is described as $\varepsilon = \varepsilon^*\,\mathrm{e}^{i\omega t}$ (Kim 2009). Consequently, the complex compliance, which is the reciprocals of the dynamic modulus, can be expressed using the following Eq. (5):

$$D^*(\omega) = \frac{\varepsilon^*}{\sigma_0} = \frac{1}{K_m} + \frac{1}{i\omega C_m} + \frac{1}{K_k + i\omega C_k} \tag{5}$$

Therefore, the dynamic modulus could be obtained as Eq. (6):

$$|E^*| = \frac{1}{|D^*|} = \frac{1}{\sqrt{\left(\frac{1}{K_m} + \frac{K_k}{K_k^2+\omega^2 C_k^2}\right)^2 + \left(\frac{1}{\omega C_m} + \frac{\omega C_k}{K_k^2+\omega^2 C_k^2}\right)^2}} \tag{6}$$

The phase angle φ can be expressed as Eq. (7):

$$\phi = \tan^{-1}\left(\frac{K_m}{\omega C_m}\frac{K_k^2 + \omega^2 C_k^2 + \omega^2 C_k C_m}{K_k^2 + \omega^2 C_k^2 + K_k K_m}\right) \tag{7}$$

The constant set of Burger's contact model were calibrated based on the procedure above by using the laboratory test results of dynamic modulus and phase angles from the whole frequency range 1 to 20 Hz. Once the macroscale parameters are obtained, the input parameters for microscale can be obtained from the following Eq. (8):

**Table 2** Constant set of Burger's model parameters for DEM input

| $K_k$ (MPa) | $K_m$ (MPa) | $C_k$ (MPa * s) | $C_m$ (MPa * s) |
|---|---|---|---|
| 12.78 | 13.47 | 0.38 | 2.31 |

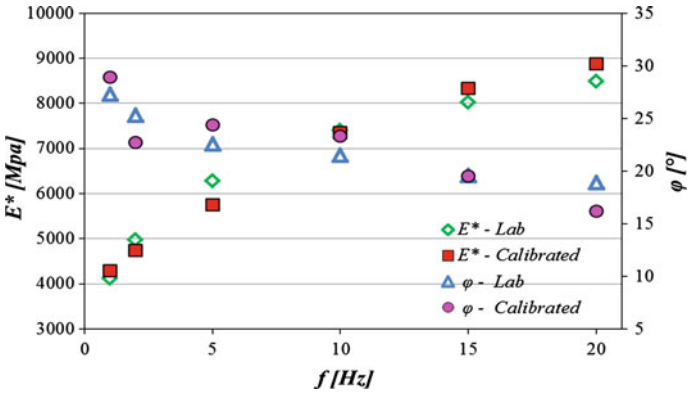


**Fig. 2** Calibration for input parameters of Burger's contact model fitted with lab test data

$$\begin{aligned} K_{mn} &= K_m L, \quad C_{mn} = C_m L \\ K_{kn} &= K_k L, \quad C_{kn} = C_k L \end{aligned} \tag{8}$$

where, $L = R(A) + R(B)$, which is the sum of the radius of two contact balls $A$ and $B$. The obtained Burger's contact model input parameters are listed in Table 2. The calibration for input parameters of Burger's contact model fitted with lab test data is shown in Fig. 2.

### 3.1.2 Variable Set of Burger's Contact Model

There are two methods available for the calibration of the variable set of Burger's contact model. The first way of calibrating the variable Burger's model set is the conventional way, in which the stiffness and viscosity of the Maxwell model were initialized first, which can be expressed as Eq. (9):

$$K_m = \lim_{\omega \to \infty} |E^*|, \quad C_m = \lim_{\omega \to 0} \left| \frac{E^*}{\omega} \right| \tag{9}$$

The actual range of frequency used in the experiments of this study is between 1 and 20 Hz. Hence the stiffness and viscosity of the Maxwell model can be approximated using the following Eq. (10), where $\omega = 125.7$ rad/s and $\omega = 6.3$ rad/s correspond to frequency $f = 20$ Hz and $f = 1$ Hz.

**Table 3** 1st set of variable Burger's parameters input for DEM

| f (Hz) | 1 | 5 | 10 | 15 | 20 |
|---|---|---|---|---|---|
| $K_k$ (MPa) | 11.55 | 15.96 | 15.12 | 14.59 | 11.54 |
| $K_m$ (MPa) | 13.47 | 13.47 | 13.47 | 13.47 | 13.47 |
| $C_k$ (MPa * s) | 0.29 | 0.47 | 0.39 | 0.33 | 0.30 |
| $C_m$ (MPa * s) | 2.31 | 2.31 | 2.31 | 2.31 | 2.31 |

**Table 4** 2nd set of variable Burger's parameters input for DEM

| f (Hz) | 1 | 5 | 10 | 15 | 20 |
|---|---|---|---|---|---|
| $K_k$ (MPa) | 12.78 | 12.78 | 12.78 | 12.78 | 12.78 |
| $K_m$ (MPa) | 12.03 | 15.16 | 13.48 | 12.92 | 13.06 |
| $C_k$ (MPa * s) | 0.38 | 0.38 | 0.38 | 0.38 | 0.38 |
| $C_m$ (MPa * s) | 2.34 | 5.32 | 5.46 | 1.82 | 0.95 |

$$K_m = \lim_{\omega \to 125.7} |E^*|, \quad C_m = \lim_{\omega \to 6.3} \left| \frac{E^*}{\omega} \right| \tag{10}$$

Substituting Eq. (10) into Eqs. (6) and (7), the stiffness and viscosity for Kelvin model can be obtained.

Different values for $K_k$ and $C_k$ were obtained for each frequency, while the values for $K_m$ and $C_m$ were kept constant for the whole frequency range used. Since the input parameters of Burger's contact model were calibrated for each frequency one by one, the calibration results fit with lab test data perfectly. The determined parameters for the 1st set of microscopic Burger's contact model are shown in Table 3.

The same procedure has been adopted for calibration of the second set of variable Burger's model. The difference is this time the Kevin model stiffness $K_k$ and viscosity $C_k$ were initialized first and were kept constant for all the frequencies, as shown in Table 4. Consequently, the same perfect match between the calibration for input parameters of Burger's contact model and lab test data was obtained.

## 4 Numerical Analysis

### *4.1 DEM Simulation of the Complex Modulus*

In this study, the model parameters for DE simulation were determined using the procedure discussed previously in this paper. The viscoelastic DE simulation was conducted with the corresponding model parameters under cyclic uniaxial compression loadings. As shown in Fig. 3a, the cylindrical model was 2 cm in height and 2 cm in diameter, which comprises 5860 spheres. Compressive dynamic loads in the z-direction were applied to the top loading plate of the digital sample, while the bottom plate of this sample was fixed in all directions. The applied load

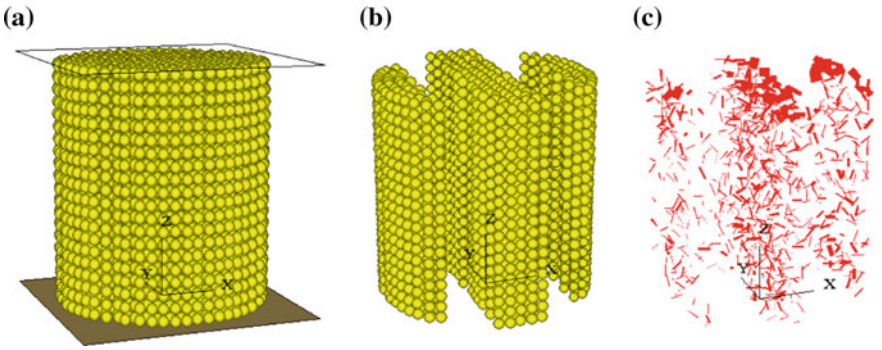


**Fig. 3** Discrete element model in $PFC^{3D}$. **a** DEM model. **b** Slices of the model. **c** Tensile forces in slice model

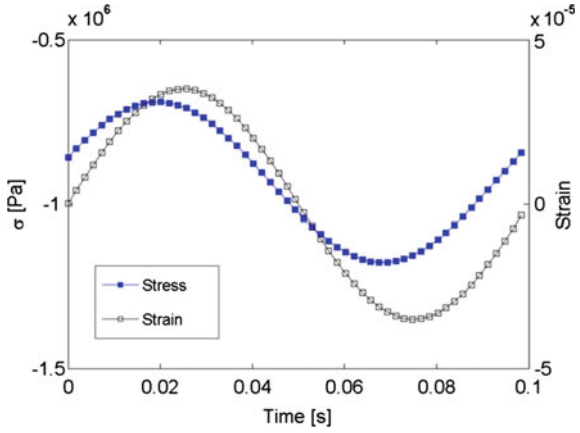


**Fig. 4** Applied strain and corresponding stress at 10 Hz in DEM simulation

frequencies were 20, 15, 10, 5 and 1 Hz. Figure 3b, c show the slices of the model and the corresponding internal tensile contact forces at the moment of peak tensile loading strain, in which the thickness of the bar is proportional to the amplitude of the force.

The motions of the spheres on the top and bottom layers were slaved to the motions of the loading plates in order to simulate the glue effect in the laboratory. Prior to the actual simulation, the sample was compacted in order to achieve an initial isotropic stress state. In order to reduce the computation time for discrete-element (DE) model of asphalt-based materials, the methodology developed by Liu and You (2011) was adopted, which is based on the frequency—temperature superposition principle. The Burger's model parameters at regular frequencies were modified to those at virtual frequencies, which were much larger than the regular frequencies, the computation time was significantly reduced.

The average stress of the model was measured by using installed measurement spheres. Figure 4 shows one of the simulation results from DEM at loading

frequency 10 Hz. The applied strain and average stress response were used for the calculation of the dynamic modulus ($E^*$) and phase angle ($\varphi$) for the whole frequency range from 1 to 20 Hz using Eq. (11).

$$E^* = \frac{\sigma_{\max} - \sigma_{\min}}{\varepsilon_{\max} - \varepsilon_{\min}} \qquad \varphi = \frac{\Delta t}{T} \times 360 \tag{11}$$

where, $\varepsilon_{max}$, $\varepsilon_{min}$, $\sigma_{max}$ and $\sigma_{min}$ = maximum and minimum values of the applied strain and the calculated stress response; $\Delta t$ = time difference between two adjacent peak strains; and $T$ = loading period, which is the inverse of the loading frequency.

The predicted dynamic modulus and phase angles from all the three different ways of calibrating Burger's contact model were compared with the laboratory test results, as shown in Figs. 5, 6, and 7. It was found that for all the three DE

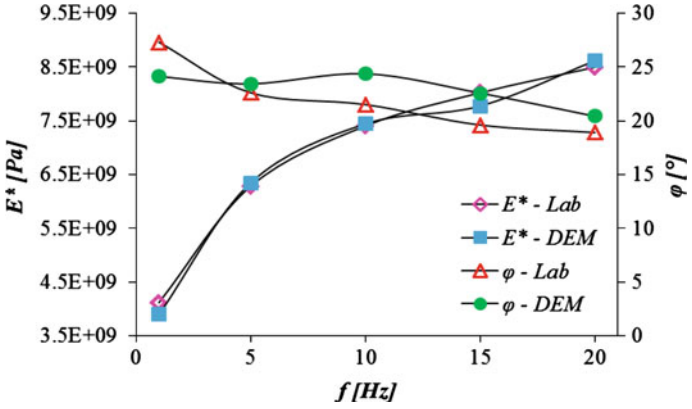


**Fig. 5** Constant Burger's contact model compared with lab test data

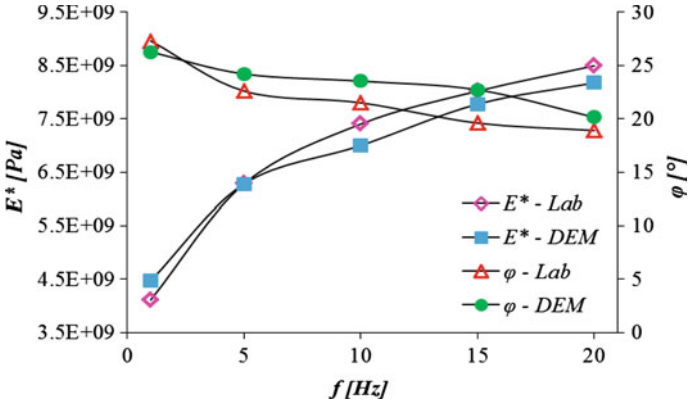


**Fig. 6** *1st* set of variable Burger's contact model, compared with lab test data

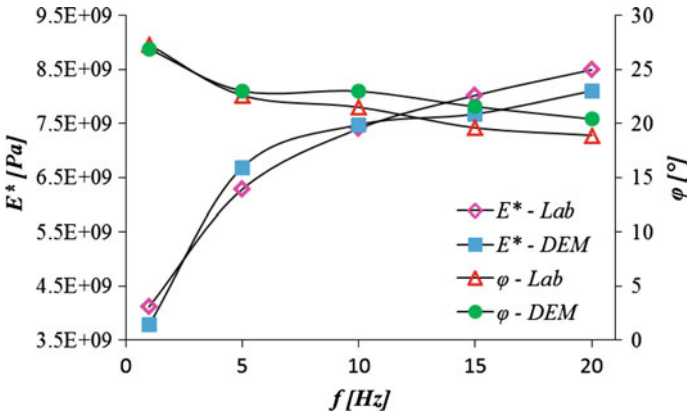


**Fig. 7** *2nd* set of variable Burger's contact model, compared with lab test data

viscoelastic models with different Burger's contact model, the predicted dynamic modulus were in general slightly lower than those from the lab tests, while the predicted phase angles were slightly higher. The 1st variable Burger's contact model has a minimum average prediction error of 1.92 % for the dynamic modulus. The minimum average prediction error for phase angle is from the 2nd variable Burgers model, which is 5.04 %. Therefore, compared to the constant set of Burger's contact model, the Burger's contact model calibrated according to each frequency can provide more accurate predictions of the viscoelastic properties of the asphalt mixtures.

## 5 Conclusions

1. The current model was able to capture the viscoelastic properties of asphalt mixtures at the investigated temperature and traffic loading frequencies, the internal mechanical response of the material at macro-scale inside the flexible pavement structure. It could provide a feasible way to study the correlation between the dissipated energy and the rolling resistance of asphalt mixtures in the future.
2. The 1nd variable Burger's contact model has a minimum average prediction error of 1.92 % for the dynamic modulus. The minimum average prediction error for phase angle is from the 2nd variable Burgers model, which is 5.04 %. Therefore, compared to the constant set of Burger's contact model, the Burger's contact model calibrated according to each frequency can provide more accurate predictions of the viscoelastic properties of the asphalt mixtures.
3. Use of the frequency-temperature superposition meant that less calculation time was needed for the viscoelastic DE simulation of asphalt mixtures.

## References

Adhikari S. and You Z. (2010) 3D discrete element models of the hollow cylindrical asphalt concrete specimens subject to the internal pressure, International Journal of Pavement Engineering. 11:5, 429-439.

Cai W., McDowell G.R. and Airey G.D. (2014) Discrete element visco-elastic modelling of a realistic graded asphalt mixture. Soil and Foundations, 54(1):12-22.

Darestani, M. Y., P. T. David, N. Andreas, and B. Daksh (2006) "Dynamic Response of Concrete Pavements under Vehicular Loads", Proc., IABSE Symposium—Response to Tomorrow's Challenges in Structural Engineering, Budapest, Hungary, pp. 104–105.

Dondi G., Vignali V., Pettinari M., Mazzotta F., Simone A. and Sangiorgi C. (2014). Modeling the DSR complex shear modulus of asphalt binder using 3D discrete element approach. Construction and Building Materials 54:236–246.

Feng H., Pettinari M., Hofko B. and Stang H. (2015) Study of the Internal Mechanical response of an asphalt mixture by 3-D Discrete Element Modeling. Construction and Building materials.

Gillespie, T. D., S. M. Karimihas, D. Cebon, M. W. Sayers, M. A. Nasim, W. Hansen, and N. Ehsan (1993) NCHRP Report 353: Effects of Heavy- Vehicle Characteristics on Pavement Response and Performance. TRB, National Research Council, Washington, D.C.

Itasca Consulting Group (2008), Inc. PFC3D Ver. 4.0, Minneapolis.

Jun C., Tongyan P., and Xiaoming H. (2011). Discrete Element Modeling of Asphalt Concrete Cracking Using a User-defined Three-dimensional Micromechanical Approach. Journal of Wuhan University of Technology-Mater. Sci. Ed. Vol. 26 No. 6.

Jun C., and Tongyan P .et al. (2012) Predicting the Dynamic Behavior of Asphalt Concrete Using 3D DEM. Journal of Wuhan University of Technology-Mater. Sci. Ed. Vol.27 No. 2.

Kim RY. (2009) Modeling of Asphalt Concrete. ASCE Press

Liu Y., Dai Q. and You Z. (2009) Viscoelastic Model for Discrete Element Simulation of Asphalt Mixtures. Journal of Engineering Mechanics. Vol. 135, No. 4.

Liu Y., and You Z. (2008), Simulation of Cyclic Loading Tests for Asphalt Mixtures using User Defined Models within Discrete Element Method, GeoCongress 2008.

Liu Y., and You Z. (2011) Accelerated Discrete-Element Modeling of Asphalt-Based Material with Frequency-Temperature superposition principle. Journal of Engineering Mechanics,. Vol. 137, No. 5.

Nillson, R.N., Hopman, P.C., and Isacsson, U. (2002) Influence of different rheological models on predicted pavement responses in flexible pavements. Road Materials and Pavement Design: An International Journal, 3, 117–149.

Uddin, W. (2003) "Effects of FWD Load-Time History on Dynamic Response Analysis of Asphalt Pavement", Presented at Pavement Performance Data Analysis Forum in Conjunction with MAIREPAV03, Guimaraes, Portugal.

Yu H., and Shen S. (2013) A micromechanical based three-dimensional DEM approach to characterize the complex modulus of asphalt mixtures. Construction and Building Materials 38 1089–1096.

# Experimental Investigation on Surface Performance and Acoustic Absorption

**Filippo Giammaria Praticò, Rosolino Vaiana and Teresa Iuele**

**Abstract** Porous European mixes and open-graded friction courses are wearing courses with well-known advantages in terms of noise reduction due to the balance between generation factors (surface texture) and absorption properties. Unfortunately, noise-oriented mix design still calls for further research and the relationship between composition and acoustic performance is mainly unknown. Consequently, the objective of this paper was to study the relationship between acoustic absorption coefficient and pavement surface performance (surface texture and drainability). The acoustic absorption coefficient was measured according to the ISO 13472-1. Acoustical absorption coefficients were analysed by taking into account contract specifications and requirements. Surface texture was investigated according to the standards ISO 13473-1; ISO/CD TS 13473-4; ISO 13473-3. In order to assess the overall state of the surface, also drainability was measured in the same points. Results were compared and analysed in terms of averages and standard deviations, studying in-depth how acoustic absorption properties vary as a function of surface texture and drainability, for a given friction course. A theoretical framework based on texture and acoustic properties was formulated. Results showed that the maximum acoustic absorption (f = 800–1000 Hz) was well correlated with drainability and Sand Height; some texture indicators (profile-based) resulted well correlated with several parameters derived from acoustic absorption spectra and/or macrotexture performance.

**Keywords** Rolling noise · Acoustic absorption · Surface texture · Profilometer

F.G. Praticò
DIIES Department, Mediterranea University of Reggio Calabria, Reggio Calabria, Italy

R. Vaiana · T. Iuele
Department of Civil Engineering, University of Calabria, Arcavacata Campus, Cosenza, Italy
e-mail: rosolino.vaiana@unical.it



F. Canestrari and M.N. Partl (eds.), *8th RILEM International Symposium on Testing and Characterization of Sustainable and Innovative Bituminous Materials*, RILEM Bookseries 11, DOI 10.1007/978-94-017-7342-3_35

## 1 Introduction and Background

Road traffic noise has been recognized as one of the most significant issues to face in order to reduce noise urban environmental pollution. In more detail, noise reduction at the source is very cost-effective, more than treatments on the buildings or on the propagation path—noise barriers. Traffic noise is primarily generated by vehicle engine, aerodynamics and tire-pavement interaction (Praticò et al. 2013, 2014; Ahammed and Tighe 2011; Freitas et al. 2012). Many innovations in the automobile manufacturing have largely reduced the noise generation of the power-train unit; on the contrary, the increase in traffic volumes and vehicles speed registered in the last decades has determined the need for reducing noise by the road pavement itself. In the mid-to-high speed range (approximately above 40 km/h for passenger cars and 70–80 km/h for trucks), the main contributor to traffic noise is tyre/road (rolling) noise (Praticò et al. 2014; Sandberg and Ejsmont 2002). As speed increases, a crossover speed is reached at that point when tire/pavement noise becomes the dominant source. This threshold value is about 40 km/h. Propulsion noise, instead, dominates the total noise at low speeds (Rasmussen et al. 2007). Tyre/road (rolling) noise derives from various and simultaneous generation mechanisms that occur at different degrees, depending on surface and tyre conditions; among them the most common are tyre vibrations, air pumping and stick/slip phenomena. Figure 1 summarizes main processes and parameters.

About 60–80 % of rolling noise is due to vibrations, characterized by a frequency of emission lower than 1000 Hz. This phenomenon is primarily determined by texture wavelengths in the range of 10–500 mm. Radial and tangential vibrations of the tread elements in road/pavement interaction determine low frequency emissions; high frequency emissions, instead, are due to aerodynamic mechanisms related to the compression and expansion of the air trapped between the tire and the surface. The air pumping mechanism is governed by texture wavelengths lower than 10 mm and the rate of noise related to the air pumping mechanism is around 10–30 %. A lower percentage of noise can be attributed to the aerodynamic flow and to the stick and slip process. Other mechanisms (horn effect, Helmholtz resonance, pipe resonance, sidewall vibrations and cavity resonance) cause the amplification of the generated noise, increasing the sound level heard (Sandberg and Ejsmont 2002; Ahammed 2009; AIPCR 2010; Vaiana et al. 2012; Losa et al. 2013). Surface texture and acoustic absorption properties of the pavement play a key role in both generation and propagation of traffic noise. The mechanism of acoustic impedance for noise reduction, in fact, is primarily related to the type of the surface (porous/non porous) and the system of the interconnected voids of the course layer (mix porosity). Furthermore, for a given layer thickness, pavement silentness mainly depends on flow resistivity and tortuosity; all these factors, in turn, depend on the properties of the bituminous mixture (Boscaino et al. 2005). Unfortunately, the relationship among the above factors is mainly unknown (Boscaino and Praticò 2001; Alvarez et al. 2012; Ahammed and Tighe 2011; Jimenez-Espadafor et al. 2011; Mak et al. 2012). By referring to surface texture influence on noise generation

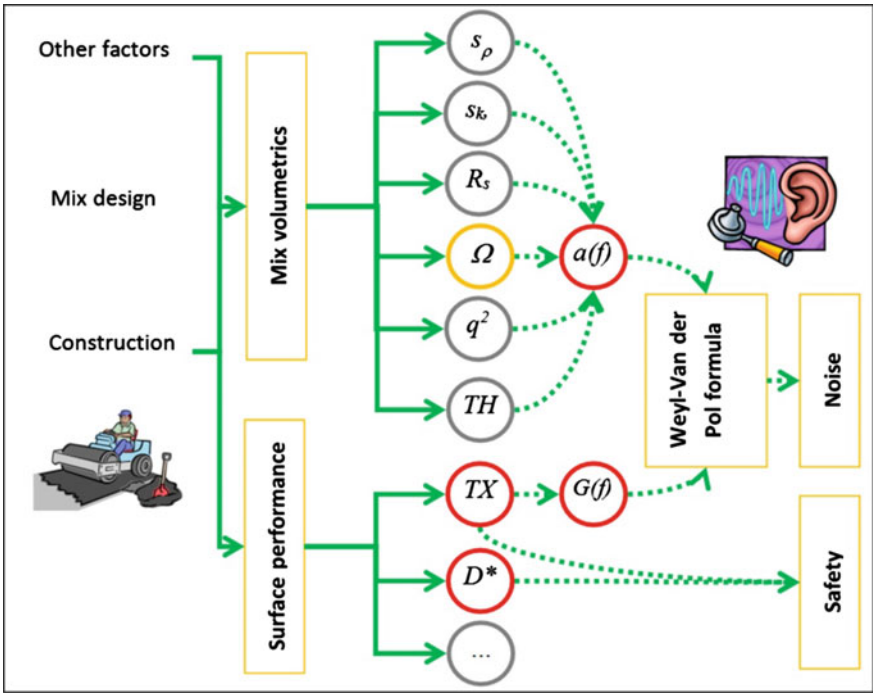


**Fig. 1** Graphical abstract of the paper. *Legend* $s_\rho$, $s_k$ viscous and thermal factors; $R_s$ resistivity (Ns/m$^4$); $\Omega$ porosity; $q^2$ tortuosity; *TH* thickness (mm); *TX* texture indicators; *G*(*f*) generation factors. (*) *D* is considered a surface performance but it strongly depends on volumetrics

and absorption, several models have been set up. Hamet and Klein (2000) focused on the envelopment of a road profile as seen by a tire, as basis for further analyses, while Praticò (2001) developed a method for considering texture influence on generation factors in Weyl-Van der Pol formula. Ongel et al. (2008), Rasmussen (2009), Reyes and Harvey (2011), Fujikawa and Tachibana (2009) developed statistical models of noise generation on asphalt and concrete pavements in which mean profile depth (MPD) or texture levels are included among the inputs which contribute to the overall on-board sound intensity (OBSI) or octave band spectra. Other authors (Brinkmeier et al. 2007; Zhang et al. 2015) approached tire-pavement noise modelling by setting up finite element models of the tire and/or of pavement surface, in order to predict radiated sound. Noise emission levels also depend on pavement maintenance conditions: a widely deteriorated surface may determine a sound level 4.5 dB higher than a new-placed layer with the same characteristics (A.A.V.V. 2001). Recently, many researches have been addressed to the design and production of "quiet" pavement surfaces aimed to absorb the sound energy preserving mechanical requirements as well as surface friction properties. Among them, the most common solutions are the well-known Open Graded Friction Courses (OGFC) or Porous European Mixes, PEMs. These last ones have

an air void content usually exceeding 20 % and act as a wearing course (often 50 mm-thick) on impermeable base courses and have well-known advantages in terms of noise reduction (Alvarez et al. 2010; Freitas 2012; Praticò and Anfosso-Lédée 2012; Praticò and Vaiana 2012; Lu and Harvey 2011). Previous studies (Ahammed and Tighe 2011; Sandberg and Ejsmont 2002) show that the range of sound energy absorption of porous pavements is between 10 and 20 %. A reduction of 3 dBA for a newly placed OGFC compared to a dense graded asphalt mix was observed in previous researches (Caltrans 2006). In Wayson (1998) authors highlighted that OGFC contribute to a reduction of the pass-by noise by 1–9 dBA (with respect to dense hot mix asphalt, HMA). These benefits, however, significantly drop in 5–7 years, thus confirming that porous pavements should be well maintained to prevent the clogging from dust and debris. Traffic post compaction actions also contribute to air voids reduction over time, even though fast traffic tends to produce a self-cleaning effect due to the tires pumping action, which preserves the noise reducing properties to some extent (Gibbs et al. 2005). In the light of the above, the objective of this paper is to better investigate on porous mixes acoustic performance in relation to surface texture and drainability. Data were collected from a survey campaign on a motorway in South Italy. In particular, surface texture was characterized by means of both profile-derived indicators (such as the mean profile depth, MPD, mm, and the texture level, LT, dB) and macrotexture measurements (sand height, SH, mm, sand patch method). The in situ absorption coefficient was measured according to the standard UNI ISO 13472-1 (2004). Finally, surface drainability was characterized in terms of outflow time measurements carried out by means of the Autostrade method (Autostrade 2001; Praticò and Moro 2006, 2007). The paper is organized as follows: in Sect. 2 some details about the experimental plan and the test methods used for the monitoring of surface performance are given. Section 3 contains experiments and results; finally, in Sect. 4 conclusions and future perspective are drawn.

## 2 Experiments and Method

As stated above, the surface performance of a porous pavement was investigated. Experiments were performed on a motorway located in South Italy. Three sections were investigated. In section 1, the following investigations were carried out (northbound carriageway): two points type T + A (T: surface profiles; A: acoustic absorption), and two points type T + SH + 2D (SH: Sand Height; D: drainability). In section 2, the following investigations were carried out: (i) (northbound): two points type T + A, and two points type T + SH + 2D; (ii) (southbound): two points type T + A, and two points type T + SH + 2D. In section 3, the same investigations above mentioned for section 1 were carried out, but in this case experiments were performed in the southbound carriageway. Note that surface texture, defined by the ISO Standards 13473-1 (1997) as “the deviation of a pavement surface from a true

planar surface", can be seen as the superposition of many elementary harmonics, each one corresponding to a specific domain associated with a wavelength range: microtexture, macrotexture, megatexture and roughness. These classes of texture are related to several phenomena that fulfil on the boundary surface between the vehicle and the pavement, where tangential contact forces are transmitted (Praticò 2001). Several methods can be used to measure pavement surface texture and surface descriptors are determined by different criteria (Boscaino and Praticò 2001). In particular, intrinsic or direct criteria are based on surface profile analysis trough which aggregate or spectral indicators can be determined. Aggregate descriptors refer to all the surveyed wavelengths, while spectral descriptors are obtained by imaging pavement profile as the superposition of "many" elementary components (harmonics). In this study both aggregate and wavenumber-related descriptors were derived. A laser profilometer based on conoscopic holography (ISO 13473-3: 2002) was used. The following indicators were derived:

- $MPD_{iso}$: Mean Profile Depth, the average value of the profile depth over a certain distance (baseline)—ISO 13473; $MPD_{aipcr}$: Mean Profile Depth—PIARC;
- Ra: Average Roughness or Centre-line average—$R_a = \Sigma_i |z_i - z_{media}| \cdot p(z_i)$; Ru: Levelling Depth—$Ru = z_{max} - z_{media}$; K: Kurtosis—$K = \sigma^{-4} \cdot \Sigma (z - z_{media})^4 \cdot p(z)$, where $z_i$ is the current value of profile height, $z_{media}$ is the arithmetic mean of $z_i$, $p(z_i)$ is the probability density, in discrete space, for the ith of the $z_i$ measurements, $z_{max}$ is the maximum value of $z_i$;
- Rm: Rut Mean Depth;
- $AAH_e$: Average Asperity Height estimated on the part of the profile above the Mean Profile Depth—$\Sigma h/n$; ASF: Average Shape Factor—$(\Sigma h/n)/(L/n)$, where h is the peak to valley height referred to the micro-texture wavelength range, n is the number of asperities, L is the total length of the specimen in question;
- LT: Texture Level (Evaluated by means of a Fourier Transforms).

The macrotexture was also measured in terms of Sand Height, SH, in mm, according to (CNR94 1983, EN 13036-1 2010, ASTM E965 2006). As for drainability, the on-site outflow time was measured according to the Autostrade method (falling head test on pavement, see Autostrade 2001; Praticò and Moro 2006, 2007). In this test, water flows through pavement, under standard test conditions, as follows: (i) the distance between the marks (reference levels marked on the drainometer) is 25 cm; (ii) the diameter of the drainometer is 14 cm; (iii) the volume of water between the marks is 3848.5 $cm^3$; (iv) the results can be expressed in terms of outflow time (s) or drainability (l/min), where l stands for liter (1000 $cm^3$) and min for minutes (60 s). Previous studies (Praticò and Moro 2006, 2007) showed that drainability depends on air voids content.

The absorption coefficient was measured according to the extended surface method (or Adrienne method, UNI ISO 13472-1:2004). This method is based on the recovering of an acoustic impulse response close to the pavement under test (Sandberg and Ejsmont 2002). A loudspeaker is placed facing the pavement and a microphone is placed between the sound source and the pavement. With the

loudspeaker emitting a transient sound, the microphone receives both the direct sound pressure wave traveling from the sound source to the pavement and the sound pressure wave reflected (including scattering) by the surface under test. The power spectra of the direct and the reflected components, corrected to take into account the path length difference of the two components, give the basis for calculating the acoustic absorption coefficient. Note that two main types of sound stimuli can be generated: MLS (maximum-length sequence) and lin-sweep (linear sweep). To obtain an MLS signal as test signal, an electro-acoustic sound source (loudspeaker) must be used, fed with an electrically generated MLS and continuously repeated. The lin-sweep stimulus consists of a sine wave that slowly changes over time from the lower to the upper edge of the spectrum. There are usually two sweep variants: the abovementioned linear sweep, where the frequency increases linearly over time, and the exponential sweep, where the frequency increases exponentially over time (sometimes referred to as a logs weep). Whatever the shape of the generated sound, the sound absorption coefficient can be expressed as a function of the impulse responses and Time windowing (Praticò et al. 2013, 2014).

## 3 Data Analysis and Results

Figures 2, 3, 4, 5, 6 and 7 illustrate the results obtained. Figure 2 shows the average absorption spectra ($a_0$ is the acoustic absorption coefficient) for both North and South monitoring sections, together with the mean values of the four sections.

As it is possible to see, two or three relative maxima were obtained in the range 0–4000 Hz. The first absolute maximum is obtained for a frequency of about 800–1000 Hz. The second one is visible in the range 2–2.5 kHz, and the third is often recorded for frequencies higher than 3 kHz (3150 Hz for sections 1-N and 3-S and 4000 Hz for sections 2-N and 2-S). Surface texture indicators, derived from profilometric analysis were correlated with both drainability and sand height measurements (see Figs. 3 and 4) for all the sections.

Note that only the aggregate indicators that exhibit correlations with R-square values higher than 0.7 are reported in Fig. 5a, b.

Other profile-based descriptors (VAR, RMS, AADe, Rt, AAD, AAHe, for symbols meaning see section 2) showed R-square values ($R^2$) in the range 0.6–0.7. Lower correlations ($R^2$: 0.3–0.5) were observed for Rm, AAH, ASF and ASFe. Note that, despite MPD (calculated by a low-pass filter, ISO 13473-1) and SH show a very good correlation ($R^2 > 0.8$), the equation is characterized by a y-intercept and a slope that differ from those of the PIARC equation for the calculation of the Estimated Texture Depth from MPD measurements (ETD = 0.8MPD + 0.2). As for drainability, the best correlations ($R^2 > 0.5$) are summarized in Fig. 5. Also in this case, other texture descriptors such as VAR, RMS, Sk, AAD, AAHe and ASFe didn't show a good correlation with drainability (R-square in the range 0.3–0.5). Note that the above relationships among drainability (D), sand height (SH), and mean profile depth (MPD) can be interpreted in terms of divergence from the

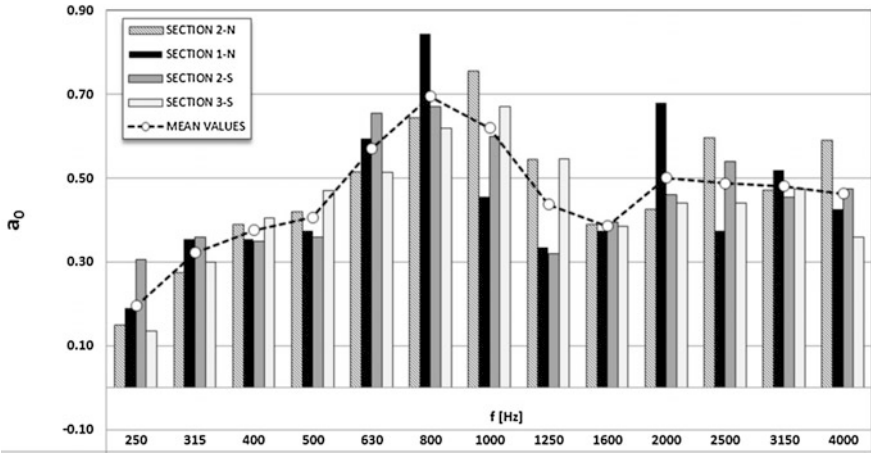


**Fig. 2** Average acoustic absorption coefficients

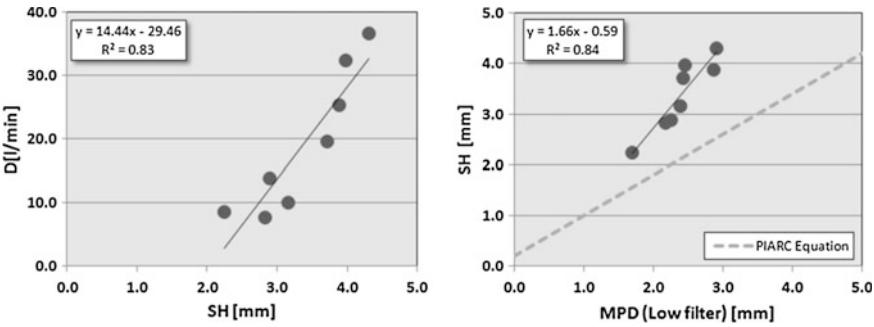


**Fig. 3** Drainability and MPD versus sand height

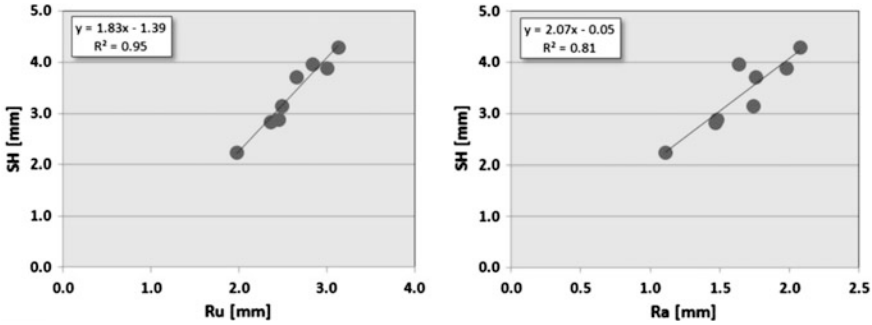


**Fig. 4** Ru and Ra versus sand height

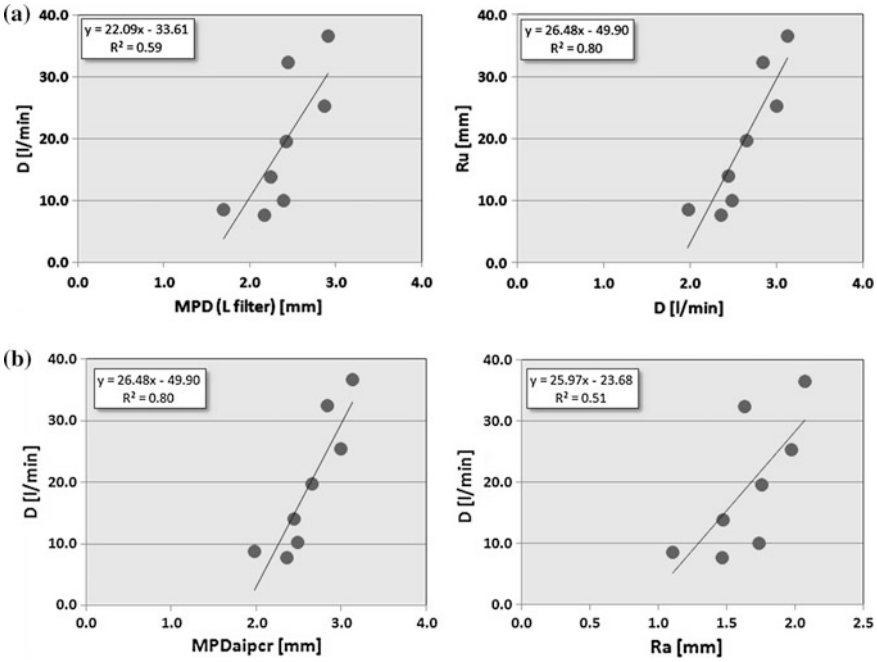


**Fig. 5** **a**, **b** MPD, Ru and Ra versus drainability

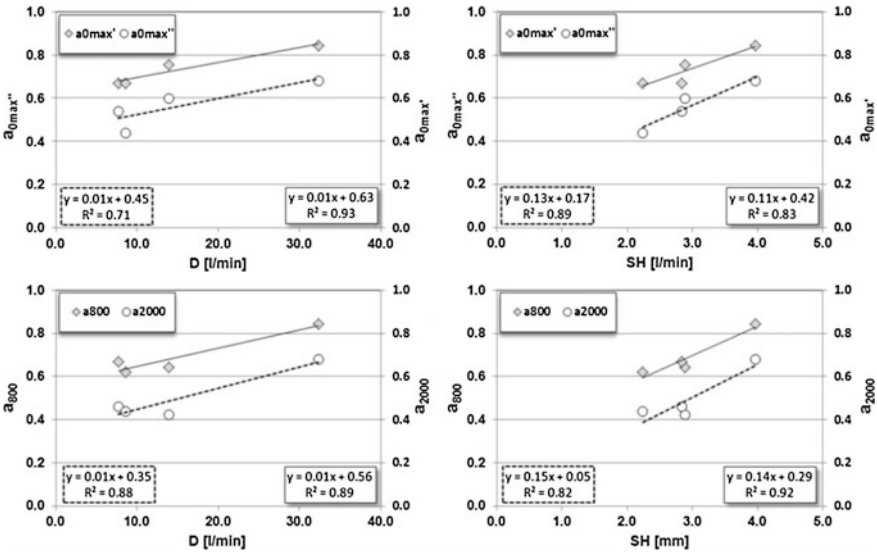


**Fig. 6** Drainability and sand height versus $a_{0max'}$, $a_{0max''}$, $a_{800}$, $a_{2000}$

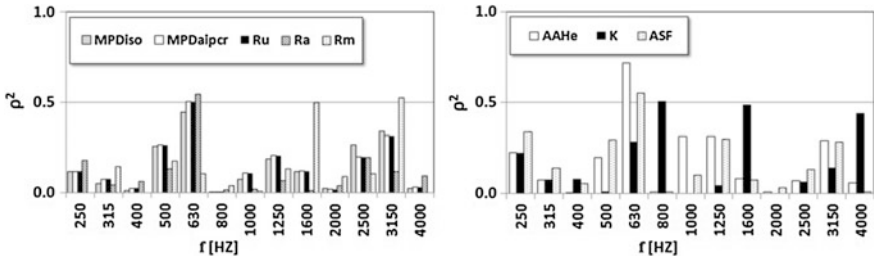


**Fig. 7** Correlations between profile-based indicators and acoustic absorption coefficient

PIARC (1995) straight line (MPD vs. SH), when porous asphalt concretes are considered. To this end it seems relevant to highlight that D-SH correlation resulted in a $R^2$ of 0.83, while D-MPD correlation yielded a lower $R^2$ (0.59). Importantly, these facts may be also interpreted in terms of significant difference between MPD and SH. Indeed, even if both refer to macrotexture, MPD explains a lower fraction of the variance of drainability. In contrast SH better explains drainability and it is derived in terms of flow through a porous skeleton. Texture spectral descriptors were expressed in terms of texture levels at different wavelengths. Importantly, texture levels corresponding to a wavelength range of 0.40–0.25 mm exhibit the best correlation with the sand height data (SH). On the contrary, R-square values are always lower than 0.5 when drainability versus texture level is considered. Acoustic data collected by means of the extended surface method were analysed in order to better investigate on how acoustic spectra correlate with sand height and drainability (Fig. 6). In Fig. 6 x-axes refer to drainability (D) and sand height (SH). Y-axes refer to the first maximum of the absorption coefficient ($a_{0max'}$), to the second (higher frequencies, $a_{0max''}$), and to the value of absorption at 800 Hz ($a_{800}$) and at 2000 Hz ($a_{2000}$). Note that frequencies around 800 and 2000 Hz yield the highest correlations with drainability and macrotexture. Figure 6 also shows that both the first absolute maximum of $a_0$ and the second one (range 0–4.0 kHz) exhibit a good correlation ($R^2 > 0.7$) with D and SH.

Correlations between profile-based indicators and acoustic absorption coefficient are summarized in Fig. 7 where the R-square values for each indicator is reported (y-axis). Note that most of the aggregate descriptors show the highest correlations for frequencies of around 500–800 Hz. Some of them (Rm, K) yield R-square values higher than 0.5 also for frequencies of 1600, 3150 and 4000 Hz. AAHe and ASF show good correlation for larger frequencies ranges.

## 4 Conclusions

Porous European mixes have well-known advantages in terms of noise reduction even if the issue of a noise-oriented mix design is still far from solved and this topic still calls for further research. Accordingly, the objective of this paper was to study

the relationship between in situ acoustic absorption coefficient (ISO 13472-1) and pavement surface performance (texture, drainability). Even if experiments and analyses are still in progress, based on the results obtained several conclusions may be drawn. Overall a relationship of the absorption coefficient with drainability and sand height was found. In more detail, the maximum acoustic absorption (f = 800–1000 Hz) resulted well correlated with drainability and SH. This fact has a great importance because macrotexture seems to affect both the generation and the absorption of rolling noise. Consequently, these correlations provide a practical and straightforward method to balance acoustical, drainability and texture characteristics in a porous asphalt concrete. The synergetic assessment of surface texture indicators permitted to understand that several profile-based indicators are rather related with a number of parameters derived from acoustic absorption spectra and/or macrotexture performance. Some indicators related to the depth of surface roughness and to asperity characteristics exhibited quite interesting correlations. Differences in r-squares, together with dissimilarities in test method and rationale behind, emerged for SH and MPD. It is recommended that future studies elaborate on modelling and causes of the obtained results. Future research will address a number of these challenges, using a systems approach to better understand how acoustic absorption and surface texture influence one another within a whole.

## References

A.A.V.V. (2001) Environment-Safety interaction in Road Infrastructures: final report. Ch.4: Noise. IASPIS Research Project (In Italian)

Ahammed MA (2009) Safe, Quiet and Durable Pavement Surfaces. Master Thesis, University of Waterloo, Ontario, Canada

Ahammed MA, Tighe SL (2011) Acoustic Absorption of Conventional Pavements. Int. J. Pavement Res. Technol. 4(1):41-47

AIPCR (2010) Attenuation of road noise. Acoustic mitigation interventions on noise sources (in Italian). XXVI Road National Conference, Roma 27 - 30 October 2010

Alvarez AE, Martin AE, Estakhri C (2010) Internal structure of compacted permeable friction course mixtures. Construction and Building Materials 24 (6):1027-1035

Alvarez de Sotomayor R, Yanguas S, Gonzalez J, Parra (2012) Measurement of Sound Absorption Coefficient of Road Surfaces in Situ. 7th Symposium on Pavement Surface Characteristics, Norfolk Waterside US, 18-21September

Autostrade s.p.a. (2001) Test method for measuring the drainage capability of road surface pavements. Internal Standard (in Italian)

Boscaino G, Praticò FG (2001) Classification et inventaire des indicateurs de la texture superficielle des revetements des chausses/A classification of surface texture indices of pavement surfaces. Bulletin des Laboratoires des Ponts et Chaussees 234: 17-34

Boscaino G, Pratico' FG, Vaiana R (2005) Tyre/road noise on different road pavements: synergetic influence of acoustical absorbing coefficient and surface texture. Paper presented at the EAEC - European Automotive Congress – Environmental impact of road transport session, Beograd (Belgrado), 30th May -1st June 2005. ISBN: 978-160423604-0

Brinkmeier M, Nackenhorst U, Biermann J, von Estorff O (2007) Prediction of tire/road noise - modelling and validation. In Proceedings of Inter-Noise 2007, Istanbul, Turkey

California Department of Transportation (Caltrans) (2006) Open Graded Friction Course. Usage Guide. Sacramento, California

Freitas E, Mendonça C, Santos JA, Murteira C, Ferreira JP (2012) Traffic noise abatement: How different pavements, vehicle speeds and traffic densities affect annoyance levels. Transportation Research Part D 17: 321- 326

Freitas, E, Mendonça C, Santos JA, Murteira C, Ferreira JP (2012) Traffic noise abatement: how different pavements, vehicle speeds and traffic densities affect annoyance levels. Transportation Research Part D 17 (4): 321–326. doi: 10.1016/j.trd.2012.02.001

Fujikawa T, Tachibana H (2009) Prediction of tire/road noise reduction by roadsurface improvements. In Proceedings of Inter-Noise 2009, Ottawa, Canada

Gibbs D, Iwasaki R, Bernhard R et al. (2005) Quiet Pavement Systems in Europe. Report No. FHWA-PL-05-01. U.S. Department of Transportation, Federal Highway Administration

Hamet JF, Klein P (2000) Road Texture and tire noise. Internoise 2000, the 29th International congress and exhibition on noise control engineering 27-30 August, Nice, France

Jimenez-Espadafor F, Becerra Villanueva JA, Torres García M, et al. (2011) Optimal design of acoustic material from tire fluff. Materials and Design 32: 3608–3616.

Losa M, Leandri P, Licitra G (2013) Mixture design optimization of low-noise pavements. Transportation Research Record, Journal of the Transportation Research Board 2372: 25-33

Lu Q, Harvey JT (2011) Laboratory evaluation of Open-Graded Asphalt Mixes with small aggregates and various binders and additives. TRB 90th Annual Meeting, Washington, D.C.,

Mak KL, Hung WT, Lee SH (2012) Exploring the impacts of road surface texture on tyre/road noise. A case study in Hong Kong. Transportation Research Part D 17: 104–107

Ongel A, Kohler E, Harvey J (2008) Principal Components Regression of Onboard Sound Intensity Levels. J. Transp. Eng. 134 (11)

PIARC (1995) International PIARC Experiment to Compare and Harmonize texture and Skid Resistance Measurements. World Road Association Mondiale de la Route

Praticò F, Vaiana R, Fedele R (2014) A study on the dependence of PEMs acoustic properties on incidence angle. International Journal of Pavement Engineering, doi: 10.1080/10298436.2014.943215

Praticò FG (2001) Roads and loudness: a more comprehensive approach. Journal of Road Materials and Pavement Design 2(4): 360-377

Praticò FG, Anfosso-Lédée F (2012) Trends and Issues in Mitigating Traffic Noise through Quiet Pavements. Procedia: Social & Behavioral Sciences, Elsevier 53:203-212 ISSN: 1877-0428

Praticò FG, Moro A (2006) Hot Mix Asphalts Drainability and Permeability: A Theoretical And experimental Investigation On Four Different Devices. Paper presented at the 10th International Conference on Asphalt Pavement, ICAP, Québec. ISBN: 978-2-550-49009-8

Praticò FG, Moro A (2007) Permeability and volumetrics of porous asphalt concrete: a theoretical and experimental investigation. Road Materials and Pavement Design 8/4: 799-817

Praticò FG, Vaiana R (2012) Improving infrastructure sustainability in suburban and urban areas: is porous asphalt the right answer? And how?. In: Urban Transport 2012. Wit Transactions On The Built Environment 128: 673-684, Southampton:Wit Press, ISBN: 978-1-84564-580-9, ISSN: 1743-3509, doi: 10.2495/UT120571

Praticò FG, Vaiana R, Iuele T (2013) Acoustic absorption and surface texture: an experimental investigation. Paper presented at the 42nd International Congress and Exposition on Noise Control Engineering, InterNoise 2013: Noise Control For Quality of Life. Innsbruck, 15-18 September 2013. ISSN: 0736-2935 ISBN: 978-163266267-5

Rasmussen R (2009) Measuring and modeling tire-pavement noise on various concrete pavement textures. Noise Control Engineering Journal 57 (2):139

Rasmussen R O, Bernhard R J, Sandberg U, and Mun E P (2007) The little Book of Quieter Pavements. FHWA, The Transtec Group, Washington, D.C.

Reyes CH, Harvey J (2011) A method for prediction sound intensity noise levels using laboratory pavement cores. In Proceedings of Noise-Con 2011, Portland, OR

Sandberg U, Ejsmont JA (2002) Tyre/Road Noise Reference Book. INFORMEX Ejsmont & Sandberg Handelsbolag, Kisa, Sweden

Vaiana R, Capiluppi GF, Gallelli V, Iuele T, Minani V (2012) Pavement Surface Performances Evolution: an Experimental Application. Procedia-Social and Behavioral Sciences

Wayson R (1998) Relationship between Pavement Surface Texture and Highway Traffic Noise. NCHRP Synthesis of Highway Practice No. 268, Transportation Research Board, Washington, D.C., USA

Zhang L, Ong GP, Fwa TF (2015) Investigating the effect of asphalt pavement texture on 1 tire/road noise: a finite element method-boundary 2 element method (fem-bem) based approach. 94th Transportation Research Board Annual Meeting.

# PSV Tyre/Test Specimen Contact

**David Woodward, Phillip Millar, Grainne McQuaid, Rebecca McCall and Oisin Boyle**

**Abstract** The PSV test has been used for many years. It is the harmonised European standard method for predicting an aggregates polishing resistance. This paper considers the test tyre/test specimen interface. This was done by painting the PSV test specimen surface and subjecting it to a period of accelerated polishing. Digital images of the test specimen were analysed using 2d and 3d techniques. Tyre/aggregate contact area was found to range from 17 to 92 % of the test specimen area. Factors such as particle shape (convex, concave, flat) and particle orientation in the test specimen influence contact. The contact interface relates to the uppermost 1–2 mm of the test specimen surface. A weak relationship was found showing contact area to increase as wet skid resistance decreased. Whilst aggregate micro-texture remains an important factor the research suggests additional scales of texture and contact influence water films at the interface. The findings of this paper impact attempts to measure road skid resistance using non-contact methods of measurement.

**Keywords** PSV tyre/test specimen interface · Contact area · 2d 3d modeling

## 1 Introduction

The Polish Stone Value (PSV) test method was developed over 60 years ago in the UK. It is now a harmonised European test method (EN 1097-8 2009) and similar versions of the method are used in many other countries around the world. There have been many research investigations into the method during its development (Hosking 1992). PSV has been considered for many years to be a measure of aggregate microtexture. At slower traffic speeds, this particle surface roughness helps break through water films that develop at the tyre/road interface in wet

D. Woodward (✉) · P. Millar · G. McQuaid · R. McCall · O. Boyle
School of Built Environment, University of Ulster, Newtownabbey, Northern Ireland, UK
e-mail: wdh.woodward@ulster.ac.uk



F. Canestrari and M.N. Partl (eds.), *8th RILEM International Symposium on Testing and Characterization of Sustainable and Innovative Bituminous Materials*, RILEM Bookseries 11, DOI 10.1007/978-94-017-7342-3_36

conditions. At higher speeds road surface macrotexture enables bulk removal of water to allow this to continue. A range of textures and contact area phenomena ranging from micro to macro are therefore involved at this tyre/road interface within the contact patch. Laboratory prediction of what happens at this contact interface and the role of different scales has been a relatively little researched area considering its relation with skid resistance, noise and rolling resistance. In contrast, specialist road assessment vehicles have been doing high speed data non-contact acquisition surveys using lasers and cameras since the late 1980s. The latest vehicles survey at speeds up to 100 km/h while measuring and spatially recording factors such as roughness, macrotexture and rut depths in the wheel-path, transverse profile edge defects, video of the view ahead, longitudinal gradient, horizontal radius of curvature and lane crossfall. The most notable factor missing from this high speed non-contact measurement is wet skid resistance.

In comparison to road surface information measured using these non-contact methods at high speeds, the PSV tyre/aggregate particle surface interface is less understood. The PSV test using single size of aggregate cannot simulate all possible uses of aggregate in the different types of surface course asphalt and concrete mixes. Rather the PSV test it is a standardised ranking method for a given set of laboratory conditions.

Change the laboratory test conditions and a different equilibrium condition is achieved for the aggregate being assessed (Woodward 2003; Roe and Woodward 2004). Although this phenomena is similar to what happens in the field, the use of single aggregate size is a restriction to the laboratory prediction of performance. This led to development of test methods that have the option of assessing aggregate, laboratory prepared asphalt test specimens and cores extracted from the road. These include the German Wehner Schulze test, the UK Road Test Machine, the Aachen Ravelling Tester and the Dutch Skid Resistance Interface Testing Machine. The German Wehner Schulze test is now known as the Friction after Polishing test (FAP) when is became a harmonised European Standard (EN 12697-49 2014). Similar to the solid rubber tyre used in the PSV test, the FAP test uses solid rubber in the form of three grooved rollers to polish the test specimen surface. Figure 1 shows good correlation between FAP and PSV test methods for German data (Huschek 2004). Although the FAP test is now a harmonised European Standard, there is relatively little experience with the equipment in many European countries. The UK has a single FAP device, located at the Transport Research Laboratory (TRL). When evaluating the FAP device at TRL, Dunford (2013) made an important finding relating to the principle of the FAP test that raises potential issues with the method. Aggregate test specimens were sprayed with yellow road marking paint to verify that stones chosen at random for further detailed assessment had come into contact with the polishing rollers. This paint erosion indication technique had been described by Parslow et al. (1997).

A painted FAP aggregate test specimen after testing is shown in Fig. 2. The centre of the FAP test specimen does not come into contact with the polishing rollers and remained covered in paint. However, there are parts of the polished area of the FAP test specimen that are still covered in paint. Dunford (2013) recognised

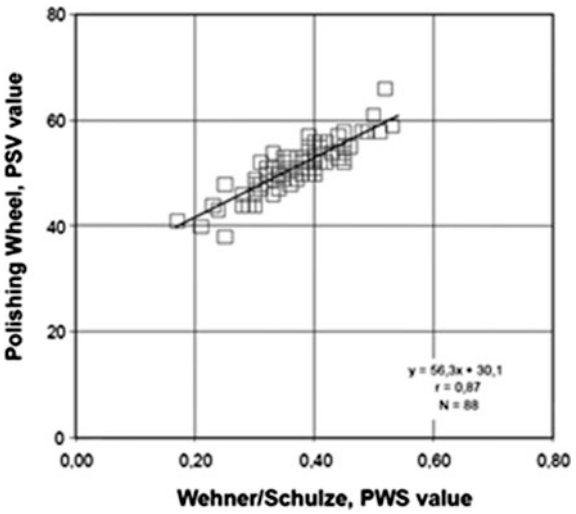


**Fig. 1** Comparison of the results of measurement with 8/11 mm coarse aggregate using the Wehner/Schulze and PSV test methods (Huschek 2004)

that because the aggregate particles were not completely flat the polishing rollers were not flexible enough to conform to all the variations in their surface. Figure 3 shows a single limestone particle before and after painting and polishing. Whilst this confirms that the majority of the stone's surface has been polished there remains a significant part that is not. This illustrates that only part of the aggregate surface is being assessed in this laboratory method and raises doubt as to its ability to adequately predict skidding resistance performance.

This prompted the authors of this paper to repeat this paint erosion experiment using PSV test specimens. The laboratory investigations had four main objectives (i) to develop a simple method to quantify aggregate particle/solid tyre contact (ii) to quantify how the solid rubber type of the PSV interacted with the aggregate

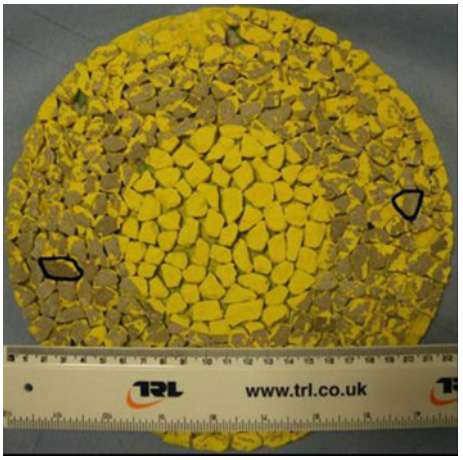


**Fig. 2** Painted FAP test specimen after testing showing roller/aggregate contact (Dunford 2013)

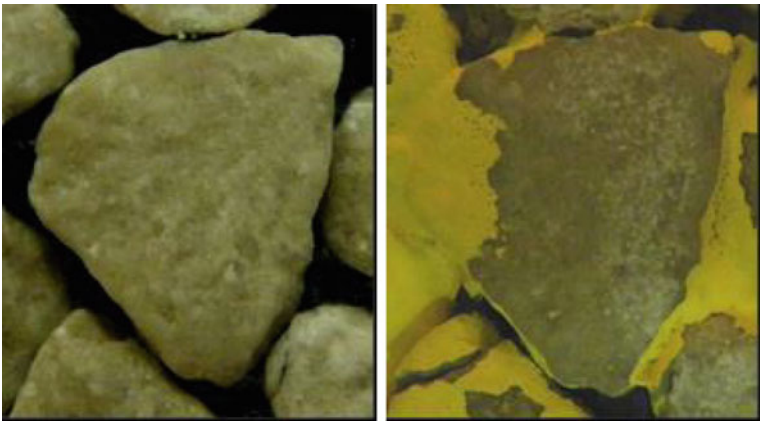

**Fig. 3** Single aggregate particle showing contact (Dunford 2013)

particles in the test specimen and (iii) to make recommendations regarding what should be considered when trying to develop high speed non-contact measurement of skid resistance either of the aggregate or road surface.

## 2 Experimental Programme

Three experimental studies are summarized in this paper. The first study developed a technique to quantify the amount of aggregate exposure using 2d digital image analysis. The second study considered paint related factors such as different types and colours that could be used and how long it would take to wear them off the PSV test specimen to expose the aggregate. The third study considered how the solid rubber tyre interacted with the aggregate particles using 3d modeling.

### *2.1 Development of a Technique to Quantify Aggregate Exposure*

A 2d image digital image analysis technique was developed to quantify the surface area of exposed aggregate during the paint erosion testing (McCall 2013). Fourteen PSV test specimens that had already been subjected to the standard 6 h test were selected to represent a range of rock types and PSV. Each was sprayed with yellow road marking paint similar to that used by Dunford (2013). They were subjected to 30 min of simulated trafficking using the accelerated polishing machine. Each PSV test specimen was washed and allowed to dry. They were photographed using a Canon 400D camera fitted with a 60 mm macro lens. A copy

stand and shutter release was used to minimise camera shake. LED lighting was used to standardise lighting conditions.

Image-Pro Premier software was used to analyse the digital image of each PSV test specimen. After the image is opened in Image-Pro, a series of functions are required to achieve the desired measurements. First, the region of interest (ROI) tool was used to select the area of the PSV test specimen image to be analysed. This was typically 44.5 mm in width and 90.6 mm in length i.e. the full area of aggregate potentially in contact with the rubber tyre. The next stage was to calibrate the image in terms of scale. This was done by include a calibration scale for reference in each image. Figure 4 shows a PSV test specimen being analysed to determine contact with the tyre.

The image in this example shows the steel rule used for scale calibration. The ruler and PSV test specimen have to be at the same height to ensure that both are in focus. After the image is calibrated to the appropriate length it can then be enhanced using different filters e.g. to adjust contrast, brightness or gamma. The count/size function in the software is applied to automatically select the exposed parts of each aggregate particle. If the image is complex these desired parts or objects can be selected manually. If undesired objects are counted, they can be excluded by editing the object size range. Image-Pro can provide many different types of measurement important to this study such as area of exposed particle area, maximum and minimum particle diameter, perimeter length and roundness. The data relating to each exposed part of each aggregate particle aggregate is exported to Excel. For the purposes of this paper only the area of exposed aggregate particles is used. The total area of exposed aggregate for each PSV test specimen is simply calculated by summing the individual objects and expressing as a percentage of the ROI.

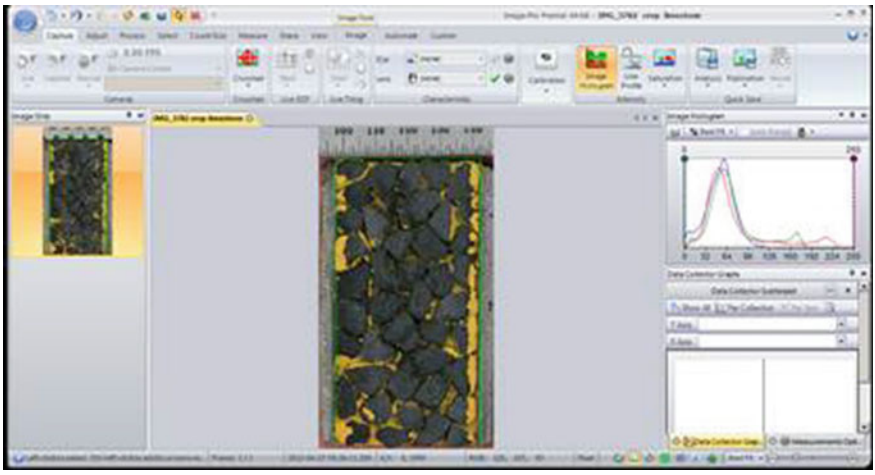

**Fig. 4** Image-Pro analysis of PSV test specimen to determine contact with tyre (McCall 2013)

## 2.2 Paint Related Factors

The second study determined (i) the best type of paint to wear off the PSV moulds (ii) which colour was best for image analysis and (iii) how long it took to wear off the paint and expose the aggregate (Boyle 2014). Dunford (2013) had used yellow road marking spray paint. However, it was felt that an alternative paint that was easier to remove may be better. This study used old PSV control stone test specimens to ensure uniformity of rock type. They were all conditioned on the accelerated polishing machine for 1 h prior to application of paint. The paints assessed included spray marker paints of different colours, paint used for steel work, exterior wall paint, enamel paint, children's water based paint and interior matt wall paint. The marker paints were sprayed with the other paints applied first with a paint brush and then finished with a fine brush. All the spaces between aggregate particles were painted to ensure that any measured aggregate exposure was due to contact with just the solid tyre of the accelerated polishing machine. The PSV test specimens were subjected to 10 min on the accelerated polishing machine. Testing was stopped at 2, 5 and 10 min to determine how the paint was wearing off. Digital images were taken and analysed using the Image-Pro technique developed by McCall (2013).

It was found that white marker spray paint did not show enough difference with aggregate where it had not been worn off. This influenced analysis and the assessment of lighter coloured rock types. Red marker spray paint became a dark red colour and did not give enough definition between the paint and the aggregate. Both the yellow and blue marker spray paints stood out from the aggregate but were too hard wearing. Paint for steel work was found to be too hard wearing and/or tended to flake off giving errors to the analysis. Exterior wall paint was found to have similar issues to the steel work paint. The bond of enamel paint was found to be too great and required too long a period on the accelerated polishing machine. Children's play paint was found to be too weak and was quickly worn off. It was concluded that of all the paints assessed a blue water based interior matt paint was best. This had the best contrast with the exposed aggregate, bonded well to the aggregate particles and did not suffer from flaking. The rate of paint erosion was then determined using aggregate from fourteen different sources. A single PSV test specimen was made from each source. They were subjected to the standard 6 h PSV test i.e. 3 h using coarse emery and 3 h using flour emery. A Canon 400D camera with 60 mm macro lens connected to a computer was used. This was fitted to a copy stand with two Led light arrays providing uniform lighting. A steel ruler was placed beside each PSV test specimen during imaging for scaling purposes during image analysis.

Each test specimen was painted using the blue interior matt paint, taking care to infill all the spaces between aggregate particles. The first period of polishing lasted 30 s after which each test specimen was removed, washed, dried and digital images taken. This was repeated after 2, 5, 10 and 30 min of accelerated polishing. It was observed that the rate of paint erosion differed for different aggregates i.e. different aggregates had different contact characteristics with the solid rubber tyre of the

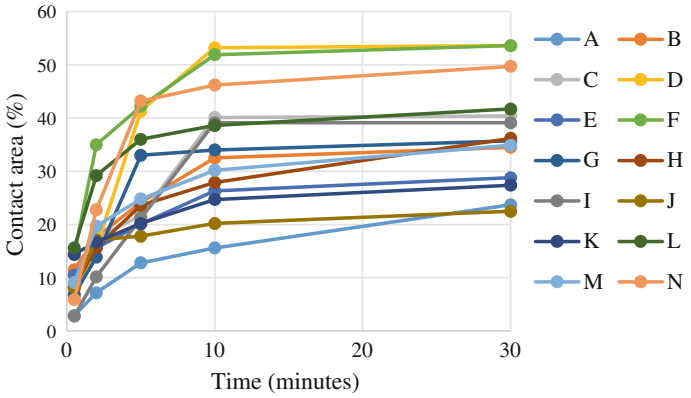


**Fig. 5** Rate of aggregate exposure (Boyle 2014)

accelerated polishing machine. Factors that influenced contact were particle shape i.e. flat, smooth or convex and texture of the aggregate particle surface.

The % contact area i.e. exposed aggregate was determined for each test period i.e. at 30 s, 2, 5, 10 and 30 min using the technique developed by McCall (2013). Figure 5 plots development of percentage contact area with time for the 14 test specimens. This measured value of solid rubber tyre/aggregate particle contact confirmed the visual observations. It was found that most paint erosion occurred during the first 10 min. The rate then decreased and equilibrium was reached by 30 min for most of the aggregates assessed.

## *2.3 Solid Rubber Tyre Interaction*

The third study used 2d and 3d techniques to better understand the solid rubber tyre/PSV test specimen interface. This involved preparing a set of 14 PSV test specimens from different sources. These were subjected to the standard 6 h PSV test. They were painted with blue interior matt paint and subjected to a further 30 min on the accelerated polishing machine. Digital images were taken of the 14 PSV test specimens for analysis. The percentage contact area was determined according to the 2d image analysis technique developed by McCall (2013). A 3d close range photogrammetry technique was developed by McQuaid (2014) to determine how the solid rubber tyre interacted with individual aggregate particles. Both the 2d and 3d techniques used images taken by a Canon 6D with a 20.2 megapixel full frame sensor and 100 mm macro lens. This was used with a tripod and remote shutter release to minimise camera shake. Two LED lighting panels and camera attached ring macro flash provided uniform lighting conditions for image capture. Manual camera settings of f/32 and shutter speed 2 s gave images

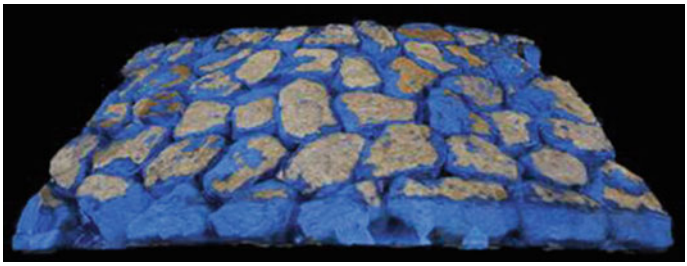

**Fig. 6** Painted PSV specimen TIN mesh after painting and accelerated polishing modelled using Zephyr

with maximum depth of field. A framework of calibrated control points allowed recovery of both surface elevation and orientation.

3DF Zephyr Pro photogrammetric software was used to combine 10 digital images to create a Triangular Irregular Network (TIN) mesh of each PSV test specimen. An example of a 3d model for a painted PSV test specimen after accelerated testing is shown in Fig. 6. This 3d model shows differing amounts of paint eroded off the surface of each aggregate particle. Digital Surf MountainsMap 7 software was used to analyze each TIN mesh. Initial operators were applied to the surface to prepare it for analysis. This included the use of the extract area operator to remove residual outskirt data. The symmetry operator was used to ensure that the TIN mesh was orientated to correspond with the actual PSV test specimen. The form removal operator was applied to the 3d model to remove the form or curvature of the PSV test specimen.

Single aggregates were selected to investigate tyre rubber/aggregate interaction using a volume of islands study. The example in Fig. 7 shows an aggregate selected for analysis. The volume of islands procedure was used to quantify parameters above a given threshold height. The area of exposed aggregate for the chosen aggregates was obtained from the 2d Image-Pro analysis. This area from the 2d analysis was used in conjunction with the volume of islands 3d analysis to threshold the surface of the aggregate particle to give a value of height. The height of the

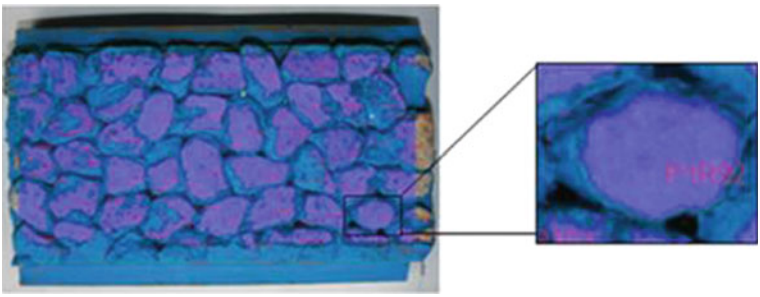

**Fig. 7** Painted PSV test specimen with a selected aggregate using Image-Pro Plus

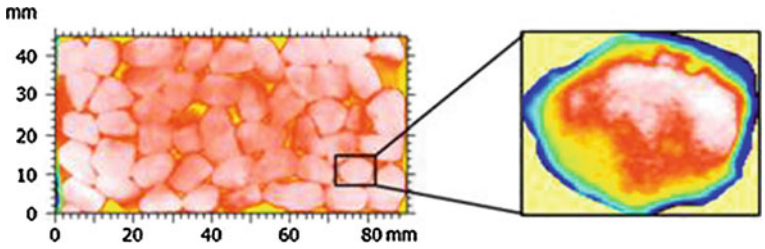


**Fig. 8** Colour depth classified painted PSV test specimen 3d model with form removed showing selected area particle using MountainsMap 7

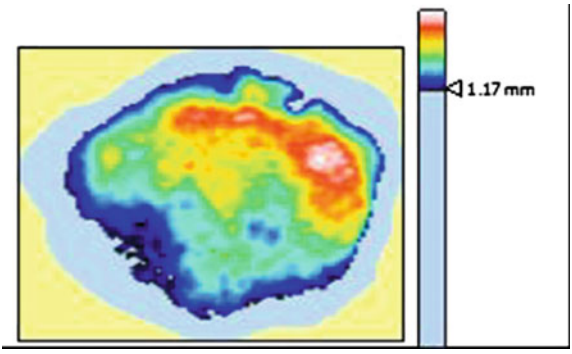


**Fig. 9** Volume of islands study for the selected aggregate particle showing tyre interaction to be 1.17 mm

threshold was adjusted to achieve an area parameter for the 3d model equivalent to that determined using the 2d analysis.

Figure 8 shows the painted PSV test specimen 3D model with form removed and the selected aggregate particle colour depth classified using MountainsMap 7. Figure 9 shows a volume of islands study for the selected aggregate particle. Assuming that both areas are the same, this example indicates that the tyre rubber/aggregate particle interface was 1.17 mm deep. It is assumed that any part of the aggregate particle above this threshold is in contact with the solid rubber accelerated polishing machine tyre. For this PSV test specimen, the depth of tyre rubber/aggregate particle interaction was found to range from 1.15 to 1.75 mm.

## 3 Discussion

This paper has summarized three studies that have involved measurement of the PSV tyre/test specimen interface. Figure 10 plots the percentage contact area after 30 min of paint erosion with pendulum value for the three studies. The combined plot shows contact area to range from 17 to 92 % with pendulum values ranging from 37 to 68.

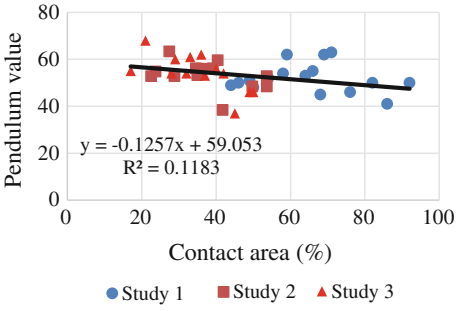


**Fig. 10** Combined pendulum and contact data from the 3 studies

The plot shows the data to have a weak overall trend i.e. as contact area increases pendulum value decreases. Initially this was unexpected. It had been assumed that greater interface area would result in greater interaction with the rubber slider during the pendulum test giving greater pendulum values. However, the data does not support this simplistic assumption. It suggests that contact area alone is not the controlling factor. This can be explained by the micro-texture of the different rock types assessed. It may be related to removal of greater films of water on the surface of the higher contact area aggregate particles. Aggregate particles with less contact area would not have such problems as the pendulum would find it easier to interact with the aggregate. The studies have shown that there is a range of textures and contacts involved from the micro-scale to a greater macro scale relating to the shape and form of the aggregate particle and its surface.

The presented data suggests that reliance on the PSV test method to predict the skid resistance performance of roads is fundamentally limited. There can be a considerable amount of the PSV test specimen and the individual aggregate particles not in contact with the solid rubber tyre. The same could be said for the solid rubber rollers of the FAP test. The German research shown in Fig. 1 found reasonable correlation between these two test methods. The studies summarized in this paper show similarity in paint erosion images for both methods. The found correlation between methods may be due to similar interface conditions i.e. the use of solid rubber rollers in the FAP test and the solid rubber tyre in the PSV test. Both images show the solid rubber not to interact with depth into the interface i.e. 1.17 mm for the PSV aggregate particle shown in Fig. 10.

In contrast, simple observation of an asphalt road surface/pneumatic tyre interface shows the depth of pneumatic tyre effect to be much greater. Obviously, the depth of rubber indentation into the texture of the asphalt/aggregate textures will depend on many factors. But, in relation to this paper and the presented data it would appear that both laboratory methods are limited in their ability to predict these actual road surface observations. With respect to non-contact 2d and/or 3d measurement, this paper raises issues that need consideration relating to the interface and the role of textures and contacts at a range of scales.

## 4 Conclusion

This paper has considered the PSV tyre/test specimen interface. The PSV solid rubber tyre/test specimen interface is similar to the FAP solid rubber grooved roller/aggregate test specimen interface. In both test methods, the rubber only interacts with the top 1–2 mm of the test specimen and its aggregate particles. Factors such as particle shape (convex, concave, flat) and particle orientation in the test specimen strongly influence this interface. Contact area was found to range from 17 to 92 % of the test specimen area. A weak relationship showing increasing contact area to be related to decreasing wet skid resistance was found. It has been proposed that the role of particle contact area may be related to either the removal or to the presence of films of water on the surface of the higher contact area aggregate particles. The authors believe that the findings of this paper impact attempts to measure road skid resistance using non-contact methods of measurement. This research has found that the laboratory prediction of aggregate friction only considers the top 1 or 2 mm of the aggregate particles. Further development of this research is currently considering differences between the laboratory prediction of skid resistance and what actually happens with real road surfaces.

## References

Boyle O (2014) Modeling PSV mould wear, MEng Civil Engineering dissertation, University of Ulster

Dunford A (2013) Friction and the texture of aggregate particles used in the road surface course. PhD Thesis, University of Nottingham

EN 1097-8 (2009) Tests for mechanical and physical properties of aggregates. Determination of the polished stone value

EN 12697-49 (2014) Bituminous mixtures – Test methods for hot mix asphalt Part 49: Determination of friction after polishing

Hosking R (1992) Road aggregates and skidding, State of the art review 4. Transport Research Laboratory, London, HMSO ISBN 0115511156

Huschek ES (2004) Experience with skid resistance prediction based on traffic simulation. 5th International Symposium on Pavement Surface Characteristics, Toronto, Canada

McCall R (2013) Development of a 2d image analysis technique to quantify aggregate exposure during paint erosion testing of PSV test specimens. Internal report, Highway Engineering Research Group, University of Ulster

McQuaid G (2014) Development of a 3d image analysis technique to quantify tyre indentation. Internal report, Highway Engineering Research Group, University of Ulster

Parslow GI, Stephenson DJ, Strutt JE and Tetlow S (1997). Paint layer erosion resistance behaviour for use in a multilayer paint erosion indication technique. Wear 212, 103-109

Roe PG and Woodward WDH (2004) Predicting skid resistance from the polishing properties of the aggregate (SKIDPREDICT). Transport Research Laboratory PR CSN/31/03

Woodward D (2003) Predicting early life skid resistance of highway surfacings (SKIDGRIP). EPSRC Grant GR/R09022/01

# Surface Performance Characterization of Single-Layer Surface Dressing: A Macrotexture Prediction Model

**Filippo Giammaria Praticò, Rosolino Vaiana and Teresa Iuele**

**Abstract** Bituminous surface treatments (seal coats, chip seals, etc.) are pavement wearing courses created using asphalt binder and aggregate. They can be applied to an existing pavement or to a base course. They can act as a waterproof, skid resistant layer, sealing cracks and raveled surfaces and increasing reflection properties of road surfaces. Their expected life ranges from two to five years and are widely used in flexible pavements maintenance and rehabilitation because of reduced costs and the easiness of application. One of the most important characteristics of bituminous surface treatments is their macrotexture (initial and over time). Indeed, it affects tire-pavement interaction in wet and dry conditions and can interact with other characteristics and distress (aggregate embedment, loss of cover aggregate, streaking, bleeding, etc.). This paper focuses on the evaluation of surface performance of laboratory slabs, produced through a single-surface dressing. Macrotexture depth was measured by the Sand Patch method. A laser profilometer was also used to survey slabs texture and both aggregate descriptors and texture levels were evaluated. Finally, skid resistance and drainability data were measured by means of the British Pendulum Tester and the Belgian Permeameter, respectively. Aggregates of different size were selected in order to investigate on the relationship between aggregate dimensions and surface performance. A model was developed, implemented and validated. Results are expected to benefit both practitioners and researchers.

**Keywords** Surface treatments · Chip seals · Surface performance · Macrotexture, laser profilometer · Friction · Safety

F.G. Praticò (✉)
DIIES Department, Mediterranea University of Reggio Calabria, Reggio Calabria, Italy
e-mail: filippo.pratico@unirc.it

R. Vaiana · T. Iuele
Department of Civil Engineering, University of Calabria, Arcavacata Campus, Cosenza, Italy



F. Canestrari and M.N. Partl (eds.), *8th RILEM International Symposium on Testing and Characterization of Sustainable and Innovative Bituminous Materials*, RILEM Bookseries 11, DOI 10.1007/978-94-017-7342-3_37

## 1 Introduction

Bituminous surface treatments (seal coats, chip seals, etc.) are wearing courses generally made of two major components: asphalt binders and natural mineral aggregate chips. These surface treatments are constructed by spraying the asphalt emulsion onto the existing asphalt pavement or on the base course and then dropping the aggregate chips into the asphalt emulsion. Afterwards, the surface is rolled to seat the chips for gaining a stronger bond between the aggregate and the binder (Wasiuddin et al. 2012; Shuler et al. 2011; Adams and Kim 2013a, b). Binder rise can change in relation to trafficking: from a minimum initial value of 35–40 % of the height of the aggregate particle to 50–60 % about two years after construction (Alderson 2006). Multiple layers may be placed and various aggregate and binder types (emulsions, performance-based asphalt cements, rubber binders, synthetic binders) can be used to address specific distress modes or traffic situations (Pasquini et al. 2014). Many benefits derive from the use of chip seal for pavements rehabilitation and maintenance: improvement of skid resistance, extension of pavement service life, preventing surface material oxidization, inhibiting raveling, and correcting surface defects.

Chip seals are often used as a wearing course on low volume roads (Li et al. 2012). Chip seals are widespread because the construction operations are less expensive and faster than those necessary for other preservation alternatives (Wasiuddin et al. 2012). However, this type of treatment does not provide positive effects on the structural performance of the existing pavement (Islam and Hossain 2012; Aktas et al. 2013). Chip seals are considered as either (TNZ 2005): (i) First coat (includes Prime coat), that is the initial seal on a prepared unsealed surface, which is usually a base-course; (ii) Reseal (includes Second coat and Pre-treatment Seal), that is any chip seal applied to a surface which has previously been sealed when it shows signs of distress such as loss of waterproofing, chip loss, cracks, loss of skid resistance. Chip seal are differentiated from each other through construction sequence, number of courses sealed, and variation in aggregate nominal size (see Fig. 1). Binder-aggregate seal coating systems refer to those solutions that require the use of both aggregate (of different dimensions) and binder (asphalt emulsions, cutback, or polymer modified binders). Asphalt seals, instead, involve the application of asphalt to an existing surface without the use of cover aggregate. Finally, reinforced seals allow enhancing the performance of a conventional chip seal over extremely oxidized or thermal cracked surfaces. Reinforced seals can be either fiber reinforced or geotextile reinforced: the first ones are used as first coat and/or reseal treatments, whereas the second ones are only reseal solutions. As regards binder-aggregate systems, it is possible to identify two main groups of seals in relation to construction and laying operations: (i) in chip seals both aggregate and binder are sprayed directly on the surface in different layers, without mixing; (ii) slurry seals require pre-mixing operations through which mixture components

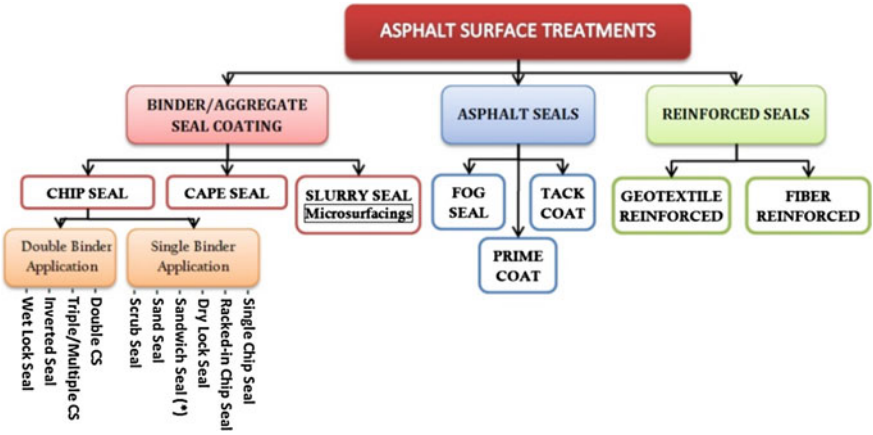


**Fig. 1** The most common solutions for asphalt surface treatments. *Note CS* chip seal; * single/double chipping

are carefully blended in a specially designed truck mounted machine. Cape seal can be considered an intermediate solution because it is a two coat system that combines a single chip seal with a fine slurry seal. For chip seal solutions, a classification according to the number of layers of binder was proposed. Within each of these main groups (single/double or multiple binder application) there are several types of treatments that can be used as both first coat and reseal treatments and other ones that are adopted only as a reseal (TNZ 2005; Li et al. 2012; Gransberg and James 2011; FHWA 2003; Holtrop 2008; Croteau et al. 2005; Kucharek 2007; Shuler et al. 2011; Nicholls 2002).

## 2 Objectives and Organization of Research

The main purpose of the research is to study the relationship between macrotexture and mix design for surface treatments (see Fig. 2).

A macrotexture prediction model, based on mix design-related factors, was formalized and calibrated by using known data from a detailed analysis of the literature review (overall 64 cases). An experimental plan was designed and carried out in the pursuit of: (i) obtaining new observations (data) of the dependent and independent variables; (ii) validate the model; (iii) investigating interrelated surface performance. Model input-output transformations (input data versus macrotexture prediction) were compared to the corresponding input-output transformations for the data derived through the new experiments, herein carried out.

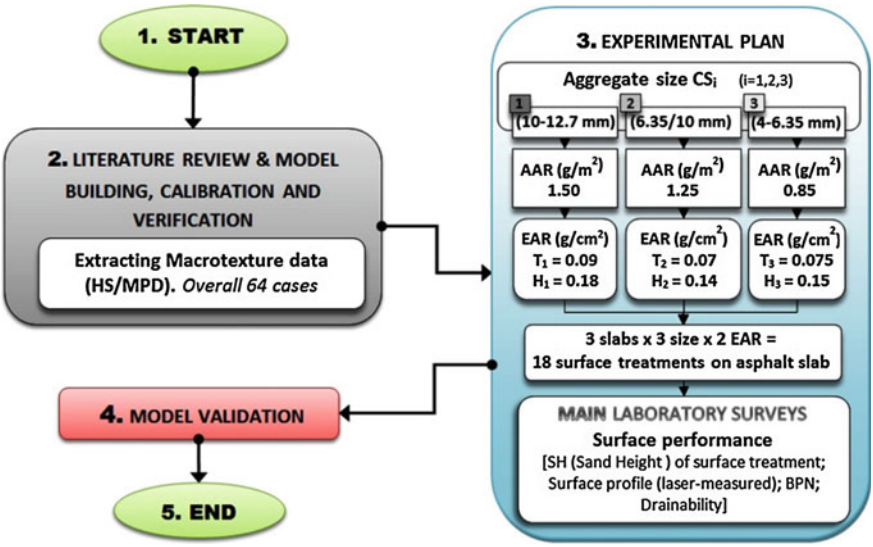


**Fig. 2** Organization of research and experimental plan

## 3 Model Building and Calibration

A model was formalized. Known data were used to calibrate and optimize the model. In more detail: (i) from Aktas et al. (2013) 8 cases were extracted; (ii) from Gurer et al. (2012) 5 main cases were extracted; (iii) from Krugler et al. (2009) 27 cases were extracted; (iv) from Adams and Kim (2013a, b) 10 cases were extracted; (v) from Zaman et al. (2013) 14 cases were used. The model here presented can be summarized into three main Eqs. (1–3) which were set up by referring to a variable-shape packing with triangular scheme The main inputs are the following: (i) AAR aggregate application rate; (ii) EAR: emulsion application rate or $Q_B$ bitumen application rate; (iii) Aggregate gradation, r. Minor inputs are: (i) z, film thickness in the upper part of grains; (ii) $SH_{INT}$: sand height of the underneath surface. Two parameters can be derived as main outputs: height of the bitumen (embedment depth, $h_B$) and sand height (SH). The model assumes that a set of quasi-spherical grains (of given radius, r, cm) is laid upon an underneath layer (of given macrotexture, $SH_{INT}$, cm, sand patch method EN 13036-1). Given the application of a given quantity of emulsified asphalt, a consequent height of bitumen ($h_B$, cm) is derived. The first equation refers to bitumen volume, VB ($cm^3$) as derived from emulsion application rate, bitumen percentage and bitumen density. $Q_B$ refers to bitumen application rate ($g/cm^2$) while $\gamma_B$ is bitumen density ($g/cm^3$) and z (cm) is the bituminous film thickness in the upper part of grains (if existing).

$$\begin{aligned} VB &= \frac{Q_B}{\gamma_B} \cdot r^2 \cdot \sqrt{3} = A + B \\ A &= r^2 \cdot \sqrt{3} \cdot h_B - \pi \frac{h_B}{6} \cdot \left(3 \cdot h_B \cdot r - h_B^2\right) \\ B &= \pi \cdot r \cdot (2r - h_B) \cdot z + r^2 \cdot \sqrt{3} \cdot SH_{INT} \end{aligned} \tag{1}$$

Note that the quantity of bitumen spread on the aggregate (left member of the equation) is used to fill the voids among the aggregate particles (first two expressions of the right member), in some cases (depending on bituminous treatment type) to have a given asphalt film thickness over the bitumen height (third term, right member), to fill the macrotexture of the underneath layer (last term). The most important unknown variable in the above equation is $h_B$, while the last two terms relate to the volume of bitumen absorbed or/and coating the grains above the $h_B$ level. The second equation refers to aggregates. The AAR (aggregate application rate, g/cm$^2$) must equal the quantity derived based on particles diameter (2r, cm) and density ($\gamma_A$, g/cm$^3$). VA (cm$^3$) and ASH (cm$^2$) represent particle volume and unit surface area, respectively.

$$AAR = \frac{V_A \cdot \gamma_A}{A_{SH}} = \pi \frac{2 \cdot r^3 \cdot \gamma_A}{3 \cdot \sqrt{3} \cdot r^2} = \pi \frac{2 \cdot r \cdot \gamma_A}{3 \cdot \sqrt{3}} \tag{2}$$

As for the second equation, note that ASH is the surface of the elementary area and that the overall area derives from the replication of many elementary areas. The third equation involves the sand volume ($V_{SH}$) and the consequent sand height (SH). This latter is usually the unknown variable.

$$\begin{aligned} SH &= \frac{V_{SH}}{A_{SH}} = C + D \quad C = \frac{2r^3 \cdot \sqrt{3} - \pi \frac{2r^3}{3} - \sqrt{3} r^2 h_B}{r^2 \cdot \sqrt{3}} \\ D &= \frac{\pi \frac{h_B}{6} \cdot \left(3 \cdot h_B \cdot r - h_B^2\right) - \pi \cdot r \cdot (2r - h_B) \cdot z - r^2 \cdot \sqrt{3} \cdot SH_{INT}}{r^2 \cdot \sqrt{3}} \end{aligned} \tag{3}$$

In order to check whether the model fits experimental measurements or other empirical data, these latter were split into two disjoint subsets: training data and verification data (see the section Experiments and verification). The training data were used to estimate the model parameters and to test for model reasonableness. The verification data even were derived from an experimental plan, ad hoc designed and carried. The verification data were used: (a) to assess model accurateness (cross-validation and extrapolation); (b) to investigate the relationship between other relevant technological issues (surface properties). As for the metric to measure the distances between observed and predicted data (especially in model training), a loss function was chosen (linear least squares). The following procedure was used during calibration: (i) input a given height of bitumen (cm) over the interface and other minor inputs such as the sand height of the underneath layer; (ii) derive the

volume of bitumen, the AAR and SH by using the first, the second and the third equation, respectively; (iii) derive the consequent error for VB, AAR and the associated error for SH; (iv) minimise the sum of errors, by changing the height of bitumen; (v) from gradation, height of bitumen, asphalt binder thickness, $SH_{int}$, through the third equation the SH is derived.

## 4 Materials and Methods

As stated above (see Sect. 2), an experimental plan was designed and carried out in order to obtain new data of the dependent and independent variables for model validation. Six test specimens were designed and produced (see Fig. 2):

- $CST_1$ (aggregate size: 10/12.7 mm; AAR = 1.50 g/cm$^2$; EAR: 0.18 g/cm$^2$);
- $CSH_1$ (aggregate size: 10/12.7 mm; AAR = 1.50 g/cm$^2$; EAR: 0.09 g/cm$^2$);
- $CST_2$ (aggregate size: 6.35/10 mm; AAR = 1.25 g/cm$^2$; EAR: 0.14 g/cm$^2$);
- $CSH_2$ (aggregate size: 6.35/10 mm; AAR = 1.25 g/cm$^2$; EAR: 0.07 g/cm$^2$);
- $CST_3$ (aggregate size: 4/6.35 mm; AAR = 0.85 g/cm$^2$; EAR: 0.15 g/cm$^2$);
- $CSH_3$ (aggregate size: 4/6.35 mm; AAR = 0.85 g/cm$^2$; EAR: 0.075 g/cm$^2$).

The average least dimension of the aggregate (ALD, defined as the average of the thickness of all individual particles when the particles lie with their least dimension upwards) was calculated for each aggregate dimension class by means of the equation suggested by Cenek and Jamieson, $ALD = 0.568 \times \mathrm{CS} - 0.142 (R^2 = 0.997)$ where CS is the average chip size (mm), (Cenek and Jamieson 2005).

For the three size of aggregate used, the following ALD values were estimated: ALD (CS1): 7.5; ALD (CS2): 5.6; ALD (CS3): 4.0. Moreover, shape factors for the three aggregate dimension classes were estimated: (i) Shape Index: SI (CS1): 2 %; SI (CS2): 15 %; SI (CS3):13 %, (EN 933-4); (ii) Flakiness Index (D/S): FI (CS1): 1.30; FI (CS2): 1.55; FI (CS3):1.41, (CNR B.U.95/84); (iii) Elongation Index (L/D): EI (CS1): 1.50; EI (CS2): 1.51; EI (CS3):1.62, (CNR B.U.95/84).

Note that the shape index is calculated as the ratio between the mass of non-cubical particles and the total mass of particles tested. Non cubical particles are those where the thickness (S) is less than 1/3 of the length (L). D is the intermediate aggregate dimension. The Flakiness index (according to Italian Standard Specifications) is defined as the ratio between the average aggregate size and the smallest size of aggregate (D/S). Aggregate properties were investigated as follows: Los Angeles Abrasion: 20.7 %, (EN 1097-2); Aggregate Specific Gravity: 2.87 g/cm$^3$, (EN 15326); Polished Stone Value: 0.39, (EN 1097-8); Resistance to wear (Micro-Deval): 6.9 %, (EN 1097-1). The binder used for the chip seal layer was a fast breaking emulsion of a SBS polymer modified binder, which is commonly used for surface treatments (both single and double layer). The main features of bitumen emulsion were the following: Water content: 31.0 %, (EN 1428); Binder content: 69.0 %, (EN 1431); Homogeneity: 0.08 %, (EN 1429); Sedimentation @

7dd: 6 %, (EN 12847); pH (acidity): 2.8, (EN 12850). As regards residual binder, the following properties were estimated: Penetration@25 °C: 60 dmm, (EN 1426); Softening Point (Ring & Ball): 80.0 °C, (EN 1427); Fraass point: −21 °C, (EN 12593); Elastic recovery@ 25 °C: 82 %, (EN 13398). Construction phases for slabs production were summarized in Fig. 3.

The chip-sealed layer was placed on a support layer made of a slab produced with traditional hot mix asphalt with a thickness of about 5 cm. The support layers were also characterized in terms of dimensional bulk specific gravity of compacted samples (according to the UNI EN 12697-33, and surface texture by means of the sand patch test, according to the EN 13036-1-9. Bulk specific gravity ranged between 2.38 ± 0.04 g/cm$^3$. A Laser Profilometer based on conoscopic holography (Praticò et al. 2014) was used and texture indicators were evaluated according to the ISO Standard 13473-3 (see Fig. 4).

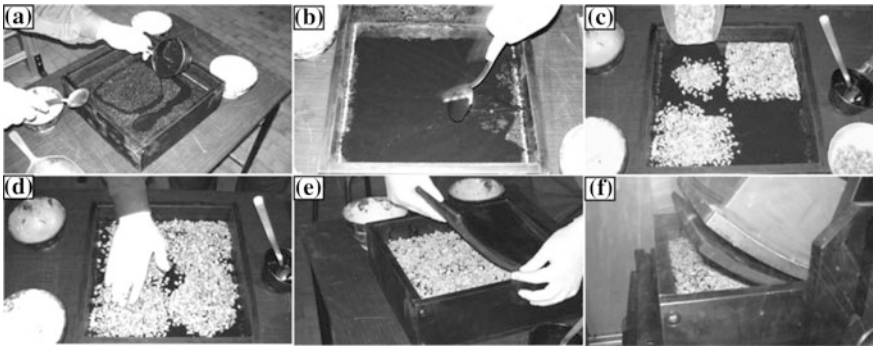


**Fig. 3** Construction phases: **a**, **b** emulsion spraying on the support layer (after storing in the oven at a temperature of 69 ± 2 °C); **c**, **d** application of a uniform layer of clean limestone aggregates; **e** a rubber sheath is laid on the surface in order to avoid the crushing of the aggregate during compaction; **f** slab compaction by means of the Unical Slab Roller Compactor (USRC) (Praticò and Vaiana 2013) (UNI EN 12697-33)

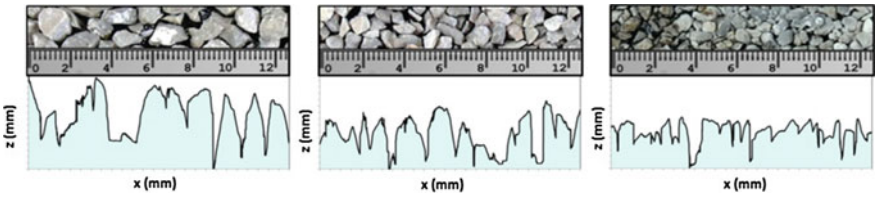


**Fig. 4** Surface images (*top*) and surface profiles (*bottom*) for each aggregate size (from CS1 on the *left* to CS3 on the *right*)

## 5 Results and Data Analysis

Figures 5, 6, 7 and Tables 1, 2, 3 summarize results obtained. Figure 5 describes how the three equations were used in model validation. The results obtained according to the model were compared to the observed values. Table 1 refers to the range of variability of sand height (EN 13036-1) and MPD (mean profile depth, Laser Profilometer). Table 2 summarizes model validation. Observed values derive from laboratory samples, while estimated values derive from the application of the model. As it is possible to see in Table 2, data well fit the statistical model. Observed values (both sand height and bitumen quantity measurements) are well replicated by the model: the variation between simulated and observed values is quite negligible. Table 3 illustrates friction performance.

Figures 6 and 7 illustrate the remaining surface performance investigated.

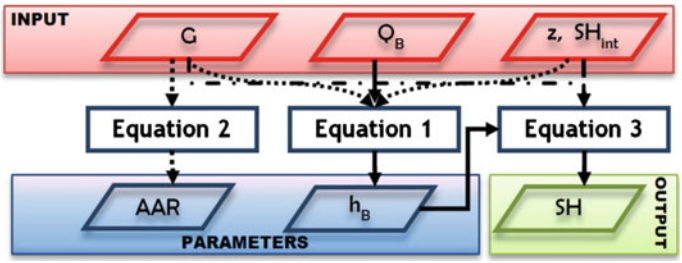


**Fig. 5** Closed-form Eqs. (1–3) to design a surface treatment based on surface properties. *Symbols* *G* aggregate grading; *z* bitumen film thickness; $h_B$ Bitumen height; *AAR* aggregate application rate, g/cm$^2$; $Q_B$ quantity of bitumen per square meter, g/m$^2$; $SH_{int}$ sand height of the underneath layer; *SH* sand height of the upper layer

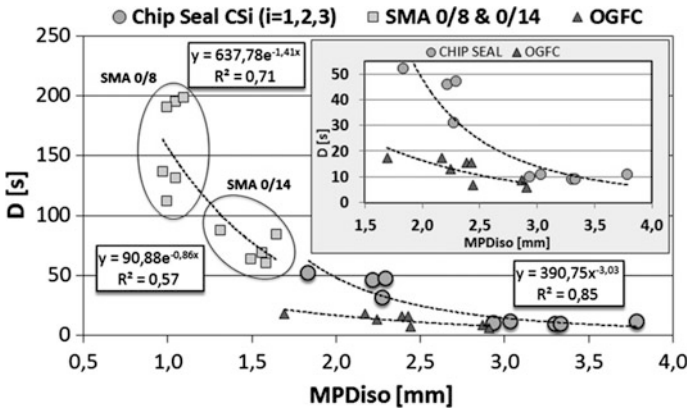


**Fig. 6** Drainability (y-axis) versus macrotexture (x-axis)

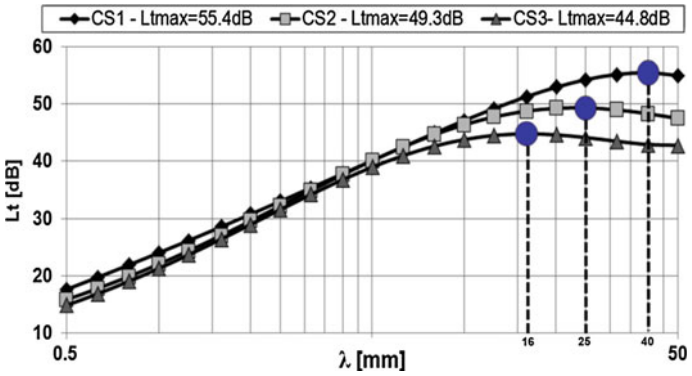


**Fig. 7** Maximum texture level and texture wavelength versus aggregate dimension

**Table 1** SH and MPD variation in relation to chip seal type

| Chip seal type | EAR (g/cm$^2$) | SH (mm) | MPD (mm) |
|---|---|---|---|
| $CSH_1$–$CST_1$ | 0.09–0.18 | 5.3–4.7 | 3.4–3.1 |
| $CSH_2$–$CST_2$ | 0.07–0.14 | 4.5–4.0 | 3.0–2.8 |
| $CSH_3$–$CST_3$ | 0.075–0.15 | 2.7–2.3 | 2.2–2.0 |

**Table 2** Model validation

| Grading[a] | 10/12.7 | 6.35/10 | 4/6.35 | 10/12.7 | 6.35/10 | 4/6.35 |
|---|---|---|---|---|---|---|
| [b] | $CST_1$ | $CST_2$ | $CST_3$ | $CSH_1$ | $CSH_2$ | $CSH_3$ |
| EAR | 0.18 | 0.14 | 0.15 | 0.09 | 0.07 | 0.075 |
| ESTSH | 4.73 | 4.01 | 2.23 | 5.31 | 4.48 | 2.72 |
| OBSSH | 4.73 | 3.95 | 2.34 | 5.30 | 4.50 | 2.70 |
| ESTBIT | 0.117 | 0.094 | 0.098 | 0.059 | 0.047 | 0.050 |
| OBSBIT | 0.117 | 0.094 | 0.100 | 0.059 | 0.047 | 0.050 |

*ESTSH* estimated SH (mm); *OBSSH* observed SH (mm); *ESTBIT* estimated Bitumen quantity ($Q_B/\gamma_B$, cm); *OBSBIT* observed bitumen quantity ($Q_B/\gamma_B$, cm); [a]mm; [b]see Table 1; *EAR* emulsion application rate (g/cm$^2$)

**Table 3** BPN values

| Chip seal type | $CSH_1$–$CST_1$ | $CSH_2$–$CST_2$ | $CSH_3$–$CST_3$ |
|---|---|---|---|
| BPN | 62–67 | 58–65 | 65–70 |

As a part of the overall study, aiming at obtaining information on surface performance, skid resistance (BPN, Table 2) and drainability (Fig. 6) data were measured (British Pendulum Tester, ASTM E303-93; Belgian Permeameter, CAM, 54.10 Belgian Specifications).

Figure 6 illustrates the relationship between outflow time (in seconds, y-axis) and macrotexture (Mean Profile Depth, x-axis) for all slab produced. Drainability (y-axis) was compared with data collected on other types of surfaces (from previous experimental investigations): (i) Splittmastixasphalts (SMA8 and SMA14, with NMAS, nominal maximum aggregate size, 8 and 14 mm, respectively, Boscaino et al. 2005); (ii) Open Graded Friction Course (NMAS = 15 mm, Praticò et al. 2013). Note that: (a) NMAS affects outflow time; (b) on average, OGFC outflow time is lower than the one obtained for surface treatments (Praticò and Moro 2006, 2007). To this end note that the Belgian drainometer was used, which is very different from Autostrade and NCAT drainometers, due to the fact that surface flow (horizontal) can be greater than the direct (vertical) flow of water from the surface to the bottom of the layer (Praticò and Moro 2005; Alvarez et al. 2014).

A deeper investigation into texture spectral descriptors was carried out as shown in Fig. 7, where the maximum texture levels ($LT_{max}$) and the corresponding texture wavelength ($\lambda_{max}$, mm) are highlighted. Note that: (i) higher NMASs yield higher SHs and correspond to higher LTs; (ii) the higher the NMAS the higher the $\lambda_{max}$; (iii) $\lambda_{max} \cong 4 \cdot S_{min}$ where $S_{min}$ refers to the lower aggregate size (e.g., 10, 6.35, 4 mm).

## 6 Conclusions

Surface treatments must allow a safe traffic for different drivers, diverse vehicles and multiple driver maneuvers. These include acceleration, deceleration, stopping at traffic lights, accelerating from a stop, braking, or having swerving response to abrupt emergencies. Pavement macrotexture can contribute to optimise the above performance especially in wet conditions and when high speeds are involved. Despite the above facts, the prediction of surface macrotexture is still far from a clear rationale. To this end the relationship between the main inputs (which refer to design and construction phases) and the output in terms of macrotexture (sand patch method) was studied and modelled through three equations. Finally, an experimental investigation was designed and carried out and this allowed validating the model and gathering valuable information on texture levels and drainability.

Based on the results obtained the following conclusions may be drawn: (i) mixture composition and surface macrotexture relate according to a rather clear rationale; (ii) the algorithm set up allows designing the bituminous surface treatment based on macro texture target. This implies that the model can be used to improve chip seal design to better their safety performance; (iii) surface performance of bituminous treatments can follow relationships which differ from the ones of other types of bituminous mixtures (OGFCs, SMAs and DGFCs). Results of this

study can benefit both researchers and practitioners. Future research will focus on two conflicting targets: (a) obtaining a more straightforward formula for macro-texture prediction; (b) introducing supplementary inputs and refining precision and reliability. Future investigations will be also focused on the evaluation of chip seal surface performance evolution in relation to embedment depth variation due to traffic actions.

## References

Adams J M and Kim Y R (2013) Mean profile depth analysis of field and laboratory traffic-loaded chip seal surface treatments. International Journal of Pavement Engineering Vol.15 (7), pp 645-656.

Adams JM, Kim Y R (2013) Mean profile depth analysis of field and laboratory traffic-loaded chip seal surface treatments, Int. J. Pav. Eng., 15 (7), 645-656.

Aktas B, Karasahi M and M Tigdemir (2013) Developing a macrotexture prediction model for chip seals. Construction and Building Materials. Vol. 41, pp. 784-789.

Alderson A (2006) Update of the Austroads sprayed Seal Design Method, Austroad Technical Report AP-T68/06, Austroad INc. 2006 ISBN192113965 X

Alvarez AE, Oscar L, Ortiz JR, Miró R, A review of the characterization and evaluation of permeable friction course mixtures, Ingeniare. Revista chilena de ingeniería, vol. 22 Nº 4, 2014, pp. 469-482.

Boscaino G, Pratico' F G and Vaiana R (2005) Tyre/road noise on different road pavements: synergetic influence of acoustical absorbing coefficient and surface texture," EAEC - European Automotive Congress – Environmental impact of road transport session, Beograd (Belgrado), 30th May -1st June ISBN: 978-160423604-0.

Cenek P D, Jamieson N J. (2005) Sensitivity of In-Service Skid Resistance Performance of Chipseal Surfaces to Aggregate and Texture Characteristics, Proc.International Surface Friction Conference, Christchurch, New Zealand.

Croteau J M, Keith Davidson J K and Houston G (2005). Seal Coat Systems in Canada: performances and practice. Annual Conference of the Transportation Association of Canada. Calgary, Alberta.

Federal Highway Administration (2003) Pavement Preservation Compendium. Publication No. FHWA-IF-03-21.

Gransberg D and D M James (2011) Chip Seal Best Practices - A Synthesis of Highway Practice. Transportation Research Board of the National Academies. Report No: NCHRP 342.

Gurer C, Karasahin M, Cetin S and Aktas B (2012) Effects of construction-related factors on chip seal performance, Constr. Build. Mat. 35, 605 –703.

Holtrop W (2008) Sprayed Sealing Practice in Australia. 1st International Sprayed Sealing Conference, Adelaide, South Australia. 27-29 July

Islam M S and M Hossain (2012) Evaluation of lightweight aggregates in chip seal. Proceedings of the 91st Transportation Research Board Annual Meeting, Washington D.C. (USA).

Krugler P E, Estakhri C K, Chang-Albitres C M, Sasser C H (2009) Synthesis study on transverse variable asphalt application rates for seal coats, Report No. FHWA/TX-09/0-5833-1

Kucharek A (2007) Measuring the Curing Characteristics of Chip Sealing Emulsions. Paper Presented at the Joint ARRA-ISSA-AEMA Meeting, Asphalt Emulsion Manufacturers Association and McAsphalt.

Li S, Noureldin S, Jiang Y and Sun Y (2012) Evaluation of Pavement Surface Friction Treatments. Joint Transportation Research Program, Indiana Department of Transportation and Purdue University, Report No.: FHWA/IN/JTRP-2012/04, West Lafayette, Indiana.

Nicholls J C (2002) Design Guide for road surface dressing. Road Note 39. 5th ed, *TRL* Ltd.

Pasquini E, Bonati, A, Giuliani, F, Canestrari, F (2014) Advanced Characterization of Clear Chip Seals. ASTM Journal of Testing and Evaluation, Volume 42, Issue 5, September 2014, doi: 10.1520/JTE20130119

Praticò F, Vaiana R, Fedele R (2014) A study on the dependence of PEMs acoustic properties on incidence angle. International Journal of Pavement Engineering, doi: 10.1080/10298436.2014.943215

Praticò FG, Moro A (2005) Experimental And Theoretical Investigation On Hot Mix Asphalts Outflow Times: Boundary Conditions Influence, 3rd SIIV International Congress, Bari. ISBN 10: 88-902409-9-7; ISBN 13: 978-88-902409-9-7.

Praticò FG, Moro A (2006) Hot Mix Asphalts Drainability and Permeability: A Theoretical And experimental Investigation On Four Different Devices. Paper presented at the 10th International Conference on Asphalt Pavement, ICAP, Québec. ISBN: 978-2-550-49009-8

Praticò FG, Moro A (2007) Permeability and volumetrics of porous asphalt concrete: a theoretical and experimental investigation. Road Materials and Pavement Design 8/4: 799-817

Praticò FG, Vaiana R, Iuele T (2013) Acoustic absorption and surface texture: an experimental investigation. Paper presented at the 42nd International Congress and Exposition on Noise Control Engineering, InterNoise 2013: Noise Control For Quality of Life. Innsbruck, 15-18 September 2013. ISSN: 0736-2935 ISBN: 978-163266267-5

Praticò FG, Vaiana R (2013) A study on volumetric versus surface properties of wearing courses, Construction and Building Materials 38, 766-775, doi:10.1016/j.conbuildmat.2012.09.021

Shuler S, Lord A, Epps-Martin A and Hoyt D (2011) Manual for emulsion-based chip seals for pavement preservation. Transportation Research Board of the National Academies, Report No.: NCHRP 680.

Transit New Zeland (2005) Chipsealing in New Zealand. Road Controlling Authorities, Roading New Zealand, Wellington, New Zealand. ISBN 0-478-10562-2.

Wasiuddin N M, Marshall A, Saltibus N E, Saber A, Abadie C and Mohammad L N (2012) Use of sweep test for emulsion and hot asphalt chip seals: laboratory and field evaluation. Proceedings of the 91st Transportation Research Board Annual Meeting Washington D.C.

Zaman M, Gransberg D, Bulut R, Commuri S, Pittenger D (2013) Develop draft chip seal cover aggregate specification based on aims angularity, shape and texture test results, Report No. OTCREOS11.1-65-F, The University of Oklahoma, Office of Research Services

# Part VII
# Environmentally Sustainable Materials and Technologies

# Effect of Rejuvenator on Performance Properties of WMA Mixtures with High RAP Content

**Mohammadreza Sabouri, Yeong-Tae Choi, Yizhuang Wang, Sungdo Hwang, Cheolmin Baek and Richard Y. Kim**

**Abstract** The production of warm mix asphalt (WMA) mixtures with high percentages of reclaimed asphalt pavement (RAP) is gaining attention as a way to save costs and efficiently utilize existing resources. However, WMA must perform at least as well as hot mix asphalt (HMA) before it can be used as a replacement for HMA. In this study, the performance of a WMA mixture with a high percentage of RAP (40 % RAP) and a WMA additive (1.5 % of binder weight) that works as a rejuvenator was evaluated and compared with the performance of a HMA mixture with the same amount of RAP in order to evaluate the effects of the WMA rejuvenator. These mixtures were evaluated in terms of fatigue cracking using the simplified viscoelastic continuum damage (S-VECD) model and in terms of rutting using the triaxial stress sweep (TSS) test. In addition, layered viscoelastic pavement analysis for critical distresses (LVECD) was used to predict the fatigue resistance of these mixtures for future use. The WMA rejuvenator was found to improve the mixing and compaction ability of the WMA mixture. Also, compared to the HMA

M. Sabouri
Braun Intertec Corporation, Minneapolis, MN, USA
e-mail: msabouri@braunintertec.com

Y.-T. Choi · Y. Wang · R.Y. Kim (✉)
Department of Civil, Construction and Environmental Engineering, North Carolina State University, Raleigh, NC, USA
e-mail: kim@ncsu.edu

Y.-T. Choi
e-mail: ychoii5@ncsu.edu

Y. Wang
e-mail: ywang70@ncsu.edu

S. Hwang · C. Baek
Highway Pavement Research Division, Korea Institute of Civil Engineering and Building Technology, Goyang, South Korea
e-mail: sdhwang@kict.re.kr

C. Baek
e-mail: cmbaek@kict.re.kr



F. Canestrari and M.N. Partl (eds.), *8th RILEM International Symposium on Testing and Characterization of Sustainable and Innovative Bituminous Materials*, RILEM Bookseries 11, DOI 10.1007/978-94-017-7342-3_38

mixture, the WMA mixture showed better fatigue resistance, but the rejuvenator found to have an adverse effect on the rutting resistance of the mixture.

**Keywords** Reclaimed asphalt pavement (RAP) · Warm mix asphalt (WMA) · Fatigue cracking · Rutting · Rejuvenator

## 1 Introduction

The Kyoto Protocol, an international agreement linked to the United Nations Framework Convention on Climate Change, has led to increased efforts in the development of warm mix asphalt (WMA) technology in recent years. The original goal of the agreement was to reduce greenhouse gas (GHG) emissions by at least 5 % from 1990 levels over the five-year period from 2008 to 2012. Recently, the Kyoto Protocol has been expanded to 2020. According to the National Asphalt Pavement Association (NAPA), "Warm-mix asphalt allows the producers of asphalt pavement material to lower the temperature at which the material is mixed and placed on the road. Reductions of 50–100 °F (10–38 °C) have been documented. Such drastic reductions have the obvious benefits of cutting fuel consumption and decreasing the production of greenhouse gases" (NAPA 2012). Other advantages of WMA include that it can be paved during cold seasons if necessary, because it remains more workable than hot mix asphalt (HMA) at low temperatures. WMA mixes also can be transported longer distances than HMA, likewise due to the fact that the mix can stay workable for longer periods. This increased workability of WMA can also lead to better density in the field (Hurley and Prowell 2006).

Another effort to increase economic efficiency and help conserve the ecosystem is to recycle construction materials. Reclaimed asphalt pavement (RAP), which is the material that remains after milling pavement, can be added as a portion of a new asphalt mixture. RAP not only decreases construction costs but also reduces environmental contamination (Mogawer et al. 2012; Bennert et al. 2014; Sabouri et al. 2014a, b). Higher percentages of RAP can be incorporated in WMA mixes than in HMA mixes due to less aging of the virgin asphalt binder used in WMA mixes, which adds to WMA's environmental advantages (Button et al. 2007).

In order to enhance the use of RAP in WMA mixtures, a rejuvenator that works as a WMA additive (hereinafter called WMA rejuvenator) was evaluated in this study. The main objective of this study is to evaluate the performance of a WMA mixture that has a high RAP content and WMA rejuvenator, referred to as the RAP-WMA mixture in this study, which was developed to lower fuel consumption and reduce GHG emissions. A comparison of the RAP-WMA mixture and a HMA mixture with RAP, referred to as the RAP-HMA mixture in this study, can help show the advantages and disadvantages of the RAP-WMA mixture.

The simplified viscoelastic continuum damage (S-VECD) model was used to evaluate the fatigue properties of the mixtures. The S-VECD model is a continuum

damage mechanics-based model. This model, coupled with its fatigue failure criterion, the $G^R$ method, has been applied effectively to predict the performance of asphalt concrete mixtures under different loading conditions (Hou et al. 2010; Underwood et al. 2012; Sabouri and Kim 2014; Norouzi et al. 2014).

The rutting performance of the mixtures was evaluated in this study using a permanent deformation model developed by Choi and Kim (2012). This so-called *shift model* can simulate the effects of temperature, pulse time, and stress on rutting using time-temperature and time-stress superposition principles. The triaxial stress sweep (TSS) test used in this project was developed to provide a simple method to calibrate the shift model.

Layered viscoelastic critical distresses (LVECD) pavement analysis was used in this study to predict the fatigue behavior of the mixtures. The LVECD program is a layered viscoelastic structural model that can calculate the stresses and strains necessary for predicting fatigue behavior using the S-VECD model (Eslaminia et al. 2012; Park et al. 2014).

## 2 Materials and Test Methods

Two different mixtures were used for this study: an HMA mixture with 40 % RAP (RAP-HMA) and a WMA mixture also with 40 % RAP as well as the WMA rejuvenator (RAP-WMA). The aggregate used for both of the mixtures was a coarse Superpave 12.5-mm blend. Samples were fabricated in the laboratory, and their gradations agreed with those found in the job mix formula to produce the same mixtures as those fabricated in the plant. In order to compare the effects of RAP and the WMA rejuvenator on the mix, the gradation was kept constant in spite of adding RAP. The asphalt content for each mixture was 5.7 % by total mix mass, and all experimental data were obtained from specimens with air void contents between 5.5 and 6.5 %. The binder grade of the virgin binder was PG 64-28.

### *2.1 Specimen Preparation*

In order to incorporate the WMA rejuvenator, the virgin binder was heated to 135 °C and mixed with the rejuvenator in 4-l cans for 3 min in order to replace 1.5 % of binder with the WMA rejuvenator. For making the specimens, aggregate stockpiles were dried and sieved into individual portions for batching individual specimen sizes. The aggregate particles were then heated to the mixing temperature (165 °C for HMA and 135 °C for WMA) for at least four hours prior to mixing. The RAP was air-dried on a flat sheet for 24 h prior to mixing and was heated to 60 °C for 2 h prior to being mixed with the virgin aggregate and asphalt binder. The RAP, virgin aggregate, and asphalt binder were mixed together for 3 min using a bucket mixer. After that, the mixtures were short-term oven-aged for 2 h at the compaction

temperature. Then, the mixtures were compacted to create specimens of appropriate geometry and air void content. All specimens were compacted to a height of 178 mm and a diameter of 150 mm using a Superpave gyratory compactor. To obtain specimens of uniform air void distribution, these samples were cored to a diameter of 100 mm and cut to height of 150 mm for dynamic modulus and TSS testing, and to 130 mm for tension testing (Lee et al. 2014). Prior to testing, all the specimens were tested for bulk specific gravity using a Corelok™ machine and vacuum bags for quality control.

## 2.2 Test Protocols

Three main mixture tests were performed in this study: (1) the dynamic modulus test to determine the linear viscoelastic characteristics, (2) the cyclic direct tension test to describe the viscoelastic damage characteristics, and (3) the TSS test to evaluate the rutting performance. Laboratory experiments were conducted according to the test protocols described in the next sections.

### 2.2.1 Dynamic Modulus Testing

Dynamic modulus testing was performed in load-controlled mode in axial compression following the protocol given in AASHTO TP 79 (2011). Tests were completed for all the mixtures at 4, 20, 40, and 54 °C and at frequencies of 25, 10, 5, 1, 0.5, and 0.1 Hz. Load levels were determined by a trial and error process so that the resulting strain amplitudes were between 50 and 75 microstrains. The testing order was from low to high temperatures and from high to low frequencies in order to minimize damage to the specimens.

### 2.2.2 Cyclic Testing Using the Simplified Viscoelastic Continuum Damage (S-VECD) Model

Cyclic testing was performed in crosshead-controlled (CX) mode of loading following the protocol given in AASHTO TP 107 (2014). In this study, all the cyclic tests were performed at three to four different amplitudes to cover a range of numbers of cycles to failure (from 1000 to 100,000).

The fatigue failure for each of the specimens tested in the CX cyclic tests was determined using Reese's approach that is based on the change in phase angle behavior (Reese 1997). The phase angle increases until strain localization occurs, and then drops suddenly. This sharp decrease in the phase angle occurs around the failure point, which makes the determination of the number of cycles to failure accurate and consistent in laboratory testing.

The S-VECD failure criterion (the $G^R$ method) also was applied to the data. According to this criterion, a characteristic relationship exists between the rate of change of the averaged released pseudo strain energy ($G^R$) during fatigue testing and the final fatigue life, defined as the number of cycles to failure ($N_f$). The $G^R$ can be calculated using Eq. (1). Details about this method can be found in Sabouri and Kim (2014).

$$G^R = \frac{\frac{1}{2}\int_0^{N_f}\left(\varepsilon_{0,ta}^R\right)_i^2(1-F_i)}{N_f^2} \tag{1}$$

where

$\left(\varepsilon_{0,ta}^R\right)_i$ pseudo strain amplitude at cycle $i$, and

$F_i$ pseudo stiffness at cycle $i$.

### 2.2.3 Permanent Deformation: Triaxial Stress Sweep (TSS) Testing

The TSS test is composed of two types of tests: a reference test at the high temperature ($T_H$) and then three multiple stress sweep (MSS) tests at three different temperatures of low, intermediate, and high ($T_L$, $T_I$, and $T_H$), respectively. The reference test in this study utilized a 0.4-s haversine pulse with a 10-s rest period. This test provided the permanent strain mastercurves by fitting the incremental model. The incremental model is expressed in Eq. (2).

$$\varepsilon_{vp} = \frac{\varepsilon_0 \cdot N_{red}}{(N_I + N_{red})^{\beta}} \tag{2}$$

where

$\varepsilon_{vp}$ viscoplastic strain (i.e., permanent strain),

$\varepsilon_0, N_I, \beta$ coefficient of the incremental model, and

$N_{red}$ number of cycles at the reference loading condition.

The MSS tests each consist of three loading blocks. In this study, the deviatoric stress was increased in each loading block while the other loading conditions were kept constant. The deviatoric stress level began at 480 kPa and then was increased to 690 and 900 kPa in the second and third loading blocks, respectively. The shift factors were obtained by shifting the permanent strain of an individual loading block toward the permanent strain mastercurve, which was obtained from the reference test. The reduced load time shift factors and deviatoric stress shift factors are shown in Eq. (3).

$$a_{\xi_p} = p_1\,\xi_p^{p_2} + p_3,$$
$$a_{\sigma_v} = d_1(\sigma_v/P_a)^{d_2} + d_3. \tag{3}$$

where

| | |
|---|---|
| $a_{\zeta_p}$ | reduced load time shift factor, |
| $a_{\sigma_v}$ | vertical stress shift factor, |
| $\xi_p$ | reduced load time, |
| $\sigma_v$ | vertical stress, |
| $p_1, p_2, p_3$ | coefficients of reduced load time shift function, |
| $d_1, d_2, d_3$ | coefficients of vertical stress shift function, and |
| $P_a$ | atmospheric pressure to normalize stress. |

Equations (2) and (3) constitute the shift model. The physical number of cycles at a given condition was converted into a reduced number of cycles using the total shift factor, which is the sum of the deviatoric stress shift factor and the reduced load time shift factor. These two shift functions utilize temperature, load time, and vertical stress to calculate the shift factors.

## 3 Results and Discussion

Dynamic modulus tests, cyclic tension fatigue tests, and rutting tests were conducted to evaluate the asphalt mixtures' performance and to provide model parameters for LVECD simulations for pavement performance evaluation.

### *3.1 Stiffness: Dynamic Modulus*

Figure 1a through Fig. 1d present comparisons of the linear viscoelastic characteristics of the mixtures in this study. The replicate averaged dynamic modulus mastercurves for the mixtures are shown in both semi-log and log-log scales, and the phase angle mastercurves and the time-temperature shift factor functions are shown as well. As these graphs suggest, incorporating the WMA rejuvenator in the RAP-WMA mixture decreased the stiffness of the mixture. Also, the RAP-HMA mixture shows a higher degree of elasticity than the RAP-WMA mixture at the high reduced frequencies, but lower elasticity at lower reduced frequencies. Using the WMA rejuvenator decreased the mixing and compaction temperatures. In other words, the WMA rejuvenator increased the workability of the mix. This phenomenon can be observed in the dynamic modulus mastercurve comparison between the RAP-HMA and RAP-WMA mixes in Fig. 1a, b. The WMA rejuvenator would likely improve the workability of the mix, and the dynamic modulus value would decrease as a byproduct.

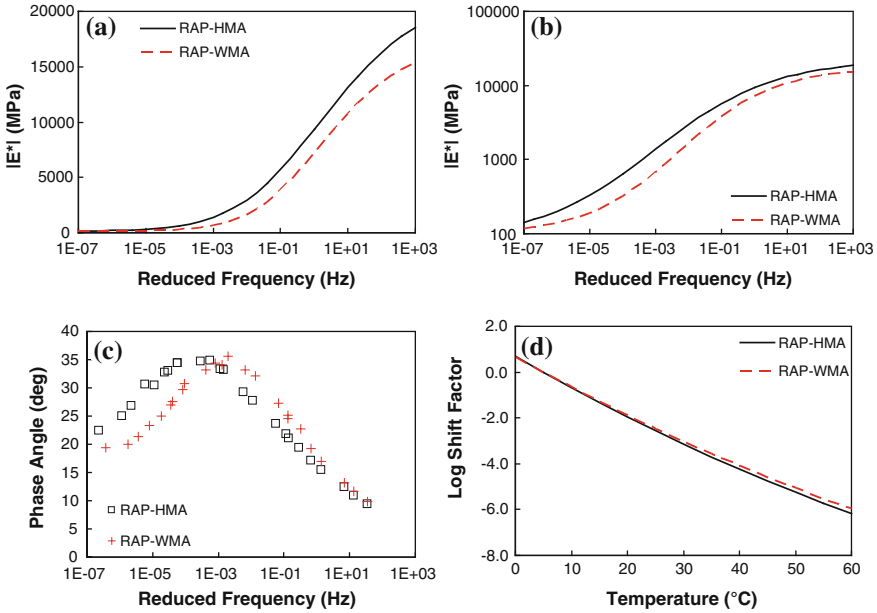


**Fig. 1** Linear viscoelastic characterization for RAP-HMA and RAP-WMA mixtures: **a** dynamic modulus mastercurve in semi-log space, **b** dynamic modulus mastercurve in log-log space, **c** phase angle mastercurve, and **d** time-temperature shift factor function

## 3.2 *Cracking Resistance Testing: S-VECD Model*

Direct tension cyclic fatigue tests of the mixtures were conducted in CX mode to characterize the S-VECD model. The pseudo stiffness (C) versus damage (S) characteristic curves were fitted using an exponential function, as described in Eq. (4).

$$C = e^{aS^b} \tag{4}$$

Figure 2a presents a comparison of the fitted C versus S curves for the study mixtures. In general, the RAP-HMA mixture has a higher curve than the RAP-WMA mixture, which could be because the WMA mixture is softer than the HMA mix.

The S-VECD failure criterion was applied to both of the study mixtures, and the results are shown in Fig. 2b. The positions of the failure criterion lines can be used as a relative comparison of the expected fatigue resistance of the mixtures. Mixtures with better fatigue resistance have failure criterion lines that are located towards the upper right corner and have shallow slopes, meaning that at the same level, the $G^R$ will correspond to a higher number of cycles to failure ($N_f$), which indicates better performance. However, in order to compare the fatigue resistance of the two

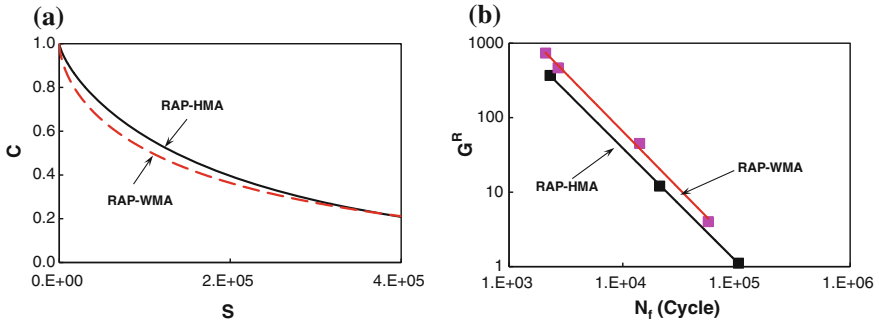


**Fig. 2** Comparison of: **a** fitted damage characteristic curves and **b** failure criterion lines for the study mixtures

mixtures, they must be considered within a specific pavement structure. This pavement evaluation was conducted for this study using LVECD software, and the results are presented in Sect. 3.4.

## *3.3 Permanent Deformation: Triaxial Stress Sweep Testing*

The rutting characterization tests, i.e., the TSS tests, were performed using the two study mixtures. Figure 3a, b show the comparison of the TSS test results between the RAP-HMA and RAP-WMA mixtures. In general, as the mixture's stiffness increases, the rutting resistance improves. This finding suggests that the dynamic modulus data, which have been captured in the viscoelastic domain, could be related to the rutting resistance of the mixtures to some extent.

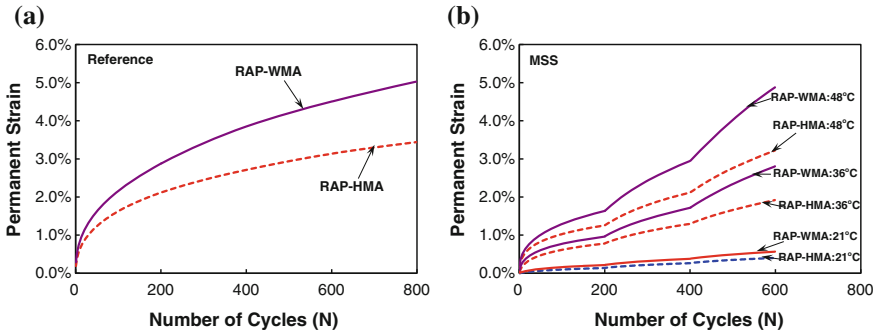


**Fig. 3** Comparison of rutting resistance between RAP-HMA and RAP-WMA mixtures: **a** reference testing and **b** MSS testing conditions

### 3.4 Pavement Analysis

The LVECD program was used to predict the fatigue behavior of the mixtures in the pavement structures. The inputs required for LVECD simulations are the design time, structural layout, traffic, and climate. The design time for this study was assumed to be 20 years.

Simulations were performed for thin and thick pavement structures that typically are considered to represent the strain-controlled and stress-controlled behavior of asphalt mixtures. In the thin pavement case, an asphalt concrete layer that was 100-mm thick with an aggregate base 200-mm thick was used, whereas for the thick pavement, a full-depth asphalt layer 300-mm thick was assumed directly on subgrade. The asphalt layer is described as a viscoelastic material with damage. Therefore, this layer can be represented by the Prony series of dynamic modulus values, time-temperature shift factors, and the S-VECD model coefficients. The aggregate base and subgrade were modeled using linear elastic properties with modulus values of 350 and 100 MPa, respectively.

A single tire with standard loading of 80 kN at the center of the pavement was assumed. The average annual daily truck traffic (AADTT) was assumed to be 2000. The climate in Boston, Massachusetts was selected for pavement analysis. Pavement temperatures were obtained from Enhanced Integrated Climatic Model (EICM) software and were input to the LVECD program. The EICM program provides hourly temperatures of asphalt pavements in terms of pavement depth.

Simulations were conducted using different properties for the asphalt layers while keeping all the other conditions constant. To evaluate fatigue, the LVECD program calculated the damage growth (i.e., reduction of the secant pseudo modulus) and the damage factor that is defined in Eq. (5) based on Miner's law. If the damage factor is equal to zero, the element does not have any damage, and a damage factor of one indicates failure of the element.

$$Damage\ Factor = \sum_{i=1}^{T} \frac{N_i}{N_{fi}} \tag{5}$$

where

T total number of periods,
$N_i$ traffic for period $i$, and
$N_{fi}$ allowable failure repetitions under conditions that prevail in period $i$.

It is noted that the fatigue performance predicted from the LVECD program has not been fully calibrated against the field performance data. A preliminary comparison of the LVECD predicted damage and the percentage of cracking areas measured from in-service pavements is presented in Norouzi and Kim (2014). However, transfer functions to convert the damage predicted from the LVECD software to the percentage of cracking areas have not yet been developed.

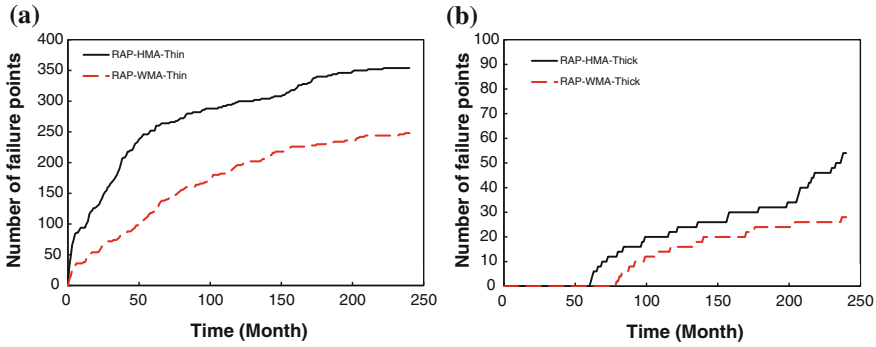


**Fig. 4** Fatigue life prediction for: **a** thin pavement and **b** thick pavement

Therefore, the LVECD predictions presented in the remaining portion of this paper use the number of failure points to evaluate the effects of different RAP mix design factors on the pavement performance.

In order to compare the fatigue resistance of the mixtures, the numbers of failure points (elements with the damage factor of '1') during the design period are shown in Fig. 4a, b for the thin and thick pavements, respectively. Comparing these two figures clearly suggests better performance of the RAP-WMA pavement compared to the RAP-HMA pavement, as the RAP-WMA pavement has fewer failure points during the design period in all the cases.

## 4 Summary and Conclusions

The production of WMA mixtures with high percentages of RAP has gained attention as a way to save costs and efficiently utilize existing resources. In this study, the performance of a WMA mixture with a high percentage of RAP (40 % RAP) and a WMA rejuvenator (1.5 % of binder weight) was evaluated and compared with the performance of a HMA mixture with the same amount of RAP in order to evaluate the effects of the WMA rejuvenator. These mixtures were evaluated in terms of fatigue cracking using the S-VECD model and in terms of rutting using the TSS test. In addition, LVECD pavement analysis was used to predict the fatigue resistance of these mixtures for future use. The WMA rejuvenator was found to improve the mixing and compaction ability of the WMA mixture. Also, compared to the HMA mixture, the WMA mixture showed better fatigue resistance, but was more sensitive to permanent strain during TSS testing. These findings suggest that using WMA rejuvenator in high RAP WMA mixtures should be considered with care, as the WMA rejuvenator improves the fatigue cracking resistance but has an adverse effect on the rutting resistance of the mixture.

## 5 Acknowledgements

The authors would like to acknowledge the financial support from the Korea Institute of Civil Engineering and Building Technology.

## References

American Association of State Highway Transportation Officials (AASHTO) (2014). AASHTO TP 107, Determining the Damage Characteristic Curve of Asphalt Concrete from Direct Tension Cyclic Fatigue Tests, AASHTO. Washington, D.C.

American Association of State Highway Transportation Officials (AASHTO) (2011). AASHTO TP 79, Standard Method of Test for Determining the Dynamic Modulus and Flow Number for Hot Mix Asphalt (HMA) Using the Asphalt Mixture Performance Tester (AMPT). AASHTO. Washington, D.C.

Bennert T, Daniel J, Mogawer W (2014). Strategies for Incorporating Higher RAP Percentages: Review of Northeast States Implementation Trials. Transportation Research Record: Journal of the Transportation Research Board. In press.

Button JW, Estakhri C, Wimsatt A (2007). A Synthesis of Warm-Mix Asphalt. Publication FHWA/TX-07/0-5597-1, FHWA and Texas Department of Transportation.

Choi Y, Kim YR (2012). Development of Calibration Testing Protocol for Permanent Deformation Model of Asphalt Concrete. Transportation Research Record: Journal of the Transportation Research Board, No. 13-2555, pp. 34-43.

Eslaminia M, Thirunavukkarasu S, Guddati MN, Kim YR (2012). Accelerated Pavement Performance Modeling Using Layered Viscoelastic Analysis. Proceedings of the 7th International RILEM Conference on Cracking in Pavements, Delft, The Netherlands.

Hou T, Underwood BS, Kim YR. (2010). Fatigue Performance Prediction of North Carolina Mixtures Using Simplified Viscoelastic Continuum Damage Model. Journal of the Association of Asphalt Paving Technologists, Vol. 79, pp. 35-80.

Hurley GC, Prowell BD (2006). Evaluation of Potential Processes for Use in Warm Mix Asphalt. Journal of the Association of Asphalt Paving Technologists, Vol. 75, Savannah, Georgia.

Lee JS, Norouzi A, and, Kim YR (2014). Determining Specimen Geometry of Cylindrical Specimens for Direct Tension Fatigue Testing of Asphalt Concrete. Submitted to ASTM Journal of Testing and Evaluation.

Mogawer WS, Bennert T, Daniel J, Bonaquist R, Austerman A, Booshehrian A (2012). Performance Characteristics of Plant Produced High RAP Mixtures. Road Materials and Pavement Design, Vol. 13, Supplement 1, pp. 183-208.

National Asphalt Pavement Association (NAPA), WMA official website. Available via http://www.warmmixasphalt.com/AboutWma.aspx, Accessed 15 Jan 2012

Norouzi A, Kim YR (2014). Mechanistic Evaluation of the Fatigue Cracking in Asphalt Pavements. Submitted to International Journal of Pavement Engineering.

Norouzi A., Sabouri M, Kim YR (2014). Evaluation of the Fatigue Performance of High RAP Asphalt Mixtures. Proceedings of 12th International Society for Asphalt Pavements, Raleigh, NC.

Park HJ, Eslaminia M, Kim YR (2014). Mechanistic Evaluation of Cracking in in-Service Asphalt Pavements. Materials and Structures, pp. 1–20.

Reese R (1997). Properties of Aged Asphalt Binder Related to Asphalt Concrete Fatigue Life. Journal of the Association of Asphalt Paving Technologists, Vol. 66, pp. 604-632.

Sabouri M, Kim YR (2014). Development of Failure Criterion for Asphalt Mixtures under Different Modes of Fatigue Loading. Transportation Research Records: Journal of Transportation Research Board. In press.

Sabouri M, Bennert T, Daniel JS, Kim YR (2014a). A Comprehensive Evaluation of the Fatigue Behavior of Plant Produced RAP Mixtures Laboratory-Produced RAP Mixtures. Submitted to Road Materials and Pavement Design.

Sabouri M, Bennert T, Daniel J, Kim YR (2014b). Evaluating Laboratory-Produced RAP Mixtures in Terms of Rutting, Fatigue, Predictive Capabilities, and High RAP Content Potential. Submitted to Transportation Research Record: Journal of the Transportation Research Board.

Underwood BS, Baek CM, Kim YR (2012). Use of Simplified Viscoelastic Continuum Damage Model as an Asphalt Concrete Fatigue Analysis Platform. Transportation Research Record: Journal of the Transportation Research Board. No 2296, pp. 36-45.

# Effect of Warm Mix Chemical Additives on the Binder-Aggregate Bond Strength and High-Service Temperature Performance of Asphalt Mixes Containing Electric Arc Furnace Steel Slag

**Marco Pasetto, Giovanni Giacomello, Emiliano Pasquini and Francesco Canestrari**

**Abstract** Warm Mix Asphalt (WMA) is a modified asphalt concrete, obtained by using organic, chemical or foaming additives, which can be produced and compacted at lower temperatures (100–140 °C). The environmental sustainability of WMA can be enhanced with the inclusion of steel slag in substitution of natural aggregates. Given this background, this paper illustrates an experimental research aimed at characterizing WMA containing steel slag. Rheological tests were carried out on asphalt binders in order to investigate the effect of the WMA additive on high-service temperature properties. Then, the bond strength between asphalt binders and aggregates (limestone and steel slag) was investigated. Finally, compactability and permanent deformation resistance of the studied mixtures were also evaluated. Results mainly showed that, regardless the presence of steel slag, the studied additive allowed adequate mixing and compaction at lower temperatures, improving the bond strength between binder and aggregates without affecting permanent deformation resistance of asphalt mixes.

**Keywords** WMA mixtures · Steel slag · Rutting potential · Bond strength

M. Pasetto · G. Giacomello
University of Padua, Padua, Italy
e-mail: marco.pasetto@unipd.it

G. Giacomello
e-mail: giovanni.giacomello@unipd.it

E. Pasquini (✉) · F. Canestrari
Polytechnic University of Marche, Ancona, Italy
e-mail: e.pasquini@univpm.it

F. Canestrari
e-mail: f.canestrari@univpm.it



F. Canestrari and M.N. Partl (eds.), *8th RILEM International Symposium on Testing and Characterization of Sustainable and Innovative Bituminous Materials*, RILEM Bookseries 11, DOI 10.1007/978-94-017-7342-3_39

## 1 Introduction

WMA is a modified asphalt concrete, obtained by using organic (wax), chemical or foaming additives, which can be produced, applied and compacted at lower temperatures (100–140 °C) than HMA. The use of WMA can lead to environmental benefits (reduced energy consumption, gas and fume emissions) as well as to economic/operational advantages such as lower production costs, longer hauling distances and extended construction periods (D'Angelo et al. 2008; Capitao et al. 2012; Rubio et al. 2012; Kheradmand et al. 2014).

Mechanical properties of WMA mixes can vary in a large range mainly depending on the amount of additive and the type of WMA technology used (Capitao et al. 2012). Generally, the most documented drawbacks related to the reduction of mixing and compaction temperatures are related to greater moisture susceptibility, higher rutting potential as well as coating and bonding problems. Moreover, uncertainties regarding long-term performance also exist (Capitao et al. 2012; Rubio et al. 2012; Kheradmand et al. 2014).

In particular, as far as WMA chemical additives concern, it should be noted that these materials are usually formed by a package of products such as emulsification agents, surfactants, polymers and additives as well as adhesion promoters (D'Angelo et al. 2008; Capitao et al. 2012; Rubio et al. 2012; Kheradmand et al. 2014). They should be able to achieve lower mixing and compaction temperatures without affecting viscosity and performance grade of the binder. This should be accomplished thanks to the reduced friction at the interface between bitumen and aggregates provided by the presence of surfactants. In fact, surfactants should reduce the surface tension of the asphalt binder acting as an emulsifier (D'Angelo et al. 2008; Capitao et al. 2012). In this sense, different studies (Sanchez-Alonso et al. 2011; Morea et al. 2012; Xiao et al. 2012) showed that viscosity of plain asphalts is not significantly affected by the addition of chemical tensoactive WMA additives notwithstanding they are able to guarantee good workability at lower temperatures (Hurley and Prowell 2006; Sanchez-Alonso et al. 2011).

However, several researches demonstrated that reducing mixing and compaction temperatures could lead to possible drawbacks. In particular, increased rutting potential in the case of WMA prepared with chemical additive was reported by several authors (Hurley and Prowell 2006; Morea et al. 2012). A further issue related to the reduced mixing and compaction temperatures of WMA could be related to the correct bonding between asphalt and aggregates. Huge research indirectly investigated this issue through the assessment of moisture sensitivity of WMA since a poor adhesion at the binder-aggregate interface can lead to moisture damage. On the contrary, only few studies were addressed to the direct assessment of the bond between warm-modified binders and aggregates (Mogawer et al. 2011).

The environmental sustainability of asphalt mixes can be strongly enhanced with the inclusion of steel slag in substitution of natural aggregates allowing both saving natural resources and re-using industrial waste.

The types of primary steel slag are usually classified on the basis of the furnace type. In this sense, the more common steel slags are basic oxygen furnace (BOF) steel slag and electric arc furnace (EAF) steel slag (Yildirim and Prezzi 2011; Piatak et al. 2014).

EAF steel slag appears as hard, wear-resistant, adhesive and rough material. Thus, it can be considered suitable to be used as high quality aggregate in road pavements (Motz and Geiseler 2001; Yi et al. 2012). However, the high bulk density of such material limited its extensive use in road construction, mainly due to the consequent higher transportation costs. On the other hand, several studies demonstrated that mechanical properties and durability of asphalt mixtures can be improved thanks to the partial replacing of mineral aggregates with steel slag (Ahmedzade and Sengoz 2009; Pasetto and Baldo 2010, 2011, 2012, 2013).

## 2 Research Objectives and Approach

Despite the huge literature concerning WMA as well as the numerous studies carried out about the use of steel slag in asphalt mixtures, the possibility of using steel slag in WMA has received very little attention (Ameri et al. 2013).

Given this background, the main goal of this experimental research is the evaluation of the feasibility of using EAF steel slag as aggregate in dense graded WMA mixes containing a chemical tensoactive additive. This was accomplished by evaluating compactability and permanent deformation resistance of such WMA mixes compared to WMA containing only mineral aggregates. The bonding conditions between warm-modified binder and steel slag were also investigated.

Secondly, as the bonding tests were performed on limestone and steel slag surfaces using plain and warm-modified binders, the evaluation of the influence of the selected warm additive on the binder adhesion properties was also allowed.

Finally, the rutting potential of the selected warm technology, regardless of the use of EAF steel slag aggregates, was evaluated through rheological tests on plain and warm-modified binders and performance-related tests on hot and warm asphalt mixtures.

The experimental plan schematized in Fig. 1 was developed to achieve the research objectives mentioned above.

Plain and warm-modified asphalt binders were subjected to rheological tests through a dynamic shear rheometer (DSR) in order to investigate the effect of the studied additive on high-service temperature properties (rutting potential). Moreover, the bond strength between asphalt binders and aggregate surfaces (limestone and steel slag) were investigated through binder bond strength (BBS) tests carried out in dry conditions.

Three different dense graded mixtures (one HMA containing only limestone aggregates and two warm mixtures containing limestone with or without EAF steel slag aggregates) were prepared with the studied binders. HMA was produced at 150 °C and compacted at 140 °C on the basis of the viscosity of the plain bitumen P

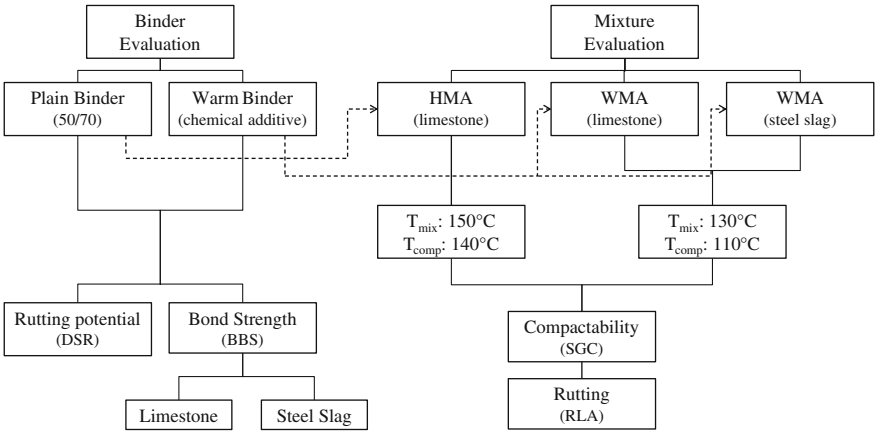


**Fig. 1** Experimental plan

whereas, in the case of WMAs, arbitrary values of 130 and 110 °C were respectively chosen for mixing and compaction temperatures to simulate real scale applications. In fact, preliminary viscosity tests demonstrated that, according to other authors (Morea et al. 2012; Xiao et al. 2012), the addition of warm chemical additive did not influence the viscosity. Thus, it was confirmed that the assessment of mixing and compaction temperatures cannot be viscosity based when a warm chemical additive is used (Capitao et al. 2012; Rubio et al. 2012).

Compactability and permanent deformation (rutting) resistance of the studied mixtures were evaluated through performance-related tests. In particular, cylindrical specimens were prepared through a Superpave gyratory compactor (SGC) and air void contents as well as densification curves have been analyzed. Then, such specimens were subjected to repeated load axial (RLA) tests using a dynamic test equipment.

## 3 Materials and Methods

### *3.1 Materials, Mix Design and Specimen Preparation*

A 50/70 penetration grade bitumen was selected as the base binder for this study. This bitumen was modified by adding a commercial chemical WMA additive. The additive is a water-free liquid product containing surface active agents. A WMA additive dosage of 0.5 % by weight of binder was selected as recommended by the producer. The binder modification was obtained in the laboratory where the prefixed amount of liquid additive was added to the hot binder (150 °C) with a portable mixer operating at high stirring rates.

Crushed limestone aggregates and EAF steel slag were used to prepare tested mixtures. Limestone was provided in four different fractions (0/4, 4/8, 8/12, 12/20 mm) whereas three fractions of steel slag were available (0/4, 4/8, 8/12 mm). A mineral limestone filler was also used.

Three dense graded asphalt mixtures with similar gradation and bitumen content were prepared to accomplish the objectives of this study. In particular, to evaluate the possible use of EAF steel slag in WMA, two warm mixes were selected: the first one prepared with limestone aggregates (WL) and the other one containing EAF steel slag in partial substitution of both coarse and fine mineral aggregates (WS). Moreover, a plain HMA prepared with limestone (HL) was also used for comparison purpose to assess the influence of the selected warm additive.

It is worth noting that the mixtures prepared with limestone had the same composition regardless of the binder type whereas, in the WS mixture, steel slag was added with a dosage of 40 % by the weight of total aggregates. In fact, it is recognized that higher dosages of EAF steel slag are not recommended mainly due to the high bulk density of steel slag (excessive increase of transportation costs). The proportions of the different fractions were selected in order to obtain a grading curve fulfilling typical Italian technical specifications for dense graded wearing courses. Since the apparent specific gravity of steel slag (3.86 g/cm$^3$) is significantly higher than that of mineral aggregate (2.74 g/cm$^3$), the substitution was made by volume to maintain the same proportions in the granular skeleton. Hence, the content of steel slag was 40 % by weight or about 32 % by volume of the overall mixture. Similarly, the binder content should also refer to the effective (mineral and steel slag) aggregate weight. Therefore, since limestone mixtures were prepared with a typical bitumen dosage of 5.5 % by weight of aggregates, WS mix contains 4.9 % warm binder content that corresponds to 5.5 % if compared to the isovolumetric control mixture prepared with natural mineral aggregates.

For each material, four cylindrical specimens (diameter = 150 mm) were prepared using a Superpave gyratory compactor (vertical pressure = 600 kPa, rotation speed = 30 rpm, compaction angle = 1.25°) with a target air void content of 3 %. Specimens were manufactured applying 100 gyrations to 6000 g of limestone mixtures and 6900 g of warm mixture containing steel slag in order to achieve almost the same volume (height ≈ 140 mm). Each sample was aged for two hours at its corresponding compaction temperature prior to compaction. As anticipated, on the basis of binder viscosity, 150 and 140 °C were respectively selected as the mixing and compaction temperatures for the control HL mixture whereas, in the case of warm mixes, such temperatures were lowered to 130 and 110 °C, respectively. After compaction, each sample was sawed to obtain two cylindrical specimens (height ≈ 65 mm) for rutting tests.

## 3.2 Test Methods

### 3.2.1 DSR Tests

Linear viscoelastic properties of the studied binders were determined through a dynamic shear rheometer (DSR) according to AASHTO TP5 in order to evaluate the high-service temperature resistance (rutting potential). DSR tests for both binders were repeated at five temperatures ranging from 66 to 90 °C, with an interval of 6 °C, performing two replicates for each testing condition. Norm of the shear complex modulus (|G*|) and phase angle (δ) were measured during the tests allowing the assessment of the superior failure temperature (continuous high-temperature grade) in accordance with Superpave specifications (AASTHO MP1). Since the assessment of a reliable laboratory procedure for a representative short term aging of warm binder is still a subject of debate and taking also into account that the Superpave specifications for short term aged binders refer to the traditional aging procedure, only virgin binders were tested in this phase.

### 3.2.2 BBS Tests

The binder bond strength (BBS) test is a pneumatic adhesion test, recently accepted as a provisional AASHTO Test Method (TP-91), carried out through a specific device. More details concerning testing instrumentation and procedure are given elsewhere (Canestrari et al. 2010; Moraes et al. 2011; Pasquini et al. 2014).

In this study, the bond strength of plain and warm-modified binders with limestone and EAF steel slag aggregate substrates was evaluated. In order to reproduce mixture preparation procedures, the asphalt samples were heated and applied on the substrate at 150 °C whereas the testing surfaces (limestone and steel slag substrates) were heated at 150 and 130 °C in the case of the application of plain bitumen P and warm modified binder W, respectively. BBS tests were carried out in dry conditions at 25 °C. Before testing, specimens were conditioned at the test temperature for 24 h. Four replicates were carried out for each test configuration.

### 3.2.3 Mixture Compactability

The compaction characteristics of the studied mixtures were evaluated not only through the assessment of final air void content of specimens compacted through the gyratory compactor but also analyzing the densification curves obtained plotting the degree of compaction against the number of gyrations.

In particular, the densification curves were analyzed in terms of the compaction energy index (CEI) introduced by Bahia and Paye (2004). CEI is defined as the area under the densification curve from the 8th gyration to 92 % of $G_{mm}$. It should represent the work applied by the roller for compacting the mixture to the required

density during construction. In this sense, eight gyrations are generally selected to simulate the effort applied by the paver, whereas the 92 % of $G_{mm}$ is typically the minimum allowable density for opening to traffic. Asphalt mixtures with lower values of CEI are desired because they have better compaction properties. In this study, CEI values were calculated as the average of four repetitions for each mixture.

### 3.2.4 RLA Tests

The permanent deformation resistance of studied mixtures has been investigated through repeated load axial (RLA) tests carried out with confinement according to EN 12697-25/Method A. For each mixture, three replicates were tested at a test temperature of 40 °C after a conditioning period at the same temperature of at least four hours. In order to compare the rutting potential of the tested mixtures, the cumulative axial strain at the end of the test was taken into account. Moreover, test results were also analyzed in terms of creep rate and creep modulus at the end of the test calculated according to EN 12697-25.

## 4 Results and Analysis

### *4.1 High-Service Temperature Binder Properties*

The average results of the oscillatory shear analysis aimed at assessing the high-service temperature properties of the studied binders are summarized in Fig. 2.

It can be observed that, differently to what found by other researchers (Xiao et al. 2012; Morea et al. 2012), the chemical warm additive produced a small decrease of $|G^*|/\sin\delta$ at all test temperatures in unaged condition leading to a slightly higher rutting potential of the warm bitumen. In these sense, based on the limit condition $G^*|/\sin\delta = 1.0$ kPa, the addition of such an additive determined a continuous

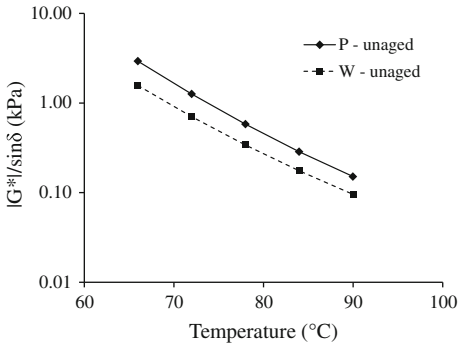


**Fig. 2** DSR mean test results

high-temperature grade of 69.3 °C whereas plain binder P was characterized by a failure temperature of 74.2 °C causing a shift in the binder superior performance grade from 70 to 64 °C.

## 4.2 Binder-Aggregate Bond Strength

The BBS experimental results in terms of mean pull-off tensile strength are shown in Fig. 3, along with error bars reporting the minimum and the maximum value obtained for each testing condition.

First of all, it is worth noting that the experimental results in the case of limestone aggregate plate were consistent with those found by Mogawer et al. (2011), confirming the reliability of test data.

Steel slag aggregates showed lower bond strength than limestone aggregates with both plain (−49 %) and warm-modified (−40 %) binders. This fact can be due to lower chemical affinity of EAF steel slag with bitumen with respect to limestone being EAF steel slag characterized by a lower alkalinity (i.e. the ratio between CaO and $SiO_2$ content) than limestone. In fact, it is commonly recognized that higher alkalinity leads to a stronger bond with asphalt. In this sense, Xie et al. (2014) reported higher asphalt affinity of BOF steel slag in comparison with basalt and granite just due to the noticeably higher alkalinity of BOF steel slag with respect to that aggregates. Thus, based on the present experimental data, it is possible to affirm that the presence of EAF steel slag aggregates could reduce the bonding with bitumen with respect to limestone, thus affecting mixture durability. As a consequence, further specific studies addressing this aspect, in particular with respect to water resistance, seem necessary.

On the other hand, the addition of the chemical tensoactive additive led to an increase in bond strength for both limestone (+10 %) and steel slag (+31 %) aggregates notwithstanding the lower application temperature of substrates (130 °C). These findings demonstrate that the selected warm additive package is able to guarantee improved adhesion between asphalt binders and aggregates thanks to its chemical composition which includes adhesion promoters.

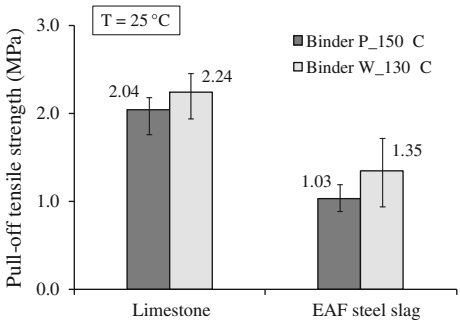


**Fig. 3** BBS mean test results

### 4.3 Mixture Compactability

The densification curves obtained from the SGC (average of four specimens) are reported in Fig. 4a. The curves clearly show that all the studied mixes were characterized by very similar final air void content (≈2.6 %).

The fact that WMA materials, mixed and compacted at lower temperatures (130 and 110 °C, respectively), are able to guarantee the same volumetric properties of the reference HMA mixture, prepared at usual mixing and compaction temperatures (150 and 140 °C, respectively), seems to demonstrate the effectiveness of the selected WMA additive in promoting compaction (Sanchez-Alonso et al. 2011; Rubio et al. 2012).

However, the final air void content after SGC compaction could not be a sufficient evidence to evaluate the potentialities of the warm additive since it is recognized that final air void content is not very sensitive to temperature changes in the case of SGC compaction (Hurley and Prowell 2006; Sanchez-Alonso et al. 2011). Nevertheless, a careful observation of densification curves (Fig. 4a) shows that warm mixtures were characterized by a slightly higher degree of compaction than control HMA during the first phase of compaction, thus denoting a higher workability.

This fact is clearly demonstrated by the average CEI values of the studied materials reported in Fig. 4b along with the error bars indicating the maximum and minimum calculated value. In fact, experimental data show a decrease in the CEI value of the warm mixtures compared to the control HMA denoting better compaction properties of WMA. Such experimental findings confirmed that CEI is a valuable indicator to be successfully used for the proper assessment of mixture workability, especially in the case of WMA (Sanchez-Alonso et al. 2011; Capitao et al. 2012).

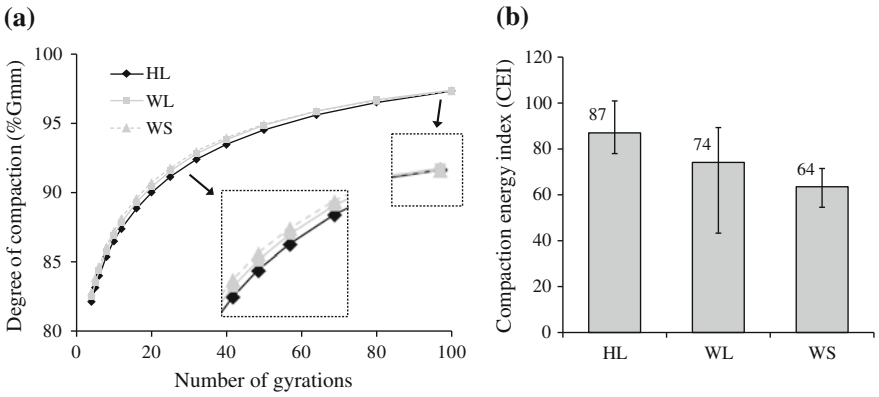


**Fig. 4** Mixture compactability: **a** SGC compaction curves, **b** compaction energy index (CEI)

CEI values also show a further increase in workability for warm mix containing EAF steel slag. According to previous studies (Pasetto and Baldo 2010), this easier compaction should be likely due to the better morphological properties (reduced shape and flakiness indexes) of EAF steel slag with respect to limestone.

## 4.4 Permanent Deformation Resistance

Table 1 reports the mean results in terms of final cumulative axial strain, creep modulus and creep rate of the studied materials subjected to the repeated load axial tests.

Experimental data did not give a clear picture of rutting behavior of studied materials. In fact, warm mixtures showed higher final cumulative axial strain and consequently a lower creep modulus (according to the results of DSR tests on binders), but they showed a lower rate of increase of permanent deformations compared to the control HMA. In this sense, conflicting results about rutting behavior of warm mix prepared with chemical tensoactive technology were also found in literature since some studies documented increased performance of WMA (Hurley and Prowell 2006; Kheradmand et al. 2014) whereas other authors reported opposite results (Capitao et al. 2012; Rubio et al. 2012; Sanchez-Alonso et al. 2013).

Moreover, the presence of EAF steel slag in partial substitution of limestone seems to negatively affect permanent deformation resistance. This was also in contrast with other research studies which demonstrated that the peculiar morphological, physical and mechanical properties of EAF steel slag should be able to provide increased stability at high temperature, thus improving rutting resistance (Pasetto and Baldo 2010, 2011, 2012). However, it should be remarked that Ameri et al. (2013) also found a decrease in permanent deformation resistance of hot mix asphalts when steel slag is used within the fine fraction of the mix.

Overall, it can be asserted that all the studied mixtures, with the given aggregate gradation, were characterized by comparable performance showing virtually no deformation (<0.6 %). Thus, warm mix technology and/or EAF steel slag did not seem to penalize permanent deformation resistance of studied asphalt mixtures.

**Table 1** Final cumulative strain, creep modulus and creep rate of studied mixtures

| Mixtures | Cumulative strain (%) | Creep modulus (MPa) | Creep rate (μ strain/cycle) |
|---|---|---|---|
| HL | 0.47 | 21.15 | 0.28 |
| WL | 0.49 | 20.35 | 0.22 |
| WS | 0.58 | 17.30 | 0.26 |

## 5 Conclusions

This paper presents a first step of a comprehensive experimental study essentially aimed at evaluating the feasibility of using electric arc furnace steel slag in partial substitution of mineral aggregates within dense graded warm mix asphalts. A chemical tensoactive additive was selected as warm technology in this study.

Based on the analysis of the experimental data, the following main conclusions can be drawn:

- the studied warm additive produces a little decrease of the continuous high-temperature grade but it is also able to slightly improve the bond strength between binder and aggregates;
- with respect to limestone, lower bond strength exists between asphalt binders and EAF steel slag due to the lower alkalinity of such an aggregate;
- the studied warm asphalt mixes are characterized by similar or even improved workability with respect to the corresponding HMA produced and compacted at higher temperatures;
- the selected WMAs, with or without steel slag, are able to guarantee high resistance to permanent deformations.

Based on the above-mentioned promising results, further research is needed to obtain a more exhaustive picture of the main mechanical properties and durability of dense graded WMAs containing EAF steel slag. In particular, fatigue and low temperature cracking resistance as well as moisture susceptibility should be investigated taking also into account different base binders and warm additives.

## References

Ameri M, Hesami S, Goli H (2013) Laboratory evaluation of warm mix asphalt mixtures containing electric arc furnace (EAF) steel slag. Constr Build Mater 49:611–617. doi: 10.1016/j.conbuildmat.2013.08.034.

Ahmedzade P, Sengoz B (2009) Evaluation of steel slag coarse aggregate in hot mix asphalt concrete. J Hazard Mater 165(1–3):300–605. doi: 10.1016/j.jhazmat.2008.09.105.

Bahia HU, Paye BC (2004) Using the gyratory compactor to measure mechanical stability of asphalt mixtures. Wisconsin Highway Research Program 05–02, Department of Civil and Environmental Engineering, University of Wisconsin, Madison, WI, USA.

Canestrari F, Cardone F, Graziani A, Santagata FA, Bahia HU (2010) Adhesive and cohesive properties of asphalt-aggregate systems subjected to moisture damage. Road Mater Pavement 11(sup1):11–32. doi: 10.1080/14680629.2010.9690325.

Capitao SD, Picado-Santos LG, Martinho F (2012) Pavement engineering materials: review on the use of warm-mix asphalt. Constr Build Mater 36:1016–1024. doi: 10.1016/j.conbuildmat.2012.06.038.

D'Angelo J, Harm E, Bartoszek J, Baumgardner G, Corrigan M, Cowsert J., Harman T, Jamshidi M, Jones W, Newcomb D, Prowell B, Sines R, Yeaton B (2008) Warm-Mix Asphalt: European Practice. Report no. FHWA PL-08-007007007, Alexandria, VA, USA.

Hurley GC, Prowell BD (2006) Evaluation of Evotherm® for use in warm mix asphalt. NCAT Report 06-02, Auburn University, Auburn, AL, USA.

Kheradmand B, Muniandy R, Hua LT, Yunus RB, Solouki A (2014) An overview of the emerging warm mix asphalt technology. Int J Pavement Eng 15(1):79–94. doi: 10.1080/10298436.2013.839791.

Mogawer WS, Austerman AJ, Bahia HU (2011) Evaluating the Effect of Warm-Mix Asphalt Technologies on Moisture Characteristics of Asphalt Binders and Mixtures. Transp Res Record 2209:52–60. doi: 10.3141/2209-07.

Moraes R, Velasquez R, Bahia HU (2011) Measuring effect of moisture on asphalt-aggregate bond with the bitumen bond strength test. Transp Res Record 2209:70–81. doi: 10.3141/2209-09.

Morea F, Marcozzi R, Castano G (2012) Rheological properties of asphalt binders with chemical tensoactive additives used in Warm Mix Asphalts (WMAs). Constr Build Mater 29:135–141. doi: 10.1016/j.conbuildmat.2011.10.010.

Motz H, Geiseler J (2001) Products of steel slag an opportunity to save natural resources. Waste Manage 21(3):285–293. doi: 10.1016/S0956-053X(00)00102-1.

Pasetto M, Baldo N (2010) Experimental evaluation of high performance base course and road base asphalt concrete with electric arc furnace steel slags. J Hazard Mater 181(1–3):938–948. doi: 10.1016/j.jhazmat.2010.05.104.

Pasetto M, Baldo N (2011) Mix design and performance analysis of asphalt concrete with electric arc furnace slag. Constr Build Mater 25(8):3458–3468. doi: 10.1016/j.conbuildmat.2011.03.037.

Pasetto M, Baldo N (2012) Performance comparative analysis of stone mastic asphalts with electric arc furnace steel slag: a laboratory evaluation. Mater Struct 45(3):411–424. doi: 10.1617/s11527-011-9773-2.

Pasetto M, Baldo N (2013) Fatigue performance of asphalt concretes made with steel slags and modified bituminous binders. Int J Pavement Res Technol 6(4):294–303.

Pasquini E, Bonati A, Giuliani F, Canestrari F (2014) Advanced characterization of clear chip seals. J Test Eval 42(5):1213–1227. doi: 10.1520/JTE20130119.

Piatak NM, Parsons MB, Seal II RR (2014) Characteristics and environmental aspects of slag: a review. Appl Geochem. doi: 10.1016/j.apgeochem.2014.04.009.

Rubio MC, Martinez G, Baena L, Moreno F (2012) Warm-mix asphalt: an overview. J Clean Prod 24:76–84. doi: 10.1016/j.jclepro.2011.11.053.

Sanchez-Alonso E, Vega-Zamanillo A, Castro-Fresno D, DelRio-Prat M (2011) Evaluation of compactability and mechanical properties of bituminous mixes with warm additives. Constr Build Mater 25(5):2304–2311. doi: 10.1016/j.conbuildmat.2010.11.024.

Sanchez-Alonso E, Vega-Zamanillo A, Calzada-Perez MA, Castro-Fresno D (2013) Effect of warm additive on rutting and fatigue behaviour of asphalt mixtures. Constr Build Mater 47:240–244. doi: 10.1016/j.conbuildmat.2013.05.083.

Xiao F, Punith VS, Amirkhanian SN (2012) Effects of non-foaming WMA additives on asphalt binders at high performance temperatures. Fuel 94:144–155. doi: 10.1016/j.fuel.2011.09.017.

Xie J, Chen Z, Pang L,Wu S (2014) Implementation of modified pull-off test by UTM to investigate bonding characteristics of bitumen and basic oxygen furnace slag (BOF). Constr Build Mater 57:61–68. doi: 10.1016/j.conbuildmat.2014.01.083.

Yi H, Xu G, Cheng H, Wang J, Wan Y, Chen H (2012) An overview of utilization of steel slag. Procedia Env Sci 16:791–801. doi: 10.1016/j.proenv.2012.10.108.

Yildirim IZ, Prezzi M (2011) Chemical, mineralogical, and morphological properties of steel slag. Adv Civ Eng 2011:1–13. doi: 10.1155/2011/463638.

# Influence of Aging on the Rheological Behavior of Warm Mix Asphalt Binders

**K. Lakshmi Roja, Neethu Roy and J. Murali Krishnan**

**Abstract** The Warm Mix Asphalt (WMA) technologies allow a significant reduction in mixing and compaction temperatures of asphalt mixtures through lowering the viscosity of binders. In WMA, different types of additives are added to the binder depending on the technology used and such addition of these materials brings down the viscosity drastically thus reducing the temperature to which the aggregates and binders have to be heated during mixing and compaction. During mixing and compaction of WMA mixture, the binders are subjected to reduced aging compared to conventional Hot Mix Asphalt (HMA) mix. This study is conducted to quantify the influence of short-term aging on the rheological properties of WMA binder at pavement working temperatures. Two types of WMA binders were studied, the first one is Evotherm modified binder and the second one is Sasobit modified binder. A viscosity grade binder (VG30) was used as the control material. All the binders were tested at unaged and short-term aged conditions. All the three samples at two aging conditions were subjected to frequency sweep tests at 25, 35, 45, 55, 65 and 75 °C from 50 to 1 Hz frequency at a rate of 0.1 Hz per second using appropriate parallel plate geometry in a dynamic shear rheometer. Master curves were constructed for all the binders tested. Parametric analysis of the master curve was carried out to quantify the difference in binder response.

**Keywords** Warm mix asphalt · Aging · Rheology · Master curve models · Sasobit · Evotherm

K. Lakshmi Roja · J. Murali Krishnan (✉)
Department of Civil Engineering, Indian Institute of Technology Madras, Chennai 600036, India
e-mail: jmk@iitm.ac.in

K. Lakshmi Roja
e-mail: lakshmiroja1988@gmail.com

N. Roy
Department of Civil Engineering, Mar Baselios College of Engineering and Technology, Thiruvananthapuram 695015, India
e-mail: neethu.roy@mbcet.ac.in



F. Canestrari and M.N. Partl (eds.), *8th RILEM International Symposium on Testing and Characterization of Sustainable and Innovative Bituminous Materials*, RILEM Bookseries 11, DOI 10.1007/978-94-017-7342-3_40

# 1 Introduction

In order to reduce the energy consumption and associated emission during mixing and compaction of hot mix asphalt (HMA), warm mix asphalt (WMA) technologies are developed. In WMA, the aggregate heating, mix production and compaction temperatures can be reduced substantially by 20–30 °C compared to that of HMA. While such technologies are clearly the need of the hour, one needs to understand how such WMA technologies change the rheological properties of binder at pavement service temperatures.

There are different types of warm mix asphalt technologies available in practice and these include chemical additives and wax based additives. Chemical additives improve the workability of an asphalt mix by reducing the friction (due to reduction of surface tension of binder in the Newtonian regime) between the asphalt binder and aggregates (Bower 2011). Wax based additive contains long chain hydrocarbons that offer lower viscosity at mixing and compaction temperature when compared to conventional binder.

During mixing and compaction of WMA mixture, the binders are subjected to reduced aging compared to HMA mixture. One of the concerns related to WMA mixture is the reduced stiffness of the mixture during service due to the reduced aging of the binder. Such behavior is expected to result in increased rutting of the asphalt concrete layer, however this might result in improved fatigue resistance of WMA mixtures. Due to the widely varying manner in which different additives impart reduced viscosities to the WMA binder during mixing and compaction, it is expected that the rheological properties of the binder will also vary during service temperatures. It is required to understand how the chemical additives and wax-based additives manifest such changes in the WMA binder.

The investigation presented here is part of a detailed study currently being carried out at IIT Madras in an attempt to understand the rheological behaviour of WMA binder. The objective of this investigation is to quantify the response of binders over a wide range of frequencies, temperatures and see how the response manifest differently under short-term aging conditions.

# 2 Experimental Investigations

## *2.1 Materials*

In this investigation, two types of WMA technologies were used and they are chemical additive (Evotherm) and wax based additive (Sasobit). Three types of samples namely, unmodified base binder (VG30, viscosity grade as per IS73:2013, 2013), Evotherm treated binder and Sasobit treated binder were tested for determining the rheological properties. The basic properties of VG30 binder are listed in Table 1. All the samples were tested under unaged and short-term aged conditions.

**Table 1** VG30 binder properties

| Test | Value | Specification limits as per IS73:2013, 2013 |
|---|---|---|
| Absolute viscosity at 60 °C (Poise) | 2989 | 2400–3600 |
| Kinematic viscosity at 135 °C (cSt), Min. | 515 | 350 |
| Penetration at 25 °C, Min. | 60 | 45 |
| Softening Point (R&B) ( °C), Min. | 52 | 47 |
| Tests on residue from rolling thin film oven test: Viscosity ratio at 60 °C, Max. | 2 | 4 |

**Table 2** WMA additives dosage and binder heating temperatures

| Description | Evotherm | Sasobit |
|---|---|---|
| Bitumen heating temperature (°C) | 155 | 130 |
| Dosage of additive | 0.4 % by weight of bitumen | 1.5 % by weight of bitumen |

Short-term aging of VG30 binder was carried out at 163 °C in rolling thin film oven as per ASTM D2872-12 (2012). In the absence of established protocols for short-term aging temperature of binder used for WMA, a temperature of 143 °C was selected in the current investigation for WMA additive treated binders (Biro et al. 2009). This temperature is 20 °C lower than the conventional temperature used, which is also the typical reduction in mixing temperature that is achieved with the warm mix asphalt technology. WMA additives were blended into hot binder at specific temperatures according to their dosage as given in Table 2.

## *2.2 Rheological Investigations at Pavement Service Temperatures*

An Anton-Paar dynamic shear rheometer (DSR), model MCR301 was used to conduct the strain amplitude sweep test and the frequency sweep experiments in the temperature range of 25–75 °C. In this investigation, parallel plate geometry of 25 mm diameter with 1 mm gap setting was used. The sample preparation and testing was carried out according to ASTM D7175-08 (2008).

### 2.2.1 Strain Amplitude Sweep Test

This test was conducted to find the linear viscoelastic (LVE) limit by subjecting the binder to strain sweep in oscillatory mode. In a strain sweep test, the dynamic modulus values of the specimen are captured over a range of strain amplitudes. In order to fix the linear viscoelastic limit for this material, the strain value corresponding to 95 % of the initial modulus was considered. The strain was increased

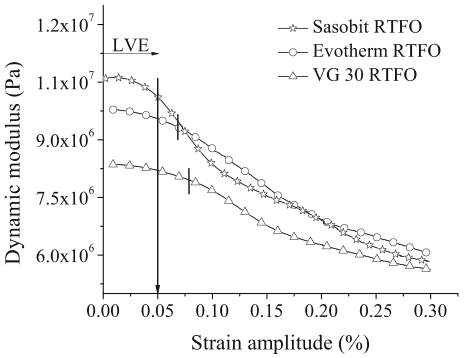


**Fig. 1** LVE limits for different samples at 25 °C

from 0.001 to 0.3 % at the rate of 0.001 % per second. The test was conducted at 25 °C and the frequency selected was 35 Hz. Short-term aged samples of VG 30, Evotherm and Sasobit treated binders were subjected to the strain sweep test to establish the linear viscoelastic limit. From Fig. 1, it was observed that the Sasobit treated sample has the lowest strain amplitude of 0.05 %, corresponding to the LVE limit. Hence the strain amplitude of 0.05 % was selected for all samples for frequency sweep test.

### 2.2.2 Frequency Sweep Test

Parallel plate geometry of 25 mm diameter with 1 mm gap setting was used to conduct the test in oscillatory shear mode. The frequency sweep test was carried out at 25, 35, 45, 55, 65 and 75 °C for all unaged and short term aged samples with a strain amplitude of 0.05 %. The tests were conducted from 50 to 1 Hz frequency at the rate of 0.1 Hz per second. Dynamic modulus and phase angle of all the three samples at different temperatures were compared for both unaged and short-term aged conditions. The storage and loss modulus for these binders were also analysed to check the crossover frequency and identify the sol-gel transition, as reported in the work carried out by Padmarekha and Krishnan (2013).

Master curves were constructed for the frequency range of 0.01–100 Hz by appealing to Time-Temperature Superposition Principle and parametric analysis of the master curves was carried out to quantify the variation in binder response.

## 3 Results and Discussions

### *3.1 Frequency Sweep Test*

Linear viscoelastic parameters such as storage modulus (G′), loss modulus (G″) and phase angle were recorded using Rheoplus software available in the dynamic shear rheometer. Dynamic modulus and phase angle of all the three samples at different

temperatures were compared for both unaged and short term aged conditions (Fig. 2).

The dynamic modulus of sasobit treated binders under unaged and short-term aged conditions exhibited higher values at all temperatures excepting 75 °C. Since sasobit starts melting at 85 °C and is completely dissolved at 115 °C, one can understand the reduction of the dynamic modulus when the temperature reaches 75 °C (Jamshidi et al. 2013). For all the temperatures and aging conditions, Evotherm treated samples exhibited the lowest dynamic modulus and the highest

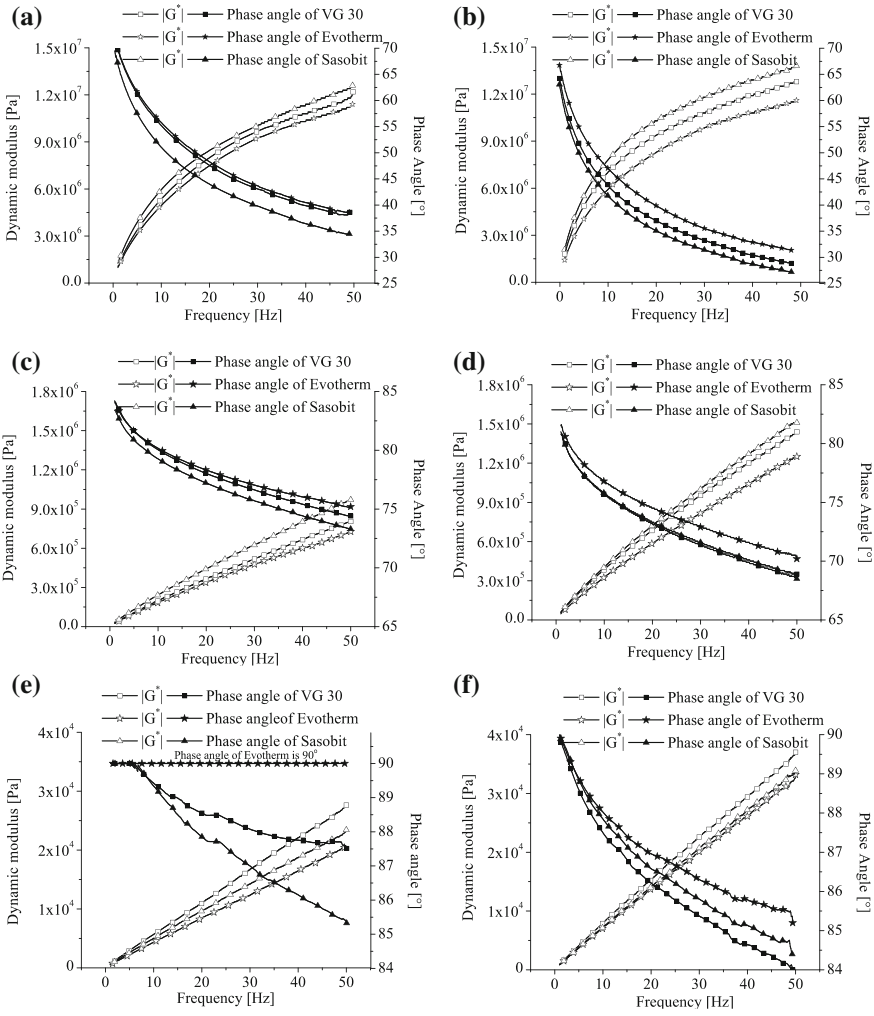


**Fig. 2** Dynamic modulus of different samples at different temperatures. **a** Unaged samples at 25 °C. **b** RTFO aged samples at 25 °C. **c** Unaged samples at 45 °C. **d** RTFO aged samples at 45 °C. **e** Unaged samples at 75 °C. **f** RTFO aged samples at 75 °C

phase angle. Infact, at 75 °C under unaged condition, Evotherm treated binder exhibited 90° phase angle thus showing a pure linearly viscous behavior. The evolution of the viscoelastic properties of VG30 binder shows expected pattern. As the temperature increases, the reduction in dynamic modulus and increase of phase angle is apparent and the material response is always in between that of Evotherm and Sasobit treated binders. At higher temperature (75 °C) as Sasobit starts dissolving, VG30 binder shows increased dynamic modulus when compared to the WMA binders. Such increased modulus values are not due to any anomalous behavior of the binder, rather the Sasobit binder shows "softer" response due to reasons mentioned above.

## *3.2 Crossover Frequencies of G'-G"*

One of the most commonly used methods for characterizing the viscoelastic fluid to viscoelastic solid transitory behavior is through small amplitude oscillatory shear experiments using a frequency-dependent storage modulus (G′) and loss modulus (G″) crossover. For a material with viscoelastic solid response, the storage modulus values are greater than the loss modulus and for viscoelastic fluid response, loss modulus values are greater than the storage modulus. On the basis of the experimental observations and the analysis of data using G′-G″ crossover, one can divide the material response into two regimes and they are viscoelastic solid regime and viscoelastic fluid regime. The crossover frequencies are represented in Fig. 3 for all the three samples for both unaged and short term aged conditions. It was observed that all the samples were showing crossover point at 25 °C within the tested frequencies. At all remaining temperatures, loss modulus values were greater than the storage modulus values and the crossover point was not seen within the tested frequencies.

The transitory behaviour of the binder is frequency dependent. Figure 3a shows the storage and loss modulus of VG30 binder at 25 °C for both unaged and short-term aged conditions. For unaged condition, the loss modulus was greater than the storage modulus for the frequency less than 25.6 Hz. When the tested frequency is less than 25.6 Hz, the viscous behavior dominates and at higher frequencies above 25.6 Hz, the elastic response dominates. When the material is subjected to aging, the crossover occurs at lower frequencies. The lower crossover frequency of 10 Hz was seen for short-term aged VG30 material.

In Fig. 3c, the crossover frequencies of Sasobit samples were lower than VG30 samples for both unaged (8.1 Hz) and short-term aged conditions (18.8 Hz). It shows the Sasobit treated sample is stiffer than VG30 sample for both unaged and short-term aged conditions at 25 °C. Figure 3e shows the crossover frequencies of Evotherm samples. It was seen that the crossover frequency of unaged Evotherm sample (26.9 Hz) was similar to unaged VG30 sample (25 Hz) and for short-term aged condition, slight increment was observed (13 Hz).

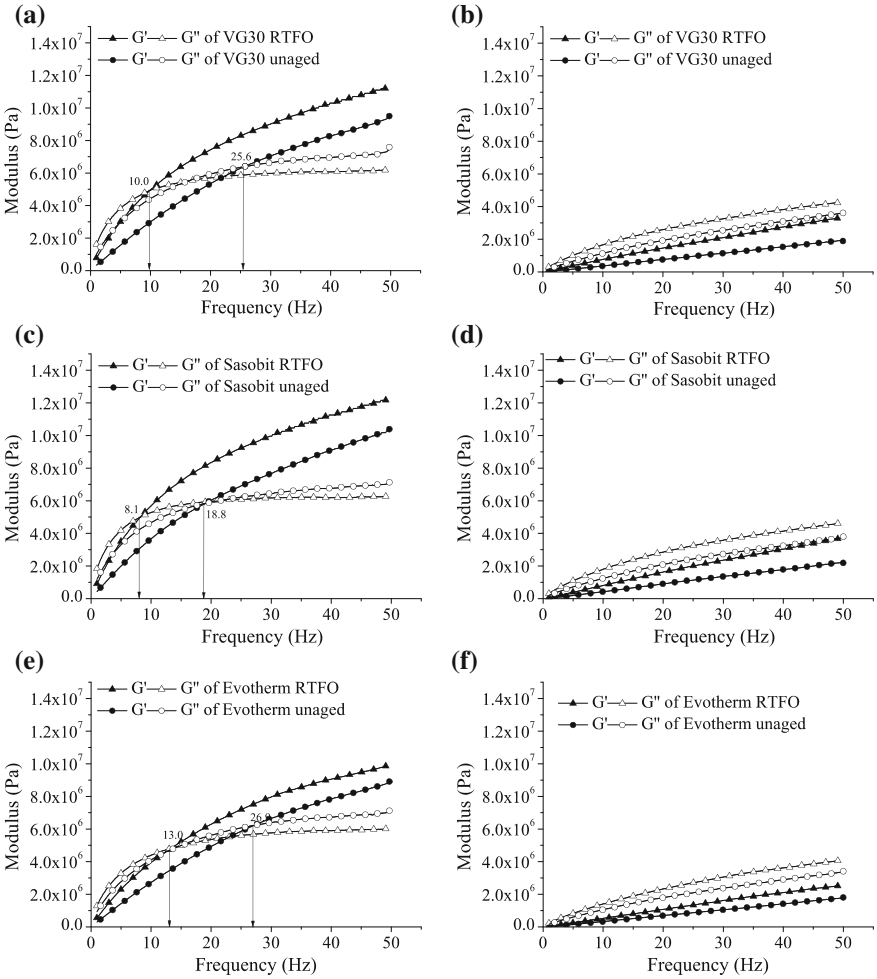


**Fig. 3** Crossover frequency of G′-G″ **a** VG30 at 25 °C **b** VG30 at 35 °C **c** Sasobit at 25°C **d** Sasobit at 35 °C **e** Evotherm at 25 °C **f** Evotherm at 35 °C

## *3.3 Master Curve Construction*

In this investigation, master curves were generated using RHEA software [RHEA version 1 (2012)]. This software can analyze the viscoelastic data of binder and generate the master curve. Master curve construction follows the pair-wise shifting technique. Initially rough shift factors are determined using William-Landel-Ferry (WLF) equation and then modulus values are shifted from successive pairs of isotherms to form a smooth master curve. Every time shift factors will be generated according to the modified fit for the finally constructed master curve. In this

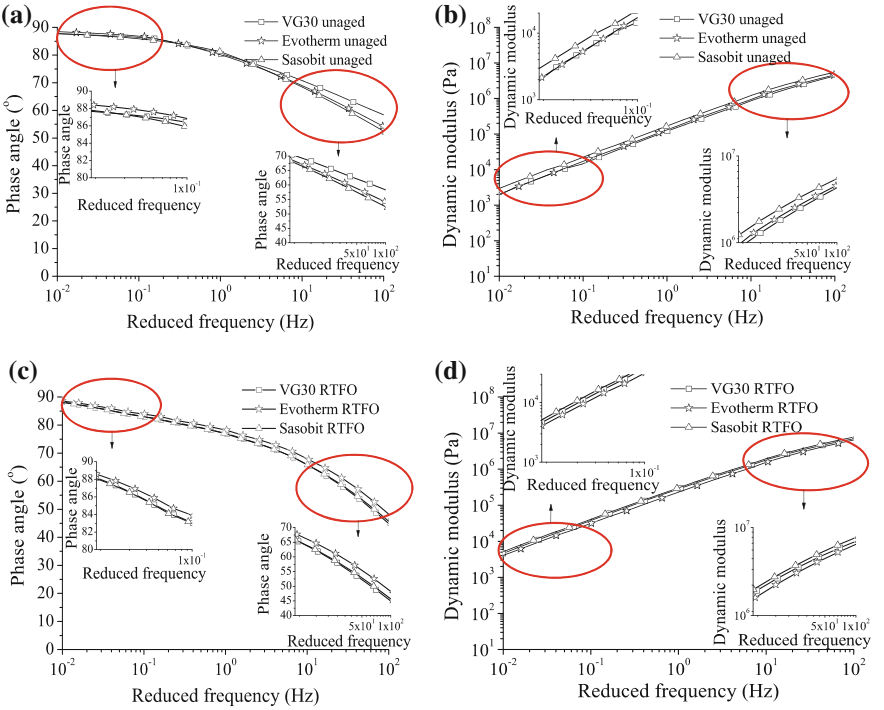


**Fig. 4** Master curves at reference temperature of 35 °C. **a** Phase angle master curves for unaged samples. **b** Dynamic modulus master curves for unaged samples. **c** Phase angle master curves for short-term aged samples. **d** Dynamic modulus master curves for short-term aged samples

investigation, phase angle and dynamic modulus master curves were constructed with the reference temperature of 35 °C.

Though the dynamic modulus values measured at 75 °C for sasobit treated samples were lower than VG30, when the master curves were fit and when the values are compared across a range of reduced frequencies, it was seen that the dynamic modulus of Sasobit treated sample was higher than the VG30 and Evotherm treated samples for all the aging conditions. As expected, there was not much difference between VG30 and Evotherm treated samples for the full range of frequency (Fig. 4).

## *3.4 Master Curve Modelling*

Master curve modelling was carried out using Christensen and Anderson (Christensen and Andersen 1992) and Christensen, Anderson and Marasteanu model (Marasteanu and Andersen 1999) to characterize the master curve and to

describe the viscoelastic behaviour of binder by using dynamic modulus-reduced frequency or phase lag-reduced frequency relationship.

### 3.4.1 Christensen and Anderson Model

To characterize the binders using CA model, four parameters are required and they are glassy modulus ($G_g$), steady state viscosity ($\eta_{ss}$), cross-over frequency ($\omega_c$) and rheological index (R). This model can predict the dynamic modulus/phase angle responses in the temperature range of 10–70 °C. R represents the rheological nature of the material and it indicates the temperature susceptibility of the material. R is the difference between the glassy modulus and the dynamic modulus value at the cross-over frequency. A higher R value indicates that the material has good temperature susceptibility characteristics (Christensen and Andersen 1992). Equations (1) and (2) shows the dynamic modulus- frequency and phase lag-frequency relationships given by Christensen and Andersen (1992).

$$|G^*(\omega)| = G_g\left[1 + \left(\frac{\omega_c}{\omega}\right)^{\frac{\log 2}{R}}\right]^{\frac{-R}{\log 2}} \tag{1}$$

$$\delta(\omega) = \frac{90}{\left[1 + \left(\frac{\omega_c}{\omega}\right)^{\frac{\log 2}{R}}\right]} \tag{2}$$

Here
$G_g$ = Glassy modulus
$\omega_c$ = Crossover frequency
R = Rheological index

While the glassy modulus value was assumed as 1 GPa in CA model, in this study, it is kept as a variable parameter and was found to be in the range of 1E7–1E9 Pa (Table 3). The fitting was carried out using non-linear curve fit tool in

**Table 3** CA model parameters

| Description | $G_g$ (Pa) | $\omega_c$ (Hz) | Susceptibility parameter, R | $\eta_{ss}$ (Pa.s) | Goodness of fit, $R^2$ |
|---|---|---|---|---|---|
| *Unaged* | | | | | |
| VG 30 | 3.32E + 08 | 1452 | 1.22 | 2.29E + 05 | 0.999 |
| Evotherm | 8.49E + 07 | 398.3 | 0.94 | 2.13E + 05 | 0.999 |
| Sasobit | 9.73E + 07 | 276.3 | 1.04 | 3.52E + 05 | 0.999 |
| *RTFO aged* | | | | | |
| VG 30 | 5.62E + 07 | 110.3 | 0.90 | 5.10E + 05 | 0.999 |
| Evotherm | 1.00E + 08 | 198.1 | 1.05 | 5.05E + 05 | 0.999 |
| Sasobit | 7.26E + 07 | 128.7 | 0.92 | 5.64E + 05 | 0.999 |

**Table 4** CAM model parameters

| Description | $G_g$ (Pa) | $\omega_c$ (Hz) | R | w | $R^2$ |
|---|---|---|---|---|---|
| *Unaged* | | | | | |
| VG 30 | 3.34E + 08 | 1179 | 1.23 | 1.03 | 0.999 |
| Evotherm | 8.47E + 07 | 497.7 | 0.93 | 0.96 | 0.999 |
| Sasobit | 9.60E + 07 | 740.2 | 0.98 | 0.84 | 0.999 |
| *RTFO aged* | | | | | |
| VG30 | 5.60E + 07 | 180.4 | 0.87 | 0.90 | 0.999 |
| Evotherm | 9.91E + 07 | 399.3 | 1.01 | 0.88 | 0.999 |
| Sasobit | 7.23E + 07 | 196.9 | 0.90 | 0.92 | 0.999 |

MATLAB. The rheological index, R was calculated using Eq. (1). The viscous asymptote $\eta_{ss}$ is calculated as $\eta_{ss} = G_g/\omega_c$. The obtained CA model parameters $G_g$, $\omega_c$, and R for each sample at both unaged and short-term aged conditions are shown in Table 4.

From Table 3, it was observed that the unaged VG30 sample has higher R value than Sasobit treated samples, followed by Evotherm treated sample. In short- term aged samples, Evotherm treated sample has higher R value than Sasobit treated sample, followed by VG30.

### 3.4.2 Christensen, Anderson and Marasteanu Model

Marasteanu and Anderson (1999) modified the CA model to improve the fitting, particularly in the lower and higher frequency range of binders. Equations (3) and (4) shows the dynamic modulus- frequency and phase lag-frequency relationships used for CAM model.

$$|G^*(\omega)| = G_g\left[1 + \left(\frac{\omega_c}{\omega}\right)^v\right]^{\frac{-w}{v}} \tag{3}$$

$$\delta(\omega) = \frac{90\ w}{\left[1 + \left(\frac{\omega_c}{\omega}\right)^v\right]} \tag{4}$$

where
v = log 2/R and R is the rheological index

By using CA model, the lack of fit may occur at two asymptotes, one is at glassy modulus as the frequency goes to infinity and another is at steady state viscosity as the frequency goes to zero. In CAM model, the parameter 'w' was introduced to improve the fit by determining the crossover point of these two asymptotes. The model parameters of CAM model are shown in Table 4.

The temperature susceptibility parameter, R obtained from CAM model and CA model were found to be more or less identical for all the binders considered in the study. It can be seen that the material behaviour is highly dependent on the aging conditions. In the unaged condition, VG30 binder has high R value compared to the WMA binders and can be expected to have good temperature susceptible characteristics. However, in HMA the binder is subjected to severe aging while mixing and compaction and such aging conditions deteriorate the binder's temperature susceptible properties, as can be seen from the R value of the RTFO aged VG 30 binder.

Evotherm and Sasobit modified binders are prepared by heating the parent binder to a temperature of 155 and 130 °C respectively. This process essentially cause a certain degree of aging in the material. Hence it will be interesting to note the difference in properties of short-term aged VG30 and the unaged Evotherm and Sasobit binders. For instance in CAM model, it is seen that the short-term aged VG30 has a reduction of 84.7 % in crossover frequency at 35 °C when compared with the unaged VG30 binder. Unaged Evotherm and Sasobit had higher R values compared to the aged VG30 binder. A further aging of the Evotherm and Sasobit samples using RTFO has decreased the crossover frequencies by 19.7 and 73.3 % respectively.

## 4 Conclusion

To characterize the binder response at pavement service temperatures, it is necessary to understand the behavior of binder over a wide range of frequencies and temperatures. Most of the current developments have paid more attention on reduction of temperatures during production process and the associated mix design issues. From the perspective of material behaviour at pavement working conditions, it is necessary that one characterizes the response of material in such temperature and frequency regime.

In this investigation, the response of the WMA and parent unmodified binders at various pavement service temperatures was characterized. It was seen that the stiffness of Sasobit treated sample was higher at low test temperatures for both unaged and short-term aged conditions, possibly due to the formation of solid crystalline structure in the binder. The higher stiffness values of Sasobit in the unaged condition could also be a result of certain amount of ageing in the material while blending the additives to binder.

To understand how the rheological behavior of the material varies over a range of temperatures and frequencies, master curves were constructed and analyzed using two master curve model functions, namely CAM model and CA model. Both models captured the response of the material identically for all the binders considered in the study. It was observed that the temperature susceptibility parameter, R and the dynamic modulus values could explain the response of the material due to aging conditions. However, the nature of aging conditions vary between the

unmodified binder and the WMA binders and there could be variations in the chemical and physical interactions in the materials due to the addition of an additive. Also it is important to understand the response of these materials in the asphalt concrete mixtures and such studies are currently underway at IIT Madras.

## References

ASTM D2872-12 (2012) Standard Test Method for Effect of Heat and Air on a Moving Film of Asphalt (Rolling Thin-Film Oven Test), ASTM International, West Conshohocken, Pennsylvania, USA.

ASTM D7175-08 (2008) Standard Test Method for Determining the Rheological Properties of Asphalt Binder Using a Dynamic Shear Rheometer, ASTM International, West Conshohocken, Pennsylvania, USA.

Biro S, Gandhi T, Amirkhanian S (2009) Midrange Temperature Rheological Properties of Warm Asphalt Binders. J. Mater. Civ. Eng 21(4): 316-323.

Bower N (2011) Laboratory Evaluation of Performance of Warm Mix Asphalt in Washington State. Master of Science thesis, Washington University.

Christensen DW, Andersen DA (1992) Interpretation of Dynamic Mechanical Test Data for Paving Grade Asphalt Cements. Proceedings of American Association of Paving Technologists, vol 61, p 67-98.

IS: 73-2013 (2013) Indian standard for Paving Bitumen-Specification (Fourth Revision), Bureau of Indian Standards, New Delhi, India.

Jamshidi A, Hamzah MO, Zhanping Y (2013) Performance of Warm Mix Asphalt Containing Sasobit: State-of-the-Art. Journal of Construction and Building Materials, p 530-553.

Marasteanu O, Andersen DA (1999) Improved Model for Bitumen Rheological Characterization, Eurobitume Workshop on Performance Related Properties for Bituminous Binder, Luxembourg, p 133.

Padmarekha A, JM Krishnan (2013) Viscoelastic Transition of Unaged and Aged Asphalt. Journal of Materials in Civil Engineering, 25:1852-1863.

RHEA version 1 (2012) Rheology Analysis Software, ABATECH., Philadelphia, USA. <http://www.abatech.com/RHEA.htm>. Accessed on 15 Oct 2014.

# Laying of Warm Mix Asphalt: Study of the Feasibility of the Workability Measure Modifying the Parameters of the Standard Gyratory Shear Compactor

**Angélique Fabre des Essarts, Anne Dony and Stéphane Faucon-Dumont**

**Abstract** The development of Warm Mix Asphalt (WMA) created a workability issue on road site, which did not exist or was not as noticeable in the case of conventional Hot Mix Asphalt (HMA), especially during manual laying. The study presented in this paper is an experimental project carried out by the French ESTP (Ecole Spéciale des Travaux Publics) in partnership with Eurovia, to complete a PhD thesis being written on the workability of Warm Mix Asphalt. It aims to change some conventional parameters of classical road laboratory equipment by means of the Gyratory Shear Compactor test (vertical strength and rotation speed) to characterize and evaluate the workability of asphalt mixes, and particularly of Warm Mix Asphalt. Some Nynas workability device tests will also be carried out for the sake of comparison. This paper will explain the choice of the new parameters in terms of the capacity of the equipment. It will also present the results of the experimental study carried out on a classic asphalt formula (a semi-coarse asphaltic concrete 0/10), varying the temperature, the presence of a WMA additive and the bitumen grade, to create mixes of really different workabilities. It will show that the GSC, even set with lower parameters, is not able to characterize workability properties of asphalt mixtures.

**Keywords** Gyratory shear compactor · Warm mix asphalt · Workability · Temperature

A. Fabre des Essarts (✉) · A. Dony
Université Paris-Est, ESTP-IRC, 94230 Cachan, France
e-mail: afabre@adm.estp.fr

A. Dony
e-mail: adony@adm.estp.fr

S. Faucon-Dumont
Eurovia, Centre de Recherche, 33703 Mérignac, France
e-mail: stephane.faucondumont@eurovia.com



F. Canestrari and M.N. Partl (eds.), *8th RILEM International Symposium on Testing and Characterization of Sustainable and Innovative Bituminous Materials*, RILEM Bookseries 11, DOI 10.1007/978-94-017-7342-3_41

## 1 Introduction

In the past few decades, the topic of sustainable development has been of prime importance to European road industries. They have focused their research on lowering the mixing and laying temperatures of Hot Mix Asphalt (HMA), from 30 to 50 °C, by developing Warm Mix Asphalt (WMA) technologies. But these new WMA created a workability issue that was not as important in the case of conventional HMA, especially during manual implementation, largely due to the viscous properties of bituminous binders and their thermal susceptibility.

To develop warm mix technologies and additives that assure a good workability of asphalt mixes in spite of mixing and laying temperature reduction, it is necessary to develop a laboratory procedure to characterize this workability property. An important work described in NCHRP Report 691 (Bonaquist 2011) has synthesized several possible devices that could assess asphalt mixtures workability.

One of these devices, the Gyratory Shear Compactor (GSC), is an essential tool to formulate bituminous mixtures and measure their compactibility properties, because it is sensitive to their granular formula and their binder content (Delorme and La Roche 2007). It can be used to measure void content and shear strength according to rotation number. Nevertheless, many published studies (Bennert et al. 2010; (Dony et al. 2010) illustrate the fact that the GSC test is insensitive to mixing and testing temperature reduction, and so is insensitive to workability differences.

Another device described in NCHRP Report 691 (Bonaquist 2011) is the Asphalt Workability Device (AWD). This test is an experiment developed by the University of Massachusetts Dartmouth. The AWD rotates in the asphalt mix sample at constant speed and the torque needed for the rotation is measured. The sample temperature is also recorded during the test. In Bennert's study (Bennert et al. 2010), the AWD tests show important workability differences between the bituminous mixtures tested, according to the temperature and the warm mix additives. Several WMA tested seem to keep a better workability than the HMA control sample does, when the temperature decreases.

Meanwhile, the Nynas workability device test was developed to characterize the workability of Cold Mix Asphalt (CMA) and has recently been standardized for its use on CMA, WMA and HMA (NF EN 98-258-1). It measures the strength needed to spread an asphalt mix sample, simulating the mechanized and manual laying on a road work (Brion et al. 1999). In the study conducted by Olard and Gaudefroy (2011), the Nynas workability device was used to test some half-warm mix technologies (LEA technologies), identifying lower workability properties for HWMA compared with HMA.

As said before, the workability of asphalt mixes is largely due to the viscous properties of bituminous binders and to their thermal susceptibility. Nevertheless, some warm mix additives have no incidence on binder viscosity. Some American studies (Bennert et al. 2010; Hanz et al. 2010) show that these additives, while they do not reduce binder viscosity, increase the workability properties of the bituminous mixtures. This increase in workability would be due to the reduction of the friction

coefficient, measured by the Asphalt Lubricity test developed at the University of Wisconsin-Madison (Hanz et al. 2010, 2011).

## 2 Objectives

The Gyratory Shear Compactor, described above and set with the parameters given by the European normative NF EN 12 697-31, is the first tool used in every French road laboratory to characterize the compactibility of asphalt mixes and verify the proper sizing of a road. On the other hand, as shown in several studies (Bennert et al. 2010; Dony et al. 2010), this Gyratory Shear Compactor (GSC) is insensitive to the lowering of temperature, to the bitumen grade and to the presence of a warm mix additive. In conclusion, the GSC test set with the European normative parameters is not able to characterize the workability of a bituminous mixture.

The objective of the study presented in this paper is to lower the vertical strength and the rotation speed of the GSC to less load the asphalt mix during the test and get into the workability field. Once the new parameters are chosen, various mixes of different workability will be tested. The several workabilities will be created by changing the mixing and testing temperature, the bitumen grade, and by adding a warm mix additive (a viscosity reducer developed by Eurovia). The results obtained with the GSC test will be compared to the one obtained with a Nynas workability device. Using the GSC as a workability test would be a very interesting goal because this tool is present and well known in every road laboratory.

## 3 Experimental Materials, Techniques and Parameters

### *3.1 Materials*

The bituminous mixture formula used in this study is a classic semi-coarse asphaltic concrete 0/10 (French BBSG 0/10), with diorite aggregates coming from the French Noubleau Quarry and Total bituminous binders.

As regards the binders, two bitumen manufactured by Total and having different grades were used: a classic bitumen 35/50 and a softer one 160/220. Their viscosity was measured with a Dynamic Shear Rheometer (DSR), with a cone and plate geometry, according to the NF EN 13702 standard (Table 1).

The warm mix additive is a viscosity reducer (a wax) developed by the French company Eurovia and is added to the mixture with 35/50 asphalt binder at a dosage rate of 0.3 %.

Afterwards, the three asphalt mixes tested will be identified as:

- Mixture 1: with pure 35/50 binder
- Mixture 2: with pure 160/220 binder
- Mixture 3: with 35/50 binder + warm mix additive (0.3 %).

**Table 1** Bitumen characteristics

| | 35/50 binder | 160/220 binder |
|---|---|---|
| Penetration (25 °C) (1/10 mm) | 43 | 188 |
| Ring and Ball Point (°C) | 52.4 | 40.8 |
| Viscosity (Pa.s) | | |
| 90 °C | 22.2 | 2.2 |
| 110 °C | 4.3 | 0.6 |
| 130 °C | 1.2 | 0.2 |
| 160 °C | 0.3 | 0.1 |

The workability of mixture 1 decreases when the mixing and testing temperatures are lower. By reducing binder viscosity, using the softer binder (160/220) and the warm mix wax, mixtures 2 and 3 will have a better workability than mixture 1, when the temperature decreases.

## *3.2 Experimental Techniques and Parameters*

### 3.2.1 Gyratory Shear Compactor Test

A large part of the experimental study was conducted with a French GSC manufactured by Vectra. The parameters recommended for use according to the NF EN 12 697-31 standard are a vertical strength F of 11.7 kN, a rotation speed of 30 rpm, an inclination angle α of 1° and three specimens tested for one GSC test.

The vertical strength of the GSC may be changed by varying the gauge pressure. The gauge calibration is presented in Table 2. As regards rotation speed, it may be changed with a potentiometer from 3 to 30 rpm. The other parameters do not vary.

A first experimental study was carried out to determine which new GSC parameters will be used (vertical strength and rotation speed). To do that, mixture 1 has been tested with these parameters:

**Table 2** GSC gauge calibration

| Gauge pressure [bar] | Vertical strength [kN] |
|---|---|
| 30 | 11.70 |
| 25 | 10.22 |
| 20 | 8.33 |
| 15 | 6.46 |
| 10 | 4.54 |
| 5 | 2.67 |
| 4 | 2.27 |
| 3 | 1.95 |

- Two temperatures: 110 and 160 °C
- Two vertical strengths: 11.7 kN (30 bar) and 1.95 kN (3 bar)
- Two rotation speeds: 30 and 3 rpm

The results obtained (mean of 3 trials) are shown in Figs. 1 and 2 and in Table 3.

A difference of void content was noticed between the two vertical strengths: the level of compaction is higher at 11.7 kN than at 1.95 kN. The difference between tests at 160 and 110 °C is higher at 1.95 kN (3 bar) than at 11.7 kN (30 bar). At 1.95 kN, this gap is higher than the GSC test repeatability recommended by NF EN 12 697-31 standard (repeatability = 1 %).

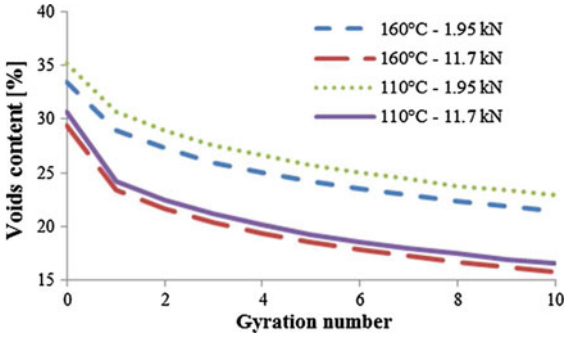


**Fig. 1** GSC tests varying the vertical strength, at 30 rpm

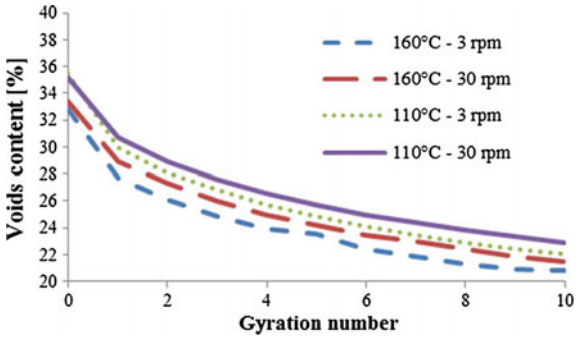


**Fig. 2** GSC tests varying the rotation speed, at 1.95 kN

**Table 3** Difference between void content at 160 and 110 °C, according to vertical strength, at 30 rpm

| Gyration number | Difference between 160 and 110 °C at 11.7 kN | Difference between 160 and 110 °C at 1.95 kN |
|---|---|---|
| 1 | 0.8 | 1.8 |
| 2 | 0.8 | 1.6 |
| 3 | 0.8 | 1.6 |
| 4 | 0.8 | 1.6 |
| 5 | 0.8 | 1.5 |
| 10 | 0.8 | 1.4 |

Thus, only the vertical strength of 1.95 kN was used for the end of the study.

The gap between 160 and 110 °C tests is a little higher at 3 rpm than at 30 rpm. Even if this gap were negligible, the next GSC tests would have to be run at a rotation speed of 3 rpm, to reduce the load applied on asphalt mix specimens.

In conclusion, the parameters of the GSC tests would be:

- Vertical strength: 1.95 kN
- Rotation speed: 3 rpm
- Mixing and testing temperatures: 160, 110 and 90 °C
- Mixes tested: mixture 1, 2 and 3

#### 3.2.2 Nynas Workability Device Test

The second experimental tool used is a Nynas workability device manufactured by the French company ICS (Instrumentation Contrôle Service), according to the standard. The model used is equipped with several jacks that can be used to perform tests at various speeds from 0.01 to 4 cm/s, and with two molds, a large one (6600 $cm^3$ containing approximately 11 kg of asphalt mixture) and a smaller one (3300 $cm^3$ for a specimen of approximately 5 kg).

In a previous study (Fabre des Essarts et al. 2014), the influence of several parameters of the Nynas workability device test were analyzed, and two experimental procedures were developed: the first one keeping a constant volume leveling the asphalt (according to NF EN 98-258-1 standard), and the second one keeping constant mass and volume regardless of the temperature, to test every specimen at constant density. The second procedure (constant density) is the one chosen here. The other parameters chosen are:

- The smallest mold: 3300 $cm^3$
- The specimen mass: 4.9 kg
- Testing speed: 3 cm/s
- Mixing and testing temperatures: 160, 130, 110 and 90 °C
- Mixes tested: mixtures 1 and 2 (with pure 35/50 and 160/220 binders).

## 4 Tests Results

### *4.1 Void Content*

#### 4.1.1 Impact of the Temperature

GSC tests were carried out on mixture 1, with the new parameters chosen (vertical strength of 1.95 kN and rotation speed of 3 rpm), varying the temperature. The results obtained are illustrated in Fig. 3.

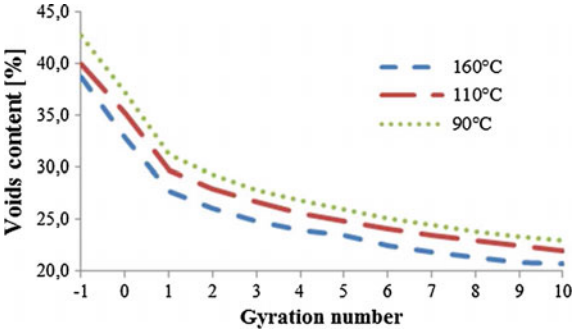


**Fig. 3** GSC tests on mixture 1, at 3 rpm and 1.95 kN, varying the temperature

The void content at gyration number −1 represents the void content of the mixture sample just poured into the mold, before putting the mold into the GSC and applying the preload. This void content has been measured manually. The void content at gyration number 0 represents the void content of the sample after applying the preload (15 N). This preload could not be changed on the GSC. From gyration number 1, the GSC test begins.

Figure 3 shows logical results: the void content is higher when the temperature is lower. But even if the gap between tests at 160 and 110 °C is higher than 1 % (repeatability according NF EN 12 697-31 standard), it is lower than 2.5 %. This gap is not enough to characterize the workability differences between mixture 1 at 160 and 110 °C observed during the laboratory experiments.

The same conclusion may be drawn from the tests at 160 and 90 °C: the gap is lower than 4.5 %; nevertheless, mixture 1 at 90 °C has a much lower workability rate than at 160 °C, as the Nynas device test will show.

### 4.1.2 Impact of the Mixture

The three different mixtures are tested at the three temperatures (160, 110 and 90 °C). The results obtained at 110 and 90 °C are shown in Figs. 4 and 5.

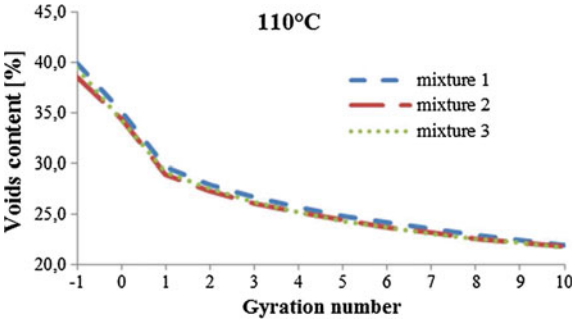


**Fig. 4** GSC tests on mixture 1, 2 and 3, at 3 rpm, 1.95 kN and 110 °C

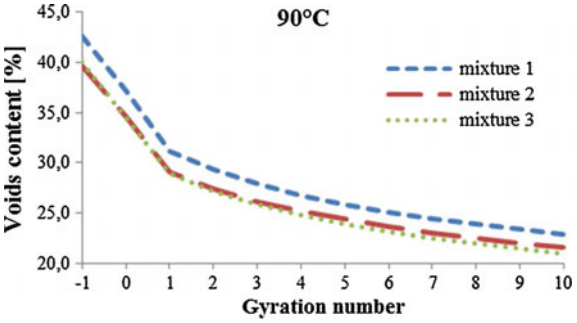


**Fig. 5** GSC tests on mixture 1, 2 and 3, at 3 rpm, 1.95 kN and 90 °C

The void content at gyration number −1 represents the void content of the mixture sample just put into the mold, before putting the mold into the GSC and applying the preload. This void content has been measured manually. The void content at gyration number 0 represents the void content of the sample after applying the preload (15 N). From gyration number 1, the GSC test has begun.

At 110 °C, the evolution of the void content is nearly the same for the three mixtures, whereas mixture 1 (with 35/50) is largely less workable than mixtures 2 and 3 at 110 °C.

The curves at 90 °C show a certain gap between mixture 1 and mixtures 2 and 3, but this gap is less than 3 %, and so, insufficient to characterize the workability differences observed during the laboratory experiments.

## *4.2 Shear Strength*

During every GSC test, the shear strength applied to the samples was measured and analyzed for the first 11 gyrations. The shear strength at gyration number 0 represents the shear strength on the sample, after applying the preload (15 N). From gyration number 1, the GSC test has begun. Figure 6 shows the results obtained for mixture 1 according to the testing temperatures.

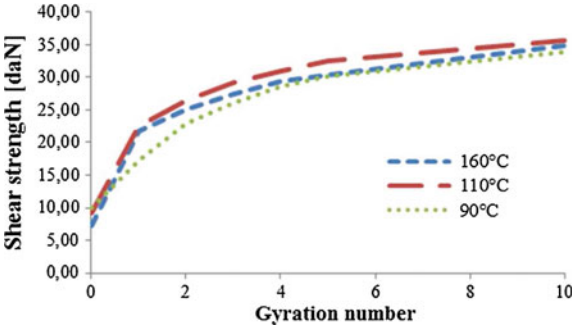


**Fig. 6** Shear strength evolution during GSC tests on mixture 1, at 3 rpm and 1.95 kN, varying the temperature

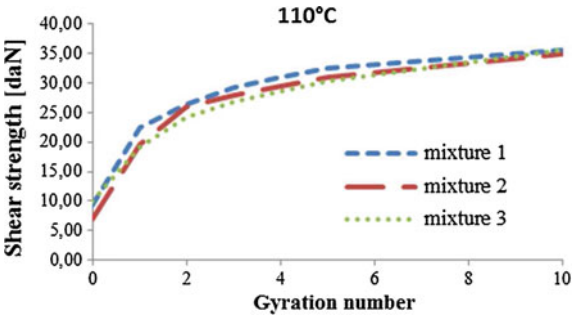


**Fig. 7** Shear strength evolution during GSC tests on mixtures 1, 2 and 3, at 3 rpm, 1.95 kN and 110 °C

The shear strength curves shown on Fig. 6 do not allow a classification of the tested samples in terms of workability. Indeed, the shear strength applied on the specimen at 90 °C is lower than the one applied at 110 or 160 °C, while mixture 1 is less workable at 90 °C than at 110 and 160 °C.

If the shear strength measured was a workability criterion, it should be significantly lower at 160 °C than at 110 and 90 °C, for mixture 1 (with 35/50 binder and without warm mix additive).

Figure 7 gives the evolution of shear strength for the three mixtures at 110 °C. The results obtained at 110 °C are almost the same for the three mixtures, while mixture 1 is less workable than mixtures 2 and 3 at 110 °C.

## *4.3 Nynas Workability*

To compare the GSC test method with another workability testing method, some experiments were made with the Nynas workability device. The results obtained are analysed in Fig. 8.

Figure 8 shows that the maximal strength measured by the Nynas device significantly increases for mixtures 1 and 2 when the temperature decreases. That confirms what is really observed (during laboratory tests and on road sites): the fact that mixtures 1 and 2's workability decreases when the temperature decreases.

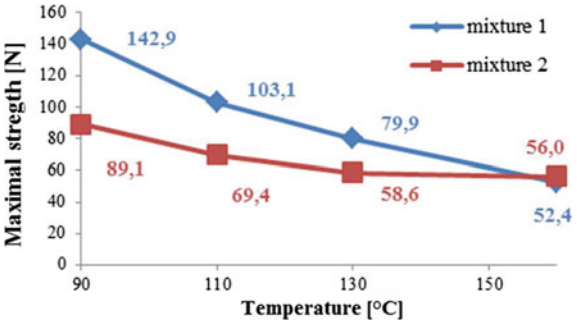


**Fig. 8** Maximal strength obtained with the Nynas workability device for mixtures 1 and 2

It is also notable that mixture 2 keeps a higher workability rate than mixture 1. Indeed, the maximal strength of mixture 1 increases 173 % between 160 and 90 °C, whereas mixture 2's increases 59 %. These results could be explained by the difference of viscosity between the 35/50 and the 160/220 binders: there is a 30 °C temperature difference for the same viscosity of 35/50 and 160/220. These results may be compared to the GSC tests results highlighting that the GSC is insensitive to workability lowering.

## 5 Conclusions

The aim of this study was to change the standard parameters of the Gyratory Shear Compactor test, well-known and practiced in every road laboratory, to use it as a WMA workability characterization device. The GSC vertical strength and rotation speed were lowered to the minima which could be set on the device, and an experimental study was carried out on the three mixtures with really different workabilities. In parallel, Nynas workability device tests were practiced for the sake of comparison.

The results obtained with the GSC in terms of void content and shear strength highlighted the fact that this device, even set with minimal parameters, is insensitive to workability lowering. Indeed, the values of the void content and the shear strength were essentially the same while the temperature (160, 110 and 90 °C) was lowered and the mixture (with 35/50, with 160/220, with warm mix additive) was changed.

On the contrary, the results of the Nynas workability device tests showed important workability differences according to temperature (160, 130, 110 and 90 °C) and to mixture (with 35/50 and with 160/220). Indeed, the maximal strength applied by the Nynas device increased when the temperature decreased, and this maximal strength presented a higher increase for mixture 1 than for mixture 2.

To conclude, even set with minimal vertical strength and rotation speed, the GSC cannot be used as a workability measure device, whereas the Nynas device gives conclusive results. Indeed, the strength levels (some newton) measured by the Nynas device are much lower than those applied by the GSC (some kilonewton).

**Acknowledgments** The authors would like to thank all the participants of this study, and especially Ronan Gueguen and François Rudelle, ESTP students, who performed all the GSC tests. Additionally, the authors would like to thank the EUROVIA laboratory in Saclay (France) for its hospitality and assistance during this study.

## References

Bennert T, Reinke G, Mogawer W, Mooney K (2010) Assessment of Workability/Compactability of Warm Mix Asphalt. In Transportation Research Record: Journal of the Transportation Research Board, No. 2180, Transportation Research Board of the National Academies, Washington, D.C., 2010, pp. 36-47

Bonaquist R (2011) NCHRP Report 691: Mix Design Practices for Warm Mix Asphalt. Transportation Research Board of the National Academies, Washington, D.C., 2011

Brion Y, Le Roux C, Linder R, Moonen R (1999) Mesure de l'évolution de la cohesion à l'émulsion au jeune âge par le maniabilimètre Nynas. Revue Générale des Routes et des Aérodromes, Vol. 769, 1999

Delorme J-L, La Roche C, Wendling L (2007) Manuel LPC d'aide à la formulation des enrobés, Groupe de travail RST « Formulation des enrobés » , Paris, Laboratoire des Ponts et Chaussées, 2007

Dony A, Maillard-Nunes P, Klincevicius M, Motta R, Bernucci L, Del Priore C, Brosseaud Y, Gaudefroy V (2010) Laboratory assessment of Warm Mixes Asphalt by means of two mix design methods. The 16th World Meeting International Road Federation, Lisboa, 2010

Fabre des Essarts A, Dony A, Roux J-N, Gaudefroy V (2014) Maniabilité des enrobés bitumineux tièdes aux températures de mise en œuvre. 32èmes Rencontres de l'AUGC, Polytech Orléans, 2014

Hanz A, Faheem A, Mahmoud E, Bahia H (2010) Measuring Effects of Warm Mix Additives: Use a Newly Developed Binder Lubricity Test for the Dynamic Shear Rheometer. In Transportation Research Record: Journal of the Transportation Research Board, No. 2180, Transportation Research Board of the National Academies, Washington, D.C., 2010, pp. 85-92

Hanz A, Mahmoud E, Bahia H (2011) Asphalt Lubricity Test Evaluation and Relationship to Mixture Workability. Transportation Research Board of the National Academies, Washington, D.C., 2011

Olard F, Gaudefroy V (2011) Laboratory assessment of mechanical performance and fume emissions of LEA Half-Warm Mix Asphalt versus traditional Hot Mix Asphalt. The 2nd International Conference on Warm Mix Asphalt, St-Louis, 2011

# Laboratory Evaluation of Complex Modulus and Fatigue Resistance of Asphalt Mixtures with RAP

**A. Basueny, A. Carter, D. Perraton and M. Vaillancourt**

**Abstract** The evaluation of the performance of recycled asphalt mixtures is a priority for the asphalt materials community. The results of the investigation dealing with the linear viscoelastic properties and fatigue resistance on RAP mixtures are presented. Complex modulus and fatigue properties of recycled asphalt mixtures are investigated on tension–compression tests (T-C). Four asphalt mixtures including four RAP contents (0, 15, 25, 40 %), one virgin aggregate, and one asphalt binder (PG 64-28) were investigated in this study. In general, the results of this study indicate that: 1) the asphalt mixtures containing RAP have higher or similar stiffness with the control mixture containing no RAP, 2) the asphalt mixtures containing 25 % RAP have the highest stiffness at lower temperatures or high frequencies, and 3) no general trend was found between the amount of RAP and the number of cycles to reach fatigue failure. In addition, high fatigue resistance was observed in mixtures containing 40 % RAP.

**Keywords** Asphalt mixtures · Reclaimed asphalt pavement (RAP) · Complex modulus · Stiffness · Fatigue resistance

## 1 Introduction

The stiffness of asphalt mixtures as defined by the complex modulus is related to the major distress modes, such as rutting, fatigue, and thermal cracking. An updated mechanistic-empirical pavement design guide (MEPDG) proposed the stiffness of asphalt mixtures as the key parameter in the flexible pavement design that controls the rutting resistance and fatigue cracking resistance of asphalt pavements. Therefore, the evaluation of the properties of asphalt mixtures containing RAP is of interest to owners and agencies seeking better performing pavements.

A. Basueny · A. Carter (✉) · D. Perraton · M. Vaillancourt
École de technologie supérieure, Montréal, Canada
e-mail: alan.carter@etsmtl.ca



F. Canestrari and M.N. Partl (eds.), *8th RILEM International Symposium on Testing and Characterization of Sustainable and Innovative Bituminous Materials*, RILEM Bookseries 11, DOI 10.1007/978-94-017-7342-3_42

In spite of the wide application of RAP materials today, the use of RAP in new pavements has always been a sensitive issue. The main concern about its use (especially in significant quantity) is the fatigue resistance of HMA mixture with RAP material (Huang et al. 2004a). Furthermore, there is little information available about the effect of RAP on fatigue resistance of the resulting asphalt mixture (Li et al. 2008). For this reason, contractors in Quebec are particularly reluctant to use more than 25 % RAP (Ambaiowei et al. 2013).

Generally, we assumed that the inclusion of RAP in HMA mixtures will blend the aged binder present in RAP with the new asphalt binder (Huang et al. 2004a). The properties of the mixtures containing RAP are influenced mainly by the aged binder properties from RAP and the content of RAP in the mixture. Aging causes an increase in viscosity and modulus of the asphalt which is beneficial to improve rutting resistance (Xiao et al. 2009), but it also increases the risk of cracking due to the increased brittleness of the aged RAP binder.

There are varied opinions on the RAP effect on a recycled mix. Some conclude that the amount of RAP used in the recycled mix affects the property of the mix (Huang et al. 2004a; McDaniel et al. 2000), whereas, other researchers conclude that mix property is not significantly affected by the quantity of RAP used (Servas et al. 1987). Some studies found the stiffness modulus of recycled mix to be higher with respect to the virgin mix (Huang et al. 2004a; Servas et al. 1987), whereas other studies found similar or lower stiffness (Noureldin and Wood 1990; Sondag et al. 2002). Fatigue performance of recycled mix, are observed to be poorer than its corresponding virgin mix, although other study suggests that it could be similar to or better than the virgin mix (Huang et al. 2004a, b), especially for the situation when RAP content with respect to the total mix is less than 30 %. This conclusion appears to contradict the common belief: the more RAP, the more brittle the mixture, thus, the lower the fatigue resistance. However, similar results were reported by Malpass (2003), Raghubar Shrestha (2009) and results were even supported by some of the fatigue test results from the NCHRP 9-12 study (McDaniel et al. 2000).

In general, most studies on laboratory-produced mixtures concluded that the effect of RAP on mixtures' properties is negligible at low RAP contents of 15-20 % (Li et al. 2008; McDaniel et al. 2000, 2007). However, the increase in RAP content beyond 20 % increases the mixture stiffness and strength resulting in an increase in rutting resistance (Li et al. 2008; McDaniel et al. 2007). When no change to the virgin binder grade is made, higher RAP contents (>40 %) result in a significant increase in the stiffness of the mix at high, intermediate, and low temperatures (McDaniel et al. 2000) and a reduction in the low temperature cracking resistance (Li et al. 2008; Daniel and Lachance 2005).

Fatigue resistance of a bituminous mixture is of great importance because it shows the ability of the mix to withstand repeated loading without fracture. Fatigue is one of the main failure modes and manifests itself in the form of cracking in the wheelpaths resulting from repeated number of cyclic loading (Perraton et al. 2011, 2014; Tayebali et al. 1992). In the pavement design procedures, it is necessary to have a measure of the fatigue characteristics of specific mixtures over a range of

traffic and environmental conditions so that fatigue consideration can be incorporated in the design process.

The fatigue characteristics of asphalt mixtures are usually expressed as relationships between the initial stress or strain and the number of load repetitions to failure determined using fatigue tests performed at several stress or strain levels (Wöhler curve).

During fatigue tests, the stiffness decreases following three distinctive phases. Phase I shows a rapid evolution of the stiffness linked to heading of the specimen and to thixotropy. It is followed by phase II, which corresponds to a more regular stiffness decrease. The specimen fracture then occurs in Phase III, due to macro crack propagation in the material.

Fatigue degradation is initially related to the micro-crack network growing uniformly in the material, affecting the rigidity of the material which implies a decrease of the modulus (Perraton et al. 2014; Di Benedetto et al. 2004). Phase II is associated with the degradation resulting from damage that uniformly spread out across the entire volume of the sample under testing. Hence, this phase is manifested by the initiation and propagation of a 'micro-crack' network in a different way. Phase III corresponds to the coalescence of micro-cracks, up to the point where a 'macro-crack' appears and propagates within the material. The coalescence appears at a certain value of micro-cracking (or level of damage or level of fatigue). During fatigue tests of asphalt mixtures, phase II and III can be considered as appearing successively, or for some test geometries, parallel in time.

To obtain accurate fatigue modelling of a mix measurement in pavement design procedure, Wöhler law must well present the transition zone between phase II and III. It is important to note that the stiffness reduction can correspond to other phenomena than fatigue. These phenomena are (Perraton et al. 2014): (1) self-heating caused by dissipated energy generation resulting from the tested material's inherent viscous property, and (2) binder thixotropy.

## 2 Objectives

The objective of this study is to evaluate the effect of RAP proportion on complex modulus and fatigue life of asphalt mix. The properties of the mixtures were evaluated through laboratory performance tests in tension-compression (T-C). A dense graded asphalt mixtures, typically used as based course in flexible pavements, GB-20, containing 0 % RAP was the control mix for evaluating properties of mixtures containing 15, 25, and 40 % RAP. One type of aggregate, a PG64-28 asphalt binder and cold RAP addition were considered in this paper.

## 3 Materials and Mix Design

Four laboratory-prepared asphalt mixtures were studied, considering one source of RAP, four percentages of RAP: 0, 15, 25, and 40 %, one asphalt binder (PG 64-28), at 4.5 % by weight. Each mix has at least two slabs of 500 × 1800 × 100 $mm^3$ (P1 to P4). For asphalt mixtures containing RAP, the RAP at room temperature was added and mixed with the overheated virgin aggregates (300 °C) for about 2–4 min depending upon the amount of RAP included in the mixture, till reaching the mixing temperature. After RAP-virgin aggregate blending, the pre-heated virgin binder (160 °C) was added and mixed for an additional 4 min. Immediately after mixing, the hot asphalt mixture was conditioned in a covered pan for 2 h in a draft oven at the compaction temperature (153 °C). After conditioning, slabs (500 × 180 × 100 mm) were compacted using the LCPC rolling wheel compactor (NF EN 1267-33). Cylindrical specimens were cored from slabs for rheological measurements (ϕ75 mm × 120 mm in length).

The RAP materials were sampled in an asphalt plant near Montreal (Canada). The nominal maximum of the aggregates in the RAP is 10 mm. RAP contains a mix of recycled asphalt pavement with an asphalt content of 4.0 %. The RAP materials yield a specific gravity value of 2.679. The performance grade (PG) of the extracted RAP binder is PG 82-18. The details of the RAP characterisation analysis are reported in Basueny et al. (2014).

Note that the mix designations consist of the following sequence: percentage of RAP added (0, 15, 25, 40 %), followed by the added binder grade PG 64-28, identified as 28. The mix design followed the MTQ (Ministère des Transports du Québec) method which is essentially based on the superpave mix design procedure (Langlois 2003). A control mixture was first designed to serve as a base line to compare with other mixtures which all have very similar gradation in an effort to minimize additional factors that can affect the results. It is important to note that as more RAP was added, the finer fractions of the mix tended to increase as shown in Fig. 1.

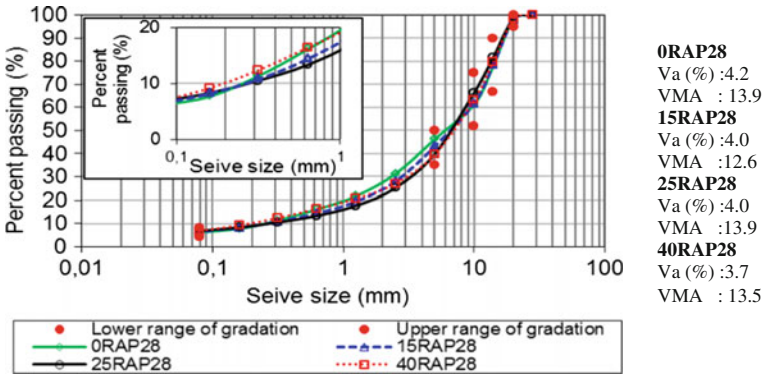


**Fig. 1** Asphalt mixtures gradations and characteristics

## 4 Testing Set-up and Procedures

The test setup on a servo-hydraulic testing system (MTS 810) was the same for both the complex modulus and fatigue tests. The axial strain was measured on the middle part of the specimen using three 50 mm extensometers, placed 120° apart.

Complex modulus testing was performed on one sample for each mix. Each specimen was subjected to cyclic sinusoidal loading in tension and compression along the axial direction. Tests were performed under strain control with target amplitude of 50 μm/m (average of three extensometers). The cylindrical specimens were loaded at 8 frequencies (20–0.01 Hz) and 8 temperatures (−35 to 35 °C). Air voids of the specimens used of complex modulus measurement were in the range of 3.8 ± 1.3 %, except for one of the mixes (15RAP28 (mix No. 2)) which had a higher air void (3.8 ± 2.2 %).

In this study, fatigue characterization was done at 10 °C and 10 Hz under strain control. The advantage of this test is the homogeneous state of stresses and strains within the specimen. With such homogeneous conditions, there is no need to assume the behaviour law (Di Benedetto and De la Roche 1998). The analysis of the observed scattering among the three measurements given by the extensometers provides clear information about the homogeneity of the strains in the sample. In a perfectly homogeneous test, these values should be identical.

For the fatigue tests, at least five specimens of each mix were tested. The air voids of the tested specimens were in the ranges from 2.1 to 7.4 %.

## 5 Complex Modulus Results

A rheological model (2S2P1D) developed at the ENTPE/DGCB laboratory in France is used to simulate the experimental results for all the materials. At a given temperature, the model has 7 constants and its complex modulus (E*(iωτ)) is given by the Eq. 1 (Olard and Di Benedetto 2003):

$$E^*_{2S2P1D}(i\omega\tau_E) = E_{00} + \frac{E_0 - E_{00}}{1 + \delta(i\omega\tau_E)^{-k} + (i\omega\tau_E)^{-h} + (i\omega\beta\tau_E)^{-1}} \quad (1)$$

where:

- i complex number defined by $i^2 = -1$;
- Ω pulsation, $\omega = 2\pi f$, (f is the frequency);
- k, h constant exponents such as $0 < k < h < 1$; δ: constant;
- $E_{00}$ the static modulus when $\omega \rightarrow 0$;
- $E_0$ the glassy modulus when $\omega \rightarrow \infty$;
- β parameter linked with η of the dashpot, $\eta = (E_0 – E_{00})\beta\tau_{E;}$
- $\tau_E$ characteristic time value;

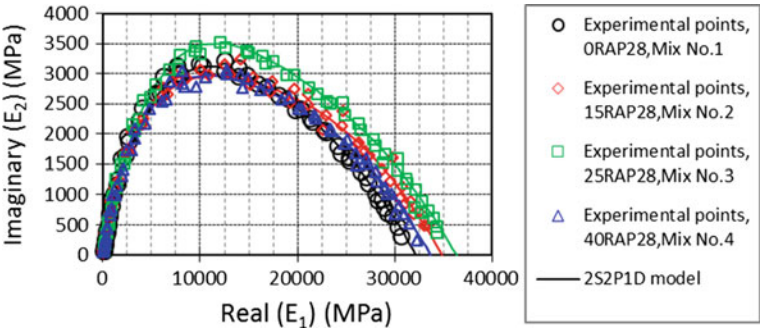


**Fig. 2** Complex modulus results in Cole-Cole plan and 2S2P1D and WLF parameters

$\tau_E$ is a function of the temperature (T), which takes into account the Time-Temperature Superposition Principle (TTSP).

Experimental results (dot marks) and the adjusted 2S2P1D models (lines) are presented in the Cole-Cole plan in Fig. 2. 2S2P1D parameters and the $C_1$ and $C_2$ constants (for WLF) are also reported in Fig. 2. On Fig. 2, mixes can be ranked by stiffness at high frequency and/or low temperature starting with the control mix as the lowest, then followed by the 40 % RAP mix and the 15 % RAP mix, the 25 % RAP mix as the stiffest. Those results are unexpected, since, as shown in the literature review, the addition of RAP usually increases the stiffness of a mix as we found at high frequency and/or low temperature.

| Mix ID | E* | | | | | | | WLF | |
|---|---|---|---|---|---|---|---|---|---|
| | $E_0$ (MPa) | $E_{00}$ (MPa) | δ | k | β | h | $\tau_{0E}$ (s) | $C_1$ | $C_2$ |
| 0RAP28 | 32,200 | 100 | 1.82 | 0.182 | 500 | 0.530 | 0.135 | 20.96 | 148.09 |
| 15RAP28 | 34,900 | 60 | 2.30 | 0.177 | 500 | 0.544 | 0.180 | 27.38 | 178.00 |
| 25RAP28 | 36,350 | 127 | 1.81 | 0.177 | 500 | 0.544 | 0.210 | 26.13 | 179.53 |
| 40RAP28 | 33,700 | 110 | 2.15 | 0.177 | 500 | 0.544 | 0.220 | 22.26 | 150.16 |

Generally, The effect of the stiffer asphalt binder contained in the RAP is responsible for higher stiffness values for the mixtures containing RAP (Li et al. 2008). The behaviour of asphalt mixtures are mainly determined by the asphalt binder and a stiffer asphalt binder results in a mix with a higher modulus. Other researchers did find similar conclusions related to the scatter in the data for the mixes containing RAP (Li et al. 2008; Sondag et al. 2002). We hypothesize that the addition of aged and brittle binder coming from RAP mixtures results in a formation of micro cracks to explain the properties of asphalt mixtures at low temperatures as it was mentioned in the literature review.

### 5.1 Normalized Results

The normalized complex modulus ($E^*_{norm}$) as proposed by Di Benedetto is introduced in Eq. 2 (Nguyen et al. 2013):

$$E^*_{norm} = \frac{E^* - E_{00}}{E_0 - E_{00}} \tag{2}$$

where $E_{00}$ and $E_0$ are asymptotic values of the norm of complex modulus when the frequency tends towards 0 and infinity.

On Fig. 3, the normalized moduli of mixtures with different percentages of RAP are superimposed in a Cole-Cole plan. The lines shown in this Figure show the normalized complex modulus results ($E^*_{norm}$) as a vector for the different materials. The group of dotted lines shown in the middle of the curves represents the results at the same temperature and frequency (5 °C, 3 Hz) and the other group, continuous lines, represented the results at low temperature −33 °C and at 3 Hz. From this, it can be seen that there is a small difference in the ranking according to temperature.

## 6 Fatigue Test Results

Table 1 summarized the fatigue tests performed on the four recycled mixes.

The initial modulus $|E^*_{00}|$ is determined as the value of the y-coordinate of the extrapolated value at cycle 1 by assuming a linear fitting of complex modulus measurements from cycles 2 to 50.

As shows in Table 1, the samples' air voids are different. To be able to compare the fatigue resistance between mixes, Wöhler curve of samples tested at similar air void content need to be built. Since, it is not our case, all the fatigue tests results are corrected based on their air voids' content. To do this, the strain values were

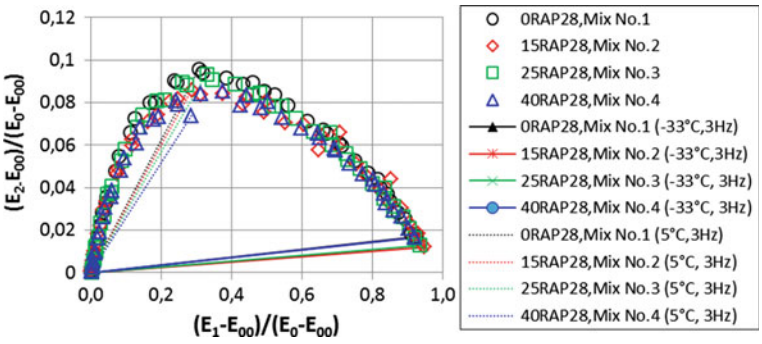


**Fig. 3** Normalized complex modulus results for the mix tested

**Table 1** Summary table of the performed fatigue test (10 °C; 10 Hz)

| Test name | Air voids (%) | Initial modulus, $\|E_{00}^*\|$(MPa) | | | Average measured strain (μdef) |
|---|---|---|---|---|---|
| | | Value | Average | Deviation | |
| 0RAP-(P1-A2)-D150[a] | 4.0 | 10,540 | 10,756 | 723 | 145.3 |
| 0RAP-(P1-A5)-D140 | 4.1 | 11,089 | | | 134.8 |
| 0RAP-(P2-A4)-D130 | 4.5 | 12,057 | | | 124.7 |
| 0RAP-(P1-A3)-D140 | 3.9 | 11,475 | | | 132.6 |
| 0RAP-(P3-A3)-D110 | 6.7 | 10,393 | | | 112.1 |
| 0RAP-(P3-A5)-D105 | 6.8 | 10,036 | | | 107.9 |
| 0RAP-(P4-A5)-D115 | 5.1 | 10,436 | | | 112.1 |
| 0RAP-(P3-A4)-D115 | 6.6 | 10,023 | | | 116.4 |
| 15RAP-(P2-A1)-D150 | 6.3 | 9,607 | 10,327 | 771 | 149.0 |
| 15RAP-(P2-A2)-D120 | 6.7 | 9,193 | | | 118.7 |
| 15RAP-(P1-A3)-D115 | 5.9 | 10,920 | | | 112.2 |
| 15RAP-(P2-A3)-D130 | 6.3 | 10,861 | | | 129.4 |
| 15RAP-(P1-A2)-D140 | 6.7 | 11,054 | | | 140.1 |
| 25RAP-(P4-A2)-D120 | 6.1 | 12,090 | 10,916 | 1477 | 119.0 |
| 25RAP-(P4-A4)-D140 | 5.6 | 10,123 | | | 135.4 |
| 25RAP-(P4-A5)-D130 | 5.8 | 11,962 | | | 128.5 |
| 25RAP-(P3-A1)-D150 | 6.8 | 11,909 | | | 151.1 |
| 25RAP-(P1-A2)-D110 | 6.2 | 8,760 | | | 108.8 |
| 40RAP-(P1-A2)-D130 | 3.3 | 11,932 | 11,930 | 539 | 130.5 |
| 40RAP-(P2-A3)-D140 | 3.8 | 12,307 | | | 137.5 |
| 40RAP-(P2-A2)-D150 | 2.1 | 12,541 | | | 147.0 |
| | 3.6 | 11,469 | | | 158.3 |

(continued)

**Table 1** (continued)

| Test name | Air voids (%) | Initial modulus, $\|E_{00}^*\|$(MPa) | | | Average measured strain (μdef) |
|---|---|---|---|---|---|
| | | Value | Average | Deviation | |
| 40RAP-(P1-A3)-D160 | | | | | |
| 40RAP-(P1-A4)-D170 | 2.7 | 11,125 | | | 168.0 |
| 40RAP-(P1-A2)-D180 | 2.5 | 12,203 | | | 178.0 |

[a]A is the sample's number according to the position in the slab, and D is the level of imposed strain

corrected based on Moutier's approach and the life duration $N_f$ value was not corrected. In this study, the average air void, for all the specimens for fatigue test is 5.1 %. This average void ($\bar{V}$) was used to calculate the corrected value of deformation $\varepsilon_{cor}$ based on the corresponding processed value of imposed deformation $\varepsilon_m$. This calculation is performed using the value of $\varepsilon_m$ measured for a recycled mixture which the air void content of its tested specimen is $V_{sample}$ according to the calculation specified by Moutier (1991):

$$\varepsilon_{cor} = \varepsilon_m + 3.3(V_{sample} - \bar{V}) \tag{3}$$

The corrected value of strain ($\varepsilon_{cor}$) was used to define the Wöhler curve based on $\bar{V}$ equal to 5.1 % in this study.

For fatigue testing, the number of cycles required for the specimen to fail, $N_f$, is determined based on failure criteria proposed in the literature (Tapsoba et al. 2013). In our experimental program, the determination of the fatigue life of tested samples is based on two criteria which are: 1) the criteria based on the evolution of the stiffness modulus (classic method or $N_{f50\ \%}$), and 2) the criteria of the end of phase II. The complete explanation of those criteria is given elsewhere (Perraton et al. 2014; Tayebali et al. 1992; Baaj 2002; Di Benedetto et al. 2004).

For each mix, the fatigue lines (Wöhler curve) were plotted on the axes log ($N_f$) versus log ($\varepsilon_0$) and the coefficient of determination $R^2$ were determined (Fig. 4). From these lines, it is possible to determine the constants of the fatigue lines (Table 2).

Figure 4 shows that the Wöhler curve obtained from the mixtures containing 0, 15, and 25 % of RAP by considering the $N_{f50\ \%}$ or $N_{fII/III}$ values are more or less similar. However, a clearly different tendency for the fatigue test results of the mixture containing 40 % RAP is seen. This illustrates that using the $N_{f50\ \%}$ and $N_{fII/III}$ criteria to predict the fatigue life of asphalt mix can show different tendency as it was discussed elsewhere (Perraton et al. 2014). That study shows that it could happen in some cases for the fatigue test results for asphalt mixes made with polymer modified binders. The artefact effects are probably the main explanations for the fatigue life obtained from the $N_{f50\ \%}$ criteria which fails to well define the beginning of the micro-cracking process in a material containing high percentage of

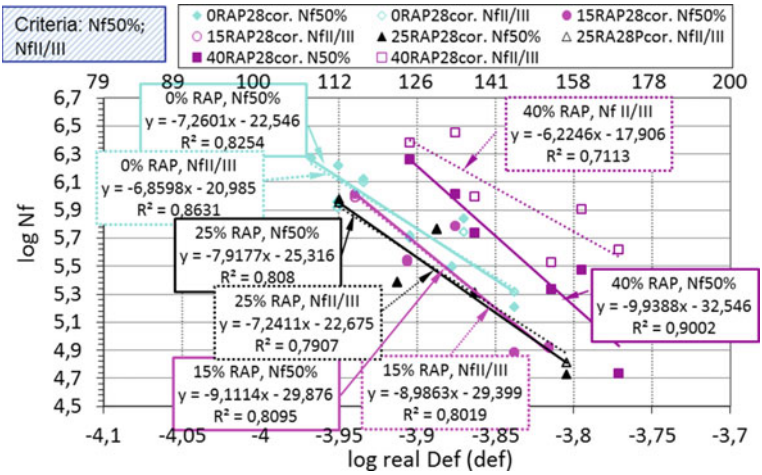


**Fig. 4** Wöhler curves for the four mixes after correcting to air void of 5.1 % determined by the classical criterion and the criterion of the end of phase II

**Table 2** Characteristics of the fatigue lines corrected for 5.1 % air voids (10 °C; 10 Hz)

| Mix | Number of tests | Failure criterion | $k_{1,cor}$ | $k_{2,cor}$ | $\varepsilon_{6,\ cor}$ | $b_{cor} = -1/k_{2cor}$ | $R^2$ | Voids mean (Std. dev.) |
|---|---|---|---|---|---|---|---|---|
| 0RAP28 | 8 | $N_{f50\ \%}$ | 2.8E-23 | 7.3 | 117 | −0.138 | 0.83 | 5.1 (1.504) |
| | | $N_{fII/III}$ | 1.0E-21 | 6.9 | 116 | −0.146 | 0.86 | |
| 15RAP28 | 5 | $N_{f50\ \%}$ | 1.3E-30 | 9.1 | 115 | −0.110 | 0.81 | |
| | | $N_{fII/III}$ | 4.0E-30 | 9.0 | 115 | −0.111 | 0.80 | |
| 25RAP28 | 5 | $N_{f50\ \%}$ | 4.8E-26 | 7.9 | 110 | −0.126 | 0.81 | |
| | | $N_{fII/III}$ | 2.1E-23 | 7.2 | 109 | −0.138 | 0.79 | |
| 40RAP28 | 6 | $N_{f50\ \%}$ | 2.8E-33 | 9.9 | 132 | −0.101 | 0.90 | |
| | | $N_{fII/III}$ | 1.2E-18 | 6.2 | 143 | −0.161 | 0.71 | |

RAP. As the RAP percentage increases some effects on the mixture properties is noted. This could be explained by the fact that when the percentage of RAP in the mix is high enough, the RAP binder creates a significant change in the mixture properties and therefore it can be concluded that the influence of RAP on the final HMA property also varies with the amount of RAP.

A classification using the two criteria for our mixes based on $\varepsilon_6$ was donebecause it is a simple way for showing the difference between mixes. $\varepsilon_6$ refers to the strain for which the life duration is equal to 1 million cycles of solicitation for a mixture tested at a given temperature and frequency. As shown in Table 2, even if the $\varepsilon_6$ is different for both criteria the classification remains the same: 25 % RAP is the least resistant to fatigue cracking, followed by the reference mix and the 15 % which have very similar results, and the 40 % RAP has the best fatigue resistance.

It is possible that the addition of 40 % RAP could provide a good aggregate structure which lead to increase mixture stiffness and ultimately the estimated

fatigue performance. This supports the reason for considering the RAP aggregate shape, gradation and quality. Therefore, it is recommended to provide the properties of the RAP material properly to be accounted for the mix design process to produce a mixture with RAP that can perform very well for fatigue resistance. It is important to note that this analysis is based on fatigue behavior on the material level, as it is commonly done; differences between laboratory and service conditions must be considered by pavements designer.

## 7 Conclusion

Experimental results indicate that the addition of RAP in asphalt mixtures does affect the complex modulus and the fatigue life. For the complex modulus, the results did not show a clear trend between the stiffness and the amount of RAP. In this case, the mix with 25 % RAP was stiffer than the mix with 40 % RAP. For fatigue, no clear trend was seen either. Further research in this area is needed to determine whether this holds true for other RAP sources and if the results vary significantly depending on the method chosen to add RAP in the lab.

## References

Ambaiowei D., Sanchez X., Safiuddin M.D., Aurilio V., Susan L. (2013) Investigation thermal cracking potential of Ontario RAP-HMA Mixtures. In 2013 Conference of the Transportation Association of Canada

Baaj H. (2002) Comportement à la fatigue des matériaux granulaire traites au liant hydraulique. Mécanique, énergétique. ENTPE and INSA Lyon, 247 p

Basueny A., Perraton D., Carter A. (2014) Laboratory study of the effect of RAP conditioning on the mechanical properties of hot mix asphalt containing RAP. Materials and structures, vol. 47, p. 1425-1450

Daniel J.S., Lachance A. (2005) Mechanistic and Volumetric Properties of Asphalt Mixtures with RAP. the Transportation Research Board 84th Annual meeting compendium of papers CD-ROM, TRB, National Research Council

Di Benedetto H., De la Roche C., Baaj H., Pronk A. et lundsrtom R. (2004) Fatigue of bituminous mixtures. Materials and structures, vol. 37, p. 202-216

Di Benedetto H., De La Roche C. (1998) State of the art on stiffness modulus and fatigue of bituminous mixtures. Rilem Rep. No. 17, Bituminous Binders and Mixtures, L Francken, ed., E&FN Spon, London

Huang B., Zhang Z., Kingery W. (2004)a Fatigue crack characteristics of HMA mixtures containing RAP. In 5 th International RILEM conference on cracking in pavements (May 5-7). p. 631-638. Limoges, France

Huang B., Kingery R.,. Zhang Z, Zuo G. (2004)b Laboratory study of fatigue characteristics of HMA surface mixtures containing RAP. In International symposium on long performing asphalt pavements (june 7-9). p. 501-22. Auburn, Ala

Langlois P. (2003) Hot mix asphalt: LC method of mix design. Québec: Ministère des transports. Québec (Province), Ministère des transports., Québec (Province) et Laboratoire des chaussées

Li Xinjun, Marasteanu M. O., Williams R.Ch., Clyne T. R. (2008) Effect of Reclaimed Asphalt Pavement (Proportion and Type) and Binder Grade on Asphalt Mixtures. Transportation Research Record: Journal of the Transportation Research Board, n° 2051, p. pp 90-97

Malpass G.A. (2003) The use of reclaimed asphalt pavement in new Superpave asphalt concrete mixtures. Raleigh, North Carolina State University

McDaniel R.S., Shah A., Huber G.A., Gallivan V. (2007) Investigation of properties of plant-produced RAP mixtures. In Transportation Research Board 86th annual meeting (CD-ROM), Transportation Research Board, National Rsearch Council. Washington, D.C

McDaniel R. S., Soleymani H., Michael Anderson R., Turner P., Peterson R. (2000) Recommended use of Reclaimed Asphalt Pavement in the Superpave Mix Design Method. NCHRP Web. Document 30 (Project D9-12): Contractor's Final Report

Moutier F. (1991) Etude statistique de l'effet de la composition des enrobés bitumineux sur leur comportement en fatigue et leur module complexe. Bulletin de liaison des laboratoires des ponts et chaussées, vol. 172, p. 33-41

Nguyen QT., Di Benedetto H., Sauzéat C. (2013) Prediction of Linear Viscoelastic Behaviour of Asphalt Mixes from Binder Properties and Reversal. Multi-Scale Modeling and Characterization of Infrastructure Materials RILEM, vol. 8, p. 237-248

Noureldin A.S., Wood L.E (1990) Laboratory evaluation of recycled asphalt pavement using nondestructive tests. Transportation Research Record: Journal of the Transportation Research Board. Washington, DC:National Research Council, vol. 1269, n° 92–100

Olard F., Di Benedetto H. (2003) General "2S2P1D" model and relation between the linear viscoelastic behaviors of bituminous binders and mixes. Road materials and pavement design, vol. 4, n° 2/2003, p. 1-40

Perraton, D., Touhara, R., Di Benedetto, H., Carter, A., 2014, Ability of the classical fatigue criteria to point out the macro-crack growth, Materials and Structures/Matériaux et Constructions, sous presse

Perraton, D., Di Benedetto, H., Carter, A., 2011, Correspondances entre les coefficients des modèls de fatigue de méthode mécanistique-empiriques de dimensionnement de chaussées souples, Can. J. Civ. Eng., 38 (12), pp. 1287-1299

Raghubar Shrestha P.E. (2009) The effects of Reclaimed asphalt pavement (RAP) on the laboratory performances of hot mix asphalts. Nevada, Reno

Servas V.P., Edler A.C., Ferreira M.A., Van Assen E.J. (1987) Fundamental Properties of Recycled Asphalt Mixes. In Proceedings of the 6th international conference on structural design of asphalt pavements. Vol. 1, p. 455-65. Ann Arbor, Michigan

Sondag M., Chadbourn B. A., Drescher A. (2002) Investigation of Recycled Asphalt Pavement (RAP) Mixtures. Minnesota Department of Transportation Research Report MN/RC 2002-15

Tapsoba N., Sauzéat C., Di Benedetto H. (2013) Analysis of Fatigue Test for Bituminous Mixtures. Materials in civil engineering, vol. 26, n° 6, p. 701-710

Tayebali A.A., Rowe G.M, Sousa J. B. (1992) Fatigue response of asphalt-aggregate mixtures. Association of Asphalt Paving Technologists

Xiao F., Amirkhanian S.N., Juang H. (2009) Prediction of fatigue life of rubberized asphalt concrete mixtures containing reclaimed asphalt pavement using artificial neural networks. Materials in civil engineering, vol. 21

# Laboratory Testing Methods for Evaluating the Moisture Damage on the Aggregate-Asphalt System

**Sara Anastasio, Inge Hoff, Carl C. Thodesen and Hussain U. Bahia**

**Abstract** The durability of the bitumen-aggregate system is a critical factor affecting the performance of asphalt pavements. It is achieved by a careful selection of the materials based on the analysis of their compatibility and their water sensitivity. Currently, a variety of analytical test methods are used to evaluate the power of the binder to adhere to various aggregates and their susceptibility to moisture. Many of these methods are time consuming and/or require sophisticated and expensive instrumentation. The most common procedure, the indirect tensile strength (ITS) test, has been questioned by many researchers and simpler testing procedures, such as the rolling bottle test, are considered to be an indicative measure. Several studies have introduced a new test procedure, the binder bond strength (BBS) test. The test, based on the pull-off strength of the bond between asphalt and aggregate measured before after water conditioning, has shown good repeatability, reliability and the ability to determine the effects of different aggregate type, conditioning time and moisture on the aggregate-asphalt system. This paper explores the potential of the BBS test by correlating the results of test methods presently used to evaluate the strength of the bond of the asphalt-aggregate system measured with the BBS test. Four different aggregate types and a traditional bitumen were tested according to the respective European standard, including type, length and temperature of conditioning. However, the different aspects of the

S. Anastasio (✉) · I. Hoff · C.C. Thodesen
Department of Civil and Transport Engineering,
Norwegian University of Science and Technology, Trondheim, Norway
e-mail: sara.anastasio@ntnu.no

I. Hoff
e-mail: inge.hoff@ntnu.no

C.C. Thodesen
e-mail: carl.thodesen@ntnu.no

H.U. Bahia
Department of Civil and Environmental Engineering,
University of Wisconsin, Madison, USA
e-mail: hubahia@wisc.edu



F. Canestrari and M.N. Partl (eds.), *8th RILEM International Symposium on Testing and Characterization of Sustainable and Innovative Bituminous Materials*, RILEM Bookseries 11, DOI 10.1007/978-94-017-7342-3_43

mixture considered in each test method determine a poor agreement of the results. Comparable levels of moisture resistance are observable only in the long term.

**Keywords** Asphalt durability · Moisture sensitivity · BBS test · ITS test · Rolling bottle

## 1 Introduction

Bitumen-aggregate interaction is known to influence the overall performance of asphalt pavements. It depends on various physical and chemical characteristics that determine the strength of the adhesive bond between the two materials. Its failure, due to the separation or stripping of the bitumen coating from the aggregate surface, is caused by the action of moisture at the bitumen-aggregate interface (Figueroa et al. 2013). Detachment, displacement, spontaneous emulsification, pore pressure, hydraulic scour, pH instability, environment or climate are considered being behind this degradation process (Kiggundu and Roberts 1988; Little and Jones 2003). A cohesive failure, due to the separation of molecules within the bitumen film, can also lead to adhesive failure when the moisture dispersed in the asphalt reaches the aggregate surface (Canestrari et al. 2010).

The resistance of the adhesive bond to moisture damage relates to surface charge, polarity, porosity, type of adsorption sites and surface energy of the aggregate surface. These characteristics are directly defined by the constitutive minerals (Bagampadde et al. 2005) and therefore vary significantly between different rock types. The aggregate chemistry has been shown to be much more influential than asphalt chemistry for both adhesion and sensitivity to water by Curtis et al. (1993) who evaluated asphalt-aggregate interactions in terms of adsorption and desorption isotherm behavior. The same study showed also that the bitumen components that had the most affinity for the aggregates also tended to have the highest sensitivity to water.

In addition to the characteristics of the mixture and its constituents, traffic load, speed, snow, ice and winter maintenance should also be added to the equation making the evaluation of moisture damage on asphalt pavements an extremely complicated issue.

Currently the laboratory test method for evaluating the water sensitivity of asphalt mixtures consists of an indirect measurement of the tensile strength of compacted samples before and after water conditioning. The affinity between bitumen and aggregate is based on the indirect measurement of the power of a binder to adhere to the aggregates through a visual estimation of the degree of bitumen coverage on uncompacted bitumen-coated aggregate particles after storage in water. The outcome of these tests has been questioned by many researchers as the process tends to be rather subjective (Airey and Choi 2002; Solaimanian et al. 2003; Berger et al. 2003). The bitumen bond strength (BBS) test was recently developed

with the purpose of improving the characterization of the asphalt-aggregate system. It consists of a pull-off test where bitumen is used as glue between a metallic stub and an aggregate substrate. The test focuses on the pull-off strength of the bond between asphalt and aggregate measured before after water conditioning. Positive characteristics of the BBS pull-off test include repeatability, reliability and the ability to determine the effects of different aggregate type. Additionally wet and dry conditioning time can also be taken into account (Moraes et al. 2011; Canestrari et al. 2010; Figueroa et al. 2013).

Since it is very difficult to obtain a good field calibration it is not possible to determine which of the laboratory tests is objectively effective in evaluating water sensitivity. In this paper we have tried to compare them and look at their relative differences to be able to recommend a test method.

## 2 Experimental Overview

### *2.1 Materials*

The samples were produced with four aggregate types commonly used as pavement construction materials in Norway: a metasandstone (hereinafter A), a metagabbro (B), a rhyolite (C) and a greywacke (D); crushed and whole rocks originating from the same quarry. Different geometrical, volumetric and mineralogical properties characterize the four rock materials.

A traditional 70/100 bitumen was used. A water absorption of 0.18, 0.22, 0.22, 0.25 % was measured respectively for A, B, C and D.

### *2.2 Testing Methods*

Four dense graded asphalt mixtures, each one with one type of aggregate (A, B, C and D), were designed using the Marshall design. The AC 11 mixtures, prepared with a binder content of 5.9, 5.1, 6 and 5.8 % respectively, recorded an average air voids content of 3 %. The experimental plan consisted of testing the four asphalt mixtures with three different methods: indirect tensile strength (ITS) test, rolling bottle test and the bitumen bond strength (BBS) test. Each of these was performed according to the respective standard or draft standard.

#### 2.2.1 Indirect Tensile Strength Test

The ITS test determines the effect of saturation and accelerated water conditioning on the indirect tensile strength of cylindrical specimens of bituminous mixtures (CEN 2008). Six samples per mixture were prepared according to EN 12697-30

(CEN 2012a) with 25 blows per each side of the samples. The samples were afterwards divided in two groups having approximately the same average height and average bulk density. The first group was stored dry at room temperature and the second one, once fully saturated using a vacuum system, in a water bath at 40 °C for 72 h. Prior testing both groups were brought at testing temperature of 25 °C.

In order to determine the water sensitivity of the mixture, the indirect tensile strength ratio (ITSR) is generally evaluated as:

$$\mathrm{ITSR} = \frac{\mathrm{ITS_w}}{\mathrm{ITS_d}} \cdot 100\,[\%] \tag{1}$$

where, $\mathrm{ITS_w}$ is the average indirect tensile strength of the wet group [kPa] and $\mathrm{ITS_d}$ is the average indirect tensile strength of the dry group [kPa].

According to the Norwegian Pavement Design Guide (NPRA 2014), this value should not be lower than 70 %.

Since the sample preparation procedure requires a lower degree of compaction compared to the mixture design procedure, the tested samples measured an average air voids of 15.77, 9.05, 16.66, 4.33 % respectively for A, B, C and D.

### 2.2.2 Rolling Bottle Test

EN 12697-11 (CEN 2012b) was used to evaluate the affinity between bitumen and aggregates on loose mix. According to the standard procedure, three bottles per each stone material, filled with 150 g of aggregates coated with bitumen and distilled water, were placed in the bottle rolling machine. After 6, 24, 48 and 72 h the aggregate particles were emptied from the bottle into a test bowl filled with water and the degree of coverage (%) was visually investigated by two operators.

According to the Norwegian Pavement Design Guide (NPRA 2014), degree of coverage, evaluated after 48 h, should not be lower than 25 %.

### 2.2.3 Bitumen Bond Strength Test

The BBS test was performed according to the Bitumen Bond Strength (BBS) test (AASHTO 2013) in order to evaluate the strength of the bond between the aggregate surface and bitumen. The test consists in using bitumen as glue media between the polished rock surface and a stub (Fig. 1).

The samples were prepared at a temperature of 165 °C. Four stubs were positioned on each stone surface. The samples were tested at different time intervals (24, 48, 96, 240 h) after conditioning in a climatic chamber at 25 °C and 30 % humidity (dry conditioning) and in a filtered water bath at 40 °C (wet conditioning). The wet samples were further conditioned for one hour in dry conditions at 25 °C prior testing.

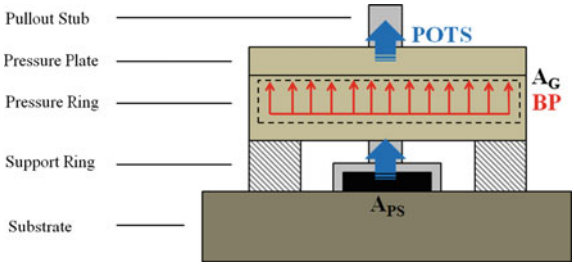


**Fig. 1** Bitumen bond strength test: schematic representation of the test. The different components used to evaluate the pull off tensile strength (POTS) are highlighted: the contact area between the gasket and the pressure plate ($A_G$); the burst pressure (BP) and the area of the pull off stub ($A_{PS}$)

After testing, the maximum pull-off tension was recorded and the failure type observed. If less than 50 % of the substrate surface is exposed, the failure was considered cohesive, otherwise adhesive.

The pull-off tensile strength (POTS) is determined as:

$$\text{POTS} = \frac{(\text{BP} \cdot \text{A}_\text{G}) - \text{C}}{\text{A}_\text{PS}} \text{ [kPa]} \tag{2}$$

where, BP is the burst pressure [kPa], $A_G$ the contact area of the gasket with the reaction plate [$mm^2$], C is the piston constant and $A_{PS}$ the area of the pull-off stub [$mm^2$].

In order to compare the results from the different tests, a pull-off tensile strength ratio (POTSR) was evaluated as:

$$\text{POTSR} = \frac{\text{POTS}_\text{w}}{\text{POTS}_\text{d}} \cdot 100 \, [\%] \tag{3}$$

No particular limitations on the pull-off strength value are suggested by the draft standard or the literature.

## 3 Analysis and Discussion of the Results

The maximum ITS for the four mixtures was measured for two different conditions, dry and wet. The results are presented in Fig. 2. These results indicate that the tensile strength depends on the type of conditioning and significantly decreases when the samples are stored in water. The metasandstone and greywacke (A and C) mixtures showed similar susceptibility to water conditioning and recorded the lower ITS values. These mixtures also measured the higher average air voids content after the 25 blows compaction. Moreover, A and D record a high standard deviation in the wet samples of 33.6 and 35.3 kPa respectively.

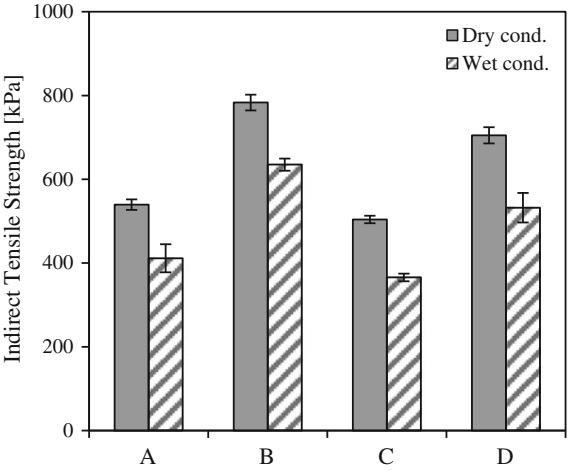


**Fig. 2** Maximum indirect tensile strength of the mixtures after dry and wet conditioning

The ITSR results are 76.24 % for A, 81.06 % for B, 72.55 % for C and 75.46 % for D. The Norwegian specification requires a minimum value of 70 % (NPRA 2014). In this case all the asphalt mixtures performed within the limits of this specification.

Figure 3 shows the results obtained from the rolling bottle test for the different aggregate types. As the rolling time increases, the degree of coverage of B, C and D decreases almost uniformly, reaching a final value, after 72 h of 28, 35 and 40 % respectively. Conversely, A's aggregates show a sudden significant drop in the degree of coverage and appeared completely washed off of the bitumen at the end of the test. The deviation of the results was not included in the graph in favor of a better readability; the standard deviation did not exceed 5 %. Moreover, since the Norwegian specification limits the minimum degree of coverage after 48 h to 25 % (NPRA 2014), the mineral aggregate A combined with the bitumen used in this study, would be rejected.

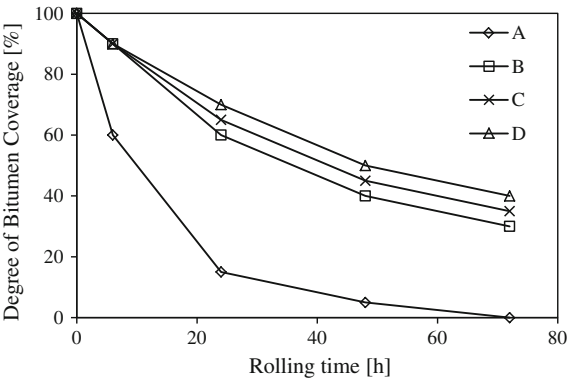


**Fig. 3** Degree of coverage of the aggregates after 24, 48 and 72 h for A (**a**), B (**b**), C (**c**) and D (**d**)

The aggregate-bitumen bond strength was determined using the BBS test. In Fig. 4a distinct difference between the dry and the wet conditioning is already visible in the A, C, and D samples conditioned after 6 h and increases with the time. A rapid worsening of the pull-off strength of the wet group is measured between the 48/96 and 240 h conditioning while the dry group tends to stabilize very quickly. B also shows a clear difference between wet and dry samples but only in the last measurement. A higher standard deviation, of up to 0.16 MPa is calculated for the $POTS_w$ of A and C after 96 and 240 h respectively. A cohesive failure type (within the bitumen layer) is observed in all cases.

A summary of the measured values recorded after the prescribed conditioning time, and the POTSR calculated at the different intervals is given in Table 1.

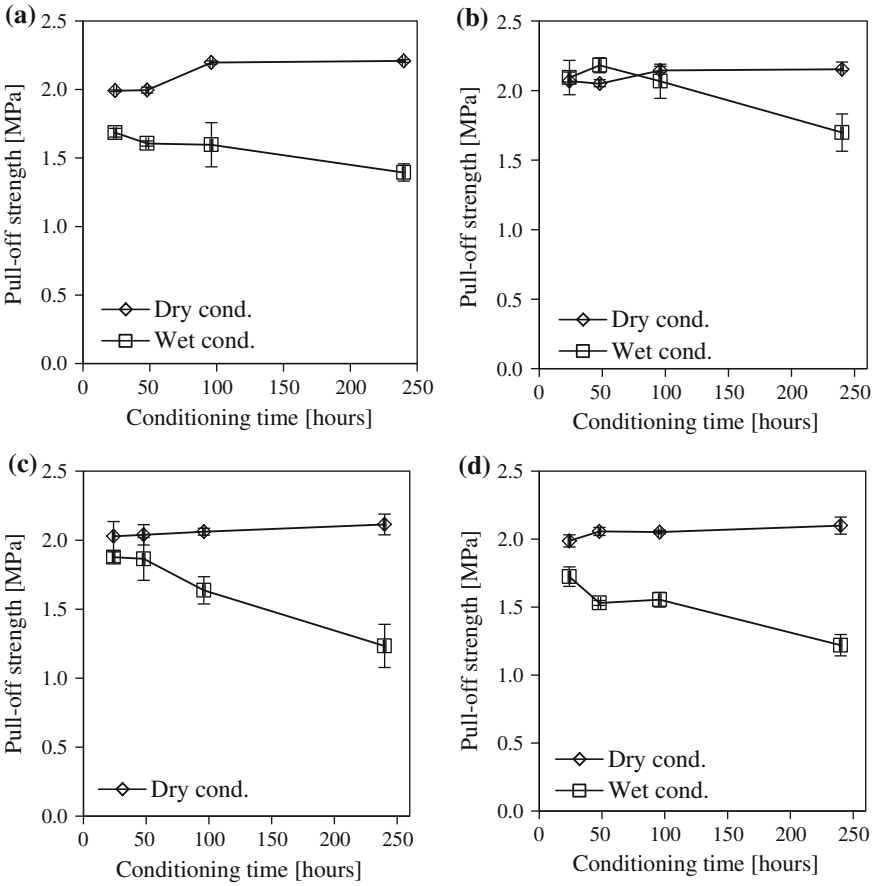


**Fig. 4** Influence of conditioning and time on the pull-off strength for the different substrates, A (**a**), B (**b**), C (**c**) and D (**d**)

**Table 1** Evaluation of the moisture susceptibility

| | Cond. time (h) | A | B | C | D |
|---|---|---|---|---|---|
| ITSR (%) | 72 | 76.2 | 81.1 | 72.6 | 75.5 |
| RB (%) | 48 | 5.0 | 40.0 | 45.0 | 35.0 |
| POTSR (%) | 24 | 84.6 | 101.2 | 92.5 | 86.8 |
| POTSR (%) | 48 | 80.5 | 106.5 | 91.5 | 74.4 |
| POTSR (%) | 96 | 72.7 | 96.4 | 79.4 | 75.8 |
| POTSR (%) | 240 | 63.1 | 78.9 | 58.4 | 58.1 |

As both the ITS and the rolling bottle test are routine test methods, clear directions to evaluate the conformity to the requirements are provided. After respectively 72 and 48 h of conditioning in water, the water susceptibility of the specimens is evaluated. A minimum requirement for the pull-off test is instead needed.

Table 2 shows how the different mixtures were ranked in the ITS test and rolling bottle test according to the specifications. Although the samples B, C and D scored similar results in the rolling bottle test, differences are visible between the outcomes of this tests and of the ITS test. The POTSR evaluated at different time intervals are instead reasonably congruent (see also Table 1). However, the ranking of the different mixtures does not agree with the ITS and rolling bottle test.

In Figs. 5 and 6a Bland-Altman plot (or difference plot) was used to show any agreement between the different test methods and estimating their total error. The Bland-Altman method is based on visualization of difference of the measurements by two methods using a graphical method to plot the difference against the mean of the measurements. Given that different test methods designed to evaluate the same property should have a good correlation, the difference plots show the difference between the values recorded in the two different test methods on the vertical axis (POTSR—ITSR in Fig. 5 and POTSR—degree of coverage in Fig. 6), against the values belonging to the traditional test method (ITSR firstly and degree of coverage secondly) on the horizontal axis. In each chart, the differences between the two procedures are evaluated for the POTSR measured after the different conditioning periods. A horizontal line represents the error between the two test methods. It is calculated as the average value per each conditioning period.

**Table 2** Ranking of the aggregates depending on moisture susceptibility

| | Cond. time (h) | A | B | C | D |
|---|---|---|---|---|---|
| ITSR (%) | 72 | 2 | 1 | 4 | 3 |
| RB (%) | 48 | 4 | 2[a] | 3[a] | 1[a] |
| POTSR (%) | 24 | 4 | 1 | 2 | 3 |
| POTSR (%) | 48 | 3 | 1 | 2 | 4 |
| POTSR (%) | 96 | 4 | 1 | 2 | 3 |
| POTSR (%) | 240 | 2 | 1 | 3 | 4 |

[a]Very close degree of coverage of the mixtures after 48 h

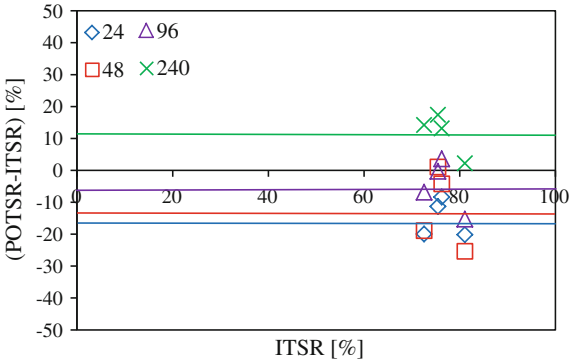


**Fig. 5** Bland-Altman plot between POTSR and ITSR

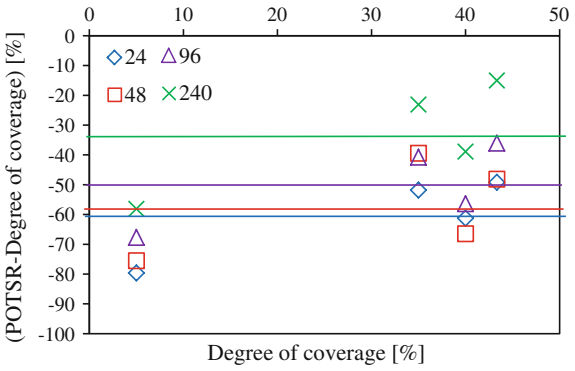


**Fig. 6** Bland-Altman plot between POTSR and the degree of coverage of the aggregates measured with the rolling bottle test

With an average value of −5 and −34, the 96 and 240 h conditioning period appear to give the best correlation respectively with the ITS test and with the rolling bottle test.

## 4 Conclusions

As suggested by the literature, water sensitivity of the asphalt pavements is directly related to the chemical interaction of its constituents, asphalt and mineral aggregates. However the complexity of the phenomenon makes it difficult to estimate the propensity of the mixture towards moisture damage. This study has attempted to compare routinely used moisture sensitivity tests (i.e. the indirect tensile strength test, the rolling bottle test and the bitumen bond strength test) for the purpose of evaluating their relative ability to estimate water damage on asphalt mixtures.

Although the sample size is small in this study, the following indications are clear from the analysis of the results:

- In all cases it is possible to measure an effect of water conditioning. However the magnitude of the effect measured per asphalt mixture, differs depending on the testing method.
- There is no strong relationship between the rolling bottle values and the moisture sensitivity measured with the ITS and BBS test. On the other hand, the ITS test and the BBS test appear to sufficiently agree in discriminating the best performing mixture from the others.
- A statistical analysis suggested that a conditioning time of 96 and 240 h in water for the BBS samples, gives the most similar results to the ITS and rolling bottle specimens respectively (evaluated after 72 and 48 h of conditioning).

Based on the testing procedures and on the results, it is possible to conclude that the tests estimate the moisture damage of asphalt mixtures in different terms and taking into account different characteristics of the mixture. While it is not possible to clearly identify which method better fulfill its scope, because of the difficulty in designing an effective test method but also in evaluating the moisture damage on the field pavement performance, the results presented in this paper suggest the BBS as a more viable option. Compared to the ITS test it largely reduces the test variables associated with the mixture design, while compared to the rolling bottle test it greatly improves the objectivity of the results focusing on both cohesion and adhesion of the aggregate-bitumen system.

**Acknowledgements** This research was sponsored by the Norwegian Public Road Administration and AVINOR. The authors thank the Modified Asphalt Research Center and its technical staff.

## References

AASHTO 2013. Determinating Asphalt Binder Bond Strength by Means of the Binder Bnd Strength (BBS) Test (Draft).

AIREY, G. D. & CHOI, Y.-K. 2002. State of the art report on moisture sensitivity test methods for bituminous pavement materials. *Road Materials and Pavement Design,* 3, 355-372.

BAGAMPADDE, U., ISACSSON, U. & KIGGUNDU, B. 2005. Influence of aggregate chemical and mineralogical composition on stripping in bituminous mixtures. *The international journal of pavement engineering,* 6, 229-239.

BERGER, E., MONISMITH, C., KWONG, J. & NODES, J. Summary Report: Breakout Session 2—Testing and Treatments. Moisture Sensitivity of Asphalt Pavements, A National Seminar, 2003. 293-301.

CANESTRARI, F., CARDONE, F., GRAZIANI, A., SANTAGATA, F. A. & BAHIA, H. U. 2010. Adhesive and cohesive properties of asphalt-aggregate systems subjected to moisture damage. *Road Materials and Pavement Design,* 11, 11-32.

CEN 2008. Bituminous mixtures – Test methods for hot mix asphalt. *Part 12: Determination of the water sensitivity of bituminous specimens.*

CEN 2012a. Bituminous mixtures – Test methods for hot mix asphalt. *Part 30: Specimen preparation, impact compactor.*

CEN 2012b. Bituminous mixtures – Test methods for hot mix asphalt. *Part 11: Determination of the affinity between aggregate and bitumen.*

CURTIS, C. W., ENSLEY, K. & EPPS, J. 1993. Fundamental properties of asphalt-aggregate interactions including adhesion and absorption. National Research Council. Strategic Highway Research Program.

FIGUEROA, A. S., VELASQUEZ, R., REYES, F. A. & BAHIA, H. 2013. Effect of Water Conditioning for Extended Periods on the Properties of Asphalt Binders. *Transportation Research Record: Journal of the Transportation Research Board,* 2372, 34-45.

KIGGUNDU, B. M. & ROBERTS, F. L. 1988. Stripping in HMA mixtures: State-of-the-art and critical review of test methods. National Center for Asphalt Technology Auburn, AL.

LITTLE, D. N. & JONES, D. Chemical and mechanical processes of moisture damage in hot-mix asphalt pavements. National seminar on moisture sensitivity of asphalt pavements, 2003. San Diego California, 37-70.

MORAES, R., VELASQUEZ, R. & BAHIA, H. U. 2011. Measuring the effect of moisture on asphalt-aggregate bond with the bitumen bond strength test. *Transportation Research Record: Journal of the Transportation Research Board,* 2209, 70-81.

NPRA 2014. Håndbok N200 Vegbygging.

SOLAIMANIAN, M., HARVEY, J., TAHMORESSI, M. & TANDON, V. Test methods to predict moisture sensitivity of hot-mix asphalt pavements. Transportation Research Board National Seminar. San Diego, California, 2003. 77-110.

# Hydrothermal Study of Roads with De-freezing Surface, Obtained by the Circulation of a Warm Fluid in a Bonding Porous Asphalt Layer

**S. Asfour, F. Bernardin, C. Mauduit, E. Toussaint and J.M. Piau**

**Abstract** Winter maintenance operations for road networks are an important issue for maintaining mobility in downgraded situations, but generate high exploitation cost and carry environmental impact. This article deals with the study of a road structure free of such constraints, thanks to a bonding porous asphalt layer, circulated by a warm fluid, to prevent ice formation at the road surface. As part of an integrated vision promoting the use of renewable energy, such device could be used to capture the thermal energy available at the road surface during warm periods, to transport it to a storage place (e.g. geothermal) and use it during cold periods. Here we focus on the heat exchange function between the fluid and the road, the storage function, external to the road, being not addressed. Neither do we address here the mechanical and durability aspects of such pavement structures, which of course remain an important issue for the applicability of the innovation. The pavement structure to be considered has three asphalt layers with 2–3 % transversal slope. The wearing course layer and the base course layer are formed of usual materials with hydrocarbon-based binders. The material of the bonding course layer has a porosity of 20 %. Firstly a thermo-hydraulic 2D model is developed to simulate the temperature field in the road structure when the fluid is injected at the upper part of the transversal slope with a target temperature at the surface. Secondly, the sensitivity of the temperature distribution at the road surface is analysed by varying different model parameters such as hydraulic conductivity, transversal slope, thermal conductivities and heat capacities. In each case the minimum fluid injection

S. Asfour · F. Bernardin (✉) · C. Mauduit
Centre for Studies and Expertise on Risks, Environment, Mobility, and Urban and Country Planning (Cerema), Clermont-Ferrand, France
e-mail: frederic.bernardin@cerema.fr

E. Toussaint
Université Blaise Pascal, Clermont Université, Institut Pascal, 10448, 63000 Clermont-Ferrand, France and UMR 6602, CNRS, Institut Pascal, 63171 Aubière, France

J.M. Piau
French Institute of Science and Technology for Transport, Development and Networks (Ifsttar), Nantes, France



F. Canestrari and M.N. Partl (eds.), *8th RILEM International Symposium on Testing and Characterization of Sustainable and Innovative Bituminous Materials*, RILEM Bookseries 11, DOI 10.1007/978-94-017-7342-3_44

temperature is determined in order to keep positive the road surface temperature at any point for given meteorological data.

**Keywords** Road · Porous asphalt · Heat transfer fluid · Renewable energy · Surface temperature control · Thermo/hydraulic model

## 1 Introduction

In order to guarantee the safety and mobility of road users during the winter, ensuring the viability of road networks necessitates the mobilisation of significant material and financial resources to maintain adequate quality of services. In addition to these economic factors, the use of road de-icers is a considerable source of environmental stress, as well as a cause of damage to the bodies of vehicles.

For these reasons, research has been undertaken in recent years to study alternative measures that will prevent the formation of black ice and snow deposits on road surfaces. Various innovations have been studied; among these are the use of electric heating elements inserted into the material of the roadway (Tang et al. 2005). However, this method requires large amounts of (electrical) energy. Another method consists of inserting heating coils into the wearing course and circulating a heat-transferring fluid in them in order to capture and store energy in warm periods and use it to heat roads in winter. Eugster (2007), Zhang and Debendra (2009), Yu et al. (2014) cite several operational projects of this type, including the Serso project in Switzerland, a test bridge in Berkintin, China, and a railroad application in Germany, as well as projects in the United States and Japan.

These measures, which are of interest from an energy-related perspective, nevertheless present elevated risks of deterioration under the effects of mechanical stresses on roadways caused by traffic, in particular, and have significant disadvantages for road upkeep, notably when surface-layer repairs become necessary.

This is why, in keeping with these types of measures, we have chosen to examine an alternative that will allow us to avoid the insertion of a "physical circuit" in the body of the roadway. Our proposal is based on the use of draining asphalt in the bonding course layer, enabling the circulation of heat-transferring fluid via gravitational flow and benefiting from the transversal slope present in standard roadway sections. A very recent study of a similar measure was conducted independently by Schacht et al. (2014).

In this paper we will develop a thermohydraulic model used to simulate the thermal exchanger function of a road where heat-transferring fluid circulates in its bonding course layer and undergoes a convection phenomenon at its surface. A study of surface-temperature sensitivity has been conducted in terms of various road parameters (thermal and hydraulic) and of the fluid injection temperature upstream of the transversal slope. The results presented are based on experiments conducted on a laboratory model to assess the hydraulic conductivity of the

draining layer. In the final section of this paper, we will establish the relationship between the injection temperature of the fluid and the convective exchange coefficient at the surface, which will enable us to guarantee the maintenance of the entire road surface under frost-free conditions at a given outside temperature.

This research falls within the scope of the European "Forever Open Road" project, supported by the Forum of European Highway Research Laboratories (FEHRL), as well as of the French "Route de cinquième génération" ["Fifth-generation road"] (R5G) project, led by IFSTTAR and CEREMA (French Institute of Science and Technology for Transport, Development, and Networks; Centre for Study and expertise on Risks, the Environment, Mobility, and Development), which work to promote the precepts of ecology and the use of renewable energy.

The mechanicals aspects and durability of the proposed solution, both in terms of materials that regardless of the pavement structure, are not treated in this paper.

## 2 Hydrothermal Study of Concept

The road surface being studied is composed of three bituminous layers, with the central layer composed of highly porous draining asphalt allowing the circulation of a heat-transferring fluid via gravitational flow under a transversal slope effect. The formulation of the bituminous layers follows the French standards (gyratory shear compactor test, Duriez compression tests, etc.).

The space variables of the model (Fig. 1) are dimension $y$ according to the inclined sub-vertical axis of transversal slope angle $\beta$ and abscissa $x$ transversal to the road (the road is assumed to have no longitudinal slope and to be infinite in its third dimension). We use $h$ to denote the height of the road surface; and $L$ for its length. The hydraulic system is assumed to be stationary and independent of temperature. Thermal stresses may be transient. This gives us the following model (Reddy and Gartling 2010), where $i$ designates the index of the layer being considered. For $0 \leq x \leq L$ and $0 \leq y \leq h$,

$$\begin{cases} (\rho C)_i \dfrac{\partial T}{\partial t}(t,x,y) = \lambda_i \Delta T(t,x,y), \ i = 1 \ or \ i = 3 \\ (\rho C)_2 \dfrac{\partial T}{\partial t}(t,x,y) + (\rho C)_f v \dfrac{\partial T}{\partial x}(t,x,y) = ((1-\phi_2)\lambda_2 + \phi_2 \lambda_f)\Delta T(t,x,y) \\ v = -K \dfrac{\mathrm{H}_2 - \mathrm{H}_1}{\mathrm{L}} \end{cases} \quad (1)$$

where $(\rho C)_i, \lambda_i, \phi_i, (\rho C)_f, \lambda_f, v$ and $K$ designate density, thermal conductivity and porosity of layer $i$, specific heat and thermal conductivity of the fluid, Darcy speed of the fluid and hydraulic conductivity of the draining asphalt, respectively. $H_1$ and $H_2$ are the hydraulic loads imposed upstream and downstream of the circulation of fluid in the porous asphalt layer. Our interest is in studying flow in a saturated environment, due to the difference of hydraulic heads $\mathrm{H}_1 - \mathrm{H}_2 \geq \beta L$ with $\beta$ = transversal

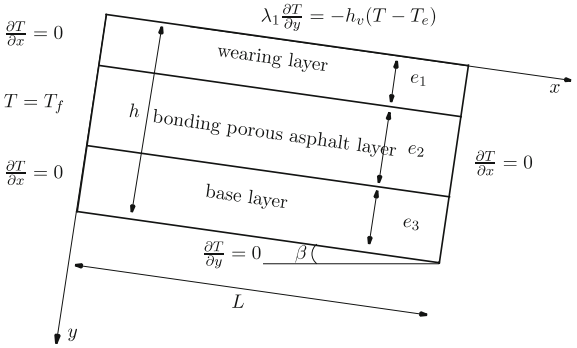


**Fig. 1** Schema of roadway with its limit conditions ($T_f$ and $T_e$ are the injection temperature of the fluid and the temperature of the outside air, respectively)

slope angle. Field $T$ is the temperature in the body of the roadway (we are assuming equality at all points between the temperatures of the fluid and the draining asphalt). At the interfaces between layers, conditions of continuity of temperature and thermal flow are imposed. The limit conditions used in the study are shown in Fig. 1. The model is simulated via discretisation at finite differences in space and a Euler schema that is implicit in time. The associated code was applied in Fortran 90.

## 3 Sensitivity Study

The model above has enabled us to study the thermal response of the road and its sensitivity to a number of parameters: the temperature of the outside air $T_e$, the convective exchange coefficient at the surface $h_v$, the specific heats $(\rho C)_i$ and thermal conductivities $\lambda_i$ of the layers of the roadway, the hydraulic conductivity $K$, the transversal slope $\beta$, the thickness of the porous asphalt layer $e_2$, the injection temperature of the fluid $T_f$, and the specific heat of the fluid $(\rho C)_f$.

For this sensitivity study we have used the Sobol indices Salteli et al. (2008). This is an overall sensitivity analysis that allows us to assign an index $S_i$ of between 0 and 1 to each parameter to which the surface temperature is sensitive. We can write formally, for any point $x$ of the surface:

$$T_s(x) = f_x(p_1, \ldots, p_n)$$

where $T_s(x)$ is the surface temperature at point $x$ and $p_1, \ldots, p_n$ are the input parameters of the model. By assigning a law of probability to each of the parameters $p_1, \ldots, p_n$, which we assume to be independent of one another, we calculate the Sobol indices of each parameter $p_i$ by:

$$S_i = \frac{V(E(T_s(x)|p_i))}{V(T_s(x))}, \qquad \begin{array}{l} E(\cdot|\cdot) : \text{ conditional expectation} \\ V : \text{ variance} \end{array}$$

The laws of probability chosen are uniform laws, the standard deviation of which is 10 or 20 % of their average. Conditional expectations and variances are calculated using a quasi-Monte Carlo method (10,000 samples instead of the several million made in the classic Monte Carlo method). The average values considered are listed in Table 1 and drawn from NF P98-150-1 (2010), Lui (2012).

The exchange coefficient $h_v$ is dependent on the wind speed $V_{vent}$ according to Mcinerney et al. (2006):

$$\begin{cases} h_v = 5.6 - 4V_{vent} & \text{if } V_{vent} \leq 5 \text{ m s}^{-1} \\ h_v = 7.2V_{vent}^{0.78} & \text{if } V_{vent} \geq 5 \text{ m s}^{-1} \end{cases}$$

We will assume in the following a wind speed varying between 0 and 8 m $s^{-1}$, which leads to a coefficient $h_v$ varying between 5.6 and 36.5 $Wm^{-2}K^{-1}$. Here, we will consider a value $h_v = 21$ $Wm^{-2}K^{-1}$.

The values of the parameters in Table 2 are the values used for a pure water-type fluid.

The values of the parameters in Table 3 are the values of the experimental model discussed in Sect. 4 with the exception of the parameter L, which has been set at 4 m to represent the average width of a real road, instead of 1 m for the laboratory model.

Sobol indices are shown in Fig. 2 for a standard deviation of 10 % depending on position $x$ (similar results with 20 % are not shown here).

The lowest surface temperature is obtained when $x = L$ (4 m). According to Fig. 2, this is highly sensitive to the outside temperature (45 % sensitivity). It then comes down equally to hydraulic conductivity, thickness of porous asphalt layer, transversal slope, and thermal capacity of the fluid, each of them explaining 10–12 % of the sensitivity, convection coefficient, and fluid injection temperature, with each explaining around 4 % of the sensitivity (in comparison to 70 % for both at $x = 0$). The other parameters (thermal parameters of the roadway) have sensitivities lower than 1 %.

According to these results, aside from the geometric parameters (transversal slope, thickness of porous asphalt layer) and those related to the fluid (thermal capacity, injection temperature), two parameters related to the road come into play: the coefficient of exchange via surface convection, and the hydraulic conductivity

**Table 1** Average values used for thermohydric parameters

| Parameter | $\lambda_{1,3}$ ($Wm^{-1}K^{-1}$) | $\lambda_2$ ($Wm^{-1}K^{-1}$) | $(\rho C)_{1,3}$ ($Jm^{-3}K^{-1}$) | $(\rho C)_2$ ($Jm^{-3}K^{-1}$) | $K$ ($ms^{-1}$) | $h_v$ ($Wm^{-2}K^{-1}$) | $T_e$ (°C) |
|---|---|---|---|---|---|---|---|
| Value | 1.4 | 1.03 | 2,254,000 | 1,840,000 | 0.008 | 21 | −10 |

**Table 2** Fluid parameter values

| Parameter | $T_f$(°C) | $(\rho C)_f$ ($Jm^{-3}K^{-1}$) | $\lambda_f$ ($Wm^{-1}K^{-1}$) |
|---|---|---|---|
| Value | 22 | 4,181,000 | 0.6 |

**Table 3** Values of geometric roadway parameters

| Parameter | $L$ (m) | $e_1$ (m) | $e_2$ (m) | $e_3$ (m) | $\beta$ (–) | $\phi_2$ (–) |
|---|---|---|---|---|---|---|
| Value | 4 | 0.06 | 0.08 | 0.05 | 0.01 | 0.2 |

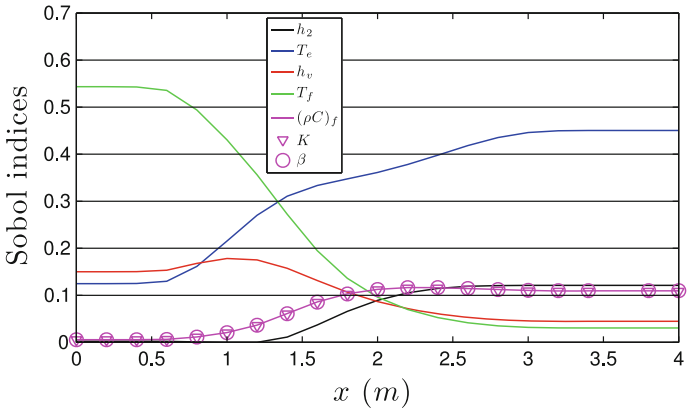


**Fig. 2** Sobol indices for a standard deviation of 10 %

of the porous asphalt layer. In the following, we will focus on the experimental measurement of the latter, and then on the influence of the exchange coefficient and outside temperature on the temperature of the injected fluid, with the latter being the sole controllable variable after the construction of the pavement to keep the road surface above the freezing point.

## 4 Hydraulic Study Conducted on a Laboratory Model

### *4.1 Experimental Apparatus*

In this section we describe the laboratory model set up in the Laboratory Department of Clermont-Ferrand under the regional East-Central direction of CEREMA. The model was drawn from a sample 1 m in length, 0.8 m in width, and 0.19 m in height, built on an experimental roadway constructed in 2013 at Egletons, France. The road is composed of three layers: a wearing course layer of semi-phaneritic asphalt concrete 0.06 m thick; a bonding course layer of 0/14 porous asphalt 0.08 m thick; and a base layer of asphalt concrete with a scaled-up thickness of 0.05 m.

The sample, with a transversal slope of 1 %, was placed on a waterproofed wooden slab and enclosed lengthwise by Plexiglas plates. Two plates of Plexiglas upstream and downstream were used to construct two tanks for the supply and recovery of fluid circulating in the bonding course layer (see Fig. 3a). A pump was

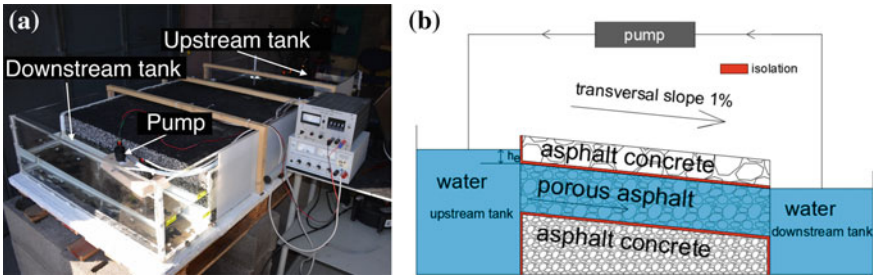


**Fig. 3** Laboratory mock-up photograph (**a**) and operating schema (**b**)

used to remove fluid from the downstream tank and reinject it into the upstream tank. The pump's power was adjusted to achieve stationary hydraulic regime corresponding to different losses of hydraulic heads between the upstream and downstream sites (fluid levels in the tanks). Fluid circulation was maintained in the porous asphalt layer by a watertight seal between it and the underlying layer. A schema of the mock-up is shown in Fig. 3b.

## *4.2 Determination of Saturated Hydraulic Conductivity of Porous Asphalt Layer*

The objective was to measure the hydraulic conductivity of the porous asphalt layer in a quasi-horizontal position, based on the relationship linking the outputs measured experimentally to the hydraulic loads imposed upstream and downstream.

To ensure total saturation of the entire porous asphalt layer, the pump is adjusted so that the fluid is located upstream and downstream respectively, above, and at the level of the upper surface of the porous asphalt layer,.

The fluid circulates in this layer from the upstream reservoir to the downstream reservoir via gravity under the effect of a 1 % transversal slope. Differences of hydraulic head between upstream and downstream of +1, +2, +3, and +4 cm were tested, which take into account the value $\beta L = 1$ cm, corresponding to a fluid level $h_e$ in the upstream reservoir higher than the upper face of the porous asphalt layer of 0, +1, +2, and +3 cm, respectively (see Fig. 4).

The outputs of the pump in a stationary rate of flow were measured in each of the cases and are shown in Table 4.

According to Darcy's law, $Q = KA\frac{\Delta H}{L}$ where $L = 1$ m and $A = 0.8 * 0.08$ m$^2$ are the flow length and the length of the porous asphalt layer section, respectively. Figure 5 shows the experimental points from Table 3 and the associated line of linear regression. We can see that the experimental results take into account a linear relationship between $Q$ and $\Delta H$, corresponding to $K = 0.0218$ ms$^{-1}$. This value is significantly higher than the one in Table 1 (0.0081 ms$^{-1}$); this is due to the use of a 0/14 draining asphalt containing 10_14 aggregates proportion of 47 %.

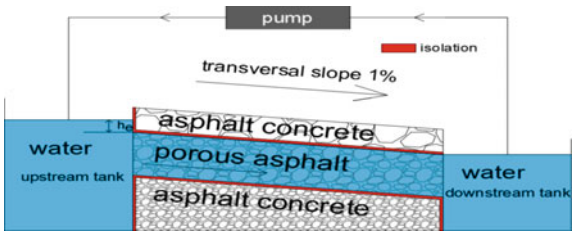


**Fig. 4** Schema of fluid circulation at saturation

**Table 4** Experimental outputs depending on the differences in hydraulic load between the upstream and downstream tanks, with saturation of the porous asphalt layer

| $\Delta H = H_1 - H_2(m)$ | 0.0 | 0.01 | 0.02 | 0.03 | 0.04 |
|---|---|---|---|---|---|
| $Q(\mathrm{m}^{-3}\ \mathrm{s}) * 10^{-5}$ | 0.0 | 1.72 | 3.04 | 4.64 | 5.53 |

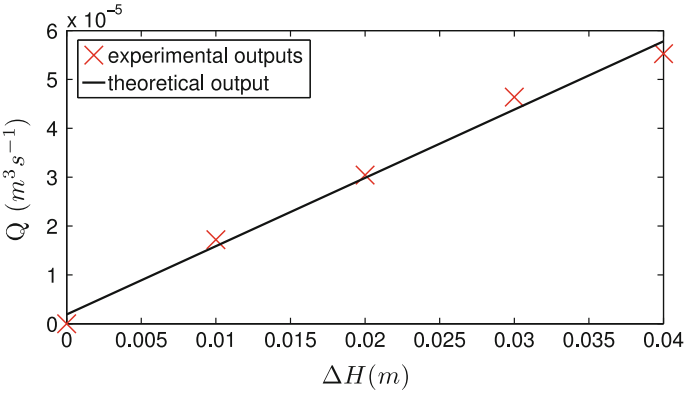


**Fig. 5** Experimental outputs according to difference in load and associated line of linear regression

## *4.3 Determination of the Hydraulic Conductivity for a Free-Surface Flow in the Draining Layer*

In the case of flow at saturation, the relationship between flow output and difference in hydraulic load is linear. In the case of a free-surface flow, it is necessary to define this relationship in order to back-calculate the conductivity. To do this, a groundwater model has been adjusted below in order to measure this conductivity indirectly.

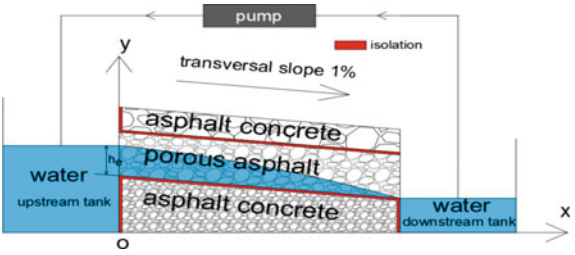


**Fig. 6** Circulation schema of fluid in free-surface flow

In this case, the downstream fluid level is maintained at the level of the lower surface of the porous asphalt layer, whereas the upstream level is fixed between the lower and upper surfaces (see Fig. 6). This level $h_e$ is chosen to vary upstream at +2, +4, +6, and +8 cm above the lower surface of the porous asphalt layer.

The results of the measurement of the experimental output $\boldsymbol{Q_{exp}}$ depending on $\boldsymbol{h_e}$ are given in Table 5.

As we will show, the results of Table 5 are consistent with a hydraulic conductivity $\boldsymbol{K}$ determined on the basis of the model given by Eq. 2.

Consider the reference point (0, $x$, $y$) defined on the schema in Fig. 1. The upstream and downstream surfaces of the porous asphalt layer have the equations $x = 0$ and $x = L(\cos(\beta) \approx 1)$, respectively. We write $y_s(x) = -\beta x$ as the equation for the lower surface of the porous asphalt layer and $y_l(x)$ for that of the free surface. For $0 \le x \le L$ and $0 \le y \le y_l(x)$, the hydraulic head at point ($x$, $y$) is equal to $H(x, y) = y_l(x)$. The output $Q$ crossing the section at $x$ of the groundwater table is constant, independent of x, and by integration into the height of the groundwater table of the local Darcy's law, we get:

$$\begin{aligned} Q &= -K \int_{y_s(x)}^{y_l(x)} \frac{dy_l(x)}{dx} dx' = (y_l(x) - y_s(x)) \frac{dy_l(x)}{dx} \\ &= constant \end{aligned} \tag{2}$$

Knowing that $y_l(0) = h_e$ and $y_l(L) = 0$, it is possible to integrate the differential equation given by Eq. 2 with unknown function $y_l$ in order to obtain the implicit equation Eq. 3 to determine the output $Q$:

$$X \ln\left(1 - \frac{1}{X}\right) = -\left(1 + \frac{\beta L}{h_e}\right) \tag{3}$$

**Table 5** Experimental output depending on water height upstream with free-surface circulation in the porous asphalt layer

| $\Delta H = H_1 - H_2(m)$ | 0.0 | 0.02 | 0.04 | 0.06 | 0.08 |
|---|---|---|---|---|---|
| $Q(\mathrm{m}^{-3}\ \mathrm{s}) * 10^{-5}$ | 0.0 | 0.31 | 1.34 | 4.06 | 6.69 |

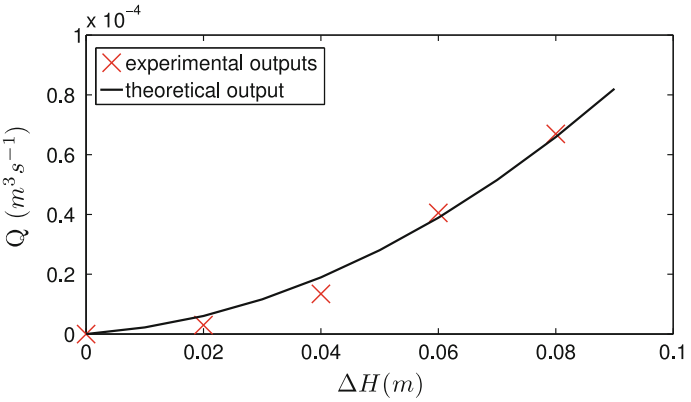


**Fig. 7** Experimental and theoretical outputs depending on difference in load

with $Q = \beta h_e KX$. A hydraulic conductivity value of $0.022\,\mathrm{ms}^{-1}$ leads to the best adjustment between the model and the experimental points in Table 5 (see Fig. 7), giving us a value very close to the hydraulic conductivity previously determined in the saturated case.

However, it seems that from an operational point of view, it would be of interest to target flow conditions of the type envisaged in Sect. 4.2, enabling the total saturation of the whole draining asphalt layer and favoring exchanges of heat with the surface layer by eliminating any air gap liable to act as a thermal insulator. However, we must also ensure that the water pressure applied to the upper surface of the porous asphalt layer remains weak enough not to cause de-cohesion of its interface with the surface layer at long run.

## 5 Optimisation of Fluid Injection Temperature to Keep Road Surface Above Freezing

In this section, we wish to test the efficiency of the innovation at maintaining the road surface temperature above zero at all points. To do this, we must define the lowest possible fluid injection temperature value $\theta_{min}^{fluid\ inj}$ for various values of the exchange coefficient by convection and outside temperatures, leading to a temperature that is only just zero at $x = L$.

We recall that our thermohydraulic model is based on Eq. 1 (flow at saturation) with the limit conditions given in Fig. 1. We will use the parameter values from Tables 1, 2, and 3, except for the hydraulic conductivity value, which is considered to be equal to $0.02\,\mathrm{ms}^{-1}$ according to the results of Sect. 4.2. The road width $L$ is considered to be 4 m.

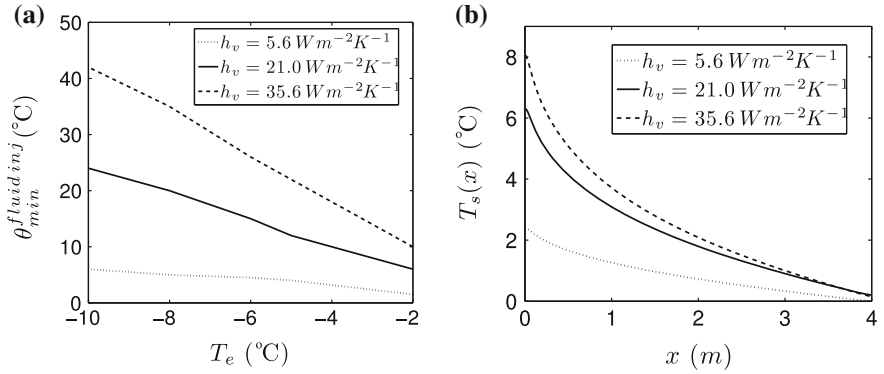


**Fig. 8** **a** Evolution of minimum fluid injection temperature with outside temperature for $h_v$ = 5.6, 21, and 36.5 $\mathrm{Wm^{-2}K^{-1}}$ for abscissa $L = 4$ m and **b** profile of surface temperature with fluid circulation for different values of $h_v$ and $T_e = -10\,^{\circ}\mathrm{C}$.

Figure 8 shows, for these conditions, the relationship between $\theta_{min}^{fluidinj}$ and the outside temperature for three values of exchange coefficients ($h_v = 5.6, 21,$ and 36.5 $\mathrm{Wm^{-2}K^{-1}}$.

We can see in Fig. 8a that, for a moderate case in which $h_v = 21\mathrm{Wm^{-2}K^{-1}}$, the minimum fluid injection temperature must be 24 °C for an outside temperature of −10 °C in order to ensure a positive surface temperature for the whole width of the road. Figure 8b shows the surface temperature profiles according to the flow distance for an outside temperature of −10 °C and for values of $h_v$ : 5.6 $\mathrm{Wm^{-2}K^{-1}}$, 21 $\mathrm{Wm^{-2}K^{-1}}$, and 36.5 $\mathrm{Wm^{-2}K^{-1}}$.

## 6 Conclusion

In this article, we have presented a thermo-hydraulic model used to simulate thermal exchanges between a road in which a heat-transferring fluid is circulating in a porous bonding course layer and where the ambient environment on the surface is represented by an outside temperature and a convection coefficient. A sensitivity study of the road surface temperature was conducted depending on various pavement parameters (thermal and hydraulic) and on the fluid injection temperature upstream of the transversal slope. The presented results are based on experiments conducted on a laboratory mock-up to assess the hydraulic conductivity of the porous asphalt layer.

The sensitivity study of surface temperature depending on thermo-hydraulic parameters showed that the most influential parameters are the injection temperature of the heat-transferring fluid, its calorific capacity and the hydraulic conductivity of the porous asphalt layer.

Experiments on a laboratory mock-up were used to determine the hydraulic conductivity value of the porous asphalt layer, which is found to be about 2 cm $s^{-1}$.

Numerical simulations done with this value show the potential efficiency of this innovative construction technique in adverse weather conditions. An injection temperature of 24 °C would enable road surfaces to be kept above freezing at an outside temperature of −10 °C, and for an average convective exchange coefficient on the surface. More extensive simulations would make it possible to estimate the effectiveness of the system during snowy weather, at outside temperatures that would be theoretically higher than those here considered, but for conditions that would need additional energy to melt snow and counteract its latent heat.

Given the results of this project, an experimental study under meteorological stress will also be conducted on the same mock-up in order to validate our theoretical results.

## References

Eugster, W. (2007) Road and Bridge Heating Using Geothermal Energy, Proceedings European geothermal Congress 2007, Unterhaching, Germany, 30 May-1 June 2007

Liu, Q. (2012) Induction Healing of Porous Asphalt Concrete, Master of Science in Materials Science Wuhan University of Technology, P.R China, GeborenteXihua Henan, P.R China, October 2012

Mcinerney, M. Trvillion, J. Lozar, R. Abdallah, T. Majumdar, A. (2006) Classifying infrastructure using thermal IR signatures, U.S. Army Engineer Research and Development Center (ERDC) Construction Engineering Research Laboratory (CERL): ASPRS 2006 Annual Conference, Reno, Nevada, May 1-5, 2006

NF P98-150-1 (2010) Bituminous asphalts - Laying of pavement bases, binder and wearing courses - Part 1: hot-mix asphalts - Constituents, formulation, fabrication, transport, laying and site inspection

Reddy,J.N., Gartling, D.K, (2010) The Finite Element Method in Heat Transfer and Fluid Dynamics, Third Edition, CRC Press, 2010

Salteli, A. Ratto, M. Andres, Terry. Campolongo, F. Cariboni, J. Gatelli, D. Saisana, M. Tarantola, S. (2008) Global Sensitivity Analysis: The Primer, John Wiley & Sons, 2008

Scaht, A. Munk, M. Busen, C. Osser, M. Steinauer, B.(2014) Application of a porous interlayer for road temperature control, Institute for road and traffic engineering, RWTH Aachen university, Deutschland, PIARC, XIV International Winter Road Congress, 4-7 February 2014, Andoraa la Vella

Tang, Z. Li, Z. Quian, J. Wang, K. (2005) Experimental study on de-icing performance of carbon-Fiber Reinforced Conductive Concrete, J. Master. Sci. Technol, vol.21, No.1, 2005

Yu, WB., Yi, X., Guo, M., Chen, L. (2014) State of the art and practice of pavement anti-icing and de-icing techniques, Sciences in Cold and Arid Region, Vol.6, Issue1, February, 2014

Zhang, J. Debendra, K. (2009) Selection of Effective and Efficient Snow Removal and Ice control Technologies for Cold-Region Bridges, Journal of Civil, Environmental, and Architectural Engineering, Vol.3, Issue.1, 2009

# Mechanical Behaviour of Asphalt Concrete Containing C&D Recycled Materials

**Edoardo Bocci, Gianluca Cerni and Sandro Colagrande**

**Abstract** Recycling of waste materials is actually one of the main targets in civil engineering, because of economic and environmental features. To this aim, the field of road engineering offers many technical solutions, including the use of recycled materials from construction and demolition of civil works (C&D) in pavement layers. These materials have been investigated to be used as aggregate in asphalt concrete base layers for flexible road pavements. Different percentages (0, 15, 30 and 50 %) of C&D materials were used in order to determine the most suitable solution. The scope was to evaluate both static and dynamic mechanical properties of the mixtures. In particular, a servo-hydraulic control static press was used to run indirect tensile tests and a Nottingham Asphalt Tester was used to determine indirect tensile stiffness modulus and fatigue strength. Specimens were manufactured by mixing the aggregate with 5 % of bitumen and compacted with a shear gyratory compactor to a fixed height, in order to have a constant air voids content equal to 5 %. Experimental results showed that C&D materials can conveniently be used in asphalt concrete for base layers (up to maximum 30 %) without penalizing the mechanical performance of the mixture.

**Keywords** C&D · Recycling · Asphalt concrete · Waste

E. Bocci (✉)
eCampus University, Via Isimbardi, 10, 22060 Novedrate, CO, Italy
e-mail: edoardo.bocci@uniecampus.it

G. Cerni
Università degli Studi di Perugia, Via G. Duranti, 93, 06125 Perugia, Italy
e-mail: gianluca.cerni@unipg.it

S. Colagrande
Università degli Studi dell'Aquila, Via Campo di Pile, 67100 L'Aquila, Italy
e-mail: sandro.colagrande@univaq.it



F. Canestrari and M.N. Partl (eds.), *8th RILEM International Symposium on Testing and Characterization of Sustainable and Innovative Bituminous Materials*, RILEM Bookseries 11, DOI 10.1007/978-94-017-7342-3_45

## 1 Introduction

In the last decades the growing environmental sensitivity and the poor availability of natural resources has been determining an increasing interest in the identification of alternative materials to be used for road construction (Grau 1980). To this aim, the use of debris from the construction and demolition (C&D) of civil structures represents a suitable solution to reduce the employment of the virgin aggregate and the disposal of the waste materials.

According to European Waste Catalogue (EPA 2002), C&D materials are classified in the group 17 09 04, which generically includes "mixed construction and demolition wastes". These materials are typically:

- obsolete, because they completed their service life as concrete structures, piles or railway ties;
- deteriorated, as they include parts of partitions, plasters, tiles and bricks from building renovations, which would need extraordinary maintenance;
- remained, i.e. they can include the surplus from the production of cement concretes and mortars.

C&D materials need to be treated before being used. This treatment, including the crashing, in order to obtain a suitable gradation, and the removal of foreign matters such as iron, paper, wood, plastics, natural and synthetic fibres, can be easily performed by specific plants. In Italy, the most common system for C&D treatment is the Homogenized Recovery of Building Waste—the Italian acronym is ROSE (Cupo-Pagano et al. 1994)

According to the National Association of Recycled Aggregate Producers, 40 % of the waste materials produced in Italy, corresponding to about 35 million t, comes from C&D activities (Bressi and Pavesi 2010). Approximately, they are generated by (ARPAV 2014):

– demolition for maintenance works in small-size residential buildings (53 % by weight);
– demolition for maintenance works of large-size public or industrial buildings (39 % by weight);
– total demolition of buildings (8 % by weight).

Only 10 % of C&D results to be contaminated by dangerous substances as amianthus, oils, solvents, paints and other harmful materials which can hinder the reusing. The remaining 90 % could be actually considered as a resource and largely exploited in road and building construction, allowing to reduce the environmental impact (Benedetti 2001). However, about 5 % of C&D materials is recycled at present (Barbaro 2012), as shown in Table 1.

Nowadays the interest in reusing C&D materials is rapidly increasing worldwide (Chong 2009). The European Union identified the problem of C&D disposal as a priority and defined the strategies to be actuated in each country in order to exploit

**Table 1** Production of C&D in Europe

| Nation | Production of C&D [$10^6$ t] | Reused fraction [%] |
|---|---|---|
| Netherlands | 14 | 60 |
| United Kingdom | 45 | 51 |
| Germany | 53 | 28 |
| Denmark | 2 | 25 |
| France | 25 | 10 |
| Italy | 35 | 5 |
| Spain | 13 | 4 |
| Belgium | 9 | 2 |

C&D as a resource (Symonds Group Ltd. 1999). In particular, the EU Directive 2008/98/EC on waste fixes the objective to recycle at least 70 % of C&D within 2020.

The continual evolution of environmental laws and, in the meantime, the real difficulties on both interpreting the new rules and coordinating them with the previous ones, not expressly or only partially repealed, make the norm fulfilment complex to engineers and companies.

In the field of road engineering, where the reuse of C&D is scanty because of the non-pursuance of the laws (Italian decree DM 203/03 establishes the use of at least 30 % of recycled materials in public works) and the strong cultural resistance, recycled aggregates are typically considered to be a waste rather than a resource, and consequently are mainly used to build embankments or foundation layers (Bocci and Colagrande 1999; Pasetto 2000; Cerni and Colagrande 2012). However, the good physical and mechanical properties of C&D could be exploited in more important layer, as base courses (Herrador et al. 2012; Leite et al. 2011).

## 2 Objective and Experimental Programme

The present paper deals with the investigation on the mechanical characteristics of an asphalt concrete (AC) for base layer containing C&D waste materials.

The objective of the research is to study the behaviour of AC mixtures produced with different percentages of C&D and compare them with a reference AC containing only virgin aggregate (0 % of C&D). In particular, 3 amounts of C&D, corresponding to 15, 30 and 50 %, were evaluated.

Specimens were manufactured with a shear gyratory compactor and were subjected to indirect tensile stiffness modulus (ITSM), indirect tensile fatigue (ITF) and indirect tensile strength (ITS) tests.

ITSM was determined through a servo-pneumatic testing machine, according to EN 12697-26. The applied impulsive load, with a rise time of 124 ms, was adjusted to achieve a target horizontal deformation of 5 μm. During the ITSM test, fifteen

conditioning pulses were followed by five test pulses. The measurements were repeated across two diameters and an average ITSM was calculated by adopting a Poisson's ratio of 0.35 (Graziani et al. 2014). The tests were carried out at 20 °C and 9 repetitions were provided for each mixture.

ITF was determined according to EN 12697-24 by means of the same servo-pneumatic machine. The test was carried out in control load configuration with the aim to measure the number of load cycles which bring the specimen to failure. The ITSM measured, for each mixture, on the same specimens allowed to adjusted the target load. The specimen was considered broken when its two parts completely separated or when a target vertical displacement of 10 mm was reached. Test temperature was fixed to be 20 °C and the number of replicates was 2 for each stress levels, for a total of 6 specimens for each mixture.

A servo-hydraulic testing machine was used to measure the ITS of dry specimens. Specifically, the equipment applies a compression force along the two generatrices until the specimen reaches breaking. A constant rate of deformation of 50 ± 2 mm/min (EN 12697-23) is applied in a continuous manner. The ITS is the maximum tensile stress that causes the conventional failure of a cylindrical specimen. Before testing, each specimen was stored for 4 h in a thermostatically controlled air chamber at 25 °C. Four repetitions were provided for the different mixtures. The ITS was measured the same specimens subjected to ITSM test.

## 3 Materials and Specimen Preparation

The C&D material used was taken from a recycling plant located in the Central Italy while the virgin aggregate was a limestone coming from a crushing plant. The planned production procedures of the recycling plant, based on preliminary sorting and separation processes, create a homogenous material without undesirable component as wood, plastic, metal, paper and glass. Table 2 shows the results of the physical characterization performed on C&D material according to EN 13285.

The grading envelope for base layers provided by Technical Norms of CIRS (CIRS 2003) was chosen as reference to build the gradation curves. In order to avoid compaction problems related to the dimensions of aggregate particles and moulds, the particles retained to the 19.5 mm-sieve were excluded. Figure 1 shows the gradation curve adopted.

The binder was a 70/100 penetration bitumen. A constant amount of bitumen, equal to 5 % by mix weight, was adopted for all the mixtures.

Materials were mixed at the temperature of 150 °C and compacted with a shear gyratory compactor. In this experimental study, the compaction protocol provided: 100 mm diameter mould, constant pressure of 600 kPa, speed of 30 rpm and constant angle of inclination of 1.25°. The number of gyrations was adjusted to reach the target height of 63.5 mm, corresponding to a geometric air voids content of about 5 % (Mahmoud and Bahia 2004).

**Table 2** Physical properties of C&D

| Property | Result | Technical requirement |
|---|---|---|
| Bituminous material ($R_a$) | 2.0 % | <5 % |
| Bricks, ceramics, tiles ($R_b$) | 29.5 % | |
| Concrete, concrete products, mortar ($R_c$) | 25.6 % | >90 %[a] |
| Unbound aggregates, natural stone ($R_u$) | 42.0 % | |
| Glass ($R_g$) | 0.6 % | <5 % |
| Metals, plastic, rubber, gypsum ($X_1$) | 0.2 % | <0.4 % |
| Wood, paper, cellulose ($X_2$) | 0.1 % | <0.1 % |
| Maximum aggregate size | 16 mm | <63 mm |
| Particle density | 2.57 Mg/m$^3$ | – |
| Water absorption | 7.7 % | – |
| Sand equivalent | 27.4 | >40 % |
| Plasticity index | NP | NP |
| Crushed particles | 72 % | >60 % |
| Shape index | 28 % | <40 % |
| Flakiness index | 26.5 % | <35 % |

[a]Requirement on ($R_b$ + $R_c$ + $R_u$)

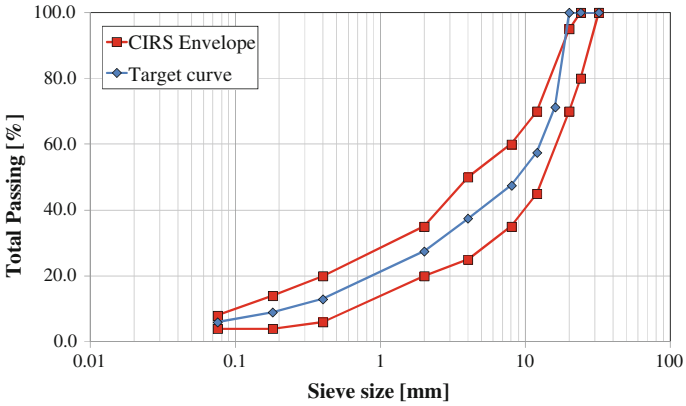


**Fig. 1** Gradation curve of the aggregate blend

## 4 Result Analysis

In the following section the results from ITSM, ITF and ITS tests are presented and discussed, with particular emphasis on the effect of C&D percentage on the mixture properties.

**Table 3** Results from ITSM tests

| | 0 % C&D | | 15 % C&D | | 30 % C&D | | 50 % C&D | |
|---|---|---|---|---|---|---|---|---|
| | ITSM [MPa] | Dev. [%] | ITSM [MPa] | Dev. [%] | ITSM [MPa] | Dev. [%] | ITSM [MPa] | Dev. [%] |
| | 2475 | 16.4 | 3910 | −32.2 | 2818 | 15.9 | 9072 | −24.2 |
| | 3148 | −6.3 | 3673 | −24.2 | *2114* | *36.9* | 8133 | −11.4 |
| | 2678 | 9.5 | 2793 | 5.5 | 2665 | 20.5 | 9277 | −27.0 |
| | 2588 | 12.6 | 2392 | 19.1 | 2932 | 12.5 | 5930 | 18.8 |
| | 3742 | −26.4 | 2490 | 15.8 | 3266 | 2.5 | 5453 | 25.3 |
| | 3432 | −15.9 | 2866 | 3.1 | 3132 | 6.5 | 6008 | 17.7 |
| | 2406 | 18.7 | 2584 | 12.6 | 3436 | −2.6 | 6552 | 10.3 |
| | 3151 | −6.4 | 3198 | −8.2 | *4994* | *−49.1* | 7374 | −1.0 |
| | 3025 | −2.2 | 2703 | 8.6 | *4793* | *−43.1* | 7924 | −8.5 |
| Mean [MPa] | 2961 | | 2957 | | 3041 | | 7303 | |
| St. Dev. [MPa] | 456.9 | | 530.8 | | 289.3 | | 1398.9 | |
| CV [%] | 15 % | | 18 % | | 10 % | | 19 % | |

## 4.1 Stiffness Modulus

The ITSM values obtained from the specimens containing different percentages of C&D are shown in Table 3. For each specimen the deviation from the mean value, expressed in percentage, is reported. The specimen that showed a deviation higher than 35 % (in italic) were excluded from the analysis. Thus, the mean, standard deviation and coefficient of variation in Table 3 were calculated considering only the consistent values.

From the results it can be noted that the mixtures with 15 and 30 % of C&D showed a ITSM comparable with the reference mix. This indicates that amounts of C&D up to 30 % can be reused in AC for base layers without significantly increasing the stiffness of the mixture. However, when the percentage of C&D was higher, the ITSM noticeably increased, as the stiffness was about twice than the one of the AC without C&D.

## 4.2 Indirect Tensile Fatigue

According to ISTM results, IFT tests were carried out by fixing the target horizontal stresses of 200, 250 and 300 kPa for the mixtures containing 0, 15 and 30 % of C&D. As the mixture with 50 % of C&D showed higher ITSM values, target horizontal stresses of 300, 400 and 500 kPa were fixed. The specimens that reached the failure with a number of cycle $N_f$ lower than 3000 had been excluded from the analysis.

The results of two fatigue tests, performed on specimens containing 30 and 50 % of C&D respectively, are shown as example in Fig. 2. Fatigue deformation storage curves typically presents 3 parts which are, in order: initial settlement zone, stable zone and failure zone. The shape of the third part indicates the type of failure that the specimen experiences: if the displacement quickly increases in few cycles, the failure is fragile whereas, if the displacement storage is gradual, the failure is ductile.

As it is shown in Fig. 2, the presence of C&D up to 30 % did not induced a fragile failure in the specimen, but a gradual increasing of the displacement was measured. A ductile failure was also observed for the other tested specimens with 0, 15 and 30 % of C&D. On the other hand, when 50 % of C&D was used, the failure was fragile. In fact, as it can be observed in Fig. 2, after the value of about 6 mm, no more displacement data were recorded as the specimen collapsed.

Such behavior could also be noted by simply observing the specimen conditions at the end of the fatigue test (Fig. 3).

Figures 4 and 5 respectively show the horizontal stress and the initial horizontal strain as a function of the number of cycles which brought the specimens to failure. The initial horizontal strain $\varepsilon_{h,i}$ represents the strain at the beginning of the test, when the specimen was undamaged thus its modulus was maximum, and was calculated through Eq. 1.

$$\varepsilon_{h,i} = \sigma_h \frac{(1 - 3\upsilon)}{E_i} \tag{1}$$

where $E_i$ is the ITSM at the beginning of the test, $\sigma_h$ is the horizontal stress and $\nu$ is the Poisson's ratio, supposed equal to 0.35. In both the graphs of Figs. 4 and 5 the results for each mixture were interpolated through a power law, which have a linear trend in bi-logarithmic scale.

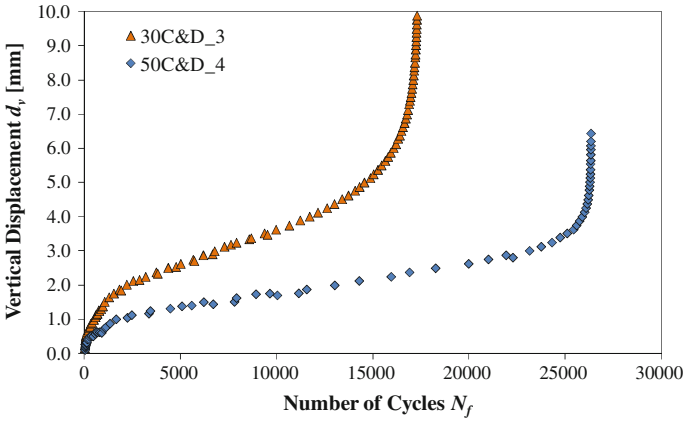


**Fig. 2** Fatigue deformation storage curve of specimens containing 30 % and 50 % of C&D


**Fig. 3** Type of fatigue failure: **a** Ductile. **b** Fragile

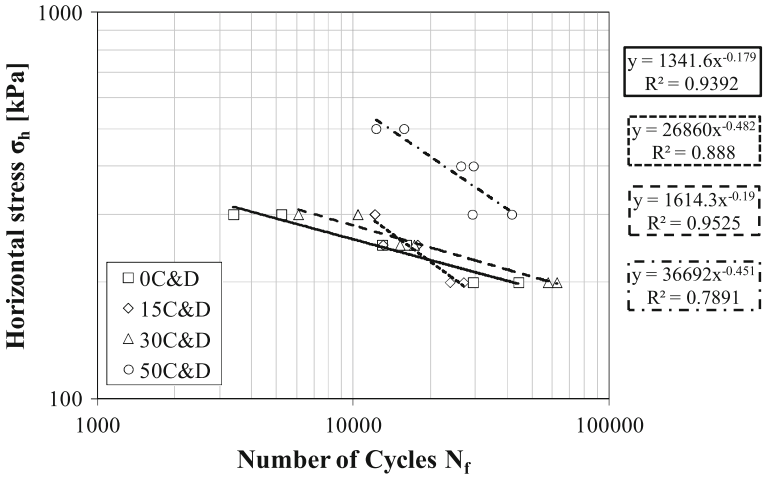


**Fig. 4** Fatigue curves in terms of horizontal stress as a function of number of cycles

From the results it can be noted that the curves for the mixtures containing 15 and 30 % of C&D are close to the one related to the reference mix in both the plots of Figs. 4 and 5. This indicates that the fatigue behavior of the mixtures is basically similar.

ITF results in Fig. 4 shows that the mix with 50 % of C&D could withstand a number of cycles comparable to that of the other mixes, even if the horizontal stresses applied were higher. On the contrary, the graph on Fig. 5 shows that the

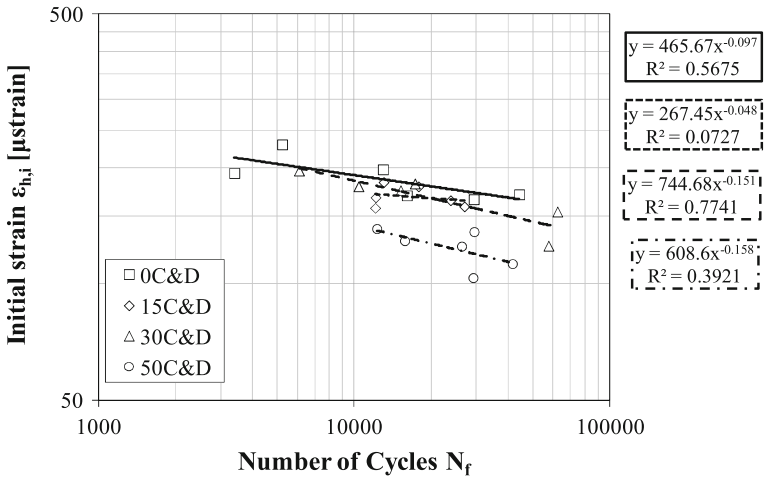


**Fig. 5** Fatigue curve in terms of initial horizontal strain as a function of number of cycles

curve of the mix with 50 % of C&D positioned below the others, denoting that, as the mix stiffness was higher, the strain applied in each cycle was lower. This confirmed that the presence of high percentages of C&D, equal or higher than 50 %, induced a fragile behavior on the mix. Thus, particular attention should be paid when designing pavements by using such a mixture, as it provides a good stiffness but it may not resist to high deformations.

## *4.3 Indirect Tensile Strength*

The ITS values of the specimens containing different percentages of C&D are shown in Table 4. In addition the indirect tensile coefficient (ITC) values, determined by using Eq. 2, are shown in Table 5.

$$ITC = \frac{\pi \cdot d \cdot ITS}{2 \cdot d_v} \tag{2}$$

where $d$ the specimen diameter and $d_v$ is the vertical displacement measured when the maximum load is reached. Essentially, ITC is related to the slope of the ITS-$d_v$ curve and gives a further indication on material stiffness.

As for ITSM results, for both ITS and ITC the mean, the standard deviation, the coefficient of variation and the deviation from the mean value, expressed in percentage, are reported.

**Table 4** ITS values

| | 0 % C&D | | 15 % C&D | | 30 % C&D | | 50 % C&D | |
|---|---|---|---|---|---|---|---|---|
| | ITS [MPa] | Dev. [%] | ITS [MPa] | Dev. [%] | ITS [MPa] | Dev. [%] | ITS [MPa] | Dev. [%] |
| | 1.00 | 10.8 | 1.10 | −6.9 | 1.53 | −0.6 | 1.83 | −8.2 |
| | 1.13 | −0.4 | 0.97 | 5.7 | 1.34 | 11.5 | 1.53 | 9.5 |
| | 1.10 | 2.0 | 1.08 | −5.0 | 1.60 | −5.1 | 1.62 | 3.9 |
| | 1.26 | −12.4 | 0.97 | 6.2 | 1.61 | −5.8 | 1.78 | −5.2 |
| Mean [MPa] | 1.12 | | 1.03 | | 1.52 | | 1.69 | |
| St. Dev. [MPa] | 0.11 | | 0.07 | | 0.12 | | 0.14 | |
| CV [%] | 10 % | | 7 % | | 8 % | | 8 % | |

**Table 5** ITC values

| | 0 % C&D | | 15 % C&D | | 30 % C&D | | 50 % C&D | |
|---|---|---|---|---|---|---|---|---|
| | ITC [MPa] | Dev. [%] | ITC [MPa] | Dev. [%] | ITC [MPa] | Dev. [%] | ITC [MPa] | Dev. [%] |
| | 111.5 | −8.7 | 103.7 | 10.2 | 119.8 | 21.8 | 245.2 | −13.5 |
| | 103.6 | −1.0 | 114.5 | 0.9 | 118.8 | 22.5 | 253.4 | −17.3 |
| | 100.5 | 2.0 | 146.9 | −27.1 | 165.9 | −8.3 | 196.9 | 8.9 |
| | 94.8 | 7.6 | 97.2 | 15.9 | 208.4 | −36.0 | 168.5 | 22.0 |
| Mean [MPa] | 102.6 | | 115.6 | | 153.2 | | 216.0 | |
| St. Dev. [MPa] | 7.0 | | 22.1 | | 42.9 | | 40.3 | |
| CV [%] | 7 % | | 19 % | | 28 % | | 19 % | |

From the results it can be noted that ITS raised when increasing the percentage of C&D in the mixture. In particular, the ITS of the AC with 15 % of C&D was similar to that of the reference AC, but an important increase was observed for 30 % C&D and 50 % C&D mixtures, with ITS values higher than 1.50 MPa.

From Table 5 it can be observed that, when increasing the content of C&D, the mixture showed a stiffer behavior related to higher values of ITC. This result mainly confirmed the ISTM findings, even if a higher statistical dispersion was noticed, especially for the AC containing 30 % of C&D.

An explanation for the results obtained can be related to the high absorbing capacity of the recycled materials. As indicated in Table 2 and reported by different authors (Melbouci 2009; Cerni et al. 2012), C&D has a high water absorption, which may determine a reduction of the thickness in the bituminous mastic which covers the aggregate particles (Lee et al. 1990).

Therefore, it can be supposed that, when increasing the percentage of C&D in the mix, the mastic film around the aggregates became thinner, determining the increase in stiffness and strength but also a fragile-type failure.

## 5 Conclusions

As nowadays the interest in reusing C&D materials is rapidly increasing and European policy is actually pushing in this direction, the present research has been carried out with the scope to study the behaviour of AC mixtures for base layers, containing with different percentages of C&D. In particular, mixes with 5 % of bitumen and 0, 15, 30 or 50 % of C&D were compacted with a shear gyratory compactor to a target air voids content of 5 % and subjected to indirect tensile stiffness modulus (ITSM), indirect tensile fatigue (ITF) and indirect tensile strength (ITS) tests.

From the ITSM values it can be noticed that amounts of C&D up to 30 % did not importantly increased the stiffness of the mixture. However, when the percentage of C&D was higher (50 %), the ITSM significantly raised.

ITF tests showed a similar performance between the mixture containing 0, 15 and 30 % of C&D, with a comparable fatigue resistance and a ductile-type failure. Differently, the mix with 50 % of C&D had a fragile-type failure, proving to have a good resistance to high horizontal stresses but a lower ability to withstand high deformations.

Static indirect tensile tests showed that both ITS and ITC raised when increasing the percentage of C&D in the mixture.

An explanation for these results can be related to the high absorbing capacity of C&D. Thus, it can be supposed that, when increasing the percentage of C&D in the mix, the mastic film around the aggregates became thinner, determining the increase in stiffness and strength but also a fragile-type failure.

Finally, at the light of the findings of the present research it can be concluded that C&D materials up to 30 % can be used with profit in AC mixtures for base course without importantly modifying the performance of the layer. The percentage could even be raised to 50 %, but particular attention should be paid when designing pavements by using such a mixture, as it provides a good stiffness but it may not resist to high deformations.

## References

ARPAV (2014) Rifiuti da Costruzione e Demolizione (C&D). Available via dialog. http://www.arpa.veneto.it/temi-ambientali/rifiuti/rifiuti-speciali/particolari-categorie-di-rifiuto/rifiuti-da-costruzione-e-demolizione. Accessed 31 Jul 2014.

Barbaro G (2012) Rifiuti speciali non pericolosi da C&D: la gestione eco-efficiente in Italia. Available via dialog. http://www.architetturaecosostenibile.it/materiali/smaltimento-e-riciclo/rifiuti-speciali-non-pericolosi-ced-gestione-eco-efficiente-italia-760. Accessed 31 May 2014.

Benedetti F (2001) Dati e logiche del mercato dei rifiuti. Paper presented at Giornata di studio – Il recupero dei rifiuti nelle costruzioni stradali, Roma, 7 June 2001.

Bocci M, Colagrande S (1999) The use of recycled materials obtained from demolition within the road works sector. Proceedings of the 3rd European Symposium on Performance & Durability of Bituminous Materials and Hydraulic Stabilised Composites, Leeds, 8-9 April 1999.

Bressi G, Pavesi E (2010) Rapporto ANPAR 2010 sul settore del riciclaggio dei rifiuti inerti. Associazione Nazionale Produttori Aggregati Riciclati.

Cerni G, Cardone F, Bocci M (2012) Permanent deformation behaviour of unbound recycled mixtures. Constr Build Mater 37:573-580. doi:10.1016/j.conbuildmat.2012.07.062.

Cerni G, Colagrande S (2012) Resilient modulus of recycled aggregates obtained by means of dynamic tests in a triaxial apparatus. Procedia - Social and Behavioral Sciences 53:475-484. doi: 10.1016/j.sbspro.2012.09.898.

Chong WK (2009) The forward path of construction and demolition waste reuse and recycling: market forces, regulatory efforts and actions from construction stakeholders. Proceedings of the 88th TRB annual meeting, Washington DC, 11-15 January 2009.

CIRS (2003) Norme tecniche di tipo prestazionale per capitolati speciali d'appalto.

Cupo-Pagano M, D'Andrea A, Giavarini C, Marro C (1994) Use of building demolition waste for asphalt mixes: first results. Proceedings of the 3rd international congress of energy, environment and technological innovation, Caracas, 5-11 November 1994.

EPA (2002) European waste catalogue and hazardous waste list. Environmental Protection Agency, Ireland, 2002.

Grau RW 1980 Utilization of marginal aggregate materials for secondary road surface layers. In: Performance of pavements designed with low-cost materials. Transport Res Rec 741:1-5.

Graziani A, Bocci E, Canestrari F (2014) Bulk and shear characterization of bituminous mixtures in the linear viscoelastic domain. Mech Time-Depend Mat 18,3:527-554.

Herrador R, Pérez P, Garach L, Ordóñez J (2012) Use of recycled construction and demolition waste aggregate for road course surfacing. J Transp Eng 138,2:182-190. doi: 10.1061/(ASCE)TE.1943-5436.0000320.

Lee DY, Guinn JA, Kandhal PS, Dunning RL (1990) Absorption of asphalt into porous aggregates. Report SHRP-A/UIR-90-009. National Research Council, Washington DC, 1990.

Leite FC, Motta RdS, Vasconcelos KL, Bernucci L (2011) Laboratory evaluation of recycled construction and demolition waste for pavements. Constr Build Mater 25:2972–2979. doi:10.1016/j.conbuildmat.2010.11.105.

Mahmoud AFF, Bahia H (2004) Using the gyratory compactor to measure the mechanical stability of asphalt mixtures. Wisconsin Highway Research Program WHRP 05-02 (0092-01-02).

Melbouci B (2009) Compaction and shearing behaviour study of recycled aggregates. Constr Build Mater 23:2723–2730. doi:10.1016/j.conbuildmat.2009.03.004.

Pasetto M (2000) The re-utilisation of discarded building materials in cement-stabilised layers of road and airfield pavements. Proceedings of WASCON 2000, Harrogate, May-June 2000.

Symonds Group Ltd. (1999) Construction and demolition waste management practices and their economic impact. Report to DGXI, European Commission. Available via dialog. http://ec.europa.eu/environment/waste/studies/cdw/cdw_report.htm. Accessed 30 Oct 2014.

# Reuse of Waste Foundry Sand Mixed with Lateritic Clayey Soils in Pavement Bases and Sub-bases Courses

**Luis Miguel Gutiérrez Klinsky, Glauco Tulio Pessa Fabbri and Vivian Silveira dos Santos Bardini**

**Abstract** This paper evaluated the reuse of WFS mixed with lateritic clayey soils in pavements sub-bases and bases. Two lateritic clayey soils and one chemically bonded WFS were used in this study. A laboratory program was conducted on mixtures of lateritic clayey soils and WFS. Atterberg Limits, Particle Size Distribution, mini-CBR, CBR, hydraulic conductivity and Cyclic Triaxial Tests were used to assess mechanical properties of soil-sand mixtures. Environmental test was performed to determine leaching potential of the WFS. The results showed that soil-sand mixtures containing WFS have mechanical properties similar to the materials commonly used in bases and sub-bases courses.

**Keywords** Waste foundry sand · Soil stabilization · Base and Sub-base courses · CBR · Resilient modulus

L.M.G. Klinsky (✉)
Highways Research Center, CCR, Presidente Dutra Road km 184.3, Santa Isabel, SP, Brazil
e-mail: luis.gutierrez@grupoccr.com.br

G.T.P. Fabbri
Department of Transportation, University of São Paulo, Av. Trabalhador Sãocarlense 400, São Carlos, SP, Brazil
e-mail: glauco@sc.usp.br

V.S. dos Santos Bardini
Department of Environmental Engineering, State University of São Paulo, Presidente Dutra Road km 138.5, São José dos Campos, Brazil
e-mail: vivian.bardini@ict.unesp.br



F. Canestrari and M.N. Partl (eds.), *8th RILEM International Symposium on Testing and Characterization of Sustainable and Innovative Bituminous Materials*, RILEM Bookseries 11, DOI 10.1007/978-94-017-7342-3_46

## 1 Introduction

One of the biggest challenges of the modern world is to dispose the solid waste in appropriate ways, mainly those resulting from industrial activities. The purpose is to recover material and energy, so natural resources can be preserved and environment degradation could be reduced.

The foundry industry uses sand in the mould and core-making processes, for several reasons: it is readily available almost everywhere, inexpensive and highly refractory (Javed and Lovell 1994). The largest volumes of foundry sand are used as "green sand" (clay-bonded), which consists of high-quality silica sand, approximately 10 % bentonite clay and 2 to 5 % water. Chemically bonded sand cast systems use one or more organic binders mixed with catalysts and hardeners. Chemically bonded sand is typically 97 % silica sand by weight (Winkler and Bolshakov 2000). The most common types of binders are sodium silicate, phosphate, phenolic and furan resins.

The high temperatures (1000 °C) used by foundries degrade and oxidize the binders and the sand, transforming them in a useless waste for the casting process. Therefore, the WFS must be disposed in sanitary landfills, which increase the operating costs of the foundry industry. For each ton of metal molten results approximately one ton of WFS (McIntyre et al. 1992).

In Brazil, the Waste Foundry Sand production raised considerably in the lasts years, more than three million tons of metal castings were produced in 2008 (ABIFA 2011); as a result, the requirement of new sanitary landfills increased. Therefore, the reuse of WFS becomes an important issue for the foundry industries and for the environment preservation.

Investigations have been made in recent years to reuse WFS in civil engineering constructions. The sand has appropriate characteristics for its use as aggregate in asphalt concrete (Javed and Lovell 1994), concrete products (Naik et al. 1994; Guney et al. 2010), flowable fills (Deng and Tikalsky 2008) and pavement bases and sub-bases courses (Fox and Mast 1998; Partridge and Alleman 1998; Kleven et al. 2000). The roadway construction demands high volume of natural resources, so it becomes an ideal destination for the WFS reuse. However, mechanical and environment properties must be studied to reuse the WFS in appropriate proportions.

On the other hand, lateritic soils are widely used in the State of São Paulo, Brazil, as sub-base and base courses, even though not recommended by traditional procedures (Nogami and Villibor 1991). These soils are mainly used in low volume traffic roads ($<10^7$ applications of Standard Axle Load of 80 kN). Additionally, some regions present lateritic clayey soils without the appropriate characteristics for its use in pavement layers; however the addition of sand to these soils makes them suitable for its use in road structures. Villibor et al. (2007) recommend adding natural sands to the lateritic clayey soils to improve the bearing capacity of the material.

Investigations showed that clay-bound foundry sands and WFS containing bentonite have acceptable mechanical properties for its use as an aggregate in sub-base and base courses under flexible pavements (Kleven et al. 2000; Goodhue et al. 2001; Abichou et al. 2004a). Furthermore, the clay encapsulates the WFS, reducing the risks of environmental pollution (Abichou et al. 2004b).

## 2 Research Significance

This investigation evaluated the reuse of Waste Foundry Sand mixed with lateritic clayey soils in bases and sub-bases courses. The region close to the city of Sertãozinho (State of São Paulo) was investigated because of its high foundry industry concentration. Also, that region has many deposits of lateritic clayey soils, but no sands or sandy soils deposits nearby. Therefore, the WFS mixed to lateritic clayey soils could be used in bases and sub-bases courses of suburban and low volume traffic roads.

A laboratory program was conducted to assess the mechanical properties of soil-sand mixtures containing WFS and lateritic clayey soils. Also, environmental tests were performed in the mixtures to determine the pollution risks of WFS reuse.

## 3 Materials and Methods

### *3.1 Waste Foundry Sand*

The WFS used in this study was collected from "Pama Mecânica e Fundição Ltda." located at the city of Sertãozinho, State of São Paulo, Brazil. According to the company, it is used a sand mix containing 98.56 % of sand; 1.2 % of phenolic resin as a binder and 0.24 % of catalyst. The particle size distribution curve of the WFS is presented in Fig. 1. Table 1 shows that WFS is classified as A-3 (AASHTO) or SP (USCS).

### *3.2 Soils*

Two lateritic clayey soils were used in this study. Soil 1 (S1) and Soil 2 (S2), both collected nearby the city of Sertãozinho. Figure 1 presents the particle size distribution of the soils and Table 1 shows index characteristics and the soils classification according to AASHTO and USCS systems.

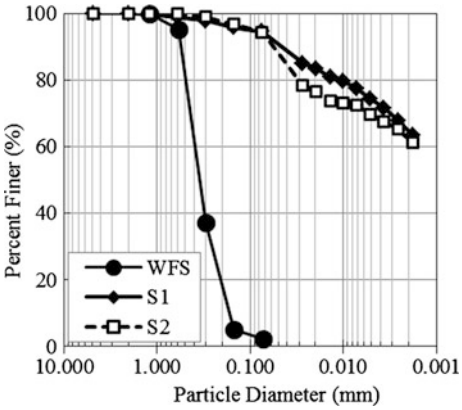


**Fig. 1** Particle size distribution curves of collected materials

**Table 1** Index properties of soils

| Materials (1) | Specific gravity[a] (2) | Atterberg limits[b] | | | Classification[c] | |
|---|---|---|---|---|---|---|
| | | Liquid limit (3) | Plastic limit (4) | Plastic index (5) | AASHTO (6) | USCS (7) |
| Soil S1 | 3.13 | 47 | 28 | 19 | A-7-6 | ML |
| Soil S2 | 3.12 | 47 | 31 | 16 | A-7-5 | ML |
| Waste foundry sand | 2.64 | NP | NP | NP | A-3 | SP |

[a]*ASTM D854*
[b]ASTM D4318
[c]ASTM D2487

## *3.3 Experimental Program and Tests*

Soil S1 was used to compose soil-sand mixtures containing 20, 40, 60 and 70 % of WFS. Particle Size Analysis (ASTM D422) and Atterberg Limits Tests (ASTM D4318) were performed to obtain the required parameters to classify the soil-sand mixtures according to USCS (ASTM D2487) and AASHTO Soil Classification (M145). Even these classifications systems were not idealized for soil mixtures, they could provide some idea of the soil-sand mixtures behavior.

The Optimum Moisture Content (OMC) and maximum dry unit weight ($\gamma_{dm}$) of the soil-sand mixtures were obtained through the mini-CBR test (DNER-ME254-97). The mini-CBR test is a modification of the Iowa Bearing Value (Lafleur et al. 1960) developed in Brazil (Nogami and Villibor 1991) to determine the bearing capacity of fine grained lateritic soils using reduced size specimens. Villibor and Nogami (2009) also nominate the mini-CBR test as mini-Proctor test, because the OMC and $\gamma_{dm}$ obtained from this test at Standard

Effort are similar to the OCM and $\gamma_{dm}$ obtained from Proctor Test (ASTM D698). The mini-CBR or mini-Proctor test uses specimens of 50 mm in diameter and 50 mm in height. The Standard Effort (690 kN-m/m$^3$) and the Intermediate Effort (1660 kN-m/m$^3$) are commonly used in this test. The Intermediate Effort was used in this research according to the recommendations of the State Department of Highways of São Paulo (DER-SP 2005) for compaction of sub-bases and bases courses of pavements with low volume traffic.

The mini-CBR test also provides the bearing capacity, swell (after 24 h soaking) and hydraulic conductivity (DER–SP ME 194-88) of the soil-sand mixtures. As well, the California Bearing Ratio (CBR) test (ASTM D1883) was performed on the mixtures. Three specimens of 100 mm in diameter and 200 mm in height were used in the Cyclic Triaxial Test, according to AASHTO T 307-99, to obtain de resilient modulus (MR) of each soil-sand mixture.

From results observed in soil-sand mixtures containing soil S1, was determined a suitable percentage of WFS to be used in bases courses. WFS was also added to soil S2 at that suitable percentage, to compare the mechanical behavior with soil S1 mixtures, through mini-CBR and Cyclic Triaxial Test.

Finally, the Leaching Test (ABNT 10006-2004) was performed to assess the environmental risks of WFS reuse. Soil S1, WFS and a soil-sand mixture containing 50 % of soil S1 and 50 % of WFS were used to perform this test.

## 4 Results and Discussion

### *4.1 Size Distribution Curves and Atterberg Limits*

The size distribution curves of the soil-sand mixtures containing soil S1 and WFS are presented in Fig. 2. As expected, high percentages of WFS reduces the content of particles smaller than 0.075 mm. The Index Properties of soil-sand mixtures obtained using soil S1 and WFS are presented in Table 2. The specific gravity of soil S1 decreased as WFS increased. Soil-sand mixtures with 60 and 70 % of WFS showed Atterberg Limits much lower than for soil S1. According to USCS and AASHTO classifications, S1 + 60 % WFS and S1 + 70 % WFS are expected to have similar behavior to SM-SC and A-4 and A-2-4, respectively; which are suitable to be used as subgrade materials.

### *4.2 Mini-CBR and CBR Test*

Optimum Moisture Content (OMC) and maximum dry unit weight ($\gamma_{dm}$) of the soil-sand mixtures were obtained through the mini-CBR test. Figure 3 shows that adding WFS to soil S1 reduced the OMC, otherwise increased the $\gamma_{dm}$.

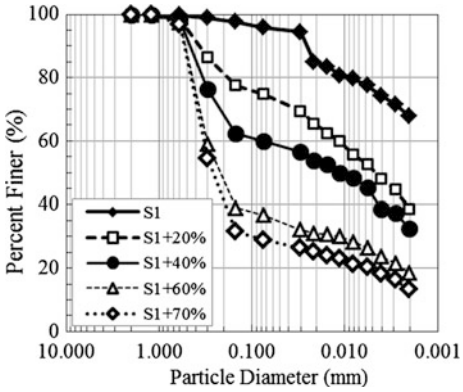


**Fig. 2** Particle size distribution curves of soil-sand mixtures (S1 + WFS)

**Table 2** Index properties of soil S1 containing waste foundry sand

| Materials (1) | Specific gravity[a] (2) | Attenberg limits[b] | | | Classification[c] | |
|---|---|---|---|---|---|---|
| | | LL (3) | LP (4) | IP (5) | AASHTO (6) | USCS (7) |
| S1 | 3.124 | 47 | 31 | 16 | ML | A-7-5 |
| S1 + 20 % | 2.964 | 40 | 24 | 16 | CL | A-6 |
| S1 + 40 % | 2.812 | 32 | 20 | 12 | CL | A-6 |
| S1 + 60 % | 2.782 | 27 | 19 | 8 | SM-SC | A-4 |
| S1 + 70 % | 2.724 | 23 | 15 | 8 | SM-SC | A-2-4 |

[a,b,c] indicate the technical standards corresponding to the specific measurement or classification.

Abichou et al. (2004b) compacted WFS (containing 9.3 % of bentonita) at Proctor Standard Effort and Modified Effort, and the $\gamma_{dm}$ ranged from 17 to 19 kN/m$^3$, with OMC values between 5 and 15 %. As presented in Fig. 3, higher values of $\gamma_{dm}$ were obtained for soil-sand mixtures containing 60 and 70 % of WFS.

The specimens used to obtain OMC and $\gamma_{dm}$ were also used to determine the mini-CBR value and swell, after 24 h soaking. The addition of WFS to soil S1 increased the mini-CBR value, as presented in Fig. 4. This behavior was also observed in CBR results. Further, both tests showed that the higher values were obtained for mixtures containing 60 % of WFS. Kleven et al. (2000) affirm that the average CBR of WFS is 20 %. Though, the results obtained here proved that much higher CBR values can be obtained mixing the WFS to lateritic clayey soils.

Figure 5 illustrates the swell obtained from mini-CBR and CBR tests in soil-sand mixtures. There was no swell or in S1 or in any soil-sand mixture according to the results of the mini-CBR test. The swell (obtained from CBR test) of soil S1 was 0.5 % and it was reduced to less than 0.1 % when 70 % of WFS was added. The specimens of CBR were soaked for 96 h, while the reduced-size specimens of mini-CBR were soaked for only 24 h. Probably, 24 h is not enough time to activate

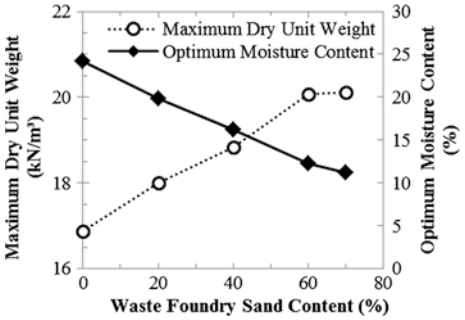


**Fig. 3** Optimum moisture content and maximum dry unit weight of soil-sand mixtures (S1 + WFS)

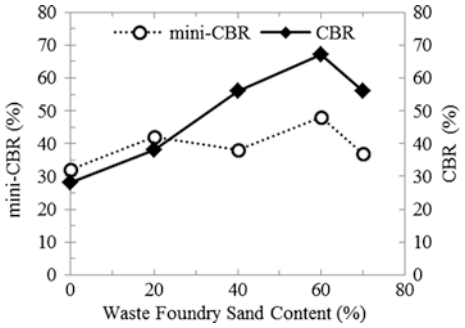


**Fig. 4** CBR and mini-CBR of soil-sand mixtures (S1 + WFS)

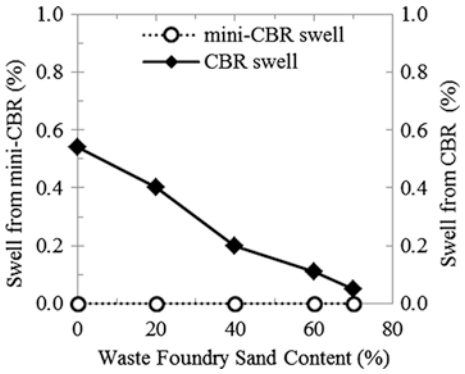


**Fig. 5** CBR swell and mini-CBR swell of soil-sand mixtures (S1 + WFS)

the swell potential of the lateritic clayey soil, even for reduced-size specimens. Additionally, soil-sand mixture containing 60 % of WFS showed similar mini-CBR and CBR characteristics to typical lateritic sandy soils used as sub-base and base course materials of low volume traffic roads, according to the Pavement Manual of the Brazilian Standards (DNIT 2006).

The suitable percentage of WFS to be added to lateritic clayey soils was fixed as 60 %. Soil S2 + 60 % WFS showed similar mini-CBR values, compared to the S1 + 60 % WFS, as illustrated in Fig. 6.

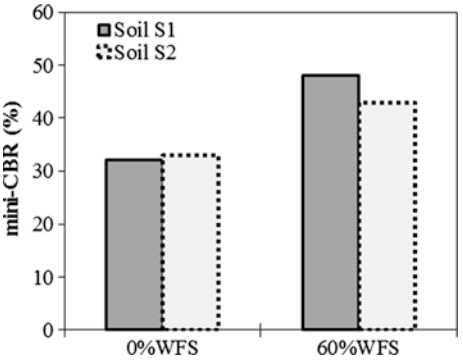


**Fig. 6** Mini-CBR results for Soils S1 and S2 containing waste foundry sand (WFS) and clean sand (CS)

## *4.3 Hydraulic Conductivity*

This test was performed using a fixed wall permeameter with falling head method. The specimens were compacted at OMC and $\gamma_{dm}$ using specimens obtained from mini-CBR test at intermediate effort. The hydraulic conductivity value of soil S1 was $1.0e^{-08}$ cm/s. Nogami and Villibor (1991) affirm that sandy lateritic soils have permeability values smaller than cm/s. Figure 7 shows the effects of adding WFS to soil S1. The addition of the residue did not significantly increase the hydraulic conductivity. The soil-sand mixtures with 70 % of WFS had a hydraulic conductivity of cm/s.

Fox and Mast (1998) performed hydraulic conductivity tests on WFS specimens using the miniature Harvard compaction device and obtained values ranging from $1.0e^{-08}$ cm/s to cm/s. Also Abichou et al. (2004b) determined that WFS containing 9.3 % of bentonite has hydraulic conductivity ranging from 10–7 to 10–8 cm/s. These values can be compared to hydraulic conductivity observed in soil S1 containing 60 and 70 % of WFS.

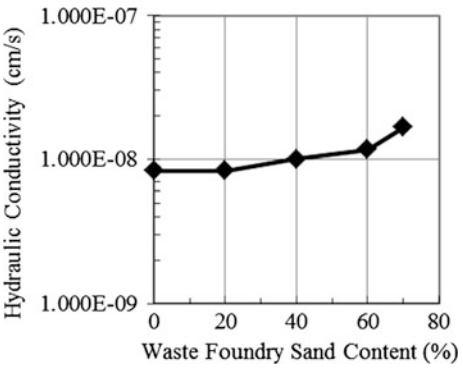


**Fig. 7** Hydraulic conductivity of soil-sand mixtures (S1 + WFS)

### 4.4 Cyclic Triaxial Test

Three specimens for each soil-sand mixture were compacted at OMC and $\gamma_{dm}$ using intermediate effort. Equation 1, recommended by NCHRP 1-28 (1997), was used to obtain the resilient modulus of the soil-sand mixtures. Table 3 shows the models of the resilient modulus of soil-sand mixtures and the coefficient of determination ($R^2$) of the models. It is verified that the adjustment of the NCHRP 1-28 equation was excellent ($R^2 > 0.90$) for all the materials but soil S2.

$$MR = K_1 \sigma_3^{k_2} \sigma_d^{k_3} \tag{1}$$

A common pavement structure of low volume traffic road was used to obtain the stresses of base courses composed by soil-sand mixtures. The initial characteristics of the pavement structure are described in Table 4. Single Load and Double Load were studied on the pavement structure. The Single Load was 40 kN and 0.56 MPa of tire pressure. The Double Load was constituted of two loads of 20 kN spaced 300 mm and 0.56 MPa of tire pressure.

ELSYM5 software was used to determine the stresses in the middle of the base layer. The stresses were used to calculate iteratively the Resilient Modulus (MR) of the soil-sand mixtures, as recommended by Huang (2004). The Resilient Modulus obtained applying Single Load is named MR1 and the Resilient Modulus obtained applying Double Load is named MR2. MR1 and MR2 values are also showed in Table 3.

Soil S1 had an average MR of 400 MPa for a Single Load applied in the low volume traffic road structure. Results shown in Fig. 8 reflect that MR decreased as WFS increased. However, mixtures containing 40, 60 and 70 % of WFS presented MR between 103 and 120 MPa. Figure 8 also shows that similar values of MR were obtained using Single Load and Double Load.

Kleven et al. (2000) performed cyclic triaxial tests on 13 waste foundry sands. The MR of the studied sands ranged from 90 to 200 MPa for different deviator and confining stresses. The study compares these values to traditional sub-base materials used in pavement construction. Thus, MR results of this study shows that clayey soils containing WFS could be used in sub-base pavement courses.

Soil S2 had a resilient modulus of 380 MPa, similar to soil S1. Also, when 60 % of WFS was added to S2, the MR decreased as observed in mixtures obtained from soil S1, as is shown in Fig. 9.

### 4.5 Environmental Tests

Leaching Test was performed on three samples: (1) Waste Foundry Sand; (2) Soil S1; (3) Mixture of Soil S1 containing 50 % of WFS. In this study the ABNT NBR 10006:2004 (Brazilian Standard) was used as reference framework to assess the

**Table 3** Resilient modulus models of soil-sand mixtures

| Material | Model parameters | | | | Resilient modulus | | | | | |
|---|---|---|---|---|---|---|---|---|---|---|
| | K1 | K2 | K3 | R2 | Resilient modulus MR1 | | | Resilient modulus MR2 | | |
| | | | | | Value (MPa) | Average (MPa) | Standard desviation | Value (MPa) | Average (MPa) | Standard desviation |
| S1 | 400.72 | 0.066 | −0.020 | 0.92 | 439 | 400 | 43 | 445 | 403 | 47 |
| | 548.49 | 0.086 | −0.099 | 0.91 | 407 | | | 413 | | |
| | 672.35 | 0.051 | −0.143 | 0.96 | 353 | | | 352 | | |
| S1 + 20 % of WFS | 1109.16 | 0.037 | −0.293 | 0.97 | 241 | 275 | 30 | 247 | 272 | 23 |
| | 948.53 | 0.033 | −0.231 | 0.97 | 286 | | | 279 | | |
| | 987.92 | 0.010 | −0.217 | 0.99 | 299 | | | 291 | | |
| S1 + 40 % of WFS | 215.16 | 0.444 | −0.499 | 0.91 | 87 | 103 | 15 | 89 | 106 | 15 |
| | 193.46 | 0.303 | −0.332 | 0.91 | 108 | | | 110 | | |
| | 253.24 | 0.285 | −0.348 | 0.95 | 115 | | | 118 | | |
| S1 + 60 % of WFS | 75.30 | 0.555 | −0.320 | 0.93 | 120 | 112 | 11 | 137 | 126 | 16 |
| | 67.04 | 0.574 | −0.320 | 0.94 | 117 | | | 134 | | |
| | 112.02 | 0.629 | −0.493 | 0.95 | 100 | | | 108 | | |
| S1 + 70 % of WFS | 10.05 | 0.851 | −0.173 | 0.97 | 127 | 120 | 9 | 148 | 142 | 9 |
| | 7.84 | 0.945 | −0.224 | 0.98 | 110 | | | 132 | | |
| | 8.96 | 0.877 | −0.183 | 0.98 | 122 | | | 145 | | |
| S2 | 651.88 | 0.021 | −0.107 | 0.97 | 380 | 379 | 16 | 377 | 375 | 17 |
| | 656.26 | 0.019 | −0.100 | 0.84 | 394 | | | 391 | | |
| | 919.20 | 0.042 | −0.188 | 0.88 | 362 | | | 358 | | |
| S2 + 60 % of WFS | 36.64 | 0.762 | −0.352 | 0.97 | 115 | 121 | 10 | 138 | 143 | 6 |
| | 23.72 | 0.735 | −0.230 | 0.96 | 133 | | | 150 | | |
| | 21.33 | 0.766 | −0.256 | 0.97 | 116 | | | 141 | | |

**Table 4** Initial characteristics of the pavement structure of a low volume traffic road

| Layer | Thickness (mm) | MR (MPa) | Poisson |
|---|---|---|---|
| Top asphalt Layer | 25 | 1500 | 0.35 |
| Base | 150 | 200 | 0.40 |
| Sub-base | 150 | 100 | 0.40 |
| Subgrade | Semi-infinite | 50 | 0.45 |

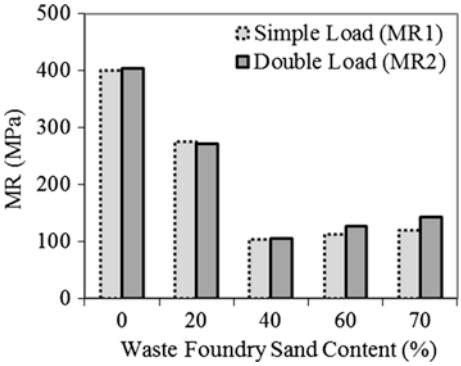


**Fig. 8** Average MR values of soil-sand mixtures (S1 + WFS) in a low volume traffic road structure, for double load and simple load

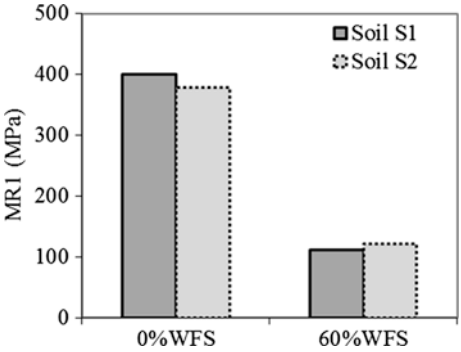


**Fig. 9** Average MR values of soil-sand mixtures using control materials in a low volume traffic road structure, for simple load

studied materials. This standard is based on U.S. Environmental Protection Agency standards.

Table 5 presents the results of Leaching Test. The soil S1 containing 50 % of WFS did not attend the Brazilian Standards. Phenol and Iron content exceeded the limits. However, Table 5 shows that even the pure soil S1 did not attend these standards. The soils of the studied region are characterized by high Phenol and Iron content and are widely used in pavement activities. On the other hand, Environmental Standards in Brazil are being changed to encourage the reuse of Waste Materials. For example, for the Environmental Agency of São Paulo State

**Table 5** Leaching characteristics of soil S1, WFS and S1 containing 50 % of WFS

| Parameter (1) | Soil S1 (mg/l) (4) | Waste foundry sand (mg/l) (2) | Soil S1 + 50 % of WFS (mg/l) (3) | ABNT NBR (10006:2004) limit (mg/l) (5) |
|---|---|---|---|---|
| pH | ND | ND | ND | - |
| Arsenic | ND | ND | ND | 0.01 |
| Barium | ND | ND | ND | 0.7 |
| Cadmium | ND | ND | ND | 0.005 |
| Chromium | ND | ND | ND | 0.05 |
| Iron | 3.2 | 0.07 | 9.28 | 0.5 |
| Lead | ND | ND | ND | 0.01 |
| Manganese | ND | 0.07 | 0.01 | 0.1 |
| Mercury | <0.0001 | <0.0001 | <0.0001 | 0.001 |
| Phenol | 0.04 | 0.06 | 0.06 | 0.01 |
| Selenium | ND | ND | ND | 0.01 |
| Zinc | 0.11 | 0.1 | 0.12 | 5 |

(CETESB), the mixture of Soil S1 containing 50 % of WFS attends to the required specifications for its use in pavement construction.

## 5 Conclusions

This research assessed the feasibility of using Waste Foundry Sand mixed with clayey soils as a roadway sub-base and base course material. Lateritic clayey soils and chemically bonded WFS were used to assemble soil-sand mixtures. Mechanical properties of the soil-sand mixtures were investigated in a laboratory program. Also, Leaching Test was performed to investigate the environmental risks of their use.

The following conclusions are drawn based on results obtained in this study:

- Atterberg Limits were affected by the addition of Waste Foundry Sand. The Liquid Limit (LL) and Plastic Index (PI) decreased as WFS content increased.
- Addition of WFS decreased the Optimum Moisture Content of clayey soils. The Maximum Dry Unit Weight increased as the amount of WFS increased.
- CBR and mini-CBR results showed that soil S1 containing 60 % of WFS had similar characteristics to lateritic sandy soils used as base course materials.
- Hydraulic Conductivity of soil S1 did not significantly change as WFS content increase. Even the soil-sand mixture containing 70 % of the residue had a very small hydraulic conductivity.
- A low volume traffic road structure analysis showed that the addition of waste foundry sand to lateritic clayey soils decreased the Resilient Modulus (MR); but

the soil-sand mixtures presented appropriate MR values for its use in sub-bases courses;

- Leaching tests showed that foundry sand could not be used as pavement material according to the actual Brazilian Environmental Standards. Iron and Phenol content exceeded the recommended limits. However, even the natural soil, which is widely used in the studied region, exceeded the same parameters.

The laboratory results showed that soil-sand mixtures containing lateritic clayey soils and Waste Foundry Sand have mechanical properties similar to the commonly materials used in bases and sub-bases courses. Therefore, Waste Foundry Sand mixed with clayey soils could be reused as a partial substitute of commonly used materials. However, is recommended to perform field investigations to assess mechanical properties and environmental risks of the reuse of each kind of WFS. Finally, the beneficial reuse of Waste Foundry Sand could reduce the operating costs of foundry industries by reducing the use of sanitary landfills.

## References

Abichou T, Edil T B, Benson C H, Bahia H (2004a) Beneficial Use of Foundry By-Products in Highway Construction. In: Geotechnical Engineering for Transportation Projects : Proceedings of GeoTrans 2004, jul 27-31 2004. Los Angeles, CA, United States: ASCE, Reston, VA 20191-4400.

Abichou T, Edil T B, Benson C H, Tawqif K (2004b) Hydraulic Conductivity of Foundry Sands and their Use as Hydraulic Barriers. Recycled Materials in Geotechnics (GSP 127), A. H. Aydilek and J. Wartman, eds., Geotechnical Special Publication;127, ASCE, New York, United States.

ABIFA (2011) Associação Brasileira da Industria de Fundição. Online Report. São Paulo. Brazil.

Deng A, Tikalsky P J (2008) Geotechnical and leaching properties of flowable fill incorporating waste foundry sand. Journal of Waste Management, Elsevier. 2008:28; Issue 11:2161-2170.

DER-SP (2005) Especificações Técnicas – Pavimentação. ET-DE-P00-015A, Sub-base ou Base de Solo Arenoso Fino de Comportamento Laterítico - SAFL. Departamento de Estradas de Rodagem, São Paulo. Brazil.

DNIT (2006) Manual de Pavimentação. Publicação IPR-179. Departamento Nacional de Infra-estruturas de Transportes. Rio de Janeiro, Brazil.

Fox P J, Mast D G (1998) Geotechnical Performance of Highway Embankment Constructed Using Waste Foundry Sand. FHWA/IN/JTRP-98/18. Joint Transportation Research Program. Indiana Department of Transportation and Purdue University. West Lafayette. Indiana, United States.

Goodhue M J, Edil T B, Benson C H (2001) Interaction of Foundry Sands with Geosynthetics. Journal of Geotechnical and Geoenvironmental Engineering. ASCE. 127:353-362.

Guney Y, Sari Y D, Talcin M, Tuncan A, Donmez S (2010). Re-usage of Waste Foundry Sand in High-Strength Concrete. Journal of Waste Management, Elsevier. 2010:30; Issues 9-8:1705-1713.

Huang Y (2004) Pavement Analysis and Design. Book. Second Edition. Prentice Hall.

Javed S, Lovell C W (1994) Uses of Waste Foundry Sands in Civil Engineering. Transportation Research Record. 1994:1486:109-113.

Kleven J R, Edil T B, Benson C H (2000). Evaluation of Excess Foundry System Sands for Use as Sub-Base Material. Transportation Research Board.1714:40-48.

Lafleur J D, Davidson D T, Katti R J, Gurland J (1960) Relationship Between California bearing ratio and Iowa bearing value. Methods of Testing Engineering Soils. Iowa State University. Ames. Ia. 1960:48-63.

McIntyre S W, Rundman K B, Baillod C R, Sandell P R, Stillwell B (1992). Beneficiation and Reuse of Foundry Sand Residuals: A Preliminary Report. Transactions of the American Foundrymen's Society. 1992:100;201-208.

Naik T R, Patel V M, Parikh D M, Tharaniyil M P (1994) Utilization of Used Foundry Sand in Concrete. Department of Civil Engineering & Mechanics. University of Wisconsin – Milwaukee. United States.

NCHRP (1997) Laboratory determination of resilient modulus for flexible pavement design. NCHRP Web Document 14 for Project 1-28. Transportation Research Board, Washington, D. C. United States.

Nogami J S, Villibor D F (1991) Use of Lateritic Fine-Grained Soils in Road Pavement bases courses. Geotechnical and Geological Engineering.9:167-182.

Partridge B K, Alleman J E (1998) Field Demonstration of Highway Embankment Constructed Using Waste Foundry Sand. FHWA/IN/JTRP-98/8. Joint Transportation Research Program. Indiana Department of Transportation and Purdue University. West Lafayette. Indiana. United States.

Villibor D F, Nogami J S, Cincere J R, Serra P R M, Zuppolini A N (2007) Pavimentos de Baixo Custo para Vias Urbanas. Bases alternativas com solos lateríticos. Book. Ed. Arte e Ciência. São Paulo. Brazil.

Villibor D F, Nogami J S (2009) Pavimentos Econômicos. Tecnologia do Uso dos solos finos lateríticos. Book. Ed. Arte e Ciência. São Paulo. Brazil.

Winkler E S, Bolshakov A A (2000) Characterization of Foundry Sand Waste. Chelsea Center for Recycling and Economic Development. University of Massachusetts at Lowell. United States.

# A Comparative Study of Bituminous Mixtures with Recycled Polyethylene Added by Dry and Wet Processes

**Silvia Angelone, Fernando Martinez and Marina Cauhape Casaux**

**Abstract** The use of "silo bags" is a common technique developed in Argentina for the low cost on farm storage of grains and nowadays, they are extensively used in different countries all around the world. They are big plastic bags made of three layers of polyethylene where different types of dry grains can be stored in a hermetic ambient. After several uses the silo bags are damaged and must be replaced. These materials are hardly biodegradable and they occupy an important volume in landfills. This paper presents a comparative laboratory study about the influence of different percentages of recycled polyethylene from silo bags added by dry and wet processes on a bituminous mixture compared to two other mixtures containing conventional bitumen and polymer modified bitumen. The obtained results are presented and discussed showing that the reuse of recycled polyethylene from silo bags in bituminous mixtures is an environmental friendly alternative.

**Keywords** Bituminous mixtures · Recycled polyethylene · Mechanical properties

## 1 Introduction

Sustainability has become a keyword in road engineering with economic, social and environmental dimensions. It is a concept related to more reliable pavement design procedures based on mechanistic principles, longer pavement design lives, more efficient pavement conservation strategies, lower mixing and compaction temperatures for asphalt materials and lower energy consumptions during the overall construction process. Also, the construction of roads is one of the most material demanding industries in the world with great economic as well as environmental impacts.

S. Angelone · F. Martinez (✉) · M. Cauhape Casaux
Road Laboratory School of Engineering, University of Rosario, Rosario, Argentina
e-mail: fermar@fceia.unr.edu.ar



F. Canestrari and M.N. Partl (eds.), *8th RILEM International Symposium on Testing and Characterization of Sustainable and Innovative Bituminous Materials*, RILEM Bookseries 11, DOI 10.1007/978-94-017-7342-3_47

Technological development, increase of the population and use of natural resources are generating large volume of waste and as a consequence, the mitigation of this serious environmental problem is a guiding parameter in projects of any nature including road construction.

In order to reduce the negative impacts of these human activities, significant efforts are carried out in terms of recycling and reuse of pavement materials and incorporating waste products such as old tires, factory rejected roofing shingles, slag aggregates from steel production, sand from metal casting foundries and waste glass in pavement materials.

Huang et al. (2007) have reviewed the use of recycled solid waste materials in asphalt pavements and they concluded that the use of recycled materials in asphalt pavements represents a valuable outlet for such materials.

The potential physical-chemical compatibility between bitumen and plastics (both from petrochemical industry) and the significant volume of materials used in asphalt road construction show the roads as a good place to dispose this kind of waste.

In particular, Ho et al. (2006), Al-Hadidy and Yi-Qiu (2009) and Fawcetta et al. (1999) have investigated the use of polyethylene in bitumens and asphalt mixtures. Hinishoglu and Agar (2004) reported the use of high density polyethylene waste as bitumen modifier and they concluded that the mixtures containing this material provide better resistance against permanent deformations. The viability of using high density polyethylene as a modifier for asphalt paving bitumen was also investigated by Attaelmanan et al. (2011) showing that the performance of the modified asphalt mixtures is better than the conventional ones with a reduced moisture and temperature susceptibility. Analogous results are reported by Zoorob and Suparma (2000).

The use of "silo bags" is a common technique developed in Argentina for the low cost on farm storage of grains and nowadays, extensively used in different countries all around the world. Silo bags are big plastic bags approximately 60–80 m long and 3–4 m in diameter made with a membrane combining three very thin layers of a low-density polyethylene, a high-density polyethylene and a UV resistant layer as a composite where the different types of dry grains can be stored in a hermetic ambient. After several uses and due to the action of cattle, birds, rodents and the machinery used to fill and empty the grain, the silo bags are damaged and must be replaced. These materials are hardly biodegradable and they occupy an important volume in landfills and, as a consequence, large amounts of polyethylene are available for recycling.

This paper presents a comparative laboratory study about the influence of different percentages of recycled polyethylene from silo bags added by dry and wet processes on a bituminous mixture compared to two other mixtures containing conventional bitumen and polymer modified bitumen. The resulting mixtures were analyzed considering their volumetric parameters and the values from diverse laboratory mechanical tests.

This study is part of an ongoing research project being carried out at the University of Rosario, Argentina and the reported results are those obtained until this paper was prepared.

The large volume of consumed materials and the significant increase in the number of overloaded trucks require higher performance materials. For this reason, the use of plastic waste in pavement production is a valid disposal waste option that must be evaluated. This is true regardless of whether the addition gives better asphalt features, because if its incorporation is neutral, this waste disposal option is in itself an important contribution to the preservation and enhancement of the environment.

## 2 Materials and Specimen Preparation

The recycled polyethylene (RP) from silo bags used in this study is produced in a recycling company where the polyethylene is washed, dried and chopped in scales with a maximum size between 6 and 10 mm. This RP was incorporated to the asphalt mixtures by two different procedures: Wet and Dry.

The Wet process refers to modification of bitumen with different percentages of RP at an elevated temperature including the blending of them.

On the other hand, the Dry process includes mixing the scales of RP with aggregates prior to addition to bitumen. This process provides a way to blend the RP with the bitumen and aggregate without the use of the previous preparation needed in the Wet process.

### *2.1 Modified Bitumen with RP*

For the modification of a conventional B-AC30 bitumen by the Wet process, different percentages of RP in solid scale form was mixed at 170 °C using a high-speed stirrer rotating at a speed of 11,000 rpm, and blended for a period of 20 min. With this procedure, a homogeneous dispersion of the recycled polyethylene into the bitumen was achieved as it was checked through micro photographs of the blends. Modified bitumens with percentages of 2 and 3 % of RP by weight of the bitumen were elaborated to be used in the preparation of different asphalt mixtures. These modified bitumens were named as B-2%MRP and B-3%MRP respectively. Also a SBS Polymer Modified Bitumen, identified as B-AM3, was considered for comparison purposes. The main properties of these bitumens are presented in Table 1.

The addition of RP influences the characteristics of the bitumen with a decreasing of the Penetration at 25 °C and an increasing of the Softening Point, the Rotational Viscosity and the Elastic Recovery. Also, the bitumens modified with RP show smaller temperature susceptibility compared to the conventional bitumen

**Table 1** Characteristics of the considered bitumens

| | B-AC30 | B-2%MRP | B-3%MRP | B-AM3 |
|---|---|---|---|---|
| Penetration 25 °C (1/10 mm) | 55 | 18 | 17 | 62 |
| Softening point (°C) | 49 | 63 | 68 | 65 |
| Penetration index | −1.2 | −0.6 | +0.2 | +2.5 |
| Rotational viscosity @ 85 °C (dPas) | 165 | 760 | 1840 | 1690 |
| Rotational viscosity @ 110 °C (dPas) | 23 | 69 | 130 | 109 |
| Elastic recovery (%) | 0 | 7 | 6 | 65 |

with greater Penetration Indexes. The storage stability of the modified bitumens with RP was poor as samples taken from the upper and lower parts of each container were observed with a microscope. So, they were energetically stirred before the addition of the bitumen to the aggregates. Nowadays, the addition of an additive to improve this condition is being investigated.

## *2.2 Asphalt Mixtures*

In this study, a dense asphalt concrete for base layers with the conventional bitumen was considered as the control mixture and it was identified as AC30. This mixture was designed according to the Marshall Mix Design Procedure. Granitic aggregates and hydrated lime were used according to the requirements established in Argentina for this kind of asphalt mixtures. The resulting Optimum Asphalt Content was 4.9 % by weight. Then, other asphalt mixtures were formulated as follows.

Two asphalt mixtures were prepared replacing the conventional bitumen with the same amount of the RP modified bitumens considered previously. These mixtures were identified as 2%WRP and 3%WRP.

Other three asphalt mixtures were prepared by the Dry process adding 2, 4 and 6 % of the chopped RP by the total weight of the mixture to the control mix, without any replacement of the aggregates. These mixtures were identified as 2% DRP, 4%DRP and 6%DRP and they were prepared mixing the hot aggregates, the hydrated lime and the recycled polyethylene first. Then, the amount of bitumen resulting from the Marshall Mix Design procedure for the mixture without RP was added and mixed. The mixture in a loose condition was placed in an oven at 160 °C during 1 h covered with an aluminum foil. Then, the mixture was taken off the oven, mixed again and compacted. This procedure was adopted in order to simulate the period of time the asphalt mixture is carried from the production facility to the construction location at high temperature.

Finally, an additional mixture was prepared resembling the control mixture but replacing the conventional bitumen by the SBS polymer modified. This mixture was identified as AM3.

**Table 2** Volumetric properties of the mixtures

| | AC30 | AM3 | 2% WRP | 3% WRP | 2% DRP | 4% DRP | 6% DRP |
|---|---|---|---|---|---|---|---|
| Gmm (kg/m$^3$) | 2.591 | 2.583 | 2.607 | 2.567 | 2.503 | 2.421 | 2.364 |
| Dm (kg/m$^3$) | 2.490 | 2.486 | 2.452 | 2.441 | 2.39 | 2.299 | 2.232 |
| Va (%) | 3.9 | 3.8 | 5.9 | 4.9 | 4.5 | 5.0 | 5.6 |
| VMA (%) | 16.1 | 15.9 | 18.0 | 16.9 | 16.2 | 16.3 | 16.5 |
| VFA (%) | 75.8 | 76.4 | 66.9 | 70.9 | 72.2 | 69.1 | 66.2 |

It should be emphasized that these mixtures containing RP are not directly comparable among them because in the cases of the RP added by the Wet process (2%WRP and 3%WMP), the amount of RP is related to the total amount of bitumen in the mixture while in the case of the RP added by the Dry process (2%DRP, 4% DRP and 6%DRP), this amount is referred to the total weight of the mixture.

The average volumetric properties of the 7 mixtures are presented in Table 2 where Gmm is the maximum specific gravity of the mixture, Dm is the bulk specific gravity (kg/m$^3$), Va are the air voids content in the mix, VMA are voids in the mineral aggregates and VFA are voids filled with asphalt.

The seven asphalt mixtures meet the volumetric requirements used in Argentina for this kind of materials for base courses of asphalt pavements.

## 3 Mechanical Properties of the Asphalt Mixtures

The mechanical properties of the considered asphalt mixtures were comparatively evaluated with different laboratory tests including Marshall, indirect tensile strength, moisture susceptibility, dynamic modulus and wheel tracking tests as it is described in the following paragraphs. Due to the lack of space, only average results are presented but in general, the dispersion of the results is of the same order as obtained with conventional asphalt mixtures.

### *3.1 Marshall Tests*

Marshall Tests were carried out according to the procedure described in EN-12697-34 (2004). The average Marshall Stability and Flow results are shown in Fig. 1a while Fig. 1b shows the Marshall Quotient (MQ) defined as the relationship between stability and flow.

All the mixtures meet the requirements used in Argentina for this kind of mixtures with a Marshall Stability greater than 9 kN.

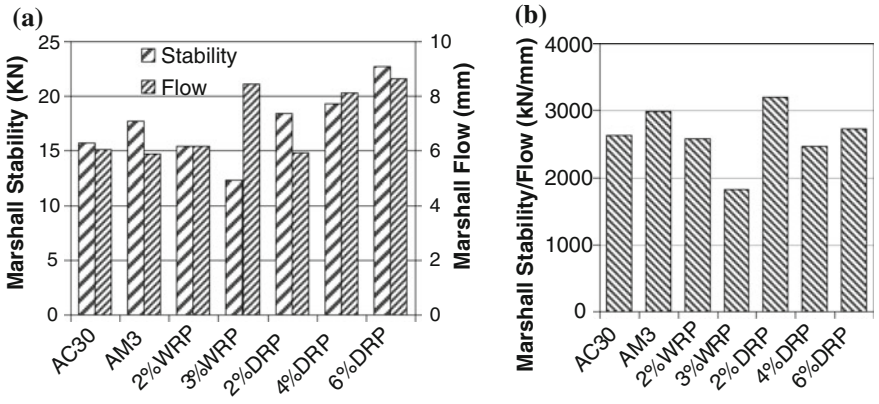


**Fig. 1** Marshall test results: **a** Stability and flow. **b** Marshall quotient

The mixtures containing RP added by the Wet process have smaller stabilities and greater flows compared to the AC30 mixture (control). Both, the stability and the flow increase with increasing the RP content added by the Dry process. The mixture 6%DRP has a Stability approximately 1.5 times greater than the AC30 mix.

Since the Marshall Quotient (MQ) could be considered as an indicator of the resistance against the deformation of the asphalt mixture, a higher value of MQ could indicate a stiffer and more resistant mixture. The maximum MQ is reached for the mixture containing 2 % of RP added by the Dry process and the minimum MQ is for the 3%WRP mixture.

## *3.2 Indirect Tensile Strength, ITS*

Indirect tensile strength tests were carried out following a procedure very similar as it is described in EN-12697-23 (2004) at a temperature of 10 °C and at a constant rate of deformation of 6.35 mm/min. The average ITS results for the seven asphalt mixtures are presented in Fig. 2a.

Also the Fracture Energy FE, calculated from the area under the load-vertical deformation curve, was measured for the 7 mixtures (Witczak et al. 2002). The resulting values are shown in Fig. 2b. It has been reported that the FE is a good indicator of the fatigue and thermal cracking resistance of asphalt mixtures.

In general, ITS decreases as the amount of RP increases for the mixtures containing recycled polyethylene added by the two processes. For the mixtures with RP added by the Dry process, the fracture energy increases as the amount of RP increases with fracture energies higher than that for the control mixture. The increase in fracture energy represents a potential for improving asphalt fatigue life and also, lower thermal cracking should be expected as the fracture energy is increased (Lee et al. 2005).

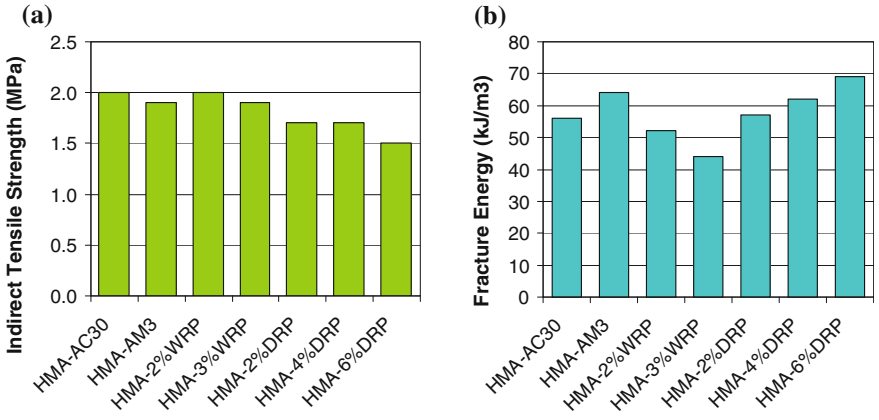


**Fig. 2** **a** Indirect tensile strength. **b** Fracture energy for the seven mixtures

## 3.3 *Moisture Susceptibility Tests*

The moisture susceptibility tests were carried out following a procedure very similar as it is described in EN-12697-12 (2003a). The tests were performed on the seven mixtures, which were compacted to an average air void content of 7 %. Two Marshall specimens for the dry group and two for the wet group were prepared. A tensile strength ratio (TSR) of wet group to dry group was computed from the results of the indirect tensile strength test (ITS) at 25 °C and at a constant rate of vertical deformation of 50 mm/min.

The higher the TSR value, the less the strength is influenced by the water soaking condition. The average test results are presented in Table 3. Normal specification used in Argentina requires a TSR value of 80 % or more. The 7 mixtures meet this requirement. The highest TSR values were obtained with the mixtures containing 4 and 6 % RP added by the Dry process.

## 3.4 *Dynamic Modulus Tests*

The dynamic modulus E* is the main input material property of asphalt mixtures for the modern mechanistic-empirical flexible pavements design methods. It determines the distribution of stress and strains into the pavement structure and also, it can be correlated with the rutting and fatigue cracking behavior of the bituminous layers (National Research Council 2004).

**Table 3** Moisture susceptibility results

| | AC30 | AM3 | 2%WRP | 3%WRP | 2%DRP | 4%DRP | 6%DRP |
|---|---|---|---|---|---|---|---|
| TSR (%) | 97 | 84 | 87 | 97 | 94 | 100 | 100 |

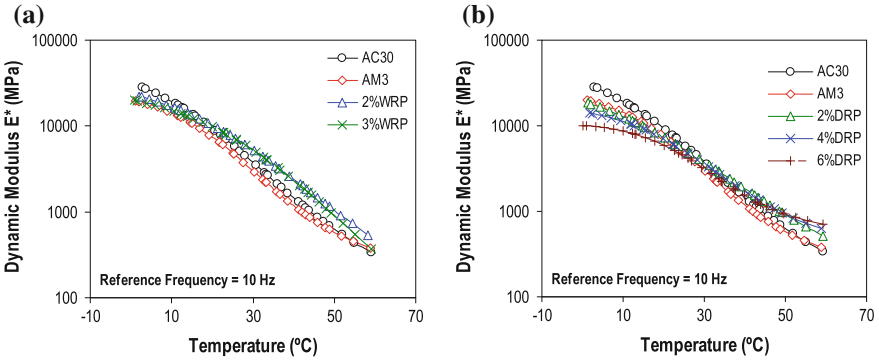


**Fig. 3** Variation of E* as a function of the temperature for the mixtures containing RP **a** added by the wet process, **b** added by the dry process

The Dynamic Modulus E* was experimentally measured with the Indirect tension (IDT) mode with sinusoidal (haversine) loadings as it was developed in a previous paper (Martinez and Angelone 2012). A cylindrical specimen is subjected in the IDT mode to two sinusoidal strips loads on a vertical direction and the resulting deformations are measured along the horizontal diameter. Then the relationship between the developed stress and strains allows the calculation of the dynamic modulus E*. In this study, five temperatures (0, 10, 20, 30 and 40 °C) and seven frequencies (5, 4, 2, 1, 0.5, 0.25 and 0.1 Hz) were used. Based on the frequency-temperature superposition principle, average master curves showing the variation of the dynamic modulus E* as a function of the temperature for a reference frequency of 10 Hz were developed according to models and equations that were analyzed in a previous paper (Angelone et al. 2013). This frequency was arbitrarily selected because is approximately equal to the loading frequency of trucks moving at 80 km/h on conventional asphalt pavements.

The dynamic modulus E* curves for the mixtures containing RP added by the Wet and the Dry processes are presented in Fig. 3a, b respectively. On both cases and for comparison purposes, the E* curves for the AC30 and AM3 mixtures are also presented.

Based on the experimental results and the frequency-temperature superposition principle, the dynamic moduli E* in two different conditions were calculated: at (10 °C/10 Hz) and at (60 °C/1 Hz). These values are shown in Fig. 4.

The five mixtures containing RP have lower E* values at low temperature and high frequency compared to the AC30 mix and, higher E* values at high temperature and low frequency. Thus, the thermal susceptibility of the mixtures containing RP is smaller than the AC30 mix and in several cases, even smaller than the AM3 mixture.

This behavior was considered very promising against the two major distress types in asphalt pavements: fatigue cracking and rutting. At low temperatures, the mixtures containing RP are softer than the AC30 mix and hence, better adapted to

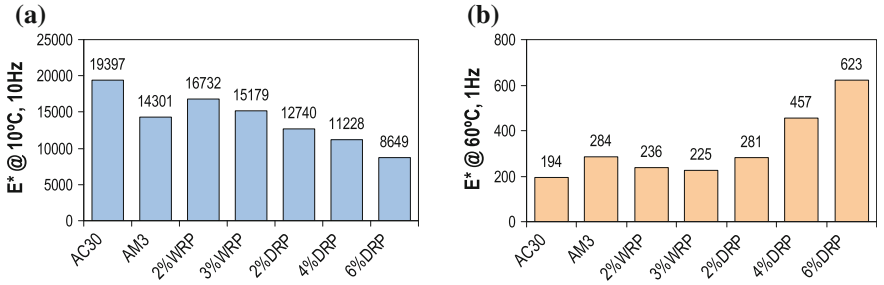


**Fig. 4** Comparison of measured E* **a** at 10 °C and 10 Hz, **b** at 60 °C and 1 Hz

resist fatigue damage. At high temperatures, the mixtures containing RP are stiffer compared to the AC30 mixtures and then, more resistant to the development of permanent deformations.

## *3.5 Permanent Deformation Tests*

The susceptibility of the asphalt mixtures to deform under repeated load was evaluated according to the EN-12697-22 procedure (European Committee for Standardization 2003) using a small-size device in air (procedure B). The tests were performed at 60 °C with a wheel load equal to 700 N during 10,000 cycles. At least two specimens were tested and the obtained average results are shown in Table 4.

where $d_i$ is the rut depth after i cycles, $PRD_{10000}$ is the proportional rut depth for the material under test at 10,000 cycles and $WTS_{AIR}$ is the wheel-tracking slope calculated from $d_{5000}$ and $d_{10000}$.

Figure 5 shows the average evolution of the rut depth as a function of the number of cycles for the mixtures considered in this study.

As it can be observed, the rut depths $d_{10000}$ of the mixtures containing RP are smaller than the control mix and the wheel-tracking slopes $WTS_{AIR}$ are 2 to more than 10 times smaller than the AC30 mixture. These values are also smaller than that obtained for the AM3 mixture elaborated with the polymer modified bitumen.

**Table 4** Permanent deformation results

| | AC30 | AM3 | 2%WRP | 3%WRP | 2%DRP | 4%DRP | 6%DRP |
|---|---|---|---|---|---|---|---|
| $d_{5000}$ (mm) | 3.2 | 1.9 | 1.4 | 2.8 | 0.8 | 0.8 | 0.3 |
| $d_{10000}$ (mm) | 3.9 | 2.3 | 1.7 | 3.3 | 0.9 | 0.9 | 0.4 |
| $PRD_{10000}$ (%) | 7.8 | 4.6 | 3.3 | 6.5 | 1.8 | 1.9 | 0.7 |
| $WTS_{AIR}$ (mm/1000 cs) | 0.148 | 0.072 | 0.041 | 0.090 | 0.016 | 0.028 | 0.009 |

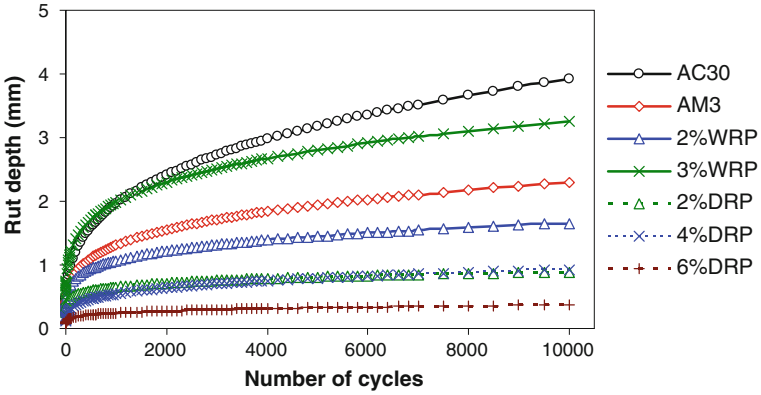


**Fig. 5** Evolution of the rut depth for the analyzed mixtures

Thus, the incorporation of RP in the mixture strongly reduces the permanent deformation susceptibility of the mixture.

## 4 Conclusions

This paper presents the results obtained about the use of recycled polyethylene (RP) in asphalt mixtures. Mixtures containing recycled polyethylene RP from silo-bags incorporated by wet and dry processes were used in this laboratory study to evaluate the performance characteristics of the resulting modified bitumens and the corresponding mixtures.

The obtained data showed that the use of RP modified the bitumen´s and the mixture's performances in several ways as summarized below:

The addition of RP influences the characteristics of the base bitumen with a decreasing of the Penetration at 25 °C and an increasing of the Softening Point, the Rotational Viscosity and the Elastic Recovery.

The mixtures prepared with RP added by the Dry and the Wet processes meet the volumetric and mechanical requirements used in Argentina for base courses of asphalt pavements.

The mixtures containing RP added by the Wet process have smaller stabilities and greater flows compared to the control mixture but the stability and the flow increase with increasing the RP content added by the Dry process.

The Indirect Tensile Strength decreases as the amount of RP increases for the mixtures containing recycled polyethylene added by any of the two processes. However, for the mixtures with RP added by the Dry process, the fracture energy increases as the amount of RP increases with fracture energies higher than that for the control mixture.

All mixtures with RP satisfy the requirements relating to the moisture susceptibility.

The five mixtures containing RP have lower dynamic modulus values at low temperature and high frequency compared to the AC30 mix and, higher dynamic modulus values at high temperature and low frequency. Thus, the thermal susceptibility of the mixtures containing RP is smaller than the AC30 mix and in several cases, even smaller than the AM3 mixture. At high temperatures, the mixtures containing RP are stiffer compared to the AC30 mixtures and then, more resistant to the development of permanent deformations.

The rut depths at the end of the permanent deformation tests for the mixtures containing RP are smaller than the control mix and the wheel-tracking slopes are 2 to more than 10 times smaller than the AC30 mixture. Thus, the incorporation of RP in the mixture strongly reduces the permanent deformation susceptibility of the mixture.

Beyond the modifications of the mechanical properties for the mixtures containing RP, this paper shows that the addition of this kind of plastic waste is feasible and it could have a positive effect on the sustainability, turning into an environmental friendly alternative in the asphalt pavements industry.

This study is part of an ongoing research project at the University of Rosario, Argentina. Other subjects such as fatigue test results, the use of additives to improve the storage stability of the blends and other percentages of added RP are being investigated and will presented in future papers.

## References

Al-Hadidy AI, Yi-qiu T (2009) Effect of polyethylene on life of flexible pavements. Construction and Building Materials 23: 1456–1464. Doi: 10.1016/j.conbuildmat.2008.07.004.

Angelone S, Borghi M, Cauhape Casaux M and Martinez F (2013) Evaluation of Different Procedures and Models for the Construction of Dynamic Modulus Master Curves of Asphalt Mixtures. Paper presented at the 9th International Conference on the Bearing Capacity of Roads, Railways, and Airfields, Trondheim, Norway.

Attaelmanan M, Feng CP and Al-Hadidy A (2011) Laboratory evaluation of HMA with high density polyethylene as a modifier. Construction and Building Materials 25: 2764–2770. doi: 10.1016/j.conbuildmat.2010.12.037.

European Committee for Standardization (2003) Bituminous mixtures - Test methods for hot mix asphalt – Part 12: Determination of the water sensitivity of bituminous specimens, EN 12697-12:2003: E.

European Committee for Standardization (2003) Bituminous mixtures - Test methods for hot mix asphalt – Part 22: Wheel tracking, EN 12697-22:2003: E.

European Committee for Standardization (2003) Bituminous mixtures - Test methods for hot mix asphalt – Part 23: Determination of the indirect tensile strength of bituminous specimens, EN 12697-23:2003: E.

European Committee for Standardization (2004) Bituminous mixtures - Test methods for hot mix asphalt – Part 34: Marshall test, EN 12697-34:2004: E.

Fawcetta AH, McNallya T, McNallyb GM, Andrewsc F and Clarkec J (1999) Blends of bitumen with polyethylenes. Polymer 40: 6337–6349. PII: S0032-3861(98)00779-4.

Hinishoglu S and Agar E (2004) Use of waste high density polyethylene as bitumen modifier in asphalt concrete mix, Materials Letters 58: 267– 271. doi: 10.1016/S0167-577X(03)00458-0.

Ho S, Church R, Klassen K, Law B, MacLeod D and Zanzotto L (2006) Study of recycled polyethylene materials as asphalt modifiers, Can. J. Civ. Eng., 33-8: 968-981.

Huang Y, Bird RN and Heidrich O (2007) A review of the use of recycled solid waste materials in asphalt pavements. Resources, Conservation and Recycling 52: 58–73. doi: 10.1016/j.resconrec.2007.02.002.

Lee SJ, Rust JP, Hamouda H, Kim YR, Borden RH (2005) Fatigue Cracking Resistance of Fiber-Reinforced Asphalt Concrete. Textile Research Journal, 75: (2): 123-128. doi: 10.1177/0040517505075002O6.

Martinez F and Angelone S (2012) The indirect tensile test configuration in the determination of the complex modulus of asphalt mixtures. Paper presented at the 5th Eurasphalt & Eurobitume Congress, Istanbul, Turkey.

National Research Council (2004) Mechanistic-Empirical design of new and rehabilitated pavement structures. Draft Report, NCHRP 1-37a.

Witczak M, Kaloush K, Pellinen T, El-Basyouny M and Von Quintus H (2002) Simple Performance Test for Superpave Mix Design. NCHRP Report 465, NCHRP Program, National Academy Press, Washington, D.C.

Zoorob SE and Suparma LB (2000) Laboratory design and investigation of the properties of continuously graded Asphaltic concrete containing recycled plastics aggregate replacement (Plastiphalt). Cement & Concrete Composites 22 (2000) 233-242.

# Rheological Characterization of Bituminous Mastics Containing Waste Bleaching Clays

**Francesco Mazzotta, Cesare Sangiorgi, Valeria Vignali, Claudio Lantieri and Giulio Dondi**

**Abstract** Bleaching clays are mostly used in food industries to clarify vegetal oils. After use they are generally dumped as waste (stage 1) or used in green innovative plants to feed biogas reactors (stage 2). In latter stage the initial residual oil content (approx. 25 % by mass) is reduced to less than 1 % by the biological process. In this study the bleaching clays effects on bituminous mastics of a traditional binder course Hot Mix Asphalt have been investigated. The physical characteristics of the two bleaching clays and of a traditional limestone filler were also studied. DSR rheological tests at high and low temperatures were performed on mastics samples containing different amounts of fillers (limestone, stage 1 or stage 2). The addition of the different waste bleaching clays significantly affects the rheological behavior of the mastics: the filler from stage 2 increases the mastic stiffness improving the resistance to permanent deformations as shown by repeated creep tests, while the filler from stage 1 strongly interacts with the bitumen reducing the mechanical characteristics of the mastics at all temperatures.

**Keywords** Bleaching clays · Bituminous mastics · Dynamic shear rheometer · Recycling

## 1 Introduction

The analysis of the response to load and temperature stresses of the asphalt pavement cannot be separated from the rheological study of the asphalt mastic. The latter, in fact, has a significant impact on the road performance and on the service life of the asphalt mixture. Asphalt-filler mastic consists of bitumen and mineral filler that is defined as the portion of aggregates passing the 63 μm sieve (EN

F. Mazzotta (✉) · C. Sangiorgi · V. Vignali · C. Lantieri · G. Dondi
Department of Civil, Chemical, Environmental, and Materials Engineering—DICAM, University of Bologna, Bologna, Italy
e-mail: francesco.mazzotta2@unibo.it



F. Canestrari and M.N. Partl (eds.), *8th RILEM International Symposium on Testing and Characterization of Sustainable and Innovative Bituminous Materials*, RILEM Bookseries 11, DOI 10.1007/978-94-017-7342-3_48

13043) and that is generally added to the aggregate mixture during the asphalt mixing process.

Numerous research works show that the mechanical performance of asphalt mastics is largely dependent on fillers properties and on the way they interact with the bitumen (Vignali et al. 2014; Delaporte et al. 2007). This also happens when alternative materials are used instead of common fillers. There are now many studies on scrap and/or waste materials used as fillers in addition or in substitution of raw materials in the production of asphalt concretes (Santagata et al. 2014). Sangiorgi et al. (2014) have examined two different types of bentonite clays as replacement of limestone filler for the production of binders course HMAs. The bentonites come from two consecutive industrial processes: spent bentonite (Ut) obtained from a vegetable oil bleaching process (stage 1), and digested spent bentonite (Ud) the result of the anaerobic digestion of spent bentonite within a reactor producing biogas (stage 2). From the analysis of Indirect Tensile Strength and Indirect Tensile Stiffness Modulus data, it was found that the presence of Ut or Ud fillers has a totally different effect on the bituminous mixture's mechanical properties. While digested spent bentonite clay determines an increase in indirect tensile strength and stiffness compared to the mixture with limestone filler, the presence of Ut filler results in an evident reduction of these properties. Besides from the analysis of the dynamic creep test, it was concluded that the substitution of the limestone filler with the Ut filler determines a reduction of resistance to permanent deformations, which is, however, improved using the Ud filler.

Based on these findings the main objective of the present research is to investigate the rheological properties of bituminous mastics containing Ut and Ud fillers, to compare with a traditional mastic containing limestone filler. The mastic stress-strain response is studied through Frequency Sweep (FS), Repeated Creep Recovery (RCR) and Multiple Stress Creep Recovery (MSCR) tests.

## 2 Materials

In this study three different mastics were produced with a hot mixing process using a 50/70 penetration grade bitumen. The characteristics of the bitumen are shown in Table 1. Three fillers were used: limestone filler, spent bentonite (Ut) and digested spent bentonite (Ud). The following mastics were produced according to the proportions of the AC mixtures studied by Sangiorgi et al. (2014) and summarized in Table 2.

**Table 1** Properties of the 50/70 pen bitumen

| | Unit | Characteristic value | Standard |
|---|---|---|---|
| Penetration @ 25 °C | dmm | 50–70 | EN 1426 |
| Soft. point | °C | 50 | EN 1427 |
| Dynamic visc. @ 60 °C | Pa s | 145 | EN 12596 |
| Fraass | °C | −8 | EN 12593 |

**Table 2** Weights percentages of fillers on bitumen

| Mastic | Limestone filler (%) | Ut | Ud |
|---|---|---|---|
| Mff | 70.6 | – | – |
| MUt | 41.8 | 28.8 % | – |
| MUd | 41.8 | – | 28.8 % |

**Table 3** Main fillers characteristics

| | Standard | Limestone filler | Ut filler | Ud filler |
|---|---|---|---|---|
| Particle density (Mg/m$^3$) | EN 1097-7 | 2.73 | 1.59 | 1.84 |
| Rigden voids (%) | EN 1097-4 | 33.82 | 31.69 | 53.75 |
| Δ Ring and Ball (°C) | EN 13179-1 | 8 | −22 | 32 |

- mastic Mff: 50/70 bitumen with limestone filler;
- mastic MUt: 50/70 bitumen with spent bentonite Ut and limestone filler;
- mastic MUd: 50/70 bitumen with digested bentonite Ud and limestone filler.

### *2.1 Fillers from Bleaching Clay*

Two different bentonite fillers were used in the experimental study obtained from two consecutive phases in the process of bleaching vegetable oils and producing energy from biogas. The filler labelled Ut was derived directly from the bleaching phase (stage 1) and, for this reason, its oil content ranges between 20 and 25 % of its dry weight. The other filler, Ud, i.e. the digested spent bentonite, is the result of the anaerobic digestion of the Ut filler during the process to produce biogas (stage 2). This phase of biochemical conversion determines a reduction of the content of residual oils, to below 1 %.

In order to be used as fillers, both spent bleaching clays were geometrically characterized through a gradation analysis (EN 933-10) and volumetrically, determining their volumetric mass (EN 1097-7) and Rigden Voids (EN 1097-4) (Sangiorgi et al. 2014). Delta Ring and Ball test was also performed according to EN 13179-1. Table 3 shows the fillers characteristics.

## 3 Test Method and Procedures

### *3.1 Frequency Sweep Test*

Rheological measurements were performed using a stress/strain controlled Dynamic Shear Rheometer equipped with a parallel plate and plate geometry. The frequency sweep (FS) test was performed in strain control configuration, where the

strain amplitude was limited within the linear viscoelastic (LVE) range. Linear behavior should be considered, to obtain the stress–strain state in the pavement structure under traffic or climatic loadings, when a rational mechanical approach is applied (Di Benedetto et al. 2007). Amplitude Sweep (AS) tests were preliminary carried out, to investigate the viscoelasticity region at 10 °C, applying a constant frequency of 10 rad/s (1.59 Hz). Linear visco-elastic deformations, $\gamma_{LVE}$, found for the three mastic were: 1.5 % for Mff, 2.5 % for MUt and 1.0 % for MUd. FS test was conducted in a range of frequencies between 0.01 and 10 Hz, at the temperatures of 0, 10, 20, 30, 40, 50 and 60 °C. The 8 mm plate with a 2 mm gap was adopted in all the range of temperatures (Dondi et al. 2014). With the FS test the complex shear modulus (G*) and the phase angle (δ) were measured.

### 3.2 Repeated Creep Recovery Test

Repeated Creep Recovery tests (RCR) were conducted with 25 mm parallel plates (PP) and a 1 mm gap under three different temperature conditions 46, 58 and 64 °C. The testing temperatures were selected in agreement with AASHTO M-320 (2015). Mff, MUt and MUd were tested with 100 cycles at a stress level of 1 kPa. Each loading cycle consisted of 1 s creep and 9 s recovery (NCHRP Report 459). The accumulated strain was calculated for each test at the end of 100 cycles.

### 3.3 Multiple Stress Creep Recovery Test

The Multiple Stress Creep and Recovery test (MSCR) was run according to the AASHTO TP 70–07 (2013) "*Standard Method of Test for Multiple Stress Creep and Recovery* (*MSCR*) *of Asphalt Binders using a Dynamic Shear Rheometer*". According to this standard, mastic sample is loaded at a constant creep stress for 1 s, followed by a zero stress recovery of 9 s. Ten cycles of creep and recovery are run at 0.1 kPa creep stress, followed by ten at 3.2 kPa creep stress. The non-recoverable compliance ($J_{nr}$) and the percent recovery after ten cycles at 0.1 and 3.2 kPa were studied. The $J_{nr}$ value was calculated as the ratio between the average non recoverable strain for 10 creep and recovery cycles, and the applied stress for those cycles. The testing temperatures of 46, 58 and 64 °C were adopted.

## 4 Results and Discussion

### 4.1 Frequency Sweep Test

The complex modulus G* and phase angle δ of mastics MUt, Mff and MUd are represented in terms of master curves in Fig. 1. Using the principle of

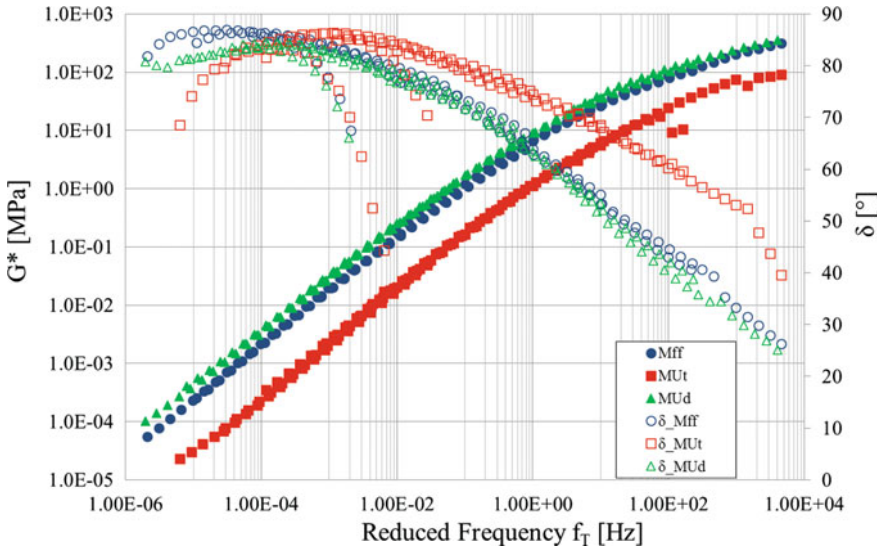


**Fig. 1** Master curves for Mff, MUt, and MUd mastics at 20 °C

time-temperature superposition (TTS) the master curves of G* and δ were plotted at the reference temperature of 20 °C. The Williams-Landel-Ferry model was used to obtain the temperatures shift factors.

Results show that in all range of frequencies the mastic containing the spent bentonite Ut attains G* values lower than the Mff and MUd mastics ones. Given the nature of the two recycled fillers it can be stated that this difference is mainly due to the different content in residual oil. This is evident at low temperatures or high frequencies where the behavior of the Ut mastic should be dominated by the properties of the base bitumen, but which, in this case, does not tend to the glassy modulus as the Mff and MUd mastics do.

Consistent differences between Mff and MUd mastic can be seen at low frequencies, where the MUd mastic shows higher moduli. It can be inferred that if the presence of filler Ud increases the mastic stiffness at low frequencies it will potentially increase also the resistance to permanent deformations. This can be traced back to the high level of Rigden voids that can demonstrate the stiffening power of the Ud filler (Faheem et al. 2012).

The mastic containing Ut filler exhibits higher phase angles at medium and low temperatures than Mff and MUd phase angles. At the high temperatures the MUt phase angle decreases, but this effect is significantly far from the one of polymers in polymer modified bitumens. The Mff and MUd δ values are approximately equivalent at medium and high frequencies, and in particular at high frequencies/low temperatures the mastics response is almost elastic (30°). At high temperatures, on the contrary, the MUd phase angle shows a significant reduction compared to Mff phase angle.

**Table 4** Rutting parameters of Mff, MUt and MUd

| Mastic | Temperature (°C) | G*/senδ (kPa) |
|---|---|---|
| Mff | 60 | 7.0 |
| MUt | 60 | 2.5 |
| MUd | 60 | 9.5 |

The presence of digested bentonite Ud shifts the rutting parameter G*/senδ to higher values. This could be seen in Table 4, in which G*/senδ values are reported for the three mastics at 60 °C.

## *4.2 Repeated Creep Recovery Test*

In order to investigate the materials response to permanent deformations RCR test in plate-plate (PP) configuration were performed at the temperatures of 46, 58 and 64 °C. Figure 2 shows, as an example, the test results at the temperature of 46 °C. In this case, the mastic containing the digested bentonite Ud has accumulated less deformations compared to Mff and MUt that has reached shear strain values close to 100.

Figure 3 shows the test results of the first cycle at 1 kPa at the three test temperatures. The MUt shows considerable higher creep strain at all test conditions. In particular, at 58 °C the mastic containing the spent bentonite reaches a peak of deformation even higher than the Mff and MUd peaks strain at 64 °C. The MUd mastic shows less sensitivity to deformation in all test conditions.

As shown in Fig. 4 this mastics relative behavior is enhanced at the end of the 100th cycle. In fact, MUt has accumulated 461 and 961 strain at 58 and 64 °C respectively, while Mff and MUd that have reached 75 and 158 strain at 58 °C and 197 and 295 strain at 64 °C. The accumulated strain difference between the Mff and

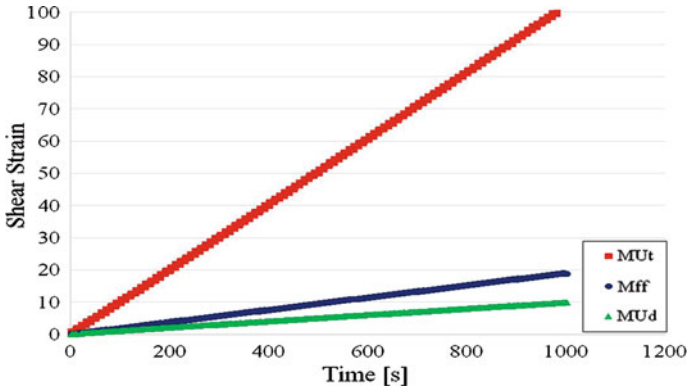


**Fig. 2** Results of the accumulated strain under repeated creep testing @ 46 °C

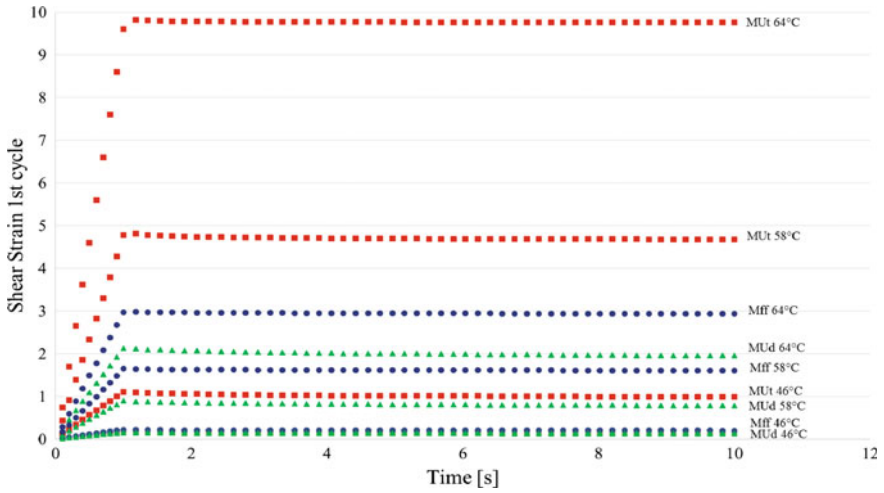


**Fig. 3** Strain/time for the first cycle of RCR test at 1 kPa at 46, 58 and 64 °C

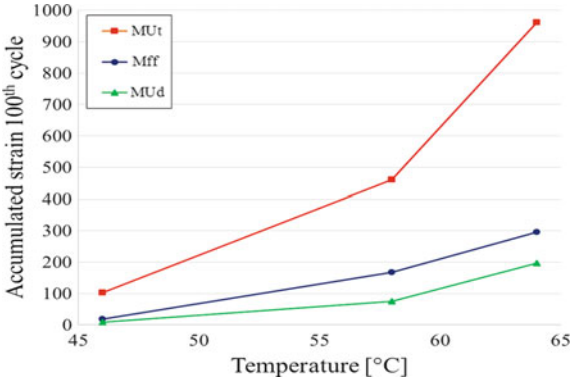


**Fig. 4** Accumulated strain values at the end of 100th cycle at @ 46, 58 and 64 °C

MUd mastics is close to 10 at 46 °C and undergoes a significant increase to 96 at the temperature of 58 °C, remaining constant up to 64 °C.

From this analysis, it is possible to confirm the repeated load axial test results on binder course mixtures presented by Sangiorgi et al. (2014) where the presence of Ud filler used in substitution of the traditional limestone filler decreases the accumulated strain compared to the adopted control mixture.

The percentage of recovery from RCR tests was also obtained and calculated as the ratio between recovered strain and peak strain at the 1st cycle and at the 100th cycle. In Fig. 5, the MUd mastic has higher recovery than Mff and MUt at the three test temperatures. Mff and MUt have the same recovery for each test configuration. For MUd there is a constant decrease of 25 % of recovery with increasing temperature than Mff and MUt mastics for which there is a decrease of 80 % of

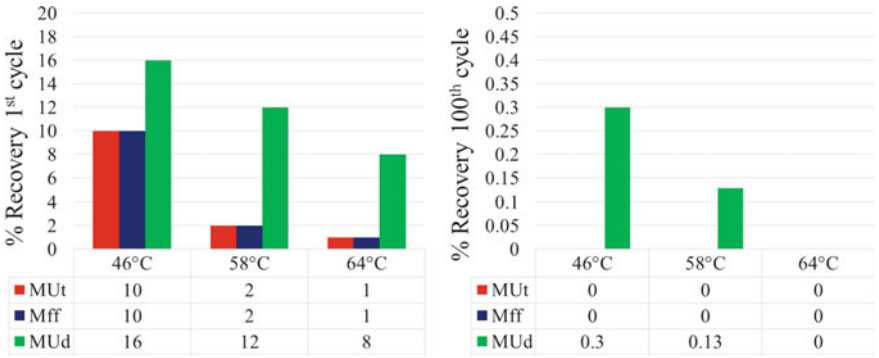


**Fig. 5** Comparison of RCR percentage recovery at the 1st and 100th cycle @ 46, 58 and 64 °C

recovery from 46 to 58 °C. At the last load cycle for MUt and Mff mastics the percentage of recovery is 0 at all temperatures. The MUd is the only mastic that shows a small percentage of recovery of 0.3 % at 46 °C and 0.13 % at 58 °C.

## *4.3 Multiple Stress Creep Recovery Test*

The multiple stress creep-recovery (MSCR) test was developed based on creep studies conduct during the NCHRP 9-10 research program (Bahia and Hanson 2001). According to the literature (D'Angelo et al. 2007; D'Angelo 2009; Wasage et al. 2010), this test can predict the deformation behavior of binders. By applying different stress levels, it can identify binders that are overly stress sensitive in the nonlinear region (Soenen et al. 2013). For this reason it was chosen to investigate further the potential rutting of the three mastics Mff, MUt and MUd through MSCR test run at 0.1 and 3.2 kPa. Figure 6 shows the test results at the temperature of 46 °C. Also in this test configuration the mastic containing the digested bentonite Ud always exhibits the stiffer behavior, accumulating less deformation at the end of the 10 cycles at 3.2 kPa.

As shown in Fig. 7 the mastic MUt has accumulated the largest deformation under the two stress conditions, while the MUd mastic shows the lower values of deformation, even when the temperature increases. For the MUt mastic most part of the strains was developed at the higher stress level.

Table 5 shows the average percentage of recovery of the three mastics under 3.2 kPa shear load at the three test temperatures of 46, 58 and 64 °C. At the temperature of 46 °C the MUd mastic attains an average recovery percentage value higher than Mff and MUt; in particular, the average recovery percentage of mastic containing digested bentonite reaches 3 %. At 58 °C Mff and MUt do not recover and MUd recovers only the 0.25 % of deformation. At the highest test temperature of 64 °C all the mastics have no recovery.

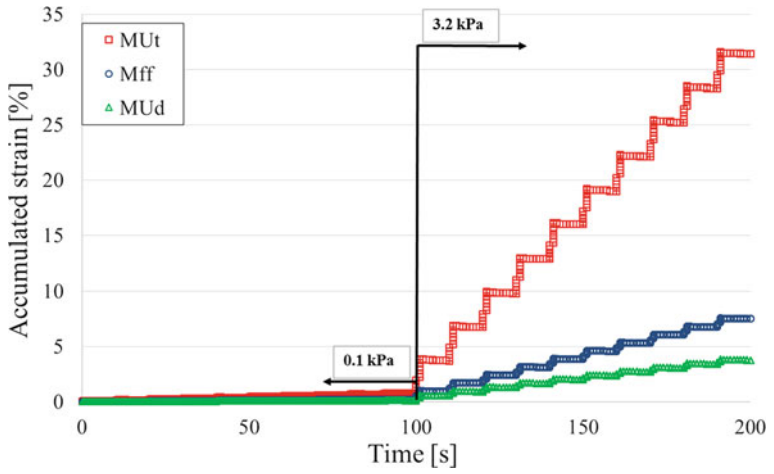


**Fig. 6** MSCR test results at @ 46 °C

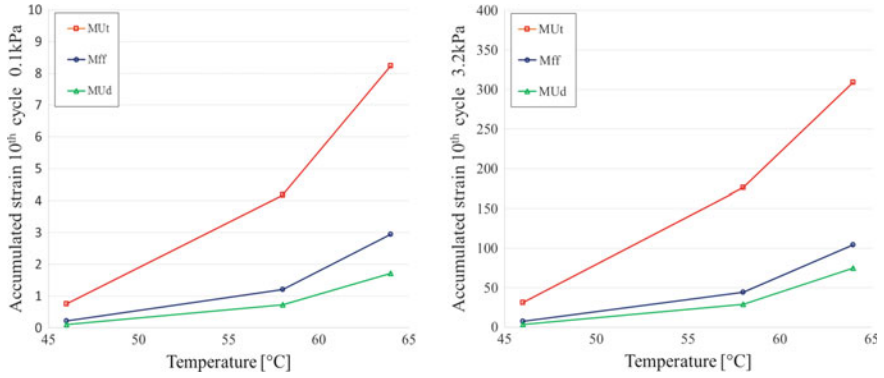


**Fig. 7** Accumulated strain values at the end of 10th cycle at 0.1 and 3.2 kPa

**Table 5** Mff, MUt and MUd average percentage of recovery at 3.2 kPa

| Mastic | Temperature (°C) | | |
|---|---|---|---|
| | 46 | 58 | 64 |
| | Average percentage recovery | Average percentage recovery | Average percentage recovery |
| Mff | 1.00 | 0 | 0 |
| MUt | 0.42 | 0 | 0 |
| MUd | 3.07 | 0.25 | 0 |

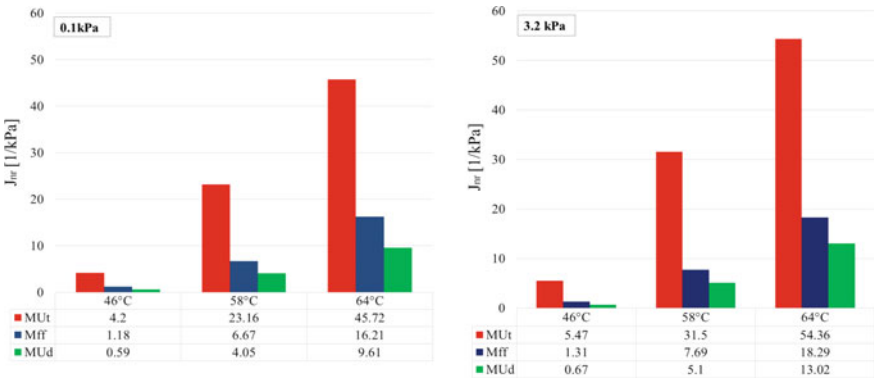


**Fig. 8** Mff, MUt and MUd non recoverable compliance at 0.1 and 3.2 kPa

The creep compliance $J_{nr}$ parameter is a measure of the non-recoverable behavior of a binder caused by creep-recovery cycles, and it is therefore suggested to describe the binder contribution to asphalt mixture permanent deformations (D'Angelo et al. 2006). The $J_{nr}$ values were calculated for the three mastics under 0.1 kPa (Fig. 8a) and 3.2 kPa (Fig. 8b) shear stresses at the three test temperatures of 46, 58 and 64 °C. The MUd mastic has lower values of non recoverable compliance at both shear stresses, showing a less sensitivity of the mastic to permanent deformations. In particular, at 3.2 kPa the mastic containing the Ud filler shows a $J_{nr}$ value of 13.0 l/kPa at 64 °C while the $J_{nr}$ value of mastic containing only limestone filler that is of 18.3 l/kPa at the same shear stress and temperature. The MUt mastic has the higher values of $J_{nr}$ under all test conditions, it is once again proven that the 25 % of oil in the Ut filler acts on the base bitumen and makes the mastic softer and more susceptible to permanent deformations.

## 5 Conclusions

On the basis of the experimental data presented in this study the following conclusions can be drawn:

- the comparison of the mastics master curves from FS and AS tests show that the substitution of part of the filler in the mixture with the proposed bleaching clays fillers is significantly effective on altering their rheological behavior. Substitutions were made so as to replicate the actual binding mastics of the HMAs tested in previous research. In particular, the study at the mastic scale confirmed that the Ud filler stiffens the base bitumen, while the Ut filler softens the mastic by a considerable amount. Positive aspects with reference to the possible use of mastics in road bituminous pavements are related to the fact that the MUt mastic does not reach the glassy modulus at high frequencies (low

temperatures) and that the MUd mastic is stiffer than the Mff mastic at the high temperatures (low frequencies). This is more likely due to the higher value of Ridgen voids of the Ud filler;

- the RCR and MSCR tests results corroborate the repeated load axial test results from previous research on HMAs. The Ut filler reduces the resistance to permanent deformations, while the Ud filler increases it at the different testing temperatures. Also the $J_{nr}$ analysis confirms that the non recovered deformations are reduced in the MUd mastic. Again the rheological effect of the Ut filler is more evident in comparison with the traditional mastics containing only limestone filler. The residual oil in the Ut filler is evidently interacting with the bituminous phase more than the mineral particles, thus reversing the effects of the Ud filler;
- the overall rheological analysis confirms that the Ud filler appears to have more positive effects on the mastic of an HMA and this is mainly due to the stiffening power of this digested bleaching clay; nevertheless some positive aspects of the use of Ut filler in mastics can be capitalized on the production of bituminous sealants or membranes were high percentages of fillers are used;
- the presented results are part of a larger study where it is foreseen the optimization of waste bleaching clay fillers volumetrics in the bituminous mixtures. This is to overcome the gradation issues related to the lower particle densities and to take advantage of the high stiffening power of the Ud filler and of the bitumen interaction of the oil in the Ut filler.

## References

AASHTO M-320. (2015) Standard specification for performance – graded asphalt binder.

AASHTO TP 70–07. (2013) Standard Method of Test for Multiple Stress Creep Recovery (MSCR) Test of Asphalt Binder Using a Dynamic Shear Rheometer (DSR).

Bahia HU, Hanson DI, Zeng M, Zhai H, Khatri MA, Anderson RM (2001) Characterization of modified asphalt binders in superpave mix design (No. Project 9-10 FY'96).

D'Angelo J (2009) The relationship of the MSCR test to rutting. Road Materials and Pavement Design Special Issue, 10: 61–80. doi: 10.3166/RMPD.10HS.61-80

D'Angelo J, Dongre R, Reinke G (2006) Evaluation of repeated creep and recovery test method as analternative to SHRP requirements for polymer modified asphalt binders.

D'Angelo J, Kluttz R, Dongre RN, Stephens K, Zanzotto L (2007) Revision of the Superpave high temperature binder specification: The multiple stress creep recovery test. Association of Asphalt Paving Technologists – Proceedings of the Technical Sessions 76: 293–331.

Delaporte B, Di Benedetto H, Chaverot P, Gauthier G (2007) Linear viscoelastic properties of bituminous materials: From binders to mastics. Association of Asphalt Paving Technologists-Proceedings of the Technical Sessions 76: 455-494.

Di Benedetto H, Delaporte B, Sauzéat C (2007) Three-Dimensional Linear Behavior of Bituminous Materials: Experiments and Modeling. International Journal of Geomechanics 7, No. 2, 149-157. doi:10.1061/(ASCE) 1532-3641(2007)7:2(149)

Dondi G, Vignali V, Pettinari M, Mazzotta F, Simone A, Sangiorgi C (2014) Modeling the DSR complex shear modulus of asphalt binder using 3D discrete element approach. Construction and Building Materials 54: 236–46. doi: 10.1016/j.conbuildmat.2013.12.005

Faheem AF, Hintz C, Bahia H, Al-Qadi I (2012) Influence of filler fractional voids on mastic and mixture performance. Paper presented at the Transportation Research Board Annual Meeting, Washington, D.C., January 22-26.

Sangiorgi C, Tataranni P, Simone A, Vignali V, Lantieri C, Dondi G (2014) Waste bleaching clays as fillers in hot bituminous mixtures. Construction and Building Materials 73: 320–325. doi: 10.1016/j.conbuildmat.2014.09.076

Santagata E, Bassani M, Baglieri O (2014) Use of vitrified municipal solid waste bottom ash as a filler substitute in asphalt mixtures. Sustainability, Eco-Efficiency and Conservation in Transportation Infrastructure Asset Management - Proceedings of the 3rd International Conference on Transportation Infrastructure, ICTI: 15-21. Code 103391

Soenen H, Blomberg T, Pellinen T, Laukkanen O (2013) The multiple stress creep – recovery test: a detailed analysis of repeatability and reproducibility. Road Materials and Pavement Design Vol. 14, No. S1: 2–11. doi: 10.1080/14680629.2013.774742

Vignali V, Mazzotta F, Sangiorgi C, Simone A, Lantieri C, Dondi G (2014) Rheological and 3D DEM characterization of potential rutting of cold bituminous mastics. Construction and Building Materials 73: 339-349. doi: 10.1016/j.conbuildmat.2014.09.051

Wasage T, Stastna J, Zanzotto L (2010) Repeated loading and unloading tests of asphalt binders and mixes. Road Materials and Pavement Design 11: 725–744. doi: 10.3166/RMPD.11.725-744

# Asphalt Mixture with RAP: Mix Design Optimization

**N. Bueche, A.-G. Dumont, M. Pittet and S. Bressi**

**Abstract** The addition of reclaimed asphalt pavement (RAP) in hot mix asphalt is now common practice in Switzerland. With the increases of RAP content in asphalt mixture, the problematic of the mix design optimization becomes an important issue to be considered. The described project deals with the mix design optimization of hot mix asphalt containing 40 % RAP. In a first phase, an analytical mix design has been conducted. The use of such a numerical method presents in particular the advantages of optimizing laboratory testing and allowing the realization of sensitivity analysis. An extensive laboratory study has been conducted in a second phase. This study permitted to clearly identify and quantify the impacts of the aggregates quality and binder content on the final mixture performances. The various tests achieved highlighted that rutting susceptibility is one of the suitable indicators for the assessment of a mix design performances. The research carried out finally permitted to highlight the benefits of an analytical mix design in a mixture optimization process. The major factors influencing the mix design have been identified and quantified through laboratory testing and some recommendations concerning the tests to carry out are also provided.

**Keywords** Reclaimed asphalt (RAP) · Mix design · Asphalt mixture · Mechanical performances

## 1 Context and Knowledge Update

The addition of reclaimed asphalt pavement (RAP) in hot mix asphalt (HMA) is now common practice in Switzerland. With the increases of RAP content in asphalt mixtures, the problematic of the mix design optimization becomes an important

N. Bueche (✉) · A.-G. Dumont · M. Pittet · S. Bressi
Traffic Facilities Laboratory (LAVOC), Ecole Polytechnique Fédérale de Lausanne (EPFL), Station 18, 1015 Lausanne, Switzerland
e-mail: nicolas.bueche@epfl.ch



F. Canestrari and M.N. Partl (eds.), *8th RILEM International Symposium on Testing and Characterization of Sustainable and Innovative Bituminous Materials*, RILEM Bookseries 11, DOI 10.1007/978-94-017-7342-3_49

issue to be investigated. The present research, financed by the Federal Road Administration (FEDRO) in Switzerland, is part of a wider research project dealing with the addition of RAP in asphalt pavements.

The mechanical behavior of asphalt mixture containing RAP has been investigated within various projects during the last decade. One can for instance mention the European research projects PARAMIX (Road Pavement Rehabilitation Techniques Using Enhanced Asphalt Mixtures, 2001–2004), SAMARIS (Sustainable and Advanced Materials for Roads and Infrastructures, 2002–2006), Re-Road (End of Life Strategies of Asphalt Pavements, 2009–2012) and Direct-MAT (Dismantling and recycling techniques for road materials, 2009–2011).

The mix design optimization of asphalt mixtures containing RAP have been also addressed by some authors, but mainly through empirical researches without specific sensitivity analyses on key parameters. For instance, some interesting information can be found in the FHWA report (Copeland 2011) and NCHRP Project 9–12 (McDaniel et al. 2000). The work performed by (Al-Qadi et al. 2007), (Valdès Vidal et al. 2010) who studied an experience of asphalt mixture with 40 and 60 % RAP laid on the Highway and (Widyatmoko 2008) who performed an extensive laboratory study can also be highlighted. Some authors also investigated the interaction mechanisms between new bitumen and RAP binder, as for instance (Nguyen 2009; El Bèze 2008) where the author reports that the binder mixing appears but in an inhomogeneous way, or (Yousefi Rad 2013) who applied a laboratory method investigating the blending ratio between fresh and RAP binder.

## 2 Project Objectives and Organization

The main objectives of the project related to the mix design of HMA with RAP are followings:

- Highlight the major parameters governing the mix design procedure.
- Identify the laboratory testing to be performed for a proper evaluation of such asphalt mixtures.
- Determine if the current standards related to material characterization are sufficient in order to guarantee an asphalt mixture at least as good as a mixture without RAP.
- Define the methodology that should be applied in laboratory for the production, conditioning and reheating process of such mixtures.

The first two objectives will be discussed in this paper. For some more information, one can recommend (Dumont and Pittet 2012; Bueche et al. 2014; Fénart et al. 2012).

## 3 Base Parameters

In the whole research, a Swiss asphalt mixture for top layer AC 11 S (i.e. max aggregate size 11 mm) (Fig. 1) with 40 % RAP has been considered. The total binder content (reference value) is 6.10 %/mixture (6.50 %/aggregates) and the richness modulus 3.9.

A similar RAP 0/11 has been used for the whole research, with a (not modified) binder content of 5.70 %/mixture (6.04 %/aggregates) and a richness modulus of 3.37. The reclaimed asphalt contains a relatively high portion of filler (11.7 %) that can impact the mechanical performances of the final mixture.

In addition to a reference pen 160/220 bitumen, two new binders (or fresh binders) have been considered namely a pen 70/100, and a PmB Styrelf C85. The characteristics of the new bitumen as well as RAP binder (solvent extraction) are reported in Table 1.

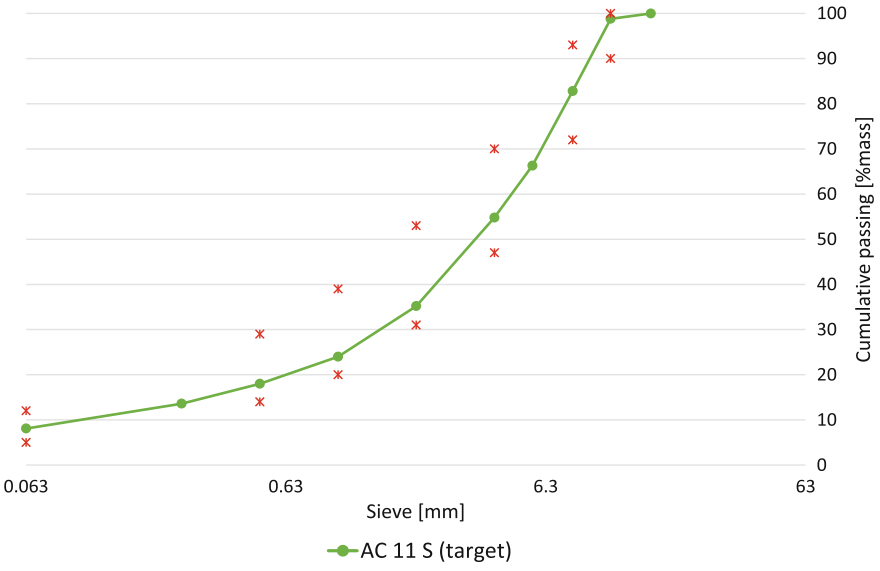


**Fig. 1** Grading curve of AC 11 S (reference mixture)

**Table 1** Binder characteristics

| | Pen @ 25 °C ($10^{-1}$ mm) | R&B Temp (°C) | IP (−) |
|---|---|---|---|
| New bitumen 160/220 (REF) | 192 | 39.6 | −0.4 |
| New bitumen 70/100 | 74 | 48.1 | −0.7 |
| New bitumen PmB C85 | 74 | 54.1 | 0.8 |
| RAP Binder | 52 | 52.2 | −0.6 |

## 4 Analytical Mix Design

In a first phase, an analytical mix design has been performed by applying the method developed by BRRC (Belgium) and implemented in PradoWin® software. This empirical method is based on a volumetric approach (Steuperaert and Vanelstraete 1997; Franken and Vanelstraete 1993). The calculation requires in particular binder (Pen, R&B, density, viscosity) and aggregates (density, grading curve, angularity) properties as input values and then calculates the voids contents for a given binder content (or otherwise). Note that the software contains a section that allows calculating some mixture characteristics and performances (e.g. stiffness, fatigue). The use of an analytical mix design method permits decreasing the amount of laboratory testing and measurements, and also contributes to a better understanding of the mechanical behavior of asphalt mixtures. Besides, the method permits to achieve some sensitivity analyses.

In a first phase, the reference mixture (AC 11S, 40 % RAP, B160/220) has been modelled and the void content calculated for the reference binder content (6.10 %). The comparison between calculated (i.e. PradoWin®) and measured (i.e. lab. hydrostatic measurement, mean of 4 replicates) void content can be found in Fig. 2. A good correspondence between both values has been found, this being due in particular to the aggregates characteristics (angularity, grading) definition. The recipe with 40 % RAP appears to have a high level of compaction. For the mixtures without RAP, the compaction level proves to be more in adequacy with the required values (Swiss standards: voids 3–6 %). These results highlight a potential mixture optimization in case of RAP, this for instance by decreasing the binder content but

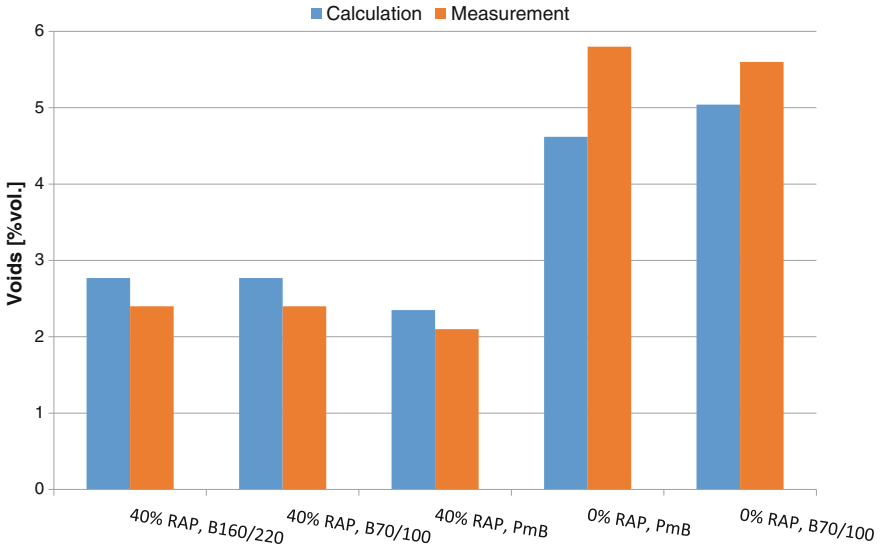


**Fig. 2** Difference between calculations and measurements for reference AC 11 S (6.10 % binder)

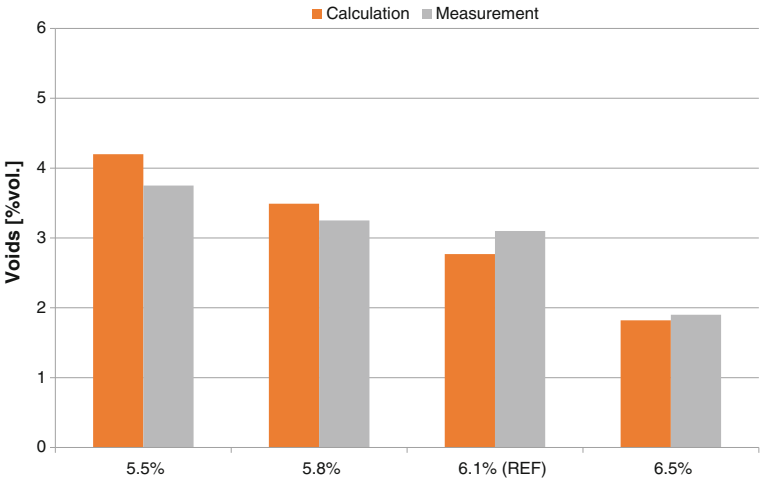


**Fig. 3** Mix design optimization: void content calculation (AC 11 S, 40 % RAP, B160/220)

still considering the required mastic film thickness (characterized by the richness modulus of mastic stiffness indicator MSI).

In a second phase, a mix design optimization has been investigated using the volumetric method. Various parameters have been considered: grading curve (especially filler and sand), aggregates quality (angularity), binder type and binder content. The results for different binder content (5.5–6.5 %) are presented in Fig. 3 for the reference mixture containing 40 % RAP. As expected, a decrease of the binder content permits to increase the voids while maintaining a sufficient film thickness. Based on this, one can suggest that the binder content that will lead to the best overall performances should be between 5.5 and 5.8 % for the mixture with 40 % RAP. A similar trend has been observed for the mixture without RAP; the optimal binder content being slightly higher (≥5.8 %).

It finally appears that the results of the calculations performed are consistent with the punctual laboratory testing performed. The method permits to quantify the impact of various parameters on the mixture mechanical behavior and on the volumetric characteristics. The calculation also highlighted a potential optimization stream for the reference mix design.

## 5 Laboratory Study

In a second phase, an extensive laboratory study has been conducted, this in order to identify the suitable tests methods and critical parameters governing the mix design procedure. The optimization of the reference mixture has also been studied.

## 5.1 Aggregates Extensive Characterization

Based on the analytical mix design, it appears that some characteristics of the raw materials have an important impact on the mechanical behavior of the asphalt mixture. Increasing the RAP content, it becomes necessary to have a better knowledge of its characteristics. Thus, in addition to the grading curve and density, the following parameters have been investigated on RAP and virgin aggregates:

- Percentage of crushed and broken surfaces in coarse aggregate particles (EN 933-5)
- Aggregates flow coefficient for 4/11 fraction (EN 933-6)

The results of crushed and broken surfaces in RAP are indicated in Table 2. Swiss standards do not contain limit values for AC 11 S aggregates. Nevertheless the uses of aggregates with an important proportion of rounded aggregates can lead to a higher rutting susceptibility, especially in case of wearing courses. It is therefore important to pay attention to the aggregates rounded part.

The flow coefficient of RAP and virgin aggregates can be found in Table 3. There is no Swiss standard providing limit values and the results have been evaluated through the comparison with some other aggregates (internal database). Both tested materials appear to be "semi-rubbing" that corresponds to an average or low mechanical behavior. In particular, the flow coefficient of the sand fraction is comparable to rounded sand.

A visual inspection of virgin aggregates (4/8, 8/11, 11/16, 16/22) confirmed that the virgin aggregates have partially damaged ridges that could lead to a weaker rutting resistance. Based on the extended tests on RAP and virgin aggregates, a sensitivity of the asphalt mixture to permanent deformation could be expected.

**Table 2** Crushed and broken surfaces in RAP 0/11

| Aggregates d/D (mm) | Totally crushed tc (%) | Partially crushed c (%) | Partially rounded r (%) | Totally rounded tr (%) | Category C |
|---|---|---|---|---|---|
| 8/11 | 42.5 | 30.5 | 14.3 | 12.7 | $C_{50/30}$ |
| 4/8 | 61.6 | 16.9 | 14.0 | 7.5 | $C_{70/10}$ |

**Table 3** Flow coefficient of RAP and virgin aggregates

| | Virgin aggregates flow coeff. (s) | RAP flow coeff. (s) |
|---|---|---|
| Sand 0.063/2 mm | 34 | 32 |
| Sand 0.063/4 mm | 18 | 16 |
| Aggregates 4/11 mm | 112 | 108 |

## 5.2 Tests Overview

As mentioned in Sect. 3, a similar grading curve has been used for the whole project as well as the same RAP sort. In other word, it is assumed that the optimal grading curve is similar for a mixture with and without RAP. Considering the importance of the virgin aggregates, four different origins (and quality) have been further investigated:

- BERAG: Reference aggregates, Bern region
- Bourgeoisie de Sion: Gravel pit aggregates, Sion region (Valais)
- Famsa: Quarry aggregates from Choëx-Massongex (high quality sandstone)
- Balmholz: Quarry aggregates from Swiss center part (siliceous stone)

The parameters finally considered are the virgin aggregate and the new bitumen. The mixtures and tests performed are summarized in Fig. 4 where the results discussed in this paper are indicated in green, while grey cells correspond to test performed but not discussed in the paper. Note that fatigue has not been investigated, this because of the mixture type (top layer).

In addition to this, a few specific investigations that will not be further discussed have been carried out. These investigations concern in particular the effect on laboratory/plant production, the impact of curing time and aggregates temperature on the mixture rutting susceptibility and the effect of the conditioning and asphalt

| N° | Recipe | Production | Aggregates | New binder | Marshall testing (S&F) | Water sensitivity (ITSR) | Rutting susceptibility | Giratory compactor | Complex modulus | Granulometry and binder content | Binder recovery and analysis (Pen, R&B, IP) |
|---|---|---|---|---|---|---|---|---|---|---|---|
| 1-C | AC 11S, 40% RAP | Plant | BERAG | 160/220 | | | | | | | |
| 2-C | | Plant* | BERAG | 160/220 | | | | | | | |
| 2-L | | Laboratory | BERAG | 160/220 | | | | | | | |
| 3-L | | Laboratory | Bour. Sion | 160/220 | | | | | | | |
| 4-L | | Laboratory | Famsa | 160/220 | | | | | | | |
| 5-L | | Laboratory | Balmholz | 160/220 | | | | | | | |
| 6-L | | Laboratory | BERAG | 70/100 | | | | | | | |
| 7-L | | Laboratory | BERAG | PmB | | | | | | | |
| 8-L | AC 11S, 0% RAP | Laboratory | BERAG | 50/70 | | | | | | | |
| 9-L | | Laboratory | BERAG | PmB | | | | | | | |
| 10-L | | Laboratory | BERAG | 70/100 | | | | | | | |
| 11-L | | Laboratory | Bour. Sion | 70/100 | | | | | | | |
| 12-L | | Laboratory | Famsa | 70/100 | | | | | | | |
| 13-L | | Laboratory | Balmholz | 70/100 | | | | | | | |

* AASHTO ageing

**Fig. 4** Overview of the laboratory testing

reheating method (extensive testing on a high modulus asphalt—EME). Some details about these investigations can be found in (Bueche et al. 2014).

## 5.3 Tests Results and Discussion

The results of Marshall testing (EN 12697-34) are presented in Table 4. Following comments can be made:

- The reference mixtures produced in plant (1-C) and in lab (2-L) have comparable results for Marshall flow and stability; the voids content is higher for the plant produced mixture.
- In general, the mixtures containing 40 % RAP have too low voids content; this especially for the laboratory produced mixtures. This is due in particular to the RAP aggregates characteristics discussed in Sect. 5.1. A decrease of the binder content would allow increasing the voids content.
- The effect of the binder type cannot be highlighted with these tests results. The testing method might not be sensitive enough.
- Mixtures without RAP appear to have substantially higher voids content and also a decrease in the Marshall flow. This can be linked to the RAP aggregates geometrical characteristics discussed in Sect. 5.1.

The water sensitivity of the various mixtures has been investigated through ITSR testing (EN 12697-12). The results are presented in Fig. 5 for the mixture containing 40 % reclaimed asphalt. The results highlight the effect of the new binder on both the pressures and ITSR ratio. The effect of PmB is substantial with an increase

**Table 4** Marshall test results (-: not measured)

| N° | RAP (%) | Aggregates | Binder | Binder content (%/M) | Voids Vm (%) | Stability SM (kN) | Flow (mm) |
|---|---|---|---|---|---|---|---|
| 1-C | 40 | BERAG | 160/220 | 5.87 | 3.2 | 9.0 | 3.5 |
| 2-L | 40 | BERAG | 160/220 | 6.10 | 1.6 | 9.0 | 3.5 |
| 3-L | 40 | Bour. Sion | 160/220 | 6.10 | 0.9 | – | – |
| 4-L | 40 | Famsa | 160/220 | 6.10 | 1.2 | – | – |
| 6-L | 40 | BERAG | 70/100 | 6.10 | 2.4 | 8.8 | 3.7 |
| 7-L | 40 | BERAG | PmB | 6.10 | 2.1 | – | – |
| 9-L | 0 | BERAG | PmB | 6.10 | 5.8 | – | – |
| 10-L | 0 | BERAG | 70/100 | 6.10 | 5.6 | 6.0 | 2.9 |
| 11-L | 0 | Bour. Sion | 70/100 | 6.10 | 1.9 | 8.9 | 3.2 |
| 12-L | 0 | Famsa | 70/100 | 6.10 | 3.7 | 9.0 | 3.5 |
| 13-L | 0 | Balmholz | 70/100 | 6.10 | 5.8 | 6.0 | 3.3 |

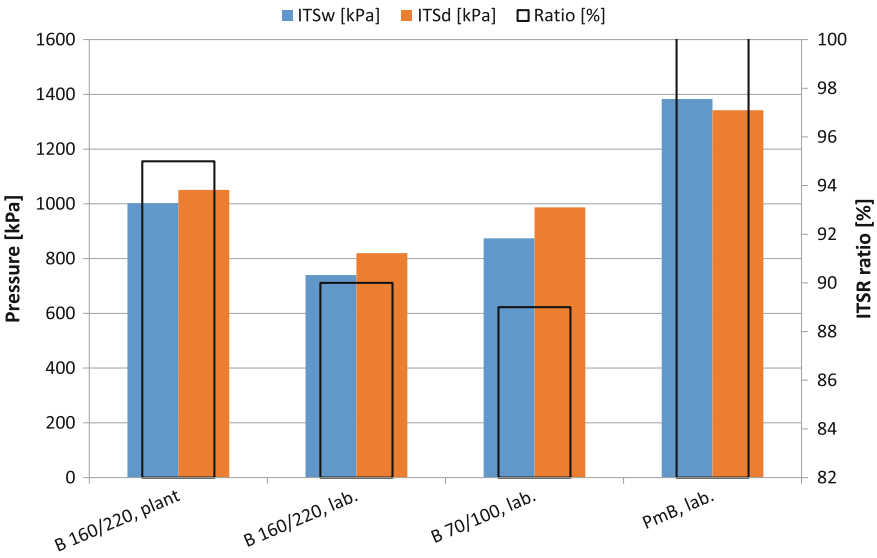


**Fig. 5** Water sensitivity (ITSR)—AC 11 S 40 % RAP (reference virgin aggregates)

of 14 % for ITSR ratio (64 % for $ITS_d$ and 87 % for $ITS_w$) in comparison with the reference mixture (B 160/220).

The effect of the aggregates sort has also been investigated through ITSR. BERAG (ref) and Balmholz aggregates appears to be comparable with a ITSR ratio >90 % but lower pressure than the two other aggregates (Bourgeoisie Sion and Famsa) that proves to have higher pressure but ITSR ratio <80 %.

Wheel tracking test (EN 12697-22) permitted to make some additional distinctions between the different mixtures (Table 5):

- The test with the laboratory produced reference mixture (2-L) has been stopped after 3000 cycles, due to the very important measured rut depth.
- For a comparable void content, the various mixtures tested do not meet the requirements (max. 10 % @ 10,000 cycles). This can be explained in particular by RAP and virgin aggregates characteristics. Indeed, a clear impact can be observed with Famsa (4-L) or Balmholz (5-L) aggregates in comparison with the reference (2-L).
- The binder choice has also a significant impact on the rutting susceptibility (comparison 2-L versus 6-L and 7-L).
- The plant produced mixture is less sensitive to rutting (ageing effect).

**Table 5** Wheel tracking tests results AC 11 S, 40 % RAP (slab thickness 50 mm, Temp = 60 °C, binder content 6.1 %)

| N° | 1-C | 2-L | 3-L | 4-L | 5-L | 6-L | 7-L |
|---|---|---|---|---|---|---|---|
| RAP content (%) | 40 | 40 | 40 | 40 | 40 | 40 | 40 |
| Production | Plant | Lab. | Lab. | Lab. | Lab. | Lab. | Lab. |
| Aggregates | BERAG | BERAG | Bourg. | Famsa | Balmh. | BERAG | BERAG |
| Binder | 160/220 | 160/220 | 160/220 | 160/220 | 160/220 | 70/100 | PmB |
| Voids (%) | 4.3 | 3.4 | 4.0 | – | 4.5 | 3.9 | 3.7 |
| 3000 cycles (%) | 7.1 | 20.1 | 12.6 | 8.6 | 8.0 | 10.5 | 9.5 |
| 10,000 cycles (%) | 10.3 | – | 17.5 | 12.6 | 12.8 | 14.9 | 13.0 |
| Slope (−) | 0.313 | 0.401 | 0.273 | 0.317 | 0.427 | 0.292 | 0.265 |
| Pen @ 25 °C ($10^{-1}$ mm) | – | 67 | – | – | – | 20 | 35 |
| R&B (°C) | – | 51.3 | – | – | – | 85.7 | 63.0 |

## 5.4 Mix Design Optimization

The analytical mix design (Sect. 4) demonstrated that binder content could be decreased while the grading curve does not play a significant role (based on the PradoWin® analysis of several grading curves, not included in this paper). Thus, the mix design optimization has been performed by varying the bitumen content for both 40 and 0 % RAP mixtures and a reference binder (160/220 resp. 70/100). Marshall testing, water sensitivity and rutting resistance are discussed below.

The results of Marshall testing are indicated in Table 6:

- The decrease of the binder provokes an increase of the Marshall voids while Marshall flow also decreases. The same trend is observed for both mixtures with and without RAP but in a different void domain.
- The RAP aggregates effect on voids content can again be observed. Based on this, the binder content of the mixture with 40 % RAP should be reduced.
- Decreasing the binder content and consequently increasing the void content does not guarantee an improved mechanical behavior of the asphalt mixture. Further test are required.

Water sensitivity testing highlighted a stable ITSR ratio (92 % for 5.5 % bitumen, 90 % for 6.1 % bitumen) for the mixture containing 40 % RAP but an increases of measured pressures (+27 % for $ITS_w$ and +25 % for $ITS_d$) for 5.5 % binder.

Wheel tracking tests results can be found in Table 7 for the RAP mixture. The mixture containing 5.5 % binder proves to have better rutting resistance and being in accordance with the Swiss standards (10 % @ 10,000 cycles). In comparison with the reference mixture, rut depth decreases by approx. 56 % at 10,000 cycles. The slope also decreases substantially that indicates a less sensitive mixture.

**Table 6** Mix design optimization: Marshall tests results

| N° | RAP (%) | Binder | Binder content (%/M) | Voids Vm (%) | Stability SM (kN) | Flow (mm) | Flow tan. Ft (mm) |
|---|---|---|---|---|---|---|---|
| O-1 | 40 | 160/220 | 5.5 | 4.5 | 7.7 | 2.6 | 1.5 |
| 0-2 | 40 | 160/220 | 5.8 | 3.0 | 7.9 | 2.7 | 1.6 |
| O-3 | 40 | 160/220 | **6.1** | 3.0 | 9.9 | 3.1 | 1.5 |
| O-4 | 40 | 160/220 | 6.4 | 1.9 | 7.5 | 3.6 | 1.9 |
| O-5 | 0 | 70/100 | 5.5 | 8.8 | 5.1 | 2.5 | 1.4 |
| O-6 | 0 | 70/100 | 5.8 | 7.7 | 5.8 | 2.8 | 1.8 |
| O-7 | 0 | 70/100 | **6.1** | 6.5 | 6.2 | 2.7 | 1.7 |
| O-8 | 0 | 70/100 | 6.4 | 6.5 | 5.6 | 2.1 | 1.3 |

Reference value in bold

**Table 7** Mix design optimization: wheel tracking tests results AC 11 S, 40 % RAP

| N° | O-1 | O-3 |
|---|---|---|
| Binder | 160/220 | 160/220 |
| Binder content | 5.5 | 6.1 |
| Voids (%) | 3.5 | 4.6 |
| 3000 cycles (%) | 6.0 | 11.6 |
| 10,000 cycles (%) | 7.9 | 17.8 |
| Slope (−) | 0.218 | 0.359 |

## 6 Conclusions and Recommendations

The presented research project aims at analyzing the mix design as well as highlighting the major parameters governing an optimization procedure of mixture containing RAP.

In case of high RAP content (>25 %), literature analysis and laboratory results both highlight the complexity of the mix design procedure as well as the various consequences on the final mixture characteristics and performances.

In a first phase, an analytical mix design has been performed. This procedure permitted to highlight the potential optimization of the reference mixture as well as quantify the impact of various parameters such as binder type on the volumetric compositions and mixture mechanical performances. The results of the calculations performed are also consistent with the punctual laboratory testing carried out.

Based on the extensive laboratory study on an AC 11 with 40 % RAP, one can mention that wheel tracking and water sensitivity testing are pertinent indicators for the evaluation of the mechanical behavior. Following parameters have been found

important in the framework of a mix design of mixture containing RAP, and their related effect quantified:

- RAP homogeneity: stock pile management.
- RAP quality (percentage of crushed and broken surfaces, edge sharpness,…).
- RAP bitumen characteristics.
- Mixture production conditions in plant.
- Choice of the new binder.

The results finally permit to propose some recommendations for the control and analysis of asphalt mixtures containing a high RAP content. An optimized control procedure will further permit to increase the RAP content while maintaining satisfactory performances.

## References

Al-Qadi I. et al. (2007) Reclaimed Asphalt Pavement – A Literature Review. Illinois Center for Transportation.

Bueche et al. (2014) Recyclage à chaud des enrobes bitumineux. EP-5 : Formulation. Projet VSS 2005/456.

Copeland A. (2011) Reclaimed Asphalt Pavement in Asphalt Mixtures : State of the Practice. Publication No. FHWA-HRT-11-021.

Dumont A.-G. & Pittet M. (2012) Vieillissement thermique des enrobés bitumineux en laboratoire. Mandat de recherche VSS 2000/434.

El Bèze L. (2008) Recyclage à chaud des agrégats d'enrobés bitumineux : Identification de traceurs d'homogénéité du mélange entre bitume vieilli et bitume neuf d'apport. Thèse Université Paul Cézanne Aix-Marseille III.

Fénart M.-A. et al (2012) Realistic laboratory curing of bituminous mixtures. EATA conference, Braunschweig, Geermany.

Franken L. & Vanelstraete A. (1993) New Developments in Analytical Asphalt Mix Design. 5th Eurobitume Congress, Stockholm, Suède.

McDaniel R. et al. (2000) Recommended Use of Reclaimed Asphalt Pavement in the Superpave Mix Design Method. NCHRP Project 9-12.

Nguyen V. H. (2009) Effects of Laboratory Mixing Methods and RAP Materials on Performances of Hot Recycled Asphalt Mixtures. Thesis University of Nottingham.

Steuperaert J. & Vanelstraete A. (1997) Code de bonne pratique pour la formulation des enrobés bitumineux. CRR, Bruxelles.

Valdès Vidal G. et al. (2010) Experimental study of recycled asphalt mixtures with high percentages of reclaimed asphalt pavement (RAP). TRB Annual Meeting. 2010.

Widyatmoko I. (2008) Mechanistic-empirical mixture design for hot mix asphalt pavement recycling. Construction and Building Materials 22.

Yousefi Rad F. (2013) Estimating Blending Level of Fresh and RAP Binders in Recycled Hot Mix Asphalt. Master of Science, University of Wisconsin Madison.

# Sustainable Urban Surface Asphalt Layers

**Ramón Botella, Rodrigo Miró Recasens, Patricia Díaz Martín, Antonio Ramírez Rodríguez, Francisco Guisado Mateo and Emilio Moreno Martínez**

**Abstract** Nowadays, given the current growing awareness about the preservation of the environment, asphalt technicians are assessing and trying to correct resulting impacts from the manufacture and application of bituminous mixtures. The concept of sustainability has come to the field of bituminous mixtures with two main components: reducing emissions and reducing the consumption of raw materials, preserving resources for the future. Conservation and rehabilitation activities of road pavements generate an increasing amount of waste from the milling of the layers of damaged asphalt mixtures. This material, which has great costs and exceptional properties, should be reused in manufacturing new mixtures of the same type and function. Moreover, it is necessary to reduce the emissions from the manufacturing and application of asphalt mixtures. This paper presents the efforts carried out to develop a technology that allows manufacturing and applying half-warm mix asphalt in surface layers of low speed roads at low temperatures using high percentages of reclaimed asphalt pavement. The research project focused on designing asphalt mixtures to be placed in urban areas. Continuously graded mixtures were manufactured at 100 °C and compacted at 80 °C with different percentages of RAP, ranging from 50 to 100 %. The results obtained from testing laboratory specimens indicated that their mechanical properties, regarding cracking resistance and fatigue resistance, were very close to those expected from regular HMA mixtures.

**Keywords** Asphalt · Half-warm mixtures · Emulsions · Reclaimed asphalt pavement

R. Botella (✉) · R.M. Recasens
Technical University of Catalonia UPC-BarcelonaTech, Barcelona, Spain
e-mail: ramon.botella@upc.edu

P.D. Martín · A. Ramírez Rodríguez
Sacyr Construcción, Madrid, Spain

F.G. Mateo · E.M. Martínez
Repsol Technology Center, Madrid, Spain



F. Canestrari and M.N. Partl (eds.), *8th RILEM International Symposium on Testing and Characterization of Sustainable and Innovative Bituminous Materials*, RILEM Bookseries 11, DOI 10.1007/978-94-017-7342-3_50

## 1 Introduction

The environmental impact of the Hot Mix Asphalt concrete (HMA) is not at all negligible. Without accounting from the manufacture processes to obtain aggregates and asphalt binders, the production alone of the HMA mixtures requires a high amount of energy consumption that inevitable leads to a high amount of greenhouse gases emissions. Moreover, the maintenance and rehabilitation tasks performed on bituminous layers generate a large amount of waste material from the milling of the damaged layers. This material has excellent properties and it should be recycled to produce mixtures of the same type and with the same goal.

Recently, there have been some research projects that have followed that line of work. Soenen et al. (2010) studied the half-warm techniques producing mixtures using foamed bitumen and wet aggregates at 90 °C. They analyzed how different variables affected the properties of the final mixture, such as moisture content of the aggregates at mixing, the time lag between mixing and compaction of the asphalt, the influence of adding active filler, and the effect of foaming the binder versus just adding hot bitumen to the mixture. Later van de Ven et al. (2012) researched about the application of half-warm foamed bitumen mixtures compacted between 90 and 100 °C for their application on binder and base layers. They showed that the compaction of these kinds of mixtures can be managed. More recently, Punith et al. (2013) applied the half-warm foaming techniques to a wide variety of mixtures, some of them containing recycled materials such as reclaimed asphalt pavement (RAP) and roofing shingles. After performing different mechanical tests they showed that the addition of RAP materials did not affect the performance of these mixtures, even though they were compacted at 85 °C.

The work described in this project has gone one step further. The main goal was to produce mixtures intended for surface layers in urban areas reducing the compaction and fabrication temperatures and reducing or avoiding altogether the use of new aggregates. Using three different types of bitumen emulsions three mixtures were manufactured with a 100 % of RAP coming from AC mixtures. The mixing temperatures ranged between 90 and 100 °C and the compacting temperatures were between 70 and 80 °C.

## 2 Test Methods and Materials

This section provides an overall view of the whole research project, describes the test methods applied in the characterization of the half-warm mixtures studied and the materials from which these mixtures were manufactured.

## 2.1 Research Plan and Test Materials

The study consisted on analyzing the properties of three different mixtures produced with three different bituminous emulsions and a 100 % of RAP. To do two test procedures were considered, Fenix test and EBADE test, and three different test temperatures, +20, +5 and −5 °C. Additionally the Fenix tests were also conducted at −15 °C.

The three emulsions were composed of three different binders, a 35/50 binder a 50/70 binder and a Latex modified binder. From now on each mixture will be refer to as 35/50, 50/70 or Latex.

The RAP employed was from an old AC mixture. It was separated by size fractions and the final mixture contained 68 % from the 0/5 mm fraction and 32 % from the 5/25 mm fraction. The amount of old binder in this RAP was 4.5 % in aggregate mass while the emulsions had a 60 % of asphalt binder on it. The final mixture was designed to have between 6.0 and 6.2 % bitumen in aggregate mass; therefore the amount of emulsion added to the RAP was between 2.55 and 2.75 % in aggregate mass. The RAP was heated to 100 °C while the emulsions' temperature was 60 °C. The mix was conducted at temperatures ranging between 90 and 100 °C and the final compaction was made at temperatures between 70 and 80 °C. The specimen compaction was conducted using the gyratory compactor during 65 cycles at a pressure of 0.6 MPa and an angle of 0.82°.

## 2.2 Fenix Test

The Fenix test is a direct tension test developed at the Technical University of Catalonia UPC-BarcelonaTech aimed to characterize the fracture properties of bituminous mixtures (Pérez-Jiménez et al. 2010). Using and hydraulic press a 1 mm/min constant displacement rate is applied to a half cylindrical notched specimen (Fig. 1).

The two main parameters obtained from the test that are used to characterize mixtures are the tensile stiffness index (IRT) and the fracture energy defined by Eqs. 1 and 2:

$$IRT = \frac{\frac{1}{4}F_{\max}}{\Delta_{\frac{1}{2}F_{\max}} - \Delta_{\frac{1}{4}F_{\max}}} \tag{1}$$

$$G_F = \frac{W}{S_F} \tag{2}$$

where, W is the work done during the test and $S_F$ is the cross-section area of the specimen. The IRT parameter quantifies the stiffness of the mixture during the test, since it is the slope of the loading curve in the linear domain.

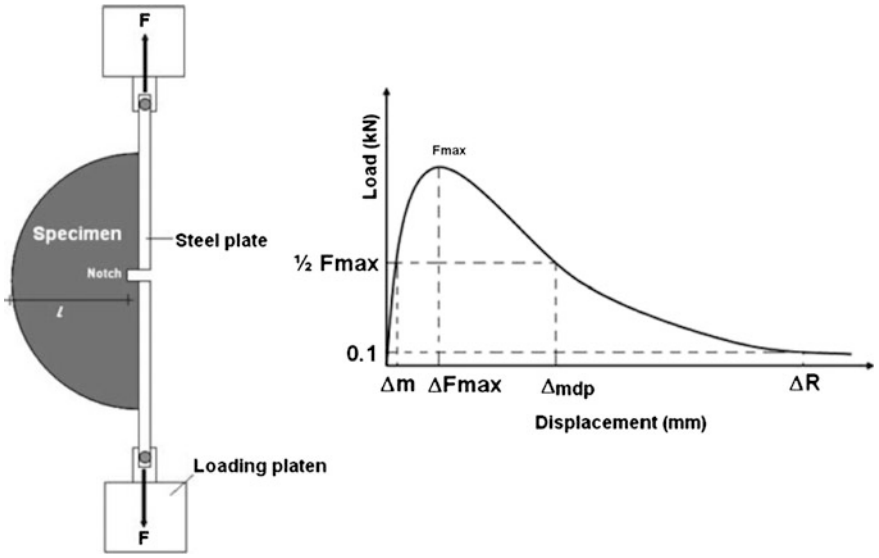


**Fig. 1** Fenix test setup and load-displacement. Output curve (Pérez-Jiménez et al. 2010)

## 2.3 EBADE Test

The Technical University of Catalonia UPC-BacelonaTech has developed a cyclic uniaxial tension-compression strain sweep test that uses prismatic specimens carved from cylindrical ones (Pérez-Jiménez et al. 2011). The test is called EBADE that stands for strain sweep test in Spanish (*Ensayo de BArrido de DEformaciones*) (Fig. 2). In this test the strain amplitude is increased every 5000 cycles, each block of 5000 cycles is called a *strain step*. The first strain amplitude applied is $25 \times 10^{-6}$ and it increases in the same amount every 5000 cycles, i.e., in the second step the strain amplitude is $50 \times 10^{-6}$, in the third $75 \times 10^{-6}$ and so on. The tests frequency chosen for the test is 10 Hz.

During the test the stress amplitude, the complex modulus and the dissipated energy density is recorded every 100 cycles. The dissipated energy density is calculated by computing the stress-strain loop area using the Gauss determinant formula.

The stress amplitude, the complex modulus and the dissipated energy density is recorded every 100 cycles. From this data two parameters are calculated:

- Initial complex modulus: Average of the 50 complex modulus values recoded during the first 5000 cycles of the test at which the strain applied is $25 \times 10^{-6}$.
- Failure strain: Strain amplitude at which the dissipated energy density drops below 50 % the maximum value reached during the test.

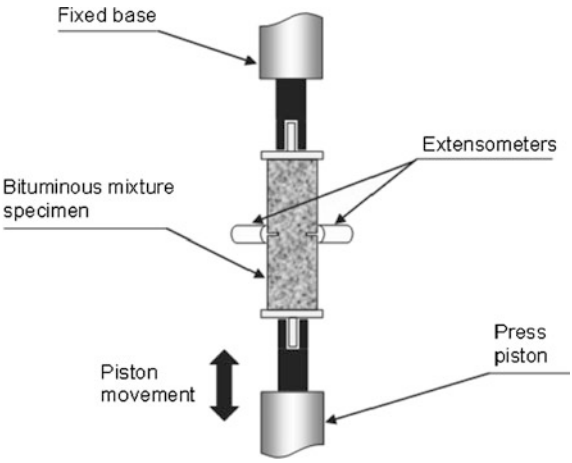


**Fig. 2** EBADE test set up (Pérez-Jiménez et al. 2011)

Using these two parameters it is possible to compare the behaviour of different mixtures under cyclic conditions.

## 3 Results

The results discussion is divided in two sections. One presents the results obtained in the Fenix tests and the other one the results obtained in the EBADE test.

### *3.1 Fenix Tests Results*

The Fenix tests load-displacement curves are shown in Fig. 3 for the tests performed at 20 and −5 °C.

The behavior of the three mixtures was very similar. The latex modified emulsion showed small increase in ductility in relation with the other two mixtures. The AC16S 50/70 mixture that appears in Fig. 3 is an HMA mixture used to compare the behavior of these three half-warm recycled mixtures with a regular one. As seen in Fig. 3, the three mixtures presented (Table 1).

Figure 4 clearly shows how the Latex emulsion produced the most ductile mixture of all three, since its fracture energy was higher at +5 and −5 °C and the second highest at +20 °C. It is interesting to note that the conventional HMA mixture presented similar or lower fracture energy values that the half-warm recycled mixtures.

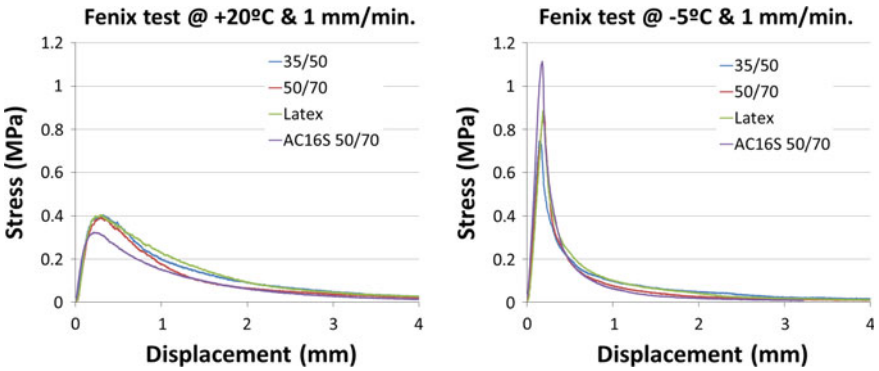


**Fig. 3** Load displacement curves obtained in the Fenix tests performed at +20 and −5 °C

**Table 1** Parameters obtained in Fenix tests

| Mixture | Temperature (°C) | IRT (KN/mm) | $G_F$ (J/m$^2$) |
|---|---|---|---|
| 35/50 | 20 | 8 | 622 |
| | 5 | 15 | 649 |
| | −5 | 15 | 440 |
| | −15 | 15 | 302 |
| 50/70 | 20 | 8 | 555 |
| | 5 | 15 | 649 |
| | −5 | 15 | 360 |
| | −15 | 17 | 252 |
| Latex | 20 | 8 | 588 |
| | 5 | 15 | 762 |
| | −5 | 15 | 602 |
| | −15 | 18 | 251 |
| AC16S 50/70 1 | 20 | 4 | 290 |
| | 5 | 12 | 612 |
| | −5 | 14 | 345 |
| | −15 | 16 | 300 |

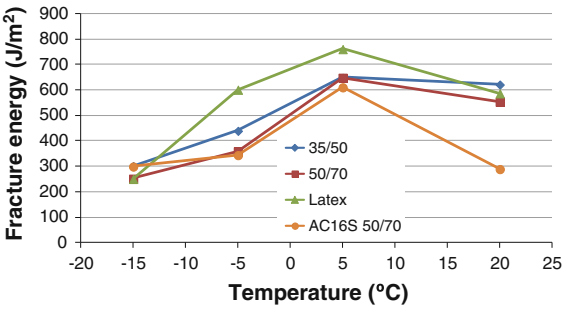


**Fig. 4** Fracture energy evolution with test temperature in Fenix tests

## 3.2 EBADE Tests Results

The EBADE results showed that at 20 °C, Fig. 4, the Latex modified emulsion produced the most ductile mixture. Its initial complex modulus was similar to the 50/70 mixture and slightly lower than the 35/50 and the HMA mixture used as reference (Fig. 5).

Figure 6 shows the representation of the initial complex modulus versus the failure strain for all the test temperatures. This kind of plot allows to analyze the change in properties of the mixtures with the temperature and to compare between them how their increase in modulus when the temperature is reduced affects their ability to sustain deformations under cyclic loading (failure strain) (Table 2).

As expected, among the half-warm mixtures, the one produced with the 35/50 emulsion was the one with higher initial complex modulus, while the mixture manufactured with the latex modified emulsion obtained higher failure strain values.

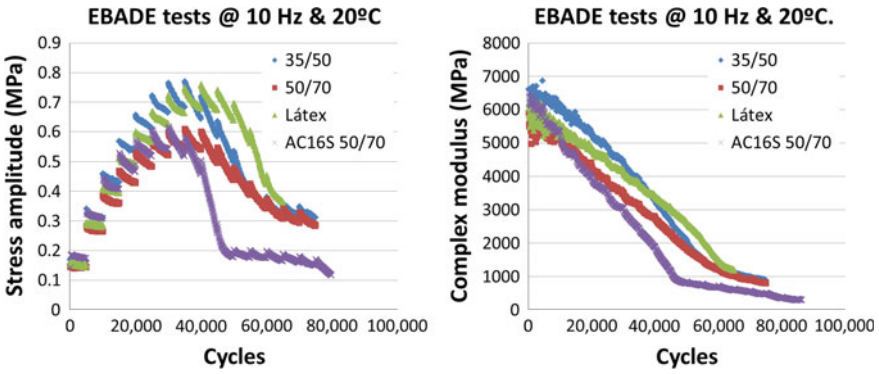


**Fig. 5** Stress amplitude and complex modulus versus the number of cycles in the EBADE tests

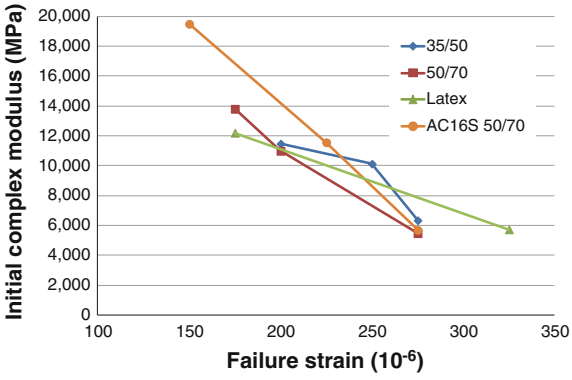


**Fig. 6** Initial complex modulus versus failure strain

**Table 2** Parameter obtained in the EBADE tests

| Mixture | Temperature (°C) | Initial complex modulus (MPa) | Failure strain ($10^{-6}$) |
|---|---|---|---|
| 35/50 | 20 | 6347 | 275 |
| | 5 | 10,128 | 250 |
| | −5 | 11,471 | 200 |
| 50/70 | 20 | 5483 | 275 |
| | 5 | 10,991 | 200 |
| | −5 | 13,801 | 175 |
| Latex | 20 | 5741 | 325 |
| | 5 | – | – |
| | −5 | 12,203 | 175 |
| AC16S 50/70 | 20 | 5698 | 275 |
| | 5 | 11,561 | 225 |
| | −5 | 19,485 | 150 |

Regarding the comparison with the reference mixture, at 20 °C all mixtures showed similar initial complex modulus while at −5 °C the HMA mixture modulus was a 35 % higher than the average of the three half-warm mixtures. In addition the failure strain of these mixtures was higher than the one corresponding to the AC16S 50/70 mixture.

## 4 Conclusions

This research project has studied the possibility of using three different emulsions to produce bituminous mixtures for surface layers of urban areas using a 100 % of Reclaimed Asphalt Pavement. Two of the emulsions were manufactured with conventional medium and hard binders (35/50 and 50/70 penetration ranges) and a third one was modified with latex.

The differences between the mixtures were very small, however the modified emulsion produced a mixture with similar stiffness and higher ductility (higher fracture energy and failure strain values).

The most important result of this project is that all three mixtures manufactured and compacted at temperatures below 100 °C using only reclaimed asphalt pavement obtained results very similar, and slightly better in some conditions, than a regular Hot Mix Asphalt mixture manufactured with a similar gradation and a similar penetration binder (AC16S 50/70 mixture).

In addition, the Fenix and EBADE tests have provided very valuable information of the mechanical characteristics of the mixtures and have been able to compare and rank them on terms of their performance.

**Acknowledgements** The work presented on this paper is part of the research project "Rodaduras Urbanas Sostenibles" (Sustainable urban surface asphalt layers), reference number IPT-2012-0316-370000, funded by the Spanish Ministry of Economy and Competitively, through the call INNPACTO 2012, and the European Regional Development Fund from the European Union.

## References

Pérez-Jiménez, F., Valdés, G., Miró, R., Martínez, A., Botella, R. (2010) Fénix Test.Development of a New Test Procedure for Evaluating Cracking Resistance in Bituminous Mixtures. Transportation Research Record: Journal of the Transportation Research Board 2181: 36-43.

Pérez-Jiménez, F., Valdés, G., Miró, R., Botella, R., Campana, J.M. (2011) Effect of Thermal Stresses on Fatigue Behavior in Bituminous Mixes. Transportation Research Record: Journal of the Transportation Research Board 2210: 90-96.

Punith, V.S., Xiao, F., Wingard, D. (2013) Performance characterization of half warm mix asphalt using foaming technology. Journal of Materials in Civil Engineering V.25 I.3: 382-392.

Soenen, H., de Visscher, J., Vervaecke, F., Vanelstraete, A., Redelius, P. (2010) Foamed bitumen in half-warm asphalt: A laboratory study. International Journal of Pavement Research and Technology V.3 I.4: 199-206.

van de Ven, M.F.C., Sluer, B.W., Jenkins, K.J., van den Beemt, C.M.A. (2012) New developments with half-warm foamed bitumen asphalt mixtures for sustainable and durable pavement solutions. Road Materials and Pavement Design V.13 I.4: 713-730.

# Part VIII
# Advances in Laboratory Characterization of Bituminous Materials

# Experimental Investigation on the Combined Effects of Physical Hardening and Chemical Ageing on Low Temperature Properties of Bituminous Binders

**Ezio Santagata, Orazio Baglieri, Davide Dalmazzo and Lucia Tsantilis**

**Abstract** Physical hardening is a phenomenon that takes place at low temperatures, producing time-dependent isothermal changes in the rheological properties of bituminous binders. Stiffening effects caused by physical hardening combine with those consequent to chemical ageing, thus promoting the build-up of thermally-induced stresses which may lead to premature pavement failure. The main goal of this paper was to investigate the influence of physical hardening on low temperature properties of bituminous binders tested in different ageing conditions. Moreover, reversibility of hardening phenomena was directly assessed by means of a dedicated testing protocol. The study, carried out by making use of the Bending Beam Rheometer (BBR), considered four binders of different type and origin (two neat bitumens and two commercial SBS polymer-modified binders) and three ageing conditions (original, short-term ageing and long-term ageing). Obtained results, expressed in terms of a Physical Hardening Rate (PHR), showed a significant effect of chemical ageing on low temperature hardening of binders. In particular, rate of hardening was found to vary with temperature and to decrease with degree of ageing. Reversibility of the hardening process was also verified.

**Keywords** Physical hardening · Chemical ageing · Hardening reversibility · Bituminous binders · Creep stiffness · Thermal cracking

E. Santagata (✉) · O. Baglieri · D. Dalmazzo · L. Tsantilis
Department of Environment, Land and Infrastructure Engineering, Politecnico di Torino, 24, corso Duca degli Abruzzi, 10129 Turin, Italy
e-mail: ezio.santagata@polito.it

O. Baglieri
e-mail: orazio.baglieri@polito.it

D. Dalmazzo
e-mail: davide.dalmazzo@polito.it

L. Tsantilis
e-mail: lucia.tsantilis@polito.it



F. Canestrari and M.N. Partl (eds.), *8th RILEM International Symposium on Testing and Characterization of Sustainable and Innovative Bituminous Materials*, RILEM Bookseries 11, DOI 10.1007/978-94-017-7342-3_51

## 1 Introduction

The term "physical hardening" refers to time-dependent isothermal changes in visco-elastic properties of bituminous binders which occur within their glass transition region (Bahia and Anderson 1993; Anderson et al. 1994; Santagata et al. 1996; Hesp et al. 2007).

Physical hardening is commonly explained by using the free volume theory, originally proposed by Struik (1978) and Ferry (1980) for amorphous polymers. Such a theory assumes the total volume of material to be constituted by two fractions: (1) occupied volume, which is the volume of molecules including their vibrational motions, and (2) free volume, which is the volume of voids between molecules due to packing irregularities.

When a bituminous binder is subjected to cooling, starting from a temperature far above the glassy state, its molecular mobility and molecular free volume decrease simultaneously and thermodynamic equilibrium is maintained throughout the cooling process. In these conditions, specific volume is proportional to molecular volume and varies linearly with temperature. At temperatures approaching the glass transition region, reductions of molecular mobility and free volume start to take place at different rates, thus leading to a relative growth of the free volume fraction. Specific volume is no longer proportional to molecular volume and its variation as a function of temperature deviates from the linear equilibrium line (Fox and Loshaek 1955; Struik 1978).

The glass transition of bitumen region is very wide, covering a range broader than 50 °C due to the occurrence of several transitions that can partially overlap taking place at different temperatures in the different bitumen fractions (Daly et al. 1996). A glass transition temperature (Tg) can thus be defined, located within the overall transition range. Such a temperature results from the combination of the different glass transition temperatures of bitumen fractions.

The glassy state is meta-stable and if the material is held at constant temperature for a sufficient amount of time, it shows a slow tendency to attain structural equilibrium as a result of free volume collapse. Density increases and an overall hardening of the binder is observed (Struik 1991). In addition to free volume collapse, some researchers have postulated that physical hardening is caused by the formation of crystalline fractions (Anderson and Marasteanu 1999), especially in those materials characterized by high wax content (Kriz et al. 2008).

Chemical ageing is caused by the combination of several phenomena which produce irreversible changes in molecular structure of asphalt binders. Such phenomena include oxidation reactions, polymerization and evaporation of lighter components (Traxler 1961; Bell 1989). Susceptibility of a given binder to chemical ageing depends upon its crude source and manufacturing process (Lesueur 2009). In road paving applications, a distinction is generally made between short-term and long-term chemical ageing, with the first one occurring during hot mix asphalt production, lay-down and compaction, and the second one occurring in situ during pavement service life.

In terms of fractional components, it has been demonstrated that ageing determines a decrease of the aromatics content with a consequent increase of relative amounts of resins and asphaltenes (Moschopedis and Speight 1977; Siddiqui and Ali 1999). This is due to the fact that aromatics generate resins that in turn generate asphaltenes. These chemical changes involve larger and more polar molecules (Bahia and Anderson 1995), revealed by the formation of new functional groups such as carbonyls and sulfoxides (Siddiqui and Ali 1999; Leuseur 2009).

From a rheological point of view, chemical ageing reflects on binder viscosity and stiffness that may increase up to four times with respect to those of the unaged material (Bell 1989).

Stiffening effects caused by physical hardening combined with those due to chemical ageing promote the build-up of thermally-induced stresses which can lead to premature pavement failure. As a consequence, in binder characterization mutual interactions between the two phenomena need to be taken into account in order to fully appreciate the performance-related value of considered materials.

The main goal of the experimental study described in this paper was to investigate the influence of physical hardening on low temperature properties of bituminous binders tested in different ageing conditions. Following an approach common to that proposed by other researchers (Anderson et al. 1994; Lu and Isacsson 2000; Soenen et al. 2004), the study was based on the use of the Bending Beam Rheometer (BBR). Reversibility of hardening phenomena was also investigated by means of a dedicated testing protocol.

## 2 Materials and Methods

The set of materials employed in the experimental investigation included two neat and two polymer-modified binders. Neat binders were 50/70 (NA) and 70/100 (NB) penetration grade bitumens sampled from two refineries which operate on crudes of different origin and source. Modified binders (MA and MB, both belonging to the 50/70 penetration grade) were characterized by a high percentage of styrene-butadiene-styrene (SBS) polymer and were produced according to undisclosed processing schemes.

In order to simulate the occurrence of chemical ageing phenomena in short-term and long-term conditions, all binders were subjected to the Rolling Thin-Film Oven Test (RTFOT), according to AASHTO T240 (2009), followed by a Pressure Aging Vessel (PAV) treatment, according to AASHTO R28 (2009).

A preliminary rheological characterization was also carried out, with the purpose of determining Performance Grade (PG) in accordance with AASHTO M320 (2010) procedures.

Description of the materials, including their PG determined as specified above, is given in Table 1.

The procedure adopted to evaluate physical hardening consists in creep tests carried out with the BBR at successive isothermal conditioning times (5 and

**Table 1** Materials used in the experimental investigation

| Binder | Description | Penetration grade | Performance grade | Ageing condition | Code |
|---|---|---|---|---|---|
| NA | Neat | 50/70 | 64–16 | Original | $NA_{OR}$ |
| | | | | Short-term aged | $NA_{RTFOT}$ |
| | | | | Long-term aged | $NA_{PAV}$ |
| NB | Neat | 70/100 | 64–16 | Long-term aged | $NB_{PAV}$ |
| MA | Modified with SBS | 50/70 | 76–22 | Original | $MA_{OR}$ |
| | | | | Short-term aged | $MA_{RTFOT}$ |
| | | | | Long-term aged | $MA_{PAV}$ |
| MB | Modified with SBS | 50/70 | 76–22 | Original | $MB_{OR}$ |
| | | | | Short-term aged | $MB_{RTFOT}$ |
| | | | | Long-term aged | $MB_{PAV}$ |

30 min; 1, 2 and 22 h). Single measurements were performed in the three-point bending configuration with a constant load of 980 mN applied for 240 s. During the tests, beam deflection was recorded at six predefined time steps (8, 15, 30, 60, 120 and 240 s).

Immediately after BBR tests, at each isothermal conditioning time specimens were flattened out by placing them upside down in the loading frame and by applying the same vertical load for the same time used for creep measurements.

Beams were manufactured by employing modular aluminum molds in accordance with AASHTO T313 (2010).

The testing program was defined with the purpose of analyzing the role played in physical hardening by critical factors such as temperature and degree of ageing, and at the same time to limit to a reasonable extent total number of tests. On the basis of this rationale, a restricted group of binders was tested at multiple temperatures, whereas remaining materials were evaluated at a single one. In this last case selected test temperature coincided with glass transition temperature at which maximum physical hardening is expected to occur (Tabatabaee et al. 2012). Tg values were determined in a previous study (Baglieri et al. 2012) by means of a dilatometric system following the procedure developed by Nam and Bahia (2004).

In the case of binders tested at their glass transition temperature, the testing protocol was modified by adding a second identical set of creep tests carried out on the same specimen. Between the end of the first run and the beginning of the second run, specimens were stored at ambient temperature for a given period (3 h) in order to allow them to return to their original state. This protocol was used with the

**Table 2** Conditioning temperatures, protocols and replicate beams used for testing

| Binder code | Test temperature (°C) | Protocol | Replicate beams |
|---|---|---|---|
| $NA_{OR}$ | −18, −24, −30<br>−15* | Single run<br>Double run | 2<br>4 |
| $NA_{RTFOT}$ | −15* | Double run | 4 |
| $NA_{PAV}$ | −19* | Double run | 4 |
| $NB_{PAV}$ | −6, −18, −30 | Single run | 2 |
| $MA_{OR}$ | −18, −24, −30<br>−19* | Single run<br>Double run | 2<br>4 |
| $MA_{RTFOT}$ | −17* | Double run | 4 |
| $MA_{PAV}$ | −16* | Double run | 4 |
| $MB_{OR}$ | −18, −30 | Single run | 2 |
| $MB_{RTFOT}$ | −18, −30 | Single run | 2 |
| $MB_{PAV}$ | −18, −30 | Single run | 2 |

*Tg (from Baglieri et al. 2012)

specific goal of verifying reversibility of physical hardening phenomena by comparing material response exhibited during first and second run.

Summary of test temperatures, adopted protocols and number of replicate beams used for each binder considered in the study is provided in Table 2.

## 3 Experimental Results

Physical hardening effects in bituminous binders are generally evaluated by considering changes in mechanical properties consequent to increasing isothermal conditioning times. However, different methods and parameters have been used to determine material susceptibility to physical hardening on a quantitative basis.

A first method refers to the time-temperature superposition principle by using one-dimensional horizontal shift factors to generate master curves and thereafter to calculate the so-called Shift Rate (SR) (Anderson et al. 1994; Anderson and Marasteanu 1999; Lu and Isacsson 2000). Such a parameter represents the slope of the curve obtained by plotting horizontal shift factors against conditioning time on a bi-logarithmic scale. SR definition and validity is founded on the hypotheses that the material is thermo-rheologically simple and that isothermal hardening does not affect the shape of master curves. Nevertheless, other authors observed that for some bitumens horizontal shifting may not be sufficient to obtain single master curves and additional vertical shifting can be necessary (Kriz et al. 2008).

An alternative approach is that based on the determination of a Hardening Index (HI), given by the ratio of stiffness measured after a given isothermal conditioning time to stiffness measured after a reference conditioning time (Soenen et al. 2004; Lu and Isacsson 2000; Baglieri et al. 2012). Similar to HI is the Hardening Rate

(HR) proposed by Tabatabaee et al. (2012), that considers the relative increase in stiffness caused by an increase of storage period.

In this study, the HI employed to quantify magnitude of physical hardening occurring in bituminous binders was determined from BBR test data as follows:

$$HI = \frac{S_{60,i}}{S_{60,1\,\mathrm{h}}} \tag{1}$$

where $S_{60,i}$ is creep stiffness at 60 s corresponding to conditioning time $t_i$ and $S_{60,1h}$ is reference stiffness measured after 1 h conditioning.

An example of HI values plotted versus conditioning time in the semi-logarithmic scale is shown in Fig. 1, which refers to neat binder NA tested in its short-term ageing state. It can be observed that HI increased monotonically, following a linear trend over the entire time interval explored with measurements. It should be pointed out that alignment of data points along the characteristic line of the binder was observed even in the case of those collected in the early phases of conditioning. Such points were excluded by other Authors from similar analyses due to the initial very high hardening rate (Lu and Isacsson 2000).

Results similar to those depicted in Fig. 1 were obtained for all other materials and test conditions used in the investigation.

A Physical Hardening Rate (PHR) was calculated as the slope of hardening curves according to the following equation:

$$PHR = \frac{d(HI)}{d(\log\, t_i)} \tag{2}$$

where PHR provides a measure of the tendency of the material to harden and therefore to promote the build-up of thermal stresses when subjected to isothermal conditions.

Figure 2 displays the variation of PHR as a function of storage temperature for binders $NA_{OR}$, $NB_{PAV}$ and $MA_{OR}$. In all cases, data points seem to follow a

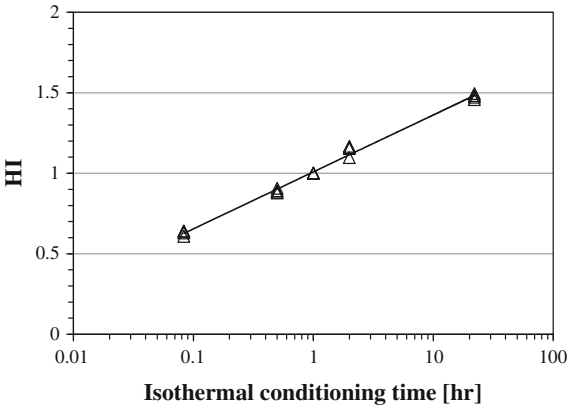


**Fig. 1** HI values plotted as a function of conditioning time ($NA_{RTFOT}$ tested at −15 °C)

bell-shaped curve characterized by the presence of a peak hardening rate value. For two binders ($NA_{OR}$ and $MA_{OR}$), such a peak was achieved at the glass transition temperature in accordance with expectations, whereas for the third binder ($NB_{PAV}$) this cannot be definitely stated due to lack of information on its Tg.

It is interesting to note that at −30 °C all materials exhibited minimum PHR values which were very close to each other. Such evidence supports the hypothesis of the existence of a limiting low temperature below which physical hardening no longer takes place within experimental time.

Findings reported above are coherent with those reported by Tabatabaee et al. (2012). They can be explained by considering that at temperatures lower than a certain limit, specific volume tends to a new thermodynamic equilibrium with an energy level higher than that of temperatures far above the glass transition region. As a consequence, a second equilibrium asymptote is present in the specific volume —temperature curve and Tg can be identified by considering the intersection of the two asymptotes. At such a temperature, deviation of specific volume from equilibrium is maximum and therefore coherent with the corresponding hardening peak observed in Fig. 2.

Influence of chemical ageing on binder susceptibility to physical hardening was analyzed by comparing PHR values obtained in unaged conditions with those obtained after RTFO and PAV treatments. Results are shown in Fig. 3, which refers

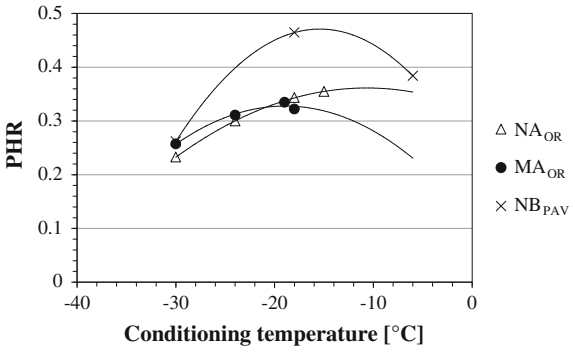


**Fig. 2** Variation of PHR as a function of conditioning temperature

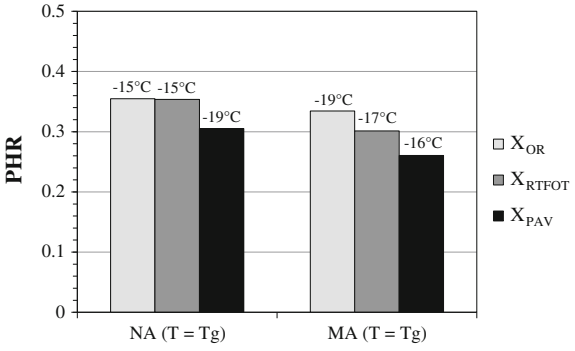


**Fig. 3** PHR values corresponding to different ageing conditions (NA and MA tested at Tg)

to binders NA and MA (tested at Tg), and in Fig. 4, which refers to binder MB (tested at −18 and −30 °C).

In all cases it was observed that physical hardening rate progressively decreased passing from original to short-term and thereafter from short-term to long-term ageing conditions. Such evidence can be explained by referring once again to free volume theory. The occurrence of chemical ageing phenomena produces an increase of asphaltenes content that leads, in turn, to a higher degree of molecular packing. Consequently, free volume and associated collapse are greatly reduced, making the aged binder less prone to harden when stored in isothermal conditions.

From a rheological point of view the reduction of physical hardening rate with chemical ageing can be justified by considering that an increment of asphaltenes, that exist in bitumen as dispersed solid particles, produces an increase in viscosity that contrasts reorganization of molecules while tending to structural equilibrium.

From the comparison between neat bitumen (NA) and modified binders (MA and MB), it can also be highlighted that relative reductions of PHR values due to chemical ageing were more pronounced in presence of SBS polymer. This is due to the diffused presence of a rubber-like network which changes the internal structure of the material and hence its thermodynamic equilibrium conditions.

Finally, data presented in Fig. 4 show that binder MB exhibited a PHR reduction when decreasing conditioning temperature. This finding is coherent with trends displayed in Fig. 2 and corroborates the existence of a threshold temperature below which limited physical hardening occurs.

Analysis of physical hardening reversibility was carried out by considering results obtained from binders subjected to the previously described double test runs (NA and MA). All samples during the second run of tests exhibited an increase in $S_{60}$ which was close to that measured during the first run. Reversibility of physical hardening was then assessed by comparing hardening rates calculated for the two testing stages. However, since the phenomenon under evaluation is extremely complex and characterized by a significant variability which affects both materials and methods, a statistical approach was considered necessary to discuss the issue of reversibility on a quantitative basis.

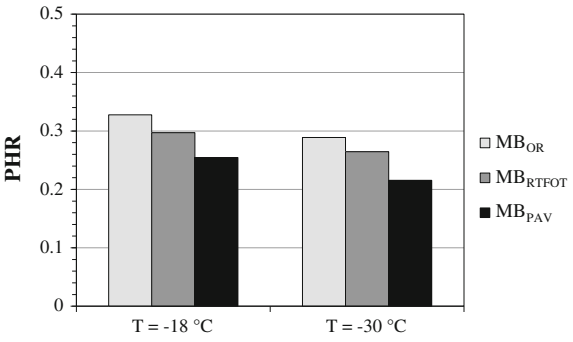


**Fig. 4** PHR values corresponding to different ageing conditions (MB tested at −18 and −30 °C)

**Table 3** Two sample t test analysis on reversibility of physical hardening

| Binder code | PHR | | | | | | Two sample t test | |
|---|---|---|---|---|---|---|---|---|
| | First run | | Second run | | n | $\bar{x}_1 - \bar{x}_2$ | $t_{\alpha/2,df}$ | $t_{calc}$ |
| | $\bar{x}_1$ | $s_1$ | $\bar{x}_2$ | $s_2$ | | | | |
| $NA_{OR}$ | 0.355 | 0.029 | 0.421 | 0.014 | 3 | −0.066 | 4.30 | 3.59 |
| $NA_{RTFOT}$ | 0.354 | 0.014 | 0.358 | 0.010 | 4 | −0.004 | 3.18 | 0.46 |
| $NA_{PAV}$ | 0.305 | 0.026 | 0.276 | 0.006 | 4 | 0.029 | 3.18 | 2.14 |
| $MA_{OR}$ | 0.335 | 0.024 | 0.327 | 0.016 | 4 | 0.008 | 3.18 | 0.54 |
| $MA_{RTFOT}$ | 0.301 | 0.003 | 0.269 | 0.016 | 4 | 0.032 | 3.18 | 3.83 |
| $MA_{PAV}$ | 0.261 | 0.021 | 0.252 | 0.012 | 4 | 0.009 | 3.18 | 0.71 |

Although the number of replicates was limited, a two sample t test was performed in order to verify whether the differences between mean PHR values corresponding to first and second run were due to actual variations in material properties. As a null hypothesis it was assumed there is no difference between mean PHR values, while the alternative hypothesis was formulated by considering a difference, either positive or negative, derived by using a significance level α of 0.05 in a two-tailed unpooled test.

Table 3 provides a synthesis of test data and results of the statistical analysis. In particular, $\bar{x}_1$ and $\bar{x}_2$ are the mean PHR values of first and second run, $s_1$ and $s_2$ are the corresponding standard deviations, and n is the sample size corresponding to number of test repetitions. Degrees of freedom (df) were assumed equal to $n - 1$.

Results of the statistical test indicate that critical t values ($t_{\alpha/2,df}$) are usually larger than computed ones ($t_{calc}$), with the only exception of $MA_{RTFOT}$. This means that from a statistical point of view the null hypothesis of equal means cannot be rejected. As a consequence, experimental data suggest that physical hardening may be considered as a reversible phenomenon.

## 4 Conclusions

The experimental investigation described in the paper focused on the combined influence of physical hardening and chemical ageing on low temperature properties of bituminous binders. The study was carried out by making use of the Bending Beam Rheometer and involved four binders of different type and origin (both neat and polymer-modified). Chemical ageing occurring in short-term and long-term conditions were simulated with RTFO and PAV treatments, respectively. In addition, reversibility of physical hardening was directly assessed by comparing material response under creep loading at increasing isothermal conditioning times before and after being stored at ambient temperature for a given period of time.

Aptitude of binders to harden with time, expressed in terms of Physical Hardening Rate (PHR), varied as a function of conditioning temperature following a bell-shaped trend characterized by the presence of a peak value which was found to be achieved at the glass transition temperature.

Chemical ageing phenomena were observed to significantly influence PHR, which progressively decreased as degree of ageing increased. Such evidence can be associated to a free volume reduction caused by the increase of asphaltenes generated by ageing treatments. Moreover, relative reduction of hardening rate consequent to chemical ageing was more pronounced for SBS polymer-modified binders as a consequence of the presence of an internal rubber-like network.

Results of a statistical test performed on mean PHR values obtained from first and second test runs support the hypothesis of reversibility of the phenomenon.

Further research is needed to validate the results obtained from this study. This should be done by extending the investigation to other materials and testing temperatures and by performing chemical analyses in order to directly link variations in rheological properties due to physical hardening to changes in the colloidal structure of binders consequent to ageing phenomena.

## References

AASHTO M320 (2010) Performance-Graded Asphalt Binder. American Association of State Highway Transportation Officials, Washington, D.C.

AASHTO R28 (2009) Accelerated Aging of Asphalt binder Using a Pressurized Aging Vessel (PAV). American Association of State Highway Transportation Officials, Washington, D.C.

AASHTO T240 (2009) Effect of Heat and Air on a Moving Film of Asphalt Binder (Rolling Thin-Film Oven Test). American Association of State Highway Transportation Officials, Washington, D.C.

AASHTO T313 (2010) Determining the Flexural Creep Stiffness of Asphalt Binder Using the Bending Beam Rheometer (BBR). American Association of State Highway Transportation Officials, Washington, D.C.

Anderson DA, Christensen DW, Bahia HU, Dongre R, Sharma MG, Antle CE (1994) Binder characterization and evaluation. Volume 3: Physical characterization. SHRP Report A-369. Strategic Highway Research Program, Transportation Research Board, National Research Council, Washington, D.C.

Anderson DA, Marasteanu MO (1999) Physical hardening of asphalt binders relative to their glass transition temperatures. Transportation Research Record 1661: 27-34.

Baglieri O, Dalmazzo D, Barazia M, Tabatabaee HA, Bahia HU (2012) Influence of physical hardening on low temperature properties of bitumen and asphalt mixtures. Procedia – Social and Behavioral Sciences 53: 504-513.

Bahia HU, Anderson DA (1993) Glass transition behavior and physical hardening of asphalt binders. Journal of the Association of Asphalt Paving Technologists 62: 93-129.

Bahia HU, Anderson DA (1995) The Pressure Aging Vessel (PAV): a test to simulate rheological changes due to field aging. American Society for Testing and Materials, Philadelphia.

Bell CA (1989) Summary report on aging of asphalt aggregate system. SHRP Report A-305. Strategic Highway Research Program, Transportation Research Board, National Research Council, Washington, D.C.

Daly WH, Qiu Z, Negulescu I (1996) Differential scanning calorimetry study of asphalt cristallinity. Transportation Research Record 1535: 54-60.

Ferry JD (1980) Viscoelastic properties of polymers. Wiley, New York.

Fox TG, Loshaek S (1955) Influence of molecular weight and degree of crosslinking on the specific volume and glass temperature of polymers. Journal of Polymer Science 15: 371-390.

Hesp SAM, Iliuta S, Shirokoff JW (2007) Reversible aging in asphalt binders. Energy Fuels 21: 1112-1121.

Kriz P, Stastna J, Zanzotto L (2008) Physical aging in semi-crystalline asphalt binders. Journal of the Association of Asphalt Paving Technologists 77: 795-825.

Leuseur D (2009) The colloidal structure of bitumen: consequences on the rheology and on the mechanisms of bitumen modification. Advances in Colloid and Interface Science 145: 42-82.

Lu X, Isacsson U (2000) Laboratory study on the low temperature physical hardening of conventional and polymer modified binders. Construction and Building Materials 14: 79-88.

Moschopedis SE, Speight JG (1977) The effect of air blowing on the properties and constitution of a natural bitumen. Journal of Materials Science 12: 990-998.

Nam K, Bahia HU (2004) Effect of binder and mixtures variables on glass transition behavior of asphalt mixtures. Journal of the Association of Asphalt Paving Technologists 73: 89-121.

Santagata E, Anderson DA, Marasteanu MO (1996) A rheological investigation on the physical hardening of modified asphalt binders. Paper presented at the 1st Eurasphalt and Eurobitume Congress, Strasbourg, 7-10 May 1996. Vol. 3, E&E5.151.

Siddiqui MN, Ali MF (1999) Studies on ageing behavior of the Arabian asphalts. Fuel 78: 1005-1015.

Soenen H, Ekblad J, Lu X, Redelius P (2004) Isothermal hardening in bitumen and in asphalt mix. Paper presented at the 3rd Eurasphalt and Eurobitume Congress, Wien, 12-14 May 2004. Vol. 2: 1364-1375.

Struik LCE (1978) Physical aging in amorphous polymers and other materials. Elsevier, Amsterdam.

Struik LCE (1991) Some problems in the non linear viscoelasticity of amorphous glassy polymers. Journal of Non-Crystalline Solids, 131-133: 395-407.

Tabatabaee HA, Velasquez R, Bahia HU (2012) Predicting low temperature physical hardening in asphalt binders. Construction and Building Materials 34: 162-169.

Traxler RN (1961) Relation between asphalt composition and hardening by volatilization and oxidation. Journal of the Association of Asphalt Paving Technologists 30: 359-372.

# Rheological Testing of Bitumen at Low Temperatures with 4-mm DSR

**Xiaohu Lu, Petri Uhlback and Hilde Soenen**

**Abstract** To measure bitumen low temperature rheological properties, a new test protocol using a dynamic shear rheometer with 4 mm parallel plates (or called 4-mm DSR) has been proposed in the US. In this paper, a series of experiments including different procedures of sample preparation were carried out to evaluate the 4-mm DSR. Comparison was made with the bending beam rheometer (BBR). The results obtained show that the 4-mm DSR can perform rheological tests at very low temperatures (down below −30 °C). With this new geometry, very little amount of sample is required, making it particularly suitable for study of field aging. There are correlations between complex modulus measured by the 4-mm DSR and creep stiffness by BBR, between phase angle and m-value, as well as between the limiting temperatures determined by the two test methods. With BBR data at 60 s loading time, higher correlation coefficients were observed at lower DSR frequencies or at a frequency corresponding to the 60 s loading time. The correlations seem also to be affected negatively by the waxes of bitumen, probably due to large differences in sample sizes that cause different thermal histories in DSR and BBR, making wax crystallization or physical hardening and its effect on rheology very different. In addition, common DSR with 8-mm plates can be applied to certain low temperatures, depending on instrument compliance and binder stiffness.

**Keywords** Low temperature rheology · Dynamic shear rheometer · 4-mm DSR · Bending beam rheometer

X. Lu (✉) · P. Uhlback
Nynas AB, SE-149 82 Nynäshamn, Sweden
e-mail: Xiaohu.lu@nynas.com

P. Uhlback
e-mail: Petri.uhlback@nynas.com

H. Soenen
Nynas NV, 2030 Antwerp, Belgium
e-mail: Hilde.soenen@nynas.com



F. Canestrari and M.N. Partl (eds.), *8th RILEM International Symposium on Testing and Characterization of Sustainable and Innovative Bituminous Materials*, RILEM Bookseries 11, DOI 10.1007/978-94-017-7342-3_52

# 1 Introduction

In cold climates, preventing low temperature cracking is of great importance to ensure the lifetime of an asphalt pavement. There are many types of factors that may affect asphalt low temperature cracking, including material-, structure-, and environmental-related factors (Haas and Phang 1988). Among the material factors, the properties of bituminous binders are probably the most critical (Isacsson and Zeng 1998). Thus, in many countries, binder specifications always include tests and criteria at low temperatures. One example is the standardized test method called the Fraass breaking point (EN 12593 2007). Although this test method has been employed widely for a long time, it is empirical in nature and is often difficult to achieve good precision.

Another low temperature test method, which has also been standardized and commonly used, is the one based on the bending beam rheometer (BBR) (EN 1477 2012). This however requires relatively large amounts of sample, and can be difficult for the binders recovered from a pavement, particularly when a thin asphalt layer is considered. Low-temperature measurements may also be carried out using a dynamic shear rheometer (DSR) with 8 mm parallel plates. However, it is claimed that the 8-mm geometry cannot go down to very low temperatures because of instrument compliance. To solve these problems, a new test protocol using parallel plates of 4 mm in diameter (or called 4-mm DSR) has been proposed by Western Research Institute (WRI) in the US (Sui et al. 2010, 2011).

The main objective of this paper is to experimentally evaluate 4-mm DSR. Various comparisons were made with BBR measurements.

# 2 Materials and Test Procedures

## *2.1 Bitumen Samples*

In this study, eight bitumens were tested (and further samples will include polymer modified binders). The selected samples differ in crude origin and/or penetration grade. Samples B and G are non-waxy bitumens, while others contain different amounts of natural waxes (up to 6 % for sample D) as measured by differential scanning calorimetry (DSC). The conventional properties of the samples are shown in Table 1.

## *2.2 Specimen Preparation and Test Procedures*

With 4-mm parallel plates, frequency sweeps from 0.1 to 100 rad/s were carried out at various temperatures. For this new geometry, great efforts were made to find a

**Table 1** List of bitumen samples

| Samples | Sources | Pen @ 25 °C, 0.1 mm | Softening point (°C) | Visc. @ 135 °C, cSt | Fraass breaking (°C) |
|---|---|---|---|---|---|
| A | Mixed | 61 | 49.0 | 468 | −15 |
| B | Venezuela | 83 | 45.4 | 345 | −21 |
| C | Russia | 86 | 47.4 | 238 | −17 |
| D | Unknown | 86 | 46.4 | 181 | −16 |
| E | Mid-East | 93 | 45.5 | 396 | −17 |
| F | Mexico | 101 | 45.1 | 325 | −16 |
| G | Venezuela | 192 | 37.8 | 199 | −21 |
| H | Mid-East | 205 | 39.2 | 225 | −22 |

proper way to prepare sample specimens of such a small size and to optimize testing procedures. After many trials, the following procedures were used.

First the gap of the DSR instrument was zeroed, and the upper 4 mm plate was released and equipped with a silicone mold. The depth of the mold was adjusted close to 2 mm (see Fig. 1). Then a small amount of sample was taken with a modified solder normally used in electronics and poured into the mold on the upper plate. The heating head of the solder was modified as a small spoon in order to make the bitumen flow. The temperature of the head was adjusted to 150–200 °C depending on the type of bitumen sample, lower for bitumen with a high penetration, and higher for low penetration bitumen. After naturally cooling to ambient temperature, excess sample in the mold was removed with a heated spatula.

The next step was to put the 4-mm plate with the silicone mold and bitumen sample in a refrigerator at 6 °C for about 15 min. Then the silicone mold was released and the plate with the bitumen specimen was placed back in the instrument. The lower plate was then heated to 30 °C and the upper plate with the

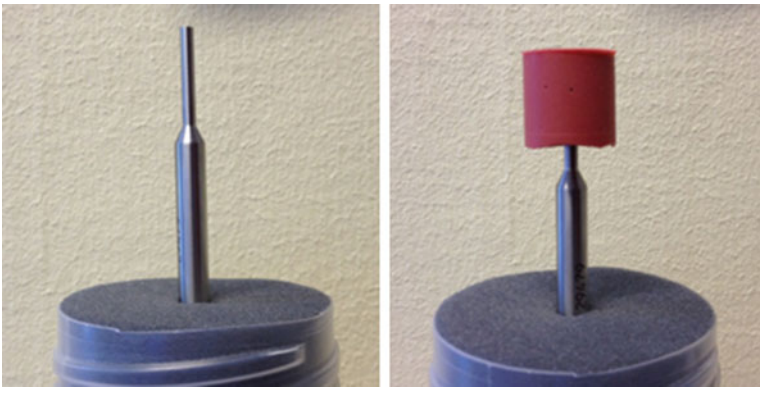

**Fig. 1** Preparation of a sample specimen on 4-mm plate

bitumen specimen was brought together with the lower plate in order to get a good bond between the sample and plates. Also the gap was thus adjusted (2 mm). Test was then started with cooling the sample to the test temperature, for which about 30 min were taken. The sample was then kept at the test temperature further 10 min before starting measurement. The normal force was set to be automatically zero to avoid any cracks or ruptures of the specimen during cooling and measurement. For each test temperature, a new specimen was prepared.

Initially, tests were conducted in constant strain mode, but in many cases the specimens broke when testing at higher frequencies. Therefore, the results presented in this paper were obtained by the stress-controlled mode. All the measurements were carried out at a stress level of 1 MPa with a rheometer Physica MCR 501 from Anton Paar.

## 3 Results and Discussion

### *3.1 DSR Tests Using Parallel Plates of Different Diameters*

DSR frequency sweeps from 0.1 to 100 rad/s were performed using parallel plates of different diameters at various temperatures ranging from −35 to 0 °C for 4 mm plates, −30 to 30 °C for 8 mm plates, and 10 to 100 °C for 25 mm plates. The test results obtained are shown as black curves in Fig. 2. Generally, at very low temperatures and/or high frequencies, with correct measurements the complex modulus G* should be a linear function of phase angle, and G* is about 1 GPa as phase angle

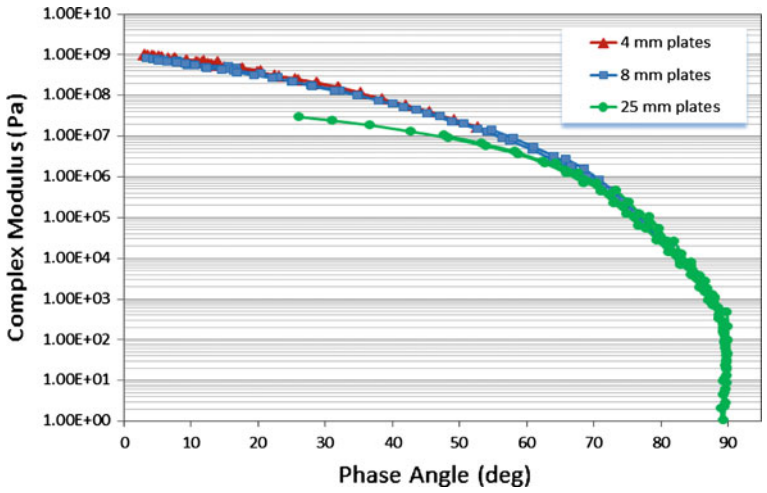


**Fig. 2** Examples of complex modulus versus phase angle obtained by parallel plates of different diameters (sample B)

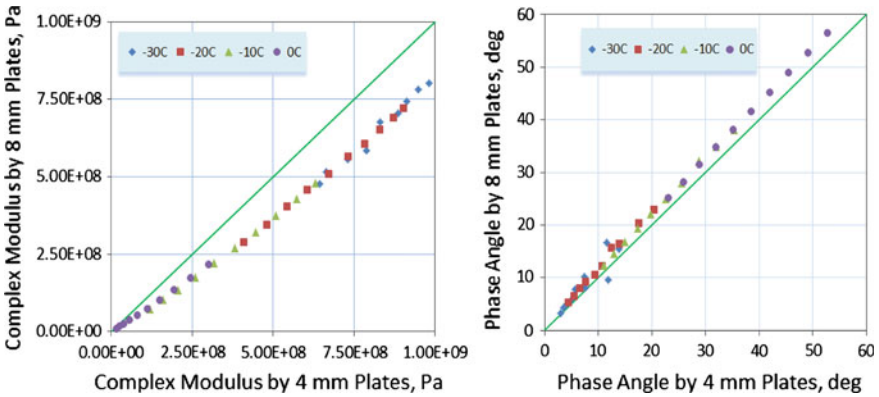


**Fig. 3** Comparison between 4 and 8 mm plates (sample B)

approaches zero. These trends likely hold for 4 and 8 mm plates. But for 25 mm plates, a clear deviation can be seen, indicating measurement errors caused by instrument compliance of the geometry at temperatures below about 20 °C.

Closer comparisons between 4 and 8 mm plates are shown in Fig. 3. As indicated, the complex moduli measured by 8 mm plates are systematically lower as compared with 4 mm ones, indicating compliance effects of the larger geometry. It was also observed that the lowest temperature where tests can be performed using 8 mm plates was −30 °C, below which the specimen was broken. However, no problem was found for 4 mm plates even at −35 °C. Also due to the smaller area of the 4 mm geometry, a higher torque can be applied to the sample without increasing too much torque in the instrument.

## *3.2 Rheological Tests at Low Temperatures with 4-mm DSR*

Three low temperatures, −15, −25 and −35 °C, were selected to closely assess 4 mm geometry. Frequency sweeps from 0.1 to 100 rad/s were carried out on a number of bitumen samples. It is known from the time-temperature superposition principle (TTSP) that time and temperature have related effects on rheological properties. Cooling a material has the same or similar effect as putting it under a short period of stress (or under a high frequency), both leading to an increase in stiffness. This is however only true for thermo-rheologically simple materials, i.e. for those which do not fundamentally change their structural character within the observed temperature range. As mentioned earlier, some samples contain waxes and their structure may change with temperature, thus making TTSP invalid (Champion et al. 1999). In the tests reported here, this should not be a problem since waxes of bitumen will crystallize at the low temperatures investigated (Lu et al. 2005), and significant changes in wax structures are not expected. Master curves at a reference

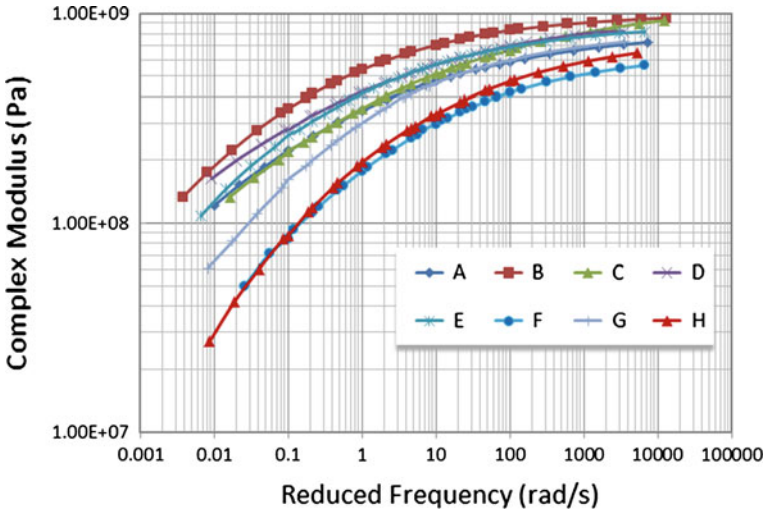


**Fig. 4** Master curves at reference temperature of −25 °C

temperature of −25 °C are shown in Fig. 4. A software module available in the rheometer was used to generate the master curves by horizontal shifts.

It is worth mentioning that at low temperatures bitumen becomes stiff and brittle, thus breaking of specimen and/or loss of contact between the sample and DSR plate may occur. These types of failure can be seen from irregular responses either in rheological results or in instrument raw data, as illustrated by Fig. 5. In the plots of raw value torque ($M_{raw}$) versus real angular movement, correct measurements are shown by a regular pattern in green.

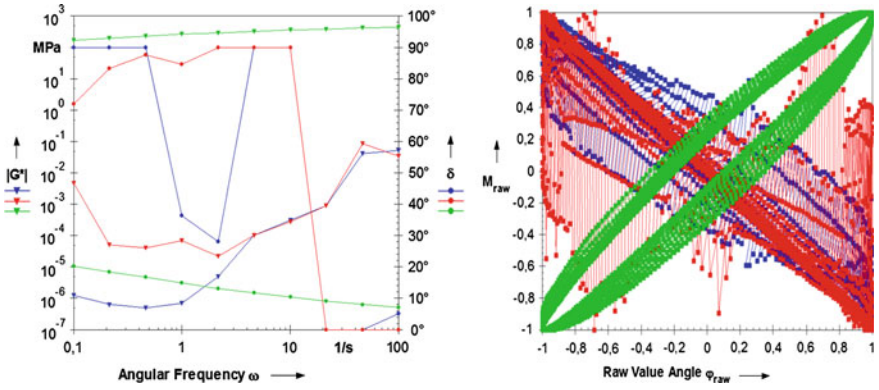


**Fig. 5** Plots showing correct (*green*) and improper (*red* and *blue*) measurements

### 3.3 Correlation Between 4-mm DSR and BBR

To examine the reliability of the 4-mm DSR, low temperature rheological tests were performed using BBR, and test results at a loading time of 60 s are summarized in Table 2. Then simple comparisons are made between the complex modulus measured using 4-mm DSR and the creep stiffness by BBR. As shown in Fig. 6 and Table 3, at the same low temperatures, correlations between the two test methods in general are not very strong, but become better when DSR run at lower frequencies.

It is known that inter-conversion between dynamic complex modulus (G*) and creep stiffness (S) may be described by the following equation (Anderson et al. 1994):

$$S(t) \approx \frac{3G^*(\omega)}{[1 + 0.2\sin(2\delta)]} \tag{1}$$

$$t \rightarrow 1/\omega$$

**Table 2** Results of BBR measurements

| | Limiting temp (°C) | | BBR at −15 °C | | BBR at −25 °C | |
|---|---|---|---|---|---|---|
| | LST | LmT | Stiffness (MPa) | m-value | Stiffness (MPa) | m-value |
| A | −20.6 | −27.0 | 123 | 0.43 | 580 | 0.32 |
| B | −18.5 | −23.3 | 171 | 0.47 | 825 | 0.26 |
| C | −22.0 | −29.0 | 105 | 0.38 | 415 | 0.33 |
| D | −20.0 | −21.0 | 143 | 0.37 | 524 | 0.26 |
| E | −18.5 | −23.2 | 146 | 0.42 | 677 | 0.28 |
| F | −22.7 | −25.5 | 85 | 0.46 | 440 | 0.33 |
| G | −23.0 | −28.3 | 45 | 0.63 | 446 | 0.38 |
| H | −23.7 | −28.0 | 58 | 0.53 | 365 | 0.35 |

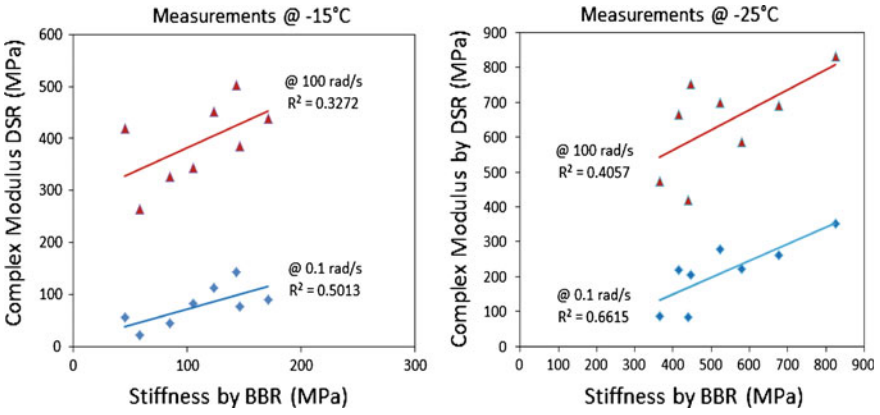


**Fig. 6** Correlation between complex modulus by 4-mm DSR and stiffness by BBR

**Table 3** Correlation coefficients ($R^2$) observed for DSR complex modulus at different frequencies versus BBR creep stiffness at a loading time of 60 s

| Temperature | 0.1 rad/s | 1 rad/s | 10 rad/s | 100 rad/s |
|---|---|---|---|---|
| −15 °C | 0.5013 | 0.5532 | 0.4782 | 0.3272 |
| −25 °C | 0.6615 | 0.6155 | 0.5268 | 0.4057 |

First, a further approximation is to let $S(t) \approx 3G^*(\omega)$ by assuming bitumen samples are very elastic with low phase angles at low temperatures. As shown in Fig. 7, the calculated stiffness moduli from 4-mm DSR are comparable to the BBR measurements.

Closer comparison between 4-mm DSR and BBR is also carried out by using exactly the inter-conversion shown above. According to this equation, at a loading time of 60 s in BBR, the corresponding angular frequency for DSR would be 0.0167 rad/s. Then complex moduli and phase angles at this frequency are extracted from the master curves in Fig. 4 (master curves for phase angles are not shown). Figure 8 shows correlation exists between 4-mm DSR and BBR, but deviation does exist. This might be attributed to waxy bitumens which had different degrees of wax crystallization or physical hardening due to different thermal histories caused by large differences in specimen sizes. By removing a waxy bitumen (sample D, containing about 6 % wax by DSC), the correlation was improved ($R^2$ increased from 0.64 to 0.77).

Correlation between phase angle (δ) and m-value is also examined. According to SHRP-A-369, at specific conditions, m-value may be simply estimated as δ/90. This is shown in Fig. 9. Also in this case, better correlation is seen at a lower frequency for DSR.

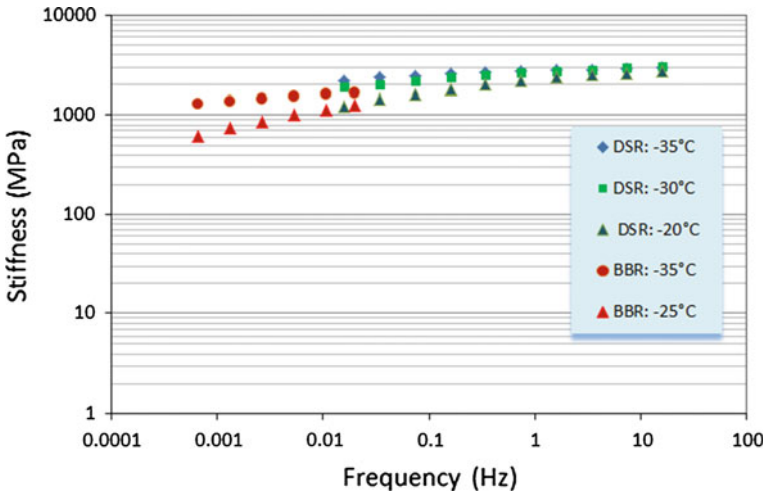


**Fig. 7** Stiffness moduli calculated from G* by 4-mm DSR or measured by BBR (sample B)

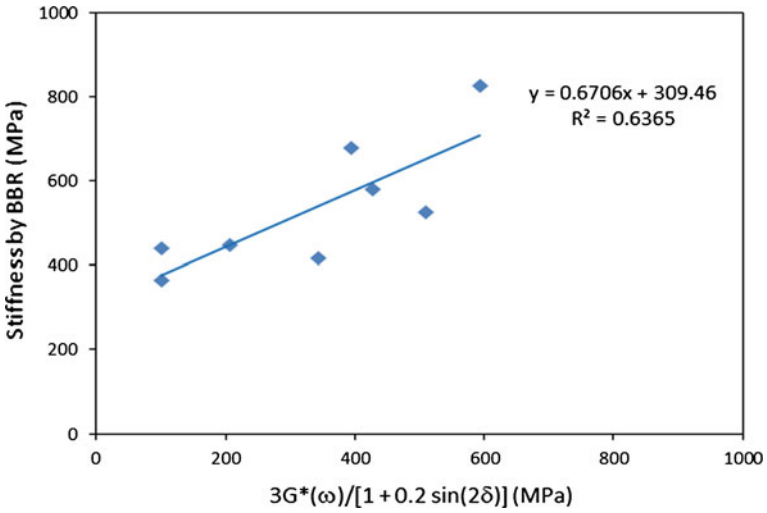


**Fig. 8** Correlation between 4-mm DSR at 0.0167 rad/s estimated from master curves at a reference temperature of −25 °C and BBR stiffness measured at the same temperature

Further comparison between 4-mm DSR and BBR is made by using different limiting temperatures, i.e. for BBR the temperatures at stiffness of 300 MPa and for DSR at complex modulus of 200 MPa. As illustrated in Fig. 10, the two test methods rank the bitumen samples quite similarly, and correlation coefficient was found above 0.70, implying reliability of the 4-mm DSR.

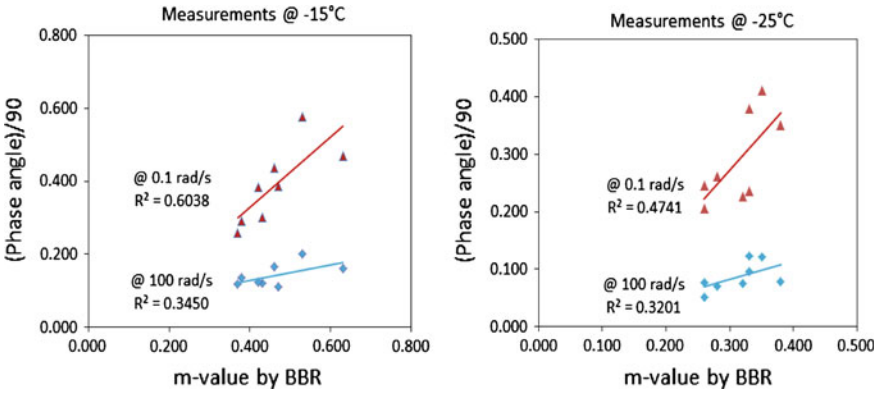


**Fig. 9** Comparison between phase angle by 4-mm DSR and m-value by BBR

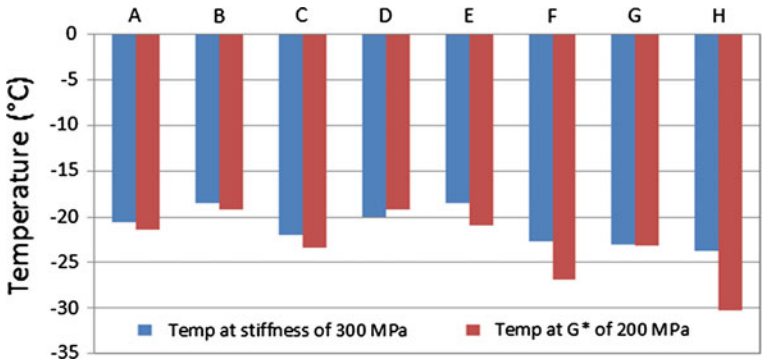


**Fig. 10** Comparison between the temperature at 200 MPa complex modulus (at 0.1 rad/s) and the temperature at 300 MPa stiffness

## 4 Conclusions

DSR with 4-mm plates has been used to measure bitumen rheological properties at low temperatures. For comparison, measurements with BBR were also carried out. The results obtained show that the 4-mm DSR can perform rheological tests at very low temperatures (down below −30 °C). With this geometry, very little amount of sample is required, which makes it particularly suitable for study of field aging for example in a thin asphalt layer. Because of very small size, a proper procedure is needed for preparing specimens, and caution also needs to be taken when running the tests.

It has been shown that correlations exist between complex modulus measured by the 4-mm DSR and creep stiffness by BBR, between phase angle and m-value, as well as between the limiting temperatures determined by the two test methods. With BBR data at 60 s loading time, higher correlation coefficients were seen at lower DSR frequencies or at a frequency corresponding to the 60 s loading time of the BBR.

The correlations between 4-mm DSR and BBR seem to be affected negatively by the waxes of bitumens. This is probably due to large differences in sample sizes that cause different thermal histories in DSR and BBR, making wax crystallization or physical hardening and its effect on rheology very different.

In addition, common DSR with 8-mm plates can be applied down to certain low temperatures. This is very much dependent on the compliance of the instrument used, as well as the stiffness of the sample to be tested.

## References

Anderson DA, Bahia HU, Dongre R, Sharma MG, Antle CE, Button J (1994) Binder characterization and evaluation, Volume 3: Physical characterization, SHRP-A-369

Champion L, Gerard JF, Planche JP, Martin D, Anderson D (1999) Asphaltenic – waxy bitumens: Limitations to the Time – Temperature Superposition principle, Eurobitume Workshop 99, Luxembourg, May 3–6, 1999

EN 12593 (2007) Bitumen and bituminous binders – Determination of the Fraass breaking point, European Committee for Standardization, CEN, Brussels

EN 1477 (2012) Bitumen and bituminous binders – Determination of the flexural creep stiffness – Bending Beam Rheometer (BBR), European Committee for Standardization, CEN, Brussels

Haas RCG, Phang WA (1988) Relationships between mix characteristics and low temperature pavement cracking, Proceedings of the Association of Asphalt Paving Technologists, Vol. 57, pp.290–319

Isacsson U, Zeng H (1998) Cracking of asphalt at low temperature as related to bitumen rheology, Journal of Materials Science, Vol. 33, pp.2165–2170

Lu X, Langton M, Olofsson P, Redelius P (2005) Wax morphology in bitumen, Journal of Materials Science, Vol. 40, pp. 1893–1900

Sui C, Farrar MJ, Tuminello WH, Turner TF (2010) New technique for measuring low-temperature properties of asphalt binders with small amounts of material, TRR 2179, pp.23–28

Sui C, Farrar MJ, Harnsberger PM, Tuminello WH, Turner T F (2011) A new low-temperature performance-grading method using 4-mm parallel plates on a dynamic shear rheometer, TRB Annual Meeting 2011

# Fatigue Rheological Characterization of Polymer-Modified Bitumens and Mastics

**Francesca Frigio, Gilda Ferrotti and Fabrizio Cardone**

**Abstract** Fatigue is one of the major distresses of flexible pavements and is mainly related to the rheological properties of the bituminous components of mixtures. In particular, bitumen and mineral filler create a blend called mastic that significantly influences the service life of asphalt pavements depending on its nature and composition. The purpose of this study is to investigate the effects of different polymer types and mineral fillers on the rheological behavior of a plain bitumen. Two types of polymer (an elastomer and a plastomer) were employed to produce polymer modified bitumens (PMBs) through laboratory mixing. Moreover, two fillers characterized by a different mineralogical nature (limestone and basalt) were selected in order to obtain several mastics. The dynamic shear rheometer (DSR) was used to study the fatigue behavior of all materials. Experimental data show that the effect of both polymer types is similar on mastics and bitumens as the presence of the elastomer leads to an improvement in fatigue life whereas the presence of the plastomer leads to a slight decrease in fatigue performance with respect to the plain bitumen, regardless of the mineral filler type. Moreover, the stiffening effect of mineral fillers was found to be significant regardless of filler mineralogy and bitumen type leading to a decrease in fatigue life with respect to bitumens. All mastics were less sensitive to the strain level applied as compared to the corresponding bitumens.

**Keywords** Bituminous mastics · Fatigue properties · Mineral filler · Modified bitumens

F. Frigio (✉) · G. Ferrotti · F. Cardone
Dipartimento di Ingegneria Civile Edile e Architettura, Università Politecnica delle Marche, Via Brecce Bianche, 60131 Ancona, AN, Italy
e-mail: f.frigio@univpm.it

G. Ferrotti
e-mail: g.ferrotti@univpm.it

F. Cardone
e-mail: f.cardone@univpm.it



F. Canestrari and M.N. Partl (eds.), *8th RILEM International Symposium on Testing and Characterization of Sustainable and Innovative Bituminous Materials*, RILEM Bookseries 11, DOI 10.1007/978-94-017-7342-3_53

## 1 Introduction

Fatigue is one of the major distresses that asphalt pavements experience during their service life and it is considered a very complicated damage phenomenon. Although the scientific community debates if fatigue cracking is due to a structure problem or a mixture problem, it is widely recognized that the cracks form and propagate through the bituminous components. Thus, fatigue needs to be studied as bitumen-associated damage phenomenon (Bahia et al. 2001).

In this sense, the use of polymer modification in road paving applications has been growing rapidly over the last decade as it allows significant enhancements in bitumen properties with consequent improvement in pavement service life. In fact, polymers are traditionally used with bitumen in order to increase its stiffness at high service temperatures and reduce it at low service temperatures (Airey 2002; Collins et al. 1991). This leads to enhanced pavements having lower thermal susceptibility, fatigue damage and stripping as well as higher resistance to rutting and thermal cracking (Yildrim 2007; Santagata et al. 2013).

Moreover, it is well recognized that the mechanical properties of asphalt mixtures are closely controlled by the behavior of bitumen-filler mastics (Anderson et al. 1992). In particular, bitumen and mineral filler create a blend that significantly influences the service life of asphalt pavements depending on its nature and composition. Filler plays a dual role in the asphalt mixtures: it is part of the mineral aggregates as it fills the interstices between larger aggregates and it may become incorporated into the bitumen acting as a mastic that bonds the aggregates together. Indeed, it well known that hot mix asphalt mixtures should be considered as mixes of mastic-coated aggregates rather than pure-bitumen-coated aggregates (Wang et al. 2011).

Given the fundamental role of bituminous components in the fatigue life of asphalt mixtures, this paper presents an experimental investigation where the fatigue properties of both bitumens and mastics were evaluated. Both plain and modified bitumens were considered by adding two types of polymers (an elastomer and a plastomer) at different contents, in order to evaluate the influence of both polymer type and concentration on bitumen fatigue behavior. Moreover, since bitumen-filler mastic properties are more strictly related to the asphalt mixture performance, selected bitumens were used to produce mastics by adding two types of filler (basalt and limestone) at a fixed concentration. In this way, a comparative evaluation of fatigue damage between bitumens and mastics was carried out.

## 2 Background on Fatigue Analysis

In the existing Superpave specifications, the fatigue damage is controlled by limiting the loss portion of the bitumen complex modulus ($G^* \sin \delta$) under defined test and aging conditions. However, such a parameter showed a lack of correlation with

mixture fatigue performance especially when modified bitumens are involved. Thus, it has been considered inadequate to describe fatigue damage as it cannot fully represent the effect of repeated loading cycles and the changes in bitumen properties due to damage accumulation (Bahia et al. 2001).

Therefore, in order to satisfy the need of an effective bitumen fatigue-cracking criterion that is valid and applicable to all types of bitumens, the NCHRP Report 459 (Bahia et al. 2001) provided a new method to predict bitumen fatigue properties by performing repeated loading time sweep tests with the DSR (Dynamic Shear Rheometer) equipment. The corresponding evaluation criterion is not based on the analysis of a single parameter but on the study of the fatigue damage development by computing the total dissipated energy during loading cycles. In particular, during fatigue tests the complex modulus ($G^*$) and the phase angle ($\delta$) can be obtained as a function of loading cycles and the corresponding dissipated energy per cycle $W_i$ can be written as a function of the stress $\sigma_i$ and the strain $\varepsilon_i$ amplitudes at the ith cycle, as follows:

$$W_i = \pi \sigma_i \varepsilon_i \sin(\delta_i) \tag{1}$$

where $\delta_i$ is the phase angle at the ith cycle.

Thus, the damage accumulation can be evaluated through the change in the Dissipated Energy Ratio (DER) over loading cycles:

$$DER = \frac{\sum_{i=1}^{n} W_i}{W_n} \tag{2}$$

where $W_n$ is the dissipated energy at the nth cycle.

In strain-controlled tests, the curve of DER versus number of cycles (Fig. 1) shows an initial linear part that is indicative of no damage as the energy dissipated per cycle is constant. Then, when cracks form and start to propagate, the dissipated energy per cycle tends to rapidly increase experiencing no recoverable fatigue damage. From this curve, two points can be conventionally selected as fatigue

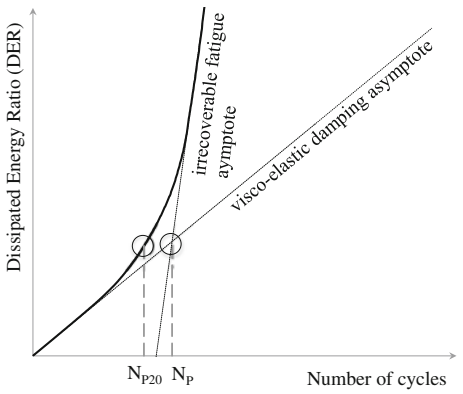


**Fig. 1** Typical plot of DER as a function of number of cycles in strain controlled tests

failure parameters: $N_{P20}$ is defined as the number of cycles to achieve 20 % deviation of DER from the no damage stage (Bonnetti et al. 2002) and represents the crack initiation condition, whereas $N_P$ is defined as the number of cycles where crack propagation starts.

## 3 Materials

A plain bitumen was used to produce four polymer modified bitumens (PMBs) by adding two types of polymer (an elastomer SBS and a plastomer PO) at two different contents (2 and 4 %).

Moreover, the plain and the modified bitumens at 4 % of polymer content were selected to produce six mastics by adding two types of filler (basalt and limestone) dosed at a constant filler/bitumen ratio equal to 1.2 by mass, in accordance with the Superpave specifications which recommend a ratio between 0.6 and 1.2.

Table 1 reports the codes used to identify all materials tested.

A 70/100 penetration-grade bitumen from an Italian oil refinery was selected as plain bitumen.

A radial styrene-butadiene-styrene (SBS) polymer with 30 % styrene and a density of 0.94 g/cm$^3$, and a polyolefin (PO) polymer having a density of 0.94 g/cm$^3$, were selected as modifying agents for the production of four PMBs.

All modified bitumens were produced in the laboratory using a ROSS high-shear mixer, operating at a rotation speed of 3000 rpm at 180 °C. Initially, 700 g of bitumen contained in a 1000 ml cylindrical can were heated to fluid conditions. Up on reaching 180 °C, the polymer was added slowly to the bitumen in order to prevent any polymer aggregation during the mixing process, which continued for 3 h. Table 2 shows the physical properties of the plain and the polymer modified bitumens, according to European specifications.

Only the plain bitumen and the PMBs including 4 % of polymers were selected to prepare mastics, by using two types of filler: basalt and limestone. The mastics were produced following a standardized experimental protocol, optimized in order to obtain homogeneous bitumen-filler mastics. The mineral filler and the bitumen were heated in the oven at 170 °C for 2 h. Then, the filler was slowly added to the

**Table 1** Codes of bitumens and mastics

| Polymer type | Polymer content (%) | Binder code | Mastic code | |
|---|---|---|---|---|
| | | | Basalt filler | Limestone filler |
| No polymer | – | B_Plain | M1_Plain | M2_Plain |
| SBS | 2 | B_SBS2 | – | – |
| | 4 | B_SBS4 | M1_SBS4 | M2_SBS4 |
| PO | 2 | B_PO2 | – | – |
| | 4 | B_PO4 | M1_PO4 | M2_PO4 |

**Table 2** Physical properties of the plain and the polymer modified bitumens

| Materials | Penetration at 25 °C 0.1 mm | Softening point °C | Dynamic viscosity at 135 °C Pa s |
|---|---|---|---|
| | (EN 1426) | (EN 1427) | (EN 12595) |
| B_Plain | 72 | 47.7 | 0.31 |
| B_SBS2 | 58 | 50.4 | 0.55 |
| B_SBS4 | 54 | 69.5 | 0.91 |
| B_PO2 | 64 | 52.4 | 0.54 |
| B_PO4 | 53 | 55.8 | 0.78 |

bitumen and blended in a mixer at 170 °C, increasing gradually the speed with the increase of the material density. The filler addition was completed in about 10 min and the mixing process was continued for 30 min in order to avoid the filler segregation.

In order to reproduce as well as possible the real field condition during service life, the produced materials were both short and long term aged. Two different short term aging procedures were used for bitumens and mastics: the rolling thin-film oven (RTFO) procedure for bitumens, whereas the thin-film oven (TFO) procedure. Finally, the long term aging was simulated using the pressure aging vessel (PAV) procedure for both bitumens and mastics.

## 4 Experimental Program and Testing Protocol

This study investigated the fatigue damage behavior of bitumens and mastics with a twofold objective. First, it allows the evaluation of the effect of polymer type and content on the bitumen fatigue behavior. Second, it assesses the effect of the addition of different mineral fillers on fatigue properties of plain and polymer modified bitumens.

All materials were subjected to fatigue tests carried out with a DSR device, using 8 mm parallel-plate-geometry and 2 mm-gap. Repeated loading cycles were applied at a temperature of 10 °C and a loading frequency of 10 Hz. Tests were carried out in a strain-controlled mode by adopting three different strain levels for each material.

A preliminary investigation concerning the linear visco-elastic (LVE) threshold allowed the definition of a suitable range of strain levels for both bitumens and mastics. Then, the choice of the applied strain levels derived from operative reasons in order to ensure that the analysis period was compatible with laboratory work constraints. The summary of the fatigue testing performed is given in Table 3. In the case of mastics, the applied strains were significantly lower than those applied for the bitumens as the presence of the mineral filler stiffs the material and thus the LVE shifts on lower strain ranges.

**Table 3** Strain levels applied for the fatigue tests

| Materials | Applied strain (%) | | | | | | | |
|---|---|---|---|---|---|---|---|---|
| | 0.3 | 0.4 | 0.6 | 0.7 | 0.8 | 0.9 | 1.2 | 1.5 |
| B_Plain | | | • | | | • | • | |
| B_SBS2 | | | | | | • | • | • |
| B_SBS4 | | | | | | • | • | • |
| B_PO2 | | | • | | | • | • | |
| B_PO4 | | | • | | | • | • | |
| M1_Plain | • | • | • | | | | | |
| M1_SBS4 | | | • | • | • | | | |
| M1_PO4 | • | • | • | | | | | |
| M2_Plain | • | • | • | | | | | |
| M2_SBS4 | | • | • | • | | | | |
| M2_PO4 | • | • | • | | | | | |

## 5 Results and Analysis

In order to investigate the fatigue damage, two different analysis approaches were selected. The first is based on monitoring the trend of complex modulus versus loading cycles and defining as conventional failure the number of cycles ($N_{50}$) at which the modulus $G^*$ decreases of 50 % with respect to its initial value. The second approach is based on the computation of the changes in the dissipated energy, according to Eqs. 1 and 2, studying $N_P$ and $N_{P20}$ values.

### *5.1 Bitumens*

The overall results of the plain and the PMBs are summarized in Table 4.

As regards the initial complex moduli $G^*_{in}$ recorded at the beginning of each fatigue test (i.e. immediately after the conditioning phase), the value obtained for each material decreases as the applied strain increases (except in one case) meaning that the materials are strain sensitive. The comparison of the initial complex modulus recorded for the different bitumens at the same applied strain shows that $G^*_{in}$ of PMBs including SBS decreases with respect to the plain bitumen, whereas PMBs including PO demonstrate a clear increase of $G^*_{in}$. Such a result indicates that the presence of the elastomeric polymer tends to soften the bitumen whereas the presence of the plastomeric polymer tends to stiffen the bitumen, as expected.

The numbers of cycles at which the materials reach the conventional fatigue failures ($N_{50}$, $N_P$, $N_{P20}$) are also reported for each bitumen and applied strain as the average of two repetitions. It is interesting to notice that, for each applied strain and for almost all materials tested, the number of loading cycles corresponding to a 50 % loss in modulus ($N_{50}$) is higher than the two fatigue parameters ($N_P$, $N_{P20}$) defined using the dissipated energy. Thus, in general, the DER approach results in

**Table 4** Fatigue test results of bitumens

| Bitumens | Applied strain γ | Initial complex modulus $G^*_{in}$ | Initial phase angle δ | $N_{50}$ | $N_P$ | $N_{P20}$ |
|---|---|---|---|---|---|---|
| | (%) | (kPa) | (°) | (−) | (−) | (−) |
| B_Plain | 0.6 | 67,050 | 34.3 | 629,250 | 452,400 | 344,700 |
| | 0.9 | 60,050 | 35.8 | 214,000 | 199,050 | 187,050 |
| | 1.2 | 58,850 | 36.4 | 98,813 | 90,900 | 79,050 |
| B_SBS2 | 0.9 | 53,900 | 34.7 | 742,500 | 655,800 | 652,800 |
| | 1.2 | 50,100 | 34.8 | 295,000 | 228,300 | 170,400 |
| | 1.5 | 52,100 | 36.1 | 118,125 | 95,850 | 88,350 |
| B_SBS4 | 0.9 | 57,933 | 33.1 | 974,667 | 861,662 | 987,750 |
| | 1.2 | 55,033 | 35.1 | 334,250 | 214,650 | 239,700 |
| | 1.5 | 53,800 | 34.8 | 130,500 | 141,900 | 123,900 |
| B_PO2 | 0.6 | 67,550 | 33.5 | 1,051,500 | 813,600 | 889,050 |
| | 0.9 | 64,600 | 33.9 | 201,920 | 152,400 | 227,400 |
| | 1.2 | 63,450 | 34.5 | 54,888 | 48,150 | 39,600 |
| B_PO4 | 0.6 | 72,150 | 32.3 | 597,000 | 453,750 | 385,200 |
| | 0.9 | 71,400 | 32.5 | 167,500 | 136,950 | 109,800 |
| | 1.2 | 69,150 | 33.0 | 82,250 | 73,950 | 64,950 |

more precautionary fatigue response with respect to the approach based on 50 % decrease in $G^*$. This can be explained with the fact that, as the dissipated energy approach allows the identification of the crack initiation and propagation condition, the material does not reach the stage where fatigue damage became irrecoverable.

Results also allowed a direct comparison between the fatigue behavior of the different bitumens studied in order to evaluate the effect of polymer type and content. The presence of SBS polymer leads to an improvement in fatigue life with respect to the plain bitumen, regardless of the analysis approach. In particular, for a given strain level, as the amount of SBS increases, the fatigue life tends to increase as well. Whereas, the presence of PO polymer tends to generally decrease the fatigue life with respect to the plain bitumen with the exception of B_PO2 that showed an improvement in fatigue life at low strain level.

The overall results can be better observed in Fig. 2 where the bitumen fatigue curve are represented in terms of $N_{P20}$, that is considered the best indicator of fatigue life (Bahia and Delgadillo 2005). Figure 2a shows a clear improvement in fatigue life due to the presence of SBS as fatigue curves are right-shifted with the increase of polymer amount. Moreover, the slope of the fatigue curves tends to decrease with the presence of SBS, meaning that those PMBs are less sensitive to the strain level applied with respect to the plain bitumen. On the contrary, Fig. 2b shows that the presence of PO results in a different fatigue response depending on the strain level applied, even if a general decrease of fatigue life is observed when PO polymers are considered.

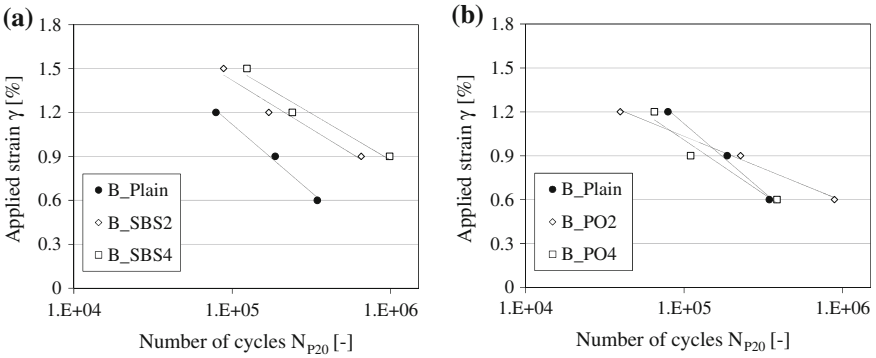


**Fig. 2** Fatigue curves in terms of $N_{P20}$ for all bitumens: **a** Plain and PMBs with SBS. **b** Plain and PMBs with PO

## *5.2 Mastics*

A similar approach was used to analyze the mastics and the overall results are summarized in Table 5.

As already shown in the case of bitumens, the initial complex moduli of mastics tend to decrease as the applied strain increases, for almost all materials. The comparison between $G^*_{in}$ obtained for bitumens and mastics (Tables 4 and 5) confirms that the presence of mineral fillers significantly stiffens the material, as already shown by many researchers (Mitchell and Lee 1939; Ridgen 1947; Kallas and Puzinauskas 1961; Tunnicliff 1962). According to Buttlar et al. (1999), the mastic behavior can be considered as an effect of three main mechanisms: volume-filling reinforcement (the presence of a rigid inclusion in a less rigid matrix causes the stiffening effect), physico-chemical reinforcement (the stiffening is caused by interfacial effects between bitumen and filler particles) and particle-interaction reinforcement. The latter effect was found to play a minor role in explaining the stiffening effect of filler and it is usually considered negligible.

As regards the number of cycles at which the materials reach the conventional fatigue failure ($N_{50}$, $N_P$, $N_{P20}$), the DER approach results in more precautionary fatigue parameters with respect to the conventional $N_{50}$, confirming the results obtained for bitumens.

The mastic fatigue behavior can be evaluated through a direct comparison between the fatigue curves reported in Fig. 3 in terms of $N_{P20}$. Results show that the presence of SBS polymer leads to significant improvements in fatigue life for both types of mastics, confirming the results obtained by Bahia et al. (2010). In the case of mastics containing basalt filler (M1) the presence of PO leads to a slight decrease in fatigue life with respect to the plain mastic whereas no significant differences are shown in the case of mastics containing limestone (M2). For both filler types, these results seem to confirm what was obtained with polymer modified bitumens (Fig. 2)

**Table 5** Fatigue tests results of mastics

| Mastics | Applied strain $\gamma$ | Initial complex modulus $G^*_{in}$ | Initial phase angle $\delta$ | $N_{50}$ | $N_P$ | $N_{P20}$ |
|---|---|---|---|---|---|---|
| | (%) | (kPa) | (°) | (−) | (−) | (−) |
| M1_Plain | 0.3 | 198,333 | 30.7 | 1,295,667 | 928,700 | 1,166,491 |
| | 0.4 | 189,500 | 31.8 | 325,500 | 185,400 | 601,200 |
| | 0.6 | 169,000 | 33.8 | 22,950 | 15,000 | 61,950 |
| M1_SBS4 | 0.6 | 201,000 | 32.6 | 674,500 | 461,400 | 438,900 |
| | 0.7 | 185,500 | 36.9 | 90,800 | 84,900 | 179,400 |
| | 0.8 | 188,000 | 35.9 | 12,900 | 11,400 | 15,000 |
| M1_PO4 | 0.3 | 279,000 | 29.4 | 946,000 | 596,850 | 640,835 |
| | 0.4 | 266,000 | 29.7 | 103,300 | 139,350 | 187,950 |
| | 0.6 | 229,000 | 32.1 | 6800 | 5100 | 6500 |
| M2_Plain | 0.3 | 251,000 | 30.4 | 3404,000 | 3,458,700 | 2,973,900 |
| | 0.4 | 253,500 | 30.6 | 552,500 | 448,950 | 440,550 |
| | 0.6 | 207,500 | 33.9 | 2100 | 9750 | 1050 |
| M2_SBS4 | 0.4 | 209,000 | 30.3 | 3,274,000 | 3,136,200 | 3,218,100 |
| | 0.6 | 192,000 | 32.0 | 293,000 | 244,800 | 265,200 |
| | 0.7 | 193,000 | 33.2 | 6000 | 49,800 | 4800 |
| M2_PO4 | 0.3 | 276,000 | 28.5 | 3,584,000 | 3,383,400 | 3,341,400 |
| | 0.4 | 275,500 | 29.2 | 446,000 | 353,850 | 337,050 |
| | 0.6 | 256,500 | 31.2 | 3900 | 17,400 | 2700 |

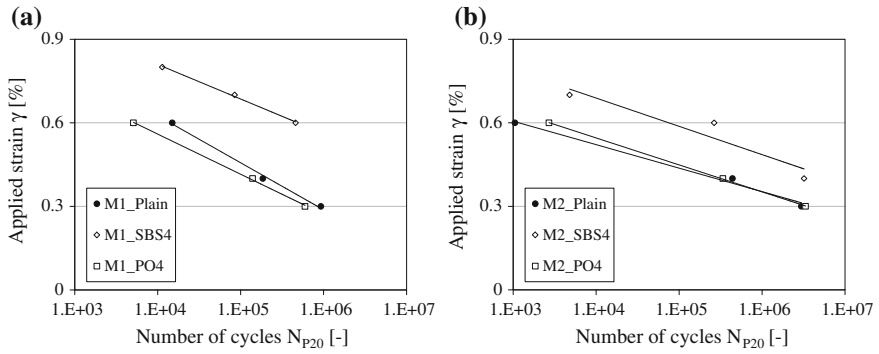


**Fig. 3** Fatigue curves in terms of $N_{P20}$: **a** Mastics M1. **b** Mastics M2

for which, with respect to the plain bitumen, a clear improvement in fatigue life with B_SBS4 and a general decrease in fatigue life with B_PO4 were observed.

In Fig. 4, the comparison between the fatigue curves of bitumens and mastics is shown for both PMBs. It is possible to observe that the addition of filler results in

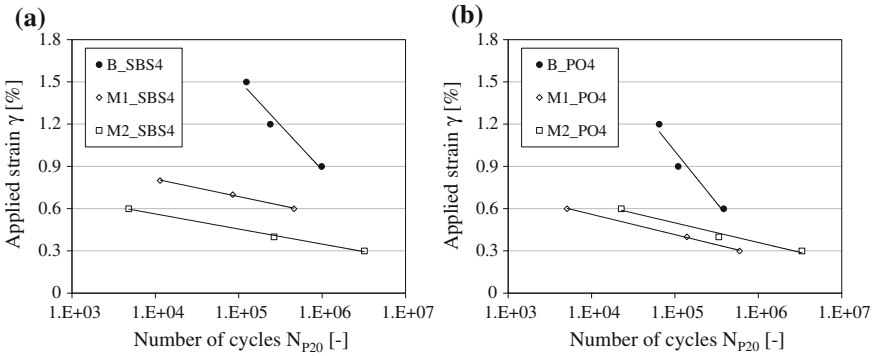


**Fig. 4** Comparison between bitumens and mastics fatigue curves in terms of $N_{P20}$: **a** Materials modified with SBS. **b** Materials modified with PO

a significant decrease in fatigue performance with respect to the corresponding bitumen, for both filler types, according to Airey et al. (2006) findings. Furthermore, all mastics show a less strain dependent fatigue behavior with respect to the corresponding bitumens for both filler types, confirming previous results (Santagata et al. 2008). From these results it is possible to conclude that the stiffening effect of the mineral filler leads to a premature fatigue failure and less strain susceptibility.

Finally, the comparison between the two types of mastics (M1 and M2) shows differences in the fatigue behavior of the two polymer modified materials. In the case of SBS polymer, the basalt mastic (M1) shows a higher fatigue life than the limestone mastic (M2), whereas the effect is reversed in the case of PO polymer. Such a result seems to suggest that some sort of physico-chemical interaction between mineral fillers and PMBs may occur affecting mastic rheological properties as fatigue performance (Shivokhin et al. 2012).

## 6 Conclusions

In this study, the fatigue damage behavior of bitumens and mastics was evaluated. A plain bitumen was used to produce modified bitumens by adding two polymer types (an elastomer SBS and a plastomer PO) at two different contents (2 and 4 %). Moreover, bituminous mastics with a filler/bitumen ratio equal to 1.2 were produced blending two types of filler (basalt and limestone) with the plain bitumen and with the modified bitumens at 4 % of polymer content.

Fatigue resistance characterization consisted of “time-sweep” tests at a loading frequency of 10 Hz and a temperature of 10 °C in a strain-controlled mode by means of a Dynamic Shear Rheometer.

Conventional failure criterion, based on the monitoring of the complex modulus decrease until 50 % of its initial value, and dissipated energy based approach were used to investigate fatigue behavior.

From the experimental results, the following conclusions can be drawn:

- the dissipated energy approach results in more precautionary fatigue response with respect to the conventional failure criterion ($N_{50}$), for both bitumens and mastics;
- in comparison with plain bitumen, polymer modified bitumens containing SBS show a clear improvement in fatigue life with the increase of polymer content and a less strain sensitive fatigue behavior, whereas the fatigue life tends to decrease due to the presence of PO polymers;
- the stiffening effect of mineral fillers was found to be significant regardless of filler mineralogy and bitumen type and leads to a decrease in fatigue life with respect to bitumens;
- all mastics were found to be less sensitive to the strain level applied as compared to the corresponding bitumens;
- the effect of both polymer types on mastics and bitumens was similar: the presence of SBS leads to an improvement in fatigue life while the presence of PO leads to a slight decrease in fatigue performance with respect to the plain bitumen, regardless of the mineral filler type;
- the filler type affects differently the fatigue performance of mastics depending on the polymer modified bitumens considered. This suggests that some possible physic-chemical interaction between mineral fillers and polymers may occur.

**Acknowledgements** This work was supported by the MIUR project "Damage and healing of innovative nano-structured and polymer-modified bituminous materials" (Grant RBFR10JOWO) under the "FIRB—Futuro in Ricerca 2010" funding program.

## References

Airey GD (2002) Rheological evaluation of ethylene vinyl acetate polymer modified bitumens. Constr Build Mater 16: 473-87.

Airey GD, Liao MC, Thom NH (2006) Fatigue Behaviour of Bitumen-Filler Mastics. 10th International Conference on Asphalt Pavements, Quebec city – Canada, 1:485-495.

Anderson DA, Bahia HU, Dongre R (1992) Rheological Properties of Mineral Filler-Asphalt Mastics and Its Importance to Pavement Performance. ASTM STP 1147, American Society for Testing and Materials.

Bahia HU, Hanson DI, Zeng M, Zhai H, Khatri MA, Anderson RM (2001) NCHRP Report 459: Characterization of Modified Asphalt Binders in Superpave Mix Design. Transportation Research Board of the National Academies, Washington, D.C.

Bahia HU, Delgadillo R (2005) Rational Fatigue Limits for Asphalt Binders Derived from Pavement Analysis. J Assoc Asphalt Paving Technol 74.

Bahia HU, Al-Qadi IL, Faheem AF, Fini E, Wen H, Desouky S (2010) NCHRP Project 9-45: Test Methods and Specification Criteria for Mineral Filler Used in HMA. Interim Report. Transportation Research Board of the National Academies, Washington, D.C.

Bonetti KB, Nam K, Bahia HU (2002) Measuring and defining fatigue behavior of asphalt binders. J Transp Res Rec 1810: 33-43.

Buttlar WG, Bozkurt D, Al-Khateeb GG, Waldhoff AS (1999) Understanding asphalt mastic behavior through micromechanics. Transport Res Rec 1681: 157-169. doi: 10.3141/1681-19

Collins JH, Bouldin MG, Gelles R, Berker (1991) A Improved performance of paving asphalts by polymer modification. J Assoc Asphalt Paving Technol 60: 43-79.

Kallas BF, Puzinauskas VP (1961) A study of mineral fillers in asphalt paving mixtures. J Assoc Asphalt Paving Technol 10:493-528.

Mitchell JG, Lee AR (1939) Evaluation of fillers for tar and other bituminous surfacings. J Soc Chem Industry 58: 299.

Rigden PJ (1947) The use of fillers in bituminous road surfacings. A study of filler binder systems in relation to filler characteristics. J Soc Chem Industry 66(9): 299-309. doi: 10.1002/jctb.5000660902

Santagata E, Baglieri O, Dalmazzo D (2008) Experimental Investigation on the Fatigue Damage Behaviour of Modified Bituminous Binders and Mastics. J Assoc Asphalt Paving Technol 77: 851-883.

Santagata E, Baglieri O, Dalmazzo D, Tsantilis L (2013) Evaluation of the anti-rutting potential of polymer-modified binders by means of creep-recovery shear tests. Mater Struct 46: 1673-82.

Shivokhin M, García-Morales M, Partal P, Cuadri AA, Gallegos C (2012) Rheological behaviour of polymer-modified bituminous mastics: A comparative analysis between physical and chemical modification. Constr Build Mater 27(1): 234-240.

Tunnicliff DG (1962) A review of mineral filler. J Assoc Asphalt Paving Technol 31: 118-150.

Wang H, Al-Qadi I, Faheem AF, Bahia HU, Yang SH, Reinke GH (2011) Effect of Mineral Filler Characteristics on Asphalt Mastic and Mixture Rutting Potential. Transport Res Rec 2208: 33-39. doi: 10.3141/2208-05

Yildrim Y (2007) Polymer modified asphalt binders. Constr Build Mater 21: 66-72.

# Influence of Hydrated Lime on Linear Viscoelastic Properties of Bituminous Mixtures

**Cong Viet Phan, Hervé Di Benedetto, Cédric Sauzéat and Didier Lesueur**

**Abstract** An experimental campaign on the characterization of the tri-dimensional linear viscoelastic (3D LVE) behaviour of 2 bituminous mixtures was carried out. These 2 different mixtures were produced using the same aggregates and bitumen. As additives, two types of fillers, hydrated lime and limestone filler, were used. The goal was to evaluate the influence of hydrated lime on linear viscoelastic properties of bituminous mixtures. The linear viscoelastic behaviour of bituminous mixtures was studied using complex modulus tests (tension-compression test on cylindrical specimens) at different temperatures (from −25 to +52 °C) and frequencies (from 0.003 to 10 Hz). Sinusoidal cyclic loadings of 50 μm/m axial strain amplitude were applied. In addition to axial stress and axial strain, radial strains were also measured. The complex modulus E* and the complex Poisson's ratios ν* were then obtained and the three-dimensional (3D) LVE behaviour (with isotropy hypothesis) was then completely described. The Time-Temperature Superposition Principle (TTSP) was verified with good approximation. The same values of shift factor were obtained for uni-dimensional (1D) and tri-dimensional (3D) conditions. The 2S2P1D model (3D) developed by ENTPE team was used for modelling linear viscoelastic properties of the two mixtures. Effect of hydrated lime is discussed.

**Keywords** Linear viscoelastic properties · Bituminous mixtures · Hydrated lime · Complex modulus test

C.V. Phan (✉) · H. Di Benedetto · C. Sauzéat
Laboratoire Génie Civil et Bâtiment & LTDS (UMR CNRS 5513), University of Lyon, ENTPE, Rue Maurice Audin, 69518 Vaulx-en-Velin Cedex, France
e-mail: congviet.phan@entpe.fr

H. Di Benedetto
e-mail: herve.dibenedetto@entpe.fr

C. Sauzéat
e-mail: cedric.sauzeat@entpe.fr

D. Lesueur
Materials R&D, Lhoist Recherche et Développement Rue de L'Industrie, 31 B, 1400 Nivelles, Belgium
e-mail: didier.lesueur@lhoist.com



F. Canestrari and M.N. Partl (eds.), *8th RILEM International Symposium on Testing and Characterization of Sustainable and Innovative Bituminous Materials*, RILEM Bookseries 11, DOI 10.1007/978-94-017-7342-3_54

## 1 Introduction

Hydrated lime has been known as an additive for asphalt mixtures from the very beginning. It is estimated that about 40 Mt of asphalt mixtures are produced each year in the USA with hydrated lime. Although hydrated lime has been successfully used in asphalt mixtures for a long time, it is still an active research field as demonstrated by the high number of recent publications. Several authors (Stroup-Gardiner and Epps 1987; Pickering et al. 1992; Epps et al. 1992; Ghouse Baig and Al-Abdul Wahhab 1998; Mohammad et al. 2000; McCann and Sebaaly 2006; Witczak and Bari 2004; Jaskula and Judycki 2005; Khattak and Kyatham 2008; Vural and Yilmaz 2009; among others), investigated on the influence of hydrated lime on mechanical properties of asphalt mixtures. The general conclusion of these studies is that hydrated lime does not always increase the modulus of asphalt mixtures. In particular, among the 71 mix formulas considered in the mentioned studies, only 42 mix formulas (59 %) showed a higher modulus due to the addition of hydrated lime. More research on this topic is needed.

Within the framework of a partnership between the LGCB/LTDS of the ENTPE and the LHOIST Group a research project is currently ongoing, focusing on the characterization of bituminous mix with hydrated lime was initiated.

An investigation the Linear Viscoelastic (LVE) behaviour of two different bituminous materials is presented in this paper. The LVE properties of the materials are measured by means of complex Young's modulus tests (tension-compression) at selected temperatures and frequencies. The three-dimensional (3D) LVE behavior of the tested materials is completely determined. 2S2P1D (2 Springs, 2 Parabolic creep elements and 1 Dashpot) model, developed at ENTPE laboratory (Olard and Di Benedetto 2003; Di Benedetto et al. 2007, 2009; Mangiafico et al. 2013; among others) is used to simulate experimental results.

This article focuses on the effect of hydrated lime on linear viscoelastic properties of bituminous mixtures. In particular, the linear viscoelastic properties (complex Young's modulus $|E^*|$, complex Poisson's ratio $|\nu^*|$, the shift factor values $a_T$ used for the construction of the master curves in the whole range of considered temperatures and frequencies) of two materials, with and without hydrated lime are compared.

Sections 2 and 3 present respectively the testing procedure and the experimental complex modulus tests results for the 2 different tested mixtures. Section 4 presents the 2S2P1D model which is used for simulation. Section 5 focuses on the analysis of the influence of hydrated lime on linear viscoelastic properties of bituminous mixtures.

## 2 Experimental Procedures and Materials

### 2.1 Test Equipment

Sinusoidal cyclic tension-compression tests were carried out on cylindrical specimens (diameter: 75 mm; height: 140 mm, glued to aluminum caps with a two-component epoxy adhesive) using a hydraulic press. Load cell (±25 kN range) fixed out of the thermal chamber provides axial stress.

A thermal chamber was used for thermal conditioning of the specimens during the test. The temperature was measured using a thermal gauge (PT100 temperature probe) fixed on the surface of the specimen.

Three axial extensometers located at 120° around the specimen were used to measure axial displacement (Fig. 1). The axial strain was obtained from the average of the three measurements (which is also used for monitoring applied loading). Two radial strains in two radial directions were obtained from two pairs of non-contact displacement transducers (range 500 μm) that measured diameter changes at mid-height of the specimen.

A general view of the specimen and a schema of the strain measurement are shown in Fig. 1.

### 2.2 Test Procedures

Advanced complex modulus tests were carried out using the described equipment. A schema of the test procedure is shown in Fig. 2. Specimens were loaded at

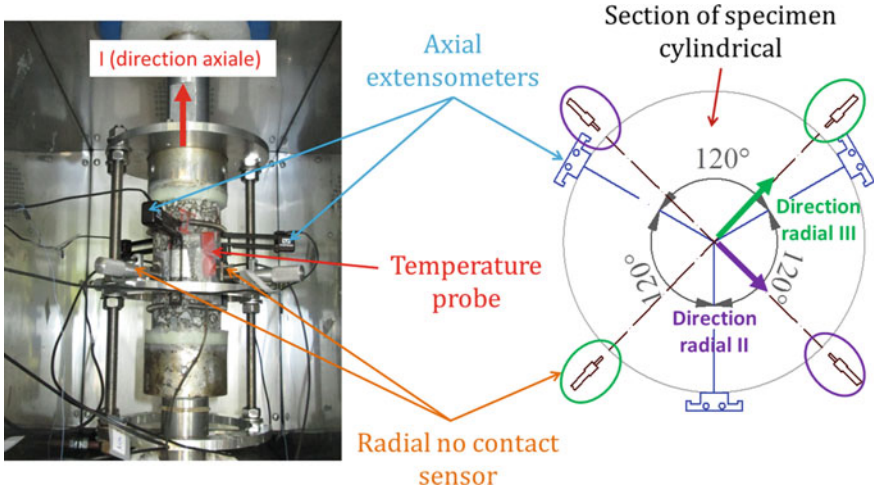


**Fig. 1** *Left* general view of the experiment developed at ENTPE to measure the axial strain and the radial strain. *Right* section of the cylindrical specimen and strain measurement devices

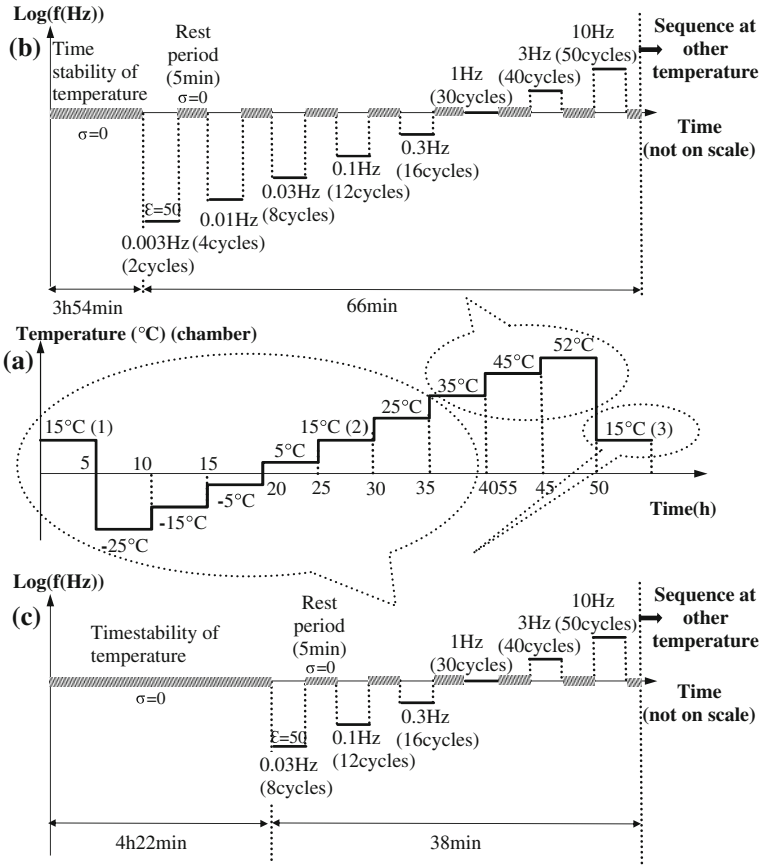


**Fig. 2** Temperature chronology of each test (**a**) and chronology of frequencies at each temperature: 35, 45 and 52 °C (**b**) and from 10 to 25 °C (**c**). All cyclic loadings at fixed strain amplitude of 50 μm/m

6 frequencies (0.03, 0.1, 0.3, 1, 3 and 10 Hz) and at 9 temperatures [from −25 to 52 °C: 15 °C (1), −25, −15, −5, 15 °C (2), 25, 35, 45, 52, 15 °C (3)], in addition 2 smaller frequencies (0.003 and 0.01 Hz) were added at high temperatures (35, 45 and 52 °C), in order to determine the viscoelastic properties of tested materials on a wider range. Tests were conducted in strain control mode. The amplitude of axial strain during cyclic loading was 50 μm/m. As shown in the Table 1, the number of

**Table 1** Frequencies and number of cycle for each tested temperature

| Frequency (Hz) | 0.003 | 0.01 | 0.03 | 0.1 | 0.3 | 1 | 3 | 10 |
|---|---|---|---|---|---|---|---|---|
| Number of cycle | 2 | 4 | 8 | 12 | 16 | 30 | 40 | 50 |
| Analyzed cycle | 2 | 2–3 | 2–7 | 2–11 | 2–15 | 2–29 | 2–39 | 10–49 |

loading cycles varied from 2 cycles up to 50 cycles. A rest period of 300 s was applied between two successive cyclic loading periods (i.e., between each frequency change). This represents a test duration of 38 min approximately for 6 temperatures (from −25 to 25 °C with 3 tests at 15 °C) and of 66 min approximately for 3 temperatures (35, 45 and 52 °C). A conditioning period of 4 h and 22 min approximately for 6 temperatures (from −25 to 25 °C with 3 tests at 15 °C) and of 3 h and 54 min approximately for 3 temperatures (35, 45 and 52 °C) was also considered when the temperature was changed to ensure an homogeneous temperature inside the specimen. During conditioning periods, stress control mode is used. The axial stress applied on the specimen is maintained equal to 0 MPa by the press monitoring system.

A sinusoidal axial strain ($\varepsilon_{ax}$) (average of three extensometers) was applied and the sinusoidal axial stress ($\sigma_{ax}$) was measured using a load cell. The sinusoidal radial strains in the directions II and III are respectively $\varepsilon_{rad\ II}$ and $\varepsilon_{rad\ III}$. They were obtained from the pairs of non-contact sensors (Fig. 1). The following equations describe these quantities:

$$\varepsilon_{ax}(t) = \varepsilon_{Aax} \sin(\omega t) \tag{1}$$

$$\sigma_{ax}(t) = \sigma_{Aax} \sin(\omega t + \varphi_E) \tag{2}$$

$$\varepsilon_{rad\,II}(t) = -\varepsilon_{Arad\,II} \sin(\omega t + \varphi_{v\,II}) \tag{3}$$

$$\varepsilon_{rad\,III}(t) = -\varepsilon_{Arad\,III} \sin(\omega t + \varphi_{v\,III}) \tag{4}$$

where $\varphi_E$ is the phase angle between the axial strain and the axial stress; $\varphi_{v\ II}$ and $\varphi_{v\ III}$ are the phase angles between the axial strain and the radial strains in the directions II and III, respectively; $\varepsilon_{Aax}$, $\varepsilon_{Arad\ II}$, $\varepsilon_{Arad\ III}$ and $\sigma_{Aax}$ are the axial strain amplitude, the radial strain amplitudes in the directions II and III, and the axial stress amplitude, respectively.

From Eqs. 1 to 4 the complex modulus (E*) and the complex Poisson's ratios in the directions II and III ($\nu^*_{II\text{-}I}$ and $\nu^*_{III\text{-}I}$, respectively) can be calculated as follows:

$$E^* = \frac{\sigma_{Aax}}{\varepsilon_{Aax}} e^{j\varphi_E} = |E^*| e^{j\varphi_E} \tag{5}$$

$$\nu^*_{II-I} = -\frac{\varepsilon_{AradII}}{\varepsilon_{Aax}} e^{j\varphi_{vII}} = |\nu^*_{II-I}| e^{j\varphi_{v\,II}} \tag{6}$$

$$\nu^*_{III-I} = -\frac{\varepsilon_{AradIII}}{\varepsilon_{Aax}} e^{j\varphi_{vIII}} = |\nu^*_{III-I}| e^{j\varphi_{v\,III}} \tag{7}$$

where $|E^*|$ is the norm of complex modulus; $|\nu^*_{II\text{-}I}|$ and $|\nu^*_{III\text{-}I}|$ are, respectively, the norms of Poisson's ratio in the directions II and III and j is the complex number defined by $j^2 = -1$.

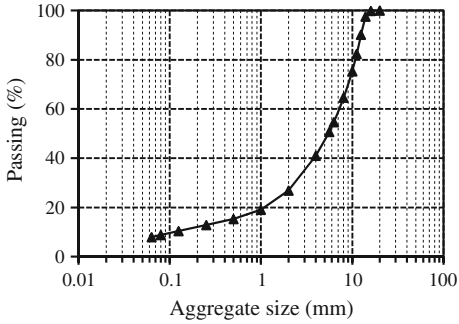


**Fig. 3** Aggregate grading curves of the 2 tested materials

**Table 2** Name and void content of tested specimens

| Material | Specimen | % voids |
|---|---|---|
| No hydrated lime (named N) | N8 | 5.2 |
| | N6 | 4.4 |
| With hydrated lime (named W) | W2 | 4.1 |
| | W1 | 4.3 |

### *2.3 Tested Materials*

Two different mixtures were produced using the same bitumen and aggregates the grading curve is presented in Fig. 3. Two types of fillers, hydrated lime and limestone filler, were used. Only the filler (particle, below 63 μm) differs between the two mixtures. One mixture contains only limestone filler while less than 1/3 of limestone was replaced by same weight of hydrated lime for the second mixture. The goal was to evaluate the influence of hydrated lime on linear viscoelastic properties of bituminous mixtures. A French rolling compactor (NF EN 12697-33 + A1) was used to produce a 600 × 400 × 150 mm slab for each material. Two specimens were tested for each material. The specimens used for complex modulus tests were cored and sawn from each slab. The void contents of all tested specimens are given in Table 2. Direction I of the sample corresponds the horizontal direction parallel to the wheel displacement. Direction II of the sample is the vertical direction when compacting the slab.

## 3 Experimental Results

### *3.1 Complex Modulus E**

Figure 4 shows the curves in the Cole-Cole and in the Black's spaces for the tested materials. The Cole-Cole diagram plots the imaginary part of complex modulus (E*) as a function of its real part. The curve in Black's space plots the norm of E* as

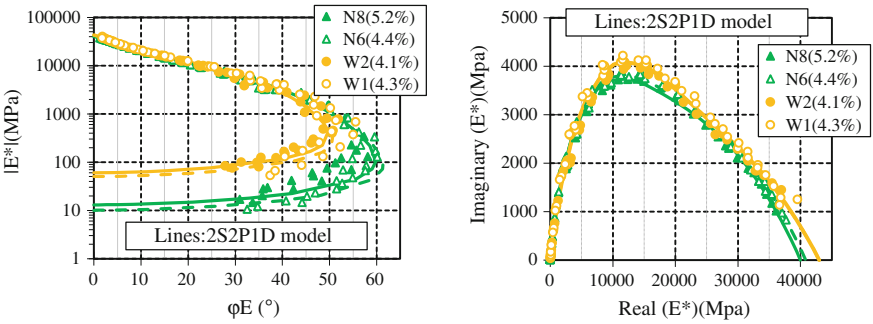


**Fig. 4** Experimental results for tested materials: complex modulus in cole-cole axes; complex modulus in black diagram. 2S2P1D model was used to simulate data (Table 3)

a function of its phase angle. The observed unique curve for each specimen validates the Time–Temperature Superposition Principle (TTSP) in the linear viscoelastic (LVE) domain for all the materials.

The master curves for the norm of the complex modulus (|E*|) and for its phase angle ($\varphi_E$) are plotted in Fig. 5 (reference temperature $T_R$ equal to 15 °C). The horizontal axis is the equivalent frequencies (which is equal to $a_T$ multiplied by the frequency (f) at tested temperature) and the vertical axis are the norm of the complex modulus and the phase angle, respectively. The shift factors ($a_T$) are presented in Fig. 6.

## 3.2 *Complex Poisson's Ratio ν**

The values obtained in radial directions II and III are rather similar showing no anisotropy on these parameters. In Fig. 7, average Poisson's ratio $\nu^*_{av}$ was considered (Eq. 8)

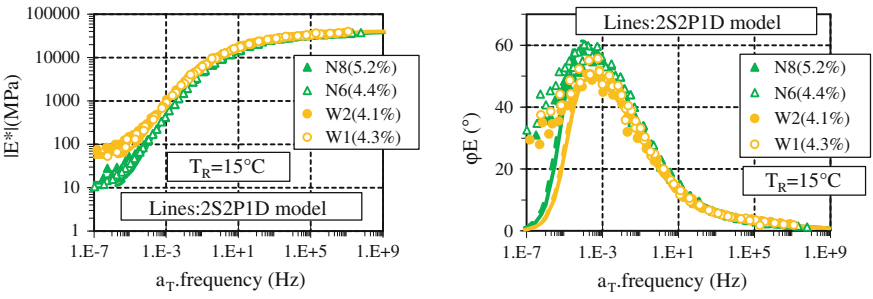


**Fig. 5** Experimental results for tested materials: master curves of the complex modulus (norm and phase angle). 2S2P1D model was used to simulate data (Table 3)

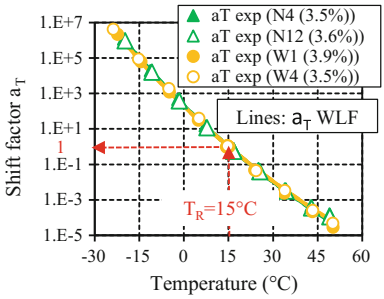


**Fig. 6** Shift factors $a_T$ identical for E* and ν* of the tested materials and WLF fitting law (Eq. 9) (constants given in Table 3)

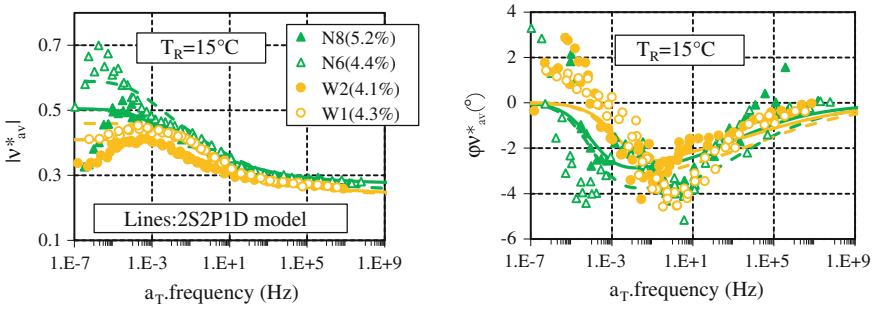


**Fig. 7** Master curves of the Poisson's ration "average" (norm and phase angle). 2S2P1D model was used to simulate data (Table 3)

$$\nu^*_{av} = \frac{\nu^*_{II-I} + \nu^*_{III-I}}{2} \tag{8}$$

These results show that the Time–Temperature Superposition Principle (TTSP), commonly observed in the one-dimensional case, can be extended to the three-dimensional behavior of bituminous mixtures. Moreover, the shift factors $a_T$ used for $|\nu^*|$ and $\varphi_\nu$ are identical to those used for $|E^*|$ and $\varphi_E$. The same results were observed in other studies (Di Benedetto et al. 2007; Nguyen et al. 2012; among others).

## 3.3 *Shift Factors*

The shift factor values used for the construction of the master curves of the tested materials are presented in Fig. 7 as a function of temperature. Values of $a_T$ are close

**Table 3** Constants of the 2S2P1D model and WLF parameters for the tested mixes (reference temperature: 15 °C)

| Specimen | E* | | | | | | | | |
|---|---|---|---|---|---|---|---|---|---|
| | $E_{00}$ (MPa) | | $E_0$ (MPa) | | k | h | δ | $\tau_{0E}$ (s) | β |
| N8 | 13 | | 40,000 | | 0.179 | 0.59 | 2.1 | 0.13 | 70 |
| N6 | 10 | | 40,800 | | | | | 0.13 | |
| W2 | 60 | | 43,000 | | 0.155 | 0.54 | 1.68 | 0.15 | 120 |
| W1 | 50 | | 43,000 | | | | | 0.15 | |
| Specimen | $\nu^*_{II-I}$ | | $\nu^*_{III-I}$ | | | $\nu^*_{av}$ | | WLF | |
| | $\nu_{00}$ | $\nu_0$ | $\nu_{00}$ | $\nu_0$ | $\tau_{0\nu}$(s) | $\nu_{00}$ | $\nu_0$ | $C_1$ | $C_2$ |
| N8 | 0.51 | 0.25 | 0.50 | 0.30 | 79.8 | 0.51 | 0.28 | 31.83 | 212.94 |
| N6 | 0.59 | 0.23 | 0.59 | 0.28 | 79.8 | 0.59 | 0.26 | | |
| W2 | 0.45 | 0.28 | 0.37 | 0.21 | 3.4 | 0.41 | 0.25 | 31.82 | 212.91 |
| W1 | 0.51 | 0.23 | 0.41 | 0.24 | 3.3 | 0.46 | 0.24 | | |

for all tested materials. The constants $C_1$ and $C_2$ of the WLF law (Eq. 9) used to fit $a_T$ data, are given in Table 3.

$$\log(a_T) = -\frac{C_1(T - T_{ref})}{C_2 + T - T_{ref}} \tag{9}$$

## 4 Linear Viscoelastic 2S2P1D Model

The 2S2P1D model, developed at the University of Lyon/ENTPE, is a generalization of the Huet-Sayegh model (Olard and Di Benedetto 2003). This model is based on a simple combination of physical elements (spring, dashpot and parabolic creep element). The graphical representation of the 2S2P1D model is given in Fig. 8. This model is widely used to model the linear viscoelastic unidimensional and tridimensional behavior of bituminous materials (including binders, mastics and mixes) (Pouget et al. 2010; Tiouajni et al. 2011; Mangiafico et al. 2014).

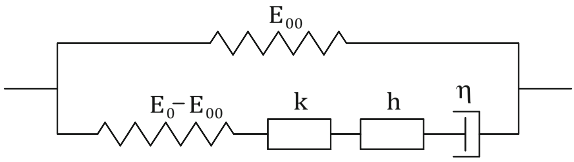


**Fig. 8** Analogical representation of 2S2P1D model (Olard and Di Benedetto 2003; Di Benedetto et al. 2007)

The complex modulus and the Poisson's ratio, at a given temperature, are given by Eqs. 10 and 11, respectively:

$$E^*_{2S2P1D}(\omega) = E_{00} + \frac{E_0 - E_{00}}{1 + \delta(j\omega\tau_E)^{-k} + (j\omega\tau_E)^{-h} + (j\omega\beta\tau_E)^{-1}} \quad (10)$$

$$\nu^*_{2S2P1D}(\omega) = \nu_{00} + \frac{\nu_0 - \nu_{00}}{1 + \delta(j\omega\tau_\nu)^{-k} + (j\omega\tau_\nu)^{-h} + (j\omega\beta\tau_\nu)^{-1}} \quad (11)$$

where

| | |
|---|---|
| $\omega$ | is the pulsation, $\omega = 2\pi f$, (f is the frequency) |
| k, h | constant such as $0 < k < h < 1$; $\delta$: constant |
| $E_{00}$ | the static modulus when $\omega \to 0$; $E_0$ the glassy modulus when $\omega \to \infty$ |
| $\nu_{00}$ | the static Poisson's ratio when $\omega \to 0$; $\nu_0$: the glassy Poisson's ratio when $\omega \to \infty$ |
| $\beta$ | parameter linked with $\eta$, the Newtonian viscosity of the dashpot, $\eta = (E_0 - E_{00})\beta\tau_E$ |
| $\tau_E$ and $\tau_\nu$ | characteristic time values, which are the only parameters depending on temperature and have a similar evolution: |

$$\tau_E(T) = a_T(T) \cdot \tau_{0E} \quad \text{and} \quad \tau_\nu(T) = a_T(T) \cdot \tau_{0\nu} \quad (12)$$

where $a_T$ is the shift factor at temperature T. At reference temperature $T_{ref}$, $\tau_E = \tau_{0E}$ and $\tau_\nu = \tau_{0\nu}$. Ten constants ($E_{00}$, $E_0$, $\delta$, k, h, $\beta$, $\nu_{00}$, $\nu_0$, $\tau_{0E}$, $\tau_{0\nu}$) are therefore required to completely characterize the 3D LVE properties (with isotropy hypothesis) of the tested material at a given temperature. The evolutions of $\tau_E$ and $\tau_\nu$ were approximated by WLF law (Eq. 9). $\tau_{0E}$ and $\tau_{0\nu}$ were determined at the chosen reference temperature $T_{ref} = 15$ °C. When the temperature effect is considered, the number of constants becomes twelve, including the two WLF constants ($C_1$ and $C_2$ calculated at the reference temperature) (Eq. 9).

2S2P1D simulations of the E* and ν* master curves for the tested asphalt mixes are presented in Figs. 4, 5 and 6. As can be seen in these figures, the model fits rather well the data on the whole range of temperatures and frequencies. Used 2S2P1D parameters are reported in Table 3 for all specimens.

## 5 Analysis of Results

As explained before, the two different mixtures were produced using the same bitumen and aggregates with and without hydrated lime. The comparison between the results obtained for the two materials, with and without hydrated lime, allows estimating the effect of hydrated lime on linear viscoelastic properties of bituminous mixtures. Controlling measured temperature was not exactly the targeted temperature. The effect on data, of the small difference between these temperatures, were

corrected using 2S2P1D model to obtain experimental result at the targeted temperature. These corrected data were used below for comparing in our analyses. For each material, two specimens were tested so the values used for the comparison are average values of duplicated tests.

The norm and the phase angle of the complex modulus ($|E^*|$ and $\varphi_E$), the norm and the phase angle of the Poisson's ratio ($|\nu^*_{av}|$ and $\varphi_{\nu^*av}$) and the shift factors $a_T$ are considered for the analysis. The results are shown in Figs. 9, 10 and 11. 2S2P1D curves are obtained by averaging the curves fitted for the two samples of each material.

In Fig. 9, the relative difference of the norm of the complex modulus, was plotted as a function of equivalent frequency: $(|E^*|_W - |E^*|_N)/|E^*|_N$, where $|E^*|_W$ and $|E^*|_N$ are, respectively, the norm of complex modulus for the mixture with and without hydrated lime. This figure reveals that the mixture with hydrated lime exhibits a stiffer modulus $|E^*|$ than the one of the mixture without hydrated lime. At 15 °C and 10 Hz, which accounts for the French pavement design method, this effect is close to 18 %. The increment of complex modulus increases with temperature and reaches nearly 500 % at 52 °C and 0.003 Hz. Clearly, these results strongly suggest that the stiffening effect of hydrated lime is temperature-dependent, as was already observed on mastics (Wortelboer et al. 1996; Lesueur et al. 2013) but, to our knowledge, never confirmed on asphalt mixtures.

A comparison was also made for the phase angle values using the parameter $(\varphi_{EW} - \varphi_{EN})$, where $\varphi_{EW}$ and $\varphi_{EN}$ are the phase angles of the complex modulus for the mixture with and without hydrated lime, respectively. This parameter is always negative, showing that the use of hydrated lime filler (instead of limestone filler) causes a reduction of the phase angle of the mixture, it can be concluded again that asphalt mix containing hydrated lime exhibits less viscous properties.

Regarding the complex Poisson's ratio, parameters $(|\nu^*_{avW}| - |\nu^*_{avN}|)$ and $(\varphi\nu_{avW} - \varphi\nu_{avN})$ are plotted in Fig. 10, as a function of equivalent frequency. The changes of these parameters are small (parameter $(|\nu^*_{avW}| - |\nu^*_{avN}|$ is often smaller than 0.1 in absolute value) and mostly within scattering of measurement. Therefore, the Poisson's ratio of both mixes can be considered as close. For information, a

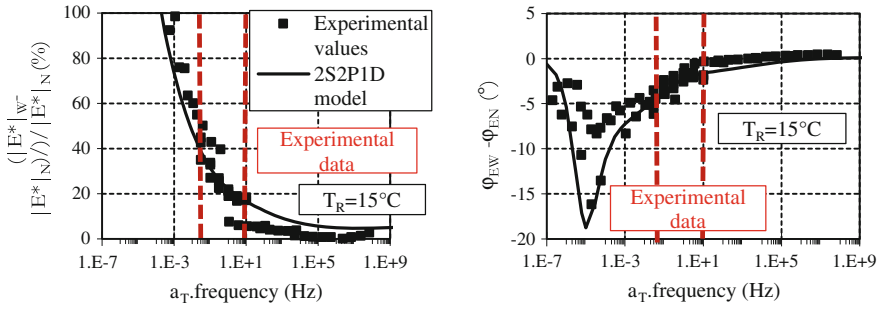


**Fig. 9** Difference between the two types of mixtures with and without hydrated lime on the complex modulus (norm and phase angle)

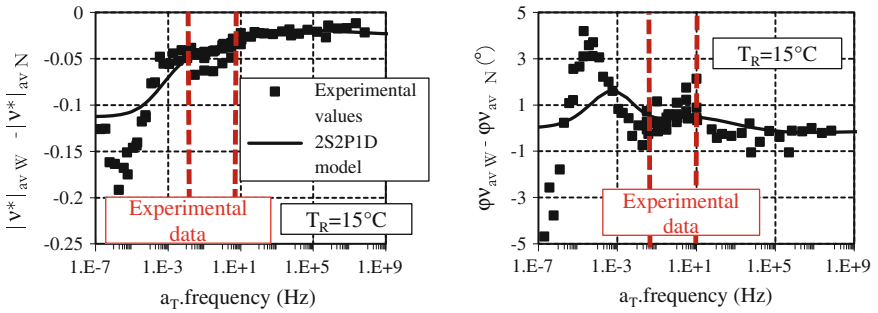


**Fig. 10** Difference between the two types of mixtures with and without hydrated lime on the Poisson's ration "average" (norm and phase angle)

difference of Poisson's ratio values of 0.03 corresponds to a variation of the diameter of the specimen of about 0.11 μm.

Figure 11(left) shows the relative difference of the shift factors $(a_{TW} - a_{TN})/a_{TN}$ (%). This figure reveals that shift factors $a_T$ of both mixes are very close (less than 6 % in absolute value, in the whole considered range). For information, a relative difference of the translation coefficients of 5 % corresponds to a variation of temperature of about 0.14 at 15 °C.

The shape of the Cole-Cole curves was changed by introduction of hydrated lime. Regarding 2S2P1D parameters, several research studies (Olard and Di Benedetto 2003; Delaporte et al. 2007) have shown that different bituminous mixtures produced with the same base binder have the same values of 4 model constants (k, h, δ, β). However, in this case, although the two tested mixtures were produced using the same binder, these 2S2P1D parameters showed non-negligible differences. It can be concluded again that hydrated lime changed the linear viscoelastic properties of bituminous mixtures. In order to evaluate the influence of hydrated lime, the relative difference of the area of Cole-Cole curves was calculated as $(A_W - A_N)/A_N = 8.1$ (%). Where $A_W$ and $A_N$ are respectively the area of Cole-Cole curves for the mixture with and without hydrated lime (Fig. 11, right).

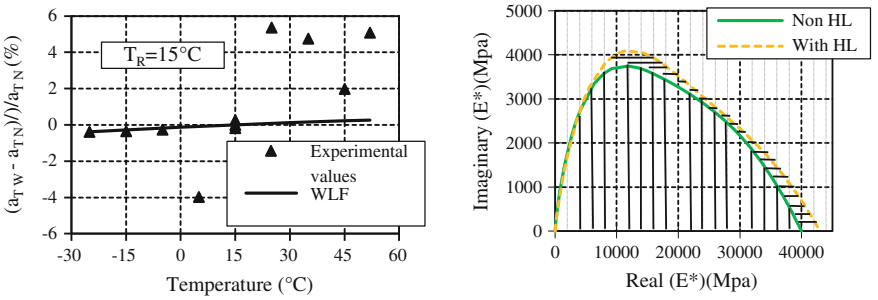


**Fig. 11** Difference between the two types of mixtures with and without hydrated lime on the shift factors $a_T$ (*left*) and on the area of cole-cole curves (*right*)

## 6 Conclusions

The objective of the research work presented in this paper was to study the linear viscoelastic behaviour of bituminous mixtures containing hydrated lime. Two mixtures with and without hydrated lime were tested. The following conclusions can be drawn from the obtained results:

- The Time-Temperature Superposition Principle was verified for the two bituminous mixtures.
- The shift factors used for the construction of the master curves were the same for the complex modulus and for the complex Poisson's ratios in directions II and III. The same shift factors were obtained for the two mixtures with and without hydrated lime.
- The 2S2P1D model simulates correctly the complex modulus and the complex Poisson's ratios data on the whole range of considered temperatures and frequencies.
- The use of hydrated lime filler (instead of limestone filler) causes an increase of complex modulus and a reduction of its phase angle. The observed differences depend on temperature and frequency, and are more pronounced at high temperature/low frequency. This fact was already observed on mastics but, to our knowledge, never documented for asphalt mixtures. A negligible influence was observed for Poisson's ratio. Linear viscoelastic properties were changed (shape of Cole-Cole curves and 2S2P1D model parameters).

## References

Di Benedetto H, Delaporte B, Sauzeat C (2007) Three dimensional linear behavior of bituminous materials: experiments and modeling. International Journal of Geomechanics 7:149–157. doi: 10.1061/(ASCE)1532-3641(2007)7:2(149)

Ghouse Baig M, Al-Abdul Wahhab HI (1998) Mechanistic evaluation of hedmanite and lime modified asphalt concrete mixtures. J. Materials in Civil Engineering 10(3):153-160

Jaskula P, Judycki J (2005) Evaluation of effectiveness of hydrated lime additive in protecting asphalt concrete against water and frost, Proc. 6th Int. Conf. on Environmental Engineering, Vilnius, May 2005

Khattak MJ, Kyatham V (2008) Viscoelastic behavior of hydrated lime-modified asphalt matrix and hot-mix asphalt under moisture damage conditions. Transportation Research Record 2057: 64-74

Lesueur D, Petit J, Ritter H-J (2013) The mechanisms of hydrated lime modification of asphalt mixtures: a state-of-the-art review. Road Materials and Pavement Design 14(1):1-16. doi:10.1080/14680629.2012.743669

McCann M, Sebaaly PE (2006) Evaluating the performance of lime in hot-mix asphalt mixtures, Proc. American Soc Civil Engineers Meeting on Airfield and Highway Pavements, p 614-624

Mohammad LN, Abadie C, Gokmen R, Puppala AJ (2000) Mechanistic evaluation of hydrated lime in hot-mix asphalt mixtures, Transportation Research Record 1723:26-36

Mangiafico S, Di Benedetto H, Sauzéat C,Olard F, Pouget S, Planque L (2013) Influence of reclaimed asphalt pavement content on complex modulus of asphalt binder blends and corresponding mixes: experimental results and modelling. Road Materials and Pavement Design 14(1):132-148. doi 10.1080/14680629.2013.774751

Mangiafico S, Di Benedetto H, Sauzéat C, Olard F, Pouget S, Planque L (2014) New method to obtain viscoelastic properties of bitumen blends from pure and reclaimed asphalt pavement binder constituents. Road Materials and Pavement Design 15(2). Doi 10.1080/14680629.2013.870639

Nguyen HM, Pouget S, Di Benedetto H, Sauzéat C (2009) Time-Temperature Superposition Principle for bituminous mixtures. Europ. Jl of Environmental and Civil Engineering: 1095-1107. doi:10.3166/ejece.13.1095-1107

Nguyen QT, Di Benedetto H, Sauzéat C (2012) Determination of Thermal properties of Asphalt mixtures as another output from cyclic Tension-Compression Test. Road Materials and Pavement Design 13(1):85-103. doi: 10.1080/14680629.2011.64408

Olard F, Di Benedetto H (2003) General "2S2P1D" model and relation between the linear viscoelastic behaviors of bituminous binders and mixes. Road Materials and Pavement Design 4(2):185-224

Pickering K, Sebaaly PE, Stroup-Gardiner M, Epps JA (1992) Evaluation of New generation of antistripping additives, Transportation Research Record 1342:26-34

Pouget S, Sauzéat C, Di Benedetto H, Olard F (2010) Numerical simulation of the five-point bending test designed to study bituminous wearing courses on orthotropic steel bridge. Materials and Structures 43(3): 319-330. doi: 10.1617/s11527-009-9491-1

Stroup-Gardiner M, Epps JA (1987) Four variables that affect the Performance of Lime in Asphalt-Aggregate Mixtures, Transportation Research Record 1115:12-22

Tiouajni S, Di Benedetto H, Sauzéat C, Pouget S (2011) Approximation of linear viscoelastic model by generalized Kelvin Voigt or generalized Maxwell Models: Application to bituminous materials in the 3 dimensional case. Road Materials and Pavement Design 12(4): 897-930. doi: 10.3166/RMPD.12.897-930

Vural KB, Yilmaz M (2009) The effect of using lime and styrene-butadiene-styrene on moisture sensitivity resistance of hot mix asphalt, Construction Building Materials 23:1999-2006

Witczak MW, Bari J (2004) Development of a Master Curve (E*) Database for Lime Modified Asphaltic Mixtures, Arizona State University Research Report, Tempe (Arizona,USA): Arizona State University

Wortelboer JP, Hoppen HJ, Ramond G, Pastor M (1996) Rheological properties of bitumen/filler mixtures. Proceedings of the 1st Eurasphalt & Eurobitume Congress, paper 4.079. Brussels, Belgium: Eurobitume and European Asphalt Pavement Association (EAPA).

# Influence of Mineral Fillers and Their Fractional Voids on Mastic Rheological and Mechanical Properties

**Elena Romeo, Valeria Ghizzardi, Silvia Rastelli and Antonio Montepara**

**Abstract** Mineral fillers are added into asphalt mixtures to stiffen asphalt binder and improve mixture density and strength. The stiffness of the mastic affects the ability of the mixture to resist permanent deformation at higher temperatures, influences stress development and fatigue resistance at intermediate temperatures, and influences stress development and fracture resistance at low temperatures. In this study, the effect of mineral fillers and their fractional voids on mastic rheological and mechanical properties is evaluated. Four types of filler with different physical properties were investigated. The fillers were associated to four asphalt binders, including unmodified and polymer modified binders, to obtain 16 asphalt mastics. The rheological properties of the mastics were evaluated conducting Superpave testing procedures, including the dynamic shear rheometer (DSR) and the bending beam rheometer (BBR). Their mechanical response was investigated using a Modified Direct Tension Test (MDTT), also employing a completely redesigned in-house developed Digital Image Correlation System (DIC) capable of accurately capturing localized or non-uniform stress distributions. The results showed that the Rigden fractional void is an effective indicator of filler stiffening effect, but it cannot be employed to evaluate the interaction between asphalt binder and filler. The effect of filler volume fraction on mastic performance depends on the binder employed.

**Keywords** Mineral fillers · Asphalt mastics · Rigden void · Filler-asphalt interaction

E. Romeo (✉) · V. Ghizzardi · S. Rastelli · A. Montepara
Department of Civil and Environmental Engineering and Architecture, University of Parma, Parma, Italy
e-mail: elena.romeo@unipr.it

V. Ghizzardi
e-mail: valeria.ghizzardi@studenti.unipr.it

S. Rastelli
e-mail: silvia.rastelli@unipr.it

A. Montepara
e-mail: antonio.montepara@unipr.it



F. Canestrari and M.N. Partl (eds.), *8th RILEM International Symposium on Testing and Characterization of Sustainable and Innovative Bituminous Materials*, RILEM Bookseries 11, DOI 10.1007/978-94-017-7342-3_55

## 1 Introduction

It's widely recognized that fracture in asphalt mixture is governed by the properties of both asphalt binder and filler properties and on their physico-chemical interaction (Anderson and Goetz 1973; Craus et al. 1976). As discussed by many authors (Zeng and Wu 2008; Faheem and Bahia 2009; Delaporte et al. 2008; Wang et al. 2011; Yi-qiu et al. 2010) the stiffness of the mastic affects the ability of the mixture to resist permanent deformation at higher temperatures, influences stress development and fatigue resistance at intermediate temperatures, and influences stress development and fracture resistance at low temperatures. Mineral filler fractional voids value has been used as an indicator of filler stiffening effect since the introduction of the test by Rigden in 1947. He considered the asphalt required to fill the voids in the dry compacted bed as fixed asphalt, while asphalt in excess of that amount was defined as free asphalt, indicating that the percent free asphalt is the main factor defining the consistency of the filled system. Many studies were later conducted to evaluate the influence of the filler's fractional voids on the performance of mastic and mixtures (Kim and Little 2004; Lackner et al. 2005; Little and Petersen 2005). All these studies agree that the stiffness of the mastic is higher than that of the binder and also that such stiffening effect increases as the fractional voids increase. More recently, Faheem and Bahia (2010) performed an important study to evaluate the effect of Rigden Void (RV) test values on the stiffening effect of fillers as determined by measuring the viscosity of the unfilled binders and filled mastics system. They found that the RV can demonstrate the potential of stiffening effect of fillers, but showed that, when the same filler is blended with different asphalt binders, the measured RVs of the fillers cannot provide sufficient guidance on the interaction between the filler and the binder. In summary, fractional void test has been proven to not be sufficient for explaining the complex interaction between binders and fillers. Moreover, very few studies were conducted to better understand the role of fillers and their fractional voids on the cracking behavior of mastics. To this scope, accurate description of strain evolution and distribution in mastics is essential for revealing significant information on the binder-filler interaction.

The present study evaluates the influence of mineral fillers and their fractional voids on mastic rheological properties and fracture behavior. Four different fillers where associated to four asphalt binders (two unmodified and two polymer modified) to obtain 16 asphalt mastics. The filler fractional voids were calculated according to the European Norms procedure (EN 1097-4). The rheological properties of the mastics were evaluated conducting Superpave testing procedures, including the DSR and BBR over a wide range of temperatures. The cracking behavior of the mastics was investigated using a Modified Direct Tension Test (MDTT) developed at the University of Parma (Montepara et al. 2011). Strain localization and damage distribution were observed using a completely redesigned in-house developed DIC software code called DICe, which was initially designed to facilitate the quantification of strains in the mastic in between the aggregates in a typical asphalt mixture (Birgisson et al. 2009). Finally, the interaction between

binder and filler was investigated using a X-ray diffractometer to analyze possible crystallographic alteration in the fillers when mixed with the asphalt binder.

## 2 Materials

Sixteen asphalt mastics were used in this study. The mastics were composed by four different asphalt binders, labeled as NV, N2, MR and ML. NV and N2 are two unmodified binders, graded as PG64-28 and PG58-22 respectively. MR and ML, graded as PG64-22 and PG70-22, are two polymer modified binders obtained blending the N2 unmodified one with a 3.5 % of SBS cross-linked and SBS linear polymers, respectively. The SBS was blended with the base asphalt by the manufacturer using high shear milling. Four fillers were associated to the four binders: a limestone filler, a clay filler, and two combinations of limestone + hydrated lime (20 % weight) and clay filler + hydrated lime (20 % weight). The selected filler concentration was 60 % by weight for all mastic formulations.

Fractional voids were calculated for the fillers according to the European Norms procedure (EN 1097-4) rather than the National Asphalt Pavement Association (NAPA) version, due to larger sample used and availability of equipment. Properties of the filler are listed in Table 1.

## 3 Mastic Rheological Analysis

The influence of mineral fillers and their fractional voids on mastic rheological properties was investigated using the Dynamic Shear Rheometer (DSR) and the Bending Beam Rheometer (BBR). The DSR was used to measure the complex dynamic shear modulus (G*) at 25 and 60 °C. The appropriate applied stress amplitude for each test temperature was determined by conducting a stress sweep at a constant frequency of 10 radians/s. With known stress and measured shear strain values, the linear range of the materials behavior was determined. The testing was conducted with an 8-mm plate with a 2-mm gap and a 25-mm plate with a 1-mm

**Table 1** Properties of the fillers

| | Density (g/cm$^3$) | Spec surface area (m$^2$/g) | pH | Rigden void (%) |
|---|---|---|---|---|
| Limestone | 2.65 | 0.28 | 9 | 36.6 |
| Clay | 2.8 | 0.32 | 7 | 46.6 |
| Hydrated lime (HL) | 2.34 | 13.5 | 12.5 | – |
| Limestone + HL | – | – | – | 49.1 |
| Clay + HL | – | – | – | 55.5 |

gap at 25 and 60 °C, respectively. The BBR was used to determine the stiffness of the binder and mastics at −25, −12 and −5 °C. A constant load of 980 mN was applied for 240 s, and the creep stiffness at 60 s was determined.

To evaluate the effect of filler on mastic workability, viscosity was measured at 135 °C using a Brookfield Rotational Viscometer. The distribution of mastic viscosity and relative viscosity with respect to RV values is displayed in Fig. 1. Relative values were computed by dividing mastic measurements by measurements on the binder in that mastic.

It is clear that mastic viscosity increases as the fractional voids increase. The mastics containing SBS exhibit consistently higher viscosities than the mastic prepared with the base binder, indicating SBS modification has the greatest effect on mastic viscosity. SBS modified mastics exhibited the highest variation in viscosity values with filler type with a maximum mastic viscosity 2 times the minimum due to filler effect alone, suggesting the significant impact of filler type on binders containing SBS.

Figure 2 shows the results obtained from DSR at 60 and 25 °C.

Results of DSR at 60° indicates that filler effect is more dominant than the binder showing that $G^*/\sin\delta$ increases with the increase of RVs. Conversely, at 25 °C there is considerable variation in mastic $G^* \cdot \sin\delta$ with both filler and binder type. There appears to be no consistent pattern in the effect of filler type on $G^* \cdot \sin\delta$ as the values among different binders do not follow any pattern. Additionally, it is difficult to distinguish between mastics containing different binders.

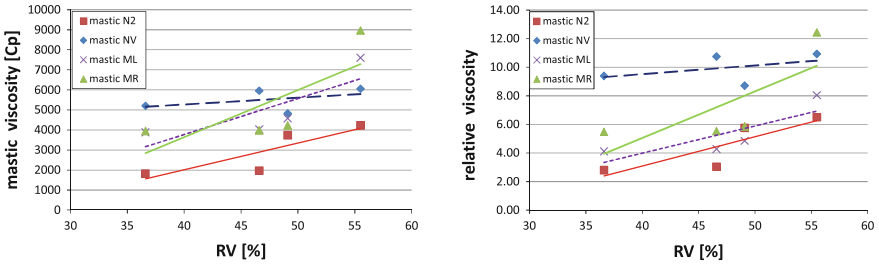


**Fig. 1** Influence of RV on mastic viscosity and relative viscosity

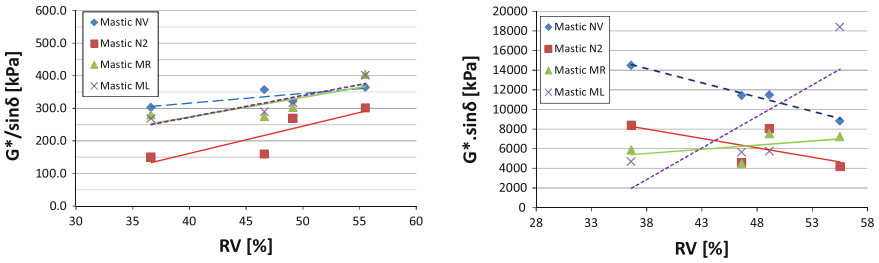


**Fig. 2** Results of DSR at 60 and 25 °C in function of filler RVs

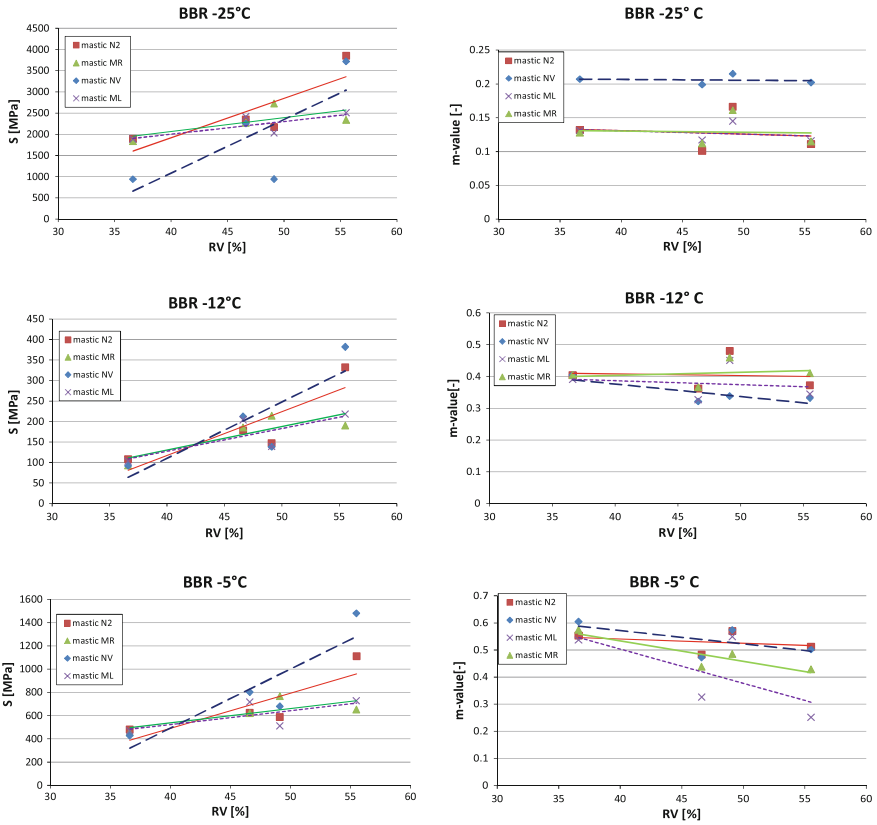


**Fig. 3** Results of BBR at −5, −12, −25 °C in function of filler RVs

Results reported for the BBR test included the stiffness and m-value at 60 s and are shown in Fig. 3.

The results clearly show that both binder and filler type affect stiffness of mastics. The mastics with the two neat binders generally exhibit higher stiffness than the modified mastics. Filler clay + hydrated lime produces a very high stiffness when combined with the two neat binders but not with the two modified binders. This indicates that the binder modification mitigates the stiffening effect of some fillers at low temperatures. There is less variability in mastic m-value with filler type than with stiffness.

## 4 Mastic Fracture Behavior

The cracking behavior of the mastics was investigated using a Modified Direct Tension Test (MDTT) developed on purpose to identify crack initiation and interpret mastic fracture response at intermediate temperature. The test was

developed modifying the Standard SuperPave™ DTT test for asphalt binders. All the details can be found elsewhere (Montepara et al. 2011).

## 4.1 Specimen Preparation

The mastic specimens were prepared following the improved SuperPave™ binder testing specimen preparation procedure. For each specimen, 28 g of asphalt binder and 42 g of filler were prepared and heated at mixing temperature (150 °C for unmodified binders and 175 °C for modified ones) in separate tins for 30 min. Then, the filler was slowly added to the asphalt in the oven. A mechanical mixer, with a maximum nominal angular speed of 8000 rpm, was used to blend the materials at mixing temperatures. The mixing process was carefully followed so that the filler was homogeneously dispersed in the binder. The mastic was continuously stirred as it cooled to prevent settling and then was poured to the preheated dog-bone shaped aluminum mold. The specimen is allowed to cool to room temperature for 1 h and de-molded. It is then placed in the environmental control chamber for 1 h at testing temperature before the test is performed.

## 4.2 Fracture Identification and Strain Analysis

Mastic strain localization and damage distribution analysis is simplified by field measurements of deformation over an area of finite extent through a Digital Image Correlation (DIC)-based method. MDTT strains were evaluated using a completely redesigned in-house developed DIC software code called DICe, which was initially designed to facilitate the quantification of strains in the mastic in between the aggregates in a typical asphalt mixture (Birgisson et al. 2009). The new DICe software code implements, for the image correlation step, a fairly innovative Least Squares Matching approach that uses higher order polynomial shape functions to model the displacement field between the reference and the measured image of the DIC sequence: proposed also by other authors in different application fields (Bethmann and Luhmann 2010). The technique is, for the first time, applied to this kind of DIC scenario. The most important issue addressed by the new code is that, when high strain occurs, the strain distribution measured by the pinpoint Least Squares Matching measure can be considered strictly constant, even if that area is small. Hence, with lower order shape function (e.g. with (linear) affine transformation models) higher residuals can be expected in the estimation process. In this case, statistical error rejection techniques (i.e. observation data snooping) are harder to be applied, and lower levels of accuracy can be expected. The previous DIC system has shown to achieve satisfactory accuracy compared to strain gauges, resulting in 0.04 % accuracy in compressive/tensile strains and 0.03 % accuracy in shear strains [further details on the method are discussed elsewhere, Birgisson et al.

(2009)]. In this case, due to the peculiar, localized, behavior of the mastic, it's hard to perform the same comparison with the new technique. Nonetheless, assuming that the nonlinearity of the displacement field can be considered similar to the ones obtained in the schematic (and general) tests performed in (Bethmann and Luhmann 2010), smaller errors (up to a factor of 4) can be expected. Further investigation and a rigorous evaluation of the accuracy performance of the new algorithm should be performed in the future.

A digital camera Basler piA1600-35gm (resolution 1608 × 1308, focal length 8 mm, pixel size 7.4 μm, 35 fps@max resolution), directly connected to the testing control system, is located on a support inside the climatic chamber where tests are performed. The chamber is provided with a proper LED lighting system which assure good illumination without heating up the specimen. Since the crack phenomenon is very fast and short-lasting (1 ÷ 2 s), the camera was properly set up to acquire the images in a smaller area of the sensor (1600 × 500 pixel) reducing the bandwidth required for transmitting each frame and, consequently, allowing a higher frame rate (ca. 80 fps). Thanks to the elongated shape of the specimen, once provided an optimal imaging geometry, the reduced size of the images still allowed the complete acquisition of the whole specimen surface. The images are automatically processed by the software, providing accurate displacement/strain fields. To achieve high accuracies in the strain field measurements, the specimen surface must present a well-contrasted grey scale speckle pattern, easily obtainable by a water paint-based treatment (Romeo 2013).

### 4.3 Test Procedure

MDTT tests were performed on three replicates at 10 °C using an MTS closed-loop servo-hydraulic loading system adopting a 2.5 kN load cell. The specimen was fixed at one end and pulled from the other end applying a constant stroke of 1.68 mm/s until rupture occurs (Montepara et al. 2011).

The engineering stress was computed according to the SuperPave™ binder specification:

$$\sigma_f = \frac{P_f}{A_0} \tag{1}$$

where: $\sigma_f$ = failure stress; $P_f$ = measured load at failure; $A_0$ = original cross-sectional area.

Failure is defined as the point on the stress-strain curve where the load reaches its maximum. The rapid loading rate and the interpretation of the test only up to fracture allow for a continuum representation. Strains were obtained from DIC system, interpolating all the strain values of the grid points located at the 46 × 20 mm specimen central cross-sectional area. The test configuration is shown in Fig. 4.

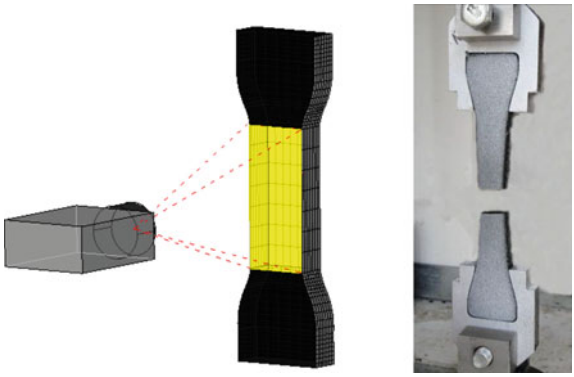

**Fig. 4** Mastic modified direct tension test configuration

## *4.4 Results*

Tensile strengths and Fracture Energy (FE) densities computed as the area under the stress-strain curve at fracture initiation (Roque et al. 2002) were compared. Tensile strengths of the mastics are shown in Fig. 5a. The results clearly show that the nature of filler influences the resistance of the mastics, since all the clay-composed materials result in a higher tensile strength. Conversely, the influence of hydrated lime on ultimate strength is not clear: it seems capable of either enhancing/decreasing (+50 % for MLA; −38 % for N2LA) the mastic resistance not making any difference (for NV and MR). More significant are the fracture energy results shown in Fig. 5b. The filler nature plays an important role in defining this failure parameter: clay-filler mastics exhibit higher fracture energies. Moreover, the presence of hydrated lime in unmodified mastics significantly enhances the fracture limit, while in polymer modified ones gives a negative contribution.

Figure 6 shows the role of filler fractional voids in defining tensile failure limits of mastics. Fracture energy densities increase with the increase of RVs only when neat binder is used. SBS modified mastics show the opposite trend demonstrating

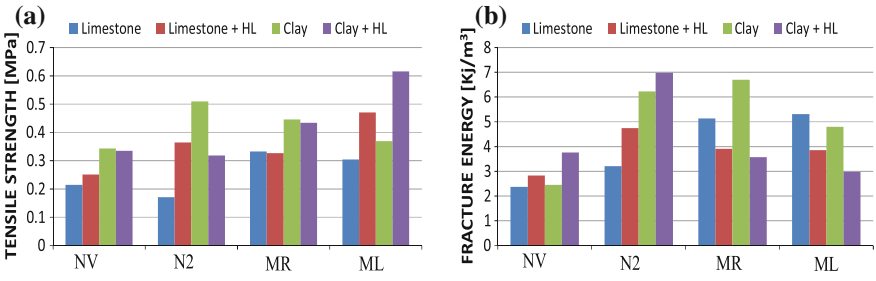


**Fig. 5** Effect of filler on mastics tensile limits. **a** Tensile strength, **b** Fracture energy

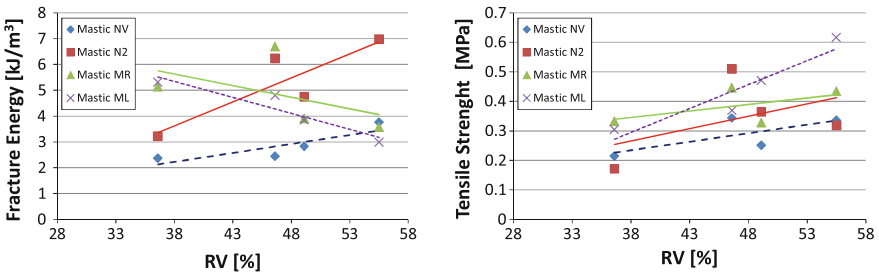


**Fig. 6** Influence of filler fractional voids on mastics tensile limits

that the interaction between SBS polymer modified binders and high RV fillers makes the mixture weaker in terms of fatigue/fracture resistance. Conversely, tensile strengths results confirm the general trend of stiffening effect increase with the increase of fractional voids.

Figure 7 shows full-field tensile strain maps at crack initiation for 8 representative mastics, in detailed those obtained with N2 binder and ML binder (SBS linear modified binder obtained mixing N2 with 3.5 % of modifier). The most important observation is that neat and modified binders assume opposite behaviors when mixed with the same filler. Neat mastics containing limestone fillers exhibit distributed damage in the all area, showing different points of micro-crack coalescence while, those containing clay fillers, show high strains localized solely along the fracture path. Conversely, modified mastics containing only limestone filler result in a more localized damage concentration, while the mastics containing clay filler exhibit different areas of excessive damage. The most likely reason for the observed trends is attributable to the physico-chemical interactions between binders and fillers and thereby to the particular network established within the mastic. Indeed, while the result of the reaction between unmodified binders and clay fillers is a toughened matrix capable of redistributing part of the stress, modified binders combined with the same clay fillers result in a weaker matrix which allows for the development of highly distributed micro-crack.

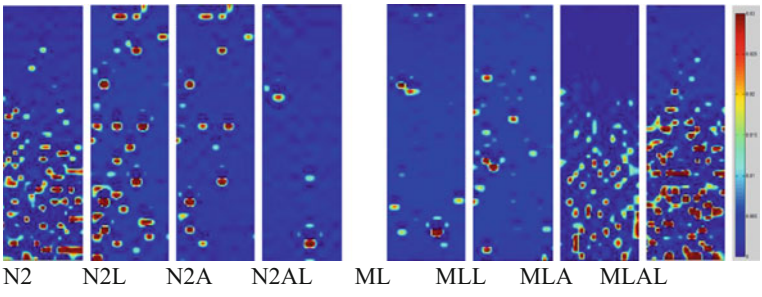


**Fig. 7** Mastics full-field strain maps

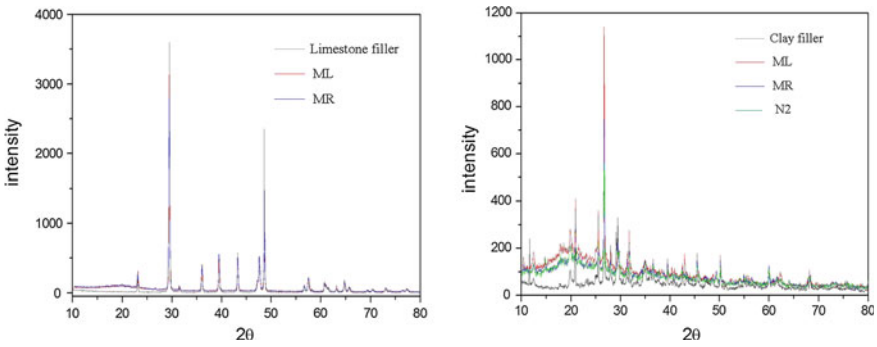


**Fig. 8** Diffraction patterns for the mastics and the related filler

## 5 X-ray Diffractometric Analysis

X-ray diffraction is a tool used for identifying the atomic and molecular structure of minerals and crystalline materials. It allows for determining the relationship between the material structure and its physico-chemical properties. X-ray diffraction (XRD) was performed using a Diffractometer model ARL X'TRA (TTK 450 climatic chamber operating at a range of temperature between −190 and 450 °C, goniometer 0–160°, Peltier cooled Si(Li) solid state detector) and the data analyzed using a WinXRD software. X-ray diffraction analyses were performed on the fillers themselves and on the mastics to individuate possible changes on the material structure. The diffraction patterns for the mastics and the related filler are shown in Fig. 8.

It's clearly evident that the phases observed for the filler are in a very good agreement with the phases observed for the mastics containing the same filler. This is true for both limestone and clay fillers. The results indicates that the intensity of the diffraction can be attributable only to the filler crystalline structure meaning that the binder-filler interaction does not lead to significant crystallographic changes of the mineral filler properties.

## 6 Summary and Conclusions

Based on the results and analysis conducted, the following findings can be summarized:

1. Rigden Voids value was identified as the filler property that has important influence on mastic viscosity and mixture workability.
2. According to DSR results, mastic rutting resistance is slightly filler specific, while mastic fatigue resistance was found to vary significantly based on fillers used. The role of fillers in mastic fatigue was found highly dependent on binder modification type.

3. Mastic low temperature stiffness and creep rate were found to be sensitive to type of filler and binder modification. It was found, as expected, that all fillers increase binder stiffness, but fillers can increase or decrease m-value, depending on modification type.
4. Mastic fracture parameters have shown to be binder specific with limited influence of filler properties. The filler nature influences the stiffness and the resistance of the mastics, but energy parameters are mostly dependent on binder modification.
5. DIC analyses allowed to observe that each filler interacts uniquely with different binders and modifiers. The different trends which characterize the behavior of mastics can be explained by the physico-chemical properties of the filler at the filler-binder interface.
6. X-RD analyses indicate that the binder-filler interaction does not affect the mineral filler crystallographic structure.

It can be concluded that Rigden Fractional voids are a good indicator of the stiffening potential of the mineral filler. The effect of filler volume fraction on mastic performance depends on the binder employed. This study indicated that the interaction between binder modification and the filler may enhance the role of the modifier or reduce it. This interaction needs to be studied further for a better understanding of the filler influence on mastic and mixture performance.

**Acknowledgments** This research has been supported by the Italian Ministry of University and Research within the project "FIRB-Futuro in Ricerca 2010"—Subpixel techniques for matching, image registration and change detection.

## References

Anderson DA, Goetz WH (1973) Mechanical Behavior and Reinforcement of Mineral Filler-Asphalt Mixtures. Journal of The Association of Asphalt Paving Technologists, 42:37-66.

Bethmann F, Luhmann T (2010) Least-squares matching with advanced geometric transformation models. International Archives of Photogrammetry, Remote Sensing and Spatial Information Sciences, Vol. XXXVIII, 5:86-91.

Birgisson B, Montepara A, Romeo E, Roque R, Roncella R, Tebaldi G (2009) An Optical Strain Measurement System for Asphalt Mixtures. Materials and Structures, 42:427-441.

Craus J, Ishai I, Sides A (1976) Some Physiochemical Aspects of the Effect and Role of the Filler in Bituminous Paving Mixtures. Journal of The Association of Asphalt Paving Technologists, 45:558-588.

Delaporte B, Di Benedetto H, Chaverot P, Gauthier G (2008) Effect of Ultrafine Particles on Linear Viscoelastic Properties of Mastics and Asphalt Concretes. Transportation Research Record, 2051:41–48

European Committee for Standardization EN 1097-4 (1999) Tests for Mechanical and Physical Properties of Aggregates, Part 4, Determination of the Voids of Dry Compacted Filler. Brussels: CEN.

Faheem AF, Bahia UH (2009) Conceptual Phenomenological Model for Interaction of Asphalt Binders with Mineral Fillers. Journal of the Association of Asphalt Paving Technologists, 78:680–717.

Faheem AF, Bahia HU (2010) Modeling of Asphalt Mastic in Terms of Filler-Bitumen Interaction. Road Materials and Pavement Design, 11(1):281-303

Kim YR, Little DN (2004) Linear Viscoelastic Analysis of Asphalt Mastics. Journal of Materials in Civil Engineering, 16(2):122-132.

Lackner R, Spiegl M, Blab R, Eberhardsteiner J (2005) Is Low-Temperature Creep of Asphalt Mastic Independent of Filler Shape and Mineralogy? Arguments from Multiscale Analysis. Journal of Materials in Engineering, 17(5):485-491.

Little D, Petersen JC (2005) Unique Effects of Hydrated Lime Filler on the Performance Related Properties of Asphalt Cements: Physical and Chemical Interactions Revisited Journal of Materials in Civil Engineering, 17(2):207-218.

Montepara A, Romeo E, Isola M, Tebaldi G (2011). The role of fillers on cracking behavior of mastics and asphalt mixtures Journal of the Association of Asphalt Pavement Technologists, 80:161–191.

Romeo E (2013) Two-dimensional digital image correlation for asphalt mixture characterisation: interest and limitations Road Materials and Pavement Design, 14(4):747-763

Roque R, Birgisson B, Sangpetgnam B, Zhang Z (2002) Hot Mix Asphalt Fracture Mechanics: A Fundamental Crack Growth Law for Asphalt Mixtures Journal of the Association of Asphalt Paving Technologist, 71:816-827.

Wang, H., Al-Qadi, I. L., Faheem, A. F., Bahia, H. U., Yang, S.-H., and, G. H., (2011). Effect of mineral filler characteristics on asphalt mastic and mixture rutting potential. Transportation Research Record, 2208: 33-39.

Yi-qiu, T., Li, Z-H., Zhang, X-Y. and Dong, Z-J. (2010). Research on high- and low-temperature properties of asphalt-mineral filler mastic, Journal of Materials in Civil Engineering, 22(8): 811-819.

Zeng, M and Wu, C., (2008). Effects of type and content of mineral filler on viscosity of asphalt mastic and mixing and compaction temperatures of asphalt mixture, Transportation Research Record, 2051: 31-40.

# Energy Dissipation in Asphalt Mixtures Observed in Different Cyclic Stress-Controlled Fatigue Tests

**Ivan Isailović, Augusto Cannone Falchetto and Michael P. Wistuba**

**Abstract** During cyclic fatigue testing of hot mix asphalt (HMA) under stress control, a continuous change of the strain amplitude is observed in each loading cycle either under pure tensile or under tensile-compressive stress conditions. Depending on the type of the applied load and on the specific viscoelastic behavior of the HMA this strain change can dramatically vary in association with a change in various mechanical properties. In order to study the variation of mechanical properties during cyclic fatigue tests under stress control an experimental program was performed using an approach based on dissipated energy. This study considers the following stress-controlled fatigue tests: indirect tensile test, uniaxial tension test and uniaxial tension-compression test. The hysteresis loops are drawn, and the dissipated energy is calculated. Based on the similar number of loading repetitions at failure, the tests are comparatively analyzed, and the changes in mechanical properties are identified. As a result, the tension-compression test shows low permanent deformation and high variation of dissipated energy which can be attributed to a distinct change in the material's mechanical properties. On the other hand, the uniaxial tension test and indirect tensile test exhibit high accumulation of permanent deformation with very few changes in mechanical properties during cyclic excitation. Based on these results the uniaxial tension test and the indirect tensile test in stress control are not well-suited for fatigue analysis since failure most likely occurs by accumulation of permanent deformation.

**Keywords** Dissipated energy · Hysteresis loop · Mechanical properties · Permanent deformation

I. Isailović (✉) · A.C. Falchetto · M.P. Wistuba
Braunschweig Pavement Engineering Centre, Technische Universität Braunschweig, Braunschweig, Germany
e-mail: i.isailovic@tu-bs.de

A.C. Falchetto
e-mail: a.cannone-falchetto@tu-bs.de

M.P. Wistuba
e-mail: m.wistuba@tu-bs.de



F. Canestrari and M.N. Partl (eds.), *8th RILEM International Symposium on Testing and Characterization of Sustainable and Innovative Bituminous Materials*, RILEM Bookseries 11, DOI 10.1007/978-94-017-7342-3_56

# 1 Introduction

Fatigue is a major distress that leads to early failure of pavement materials. It results in material cracking under the effect of repeated loading. Even though the individual load is lower than the material's ultimate strength, due to the gradual increase in the load repetitions, micro cracks initiate and accumulate, coalescing into macro cracks that finally lead to failure (Dowling 1999).

Fatigue properties of hot mix asphalt (HMA) are generally determined using different laboratory tests under different loading modes: uniaxial, indirect, bending, in tension, compression or both (cp. EN 12697-24). Conventionally two loading modes are used: constant stress control for relatively thick pavements, and constant strain control for conventional flexible pavements.

Especially as regards test methods with dominant tensile loading (e.g. the indirect tensile test), depending on the type of binder, its rheological properties and aggregate gradation used, these tests can generate a substantial plastic (irreversible) strain as a consequence of material viscous properties under tensile load. According to the work of Di Benedetto et al. (2004) the irreversible accumulated strain in fatigue tests can hide the effects associated to fatigue which is quite detrimental for analysis purposes. Consequently failure occurs probably by accumulation of permanent strain (Di Benedetto 2013).

A laboratory analysis was therefore performed in order to observe the evolution of the material mechanical properties and of the permanent deformation during indirect tensile fatigue test (ITT). Uniaxial tension test (UTT) and uniaxial tension-compression test (UTCT) in stress control were also used in this investigation for the purpose of employing different specimen geometries and loading conditions. The analysis of the mechanical properties evolution was performed using the dissipated energy approach that is a fundamental instrument for observing the difference in material behavior during cyclic loading (Carpenter and Shen 2006).

# 2 Experimental Study

## *2.1 Material Composition*

The experimental investigation was carried out using an asphalt mixture for surface course, i.e. asphalt concrete of the type AC 11 DS for highest road category prepared with aggregates having maximum grain size of 11 mm and with a bitumen with penetration grade 50/70 (acc. to EN 1426) in percentage of 5.9 % by total mixture weight. Figure 1 represents the aggregate gradation curve. The tested specimens had an air voids content of 2.5 %.

Test specimens were cut from slabs made with a Rolling Sector Compactor Using this compaction device it is possible to produce HMA slabs with adequate

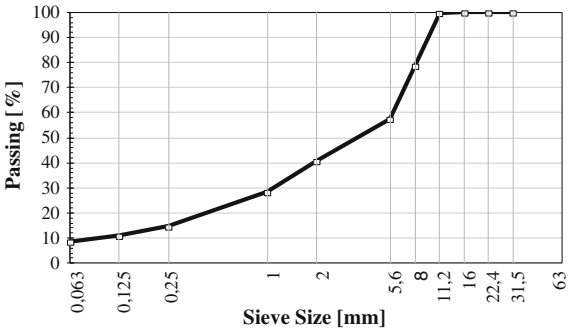


**Fig. 1** Aggregate gradation curve used to prepare HMA specimens

mechanical characteristics compared to those in the field (Renken 2000). The compactor uses a steel roller cylindrical sector to produce a kneading action and a downward force to the specimen in both pre-compaction and main compaction phase (Wistuba 2014). The pre-compaction is displacement controlled and simulates the compaction effort of paver, and main compaction is force controlled and simulates the effective compaction by roller compactors in the field. Each phase consists of 12 roller passes.

## 2.2 *Fatigue Analysis*

Fatigue analysis of the selected HMA was performed using three different fatigue tests: indirect tensile test (ITT), uniaxial tension test (UTT) and uniaxial tension-compression test (UTCT). In ITT test a vertical acting compressive stress induces in the specimen a non-homogeneous stress state, where in the middle portion of the specimen a horizontal tensile stress is observed (Fig. 2). This tensile horizontal stress leads primarily to the specimen failure. In opposite to ITT test, in UTT and UTCT constant stress and strain fields are imposed.

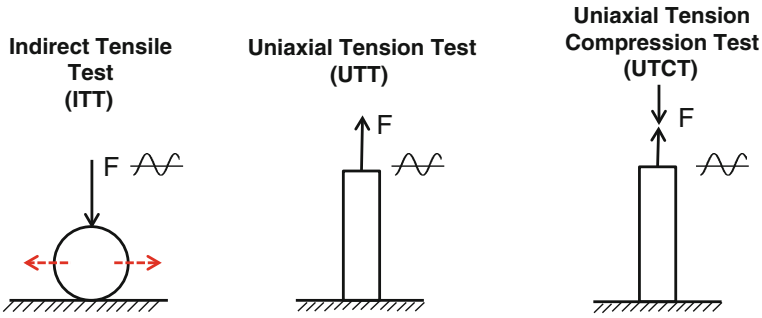


**Fig. 2** Principles of the indirect tensile test (*left*), uniaxial tension test (*middle*) and uniaxial tension compression test (*right*)

A sinusoidal cyclic stress was selected under load control mode at a frequency of 10 Hz and at a test temperature of 20 °C. The amplitudes were chosen through a pre-testing procedure in such a way that the different types of tests give similar fatigue lives (number of loading cycles at failure). As a result the following stress amplitudes were chosen:

- ITT: induced horizontal stress amplitude = 0.133 MPa
- UTT: axial stress amplitude = 0.18 MPa
- UTCT: axial stress amplitude = 1.05 MPa.

The most important parameters for material analysis were monitored and recorded during the entire tests duration. For the evaluation of the number of loading repetitions at failure the Energy Ratio (*ER*) approach proposed by Hopman et al. (1989) was used. *ER* represents the ratio between the initial dissipated energy ($W_0$), to the dissipated energy at cycle $n$ ($W_n$), multiplied by the load cycle value $n$:

$$ER_n = \frac{n \cdot W_0}{W_n}, \tag{1}$$

where:
$n$ cycle number,
$W_0$ initial dissipated energy (for 100th cycle),
$W_n$ dissipated energy at cycle $n$

A typical example of the Energy Ratio evolution is shown in Fig. 3.

By plotting *ER* versus the number of loading cycles, fatigue life is defined as the number of loading cycles for which *ER* achieves the maximum. The so-obtained point represents the transition between micro and macro cracking and is specified as $N_{Macro}$.

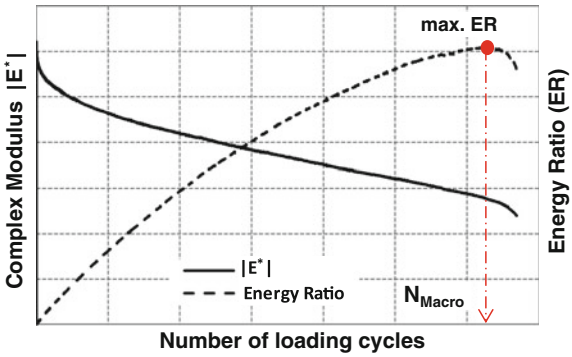


**Fig. 3** Typical evolution of the complex modulus $|E^*|$ and of the energy ratio (*ER*) over the number of loading cycles in a uniaxial tension-compression fatigue test

## 2.3 Analysis of Change in Mechanical Properties Using Dissipated Energy Approach

The energy dissipated within one loading cycle represents the difference between the energy provided to the material during the loading phase and the energy released during unloading. If a material is perfectly elastic, the loading and unloading curves follow the same paths, meaning that all the energy is recovered, without any energy dissipation (Fig. 4 left). In case of viscoelastic materials such as HMA loading and unloading curves do not overlap, which indicates loss of energy within the material. Part of the energy is dissipated from the system through external work, heating or damage (Ghuzlan and Carpenter 2000).

The ellipse generated by the loading and unloading phases is called hysteresis loop and its area corresponds to the energy dissipated in one loading-unloading cycle (Fig. 4 right). For the calculation of dissipated energy in one loading cycle the following equation can be used:

$$W_n = \pi \cdot \sigma_n \cdot \varepsilon_n \cdot \sin \phi_n, \tag{2}$$

where:

$W_n$ dissipated energy in cycle n (J/m$^3$),
$\sigma_n$ stress amplitude in cycle n (MPa),
$\varepsilon_n$ strain amplitude in cycle n (‰),
$\phi_n$ phase angle in cycle n (°)

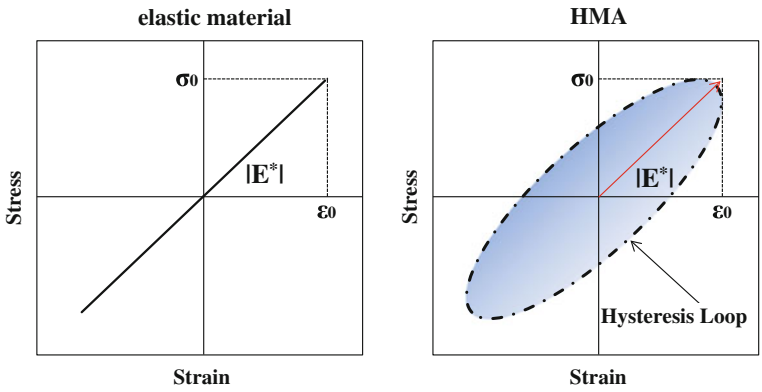


**Fig. 4** Loading cycle in a strain-stress diagram for a perfectly elastic material (*left*), and for a viscoelastic material, such as hot mix asphalt (HMA) (*right*)

The dissipated energy ($W$) can be used for investigating the change in mechanical properties during fatigue tests, since it considers variations both in the phase angle and in the strain or stress state (depending on the loading mode) during the material damage evolution. In stress controlled fatigue test the dissipated energy increases while it decreases in strain controlled mode.

Based on the work of Di Benedetto (2013) the material behavior in a cyclic test can be characterized by the change of the form and position of the hysteresis loop in each loading cycle. Rotation and expansion of the hysteresis loops with increasing number of loading cycles is primarily due to material fatigue (or effects associated with fatigue) (Fig. 5 left), while horizontal shifting along the strain axis can be interpreted as a permanent deformation of the specimen (Fig. 5 right). On this basis, the evaluation of the mechanical properties during fatigue tests can be performed.

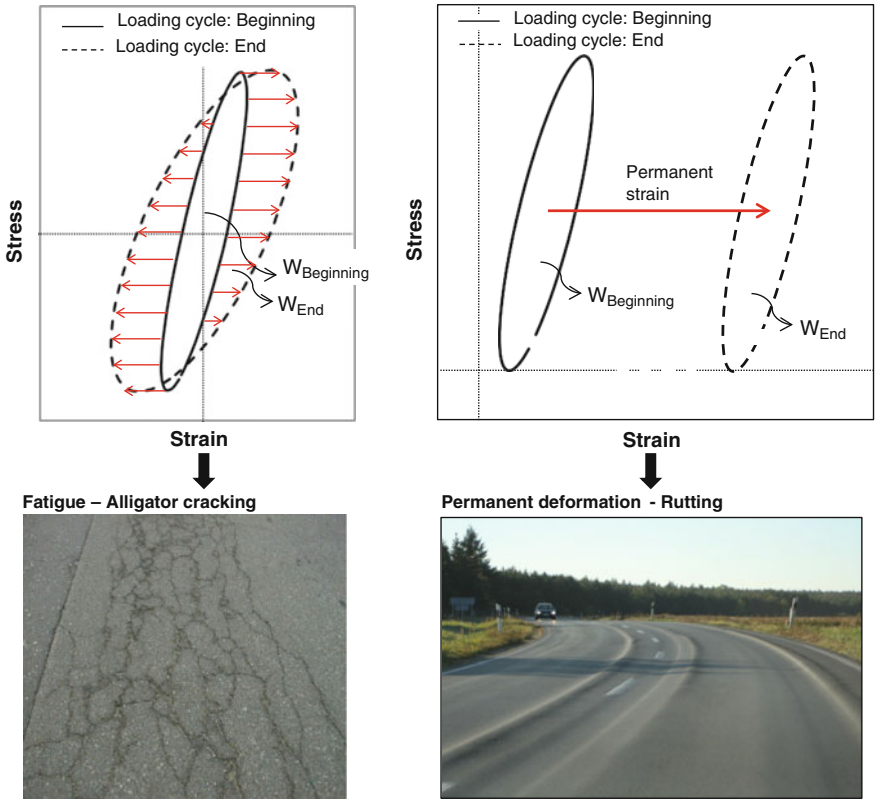


**Fig. 5** Interpretation of a fatigue test (*left*) and a permanent deformation test (*right*); hysteresis loops for the loading cycles at the beginning and at the end of the test (cf. Di Benedetto 2013)

## 3 Test Results and Analysis

The change in mechanical properties is evaluated in three different fatigue tests with similar fatigue life durations. Using the *ER* proposed by Hopman, the following numbers of loading repetitions at failure ($N_{Macro}$) were achieved (see Fig. 6):

- Indirect tensile test (ITT): 8650 cycles,
- Uniaxial tension test (UTT): 8501 cycles,
- Uniaxial tension-compression test (UTCT): 8580 cycles.

Based on the almost same number of loading repetitions at failure it is possible to conduct a reasonable comparison between these three tests by determining the individual changes in mechanical properties. As reported by Di Benedetto (2013)

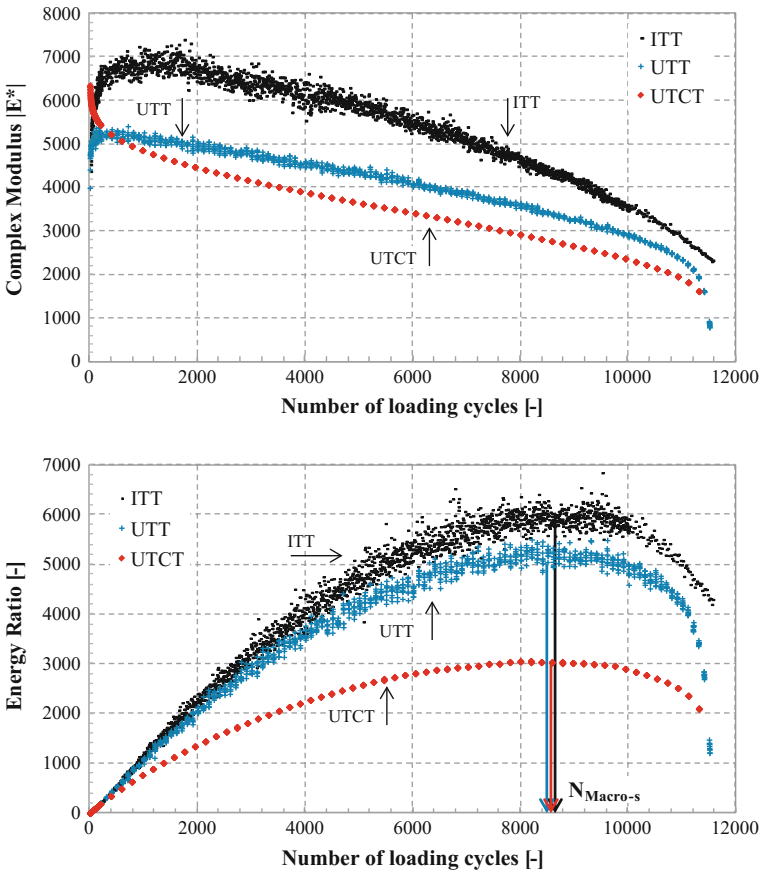


**Fig. 6** Evolution of absolute value of complex modulus and energy ratio over the number of loading cycles and achieved $N_{Macros}$ in indirect tensile test (ITT), uniaxial tension test (UTT) and uniaxial tension-compression test (UTCT)

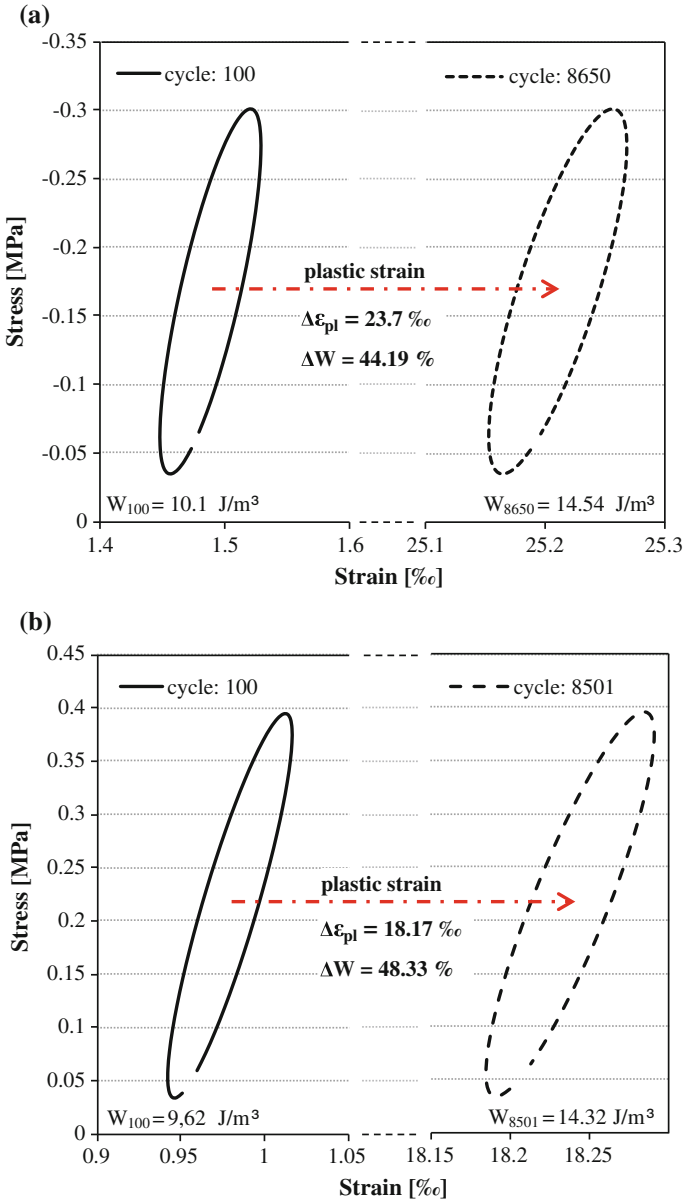


**Fig. 7** Hysteresis loops at cycle 100 and at failure (cycle $N_{Macro}$) for indirect tensile test (**a**) and uniaxial tension test (**b**)

the change in mechanical properties of HMA in a fatigue test can be characterized by the change of the hysteresis loop form during cyclic loading, which directly corresponds to the change in dissipated energy. For this reason the hysteresis loops

at the beginning of the test (at cycle 100) and at failure (for $N_{Macro}$) are drawn and dissipated energy change between these loading cycles is comparatively calculated for each type of fatigue test performed. The test results are plotted in Figs. 7 and 8.

The test results show that testing procedures including only tensile stress condition such as in ITT and UTT lead to relatively slow increase in dissipated energy (ΔW) between the beginning of the testes and failure, with 44.19 and 48.33 % respectively. The hysteresis loops represented in Fig. 7 show relatively small change in shape with significant horizontal shifting associated to plastic deformation, which in ITT test exceed 23 ‰.

On the other hand the UTCT shows a distinct change in the shape of the hysteresis loop with 182.3 % growth of dissipated energy at failure (Fig. 8). The plastic strain of UTCT is smaller compared to ITT and UTT tests (0.31 ‰) and can be assumed as negligible.

The higher dissipated energy change observed in the stress controlled tension-compression test compared to the other tests is a consequence of the significant increase of elastic strain amplitude and phase angle as loading repetitions increase. This implies that the material is experiencing higher loss in stiffness and delayed response over time with respect to ITT and UTT. This is associated to remarkable change in mechanical properties.

Generation of large plastic deformation in ITT and UTT is a consequence of stress conditions coupled with material's rheological characteristics. If only tensile stress acts in the specimen and material viscosity is low it will result in additional

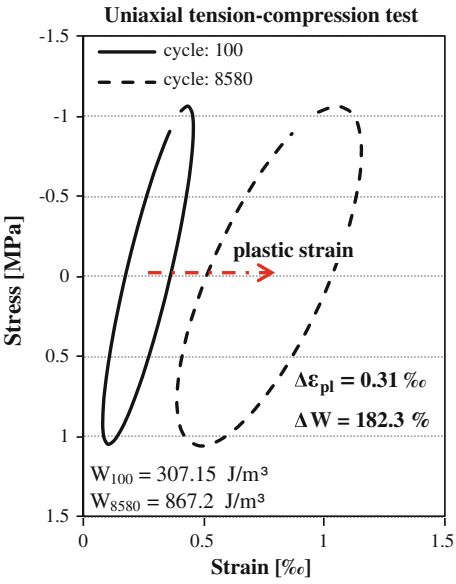


**Fig. 8** Hysteresis loops at cycle 100 and at failure (cycle $N_{Macro}$) for uniaxial tension-compression test

plastic deformation in each loading cycle. On the other hand in UTCT the compressive stress part in each loading cycle develops inverse plastic deformation (partially or entirely) and prevents the evolution of disproportional permanent deformation.

## 4 Summary

In this study, a dissipated energy approach is applied to investigate the change of mechanical properties in three stress controlled fatigue tests: indirect tensile test, uniaxial tension test and uniaxial tension-compression test. Based on the almost same number of loading repetitions at failure it was possible to conduct a reasonable comparison between these three tests.

The test results show that indirect tensile test and uniaxial tension test present comparatively little change in the material mechanical properties, with high accumulation of plastic deformation. On the other hand the uniaxial tension-compression test shows significant change in mechanical properties (approx. four times higher), with minimal plastic deformation.

According to the test results, it can be concluded that indirect tensile test and uniaxial tension test are not well-suited for fatigue analysis, because the failure is primarily associated to the accumulation of permanent deformation, and not in consequence of fatigue damage.

More research on this field is needed in order to examine the change of mechanical properties more in detail by unraveling the effects of thixotropy and material heating during cyclic loading. Further mixes should be investigated in order to check if these three tests yield the same fatigue ranking.

## References

Carpenter, S., and Shen, S. (2006). A Dissipated Energy Approach to Study HMA Healing in Fatigue. In Transportation Research Record (TRR): Journal of the Transportation Research Board, No 1970, pp. 178-185.

Di Benedetto, H. (2013). Fatigue and other Phenomena during Cyclic Loading of Bituminous Materials. Keynote at EATA 2013 Conf., Braunschweig, Germany, 06/2013.

Di Benedetto, H., de La Roche, C., Baaj, H., Pronk, A., and Lundström, R. (2004). Fatigue of bituminous mixtures. Materials and Structures, Vol. 37, pp. 202-216.

Dowling, N. E. (1999). Mechanical Behavior of Materials, Engineering Methods for Deformation, Fracture, and Fatigue. Second Edition. Prentice Hall, Upper Saddle River, New Jersey.

EN 12697-24 (2012). Test methods for hot mix asphalt – Part 24: Resistance to fatigue. 2012.

EN 1426 (2013). Bitumen and bituminous binders - Determination of needle penetration. 2013.

Ghuzlan, A., and Carpenter, S. (2000). An Energy-Derived / Damage-Based Failure Criteria for fatigue Testing. Proc. Transportation Research Board Meeting, Washington, D.C., 2000.

Hopman, P., Kunst, P., and Pronk, A. (1989). A Renewed Interpretation Model for Fatigue Measurement. Verification of Miner´s Rule. 4th Eurobitumen Symposium, October 4th, 1989, Madrid.

Renken, P. (2000). Influence of Specimen Preparation onto the Mechanical Behavior of Asphalt Aggregate Mixtures. 2nd Eurasphalt & Eurobitumen Congress Barcelona, 2000.

Wistuba, M. P. (2014). The German segmented steel roller compaction method – state-of-the-art report. Int. Journal of Pavement Engineering. Taylor and Francis, London 2014.

# Deterioration of HMA Partially Saturated with Water or Brine Subjected to Freeze-Thaw Cycles

**Sébastien Lamothe, Daniel Perraton and Hervé Di Benedetto**

**Abstract** In the province of Quebec, during winter and spring, hot mix asphalt (HMA), constituting the pavement, is subjected to freeze-thaw cycles (FTC). This paper presents a part of a general research program aimed at characterizing damage generated on bituminous mixes by thermal tests, including FTC, under dry (D) and partially saturated (PS) conditions, with water (PSW) or brine (PSB). The samples were subjected to mechanical testing and the complex modulus test is used to assess the evolution of their damage after different sequences of FTC. The test results and rheological model 2S2P1D were used to simulate the behaviour of the HMA according to the various states. The 2S2P1D model simulates the linear viscoelastic behaviour of the asphalt mix following different states very well. Over FTC, damage is observed for all samples, but is seen to be much higher for the PSW sample. Moreover, for PS samples, the principle of equivalent temperature-time is less valid over the FTC, and a double behaviour is observable: below and above the ice formation. Indeed, damage to the asphalt mix seems to have a greater impact at high temperatures and low frequencies.

**Keywords** Asphalt mixture · Water · Brine · Complex modulus

S. Lamothe (✉) · D. Perraton
Département de génie de la Construction, École de Technologie Supérieure (ETS), 1100 Notre-Dame Street West, Montréal, Canada
e-mail: sebastien.lamothe.1@ens.etsmtl.ca

D. Perraton
e-mail: daniel.perraton@etsmtl.ca

H. Di Benedetto
LGCB, LTDS (CNRS 5513), École Nationale des Travaux Publics de l'État (ENTPE), Maurice Audin Street, 69518 Vaulx en Velin, France
e-mail: herve.dibenedetto@entpe.fr



F. Canestrari and M.N. Partl (eds.), *8th RILEM International Symposium on Testing and Characterization of Sustainable and Innovative Bituminous Materials*, RILEM Bookseries 11, DOI 10.1007/978-94-017-7342-3_57

## 1 Introduction

The emergence of cracks observed on wheel tracks during thawing is often associated with the fatigue phenomenon (St-Laurent and Roy 1995). Wheel track damage recorded for three years on two observation sites in the province of Quebec indicates that the annual damage can reach 85 % during the winter and spring thaws (MTQ 2003). The level of damage is especially higher for secondary roads. This premature damage seems to be directly related to severe conditions prevailing on the roadway during winter and spring. In Quebec, the number of FTC averages between 40 and 51 per year (Tremblay 2006; Fortin 2006).

This paper presents a part of a general research program aimed at characterizing damage generated by freeze and thaw cycles (FTC) under dry (reference) and partially saturated (with water or brine) conditions. Two groups of samples having the same characteristics were tested. One samples group was used for thermal, contraction and expansion (TCE) analyses, while the other samples group was subjected to complex modulus testing (E*), after a given number of freeze-thaw cycles. The results for TCE analyses can be found in Lamothe et al. (2014) and Lamothe (2014). The results from E* are examined in this paper.

## 2 Experimental Program

A group of five instrumented samples was tested. One sample was in dry condition (D), one partially saturated with water (PSW), and three were partially saturated with brine, at different salt concentrations (7, 14 and 19 weight percent salt in solution, wt%). E* were used to follow the sample damage under FTC.

Figure 1 shows the sequences and times for the realization of the FTC followed during our testing program.

The program was divided into six distinctive sequences of FT cycle series and so-called thermal tests (TT) sequence, from points $A_j$ to $J_j$ (with j = 1–6),

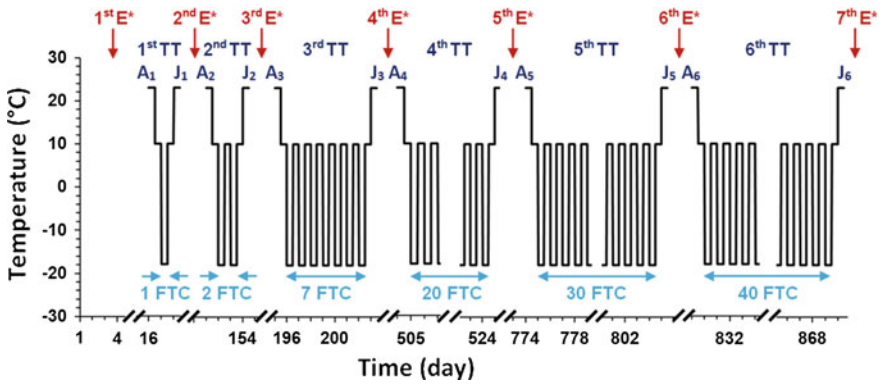


**Fig. 1** Six thermal test (TT) sequences of freeze-thaw cycles (FTC) applied to the samples

as shown in Fig. 1. A different number of FTCs were applied for each TT: 1, 2, 7, 20, 30, and 40. To quantify the damage generated by FT cycles, E* was measured before and after each TT sequence. It takes three days to perform the E* test, which explains the peculiar FT cycles chronology applied to the samples group. Moreover, before and after each TT, a period of 15 days is allowed for preparation, measurements and results processing.

## 3 Material, Samples Preparation and Conditioning Procedure

A bituminous mixture with a nominal aggregate size of 0/14 mm (EB14, Quebec standard) of high quality, fully-crushed aggregates and a bitumen classified PG 70-28 was used. The bitumen content was 4.8 % of the weight of the mixture. The EB14 mix was prepared with sampled material from a batch plant. The EB14 is commonly used for surface, single and base courses. Figure 2 presents the specifications (Ministry of Transportation of Quebec, MTQ standard) and aggregate grading curve of the EB14 mixture.

The EB14 asphalt mixture was compacted with the French laboratory compactor. The dimensions of the compacted slabs were 125 × 400 × 600 $mm^3$. After a minimum curing time of two weeks, samples 80 mm in diameter were cored in the thickness of the slabs in the direction of the wheel compactor displacement. The samples were then trimmed to 120 mm.

To introduce liquid in the sample voids network, a saturation process under vacuum was used. Two steps were considered. First, the sample was placed in a desiccator whose pressure (P) was kept below or equal to 4 kPa. Then, after 30 min, the desiccator was filled with a de-aerated water (or brine), always under vacuum. The sample was kept under submersion for at least 90 min. After removing the sample from the desiccator, a latex membrane was placed around it.

After each saturation time, samples were weighted to quantify the amount of liquid within the material and thereby determine the degree of saturation (DS). During the testing program, it was necessary to re-saturate the samples due to leaks. Notably, the re-saturations are carried out to maintain a DS higher than 40 %. Table 1 shows the DS of tested samples, before and after each TT sequence.

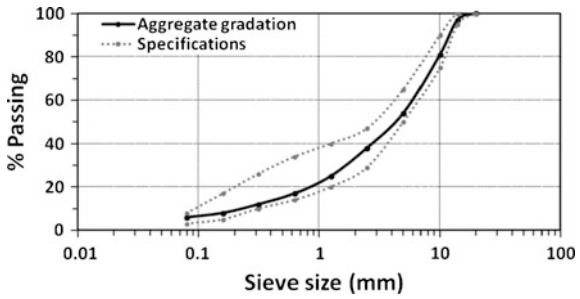


**Fig. 2** Specifications for EB14 mix type (MTQ standard) and aggregate gradation

**Table 1** Evolution of the degree of saturation of tested samples before and after each TT

| Voids (%) | State | Degree of saturation: DS % = volume of absorbed liquid/pore volume × 100 % | | | | | | | | | | | |
|---|---|---|---|---|---|---|---|---|---|---|---|---|---|
| | | 1st TT | | 2nd TT | | 3rd TT | | 4th TT | | 5th TT | | 6th TT | |
| | | 1st FT | | 2nd–3rd FT | | 4th–10th FT | | 11th–30th FT | | 31st–60th FT | | 61th–100th FT | |
| | | Bef. | Aft. | Bef. | Aft. | Bef. | Aft. | Bef. | Aft. | Bef. | Aft. | Bef. | Aft. |
| 4.8 | D | 0 | 0 | 0 | 0 | 0 | 0 | 0 | 0 | 0 | 0 | 0 | 0 |
| 3.4 | PSW | 46 | 46 | 46 | 46 | 36 | 36 | 88 | 74 | 103 | 79 | unkn. | 104 |
| 4.2 | PSB7 | 54 | 53 | 78 | 73 | 63 | 48 | 82 | 73 | 88 | 78 | unkn. | 86 |
| 3.1 | PSB14 | 54 | 54 | 57 | 54 | 44 | 35 | 65 | 57 | 64 | 53 | unkn. | 73 |
| 4.3 | PSB19 | 50 | 50 | 67 | 61 | 57 | 48 | 75 | 64 | 77 | 69 | unkn. | 71 |

## 4 Thermal Test and Freeze-Thaw Cycles

For thermal test (TT) sequences, samples were placed horizontally on a bed of crushed sand (2.5/5 mm) in a thermal controlled chamber, called the cabinet. The sand prevents creep deformation of the samples under storage and during TT in the cabinet. The samples were placed in three metallic vessels which are distributed over three shelves in the cabinet. The TT sequence is shown in Figs. 1 and 3.

Prior to start freeze-thaw (FT) cycle(s), steps $D_{ij}$–$H_{ij}$ in Fig. 3, the temperature of the cabinet was maintained at +23 °C for 11.5 h. In Figs. 1 and 3, the letter "j" is used to indicate the TT sequence number, while the letter "i" is used to indicate the FTC number. For each FTC, two different temperature levels were targeted: −18 and +10 °C. At each level, the temperature was kept constant for a period of 11.5 h. Finally, after the last FTC of a specific TT sequence, a +23 °C constant temperature period was maintained for 11.5 h ($I_j$–$J_j$ in Fig. 3). Temperatures were kept constant for 11.5 h periods (A–B, C–D, E–F, G–H and I–J) to ensure that the temperature within the sample, as well as the strain, was stabilized. It should be noted that the time of stabilization is approximately 10 h and 15 min (Lamothe et al. 2014). The temperature rate of the cabinet between each step is indicated in Fig. 3, and is either 56 °C/h (between points D–E and F–G) or 26 °C/h (between points B–C and H–I). However, the temperature rate within the samples was much lower (maximum of 7–8 °C/h).

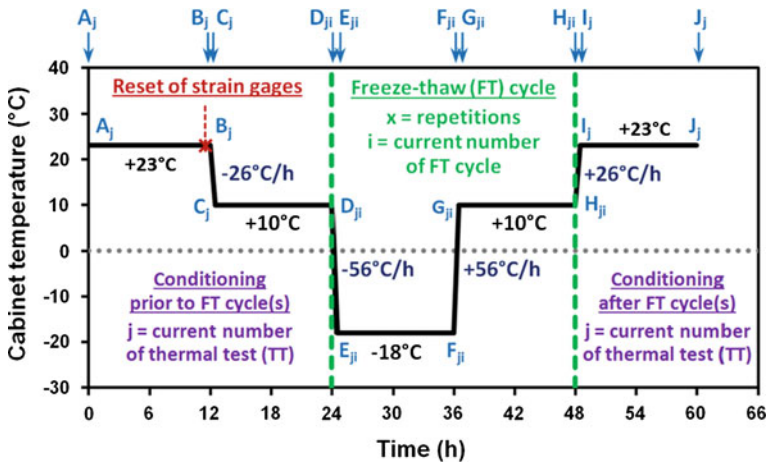


**Fig. 3** Cabinet temperature history during thermal test sequence (TT): "j" is the current number of TT (Fig. 1) and "i" is the current number of freeze-thaw (FT) cycles (Lamothe et al. 2014)

## 5 Test Equipment, Data Acquisition and Calculations

The sinusoidal loading in tension and compression was applied on the sample along direction 1 using a hydraulic press having a maximum capacity of ±100 kN and a ±50 mm axial stroke. The axial strain of the sample was measured with two strain gages glued vertically, in direction 1, on the surface in the middle part of the sample. Also, the axial strain was measured on the full height of the sample using three extensometers 165 mm in length (Fig. 4a, b), located at 120° around the sample, and used to drive the test under strain control. As the strain gages became non-functional due to surface alteration under FTC, a correlation between the proper strain gage measurements and the corresponding extensometer strain measurements was established to correct extensometer measurements.

A thermal chamber was used to control the temperature of the sample during the test. The temperature was measured with a thermal gage placed on the sample surface and held with a rubber band. The cylindrical sample was loaded at 6 frequencies (f = 0.03 to 10 Hz) and 9 temperatures (T = −35 to 35 °C). The sinusoidal axial strain ($\varepsilon_1$) (average of three extensometers) was used for monitoring. The amplitude of axial strain during cyclic loading was 50 μm/m. The number of cycles applied at each frequency was small (less than 100), and as a result, heating problems due to viscous dissipation were negligible (Di Benedetto et al. 2011; Nguyen et al. 2012). The axial stress ($\sigma_1$) was obtained from the load cell.

Sinusoidal curves of strain and stress were fitted to the experimental data ($\varepsilon_1$ and $\sigma_1$, Fig. 4c) and used to calculate the norm and phase angle of the complex modulus (E*) using "Eqs. 1–3", where $\varepsilon_{01}$ and $\sigma_{01}$ were the axial strain amplitude and the axial stress amplitude, respectively. As three extensometers were used for axial strain measurement, sinusoidal strains were first fitted to data for all single extensometers, and mean values of axial amplitudes and phase angles were used as $\varepsilon_{01}$ and $\varphi_{\varepsilon 1}$ in all calculations. Furthermore, $\varphi_E$ is the phase angle between the axial stress and the mean axial strain, $|E^*|$ is the norm of the complex modulus and j is the complex number defined by $j^2 = -1$.

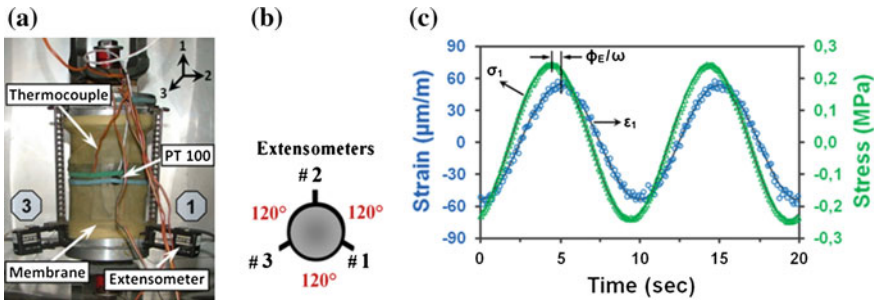


**Fig. 4** Setup used to measure E*: **a** specimen and measurement system, **b** top view, **c** example of stress-strain measurements and sinusoidal fitting curves (f = 0.1 Hz and T = 15 °C)

$$\varepsilon_1(t) = \varepsilon_{01}\sin(\omega t + \varphi_{\varepsilon 1}) \tag{1}$$

$$\sigma_1(t) = \sigma_{01}\sin(\omega t + \varphi_{\sigma 1}) \tag{2}$$

$$E^* = \frac{\sigma_{01}}{\varepsilon_{01}}\, e^{j(\varphi_{\sigma 1} - \varphi_{\varepsilon 1})} = |E^*|\, e^{j\varphi_E} \tag{3}$$

The complex modulus is given by "Eq. 4" in the 2S2P1D model (Olard and Di Benedetto 2003; Di Benedetto et al. 2004):

$$E^*_{2S2P1D}(j\omega\tau_E) = E_{00} + \frac{E_0 - E_{00}}{1 + \delta(j\omega\tau_E)^{-k} + (j\omega\tau_E)^{-h} + (j\omega\beta\tau_E)^{-1}} \tag{4}$$

where $\omega$ is the pulsation ($\omega = 2\pi f$, f is the frequency); k and h are constant exponents such as $0 < k < h < 1$; $\delta$ is a constant; $E_{00}$ is the static modulus when $\omega \to 0$; $E_0$ is the glassy modulus when $\omega \to \infty$; $\beta$ is a parameter linked with $\eta$, the Newtonian viscosity of the dashpot, $\eta = (E_0 - E_{00})\,\beta\tau_E$ and $\tau_E$ is a characteristic time values, which are only parameters depending on temperature and define as "Eq. 5".

$$\tau_E(T) = a_T(T) \cdot \tau_{0E} \tag{5}$$

where $a_T$ is the shift factor at temperature T, $\tau_E = \tau_{0E}$ at reference temperature $T_0$. $\tau_E$ is determined at each isotherm by minimizing the error between $|E^*_{measured}|$ and $|E^*_{2S2P1D}|$. Seven constants ($E_{00}$, $E_0$, $\delta$, k, h, $\beta$ and $\tau_{0E}$) are required to completely characterize the linear viscoelastic (LVE) properties of the tested material at a given temperature. The evolutions of $\tau_E$ was approximated by the WLF model ("Eq. 6"). $\tau_{0E}$ was determined at a chosen reference temperature $T_0$. When the temperature effect is considered, the number of constants becomes nine, including the WLF constants ($C_1$ and $C_2$ calculated at the reference temperature).

$$\log(a_T) = -\frac{C_1(T - T_0)}{C_2 + T - T_0} \tag{6}$$

## 6 Test Results

### 6.1 *Evolution of Complex Modulus (E*) with Number of FTC*

For each of the five saturation states studied, the E* measurement carried out following the imposed FTC helped monitor induced damage in the samples. Thirty-four E* tests were carried out (thirty valid results). E* results were traced in different domains, and parameters of the 2S2P1D analogue model were stated.

The 2S2P1D model helps describe rheological behaviour in small strain domain for a large spectrum of solicitations, and thus facilitates results analysis. Also, we used the normalization of results (detailed analysis) to verify whether the materials with similar behaviour (Lamothe 2014). Except PSW material, their behavior is similar, which allows to fix the parameters k, h, δ and β of the 2S2P1D analogue model. Indirectly, this allows an easier comparison between test results. Then the PSW material has its own values for these parameters, but fixed an E* to another.

Test results show that in the course of the FTCs, the complex modulus of the partially saturated bituminous material evolves. Figure 5 shows an example of complex modulus (5a) and relaxation time (5b) evolutions in the PSW sample.

A large part of the partially saturated samples demonstrated peculiar rheological behaviour in the course of the FTCs. Figure 6 shows complex modulus results in

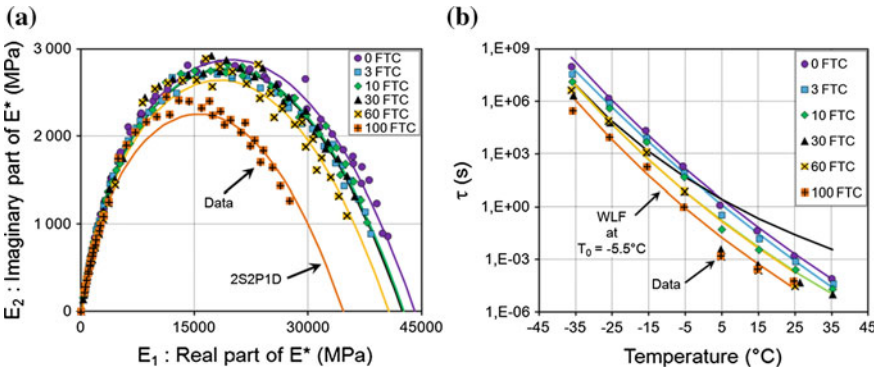


**Fig. 5** E* results in accordance with FTC of the PSW sample: **a** cole-cole plane, **b** relationship between the relaxation time and the E* testing temperatures

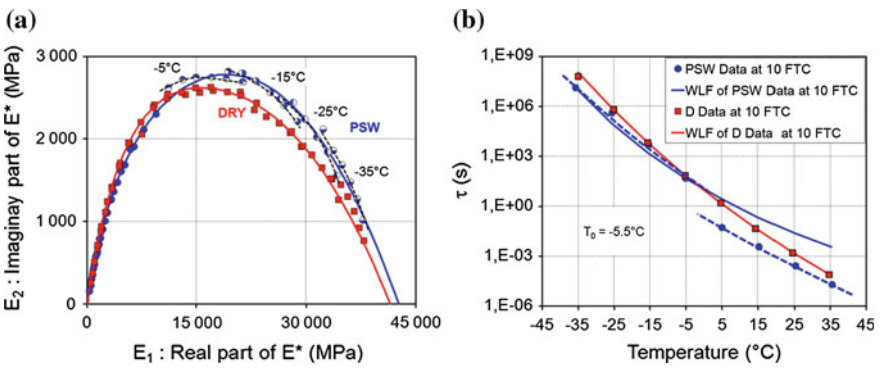


**Fig. 6** E* results obtained for the first 10 FTC of the PSW and D samples: **a** cole-cole plane, **b** relationship between the relaxation time and the E* testing temperatures

the Cole-Cole plane obtained in accordance with the 10th FTC for the (partially saturated with water) PSW and dry (D) samples. The results in Fig. 6 shows that complex moduli of the PSW sample for test temperatures lower than −5 °C, that is, temperatures lower than that at which ice forms inside pores in the bituminous mixture, are different from those obtained for higher temperatures. Furthermore, an analysis of the full results obtained with this research program show that the range of this difference increases with the FTCs. Figure 6b shows that the relationship between the relaxation time and temperature for the dry sample (D) is unequivocal while that of the PSW sample is bivalent. Therefore, the WLF approach function, established for all the PSW sample results, is not precise. Figure 6b shows a discontinuity in the relationship, situated between −5 and 5 °C, a temperature range which here is associated with ice formation, which leads to a translation of points on both sides of this range (Fig. 6b). Also, the relationship has been established for a reference temperature ($T_0$) of 4.7 °C to allow the correction of experimental values.

An analysis of the overall results for samples partially saturated with brine shows a similar behaviour to PSW samples, but for differentiated and increasingly lower temperatures, because the ice-forming temperature gets lower with increasing salt concentrations. Table 2 shows the ice formation temperatures obtained through the measurement of surface temperatures and temperatures inside the samples during the FTC. The ice formation temperature for the PSW sample, at −1.0 °C, is lower than 0 °C because part of the water is absorbed into pore walls.

Complex modulus results clearly show that ice formation in the microstructure of the bituminous mixture causes greater rigidity in the material at low temperatures on the one hand, and a distinct evolution in the rheological behaviour from that seen at higher temperatures, on the other. This observation highlights the difficulty in modelling the rheological behaviour of the PSW bituminous material by means of an analogue model. The presence of a liquid in the microstructure of the bituminous material causes a distinct evolution in the rheology of material as soon as ice formation sets in: the curve in the Cole-Cole plane ceases from being unique and becomes ambivalent, as if it were manifesting the behaviour of two distinct materials. Whatever the case, an analysis done, taking the 2S2P1D model into account enables first level separation of the behavioural differences of the partially saturated materials in the course of the FTCs.

**Table 2** Measured freezing points of testing samples (Lamothe et al. 2014)

| Element | Brine concentration (%) | | | |
|---|---|---|---|---|
| | 0 | 7.4 | 13.8 | 19.4 |
| Sample | PSW | PSB7 | PSB14 | PSB19 |
| Freezing point (°C) | −1.0 | −8.8 | −14.7 | <−18 |

## 6.2 *Effect of FTC on Rheology of PS Bituminous Mixtures*

To demonstrate the effect of the FTCs on the rheology of the partially saturated (PS) bituminous materials, we should consider its behaviour depending on whether the infiltrating liquid is in a fluid (effect of liquid) or solid state (effect of ice) within the microstructure of the material.

### 6.2.1 Effect of Liquid

The results are presented such as to show, firstly, the effect of the liquids on the rheology of the material even before it is subjected to the FTCs and, and secondly, the effect of the liquid on rheology in the course of the FTCs.

*Effect of the liquid on rheology before the FTCs*—The effect of the liquid in its microstructure on the rheology of the bituminous material in small strains domain can be demonstrated through the E* test results obtained for all the states studies as compared to those for tests on the dry sample, D. To simplify the presentation of these results, the relaxation time per reference temperature, $\tau_{0E}$, values which are characteristic of the E* test for each of the state studied. It should be recalled that the relaxation time is directly linked to the rheological behaviour of the material. For a given material, the reduction of relaxation time is observable when the temperature rises. Besides, a reduction of relaxation time in accordance with a given temperature, reveals a drop in the rigidity of the material.

For the liquid effect to be taken into consideration, $\tau_{0E}$, values have been considered for two (2) reference temperatures set on both sides of the temperature of ice formation obtained for sample D (−5.5 and 4.7 °C). Figure 7 shows the relationship between the relaxation rates of different states considered normalised in reference to

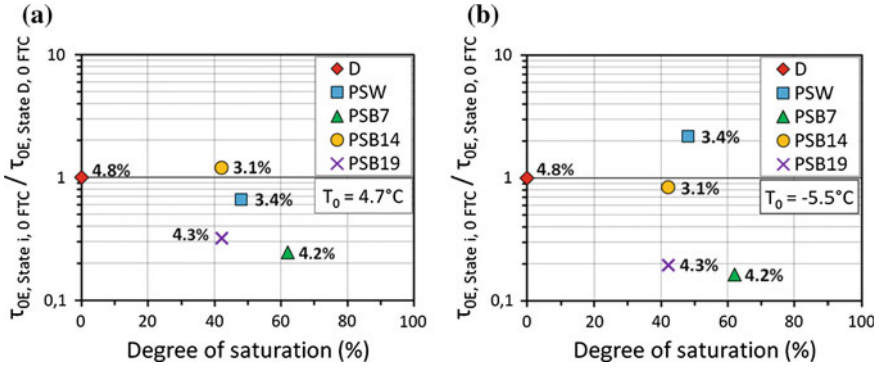


**Fig. 7** Relationship between the relaxation time established for a specific saturation state "i" ($\tau_{0E,\text{state i,0 FTC}}$), expressed relatively to the relaxation time obtained for the dry (D) sample ($\tau_{0E,\text{state D,0 FTC}}$), and the degree of saturation, before to apply any FT cycles (void content of samples indicated): **a** $T_0 = 4.7$ °C, **b** $T_0 = -5.5$ °C

that obtained for sample D, as a function of the degree of saturation in the sample prior to the launching of the FTCs. The results of Fig. 7a prove that the presence of the liquid in the microstructure of the material reduces its degree of rigidity. Figure 7b further shows that when a reference temperature lower than that associated with ice formation is considered, water solidification has the effect of making the material rigid. For samples partially saturated with brine (PSB), it should be noted that ice formation is inexistent at the temperatures studied in Fig. 7. Furthermore, consideration of the overall results of the experimental program, the general conclusion is that the presence of water in the material leads to an 8–10 % fall in rigidity at 15 °C and 10 Hz (Lamothe 2014).

*Effect of liquid and FTCs*—To demonstrate the effect of the liquid on the rheology of the material as the FTCs go by, the evolution of the relaxation time determined for each of the states studied and normalised in reference to the relaxation times obtained for each of the states before they were subjected to the FTCs, was traced. Figure 8 enables an evaluation of the combined effect of the liquid and the FTCs on the rigidity of the material in the course of the FTCs. It clearly shows that the relaxation time, normalised in reference to that of sample D at 0 FTC, is not highly influenced as the FTCs go by, for the D and the PSB19 samples. The results for the other three samples tested were different (PSW, PSB7 and PSB14). For the later, the low temperature reached during an FTC leads to ice formation inside the microstructure of these samples.

Consequently, it can be admitted that the loss of rigidity in the partially saturated samples in the course of the FTCs is caused by physical damage rather than a chemical attack by the salt present in the pores.

It should also be noted that at 4.7 °C, a ten unit drop in relaxation time generally corresponds to a rigidity loss of between 15 and 20 % in the sample. As such, after 100 FTCs, the PSW material shows a rigidity loss of 65 % at 4.7 °C.

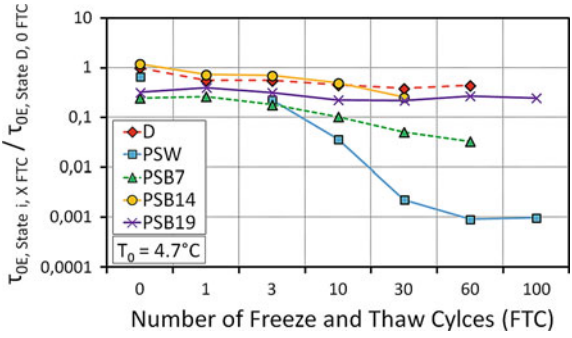


**Fig. 8** Relationship between the relaxation time established at $T_0$ of 4.7 °C for a specific saturation state "i" ($\tau_{0E,state\ i,X\ FTC}$), expressed in reference to the relaxation time obtained for the D sample ($\tau_{0E,state\ D,0\ FTC}$), and the number of FTC

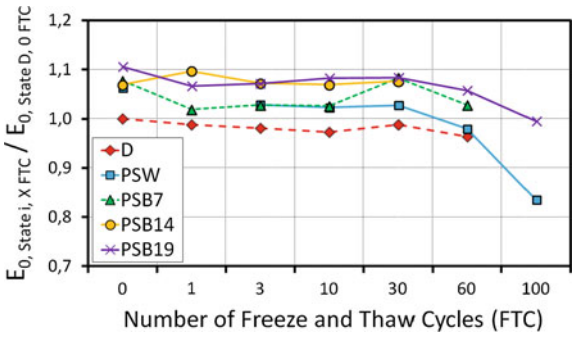


**Fig. 9** Relationship between the evolution of the glassy modulus established for each saturation state "i" ($E_{0,state\ i,0\ FTC}$) expressed relatively to the glassy modulus of the tested dry sample before to be submit to FTC

### 6.2.2 Effect of Ice on the Rheology of the Bituminous Mixture

In order to quantify the effect of ice formation on the rheology of the partially saturated material, it is wise to refer to the glassy modulus results ($E_0$) as determined through modeling of the complex modulus results from the 2S2P1D.

Glassy modulus results obtained before samples were subjected to FTCs that the $E_0$ of the partially saturated samples are 6–11 % higher than the $E_0$ of the dry tested sample (D) and this, despite the fact that all the tested samples were very low in pores (<4.3 %). It is highly probable that the effect of rigidification of the water saturated material at low temperatures will be greater at higher voids contents (7–9 %), as compared to their dry state.

*Effect of Ice and FTCs*—Fig. 9 shows the evolution of the glassy modulus for samples tested in different states ($E_{0,state\ i,X\ FTC}$) and normalised with reference to the glassy modulus of the dry tested sample before subjection to FTCs $E_0$, state S, ($E_{0,state\ D,0\ FTC}$). Figure 9 shows that the effect of ice is not significant on the glassy modulus values ($E_0$) of the tested material in accordance with FTCs. The effect of ice is essentially notable only for the PSW sample. In sum, the rheology, that is, mechanical properties, of the bituminous material remains the same at very low temperatures when ice has formed in the interstitial spaces during the FTCs.

## 7 Conclusion

The test results show that:

1. The complex modulus of the partially saturate material evolves under the action of the freeze-thaw cycles (FTCs) while it remains relatively stable for the dry tested sample (reference sample);

2. The small strains behaviour of the tested partially saturated samples distinctly evolves depending on whether temperatures are above or below the temperature at which ice forms in the pore spaces of the material: the presence of ice leads to an increase in rigidity of the material and the presence of liquid in the material, at high temperatures, reduces its rigidity. Then a double behaviour is observable for the same sample (or partially saturate mix);
3. The FTCs cause damages in the microstructure of the bituminous material if ice formation is effective. In the microstructure of HMA, the ice formation is effective at −1.0, −8.8, −14.7 and <−18 °C for water and brine at 7, 14 and 19 % of salt, respectively;
4. Rising the salt concentration in the liquid reduces ice formation and thus limits the damage generated by FTCs (temperature ranging from −18 to +10 °C);
5. After 100 FTCs, the PSW sample shows the higher rigidity loss: 65 % at 4.7 °C.

## References

Di Benedetto H, Olard F, Sauzéat C, Delaporte B (2004) Linear viscoelastic behaviour of bituminous materials: From binders to mixes. RMPD, 5(Special Issue EATA): 163–202.

Di Benedetto H, Nguyen QT, Sauzéat C (2011) Nonlinearity, Heating, Fatigue and Thixotropy during cyclic loading of Asphalt Mixtures. RMPD 12:1 129–158.

Fortin G (2006) Variabilité et fréquence des cycles de gel-dégel dans la région de Québec, 1977-2006. Le Géographe canadien, 54, 2, p 196–208 [In French].

Lamothe S (2014) Endommagement d'un enrobe bitumineux partiellement saturé en eau ou en saumure soumis à des sollicitations cycliques de gel-dégel et mécanique. ETS and ENTPE, PhD Thesis, 467 p [In French]

Lamothe S, Perraton D, Di Benedetto, H (2014) Contraction and expansion of partially saturated hot mix asphalt samples exposed to freeze–thaw cycles. RMPD.

MTQ (2003) Impact des restrictions de charges en période de dégel. Ministère des Transports du Québec, Info DLC, Vol. 8, No. 11, 2 p [In French]

Nguyen QT, Di Benedetto H, Sauzéat C (2012) Determination of Thermal properties of Asphalt mixtures as another output from cyclic Tension-Compression Test. RMPD 13:1 85–103

Olard F, Di Benedetto H (2003). General 2S2P1D model and relation between the linear viscoelastic behaviors of bituminous binders and mixes. RMPD 4:2, 185–224

St-Laurent D, Roy M (1995) Évaluation structurale de chaussées souples dans un contexte climatique nordique, Report GCS-95-05, Université Laval, Québec, 238 p [In French]

Tremblay M (2006) Étude de la fréquence des événements météorologiques précurseurs des nids-de-poule: le Québec un cas particulier? http://ptaff.ca/routes_du_quebec/ [In French]

# Experimental Study of Moisture Sensitivity of Aggregate-Bitumen Bonding Strength Using a New Pull-Off Test

**Jizhe Zhang, Alex K. Apeagyei, James Grenfell and Gordon D. Airey**

**Abstract** Moisture damage in asphalt mixtures is a complicated mode of pavement distress that results from the loss of interfacial adhesion between the aggregate and bitumen and/or the loss of cohesion within the bitumen. Both adhesive and cohesive strength of aggregate-bitumen bonds can be determined in the tensile testing mode. This paper presents the development of suitable procedure consisting of an innovative sample preparation, controlled moisture conditioning and new pull-off test set-up to characterise moisture damage resistance of the bonding strength of aggregate-bitumen samples that is sensitive to the mineralogical and physico-chemical properties of the aggregates as well as key bitumen physical properties. The test set-up consists of three main parts: a moisture conditioning step designed to ensure characteristic moisture diffusion into the aggregate-bitumen interface, accurate determination of bitumen film thickness using a modified dynamic shear rheometer and direct tension fixtures mounted on an Instron universal testing machine. The capability to vary loading rate, accurately control film thickness and ensure moisture diffusion to the aggregate-bitumen interface are an important improvement over most existing pull-off tests. The test was also found to be sensitive to moisture conditioning time, moisture uptake and the type of aggregate. All samples were subjected to the pull-off test to characterise their tensile strengths before and after moisture conditioning. The results show that the magnitude of the aggregate-bitumen bonding strength in the dry condition is mainly influenced by bitumen. However, the magnitude of the tensile strength after moisture conditioning was found to be influenced by mineralogical composition as well as the moisture

J. Zhang (✉) · A.K. Apeagyei · J. Grenfell · G.D. Airey
Nottingham Transportation Engineering Centre, Department of Civil Engineering, University of Nottingham, University Park, Nottingham NG7 2RD, UK
e-mail: evxjz3@nottingham.ac.uk

A.K. Apeagyei
e-mail: alex.apeagyei@nottingham.ac.uk

J. Grenfell
e-mail: james.grenfell@nottingham.ac.uk

G.D. Airey
e-mail: gordon.airey@nottingham.ac.uk



F. Canestrari and M.N. Partl (eds.), *8th RILEM International Symposium on Testing and Characterization of Sustainable and Innovative Bituminous Materials*, RILEM Bookseries 11, DOI 10.1007/978-94-017-7342-3_58

diffusion properties of the aggregates. The new test was found to be repeatable with variability comparable to most advanced tensile testing systems for bitumen.

**Keywords** Pull-off test · Bitumen · Aggregate · Moisture conditioning

## 1 Introduction

Asphalt mixtures are widely used as road construction materials. During their service life, asphalt pavements have to sustain harsh traffic loads and environmental conditions, which progressively deteriorate their structural capacity and performance with the passage of time. Moisture damage is considered to be one of the major causes of failure in asphalt pavements. Although not all damage is caused directly by moisture, its presence increases the extent and severity of existing distresses like cracking, potholes and rutting (Grenfell et al. 2014).

Moisture damage is a very complex phenomenon because it represents the combined action of various chemical, physical and mechanical processes that occur simultaneously at different intensities and rates (Caro et al. 2010). Existence of moisture in the pavement gradually reduces the overall functionality of asphalt mixtures due to the loss of cohesion within the bituminous binder itself (cohesive damage) and/or the loss of interfacial adhesion between binder and the aggregates (adhesive damage) (Grenfell et al. 2014). There are several parameters which may influence the durability of asphalt mixtures to moisture attack: porosity and roughness of the aggregates, wettability between bitumen and aggregates and chemical interaction at the interface (Horgnies et al. 2011). According to previous researchers, aggregate which has a porous, slightly rough surface and contains more calcium, aluminium and magnesium exhibits relative high moisture sensitivity (Bagampadde et al. 2004), whereas, bitumen which has more carboxylic acids and sulfoxides and good wettability will bond well with aggregate (Petersen and Plancher 1998). Moreover, other researchers demonstrated that the surface energy of the materials could control the wettability between bitumen and aggregate so as to influence the moisture sensitivity (Grenfell et al. 2014).

There are many experimental methods designed and used to characterise the moisture induced damage of bituminous mixtures over the last three decades. Testing methods such as the boiling water test and immersion test are used to characterise the adhesive properties of uncompacted mixes (Liu et al. 2014). The Indirect Tensile Test (Lottman 1982), Hamburg Wheel Tracking Device (Aschenbrener 1995) and Saturation Ageing Tensile Stiffness test (Aschenbrener 1995) are methods which focus on compacted mixtures to predict their degradation under simulated moisture conditioning. It can be seen that the most researches on moisture damage focused on loose bitumen-coated aggregate mixtures and compacted asphalt mixtures, whereas the degradation of bonding strength of bituminous film or aggregate-bitumen interfaces were less investigated. A major limitation of

some aggregate-bitumen bonding strength tests is the lack of capability to precisely control loading rate (Kim et al. 2012). For a better understanding the performance of the aggregate-bitumen interface when exposed to moisture, this paper presents the development of a suitable procedure consisting of an innovative sample preparation, controlled moisture conditioning and new pull-off test set-up.

## 2 Materials

Two bituminous binders (B1 and B2) with the penetration grades of 40/60 and 70/100 respectively and similar chemical compositions were used in the study. The physical properties of the bitumen were characterised using softening point and penetration tests. Based on the tests, the softening points (ASTM D36) of B1 and B2 were 51.2 and 45.2 °C respectively, whereas the measured penetration (ASTM D5) of B1 at 25 °C was 46 (0.1 mm) compared with 81 (0.1 mm) for B2.

The dynamic shear rheometer (DSR) was adopted to characterise the visco-elastic behaviour of bitumen binders from 10 to 80 °C. Figure 1 shows the shear complex modulus and phase angle master curves for the two bituminous binders used in this research. Data in this figure were produced by means of DSR testing performed within the linear visco-elastic range. The reference temperature is 30 °C. According to the time-temperature superposition principle (TTSP), low shear frequencies correspond to high temperatures while the high frequencies correspond to low temperatures. It was found that bitumen B1 presents higher shear complex modulus than bitumen B2 from low to high shear frequency. With respect to the phase angle, the data seems to overlap as the frequency becomes lower than 10 Hz. However, the phase angle of bitumen B1 is somewhat higher than that of bitumen B2 as the frequency becomes greater than 10 Hz, but the difference is relatively minor. Bitumen showing higher complex modulus is likely to form a stiffer bond to resist the direct tensile forces.

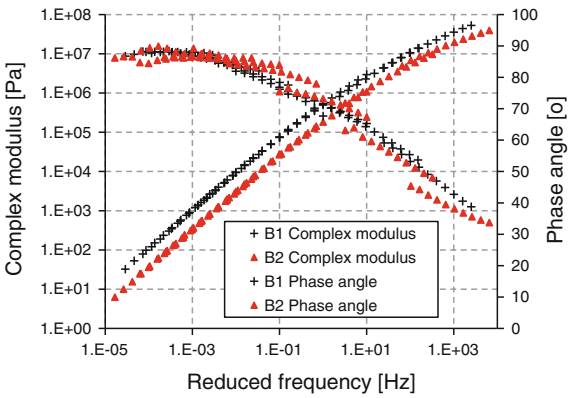


**Fig. 1** Master curves of shear complex modulus and phase angle at a reference temperature of 30 °C for two bituminous binders B1 and B2. Data suggest B1 is stiffer than B2

Three types of aggregate from different quarries were selected as substrates. They included one limestone aggregate (L1) and two granite aggregates (G1 and G2). These aggregates are known to have different moisture sensitivity due to their mineralogical composition. Based on their mineral compositions, two of the aggregates (G1 and G2) can be classified as acidic and the third aggregate (L1) is considered basic.

## 3 Test Methods

The main objective of this paper is characterising the moisture sensitivity of aggregate-bitumen bond using a new designed pull-off test. This test is sensitive to the mineralogical and physicochemical properties of the aggregates as well as key bitumen physical properties. So, the mineralogical composition and moisture absorption of the selected aggregates were first studied. The test set-up consists of three main parts: a moisture conditioning step designed to ensure characteristic moisture diffusion into the aggregate-bitumen interface, accurate determination of bitumen film thickness using a modified dynamic shear rheometer (DSR) and direct tension fixtures mounted on an Instron universal testing machine. The capability to vary loading rate, accurately control film thickness and ensure moisture diffusion to the aggregate-bitumen interface is an improvement over most existing pull-off tests.

### *3.1 Mineral Liberation Analyser (MLA) Test*

The mineralogical compositions of aggregates have a significant influence on moisture damage susceptibility of asphalt mixtures. The mineralogy of the different aggregates was studied using a Mineral Liberation Analyser (MLA) in order to understand the effect of their morphology on moisture damage resistance of aggregate-bitumen bonds. The experimental procedures used for the MLA included the following steps. Aggregates were first washed in water and then dried in an oven at 40 °C for 24 h. The oven-dried aggregates were cast in resin moulds with 25 mm diameter and 20 mm height, followed by polishing of the surface using a rotary polishing machine. Then, carbon coating was applied to get an electron conductive surface. An FEI Quanta 600 Scanning Electron Microscopy (SEM) with MLA capability was used for the mineral analysis. During testing, the SEM collects Back-scattered Electron (BSE) images and energy dispersive X-ray data for a series of frames step by step across the specimen surface. Measurement of the back-scattered electron intensities allows for the segmentation of mineral phases within each particle section, while Energy Dispersive X-ray (EDX) analysis of a given phase allows for phase identification (Grenfell et al. 2012).

## 3.2 Aggregates Moisture Absorption

Another important parameter that influences moisture-induced damage in asphalt mixtures is the rate and amount of water absorption of the aggregates. This approach is in contrast to most previous studies that only consider conditioning time when evaluating moisture damage. The current approach recognises the differences in moisture absorption characteristics of different aggregates. To perform the moisture absorption experiments, rectangular aggregate beams with the dimension of 100 mm × 20 mm × 10 mm were first cut from boulders. Then the aggregate beams were cleaned using deionised water and dried in an oven at 40 °C for 24 h to remove all the moisture. The weight of each beam in the dry condition was measured using a balance with the precision of 0.1 µg. The aggregates were moisture conditioned by placing them in baths containing deionised water at 20 °C and weighing them periodically until steady conditions were reached. The results were used to calculate the mass of water absorbed by aggregate as a percentage of the dry aggregate weight (Eq. 1).

$$Mass\ uptake(\%) = M_t = \frac{w_t - w_0}{w_0} \tag{1}$$

where $M_t$ is the moisture uptake at time $t$, $w_0$ is the initial mass of the aggregate in dry condition, $w_t$ is the mass of aggregate after time $t$ of immersion.

## 3.3 Bonding Strength Evaluation

The innovation of this test is the ability to accurately determine bitumen film thickness using a modified dynamic shear rheometer, small aggregate substrate size that permits realistic moisture conditioning and simplified custom-made direct tension fixtures that can be easily mounted on an Instron universal testing machine. The pull-off test set-up has been successfully used in the past to evaluate aggregate-asphalt mastic bonds (Apeagyei et al. 2014).

### 3.3.1 Aggregate-Bitumen Sample Preparation and Conditioning

Figure 2 shows the whole procedure in terms of sample preparation. For sample preparation, boulders of each aggregate were first drilled using a coring tool to get aggregate cylinders with 25 mm diameter. A trimming saw was used to cut the aggregate cylinders into discs with 5 mm thickness. To obtain a relatively constant surface roughness, both surfaces of the aggregate discs were polished using a rotary polishing machine. All discs were cleaned in an ultrasound cleaning machine for

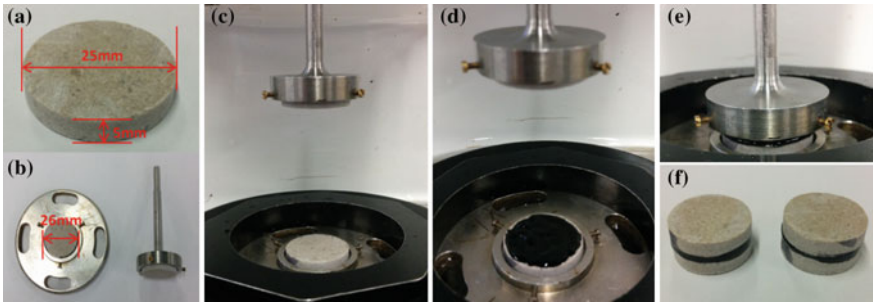


**Fig. 2** Aggregate-bitumen sample preparation procedures

15 min and dried in an oven at a temperature of 40 °C for 24 h. The finished polished aggregate substrate is shown in Fig. 2a.

Two aluminum specimen holding plates (Fig. 2b) were specially designed (diameter and thickness) and fabricated to fit in a standard DSR (Gemini DSR). The plates had dimensions (diameter and thickness) which were similar to a DSR. They differ from a DSR top and bottom plate in terms of the provision of sample holders (2 mm tall rings with 3 screen pins, Fig. 2b).

With a view to precisely controlling the film thickness of the bitumen, two modified fixtures were designed to clamp the discs (Fig. 2b) and then fixed into the DSR machine (Fig. 2c). Firstly, the gap between upper and lower surfaces should be set to zero and these two surfaces should be parallel. After establishing the zero gap and ensuring that the discs are parallel, a small amount of hot bitumen was placed on the lower aggregate surface (Fig. 2d) and then pressed with the upper aggregate to achieve the required bitumen film thickness (Fig. 2e), with a gap resolution of 1 μm. It is found that the minimum bitumen film thickness between two substance surface was approximately 20 μm (Marek and Herrin 1968). So, in this research the sample was removed from the DSR after about 15 min of cooling and then the excess asphalt binder removed by means of a heated pallet knife, as shown in Fig. 2f.

The samples were then stored at 20 °C in water (as shown in Fig. 3) and periodically removed and tested using the pull-off test setup. During the moisture

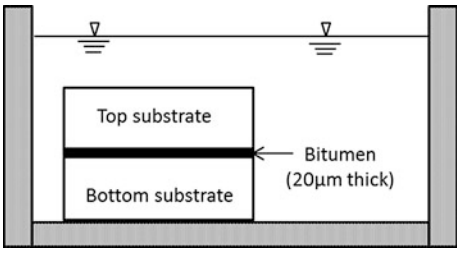


**Fig. 3** Specimen of aggregate-bitumen bond submerged into water

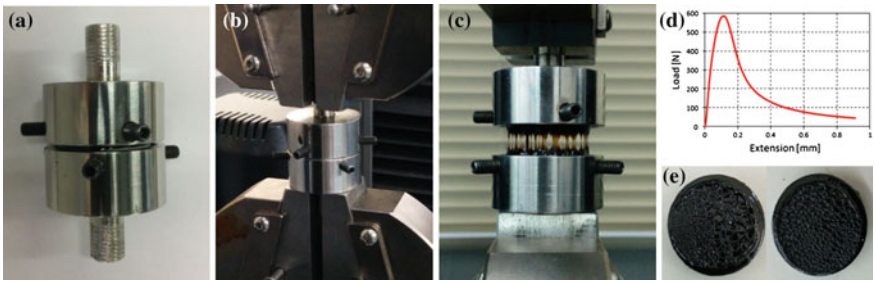


**Fig. 4** Procedures for bonding strength evaluation

conditioning, moisture could reach the aggregate-bitumen interface in three different ways: through the top and bottom aggregate, through the edge of aggregate-bitumen interface and through the bitumen film.

### 3.3.2 Pull-Off Test

Before the pull off test, the prepared sample was first fixed by two direct tension fixtures with three screws on each, as shown in Fig. 4a. These two fixtures were then installed on the Instron machine (Fig. 4b). An extension speed of 10 mm/min and a temperature of 20 °C were applied to break the interface (Fig. 4c). During the test, the pull force as a function of elongation was recorded (Fig. 4d) and the failure surfaces of each broken sample were taken with a camera (Fig. 4e). At least four repeat tests were made for each aggregate-bitumen sample. The results were used to calculate the tensile strength. Tensile strength TS (kPa) was computed as the ratio of the peak load divided by the cross-sectional area of the bitumen film as follows:

$$TS = \frac{F}{\pi r^2} \tag{2}$$

where $F$ is the Peak tensile force (N) and $r$ is the Radius of aggregate disc (m).

## 4 Results and Discussion

### *4.1 Mineralogy of Aggregates*

Figure 5 shows the mineralogical composition and distribution of the aggregates obtained from the Mineral Liberation Analyzer. As shown in this figure, minerals in the granite sample (G1 and G2) exhibit considerable texture and the distribution is more complex, while the limestone surface is simple and calcite makes up almost all of the area. For the limestone (L1) sample, calcite is the predominant phase

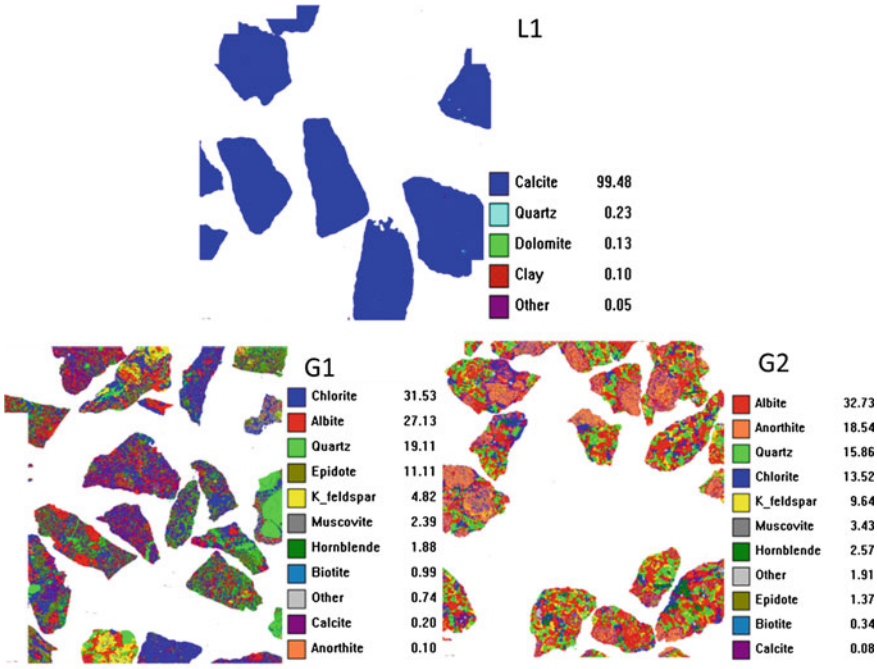


**Fig. 5** Mineral mosaic of three aggregates

when compared to the other minerals present, with 99.48 % by weight. However, granite is made up of a number of different mineral phases. Chlorite and Albite are the dominant minerals in G1 with a presence of 31.53 and 27.13 % by weight, followed by quartz, epidote and K-feldspar, which account for 19.11, 11.11 and 4.82 %, respectively. Different from G1, albite and anorthite are the predominant content minerals in G2, which account for 32.73 and 18.54 % by weight, but quartz and chlorite also have significant quantities. It is believed that the large proportion of the albite and quartz phases have the potential to lead to moisture damage, due to the poor adhesion between quartz and bitumen. Though Albite can form strong bond with bitumen in the dry condition, this bond is quickly broken in the presence of water. There is also evidence that feldspar is responsible for interfacial failure between bitumen and aggregate (Horgnies et al. 2011).

## *4.2 Water Absorption of Aggregate*

Water absorption data were obtained from these three aggregates used for substrates in this research. In order to measure how much water was absorbed into aggregate during the conditioning time, the water absorption test was performed and the

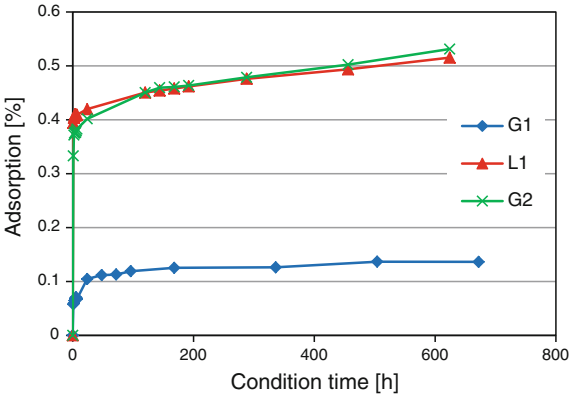


**Fig. 6** Water absorption of three aggregates used in this research

results of the three aggregates are shown in Fig. 6. It can be seen that for the aggregates considered, more than 80 % of the moisture was absorbed during the first 24 h of water conditioning. After that, the water absorption of L1 and G2 experienced a slow increase in comparison with the first 24 h and finally reached marginally over 0.5 % although the water absorption of L1 and G2 still seems to be increasing and has probably not reached their equilibrium. G1 showed the lowest water absorption with the value being only 0.13 % even after 600 h conditioning. The differences in the rate and amount of moisture absorption could be due to the effect of mineral composition and the structure of the aggregates.

## *4.3 Influence of Aggregate and Bitumen on Dry Bond Strength*

Four replicate tests were performed on each aggregate-bitumen combination. The average tensile strength of each aggregate-bitumen bond in the dry condition was calculated according to Eq. 2. The results are depicted in Table 1 together with the test variability (standard deviation); the latter suggesting the new pull-off test has low variability with a coefficient of variability ranging from about 5–16 %. It can be seen from Table 1 that samples prepared with bitumen B1 have higher bonding strength in comparison with bitumen B2. This phenomenon correlates well with the DSR results with shear complex modulus higher for B1 than B2. In addition, bitumen B1 has a higher softening point and lower penetration than B2. It can be demonstrated that bitumen with higher shear complex modulus results in higher tensile strength. In terms of the same bitumen, samples prepared with different aggregates tend to yield similar tensile strength. This suggests that, in the dry condition, the tensile strength of samples is controlled mainly by the bitumen properties, aggregate effects appear minimal. One confirmation of this observation is that damage was mainly cohesive (i.e. within the bitumen) and not interfacial.

**Table 1** Dry tensile strength (kPa) of aggregate-bitumen at 20 °C

| Sample ID | L1 | | G1 | | G2 | |
|---|---|---|---|---|---|---|
| | Mean | Std | Mean | Std | Mean | Std |
| B1 | 1920 | 103 | 1947 | 199 | 1938 | 312 |
| B2 | 1425 | 147 | 1386 | 72 | 1413 | 128 |

B1 = 40/60 pen bitumen; B2 = 70/100 pen bitumen; L1 = limestone; G1 = granite 1; G2 = granite 2; Std = standard deviation

## *4.4 Effect of Moisture Conditioning on Load Behaviour*

To simulate the effect of moisture on the stress-strain properties of the aggregate-bitumen samples, the pull-off tests were performed on samples moisture conditioned at 20 °C for 1 day and 7 days. Figure 7 shows the influence of increasing moisture conditioning time on the stress-strain behaviour of samples prepared with bitumen B1 and the three aggregates. From this figure it can be seen that the tensile loads for all specimens decreased after moisture conditioning. In terms of the load-extension curve, B1-L1 and B1-G2 with 1 day moisture conditioning experienced a sharp decrease once they reached the peak load, which is totally different from other specimens. This may be due to the short-term moisture conditioning for these two specimens hardening the bitumen film or acts on the

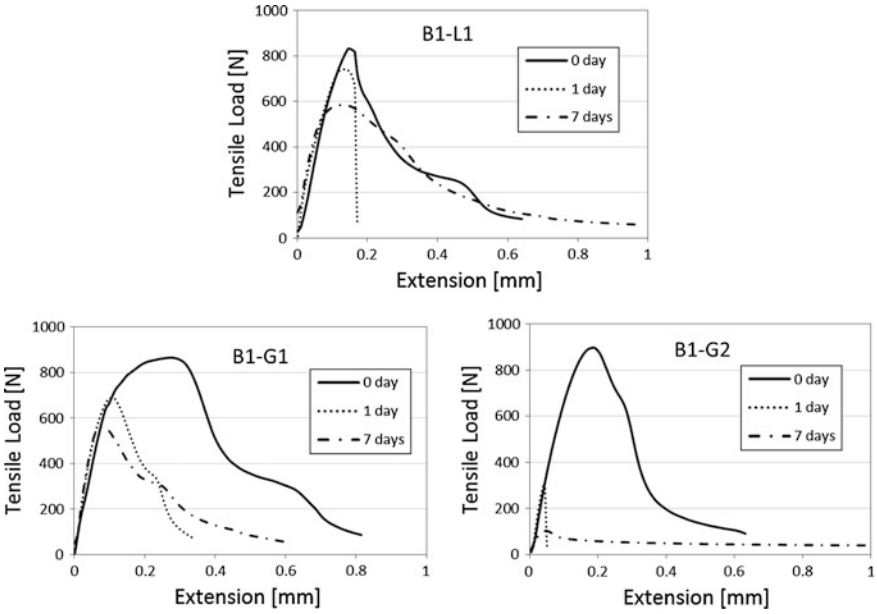


**Fig. 7** Effect of moisture on stress-strain behaviour of aggregate-bitumen combined samples before and after moisture conditioning. Samples were conditioned in water at 20 °C; loading rate was 10 mm/min

adhesion bond between the bitumen and aggregate and having no chance to release during extension. Due to the lower moisture absorption of G1 aggregate as shown in Fig. 6, it is not easy for water to penetrate into the aggregate-bitumen interface and harden the bitumen so that the sharp decrease of tensile load does not appear in B1-G1.

## 4.5 *Effect of Moisture on Retained Strength*

Retained strength, the ratio of bond strength after a given level of moisture conditioning to the dry bond strength, is a common measure of moisture sensitivity of asphalt mixtures. The higher the retained strength of an asphalt mixture, the better the moisture damage resistance of the bond. Figure 8 shows the effect of conditioning time on retained tensile strength of the aggregate-bitumen bond. From this figure it can be seen that specimens which contain L1 or G1 aggregate show good moisture resistance with over 75 % tensile strength retained after 7 days conditioning. On the contrary, the moisture effect was more pronounced in the specimens containing G2 aggregate where the strength decreased by over 80 and 40 % for B1 and B2 bitumen, respectively. Aggregate L1 and G2 have similar moisture absorption properties (as shown in Fig. 6), but they show obviously different moisture sensitivity. This result suggests that the mineralogical property of aggregate is an important indicator of moisture damage. In fact, in the sample G2 the bonds formed with bitumen are quickly broken in the presence of water due to the large amount of albite and quartz within the aggregate. The results showing better resistance to moisture-induced damage for specimens containing limestone than granite are in agreement with previous studies (Apeagyei et al. 2014; Airey and Choi 2002). However, G1 is granite, but because of its lower moisture absorption, it is hard for water to diffuse through the aggregate into the aggregate-bitumen interface so that it cannot obviously weaken the bond. On this basis, it is reasonable

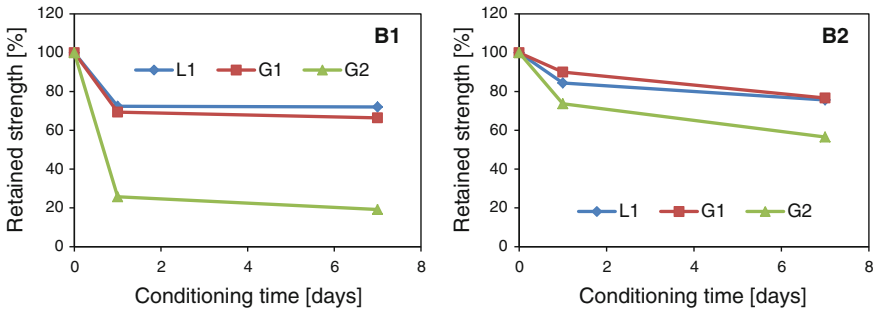


**Fig. 8** Effect of moisture conditioning time on tensile strength of different aggregate-bitumen combinations. In general acidic aggregate performed worse than basic aggregates. The combination of bitumen B1 with aggregate G2 performed worst

to state that the moisture-induced damage of aggregate-bitumen bond is not only controlled by the mineralogical composition but the moisture absorption of aggregate should also be considered. The differences in retained strengths between G1 and G2 could be attributed to higher moisture absorption of the latter. This later result combined with the L1 results previously discussed leads one to conclude that for susceptible aggregates, the amount of moisture absorption is a significant factor.

In terms of the same aggregate, specimens prepared with B2 bitumen show better resistance to moisture damage in comparison with B1. This demonstrated that softer bitumen with lower complex modulus may have better performance with the presence of moisture. However, more tests need to be done so as to confirm this conclusion.

## *4.6 Moisture Effects on Failure Type*

Figure 9 shows the effect of increasing conditioning time on the failure surface of aggregate-bitumen specimens. Without moisture conditioning, cohesive failure occurred into the bulk of the bitumen film. Under this condition, the tensile strength depends on the cohesive properties of the bitumen film. So, the same bitumen shows almost the same tensile strength, regardless of aggregate type. After moisture conditioning, the water could penetrate into the specimen and weaken the aggregate-bitumen bond. The failure tends to transfer from cohesive to an adhesive-cohesive mix with the increase of conditioning time. It can be seen that specimens prepared with L1 retained the most cohesive failure, followed by G1 and specimens with G2 showed the least cohesive failure. Specimens with G2 aggregate even show totally adhesive failure after 7 days moisture conditioning. The results demonstrated that, with similar moisture absorption properties, limestone showed better resistance to moisture-induced damage than granite.

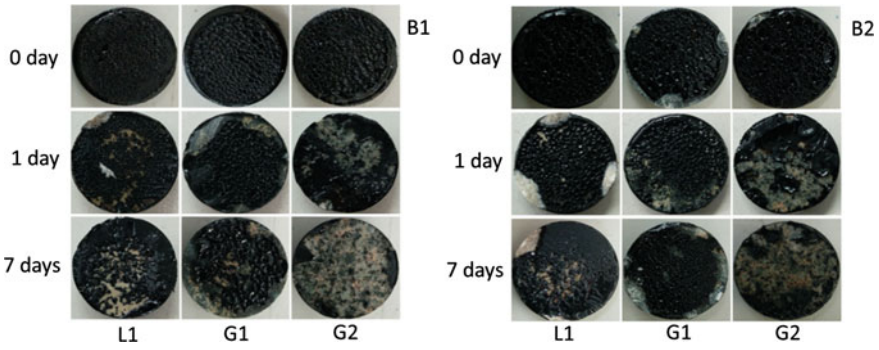


**Fig. 9** Failure surface of aggregate-bitumen bonds exposed to moisture: top bitumen B1; bottom bitumen B2. The effect of bitumen type is minimal compared with the effect of aggregate type

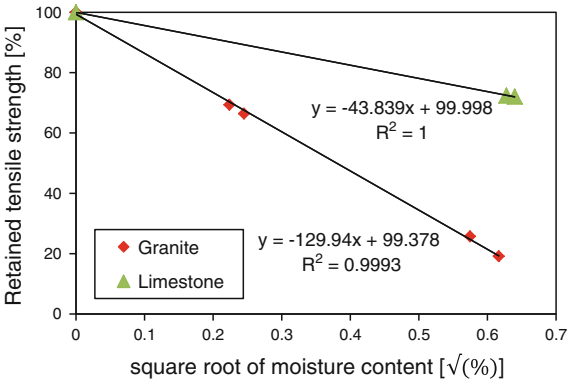


**Fig. 10** Relationship between retained tensile strength and square root of moisture content: specimens prepared by bitumen B1

### *4.7 Relationship Between Moisture Content and Retained Tensile Strength*

Results in Figs. 8 and 9 clearly showed the effect of conditioning time on the aggregate-bitumen bond strength and failure type. If taking the moisture absorption into consideration (Fig. 6), the longer the conditioning time, the greater the amount of water that can penetrate into the aggregate and reach the aggregate-bitumen interface. Also, due to the porosity difference, a porous aggregate would absorb more moisture than a less porous aggregate over the same conditioning time.

Figure 10 shows the retained tensile strength, evaluated at both moisture conditioning times, of the specimens prepared with bitumen B1 versus the square root of moisture absorption. From this figure it can be seen that a linear negative relationship was found between retained tensile strength and square root of moisture content. This suggests that, for the same type of aggregate, the amount of water absorbed by the aggregate controls the degradation of the aggregate-bitumen bond strength. As the slope of granite is bigger than limestone, it means that specimens prepared with granite are more sensitive to moisture induced damage. The specimens prepared by bitumen B2 showed the same phenomenon. So, the amount of water absorbed by the aggregate may control the degradation of the aggregate-bitumen bond strength in both basic and acidic aggregates.

## 5 Conclusions

This paper reports on the findings from an investigation on the moisture conditioning effects on the bond properties of aggregate-bitumen systems through a new procedure based on pull-off testing that allows to accurately control bitumen film thickness as well as to take into account the aggregate moisture absorption. Tensile strength and retained tensile strength were used as measures of moisture sensitivity

of aggregate-bitumen bonds. The results were also analysed by relating moisture absorption and mineralogical composition to retained tensile strength. The following conclusions were reached based on the results presented in this paper.

- The new pull-off testing system developed in this study was found to be effective in characterising the bonding strength of aggregate-bitumen system. The variability in bond strength was low with a coefficient of variation that ranged from 5–16 %. The system is capable of controlling bitumen film thickness with a resolution of 1 μm.
- In the dry state, the types of failure of all the aggregate-bitumen combinations were cohesive. The effect of bitumen grade was significant with samples prepared with 40/60 pen bitumen having higher tensile strength than those prepared with 70/100 pen bitumen. The results suggest the bitumen stiffness controls the aggregate-bitumen bond strength in the dry state to a higher extent than aggregate type.
- The bond strength of the various aggregate-bitumen combinations measured with the new pull off test was shown to be sensitive to moisture conditioning. The failure pattern was shown to change from cohesive to mixed cohesive/adhesive and even adhesive failure as the conditioning time extended.
- Results of pull off tests suggest that the moisture damage of different aggregate-bitumen combinations could be explained by the moisture absorption and mineralogical compositions of aggregates. With the same moisture absorption, limestone tends to have better resistance to moisture damage than granite. Furthermore, in terms of similar mineralogical compositions, lower moisture absorption may result in better moisture resistance.
- For both limestone and granite used in this research, there was excellent correlation between the moisture content and retained tensile strength. The significant correlation between the moisture content absorbed by aggregate and retained tensile strength of aggregate-bitumen system suggests that the water absorption process of the aggregate controls the degradation of the aggregate-bitumen bond.

## References

J. Grenfell, N. Ahmad, Y. Liu, A. Apeagyei, D. Large and G. Airey. Assessing asphalt mixture moisture susceptibility through intrinsic adhesion, bitumen stripping and mechanical damage. Road Materials and Pavement Design 2014, 15(1): 131-152.

S. Caro, E. Masad, A. Bhasin and D. Little. Micromechanical modeling of the influence of material properties on moisture-induced damage in asphalt mixtures. Construction and Building Materials 2010, 24: 1184–1192

M. Horgnies, E. Darque-Ceretti, H. Fezai, E. Felder. Influence of the interfacial composition on the adhesion between aggregates and bitumen: Investigations by EDX, XPS and peel tests. International Journal of Adhesion & Adhesives 2011, 3: 238–247

U. Bagampadde, U. Isacsson and B.M. Kiggundu, Classical and Contemporary Aspects of Stripping in Bituminous Mixes, Road Materials and Pavement Design 2004; 5(1): 7-43.

J.C. Petersen, H. Plancher, Model Studies and Interpretive Review and the Competitive Adsorption and Water Displacement of Petroleum Asphalt Chemical Functionalities on Mineral Aggregate Surfaces, Petroleum Science & Technology 1998; 16(1-2): 89-131.

J. Grenfell, N. Ahmad, Y. Liu et al. Assessing asphalt mixture moisture susceptibility through intrinsic adhesion, bitumen stripping and mechanical damage. Road Materials and Pavement Design 2014; 15(1): 131-152.

Y. Liu, A. Apeagyei, N. Ahmad et al. Examination of moisture sensitivity of aggregate-bitumen bonding strength using loose asphalt mixture and physic-chemical surface energy property tests. International Journal of Pavement Engineering 2014; 15(7): 657-670.

R.P. Lottman, Predicting Moisture-Induced Damage to Asphaltic Concrete Field Evaluation, NCHRP 246, 1982.

T. Aschenbrener, Evaluation of Hamburg wheel-tracking device to predict moisture damage in hot-mix asphalt. Transport Research Record 1995; 1492: 193-201.

Y-R Kim, I Pinto and S-W Park. Experimental evaluation of anti-stripping additives in bituminous mixtures through multiple scale laboratory test results. Construction and Building Materials 2012; 29: 386-393.

J. Grenfell, N. Ahmad, G. Airey, A. Collop and R. Elliott. Optimising the moisture durability SATS conditioning parameters for universal asphalt mixture application. International Journal of Pavement Engineering 2012; 13(5): 433-450.

A. Apeagyei, J. Grenfell, G. Airey. Moisture-induced strength degradation of aggregate–asphalt mastic bonds. Road Materials and Pavement Design 2014; 15(1): 239-262.

Marek CR, Herrin M. Tensile behavior and failure characteristics of asphalt cements in thin film. Proceeding, Association of Asphalt Paving Technologists 1968; 37: 387-421.

M. Horgnies, E. Darque-Ceretti, H. Fezai, & E. Felder. Influence of the interfacial composition on the adhesion between aggregates and bitumen: Investigations by EDX, XPS and peel tests. International Journal of Adhesion and Adhesives 2011; 31(5): 238–247.

G.D. Airey, Y.K. Choi. State of the art report on moisture sensitivity test methods for bituminous pavement materials. Road Materials and Pavement Design 2002; 3(4): 355-372.

# Effect of Fine Aggregate Composition on Moisture Susceptibility of Hot Mix Asphalt

**Gordon L.M. Leung and Alan W.G. Wong**

**Abstract** This paper discusses how the moisture susceptibility is influenced by the angularity characteristic and the composition of the fine aggregates. The results indicate that the composition of fine aggregate affects the moisture susceptibility of asphalt mixture in certain degree. By reviewing the results of the split strength ratio of bituminous mixture, the mass (in percent %) of natural sand in the fine aggregate (N/FA) ratio has an optimal value. This value is propitious to improve the workability of the asphalt mixture and enhance the compaction of mixture, and thus reduce the percent of air voids in asphalt mixture and reduce the moisture susceptibility. From the study, it was found that the optimal value of N/FA is 30 %, approximately being equal to 13 % (in weight) of the total weight of the mineral aggregates. Further increase in N/FA ratio may cause a lower adhering ability between the bitumen and aggregate. Furthermore it is considered that by viewing the FAA alone is not sufficient to justify or conclude on the possible performances of the subsequent bituminous mixtures formed.

**Keywords** Hot mix asphalt (HMA) · Moisture susceptibility · Fine aggregate angularity (FAA) · Split strength

G.L.M. Leung (✉)
Road Research Group, Department of Civil Engineering,
Chu Hai College of Higher Education, Hong Kong, China
e-mail: glmleung@chuhai.edu.hk

A.W.G. Wong
Hong Kong Road Research Laboratory, Hong Kong, China
e-mail: wgwong@chuhai.edu.hk



F. Canestrari and M.N. Partl (eds.), *8th RILEM International Symposium on Testing and Characterization of Sustainable and Innovative Bituminous Materials*, RILEM Bookseries 11, DOI 10.1007/978-94-017-7342-3_59

# 1 Introduction

The fine aggregates (i.e. 0.075 mm to 2.36 mm) used in the paving asphalt mixtures are usually consisted of stone chips, natural sand, or crushed sand. It is typically considered that the characteristics of the fines aggregate are influential to the performance of asphalt mixtures, especially on the rutting performance of the materials. Around the world, different researches drew different conclusions on this which leads to different emphasis on the material specifications. For example, (1) The specification of JTJ 032-94 (China) regulates that the fine aggregates of hot mix asphalt should be consisted of superior quality natural sands or crushed sands, of which the dosage of stone chips used in topping course or wearing course of the asphalt concrete of the expressway, first-grade highway should not exceed that of natural sands (2). The Asphalt Pavement Guide of Japan also rules that the dosage of stone chips should not exceed the dosage of natural sands in the design of mixtures (3). The Federal Highway Administration of America (FHWA) regulates that the dosage of natural sands in the total fine aggregates is 20 % approximately and also many highway authorities in the US require minimum values of FAA (43–45 %) to be used in bituminous mixtures on high traffic roads (4). In addition, the Superpave asphalt mixtures design method indicates the fine aggregates angularity (FAA) as the criteria for controlling the quality of fine aggregates (5). However, some scholars considered that, under different testing content or testing conditions, the value of FAA is not always the important factor that affects the performance of asphalt mixtures. (6) However, the Hong Kong specification does not put emphases on the properties of the fine aggregates other than specifying the requirements on gradations.

On the basis of the different viewpoints mentioned above, this study reviews the effects on the property of the asphalt mixture (i.e. moisture susceptibility) by varying the component proportion of fine aggregates (thus changing the value of FAA) by the adoption of the freeze-thaw splitting test of asphalt mixtures.

# 2 Experiment

## *2.1 Materials*

The bitumen used in the study is SK-AH-70 obtained from China and the technical specifications of the material are shown in Table 1. The crushed

**Table 1** Main technical specification of asphalt

| Specification | Tested value |
|---|---|
| Penetration ($10^{-1}$ mm) | 69 |
| 15 °C Ductility (cm) | >200 |
| Soften point ($^{o}$C) | 46 |
| Density (g/cm$^3$) | 1.018 |

gritsand was used as the coarse aggregates and its bulk specific gravity of coarse aggregate is 2.692. The fine aggregates composed of limestone chips and natural river sand. The two types of fine aggregates were mixed together according to different mass percentages to form different natural sand to total fine aggregates ratio (N/FA). The corresponding specific gravities of the different fine aggregates are shown and the associated FAAs (6) as tested based on ASTM C1252 are shown in Table 2. The mineral filler used in the mixtures was limestone powder and its apparent specific gravity was 2.720. A dense-grade aggregates gradation was selected for mixture design, and the associated gradation of the material is shown in Table 3.

## 2.2 Determination of Asphalt Content of Mixtures

Based on the aggregates gradation shown in Table 3, the bitumen content of mixtures were determined according to the composed proportion of the two fine aggregates, with the two boundary levels of 10 and 50 % of N/FA ratio (being the lower and upper limits respectively). The mixtures samples were formed by the Marshall compaction method. The Marshall test results (stability, percent air voids, flow value and percent of the voids in mineral aggregate that are filled with asphalt of bituminous mixtures) indicate that the optimum asphalt aggregate ratio of 4.7 % was achieved at the level of 10 % N/FA, and 4.6 % was obtained at the level of 50 % N/FA. Finally the asphalt aggregate ratio of 4.7 % was selected for all experiments under this study.

**Table 2** Bulk specification gravity and FAA value of fine aggregates

| N/FA (%) | Bulk specification gravity (g/cm$^3$) | FAA value (%) |
|---|---|---|
| 10 | 2.713 | 47.1 |
| 20 | 2.715 | 46 |
| 30 | 2.630 | 44.1 |
| 40 | 2.667 | 42.8 |
| 50 | 2.658 | 40.3 |

**Table 3** Aggregate gradation of asphalt concrete mixtures

| Sieve size (mm) | 16.0 | 13.2 | 9.5 | 4.75 | 2.36 | 1.18 | 0.6 | 0.3 | 0.15 | 0.075 |
|---|---|---|---|---|---|---|---|---|---|---|
| Percent passing (%) | 100 | 97 | 76 | 50 | 32 | 22 | 15 | 11 | 7 | 5 |

## 2.3 Testing of Volume Specification

By keeping the composition of the coarse aggregates (sizes from 4.75 to 13.2 mm) the same, the proportions of the fine aggregates were adjusted in five levels, being from 10 to 50 % (i.e. with 10 % interval). The ratios of mineral aggregates are shown in Table 4. Two batches of Marshall samples were made at each level, of which the asphalt aggregate ratio of 4.7 % was adopted for all the samples of the mixtures. The bulk specific gravity of samples was obtained according to ASTM D 1188-96 (7), the percentage air voids (VV), percentage of the voids in mineral aggregate (VMA) were also pursued and the results are shown in Table 5.

## 2.4 Freeze and Thaw Split Tests

A series of freeze-thaw split tests were conducted (3 nos. samples were adopted for each test). One of the two batches samples was pre-conditioned according to ASTM D4867/D4867 M-96 (8), of which the samples were frozen under the condition of −18 °C for 16 h ± 1 h and thawed at 60 °C ± 0.5 °C for 24 h. Another batch of samples (control samples) was placed under the condition of room temperature. The moisture susceptibility was evaluated based on the ratio of freeze-thaw split strength (TSR). The splitting tests were conducted at the temperature of 25 °C and the loading rate was set as 50 mm/min. The results of freeze-thaw split tests are shown in Table 6.

**Table 4** Mineral aggregate composing ratios

| d (mm) | | 13.2 | 9.5 | 4.75 | 2.36 | 1.18 | 0.6 | 0.3 | 0.15 | 0.075 | <0.075 |
|---|---|---|---|---|---|---|---|---|---|---|---|
| Ratio (%) | | 3.0 | 20.7 | 26.3 | 18.0 | 10.0 | 7.0 | 4.0 | 3.3 | 2.1 | 5.6 |
| N/FA (%) | 10 | 3.0 | 20.7 | 26.3 | 1.8[a] | 1.0 | 0.7 | 0.4 | 0.3 | 0.2 | 5.6[b] |
| | | | | | (16.2) | (9.0) | (6.3) | (3.6) | (3.0) | (1.9) | |
| | 20 | 3.0(2) | 20.7 | 26.3 | 3.6 | 2.0 | 1.4 | 0.8 | 0.7 | 0.4 | 5.6 |
| | | | | | (14.4) | (8.0) | (5.6) | (3.2) | (2.6) | (1.7) | |
| | 30 | 3.0 | 20.7 | 26.3 | 5.4 | 3.0 | 2.1 | 1.2 | 1.0 | 0.6 | 5.6 |
| | | | | | (12.6) | (7.0) | (4.9) | (2.8) | (2.3) | (1.5) | |
| | 40 | 3.0 | 20.7 | 26.3 | 7.2 | 4.0 | 2.8 | 1.6 | 1.3 | 0.8 | 5.6 |
| | | | | | (10.8) | (6.0) | (4.2) | (2.4) | (2.0) | (1.3) | |
| | 50 | 3.0 | 20.7 | 26.3 | 9.0 | 5.0 | 3.5 | 2.0 | 1.7 | 1.1 | 5.6 |
| | | | | | (9.0) | (5.0) | (3.5) | (2.0) | (1.6) | (1.0) | |

[a]In the cell, the above datum was the mass percent of nature sand against total mass of mineral aggregate, the inferior datum was the mass percent of stone chip with same dimension against total mass of mineral aggregate

[b]The ratio of the coarse aggregates (≥4.75 mm) and mineral powder (<0.075 mm) against total quantum of mineral aggregate kept constant when the N/FA varied

**Table 5** Volume specification of marshall samples

| N/FA (%) | FAA (%) | VV (%) | VMA (%) |
|---|---|---|---|
| 10 | 47.1 | 5.3 | 15.8 |
| 20 | 46.0 | 6.3 | 16.7 |
| 30 | 44.1 | 5.5 | 15.9 |
| 40 | 42.8 | 5.0 | 15.5 |
| 50 | 40.3 | 5.1 | 15.6 |

**Table 6** Testing results of freeze-thaw split

| N/FA (%) | FAA (%) | $R_{T1}^{a}$ (MPa) | $R_{T2}^{b}$ (MPa) | TSR = $R_{T2}/R_{T1}$ (%) |
|---|---|---|---|---|
| 10 | 47.1 | 1.429 | 0.945 | 66.2 |
| 20 | 46.0 | 1.377 | 0.916 | 66.5 |
| 30 | 44.1 | 1.377 | 1.026 | 74.5 |
| 40 | 42.8 | 1.287 | 0.942 | 73.2 |
| 50 | 40.3 | 1.203 | 0.855 | 71.0 |

[a]The split strength of samples that did not endure the freeze-thaw precondition
[b]The split strength of samples that endured the freeze-thaw precondition

## 2.5 Test Results

Based on the test results as shown in Table 5, the effects of N/FA on the volume properties are plotted in Figs. 1 and 2. The data indicates that, by varying the values of N/FA, the two volume properties of VV and VMA tend to vary considerably and when N/FA value is approximately at the level of 20 %, VV and VMA of samples appear to be the highest.

Based on the results of the freeze-thaw split tests, the ratio of split strength of the samples obtained under the freeze-thaw conditioning against the split strength of the control samples are demonstrated in Table 6 according to different N/FA ratios. Figures 3, 4, 5 and 6, respectively, illustrate how the FAA values, split strengths ($R_T$), and TSR(s) were affected by varying the N/FA ratio. In the meanwhile, the effects of FAA on $R_T$ and TSR are shown in Figs. 6 and 7 respectively.

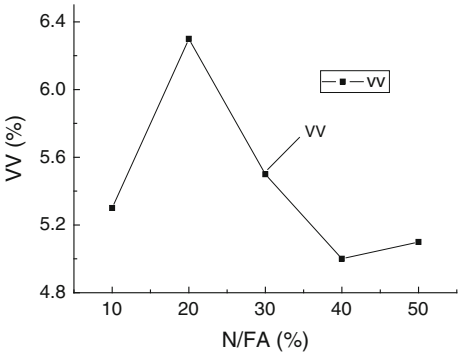


**Fig. 1** N/FA versus the percent air voids in asphalt mixtures (VV)

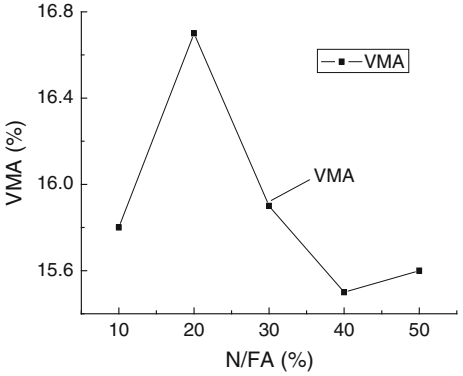


**Fig. 2** N/FA versus the total voids in mineral aggregate (VMA)

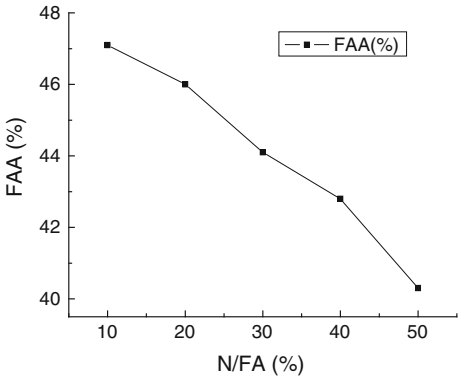


**Fig. 3** N/FA versus FAA
FAA

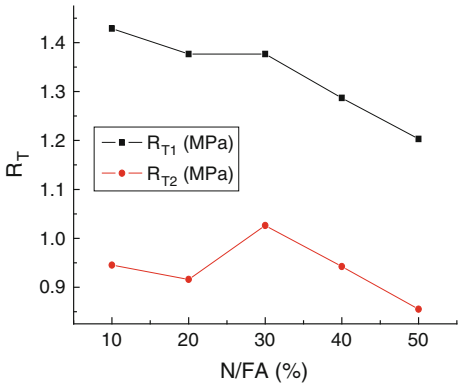


**Fig. 4** N/FA versus $R_T$

Several important trends from the results are observed, firstly, the FAA of the fine aggregates reduces considerably when the N/FA ratio increases and this trend is well expected as the increasing content of sand (with more rounded shapes) would

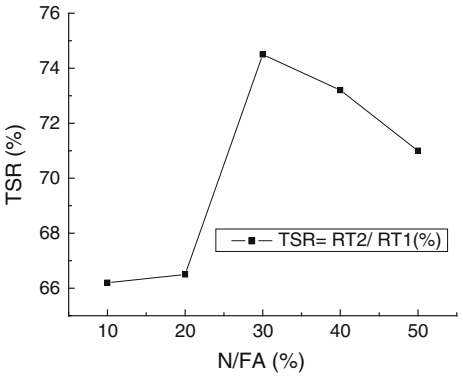


**Fig. 5** N/FA versus TSR

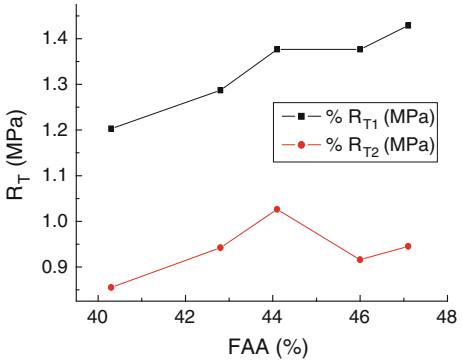


**Fig. 6** FAA versus $R_T$

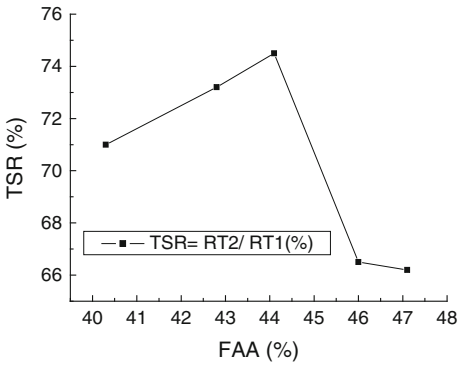


**Fig. 7** FAA versus TSR

reduce the overall angularity of the mixed fine aggregates. Secondly the split strengths ($R_{T1}$ and $R_{T2}$) and TSRs of the test samples varied significantly with the change in N/FA ratio, and it is shown that the optimum TSR (74.5 %) tends to be at the N/FA ratio of approximately 30 %, which corresponds to the ratio of natural

sand to total mineral aggregates of about 13.2 % and the associated FAA value is 44.1. Thirdly, the increase in FAA seems to enhance the split strengths (in a rather vague extent) but it shows the inability of enhancing the TSRs and subsequently the moisture susceptibility. Hence it is opined that the FAA is only a general indicator used to qualify the macro physical characteristic of fine aggregates, as there may be many other factors that may contribute to the behavior of the bituminous mixtures. The story is further complicated if different components are present (i.e. more angular aggregates and sand which is less angular).

## *2.6 Interpretation*

The shape of natural sand is generally rounder and the surface is usually smoother than the fine aggregates that are all composed of stone chips, so by varying the content of natural sand within the fine aggregates, the workability of the asphalt mixtures are expected to change accordingly. The most important factor of influencing the moisture susceptibility of asphalt mixtures, have been well recognised to be the (1) percent air voids in bituminous mixture which is affected by the workability of fresh-mix asphalt mixtures and (2) the adhering capacity between the bitumen and the aggregates.

A lower N/FA ratio is expected to produce a higher FAA, and the compaction of the bituminous mixtures would become difficult because of the poor workability, and the associated air void content is rather high and hence the TSR is rather low. With the increase in the value of N/FA ratio, the workability of the mixture would be higher and the compaction of the mixture could be correspondingly improved and thus the density of mixture would increase. Under such a condition, the volume of voids of the mixture would decrease and thus TSRs would increase correspondingly. When the N/FA ratio continually to increase, the workability of mixture would become higher and higher and finally it reaches a point that further increase in workability does not significantly reduce the Volume of Voids (i.e. change in VV (%) becomes steady and small) of the bituminous mixtures. At that point the TSR value would achieve the maximum value. Further decrease in air voids (i.e. due to the increase in workability) may not significantly affect the TSRs. Within such a range, the effect of varying air voids of mixture on changing the TSR value of mixture would not be significant. Whereas because of the increased content of the natural sand, and due to the relatively high overall roundness and smoothness of fine aggregates increase and thus it causes a reduction in the sorption of asphalt to the aggregates (last column of Table 5 refers). In the consequence of this, the proportion of adsorbed asphalt is reduced and in the meantime, the proportion of the free asphalt is increased correspondingly. As the bounding capacity of asphalt binder reduces, thus the moisture susceptibility becomes higher and hence the TSR decreases.

## 3 Conclusions and Recommendations

Several conclusions can be drawn after this study:

1. The composition of fine aggregates has apparent influence on the compaction characteristic of the bituminous mixture. The compacted characteristic and cohering characteristic of mixture that result from the variety of fine aggregate composition reduced the change of volume performance.
2. The existence of natural sand in the fine aggregates obviously cause variations on the FAA. However, it is considered that by viewing the FAA alone is not sufficient to justify or conclude on the possible performances of the subsequent bituminous mixtures formed (the moisture susceptibility is one example of the performance criteria under the study). Moreover, FAA may have different influences on the different performance criterion (rutting/fatigue, etc.) of the bituminous mixtures.
3. The composition of fine aggregate affects the moisture susceptibility of asphalt mixture in some degree. In a determined range, corresponding to the ratio of split strength of bituminous mixture, the N/FA ratio has an optimal value. This value is propitious to improve the workability of asphalt mixture and enhance the compacting degree of mixture, thus decrease the percent of air voids in asphalt mixture and reduce the moisture susceptibility. Further increase in N/FA ratio may cause a lower adhering ability between the bitumen and aggregate. For this study, the optimal value of N/FA is 30 %, approximately reach the 13 % in the total mineral aggregate.

The authors opine more detailed investigations are needed and worthwhile for further recommendations on the additional requirements of the fine aggregates (apart from gradation) used within the bituminous mixtures for construction of road pavement in Hong Kong.

## Bibliography

ASTM C1252-06 (2006), Standard Test Methods for Uncompacted Void Content of Fine Aggregate.

ASTM Designation D 1188-96 (2002), Standard Test Method for Bulk Specific Gravity and Density of Compacted Bituminous Mixtures Using Coated Samples. American Society for Testing and Materials.

ASTM Designation D4867/D4867 M-96 (2002), Standard Test Method for Effect of Moisture on Asphalt Concrete Paving Materials. American Society for Testing and Materials.

E.T. Harrigan, R.B. Leahy and J.S. Youtcheff. (1994), SHRP -A-379, The SUPERPAVE Mix Design System - Manual of Specifications, Test Methods, and Practices. Strategic Highway Research Program Strategic Highway Research Program, National Research Council, Washington, DC.

Jose Leomar fernandes, Reynaldo Roque, Mang Tia, etc (2000), Evaluation of Uncompacted Void Content of Fine Aggregate as A Quality Indicator of Materials used in Superpave Mixtures. Transportation Research Board 79th Annual Meeting. Washington, D.C.

Reed B. Freeman, Chun-Yi Kuo (1999), Quality Control for Natural Sand Content of Asphalt Concrete, Reed B. Freeman, Chun-Yi Kuo, Journal of Transportation Engineering.

The Specification of Construction Technique of Highway Asphalt Pavement (1994), People's Traffic Publishing Company, Beijing.

The Specification of Construction and Acceptance of Highway Asphalt Pavement (1994), People's Traffic Publishing Company, Beijing.

# Evaluation of Rutting Properties of Bituminous Binders by Means of Single Shear Creep-Recovery (SSCR) Tests and Correlation with Mixture Performance

**Ezio Santagata, Orazio Baglieri, Muhammad Alam and Pier Paolo Riviera**

**Abstract** One of the main distresses affecting asphalt pavements is rutting, which originates from the accumulation of permanent deformation caused by traffic loading. In order to prevent such a phenomenon, binders employed for the production of bituminous mixtures need to be selected by taking into account their temperature- and time-dependent behavior. In the experimental investigation presented in this paper, single shear creep-recovery (SSCR) tests were used to evaluate rutting properties of bituminous binders, of the unmodified and polymer-modified type, at various temperatures. Experimental results were compared with those derived from Flow Number (FN) tests carried out on bituminous mixtures prepared by employing the same binders. Analysis of experimental data revealed the existence of a strong correlation between rutting parameters of binders and permanent deformation response of mixtures. It was thus confirmed that the proposed testing procedure can be adopted for the evaluation of the rutting potential of bituminous binders and for their consequent performance-related ranking.

**Keywords** Rutting · Bituminous binders · Bituminous mixtures · Creep-recovery · Flow number

E. Santagata (✉) · O. Baglieri · M. Alam · P.P. Riviera
Department of Environment, Land and Infrastructure Engineering, Politecnico di Torino, 24, corso Duca degli Abruzzi, 10129 Turin, Italy
e-mail: ezio.santagata@polito.it

O. Baglieri
e-mail: orazio.baglieri@polito.it

M. Alam
e-mail: muhammad.alam@polito.it

P.P. Riviera
e-mail: pierpaolo.rivera@polito.it



F. Canestrari and M.N. Partl (eds.), *8th RILEM International Symposium on Testing and Characterization of Sustainable and Innovative Bituminous Materials*, RILEM Bookseries 11, DOI 10.1007/978-94-017-7342-3_60

## 1 Introduction

Rutting represents one of the main distresses affecting asphalt pavements. It derives from the accumulation of permanent deformation caused by repeated axle loadings which can be significantly enhanced at high in-service temperatures and under the effects of heavy slow-moving vehicles. Such a phenomenon is relevant in the context of pavement design and management, since formation of ruts leads to a reduction of comfort and safety perceived by road users.

In the occurrence of permanent deformation in bitumen-bound layers, binders play a major role due to their temperature- and time-dependent behavior (Cooper et al. 1985; Sousa et al. 1991). As a consequence, they need to be selected by referring to the results of reliable laboratory tests, capable of capturing their non-reversible strain response under loading and of yielding a truly performance-related ranking.

The original approach proposed in the SHRP research project, based on visco-elastic parameter $G^*/\sin\delta$ (Harrigan et al. 1994; Anderson et al. 1994), was found to be inadequate in evaluating the real anti-rutting potential of bituminous binders, especially in the case of polymer-modified products (Bahia et al. 2010; D'Angelo and Dongre 2002). A number of studies were carried out by researchers worldwide to overcome the limitations of such an approach (Bahia et al. 2010; D'Angelo et al. 2007; Santagata et al. 2013) and as a result of these efforts, several standard methods are currently available for the assessment of rutting properties of bituminous binders. These standards include:

- AASHTO TP70-10 (2010), which describes the Multiple Stress Creep-Recovery (MSCR) test protocol;
- CEN/TS 15325 (2008), which defines the procedure for determination of Zero-Shear Viscosity (ZSV);
- CEN/TS 15324 (2008), which focuses on determination of Equi-Viscous Temperature (EVT) based on the LSV concept.

More recently, Santagata et al. (2014) proposed a novel test procedure involving the use of single shear creep-recovery (SSCR) tests carried out at different temperatures and at predefined loading and recovery times. Results obtained on a wide set of materials confirmed the effectiveness of the procedure in discriminating high-temperature characteristics of bituminous binders of different types and origin. Moreover, synthetic information on resistance to flow was obtained by referring to a new control parameter, the so-called creep compliance rate (CCR), which was found to be adequate for the purpose of performance-related ranking.

The goal of the experimental investigation reported in this paper was to further verify the validity of the abovementioned test method by comparing experimental results obtained for several bituminous binders with those derived from permanent deformation tests carried out on corresponding mixtures.

## 2 Materials and Methods

Bituminous binders employed in the experimental investigation included two unmodified bitumens (B1 and B2) and one polymer-modified binder (P1), originated from base bitumen B1 by adding a high percentage of styrene-butadiene-styrene co-polymer (SBS) according to a patented processing scheme.

All binders were subjected to testing in short-term aged conditions after being treated with the Rolling Thin Film Oven Test (RTFOT) in accordance with AASHTO T240 (2009). Preliminary rheological tests were carried out in the oscillatory shear loading mode in order to determine their upper limiting performance grade (PG) temperatures ($T_{PG-U}$, corresponding to G*/sin δ equal to 2.2 kPa). Obtained results are listed in Table 1.

Rutting properties of binders were assessed by means of SSCR tests, performed by adopting a protocol very similar to that previously developed by Santagata et al. (2014). Such a protocol is composed by a single creep phase followed by a recovery phase, during which the variation of shear strain is monitored as a function of time.

In the investigation described in this paper, measurements were carried out at four temperatures (ranging from 46 to 64° in the case of bitumens B1 and B2, from 58 to 76 °C in the case of binder P1) at a single stress level (equal to 100 Pa). At least two replicates were run at each temperature and average data were considered in the analysis.

Duration of creep and recovery phases was set by making sure they would allow materials to reach steady-state flow conditions under loading and to recover most of the delayed elastic deformation after load removal. Unmodified binders were expected to flow quite quickly at the selected test temperatures, whereas in the case of the polymer-modified binder it was anticipated that achievement of steady-state conditions would require very long creep and recovery times as a result of its internal rubber-like structure. On the basis of past experience, test conditions summarized in Table 2 were adopted in the present study.

SSCR tests were carried out by means of a stress-controlled dynamic shear rheometer (DSR), equipped with a permanent magnet synchronous drive (minimum torque = 0.1 μ Nm, torque resolution < 0.1 μ Nm) and an optical incremental encoder for the measurement of angular rotation (resolution < 1 μ rad). The standard 25 mm parallel plates geometry was employed with 1.0 mm gap.

For each binder, a corresponding mixture (indicated as M-B1, M-B2 and M-P1) was prepared in the laboratory by making use of mineral siliceous aggregates

**Table 1** Upper limiting PG temperatures

| Binder code | Description | $T_{PG-U}$ (°C) |
|---|---|---|
| B1 | Unmodified | 68.3 |
| B2 | Unmodified | 66.0 |
| P1 | Modified with SBS | 81.7 |

**Table 2** SSCR test conditions

| Binder code | Temperature (°C) | Duration of testing phases (s) (Creep + Recovery) |
|---|---|---|
| B1, B2 | 46 | (600 + 1800) |
| | 52 | (240 + 600) |
| | 58 | (180 + 480) |
| | 64 | (120 + 360) |
| P1 | 58 | (10,800 + 43,200) |
| | 64 | (1800 + 21,600) |
| | 70 | (600 + 10,800) |
| | 76 | (300 + 7200) |

provided by a local contractor and Portland cement filler. The job mix formula adopted for all mixtures was defined by referring to acceptance limits given in Italian technical specifications for dense-graded wearing courses (CIRS 2001), with a maximum aggregate diameter of 16 mm. Reconstruction of target size distribution of aggregates was made by subjecting available fractions to washed sieve separation and by thereafter combining single-size fractions in the needed quantities. Binder dosage was set at 5.5 % by weight of dry aggregates.

Permanent deformation properties of bituminous mixtures were investigated by means of Flow Number (FN) tests, performed by means of the Asphalt Mixture Performance Tester (AMPT) in accordance with AASHTO TP 79 (2009). During these tests, cumulative permanent strains ($\varepsilon_p$) developed in cylindrical specimens as a consequence of repeated compressive loads are recorded as a function of the number of loading cycles (N). From the N-$\varepsilon_p$ plots derived from experimental data, three typical stages of creep behavior can be clearly identified, and in particular, the number of loading cycles required to initiate the final phase of tertiary creep, which leads to failure, is indicated as Flow Number (FN). On the basis of extensive research carried out under NCHRP project 9-19 (Witczak et al. 2002), such a parameter has been recommended as a valid indicator of the aptitude of bituminous mixtures to resist to the accumulation of permanent deformation (Witczak 2005).

In the present investigation, tests were carried out at three temperatures (46, 52 and 58 °C), with a repeated axial stress of 600 kPa and no lateral confinement. For all mixtures, three replicates were run at each test temperature and average results were considered in the analysis.

Test temperatures were selected in order to have a wide overlap with those employed for SSCR tests carried out on unmodified bitumens B1 and B2. However, higher test temperatures, which would have matched conditions adopted for characterization of binder P1, were not included in the testing program due to time constraints.

Even though it was proven that lateral confinement of test specimens provides a better simulation of stress conditions which occur in the field, in the present study FN tests were carried out with no confinement for practical reasons, mainly related

to the need of limiting total testing time. In fact, by increasing the level of confining pressure, resistance of mixtures to flow may significantly increase, resulting in very long test durations. Moreover, it was shown that in some cases deformation may not reach the tertiary creep stage, making determination of FN impossible (Bonaquist 2008). Finally, it should be mentioned that it was reported that tests carried out in confined conditions may lead to poor repeatability of test results, which have been found to be extremely sensitive to sample preparation (Bonaquist 2010).

Test specimens (100 mm diameter, 150 mm height) used in the AMPT were obtained from larger cylindrical samples (150 mm diameter, 170 mm height) prepared with the Gyratory Shear Compactor (GSC) by following instructions provided by AASHTO PP 60 (2011). In particular, over-height gyratory samples were compacted by employing the mixture mass needed to reach target air voids content, which in this study was set equal to 5.6 ± 0.5 %. 100 mm cores were then extracted from the center of gyratory samples by using a diamond coring stand. Finally, core ends were trimmed by means of a masonry saw in order to obtain smooth and parallel end surfaces.

Before FN tests, volumetric properties of specimens (air voids content v, voids in mineral aggregates VMA, voids filled with asphalt VFA) were determined in accordance with EN 12697-8 (2003). In addition, theoretical maximum density (TMD) was measured by means of the pycnometer method described in EN 12697-5 (2009). Average results of volumetric characterization are reported in Table 3.

It was observed that actual air voids of compacted mixtures were very close to the target value and that all remaining volumetric parameters were very similar for all materials. As discussed in the following, this aspect is of crucial importance for the purpose of the investigation since it allowed binder effects on permanent deformation of mixtures to be clearly highlighted.

## 3 Results and Discussion

### *3.1 SSCR Tests on Binders*

Examples of experimental data gathered from SSCR tests are given in Figs. 1 and 2, where shear strains (γ) measured during creep and recovery phases are plotted as a function of time (t). Figure 1 provides a comparison between the response of unmodified bitumens (B1 and B2) and that of the polymer-modified one (P1) at a

**Table 3** Volumetric characteristics of bituminous mixtures

| Mixture code | v (%) | VMA (%) | VFA (%) | TMD (g/cm$^3$) |
|---|---|---|---|---|
| M-B1 | 5.65 | 18.3 | 69.2 | 2.514 |
| M-B2 | 5.63 | 18.3 | 69.2 | 2.504 |
| M-P1 | 5.77 | 18.5 | 68.8 | 2.519 |

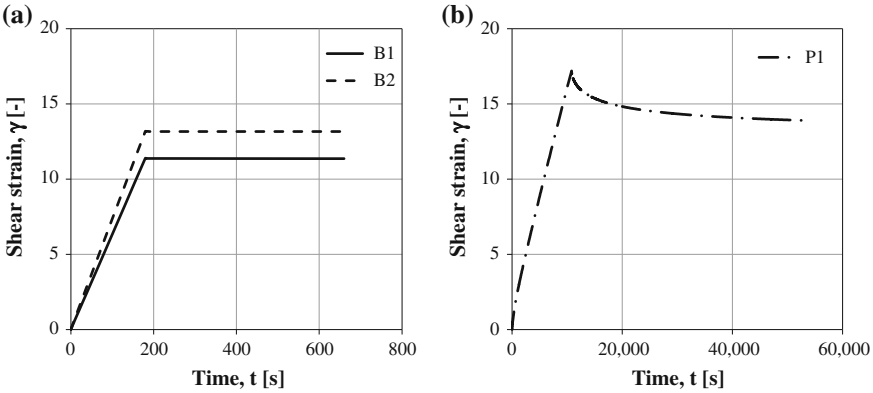


**Fig. 1** Results of SSCR tests at 58 °C: **a** unmodified bitumens, **b** polymer-modified binder

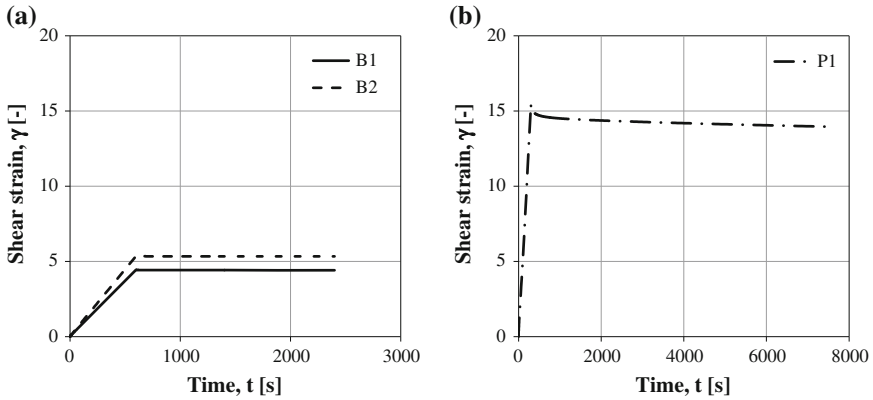


**Fig. 2** Results of SSCR tests: **a** unmodified bitumens at 46 °C, **b** polymer-modified binder at 76 °C

common test temperature (equal to 58 °C), while Fig. 2 displays their behavior at the lowest temperature investigated for unmodified bitumens (46 °C) and at the highest one considered for the polymer-modified binder (76 °C).

As expected, regardless of test temperature, t-ε curves of unmodified binders exhibited an almost constant slope throughout the creep phase, revealing the achievement of viscous flow in a very short loading time. In the case of the polymer-modified binder, initial curvature associated to the presence of an internal rubber-like network was found to gradually smoothen out for increasing test temperatures. However, in all cases duration of the creep phase was sufficient to reach a final linear trend, indicating for this material the achievement of steady state conditions.

Analysis of data corresponding to the unloading phase highlighted a pronounced delayed elasticity in the case of binder P1, which recovered a significant portion of total strain experienced under loading, especially at lower test temperatures. On the contrary, recovered strain recorded for binders B1 and B2 was negligible at all test temperatures, as demonstrated by the presence of a horizontal trend in the t-ε curve after load removal.

From the final linear portion of time-strain loading curves, creep compliance rate (CCR) values were calculated as follows:

$$\mathrm{CCR} = \frac{\mathrm{d}\left(\frac{\gamma}{\tau_0}\right)}{\mathrm{dt}} = \frac{\mathrm{dJ}}{\mathrm{dt}} \tag{1}$$

where $\gamma$ is shear strain, $\tau_0$ is applied stress, and J is creep compliance.

In Fig. 3, CCR values calculated for the three binders are plotted against test temperature in the semi-logarithmic scale. It was observed that for each binder, experimental data can be approximated by a linear function: with such a representation a clear distinction can be made between unmodified (B1 and B2) and polymer-modified (P1) materials. In terms of ranking, at all temperatures binder P1 yielded the lowest CCR value, which corresponds to the highest resistance to flow (i.e. to the highest anti-rutting potential). Small differences were detected when comparing the two unmodified binders. However, binder B1, characterized by a higher $T_{PG-U}$ value (Table 1), also showed lower CCR values at all test temperatures.

## 3.2 FN Tests on Mixtures

Typical response curves obtained from FN tests carried out on bituminous mixtures considered in the investigation are shown in Figs. 4 and 5, where cumulative axial strain ($\varepsilon_p$) is plotted as a function of number of loading cycles (N). Figure 4 displays

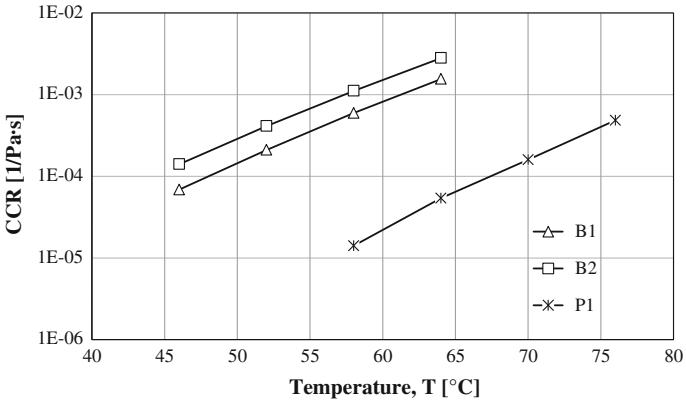


**Fig. 3** CCR values as a function of test temperature

experimental data obtained at a common test temperature (equal to 58 °C) for all mixtures, while Fig. 5 provides a comparison between curves recorded at different temperatures for mixture M-B1.

In each graph, the three classical stages of creep behavior can be clearly identified. The primary stage is characterized by a rate of strain that decreases as the number of loading cycles increases. During the subsequent secondary stage, rate of strain remains almost constant with increasing load repetitions. In the final stage (tertiary flow) strain rate rises dramatically, leading to test specimen failure.

In this study, FN values were calculated by making use of the Francken model, recently introduced in AMPT data analysis (Biligiri et al. 2007; Dongrè et al. 2009) due to its effectiveness and consistency in fitting experimental data (Bonaquist 2008). Average FN values calculated for considered mixtures at the three test temperatures are represented in Fig. 6.

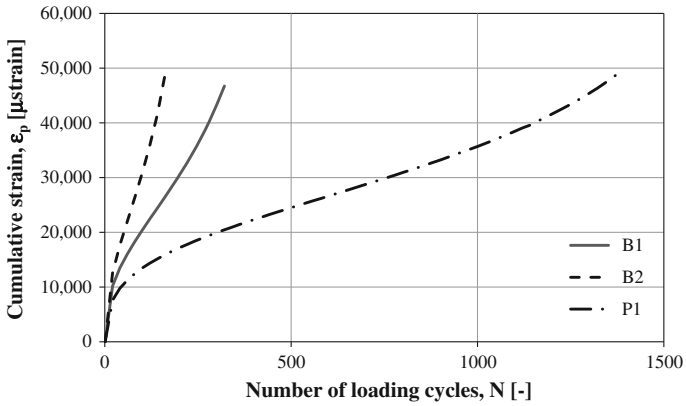


**Fig. 4** Results of FN tests carried out at 58 °C on all bituminous mixtures

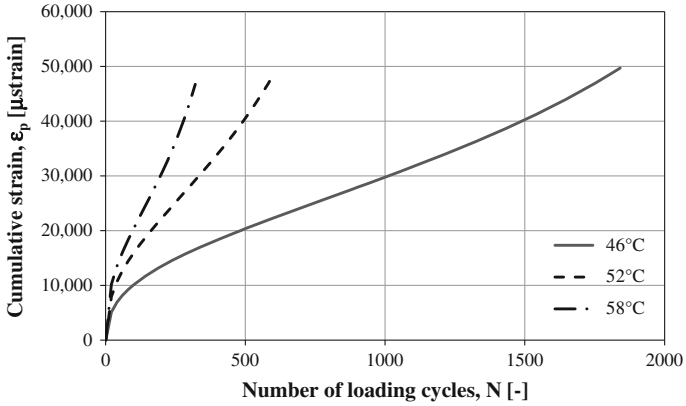


**Fig. 5** Results of FN tests carried out on mixture M-B1 at all test temperatures

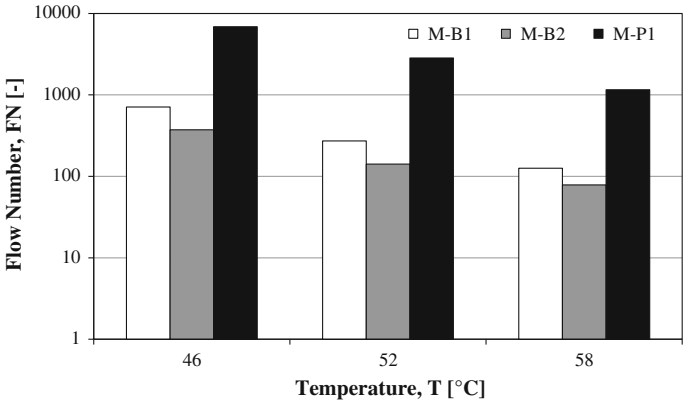


**Fig. 6** FN values as a function of test temperature

As expected, mixture M-P1 containing the polymer-modified binder exhibited the highest FN values at all test temperatures, with differences with respect to mixtures containing unmodified binders (M-B1 and M-B2) of one order of magnitude. Minor differences were also observed between mixtures M-B1 and M-B2, the former proving to be slightly more resistance to accumulation of permanent deformation. These observations are coherent with those which were made while analyzing SSCR test results, with the same relative ranking of considered materials.

## *3.3 Relationship Between Binder and Mixture Data*

CCR values obtained for binders from SSCR tests are represented in Fig. 7 as a function of FN values derived from tests carried out on the corresponding bituminous mixtures at the same test temperatures. It should be considered that SSCR tests were not performed on binder P1 at 46 and 52 °C as a result of the unpractical, too long loading and unloading durations. Corresponding CCR values were extrapolated from those recorded at higher temperatures by fitting a linear relationship to temperature-CCR data represented in the semi-log scale (Fig. 3).

Data points plotted in Fig. 7 show that a strong relationship was found between CCR and FN, with the presence in the log-log scale of a single linear decreasing trend (represented as a dashed line) which does not depend upon binder origin or type. A single power-law function can therefore be fitted to these data.

Since FN can be considered as a reliable indicator of rutting resistance, obtained results suggest that accumulation of permanent deformation in bituminous mixtures, for given composition and volumetrics, is governed by rutting properties of the binder phase as measured by SSCR tests. This finding provides evidence of the effectiveness of the proposed test protocol in capturing relevant

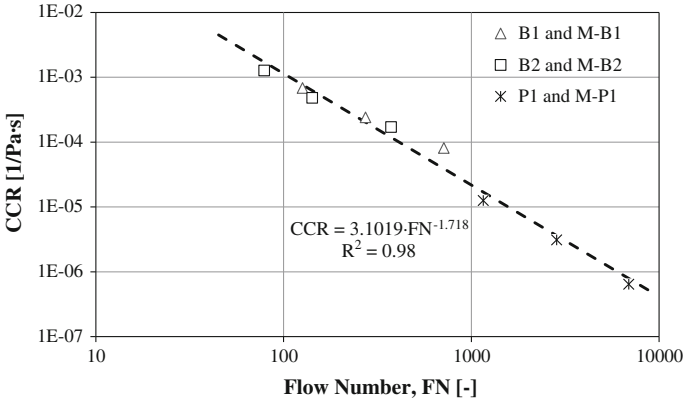


**Fig. 7** Relationship between CCR and FN

aspects of binder rheology and in providing a true performance-related binder ranking.

Finally, it should be pointed out that test results suggest that the CCR determined for binders may have the potential of being employed for the prediction of the FN of corresponding mixtures. For the composition and volumetrics considered in the investigation, this is shown in Table 4, where measured FN values are compared to those predicted from the power-law function fitted to the data plotted in Fig. 7. Overall, predictions can be considered satisfactory. This can be deduced by listed values of percent relative errors ($E_{FN}$%), which in most cases were found to be comprised within the range defined by the minimum and maximum percent deviation of measured values from the mean ($FN_{\Delta range}$%).

**Table 4** Comparison between measured and predicted FN values of bituminous mixtures

| Mixture code | Temperature (°C) | $FN_{measured}$ | $FN_{predicted}$ | $E_{FN}$% (%) | $FN_{\Delta range}$% (%) |
|---|---|---|---|---|---|
| M-B1 | 46 | 715 | 465 | −34.9 | −12.4 to +11.2 |
| | 52 | 274 | 250 | −8.8 | −17.4 to +18.0 |
| | 58 | 126 | 138 | 9.0 | −11.3 to +10.8 |
| M-B2 | 46 | 374 | 304 | −18.7 | −1.6 to +2.7 |
| | 52 | 142 | 169 | 18.4 | −15.0 to +29.3 |
| | 58 | 79 | 96 | 22.1 | −21.5 to +29.1 |
| M-P1 | 46 | 6914 | 7387 | 6.9 | −15.6 to +29.7 |
| | 52 | 2851 | 3008 | 5.5 | −14.0 to +9.7 |
| | 58 | 1160 | 1351 | 16.5 | −4.8 to +6.5 |

## 4 Conclusions

In the experimental study described in this paper, rutting properties of different bituminous binders and those of corresponding mixtures characterized by common composition and volumetrics were investigated and compared. Single shear creep-recovery (SSCR) tests were carried out on binders for the determination of their creep compliance rate (CCR), whereas bituminous mixtures were evaluated by referring to their Flow Number (FN), derived from repeated compressive loading tests carried out with the Asphalt Mixture Performance Tester (AMPT).

Analysis of experimental data showed that binders and mixtures were identically ranked in terms of their potential rutting performance. In particular, the superior performance of the polymer-modified binder and of its corresponding mixture was clearly highlighted.

A single relationship independent from binder origin and type was found between CCR and FN, thus confirming the effectiveness of the SSCR test protocol in capturing the contribution of the binder phase to accumulation of permanent deformation in mixtures. Moreover, the potentiality of employing CCR values for the prediction of FN was preliminarily explored with a satisfactory outcome.

Based on obtained results, it is envisioned that future research will focus on the validation and generalization of the abovementioned CCR-FN relationship. This will require an extension of the database to include a wider array of binders and to consider effects associated to variations in composition and volumetrics of bituminous mixtures. A comparison with results obtained from other tests carried out on binders and mixtures will also be performed in order to fully assess the advantages and/or drawbacks of the proposed characterization procedure.

## References

AASHTO TP79 (2009) Standard method of test for determining the dynamic modulus and flow number for hot mix asphalt (HMA) using the asphalt mixture performance tester (AMPT). American Association of State Highway Transportation Officials, Washington, DC.

AASHTO T240 (2009) Effect of heat and air on a moving film of asphalt binder (Rolling Thin-Film Oven Test). American Association of State Highway Transportation Officials, Washington, D.C.

AASHTO TP70 (2010) Multiple stress creep recovery (MSCR) test of asphalt binder using dynamic shear rheometer (DSR). American Association of State Highway Transportation Officials, Washington, D.C.

AASHTO PP60 (2011) Standard practice for preparation of cylindrical performance test specimens using the SUPERPAVE gyratory compactor (SGC), American Association of State Highway Transportation Officials, Washington, D.C.

Anderson DA, Christensen DW, Bahia HU, Dongre R, Sharma MG, Antle CE (1994) Binder characterization and evaluation. Volume 3: Physical characterization. SHRP Report A-369. Strategic Highway Research Program, Transportation Research Board, National Research Council, Washington, D.C.

Bahia HU, Hanson DI, Zeng M, Zhai H, Khatri MA, Anderson RM (2010) Characterization of modified asphalt binders in Superpave mix design. NCHRP Report 459. National Cooperative Highway Research Program, Transportation Research Board, National Research Council, Washington, D.C.

Biligiri KP, Kaloush KE, Mamlouk MS, Witczak MW (2007) Rational modeling of tertiary flow for asphalt mixtures. Transportation Research Record 2001: 63-72.

Bonaquist R (2008) Ruggedness testing of the dynamic modulus and flow number tests with the simple performance tester. NCHRP Report 629. National Cooperative Highway Research Program, Transportation Research Board, National Research Council, Washington, D.C.

Bonaquist R (2010) Wisconsin mixture characterization using the asphalt mixture performance tester (AMPT) on historical aggregate structure. WHRP Report 09-03. Wisconsin Highway Research Program, Wisconsin Department of Transportation, Madison, WI.

CEN/TS 15324 (2008) Bitumen and bituminous binders. Determination of equiviscous temperature based on low shear viscosity using dynamic shear rheometer in low frequency oscillation mode. European Committee for Standardization, Brussels, Belgium.

CEN/TS 15325 (2008) Bitumen and bituminous binders. Determination of Zero Shear Viscosity (ZSV) using a shear stress rheometer in creep mode. European Committee for Standardization, Brussels, Belgium.

CIRS (2001) Performance-related technical specification for the construction and maintenance of road pavements. Inter-University Road Research Center, Ancona, Italy (in Italian).

Cooper KE, Brown SF, Pooley GR (1985) The design of aggregate gradings for asphalt base course. Journal of the Association of Asphalt Paving Technologists 54: 324-346.

D'Angelo J, Dongre R (2002) Superpave binder specifications and their relationship to modified binders. Paper presented at the 47th Canadian Technical Asphalt Association Annual Meeting, Calgary, Canada, 18-20 November 2002.

D'Angelo J, Kluttz R, Dongre R, Stephens K, Zanzotto L (2007) Revision of the Superpave high temperature binder specification: the multiple stress creep recovery test. Journal of the Association of Asphalt Paving Technologists 76: 123-162.

Dongré R, D'Angelo J, Copeland A (2009) Refinement of flow number as determined by asphalt mixture performance tester. Transportation Research Record 2127: 127-136.

EN 12697-8 (2003) Test methods for hot mix asphalt. Determination of void characteristics of bituminous specimens. European Committee for Standardization, Brussels, Belgium.

EN 12697-5 (2009) Test methods for hot mix asphalt - Part 5: Determination of the maximum density. European Committee for Standardization, Brussels, Belgium.

Harrigan ET, Leahy LB, Youtcheff JS (1994) The Superpave mix design system. Manual of specifications, test methods, and practices. SHRP Report A-379. Strategic Highway Research Program, Transportation Research Board, National Research Council, Washington, D.C.

Santagata E, Baglieri O, Dalmazzo D, Tsantilis L (2013) Evaluation of anti-rutting potential of polymer modified binders by means of creep-recovery tests. Material and Structures 46(10): 1673-1682.

Santagata E, Baglieri O, Alam M, Dalmazzo D (2014) A novel procedure for the evaluation of anti-rutting potential of asphalt binders. International Journal of Pavement Engineering. DOI:10.1080/10298436.2014.942859

Sousa JB, Craus J, Monismith CL (1991) Summary report on permanent deformation in asphalt concrete. SHRP Report A/IR-91-104. Strategic Highway Research Program, Transportation Research Board, National Research Council, Washington, D.C.

Witczak MW (2005) Simple performance tests: summary of recommended methods and database. NCHRP Report 547. National Cooperative Highway Research Program, Transportation Research Board, National Research Council, Washington, D.C.

Witczak MW, Kaloush K, Pellinen T, El-Basyouny M, von Quintus H (2002) Simple performance tests for pavement Superpave mix design. NCHRP Report 465. National Cooperative Highway Research Program, Transportation Research Board, National Research Council, Washington, D.C.

# Mechanisms of Failure in Uniaxial Repeated Creep Test and the Relationship to Aggregate Packing

**Nima Roohi Sefidmazgi and Hussain U. Bahia**

**Abstract** Rutting performance characterization of asphalt mixtures has attracted lots of attentions after the Strategic Highway Research Program (SHRP). The main reason is the lack of a stability or strength test in the Superpave volumetric criteria. Different test methods and analysis have been proposed with a goal of accurately as well as simply predicting the rutting performance of designed mixtures. A uniaxial repeated creep and recovery test is recommended in NCHRP 456 report (i.e. Flow number test) as a performance characterization test method, and it is currently being used by researchers extensively. This study is focused on comparing the mechanisms and fundamental properties that control the performance of asphalt mixtures throughout the uniaxial flow number testing. It is shown that aggregate packing, as measured using an image analysis method, is the key property affecting deformation characteristics in uniaxial testing. Additionally, it is shown that the main cause of tertiary flow of mixtures in the flow number test is structural instability and bulging (dilation) of aggregate skeleton. Aggregate skeleton discontinuities at outer layers of samples are observed after failure in the tertiary zone. It is observed that mixtures with better aggregate packing showed a better rutting performance due to lower stress level within the binder phase due to aggregate skeleton serving as the main stress path, and the aggregates in proximity or contact showed a supporting structure, which delays the tertiary flow in material, and reduces the rate of permanent deformation. Based on these observations, it is shown that applying confinement has a very significant effect in preventing tertiary flow conditions by maintaining the aggregate packing, thus improving rutting resistance of asphalt mixtures.

**Keywords** Flow number · Rutting · Aggregate packing · Image analysis · Asphalt mixture

N.R. Sefidmazgi (✉)
Green Asphalt LLC, Long Island City, USA
e-mail: nroohi@greenasphaltco.com

H.U. Bahia
University of Wisconsin-Madison, Madison, USA
e-mail: hubahia@facstaff.wisc.edu



F. Canestrari and M.N. Partl (eds.), *8th RILEM International Symposium on Testing and Characterization of Sustainable and Innovative Bituminous Materials*, RILEM Bookseries 11, DOI 10.1007/978-94-017-7342-3_61

## 1 Introduction

Rutting in asphalt pavements can be defined as excessive accumulation of permanent deformation as the loading cycles increase in wheel path. The two principal mechanisms involved in rutting distress are densification and shearing deformation of one, or several pavement layers. Densification controls rutting in pavements with insufficient level of compaction and typically happens when the pavement is opened to traffic after construction; on the other hand, shearing deformation is the main cause of rutting distress in properly compacted pavements (Witczak and Kaloush 2002). The Accumulation of permanent deformation in pavement layer is maximum at the surface and decreases gradually with depth; this reduction could be due to the increase in confining pressure in deeper layers and decrease in shear stress as increasing the depth of pavement layer. The study by Witczak and Kaloush (2002) showed that rutting mainly happens as in shearing deformation due to the lateral movement of asphalt mixture. They tested asphalt mixtures both in repeated as well as constant creep and reported the accumulation of permanent deformation during loading can be classified into three zones:

- Primary zone: The permanent deformation accumulates rapidly in this zone. The main mechanism occurs is densification and reduce in volume.
- Secondary zone: The rate of permanent deformation accumulation reaches a constant value (the cumulative permanent deformation vs. number of cycles of loading plot becomes linear in this zone).
- Tertiary zone: The rate of accumulation increases and the material begins plastic flow with constant volume (as reported by Witczak and Kaloush 2002).

In repeated creep test, the cycle number in which tertiary flow begins is referred to as 'Flow Number' representing the rutting performance of mixture.

## 2 Uniaxial Test

The uniaxial testing method includes a cylindrical sample, with 100 mm diameter and 150 mm height (Fig. 1) that is tested under a haversine mode of repeated loading. Load is applied in pulses with a 0.1 s of duration followed by 0.9 s of rest. Linear Variable Differential Transformers (i.e., LVDTs) are used in order to measure the cumulative axial and radial deformation of sample. The test is performed in a temperature controlled chamber, which allows testing at different temperatures.

Current mix design procedures are focused on determining a design asphalt content to achieve a target density and volumetric characteristics. However, several studies carried out on laboratory and field produced mixtures, have shown that mixes with same density can provide significantly different rutting resistance

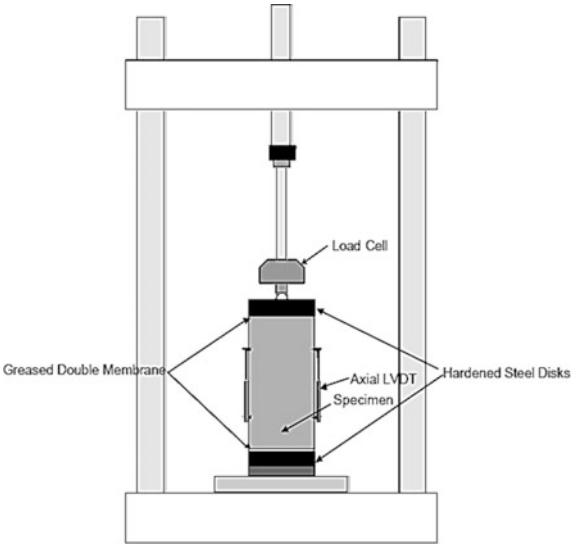


**Fig. 1** The permanent deformation test setup (after Faheem et al. 2004)

(Anderson 2002; Faheem and Bahia 2004; Roohi et al. 2012). For this reason, to achieve the expected mixture's performances, a selection of design parameters based on deeper assessment of the fundamental mixes properties that influence rutting performance, is needed.

At high service temperatures of pavements, the asphalt binder becomes relatively soft which lessens the load bearing capabilities of viscoelastic phase in mixture. Therefore, the aggregate structure is the effective skeleton resisting permanent deformation of asphalt mixtures at high service temperatures. Applying this concept, researchers has tried to characterize rutting performance of asphalt mixtures indirectly (comparing to direct mechanical testing), using indices and characteristics representing the quality of aggregate structure (Nguyen et al. 2009; Olard et al. 2010, 2012; Roohi et al. 2012; Coenen et al. 2012).

Microstructure of asphalt mixtures can be characterized using digital visualization (i.e. image processing). Analysis of digital images can be performed very efficiently today using readily available software, and can be applied to represent mixture characteristics that are more fundamentally related to mechanical performance (Masad et al. 1998, 1999; Yue et al. 1995; Shashidar et al. 2000; Tashman et al. 2007; Wang et al. 2004; Coenen et al. 2012; Roohi et al. 2012). Researchers have reported correlation between the aggregate structure indices for asphalt mixture and corresponding rutting performance (i.e. mechanical testing, SGC measured characteristics, imaging and microstructural analysis) (Anderson 2002; Roohi et al. 2012; Bahia et al. 1998). However there is still a gap of knowledge on understanding the mechanisms controlling the behavior and failure of material in rutting characterization test methods and interrelations between these mechanisms and testing results.

## 3 Objectives

The objective of this study is to understand the main mechanisms controlling the behavior and failure of asphalt mixtures during mechanical cyclic loading and relating the mechanisms to microstructural characteristics measured from 2-Dimensional image analysis.

## 4 Experimental Design

In this study, four different mixtures are designed and compacted up to target air void of 7 ± 0.5 %. Two relatively coarse (mix 1) and fine (mix 2) mixtures and a Stone-Mastic asphalt (SMA) mixture with neat and modified binder (Fig. 2) have been designed for the purpose of this study from a granite aggregate source commonly used for HMA production in Wisconsin. The optimum asphalt content of mixtures are 5.5, 5.4, and 5.4 % for Coarse, Fine, and SMA mixtures, respectively. The binders used for mixtures production is PG 64-22. The SMA mixture has been produced with neat asphalt binder and the neat asphalt blended with 0.3 % of polymer modifier and 0.4 % (by weight of binder) of fiber.

## 5 Failure Behavior in Dense Graded Mixtures

In a previous study, it is shown by Roohi et al. (2012) that there is a good correlation between aggregate structure indices (i.e. Total Proximity Length, TPL) with rutting performance (i.e. uniaxial Flow Number, FN) of mixtures produced with

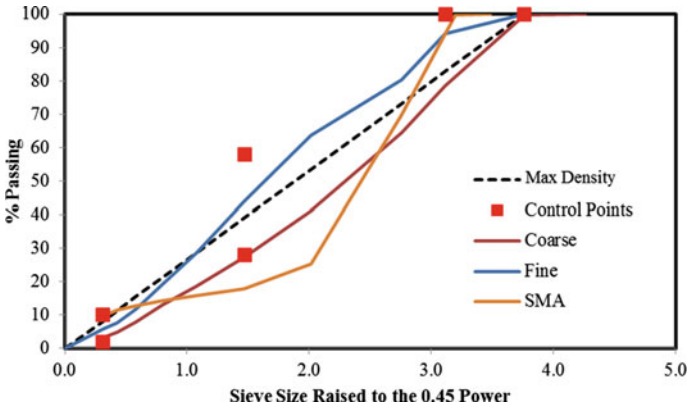


**Fig. 2** Gradations of mixtures

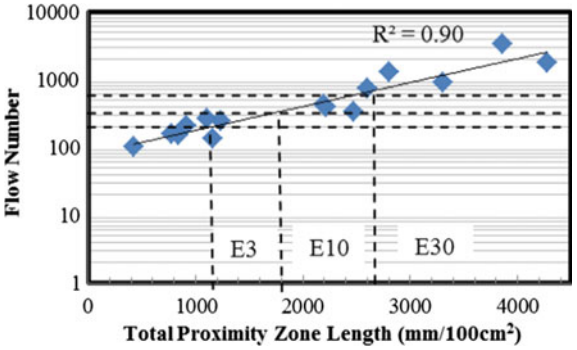


**Fig. 3** Correlation between TPL and flow number (Roohi et al. 2012)

different gradations, aggregate sources, and binder modifications (Fig. 3). However, the mechanism through which a higher aggregate packing represented by TPL leads to higher performance (i.e. FN) was still unknown. In order to understand the relation between aggregate packing and rutting performance (i.e. FN), a deeper understanding of failure in flow number test both in uniaxial and triaxial conditions is needed.

For the purpose of this study, flow number samples were prepared for the fine and coarse mixtures labeled here as mix 1 and 2 respectively. The objective was to track the change in aggregate packing and density during cyclic loading process until after failure of mixtures. Two replicate samples were tested for each mixture type to determine the flow number, and capture the different zones of behavior (i.e. primary, secondary, and tertiary zone), at the temperature of 46 °C with an axial stress level of 600 kPa. Based on the flow number test results, three numbers of loading cycles are selected to represent the primary zone, the initial stage of secondary zone, and the final loading cycles of secondary zone. The samples are loaded to the selected number of cycles and the internal structure and density were measured after testing. These results were compared with the structure and density for the unloaded and the failed samples. The permanent deformation results for each mixture types are shown in Fig. 4.

Densities of samples were measured before and after testing. The results are presented in Table 1. All samples are within the target air void of 7 ± 0.5 % before testing. It is shown that throughout loading cycles, the air void content of samples is reduced prior to start of tertiary zone. A significant densification happened in samples during the loading process; however, the air void content of samples is increased drastically in tertiary zone. This can be explained due to the significant bulging and cracks observed on the outer surface of samples. According to the literature, the main mechanism of deformation happening in the primary zone is densification. However, the dominant deformation mechanism in the secondary zone is shearing of material due to minimal change in density. This shearing deformation happens with a constant rate until a cycle of loading after which sever instability can be observed in material behavior (i.e. Flow number) with high permanent deformation. The air void contents before and during loading confirms

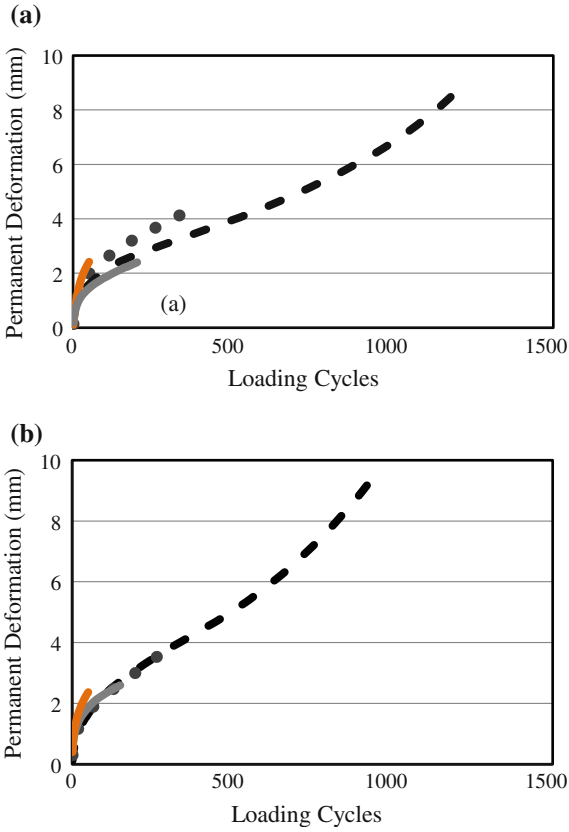


**Fig. 4** Permanent deformation for cyclic creep and recovery testing of: **a** mix 1, **b** mix 2

the fact that the main portion of densification happens in primary zone. Although some researchers have defined tertiary flow to happen with a constant density (Witczak and Kaloush 2002), it is observed that the density of samples reduced due to severe bulging and disintegration of material at samples outer layers in uniaxial testing performed in this study.

After density measurements, all samples are cut and scanned for image analysis using IPAS2 software (Roohi et al. 2012). The first observation made out of sliced samples is that, mainly the bulging of material and increase in air void after failure happened close to outer side of samples. Therefore, there are relatively minimal flaws, increase in air void sizes or any types of cracks observed as going from outside to middle of samples (Fig. 5).

All images obtained from samples are analyzed for TPL calculation. The image analysis results showed that, there is an increase in TPL during primary zone that densification happened for both mix 1 and 2. However, after primary zone (i.e. during secondary and tertiary zone) the TPL is reduced for both types of mixtures (Fig. 6). The final TPL measured for mix 1 and mix 2 after failure are 1689.9 and 1305.0 mm/100 $cm^2$. The comparison between the TPL after failure for mix 1 and

**Table 1** Air void measurements before and after loading

| Mix 1 | Air void (%) | | Mix 2 | Air void (%) | |
|---|---|---|---|---|---|
| Load cycles | Before loading | After loading | Load cycles | Before loading | After loading |
| 0 | 7.5 | – | 0 | 7.4 | – |
| 50 | 7.4 | 6.7 | 50 | 7.3 | 6.7 |
| 200 | 7.3 | 6.6 | 150 | 7.4 | 6.2 |
| 400 | 7.5 | 6.5 | 300 | 7.5 | 6.1 |
| 1200 | 7.4 | 10.3 | 920 | 7.5 | 17.2 |

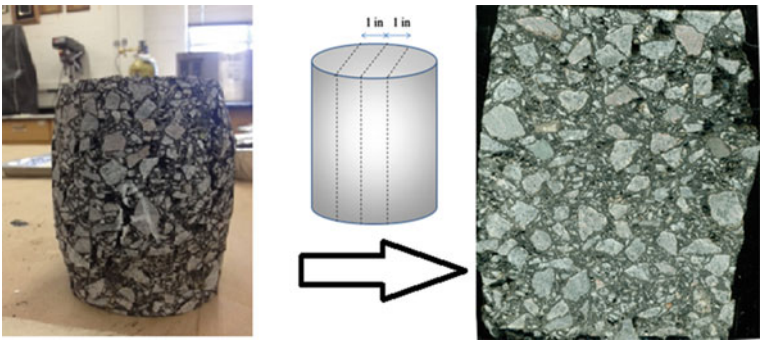


**Fig. 5** Cutting section of a failed sample

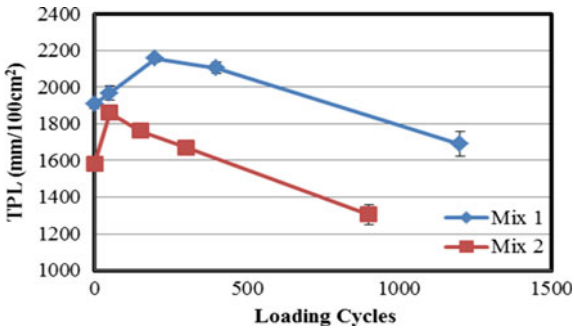


**Fig. 6** Evolve in aggregate packing during loading

mix 2 with other mixtures illustrates that mixtures with the same level of TPL should be able to resist applied loads (Fig. 3), if there is a continuous and stable aggregate skeleton in the mixture. Therefore, it is hypothesized that the failure in mixture and decrease in TPL during secondary and tertiary zone is due to some localized deformation and discontinuities in aggregate skeleton of mixes, leading to failure of the whole sample and sever reduction in load bearing capacity of mixture.

To track the connectivity of aggregate skeletons during loading, networks of aggregates in proximity or contact are plotted for samples at each stage of loading. The aggregate network plots for mix 1 and 2 are shown in Fig. 7. The lines represent a connection from centroid of one aggregate to centroid of any other aggregates that are in proximity with it. It should be noted that each aggregate network plot shown in Fig. 7 is for an individual replicate sample after loading. As it is shown in Fig. 7, the aggregate connectivity started getting damaged close to the end of secondary zone (i.e. approximately after 150–200 cycles of loading). The main discontinuity and bulging in structure happened close to outer layers of sample due to lower confinement (Fig. 8) [the same type of failure is observed for all mixtures shown in Fig. 3 prepared with different aggregate sources and gradations (Fig. 8)].

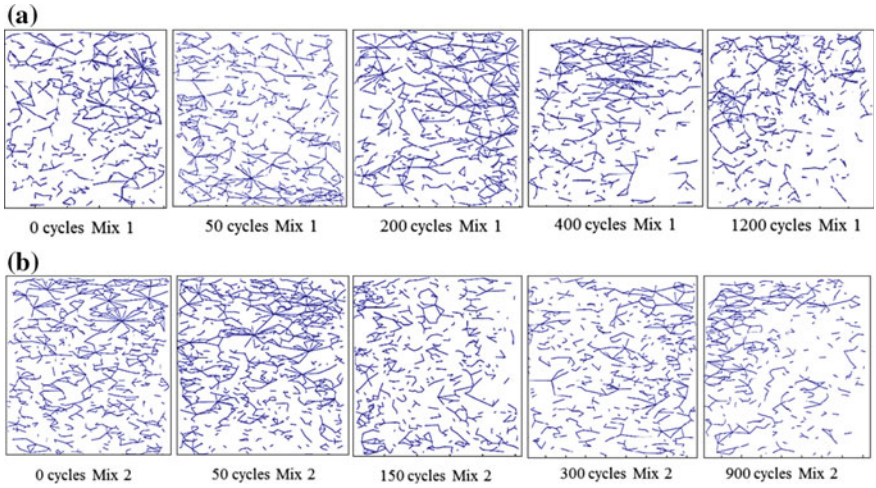


**Fig. 7** Evolve in aggregate skeleton connectivity during loading: **a** mix 1, **b** mix 2

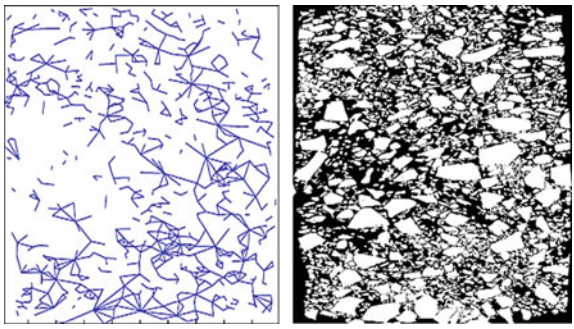

**Fig. 8** Discontinuity of aggregate structure at outer layers due to bulging represented by *black* and *white* image and aggregate skeleton network

According to the aggregate network plots, density measurements, and visualization of samples after failure, as discussed, the mechanisms of deformation and failure in uniaxial testing can be explained as follows:

- Primary zone: The main mechanism of permanent deformation in primary zone is densification. In this zone, the material mainly loses some air voids rapidly which increases aggregate packing due to proximity of more aggregates. The stiffening of mixtures after primary zone is due to the higher packed aggregates comparing to initial stage of material packing.
- Secondary zone: In secondary zone, the aggregate skeleton starts deformation due to shearing. Since the aggregate contacts are not perfectly oriented in the axial loading direction, the aggregate skeleton starts deformation along the directions that show less confinement (i.e. outside of sample). However, since the aggregate skeleton is still stable at most of the proximity zones, there is no rapid deformation or failure of sample. The bulging of aggregate skeleton is relatively higher for the aggregate skeleton near to outside of sample.
- Tertiary zone: When some parts of the aggregate skeleton as the main paths of stress in material are highly deformed (i.e. localized bulging of sample), the whole skeleton becomes statically instable due to the loss of load bearing capacity in some parts. Therefore, a drastic deformation starts after a cycle of loading which is designated as flow number (FN). In some samples localized bulging is enough for the failure to start; however, other samples may bulge under cyclic loading in a symmetric shape due to these localized failures. If the stress level is not high enough or the mixture aggregate skeleton is highly packed, the mixture may never experience the tertiary zone (Low stress level and highly packed aggregate skeleton reduce the plastic deformation in the aggregate skeleton and asphalt binder).

To further validate the concept of aggregate skeleton bulging as the main mechanism controlling tertiary flow, replicate samples of mixes 1 and 2 were prepared for testing in a fully confined condition. For this purpose, a PVC pipe with an inner diameter of 10 cm which is equal to the outer diameter of asphalt mixture samples is cut to 8 cm pieces. The distance between the edges of spots glued to sample for vertical deformation measurements (i.e. the height which the vertical LVDT measures the deformation for) is 9 cm. The PVC pipe was selected to have a sufficient stiffness at testing temperature (i.e. 46 °C) which causes a perfect confining condition meaning that the mixtures ideally cannot bulge in lateral direction. The pieces of pipes are put on samples and LVDT spots are glued (Fig. 9). Since the core diameter was slightly lower than the inner diameter of pipe, sample was fit in the pipe with minimal friction at the beginning of test.

The confined samples of mixes 1 and 2 were tested at the same testing condition of unconfined samples. The permanent deformations of confined and unconfined samples are shown in Fig. 10, which clearly shows that no tertiary flow is observed in confined testing. Furthermore, the permanent deformation measured is lower compared to the unconfined test, as expected since there is minimal lateral deformation in samples; therefore, no significant shearing deformation can occur after

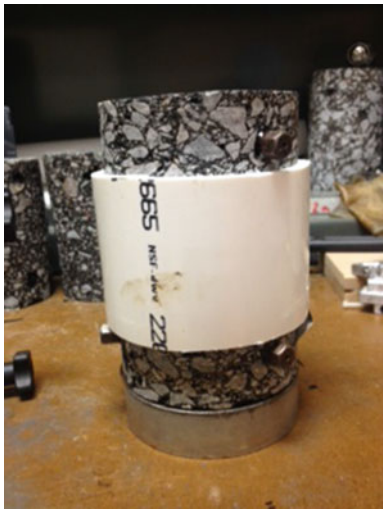

**Fig. 9** Sample confined with PVC pipe

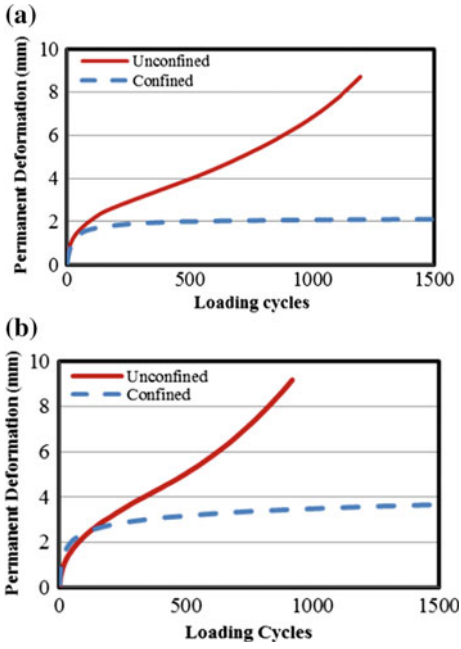


**Fig. 10** Comparison of permanent deformation between confined and unconfined test: **a** mix 1, **b** mix 2

initial densification. The densities of samples are measured before and after testing in confined condition. The air void content for mix 1 is reduced from 7.3 to 6.4 % and for mix 2, it is reduced from 7.5 to 6.1 %. The permanent deformation rate of mix 1 is close to zero after the primary densification. However, mix 2 showed a higher rate of rutting.

The confined uniaxial testing compared to unconfined condition, confirms the concept that tertiary flow in uniaxial testing mainly happens due to instability of aggregate skeleton as result of lateral bulging. This finding is in agreement with what researchers reported about the definition of tertiary zone and the Poisson's ratio at which failure happens (Witczak and Kaloush 2002). It is reported by researchers that failure in asphalt mixture cyclic creep testing (i.e. both in uniaxial and triaxial testing) happens at Poisson's ratio of 0.6–0.7. A Poisson's ratio higher than 0.5 represents dilation in material under loading. As shown in this study, the dilation of material in lateral direction happens due to bulging or buckling of aggregate skeleton since there is no confinement stress at outer layers of sample. The material in a sample itself causes a confinement for elements of material closer to middle core of sample which helps resisting dilation or bulging in the middle of sample. This is the main reason for aggregate skeleton to mostly stay connected in the middle of samples and disconnected close to the outer edges after failure.

Based on observations and experiments conducted in this study, aggregate packing can control the failure of asphalt mixtures at high service temperatures through two main mechanisms:

- Better aggregate packing (i.e. higher TPL) can reduce the stress level applied on continuous phase (i.e. asphalt binder acting as the bonding phase of aggregate skeleton) at aggregate proximity zones since mixtures with higher TPL provide an aggregates network with more stress paths in the whole mixture.
- The deformation and bulging of aggregate skeleton take place due to deformation at proximity zones and contacts of aggregates. In mixtures with higher TPL, the skeleton provides a stronger supporting structure which increases the aggregate interlock in mixture decreasing the rate of deformation, and delaying the tertiary flow at the end of secondary creep zone.

Figure 11 is prepared to verify the effect of aggregate skeleton on rutting rate. It shows the rutting rate in secondary zone (i.e. m-value) for mixtures versus TPL. As shown in Fig. 11, mixtures with higher aggregate packing show lower rate of rutting in the secondary creep zone. This data supports the finding that aggregate packing not only delays the instability of structure and tertiary flow, but also reduces the rate of permanent deformation and increases the modulus in secondary zone with a supporting structure effect for aggregate skeleton.

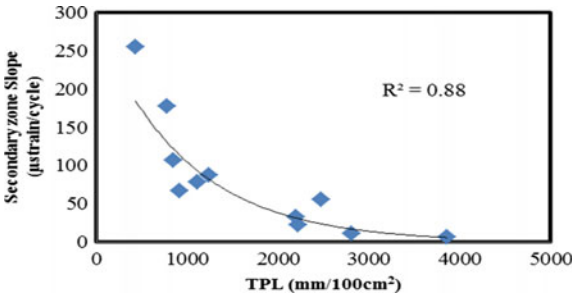


**Fig. 11** Secondary zone rutting rate versus TPL

In this part of the study the effect of binder/mastic rheology was not evaluated. It is logical to assume that binder resistance to flow has an impact as it can provide stability and confinement of the skeleton. The following section includes results collected to study the effects of binder and mastic properties on rate of rutting of mixtures.

## 6 Failure Behaviour in SMA

To further investigate the evolve in aggregate structure of asphalt mixture throughout the loading process, the SMA mixtures as introduced earlier were used to track the change in aggregate structure of both neat and fiber modified SMA mixtures. Based on the cyclic creep and recovery (Flow number) test results, the loading cycles of 30, 120, and 240 for neat SMA mixture and 200, 1000, and 2000 for fiber modified SMA mixture has been selected to assess the change in aggregate structure of mixtures during loading. The number of loading cycles has been selected to obtain samples of aggregate structure at the end of primary zone, in the middle of secondary zone, and end of secondary zone. Similar to previous section, the samples are prepared with a target density of 7 ± 0.5 % and the density of samples before and after loading are measured. The cyclic creep and recovery test results and densities of samples before and after loading are shown in Fig. 12 and Table 2.

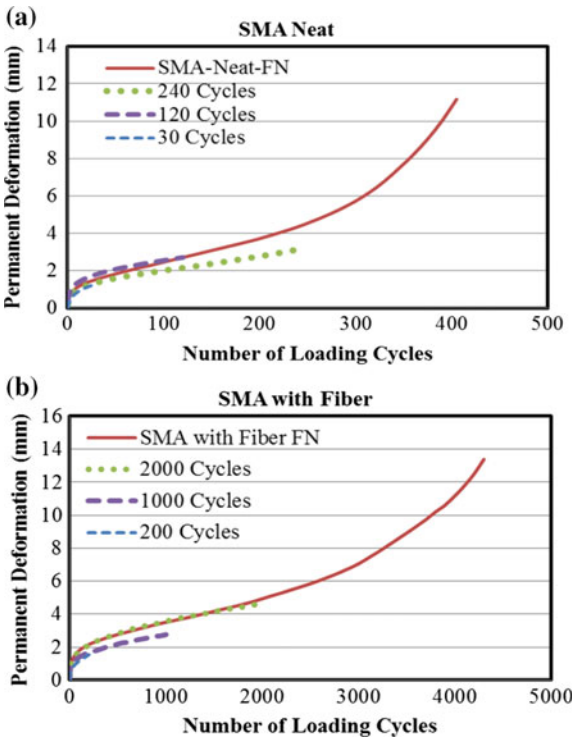


**Fig. 12** Permanent deformation for cyclic creep and recovery testing of: **a** neat SMA, **b** fiber modifier SMA

**Table 2** Air void measurements before and after loading for SMA mixtures

| SMA neat | Air void (%) | | SMA fiber | Air void (%) | |
|---|---|---|---|---|---|
| Load cycles | Before loading | After loading | Load cycles | Before loading | After loading |
| 0 | 7.2 | – | 0 | 7.0 | – |
| 30 | 7.1 | 6.2 | 200 | 7.3 | 6.1 |
| 120 | 7.5 | 5.9 | 1000 | 7.1 | 5.7 |
| 240 | 7.4 | 5.5 | 2000 | 7.5 | 5.5 |
| 405 | 7.4 | 11.4 | 4300 | 7.3 | 10.3 |

After performing density measurement on tested samples, all samples are cut in three sections and the six section faces are scanned. The obtained images are analysed using IPAS2 to measure TPL for all mixtures. The results of image analysis are shown in Fig. 13.

According to the cyclic creep test results, density measurements, and image analysis results, for the neat SMA mixture, after a short densification process (in terms of number of loading cycles), dilation of mixture and reduction in aggregate packing started. Considering that the SMA mixture is designed as a gap graded mixture, the initial aggregate packing is lower than regular HMAs. Consequently, the aggregate particles are not as stable as dense graded mixtures and additionally, in SMA mixtures a higher stress level is applied on the continuous phase. Therefore, for the neat mixture, since the continuous phase is not strong enough, the mixture started sever permanent deformation due to the bulging of aggregate structure after around 300 cycles. However, in fiber modified SMA mixture, although the initial aggregate packing is lower than neat mixture, due to the strong continuous phase that bonds the aggregate skeleton, the aggregate packing kept increasing up to 1000 loading cycles after which dilation of material started. The clear effect of continuous phase resistance to shearing deformation as well as its effect on creating a higher aggregate packing throughout loading process while keeping the mixture stable can be understood from the analysis results.

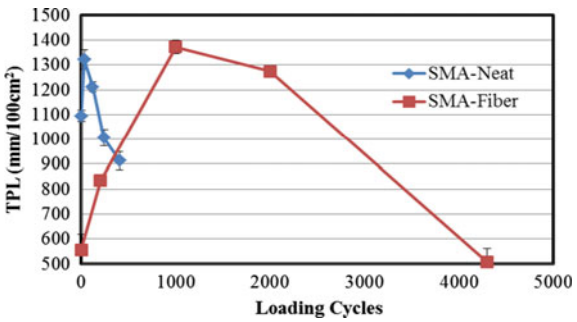


**Fig. 13** Image analysis results for SMA mixtures

## 7 Summary of Findings

The uniaxial repeated creep test is the main test method used by researchers for evaluating rutting resistance of asphalt mixtures. This study was focused on further understanding the fundamental mechanisms that control the behavior of asphalt mixtures in this test. Mechanical measurements, volumetric measurements, and imaging of samples were used to explain the changes in density and aggregate packing during various stages of each of the tests. The main findings can be summarized in the follow points:

- Mixture samples were tested and imaged after applying different cycles of loading using a uniaxial-unconfined test set-up. It is shown that the main mechanism of deformation in the primary creep zone of rutting is densification of mixture. The aggregate packing (as measured by the Total Proximity Length, TPL) increases during the primary zone for the two mixture tested. However, TPL starts decreasing when the loading cycles are increased during the secondary creep zone. It is shown that the failure and tertiary flow in mixtures happen mainly due to the instability of aggregate structure. The instability happens as a result of the aggregate skeleton bulging (dilation) in mixture samples; especially the portion of aggregate skeleton close to outer side of samples since the confinement is lower. To further verify this concept, mixtures were tested in a fully confined condition. The results showed no tertiary flow happening in the confined mixtures, and significantly lower permanent deformation is recorded. The findings in this study are in agreement with literature showing that mixtures tested in uniaxial stress conditions usually start to fail at Poisson's ratio of 0.6–0.7.
- It is shown in this study that aggregate packing and the resulting skeleton are the main aggregates' property that controls behavior of mixtures in uniaxial cyclic creep testing. Recent studies have shown that aggregate packing is mainly a function of mastic viscosity during compaction. Therefore it is expected that, for each aggregate blend, selection of proper compaction temperature and effort could be very critical to achieve better packing and better resistance to creep and instability of asphalt mixtures.
- In this study the effect of binder/mastic rheology was not studied. It is logical to assume that binder resistance to flow has an impact as it can provide stability and confinement of the skeleton. More work is planned to explore the relative importance of binder and mastic characteristics as compared to the aggregate packing.

**Acknowledgements** This research was sponsored by the Asphalt Research Consortium (ARC), which is managed by FHWA and WRI and MARC partners. This support is gratefully acknowledged. The results and opinions presented are those of the authors and do not necessarily reflect those of the sponsoring agencies.

## References

Anderson R.M., "Relationship between Superpave gyratory compaction properties and the rutting potential of asphalt mixtures", Asphalt Paving Technology, Association of Asphalt Paving Technologists-Proceedings of the Technical Sessions, Vol – 71, pp 207-740, 2002.

Bahia H.U., Friemel T., Peterson P. and Russell J., "Optimization of Constructability and Resistance to Traffic: A New Design Approach for HMA Using the Superpave Compactor", Association of Asphalt Pavement Technologies, V.67-98, p.189, 1998.

Coenen A.R., Kutay M.E., Roohi Sefidmazgi N. and Bahia H.U., "Aggregate Structure Characterization of Asphalt Mixtures Using 2-Dimensional Image Analysis", Road Materials and Pavement Design, Vol. 13, Iss. 3, 2012.

Faheem A.F., Bahia H.U., "Using the gyratory compactor to measure the mechanical stability of asphalt mixtures", Wisconsin Highway Research Program Report 05-02, Madison, Wisconsin, 2004.

Masad E., Muhunthan B., Shashidhar N. and Harman T., "Aggregate Orientation and Segregation in Asphalt Concrete", ASCE Getotechnical Special Publication No. 85, pp. 69-80, 1998.

Masad E., Muhunthan B., Shashidhar N. and Harman T.. Internal Structure Characterization of Asphalt Concrete Using Image Analysis. ASCE Journal of Computing in Civil Engineering (Special Issue on Image Processing), 13 (2), pp. 88-95, 1999.

Nguyen H.M., Pouget S., Di Benedetto H., Sauzéat C., "Time-Temperature Superposition Principle for bituminous mixtures", European Journal of Environmental and Civil Engineering, vol. 13, n°9, pp. 1095-1107, 2009.

Olard F. and Perraton D., On the Optimization of the Aggregate Packing Characteristics for the Design of High-Performance Asphalt Concretes, Road Materials and Pavement Design, Vol. 11, Iss. sup1, 2010.

Olard F., GB5 mix design: high-performance and cost-effective asphalt concretes by use of gap-graded curves and SBS modified bitumens, Road Materials and Pavement Design, Vol. 13, Iss. sup1, 2012.

Roohi Sefidmazgi N., Tashman L. and Bahia H.U., "Internal structure characterization of asphalt mixtures for rutting performance using imaging analysis", Road Materials and Pavement Design, Vol. 13, Iss. sup1, 2012.

Shashidhar N., Zhong X., Shenoy A.V. and Bastian Jr E.J., "Investigating the role of aggregate structure in asphalt pavement", International Center for Aggregates Research 8th Annual Symposium: Aggregates - Asphalt Concrete, Bases and Fines, 2000.

Tashman L., Wang L.B. and Thyagarajan S., "Microstructure Characterization for Modeling HMA Behavior Using Imaging Technology", Journal of Road Materials and Pavement Design, Vol.8, No.2, pp. 207-238, 2007.

Wang L.B., Paul H.S., Harman T. and D'Angelo J., "Characterization of Aggregates and Asphalt Concrete using X-ray Tomography", AAPT, Vol. 73, pp. 467-500, 2004.

Witczak M.W., Kaloush K.E. and Von Quintus H., "Pursuit of the Simple Performance Test for Asphalt Mixture Rutting", Asphalt Paving Technology, Association of Asphalt Paving Technologists-Proceedings of the Technical Sessions, Vol. 71, pp 783-810, 2002.

Yue Z.Q., Bekking W. and Morin I., "Application of Digital Image Processing to Quantitatively Study of Asphalt Concrete Microstructure", Transportation Research Record 1492, TRB, National Research Council, Washington, D.C., pp. 53-60 , 1995.

# Development of a Test and Classification Method to Objectively Determine the Colour of Coloured Bituminous Pavements

**Katleen Denolf, Nathalie Piérard and Ann Vanelstraete**

**Abstract** Coloured bituminous pavements are increasingly used on our roads, mostly in rural environments to increase safety, road legibility and liveability. Since the expression of a colour is different for every individual, the colours of coloured roads are quite often a subject of discussion between contractors and clients. The perception of colour depends on a variety of parameters: the observer is an important factor, but the incidence of light and the distance between the observer and the object also have a great influence. This article deals with a measurement and classification method to objectively determine the colour of coloured asphalt cores. A round robin test was carried out to verify the repeatability and reproducibility of the test method. Several coloured cores representative of the range of colours available from the Belgian asphalt producers were measured and visually inspected by the BRRC steering committee on *Coloured Bituminous Pavements*. The results were analysed and have led to a classification into different colour classes, which will be implemented in the Flemish standard specifications.

**Keywords** Asphalt pavement · Colour · Spectrophotometer

## 1 Colorimetry

### *1.1 Introduction*

Coloured asphalt can be distinguished from ordinary asphalt by its colour. This colour can be obtained by means of particular components such as coloured granulates, pigments and colourless synthetic binders. In the old Belgian specifications RAL colour charts were used to determine the colour of asphalt pavements. RAL (Reichs-Ausschuβ für Lieferbedingungen) is a colour matching system used

K. Denolf (✉) · N. Piérard · A. Vanelstraete
Belgian Road Research Centre, Woluwedal 42, B-1200, Brussels, Belgium
e-mail: k.denolf@brrc.be



F. Canestrari and M.N. Partl (eds.), *8th RILEM International Symposium on Testing and Characterization of Sustainable and Innovative Bituminous Materials*, RILEM Bookseries 11, DOI 10.1007/978-94-017-7342-3_62

in mainly in Europe, and was invented in Germany in the year 1927. The RAL colour charts form a collection of colours mostly used in the paint industry and are a good tool to determine the colour of a smooth homogeneous surface (e.g. a painted wall). Once the surface becomes textured and heterogeneous like an asphalt pavement, the use of colour charts is no longer recommendable and has led to several discussions between contractors and clients.

Unlike for length or weight, there is no physical scale for measuring colour, making it unlikely that a certain colour will be expressed in the same way by different people. Colour can only exist when three components are present: an observer, an object and light. Its perception is influenced by different factors such as:

- the observer: a coloured asphalt layer can seem different to different observers;
- the state of the object: a bituminous pavement can be wet or dry, clean or dirty, less or more compacted … In each state different colours will be observed;
- the light source: an asphalt layer can look yellow ochre on a sunny day while it may seem dark grey on a cloudy evening;
- the distance between the object and the observer;
- the angle at which the object is observed.

## *1.2 Colour Coordinates L*a*b* and L*C*h*

The L*a*b* colour space, shown in Fig. 1, was defined by the International Commission of Illumination (CIE 1971 and 1978). L*, a* and b* are dimensionless quantities, where L* denotes the lightness of a colour and varies between 0 (absolutely black) and 100 (perfect white), and a* and b* are the chromaticity coordinates and generally vary between −100 and +100: +a* is the red direction, −a* is the green direction, +b* is the yellow direction and −b* is the blue direction. The centre of the sphere is achromatic. As the absolute values of a* and b* increase, the saturation of the colour will also increase.

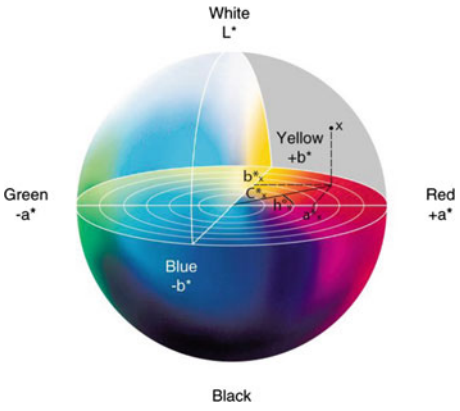


**Fig. 1** The L*a*b* colour space

The chromaticity coordinates a* and b* can also be expressed in terms of polar coordinates C* and h°, as shown in formulas 1, 2 and Fig. 1. In this case C* represents the chroma or saturation and h describes the hue.

$$C^* = \sqrt{(a^*)^2 + (b^*)^2} \tag{1}$$

$$h^\circ = \tan^{-1}\left(\frac{b^*}{a^*}\right) \tag{2}$$

As colours become more chromatic or intense, they move away horizontally from the centre of the colour space, which is completely unsaturated (i.e. grey, white or black, depending on the L* value). The hue, or h°, is expressed in degrees ranging from 0° (red) to 90° (yellow), 180° (green) and 270° (blue) and then back to 0°. The use of L*C*h° coordinates is recommended for chromatic (C* > 10) colours (Hunterlab 2001; Konica Minolta Sensing 2007; X-Rite 2007).

## 1.3 Colour Differences

To quantify colour differences between a standard and a sample, several colour difference formulas have been suggested in the course of times (CIE 1986).

In 1976 the CIE (International Commission on Illumination) released the ΔE* formula, which was written as:

$$\Delta E^* = \sqrt{(\Delta L^*)^2 + (\Delta a^*)^2 + (\Delta b^*)^2} \tag{3}$$

where Δ symbolizes the difference for each colour coordinate between a sample and a given reference (hereinafter called standard). This formula allows to quantify a colour difference by a single number and expresses the *distance* in the L*a*b* colour space between two colours. Unfortunately it has its drawbacks. It does not always match visual perception: ΔE* could be 5 for both sample 1 and sample 2 with respect to a certain standard, but for sample 1 this could mean that ΔL* = Δa* = Δb* = 2.88 and for sample 2 it could mean that ΔL* = Δb* = 0 and Δa* = 5. In the first case, for sample 1, the colour difference is divided between all the colorimetric coordinates; to the human eye the sample and the standard will have quite similar colours. In the second case the colour difference is concentrated in one parameter, a*, meaning that, as far as visual perception is concerned, sample 2 will differ more from the standard than sample 1. To avoid this problem, different limits for ΔL*, Δa* and Δb* could be defined creating a rectangular tolerance box around the standard. But this method also has its inconveniences, because the colour discrimination thresholds of the human eye in the L*a*b* colour space have the form of an ellipsoid rather than a cube or a beam.

In 1984 the Colour Measurement Committee of the Society of Dyers and Colourists of Great Britain developed the $\Delta E_{CMC}$ formula (Clarke et al. 1984). This formula defines an ellipsoid around a standard, with colour coordinates ($L_1^*$, $C_1^*$, $h_1^\circ$) as follows:

$$\Delta E_{CMC} = \sqrt{\left(\frac{\Delta L^*}{lS_L}\right)^2 + \left(\frac{\Delta C^*}{cS_C}\right)^2 + \left(\frac{\Delta H^*}{S_H}\right)^2} \tag{4}$$

where:

$$\forall L_1^* \geq 16 : S_L = \frac{0.040975 L_1^*}{1 + 0.01765 L_1^*} \tag{5}$$

$$\forall L_1^* < 16 : S_L = 0.511 \tag{6}$$

$$S_C = \frac{0.0638 C_1^*}{1 + 0.0131 C_1^*} + 0.638 \tag{7}$$

$$S_H = S_C(Tf + 1 - f) \tag{8}$$

$$f = \left(\frac{C_1^4}{C_1^4 + 1900}\right)^{1/2} \tag{9}$$

$$\forall h_1^\circ \in [0^\circ, 164^\circ] \wedge \forall h_1^\circ \in [345^\circ, 360^\circ] : T = 0.36 + 0.4\cos\left(h_1^\circ + 35\right) \tag{10}$$

$$\forall h_1^\circ \in ]0^\circ, 164^\circ[ : T = 0.56 + 0.2\cos\left(h_1^\circ + 168\right) \tag{11}$$

$$\Delta H^* = \sqrt{(\Delta a^*)^2 + (\Delta b^*)^2 - (\Delta C^*)^2} \tag{12}$$

$S_L$, $S_C$ and $S_H$ are weighing factors corresponding to the semi-axis of the ellipsoid for lightness, chroma and hue and depending on the colour of the standard. Factors l and c can be used to modify the lengths of the relevant semi-axis. A l:c ratio of 1:1 was used in this research (Kigle-Böckler 2011; Lindbloom 2009).

## *1.4 Spectrophotometers*

The devices on the market that are capable of measuring colour can generally be divided into two groups: colorimeters and spectrophotometers. In this research spectrophotometers were used to measure colour, since they have more possibilities and better accuracy. The principle of a spectrophotometer is simple: the device is placed on an object, its light source illuminates the object and the reflected light is measured by its observer.

### 1.4.1 Light Source Versus Illuminant

A light source is a physical emitter of radiation that can be characterized numerically by a spectral power distribution curve. Each spectrophotometer has a built-in light source. Since different light sources will make a colour look different, the CIE (International Commission on Illumination) has codified the spectral power distribution curve of different types of white light sources and called them "illuminants". One of the commonly used standard illuminants is the D65 illuminant, which corresponds roughly to a mid-day sun in Europe and is also called the daylight illuminant. There are no actual D65 light sources, only simulators. The spectrophotometer's built-in light source may or may not match any of the CIE illuminants. Instead, the instrument determines the data for measurements under the selected illuminant through calculations based on the data actually measured under the instrument's light source and the illuminant's spectral distribution data stored in the instrument's memory. In this research a D65 illuminant was used for all measurements.

### 1.4.2 Observer

The spectrophotometers used in this investigation offer a selection between a 2° and a 10° observer. In 1931 the CIE defined a standard observer using a 2° field of view, as it was believed that the colour-sensitive cones in the eye resided within a 2° arc of the fovea. In 1964, however, research showed that cones were present in a larger area of the eye than previously believed and the 10° standard observer was defined. The 10° observer is most often used because it gives a better correlation with the visible judgment, and was consequently used in this research.

## 2 Test Method and Precision

A test method was developed (Denolf et al. 2012) to determine the colour of small asphalt cores (∅ = ±0.1 m) or plates (of ±0.08 m by 0.08 m). It can be summarized as follows:

- before a sample is measured, its surface should be clean and dry. If the surface is contaminated, a hard brush shall be used to clean it. If the surface is wet, a hot air blower shall be used to dry it;
- before a sample is measured, its surface should be at room temperature;
- the following settings for the spectrophotometer should be used:
  - D65 illuminant;
  - 10° viewing angle;

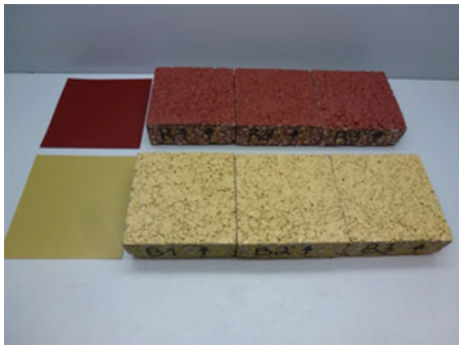

**Fig. 2** Samples measured in the round robin test

- the asphalt sample is divided into four quadrants and one measurement with the spectrophotometer is performed per quadrant. The average values for L*, a* and b* are calculated and are considered to be the colour coordinates of the core.

To determine the repeatability and reproducibility of the test method on cores, a round robin test was carried out. Eleven spectrophotometers participated in the test. Each participant received three red and three beige asphalt plates with dimensions of 8 cm by 8 cm, as shown in Fig. 2. Two reference NCS colour cards with similar colours as the asphalt plates were also added for measurement in the round robin test.

After all the data from the round robin test had been analysed, the following conclusions could be drawn:

- on the asphalt plates, spectrophotometers with a measurement window smaller than or equal to 6 mm in diameter systematically measured abnormal or isolated values for L*, a* and/or b*. For the other spectrophotometers with a measurement window of 8, 11, 14 or 25 mm this systematic deviation was not found. Furthermore, for the reference NCS colour cards the L*, a* and b* values measured with the spectrophotometers with a small window (diameter ≤ 6 mm) did not deviate from the ones with a larger window (diameter ≥ 8 mm). Only spectrophotometers with a measurement window larger than or equal to 8 mm should, therefore, be used to measure the colour of bituminous pavements;
- the average repeatability of the test method was 3 %;
- the maximum reproducibility of the test method was 9 %.

## 3 Determination of Colour Classes

### *3.1 Steering Committee on Coloured Bituminous Pavements*

A steering committee on *Coloured Bituminous Pavements* was formed by the Belgian Road Research Centre, with representatives of the Belgian asphalt sector

(road administrations and contractors). The main objective of this committee is to have requirements for the colour of coloured bituminous pavements included in the standard specifications for road construction.

In Belgium each contractor has to register his asphalt mix with the regional authorities and prove, using a type testing study, that his mixture meets certain requirements for rutting, water sensitivity, … according to certain classes defined in the European EN 13108 series of standards. For coloured bituminous mixtures the steering committee decided that colour should also be a requirement and that the determination of colour should be part of the type testing study.

To achieve this goal, a realistic view on the colours of bituminous pavements currently available on the current market is indispensable. That is why the Belgian asphalt producers were contacted and requested to provide BRRC with asphalt cores produced in their own laboratories, representative of the range of colours available.

## 3.2 Visual Inspection

All the asphalt cores provided by the Belgian asphalt producers were visually inspected by the steering committee, and the committee decided which cores had an acceptable colour and which had not. For this visual inspection the cores were placed in a colour box as illustrated in Fig. 3. This colour box provides a colour-neutral environment and a constant light source. Several light sources can be chosen, but for this exercise the D65 light source was selected in order to match the settings of the spectrophotometers (see Sect. 2). The position of the inspector with respect to the sample is also important; in this case the viewer looked down the sample at an angle of approximately 45°.

The colour coordinates of the cores that were accepted by the steering committee for the colour classes red, burgundy/brown, beige and ochre are shown in Figs. 4 and 5. A picture of a selection of cores representative of each colour class is shown in Fig. 3. For each colour class a standard was selected and is marked in Figs. 4 and 5 with a grey symbol.

## 3.3 Determination of Acceptable Tolerances—Calculation of $\Delta E_{CMC}$

For each colour class, $\Delta E_{CMC}$ with respect to the standard (see Sect. 1.3) was calculated for all the accepted cores. To verify the difference in $\Delta E_{CMC}$ between *accepted* and *rejected* cores, $\Delta E_{CMC}$ with respect to the standard was also calculated for the rejected cores. The $\Delta E_{CMC}$ values for the accepted and rejected samples are represented per colour class in Fig. 6. Each standard has a $\Delta E_{CMC}$ value of zero.


**Fig. 3** Samples representative of each colour class. The standard of each colour class is situated on the *left hand* side of the box. The remaining samples are arranged by increasing $\Delta E_{CMC}$ values

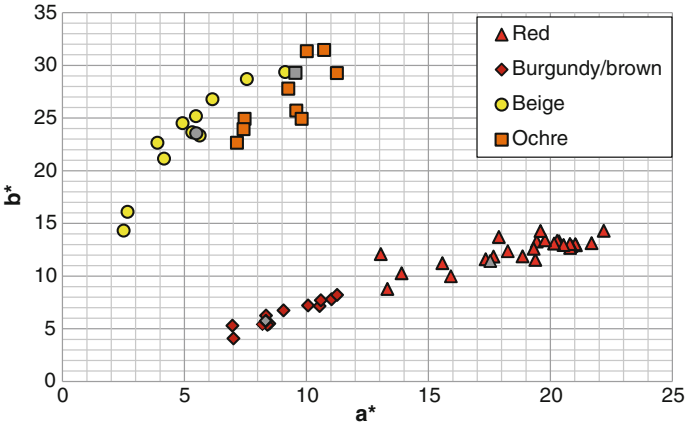


**Fig. 4** b* versus a* for the samples accepted by the steering committee. For each colour class the standard is marked in *grey*

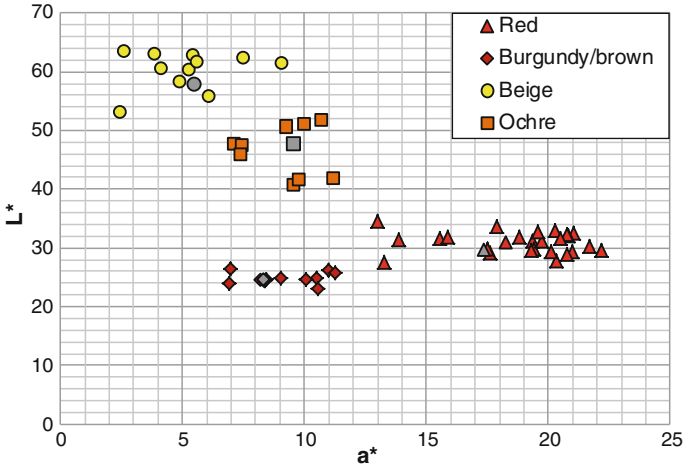


**Fig. 5** L* versus a* for the samples accepted by the steering committee. For each colour class the standard is marked in *grey*

For each colour class it can be concluded that there is a difference in $\Delta E_{CMC}$ between *accepted* and *rejected* cores. Table 1 gives for each colour class the maximum value of $\Delta E_{CMC}$ for the accepted cores and the minimum value of $\Delta E_{CMC}$ for the rejected cores. The maximum $\Delta E_{CMC}$ value should be in between these two values and has yet to be decided by the steering committee.

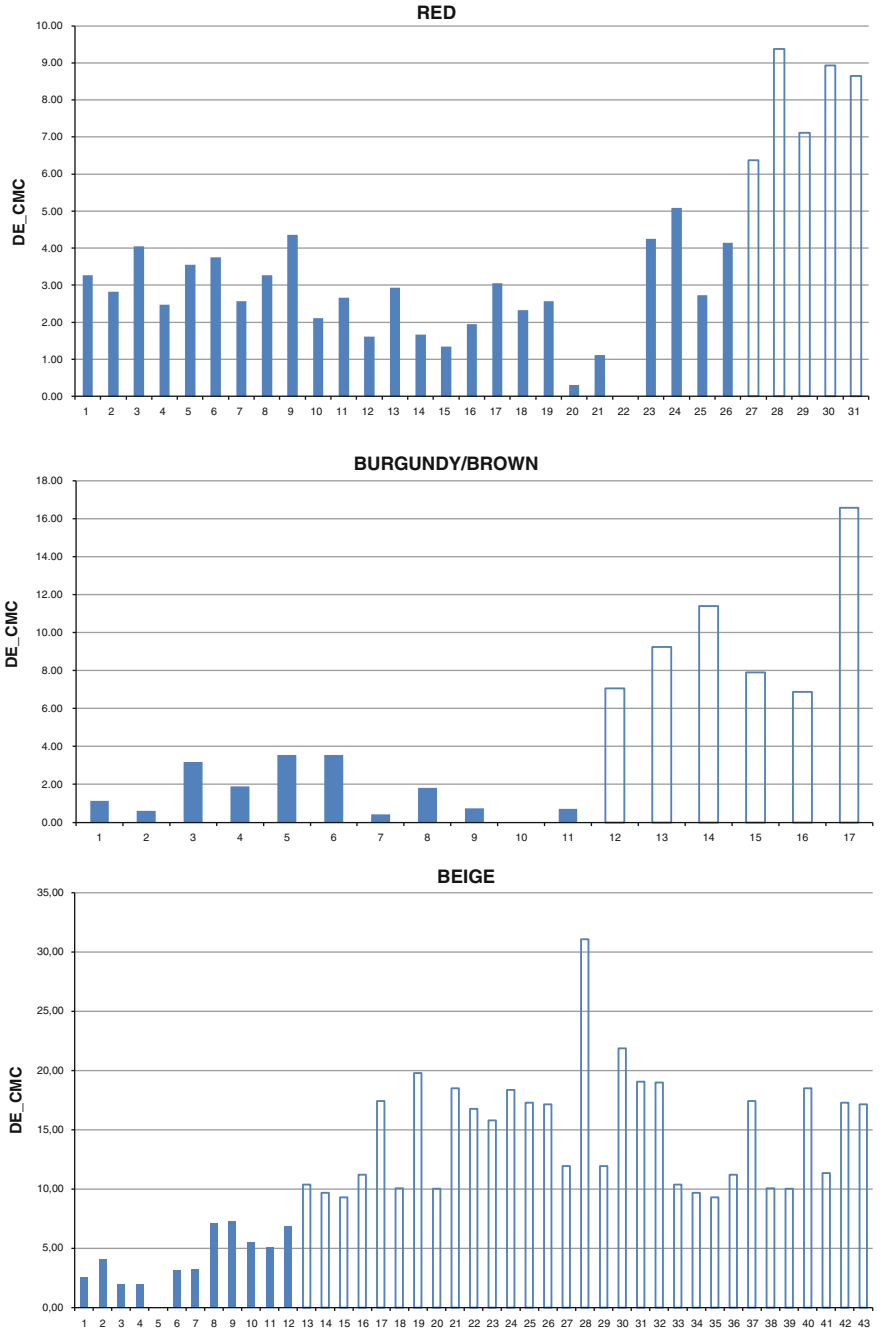


**Fig. 6** $\Delta E_{CMC}$ values for each colour class, represented with *filled bars* for the cores accepted and with *no fill* for those rejected by the steering committee

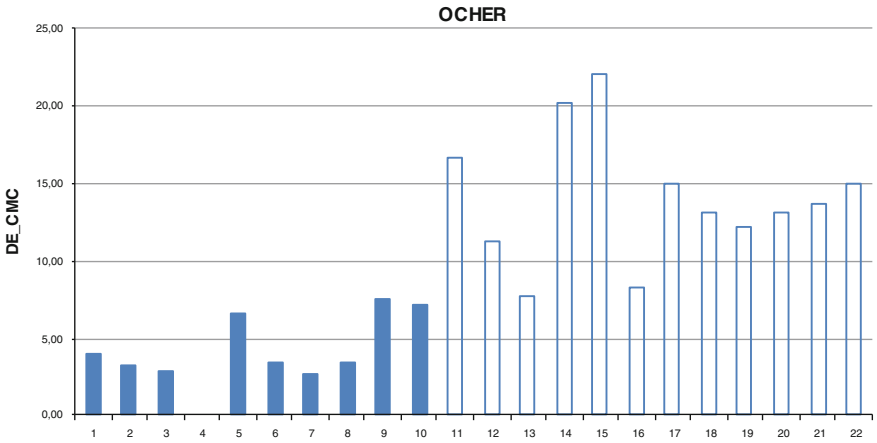


**Fig. 6** (continued)

**Table 1** Maximum $\Delta E_{CMC}$ values per colour class for the accepted cores (*first row*) and minimum $\Delta E_{CMC}$ values per colour class for the rejected cores (*second row*)

| | Red | Burgundy/brown | Beige | Ochre |
|---|---|---|---|---|
| $\Delta E_{CMC\ max}$ accepted cores | 5.1 | 3.6 | 7.3 | 7.5 |
| $\Delta E_{CMC\ min}$ rejected cores | 6.4 | 6.9 | 9.3 | 7.7 |

## 3.4 Conclusions and Future Perspectives

A test method to measure the colour of coloured bituminous samples or plates was developed and its precision was determined in a round robin test. This method was applied to several coloured asphalt samples representative of the colour range of Belgian coloured asphalts. All these samples were also visually inspected by the members of the BRRC steering committee on *Coloured Bituminous Pavements.* Four colour classes were determined (red, burgundy/brown, beige and ochre) and for each colour class a standard was chosen. A maximum tolerance value for $\Delta E_{CMC}$ was set for each colour class with respect to the standard. This procedure has been included in the Flemish tender specifications for the initial type testing for coloured asphalt mixtures.

The next challenge to the steering committee will be to compare the colour of the mixture in the laboratory study to the colour of the coloured bituminous pavement directly after laying on site.

## References

CIE International Commission on Illumination (1971 and 1978), Recommendations on Uniform Colour Spaces, colour-Difference Equations, Psychometric Colour Terms, Supplement No. 2 to CIE Publication No. 15, Colorimetry

CIE International Commission on Illumination (1986), Colorimetry, 2nd ed. Vienna: CIE Publications No15.2

Clarke F.J.J., McDonald R, Rigg B (1984) Modification to the JPC79 colour-difference formula. Jounal of the Society of Dyers and Colourist vol. 100 (4), 128-132

Denolf K, Piérard N, Vanelstraete A (2012) Development of a research method to objectively determine the colour of coloured asphalts. Paper presented at the 5th Eurasphalt & Eurobitume Congress, Istanbul, 13–15 June 2012

Hunterlab (2001) The basics of colour perception and measurement via http://www.elscolab.nl/pdf/colour.pdf. Accessed 14 Nov 2014

Kigle-Böckler G (2011) Standardized colour management system via http://www.byk.com/en/support/instruments/technical-information/colour-information.html. Accessed 14 Nov 2014

Konica Minolta Sensing (2007) Precise colour communication: colour control from perception to instrumentation via http://www.konicaminolta.com/instruments/knowledge/colour/index.html. Accessed 14 Nov 2014

Lindbloom B (2009) Useful colour equations via http://www.brucelindbloom.com/. Accessed 14 Nov 2014

X-Rite (2007) A guide to understanding colour communication via http://www.xrite.com/documents/literature/en/L10-001_Understand_Colour_en.pdf. Accessed 14 Nov 2014

# A New Performance Test for Resistance to Ravelling by Traffic: Laboratory and Field Experience in Belgium

**Joëlle De Visscher and Ann Vanelstraete**

**Abstract** The use of specially designed asphalt mixtures for thin to very thin surface courses is seen as a cost-effective solution for reducing traffic noise in Belgium. However, ravelling is a major concern for this type of mixtures and there is an urgent need for a standardized laboratory test to predict resistance to ravelling caused by shear forces (also known as "scuffing"). The Belgian Road Research Centre (BRRC) uses the Darmstadt Scuffing Device, an apparatus developed in Germany for testing porous asphalt. This paper describes the experience of BRRC with this new test device. As a first step, it was verified whether the test is capable of discriminating between mixtures other than porous asphalt, the mixture type for which the apparatus was originally designed. The second step was to verify if the ranking of mixtures is in agreement with the observations on the road. Therefore, the test was applied to mixtures from different test sections that are being monitored at regular times, a work that will be continued in the coming years. While this work is going on, CEN TC 227 WG1/TG2 is in the process of drafting a European standard for the scuffing test (prCEN/TS 12697-50). The results of this research will be used to contribute to the development of a standard European test method.

**Keywords** Scuffing test · Ravelling test · Darmstadt scuffing device · Test sections

## 1 Introduction

Asphalt mixtures for thin to very thin surface courses are seen as a cost-effective solution for reducing traffic noise on the Belgian road network. Because of their granular composition, high void content and relatively low binder content, such

J. De Visscher (✉) · A. Vanelstraete
Belgian Road Research Centre (BRRC), Woluwedal 42, B-1200, Brussels, Belgium
e-mail: j.devisscher@brrc.be

A. Vanelstraete
e-mail: a.vanelstraete@brrc.be



F. Canestrari and M.N. Partl (eds.), *8th RILEM International Symposium on Testing and Characterization of Sustainable and Innovative Bituminous Materials*, RILEM Bookseries 11, DOI 10.1007/978-94-017-7342-3_63

mixtures generally exhibit high resistance to permanent deformation. Consequently, rutting in proportion to layer thickness is not expected to be a critical performance characteristic. On the other hand, there are performance characteristics that become more critical when layer thickness tends to decrease, such as resistance to ravelling caused by shear forces (also known as "scuffing").

A European Technical Specification for the measurement of resistance to scuffing is already under preparation (prCEN/TS 12697-50). This document describes four types of device that have been developed in specialized research labs:

- ARTe or Aachener Raveling Tester (Schulze and Cyrus Gharabaghy 2008), (Jacobs et al. 2012);
- DSD or Darmstadt Scuffing Device (Root 2008);
- RSAT or Rotating Surface Abrasion Tester (Bochove 2000);
- Triboroute (Hamlat 2007).

In the period 2010–2012, BRRC decided to investigate if one of these devices would be suitable for Belgium. Because of the frequent use of stone mastic asphalt (SMA) for Belgian surface courses, capability of discriminating between SMA mixtures for ravelling resistance was seen as a requirement, in addition to capability of evaluating mixtures for thin and very thin noise-reducing surface courses. Therefore a comparative study was carried out with SMA and with asphalt concrete mixtures for very thin layers (De Visscher et al. 2012). As an outcome of this study, it was decided to acquire the so-called *Darmstadt Scuffing Device*. This device was developed at the Technical University of Darmstadt for evaluating the resistance of porous asphalt to shear forces induced by traffic (Root 2008). The design and flexibility of the apparatus, which simulates the phenomenon in a realistic way, and the reported experimental evidence were the main reasons to opt for this device.

This paper discusses the experience gained with the DSD in Belgium. After describing the test method in Sect. 2, some test results are shown in Sect. 3 to demonstrate the capability of testing SMA and very thin surface courses. In Sect. 4, the paper focusses on test results obtained from test sections with noise-reducing thin layers on a road in the Flanders region. Monitoring of the long-term behaviour of these test sections will provide the ultimate validation of the test method and allow the recommendation of adequate requirements for ravelling resistance, to be included in tender specifications.

The results of this research done at BRRC are also used to contribute to the development of the European standard test method.

## 2 Test Method

The principle of the test method is to measure the loss of material from the surface of a compacted test specimen under a combination of normal and shear stresses induced by a "scuffing" tyre.

## 2.1 Apparatus

The test device used at BRRC is the DSD (Darmstadt Scuffing Device), a picture of which is shown in Fig. 1. In this device, a pneumatic tyre is lowered with a controlled force onto the surface of a square test plate (26 × 26 $cm^2$), while the plate performs a combination of translations and rotations. This simulates the mechanical effect of vehicles when they are turning, accelerating or braking. The platform on which the test plate is fixed can be heated to allow measurements at higher service temperatures.

## 2.2 Test Conditions

The test conditions to be selected by the user are tyre pressure, vertical load, test temperature, rotating speed and number of cycles. At BRRC tests are made with a tyre pressure of 300 kPa, a vertical load of 1000 N and a rotating speed of 6 rpm.

The test temperature can be varied within the range from ambient temperature to 50 °C. However, it is difficult to set the temperature accurately. At test temperatures above ambient temperature, the actual temperature at the surface of the plate is systematically lower than the set temperature. Therefore the exact surface temperature is measured with an infrared thermometer at the start of each cycling sequence (which means every two cycles). The installation of a thermostatic enclosure could be suggested as a possible improvement of the device.


**Fig. 1** Darmstadt scuffing device (DSD) at the Belgian Road Research Centre

## 2.3 Procedure

The test plates are compacted with a plate compactor according to EN 12697-33 (CEN/TC 227 2007), using large moulds of 60 cm by 40 cm. The heavy compaction procedure is systematically used. It is crucial to check the repeatability of the compaction procedure, because the test result is highly sensitive to compaction level. After sawing off the borders of the plate, the remaining central part is cut into two test specimens of 26 cm by 26 cm (see Fig. 2a). Alternatively, the test can be applied to surface courses compacted on the road. Large cores of 400 $cm^2$, which are subsequently cast in plaster in a square test mould, are used for that purpose (see Fig. 2b).

Up to ten cycles are applied and the loss of material is measured every two cycles, to allow a graphical representation against the number of load cycles. Note that one cycle is a combination of five translations and one rotation to an angle of 180°; each movement is considered as a two-way movement. The loss of material is determined from the incremental weight of the container of a vacuum cleaner which collects the loose material every two cycles. With this procedure, there is no need to remove the plate from the device during the measurement and the loose material is systematically removed. This is a crucial point, since loose grains remaining between the tyre and plate surface accelerate the damage process. At the end of the measurement, the plate is weighed and the total difference between initial and final mass is used to verify the incremental mass of the loose material.

## 2.4 Precision

Repeatability was already investigated in the thesis of Root (2008). He performed repeated tests at five different test levels and established a linear relation between the repeatability standard deviation and the test level.

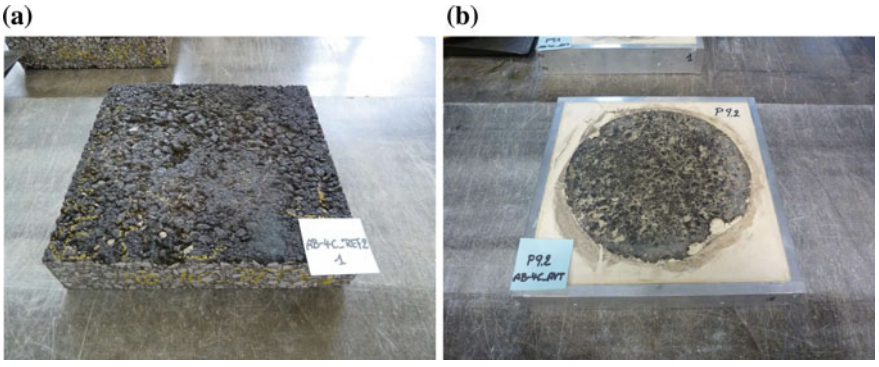


**Fig. 2** **a** Test plate compacted in the lab. **b** Test core from a road, cast in a test mould

Experience at BRRC has confirmed that precision depends on the level of ravelling. At least two (if possible four) test plates are prepared per mixture to determine resistance to ravelling with a higher precision.

In 2013–2014, BRRC together with five other laboratories participated in a ring test organized by the Technical University of Darmstadt to determine the repeatability and reproducibility of the test method. Five different test levels were considered and three repeated tests were made by each laboratory at each test level. The report was being finalized at the time of drafting of this paper.

## 3 Test Results for Mixtures Other Than Porous Asphalt

As explained in the introduction, the test method was developed specifically for porous asphalt. A standard test temperature of 40 °C is used, since this is considered to be within the critical temperature range for ravelling in Germany. In Belgium, porous asphalt is rarely used and most of the surface courses on highways are in SMA. Therefore, in the first part of this Section it is demonstrated that the test protocol is capable of discriminating between SMA mixtures with different susceptibility to ravelling. The second part of this Section shows test results on asphalt concrete for very thin layers. The mix type is called RUMG 6.3 (Revêtement Ultramince Grenu) and is used in the Walloon region (Qualiroutes 2012). It is a mixture with a stony skeleton, laid to a thickness of 15 mm. Ravelling is the most commonly observed defect in this type of surface course.

### *3.1 Stone Mastic Asphalt*

Figure 3 shows results obtained on four variants of SMA 10 with identical grading curves. The variants only differ by the type of binder and the use of hydrated lime or not. The tests were carried out on slabs following compaction according to EN 12697-33 of bulk material taken at the asphalt plant during the construction of different test sections on the N568a at Heppignies in 2013 (Vansteenkiste et al. paper submitted for E&E 2016). A substantial impact of the test temperature (27 or 40 °C) can be observed. In this temperature range, ravelling increases with temperature because of the softening of the binder. The use of a polymer modified binder (PmB) 45/80–50 significantly improves resistance to ravelling at higher service temperatures, as compared to a paving grade bitumen 50/70. However, ravelling resistance with the latter binder can also be improved by adding hydrated lime (1.5 wt% to dry mixture). The relative impact of binder type and hydrated lime is greater at the higher test temperature of 40 °C. All these observations are in agreement with general field experience with SMA containing PmB and/or hydrated lime.

The effect of a PmB is also demonstrated in Fig. 4. These tests were part of a Master's thesis by a student of the University of Antwerp (Haulet 2014), to

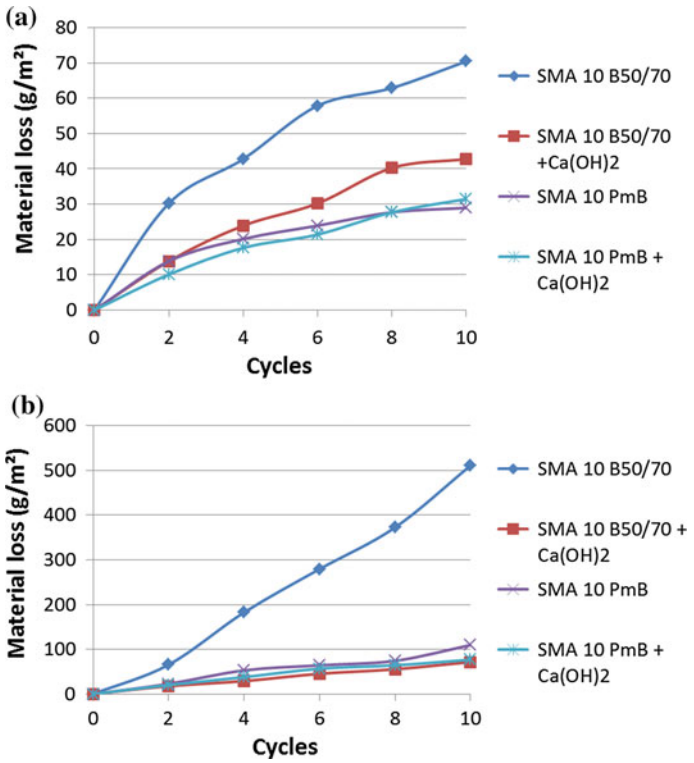


**Fig. 3** Test results for SMA 10 showing impact of binder type and use of $Ca(OH)_2$: **a** at 27 °C, **b** at 40 °C

investigate the effect of reclaimed asphalt (RA) on the performance of SMA. The test plates had been prepared at the University of Antwerp. It can be observed (also in comparison with Fig. 3) that the beneficial effect of the PmB 45/80–50 is higher for mixtures with a lower resistance to ravelling, as could be expected. For this particular mixture and under these test conditions, there is also a beneficial effect of using RA. This can possibly be explained by the contribution of the harder binder from the RA. Fracture occurred within the mastic of the SMA and therefore, a mixture with harder mastic is expected to exhibit better resistance to scuffing. The quality of the RA is probably also an important factor. Better understanding of the failure phenomena and the impact of the various factors is needed before drawing general conclusions regarding the impact of RA.

Figure 5 shows test results for two type SMA 6.3 mixtures. The tests were made on laboratory-compacted plates from bulk mixtures sampled on a road under construction. Both mixtures were prepared with a PmB 45/80–65, the same binder content (6.2 %) and the same aggregate (sandstone). The main difference between the mixtures lies in their grading: mix B is less discontinuous in grading and has a lower void content than mix A. Both mixtures exhibit little ravelling: less than

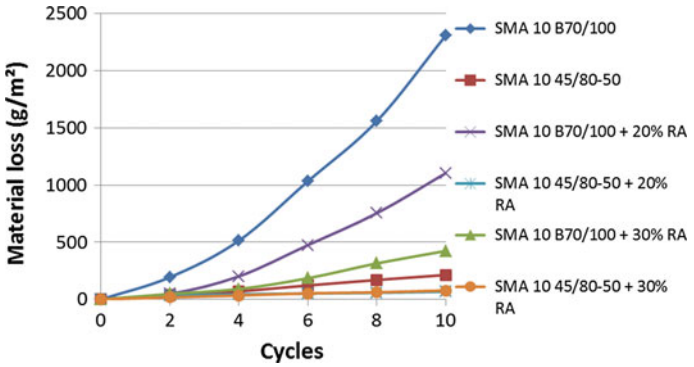


**Fig. 4** Test results for SMA 10 (different binders and use of reclaimed asphalt), at 40 °C

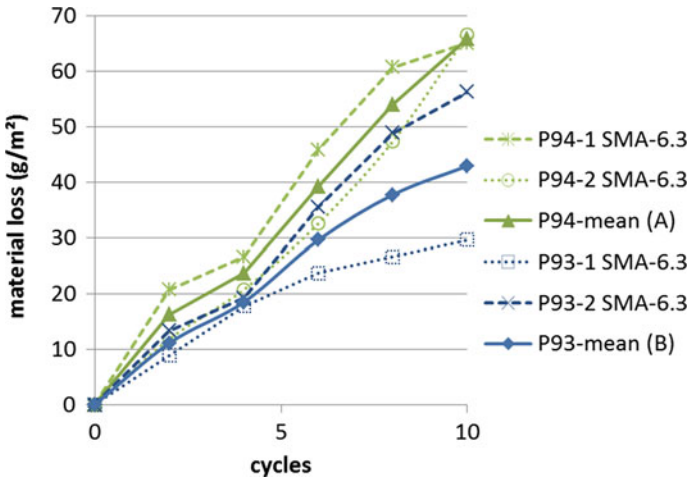


**Fig. 5** Test results for SMA 6 (mix A and B, with different grading), at 40 °C

100 g/m$^2$ loss of material after ten cycles at 40 °C. However, the ranking does correspond to the expectation that the mixture with the higher void content and more discontinuous grading would be more susceptible.

## *3.2 Asphalt Concrete for Very Thin Layers*

Two variants of the Walloon type RUMG 6.3 mixture were tested: mixture M1 with a binder content of 5.2 %, and mixture M2 with a binder content of 4.7 % and a slightly more discontinuous grading. The test plates were two-layered, consisting of

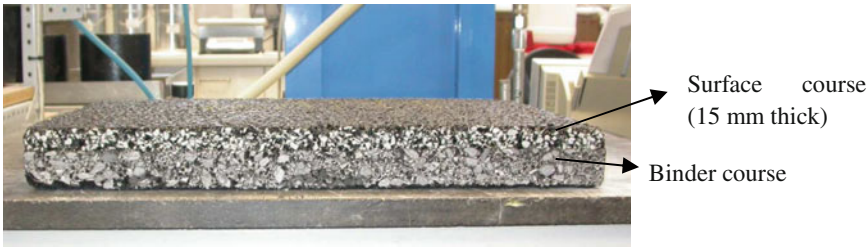


**Fig. 6** Two-layered test plate with AC 14 binder course and RUMG 6.3 surface course

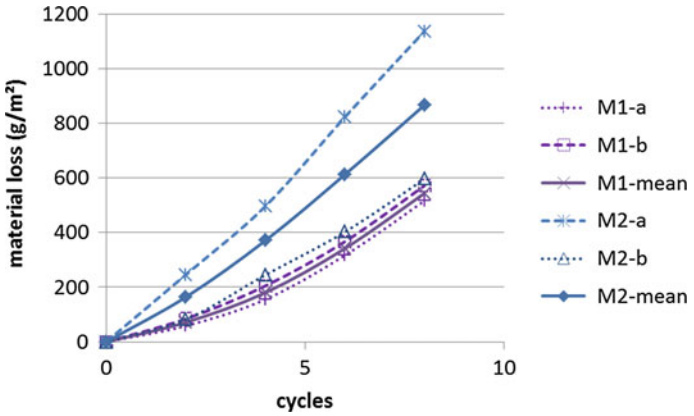


**Fig. 7** Test results for two variants of RUMG 6.3, at 20 °C (mix 1 has a higher binder content and is less discontinuous in grading than mix 2)

the same asphalt concrete binder course (AC 14), the same tack coat and the very thin surface course (Fig. 6). The tests shown in Fig. 7 were all conducted at ambient temperature. The average results match the expected ranking, but the variance of the results for the same mixture is large for the more sensitive mixture. The large variance may also be due to the complexity of specimen preparation and compaction, which has an impact on repeatability. We note that the loss of material is much greater than from SMA and that resistance to ravelling is clearly a critical performance characteristic for these mixtures.

## 4 Validation on Test Sections

In May 2012, the Flemish Agency for Roads and Traffic (AWV) constructed test sections with thin noise-reducing asphalt layers on regional road N19 Turnhout-Kasterlee. The 2 km long test stretch was divided into ten sections each

200 m in length. Through a call for tender, eight different variants of thin surface courses were selected. A noise reduction of at least 2 dB(A) with respect to the reference section (SMA 10 in test section 1) was required. Measurements were performed in cooperation between BRRC and AWV, for acoustical quality as well as mechanical performance. Durability is an important issue not only for length of life but also for the long-term development of acoustical quality.

The performance characteristics of thin layers are known to be highly sensitive to paving conditions. Adverse weather conditions, inadequate compaction temperatures or poor quality of the tack coat are some of the parameters that may seriously affect the performance of the pavement. To make a correct evaluation of the different types of surface mixture, all critical parameters were measured during and after construction. Surface temperature measurements showed large variations over the length and width of the test sections, owing to rapid cooling of the thin layers. However, final density as measured with a nuclear density gauge was sufficiently uniform within each section, thanks to the fact that the compactors followed the finisher closely and compacted the surface course correctly.

The test plates for the ravelling tests were prepared with the asphalt mixtures sampled at the construction site. The bulk mixtures were reheated and compacted in the laboratory with a plate compactor according to EN 12697-33. Tests for this study were made at ambient temperature. Two plates were tested per variant and the mean results are shown in Fig. 8. There is a clear distinction between mixes A and B, with a lot of material loss, and all the other variants, with moderate or slight material loss. Mixtures F and E exhibit good resistance to ravelling, equivalent to SMA (the reference). The high sensitivity to ravelling of mixtures A and B was explained by their composition and the related high void content.

The difference in ravelling resistance revealed by the laboratory tests was already confirmed by visual inspections after less than two years of service: both sections with variants A and B were subject to local ravelling induced by traffic (see Fig. 9).

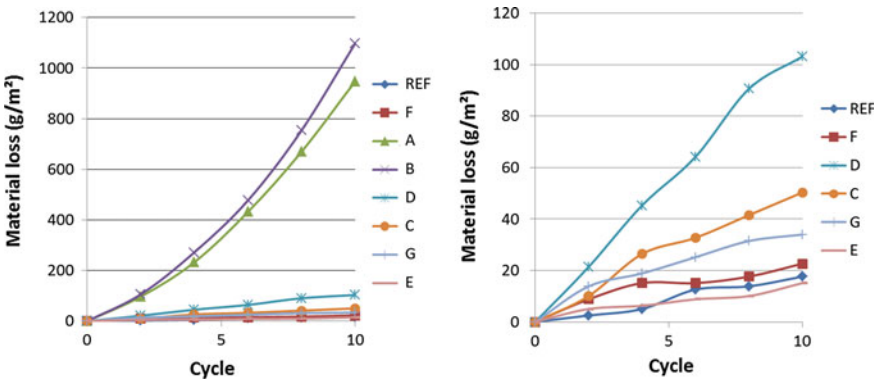


**Fig. 8** Loss of material in the raveling tester at 20 °C (the two graphs are the same, except for the scaling of the vertical axis)

**Fig. 9** Ravelling observed in test sections on the N19 Turnhout-Kasterlee

It is interesting to note that these two sections initially performed very well for noise reduction, but the results of the noise measurements over the first two years of service show that their acoustical quality is deteriorating as well.

## 5 Perspectives

Using the results from the test sections described in the previous section, the Flemish Agency for Roads and Traffic has included performance-related requirements for thin noise-reducing asphalt layers in its new standard tender specifications (SB250, version 3.1). For resistance to ravelling by traffic, a maximum allowable loss in material of 300 g/m$^2$ after ten cycles at 25 °C (±2 °C) has been specified. Additional data will be collected by testing more mixtures from test sites.

The test is further used in various projects to assess the impact of mix composition, ageing and other important parameters on resistance to ravelling and to improve our understanding of the failure mechanisms.

The experience gained by BRRC is used to contribute to the development of the future European test method.

## 6 Conclusions

The Darmstadt Scuffing Device is used at BRRC to evaluate the sensitivity of surface courses to ravelling by traffic (or scuffing). In the Belgian context the device is used on mixture types other than porous asphalt, such as SMA and mixtures for thin noise-reducing surface courses. Tests were performed at ambient temperature (approximately 25 °C) and at 40 °C on mixtures with different compositions, different binder types and with or without hydrated lime. The following conclusions follow from this study:

- the test is capable of discriminating between different variants of SMA;
- the test is capable of discriminating between different variants of mixtures for very thin surface courses;
- SMA exhibits little loss of material loss in comparison with mixtures for very thin courses;
- binder type has a greater impact on the result at 40 °C than at ambient temperature (around 25 °C);
- the test results are in line with general expectations and/or practical experience and hence confirm the relevance of this test method.

The test sections of the Flemish Agency for Roads and Traffic with thin noise-reducing surface courses on the N19 Turnhout-Kasterlee provide a first validation of the test method by field performance, since the ravelling behaviour observed on the road confirms the test results in the laboratory. This field validation has led to performance related requirements for noise-reducing surface courses in the Flemish standard tender specifications.

**Acknowledgements** The authors express their gratitude to the Belgian Bureau for Standardization (NBN) for the financial support for the development of the mechanical performance tests (CC CCN/PN/NBN-908-958). In addition the authors wish to thank the Flemish Agency for Roads and Traffic and the contractors for their cooperation in the field tests on the N19. The technical staff of BRRC is acknowledged for their technical support in the laboratory and on the test sections.

## References

Bochove G (2000), Porous asphalt (2-layered) - Optimising and Testing. Proceedings of the 2nd Eurasphalt & Eurobitume Congress 2000, paper 402-100, Barcelona, 2000

CEN/TC 227 EN 12697-33 Bituminous mixtures – Test methods for hot mix asphalt – Part 33: Specimen prepared by roller compactor, 2007

De Visscher J, Vansteenkiste S, Vanelstraete A (2012) Laboratory tests for internal cohesion of thin and ultra-thin surface courses. Proceedings of the 5th Eurasphalt & Eurobitume Congress 2012, Istanbul, June 2012

Hamlat S, Hammoum F, Hicher P-Y, Terrier J-P (2007) Laboratory evaluation of the resistance to tangential forces of road surfacing materials. IFSTTAR BLPC n° 267 2007, p 49–60, april-june 2007

Haulet J.-P. (2014) Performance characteristicsof surface courses in stone mastic asphalt with addition of reclaimed asphalt. Master thesis, Universiteit Antwerpen, Academic year 2013-2014

Jacobs M, Gharabaghy C, Schulze C, van den Bremt R (2012) Bepaling van de rafelingseigenschappen van open asfaltmengsels met de ARTe. Paper CROW infradagen 2012, The Netherlands, 2012

Qualiroutes (2012), Cahier des Charges Type, Service Public de Wallonie, version 2012

Root V (2008) Entwicklung eines Prüfverfahrens zur Beurteilung des Widerstandes von Asphaltdeckschichten gegen Schubbeanspruchungenb and der Oberfläche, Dissertation, Schriftenreihe des Instituts für Verkehrs, Technische Universität Darmstadt

Schulze C, Cyrus Gharabaghy C (2008) Kornausbrüche bei Offenporigen Asphalten - Prognoseprüfung und Bewertung, ISAC, RWTH Aachen, Germany, Powerpoint presentation, Germany, November 2008

Vansteenkiste S, De Visscher J, Denayer C Influence of hydrated lime on the field performance of SMA10 mixtures containing polymer modified binder, paper submitted to E&E congress in Prague 2016

# Part IX
# Field Measurement and In Situ Characterization

# Active Filler's Effect on In Situ Performances of Bitumen Emulsion Recycled Mixtures

**G. Betti, G. Airey, K. Jenkins, A. Marradi and G. Tebaldi**

**Abstract** This paper address the in situ performance over time of different bitumen emulsion stabilized mixtures blended with different types of fillers (cement, lime and mineral filler), monitored during the first year from construction. Results are part of a more extensive research program aimed to investigate the effects of using lime as active filler in cold recycled mixtures, both with bitumen emulsion and foam bitumen. A specific test track has been designed on a construction road near Florence in order to evaluate the evolution of mixture performance over time. Short term bearing capacity has been evaluated by means of LWD (Lightweight tests) after 4 h from compaction while FWD tests have been performed after 24 h, 14 days, 28 days and 9 months to monitor the mid-term performances. Up until mid-2014 tests road was not yet opened to traffic so the mixtures experienced only construction traffic loads. Results obtained positively support the use of lime as

G. Betti (✉) · A. Marradi
Department of Civil and Industrial Engineering, University of Pisa, L. Lazzarino, 56126, Pisa, Italy
e-mail: g.betti@dic.unipi.it

A. Marradi
e-mail: a.marradi@ing.unipi.it

G. Airey
NTEC, University of Nottingham, Pavement Research Building, University Park, Nottingham NG7 2RD Gordon, UK
e-mail: airey@nottingham.ac.uk

K. Jenkins
Department of Civil Engineering, University of Stellenbosch, Private Bag X1, Matieland 7602, South Africa
e-mail: kjenkins@sun.ac.za

G. Tebaldi
Department of Civil and Environmental Engineering and Architecture, University of Parma, Via G.P. Usberti 181/a, Parma 43124, Italy
e-mail: gtebaldi@unipr.it; gtebaldi@ufl.edu

G. Tebaldi
E.S.S.I.E, University of Florida, 365 Weil Hall, P.O. Box 116580, Gainesville, FL 32611, USA



F. Canestrari and M.N. Partl (eds.), *8th RILEM International Symposium on Testing and Characterization of Sustainable and Innovative Bituminous Materials*, RILEM Bookseries 11, DOI 10.1007/978-94-017-7342-3_64

active filler in the bitumen emulsion stabilized material and underline the effect of different blends of fillers in the material behaviour. FWD tests are scheduled to be repeated every 6 months in order to monitor the stiffness evolution of the mixtures and evaluate the nature of traffic damage.

**Keywords** Cold recycling · Performances tests · FWD · LWD

## 1 Introduction

Asphalt mixtures are the most common materials employed in road pavements around the world thanks to their availability and ease of use. In the face of benefits, the use of these kinds of materials involves many sustainability challenges. More frequently the regulation made by local agencies and public administrations are specifically devoted to reduce the amount of materials to be disposed of and encourage recycling. Accordingly, using asphalt mixtures the stakeholders have to solve different issues raising from sustainability and specifically focusing on how to reuse the materials and how they are manage after demolition.

From a general point of view, asphalt mixtures can be fully recycled in plant or in field using hot recycling techniques or cold recycling techniques (Tebaldi et al. 2012). Considering greenhouse emissions, impact on traffic and fuel consumption, from the environmental point of view the most efficient technique is the in-place full-depth reclamation using a cold recycling technique. One of the most used is the bitumen stabilization with foam bitumen or emulsions. This is most probably due to the possibility to perform stabilization using RA (Reclaimed Asphalt) aggregates from the bound layers mixed with materials coming from the unbounded pavement layers. Together with several advantages, the in situ bitumen stabilization also brings some challenges regarding the role of active fillers and their optimal use. The reasons of using active fillers in the bitumen-stabilized mixtures mainly are as follows:

- facilitate the dispersion of bitumen in the mixture: active filler's particles catch the droplets of bitumen made by the blasting of the bubbles of foam bitumen or made by the flocculation of the emulsion's bitumen and take them in the mixture;
- to have a quicker strengthening of the mixture and consequently to reach rapidly the necessary bearing capacity of the layer (cement is mainly used for this purpose);
- to control the moisture content.

In addition to previous tasks, sometimes in full depth reclamation it is necessary to stabilize clay particles found in the unbounded layer from the subgrade. To reach this goal, the most used technique involves the use of lime as a stabilization agent; it generally means that cold recycling process needs to be performed using a blend of fillers (Asphalt Academy 2009): lime for stabilization of clay particles, cement to

quickly achieve the necessary bearing capacity and mineral filler originally present in the granular material of unbounded layer.

The problems arising for the use of active fillers may be synthesized in the following questions:

- Which is the most appropriate active filler to be used?
- What is the correct amount of active filler to be used?
- In case of a blend of active fillers, what is the correct ratio between the different components?

In spite of practical experience, from a scientific point of view there are still many issues to solve. In particular, the relationship between active filler and performance of bitumen-stabilized material is unclear. Nowadays limited literature is available regarding the effect on long-term performance of cold recycled mixtures incorporating different blends of active fillers.

In an effort to develop a better understanding of the stiffness evolution of bitumen-stabilized materials (with bitumen emulsion and foam bitumen) over time related to the blends of active fillers used, a comprehensive research project was established by University of Pisa, University of Stellenbosch, University of Parma and University of Nottingham involving both laboratory and site tests. This paper presents the results of a part of the project focused on the investigation of on-site mid-term performances of fully recycled mixtures produced by adding bitumen emulsion and different blends of fillers made by cement, lime and mineral filler.

Three mixtures made with 100 % RAP (Reclaimed Asphalt Pavement), bitumen emulsion, lime, cement and mineral filler were used to build three consecutive experimental sections on a constructing road near Florence. The performance of the mixtures were investigated over time using Light Weight Deflectometer after compaction (short-term performances), and Falling Weight Deflectometer in the mid-term (24 h, 14 days, 28 days and 9 months). During this period mixtures experienced only construction traffic as the road was not yet opened to traffic; this is why, for the purpose of this paper, assessment made on performances evaluated after 9 months are considered to be related to the mixtures properties alone, without need to consider the effect of traffic and assuming mixtures are all completely cured in the same way.

The results obtained when all the mixtures can be considered to be fully cured allow some preliminary considerations and some fundamental hypotheses on behaviour of bitumen emulsion stabilized mixtures to be made; these hypotheses are under verification in the ongoing phases of the project, in particular considering weather and traffic effects.

## 2 Objective and Scope

The objective of this research work is to investigate and characterize the evolution of performance properties of bitumen emulsion stabilized mixtures containing different blends of fillers, made with cement, lime and mineral filler, over time.

Even though the in situ recycling technique could have been appropriate for full depth recycling in this case, in order to minimize the variability and to keep under control all the different components to have as much as possible homogeneous mixtures, all the mixtures was made with a mobile mixing plant using only sieved RAP and laid down with a paver.

The comparison between the performance of different mixtures was based on the elastic modulus evaluated on the basis of deflectometric tests at different times after construction. All the tests were carried out using the FWD with exception of the test, immediately after compaction, with the Light Weight Deflectometer.

In order to underline the performance evolution over time, avoiding the effect of traffic loading on mixtures curing process, pavement was completed and the road was open to traffic after 9 months; after this period it was possible to consider all mixtures to be fully cured with curing process independent from traffic loads. During the 9 months, the layer made with BSM (Bitumen Stabilized Material) was protected by weather effects with a specific surface treatment. LWD and FWD tests were made after 4 and 24 h to evaluate immediate performance. Moreover further FWD tests were made after 14 and 28 days when the setting reaction of cement may be considered to be completed. The last FWD survey have been made after 9 months, before last paving operations and traffic opening in order to focus on the midterm performances.

## 3 Materials and Investigation Method

### *3.1 Materials Mixtures and Test Track*

Test tracks have been realized using bitumen emulsion stabilized mixtures with different blends of fillers made by three component (cement, lime and mineral filler). According to Italian practice regarding cold recycling, an over stabilized bitumen emulsion was selected. These emulsion are specifically produced using special additives in order to delay (almost to stop) the breaking process and to maximize the mixture workability. Due to these specific characteristics, a minimum amount of cement is required in order to promote the development of the breaking process. The cement hydration absorbing water alters the thermodynamic equilibrium of the system triggering the emulsion breakage. The total amount of filler in the mixes was kept constant and a minimum amount of cement, considering the emulsion characteristics, of 1 % of dry aggregates weight was set. For all these reasons the evaluation of the mixtures performances should be carried out based on the hypothesis that 1 % of cement does not work as an active filler but it works to promote the development of the emulsion breaking process. In the case of the use of traditional emulsion this minimum amount of cement would be not required.

The overall characteristics of the bituminous binder used in the present research are reported in Tables 1 and 2.

**Table 1** Characteristics of the bitumen emulsion used within the present study

| Characteristics | Standard reference | Unit | Values |
|---|---|---|---|
| Water content | EN 1428 | % | 40 |
| Bitumen content | EN 1431 | % | 60 |
| pH | EN 12850 | | 3 |

**Table 2** Characteristics of the bitumen

| Characteristics | Standard reference | Unit | Values |
|---|---|---|---|
| Penetration @25 °C | EN 1426 | dmm | 70 |
| Softening point | EN 1427 | °C | 50 |
| Fraass | EN 12593 | °C | −10 |

Cold recycled mix is made by two fractions of RA aggregates to form the stone skeleton, which results made with 100 % RA aggregates. Grading composition was kept the same for all the mixtures. The total amount of filler in the mix was optimized by means of laboratory tests in order to reach the OMMC (Optimum Moisture Mixing Content). A complete report on the mix design process will be published in the near future.

Resulting mixtures mix design is presented in the following Table 3.

Test track was located on a constructing road near Florence. The test pavement included a base course comprising 17 cm of bitumen emulsion stabilized material placed over a lime stabilized subgrade. Compaction was extended until reaching the reference level of 100 % the Modified Proctor density using a combi-roller (front rubber and rear metallic drum). The pavement will be completed with additional 4 cm of asphalt concrete wearing course, laid directly over the recycled layer (laying of wearing courses has been completed after 1 year from construction of recycled layer). The entire pavement structure was specifically designed with the only aim to reach the stress and strain distribution under load allowing researchers to clearly underline the different performances of tested mixtures.

An extensive LWD test campaign was carried out before construction of the studied mixtures allowing to control the bearing capacity and compaction level achieved by the subgrade, and underline presence of weak areas (Marradi et al. 2014). Subgrade performance appeared to be very high: the resulting average Surface Modulus ranged between 350 and 450 MPa.

**Table 3** Mix design results of study mixtures

| Mixture ID | Bitumen emulsion (%) | Water add (%) | Cement (%) | Lime (%) | Mineral filler (%) |
|---|---|---|---|---|---|
| 2A | 3 | 3 | 1 | 2 | 1.5 |
| 2B | 3 | 3 | 1 | 0 | 3.5 |
| 4D | 3 | 3 | 2.5 | 0 | 2 |

Short term performance of bitumen emulsion stabilized mixtures was evaluated by means of LWD tests after 4 h and FWD after 24 h curing. Results obtained were compared with requirements provided by the Italian Road Authority ANAS specification regarding foam recycled layers in plant (*surface modulus carried out by means of LWD tests should be higher than 45 MPa after 4 h from compaction and higher than 170 MPa after 24 h*) in order to control the short term performances of the mixes and agree the completion of paving work; surface modulus undertaken both after 4 h (LWD tests) and 24 h (FWD tests due to the achieved stiffness of the mix) exceeded the previous mentioned threshold values (Betti et al. 2014).

To evaluate the mid-term performances, further FWD tests were carried out after 14 and 28 days, when the setting reaction of cement may considered completed, and after 9 months in order to have the mixtures completely cured, just before last paving operations and traffic opening. Measured deflections have been used to estimate layer moduli (Odemark Boussinesq's backcalculation model MET Method of Equivalent Thickness—Dynatest Elmod backcalculation software) and evaluate their evolution over time (last FWD survey was performed just before wearing course paving operation). A two layer model has been used for backcalculation purpose where the upper layer refers to bitumen emulsion stabilised material only. The road experienced no traffic loading during the first 9 months which meant that full curing was achieved independent of any effects that may be associated with traffic loads.

## *3.2 Materials Temperature Sensitivity Analysis*

Field tests have been performed in different seasons, consequently a significant variation of pavement temperatures was experienced. In order to take into account the changes in material's response under different climate conditions, and to gain information about mixtures temperature sensitivity, future tests will be scheduled in different seasonal periods, exploiting the variable climate conditions of the centre part of Italy during the year. This approach involves the need to develop a procedure to correct moduli evaluated at the test temperature to the 20 °C reference value.

Previous research on cement treated mixtures with high content of RA aggregates underline a variation of layer moduli from tests carried out in different seasons (winter and summer), revealing a sort of temperature sensitivity due to the presence of RA (Isola et al. 2013). Regarding bitumen stabilized materials, Plati et al. presented a specific equation, based on laboratory results, to correct layer moduli to 20 °C reference temperature. More recently the effect of temperature on Resilient Modulus of foam bitumen stabilized mixtures with different amounts of RA aggregates have been investigated: results obtained underline that high percentage of RA aggregates could led to early fatigue in the pavement as well as permanent deformation (Dal Ben 2014).

Within the present research work an innovative procedure to evaluate temperature variation of bitumen emulsion stabilized layer moduli is presented, based on assessment of FWD tests. The basic idea is to perform FWD tests in the same day (same curing level), paying attention to perform tests with significant difference in the pavement temperatures.

Measured deflections, recorded for each mixture, have been back-calculated to estimate layer moduli and estimate their variation due to only temperature. Resulting moduli at different temperatures were then used to calibrate a specific value for temperature sensitivity parameter "α" for each mixture, provided by the generalized version of the equation for temperature correction provided by the Asphalt Institute (Eq. 1) (Harichandran et al. 2000).

$$E_{Ts} = 10^{\alpha \cdot (T^2 - T_S^2)} \times E \tag{1}$$

where $E_{Ts}$ is the layer modulus at the reference temperature, E is the modulus at test temperature, T (°F) is the test temperature, $T_s$ (°F) is the reference temperature and α is a temperature sensitivity parameter. Asphalt Institute suggest a value of $\alpha = 1.47362 \times 10^{-4}$ to be applied for correction of new road asphalt mixtures layer moduli.

The experimental procedure previously described was applied to all the mixtures in order to find three different values of α to be used for correction of bitumen emulsion layer moduli at the 20 °C reference temperature. This approach has been applied to the moduli evaluated from deflections recorded during the four tests campaign after construction (24 h, 14, 28 days and 9 months). Results obtained are reported in the next graph where the trend of temperature variation of recycled layer moduli is compared to the ones obtained using the equation provided by Plati et al., Asphalt Institute equation for new asphalt mixtures (Eq. 1) and also equation provided by the HD 29/08 Standard (Fig. 1).

Results underline the significantly lower temperature sensitivity of the bitumen emulsion stabilized mixtures analysed in this research work compared to variations typical of asphalt mixtures.

This behaviour may have an important implication in pavement design; in warm climate areas, like the one experienced in Italy, stiffness variation over the year due to air temperature variation from cold to hot seasons can be considered quite low. For this reasons, regarding the temperature sensitivity of bitumen emulsion stabilized materials, they seem to perform more like a "super-performing granular material" (Collings et al. 2011) than an asphalt concrete.

The resulting average moduli for each period of testing ($E_{1t}$ at the test temperature) are presented in Table 3 together with average moduli at the 20 °C reference temperature ($E_{1ts}$). The layer temperatures, measured through a thermometer placed in a drilled hole inside the pavement, are also reported.

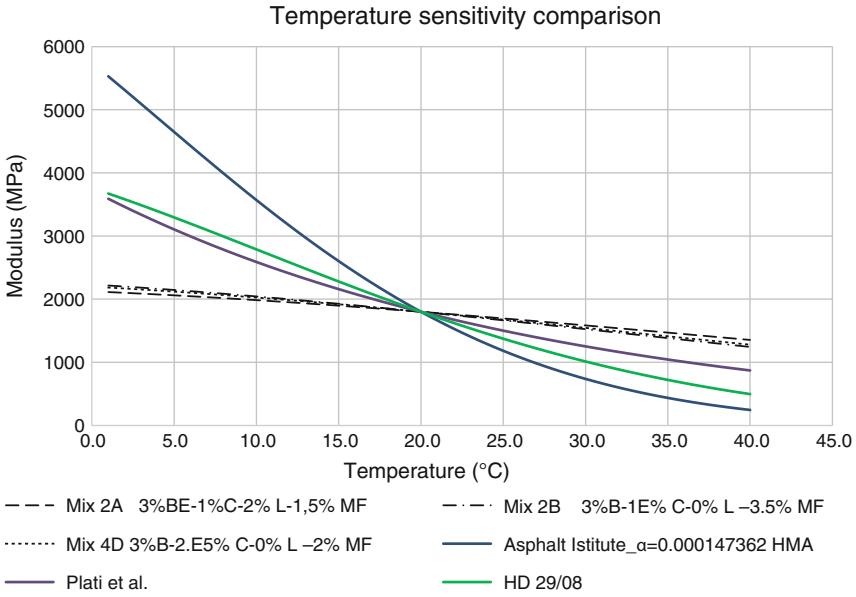


**Fig. 1** Trend of moduli variation with temperature

The approach proposed involves some approximation and is probably the reason for some scatter in the results obtained but is needed in order to have performances directly comparable (Table 4).

**Table 4** Temperature sensitivity of recycled mixtures

| Curing | E1t (MPa) | T (°C) | E1t/E1ts | α | E1ts (@20°C) (MPa) |
|---|---|---|---|---|---|
| *Mix 2A 3 %BE-1 %C-2 % L-1, 5 % MF* | | | | | |
| 24 h | 893 | 27 | 1.09 | 0.00002 | 973 |
| 14 days | 1111 | 29 | 1.12 | 0.00002 | 1245 |
| 28 days | 1415 | 16.7 | 0.97 | 0.00002 | 1366 |
| 9 months | 992 | 24.7 | 1.06 | 0.00002 | 1049 |
| *Mix 2B 3 %BE-1 % C-0 % L-3.5 % MF* | | | | | |
| 24 h | 825 | 24.5 | 1.07 | 0.000026 | 885 |
| 14 days | 1018 | 28 | 1.14 | 0.000026 | 1159 |
| 28 days | 1365 | 17 | 0.96 | 0.000026 | 1309 |
| 9 months | 1090 | 25.7 | 1.09 | 0.000026 | 1193 |
| *Mix 4D 3 %BE-2.5 % C-0 % L-2 % MF* | | | | | |
| 24 h | 774 | 29.2 | 1.15 | 0.000024 | 889 |
| 14 days | 1070 | 27.1 | 1.11 | 0.000024 | 1189 |
| 28 days | 1250 | 18 | 0.97 | 0.000024 | 1218 |
| 9 months | 1509 | 26.5 | 1.1 | 0.000024 | 1660 |

## 4 Results and Discussion

Back-calculated layer moduli are reported in the next graph comparing values obtained on each mixture for the four series of tests carried out at different curing times. Results are organized to show both values obtained on each test location (8 test locations per mixture) and average values for the four curing levels together with the coefficient of variation (CV) to underline the spatial variation of resulting moduli. LWD tests results on the subgrade are also presented in order to underline its influence on recycled mixtures performances.

Since mixtures compaction may influence the stiffness growth of mixtures containing cementitious binder (Lancieri et al. 2006), LWD average modulus obtained after 4 h from compaction are also presented.

All the tests have been carried out before opening to traffic, during the first nine months from construction. For this reason all the mixes can be considered completely cured in the same manner, without being subjected to traffic post compaction effect. Moduli reported in the next graphs are all corrected to 20 °C reference temperature, applying the procedure previously reported (Figs. 2, 3 and 4).

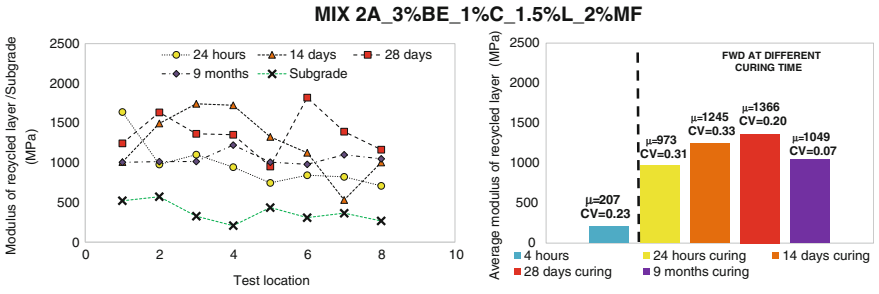


**Fig. 2** Performance over time: mixture 2A

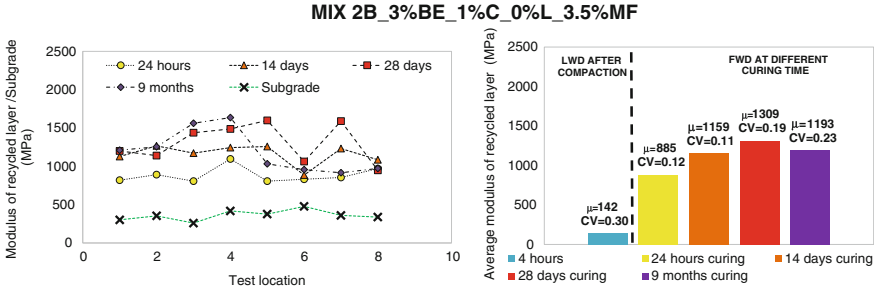


**Fig. 3** Performance over time: mixture 2B

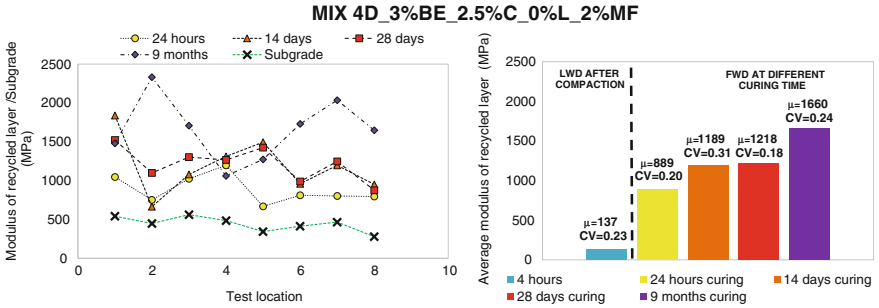


**Fig. 4** Performance over time: mixture 4D

To compare the performance evolution over time of all the mixtures analysed and evaluate the influence of the different blends of active fillers, the average values of layer moduli at different curing times are plotted together in the subsequent graph (Fig. 5).

Results presented show that stiffness of mixtures 2A, 2B increase rapidly in the first 14 days of curing and remain almost stable in the next period. On the other hand the layer modulus of mixture 4D continue to increase after 28 days of curing, reaching at the end of curing, values significantly higher than mixtures 2A and 2B. This means that mixtures without cement (2A, 2B, 1 % of cement is used only to manage the emulsion breakage) show rapid stiffness increase in the first period while mixture with an high content of cement (4D) shows the higher stiffness at the end of curing (9 months) even if the rate of stiffness growth seems to be lower. These results led to consider the behaviour of mixtures with 2.5 % of cement to be

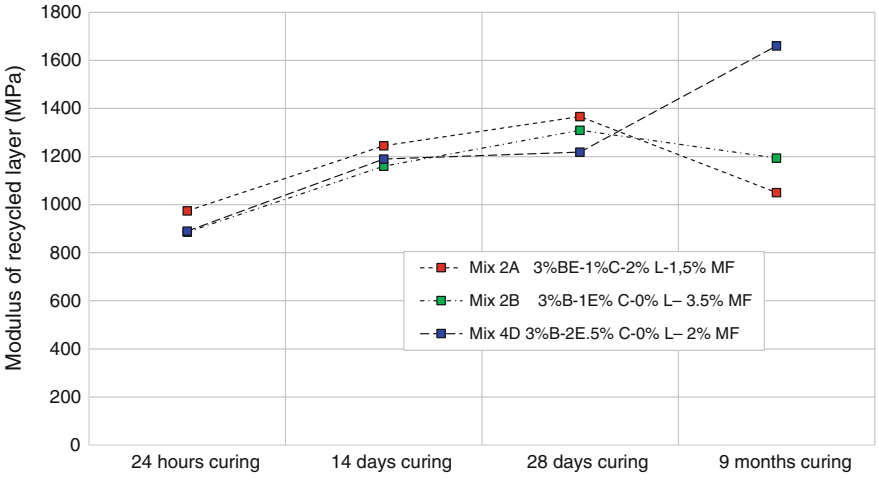


**Fig. 5** Comparison of mixtures performance over time

more likely to form a continuously bound material able to increase stiffness over time as an effect of curing. On the other hand, mixtures without cement appear to behave like a non-continuously bound material capable of rapid stiffness increase in a very short term period (14 days) and remain almost constant after that.

To verify these assumptions the test track will be monitored in the future in order to evaluate the long term performances of the mixtures. Special regard will be devoted to the effect of traffic and the consequent failure of the material in terms of fatigue cracking (reduction of stiffness for a continuously bound material) or in terms of permanent deformation (stiffness increase over time for a unbounded or un-continuously bonded material) (Collings et al. 2011). It worth also noting that, based on the Italian practice, the order of magnitude of the back-calculated moduli is in a realistic range. At the same time, the influence of traffic loading will need to be included through FWD measurements at least 3–5 years after construction, before a steady state stiffness can be determined for structural design purposes.

## 5 Summary and Conclusions

In the present study, the effect of different blends of fillers on performance evolution over time of bitumen emulsion recycled mixtures has been analysed. Results are based on FWD tests carried out on a specifically designed test track monitored within the first year. To minimize the variability and to keep under control all the different components to have as much as possible homogeneous mixtures, all the mixtures were produced with a mobile mixing plant using only sieved RA aggregates and laid down with a paver.

In order to achieve full curing avoiding any effect of traffic on mixtures performances, the road was opened after 9 from construction. During the 9 months a specific surface treatment were used to protect mixtures from weather effects. LWD and FWD tests were made after 4 and 24 h to evaluate immediate performances and further FWD tests were made after 14 and 28 days when the setting reaction of cement may be considered completed and after 9 months, before last paving operations and traffic opening, to evaluate the midterm performances.

To compare moduli obtained in different temperature conditions an innovative procedure, based on FWD tests was followed allowing authors to correct moduli at test temperature to the 20 °C reference temperature. Results obtained underline the lower temperature sensitivity of the bitumen emulsion stabilized mixtures compared to variations typical of asphalt mixtures. From a practical point of view, these results allow the stiffness variation from cold to hot seasons to be considered to be quite low. Regarding the temperature sensitivity, bitumen emulsion stabilized materials seem to performs more like a "super-performing granular material" (Collings et al. 2011) than an asphalt concrete.

In terms of performances, mixtures with no cement (2A and 2B) seem to have a quick growth of stiffness in the first period (14 days), remaining almost stable after that. On the other hand the layer modulus of mixture 4D continued to increase after

28 days of curing, reaching at the end of curing values significantly higher than mixtures 2A and 2B. These results led to consider the behaviour of mixtures with 2.5 % of cement more like that of a "continuously bound" material, able to increase stiffness over time as the primary effect of curing. On the other hand, mixtures without cement appear to behave like a non-continuously bound material capable of rapid stiffness increase in the very short-term period (14 days) and remain almost constant after that.

To verify these assumptions test track will be monitored in the future in order to evaluate the long-term performances of the mixtures. Special regard will be devoted to the effect of traffic and its influence on material failure.

## References

Asphalt Academy Technical Guideline: Bitumen Stabilized Materials. A guideline for the Design and Construction of Bitumen Emulsion and Foamed Bitumen Stabilized Materials Asphalt Academy, Pretoria South Africa, 2009.

Betti G., Cocurullo A., Marradi A., Tebaldi G., Airey G., Jenkins K., "Effect of Lime on Short-Term Bearing Capacity of Bitumen Emulsion Recycled Mixtures". Proceedings of the International Conference on Asphalt Pavement ISAP, North Carolina, USA, 2014.

Collings D., Jenkins K., "The Long Term Behaviour of Bitumen Stabilised Materials (BSMs)", proceedings of the 10th Conference on Asphalt Pavement for Southern Africa, CAPSA 2011.

Dal Ben M., "Resilient Response and Performance of Bitumen Stabilized Materials with Foam Incorporating Reclaimed Asphalt", PhD Thesis at Stellenbosh University, January 2014.

Harichandran R., Ramon C., Baladi G., "Michback User Manual", Department od Civil and Environmental Engneering, Michigan State University, 2000.

Isola M., Betti G., Marradi A., Tebaldi G., "Evaluation of Cement Treated Mixtures with High Percentage of Reclaimed Asphalt Pavement". Construction and Building Materials volume 48, pp 238-247, London 2013.

Lancieri F., Marradi A., Mannucci S., "C&D Waste for Road Construction: Long Time Performance of Roads Constructed Using Recycled Aggregates for Unbound Pavement Layers", proceedings of the 3rd International Conference on Waste Management and the Environment, Waste Management, Malta 2006.

Marradi A., Pinori U., Betti G., "Subgrade and Foundation Dynamic Performance Evaluation by Means of Light Weight Deflectometer". Proceedings of the 2014 TRB annual meeting. Paper accepted for the publication on the TRR Transportation Research Record Journal.

Tebaldi G., Dave. E., Marsac P., Muraya P., Hugener M., Pasetto M., Graziani A., Grilli A., Marradi A., Wendling L., Gaudefroy V., Jenkins K., Loizos A., Bocci M., Classification of Recycled Asphalt (RA) material. Paper presented at the 2nd International Symposium on Asphalt Pavements & Environment, ISAP TC APE, Fortaleza, Brazil, October 1-3 2012.

# Innovative Longitudinal Joints Between New and Old Porous Asphalt

**Jan Voskuilen and Lambert Houben**

**Abstract** For both lane and carriageway wide maintenance of Porous Asphalt (PA) in the Netherlands, contractors increasingly make use of so called joint protectors to prevent premature damage to longitudinal joints in the warranty period of 7 years. Mostly strips of bituminous material are placed on those joints or the joints are poured with hot bitumen and sanded, but sometimes no measures are taken. Those joint protectors can eventually go smooth and/or shiny. Rijkswaterstaat (RWS) gets relatively many complaints of especially motorcyclists, because they are more vulnerable and driving in the middle of the lane where sometimes the joint is. Claims are also made. Sometimes joint protectors are mistaken for "ghost" marking, especially during rainfall, because they are more visible than the mark. In short, RWS was not satisfied with the current joint protectors. In order to remedy this, RWS started a competition to come up with improvements. Contractors came with 11 ideas that were assessed on skid resistance, shine, traffic hindrance, environmental friendliness and costs. Five winners were selected by an independent jury. Those prize winners were able to demonstrate their idea on a PA test section on motorway A59. Cores from these test sections, drilled on the joint, were investigated in the laboratory. One year after construction the joints were visually inspected, and the skid resistance and horizontal water drainability was measured. This paper discusses the winning ideas, the construction of the test sections, the laboratory and field tests and results.

**Keywords** Longitudinal joints · Porous asphalt · Maintenance · Skid resistance

J. Voskuilen (✉)
Ministry of Infrastructure and the Environment, Rijkswaterstaat, Utrecht, Netherland
e-mail: jan.voskuilen@rws.nl

L. Houben
Delft University of Technology, Delft, Netherland
e-mail: l.j.m.houben@tudelft.nl



F. Canestrari and M.N. Partl (eds.), *8th RILEM International Symposium on Testing and Characterization of Sustainable and Innovative Bituminous Materials*, RILEM Bookseries 11, DOI 10.1007/978-94-017-7342-3_65

# 1 Introduction

Since 1990 the policy in the Netherlands is to apply only silent pavements on motorways. In 2014 more than 90 % of the motorways has a Porous Asphalt (PA) wearing course. Due to the higher traffic load, the slow lane is mostly replaced after 11 years. The average end of service life of the fast lane is 17 years. So, the most applied maintenance technique is to replace after 11 years only the slow lane PA and lay a new PA wearing course carriageway wide after 17 years. Due to the inlay after 11 years, a longitudinal joint is created between old and new PA. The purpose of joint protectors is to preserve the connection between new and old PA. Joint protectors are increasingly used by contractors in predominantly longitudinal joints to avoid premature damage during the 7 years warranty period. Damage of the joint can be caused by the fast milling speed of old PA, which can initiate micro cracks in the mortar forming bridges between the coarse aggregate. Also the bonding between hot new PA and cold old PA is not optimal. A hot to hot PA construction gives a better bonding, so this is preferred. The old PA can also be preheated with a joint heater. If a joint is widening, it is often the start of raveling and can sometimes be a slot formed in the PA.

In recent years RWS was increasingly confronted with complaints from road users about joint protectors. Joints are often poured with hot bitumen and whether or not sanded with fine mineral aggregate, bituminous strips are sometimes stuck on, there are other types of joint protectors, but sometimes also nothing is done and hot PA is directly placed to cold old PA. Many of these joint protectors become smooth or slippery over time and will shine.

There are relatively common complaints, especially from motorcyclists, about too smooth joint protectors. This is because they are more vulnerable, but there are also complaints from other road users. During rainfall they assess shiny joint protectors sometimes as ‘ghost’ markings. These ‘ghost’ markings may be specifically present in curves where the joint is between marking lines and that can lead to dangerous situations. RWS has already received claims related to motorcycle accidents due to a too smooth surface of the joints. Measurements with the Skid Resistance Tester (SRT) have confirmed this. SRT-values between 28 and 32 were found, while the requirement is ≥45.

Because traffic safety is top priority, RWS decided to challenge the market to come up with good solutions.

## *1.1 Competition Joint Protectors*

In order to improve the current protectors for longitudinal joints, RWS started a competition to challenge the contractors to come up with improvements. The main idea is to develop an innovative durable joint with good skid resistance and no

shining. The water permeability in horizontal direction should also be sufficient. The following selection criteria were applied by the jury:

1. skid resistance and no shining (weighing factor 4);
2. durability and life-time of joints (weighing factor 3);
3. minimum traffic hindrance during application (weighing factor 1);
4. environmental friendly materials and application process (weighing factor 1);
5. costs of production and application of the joints (weighing factor 1) (Figs. 1, 2, 3, 4 and 5).

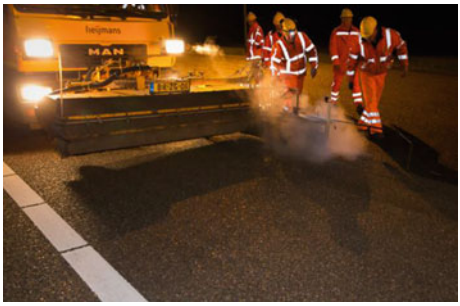


**Fig. 1** Airjetseal

**Fig. 2** Jointfix PB


**Fig. 3** Jointfix UV

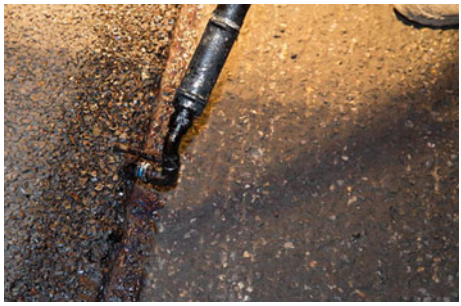

**Fig. 4** Direct vertical seal

**Fig. 5** Lassealer

Five winners got the opportunity to demonstrate their ideas on a PA test section on the motorway A59 near Waalwijk during the night from September 27 to 28, 2013. This motorway had to be maintained with an inlay in the slow lane. As shown in Table 1, in five test sections the joints between old and new PA were treated with the innovative joint protectors of the five winners. The A59 has two carriageways with 2 lanes and one emergency lane per carriageway. The slow lane was milled and a new PA mixture was laid back. The joint between old and new PA is approximately 50 mm left of the middle marking. The old PA contained crushed river gravel with a minimum PSV value of 53, the new PA contained a crushed quarry material with a minimum PSV value of 58.

**Table 1** Overview of locations test sites on motorway A59 HRL1

| Joint code | Airjet seal (H) | Reference (R) | Jointfix PB (E1) | Direct vertical seal (B) | Jointfix UV (E2) | Las-sealer (M) |
|---|---|---|---|---|---|---|
| Start (km) | 11.23 | 11.21 | 11.18 | 11.16 | 11.14 | 11.12 |
| End (km) | 11.21 | 11.18 | 11.16 | 11.14 | 11.12 | 11.10 |

Due to the fast milling process on the slow lane, the mortar bridges in the old PA on the fast lane can be damaged and initial micro cracks can grow further. To heal these micro cracks, it is a standard method in the Netherlands to apply a bitumen emulsion containing a rejuvenator on 0.5 m of the adjacent old PA. In this case, only the reference test section (R) was treated with such a product. In this project Modimuls TT was used. Also to avoid premature damage in the old PA, on Dutch motorways it is forbidden to drive with rollers on the old PA.

## 2 Research Plan

Field cores of diameter of 150 mm were drilled out of the test sections in such a way that the joint between new and old PA is in the middle of the core.

In Table 2 an overview is given of the whole test program. More background information about the lab tests can be found in (Houben et al. 2014) and more background information about the field tests carried out one year after construction can be found in (Buurman 2014).

### *2.1 Siemens CT Scanner*

The internal structure of the joint system is assessed using the Siemens medical CT scanner (on 150 mm core). Dependent on the grey scale of different compositions (stone, mortar + clogging, air voids) due to density difference, different compositions can be distinguished with a resolution of 0.3 mm. The distribution of the compositions can be obtained each 1 mm over the horizontal and vertical direction of the specimen. The internal joint system can also be visualized.

**Table 2** Overview of tests

| Test | Reasons |
|---|---|
| CT | Internal structure of the joints |
| Direct tension test (DTT) | Bonding strength at low temperature |
| Permeability test (lab) | Water permeability of the joints (lab) |
| Rotating surface abrasion test (RSAT) | Raveling resistance of the joints |
| Skid resistance test (SRT) | SRT before and after RSAT |
| Permeability test (field) | Water permeability 1 year after construction |
| SRT | In situ SRT 1 year after construction |
| Visual inspections | Performance of the joints after 1 year |

## 2.2 Permeability Tests

Permeability tests were carried out on specimens taken from the test section directly after application and in situ after one year.

### 2.2.1 Permeability Tests on Laboratory Specimens

In order to measure the bonding strength of the system a beam specimen was produced through the 150 mm samples with length * height * width of 90 * 45 * 60 $mm^3$. There is a slope of the interface between the old and new PA. A permeability test was applied to the samples. The surrounding of the specimens was sealed and a modified Becker test was designed as shown in Fig. 6. The sample is placed under the Becker test allowing water passing through from old PA (top) to new PA (bottom), simulating the water flow from the fast lane to the slow lane. 500 ml of water was applied from the top of the specimen. The time for the water draining to the bottom of the specimen was recorded.

### 2.2.2 In Situ Permeability Test for Joints

A 1.5 l PET bottle is mounted upside in a frame. The bottleneck can be closed and opened by moving a rubber ball with a steel rod. The bottleneck is placed 20 mm above the old PA and 100 mm from the joint (see Fig. 6). During the test 1 liter water flows over the old PA to the new PA due to the slope of 2 %. If there is no barricade of the joint, the water spot at the location of the joints is small. If there is a

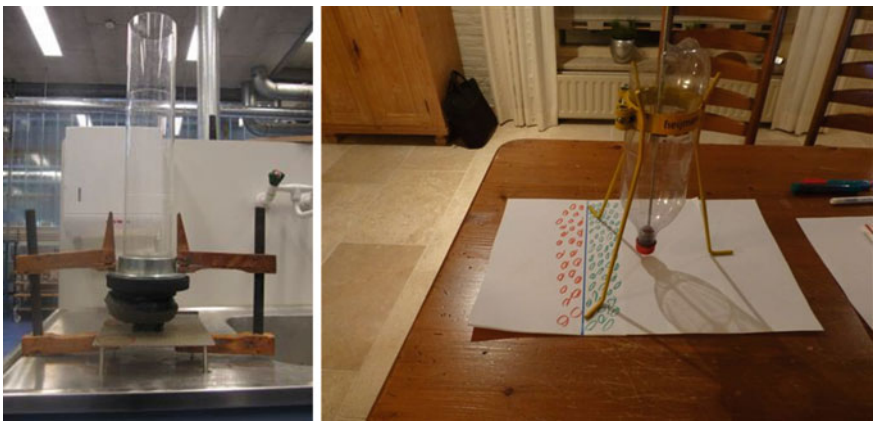

**Fig. 6** Illustration of permeability lab test (*left*) and Breda bottle test (*right*), *green* is old PA, *red* is new PA

barricade due to the joints, the water spot is wider. So the width of the water spot measured in cm is the result of the Breda Bottle test.

## 2.3 Direct Tension Test

As shown in Fig. 7, the rectangular samples were tested in the temperature controlled UTM to measure the failure strength at low temperature (−5 °C) which is most critical with respect to widening of the joints. Three LVDTs were used to control the displacement speed. The global force-displacement curve was recorded.

The direct tensile tests are carried out with a low speed of 0.012 μm/s to simulate the displacements in the PA in the field when it is cooling down in winter.

## 2.4 Raveling Resistance

In order to investigate the surface performance of the joints, RSAT tests were performed 3–4 months after application of the innovative joints. Prior to the RSAT tests the cores were stored at a temperature of 5 °C.

As shown in Fig. 8, in a RSAT test an octagonal plate of 500 mm in diameter is charged by a wheel with a solid rubber tire. Three cores with a diameter of 150 mm from the road surface are glued in a plate. The wheel is vertically loaded with a contact pressure of 0.6 MPa and tilted (33.7°) with the direction of back and forth movement to introduce horizontal forces on the surface. The entire surface of the test plate is substantially uniformly loaded by rotating the test plate during the test

**Fig. 7** Illustration of the direct tension test

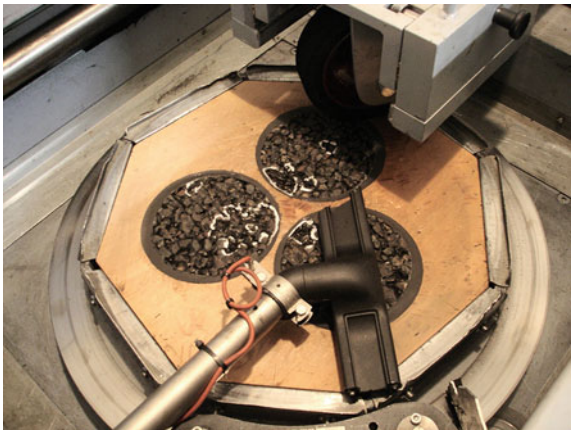

**Fig. 8** Illustration of RSAT

(496 circles per hour). During the 24 h test at a temperature of 20 °C, the loss of material from the surface is collected continuously with a vacuum cleaner. The loss of stones with a grain diameter of more than 2 mm is reported as raveling damage.

The intention was to perform a skid resistance test before and after the RSAT test, to evaluate the skid resistance of the joints before and after the accelerated loading. However, after the RSAT test the surface of all the RSAT specimens was seriously damaged, thus the skid resistance test could not be performed.

### *2.5 Skid Resistance*

The skid resistance of the joint samples taken just after construction and in situ after 1 year were measured with SRT. The requirement for joints is ≥45.

## 3 Results

### *3.1 CT Scans*

Figure 9 shows an example of a CT scan of a joint specimen. From the CT scanning, the old PA (left part of the scan) and the new PA (right part of the scan) can clearly be differentiated due to the different density of the stones. It can also be observed that the old PA has a low air voids content due to severe clogging. And the new PA has a high air voids content. As far as the interface between the new PA and the old PA is concerned, a clear interface is observed, and sometimes with slightly higher air voids content. Figure 10 also shows that beneath the new PA about 10 mm old PA is still there, so not the whole old PA layer was milled. Probably the layer was thicker than the expected 50 mm.

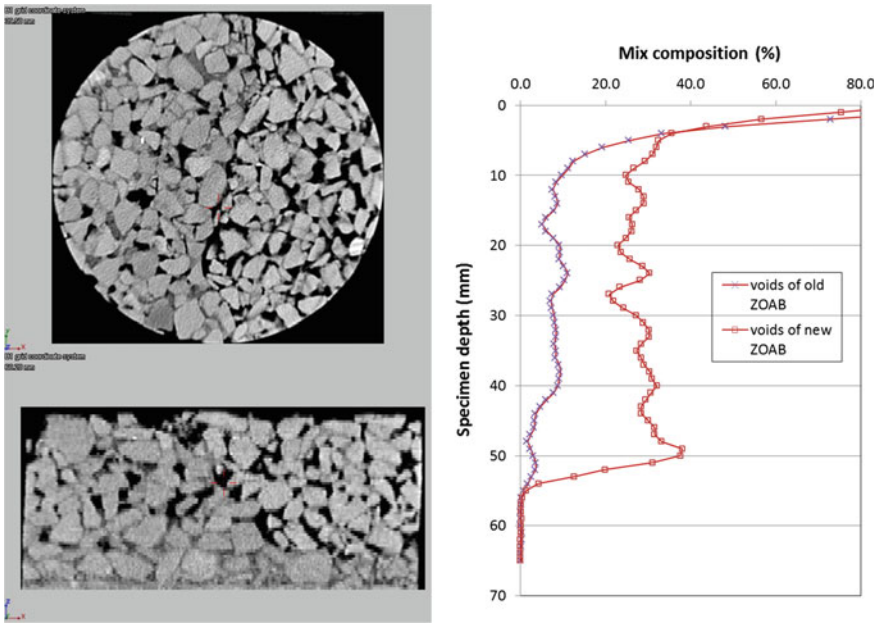


**Fig. 9** Example of CT scan. *Right graph* distribution of air voids in new PA and old PA

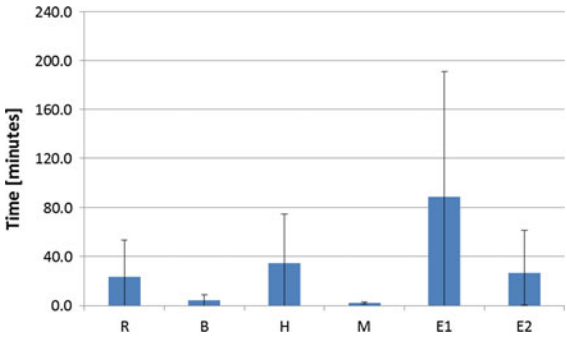


**Fig. 10** Laboratory permeability tests of beam samples

## *3.2 Permeability Tests*

### 3.2.1 Permeability Tests on Laboratory Samples

In Fig. 10 the results of the laboratory tests are presented. It can be seen that there is a huge variation in draining time between the various solutions, i.e. in the permeability in horizontal direction across the joint. It should be realized that this laboratory permeability test is different from the standard Becker test, prescribed by RWS (Morgan 2008) in which for new PA draining times up to 25 s are measured.

### 3.2.2 Permeability Field Tests

In Table 3 the results of the in situ permeability measurements, one year after construction, are presented. Besides the test sites (3 measurements per test site), also the fast lane (FL), slow lane (SL) and the Emergency lane (EL) were measured (2 measurements per test site).

Table 3 learns that the reference joint as well as all the innovative joints exhibit a smaller width of the water spot. i.e. a better permeability, than the fast lane. This means that none of the joints between the fast lane and the slow lane forms an obstacle for the water flow. It should be remarked that the permeability of the joints between the slow lane and the emergency lane was not measured. It further should be realized that in the fast lane as well as in the emergency lane old PA is present, while new PA with a much higher permeability is present in the slow lane. It is striking that the results from the laboratory permeability tests and the results from the field permeability tests after 1 year (Table 3) show the same trend.

## *3.3 Results of Direct Tensile Tests*

In Table 4 the results are given of the DTT. The following was measured or calculated: maximum strength, displacement at maximum load, initial stiffness and energy till maximum load.

DTT results indicate an improvement of the displacement at break for H, E1 and E2 joint protectors. B and M show less displacement at break. A lower strength of B is also observed. Failure of the specimens always occurred at the joints and not in the old or new PA, with the exception of the B joint protector.

**Table 3** Results of in situ permeable measurements with Breda bottle test; the numbers represent the width (mm) of the water spot at the joint (see Sect. 2.2.2)

| | R | B | H | M | E1 | E2 | FL | SL | EL |
|---|---|---|---|---|---|---|---|---|---|
| Average | 823 | 680 | 910 | 577 | 850 | 640 | 903 | 335 | 730 |
| SD | 116 | 78 | 270 | 31 | 70 | 61 | 301 | 49 | 14 |

**Table 4** Results of dry DTT

| | R | B | H | M | E1 | E2 |
|---|---|---|---|---|---|---|
| Strength (MPa) | 0.93 | 0.39 | 0.81 | 0.81 | 0.86 | 0.87 |
| Displacement (mm) | 0.025 | 0.018 | 0.028 | 0.018 | 0.037 | 0.035 |
| Initial stiffness (kN/mm) | 126 | 71.6 | 94.4 | 128.8 | 29.7 | 24.4 |
| Energy (J) | 0.020 | 0.005 | 0.016 | 0.011 | 0.022 | 0.022 |

### 3.4 Results of RSAT Tests

In Table 5 the results of the RSAT tests are given. Most of the stone loss was coming from the old PA. The E1 and E2 solutions exhibit a much higher resistance against raveling than the reference solution and the other 3 solutions, where it should be noted that the testing of the reference and B solutions had to be stopped after 17 and 18 h, respectively, because of excessive stone loss.

### 3.5 Skid Resistance

In Table 6 the results are given of the SRT measurements on drilled cores taken just after construction and in situ measurements one year after construction.

One should realize that the SRT measurements were done 1 year after construction and at that time the applied joint solutions as well as the mortar of the new PA were worn off from the pavement surface. So, actually the SRT measurements were done on the coarse aggregates of the PA. The old PA had an age of more than 10 years and contains crushed river gravel with a required PSV-value of ≥53. The new PA contains quarry aggregate with a PSV-value ≥58. Basically the skid resistance at the joint is equal to the skid resistance of the surrounding PA and not influenced anymore by the joint protector.

### 3.6 Visual Inspections

One year after construction no damage was observed of the joints. All material on the surface of the joints was weared off by traffic loading, so the surface looked like

**Table 5** Results of RSAT

| | R | B | H | M | E1 | E2 |
|---|---|---|---|---|---|---|
| Duration of the test (h) | 17 | 18 | 24 | 24 | 24 | 24 |
| Stone loss (g) | 61.7 | 83.3 | 45.7 | 95.8 | 17.0 | 21.4 |
| Stone loss (g/h) | 3.6 | 4.6 | 1.9 | 4.0 | 0.7 | 0.9 |

**Table 6** SRT results after construction and 1 year after construction

| | R | B | H | M | E1 | E2 |
|---|---|---|---|---|---|---|
| SRT joint after construction | 61 | 69 | 67 | 53 | 52 | 80 |
| SRT joint 1 year after construction | – | 51 | 53 | 45 | 52 | 48 |
| Old PA | 48 | 44 | 44 | 45 | 50 | 46 |
| New PA | 61 | 60 | 60 | 65 | 59 | 64 |

normal PA, and was not shiny. The adjacent old PA of all the joint had some light raveling caused by the poor quality of this old PA.

## 4 Conclusions and Recommendations

The five innovative joint protectors are a good alternative for the current used joint protectors: the skid resistance after construction and one year after construction is sufficient, also the permeability and bonding between old and new PA is sufficient.

Based on the experimental results, the following can be concluded:

- Innovative joint protectors can be visualized using CT scan technique;
- The permeability tests show a huge variation of the results due to clogging of the old PA. After construction the B and M joint protectors indicate better permeability than the other ones. One year after construction joint protector H performs worse in comparison with the other joint protectors. The performance of joint protectors B and M is still good, but also the performance of E1 and E2 is good;
- DTT tests indicate an improvement of the displacement at break for H, E1 and E2 joint protectors. B and M show less displacement at break. A lower strength of B is also observed. Failure of the specimens always occurred at the joints and not in the old or new PA, with the exception of the B joint protector;
- RSAT tests show a large amount of stone loss for all joint structures tested. When comparing the different joint protectors, B and M are comparable with the reference. And H, E1 and E2 show less stone loss. For these 3 innovative joints the relative low stone loss goes together with relative good mechanical performance;
- After construction SRT tests show a higher skid resistance of the B, H and E2 joint protectors when compared with the reference. Lower skid resistance values are observed for M and E1;
- The five innovative joint protector did not barricade the water flow between the old PA of the fast lane and the new PA of the slow lane;
- The Breda Bottle test is a good test to get an impression of the horizontal water flow through the longitudinal joint;
- Visual inspections one year after construction show that all joint protectors still are in good condition and meet the requirements for skid resistance;
- It is recommended to follow the performance of these innovative joints in time by measurements and visual inspections, in such a way that the findings of this laboratory and in situ research can be correlated.

## References

Buurman J., Skid resistance measurements with SRT and detailed visual inspections on test sections with joint protectors on A59 (in Dutch)

Houben L., Qiu J., Verwaal W., Poot M. and Bientjes J., Evaluating innovative longitudinal joints between old and new Porous Asphalt, report 7-14-193-1, Delft University of Technology, July 2014

Morgan P.A., Rijkswaterstaat, Scientific Strategy Document *End Report*, DVS-2008-016, March 2008.

# High Aircraft Tire Pressure Effects on HMA Airfield Pavements

**Navneet Garg, Qiang Li and Monir Haggag**

**Abstract** In November 2013, the Federal Aviation Administration (FAA) took delivery of Heavy Vehicle Simulator—Airfields (HVS-A Mark-VI). Full-scale accelerated pavement tests were performed using HVS-A to study the effect of high tire pressure effects on HMA airfield pavements. Two test pavements with 10-in. (250 mm) thick HMA surface and 12-in. (300 mm) thick aggregate base layer were trafficked bi-directionally with a radial aircraft tires (size 52 × 21.0R22) and 61,300 lbs (27.81 metric tons) wheel load. Tire pressure on one test pavement was 210-psi (1.45 MPa) and 254-psi (1.75 MPa) on the other test pavement. Embedded pavement sensors included asphalt strain gages (longitudinal and transverse) at the bottom of HMA layer, and pressure cells at the top of subgrade and aggregate base layer. Pavement performance during traffic tests was monitored by measuring surface profiles and straight-edge rut depth measurements at regular intervals. Laboratory characterization of HMA mix included dynamic modulus tests, and asphalt pavement analyzer (APA) tests. Full-scale accelerated pavement tests were completed. This paper presents the results from laboratory characterization of pavement materials, and the results of accelerated pavement tests on the effect of high aircraft tire pressures on HMA performance.

**Keywords** HMA · Tire pressure · Full-scale accelerated pavement tests

N. Garg (✉)
US Federal Aviation Administration, Washington, DC, USA
e-mail: Navneet.Garg@faa.gov

Q. Li · M. Haggag
SRA International Inc, Fairfax, USA
e-mail: Qiang.Li@sra.com

M. Haggag
e-mail: Monir.Haggag@sra.com



F. Canestrari and M.N. Partl (eds.), *8th RILEM International Symposium on Testing and Characterization of Sustainable and Innovative Bituminous Materials*, RILEM Bookseries 11, DOI 10.1007/978-94-017-7342-3_66

## 1 Introduction

The International Civil Aviation Organization (ICAO) has increased aircraft tire pressure limits on most pavement categories used in PCN (pavement classification number) methodology. The increase for Category X pavements is from 218 to 254 psi. The new aircraft, such as the Boeing 787 and Airbus 350, have tire pressures in excess of 220 psi (1.52 MPa). The effects of high tire pressure are localized and concentrated in the Hot Mix Asphalt (HMA) surface layer of the flexible pavement structure. This has necessitated the need to study the effects of high tire pressures on the HMA surfaces under full-scale aircraft loading.

In November of 2013, the Federal Aviation Administration (FAA) Airport Technology Research and Development Branch located at William J. Hughes Technical Center in Atlantic City, NJ, acquired Heavy Vehicle Simulator—Airfields Mark VI (HVS-A). A test pavement area was constructed for the acceptance testing of HVS-A. After the completion of acceptance tests, two test strips on this paved area were tested using aircraft tire at tire pressures of 210-psi (1.45-MPa) and 254-psi (1.75-MPa) respectively.

The objective of this research project was to study the effect of tire pressure increase on HMA surface performance. The paper describes the FAA's HVS-A, and summarizes the results from laboratory characterization of HMA and full-scale accelerated pavement test results.

## 2 Heavy Vehicle Simulator—Airfields (HVS-A)

The FAA's existing National Airport Pavement Test Facility (NAPTF) and test vehicle (NAPTV) is used for full scale pavement tests and is ideal for testing pavement structure as a whole (structural failure which is related to subgrade failure). NAPTF is an indoor facility and there are limitations on achievable pavement temperatures. To study the performance of surface layers such as HMA, Warm Mix Asphalt (WMA), Stone Matrix Asphalt (SMA), etc., the wheel load and tire pressures in combination with surface temperature are more critical than the gear load (due to minimum wheel load interaction affects). The work to-date for studying high tire pressures effects has primarily been based on laboratory tests. Full-scale tests are needed so that the performance prediction models for HMA from laboratory tests can be validated/calibrated to the in situ pavements. Full-scale tests at high HMA temperatures are very crucial for the success of these projects. FAA's recently acquired HVS-A provides that capability.

The HVS-A will be used for full scale testing to study the effects of high tire pressures in the pavement surface layers, testing the performance of greener/sustainable technologies (especially the upper layers) and layer materials (like HMA, WMA, SMA), and testing the effects of temperature variation in the pavement surface layers especially the effect of high temperatures on asphalt

pavements. HVS-A is 121 feet (36.9 m) long, 16 feet (4.9 m) wide, and 14 feet (4.3 m) high making it the world's largest, heaviest, and one-of-a-kind HVS in the world. The machine is capable of applying bi-directional and unidirectional loading using a single wheel [maximum wheel load of 100,000 lb (45.36 metric ton)] or dual wheel gear [maximum wheel load of 50,000 lb (22.68 metric ton)]. It has a central controller that can be programmed to provide automatic test sequencing and interfacing with the pavement instrumentation and data acquisition system. It can accommodate a lateral wander pattern up to a maximum wander width of ±3 feet [total wander 6 feet (1.83 m)]. Figure 1 shows FAA's HVS-A Mark VI. HVS-A is equipped with heaters and insulation panels and is capable of heating the test pavement surface up to 150 °F (66 °C). HVS-A will be stationed at the FAA's National Airport Pavement and Materials Research Center (NAPMRC) in Atlantic City, NJ.

**Fig. 1** FAA's heavy vehicle simulator—airfields mark VI (HVS-A)

## 3 Pavement Test Section

Figure 2 shows the test pavement layout and pavement cross-section. The test pavement thickness was determined using FAARFIELD (FAA 2009). The pavement structure was designed to prevent failure in subgrade and aggregate base. The P-401 and P-209 are FAA standard specifications for the plant mix bituminous surface, and crushed aggregate base course respectively (FAA 2014). Figure 3 shows the instrumentation (sensor) layout.

Six H-bar asphalt strain gages and two 9-in. (23 cm) diameter pressure cells were installed in each of the two test strips. Five thermocouples were installed at various depths to measure temperature gradient within the HMA layer.

## 4 P401 HMA Characterization

The HMA mix design for the test pavement was performed as per guidelines set forth in the FAA AC 150/5370-10G, Item P-401 (FAA 2014). A 75-blow Marshall mix design criterion and Performance Graded (PG) binder PG76-22 was used. The aggregates used in the HMA were argillite. Mix design properties and aggregate gradations are summarized in Table 1 and Fig. 4 respectively.

Dynamic modulus was determined in uniaxial compression using the Asphalt Mixture Performance Tester (AMPT) following the method outlined in AASHTO TP79 (AASHTO 2013). Tests were performed at three temperatures: 4, 20, and 35 °C using loading frequencies of 25, 10, 5, 1, 0.5, 0.1, and 0.01 Hz. The dynamic modulus values of the varying temperatures and loading frequencies were used to develop dynamic modulus master curves. Temperature of 20 °C was selected as reference temperature for master curves. Figure 5 shows the dynamic modulus master curve for the HMA mix.


**Fig. 2** Test pavement layout and pavement cross-section

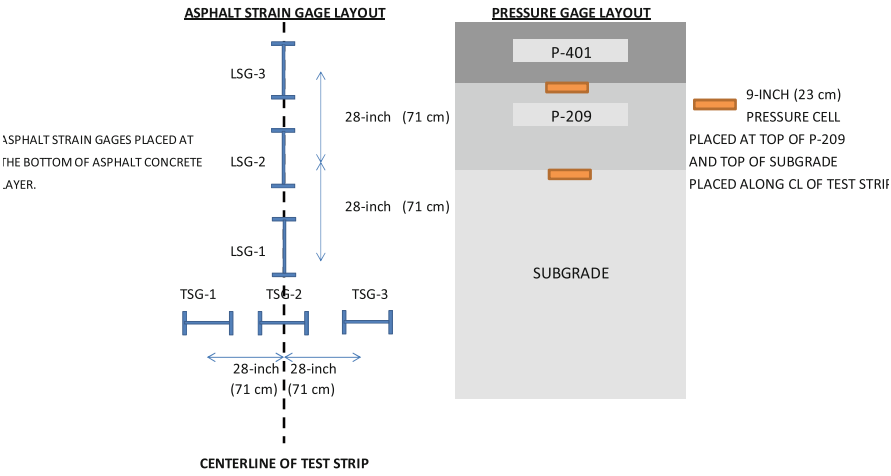


**Fig. 3** Pavement instrumentation/sensor layout

**Table 1** Mix design properties at optimum asphalt content

| Properties at optimum asphalt content | |
|---|---|
| Mixture property | Value |
| Asphalt content (%) | 5.0 |
| Air voids (%) | 3.4 |
| VMA (%) | 15.7 |
| Unit weight (lbs./ft$^3$) | 158.0 |
| Maximum theoretical specific gravity | 2.622 |
| Marshall stability (lbs.) | 3950 |
| Flow value (0.01 in.) | 12 |
| Binder grade | PG 76-22 |
| Specific gravity of binder | 1.030 |

Asphalt Pavement Analyzer (APA) has been extensively used in laboratory to characterize permanent deformation in HMA. APA measures permanent deformation in asphalt mixtures subject to a loaded wheel under repetitive loading conditions in a temperature controlled chamber to determine the rutting susceptibility of the mixtures. A number of studies (Shami et al. 1997, Kandhal and Mallick 1999, Kandhal and Cooley 2003, Rushing et al. 2012) have shown the application potential of APA to study rutting of HMA. However, the loading conditions in the APA are more commonly associated with highway conditions. FAA customized APA equipment is specifically designed to simulate high tire pressures associated with aircraft loading. It is capable of applying tire pressure representative of a heavy commercial aircraft. Hose pressures of up to 260 psi (1.79 MPa) can be achieved in the temperature range from ambient to 162 °F (72 °C). In this study APA tests were performed to study the rutting potential of the HMA used in HVS-A test strips at

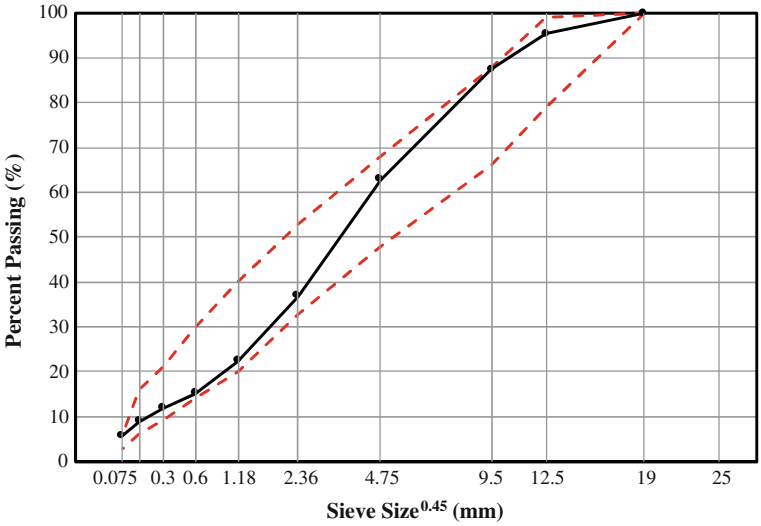


**Fig. 4** Job mix formula gradation (*dashed lines* represent FAA P-401 gradations limits)

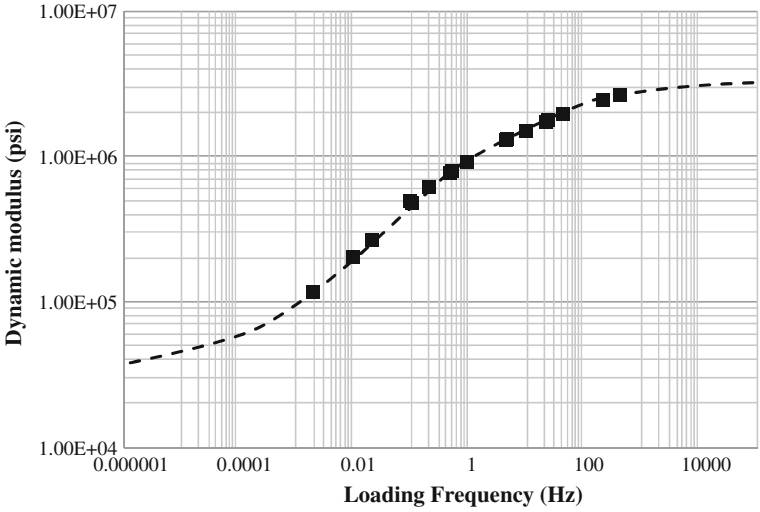


**Fig. 5** Dynamic modulus master curve (1 psi = 6.894 kPa)

two different tire pressures [210-psi (1.45 MPa) and 254-psi (1.75 MPa)] and at 120 °F (49 °C) temperature (pavement temperature for traffic tests in HVS-A). Twelve samples (six from Test Strip-1, and six from Test Strip-2) were cored out of

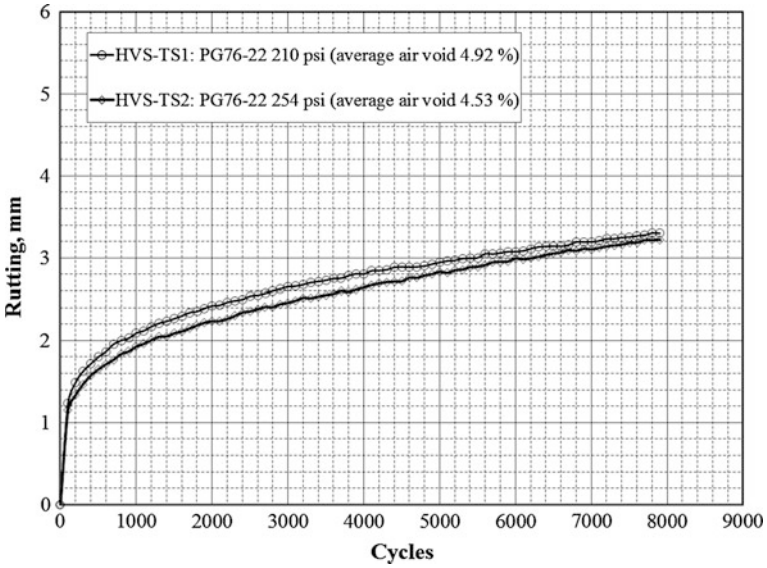


**Fig. 6** APA test results on cores extracted from HVS-A test strips

the test strip pavement for APA tests. The results are shown in Fig. 6. The APA rutting measurements shown below are average of six samples for each test strip. Similar rutting was observed at the two different tire pressures. The slight difference observed in rutting is attributed to the higher air voids in Test Strip-1 samples.

## 5 Full-Scale Accelerated Pavement Tests

Since the main objective of this study was to study the performance of HMA surface under high tire pressure, traffic tests were performed at conditions that would be deemed severe for HMA surface—slow speed and high pavement temperature. The traffic tests were performed at a pavement temperature of 120 °F (49 °C) measured 1-in. (25 mm) below the pavement surface, and at 2-mph (3.22-km/hr). Single aircraft wheel (radial tire size 52 × 21.0R22) loaded to 61,300-lbs (27.81 metric tons) was used for traffic tests. Tire inflation pressures were 210-psi (1.45 MPa) and 254-psi (1.75 MPa) for Test Strip-1 and Test Strip-2 respectively. All the test parameters were consistently monitored and recorded during the duration of tests. Tire pressure was monitored on a daily basis and adjusted as necessary. Figure 7 shows an image from infrared camera. Temperature of HMA layer surface was observed to be fairly uniform.

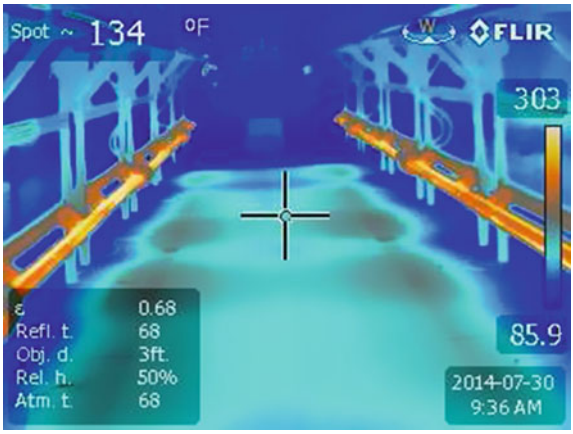


**Fig. 7** Surface temperature as measured by infrared camera

Test strips were trafficked with a pre-determined wander pattern in a bi-directional, normally distributed traffic pattern. Lateral wander positions are given in Table 2.

The failure criterion was 1-in. (25 mm) of surface rutting. However, testing was carried out well beyond the failure criterion to observe pavement behavior.

Pavement surface profiles were measured at regular intervals using on-board laser profiler. Longitudinal profile measurements were made at 4-in. (10 cm) intervals and longitudinal profile lines were spaced at 1-in. (2.54 cm) intervals in the transverse direction. Asphalt strains and pressure gage reading were recorded for each pass.

Daily routine consisted of following steps:

1. Start HVS-A heaters at 6:00 a.m. with target temperature set to 120 °F (49 °C) measured at 1-in. (25 mm) below pavement surface.
2. Straight edge rut depth and surface profile measurements were made in the morning before the start of trafficking.

**Table 2** Lateral wander positions

| Sequence no. | Track no. | Transverse wander position, in (m) | Sequence no. | Track no. | Transverse wander position, in (m) |
|---|---|---|---|---|---|
| 1 | −2 | 16 (0.41) | 10 | −1 | 26 (0.66) |
| 2 | −2 | 16 (0.41) | 11 | 0 | 36 (0.91) |
| 3 | 0 | 36 (0.91) | 12 | 0 | 36 (0.91) |
| 4 | 0 | 36 (0.91) | 13 | 1 | 46 (1.17) |
| 5 | 2 | 56 (1.42) | 14 | 1 | 46 (1.17) |
| 6 | 2 | 56 (1.42) | 15 | −1 | 26 (0.66) |
| 7 | 1 | 46 (1.17) | 16 | −1 | 26 (0.66) |
| 8 | 1 | 46 (1.17) | 17 | 0 | 36 (0.91) |
| 9 | −1 | 26 (0.66) | 18 | 0 | 36 (0.91) |

3. Monitor tire pressure. Adjust if needed.
4. Once the pavement temperature reached the target temperature, trafficking of test pavement was started.
5. Trafficking was terminated at end of work day and heaters were shut off.
6. If water accumulation was observed in the rutted area due test pavement was not tested till the pavement surface was completely dry. This was done to prevent corrosion of HVS-A parts from steam that would form once the heaters were turned on.

This resulted in traffic testing duration of about 3 to 4 h a day. Traffic tests started on Test Strip-1 and once the test strip was declared failed, additional passes were applied on the test strip to study rutting progression. After that, the HVS-A was moved and positioned on Test Strip-2 for the traffic tests.

## 6 Test Results

Figure 8 shows the rut depths for the two test strips. The rut depths are computed from the surface profile measurements and were computed as the difference between the surface profiles measured during traffic tests and the pre-traffic tests surface profile. Figures 9 and 10 show the surface profiles at different passes for Test Strips 1 and 2 respectively.

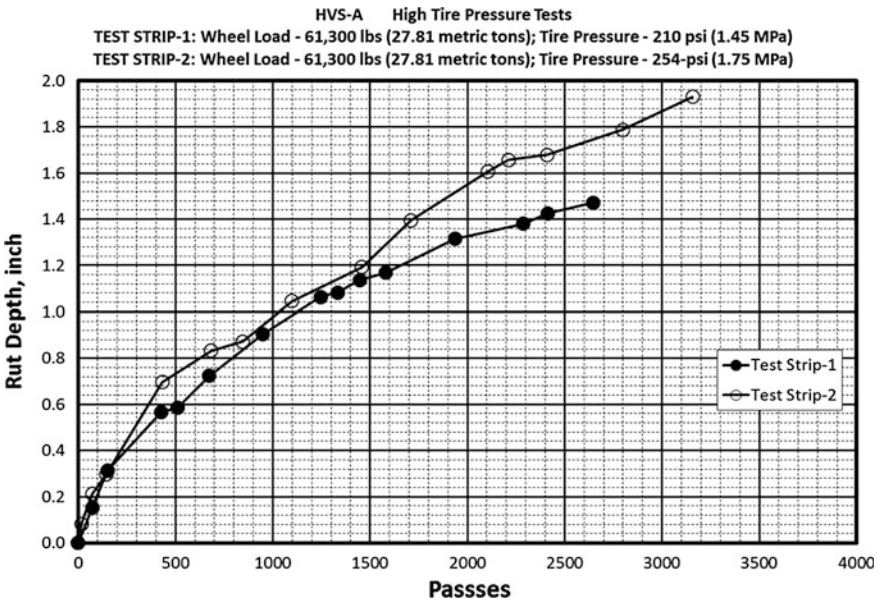


**Fig. 8** Rut depth measurements for the two test strips

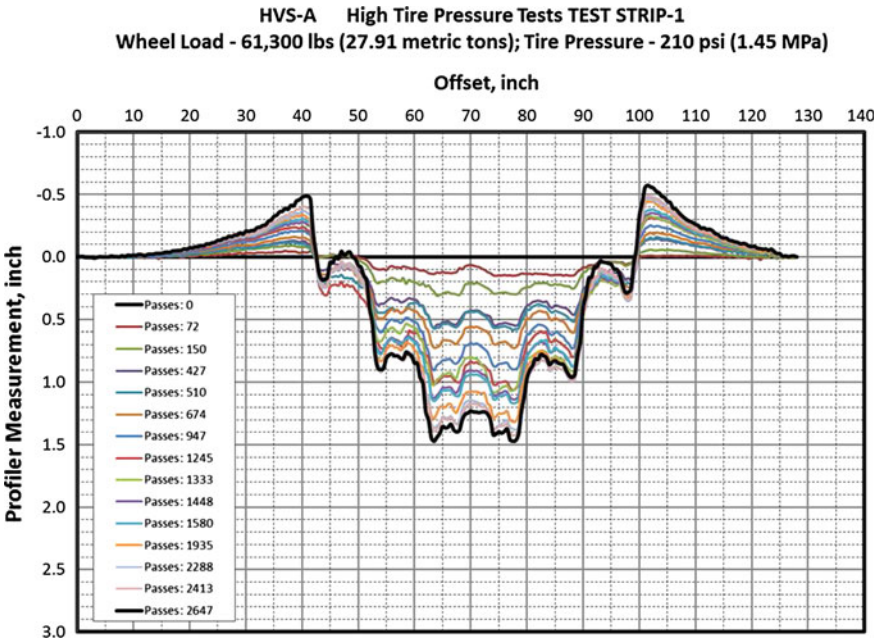


**Fig. 9** Surface profile measurements for Test Strip-1

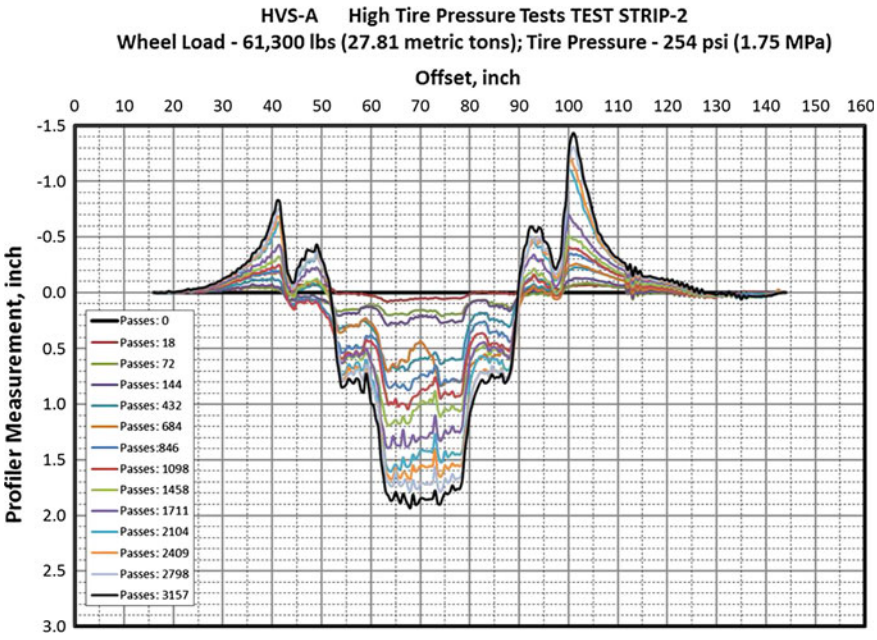


**Fig. 10** Surface profile measurements for Test Strip-2

**Fig. 11** HMA deterioration outside trafficked area in Test Strip-2

Figure 8 shows that the Test Strip-1 reached failure (1-in. (25 mm) rutting) at 1125 passes and Test Strip-2 reached failure at 1025 passes. In other words, the two Test Strips reached failure in about similar number of load repetitions showing insignificant effect of tire pressure. The effect of tire pressure was more significant beyond failure (1 in. (25 mm) of rutting). Traffic tests were continued to 2647 passes for Test Strip-1 and 3157 passes for Test Strip-2. At around 1450 passes, the surface rutting in Test Strip-2 starts accumulating at a higher rate. This is attributed to the deterioration in HMA outside the traffic area (surface cracking and tertiary flow) as shown in Fig. 11.

Figures 9 and 10 show surface upheaval outside the trafficked area in Test Strips 1 and 2 respectively. This is due to the tertiary flow taking place in HMA (outward movement of HMA). Higher amount of tertiary flow was observed in HMA in Test Strip-2—surface upheaval of about 1.5 in. (38 mm) compared to about 0.5 in. (13 mm) in Test Strip-1.

## 7 Summary

The results from laboratory characterization of pavement materials, and accelerated pavement tests using HVS-A on the effect of high aircraft tire pressures on HMA performance are presented. The pavement structure was designed using FAARFIELD in such a way so as to protect the subgrade and aggregate base layer and restrict distresses to HMA layer. The two test strips were tested at 61,300 lbs (27.81 metric tons) wheel load and tire pressures of 210-psi (1.45 MPa) and 254-psi (1.75 MPa). The results show that for the pavement structure tested and under given test conditions, increasing tire pressure from 210-psi (1.45 MPa) to 254-psi (1.75 MPa) had an insignificant effect on HMA surface rutting. Traffic tests were continued beyond the failure criterion (1 inch (25 mm) rutting). Pavement structure trafficked at higher tire pressure showed higher rate of rutting after about 1450 passes due to increased surface cracking and tertiary flow outside the

trafficked area. Additional tests are planned in the future at FAA's NAPMRC to study the tire pressure effects on HMA and Warm Mix Asphalt (WMA) with unmodified binders and polymer modified binders. The processing of asphalt strain gage and pressure cell data is currently underway. Post traffic trenches are planned in the near future to study failure in the pavement layers.

**Acknowledgments** The work described in this paper was supported by the FAA Airport Technology Research and Development Branch. The authors would also like to acknowledge the support of Murphy Flynn (FAA), Wilfredo Villafane (FAA), David Traverzo (SRA), Sean Combs (SRA), Henry Fermin (SRA), Jeffery Stein (SRA), Matthew Willson (SRA) for their support during construction of test sections, pavement instrumentation installation, and laboratory tests. Peter Millar (Dynatest) and Dennis Bataille (SRA) are acknowledged for their help in operating the HVS-A. The contents of this paper reflect the views of the authors, who are responsible for the facts and accuracy of the data presented within. The contents do not necessarily reflect the official views and policies of the FAA. The paper does not constitute a standard, specification, or regulation.

## References

AASHTO (2013) AASHTO TP 79 Standard Method of Test for Determining the Dynamic Modulus and Flow Number for Hot Mix Asphalt (HMA) Using the Asphalt Mixture Performance Tester (AMPT). American Association of State and Highway Transportation Officials.

FAA, AAS-100, Office of Airport Safety & Standards, 150/5370-10G - Standards for Specifying Construction of Airports, U.S. Department of Transportation, 2014.

FAA, AAS-100, Office of Airport Safety & Standards, 150/5320-6E - Airport Pavement Design and Evaluation, U.S. Department of Transportation, 2009.

Kandhal, P. S., and Mallick, R. B. (1999) Evaluation of Asphalt Pavement Analyzer for HMA Mix Design, NCAT Rep. No. 99-4, National Center for Asphalt Technology, Auburn, Alabama.

Kandhal, P. S., and Cooley, L. A. Jr. (2003) Accelerated Laboratory Rutting Tests: Evaluation of the Asphalt Pavement Analyzer, NCHRP Rep. No. 508, National Cooperative Highway Research Program, National Academy Press, Washington, D.C.

Rushing, J. F., Little, D. N. and Garg, N. (2012) Asphalt Pavement Analyzer Used to Assess Rutting Susceptibility of Hot Mix Asphalt Designed for High Tire Pressure Aircraft, Transportation Research Record, 2296, Transportation Research Board, Washington, D. C., 97-105.

Shami, H. I., Lai, J. S., D'Angelo, J. A., and Harman, T. P. (1997) Development of Temperature-Effect Model for Predicting Rutting of Asphalt Mixtures Using Georgia Loaded Wheel Tester, Transportation Research Record, 1590, Transportation Research Board, Washington, D. C., 17-22.

# Development of New Embedded Expansion Joint Using High Flexibility Stone Mastic Asphalt

**Nobuya Okamoto, Takagi Kinoshita and Takashi Futagi**

**Abstract** Replacement of expansion joint of highway viaducts is one of the current technical challenges in order to improve driving comfort in highway network. Generally, embedded expansion joints have been used for reinforced bridges and pre-stressed concrete bridges. As for the embedded expansion joint, base course gussasphalt strengthened with expanded metal is used for absorbing thermal expansion of adjacent bridges. This base course is generally damaged by the flexural rotation at the girder end under low temperature condition; therefore, structural improvement especially enhancing flexibility of pavement is demanded for improving durability. In this study, new asphalt material called "High flexibility stone mastic asphalt" is used as a base course, because this high flexibility asphalt is considered to accommodate the thermal expansion as well as flexural rotation even under low temperature. This new joint is adopted the urban expressway viaduct in Japan. Fundamental experiments showed high durability performance of the new joint compared to those of the conventional joint and the field strain measurement also showed good performance under actual condition. This paper summarizes the structure and performance of the new embedded expansion joint in Japan.

**Keywords** New embedded expansion joint · High flexibility stone mastic asphalt · Improving durability · Urban expressway viaduct

N. Okamoto (✉)
Hanshin Expressway Co. Ltd, Osaka, Japan
e-mail: nobuya-okamoto@hanshin-exp.co.jp

T. Kinoshita
Hanshin Expressway Engineering Co. Ltd, Osaka, Japan
e-mail: takagi-kinoshita@hex-eng.co.jp

T. Futagi
Taisei Rotec Corp, Tokyo, Japan
e-mail: takashi_futagi@taiseirotec.co.jp



F. Canestrari and M.N. Partl (eds.), *8th RILEM International Symposium on Testing and Characterization of Sustainable and Innovative Bituminous Materials*, RILEM Bookseries 11, DOI 10.1007/978-94-017-7342-3_67

# 1 Introduction

Generally, embedded expansion joints are used for replacement of old expansion joint of pre-stressed concrete bridges with the span length under 25 m and joint movement under 20 mm for improvement of trafficability in Japan. As for the embedded expansion joint, base course gussasphalt strengthened with expanded metal is used for absorbing thermal expansion of adjacent bridges. This embedded structure is generally damaged by the flexural rotation at the girder end under low temperature condition. For improvement of durability of expansion joint, structural improvement especially enhancing flexibility of pavement is highly demanded.

# 2 Outline of Conventional Embedded Expansion Joint and Technical Problem

## *2.1 Conventional Embedded Expansion Joint*

Expansion joints are absorbed the movement by temperature change and traffic. Road surface on bridge is kept level and consecutiveness.

But expansion joints are exposed to repeated lived load and easily damaged. Deteriorated expansion joints cause noise and vibration. In addition, water leakage from deteriorated expansion joints severely damaged bearings and girder end.

Conventional embedded expansion joint, as shown in Fig. 1, used gussasphalt and expanded metal as a base course. Conventional method should resist thermal expansion of girder, mainly. Whereby, sliding sheet (PM-N sheet) is placed between gussasphalt and concrete slab for relaxing frictional resistance.

The following are the factor for the deformation at the edge of girder, as shown in Fig. 2.

(a) Thermal expansion
(b) Flexural rotation by wheel load
(c) Share force by wheel load

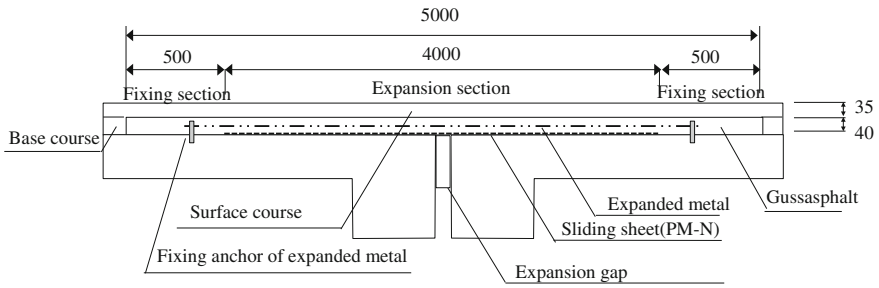


**Fig. 1** Conventional embedded expansion joint

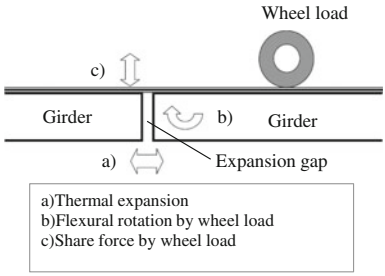


**Fig. 2** The factor for the deformation at girder end

## *2.2 Durability Problem*

The conventional embedded expansion joints have a durability problem. Although maintenance cycles of surface and expansion joints are scheduled about 8 years, they have minor cracks on expansion joint after opening to traffic in 3.3 years and major crack in 4.6 years, according to the current research. The durability of conventional expansion joint is only half terms of assumed maintenance cycle.

The durability of embedded expansion joints should be improved.

# 3 Investigation of the Cause of Damage

## *3.1 Investigation of Condition of Defects*

Typical defects on embedded expansion joint are crack and pothole. Transversal crack on pavement occurred along expansion joint and pothole occurred nearby the cracks, as shown in Fig. 3a.

Cause of defects is considered to behavior of gussasphalt. Gussasphalt used for base course has a low elasticity characteristic at low temperature condition. Temperature on the bridge surface in Japan is changed between −5 and 50 °C.

First, crack on gussaphalt happened by repeated wheel load at low temperature because of a low elasticity.

Next, reflection crack occurred on surface course. Finally, cracks expanded and pothole occurred.

The material of base course should have high elasticity at low temperature and resist repeated wheel load.

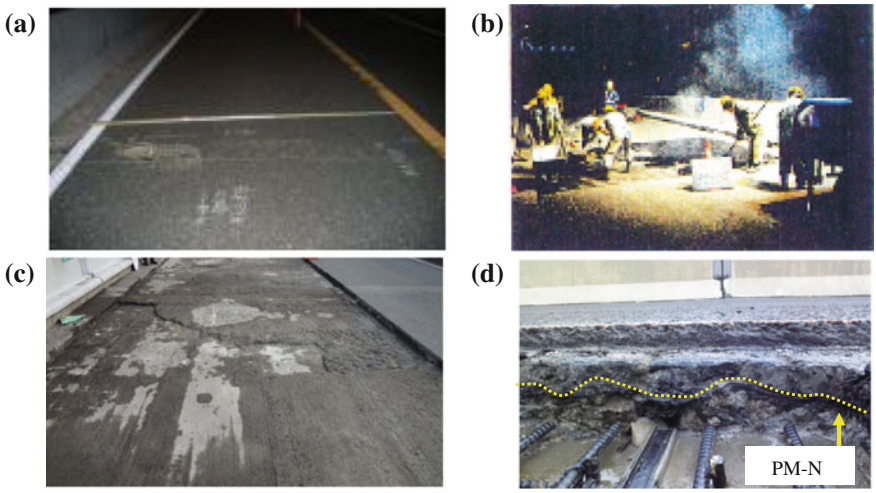


**Fig. 3** Picture of conventional method: **a** injured surface, **b** gussasphalt is constructed by human power, **c** formation level is uneven, **d** PM-N was not set on flat

## *3.2 Investigation of Construction*

Gussasphalt cannot choose but be casted by human construction, as shown in Fig. 3b. Therefore, the quality control is difficult. The base course should be casted by machine construction instead of human construction for quality control.

Expanded metal is located in the middle of gussasphalt course in design. However expanded metal were not set in right position in construction.

Also some areas have not enough thickness than design.

## *3.3 Investigation of Formation Level*

Deck surface is injured by removing existing expansion joint. Formation level is often uneven, as shown in Fig. 3c.

PM-N plays important role to absorb expansion girder. If it were not set on flat, the function of PM-N is not expected. But PM-N was not set on flat in construction, as shown in Fig. 3d.

The formation level should be flat without gap.

# 4 Development of New Embedded Expansion Joint

## *4.1 The Special Polymer Modified Asphalt Binder and High Flexibility Stone Mastic Asphalt (SMA)*

High flexibility SMA is adopted as a base course in new design instead of gussasphalt for improving elasticity at low temperature. High flexibility SMA uses special polymer modified asphalt binder, which is very flexible at low temperature.

The special polymer modified asphalt binder contains the styrene butadiene co-polymer (SBS). SBS is generally used as a reforming material. Also another special additive is included.

The specification of special polymer modified asphalt binder, which is used high flexibility SMA, are shown in Table 1, compared with Polymer modified asphalt (PMA) Type II used heavy traffic for dense-graded asphalt mixture in Japan. The asphalt content and the targeted grading of aggregate are shown in Table 2.

Stress relaxation and several performance of special polymer modified asphalt is not deteriorated at low temperature, because ductility at 4 °C is larger than polymer modified asphalt. Fraass Breaking Point is low, penetration is large and softening point is high.

**Table 1** The specification of special polymer modified asphalt

| Term | Special polymer modified asphalt | Polymer modified asphalt (PMA) Type II |
|---|---|---|
| Peneration (25 °C), 1/100 cm | 173 | 55 |
| Softenig point, °C | 79 | 61.5 |
| Ductility (15 °C), cm | 100+ | 86 |
| Ductility (4 °C), cm | 90 | 54 |
| Fraass breaking point, °C | −23 | −11 |
| Penetration index | 8.56 | 1.57 |
| Viscosity (60 °C), Pa s | 8896 | 1475 |

**Table 2** The asphalt content and the targeted grading of aggregate

| Mixture | Asphalt content (%) | Combined gradation (percentage passing %) | | | | | |
|---|---|---|---|---|---|---|---|
| | | 19 mm | 13.2 mm | 4.75 mm | 2.36 mm | 0.3 mm | 0.075 mm |
| High flexibility SMA | 6.6 | 100 | 96.9 | 39.8 | 24.4 | 15.1 | 10.4 |
| Gussasphalt | 8.6 | 100 | 98.8 | 75.1 | 53.4 | 38.2 | 23.4 |

## 4.2 Evaluation Method

Bending strength test, Bending fatigue test and penetration with crack test are conducted for evaluating of High flexibility SMA.

Bending strength test characterizes asphalt bending stiffness. Bending fatigue test characterizes asphalt bending resistance by repeated load. Penetration with crack test characterizes crack resistance of base course by repeated wheel load, as shown in Fig. 4.

## 4.3 Test Results

### 4.3.1 Result of Bending Strength Test and Bending Fatigue Test

Result of bending strength test is shown in Fig. 5a. On the both of bending strength and fracture of strain in −10 °C, SMA is higher performance than gussasphalt. SMA is more flexible than gussasphalt.

Result of bending fatigue test is shown in Fig. 5b. This test is conducted under the difference temperature 5, 0, −10 °C. SMA is higher performance than gussasphalt in every temperature.

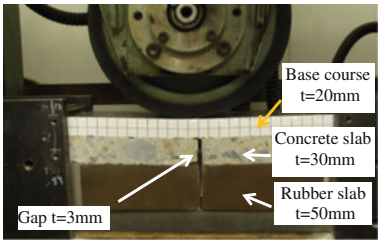


**Fig. 4** Penetration with crack test by wheel load

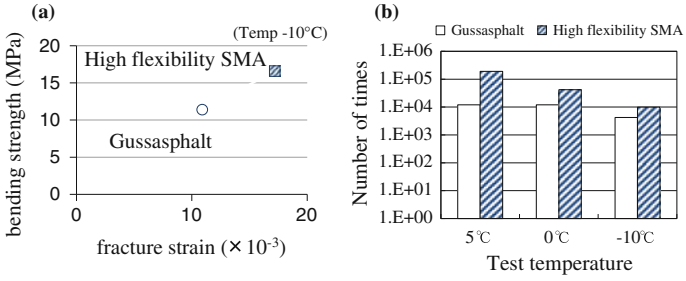


**Fig. 5** Test results: **a** bending strength and fracture of strain by bending strength test at −10 °C, **b** bended fatigue test results

### 4.3.2 Result of Penetration with Crack Test

As the result of penetration with crack test, high flexibility SMA is superior to gussasphalt for the resistance to crack by the repeated wheel load, especially big difference at low temperature, as shown in Fig. 6a. This result show the superiority of high flexibility SMA, because main cause of defects is reflection crack at low temperature.

To enhance durability more, glass fiber sheets are used under base course for reinforcement. In case of using glass fiber sheets under base course, the resistance to crack is higher than no reinforcement, as shown in Fig. 6b.

## *4.4 Design of New Embedded Expansion Joint*

New structure of embedded expansion joint is shown in Fig. 7.

High flexibility SMA with reinforcing material is used in base course, instead of gussasphalt with expanded metal.

Furthermore, high flexibility SMA is casted by machine construction for quality control to keep continuity of pavement and it make surface flat.

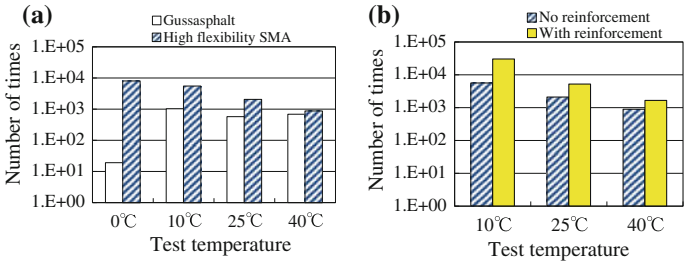


**Fig. 6** Test results: **a** penetration with crack test results, **b** compared with the effect of rein forcing material

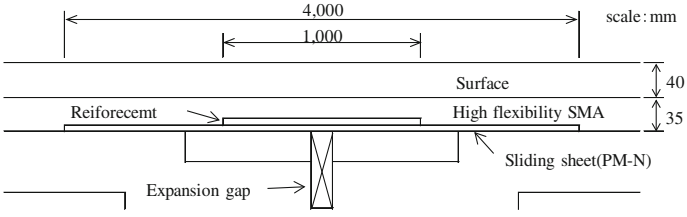


**Fig. 7** New structure of embedded expansion joint

## 5 Test Operation on Urban Expressway Viaduct

New embedded expansion joint was constructed on Hanshin Expressway in Japan in October, 2013.

### *5.1 Location*

Both of new embedded expansion joint and conventional expansion joint were constructed to make a comparison, as shown in Fig. 8.

### *5.2 Mixture Design*

Mix proportion of high flexibility SMA is shown in Table 3. The asphalt content is 6.7 %.

The condition of composition is mixing temperature 170 ± 10 °C, heating temperature of asphalt 170 ± 5 °C, heating temperature of aggregate 195 ± 10 °C, mixing time with aggregate 15 s, and mixing time with binder 45 s.

### *5.3 Procedure of Construction*

Construction is conducted by following procedure.

1. Cutting existing asphalt
2. Repaired rough surface area
   Surface of slab was not flat. Rough surface area was repaired by patching asphalt mixture, as shown in Fig. 9a.
3. Put sliding sheet and reinforce layer
   Sliding sheet was put on the expansion gap, furthermore, glass fiber sheet was put on the sliding sheet as reinforce layer.

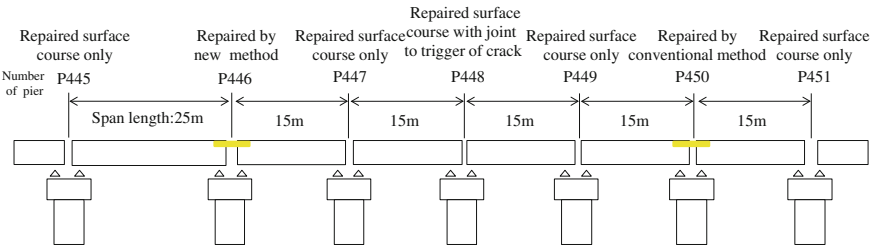


**Fig. 8** Location in test operation: P446 was repaired by new method, P450 was repaired by conventional method

**Table 3** Mix proportion of high flexibility SMA

| | 19 mm | 13.2 mm | 4.75 mm | 2.36 mm | 0.6 mm | 0.3 mm | 0.15 mm | 0.075 mm |
|---|---|---|---|---|---|---|---|---|
| Targeted gradation | 100.0 | 99.2 | 39.7 | 25.1 | 17.0 | 13.8 | 12.1 | 10.4 |
| Range of standard gradation | 100 | 95–100 | 30–50 | 20–35 | | 13–20 | | 8–13 |

Combined gradation (percentage passing %)

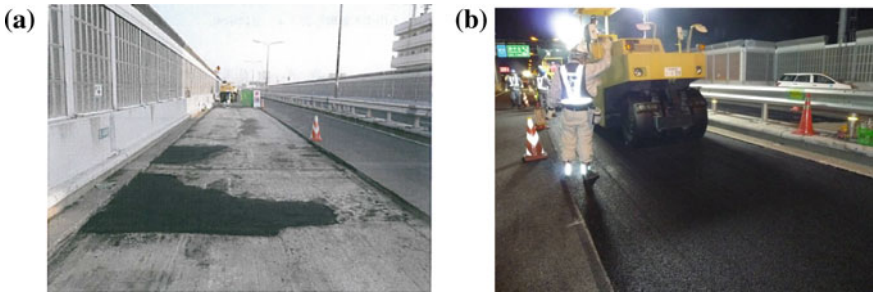


**Fig. 9** Picture of construction: **a** repaired rough surface area, **b** compaction

4. Placement of base course
   High flexibility SMA is compacted by 25 ton tire roller, 10ton macadam roller, and 4 ton tandem roller. The first compaction was 7 times by tire roller, the second compaction was 5 times by macadam roller, the finish compaction was 5 times by tandem roller. Shown in Fig. 9b
   The temperature of placement is over 155 °C, first compaction is over 145 °C, second compaction is over 105 °C, and finish compaction is over 95 °C.
   Compaction degree is targeted over 96 %. Practically, compaction degree was made over 98 % on site.
5. Placement of surface course

   After casting SMA, surface course was constructed.

# 6 Tracing Survey

## *6.1 Surface Condition*

Surface was checked at both joints after opening to traffic. Air temperature change is from −3 to 37 °C for 10 months and traffic number is about 15,000 vehicles per day at the lane.

P446 repaired by new method, and P450 repaired by conventional method have not been cracking after 10 months. Others were cracked. Shown in Table 4.

**Table 4** Surface condition

| Number of pier | P445 | P446 | P447 | P448 | P449 | P450 | P451 |
|---|---|---|---|---|---|---|---|
| Repairment | △ | ◎ | △ | ▲ | △ | ○ | △ |
| 3 months after | NG | OK | NG | OK | NG | OK | NG |
| 7 months after | NG | OK | NG | NG | NG | OK | NG |
| 10 months after | NG | OK | NG | NG | NG | OK | NG |

*Legend* ◎: Repaired by new method, ○: Repaired by conventional method, △: Repaired surface course only, ▲: Repaired surface course with joint to trigger of crack
OK: No cracking, NG: Cracking

10 months is not enough for research, because crack would averagely happen after opening to traffic in 3.3 years.

It is necessary to continue tracing survey to confirm superiority of new method.

## 6.2 *Measurement of Strain*

### 6.2.1 Location of Sensors

Static strain and dynamic strain are measured under traffic opening in site. Strain sensors are set at three point; right wheel line, left wheel line and road shoulder on the surface course and the base course, as shown in Fig. 10.

### 6.2.2 Results of Measurement of Static Strain

Static strain was measured every ten minutes for 4 months in order to measure the strain from expansion of girder by temperature change.

Results of measurement are shown in Fig. 11.

The strain range of new joint method is ±400 μm, and conventional joint method is ±600 μm.

The result shows that new joint system can absorb the strain from expansion of girder by temperature change compared with conventional one. Lower strain range in new joint method expected high durability.

### 6.2.3 Results of Measurement of Dynamic Strain

Dynamic strain was measured by loading truck weighted 196 kN. Driving speed was 30 km/h. Measurement was conducted in every three month in order to compare with different seasons.

Maximum strain of both joint methods is the same level at every season, as shown in Fig. 12.

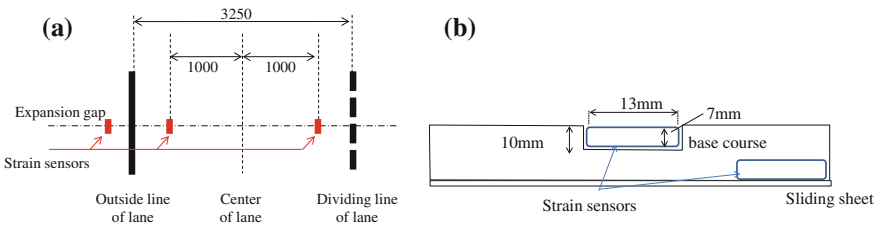


**Fig. 10** Position of strain sensors: **a** ground plan, **b** cross sector view

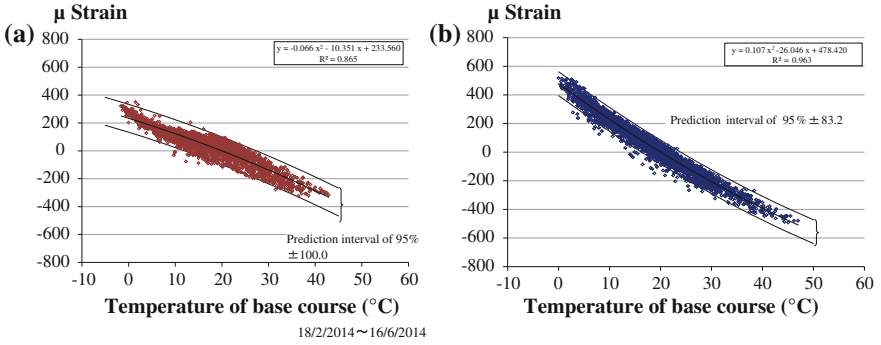


**Fig. 11** Results of static strain at road shoulder: **a** new joint method, **b** conventional joint method

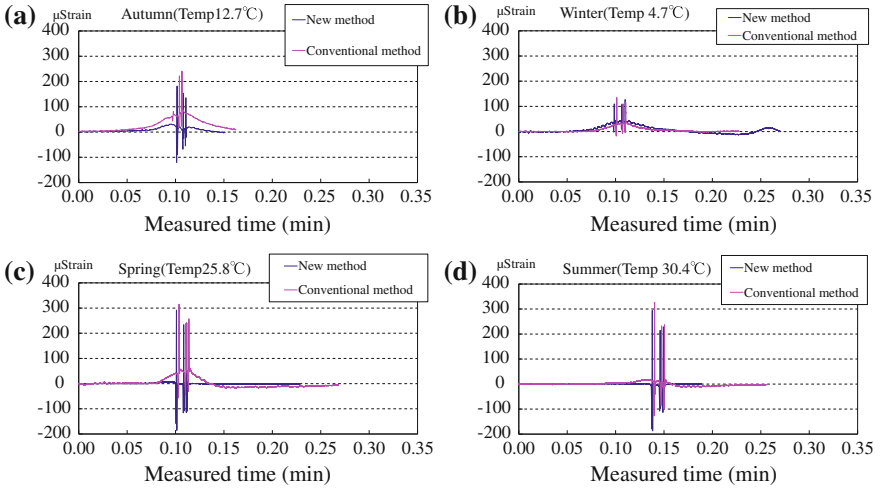


**Fig. 12** Results of dynamic strain on the base course in site: **a** results in the autumn (12 November 2013), **b** results in the winter (17 February 2014), **c** results in spring (16 June 2014), **d** results in summer (19 August 2014)

But the appearance of strain is different at autumn and spring. In case of conventional joint, strain become high before passing the truck at the expansion gap, and stayed high after the truck. In case of new joint, those were not seen. The conventional joint was affected by strain more than new joint.

The amount of energy accumulated by truck loading in conventional method is bigger than new method, as shown in Fig. 5a.

Therefore high durability is expected in new joint method.

### 6.2.4 Finding

Both joints were not cracked after opening traffic in 10 months.

Static strain of conventional joint was larger than new joint. Conventional joint have a disadvantage in durability, because the strain width is larger than new joint.

Maximum dynamic strain of both joints are the same level. However, the appearance of strain is different at autumn and spring. The amount of energy accumulated by truck loading in conventional method is bigger than new method.

High durability is expected in new joint method.

## 7 Conclusion

Deformation performance of high flexibility SMA is better than gussasphalt, especially at low temperature.

New joint system is constructed by machine construction to keep continuity of pavement and it makes surface flat.

In case of that deck surface was injured, there is necessary to be repaired by non-shrinking mortar or resin mortar.

New joint method with high flexibility SMA has not been cracked 10 months after opening traffic.

10 months is not enough for research and getting conclusions, because crack would averagely happen after opening to traffic in 3.3 years.

Tracing survey has to continue to make sure the durability of new joint method.

## Bibliography

Hanshin Expressway Co.Ltd, (1994) Design and construction manual of embedded expansion joint.

Huurman M. et al. (2010) Mechanistic Design of Silent Asphalt Mixtures. International Journal of Pavement Research and Technology, 2013.3(2)

Iguchi Y. et al. (2014) Modified research of embedded expansion joint. Paper presented at the 69th Annual Conference of the Japan Society of Civil Engineers, University of Osaka, Osaka, 10-12 September 2014

Oguri N. et al. (2010) SMA with Special Modified Asphalt Aimed to Extend Pavement Lifespan. ISAP2010

Omori A. et al. (1986) Development of embedded expansion joint method. Bridge Engineering Vol22.No.12:27-37

Partl M.N. et al. (2002) Asphalt Plug Joint Characterization and Performance Evaluation. Proceedings of 9th int. Conference on Asphalt Pavements, ISAP, Copenhagen, 2002

Partl M.N. and Hean S. (2011) Experience with Testing and Performance Evaluation of Bituminous Plug Expansion Joints on Concrete Road Bridges. International Journal of Roads and Airports (IJRA), v.1, n.1 (2011) 1-17

# Development of Specifications and Guidelines for Hot in-Place Recycling in Finland—Outline and Framework

**Michalina Makowska and Terhi Pellinen**

**Abstract** For 25 years, the hot in-place recycling (HIP-RC) has been the major pavement preservation technique in high volume roads in Finland, and currently it constitutes ca. 50 % of all road construction expenditures. The cost is ca. half of the mill and fill overlay as only up to 25 % new material is consumed. With least traffic disruption, it provides a quick refill of the rutted pavement, which is abraded due to the use of studded tires. Studded tires are used for mitigating icy roads conditions in the wintertime. However, the reduced maintenance funding has created a need to re-evaluate and better standardize the method. Therefore, a REMIX research project has been initiated, which focuses on the identification of best practices for the HIP-RC by reviewing prior construction records and their usability for the planning of future recycling and by developing enhanced performance criteria for the end product. The four-year project closely follows roads at different stages in their life cycle, which gives a unique opportunity to observe and study pavement surfaces recycled multiple times. This article presets outline and framework for the project and gives results from the initial stage of the project.

**Keywords** Hot in-place recycling · Specifications · Rejuvenators · BISOM · Hansen solubility parameters

## 1 Introduction and Background

In the 1970s, the oil crisis caused an increased interest in asphalt recycling techniques which allowed for 100 % use of an old material. Various hot in-place recycling (HIP-RC) techniques started to emerge and slowly spread around the

M. Makowska · T. Pellinen (✉)
Aalto University, Espoo, Finland
e-mail: terhi.pellinen@aalto.fi

M. Makowska
e-mail: michalina.makowska@aalto.fi



F. Canestrari and M.N. Partl (eds.), *8th RILEM International Symposium on Testing and Characterization of Sustainable and Innovative Bituminous Materials*, RILEM Bookseries 11, DOI 10.1007/978-94-017-7342-3_68

world. The benefits of HIP-RC type maintenance are plentiful (Hesham et al. 2012) and the interest in the techniques as an alternative to milling and hauling is quite high, especially in countries where high quality aggregates are required due to studded tire wear, and the road network maintenance budget is limited (Makowska et al. 2014; Li et al. 2014; Hesham et al. 2012).

Earlier studies in Finland have produced a set of guidelines which rely on bitumen penetration as the quality criteria. The statistical analysis of in-service life-cycles in the 90s has, however, suggested degrading pavement quality. As a result, the restrictions were set in place allowing the wearing course to be recycled only twice.

In 2013, the Finnish Transport Agency (FTA) commissioned a four-year project designated as "REMIX", which aims to improve the success rate of HIP-RC maintenance. The aim is first to review the previous research in Finland and elsewhere; gather empirical and tacit knowledge from the asphalt contractors. Then, to observe and identify poor construction practices and prepare enhanced specifications and quality control requirements for the HIP-RC treated pavements. The project will focus on the tender documentation in terms of required preconstruction sampling and initial material analysis; the development of the evergreen rules of rejuvenation; the development of methodologies for the proper optimization of admixtures, and techniques to allow for more than two consecutive cycles of HIP-RC treatment.

The HIP-RC recycling has been used in Finland since 1975, and based on positive laboratory and field trials early on; its use has increased considerably. At the beginning of 1990s, 1.2 million $m^2$ of roads were treated with the HIP-RC, and in 1992 the number had increased to 2.5 million $m^2$ (Wastimo 1995). The most popular technique used today is called REMIX. It consists of the in situ reheating of the pavement followed by milling, addition of the rejuvenator and fresh admixtures, and homogenization of the produced layer before the final compaction. In 2013, about 30 % of the road construction contracts in Finland were commissioned as the HIP-RC; and in the southern region alone, about 871,000 $m^2$ of roads were REMIX treated. It is expected that this trend will continue as the road maintenance expenditures are most likely not going to increase in the coming years (Lyytinen 2014).

The most common pavement distress type in Finland is rutting due to studded tire wear. The fresh mixtures are optimized against this damage and the key attention is given to the wear resistant aggregate and mixture proportioning (Saarela et al. 1993; FAS 2011). The quality criterion triggering the road maintenance is set to 12–21 mm of rut depth depending on road type and traffic (Tiehallinto 2007). The time to reach this threshold is highly dependent on the amount of traffic but also on the success of the initial construction. It has been estimated that studs abrade asphalt ca. 15–25 $kg/m^2$ for the corresponding rut depth values, which then needs to be refilled in order to sustain safe driving surfaces. The price and availability of the special hard aggregate becomes a factor encouraging Finland to recycle up to 100 % of asphalt concrete, when possible. In addition, the overall European goal of increasing independence from the crude oil will be fulfilled.

The HIP-RC is preferred on the high volume roads (speed limit between 60 and 120 km/h), where minimal traffic disturbance is desired. Therefore, a good resistance against permanent deformation and studded tire wear is needed and it has to be the main quality concern.

As the popularity of the process grew, more research projects were initiated to investigate HIP-RC maintenance. Patosalmi (1996) studied indirect tensile strength variation of mixtures due to the use of various rejuvenators. The best restoration of strength was attained with the soft penetration graded bitumen 650/900 (in some cases exceeding the values of the original mixture) compared with the original mix design and the non-rejuvenated HIP-RC treated materials. Other tested rejuvenators included softer viscosity graded bitumens (V1500, V3000), tall oil, heavy oil and bitumen emulsions. Apilo et al. (1998) investigated twice HIP-RC treated field pavements, and for the third REMIX cycle they developed an artificial laboratory aging methodology to simulate pavement performance after multiple recycling cycles. Based on their study the FTA made a decision in 1998 to limit the number of REMIX treatment cycles to two and to encourage the use of rejuvenators, although no mandating specifications were yet released at that time. Over time there have been local deviations from the general guidelines and three times REMIX treated road segments do exist. This is due to patching type maintenance operations of deteriorated road segments prior to the maintenance of the entire length of the road.

In 2009, the FTA commissioned a statistical analysis of the success rates on once and twice REMIX treated segments compared with the fresh overlays (Rantanen et al. 2009). It was found that on average pavement life decreased with every consecutive REMIX cycle. Specifically for the highly trafficked roads, the average cycle length after the 3rd HIP-RC maintenance was cut by half compared with the fresh overlay. Incidentally, the cost of milling and fresh filling with an overlay, being ca. 6.9 €/m$^2$, is almost twice as big as REMIX type maintenance (ca. 2.7 €/m$^2$) for SMA surfaces. Due to the increased risk of failure on the 3rd time REMIX treated roads, the earlier decision was sustained to allow the treatment to be conducted only twice after the fresh overlay.

In preparation for the tenders and execution of the construction, contractor is required to core at least 5 samples from the representative area of the road. Typically a gradation, bitumen penetration, maximum density and air void content are tested on the collected samples, in order to allow for a better optimization of admixtures. Although some contractors take 5 cores also from the finished road to their own quality assurance, there are no criteria set for the final product and therefore this step is not required.

After assessing the remixing work prior to this project in 2013, it became evident that if no rejuvenator was used it resulted in increased air voids and drastic decrease of in situ penetration values. Therefore, the Finnish Transport Agency decided to make it mandatory in 2008 to use soft bitumen 650/900 with the amount of 150–250 g/m$^2$ as rejuvenator in HIP-RC.

## 2 Test Road—Rehabilitation History and Observations

For the course of the study, a set of test roads will be selected based on the outcomes of the observations from the first test road. The first selected test road is Highway no. 1 (HW1) (speed limit 120 km/h, AADT 39000-56000), where 26.5 km of driving lane were let for the Remix maintenance in 2013 (REM'13). Based on FTA's database, at least seven different road segments could be identified which had different prior treatments and mix designs. Combined with maintenance records, it became evident that the road was anything but homogenous and various dominant distress types such as rutting, raveling and low temperature cracking were present. The contractor awarded for the new work in 2013 was facing the first problem of choosing a representative site to collect samples from the road. As a compromise, it was agreed on to use only one admixture throughout the 26 km stretch of road.

The rehabilitation history suggested that the selected four segments had the following history of rehabilitation work (Table 1): The 1st coring site comprised of an overlay placed over an existing overlay constructed in 2009, 2nd site had once REMIX treated overlay, 3rd site had twice REMIX treated overlay and 4th site was mill and fill overlay placed above twice REMIX treated overlay. The 4th site had essentially the same aging cycle as 1st site because twice REMIX treated surface mixture had been milled away before placing fresh overlay in 2009. The 3rd site provides us with a unique opportunity to observe how the road would perform after it has been REMIX treated three times.

At job site, decision was made to core samples from two stations 100 m apart, stations 0 and 100 before, and station 50 and 150 after the REM'13 construction. Per station we drilled the minimum of 8 cores of which minimum of 6 were taken outside of the wheel path and 2–4 from the wheel path. One of the cores per station before and after was taken as a full depth. The full cores were up to 250 mm tall. Few additional samples were taken from extremely damaged sites. Together 165 cores were collected (85 before and 80 after REM'13), transferred into the laboratory and kept in refrigerated room. Layers were then identified and top layer samples were separated with the help of a diamond saw.

Three bottom base layers were visually identified having the same material, originating from the original road construction in 1971. Above the base layers, each

**Table 1** Pavement history before REM'13 and surface mix aging cycles after

| Coring sites | Existing surface before REM13': construction year, treatment type and admixture | Prior surface treatment | Aging cycles due to/after REM'13 |
|---|---|---|---|
| 1 | 2009 glue +slab w SMA16 | Slab | 1st |
| 2 | 2008: REM w SMA16 admixture | REM | 2nd |
| 3 | 2008: REM w SMA16 admixture | 2 × REM | 3rd |
| 4 | 2009: mill + fill, slab w SMA16 | 2 × REM | 1st |


**Fig. 1** The cores from HW1 taken from locations (*1*, *2*, *3* and *4*) representative of different aging cycles of life before (*upper row*) and after REM'13 treatment (*lower row*)

of the coring locations had a different structure of asphalt layers depending on rehabilitations history.

The visual inspection of the coring sites prior to REM'13 (Fig. 1) revealed that 2nd site was particularly damaged: raveling and a lot of segregated spots could be identified, the layer thickness was on average 25 % lower than on other sites. The 1st site seemed visually good, but closer analysis revealed that there must have been originally issues with surface layer compaction, as we identified each core having visible air channels which allowed moisture infiltration to the pavement. The visual inspection of the test sites after REM'13 indicated the following: (1) there were issues with the bitumen or mastic in the 1st site, as the mastic part of the mixture became flaky; (2) the status of the 2nd site improved and no segregated spots could be identified afterwards; (3) the 3rd site was in a very good condition; (5) the 4th site got worse as pavement visually seemed to be less dense than before.

## 3 Laboratory Testing for Performance

Table 2 presents laboratory test results. The air voids of cores were tested according to the SFS-EN 12697-6 using methods B, C and D for verification. Bitumen content and gradation analysis was performed after binder extractions. The fines passing 0.125 mm sieve were analysed additionally with FT-IR in order to provide qualitative analysis. The surface area (SA) of fines passing 0.125 mm sieve in samples prior to REM'13 was measured according to the procedure described elsewhere (Makowska et al. 2014).

The FT-IR analysis was performed to double-check if the limestone filler had been substituted with fly ash in the earlier HIP-RC admixtures. FT-IR analysis and

**Table 2** The results of core and aggregate analysis per sampling location before and after REM'13 work

| Sieve size (mm) | Site 1 before | Site 1 after | Site 2 before | Site 2 after | Site 3 before | Site 3 after | Site 4 before | Site 4 after |
|---|---|---|---|---|---|---|---|---|
| 0.063 | 11.5 | 11.5 | 12.0 | 11.6 | 12.8 | 13.4 | 12.4 | 11.4 |
| 0.125 | 14.4 | 14.5 | 14.5 | 14.4 | 15.7 | 17.1 | 15.9 | 14.2 |
| 0.25 | 17.1 | 17.4 | 16.7 | 17.2 | 18.3 | 20.7 | 19.3 | 16.7 |
| 0.5 | 18.8 | 19.7 | 18.6 | 19.6 | 20.5 | 23.5 | 21.4 | 18.4 |
| 1 | 21.0 | 22.3 | 21.3 | 22.5 | 23.5 | 26.6 | 23.5 | 20.3 |
| 2 | 24.4 | 25.8 | 25.3 | 26.3 | 28.4 | 31.0 | 26.3 | 22.8 |
| 4 | 28.8 | 30.5 | 31.0 | 31.4 | 34.0 | 36.7 | 30.6 | 26.4 |
| 5.6 | 34.0 | 35.5 | 36.3 | 36.1 | 40.7 | 42.7 | 35.0 | 30.3 |
| 8 | 45.1 | 44.9 | 47.3 | 45.7 | 55.6 | 55.0 | 43.2 | 38.5 |
| 11.2 | 70.4 | 66.8 | 68.0 | 64.0 | 78.7 | 74.2 | 64.7 | 58.4 |
| 16 | 96.9 | 96.3 | 98.6 | 94.8 | 99.4 | 97.2 | 91.5 | 91.9 |
| $V_{aSSD}$ | 2.5 | 2.9 | 1.4 | 1.2 | 0.7 | 1.0 | 0.6 | 2.8 |
| $V_{aDIM}$ | 5.2 | 8.8 | 5.3 | 6.2 | 1.6 | 5.3 | 1.2 | 7.6 |
| SA[a] ($m^2/g$) | – | – | 1.24 | – | 0.98 | – | 1.11 | – |
| Fine area[b] ($m^2$) | – | – | 17,85 | – | 15,38 | – | 17,65 | – |
| $P_b$ (%) | | | 6.2 | | 6.5 | | 6.3 | |
| $P_b$/Fine area[b] ($g/m^2$) | – | – | 0.34 | – | 0.42 | – | 0.35 | – |
| Strength (kPa) | 1937 | 1685 | 2287 | 2492 | 2413 | 2356 | 2151 | 2175 |

Gradation requirements for the SMA16 according to FAS (percent passing)
[a]Fines passing 0.125 mm sieve
[b]Per 100 g of mix

construction records confirmed that 4th site had fly ash up to 9 % of filler. Interestingly, the FT-IR test was much faster than obtaining data from the registry. The 2nd site and 3rd site consisted of small amounts of limestone and based on records fly ash. The 1st site consisted of larger amounts of limestone as witnessed by the ratio of the carbonate to silica peak (0.24, 0.25 and 0.7, respectively). The low amount of bitumen per surface area in site 2 and 4 is indicative of a rather stiff mixture and expectedly problems upon reheating and compacting should occur in such cases, as was observed. Prall abrasion and pavement wear resistance (PWR) tests were conducted only on the REMIX 2013 treated samples according to the standard SFS-EN 12697-16 (method A and B) in order to evaluate the success rate and properties of the HIP-RC pavements in terms of resistance to the abrasion by studded tires. As hypothesized, the resistance to studded tire wear, for the SMA16 mixes with similar gradations, as confirmed by both methods was dependent on the air void content. The Prall abrasion increased when air void

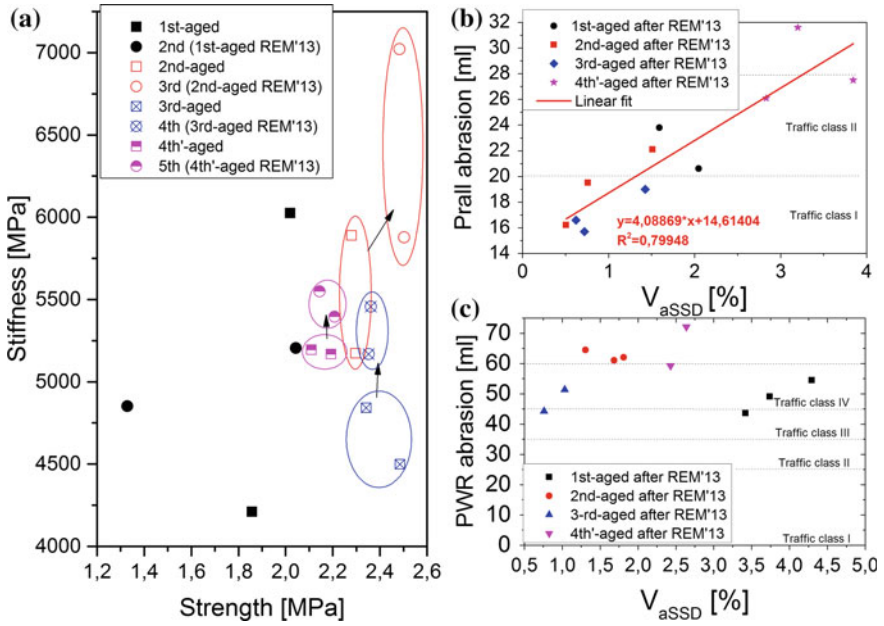


**Fig. 2** **a** Relationship of strength and stiffness between different tested locations before and after REM'13; **b** relationship of Prall abrasion from the air voids measured by surface saturated dry method; **c** relationship of pavement wear resistance to studded tires (PWR abrasion) from the air voids measured by surface saturated dry method

content increased (Fig. 2b). The PWR abrasion seemed to depend also on other mix properties (Fig. 2c).

Additionally, six samples per sampling location were subjected to indirect tensile stiffness (SFS EN 12697-26) and strength (SFS EN 12697-23) testing at 10 °C. These results will be used to develop a database of mix designs in terms of their composition and stiffness to strength ratio along the failure modes. This idea is based on proposed conceptual performance criteria by Pellinen (2003) on the strength and stiffness relationship of asphalt mixtures. The results collected on REMIX samples, averaged per sampling location, are shown in Fig. 2a. The hypotheses were confirmed that HIP-RC maintenance is in general stiffening the mixture as the binder becomes more aged. According to Pellinen (2003), a shift towards higher stiffness and strength is decreasing rutting, but at the same time decreasing durability and increasing susceptibility to thermal cracking. Fatigue failure is more ambiguous, for thick pavements higher stiffness and strength would be desirable as for thin pavements a softer mixture would give more ductility and strain tolerance. But if mixture strength is attained via dense packing, cracks may propagate faster depending on the aggregate grain size and packing.

On the basis of the obtained field data, we are focusing on material optimization and admixture design in order to retain the resistance to thermal cracking and retain

enough stiffness to withstand permanent deformation within the HIP-RC treated pavements, i.e. to further extend the life cycle of the pavement. A collaborative database is expected to provide us with an answer to the optimal stiffness/strength ratio, so far referred to as "a golden midpoint" on which further specifications could be based.

## 4 Bitumen Analysis and Selection of Rejuvenating Method

Bitumen recovery was conducted according to the norm EN 12697-1 and EN 12697-3. Samples were taken before and after REM'13 work in order to test the quality of the bitumen. To obtain minimum of 100 g bitumen required for the further Penetration testing, three or more cores were combined as one sample.

Techniques such as Penetration, Iatroscan SARA fractions, Bitumen Solubility Model (BISOM) and Solubility Parameters were applied to evaluate the initial quality of bitumen.

Penetration was conducted according to EN-1426. The BISOM titrations and calculation of characteristic parameters as well as determination of the Solubility Parameters were executed in Nynas AB laboratories according to the methodology explained elsewhere (Redelius and Soenen 2005; Redelius 2004), respectively. SARA fractions were also conducted according to the methodology described elsewhere (Simonen et al. 2013). The results of the BISOM titrations are presented in Table 3 along the Penetration values for each of the evaluated bitumens. It has been previously observed that the parameters D, H and N do not correlate well to the traditional stiffness characteristics of bitumens (e.g. Penetration) and the same can be observed from the obtained data.

According to the results obtained during the BISOM titrations, we have obtained valuable information in terms of bitumen quality at different stages in life. The parameters D, N and H (presented in Table 3) are used to designate the stability of the bitumen in terms of dispersive interactions, polar interactions and hydrogen bonding, respectively. The higher the D parameter the more stable and better quality bitumen we are dealing with. The D values falling around 2.5 and below are usually deemed unstable and of low quality. However, extremely high values, e.g. 7, are not to be aimed at (Redelius and Soenen 2005).

On the other hand, the higher the H and N parameter, the more aged the bitumen is. As weak polar and hydrogen interactions increase upon aging, the elastic behavior of the bitumen increases (Redelius and Soenen 2005).

On the basis of our results, it became obvious that the quality and need for rejuvenation of the bitumen should be evaluated case by case rather than relying on the general FTA guidelines of using soft bitumen 650/900 discussed above. The development of a proper test procedure is desirable. BISOM titration proved promising as a candidate for further research and development efforts. Clearly, the most aged bitumen which was recycled twice was also the most stable and best

**Table 3** Results of the BISOM titration experiments for non-rejuvenated bitumens extracted from test road before REM13'

| | D | $d_a$ | $D_0$ | $R^2$ | N | $n_a$ | $N_0$ | $R^2$ | H | $h_a$ | $H_0$ | $R^2$ | Pen |
|---|---|---|---|---|---|---|---|---|---|---|---|---|---|
| 1st site | 2.79 | 0.6 | 1.11 | 0.98 | 3.38 | 0.54 | 1.55 | 0.99 | 2.20 | 0.50 | 1.09 | 0.99 | 135[a] |
| 2nd site | 2.64 | 0.59 | 1.08 | 0.98 | 3.30 | 0.58 | 1.38 | 0.96 | 2.19 | 0.52 | 1.06 | 0.98 | 39 |
| 3rd site | 3.35 | 0.67 | 1.12 | 0.90 | 3.06 | 0.59 | 1.24 | 0.98 | 2.77 | 0.55 | 1.23 | 1.00 | 52 |
| 4th site | 3.05 | 0.57 | 1.30 | 1.00 | 3.30 | 0.58 | 1.38 | 0.96 | 1.83 | 0.50 | 0.91 | 1.00 | 68 |
| Deviation[b] | 0.03 | | | | 0.12 | | | | 0.08 | | | | |

[a]Solvent was confirmed not to fully evaporate during recovery, potential error
[b]Standard deviation established during optimization by Nynas laboratories for the procedure

quality one. Incidentally, bitumen from the 1st site, which had not been recycled yet, is falling very close to the edge of the stability.

The visual observation of the site indicated the improvement in pavement quality upon the start of the 3rd cycle and thus further studies of the bitumen stability improvement upon rejuvenation and HIP-RC should be studied in the next phases of the project. The first conclusions and suggestions for the future work are that the rejuvenation effort should focus on the up keeping or increasing dispersive forces within the bitumen, while not introducing more components contributing to polar or hydrogen interactions, therefore focusing on retaining the viscous properties of the bitumen. The increased elasticity of the binder creates a potential risk for damages to the HIP-RC treated pavements and, what is especially crucial in cold region engineering; it is hypothesized to increase susceptibility to thermal cracking. Our field study (Laukkanen et al. 2013) verifies findings by Redelius and Soenen (2005) that in situ aging is increasing the elasticity of the binder. But how this increased elasticity is affecting the thermal properties and the healing properties is not yet quite understood although thermal cracking may increase as there is less viscous flow and healing.

According to the general fractioning (Table 4), two times recycled (3rd site) bitumen had the least amount of asphalthenes, which shifted its composition towards resins and aromatics. According to Isacsson and Zeng (1997), the cumulative amount of asphalthenes and resins (A + R = 61.1) for this bitumen suggests that it ought to be softer and less thermal cracking prone than once recycled (2nd site) (A + R = 66.5), but harder and with lower resistance to low temperature action than the non-recycled (4th site) (A + R = 59). This is confirmed by the penetration values collected and presented in Table 3.

The bitumen solubility parameters are represented in Fig. 3 in the form of solubility spheres for bitumens recovered before REM13'. It is easily visible (Fig. 3a) that the changes between the different cycles of life are minuscule as was expected. One solvent gave clearly different solubility reading whereas with others the precipitation was a function of time rather than the solvent. The main complication on the construction site observed to occur is the loss of temperature control during HIP-RC and a risk for mixture self-ignition during the process. Therefore, we must also pay attention to the volatility of the rejuvenators used in the process. Using the rejuvenator (e.g. very soft bitumen, Fig. 3b) with a solubility sphere permeating the solubility sphere of bitumen in question facilitates the lowest risk for separation between volatile components and provides optimal opportunity for blending to occur.

**Table 4** General fractioning results for the tested bitumens before REM13'(average and standard deviation)

| | 2nd site | 3rd site | 4th site |
|---|---|---|---|
| Saturates, % | 3.3 (1.9) | 3.9 (0.1) | 4.1 (1.0) |
| Aromatics, % | 30.2 (2.5) | 35.0 (0.3) | 36.4 (3.1) |
| Resins, % | 39.2 (1.6) | 36.4 (0.4) | 31.8 (1.9) |
| Asphaltines, % | 27.3 (0.3) | 24.7 (0.7) | 27.6 (2.2) |

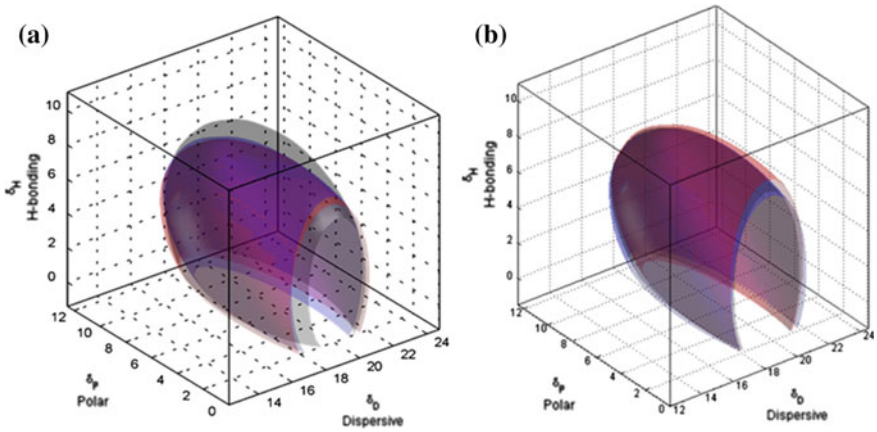


**Fig. 3** **a** Solubility parameters of recovered bitumens 2nd site (*red*), 3rd site (*blue*) and 4th site (*black*) indicating minuscule changes in solubility between the materials; **b** an example of soft bitumens solubility parameter (*red*) with bitumens from 3rd site (*blue*) and 4th site (*black*)

On the basis of the above results, and the literature review on the Finnish experience with rejuvenators in HIP-RC, it is advised that the guideline of using bitumen 650/900 as a rejuvenator during REMIX works be sustained until further studies determine the suitability of other rejuvenators (e.g. softer bitumens or artificial bitumens) or there would be data indicating lack of merit behind this decision. Because the main issue with rejuvenation is dosing, authors believe that focusing on the optimization and improvement of dosing should be the most important effort in the further steps of the project.

## 5 Concluding Remarks

An outline and framework for the criteria development for the hot-in-place recycling have been presented. The preliminary results indicate that asphalt mixture can be multiple recycled under given conditions, but the success depends on the performance criteria set for the final product. The first observations of our REMIX project suggest that the important performance related parameters to focus on are the air void content and its effect on the studded tire abrasion, the stiffness to strength ratio value in order to balance thermal and fatigue cracking and permanent deformation, and the general admixture optimization in order to improve the overall properties of the pavement in question.

**Acknowledgements** Authors wish to thank Dr. Per Redelius and Dr. Xiaohu Lu for their help and advice in conducting binder solubility testing at Nyas AB Ltd bitumen laboratory and the Finnish Road Administration and Pavement Engineer Katri Eskola for the financial support in this research.

## References

Apilo L., Eskola K., Uusiopäällystetutkimukset 1998, Helsinki 1999, Tielaitos, Tielaitoksen selvityksiä 7/1999,, ISSN 0788-3722, ISBN 951-726-497-6, TIEL 3200553

Finnish Asphalt Specifications 2011. Finnish Pavement Technology Advisory Council, PANK. Edita Ltd., Helsinki, 2011.

Hesham Ali, Ph.D., P.E., Khaled Sobhan, Ph.D, On the Road to Sustainability: Properties of Hot in-place Recycled Superpave Mix, TRB 2012 Annual Meeting, paper no 12-0771

Isacsson U., Zeng H., Relationship between bitumen chemistry and low temperature behavior of asphalt, Construction and Building Materials, Vol. 11 No. 2, 1997, pp. 83-91

Laukkanen OV, Pellinen T, Makowska M. Exploring the observed rheological behavior of in-situ aged and fresh bitumen employing the colloidal model proposed for bitumen. Multi-Scale Modeling and Characterization of Infrastructure Materials: Proceedings of the International RILEM Symposium Stockholm, June 2013 (RILEM Bookseries) RILEM, 2013

Li J., Ni F., Huang Y., New Additive Used in Hot In-place recycling to improve Performance of RAP Mix, TRB 2014, Memory stick

Lyytinen J., ”Suomen infra rapautuu lian nopeaa vauhtia!”, Teitä Varten, Päällysteallan erikoisjulkaisu 1/2014

Makowska M., Pellinen T., Martinez P. O., Laukkanen O.-V., Analytical methodology to determine the composition of filler used in HMA: Case study, TRR, 2014, Issue No: 2445, pp 12-20,

Patosalmi S., Vanhan asfalttipäällysteen sideaineen elvyttimet, Master of Science, 23.9.1996, Helsinki University of Technology, Espoo

Pellinen T.K., The effect of Volumetric Properties on mechanical behavior of Asphalt Mixtures, TRB 2003 Annual Meeting

Rantanen T., Suikki L., Uusiopäällysteiden ylläpidossa, Helsinki 2009, Tiehallinto, Tiehallinnon sisäisiä julkaisuja 56/2009, ISSN 1459-1561, TIEH 4000731-v

Redelius, P., Bitumen Solubility Model Using Hansen Solubility Parameter, Energy & Fuels 2004, 18 (4), pp. 1087-1092

Redelius P., Soenen H., Correlation between Bitumen Polarity and Rheology, Road Materials and Pavement Design, (2005), 6:3, 385-405, DOI: 10.1080/14680629.2005.9690013

Simonen, M.; Blomberg, T.; Pellinen, T.; Makowska, M.; Valtonen, J., Curing and ageing of biofluxed bitumen: a physicochemical approach, 2013, Road materials and pavement design, Vol. 14, nro 1, pp. 159-177.

Saarela, A., et al. (1993). Asfalttipäällysteiden tutkimusohjelma ASTO 1987-1992”. (Asphalt Pavements Research Program ASTO 1987-1992), Final Report. Technical Research Centre of Finland. Road, Traffic and Geotechnical Laboratory. Espoo 1993.

Tiehallinto, Päällysteiden ylläpidon toimintalinjat, ISBN 978-951-803-793-7, Edita Prima Oy, Helsinki 2007

Wastimo E., Aasfaltti- ja kevytpäällysteiden uudellenkäyttö 1973-1995, Asfaltti, 56, December 1995, pp 20-30

# Part X
# Recycling and Re-use in Road Pavements

# Rheological Investigation of Asphalt Mixtures Containing RAP and RAS

**Augusto Cannone Falchetto, Ki Hoon Moon, Michael P. Wistuba and Mihai O. Marasteanu**

**Abstract** Reclaimed Asphalt Pavement (RAP) and Recycled Asphalt Shingles (RAS) are valuable materials commonly reused in asphalt mixtures due to economic and environmental benefits. However, the aged binder in these materials may negatively influence the low temperature properties of the final asphalt mixtures. In this paper, the effect of adding RAP and RAS on low temperature properties of asphalt mixtures is investigated through Bending Beam Rheometer (BBR) tests and rheological modelling. First, a set of fourteen asphalt mixtures containing different amounts of RAP and RAS are prepared and creep stiffness experimentally measured. Then, the Huet model and the Ecole Nationale des Travaux Publics de l'Etat (ENTPE) transformation are used to back calculate the asphalt binder creep stiffness from mixture experimental data. Finally, the model predictions are compared to the creep stiffness of the asphalt binders extracted from each mixture, and the results are discussed. Experimental measurements indicate that the addition of RAP and RAS significantly affects low temperature performance of asphalt mixture. Differences between back-calculated results and experimental data suggest blending between new and old binder is only partial. Based on the recent finding on diffusion studies, this effect may be associated to mixing and blending processes, to the effective contact between virgin and recycled materials and to the variation of the total virgin-recycled thickness of the binder film which may significantly influence the diffusion process.

A. Cannone Falchetto (✉) · M.P. Wistuba
Technische Universität Braunschweig – ISBS, Braunschweig, Germany
e-mail: a.cannone-falchetto@tu-bs.de

M.P. Wistuba
e-mail: m.wistuba@tu-bs.de

K.H. Moon
Samsung Corporation, Seoul, South Korea
e-mail: moonx113@umn.edu

M.O. Marasteanu
University of Minnesota, Minneapolis, USA
e-mail: maras002@umn.edu



F. Canestrari and M.N. Partl (eds.), *8th RILEM International Symposium on Testing and Characterization of Sustainable and Innovative Bituminous Materials*, RILEM Bookseries 11, DOI 10.1007/978-94-017-7342-3_69

**Keywords** Reclaimed asphalt pavement · Recycled asphalt shingles · Back-calculation · Binder blending

## 1 Introduction

Using recycled materials such as Reclaimed Asphalt Pavement (RAP) and Recycled Asphalt Shingles (RAS) is a top priority in the pavement industry not only for reducing the construction costs but also for minimizing the environmental impact of road construction (Cannone Falchetto et al. 2013). However, the aged and brittle binder contained in RAP and RAS may negatively influence the low temperature properties of the final asphalt mixtures and, eventually, the pavement durability.

In the recent past, a number of research efforts were conducted to evaluate the effect of RAP on recycled asphalt mixtures both in the US and in Europe (McDaniel and Anderson 2002; FEHRL 2003) with the conclusion that RAP content has a significant influence on mixture properties. Specifications were also developed with recommendations for selecting RAP percentage based on traffic level up to a maximum of 40 % by weight (MnDOT 2008). More recent studies have centered their efforts in understanding and modeling the effective blending and the diffusion processes occurring at the interface between virgin and aged binder in the recycled mixtures (Mangiafico et al. 2013; Kriz et al. 2014).

Regarding the re-use of roofing asphalt shingles, two distinct categories are available in the market: Manufacturer Waste Scrap Shingles (MWSS) and Tear-off Scrap Shingles (TOSS), from old roofs that have been exposed to solar radiation and high temperatures for extended periods of time. Both TOSS and MWSS, which are generally identified as RAS, contain high amount of small aggregates and a much harder asphalt binder compared to that used in asphalt pavement mixtures: at 25 °C, the penetration values for asphalt binder in shingles ranges from 20 to 70 dmm, while traditional paving binders range from 50 to 300 dmm (Newcomb et al. 1993). Most of the past studies on RAS were devoted to identify the maximum amount of shingles that could be recycled in the new mixtures (Newcomb et al. 1993). More recently, McGraw et al. (2010) investigated the combined use of RAP and RAS showing the negative effect of TOSS on mixture strength and binder's critical cracking temperature. Recent European studies have also addressed the use of shingles (Rasmussen 2012; Tapsoba et al. 2014). In one of this research works (Tapsoba et al. 2014), both stiffness and fatigue properties of the recycled mixture were investigated showing an increase in mixture stiffness due to the inclusion of RAP and shingles (up to 5 %).

The use of RAS in hot mix asphalt has seen increased acceptance from government agencies and road authorities, however this material poses significant challenges for pavement built in cold climates where materials with good fracture resistance are required. This is particularly true for TOSS, which contain highly oxidized binders that are more prone to brittle failure. Similarly to RAP,

specifications on the use of RAS are based on content limits (5 %) with the provision that a specific percentage of new binder is used in the recycled mixture (MnDOT 2008).

## 2 Research Approach and Objectives

In this research, the addition of RAP, MWSS and TOSS to asphalt mixtures used in pavement applications is investigated based on changes in mixtures and binders low temperature properties. Huet (1963) analogical model (Sharpe 2008) coupled with the transformation proposed by the research team of the Ecole Nationale des Travaux Publics de l'Etat (ENTPE) (Di Benedetto et al. 2004) are used to investigate the effect of adding recycled material on both asphalt binder and asphalt mixture creep stiffness. Back-calculation of the asphalt binder creep stiffness is performed using mixture creep stiffness data obtained with the Bending Beam Rheometer (BBR) (AASHTO T313 2012). The goal is to determine if changes in mixture behavior are due to the addition of recycled material and more specifically to the blending of new and old binder. This is obtained by comparing the back-calculated binder creep stiffness with the corresponding extracted binder obtained from the same mixture, which represents a condition of full blending. This also provides an indication of the degree of blending between the virgin binder and the aged binder present in the added recycled materials, RAP or RAS.

## 3 Materials and Testing

Fourteen different asphalt mixtures (Table 1) prepared with two plain asphalt binders having performance grade PG58-28 and PG52-34 were used in this study (AASHTO M320 2010). Three types of virgin aggregates were blended to prepare the mixtures: pit-run-sand, quarried 3/4 in. (19 mm) dolostone, and quarried dolostone manufactured sand. The recycled material consisted of different amounts of RAP, TOSS and MWSS. Additional details on the material used for the present research can be found elsewhere (McGraw et al. 2010).

Small beams of asphalt mixtures (three replicates per mixture) were tested using the Bending Beam Rheometer (Fig. 1) following the experimental procedure proposed by Marasteanu et al. (2009). In the same study it was demonstrated that the BBR samples dimensions large enough to be considered representative of asphalt mixture and, hence, of the binder present in the mixture.

Asphalt binder was also extracted from mixtures 2–14 and BBR creep stiffness (AASHTO T313 2012) measured; the extraction and testing of the extracted binders were performed at MnDOT Office of Materials. BBR creep stiffness was also obtained on the original PG58-28 binder after RTFOT aging and next assumed as

**Table 1** Mix design for the fourteen asphalt mixtures investigated

| ID | Mix | Recycled material | | | Binder |
|---|---|---|---|---|---|
| | Description | RAP (% weight) | MWSS (% weight) | TOSS (% weight) | PG |
| 1 | Control | 0 | 0 | 0 | 58-28 |
| 2 | 15 % RAP | 15 | 0 | 0 | 58-28 |
| 3 | 25 % RAP | 25 | 0 | 0 | 58-28 |
| 4 | 30 % RAP | 30 | 0 | 0 | 58-28 |
| 5 | 15 % RAP 3 % MWSS | 15 | 3 | 0 | 58-28 |
| 6 | 15 % RAP 3 % TOSS | 15 | 0 | 3 | 58-28 |
| 7 | 15 % RAP 5 % MWSS | 15 | 5 | 0 | 58-28 |
| 8 | 15 % RAP 5 % TOSS | 15 | 0 | 5 | 58-28 |
| 9 | 25 % RAP 3 % MWSS | 25 | 3 | 0 | 58-28 |
| 10 | 25 % RAP 3 % TOSS | 25 | 0 | 3 | 58-28 |
| 11 | 25 % RAP 5 % MWSS | 25 | 5 | 0 | 58-28 |
| 12 | 25 % RAP 5 % TOSS | 25 | 0 | 5 | 58-28 |
| 13 | 25 % RAP 5 % MWSS | 25 | 5 | 0 | 52-34 |
| 14 | 25 % RAP 5 % TOSS | 25 | 0 | 5 | 52-34 |

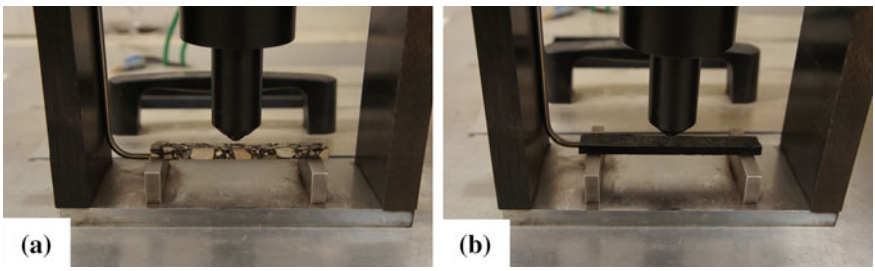


**Fig. 1** Bending beam rheometer with thin **a** asphalt mixture and **b** asphalt binder beams

control in the analysis. The same testing temperature, $T = -6$ °C, was used for binder and mixture tests to avoid any potential errors associated to time-temperature superposition.

## 4 Huet Model and ENTPE Transformation

Several analogical models are available to describe the properties of viscoelastic materials such as asphalt binder and asphalt mixture (Findley et al. 1989; Di Benedetto et al. 2004). In previous study (Cannone Falchetto et al. 2011), analogical models were used to obtain creep stiffness of asphalt binders from creep stiffness of the corresponding asphalt mixtures (inverse problem). It was found that Huet model (1963) fitted very well the experimental data obtained from BBR tests at low temperatures for both asphalt binders and mixtures. This model is composed of one spring, and two parabolic elements combined in series (Fig. 2).

The Huet model expression for creep compliance can be written as:

$$D(t) = \frac{1}{E_\infty}\left(1 + \delta\frac{(t/\tau)^k}{\Gamma(k+1)} + \frac{(t/\tau)^h}{\Gamma(h+1)}\right) \quad (1)$$

where $D(t)$ is the creep compliance, $E_\infty$ is the glassy modulus, $h$ and $k$ are exponents such that $0 < k < h < 1$, $\delta$ is a dimensionless constant, $t$ is the time variable, $\Gamma$ is the gamma function, $\tau$ is the characteristic time varying with temperature accounting for the Time Temperature Superposition Principle (TTSP): $\tau = a_T(T)\tau_0(T_S)$, $a_T$ is the shift factor at temperature $T$ and $\tau_0$ is the characteristic time determined at reference temperature $T_S$.

The authors (Cannone Falchetto et al. 2011) found the following relationship between the characteristic time of mixture, $\tau_{mix}$ and the characteristic time of the corresponding binder, $\tau_{binder}$, at the reference temperature $T$:

$$\tau_{mix}(T) = 10^{\alpha}\tau_{binder}(T) \quad (2)$$

where $\alpha$ is a regression coefficient depending on mixture type and aging (Di Benedetto et al. 2004). This expression corresponds to the equation proposed by Di Benedetto et al. (2004) and obtained from 2S2P1D model and complex modulus data. Based on Eqs. 1 and 2, a transformation that relates the creep stiffness of the asphalt binder $S_{binder}(t)$, to the creep stiffness of the corresponding asphalt mixture $S_{mix}(t)$ can be written:

$$S_{mix}(t) = S_{binder}(t10^{-\alpha}) \cdot (E_{\infty\_mix}/E_{\infty\_binder}) \quad (3)$$

where $E_{\infty\_mix}$ is the mixture glassy modulus and $E_{\infty\_binder}$ is the binder glassy modulus. Equation 3 does not depend on the original model used to obtain it and

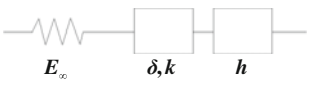


**Fig. 2** Huet model (1963)

represents the low temperatures formulation of the ENTPE transformation (Di Benedetto et al. 2004; Cannone Falchetto et al. 2011).

## 5 Back-Calculation

In this section, asphalt binder creep stiffness is back-calculated from the creep stiffness experimental data of asphalt mixture with the aim of obtaining useful information on the blending process and the degree of blending between the new virgin binder and the aged binder contained in RAP and RAS. For such a purpose, Huet model was introduced into Eq. 3 as:

$$S_{mix}(t,h,k,\delta,\tau_{mix}) = S_{binder}(t,h,k,\delta,10^{\alpha}\tau_{binder}) \cdot (E_{\infty\_mix}/E_{\infty\_binder}) \quad (4)$$

where the five constants $\delta$, $k$, $h$, $E_{\infty}$, and $\tau$ can be estimated by minimizing the sum of the distances between asphalt mixture experimental data and the predicted values obtained from Eq. 4 at n time points. In previous studies (Di Benedetto et al. 2004; Cannone Falchetto et al. 2011), it was found that Huet model parameters assume the same values for binder and corresponding mixtures. Therefore, the difference between asphalt binder and asphalt mixture is given by the characteristic times, $\tau_{binder}$ and $\tau_{mix}$, which, based on Eq. 2, are directly associated to parameter $\alpha$. In this study, the value of $\alpha$ was obtained during the minimization process starting from initial values of $\delta$, $k$, $h$, $E_{\infty}$, and $\tau$ found in literature (Huet 1963; Di Benedetto et al. 2004; Cannone Falchetto et al. 2011). In addition, the recent recommendation proposed by Moon et al. (2013), which limits the value of $k$ between 0.25 and 0.40 for asphalt binders having low PG equal to −28 and between 0.20 and 0.40 for binders with low PG equal to −34, was used. Table 2 presents the Huet model parameters for the fourteen asphalt mixtures tested at −6 °C and for the corresponding back-calculated asphalt binders; the values of $\alpha$ are given in the last column of the table.

The values of parameters $h$, $k$ and $\delta$ are in agreement with the values obtained in different research efforts (Di Benedetto et al. 2004; Cannone Falchetto et al. 2011). It is interesting to observe that $h$ is significantly higher for the control binder, compared to value obtained from the back-calculation process on the mixture containing recycled material. This confirms what found in a different study for which smaller values of $h$ are associated to aged, oxidized materials affected by air blowing or weathering during its production process or several years after its service life (Huet 1999).

As expected, there is a significant difference in the characteristic times of binders and corresponding mixtures. Nevertheless, is interesting to observe that the presence of recycled materials significantly influences this parameter (Mangiafico et al. 2013). Higher values of the transformation parameter, $\alpha$, were observed when recycled material is added to the mixture in comparison with the control mixture prepared with virgin aggregates and virgin binder. This is true both when only RAP

**Table 2** Huet model parameters for mixtures and corresponding back-calculated binders

| ID | $\delta$ | $k$ | $h$ | $E_{\infty\_binder}$ (MPa) | $E_{\infty\_mix}$ (MPa) | Log($\tau_{binder}$) | Log($\tau_{mix}$) | α |
|---|---|---|---|---|---|---|---|---|
| 1 | 2.81 | 0.25 | 0.63 | 2500 | 23,718 | −1.102 | 1.808 | 2.91 |
| 2 | 2.95 | 0.28 | 0.53 | 2500 | 20,639 | −1.046 | 3.086 | 4.13 |
| 3 | 2.84 | 0.31 | 0.49 | 2500 | 20,000 | −0.939 | 3.401 | 4.34 |
| 4 | 3.05 | 0.30 | 0.55 | 2500 | 20,016 | −0.851 | 3.199 | 4.11 |
| 5 | 2.69 | 0.26 | 0.50 | 2500 | 20,543 | −1.086 | 2.804 | 3.89 |
| 6 | 2.79 | 0.25 | 0.50 | 2720 | 20,000 | −1.125 | 3.225 | 4.35 |
| 7 | 2.81 | 0.25 | 0.49 | 2500 | 20,027 | −1.036 | 3.195 | 4.23 |
| 8 | 3.04 | 0.29 | 0.43 | 2500 | 20,837 | −1.032 | 3.701 | 4.73 |
| 9 | 2.51 | 0.25 | 0.49 | 2500 | 21,059 | −1.108 | 3.712 | 4.82 |
| 10 | 2.70 | 0.25 | 0.48 | 2500 | 23,191 | −1.119 | 3.591 | 4.71 |
| 11 | 2.61 | 0.25 | 0.49 | 2620 | 20,003 | −1.125 | 3.875 | 4.91 |
| 12 | 2.71 | 0.25 | 0.46 | 2546 | 20,037 | −1.155 | 3.645 | 4.80 |
| 13 | 1.75 | 0.25 | 0.48 | 2710 | 20,010 | −0.886 | 2.964 | 3.85 |
| 14 | 2.32 | 0.25 | 0.46 | 2826 | 20,001 | −0.959 | 2.951 | 3.91 |

is used as well as when MWSS and TOSS are included in the mix design. Nevertheless, no statistically significant differences could be detected among the values of $\alpha$ obtained for the recycled mixtures prepared with PG58-28 asphalt binder. Smaller values of the transformation parameter could be observed for the two asphalt mixtures designed with the softer PG52-34 asphalt binder.

## 6 Comparison with Experimental Data

The values of the asphalt binder creep stiffness predicted from the ENTPE transformation were compared to the creep stiffness values obtained experimentally on the RTFOT aged original binder and on the extracted asphalt binders (mixtures 2–14). Asphalt mixtures were tested for 1000 s (Marasteanu et al. 2009) while the test duration of asphalt binders was limited to 240 s as prescribed in the standard (AASHTO T313 2012). Therefore, in the following plots the curves of creep stiffness obtained from asphalt binders are shorter than those predicted through back-calculation from mixture data. Figures 3, 4, 5 and 6 present the creep stiffness obtained from extracted binders and from the back-calculated process for some of the mixtures investigated.

The ENTPE transformation provides a very accurate prediction of the creep stiffness of the RTFOT original binder, confirming the findings of previous studies on virgin materials (Di Benedetto et al. 2004; Cannone Falchetto et al. 2011). A common trend is observed for stiffness curves of asphalt binders obtained from the recycled mixtures (2–14): they are initially asymptotically close to the creep

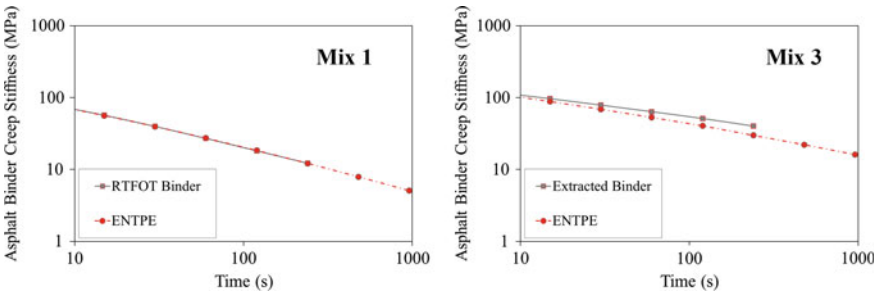


**Fig. 3** Back-calculated and extracted creep stiffness of asphalt binder: mix 1 and 3

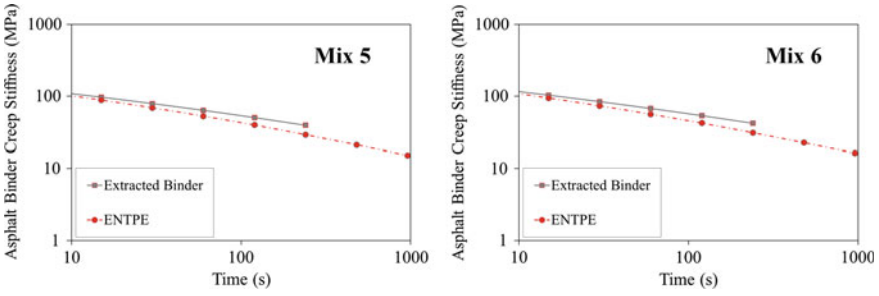


**Fig. 4** Back-calculated and extracted creep stiffness of asphalt binder: mix 5 and 6

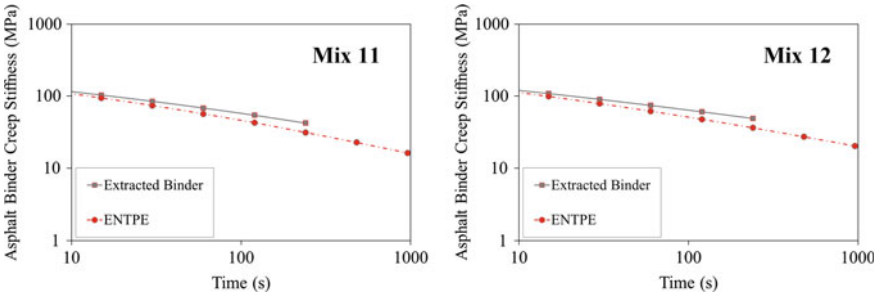


**Fig. 5** Back-calculated and extracted creep stiffness of asphalt binder: mix 11 and 12

stiffness curves of extracted binders, while they diverge toward lower stiffness values as time increases. This suggests that the relaxation properties obtained from ENTPE back-calculation are higher compared to the extracted binders.

It can be hypothesized that one of the reasons responsible for these observations is due to the presence of fine particles in the asphalt binder which could not be removed during the extraction process. However, this hypothesis would result in global higher stiffness values also for the part of the curve which is asymptotically

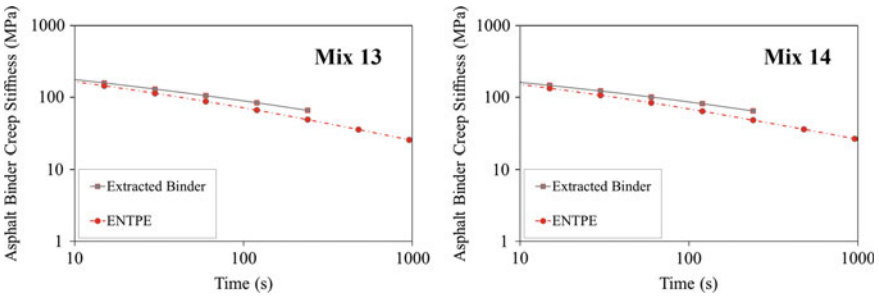


**Fig. 6** Back-calculated and extracted creep stiffness of asphalt binder: mix 13 and 14

approaching the model predictions, leading to an overall deviation of the experimental measurements from the back-calculated stiffness.

An alternative and more reasonable explanation of the difference between extracted binders and back-calculated creep stiffness curves is associated to the limited or partial blending occurring between new and recycled binder. Therefore, while the mixture creep behavior is affected by all new binder and only a part of the aged, oxidized binder, the extraction and recovery process resulted in a complete blending; this implies that the resulting blend has worse relaxation capabilities since the properties are influenced by the entire aged binder component.

Bonaquist (2007) has associated the insufficient heat transfer during mixing to partial binders blending in the mixture. An additional explanation of the limited binder blending can be provided on the basis of the work recently presented by Kriz et al. (2014); he identified two major processes which are involved in the binder blending: contact between the two binders, achieved mechanically and binder blending after contact is made, achieved mainly by diffusion and strongly influenced by the total new-aged binder thickness. The limited or partial blending may be linked to the distribution of the binder film thickness within the asphalt mixtures microstructure and to the impossibility of obtaining a proper binder contact when mixing. This can explain the discrepancy between the actual binder stiffness in the mixture and that obtained from extraction.

## *6.1 Discussion on the Characteristic Time Parameter for RAP Binder—Mixtures (Mixture 1–4)*

In this section the value of characteristic time, $\tau$, of the Huet model (1963) is further investigated for mixtures containing only RAP as recycled material in their mix design (Mixture 1, with 0 % RAP, to 4, with 30 % RAP). The other mixtures, which include MWSS and TOSS, are not addressed at this stage of the research due to the limited design combinations for this type of materials.

In a recent study it was found that, for completely blended binders, parameter $\tau$ follows a linear trend with respect to RAP content in a log scale, eventually reaching the unique RAP value of $\tau$ (Mangiafico et al. 2013). In this study the creep stiffness of the 100 % RAP binder is not known, however, it is possible to compere that characteristic time of extracted binder present in the RAP mixtures with the characteristic time obtained from back-calculation. Table 3 presents the Huet model parameters for the extracted binders of the first four mixtures, while Fig. 7 shows the comparison between the characteristic times derived from extracted binder and back-calculated creep stiffness.

It can be observed that $\tau$ of extracted binders presents a reasonable linear pattern with increasing values for higher RAP content in the log scale. This confirms what found in other investigations (Mangiafico et al. 2012, 2013). On the other hand, the characteristic time obtained from back-calculation shows a significant deviation from linearity which becomes more severe for higher amount of RAP. The latter effect can be associated to the partial blending of virgin and aged binder which may results in a substantially different material response within the binder film thickness causing a dramatic increase in the characteristic time. Nevertheless, this hypothesis needs to be further investigated

**Table 3** Huet model parameters for RTFOT and extracted RAP binders

| ID | Description | $\delta$ | $k$ | $h$ | $E_{\infty\_binder}$ (MPa) | Log($\tau_{binder}$) |
|---|---|---|---|---|---|---|
| 1 | Control | 2.81 | 0.25 | 0.63 | 2500 | −1.102 |
| 2e[a] | 15 % RAP | 3.01 | 0.32 | 0.43 | 2500 | −1.092 |
| 3e[a] | 25 % RAP | 3.04 | 0.26 | 0.44 | 2500 | −1.071 |
| 4e[a] | 30 % RAP | 3.01 | 0.29 | 0.45 | 2500 | −1.060 |

[a]e stands for extracted

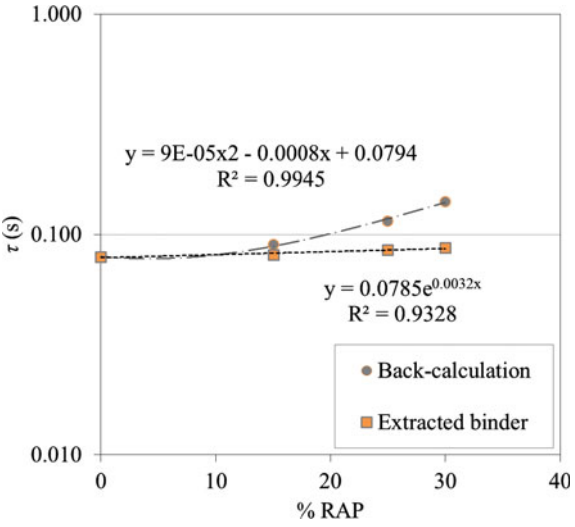


**Fig. 7** Evolution of parameter $\tau$ as function of RAP content

and validated on additional mixtures with higher RAP content, and with specific experimental and modeling tools for evaluating the effective diffusion of the new binder into the aged binder (Kriz et al. 2014).

## 7 Summary and Conclusions

In this paper, the effect on low temperature properties of asphalt mixtures due to the addition of various percentages of RAP, MWSS and TOSS was investigated. First, Bending Beam Rheometer (BBR) tests, Huet model and the transformation implemented by the Ecole Nationale des Travaux Publics de l'Etat (ENTPE) were used to back-calculate the asphalt binder creep stiffness of the binder present in fourteen mixtures. Then, the back-calculated predictions were compared to the experimental creep stiffness values measured on the short-term aged original binder and on the binders extracted from the other set of thirteen recycled mixtures prepared for this study. Finally, additional analysis was performed to further investigate the effect of RAP on the characteristic time parameter of the Huet model.

The creep stiffness of the original binder after short term aging was matched very closely by the ENTPE transformation, while the asphalt binders stiffness curves back-calculated from recycled mixtures data did not match the creep stiffness curves of extracted binders.

It is hypothesized that blending between new and aged, oxidized binder occurred only partially due to insufficient heat transfer and limited binder contact during mixing and/or to the distribution of the binder film thickness within asphalt mixtures. Therefore, the mixture creep properties were affected by all new binder and only a portion of the old binder. On the other hand, extraction and recovery process resulted in a complete blending which implies reduced relaxation capabilities since all aged binder contributed to the properties of the blend. This hypothesis seems to be further confirmed by the different trend of the characteristic times obtained on extracted binders and thorough the back-calculation procedure.

The findings of the present research indicate that the low temperature stiffness properties of asphalt mixture are influenced by the recycled materials properties. Asphalt binder blending appears to control the creep stiffness when recycled asphalt materials are added in the mixture. In addition, the use of RAP in asphalt mixture results in a blending process which may not necessarily lead to a complete blend over the year; this may be associated to an unexpected evolution of the mixture creep stiffness, potentially resulting in premature failure at low temperature cracking. Therefore, the mix design process must be very carefully considered.

**Acknowledgments** The authors gratefully acknowledge the Minnesota Department of Transportation (MnDOT) for providing the asphalt materials and the binder creep stiffness data.

## References

AASHTO M320-10-UL (2010) Standard specification for performance-graded asphalt binder. Am Assoc State Highw Transp Off.

AASHTO T313-12-UL (2012) Determining the flexural creep stiffness of asphalt binder using the Bending Beam Rheometer (BBR). Am Assoc State Highw Transp Off.

Bonaquist R (2007) Can I run more RAP? Hot Mix Asph Tech 11-13.

Cannone Falchetto A, Marasteanu MO and Di Benedetto H (2011) Analogical based approach to forward and inverse problems for asphalt materials characterization at low temperatures. J Ass Asph Pavement Tech 80:549-582.

Cannone Falchetto A, Montepara A, Tebaldi G and Marasteanu MO (2013) Microstructural characterization of asphalt mixtures containing recycled asphalt materials. J Mat Civ Eng, ASCE 25(1):45–53. doi: 10.1061/(ASCE)MT.1943-5533.0000544

Di Benedetto H, Olard F, Sauzéat C and Delaporte B (2004). Linear viscoelastic behavior of bituminous materials: from binders to mixes. Road Mat Pavement Des 5(1):163-202. doi: 10.1080/14680629.2004.9689992

FEHRL, Forum of European National Highway Research Laboratories (2003) SAMARIS: Sustainable and advanced materials for road infrastructures. Final research report on the 5th Framework Programme of the European Union.

Findley WN, Lai JS and Onaran K (1989) Creep and relaxation of nonlinear viscoelastic materials. Dover Publications, INC., New York.

Huet C (1963). Etude par une méthode d'impédance du comportement viscoélastique des matériaux hydrocarbonés. Dissertation Université de Paris.

Huet C (1999) Coupled size and boundary-condition effects in viscoelastic heterogeneous and composite bodies. Mech Mat 31(12):787-829. doi: 10.1016/S0167-6636(99)00038-1

Kriz P et al. (2014) Blending and diffusion of reclaimed asphalt pavement and virgin asphalt binders. Road Mat Pavement Des 15(1):78-112. doi: 10.1080/14680629.2014.927411.

Mangiafico S, Di Benedetto H, Sauzéat C, Olard F, Dupriet S, Planque L and Van Rooijen R (2012) Effect of reclaimed asphalt pavement on complex modulus and fatigue resistance of bitumens and asphalts. Proc 5th Euroasph Eurobitum Congr, Instabul.

Mangiafico S, Di Benedetto H, Sauzéat C, Olard F, Pouget S and Planque L (2013). Influence of reclaimed asphalt pavement content on complex modulus of asphalt binder blends and corresponding mixes: experimental results and modelling. Road Mat Pavement Des 14 (1):132-148. doi: 10.1080/14680629.2013.774751

Marasteanu M, Velasquez R, Zofka A and Cannone Falchetto A (2009). Development of a simple test to determine the low temperature creep compliance of asphalt mixture. IDEA Program Final Report NCHRP 133.

McDaniel RS. and Anderson RM (2002) Recommended use of reclaimed asphalt pavement in the superpave mix design method: technician's manual. NCHRP Report 452, Natl Coop Highw Res Progr.

McGraw J, Johnson E, Johnson G, Dai S, Linell D and Watson M (2010). Incorporation of recycled asphalt shingles in hot-mixed asphalt pavement mixtures. Final Report MN/RC 2010-08, Minnesota Department of Transportation.

Minnesota Department of Transportation, MnDOT (2008) Combined 2350/2360 plant mixed asphalt pavement, standard specifications for construction.

Moon KH, Cannone Falchetto A and Marasteanu MO (2013) Rheological modelling of asphalt materials properties at low temperatures: from time domain to frequency domain. Road Mat Pavement Des 14(4):810-830. doi: 10.1080/14680629.2013.817351

Newcomb DE, Stroup-Gardiner M, Weikle B and Drescher A (1993) Influence of roofing shingles on asphalt concrete mixture properties. Final Report, MN/RC-93-09, Minnesota Department of Transportation (MN/DOT), St. Paul, MN.

Rasmussen R (2012) From roof to road - Innovative recycling of bitumen felt roofing material. Final report LIFE07 ENV/DK/000102, Denmark.

Sharpe WN (2008) Springer handbook of experimental solid mechanics. Sharpe Editions, New York.

Tapsoba N, Sauzéat C, Di Benedetto H, Baaj H and Ech M (2014) Behaviour of asphalt mixtures containing reclaimed asphalt pavement and asphalt shingle. Road Mat Pavement Des 15(2): 330-347. doi:10.1080/14680629.2013.871091

# The Effect of Curing on the Mechanical Behavior of Cement-Bitumen Treated Materials

**Carlotta Godenzoni, Fabrizio Cardone, Andrea Graziani and Maurizio Bocci**

**Abstract** The re-use of pavement materials is an efficient and cost-effective solution in road rehabilitation and construction activities, especially when the availability of high-quality virgin aggregates is limited. In this context, cold recycling of bituminous pavements is becoming one the of most attractive and low environmental impact techniques. The use of cold-recycled pavement mixtures requires a careful assessment of their mechanical properties, which are influenced by both compositional and environmental factors. In particular, regardless of aggregate nature, binder type and dosage, a distinctive feature of cold recycled mixtures is the requirement for a certain curing period to develop the ultimate values of strength and stiffness. In this study, the mechanical behaviour of cement-bitumen treated materials (CBTM), containing high percentage of reclaimed asphalt (RA), was evaluated considering the influence of curing time and temperature. Two CBTM containing 1.0 and 2.5 % cement and 2.0 % of fresh bituminous binder were analyzed. Cylindrical specimens were compacted using a gyratory compactor and cured at 25 and 40 °C; moisture loss and indirect tensile strength (ITS) were measured at increasing curing times. Results showed that the curing temperature and time (curing conditions) significantly affect the moisture loss by evaporation that therefore can be considered a good estimator of the curing process. Moreover, the mechanical characterization indicated that the moisture loss and the cement content control the increase in strength properties of the investigated CBTM. Results also showed that the cement content strongly affects the moisture loss in addition to assure improved mechanical behavior.

C. Godenzoni (✉) · F. Cardone · A. Graziani · M. Bocci
Dipartimento di Ingegneria Civile Edile e Architettura, Università Politecnica delle Marche, via Brecce Bianche, 60131 Ancona, Italy
e-mail: c.godenzoni@pm.univpm.it

F. Cardone
e-mail: f.cardone@univpm.it

A. Graziani
e-mail: a.graziani@univpm.it

M. Bocci
e-mail: m.bocci@univpm.it



F. Canestrari and M.N. Partl (eds.), *8th RILEM International Symposium on Testing and Characterization of Sustainable and Innovative Bituminous Materials*, RILEM Bookseries 11, DOI 10.1007/978-94-017-7342-3_70

**Keywords** Cold recycling · Curing · Cement-bitumen treated materials · Indirect tensile strength

## 1 Introduction

In cold in-place recycling (CIR), the use of bituminous emulsion and cement as stabilizing agents to obtain recycled mixtures that guarantees suitable structural and durability properties is mostly used in current practice (Bocci et al. 2012; Santagata et al. 2009; Stroup-Gardiner 2011). Cold recycled mixtures (CRMs) show a mechanical behaviour strongly dependent on the properties and proportions in which binders are mixed. In particular, when the cement content is higher than 1 %, the mixtures are referred to cement-bitumen treated materials (CBTMs). In general, the addition of cement increases strength and stiffness as well as permanent deformation resistance (Du 2014; Grilli et al. 2012). Whereas, the presence of bitumen amongst the recycled aggregate affects cohesion, durability and fatigue cracking resistance and reduced moisture sensitivity of the mixture as well (Bocci et al. 2011). In addition, the visco-elastic behavior and temperature dependency of the bituminous binder confers to CBTM asphalt-like properties (Cardone et al. 2014; Grilli et al. 2012).

The curing process is a distinctive characteristic of the CBTM. Indeed, these materials require a certain curing period to develop the ultimate mechanical properties (strength and stiffness). In other words, curing can be defined as that process that controls the rate of strength and stiffness gain in the mixture over time.

Basically, the curing process of CBTM can be explained through the combination of three phenomena that occur within the recycled mixture: emulsion breaking, moisture loss and hydration of cementitious compounds (Cardone et al. 2014; Garcia et al. 2013; Kim et al. 2011). In particular, emulsion breaking takes place in the early phases (i.e. after mixing and compaction), whereas moisture loss and cement hydration continue over time. Several research studies (Cardone et al. 2014; Garcia et al. 2013; Kim et al. 2011) highlighted that while the curing process of bituminous emulsion is strictly related to moisture loss, the hydration of cement requires the presence of water.

Both moisture loss and cement hydration depend on many factors including mix composition (type and content of binders), construction features (degree of compaction, layer thickness, drainage condition, construction phase) and environmental condition (air temperature, humidity, and wind).

Therefore, a thorough understanding of the curing process of CBTM requires to define a standardized laboratory procedure that allows to control and measure the current curing mechanisms. This to evaluate the prevailing mechanism and/or possible interaction between them under specific curing conditions and how they affect the mechanical response of materials.

The objective of this paper is to analyze the curing process of CBTM mixtures by monitoring the evolution of moisture loss by evaporation and strength of laboratory prepared specimens. In particular, the influence of cement content and curing temperature were considered.

## 2 Experimental Program

### *2.1 Materials*

The CBTM samples considered in this investigation were produced in the laboratory using reclaimed asphalt (RA), virgin aggregates (VA), bituminous emulsion, Portland cement and water.

The RA was sampled from a stockpile in a recycling plant and characterized in terms of gradation (EN 933-2), particle density and absorption (EN 1097-6) and bitumen content (EN 12697-1). Results are summarized in Table 1. Before compaction, RA particles greater than 20 mm were preliminary removed to improve the homogeneity of the prepared samples.

The employed VA was a crushed limestone sand characterized by maximum dimension of 4 mm. Particle density and absorption are reported in Table 1.

Based on grading results, the RA was designated as 40RA 0/12 according to EN 13108-8, whereas the VA was designated as F 0/4 $G_F85$ (EN 13043). In addition, since for the aggregate blend design the RA was considered as "black rock", it was also designated as A 0/32 $G_A90$ with the procedure described for virgin aggregate (EN 13043).

A cationic slow-setting bituminous emulsion designed as C 60 B 6 (EN 13808) was selected in this research. This emulsion is specifically formulated for cold in-place recycling, guaranteeing high mixing stability with cement (over-stabilized emulsion) and good workability during compaction phase.

A Portland limestone cement type II/A-LL, strength class 32.5 R (EN 197-1) was used. Its composition is a combination of clinker (80–94 %) and limestone dust (20–6 %).

Two mixtures with different composition were analyzed in this study. For both mixtures, the aggregate blend was prepared by mixing 80 % RA and 20 % fine aggregate VA (Fig. 1). The gradation curve was obtained adding sand to the RA with the objective of correcting the fine fraction. As it can be observed, in the lower

**Table 1** Designation and physical properties for granular materials

| Materials | Absorption (%) | Particle density ($Mg/m^3$) | Bitumen content[a] (%) |
|---|---|---|---|
| Reclaimed aggregate | 1.0 | 2.470 | 4.84 |
| Virgin aggregate | 0.9 | 2.712 | – |

[a]by weight of mixture

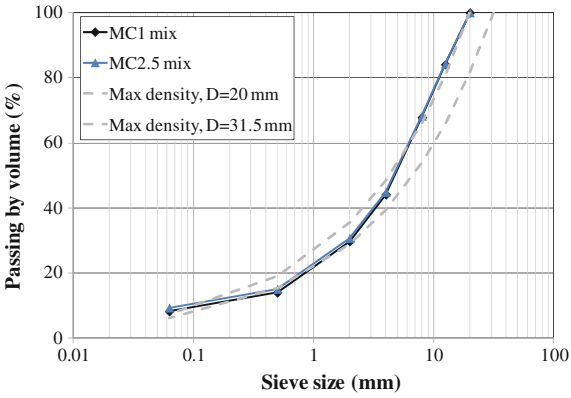


**Fig. 1** Gradation of tested mixtures (including cement)

part of the grading curve the aggregate gradation fits better the maximum density curve with D = 31.5 mm. The employed emulsion content was 3.3 % by dry aggregate weight, corresponding to 2 % of fresh bitumen. Two cement contents, 1 and 2.5 % by dry aggregate weight, were employed and the corresponding samples were coded as MC1 and MC2.5, respectively.

## *2.2 Mixing and Compaction*

In order to control the water content of the mixture, oven dried aggregates were used. The drying temperature was 105 ± 2 °C for VA and 40 ± 2 °C for RA. One batch of dried aggregate (4800 g), was used to prepare two specimens.

A total water content $w_{tot}$ = 5 % by dry aggregate weight was used for both MC1 and MC2.5. $w_{tot}$ is composed by the water from the emulsion ($w_{em}$) and additional water ($w_{add}$), which is added in two parts. The first part, related to the water absorption ($w_{add\_1} = w_{abs}$) of the constituent aggregates, was added to the dry aggregates blend the day before mixing. Then, the wet mixture (aggregate containing $w_{add\_1}$) was stored in a sealed plastic bag for 12 h at room temperature in order to ensure a homogeneous moisture condition and to allow absorption by the aggregates. Subsequently, the aggregate blend was thoroughly mixed, gradually adding the remaining part of the mixing water ($w_{add\_2}$), cement and emulsion in sequence. Samples were mixed with a mechanical mixer at room temperature for at least two minutes, time required to guarantee a good particle coating.

Immediately after mixing, specimens were compacted by means of a shear gyratory compactor (SGC) according to a standardized procedure (Bocci et al. 2011; Cardone et al. 2014; Grilli et al. 2012). In particular, the adopted protocol provided a 150 mm diameter mould, a constant pressure of 600 kPa, a gyration speed of 30 rpm and an angle of inclination of 1.25°. For each specimen about 2800 g of loose mixture were compacted with 100 revolutions obtaining a specimen

height of about 70 mm, suitable for mechanical testing. After compaction, specimens were sufficiently stable to allow extrusion and were immediately weighted to check any material loss.

### 2.3 Curing Procedure

For each mixture, two series of 24 cylindrical specimens were prepared. Each series was further divided in two groups of 12 specimens that were cured separately, at 25 ± 2 °C and 40 ± 2 °C. A constant relative humidity of 70 ± 5 % was adopted; this value was considered a reasonable compromise to achieve curing of both the bituminous components (based on moisture loss) and the cementitious components (which require a moist environment). Specimens were not sealed during curing to guarantee free water evaporation.

### 2.4 Testing Methods

Moisture loss by evaporation was measured at different curing times, by weighting two replicate specimens at 1, 3, 7, 14, 28 and 100 days (before mechanical testing).

A mechanical testing machine was used for the assessment of the indirect tensile strength (ITS) of the cured specimens. The equipment applies a compression force along the two generatrices until the specimen reaches a splitting failure. The load is applied with constant rate of deformation of 50 ± 2 mm/min (EN 12697-23).

ITS tests were carried out at 20 °C, therefore specimens cured at both 25 and 40 °C were conditioned for 4 h at 20 °C before testing. The testing program is summarized in Table 2.

## 3 Results and Analysis

### 3.1 Mixtures Volumetric Analysis

The weight loss which occurs during compaction is summarized in Fig. 2a in terms of frequency distribution, partial and cumulative. As it can be observed (Fig. 2a) the

**Table 2** Testing program summary

| | Moisture loss | ITS |
|---|---|---|
| Mixture code | MC1, MC2.5 | MC1, MC2.5 |
| Curing temperature (°C) | 25, 40 | 25, 40 |
| Curing time (days) | 1, 3, 7, 14, 28, 100 | 1, 3, 7, 14, 28, 100 |
| Testing temperature (°C) | 25, 40 | 20 |

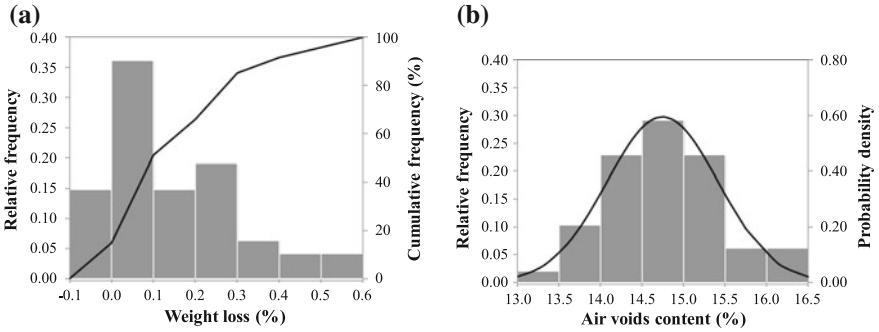


**Fig. 2** Relative frequency distribution of the measurements of weight loss (**a**) and air voids content $V_m$ (**b**)

relative frequency distribution is positively skewed and is characterized by a median value of 0.10 %. Visual observations, performed during specimen extrusion, suggested that such small loss of weight could be assumed to be exclusively a loss of water. Since the specimens are not completely saturated, the water loss can be assumed to occur only from the bottom or the top of the compacted specimens. On the basis of the previous considerations, the 85 % of the specimens had a water loss smaller than 0.3 %, hence their total water content, after compaction and before the curing phase, ranged between 5.0 % (the initial $w_{\text{tot}}$) and 4.7 %.

The compaction results were analyzed using a volumetric approach described in Grilli et al. (2012). In particular, the air voids content $V_{\text{m}}$ of the specimens was evaluated as:

$$V_m = \frac{\rho_m - \rho_d}{\rho_m} \cdot 100 \tag{1}$$

In Eq. 1, $\rho_m$ is the maximum density of the loose mixture, calculated considering aggregates, cement and bitumen (i.e. not including water), whereas $\rho_d$ is the dry density of the compacted mixture, i.e. the ratio of the total mass of solids to the total mixture volume (Grilli et al. 2012). In particular, the dry density $\rho_d$ was calculated considering the height data recorded during the SGC compaction.

The $V_m$ values at 100 gyrations, are summarized in Fig. 2b, in terms of frequency distribution histogram. As it can be observed, the distribution of the experimental results depicts a typical "bell-shaped" symmetrical trend, characterized by an average value of 14.7 % and standard deviation of 0.7 %.

In Fig. 2b, the continuous line, matching the histogram values, describes the normal distribution characterized by the previous parameters suggesting that the sample likely complies with the normal distribution. This means that the $V_m$ measurements were obtained under repeatability conditions. Since the standard deviation can be considered as an estimation of test repeatability, its low value (0.7 %) highlights the good repeatability achieved for specimen production.

Overall, the analysis of moisture loss and air voids allowed the reliability of the mixing and compaction procedure to be highlighted and therefore the adopted protocol for the production of a homogeneous specimens to be validated.

## 3.2 *Moisture Loss*

Moisture loss by evaporation (i.e. difference between the weight of specimen after compaction and the weight measured at the specific curing time), as function of curing time is shown in Fig. 3. For both mixtures (MC1 and MC 2.5) and curing temperatures (25 and 40°C), results of two replicate specimens and their average are reported.

For mixture MC1, moisture loss after one day curing was 3.0 and 1.8 % at 40 and 25 °C, respectively. This difference reduced at longer times until 100 days, when the same weight loss (4.4 %) was measured for both curing temperatures.

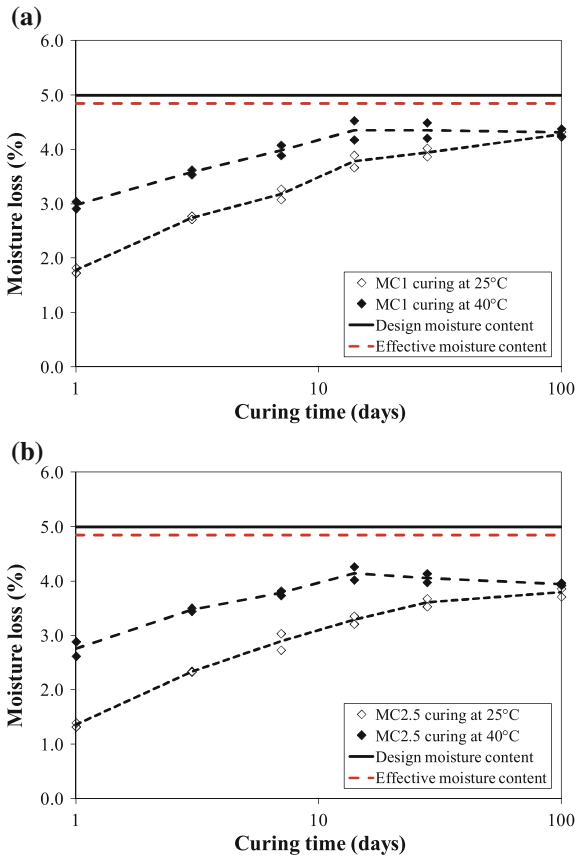


**Fig. 3** Moisture loss by evaporation for MC1 (**a**) and MC2.5 (**b**)

Analogously, for mixture MC2.5, the moisture loss after one day curing was 2.6 and 1.4 % at 40 and 25 °C, respectively. This difference reduced at longer times and at 100 days, the same weight loss (3.9 %), was measured for both curing temperatures. In addition, it can be observed that, at 40 °C, the moisture loss did not increase after 14 days anymore, whereas at 25 °C such an "equilibrium" condition was not obtained before 100 days.

Results showed that, for both mixtures, the curing temperature affected the rate of water evaporation but did not modify the water content measured after 100 days $w_{eq}$.

The value of $w_{eq}$ can be measured considering that the initial water content of the compacted specimens is comprised between 5.0 and 4.7 %. Thus, assuming an average initial value of 4.85 %, $w_{eq}$ = 0.55 % and $w_{eq}$ = 0.95 % were estimated for mixtures MC1 and MC2.5, respectively. Therefore, the moisture loss by evaporation decreased with increasing cement content. This evidence is consistent with the fact that cement reduced the evaporable water amount.

It should be considered that $w_{eq}$ contains the water required for the hydration of cement $w_{hydr}$ that is not available for evaporation. Part of $w_{hydr}$, about 23 % of cement weight, is required to form the calcium-silicate-hydrate (C-S-H) gel, whereas another part, about 19 % of cement weight, is absorbed by the nano-porosity of C-S-H gel and can be removed only at very low relative humidity (Mehta and Monteiro 1993). Hence, the amount of water needed for the hydration process can be calculated as:

$$W_{hydr} = (0.23 + 0.19) \cdot \alpha \cdot k \cdot C \tag{2}$$

where $\alpha$ is the degree of hydration of the cement paste, $C$ is the cement content within the mixture and $k$ is the fraction of Portland cement clinker in the cement.

Assuming $k$ = 0.87 (average of the clinker content range) and $\alpha$ = 0.95 at 100 days of curing (Mehta and Monteiro 1993) Eq. 2 yields $w_{hydr}$ = 0.33 % and $w_{hydr}$ = 0.82 % for mixtures MC1 and MC2.5, respectively.

The comparison between the $w_{eq}$ and $w_{hydr}$ showed that a small fraction of potentially evaporable water (= $w_{eq} - w_{hydr}$) is still contained inside the mixtures; in particular, 0.22 and 0.13 % for mixtures MC1 and MC2.5, respectively. This fraction of potentially evaporable water is probably trapped inside the surface porosity of the aggregate or inside the bituminous mortar (Garcia et al. 2013).

Since, for both mixtures $w_{eq} > w_{hydr}$, it can be hypothesized that moisture evaporation did not hinder the hydration process of cement.

## 3.3 Indirect Tensile Strength

ITS values, measured at different curing times, on the same specimens used to evaluate moisture loss, are shown in Fig. 4. For both mixtures (MC1 and MC 2.5)

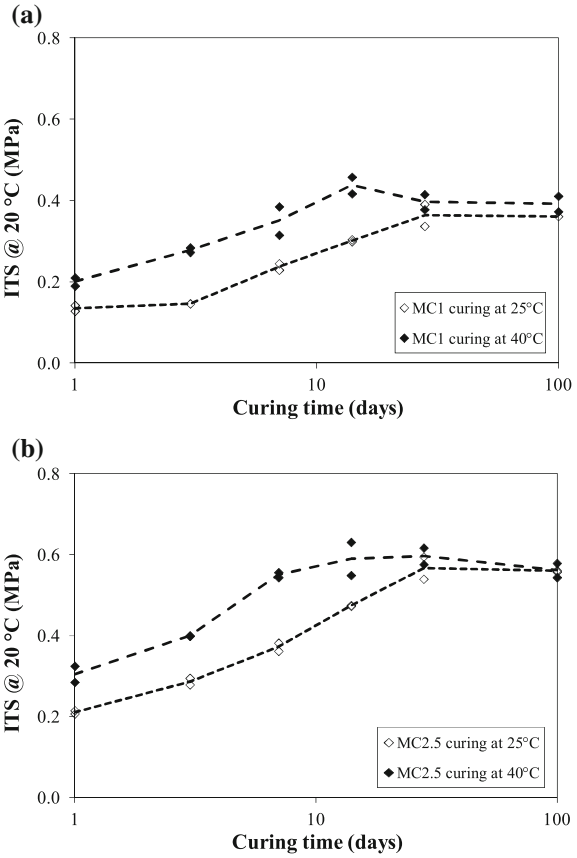


**Fig. 4** Evolution of ITS at 20 °C with curing time for MC1 (**a**) and MC2.5 (**b**)

and for curing temperatures (25 and 40 °C) results of two replicate specimens and their average are reported.

For mixture MC1, ITS after one day curing was 0.20 and 0.14 MPa at 40 and 25 °C, respectively. This difference reduced with increasing curing time, until 100 days, when about the same ITS value was obtained (0.38 MPa). A similar trend was observed for mixture MC2.5 which, after one day curing, showed ITS values of 0.31 and 0.21 MPa at 40 and 25 °C, respectively. Then, after 100 days the same ITS value was measured (0.56 MPa).

As it can be observed, for both mixtures ITS increased with increasing curing time, regardless of the curing temperature, and approached a constant value at longer curing periods (i.e. 100 days). As expected, mixture MC2.5 showed higher ITS values as compared to MC1, highlighting the strengthening contribution of hydrated cement. Specimens cured at 40 °C showed the maximum strength after 7–10 days and then a slight decrease, whereas specimens cured at 25 °C required at least 28 days to yield a similar performance. This suggests that higher curing

temperature resulted in higher rate of ITS increase, without penalizing the final mechanical performance.

The ITS increase with curing time can be explained by three phenomena: emulsion breaking, moisture loss by evaporation and cement hydration. While emulsion breaking occurs at early ages evaporation and hydration develop over time. In addition, comparing Figs. 3 and 4, similar trends are observed for moisture loss and ITS suggesting the existence of a causal relationship between them. Therefore, ITS values were plotted versus moisture loss for mixtures MC1 and MC2.5 in Fig. 5.

For MC2.5 the moisture loss showed similar effects on the ITS development, but a different trend was observed for different curing temperatures. In particular, at a specific amount of moisture loss, specimens cured at 25 °C showed slightly higher ITS with respect to the specimens cured at 40 °C. This can be explained by the fact that specimens cured at 25 °C required more curing time to achieve the same moisture loss and, during this time, the cement hydration contributed to the ITS increase. Therefore, these results confirm that for the mixture containing 2.5 %

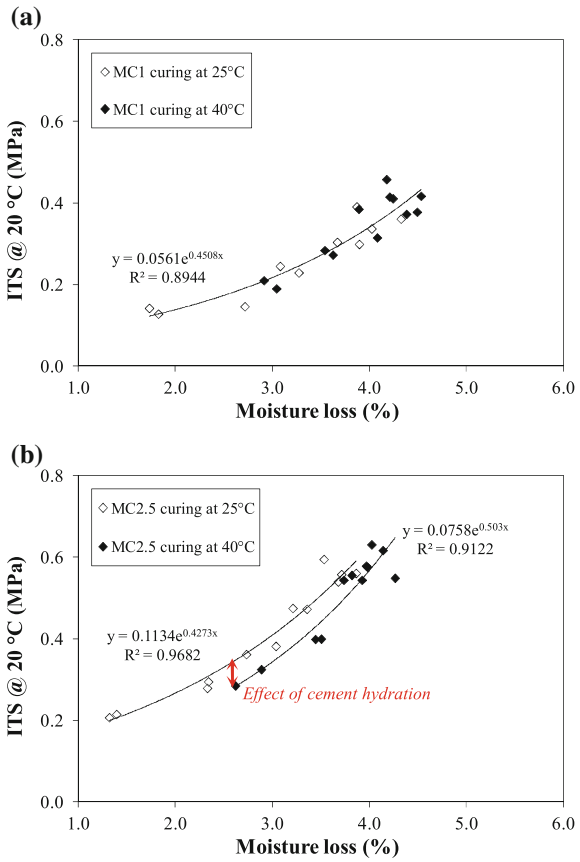


**Fig. 5** Relationship between ITS and moisture loss for MC1 (**a**) and MC2.5 (**b**)

cement, the curing level measured by ITS resulted from the combined effect of both moisture loss by evaporation and cement hydration.

On the other hand, for mixture MC1, the increase of ITS with increasing moisture loss appears to be not dependent on curing temperature. This highlights that the curing level, as measured by ITS, is controlled only by the amount of moisture loss by evaporation, whereas the temperature controls the curing rate. In addition, this suggests that for the mixture containing 1 % of cement, hydration had a negligible effect on curing process.

## 4 Conclusion

The present paper reports an experimental study concerning the analysis of the curing process of two cold recycled mixtures containing 1 and 2.5 % of cement (MC1 and MC2.5). The evolution of moisture and ITS were measured at two curing temperatures (25 and 40 °C).

All the tested specimens were prepared using a standardized mixing and compaction procedure, based on SGC. The air voids distribution of the compacted specimens was characterized by a standard deviation of 0.7 %. In addition 85 % of the specimens had a moisture loss smaller than 0.3 % during the compaction.

Results showed that the curing temperature affected the rate of water evaporation but did not modify the final water content $w_{eq}$ (i.e. after 100 days of curing). For both mixtures $w_{eq}$ exceeded the water required for the hydration of cement $w_{hydr}$ (water not available for evaporation) and therefore it can be hypothesized that moisture loss by evaporation did not hinder the hydration process of cement. For both mixtures ITS increased with increasing curing time, regardless of the curing temperature, and approached a constant value at longer curing periods (i.e. 100 days). For mixture MC1, the ITS increase with increasing moisture loss appears to be not dependent on curing temperature. This highlights that the curing level, as measured by ITS, is controlled only by the amount of moisture loss by evaporation. For MC2.5 the moisture loss showed similar effects on the ITS development, but a different trend, related to the curing temperature, was observed. This highlights that, for the mixture containing 2.5 % cement, the curing level measured by ITS, resulted from the combined effect of both moisture loss by evaporation and cement hydration.

## References

Bocci M, Grilli A, Cardone F, Graziani A (2011) A study on the mechanical behaviour of cement-bitumen treated materials. Constr Build Mater 25 (2) 773-778.

Bocci M, Grilli A, Cardone F, Ferrotti G (2012) Full Depth Reclamation for the Rehabilitation of Local Roads: a Case Study. Int J Pavement Eng 15(3):191-201.

Cardone F, Grilli A, Bocci M, Graziani A (2014) Curing and temperature sensitivity of cement–bitumen treated materials. Int J Pavement Eng. doi:10.1080/10298436.2014.966710.

Du S (2014) Interaction mechanism of cement and asphalt emulsion in asphalt emulsion mixtures. Mater Struct 47: 1149-1159. doi:10.1617/s1 1527-013-0118-1.

Garcia A, Lura P, Partl MN, Jerjen I (2013) Influence of cement content and environmental humidity on asphalt emulsion and cement composites performance. Mater Struct 46:1276-1285. doi:10.1617/s11527-012-9971-6

Grilli A, Graziani A, Bocci M (2012) Compactability and Thermal Sensitivity of Cement-Bitumen Treated Materials. Road Mater Pavement 13(4): 599-617.

Kim Y, Im S, Lee HD (2011) Impacts of Curing Time and Moisture Content on Engineering Properties of Cold In-Place Recycling Mixtures Usign Foamed or Emulsified Asphalt. J Mater Civ Eng 23(5): 542–553. doi: 10.1061/(ASCE)MT.1943-5533.0000209.

Mehta PK, Monteiro PJM (1993) Concrete: Structure, Properties, and Materials (2nd Ed). Prentice-Hall, Englewood Cliffs, NJ, USA.

Santagata FA, Bocci M, Grilli A, Cardone F (2009) Rehabilitation of an Italian Highway by Cold In-Place Recycling Techniques. Paper presented at the 7th International RILEM Symposium on Advanced Testing and Characterization of Bituminous Materials, Rhodes, Greece, 27-29 May 2009.

Stroup-Gardiner M (2011) NCHRP Synthesis 421: Recycling and Reclamation of Asphalt Pavements Using In-Place Methods. The National Academies Press, Washington DC, USA.

# Blending Simulation of RA and Virgin Binders in Hot Recycled Mixtures

**Mohamad Mohajeri, André A.A. Molenaar and Martin F.C. van de Ven**

**Abstract** In this paper the results of a model study are reported in which glass beads covered with artificially aged bitumen are mixed with superheated bold beads and virgin bitumen. The goal of the study was to simulate how aged binder and added virgin binder would distribute over RAP and virgin aggregates. Furthermore the goal of the study was to determine whether high preheating temperatures would affect the rheological properties of the binder covering the RAP and virgin aggregates. The study showed that when preheating temperature was 300 or 400 °C, the shear modulus of the binder recovered from the super-heated bold particles was about the same as the $G^*$ of the binder that was recovered from the particles that were covered with aged binder before mixing. At 300 °C the log pen rule seemed to be applicable which was not the case when the preheating temperature was 400 °C.

**Keywords** Artificially aged bitumen · Super-heated aggregate · Glass beads

## 1 Introduction

In the Netherlands, hot mix asphalt containing high percentages of reclaimed asphalt (RA) are being produced by either a batch plant to which a parallel drum is attached to preheat the RA to approximately 130 °C, or by means of a double barrel drum. In the double barrel drum virgin aggregates are preheated in the inner drum and then mixed with moist RA at ambient temperature in an outer drum which is folded around the inner drum. In the outer drum also the virgin fines (filler) and

M. Mohajeri · A.A.A. Molenaar (✉) · M.F.C. van de Ven
Delft University of Technology, Delft, South Holland, Netherlands
e-mail: a.a.a.molenaar@tudelft.nl

M. Mohajeri
e-mail: mohajeri_me@yahoo.com

M.F.C. van de Ven
e-mail: m.f.c.vandeven@tudelft.nl



F. Canestrari and M.N. Partl (eds.), *8th RILEM International Symposium on Testing and Characterization of Sustainable and Innovative Bituminous Materials*, RILEM Bookseries 11, DOI 10.1007/978-94-017-7342-3_71

bitumen are added. Since the mixing temperature is between 160 and 180 °C, the virgin aggregates have to be preheated to (very) high temperatures especially when high RA percentages are used. In the Netherlands using 50 % in RA is common practice for all base, binder and wearing course mixtures. The only exceptions are that RA is not allowed in SMA and porous asphalt concrete mixtures are only allowed to have an RA percentage of 25 %.

It is not uncommon to preheat the virgin aggregates to 320 °C and higher in the double drum mixer to obtain a mixing temperature of 160 °C. Especially when the RA is moist, moisture contents of 5 % are not uncommon, even higher preheating temperatures are required.

Also in a batch plant, the virgin aggregates are heated to fairly high temperatures even when the RA is preheated in a parallel drum to 130 °C. The virgin aggregates should be heated to higher temperatures when larger amounts of RA are used.

It might very well be that the heat transfer between superheated aggregates and binders may locally damage both the RA binder and virgin bitumen. Therefore it is essential to study the effect of this kind of harsh heat transfer on the binder properties. Doing this on real mixtures produced by real plants is a huge task and for an initial study, a model approach is more appropriate. It was therefore decided to use glass beads to replace real aggregates and artificially aged binder to replace the RA binder.

## 2 Research Approach

In the laboratory investigation that was set-up in which glass beads were used to represent the aggregates (Mohajeri 2015). Part of the glass beads was covered with aged bitumen and part of the glass beads represented the virgin aggregates.

Glass beads instead of normal aggregate were used because the major difficulty in studying the interaction between RA binder and virgin bitumen is the separation of RA aggregates from VA in the recycled mixture inasmuch as each aggregate particle is coated with black binder and the shape of the RA and VA particles is similar.

Since distinction by color differences between aggregates was not applicable, a novel method was devised in this research by using mono-size glass beads (GB) as artificial aggregates instead of real aggregates. RA could then be separated from VA because of different shapes and sizes. Furthermore the use of mono-sized beads allowed to calculate precisely the available surface area of the beads.

Two mixture combinations were designed to study the effect of superheating in HMA recycling by replacing real stone aggregates by glass beads. They will be explained in detail in one of the next sections.

The Rotating Cylinder Aging Test (RCAT) was used to create an artificial aged binder. Firstly two grades of bitumen were aged using different aging periods. Secondly, their chemical and physical properties were determined. The properties of the aged binder were compared with those of real RA binder. Then a decision was made on choosing the aging protocol.

Once artificial RA aggregates were separated from virgin aggregates, their binders were extracted for further analysis.

## 3 Materials

In this study two mixtures were tested which were composed of artificially aged binder and glass beads. Details of the aged binder and the glass beads are presented in this section.

### *3.1 Artificially Aged Binder*

The Rotating Cylinder Aging Test as developed by the Belgian Road Research Center was used to produce aged binder. Details of the test device as well as of the testing procedures can be found in (Verhasselt and Choquet 1997; Verhasselt 2002). Normally oxygen is used but since the RCAT oven that was available was not equipped with oxygen supply, air was used in the process at a flow rate of 4.5 l/h. The short term aging (STA) and long term aging (LTA) was done together using one temperature (163 °C) for a total duration of 24 h. The development of aging was monitored by taking samples at 0, 4, 8 and 24 h. These samples were used for penetration, $T_{R\&b}$, FTIR and DSR tests to study the progress of aging during the RCAT test. The results were compared with those obtained on a real RA binder which was taken as a reference. In this paper only the results of the penetration, $T_{R\&B}$ and DSR tests will be reported.

Two grades of bitumen were used in this study being a Q8 70/100 and a Q8 40/60.

### *3.2 Rheological Evaluation of Aged Binders*

As mentioned earlier, penetration and softening point tests were carried out to determine the change of these physical parameters as a function of aging time. The results are shown in Fig. 1.

A dynamic shear rheometer (AR2000ex) was used in the research to measure the complex shear modulus (G*) and the phase angle (δ) between shear stress and shear strain.The machine has a torque capacity of 0.2 Nm and is equipped with an environmental test chamber. G* and δ values are measured at different temperatures and loading frequencies. The results were used to create master curves of the shear modulus (G*) and phase angle (δ).

The master curves of the aged 70/100 pen binder along with the virgin bitumen are illustrated in Fig. 2. From the DSR measurement results it was concluded that

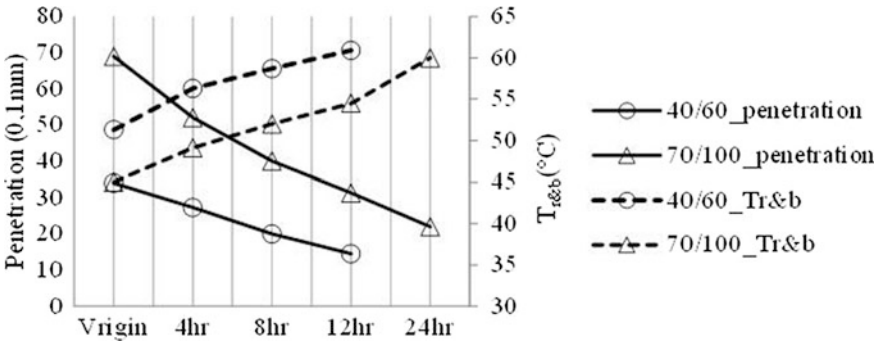


**Fig. 1** Change in penetration and softening point in relation to the nr of hours of RCAT aging

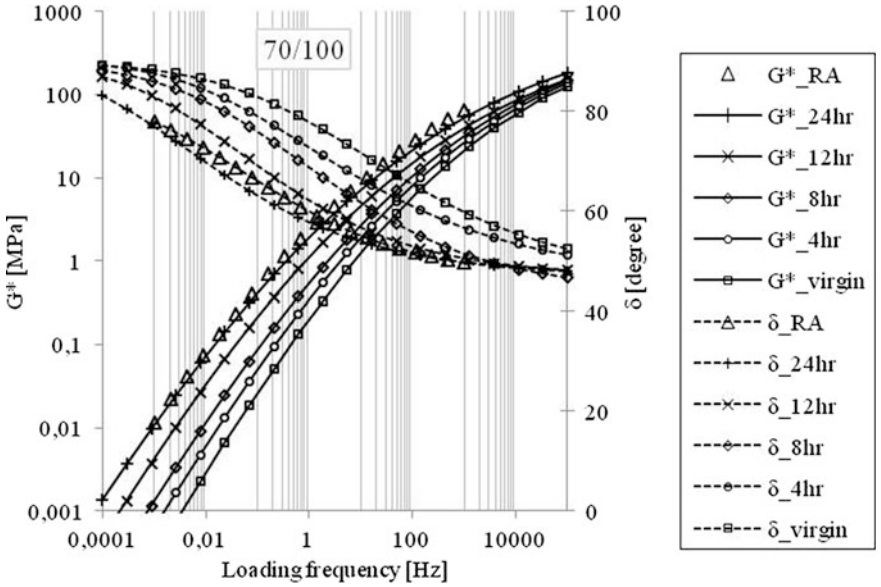


**Fig. 2** $G^*$ and δ master curves of the virgin 70/10 and 70/100 pen bitumen aged for several hours using the RCAT at 25 °C

RCAT aging of 70/100 bitumen at 163 °C and 24 h produces a binder that is closest to the real RA binder.

## *3.3 Glass Beads*

Glass beads are widely used in industry and research. They are available in different sizes and even in micro scales and their sizes are very precise.

As mentioned before, the regular size and shape of GBs was the reason for using them in this study. However the smooth surface of GBs is a critical drawback in comparison with the natural, usually rough, surface of normal aggregates.

In this research, glass beads of different sizes were used to simulate RA and VA.

Two available sizes of Borosilicate glass beads were used in mixture type 1 and 2 being 5 and 8 mm. The GBs used in this research contain primarily silica and boron oxide which is making them more resistant to thermal shocks than any other common glasses.

The volumetric properties of GB5 and GB8 are presented in Table 1. The volumetric properties are needed to determine the required amount of binder to achieve the intended film thickness. The weight of the particles of each size was calculated by dividing the weight of a number of beads by that number. It turns out that 22 g of bitumen is required to coat 1000 g of 5 mm beads with a film thickness of 40 µm.

The 40 µm film thickness was selected because this formed a stable bitumen coating around glass beads. This percentage was used later to prepare artificial RA with 5 mm beads and aged bitumen.

## 4 Mixtures

As mentioned before, two mixtures had to be prepared in the laboratory with artificial aggregates. The mixing procedure of each mix type is explained hereafter.

### *4.1 Mixture 1*

In the type 1 mixtures, GB5 had to be covered with 2 % (by weight) aged bitumen (RCAT163 °C_70/100@24 h) which was chosen during the preliminary aging tests which are discussed earlier. 2 kg of GB5 was premixed with 2 % aged binder at 150 °C to prepare the artificial RA. A Hobart pan mixer with a spiral dough hook was used to coat GB5 with aged binder within 3 min to ensure a homogenous coating. The pre-coated GB5 was cooled down with a fan while it was spread on silicone paper on a table. After cooling using the fan for 1 h, the mixture was stored for 3 h at room temperature (23 °C) and 24 h in a climate room (15 °C) to make it brittle enough to be broken into single particles by means of slight hammering. The separated particles were stored at −5 °C to avoid sticking together again.

**Table 1** Glass bead characteristics

| Glass bead | Specific density ($kg/mm^3$) | Diameter (mm) | Surface area ($mm^2$) | Volume ($mm^3$) | Mass (kg) * $10^{-4}$ | Nr. of particles in 1 kg | Total surface area in 1 kg ($mm^2$) |
|---|---|---|---|---|---|---|---|
| GB5 | 2.5 * $10^{-6}$ | 5 | 78.5 | 65.5 | 1.64 | 5634 | 4423 |
| GB8 | 2.5 * $10^{-6}$ | 8 | 201.1 | 268 | 6.7 | 1455 | 2923 |

Then 500 g of GB8 (as virgin aggregate) was preheated to 300 °C in an oven for 3 h. After this the pre-coated GB5 particles (500 g at 15 °C) were mixed in a pan mixer together with the GB8 particles for 30 s.

The heat exchange between the pre-heated bald G8 particles and the coated GB5 particles during mixing was measured by means of the infrared thermography method. The GB5 particles started to stick to each other as soon as they were added to the mixer, because of their pre-coating. For this reason manual agitation during 10 s by means of a steel spatula was done before mechanical mixing started; this improved mixing considerably. One similar mixture was prepared in which the GB8 was preheated to 400 °C. After mixing and cooling down, the particles of the mixture were also separated by means of slight hammering.

A special sieve was prepared with openings of 6 mm to separate the GB5 particles from GB8. A few small particles were still remaining on the sieve, and had to be separated manually.

In the next step the binders covering the GB5 and GB8 particles were recovered. Initially it was intended to extract binders in two stages but the GB's lost their binder as soon as they were soaked in the solvent. Two reasons caused the quick solving of the binders around the GB's being: lack of texture on the GB surface and the fact that pure bitumen (without filler) was used in the experiment.

Consequently only one stage extraction was applied on GB5 and GB8 for each mixture.

### *4.2 Mixture 2*

Mixture 2 was quite similar to mixture 1 in the sense of preheating temperature and mixing. The only two differences compared to mixture 1, were:

- GB5 is pre-coated with 1 % aged bitumen (where it was 2 % in mixture type 1)
- then the same weight of super-heated GB8 particles (VA) and 1 % virgin bitumen is added during 30 s of mixing time

Given the fact that both mix types contain 50 % GB5 and 50 % GB8, it turns out that the final binder content of all mixtures is 1 % by mass.

Other procedures such as preheating, storing, particle separation and binder extraction and recovery were similar to those used to prepare mixture 1.

## 5 Results

The extracted binders were used for rheological and chemical analyses. G* values were determined at different temperatures and frequencies by means of a Dynamic Shear Rheometer (DSR) using parallel plates with a diameter of 25 mm to create master curves.

It has to be noted once again that GB5 stands for glass bead (5 mm) which was prepared as an artificial aggregate by pre-coating it with aged binder. Artificial virgin aggregates are represented by GB8 which are superheated prior to mixing at temperatures of 300 and 400 °C. In mixture type1, GB5 was coated with 2 % aged bitumen. GB5 in mixture type 2 is pre-coated with 1 % aged bitumen and 1 % virgin bitumen which was being added during mixing. Comparison of the binder content on each group of aggregates (GB5 and GB8) will determine the amount of binder transfer from GB5 to GB8.

## 5.1 Mixture 1

Figure 3 shows that 0.8 % of GB5 binder was transferred to GB8. This implies that 1.2 % of the bitumen stayed at the GB5 particles. This can be explained in the following way. Mixture 1 contained, in terms of weight, the same amount of GB8 and GB5 particles. This implies that the total surface area of the GB5 particles was 1.6 times larger than the total surface area of the GB8 particles (see also Table 1). Given the fact that the GB5 particles, with their total surface area being 1.5 times that of the GB8 particles (see Table 1), were carrying 1.5 times more bitumen in total than the GB8 particles implies that per unit of surface area, the GB5 and GB8 particles carried the same amount of bitumen. This amount was similar at both superheating temperatures. It reveals that cold RA (GB5) could share to a large extent its binder with superheated aggregates at even short periods of mixing (30 s).

The comparison between the shear modulus of GB5 and GB8 binders (at 300 °C superheating temperature) shows no severe change or damage of the binder properties. However, superheating at 400 °C has increased the G* value of the GB5 binder as well as that of the GB8 binder. G* values of the original aged binder (being RCAT_70/100@24 h) are also shown in the charts as the property of the binder before mixing. Furthermore, the GB8 binder has become slightly stiffer than that of GB5. Direct exposure of the binder to superheated aggregates (400 °C) accounts for the difference between the binders coating GB5 and GB8.

## 5.2 Mixture 2

As it can be seen from Fig. 4, the GB8 particles are carrying the same amount of bitumen as the GB5 particles after being mixed with the GB5 particles carrying 1 % of bitumen and the 1 % added virgin bitumen. In contrary to what happened to mixture 1, the bitumen now seems NOT to be divided according to the surface area ratio of GB5 and GB8. It is however very difficult to say how much of the artificial aged binder on the GB5 particles was transferred to the

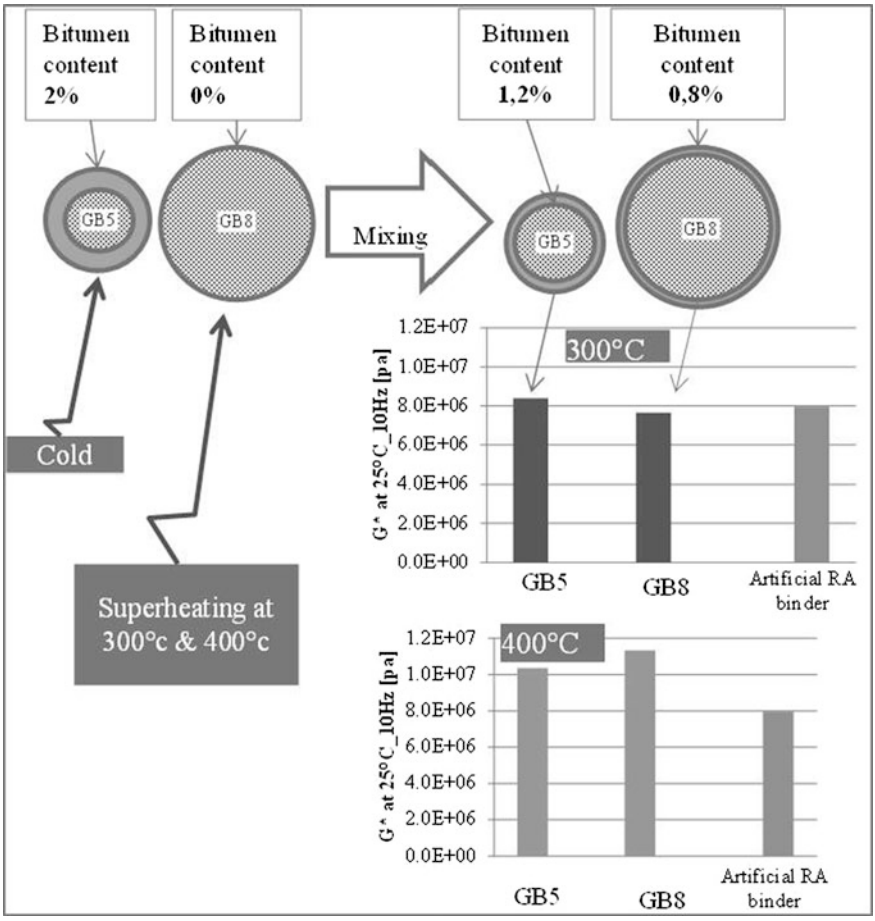


**Fig. 3** $G^*$ values of the binder recovered from the GB5 and GB8 glass beads in mixture 1

GB8 particles. Although the $G^*$ values determined on the bitumen coming from the GB8 particles is slightly higher than those determined on the bitumen coming from the GB5 particles, this does not tell anything about the composition of the binder coming from the GB5 and GB8 particles. The only conclusion that perhaps can be made is that the superheated GB8 particles had almost the same effect in terms of aging on the bitumen that finally coated both glass beads sizes.

In Fig. 4, the shear modulus of the binders extracted from GB5 and GB8 after mixing are compared with those of binders before mixing (virgin bitumen and artificial aged bitumen). At both preheating temperatures, the G* values of the GB5 and GB8 binder are between those of the original binders. It shows the effect of blending between the two binders. At 300 °C, the GB8 binder has become slightly

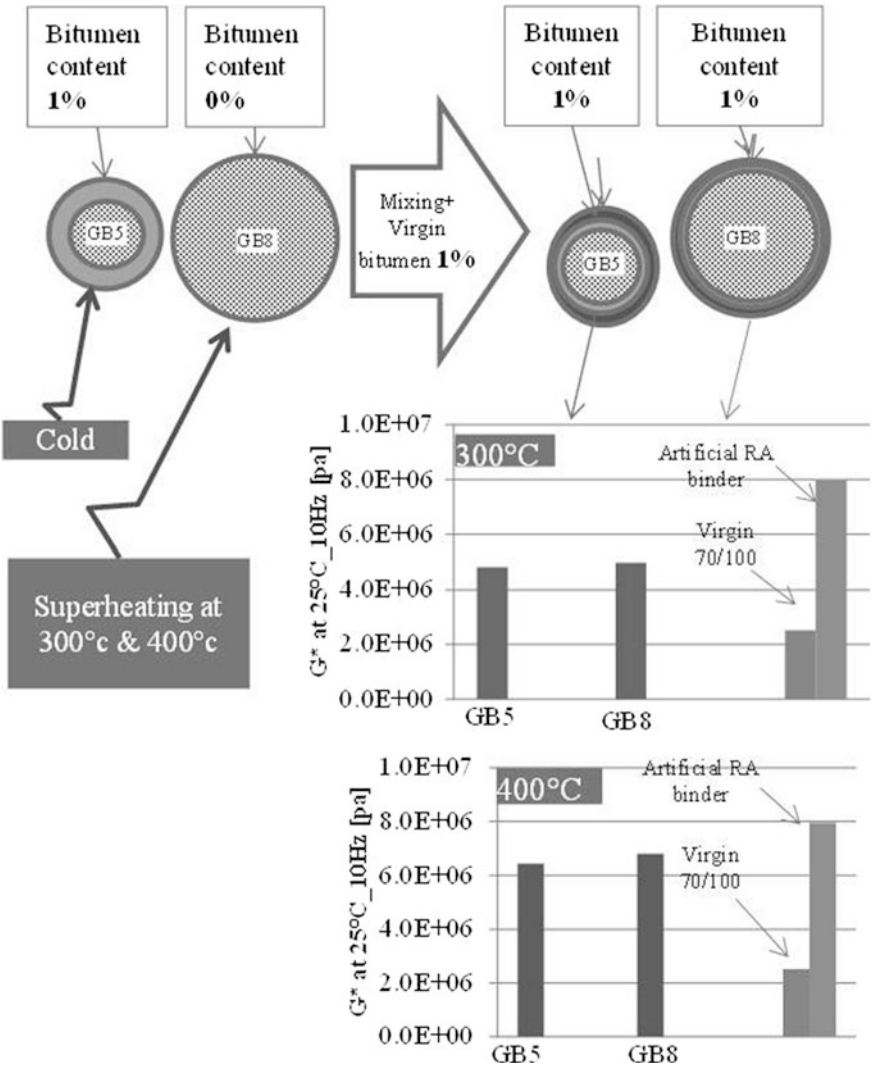


**Fig. 4** $G^*$ values of the binder recovered from the GB5 and GB8 glass beads in mixture 2

stiffer than the GB5 one, most probably because of the exposure to superheated particles. The same trend is observed in the other mixture where the superheating temperature was 400 °C.

Increasing the superheating temperature from 300 to 400 °C caused more aging on both the GB5 and GB8 binders.

The results allowed checking the validity of the log (pen) rule which is normally used to determine the grade of virgin bitumen to be used in recycling. The rule is:

$$A \log\left(pen_{virgin}\right) + B \log(pen_{RA}) = (A + B) \log(pen_{mixture}) \quad (1)$$

where A is the % of virgin bitumen, $pen_{virgin}$ is the penetration of the virgin bitumen added, B is the % of bitumen coming from the reclaimed asphalt, $pen_{RA}$ is the penetration of the bitumen of the reclaimed asphalt, $pen_{mixture}$ is the penetration of the bitumen of the completed mixture, A + B = 100.

Since there is a good relation between the pen and $G^*$ at 25 °C and 0.4 Hz, it is assumed that this rule is also applicable to determine the $G^*$ of the bitumen of the recycled mixture.

Since at 25 °C and 10 Hz, $G^*_{virgin}$ = 2.47 * $10^6$ Pa and $G^*_{aged}$ = 8 * $10^6$ Pa, one would expect the $G^*_{mixture}$ to be equal to 4.42 * $10^6$ Pa. The figure shows that in case of the 300 °C pre-heated aggregates, the $G^*$ of the bitumen coming from GB5 equals 4.82 * $10^6$ Pa and is 4.94 * $10^6$ Pa for the bitumen coming from the GB8 particles. In this case it looks like the log ($G^*$) rule seems to be valid. However it is clear that in case the virgin GB8 aggregate was pre-heated to 400 °C, the log ($G^*$) rule is not valid. The $G^*$ of the bitumen coming from both the GB5 and GB8 particles is much higher. Obviously additional aging due to the super-heated aggregates must have been occurred in this case.

Figure 5 is showing the $G^*$ values at 25 °C and 8 Hz for the bitumen recovered from the GB5 and GB8 glass beads of mixtures 1 and 2. The figure also shows the effect of super-heating the GB8 beads to 300 resp. 400 °C and of adding virgin bitumen (mixture 2).

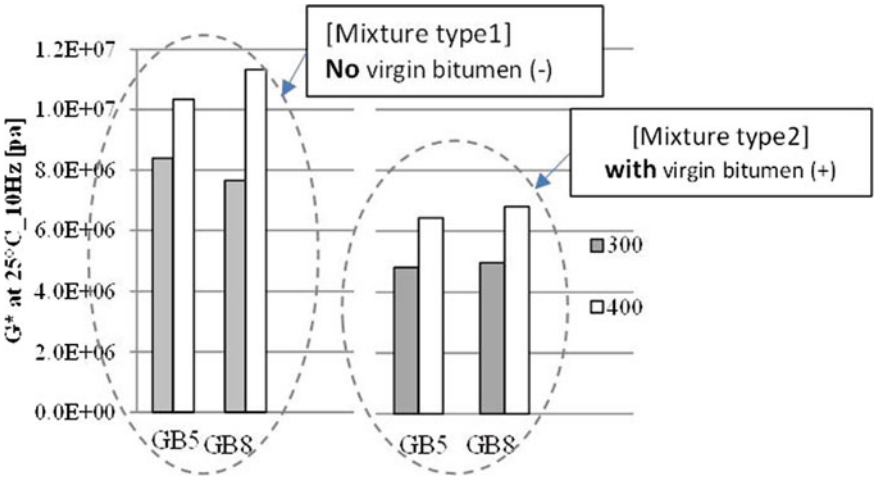


**Fig. 5** Summary and comparison of the DSR results obtained on the bitumen from the GB5 and GB8 glass beads as used in mixtures 1 and 2

## 6 Conclusions

Although it is true that the model experiments carried out are only a rude representation of what happens in practice, it is believed that they did give a good insight in what is happening when particles at ambient temperature and covered with a layer of aged bitumen are mixed with super-heated particles and virgin bitumen. From the experiments, the following is concluded:

- When mixing bitumen covered beads which are at ambient temperature with super-heated beads, then the bitumen is distributed over the glass beads according to the available surface area.
- When mixing superheated bald beads with bitumen covered beans which are at ambient temperature and virgin bitumen, the bitumen is not distributed according to the available surface area.
- When mixing superheated bald beads with bitumen covered beads which are at ambient temperature, then the log pen rule seems to be valid if the preheating temperature is 300 °C or lower. At higher temperatures the log pen rule seems to be not applicable anymore.
- The difference in $G^*$ values of the bitumen recovered from the initially super-heated beads and the beads that were covered with aged bitumen were small and seem to indicate that full blending occurred.
- From the above it seems reasonable to assume that additional aging will occur in practice when recycled mixtures are prepared using a double barrel drum when the virgin aggregates have to be preheated to very high temperatures.
- Furthermore it seems reasonable to assume that additional aging does not occur when RAP is preheated in a parallel drum to 130 °C and then mixed with virgin aggregates which are preheated to temperatures which stay below 300 °C.

## References

Mohajeri, M (2015) Hot Mix Asphalt Recycling, Practices and Principles. PhD Thesis Delft University of Technology, Delft 2015

Verhasselt, A.F., Choquet, F.S. (1997) Field Aging of Bituminous Binders: Simulation and Kinetic Approach. In: Proc. 5th RILEM Symposium om Mechanical Test Methods for Bituminous Materials, Lyon 1997

Verhasselt, A.F. (2002) Long Term Aging Simulation by RCAT Aging Test. In: Proc. 9th Int. Conf. on Asphalt Pavements, Copenhagen 2002

# Thermal and Water Effects on Virgin Bitumen, Recycled and Mastic Mixtures

**Salomé dos Santos, Lily D. Poulikakos and Manfred N. Partl**

**Abstract** Blending between aged bitumen from reclaimed asphalt pavement (RAP) and virgin bitumen is important in recycled asphalt. In this work, bitumen blends prepared by mixing virgin bitumen and recovered bitumen from RAP, were investigated as well as mastic mixtures prepared by mixing virgin bitumen with RAP. The aim of the study was to investigate the differences between virgin bitumen, bitumen blends containing different amounts of bitumen recovered from RAP, and mastic mixtures, in terms of surface microstructure, rheological properties and wetting behaviour. Thermal studies were carried out using different mixing times, annealing temperatures and cooling rates. The change in the molecular assembly was determined using attenuated total reflectance Fourier transform infrared spectroscopy; surface properties were evaluated using atomic force microscopy and the rheological properties were evaluated using dynamic shear rheometer. It was observed that the shear complex modulus and phase angle as well as the surface properties of the bitumen blends depended on the BitRAP content. The cooling rate of bitumen films influenced strongly the surface properties such as the roughness and size of the so-called "bee" structures as well as the molecular assembly. Additionally, contact angle measurements performed during dispensing of a water drop on the bitumen surface showed that in the presence of water, the viscoelastic bitumen films deformed at the three phase (bitumen-water-vapour) contact line and the deformation was influenced by the cooling rate of the bitumen films.

**Keywords** Thermal effects · Contact angle · RAP · Recycling

S. dos Santos (✉) · L.D. Poulikakos
EMPA—Swiss Federal Laboratories for Materials Science and Technology, Überlandstrasse 129, 8600 Dübendorf, Switzerland
e-mail: salome.dossantos@empa.ch

M.N. Partl
Road Engineering/Sealing Components, EMPA—Swiss Federal Laboratories for Materials Science and Technology, Überlandstrasse 129, 8600 Dübendorf, Switzerland



F. Canestrari and M.N. Partl (eds.), *8th RILEM International Symposium on Testing and Characterization of Sustainable and Innovative Bituminous Materials*, RILEM Bookseries 11, DOI 10.1007/978-94-017-7342-3_72

# 1 Introduction

The blending properties of the mixtures of virgin materials and reclaimed asphalt pavement (RAP) were the subject of several works where the combination of different measurement techniques was used, in an attempt to determine the blending state, and correlate rheological and chemical properties. Some of the relevant works are listed below. Using dynamic shear rheometer (DSR) and gel permeation chromatography (GPC) measurements, it was shown that mixing time and mixing temperature influenced the blending state (Bowers et al. 2014a). GPC and Fourier transform infrared (FTIR) spectroscopy measurements were combined to determine the blending state in different layers of the bitumen film around the RAP mineral aggregate (Bowers et al. 2014b); partial blending occurred in different layers, with the outermost layer being the softest and the innermost layer (closer to the mineral aggregate) the stiffest. Surface microstructural properties of the "blending zone" between virgin and bitumen recovered from RAP measured using atomic force microscopy (AFM), and DSR measurements were also combined in another study (Nahar et al. 2013); blended bitumen presented properties that fell in between those of the two individual bitumens (Nahar et al. 2013; Nazzal et al. 2013). The nature of blending was also investigated using a combination of DSR, electron microscopy and computer tomography (Rinaldini et al. 2014). Bitumen recovered from recycled AC mixtures (recycled bitumen) was also studied using attenuated total reflectance (ATR)-FTIR spectroscopy, DSR, differential scanning calorimetry (DSC) and AFM (dos Santos et al. 2014a); it was found that recycled bitumen showed properties e.g. degree of oxidation, rheological and thermal properties different from virgin bitumen and bitumen recovered from RAP (BitRAP) (dos Santos et al. 2014a; Poulikakos et al. 2014). Further studies are needed in order to understand the blending process between virgin bitumen and bitumen from RAP. Therefore, in the present work, rheological and microstructural properties of bitumen blends (virgin bitumen + BitRAP) and mastic mixtures (virgin bitumen + RAP) have been studied as a function of BitRAP and RAP content; the effect of mixing time, mixing temperature and cooling rate was investigated using DSR, ATR-FTIR, AFM and dynamic contact angle (CA) measurements.

# 2 Materials and Methods

## *2.1 Materials*

Standard virgin (V) bitumens referred to as V160/220 and V70/100 (penetration 160/220 and 70/100; softening point 39.8 and 46.8 °C, respectively) were used. BitRAP was recovered from RAP. RAP0.2 (RAP with fine particles smaller than 0.2 mm) was obtained by sieving RAP using a sieve with mesh size of 0.2 mm. Therefore, RAP0.2 contained (presumably aged) bitumen around the fine particles.

The amount of bitumen present in RAP0.2 sample was determined by calcination: Three RAP0.2 samples of ~5 g were first burnt under flame and thereafter placed in an oven at 650 °C for 3 h. Afterwards, the samples were removed from the oven and placed in the desiccator while cooling and before being weighed. The average organic content, which was assumed to be bitumen, was 9.89 %. Isothermal mass loss measurements (not shown), where V160/220 and BitRAP were heated at a constant temperature of 110 or 160 °C for 2 h under $O_2$, showed a mass loss of 0.11 % at 110 °C and 0.41 % at 160 °C for V160/220, and 0.52 % at 110 °C and 0.93 % at 160 °C for BitRAP. This loss of mass may be due to evaporation of water or other small molecular weight compounds. In the case of BitRAP which was recovered from RAP, water or other compounds resulting from aging and service life may be present.

## 2.2 Sample Preparation

Mastic samples were prepared by weight mixing RAP0.2 and virgin bitumen. The final mass was ~5 g. V160/220 or V70/100 and RAP0.2 were heated separately in the oven at the mixing temperature of 110 ± 2 °C or 160 ± 2 °C for 10 or 60 min. Thereafter, RAP0.2 was added to the bitumen and the mastic sample was stirred vigorously by hand for 1 min and placed back in the oven for another 10 min. Before removing the mastic sample from the oven it was stirred another minute as it cooled down. This preparation sequence was therefore designated as 10(60) + 1 + 10 + 1. Composition and preparation sequence of the mastic samples are presented in Table 1. The sample designation in Table 1 like 110_V160/220_60RAP0.2_40 corresponds to the mixture of 60 % V160/220 with 40 % RAP0.2 prepared at 110 °C.

The blends of virgin bitumen and BitRAP were prepared as follows. The bitumen blends were produced following the same preparation procedure used for the mastic. However, virgin bitumen and BitRAP were weighted in the same container, aiming at a final mass of ~5 g, and placed in the oven at the mixing temperature of 110 ± 2 or 160 ± 2 °C for 10 min. Composition and preparation sequence of bitumen blends are presented in Table 2. Sample designation like

**Table 1** Composition and preparation sequence of mastic samples containing RAP0.2

| Sample designation | Preparation sequence | Virgin/RAP0.2 (%w/w) | Bitumen from RAP (%)[a] |
|---|---|---|---|
| 110_V160/220_60RAP0.2_40 | 10 + 1 + 10 + 1 | 59.96/40.04 | 6.19 |
| 110_V160/220_60RAP0.2_40_**70** | 60 + 1 + 10 + 1 | 61.12/39.88 | 6.16 |
| 110_V160/220_20RAP0.2_80 | 10 + 1 + 10 + 1 | 20.15/79.85 | 28.15 |
| 110_V160/220_20RAP0.2_80_**70** | 60 + 1 + 10 + 1 | 19.98/80.02 | 28.37 |
| **160**_V160/220_60RAP0.2_40 | 10 + 1 + 10 + 1 | 60.04/39.96 | 6.18 |
| 110_**V70/100**_60RAP0.2_40 | 10 + 1 + 10 + 1 | 59.99/40.01 | 6.08 |

[a]Content of bitumen from RAP in the total bitumen content. n/a = not applicable

**Table 2** Composition and preparation of bitumen blends containing BitRAP

| Sample designation | Preparation sequence | Virgin/BitRAP (%w/w) |
|---|---|---|
| 110_V160/220_94BitRAP_6 | 10 + 1 + 10 + 1 | 94.01/5.99 |
| 110_V160/220_72BitRAP_28 | 10 + 1 + 10 + 1 | 71.99/28.01 |
| 110_V160/220_53BitRAP_47 | 10 + 1 + 10 + 1 | 53.02/46.98 |
| 110_V160/220_20BitRAP_80 | 10 + 1 + 10 + 1 | 20.02/79.98 |
| **160**_V160/220_53BitRAP_47 | 10 + 1 + 10 + 1 | 53.02/46.98 |
| 110_V70/100_50BitRAP_50 | 10 + 1 + 10 + 1 | 50.01/49.99 |

110_V160/220_94BitRAP_6 corresponds to the bitumen blend containing 94 % V160/220 with 6 % BitRAP prepared at 110 °C.

For dynamic shear rheometer (DSR) measurements, the samples were prepared according to the following procedure: ca. 0.25 g of bitumen blends were placed in silicone rubber molds of 8 mm diameter and 2 mm height and, subsequently, heated in a ventilated oven at 110 ± 2 °C for 20 min. After removal from the oven, the samples were left to cool down at ~23 °C and tested 24–72 h later.

For atomic force microscopy (AFM) measurements, approximately 1.5 or 8 mg of sample were spread with a spatula at ~23 °C by buttering action over a ca. 0.8 × 0.8 $cm^2$ area on a ca. 1 × 1 $cm^2$ glass slide and placed in the oven at the annealing temperature of 110 ± 2 °C for 20 or 70 min and 160 ± 2 °C for 20 or 70 min. The annealing temperature equal or above 110 °C was chosen because it is above the melting temperature of the crystalline material (e.g. wax crystallites) that can exist naturally in the bitumens investigated V160/220, V70/100 and BitRAP. Thereafter, bitumen and mastic films were either removed from the oven, covered to prevent dust deposition and allowed to cool down at room temperature (fast cooling rate—cr_fast) or left in the oven to cool down at the cooling rate of the oven after switching it off (slow cooling rate—cr_slow). The cr_fast was measured using a full colour infrared camera, 640 × 480 pixels, and the cr_slow was measured using a thermocouple placed inside the oven. The cooling rate profiles are shown in Fig. 1. After cooling, the films were conditioned at ~23 °C for less than 48 h prior to the measurements. The detail of the conditioning (annealing temperature and time, and cooling rate) of the samples, including the final film thickness calculated assuming the bitumen density equal to 1 g/$cm^3$ are presented in Table 3. Sample designation like V160/220_110_20_cr_fast corresponds to the V160/220 film prepared using the annealing temperature of 110 °C for 20 min and cr_fast.

For attenuated total reflectance Fourier transform infrared (ATR-FTIR) spectroscopy measurements, V70/100 sample was prepared in the same way as the samples used for AFM measurements. However, ca. 150 mg of V70/100 were spread using a spatula at ~23 °C by buttering action over a ca. 2 × 2 $cm^2$ area on a 2.5 × 2.5 $cm^2$ glass slide. In this case, the final film thickness was 350–400 μm.

For contact angle (CA) measurements, the films of V160/220 and V70/100 were prepared in the same way as the samples used for ATR-FTIR measurements; however, ca. 450 mg of bitumen were applied over a ca. 7 × 2 $cm^2$ area on a 7.5 × 2.5 $cm^2$ glass slide.

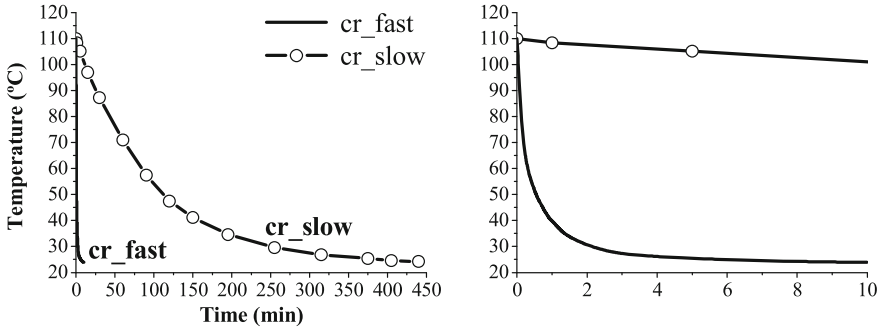


**Fig. 1** Profiles of the cooling rates cr_fast and cr_slow for V70/100 using annealing temperature of 110 °C. The plot on the *right* shows a close-up of the profiles for the first 10 min

**Table 3** Samples used for AFM measurements

| Sample designation | $T_{annealing}$ | Preparation | Thickness (μm)[a] |
|---|---|---|---|
| V160/220_110_20_cr_fast | 110 | 20 + cr_fast | 130 |
| V160/220_110_20_cr_slow | 110 | 20 + cr_slow | 128 |
| V160/220_**160**_20_cr_fast | 160 | 20 + cr_fast | 133 |
| V160/220_110_**70**_cr_fast | 110 | 70 + cr_fast | 133 |
| V160/220_110_20_cr_fast | 110 | 20 + cr_fast | **22** |
| V160/220_110_20_cr_slow | 110 | 20 + cr_slow | **22** |
| BitRAP_110_20_cr_fast | 110 | 20 + cr_fast | 133 |
| BitRAP_110_20_cr_slow | 110 | 20 + cr_slow | 134 |
| 110_V160/220_53**BitRAP**_47_cr_fast | 110 | 20 + cr_fast | 134 |
| 110_V160/220_53**BitRAP**_47_cr_slow | 110 | 20 + cr_slow | 134 |
| 110_V160/220_60RAP0.2_40_cr_fast | 110 | 20 + cr_fast | n/a |
| 110_V160/220_60RAP0.2_40_cr_slow | 110 | 20 + cr_slow | n/a |
| **160**_V160/220_60RAP0.2_40_cr_fast | 110 | 20 + cr_fast | n/a |
| **160**_V160/220_60RAP0.2_40_cr_slow | 110 | 20 + cr_slow | n/a |
| 110_V160/220_20RAP0.2_80_cr_fast | 110 | 20 + cr_fast | n/a |
| 110_V160/220_20RAP0.2_80_cr_slow | 110 | 20 + cr_slow | n/a |
| 110_V160/220_60RAP0.2_40_**70**_cr_slow | 110 | 70 + cr_slow | n/a |
| 110_V160/220_20RAP0.2_80_**70**_cr_fast | 110 | 70 + cr_fast | n/a |

[a]Calculated assuming bitumen density equal to 1 g/cm$^3$ the area 0.8 × 0.8 cm$^2$. n/a = not applicable

## *2.3 Methods*

DSR measurements were performed in a Physica MCR 301 rheometer from Anton Paar. The samples were measured within the linear viscoelastic regime at constant strain amplitude of 0.01 %, constant angular frequency of 10 rad/s (1.59 Hz) and 20 °C using 8 mm plate-plate geometry with a gap of 2 mm. The rheological

properties were collected at this temperature in accordance with other measurements that were also performed at 20 °C. The complex modulus ($|G^*|$) and phase angle (δ) were determined.

Surface characteristics were obtained using peak force tapping quantitative nanomechanical (PFT QNM) AFM measurements carried out at ~23 °C using a Bruker MultiMode 8 atomic force microscope, with a Nanoscope V controller and the software Nanoscope 8.15. Bruker TAP150A tips with the following properties: Material—0.01–0.025 Ω cm Antimony (n) doped Si coated with Al-coating on the detector side; tip height—15–20 μm; spring constant—5 N/m; resonance frequency—150 kHz;. The tip radius was calibrated and set as 20 nm. Every AFM image was built up by 256 × 256 pixels. The scan size 50 × 50 $\mu m^2$ was found to be suitable to show the overall characteristics of the surface. The scan rate was 0.5 Hz. Peak force frequency was 2 kHz and the peak force was 20 nN. The offline data analysis was performed using Bruker Nanoscope Analysis 1.40.

Molecular assembly properties were investigated using ATR-FTIR measurements performed at 23 °C in a Nicolet iS5 Fourier Transform Infrared Spectrometer in the ATR mode using a diamond crystal. The bitumen films were placed with the top surface against the diamond crystal. The spectra were collected in the 4000–600 $cm^{-1}$ range with a resolution of 4 $cm^{-1}$ and each final spectrum represented an accumulation of 32 spectra. The data were collected with the OMNIC software.

Dynamic CA measurements were performed using 40 μL-drops of water dispensed from a syringe placed very close to the bitumen surface with the dispensing rate of 0.2 μL/s. The measurements were performed at 20 °C and at relative humidity of 70 % and repeated at least three times on the same bitumen film. CA was measured using the Contact Angle System OCA20 from Data Physics with the Ellipse Fitting analysis.

## 3 Results and Discussion

The results from DSR measurements performed in the bitumen blends are presented in Fig. 2. $|G^*|$ increased non-linearly as the BitRAP content increased whereas δ decreased. In addition, the bitumen blend of 50 % BitRAP and 50 % V70/100 resulted in higher $|G^*|$ and lower δ as comparing to the corresponding blend with V160/220 because V70/100 alone was also characterized by larger $|G^*|$ and lower δ than V160/220. The blend 160_V160/220_53BitRAP_47 prepared at 160 °C did not present significant differences in $|G^*|$ and δ with respect to the blend prepared at 110 °C.

AFM results showed that the so-called “bee” structures located in the center of presumably wax crystallites (dos Santos et al. 2014b; Lyne et al. 2013), were present on the surface of all virgin bitumens, blended bitumens and mastic samples. Additionally, films prepared using cr_slow presented higher surface roughness than films prepared using cr_fast. This is shown in the images in Figs. 3 and 4. For the films prepared using cr_fast, blends containing high contents of BitRAP and mastic

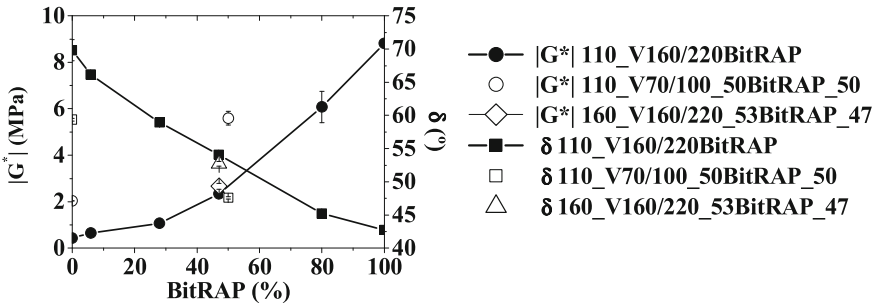


**Fig. 2** Complex modulus ($|G^*|$) and phase angle (δ) at 20 °C as a function of BitRAP content for mixtures prepared at 110 and 160 °C

samples containing high content of RAP0.2 presented smaller "bee" structures than the virgin bitumens (Fig. 4). Also, the "bee" structures were generally larger in the case of cr_slow for the same annealing temperature. If the "bee" structure is assumed to increase proportionally to the size of the wax crystallites, this observation implies that the cr_slow resulted in larger wax crystallites than cr_fast. The change in annealing temperature from 110 to 160 °C also changed the surface microstructure as seen for V160/220 (Fig. 3), resulting in larger "bee" structures at 160 °C. However, V160/220 films of smaller thickness (∼20 μm) showed no significant difference (or trend) when compared to those of thickness ∼130 μm. Despite the common effect regarding cr_slow, differences were generally found between the virgin films, BitRAP, bitumen blends and mastic samples. When using cr_slow, the roughness was larger (see z-scale in Figs. 3 and 4) for the virgin bitumens than for BitRAP, bitumen blends and mastic samples, as shown in Fig. 4. The mastic samples presented characteristics closer to the virgin bitumen as

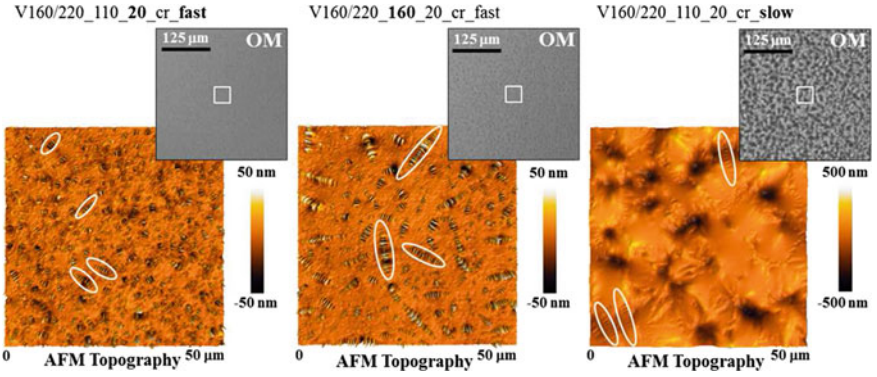


**Fig. 3** AFM topography images of the surface of V160/220_110_20_cr_fast, V160/220_160_20_cr_fast and V160/220_110_20_cr_slow. OM = optical microscopy images obtained with microscope placed above the head of the AFM instrument. The ellipses show examples of the "bee" structures. Scan area is 50 × 50 $\mu m^2$

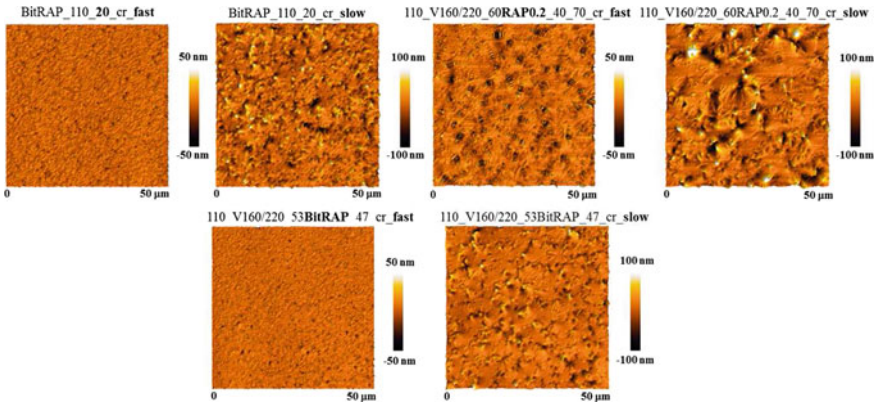


**Fig. 4** AFM topography images of the surface of different films. Scan area is 50 × 50 µm$^2$

compared with the blends for similar bitumen from RAP and BitRAP contents. This indicated that the blending between BitRAP and virgin bitumen was larger than the blending of bitumen from RAP and virgin bitumen. However, the mastic sample mixed at 160 °C, 160_V160/220_60RAP0.2_40 showed characteristics which became closer to 110_V160/220_53BitRAP_47 in terms of "bee" structure sizes and roughness. This may indicate that higher mixing temperature, 160 °C, produced better blending between the virgin bitumen and the bitumen from RAP0.2 as reported also by Bowers et al. (2014a). Regarding the mixing time, the samples prepared using 70 min of mixing, as did not show significant differences from those prepared using only 20 min.

To evaluate if the changes occurred for cr_slow observed using AFM were connected to changes in the molecular assembly, ATR-FTIR measurements were performed for V70/100. Figure 5 shows the ATR-FTIR spectrum for V70/100 film cooled using cr_fast and cr_slow. Typically, the bitumen infrared spectrum shows peaks at several wavenumbers as shown in Fig. 6a. Figure 6 displays also the changes in peaks happening at ~2920 (A), ~2850 (B), 1465–1455 (C), ~1375 (D) and 735–715 cm$^{-1}$ (E) due to the different cooling rate. An increase in absorbance for the peaks at ~2920, ~2850, ~730 and ~720 cm$^{-1}$ was observed for cr_slow as well as a clear shift in the position of the peaks as marked in A and B. Moreover, the peaks at ~1460 cm$^{-1}$ and at ~720 cm$^{-1}$ split into two clear peaks. Additionally, the distance between the peaks at 730 and 720 cm$^{-1}$ and between 1460 and 1455 cm$^{-1}$ increased. Splitting, shifting to lower wavenumbers and increasing of peak intensity are related to the increase of the crystallization degree (Borchman et al. 2011; Brubach et al. 2007; Heredia-Guerrero et al. 2012; Srivastava et al. 1993; Ungar and Masic 1985). The increase in intensity of the peak at ~720 cm$^{-1}$ is related to the increase of the amount of alkyl chains, not necessarily assembled in an organized way (e.g. hexagonal symmetry). These results showed that using cr_slow more time was available (at higher temperatures) to

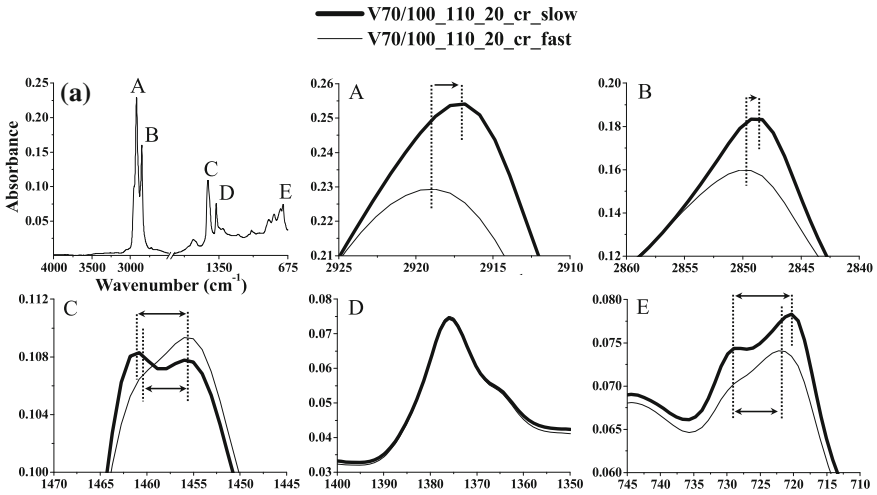


**Fig. 5** ATR-FTIR spectra for V70/100_110_20_cr_fast and cr_slow. **a** V70/100_110_20_cr_fast full spectrum. *A*, *B*, *C*, *D* and *E* show close-ups at ~2920, ~2850, 1460–1455, ~1375 and 730–720 $cm^{-1}$, respectively. The *dotted lines* and the *arrows* show shifts and splitting of the peaks

bring more long alkyl chain molecules (e.g. wax molecules) to the surface and for crystallization.

To evaluate if the changes in cooling rate produced changes in the wetting behaviour of the films, CA measurements were performed for V160/220 and V70/100 films prepared using 110 °C for 20 min. When the water drop was placed on the bitumen surface, the bitumen films deformed at the three phase bitumen-water-vapour contact line forming a ridge. As the water drop was dispensed, it stuck at the contact line and only after a variable time, depending on the film characteristics, slipped forward over a certain distance, where a new stick-slip event happened. This behaviour is commonly encountered for viscoelastic materials due to the action of the capillary pressure inside the drop and the perpendicular component of the water surface tension which pulls the material up (Carre et al. 1996). Figure 6 shows an example of this behaviour for bitumen V70/100 for cr_fast. As time increased, and thus also the volume of the water drop, the contact angle before each slip event (for instance $\theta_a$ in $Stick_5$) was larger than the previous ($\theta_a$ in $Stick_4$). Moreover, the contact angle after the slip event (for instance $\theta_a$ in $Slip_5$) was smaller than the previous ($\theta_a$ in $Slip_4$). In addition, it can be seen from the Fig. 6 that the time between the stick-slip events increased. In particular, the time between $Slip_4$ and $Stick_5$ was less than 2 s, while the time between $Slip_{11}$ and $Stick_{12}$ was close to 30 s. If, a slip frequency, $f_{slip}$, is defined as the number of slipping events that occurred for a fixed amount of time of 200 s and dispensing rate of 0.2 μL/s bitumen V160/220 showed the lowest $f_{slip}$ ($f_{slip}$cr_fast = 5.2 ± 1.2; $f_{slip}$cr_slow = 16.4 ± 1.6) as compared with bitumen V70/100 ($f_{slip}$cr_fast = 10 ± 2; $f_{slip}$cr_slow = 26.8 ± 2.8. Also, $f_{slip}$ was always lower for the same bitumen type

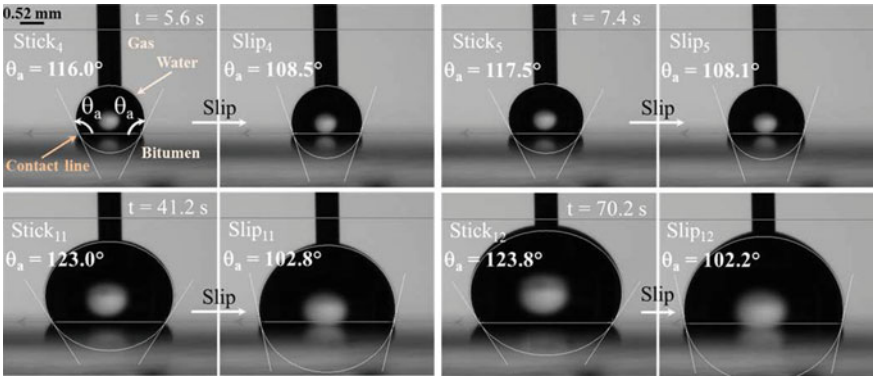


**Fig. 6** Wetting behaviour of V70/100_110_cr_fast during the dispensing of a 40 μL-water drop using the dispensing rate of 0.2 μL/s. $Stick_4$ and $Slip_4$ are the 4th stick and the 4th slip event, respectively; the stick event results in the maximum contact angle just before the slip event. $\theta_a$ is the advancing contact angle which is calculated from the average between the contact angle on the right and the left sides of the water drop

prepared using cr_slow. The differences observed between the wetting behaviour of the bitumen films may be consequence of their different rheological properties, surface roughness or chemical properties. Future studies will be performed to understand the wetting behaviour on the bitumen films.

## 4 Conclusions

A summary of the most relevant conclusions in this study follows.

- The rheological properties changed with the increase of BitRAP content in the bitumen blends probably due to the properties of BitRAP that increase the elastic response of the blend.
- Bitumen blends presented different surface properties compared to the mastics containing the same amount of bitumen indicating that the blending between bitumen from RAP and virgin bitumen followed a different mechanism.
- The cooling rate had strong influence on surface and molecular assembly properties, e.g. slow cooling resulted in larger "bee" structures and larger content of long alkyl chains at the surface.
- The wetting behaviour on the bitumen films was strongly dependent on the cooling rate.

**Acknowledgments** The authors thank the Swiss National Science Foundation (200021_140210/1 and 200020_152980/1) for financial support, Tina Künniger for helping with the CA measurements and Moises Bueno for helping with cooling rate measurements.

## References

Borchman D, Foulks GN, Yappert MC, Bell J, Wells E, Neravetla S, Greenstone V. 2011. Human Meibum Lipid Conformation and Thermodynamic Changes with Meibomian-Gland Dysfunction. Investigative Ophthalmology & Visual Science 52: 3805-3817.

Bowers BF, Moore J, Huang BS, Shu X. 2014a. Blending efficiency of Reclaimed Asphalt Pavement: An approach utilizing rheological properties and molecular weight distributions. Fuel 135: 63-68.

Bowers BF, Huang BS, Shu X, Miller BC. 2014b. Investigation of Reclaimed Asphalt Pavement blending efficiency through GPC and FTIR. Construction and Building Materials 50: 517-523.

Brubach JB, Jannin V, Mahler B, Bourgaux C, Lessieur P, Roy P, Ollivon M. 2007. Structural and thermal characterization of glyceryl behenate by X-ray diffraction coupled to differential calorimetry and infrared spectroscopy. International Journal of Pharmaceutics 336: 248-256.

Carre A, Gastel JC, Shanahan MER. 1996. Viscoelastic effects in the spreading of liquids. Nature 379: 432-434.

dos Santos S, Poulikakos LD, Partl MN. 2014a. From virgin to recycled bitumen: A microstructural view. Composites Part B: Engineering Submitted.

dos Santos S, Partl MN, Poulikakos LD. 2014b. Newly observed effects of water on the microstructures of bitumen surface Construction and Building Materials 71: 618-627.

Heredia-Guerrero JA, de Lara R, Dominguez E, Heredia A, Benavente J, Benitez JJ. 2012. Chemical-physical characterization of isolated plant cuticles subjected to low-dose gamma-irradiation. Chemistry and Physics of Lipids 165: 803-808.

Lyne AL, Wallqvist V, Rutland M, Claesson P, Birgisson B. 2013. Surface wrinkling: the phenomenon causing bees in bitumen. Journal of Materials Science 48: 6970-6976.

Nahar SN, Mohajeri M, Schmets AJM, Scarpas T, van den Ven MFC, Schitter G. 2013. First observation of the blending zone morphology at the interface of reclaimed asphalt binder and virgin bitumen. TRB Annual Meeting.

Nazzal MD, Mogawer W, Kaya S, Bennert T. 2013. Nano-scale evaluation of the effect of RAP on virgin asphalt binder properties. TRB Annual Meeting.

Poulikakos LD, dos Santos S, Bueno M, Kuentzel S, Hugener M, Partl MN. 2014. Influence of short and long term aging on chemical, microstructural and macro-mechanical properties of recycled asphalt mixtures. Construction and Building Materials 51: 414-423.

Rinaldini E, Schuetz P, Tebaldi G, Partl MN, Poulikakos LD. 2014. Investigating the blending of reclaimed asphalt with virgin materials using rheology, electron microscopy and computer tomography. Composites: Part B 67: 579-587.

Srivastava SP, Handoo J, Agrawal KM, Joshi GC. 1993. Phase-Transition Studies in N-Alkanes and Petroleum-Related Waxes - a Review. Journal of Physics and Chemistry of Solids 54: 639-670.

Ungar G, Masic N. 1985. Order in the Rotator Phase of Normal-Alkanes. Journal of Physical Chemistry 89: 1036-1042.

# Comparative Analysis of Stiffness Modulus and Fatigue Resistance of Asphalt Concretes Containing RAP Materials

**Nicola Baldo, Evaggelos Manthos, Marco Pasetto and A.F. Nikolaides**

**Abstract** The paper discusses the results of a comparative laboratory investigation on the mechanical performance of bituminous mixtures for pavement base courses, made with Reclaimed Asphalt Pavement (RAP). Five Asphalt Concretes (AC) were used in this study: a control AC mixture with limestone aggregates and two AC mixtures with 20 and 40 % RAP (by weight of aggregate) respectively. The RAP material used came from two different sources, one from Italy and one from Greece. The mix design procedure was based on the optimization of the volumetric properties and the moisture resistance of the bituminous mixtures. Then, the stiffness modulus of the mixtures was evaluated by the Indirect Tensile Stiffness Modulus test, at various temperatures and rise times. The Indirect Tensile Fatigue Test, concluded the experimental trial. Depending on the RAP sources and content, the bituminous mixtures made with RAP aggregates showed improved indirect tensile strength as well as higher stiffness modulus values and fatigue resistance, with respect to the control asphalt concrete prepared with natural aggregate.

**Keywords** RAP asphalt concrete · Stiffness modulus · Moisture resistance · Fatigue resistance

N. Baldo (✉)
Chemistry, Physics and Environment Department, University of Udine, Udine, Italy
e-mail: nicola.baldo@uniud.it

E. Manthos · A.F. Nikolaides
Department of Civil Engineering, Aristotle University of Thessaloniki, Thessaloniki, Greece
e-mail: emanthos@civil.auth.gr

A.F. Nikolaides
e-mail: anik@civil.auth.gr

M. Pasetto
Department of Civil, Environmental and Architectural Engineering, University of Padua, Padova, Italy
e-mail: marco.pasetto@unipd.it



F. Canestrari and M.N. Partl (eds.), *8th RILEM International Symposium on Testing and Characterization of Sustainable and Innovative Bituminous Materials*, RILEM Bookseries 11, DOI 10.1007/978-94-017-7342-3_73

# 1 Introduction

The use of RAP materials for the design of conventional or high performance asphalt concretes has been widely investigated by many researchers (Celauro et al. 2010; Grilli et al. 2013; Miró et al. 2011). In most cases, RAP materials come from sources located in the same country. The aim of the research described in this paper was to investigate and compare the mechanical and performance characteristics of base course asphalt concretes made with RAP materials provided by different sources, located in Italy and Greece.

A statistical study has been performed on the Stiffness Modulus values of the asphalt concretes, at different temperatures and rise time, in order to verify the effect of RAP type and content on the mechanical properties of the mixtures.

# 2 Materials and Methods

## *2.1 Materials*

Crushed limestone aggregate as well as limestone filler have been used in the investigation; both the granular materials came from a source located in the North-east part of Italy. The aggregates have been made available in four different grading fractions: 12/20, 8/12, 4/8, and 0/4 mm. Table 1 reports the physico-mechanical properties of the aggregates and the test protocols adopted.

Two different RAP materials have been integrated into the aggregate skeleton of the asphalt concretes considered in the study, but without using both of them in the same mix. The first one was obtained from the milling of an Italian motorway pavement, in the North-east area of Italy and the second one derived from the milling of a Greek highway in Northern Greece; they have been named I-RAP and G-RAP, respectively.

**Table 1** Aggregates characterization

| Physical properties | Limestone 12/20 | Limestone 8/12 | Limestone 4/8 | Sand 0/4 | I-RAP | G-RAP | Filler |
|---|---|---|---|---|---|---|---|
| Apparent particle density (g/cm$^3$) EN 1907-6 | 2.784 | 2.785 | 2.790 | 2.804 | 2.754 | 2.746 | 2.728 |
| Flakening index (%) EN 933-3 | 6.8 | 7.6 | 9.9 | – | – | – | – |
| LA coefficient (%) EN 1097-2 | 19.7 | 21.3 | 22.8 | – | – | – | – |

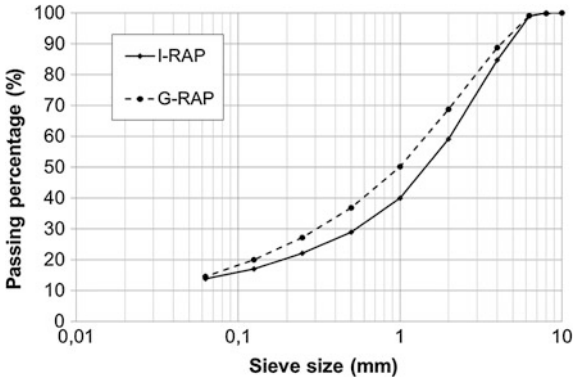


**Fig. 1** Grading curves of the RAP aggregates

**Table 2** RAP binders and conventional bitumen characterization

| Physical properties | I-RAP binder | G-RAP binder | Conventional bitumen | Standard |
|---|---|---|---|---|
| Penetration at 25 °C (mm/10) | 19 | 7 | 52 | UNI EN 1426 |
| R&B softening point (°C) | 63 | 79 | 48 | UNI EN 1427 |
| Viscosity at 160 °C (Pa s) | 0.256 | 0.66 | 0.125 | UNI EN 13302 |
| Viscosity at 100 °C (Pa s) | 13.6 | 89.6 | 3.9 | UNI EN 13302 |
| Viscosity at 80 °C (Pa s) | 113 | 1180 | 21.4 | UNI EN 13302 |

The grading curves of the RAP aggregates (UNI EN 12697-2), after extraction, are presented in Fig. 1; the Italian RAP was coarser than the Greek one. The RAP binder content, determined by means of a centrifuge extractor (UNI EN 12697-1), resulted equal to 5.2 and 4.7 %, on the weight of the aggregates, for the Italian and the Greek RAP, respectively.

The physical properties of the RAP binders, recovered by means of the Abson method (CNR 133), were also investigated. The results, reported in Table 2, show clearly that the Greek RAP binder was characterized by an extremely low penetration value and a very high viscosity, at all the temperatures investigated, so demonstrating to be much more aged than the Italian RAP bitumen. Although a RAP material with such low penetration grade, as the G-RAP, should not be used (EN 13108-8), it was decided to proceed with the investigation in order to check the effect of the very low penetration grade on stiffness and fatigue performance.

A conventional bitumen (50/70 dmm penetration grade), has been used as virgin bitumen to be added to all the mixes. As seen from Table 2, the conventional bitumen was softer than both the binders in RAP.

## 2.2 Methods

### 2.2.1 Mix Design

The mix design procedure was based on the volumetric analysis of specimens prepared by gyratory compaction and the Indirect Tensile Strength (ITS) test at 25 °C, on both dry and wet cylindrical samples, according to CIRS-Italian Ministry of Infrastructure Specifications (2001). The Tensile Strength Ratio (TSR) has been computed as the percentage ratio between the indirect tensile strength of the specimens treated by means of 15 days of immersion in a thermostatic bath at 25 °C ($ITS_{wet}$) and untreated ($ITS_{dry}$), respectively. Regarding the main gyratory test parameters, a speed of 30 gyrations/min, a pressure of 600 kPa, an angle of rotation of 1.25° and a diameter of the mould of 150 mm, were used in the gyratory compaction. The actual amount of virgin bitumen to add to the aggregate matrix was identified as that which satisfied the residual air voids ($V_a$) prerequisites in correspondence to three different gyration numbers. Moreover, the dry ITS and the TSR values of the mixtures prepared with the optimum bitumen content, should result higher than the minimum CIRS acceptance thresholds.

### 2.2.2 Performance Characterization

Indirect Tensile Stiffness Modulus (ITSM) tests, as described in Annex C of the EN 12697-26 standard, were conducted on the asphalt concretes studied, in order to characterize their dynamic response, under repeated load pulses. In the ITSM test, the Stiffness is evaluated in correspondence to the maximum vertical load that determines the controlled deformation, so it is reasonable to assume a time quadruple of that necessary for the load to reach the peak value as the "virtual" period of the cycle (Pasetto and Baldo 2006). The ITSM tests were performed at three different temperatures (10, 20 and 30 °C). At each temperature the stiffness of the asphalts was evaluated at five different rise times (125, 100, 75, 50 and 25 ms), with the same horizontal deformation (7 μm) and maintaining the pulse repetition period unvaried at 3 s. Therefore, for each mixture, 15 different testing conditions have been studied, in order to subsequently elaborate the master curves of the Stiffness Modulus. Chauvenet's criterion (Barnett and Lewis 1994), has been applied to the stiffness data, in order to verify their statistical acceptability. Moreover, an ANOVA analysis was performed on the ITSM data, to study statistically the effect of RAP on the stiffness response of the mixes. Lastly, the fatigue resistance evaluation, at a reference temperature of 20 °C, has been performed by repeated Indirect Tensile Fatigue Tests (ITFT), following the general indications given in the British Standard Draft for Development DD ABF. ITFT tests were conducted on each mixture with a rise time of 124 ms and using a single stress level, equal to 600 kPa.

# 3 Results and Discussion

## *3.1 Mix Design Results*

Both the RAP materials have been integrated in the aggregate skeleton of the asphalt concretes with two different percentages: 20 and 40 % by weight of the aggregates. The mixes produced with Italian RAP were named AC20/I and AC40/I, while the asphalts with Greek RAP have been identified by the code AC20/G and AC40/G (the numbers 20 and 40 denote the RAP content). A control mix, named AC0, produced exclusively with conventional limestone aggregate, has also been studied, in order to compare the mechanical properties. The particle size distribution of the asphalt concretes was optimized with reference to the design grading envelope of CIRS (2001) for asphalt concrete base courses. The composition of the RAP mixes has been studied in order to maintain the grading curves, as close as possible to that of the AC0. Table 3 reports the composition of the 5 mixtures studied; the corresponding grading curves are presented in Fig. 2.

According to the data presented in Table 4, the Air Voids requisites prescribed by CIRS mix design procedure, at 10, 100 and 180 revs, were completely satisfied in correspondence of a total bitumen content equal to 5 % (by weight of the aggregate), for all the mixes.

At the optimum total bitumen content, both the dry ITS and the TSR values, resulted above the CIRS acceptance prerequisites for all the asphalt concretes examined. Hence all mixes produced in this study were acceptable for road construction according to the CIRS specification. The mixes with RAP showed higher ITS values, with respect to the control asphalt concrete, varying from 12 to 56 %, depending on the RAP content and on the dry/wet condition. The strength increments are greater for the mixes made with Italian RAP, but only for the highest RAP content (40 %); in fact, at the lower RAP percentage (20 %), the ITS values resulted equal (in dry conditions) or very similar (for wet conditions).

**Table 3** Aggregate type and composition of the mixtures; quantity (%)

| Aggregate type | AC0 | AC20/I | AC40/I | AC20/G | AC40/G |
|---|---|---|---|---|---|
| Limestone 12/20 mm | 39 | 40 | 39 | 40 | 39 |
| Limestone 8/12 mm | 7 | 5 | 0 | 5 | 0 |
| Limestone 4/8 | 5 | 7 | 14 | 7 | 14 |
| Sand 0/4 mm | 46 | 27 | 7 | 27 | 7 |
| Filler | 3 | 1 | 0 | 1 | 0 |
| I-RAP | 0 | 20 | 40 | 0 | 0 |
| G-RAP | 0 | 0 | 0 | 20 | 40 |

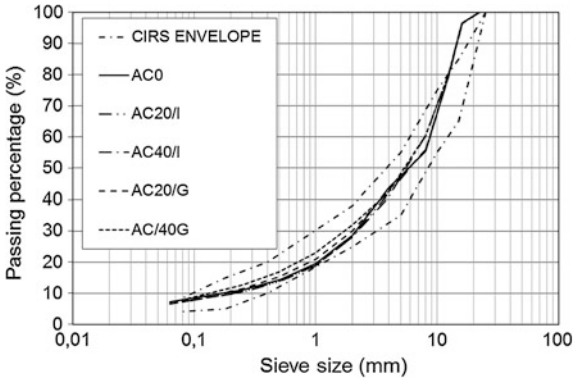


**Fig. 2** Grading curves of the mixes

**Table 4** Mix design results; total bitumen content equal to 5 %

| Property | AC0 | AC20/I | AC40/I | AC20/G | AC40/G | CIRS requisites |
|---|---|---|---|---|---|---|
| Va @ 10 revs (%) | 13.9 | 11.1 | 10.8 | 13.6 | 11.2 | 10–14 |
| Va @ 100 revs (%) | 5.0 | 3.7 | 3.3 | 4.7 | 3.5 | 3–5 |
| Va @ 180 revs (%) | 3.4 | 2.7 | 2.5 | 3.3 | 2.3 | >2 |
| Bulk density ($g/cm^3$) | 2.451 | 2.479 | 2.483 | 2.455 | 2.477 | – |
| Maximum density ($g/cm^3$) | 2.580 | 2.574 | 2.568 | 2.576 | 2.567 | – |
| $ITS_{dry}$ (MPa) | 1.51 | 1.69 | 2.35 | 1.69 | 2.23 | >0.6 |
| $ITS_{wet}$ (MPa) | 1.46 | 1.66 | 2.26 | 1.62 | 2.16 | – |
| TSR (%) | 96.7 | 98.2 | 96.2 | 95.9 | 96.9 | >75 |

## 3.2 *Performance Analysis Results*

Tables 5, 6, and 7 present the results of the ITSM tests, conducted on the samples compacted at 100 revs, where the values of the Modulus ($S_m$) for each mixture and for each testing condition, were determined as the average of 3 gyratory specimens.

In order to perform a subsequent statistical analysis of the stiffness values, it was decided to test, in addition to a first pair of randomly chosen orthogonal diameters ($D_1$, $D_2$), also a second pair of diameters ($D_3$, $D_4$) along the directions identified by the bisectors of the right angles formed by the first two diameters. Moreover, for each specimen and diameter considered, five repeated ITSM tests have been performed. Therefore, for each single specimen, at each testing condition, twenty stiffness values have been obtained; An overall number of 4500 Stiffness Modulus values were determined in the experimental investigation.

**Table 5** Stiffness modulus (MPa) and standard deviation at 10 °C, for different rise times

| Mix type | 125 ms | 100 ms | 75 ms | 50 ms | 25 ms |
|---|---|---|---|---|---|
| AC0 | 17,310 ± 766 | 18,228 ± 713 | 19,850 ± 980 | 21,369 ± 1335 | 24,506 ± 1485 |
| AC20/I | 19,979 ± 745 | 21,117 ± 860 | 22,454 ± 1018 | 23,136 ± 867 | 24,399 ± 1036 |
| AC40/I | 22,974 ± 743 | 23,917 ± 990 | 24,804 ± 951 | 26,845 ± 1213 | 28,370 ± 2459 |
| AC20/G | 18,725 ± 951 | 18,832 ± 1605 | 20,068 ± 1279 | 22,046 ± 1284 | 24,036 ± 1242 |
| AC40/G | 22,138 ± 1097 | 22,127 ± 808 | 24,234 ± 695 | 25,193 ± 1427 | 26,977 ± 1820 |

**Table 6** Stiffness modulus (MPa) and standard deviation at 20 °C, for different rise times

| Mix type | 125 ms | 100 ms | 75 ms | 50 ms | 25 ms |
|---|---|---|---|---|---|
| AC0 | 8429 ± 609 | 8738 ± 446 | 9888 ± 429 | 11,210 ± 512 | 13,575 ± 651 |
| AC20/I | 10,205 ± 400 | 10,756 ± 821 | 12,129 ± 541 | 13,055 ± 763 | 15,530 ± 639 |
| AC40/I | 14,208 ± 380 | 14,605 ± 528 | 16,247 ± 1196 | 16,993 ± 940 | 18,838 ± 1236 |
| AC20/G | 10,064 ± 982 | 10,465 ± 489 | 11,439 ± 595 | 12,758 ± 834 | 14,999 ± 1316 |
| AC40/G | 13,633 ± 391 | 15,139 ± 935 | 15,787 ± 759 | 17,155 ± 1211 | 18,552 ± 724 |

**Table 7** Stiffness modulus (MPa) and standard deviation at 30 °C, for different rise times

| Mix type | 125 ms | 100 ms | 75 ms | 50 ms | 25 ms |
|---|---|---|---|---|---|
| AC0 | 2079 ± 262 | 2322 ± 184 | 2351 ± 226 | 2755 ± 188 | 4971 ± 380 |
| AC20/I | 3040 ± 400 | 3488 ± 370 | 3741 ± 293 | 4645 ± 402 | 6694 ± 585 |
| AC40/I | 5348 ± 453 | 6092 ± 531 | 6821 ± 288 | 7649 ± 644 | 9710 ± 837 |
| AC20/G | 2947 ± 328 | 3131 ± 333 | 3206 ± 369 | 4016 ± 539 | 5945 ± 428 |
| AC40/G | 5346 ± 398 | 5343 ± 218 | 5805 ± 235 | 7423 ± 253 | 9287 ± 358 |

The mean Stiffness Modulus and the standard deviations reported in Tables 5, 6, and 7 have been computed on the basis of 60 values for each mixture and testing condition. The 60 Stiffness values, correspond to the 20 Modulus values measured for each specimen, for the three sample repetitions.

In order to statistically analyze the ITSM tests, the Stiffness values (4500 overall) have been subdivided in 225 statistical samples, which correspond to 15 physical specimens, tested under 15 different conditions. Each statistical sample includes 20 measures, given by 5 ITSM tests performed on 4 different diameters, for each gyratory specimen. Chauvenet's criterion has been applied to the 225 statistical samples, in order to determine the number of potential rejectable values, namely outliers. Chauvenet's criterion defines an acceptable scatter, in a statistical sense, around the mean value of a given sample of N measurements. The criterion states that all the data points should fall within a band around the mean value that corresponds to a probability of $1 - 1/(2N)$. In other terms, data points can be considered for rejection only if the probability of obtaining their deviation from the mean value is less than $1/(2N)$. Given N measurements ($x_1$, $x_2$, …, $x_N$) of the same parameter x (the Stiffness modulus), Chauvenet's criterion performs the calculation

of the arithmetic mean $\bar{x}$ and the standard deviation $\sigma_x$. The presence of a suspicion value within the sample, named $x_s$, is subsequently verified. The number of standard deviations of which the suspicion value $x_s$ differs from the average value $\bar{x}$, namely the value of the parameter $t_s$, is calculated as:

$$t_s = \frac{|\bar{x} - x_s|}{\sigma_x} \quad (1)$$

Subsequently, the probability that the suspicious measure $x_s$ differs from the average value $\bar{x}$ for a quantity equal to $t_s$ [namely, $P(t > t_s)$], is determined using the normal distribution function (or a table thereof) (Barnett and Lewis 1994). The expected number of suspicious measures (n), is determined as:

$$n = N \cdot P(t > t_s) \quad (2)$$

Lastly, it is verified that this number (n) results greater than a certain minimum threshold, which is fixed at 0.5. The analysis conducted with the Chauvenet's criterion has led to the rejection of only 35 stiffness values with respect to the total number of 4500 (Table 8), equal to 0.78 % of the data determined in the experimental trial.

Focusing the attention on the mechanical aspects of the Stiffness investigation, as would be expected, given the viscoelastic behavior of the bituminous mixtures, the Stiffness Modulus increases with the reduction in temperature and rise time, and is higher for the RAP mixtures than for the control one, with increments up to 33 % at 10 °C, 69 % at 20 °C and 190 % at 30 °C, in relation to the rise time, as well as to the content and type of RAP. The higher stiffness values of the RAP mixes, are primarily due to the age hardening effect of the RAP binders (Pasetto and Baldo 2012). Although the Greek RAP binder is significantly harder than the Italian one, the higher amount of virgin bitumen required by the mixes with G-RAP to achieve the optimum total bitumen content resulted to stiffness values lower than those of the I-RAP mixes. Moreover, for both the RAP types, the higher the RAP content, the greater the amount of aged binder is incorporated in the mix with, consequently, higher stiffness values of the asphalt concretes.

Applying the theory of viscoelasticity, and in particular the time-temperature superposition principle made it possible to provide a predictive interpretation of the experimental data, useful for the calculation of $S_m$ at different values of frequency (f) to that used in the study. Through a linear regression model, the Master Curves

**Table 8** Chauvenet's criterion results

| Stiffness modulus data | Accepted values (%) | Rejected values |
|---|---|---|
| Total stiffness data | 99.22 | 35/4500 |
| Stiffness modulus at 10 °C | 98.93 | 16/1500 |
| Stiffness modulus at 20 °C | 98.93 | 16/1500 |
| Stiffness modulus at 30 °C | 99.80 | 3/1500 |

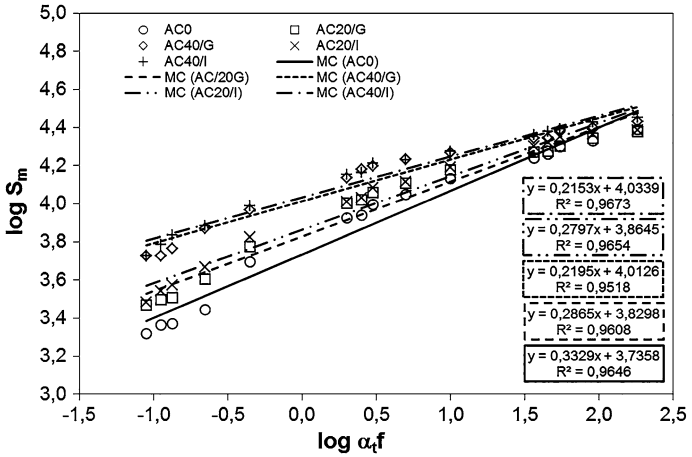


**Fig. 3** Stiffness modulus master curves at 20 °C

of the Stiffness Modulus were elaborated, starting from the data obtained with the ITSM tests, calculating the value of the factors of translation $\alpha_t$ with the Arrhenius formula: $\ln(\alpha_t) = \Delta H/R * (1/T - 1/T_s)$. In this equation $\Delta H$ is the energy of apparent activation, characteristic of the material, in the order of 210 kJ/mol; R is the constant of the perfect gasses, equal to 8314 J/(K mol); T, $T_s$ are the temperatures expressed in degrees Kelvin. On the plane log $S_m$ − log ($\alpha_t$ f) the master curves of the mixtures can be represented with equations of the type:

$$\log S_m = b \log(\alpha_t f) + c \tag{3}$$

where *b* and *c* are regression coefficients dependent on the material. Figure 3 reports the Master Curves of the mixes at the reference temperature ($T_S$) of 20 °C.

As previously discussed, integration of the RAP materials in the aggregate skeleton of the mixes involves an increase in the Modulus $S_m$, which translates into an increment of the coefficient *c*, i.e. in a shift of the Master Curves of the mixes with RAP towards higher stiffness values.

## *3.3 Statistical Analysis of the Stiffness Modulus Data*

An analysis of variance (ANOVA) was conducted on the ITSM data, with the assumption of a normal distribution, to study primarily the effect of RAP content and type on the stiffness of the asphalt concretes. Therefore, in the ANOVA studied, both the RAP type and content, but also the rise time and the temperature, were chosen as factors (*a, b, c, d*, respectively). The interactions between the factors have been also taken into account. For the multiple factors ANOVA performed

**Table 9** ANOVA test results

| Source | DF | Adj SS | Adj MS | F-value | *P*-value |
|---|---|---|---|---|---|
| a | 1 | 58,765,910 | 58,765,910 | 96.66 | 0.000 |
| b | 2 | 4,282,502,634 | 2,141,251,317 | 3522.06 | 0.000 |
| c | 4 | 3,077,469,508 | 769,367,377 | 1265.50 | 0.000 |
| d | 2 | 55,449,409,313 | 27,724,704,656 | 45,603.31 | 0.000 |
| a * b | 2 | 30,557,067 | 15,278,533 | 25.13 | 0.000 |
| a * c | 4 | 3,156,130 | 789,032 | 1.3 | 0.269 |
| a * d | 2 | 27,416,757 | 13,708,378 | 22.55 | 0.000 |
| b * c | 8 | 19,524,428 | 2,440,553 | 4.01 | 0.000 |
| b * d | 4 | 102,443,748 | 25,610,937 | 42.13 | 0.000 |
| c * d | 8 | 164,234,016 | 20,529,252 | 33.77 | 0.000 |
| a * b * c | 8 | 4,017,378 | 502,172 | 0.83 | 0.580 |
| a * b * d | 4 | 14,384,176 | 3,596,044 | 5.91 | 0.000 |
| a * c * d | 8 | 8,092,338 | 1,011,542 | 1.66 | 0.103 |
| b * c * d | 16 | 59,627,375 | 3,726,711 | 6.13 | 0.000 |
| a * b * c * d | 16 | 20,646,101 | 1,290,381 | 2.12 | 0.006 |

(Cochran and Cox 1992), the response was obviously the Stiffness Modulus; the results are presented in Table 9. At the 95 % confidence level, all the four factors were statistically significant, because the *p*-values resulted lower than 5 %, but the RAP content and the testing temperature have to be considered the most relevant variables, because of their higher F-values. However, also the RAP type has presented a significant effect on the Stiffness modulus (*p*-value equal to 0) and therefore, the differences between the stiffness values of the mixes made with Greek or Italian RAP, have to be considered as relevant. Three interactions among some of the factors, more precisely those involved with the RAP type and the rise time, resulted not statistically significant, because the *p*-values were greater than 5 %. The most significant interaction between variables, was among the RAP content and the testing temperature.

## *3.4 Fatigue Resistance Evaluation*

The results of the stress control fatigue tests, reported in Table 10, are consistent with those from the study reported by Pasetto and Baldo (2013): at the same level of stress, as the asphalt concrete's stiffness increases, fewer deformations develop and consequently the cracking resistance of the material increases.

The mixes with RAP have therefore presented a higher fatigue resistance than the control asphalt concrete, especially for the RAP content equal to 40 %. The difference in cycles to failure between mixes AC20/I and AC20/G and also between mixes AC40/I and AC40/G could be attributed to the effect of the very low

**Table 10** Fatigue tests results

| Property | AC0 | AC20/I | AC40/I | AC20/G | AC40/G |
|---|---|---|---|---|---|
| Cycles to failure | 2570 | 10,570 | 55,430 | 5150 | 43,450 |

penetration grade bitumen of the Greek RAP material. Even if the Greek RAP binder was harder than the Italian one, the Stiffness and the fatigue life of the Italian RAP mixtures were both higher than the Greek one. This could be due to a better affinity between the virgin bitumen and the softest RAP binder, namely the Italian one, that allows an improved adhesion between the Italian RAP grains and the virgin bitumen film, with positive effects in terms of Stiffness and fatigue resistance for the Italian RAP mixtures. However, the fatigue tests have been performed just on one sample per mix, because the quantity of RAP materials was limited; therefore the results should be considered very carefully.

## 4 Conclusions

All the designed bituminous mixtures with RAP, have satisfied the prerequisites for acceptance in the road sector technical standards (Air Voids, ITS, TSR), thus resulting as suitable for use in the construction of road base courses.

The performance analysis, in terms of stiffness modulus and fatigue resistance, has completely confirmed the comparative ranking of the mixtures, already outlined in the tensile strength investigation.

The ANOVA performed on the stiffness data, outlined a significant effect of the type and, especially, of the content of RAP material integrated in the mixes.

The use of RAP material containing bitumen with penetration grade below 10 mm/10, had an effect on the fatigue and not on the stiffness performance of the recycled mixtures analyzed in this study.

## References

Barnett V, Lewis T (1994) Outliers in Statistical Data (3rd ed). Wiley and Sons, Chichester

Celauro C, Celauro B, Boscaino G (2010) Production of innovative, recycled and high-performance asphalt for road pavements. Resour Conserv Recycl 54(6): 337-347. doi: 10.1016/j.resconrec.2009.08.009

CIRS-Italian Ministry of Infrastructure Specifications (2001) Norme tecniche di tipo prestazionale per capitolati speciali d'appalto. Roma. [in Italian]

Cochran W G, Cox G M (1992). Experimental designs (2nd ed). Wiley, New York

Grilli A, Bocci M, Cardone F, Conti C, Giorgini E (2013) Laboratory and in-plant validation of hot mix recycling using a rejuvenator. Int J Pav Res Technol 6(4): 364-371. doi: 10.6135/ijprt.org.tw/2013.6(4).364

Miró R, Valdés G, Martínez A, Segura P, Rodríguez C (2011) Evaluation of high modulus mixture behaviour with high reclaimed asphalt pavement (RAP) percentages for sustainable road construction. Constr Build Mater 25 (2011) 3854–3862

Pasetto M, Baldo N (2006) Critical Analysis of the EN 12697-26 Standard for the Determination of the Indirect Tensile Stiffness Modulus. Paper presented at the 10th International Conference on Asphalt Pavements, Québec City, 12-17 August 2006.

Pasetto M, Baldo N (2012) Fatigue Performance of Asphalt Concretes with RAP Aggregates and Steel Slags. In: Scarpas A et al. (ed) 7th RILEM International Conference on Cracking in Pavements, RILEM Bookseries, Volume 4, Springer Netherlands, p 719-727

Pasetto M, Baldo N (2013) Fatigue Performance of Asphalt Concretes Made with Steel Slags and Modified Bituminous Binders. Int J Pav Res Technol 6(4):294-303. doi: 10.6135/ijprt.org.tw/2013.6(4).294

# In Plant Production of Hot Recycled Mixtures with High Reclaimed Asphalt Pavement Content: A Performance Evaluation

**Arianna Stimilli, Amedeo Virgili, Felice Giuliani and Francesco Canestrari**

**Abstract** Nevertheless hot recycling process is nowadays a widespread technique, many doubts related to the in plant recycling process effects on the performance of recycled mixtures still exist and limit the maximum allowable amount of Reclaimed Asphalt Pavement (RAP). Therefore, the feasibility of an efficient production of plant hot recycled mixtures characterized by high RAP content and suitable performance should be properly addressed. To this aim, the overall performance of hot recycled asphalt mixtures produced in asphalt plant and containing high RAP content were assessed in this study. The mixtures were prepared with two different bitumens (high and low content of SBS polymer modifier) and 40 % of RAP only deriving from asphalt layers containing polymer modified bitumens. The aggregate grading curve was previously optimized through a specific laboratory study by applying the Bailey Method and using selected RAP. A third mixture, currently used for binder layers in motorway pavements, was also studied for comparative purposes. Compactability, stiffness, cracking and rutting resistance and fatigue behavior were investigated. Results of the mechanical tests suggest that mixtures containing 40 % RAP are suitable for the production of new asphalt pavements,

A. Stimilli (✉) · A. Virgili · F. Canestrari
Dipartimento di Ingegneria Civile Edile e Architettura, Università Politecnica delle Marche, via Brecce Bianche, 60131 Ancona, Italy
e-mail: a.stimilli@univpm.it

A. Virgili
e-mail: a.virgili@univpm.it

F. Canestrari
e-mail: f.canestrari@univpm.it

F. Giuliani
Dipartimento di Ingegneria Civile, Università degli studi di Parma, dell'Ambiente, del Territorio e Architettura, Parco Area delle Scienze, 181/A, 43124 Parma, Italy
e-mail: felice.giuliani@unipr.it



F. Canestrari and M.N. Partl (eds.), *8th RILEM International Symposium on Testing and Characterization of Sustainable and Innovative Bituminous Materials*, RILEM Bookseries 11, DOI 10.1007/978-94-017-7342-3_74

especially when low modified bitumens are used. In fact, the performance of such mixtures were comparable or even higher than those of the reference mixture. In particular, the specific and accurate mix design allowed the potential drawbacks due to higher RAP content to be balanced.

**Keywords** Hot recycling · RAP · Polymer modified bitumen · In plant production

## 1 Introduction

In several productive fields, recycling techniques represent one of the most promising strategies to achieve economic and environmental sustainability goals. Also in the pavement industry, recycling has gained increasing importance for the production of new asphalt mixtures. In fact, it allows the optimization of the materials in terms of costs and natural resources saving (de la Roche et al. 2013). Many laboratory studies concerning the evaluation of performance of recycled mixtures with high RAP content have been carried out (Aurangzeb et al. 2012; Frigio et al. 2014; Stimilli et al. 2013). However, it is widely recognized that mixtures prepared in plant for a large scale production could not perform as well as mixtures optimized in laboratory (de la Roche et al. 2013). Many aspects related to the in plant production process, not fully repeatable in laboratory, can alter the mixture performance. In fact, in the case of hot recycled mixtures the production process requires particular sequences to incorporate RAP in the mixture due to the impossibility of treating the milled material as a virgin aggregate for the presence of the external film of aged bitumen. The RAP aggregates need to be processed in a separated drum at low temperature or added at ambient temperature directly inside the mixer at the final stage of the production process to avoid the excessive smoke produced when RAP comes into contact with the burner flame (Kandhal and Mallick 1997). In particular, the potential detrimental effects caused by the production sequences become more evident when large amounts of RAP are incorporated in the new mixture. In this sense, laboratory studies can represent a useful tool to initially optimize the mix design of a mixture. However, a validation of the in plant production is necessary to demonstrate the actual feasibility of successfully realizing hot recycled mixtures containing high RAP content without compromising the material performance. In this context, the present study illustrates the performance evaluation of dense graded hot recycled mixtures containing 40 % of RAP produced in a central plant for the construction of a full scale trial section along an in-service Italian motorway. The mixtures were produced according to the optimized mix design addressed through a previous laboratory study based on the Bailey Method (Stimilli et al. 2015a). A wide experimental program based on different mechanical tests for the evaluation of the main properties of a flexible pavement (compactability, stiffness, cracking aptitude, rutting resistance and fatigue) was carried out.

## 2 Materials

Three dense graded mixtures containing RAP were evaluated in this study. They were produced in a double drum hot mix plant and used to realize the binder course (80 mm thick) of three full scale experimental sections as part of a motorway rehabilitation project. In the first section, the binder course was constructed using a mixture (named as *REF_situ*) prepared following the practice currently adopted for Italian motorways. The mixture is characterized by a Nominal Maximum Aggregate Size (NMAS) equal to 20 mm and includes 25 % by aggregate weight of unfractioned RAP (0/16 mm) mixed with virgin limestone aggregates and virgin "hard" polymer modified bitumen (H) which contains 3.8 % of Styrene-Butadiene-Styrene (SBS) polymer by bitumen weight. The total binder content (virgin bitumen and reclaimed bitumen from RAP) is 4.8 % by aggregate weight following the current practice. This mix was used as control mix for comparison purposes. For the construction of the other sections, two mixtures including 40 % of RAP by total aggregate weight were used. They were characterized by the same NMAS of the reference mixture. The mix design adopted was determined during a previous specific laboratory study aimed at optimizing the grading curve and the bitumen content of such mixtures (Stimilli et al. 2015a) according to the technical specifications for Italian motorway pavements. To this aim, the RAP was previously divided in two fractions (i.e. 8/16 mm and 0/8 mm). Moreover, to achieve an optimized aggregate packing and, subsequently, improved volumetric and mechanical properties to overcome potential drawbacks due to the increase in RAP content, the 40 % RAP mixtures were designed by applying the Bailey Method (Vavrik et al. 2002). The optimum binder content of the 40 % RAP mixtures was found to be equal to 5.2 % by aggregate weight. This value is higher than that of the reference mixture because of the higher amount of RAP included. In fact, not all the aged binder coming from RAP takes part in the blending process (Shirodkar et al. 2011; Frigio et al. 2014; Stimilli et al. 2015b). Therefore, as the RAP percentage increases, the amount of aged inactive binder (black aggregate) increases as well (Frigio et al. 2014). The two 40 % RAP mixtures differed for the type of virgin bitumen used. One mixture (named as 5.2 %*H_situ*) was produced with the same "hard" modified bitumen (H) employed for the reference mixture, whereas the other one (named as 5.2 %*S_situ*) was prepared using a "soft" modified bitumen (1.8 % of SBS by bitumen weight, coded as S). Binder H was selected because it corresponds to the original binder included in the RAP and is commonly used for the production of Italian motorway asphalt mixes. Moreover, a "softer" binder S was investigated for evaluating the potential benefits due to the use of a lower binder grade that compensates the stiffness increase caused by higher amount of aged binder coming from RAP. The basic characteristics of the virgin binders used are presented in previous studies (Stimilli et al. 2014). Three virgin crushed limestone aggregates (classified as 10/20, 4/10, 0/4 mm according to EN 13043) were used to produce all the mixtures along with RAP milled from binder and base courses of old motorway pavements. The RAP binder type was an SBS modified bitumen

**Table 1** Field mixtures composition

| Sieve (mm) | *REF_situ* | | 5.2 *%H_situ* | | 5.2 *%S_situ* | | Grading envelope | |
|---|---|---|---|---|---|---|---|---|
| | Passing (%) | | Passing (%) | | Passing (%) | | Passing (%) | |
| | Design | Actual | Design | Actual | Design | Actual | Max | Min |
| 31.5 | 100 | 100 | 100 | 100 | 100 | 100.0 | 100 | 100 |
| 20 | 92.4 | 93.3 | 92.3 | 95.4 | 92.3 | 94.6 | 98 | 85 |
| 14 | 80.9 | 72.7 | 79.4 | 74.8 | 79.4 | 73.5 | 87 | 70 |
| 10 | 69 | 59.4 | 64.8 | 63.1 | 64.8 | 61.1 | 78 | 58 |
| 6.3 | – | 50.8 | – | 48.6 | – | 47.9 | 66 | 46 |
| 2 | 28.7 | 28.6 | 26.9 | 27.2 | 26.9 | 26.8 | 38 | 25 |
| 0.5 | 14.1 | 12.8 | 12.9 | 13.7 | 12.9 | 12.3 | 21 | 11 |
| 0.25 | 9.4 | 9.6 | 9.4 | 9.4 | 9.4 | 9.2 | 17 | 7 |
| 0.063 | 5.2 | 6.3 | 4.8 | 6.8 | 4.8 | 5.8 | 8 | 4 |
| Bitumen (%) | 4.8 | 5.0 | 5.2 | 5.2 | 5.2 | 5.1 | 6.0 | 4.5 |

(3.8 % of SBS by bitumen weight) and its average content was 4.91 % by aggregate weight. As shown in Table 1 that summarizes the mixtures composition results directly determined through laboratory tests, the studied asphalt mixtures prepared in the asphalt plant adhered to the composition requirements developed through the laboratory study and fully respected the acceptance requirements prescribed by Italian technical specification. In particular, the bitumen content was assessed through solvent extraction.

## 3 Testing Methods and Program

During the in plant production, a given amount of each mixture was collected to perform a comprehensive laboratory study. Volumetric and mechanical properties of the mixtures were measured on laboratory specimens compacted at 160 °C immediately after the in plant production (avoiding further aging due to re-heating) using the Superpave Gyratory Compactor (SGC) with a target air voids of 3.5 % according to the limit range provided by the Italian technical specification. The air voids content was assessed by using the maximum and the bulk density of the mixtures measured according to EN 12697-05 (procedure C) and EN 12697-06 (procedure B). The Compaction Energy Index (CEI) (Mahmoud and Bahia 2004) was used to assess the compactability. Then, the cylindrical specimens prepared through the SGC were cut and cored in order to obtain samples with proper dimensions for mechanical tests (Table 2). The mechanical characterization of the mixtures was performed by means of a servo-pneumatic testing machine equipped with an environmental chamber. The experimental program involved a wide range

**Table 2** Experimental program (test repetitions)

| Mixture | CEI | Complex modulus | ITSM | SCB | ITFT | Permanent deformation |
|---|---|---|---|---|---|---|
| *REF_situ* | 5 | 2 | 6 | 4 | 6 | 2 |
| 5.2 % *H_situ* | 5 | 2 | 6 | 4 | 6 | 2 |
| 5.2 % *S_situ* | 5 | 2 | 6 | 4 | 6 | 2 |
| Specimen dimension (D × H; mm) | 150 × 100 ÷ 170 | 100 × 150 | 100 × 50 | 150 × 75 | 100 × 50 | 100 × 80 |

of performance-related tests in order to get a comprehensive picture of the mechanical properties of each investigated material. In particular, cyclic uniaxial compression tests were carried out to measure the complex modulus (E*) and the phase angle (δ) in accordance with AASHTO TP 79-09. Tests were run at five different temperatures (i.e. 10, 20, 30, 40, 50 °C) by applying a sinusoidal load at six frequencies (i.e. 0.1, 0.3, 1, 3, 10, 20 Hz) and were carried out in controlled strain mode setting 30 με as target strain level. Mixtures stiffness was also evaluated through Indirect Tensile Stiffness Modulus (ITSM) tests carried out according to EN 12697-26 at 20 °C. Semi-Circular Bending (SCB) tests were performed to evaluate the low temperature fracture resistance in accordance with EN 12697-44. Tests were run at a temperature of 10 °C using a constant vertical deformation rate equal to 5 mm/min. Cyclic indirect tension fatigue tests (ITFT) were also performed for evaluating the fracture resistance due to cycling loading according to BS DD ABF. Tests were carried out at a temperature of 20 °C in controlled stress mode, with a rise time of 124 ms. The failure was established when the complete fracture of the specimen was obtained. A minimum of 3 stress levels for each mixture was applied. Finally, the permanent deformation resistance was assessed by cyclic triaxial compression tests, according to EN 12697-25 (Method B). Tests were performed at a temperature of 40 °C with a confining pressure of 50 kPa. The overall experimental plan is summarized in Table 2.

## 4 Results and Analysis

### *4.1 Compactability*

The compactability aptitude of each mixture was assessed by means of the Compaction Energy Index (CEI). The lower the CEI, the better the compactability (Mahmoud and Bahia 2004). In fact, CEI represents the work required to achieve a target density during construction and is calculated as the area under the

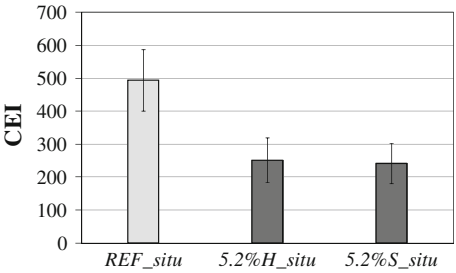


**Fig. 1** Compaction energy index results

densification curve from the 8th gyration to 92 % of the maximum theoretical density. Figure 1 shows CEI values calculated for each mixture as average of all specimens (D = 150 mm) prepared for this study along with the error bars reporting the standard deviation for each mixture investigated. The results are in accordance with those of typical dense graded mixtures (Mahmoud and Bahia 2004). In particular, the reference mixture has the worst compactability aptitude (highest CEI value), whereas the 40 % RAP mixtures were characterized by lower CEI value, regardless of the bitumen type. This finding can be attributed to the optimization of the aggregate gradation through the Bailey Method that balanced the potential negative effect due to higher amount of RAP containing stiff aged binder. Moreover, the RAP fractioning in two sizes allowed the variability often related to RAP sources to be limited with benefits in terms of the controlling of the grading curve.

## *4.2 Stiffness*

The stiffness properties of the studied mixtures obtained through cyclic uniaxial compression tests for all tested temperatures and frequencies are reported in the Cole-Cole diagram (Fig. 2) in terms of storage ($E_1$) and loss modulus ($E_2$). Figure 2 shows the impossibility of fitting the data using a unique continuous line. Such a tendency demonstrates that the mixtures cannot be considered as thermo-rheologically simple materials. This finding is consistent to what expected since a relevant content of RAP and polymer modified bitumens are used to prepare all mixtures. In fact, as previously demonstrated by other researches, aged and polymer modified bitumens do not follow the Time-Temperature Superposition Principle (Stimilli et al. 2013). However, as long as only the complex modulus norm is evaluated, the Partial Time-Temperature Superposition Principle can be considered valid (Di Benedetto et al. 2011). Thus, the master curves of Fig. 3 were determined at a reference temperature of 20 °C using a four-parameter sigmoidal function as analytical model for |E*| (Pellinen and Witczak 2002) and allowing free variation of the shift factors. Based on Figs. 2 and 3 (average of two replicates), it is possible to observe that, within the temperature/frequency range investigated,

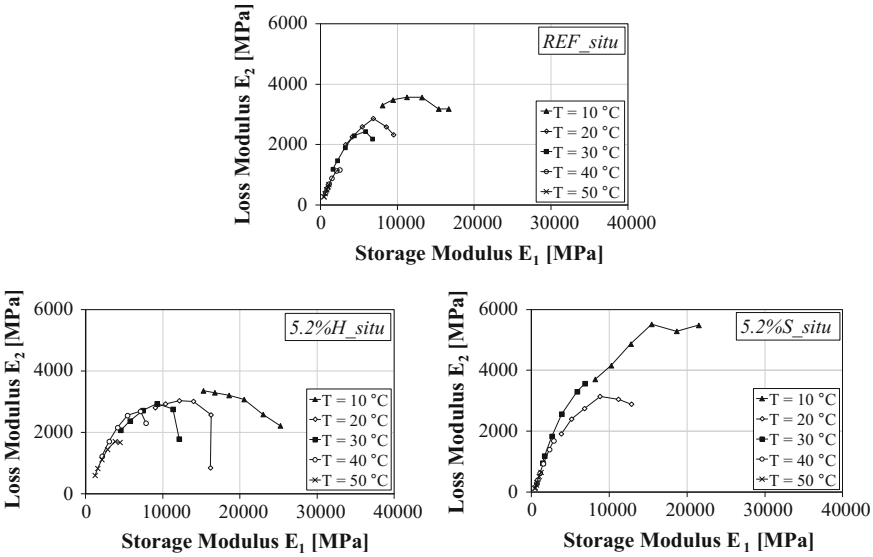


**Fig. 2** Cole-Cole diagrams

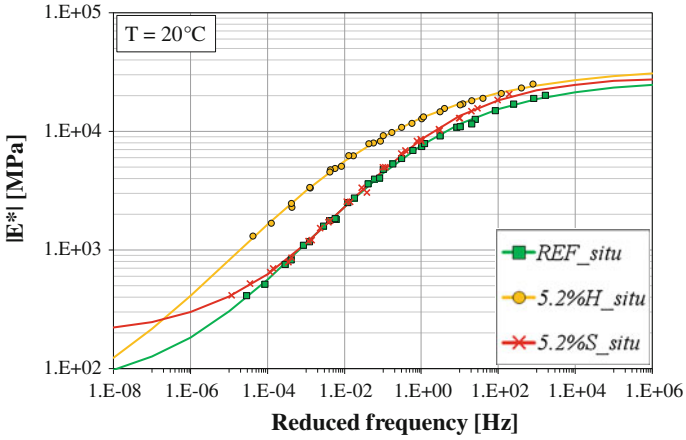


**Fig. 3** |E*| master curves at 20 °C within the temperature range investigated

significantly higher modulus values were measured for the mixture prepared with 40 % of RAP and bitumen H (5.2 *%H_situ*). Since this mixture is prepared with the same type of virgin bitumen used to prepare the reference mixture (*REF_situ*), the stiffening effect observed can be attributed only to the additional 15 % of RAP. As expected, the increment in the RAP percentage caused the presence of higher amount of aged and oxidized bitumen and, consequently, the development of a stiffer asphalt mixture. On the contrary, the use of bitumen S (mixture 5.2 *%S_situ*)

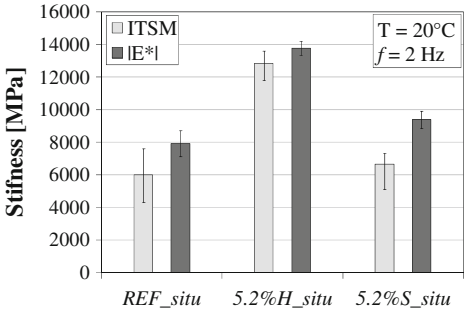


**Fig. 4** |E*| and ITSM @ 20 °C and 2 Hz (equivalent to 124 ms rise time for ITSM) with the standard deviation error bars

appeared to offset the stiffening effect due to the higher presence of milled material. In fact, the mixture 5.2 *%S_situ* was characterized by complex modulus values similar to the reference mixture. The average values of the norm of the complex modulus obtained at 20 °C and 2 Hz were also compared with ITSM values measured at the same temperature and comparable frequency (Fig. 4). Similar results were achieved using the two test configurations, validating laboratory measurements and confirming the observations drawn on the basis of the complex modulus results.

## *4.3 Cracking Aptitude*

Semi-Circular Bending (SCB) tests were performed to assess the cracking aptitude at low temperature in relation to the presence of high amount of RAP. Test data were analyzed in terms of fracture toughness *K*, function of the maximum stress at failure, and total fracture energy G, calculated as the area under the load-displacement curve normalized with respect to the area of ligament that represents the work required to increase the fractured surface until complete failure. Results, as average of four replicates, are summarized in Fig. 5 along with the error bars reporting the maximum and minimum value for each mixture investigated.

The mixture 5.2 *%S_situ* showed the best performance in terms of fracture properties. In fact, it was characterized by the highest *K* and *G* values, hence demonstrating higher resistance to crack initiation as well as ductility. This finding demonstrates that the use of a softer bitumen (low modified) can considerably improve the fracture properties of the material. On the contrary, the use of a high modified bitumen (i.e. bitumen H) combined with high percentage of RAP seems detrimental for the overall ductility of the mixture according to the increase in stiffness recorded for the mixture prepared with bitumen H (see Sect. 4.2). Therefore, it can be stated that additional 15 % of RAP (40 % instead of 25 % for the reference mixture) could even enhance the fracture properties of the mixture if a

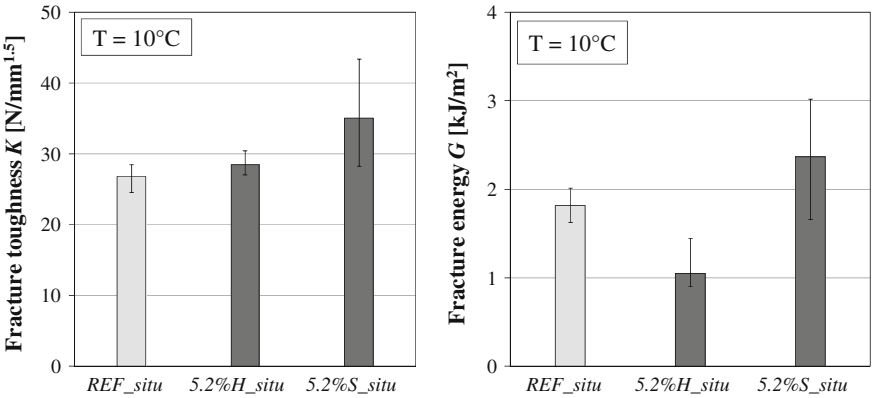


**Fig. 5** Semi-circular bending test results: fracture toughness K (*left*); fracture energy G (*right*)

low modified bitumen is used. Such a bitumen along with the implementation of the Bailey Method for the gradation design and the fractioning of RAP in two sizes compensate the potential negative effect related to the increase in RAP. In addition, the fracture resistance under repeated loading was evaluated through the cyclic indirect tension test. The results are expressed as the number of loading cycles to failure and are depicted in Fig. 6 as a function of the initial maximum horizontal strain ($\varepsilon$) calculated according to BS DD ABF. As expected, the mixture 5.2 % *H_situ* was characterized by lower cracking resistance than the reference mixture. Apparently, the higher stiffness of the 40 % RAP mixture prepared with bitumen H, induces also higher brittleness resulting in worst cracking resistance. At the same time, it is possible to observe that such a behavior associated to higher RAP content can be significantly improved by combining the inclusion of high RAP percentage with a softer bitumen. In fact, the 5.2 *%S_situ* mixture demonstrated the best performance in terms of resistance to repeated loading. These remarks also confirm the findings arising from the SCB tests.

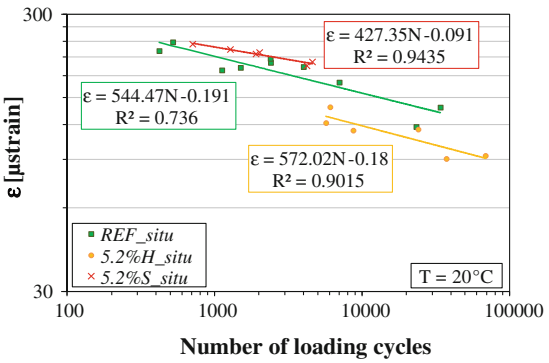


**Fig. 6** Strain versus loading cycles relationship

**Table 3** Creep rate values for the studied mixtures

| Mixture | $f_c$ |
|---|---|
| REF_situ | 7.47 |
| 5.2 %H_situ | 11.99 |
| 5.2 %S_situ | 7.39 |

### 4.4 Permanent Deformation Resistance

The permanent deformation resistance of the studied mixtures was evaluated through cyclic triaxial compression tests. As suggested by the EN 12697-25, the average creep rates ($f_c$) was used to analyze the results. The parameter $f_c$, calculated as the slope of the (quasi) linear part of the least square linear fit, represents the rate of the creep curve (cumulative axial strain vs. number of load application). The lower $f_c$, the higher the permanent deformation resistance. The average results are summarized in Table 3. Despite the presence of a softer virgin bitumen, the mixture prepared with bitumen S showed the best performance in terms of rutting behavior. The $f_c$ value is close to that one found for the reference mixture, demonstrating that in terms of rutting resistance the drawbacks related to the use of a softer bitumen are balanced by the best aggregate packing achieved by applying the Bailey Method (confirmed by CEI values as shown in Sect. 4.1) and fractioning the RAP in two sizes. The performance gap recorded between the reference and the 5.2 *%H_situ* mixture, that showed the worst rutting resistance, is mainly due to the higher bitumen content of the latter material. Considering the same type of bitumen, the higher the bitumen content, the higher the permanent deformation susceptibility. On the contrary, the use of a softer bitumen enhances the compactability aptitude achieving an optimized internal aggregate structure and aggregate packing so much to overcome the effect related to higher bitumen content. In fact, results of a previous image analysis (Stimilli et al. 2014, 2015c) showed that the mixtures prepared with bitumen S were able to achieve the best aggregate packing in terms of proximity zone length and number of contact points between aggregate particles.

## 5 Comparison Between Laboratory and Field Mixtures

As previously mentioned, the mix design followed in plant to produce the mixtures investigated in this research (hereafter named field mixtures) was optimized through a specific laboratory study (Stimilli et al. 2015a). Laboratory and field mixtures were identical in terms of raw materials and mix design, and they were subjected to the same mechanical characterization. Thus, a performance comparison between the field mixtures and the corresponding laboratory mixtures was conducted. Good correlation of the results was found between laboratory and field mixtures confirming the same performance trend, so demonstrating the goodness of the adopted laboratory practices. The laboratory research phase was representative of the real

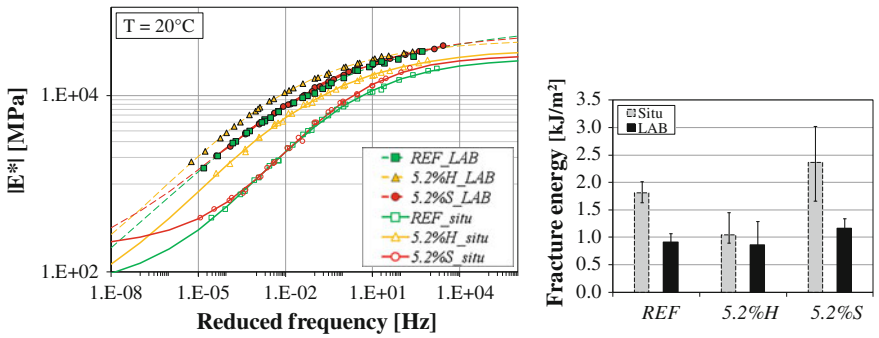


**Fig. 7** Laboratory versus field mixtures: stiffness values (*left*); fracture energy (*right*)

plant conditions and the selected mix design was accurate. Generally, the performance demonstrated by the field and the corresponding laboratory mixtures were comparable. In particular, the laboratory mixtures appeared stiffer as well as more brittle, as demonstrated by the higher stiffness values together with the improved permanent deformation resistance and the worst fracture properties. Just for example, Fig. 7 shows the master curves of E* and the fracture energy of studied laboratory and field mixtures. Such a tendency can be attributed to the more severe aging process (1 h at 160 °C in a force-draft oven) that the mixtures underwent in laboratory after the mixing procedure to simulate the oxidation phenomena related to the transportation and lay down phases (i.e. short term aging). Moreover, it must be taken into account the different production scale of the material. In laboratory the amount of mixture prepared is exactly necessary for the production of one or few samples. Therefore, the whole aggregate area, coated by the bitumen, is exposed to high temperature effects inside the oven, whereas for operational reasons during the in plant production, that involves a large amount of material, this further heating time was not taken into account.

## 6 Conclusions

This paper summarizes the results of an experimental study focused on the volumetric and mechanical properties of hot plant recycled asphalt mixtures. Three experimental sections were realized as part of an Italian motorway rehabilitation project. One reference mixture (25 % of unfractioned RAP, 4.8 % of total binder) and two recycled mixtures (40 % of selected RAP, 5.2 % of total binder) prepared with two different polymer modified bitumens (low and high modified) were investigated. The study aimed at verifying the performance of "real" mixtures directly prepared at the asphalt plant following the mix design optimized through a previous laboratory study. The experimental program carried out included the

evaluation of compactability, stiffness, cracking aptitude and rutting resistance. Experimental results allowed the following main conclusions to be drawn:

- the 40 % RAP mixtures demonstrated better compactability properties;
- all mixtures investigated cannot be considered as thermo-rheologically simple materials due to the presence of aged and polymer modified bitumens. However, the Partial Time-Temperature Superposition Principle allows the construction of the norm of the complex modulus master curve;
- the mixture with 40 % of RAP and the high modified bitumen H was characterized by significantly higher moduli than the reference mixture due to the presence of higher RAP content. However, the use of the low modified bitumen S allowed the compensation of such stiffening effects. However, the rutting resistance of the 40 % RAP mixture prepared with low modified bitumen was comparable with the reference mixture;
- the 40 % RAP mixtures prepared with the low modified bitumen was characterized by improved fracture properties. On the contrary, the combination of the high modified bitumen and high RAP contents (i.e. 40 % RAP) appeared detrimental in terms of cracking resistance and ductility.

The overall experimental results confirmed that mixtures including 40 % of RAP can behave as well as (or even better than) the reference mixture if a low modified bitumen is used. Particular attention must be focused on the aggregate gradation and the virgin bitumen type that can significantly alter the internal aggregate structure and aggregate packing with consequences on the overall mixture performance. In particular, the implementation of the Bailey Method to optimize the mix design and the fractioning of RAP in two sizes compensate the potential drawbacks related to the increase in RAP percentage and guaranteed good performance both at high and low temperature. The use of a softer virgin bitumen is therefore recommended to achieve enhanced overall performance. Finally, good correlation of the results was found between laboratory and field mixtures.

**Acknowledgments** This research was sponsored by Pavimental SpA. This support is greatly acknowledged. Data analysis and opinions are those of the authors and do not necessarily reflect those of the sponsoring agency.

## References

Aurangzeb, Q., Al-Qadi, I. L., Abuawad, I. M., Pine, W. J. & Trepanier, J. S. 2012. Achieving Desired Volumetrics and Performance for High Rap Mixtures. Trans Res Rec 2294:34-42.

de la Roche, C., Van de Ven, M., Planche, J.P., Van den Bergh, W., Grenfell, J., Gabet, T. et al. 2013. Hot Recycling of Bituminous Mixtures. In M.N. Partl, H.U. Bahia, F. Canestrari, C. de la Roche, H. Di Benedetto, H. Piber & D. Sybilski (eds) State-of-the-Art-Reports 9: Advances in Interlaboratory Testing and Evaluation of Bituminous Materials:361-428. Springer.

Di Benedetto, H., Sauzeat, C., Bilodeau, K., Buannic, M., Mangiafico, S., Nguyen, Q. T., Pouget, S., Tapsoba, N. & Van Rompu, J. 2011. General overview of the time-temperature superposition principle validity for materials containing bituminous binder. Int J Roads Airp 1(1):35-52.

Frigio F., Pasquini, E. & Canestrari, F. 2014. Laboratory Study to Evaluate the Influence of Reclaimed Asphalt Content on Performance of Recycled Porous Asphalt. JOTE 43(6).

Kandhal, P.S. & Mallick, R.B. 1997. Pavement Recycling Guidelines for State and Local Governments Participant's Reference Book. FHWA Final Report SA-97.

Mahmoud, A.F.F., & Bahia, H.U. 2004. Using the gyratory compactor to measure mechanical stability of asphalt mixtures. Wisconsin Highway Research Program WHRP 05-02 (0092-0102).

Pellinen, T.K. & Witczak, M.W. 2002. Stress Dependent Master Curve Construction for Dynamic (Complex) Modu-lus (with Discussion). J Assoc Asphalt Pav Tech 71:281–309.

Shirodkar, P., Mehta, Y., Nolan, A., Sonpal, K., Norton, A., Tomlinson, C., Dubois, E., Sullivan, P. & Sauber, R. 2011. Study of determine the degree of partial blending of re-claimed asphalt pavement (RAP) binder for high RAP hot mix asphalt. Constr Build Mater 25:150-155.

Stimilli A., Ferrotti G., Graziani A. & Canestrari F. 2013. Performance evaluation of cold recycled mixture containing high percentage of reclaimed asphalt. RMPD, 14:149-61.

Stimilli, A., Ferrotti, G., Conti, C., Tosi, G. & Canestrari F. 2014b. Chemical and rheological analysis of modified bitumens blended with "artificial reclaimed bitumen". Constr Build Mater 63:1-10.

Stimilli, A., Radicioni D., Ferrotti, G. & Canestrari F 2015a. Performance evaluation of hot recycled mixtures containing SBS modified binder, Proceedings of 6th ICONFBMP, Thessaloniki.

Stimilli A., Virgili A., Canestrari F 2015b. Original Method for Quantifying the "Re-Activated" RAP Binder in Recycled HMA, RMPD – Special Issue.

Stimilli A., Canestrari F., Teymourpour P., Bahia H.U 2015c A. Low-Temperature Mechanics of Hot Recycled Mixtures through Asphalt Thermal Cracking Analyzer (ATCA), Constr Build Mater 84:54-65.

Vavrik W.R., Huber G., Pine W.J., Carpenter S.H., Bailey R. 2002. Bailey Method for Gradation Selection in HMA Mixture Design. Transp Res Circular number E-C044, Transportation Research Board.

# Evaluation of a 100 % Rap Recycling Project in Fort Wayne, Indiana

**Geoffrey M. Rowe, John Barry and Ken Crawford**

**Abstract** A project site investigation involving a high RAP (close to 100 %) recycling has been evaluated to determine the performance differences with a control section, located in Fort Wayne, Indiana, one year after construction. The analysis involved cutting cores from the surface and determining recovered binder properties and mixture physical properties. Binder properties included standard PG grading in accordance with AASHTO M320 and the development of full master curves over the range of temperatures −30 to +80 °C. From the master curve analysis was conducted to look at parameters such as cross-over frequency, rheology index and viscos-elastic transition temperature. The data from this testing has been used in a manner to judge the effectiveness of a recycling oil, particularly when inspecting the relationship between cross-over frequency and rheological index. Mixture testing included evaluation of strength properties by conducting tests in bending beam rheometers and the development of mixture master curves. At the current time little difference is seen in the performance of the 100 % RAP section compared to the control section, which provides significant support for continuing the effort to develop technologies for high percentage RAP recycling projects.

**Keywords** Recycling · RAP · Rejuvenation · Rheology

G.M. Rowe (✉)
Abatech, Perkasie, PA, USA
e-mail: growe@abatech.com

J. Barry · K. Crawford
Crowley Chemical Company, New York, NY, USA
e-mail: jbarry@crowleychemical.com

K. Crawford
e-mail: kjjcrawford@gmail.com



F. Canestrari and M.N. Partl (eds.), *8th RILEM International Symposium on Testing and Characterization of Sustainable and Innovative Bituminous Materials*, RILEM Bookseries 11, DOI 10.1007/978-94-017-7342-3_75

## 1 Introduction

The recycling of HMA has been occurring for well over 40-years. However, due to changes in bitumen economic and environmental factors the need to recycle higher amounts of material has been increasing. The price of binder generally now tracks with other fuel commodities and the costs have risen significantly in the past years. In addition, with the increased environmental stewardship and factor such as taxes for extraction of aggregates and costs associated with disposal (if dumped) results in significant savings as the percentage of recycled material increases. This paper presents some of the trends that have been taking place in recycling in the USA and presents some of the developments that have been taking place in recent years with a high RAP hot-mix asphalt (close to 100 % RAP)—termed HyRap®.

Recycling percentages in HMA vary by state and location dependent upon local specifications. It should be noted that each state department of transport (DOT) sets its own policies with regard to the percentages of recycled asphalt pavement (RAP) that is allowed in HMA. This combined with the various toll-road authorities and other organization with responsibility for highways results in some significant variability in specifications.

Asphalt mixture designs containing RAP follows the AASHTO M-323 standard that deals with "Superpave Volumetric Mix Design." This document notes that if the RAP content is less than 15 % then no change in the binder selection is made. Above 15 % and below 25 % the recommendation by AASHTO is to use a grade softer binder. If 25 % or greater rap is used then the recommendations from blending charts would be needed. These recommendations have been in place since the late 1990s. In the current version of AAHSTO M323 the RAP content is simply expressed as a percentage. However, a proposal from the Mixture Expert Task Group is that the RAP percentage should be changed to express the content as a RAP Binder Ratio (RAPBR) within the specifications rather than the percentage of RAP when considering the need to adjust the binder grade. This places emphasis on the binder content within the RAP rather than just the percentage of RAP and should be implemented within the specifications over the next couple of years. In practice several of the State DOTs have already changed the measurement to RAPBR instead of percent RAP. At the higher RAP contents (>25 %) M323 requires a binder extraction to determine the "true" PG grade of the RAP binder. Extraction and recovery of asphalt binder is time consuming and involves hazardous chemicals creating a technical barrier for the use of higher amounts of RAP. Currently, little use is made of the extraction-recovery process; instead state specifications generally have been modified to allow use of a softer grade of asphalt binder to a higher RAP rate. The highest such upper limit has been set at 40 %.

Of course it is important to ensure that the RAP mix will have a binder blend with the correct rheology to function over the range of high and low temperature experienced by the pavement. The Indiana DOT performed two studies prior to setting new RAP binder selection grades (Beeson et al. 2011; McDaniel et al. 2012). In the first numerous stockpiles of RAP were sampled and the asphalt binder

was recovered to inventory grades of asphalt binder. Second a series of plant mixes were produced for mixtures containing up to 40 % RAP. On the basis of these studies INDOT changed the specification to allow no change of asphalt binder grade up to 25 % RAP and lowering of one grade (high temperature and low temperature) if RAP is greater than 25 % but no more than 40 %.

## 2 Black Rock or Usable Binder

One of the questions that have resulted in significant discussions is—does the binder act in a functional manner or is RAP purely "black rock." This aspect has been studied in practice by three different types of studies. These are: (1) evaluation of RAP mix stiffness properties; (2) assessment of RAP binder diffusion; and (3) determination of RAP mixture fracture properties.

In RAP mix stiffness evaluation, the predicted versus estimated complex dynamic stiffness modulus, E* of the mixture are determined. The measured results are compared to that which would be predicted from the recovered binder and aggregate properties (volumetric proportions) using the Hirsch model developed by Christensen et al. (2003). In this procedure first a complex dynamic modulus mastic curve (E*) is constructed for a mixture and then using the Hirsch relationships the binder stiffness is estimated for the blend of RAP and virgin binder. The back-calculated complex shear modulus, G*, values for the binder are then compared to those for conventional binder (containing no RAP binder) (West et al. 2013; Rowe 2012). While this method has been used to assess the incorporation of RAP binder, the changes in performance during early life (Kriz 2014) make this procedure somewhat problematic in that the degree of co-mingling of the binder can change.

The mixing of new binder with existing binder can be considered as a diffusion problem which is time and temperature dependent. Work conducted by Kriz (2014) suggests that the diffusion occurs at different rates during the early life of an asphalt mixture. The most rapid diffusion occurs while the mix is hot during the mixing and compaction process and then slows down as the mix cools. Diffusion continues during service but at a significantly reduced rate. The time for complete diffusion of a RAP binder with a new virgin binder following mixing, laydown and placement could be nearly immediate to a few months or even years depending on the thermal history provided. Kriz (2014) also noted that the effective viscosity of the blend was lower in the condition where complete diffusion had not occurred which would result in a less stiff material than would be estimated from a complete blending estimation—typically associated with the blending of recovered binders.

The evidence suggests that a large volume of the binder in the RAP can be considered as functional binder although some of the absorbed binder and/or heavily oxidized binder does not completely re-blend. The blending, while not immediate, generally appears to be relatively complete after a few months. However, effective performance is considered key, and currently most DOTs are keen for mixture tests such as those that will evaluate the fracture properties after

the material has been mixed. While this only evaluates limited conditions it is seen as a way of ascertaining the product quality and performance at the production and lay-down stage using equipment and procedures that can be easily incorporated into project specifications. Methods being considered for fracture evaluation include tensile tests, bending beam fatigue (AASHTO M321), the Texas Overlay Tester and other measures of fracture properties.

## 3 Binder Rejuvenation

Binder rejuvenation has been applied since the 1970s. While the use of softer binder grades as discussed above is used in the majority of the US market we note that the rejuvenation is now part of the process commonly used with RAP mixtures with many rejuvenators in the market place.

As binders age absorption and oxidative reactions result in significant changes to both physical and chemical properties. The changes in physical properties can be captured by conducting rheological studies of the binder. Two major effects occur, the binder hardens and the relaxation properties change consistent with the binder oxidizing. The change in rheology can be accessed via determination of the "Rheological Index" (Christensen and Anderson 1992; Rowe 2014) and the hardening can be assessed by determination of the frequency at which the phase angle is 45° at as standard temperature—often termed the crossover frequency, see Fig. 1. If we express the CA model as:

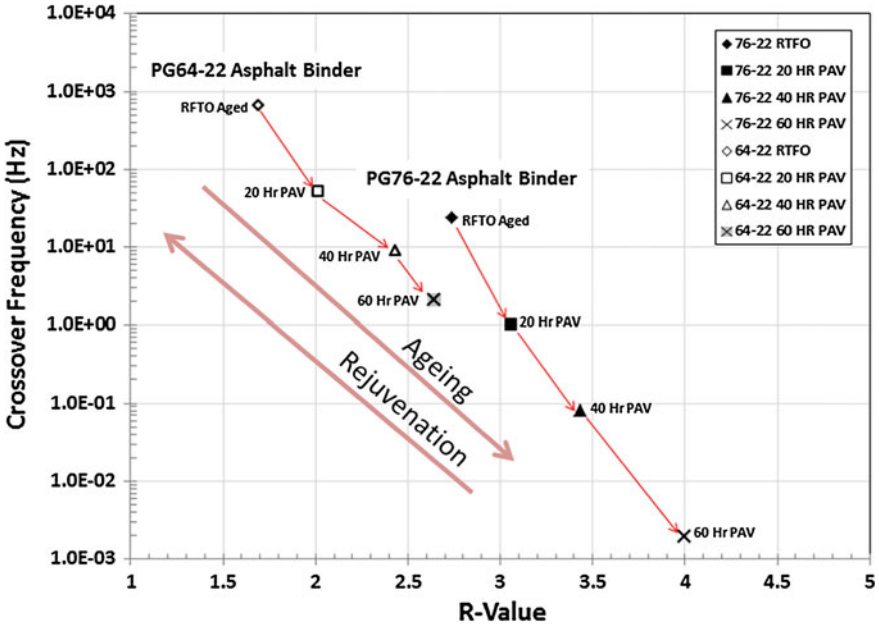


**Fig. 1** Changes to R-value and Crossover frequency during aging (after Bennert 2014)

$$G^*(T, \omega_r) = G_g\left[1 + \left(\frac{\omega_c}{\omega_r}\right)^{\beta}\right]^{\frac{-\kappa}{\beta}} \quad (1)$$

where:

| | |
|---|---|
| $G^*(T, \omega_r)$ | complex shear modulus at temperature ($T$) |
| $G_g$ | glassy modulus |
| $\omega_c$ | cross over frequency |
| $\omega_r$ | reduced frequency of interest |
| $\beta$ and $\kappa$ | fitting parameters |

When expressed in this form the "Rheological Index" or $R$ value as used in the original Christen-Anderson model is equal to (log 2)/$\beta$. If the temperature susceptibility parameters are defined with a master curve then typically either a WLF or a modified Kaelble will provide the best fit to the data (Rowe and Sharrock 2011). Since a Kaelble defaults to a WLF when data only occurs above the defining temperature this relationship is more universal in dealing with the full temperature range and consequently this method is used in developing expressions since it is more inclusive of data types. The modified Kaelble is defined as follows:

$$\log a_T = -C_1\left(\frac{T - T_d}{C_2 + |T - T_d|} - \frac{T_r - T_d}{C_2 + |T_r - T_d|}\right) \quad (3)$$

where:

| | |
|---|---|
| $T_d$ | defining temperature for inflection point |
| $T_r$ | reference temperature |
| $C_1$ and $C_2$ | fitting constants |

where the reduced frequency is expressed as:

$$\omega_r = \log a_T \times \omega \quad (\omega = frequency) \quad (4)$$

Mookhoek (2013) made use of rheological data when evaluating materials with a Black space plot of G* versus phase angle (δ). He commented about RAP mixes he evaluated that damage levels can be described by the Glover–Rowe function which describes the relationship between G* and δ. This type of evaluation has been used by several researchers recently to explain a non-load associated distress in asphalt binders since it effectively characterizes the stiffness and relaxation properties (King et al. 2012). In addition, it will be one of the methods considered in the project being conducted by Texas A&M University considering these materials (NCHRP 9-58 Effects of Recycling Agents on Asphalt Mixtures with High RAS and RAP Binder Ratios) (Daniels 2014). The cracking potential of three asphalt binders are shown at four different conditions in Fig. 2. As the binders are subjected to greater ageing they approach a region in the Black space plot shown as the damage zone.

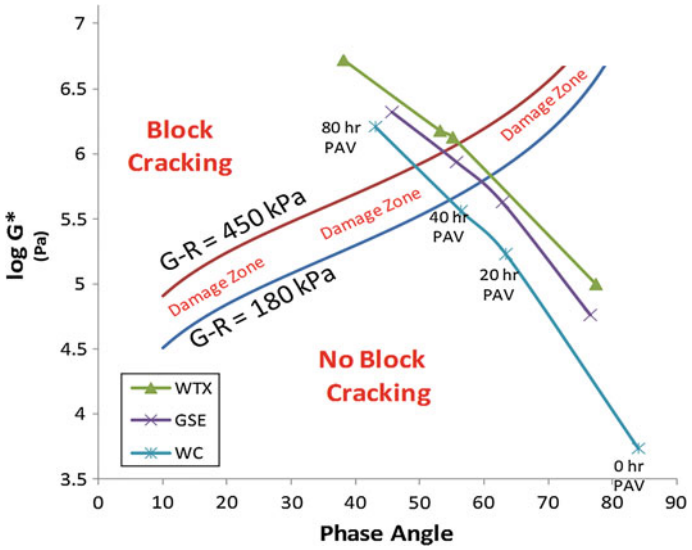


**Fig. 2** Characterization of cracking potential by the Glover-Rowe parameter within a Black-Space plot

Results below this region generally show little or no cracking whereas results above this region are generally associated with cracked pavements.

This approach is similar in concept to the understanding that is obtained by inspecting the $G^*_{VET}$ versus VET temperature that has been used to evaluate the performance of binders in the UK (Widyatmoko et al. 2004). A direct correspondence exists between the VET parameters and those of the Christensen-Anderson (CA) model has been demonstrated (Rowe 2014).

## 4 Improvement in Mix Design

The concept of a balanced mix design approach has been implemented in several projects following completion of a research study by Zhou et al. (2013). In this method the asphalt binder, aggregate and RAP are first combined in a manner that meets the requirements of a standard such as M323 in which gradation and binder properties are satisfied. The compaction to maximum density is checked to ensure that the mixture does not produce less than 2 % air voids (or is less than 98 % of the theoretical maximum density).

Two performance tests are used which relate to deformation/moisture damage and cracking propensity which are the Hamburg Wheel Tracking Test and the Texas Overlay tester respectively. A typical mix design requirement may be <0.5 in.

in the Hamburg device and >300 cycles in overlay tester. These tests are performed on specimens compacted to a nominal 7 % air void content whereas the volumetric evaluation produces void contents associated with a given number of gyrations used for conventional mixtures within that region. Each of these criteria results in allowable binder content and the design binder content is taken as the lowest binder content for cracking resistance or the highest binder content for rutting resistance. Zhou et al. (2013) did note that in some cases that the cracking criteria initially proposed had to be relaxed in designs. However, these mixes still seemed to perform better or equal to conventional mixes. If a similar scheme is implemented in other areas then the test types may change based upon the local experience of a particular agency with materials in a given region.

## 5 High Rap Mixes

HMA with high rap contents (above 75 %) have been used in the USA for a number of years in either an experimental or pioneering manner. For example a technology called CYCLEAN was implemented in the Los Angeles area of California in 1988 (Martin 1992) and was manufacturing high 100 % RAP mixtures with an oil-based rejuvenating agent added to restore flexibility to the asphalt binder (Environment and Energy Management, EPRI Industrial Program 1992). More recently other technologies have been implemented that produce mixtures to high standards with consideration of more modern design methods such as that with AASHTO M323. An example of a recent innovation in this area is the HyRap® process implemented in Fort Wayne, Indiana (Gallivan 2013). In this process fractionated RAP (FRAP) is fed through multiple entry points in a drum mix plant which has been specially modified to minimize the production of smoke from flame contact with the old RAP binder (see Fig. 3).

This plant has been in use for several years and recently Rowe et al. (2013) reported on the performance of Eggeman Road project in the area (see Fig. 4) which was cored for samples after a year in service. The roadway was originally repaved in August 2012 whereas coring took place in April 2013. At the time of construction no difference was observed between the performances of the HyRap materials versus the control sections placed. Five locations were evaluated and from each location 5 cores were taken in a line so that each core would have a similar void content and effects of any transverse variability would be minimized.

Test conducted on the cores including mixture volumetrics, binder and mix properties. The binder properties included evaluation of the master curves as shown in Fig. 5. In this testing it was not possible to distinguish between the performance of the binders and further calculations of the R-value and cross-over frequency confirmed that no significant difference existed between the Control and HyRap sections which suggested that the rejuvenator used had restored the binder. Testing of the complex modulus of the mixture also showed similar results for all the locations.

**Fig. 3** Plant used in Fort Wayne, Indiana to produced 100 % RAP mixes (after Gallivan 2013)

**Fig. 4** Eggeman road, Fort Wayne, Indiana—shortly after construction with overly containing 100 % recycled asphalt

In addition to stiffness testing the tensile strength was also evaluated. This testing was conducted on a small beam cut from the cores and done at a temperature that would result in a brittle type fracture. This revealed slightly higher strengths for the HyRap sections. However, when this was contrasted to the marginally lower void contents of these sections the performance became indistinguishable as shown

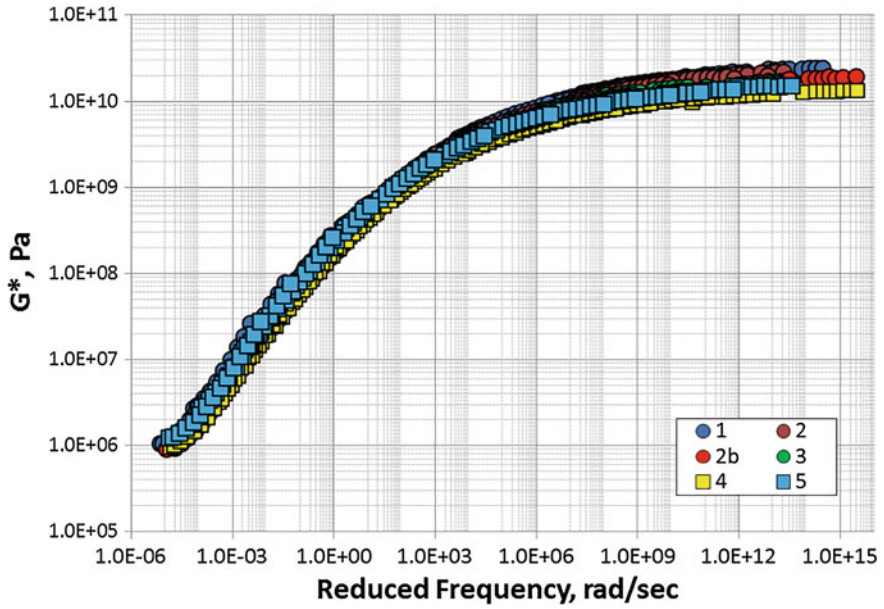


**Fig. 5** Master curves of complex modulus, G*, of the binder recovered from mix samples after one year of service ($T_{ref}$ = 25 °C)—references 1–3 are HyRap sections whereas 4 and 5 are the Control sections

in Fig. 6. This road was inspected again in June 2014 and the spring of 2015 and with the exception of some very minor distress the road appears to be functioning very well.

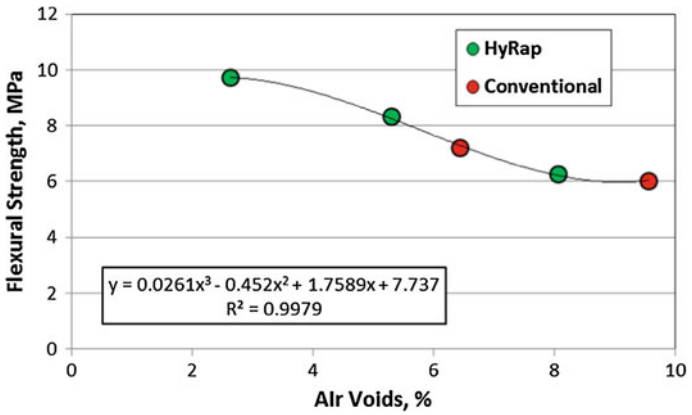


**Fig. 6** Relationship between air voids and flexural strength

## 6 Summary

The discussion in this paper provides a view on some of the implementation of RAP mixes in the USA. The use of RAP is common place. The emergence of technologies to produce high RAP mixtures is also gaining some momentum with several plant manufactures offering options for equipment that will produce mixtures with greater than 70 % RAP content.

In the design of RAP mixtures it is important to consider the binder properties that will be achieved over the full range. In the USA this is done by considering the AASHTO M320 specification properties and ensuring that high, low and intermediate properties are all satisfied when designing a RAP mixture. This is critical to ensure the range of rheological parameters for performance is obtained and to prevent early life cracking.

The concept of a balanced mix design ensures that adequate properties will be achieved for the major distress modes that affect a pavement structure and places an emphasis on the physical properties of the RAP mix rather than compliance with recipe specifications. This approach has already been shown to reduce the occurrence of cracking in some projects in Texas and shows significant promise for future implementation.

The use of high RAP mixtures have been evaluated for an example project in Fort Wayne, Indiana has illustrated that identical performance can be obtained when compared to conventional mixtures. The use of asphalt mixtures containing greater than 70 % RAP is occurring with a number of different manufactures in several USA states. This type of technology is being evaluated by various agencies and will continue to be implemented as plants and technologies improve over the years.

Environmental stewardship and economic cost savings will result in a continued use of RAP and while this type of mix was once a rarity in the asphalt industry it has now become common place along with the need for technologists to understand how these materials behave.

**Acknowledgments** The contributions made by Drs. Jo. Daniels and Tom Bennert of the University of New Hampshire and Rutgers University have been a great help to the formulation of the discussion presented in this paper. In addition, the encouragement of Mr. Lee Gallivan of the Federal Highways is acknowledged and his support for the innovation in this area of technology. Finally, the contributions of Mr. John Brooks who committed to the significant capital investment of the plant and equipment in Indiana—without whom none of this development work with HyRap would have been possible and the staff of the City of Fort Wayne for allowing trials of materials on their road network.

## References

Beeson M, Prather M and Huber G (2011) Characterization of Reclaimed Asphalt Pavement in Indiana: Changing INDOT Specification for RAP. Transportation Research Board Meeting, Washington, DC.

Bennert T (2014) Personal communications. Rutgers University, New Jersey, 2014.
Christensen, D.W. and Anderson, D.A., "Interpretation of Dynamic Mechanical Test Data for Paving Grade Asphalt," Journal of the Association of Asphalt Paving Technologists, Volume 61, 1992, pp. 67-116.
Christensen DW, Pellinen T and Bonaquist RF (2003) Hirsch Model for Estimating the Modulus of Asphalt Concrete. Journal of the Association of Asphalt Paving Technologists.
Daniels J (2014) NCHRP 9-58 Effects of Recycling Agents on Asphalt Mixtures with High RAS and RAP Binder Ratios. September Binder/Mixture ETGs.
Environment & Energy Management, EPRI Industrial Program (1992) Microwave Process for Asphalt Pavement Recycling. Techapplication, Issue No. 2.
Gallivan V (2013) Status of Reclaimed Asphalt Pavement use in North America. HighRAC Workshop, TU Delft, Netherlands.
King GN, Anderson RM, Hanson DI and Blankenship PB (2012) Using Black Space Diagrams to Predict Age-Induced Cracking. 7th Rilem International Conference on Cracking in Pavements, Delft NL.
Kriz P (2014) Asphalt Diffusion. 59th Canadian Technical Asphalt Association Annual Conference, Winnipeg, Manitoba, Canada, November, 2014.
Martin H (1992) Facility Allows City to Recycle Its Roadways: Environment: Thanks to L.A.'s Pacoima asphalt treatment plant, fewer highways end up down in the dumps. Los Angeles Times, November 2nd, 1992.
McDaniel R, Shah A, Huber G and Copeland A (2012) Effects of Reclaimed Asphalt Pavement Content and Virgin Asphalt Binder Grade on Properties of Plant Produced Mixtures," Journal of Road Materials and Pavement Design, Volume 13, No. S1, pp. 161-182.
Mookhoek SD (2013) PMB properties in 2LPA, The effect of ageing on raveling resistance. HighRAC Workshop, TU Delft, Netherlands, June 4th, 2013.
Rowe G.M (2014) Interrelationships in Rheology for Asphalt Binder Specifications.59th Canadian Technical Asphalt Association Annual Conference, Winnipeg, Manitoba, Canada, November 2014.
Rowe GM (2012) Rheology considerations for recycled and recovered binder. Presentation at the Pavement Performance Prediction Symposium - Binder Issues Affecting the Durability of RAP and WMA Pavements, Research Institute, Laramie, Wyoming, July 12th 2012.
Rowe GM and Sharrock MJ (2011) Alternate Shift Factor Relationship for Describing Temperature Dependency of Viscoelastic Behavior of Asphalt Materials, Transportation Research Record, Journal of the Transportation Research Board, No. 2207.
West R, Willis JR and Marasteanu M (2013) Improved Mix Design, Evaluation, and Materials Management Practices for Hot Mix Asphalt with High Reclaimed Asphalt Pavement Content. NCHRP Report 752, National Cooperative Highway Research Program.
Widyatmoko I, Elliott RC and Heslop MW (2004) Mapping Crack Susceptibility of Bituminous Materials with Binder Durability. 5th International RILEM Conference, Limoges, France.
Zhou F, Hu, S and Scullion T (2013) Balanced RAP/RAS Mix Design and Performance Evaluation System for Project-Specific Service Conditions. Report 0-6092-3, Texas A&M Transportation Institute.

# Hot Recycling of Reclaimed Asphalt Using a Bio-based Additive

**Andrea Grilli, Edoardo Bocci and Maurizio Bocci**

**Abstract** Hot recycling of reclaimed asphalt (RA) has increasing interest worldwide due to economical and environmental benefits. In particular, the use of RA in place of virgin aggregates reduces of aggregate supply and disposal of RA. Moreover, the hot recycling process allows reusing the aged bitumen from the RA, implying a reduction of the required amount of new bitumen. However, the ageing process, which occurs from the production throughout the service life of the pavement, affects physical and chemical properties of bitumen, determining its hardening. For this reason, when high amounts of RA has to be reused (more than 20 % by aggregate weight), the use of specific additives is strongly recommended in order to reach the desired bitumen properties and consequently to produce an asphalt concrete (AC) with high performance. This experimental project focused on the use of a bio-based additive (A) for the production of an AC for binder course with a high amount of RA. The experimental program consisted of two main phases: the first phase dealt with the mix design of three mixtures containing respectively no RA, 40 % of RA, 40 % of RA treated with A; the second phase aimed at producing and laying down in a trial section selected mixtures for the validation of the full-scale hot recycling process.

**Keywords** Hot recycling · Reclaimed asphalt · Bio-based additive · Asphalt concrete

A. Grilli
University of the Republic of San Marino, Salita Alla Rocca, 44,
47890 San Marino, San Marino Republic
e-mail: andrea.grilli@unirsm.sm

E. Bocci (✉)
eCampus University, Via Isimbardi 10, 22060 Novedrate, CO, Italy
e-mail: edoardo.bocci@uniecampus.it

M. Bocci
Marche Polytechnic University, Via Brecce Bianche, 60131 Ancona, Italy
e-mail: m.bocci@univpm.it



F. Canestrari and M.N. Partl (eds.), *8th RILEM International Symposium on Testing and Characterization of Sustainable and Innovative Bituminous Materials*, RILEM Bookseries 11, DOI 10.1007/978-94-017-7342-3_76

## 1 Introduction

The worldwide diffused maintenance technique, consisting in milling of distressed asphalt layers before overlaying, generates a large amount of reclaimed asphalt (RA) as a product of the milling operation (Bocci et al. 2010).

Since bitumen and mineral aggregates contained in RA still have important residual properties, RA must not be underestimated and demoted to a waste material (Karlsson and Isacsson 2006).

In road construction, RA can be reused by means of cold and hot recycling techniques.

Cold recycling allows reaching the highest amount of RA to be reused. The RA acts as a "black aggregate" because the bitumen is not mobilized and hardly interacts in an efficient manner with the new bitumen (Grilli et al. 2012). Therefore, RA is used as alternative to mineral aggregates.

Although hot recycling generally allows a lower amount of RA to be reused, both mineral aggregates and bitumen contained in RA can be valued (Al-Qadi et al. 2007). Even if the melting of the old bitumen contained in the RA during the AC mixing phase and the blending and the interaction of mobilized aged bitumen with the new bitumen are still phenomena under investigation, a reduction of the required amount of new bitumen for the production of AC is potentially the most ambitious target.

In this case, the maximum amount of RA to be reused in the AC production depends mainly on the heating system of the mix plant facility and on the ability to correct the physical and chemical characteristics of the aged bitumen (Frigio et al. 2014).

When using batch plants, RA can be heated through specific systems as screened-flame burners, double parallel drums and external ring around the dryer. The first technique protects the RA from direct contact with the burner flame. Nevertheless, heating high percentages of RA could cause high emissions of blue smoke that need to be specifically filtered. The second system consists in heating the RA in a separate drum at lower temperatures preventing additional emissions. Even if this facility allows the highest RA amount to be employed, the production economic benefits could be reduced by the additional energy consumption necessary to run the second drum. The ring or double barrel drum, which has concentric drums, with the RA introduced in the annular space between the inner and the outer drum walls (Brown et al. 2009) may represent a good compromise even if the amount of RA to be recycled is limited. Indeed, it does not generate emission-related matters and ensures a cost-effective process.

Considering the characteristics of the aged bitumen, it is well known that the bitumen is subjected to an aging process which causes a progressive change in its physicochemical properties (Stimilli et al. 2014). As a consequence, bitumen in the RA often shows a stiff behavior and reduced coating properties.

Therefore, when using a high amount of RA, the integration of specific additives is strongly recommended to achieve adequate workability and mechanical

performance (Chen et al. 2007; Shen et al. 2007; Grilli et al. 2013; Grady et al. 2014; Severance et al. 2014). Additives should be non-hazardous and stable over a wide range of temperatures, from production to application. In addition, they must not expertise any exudation or evaporation, in order to ensure a good performance over the designed lifetime of the asphalt pavement.

This paper focuses on the use of a specific additive to produce AC using a high amount of RA without scarifying the mix performance and complying with the Italian specifications. The research project included both laboratory and in plant experimentation. After the mix design phase developed in laboratory, a trial section was built on the A14 motorway between Senigallia and Montemarciano (Marche region, Italy).

## 2 Objective and Experimental Program

This paper deals with hot recycling of RA using a bio-based additive (A). The additive is a byproduct from the paper industry derived from pinewood, which through a specific chemical processing, can be use for the production of additives for RA recycling.

This study provides the volumetric mix design of several ACs containing no RA, 40 % RA and 40 % RA plus additive (A), as well as the full-scale validation of the optimum mixtures by means of a trial section built on an Italian motorway. The objective was to evaluate the effectiveness of A to produce AC with high percentages of RA complying Italian specifications (Autostrade per l'Italia 2008; ANAS 2010).

To this aim, the experimental program consisted of two main phases: the first one developed in laboratory and the second one carried out in field.

The first phase dealt with mix design and testing of three mixtures:

- reference AC with no RA (00RA);
- control AC with 40 % of RA, i.e. the aggregate included in the RA was 40 % by granular mixture weight including filler (40RA);
- target AC with 40 % of RA and 6 % of A by aged bitumen weight (40RA6A);

Mixtures were compacted by means of a gyratory compactor (GC) according to EN 12697-31. The mix design procedure consisted in the volumetric analysis of the mixtures, carried out through the following steps:

- selection of an appropriate constituent materials and aggregate gradation;
- production of four mixtures using different bitumen content (4.3, 4.8, 5.3 and 5.8 % by mixture weight). The bitumen contents were chosen to cover the accepted range defined by Italian specification;
- compaction of 3 specimens for each mixture by means of a GC after 200 gyrations, in order to evaluate the overall compaction curve;

- calculation of the bitumen content (optimum bitumen content) that allows 4 % of air voids content ($V_m$) to be obtained after 100 gyrations and checking of $V_m$ at 10 and 180 gyrations to respect the Italian specification;
- checking the Void in the Mineral Aggregate (*VMA*) and Void Filled with Binder (*VFB*) after 100 gyrations.

The mechanical characterization of the designed mixture followed the present protocol:

- production of the mixture using the calculated (optimum) bitumen content;
- compaction of 3 specimens by means of a GC after 100 gyrations and determination of Indirect Tensile Stiffness Modulus *ITSM* (EN 12697-26) and Indirect Tensile Strength *ITS* (EN 12697-23);
- compaction of 6 specimens using the mixture with the calculated (optimum) bitumen content by means of a GC after 50 gyrations. Dividing the 6 specimens into two subsets, one to be tested dry and one to be tested after precondition in water (EN 12697-12), and determination of Indirect Tensile Strength Ratio *ITSR*.

The second phase dealt with the in-field validation through the construction of a trial section. The ACs were produced at a mix-plant and laid down on an Italian Motorway. Two ACs were compared: a mixture currently in use in the selected mix plant which uses 15 % of RA and no additives (15RA), and the most cost-effective mixture from the mix design assessments which contained 40 % of RA and 6 % of A (40RA6A). The comparison included verification of mixture composition (gradation and bitumen content), volumetric and mechanical tests, such as *ITSM* and *ITS*, on cores extracted from the pavement.

## 3 Materials

Virgin limestone aggregates and two fractions of RA were sampled in a selected mix plant and characterized in terms of gradation (Fig. 1). In particular, the RA after bitumen extraction (gradation of the aggregates in the RA) was sieved adopting the wet sieving method. The bitumen content in the RA, measured by mix weight, was 4.6 % in the fine fraction and 3.2 % in the coarse one. In order to optimize plant RA management it was used 2/3 of fine RA and 1/3 of coarse RA for the mix design.

The recovered bitumen from RA showed a penetration of 18 dmm (EN 1426) and a softening point of 75 °C (EN 1427).

The different fractions of RA and virgin aggregates were proportioned in order to obtain gradation curves similar among the different mixtures and inside the reference envelope for a binder course.

The virgin binder was a 50/70 paving grade bitumen with a penetration of 53 dmm and a softening point of 48 °C.

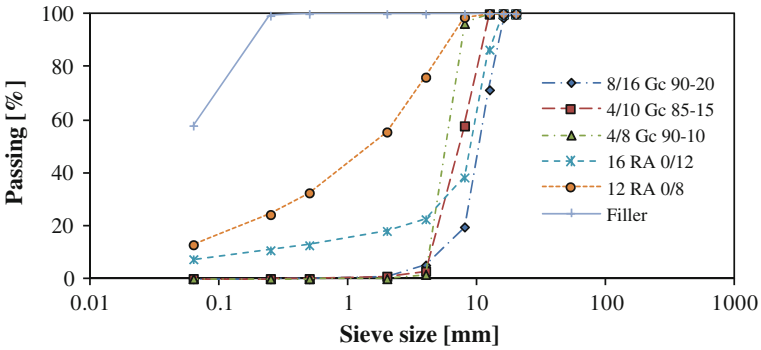


**Fig. 1** Gradation of the aggregate fractions

Based on the penetration and softening point of the bitumen in the RA and through a preliminary investigation on binder viscosity, the optimum content of A was identified to be 6 % by aged bitumen weight.

## 4 Mix Design

The 00RA mixtures, using 4 different total bitumen contents (4.3, 4.8, 5.3 and 5.8 %), were produced mixing virgin aggregate (including filler) and bitumen at 170 °C. For 40RA and 40RA6A mixtures, as the recovered aged bitumen was about 1.7 % by mixture weight, the virgin paving grade bitumen used was 2.6, 3.1, 3.6 and 4.1 %. Simulating the operative process, in this case, 25 % of RA was heated and mixed at 170 °C, whereas 15 % of RA was cold added to the mix.

Figures 2, 3, and 4 show the air voids content as a function of bitumen dosage in order to calculate the optimum bitumen content for the different mixtures.

The optimum (total) bitumen contents, corresponding to 4 % of $V_m$, were found to be 4.8, 5.0 and 4.8 % by mixture weight for 00RA, 40RA and 40RA6A, respectively. Such values allowed to comply with the Italian specifications in terms of $V_m$ at 10 and 180 gyrations ($V_{m,10}$ = 11–15 %, $V_{m,180} \geq 2$ %). In addition, the VMA and VFB limits (Cominsky 1994) were satisfied.

The mechanical characteristics (*ITS*, *ITSM* and *ITSR*) for the designed mixtures produced with the optimum bitumen content are shown in Figs. 5, 6, and 7.

Considering the *ITS* and *ITSM* values, it can be asserted that 40RA6A and 00RA achieved similar results respecting the Italian specification, while 40RA mixture showed the highest values, highlighting a stiffer behavior. Indeed, the 40RA mixture exceeded the *ITS* maximum limit defined by Italian specifications (0.75 MPa ≤ *ITS* ≤ 1.35 MPa), resulting not suitable for road construction.

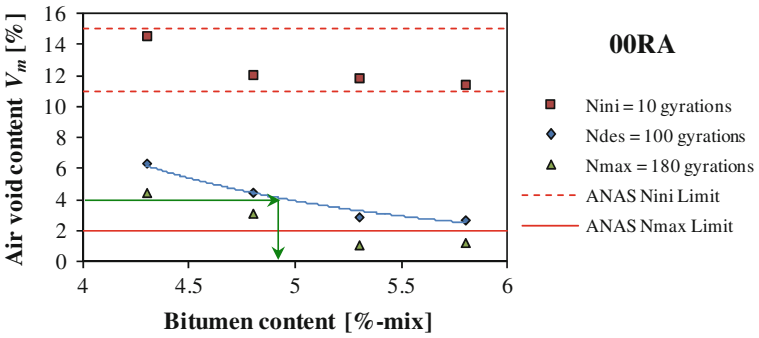


**Fig. 2** Air voids content as a function of bitumen dosage for the 00RA mixture

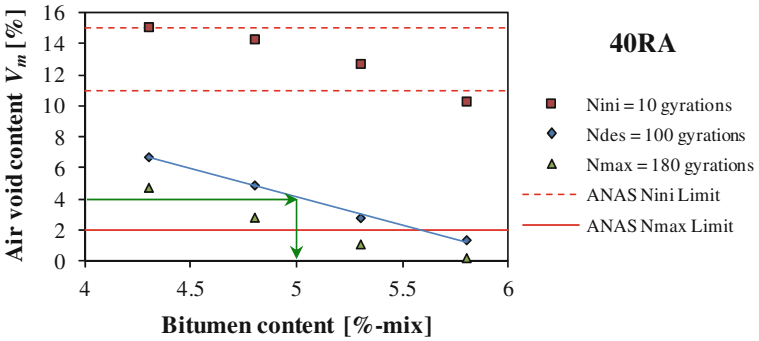


**Fig. 3** Air voids content as a function of bitumen dosage for the 40RA mixture

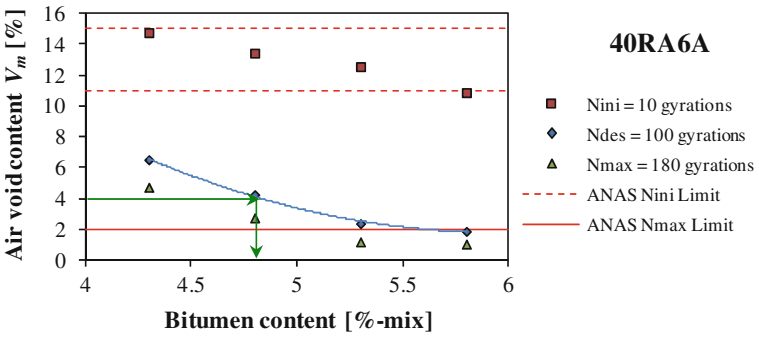


**Fig. 4** Air voids content as a function of bitumen dosage for the 40RA6A mixture

As can be noticed, *ITSR* results did not allow discriminating among mixtures since all mixtures showed no water sensitivity, probably due to the use of limestone virgin aggregates and filler.

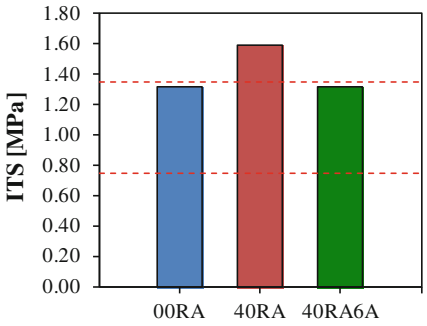


| Mixture | ITS [MPa] | St. Dev. [MPa] |
|---|---|---|
| 00RA | 1.32 | 0.06 |
| 40RA | 1.60 | 0.08 |
| 40RA6A | 1.31 | 0.04 |

**Fig. 5** *ITS* on specimens compacted under 100 gyrations, comparison with Italian specifications

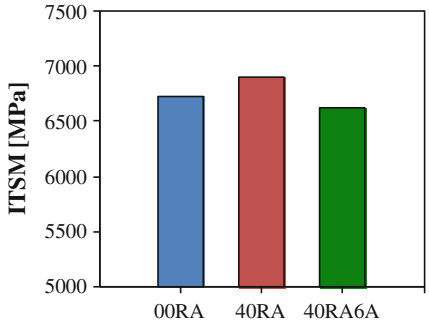


| Mixture | ITSM [MPa] | St. Dev. [MPa] |
|---|---|---|
| 00RA | 6723 | 444 |
| 40RA | 6903 | 354 |
| 40RA6A | 6624 | 118 |

**Fig. 6** *ITSM* on specimens compacted under 100 gyrations

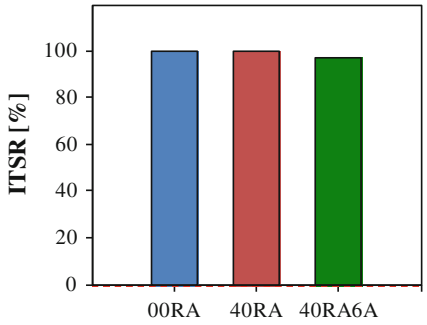


| Mixture | ITSR [%] | St. Dev. [%] |
|---|---|---|
| 00RA | 100.0 | 4.0 |
| 40RA | 100.0 | 7.1 |
| 40RA6A | 97.2 | 10.0 |

**Fig. 7** *ITSR* on specimens compacted under 50 gyrations

Table 1 summarizes the volumetric and mechanical properties of the mixtures with their respective optimum bitumen content.

From Table 1, it can be noticed that the 40RA mixture did not respect the upper *ITS* limit. However, when using a proper dosage of additive A all the volumetric

**Table 1** Characteristics of the design mixtures

| Parameter | **00RA** | **40RA** | **40RA6A** | **Acceptability range** |
|---|---|---|---|---|
| Optimum bitumen content (% by mix) | 4.8 | 5.0 | 4.8 | 4.1–5.5 |
| Virgin bitumen content (% by mix) | 4.8 | 3.3 | 3.1 | – |
| $V_m$ at 10 gyrations (%) | 12.1 | 13.2 | 13.4 | 11.0–15.0 |
| $V_m$ at 100 gyrations (%) | 4.50 | 3.81 | 4.27 | 3.0–6.0 |
| $V_m$ at 180 gyrations (%) | 3.14 | 2.39 | 2.76 | ≥2.0 |
| *VMA* at 100 gyrations (%) | 15.8 | 15.4 | 15.5 | ≥13.0 |
| *VFB* at 100 gyrations (%) | 71.5 | 75.3 | 72.4 | 65.0–75.0 |
| *ITS* at 25 °C (100 gyrations) (MPa) | 1.32 | 1.60 | 1.31 | 0.75–1.35 |
| *ITSM* at 20 °C (100 gyrations) (MPa) | 6723 | 6903 | 6624 | – |
| *ITSR* at 25 °C (50 gyrations) (%) | 100 | 100 | 97 | – |

and mechanical requirements were satisfied, attaining similar results than those of 00RA. Note that 40RA6A allowed a reduction of virgin bitumen compared to 00RA of about 30 % (from 4.8 to 3.1 % by mix weight).

# 5 In-Field Validation

## *5.1 Details of the Trial Section*

The commonly-produced mixture (15 % of RA with no additive) and the most profitable mixture from the mix design assessments (40RA6A) were manufactured in a selected batch plant. This mix plant is equipped with an RA feeding ring installed around the end of the drier, where RA (no more than 25 % by aggregate weight for this specific plant) gets heating before joining the hot virgin aggregates on the buckets in the elevator. Further RA (no more than 15 % by aggregate weight for this specific plant) goes to a specific bin on a scale, before going to the mixing chamber without any previous heating process. In the present study, the 15RA mixture was produced with only cold RA introduction, while 40RA6A mixture included 25 % of hot RA introduction and 15 % of cold RA introduction.

A dosing system was set up in order to add the correct amount of additive to the RA before mixing with aggregate and virgin bitumen.

For 15RA, the RA brought about 0.6 % bitumen by mixture weight and 4.2 % of virgin bitumen was added following the common recipe used by the producer. For 40RA6A, the recycled aggregate brought 1.7 % bitumen by mixture weight, therefore 3.1 % of virgin bitumen was added. Even if a low content of virgin bitumen was used, the 40RA6A showed a good aggregate coating and appeared easy to lay-down and to compact.

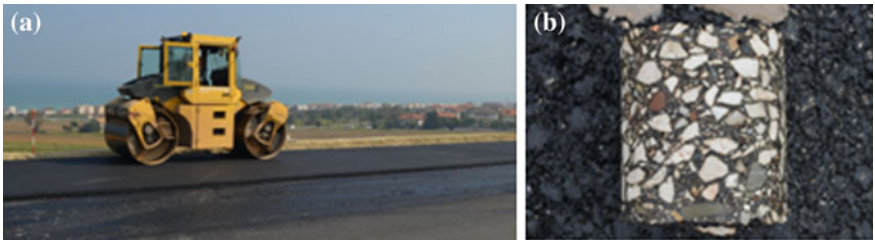


**Fig. 8** In-field validation: **a** compaction of the recycled layer, **b** extracted core

The temperature of ACs, measured directly on the selected trucks after AC discharge at the mix plant, resulted to be 162 and 170 °C for the 15RA and 40RA6A, respectively. The temperature of ACs behind the paver was 146 and 137 °C for the 15RA and 40RA6A, respectively. The ACs were laid down by means of a paver and compacted through a 10 tons double-drum vibratory roller (Fig. 8a). Considering a lane width of 3.50 m, a target density of 2.400 kg/m$^3$ and a layer thickness of 0.05 m (after compaction), one truck (30 t) provided the material to pave a lane length of about 70 m. Cores were extracted 5 days after construction (Fig. 8b).

## 5.2 *Core Analysis*

Table 2 reports the gradation and bitumen content of each mixture. Compared with the optimum bitumen content defined through the mix design, the bitumen content of 40RA6A mixture (4.3 % by weight) was less than the target value (4.8 % by weight).

The 15RA mixture complied with the Italian specification in terms of gradation. While, it can be noticed that the 40RA6A mixture has far lower sand content in comparison with the design gradation established in the mix design. Approximately, the recycled 40RA6A mixture has a lower bitumen content (almost 1 %) and sand content (about 10 %) than the reference mixture. This could be due to the mix plant changing the materials proportions from a 15RA to 40RA mixture in a short period of time for trial purposes, this is not expected to happen in day-to-day continuous production.

Figure 9 shows the volumetric properties of the cores extracted from the trial section. The results demonstrate that both mixtures satisfied the Italian specification in terms of air voids content (3 % ≤ $V_m$ ≤ 8 %) even if the poor bitumen and sand contents influenced the compactability of the mixture with 40RA6A.

The compactability of the mixtures can be also evaluated by means of *VMA* and *VFB*. It can be affirmed that 15RA and 40RA6SR showed similar *VMA* (Fig. 9), though the mixture with 40RA6A showed a lower *VFB* value, obviously related to the poor bitumen content.

**Table 2** Gradation of the mixture from the trial section

| Sieve (mm) | 15RA | 40RA6A |
|---|---|---|
| 12 | 100 | 100 |
| 10 | 71 | 61 |
| 8 | 66 | 56 |
| 4 | 44 | 36 |
| 2 | 30 | 23 |
| 1 | 20 | 18 |
| 0.5 | 15 | 14 |
| 0.25 | 12 | 11 |
| 0.125 | 9 | 8 |
| 0.063 | 6.5 | 6.1 |
| Bitumen (% by mix) | 5.2 | 4.3 |

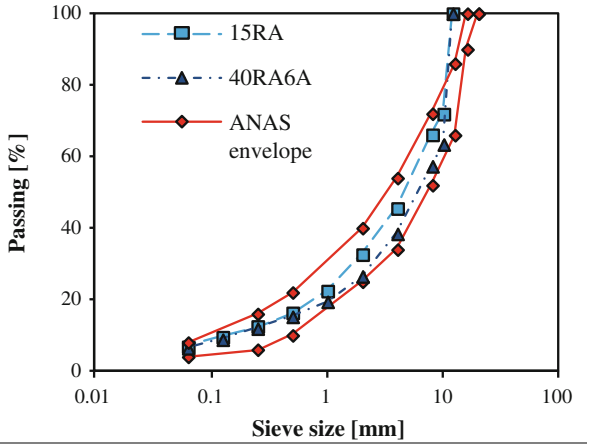


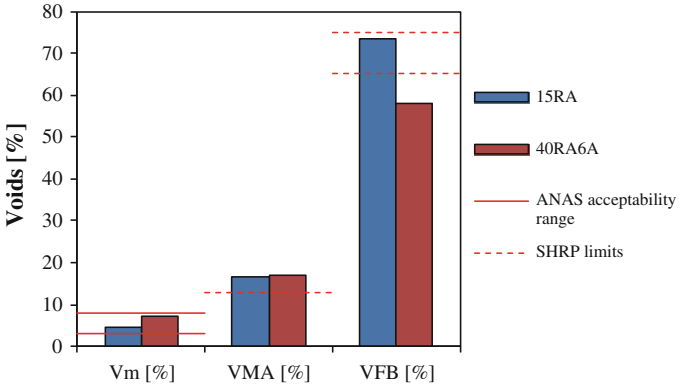


**Fig. 9** Volumetric properties of the cores

The mechanical properties of the cores are plotted in Fig. 10. The *ITSM* values were similar between the mixtures and the small difference should not significantly influence the service life of the pavement. In particular, 40RA6A mixture has higher *ITSM* than 15RA mixture (about 15 %) probably because it contains a lower bitumen content. However, all the *ITSM* values are consistent and respect the common attitude for a binder course mixture.

Also *ITS* results were similar for both mixtures, satisfying the Italian requirements.

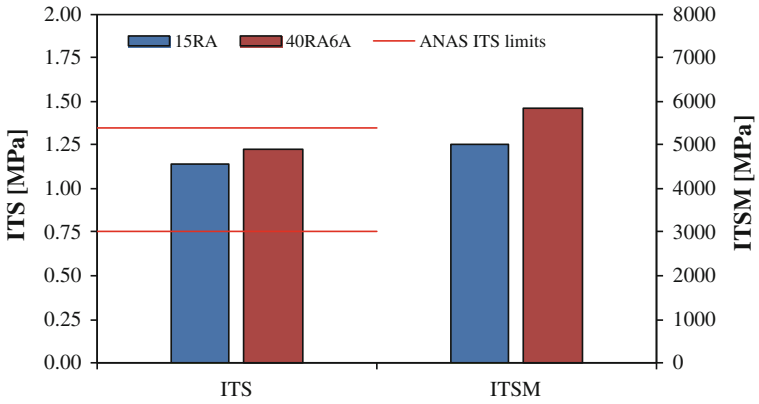


**Fig. 10** *ITS* and *ITSM* values of the cores

## 6 Conclusion

The research project described in the present paper aimed at the use of a specific Bio-based Additive (A) to produce AC using a high amount of RA without scarifying the mix performance and complying with the Italian specifications.

The experimental program consisted of two main phases. The first one focused on mix design of three mixtures containing respectively no RA, 40 % of RA, 40 % of RA treated with A. The second one was intended to the full-scale validation of the recycled mixture through the construction of a trial section comparing the commonly-produced mixture (15 % of RA with no additive) and the most profitable mixture from the mix design assessments (40RA6A).

This study demonstrates that a dosage of 6 % of additive A allowed the AC containing 40 % of RA to comply with Italian specifications in terms of volumetric and mechanic characteristics.

The hot-recycling technique with the additive A required a low amount of new (virgin) bitumen. This issue is particularly significant as it highlights the capability of the additive A to mobilize and restore the RA bitumen, with consequent economical benefits related to the use of a low amount of virgin bitumen.

**Acknowledgments** The Authors wish to thank Arizona Chemical and Pesaresi S.p.A. that provided materials and support to the research project.

## References

Al-Qadi I, Elseifi M, Carpenter SH (2007) Reclaimed asphalt pavement – A literature review. Illinois center of transportation, report No. FHWA-ICT-07-001.

ANAS (2010) Capitolato speciale di appalto, Parte 2ª Norme tecniche per pavimentazioni stradali/autostradali

Autostrade per l'Italia (2008) Capitolato speciale di appalto, parte seconda, opere civili

Bocci M, Canestrari F, Grilli A, Pasquini E, Lioi D (2010) Recycling techniques and environmental issues relating to the widening of a high traffic volume Italian motorway. Int J Pavement Res Tech, 3(4):171-177

Brown ER, Kandhal PS, Roberts FL, Kim YR, Lee DY, Kennedy TW (2009) Hot mix asphalt material, mixture design and construction, Third Edition. NAPA Research and Education Foundation, Lanham (USA)

Chen JS, Huang CC, Chu PY, Liu KY (2007) Engineering characterization of recycled asphalt concrete and aged bitumen mixed recycling agent. J Mater Sci 42:9867-9876

Cominsky RJ (1994) The Superpave mix design manual for new construction and overlays. Washington, DC: Strategic Highway Research Program, SHRP-A-407.

Frigio F, Pasquini E, Partl M, Canestrari F, (2014) Use of reclaimed asphalt in porous asphalt mixtures: laboratory and field evaluations. J Mater Civil Eng 04014211. doi:10.1061/(asce)mt.1943-5533.0001182

Grady W, Silverberg R, Severance R, Porot L, Broere D, Gomes V, (2014) Rejuvenecimiento del ligante viejo para su reutilización en mezclas bituminosas con alta tasa de asfalto recuperable (RA). Jornada Nacional ASEFMA, Comunicación 34.

Grilli A, Graziani A, Bocci M, (2012) Compactability and Thermal Sensitivity of Cement-Bitumen Treated Materials, Road Mater Pavement 13(4):599-617. doi:10.1080/14680629.2012.742624

Grilli A, Bocci M, Cardone F, Conti C, Giorgini E (2013) Laboratory and in-plant validation of hot mix recycling using a rejuvenator. Int J Pavement Res Technol 6(4):364-371. doi:10.6135/ijprt.org.tw/2013.6(4).364

Karlsson R, Isacsson U (2006) Material-related aspects of asphalt recycling: State-of-the-art. J Mater Civil Eng, 18(1):81-92. doi: 10.1061/(ASCE)0899-1561(2006)18:1(81)

Severance R, Porot L, Felipo J, López J, (2014) Empleo de rejuvenecedores en reciclado de mezclas bituminosas. Asfalto Y Pavimentación, 14(4):39-49

Shen J, Amirkhanian S, Miller JA (2007) Effects of rejuvenating agents on superpave mixtures containing reclaimed asphalt pavement. J Mater Civil Eng 19(5):376–384

Stimilli A, Ferrotti G, Conti C, Tosi G, Canestrari F (2014) Chemical and rheological analysis of modified bitumens blended with "artificial reclaimed bitumen". Constr Build Mater 63:1-10. doi: 10.1016/j.conbuildmat.2014.03.047

# Tests Campaign Analysis to Evaluate the Capability of Fragmentation Test to Characterize Recycled Asphalt Pavement (RAP) Material

**D. Perraton, G. Tebaldi, E. Dave, F. Bilodeau, G. Giacomello, A. Grilli, A. Graziani, M. Bocci, J. Grenfell, P. Muraya, M. Pasetto, K. Kuna, A. Apeagyei, D. Lo Presti, G. Airey, K. Jenkins, E. Hajj, M. Hugener and P. Marsac**

**Abstract** Cold and hot recycling of reclaimed asphalt pavement (RAP) is increasingly gaining in popularity worldwide due to the need to increase the sustainability of asphalt pavement, both from environmental and economic perspectives. Despite the increasing of use of these techniques, we are still faced with the problem of correctly characterizing RAP. In the framework of the RILEM TC 237-SIB TG6, a Round Robin Test (RRT) was performed in order to evaluate the capacity of the fragmentation test to characterize RAP materials. A total of 5 laboratories located in 4 different countries were involved in the testing program. This paper focuses on the presentation of the fragmentation test method and the results of the RRT performed on different sources of RAP. To differentiate RAP materials in terms of size alteration vulnerability, fragmentation tests were performed at three different temperatures (5, 20 and 40 °C) on different sources of RAP. Fragmentation testing consists in evaluating the amount of materials passing through a control sieve of a coarse uniform RAP material after a fixed series of strokes carried out with a normalized falling mass. Results show that fragmentation is reduced when the testing temperature increases. Fragmentation tests performed on natural aggregates indicate that they do not vary with the testing temperature, and such test results are a function of the amount of foreign matter in the RAP. The results also show that the test is suitable for differentiating RAP materials from different sources.

Work from RILEM TC 237-SIB, "Testing and Characterization for Sustainable Innovative Bituminous Materials and Systems".

D. Perraton (✉) · G. Tebaldi · E. Dave · F. Bilodeau · G. Giacomello · A. Grilli · A. Graziani
M. Bocci · J. Grenfell · P. Muraya · M. Pasetto · K. Kuna · A. Apeagyei · D. Lo Presti
G. Airey · K. Jenkins · E. Hajj · M. Hugener · P. Marsac
École de technologie supérieure, Montréal, Canada
e-mail: daniel.perraton@etsmtl.ca



F. Canestrari and M.N. Partl (eds.), *8th RILEM International Symposium on Testing and Characterization of Sustainable and Innovative Bituminous Materials*, RILEM Bookseries 11, DOI 10.1007/978-94-017-7342-3_77

**Keywords** Fragmentation · Recycled asphalt pavement (RAP) · Aggregate · Round robin test (RRT)

## 1 Introduction

Incorporating high amounts of RAP into a newly constructed pavement structure can provide major economic and environmental benefits, but this needs to done properly in order to guarantee that the mixtures perform as intended, and consequently, that the pavements will as well. The process requires the realization of a proper mix design, after which materials in agreement with that mix are used. The latter point is what we need to verify and guarantee through quality control, but if it simple with bitumen and aggregates, it is not exactly simple with RAP.

One of the main critical points with using RAP is the grading curve of mixtures. RAP is not always composed of aggregates covered by old bitumen, but rather, it is also composed of conglomerates of small aggregates glued together by mastic produced by the milling machine as it breaks the pavement layers. These conglomerates can be broken during compaction, or, in the case of hot recycling, by the impact with other aggregates during the mixing operation, when the bitumen that binds the agglomerates becomes soft. As recently demonstrated at the University of Florida (Isola 2014), even small changes in the grading curve can have huge impacts on the mixture performance, and as a result, it is extremely important to keep the aggregate sizes and their distribution under control. Because RAP is extreme heterogeneous, this is not a simple challenge, particularly during the quality control phases. The main difficulty lies in the fact that the traditional method used to classify RAP does not involve quick and simple tests that can be used in the laboratory to produce reference values, and in the field to secure fast data that may be compared with those references values.

A potential solution was proposed by Perraton at École de technologie supérieure, requiring the use of fragmentation tests to characterize aggregates (NFP 18-574) for the characterization of RAP materials.

The characteristics of RAP need to be determined in order to enable predictions of influence of the RAP on a new, blended material. Incorporating high amounts of RAP into a newly constructed pavement structure can provide major benefits.

In the framework of the RILEM TC 237-SIB TG6, a protocol for using the fragmentation test on RAP was produced, and an RRT was performed in order to evaluate the capacity of the fragmentation test to characterize RAP materials. A total of 5 laboratories located in 4 different countries were involved in the testing program. This paper focuses on the presentation of the fragmentation test method and on the results of the RRT performed on different sources of RAP. The results shown here fill a gap in existing international standards, as is possible to verify in

the review of international standards made during the activities of TG6 (Tebaldi[a] et al. 2012, Tebaldi[b] et al. 2012, Tebaldi et al. 2014).

## 2 Objectives

When the researchers of Task Group 6 of RILEM TC 237-SIB designed the protocol to use the fragmentation test for RAP characterization they had in mind to define a tool able to provide a quick and clear parameter that can be evaluated on the RAP used for mix design and that can be evaluated on the material used in the field in an amount of time compatible with the times of construction work plan. The goal is to have a quick test able to clearly say that the final gradation of the mix that the contractor is making in the field it is with a certain level of tolerance the same that the mixture made in laboratory during mix design had. The fragmentation test give more information that a simple grading analysis because it take in consideration the changes made by the breaking of conglomerates that are in the RAP. In very simple words the concept that the TG6's researchers wanted to prove it was: if two RAP has the same (or similar) fragmentation characteristic they are similar, if two RAP has different fragmentation test they are different.

Specifically, the goal of RRT shown in this paper is to show that fragmentation test is able to identify if two RAP coming from different sources are different.

## 3 RAP Characteristics and Tested Sample

Each laboratory involved in the RRT selected a local source of RAP, currently used in their country, in order to thoroughly analyze the RAP classification process. Considering the "common" heterogeneity of RAP, the selection of materials for test campaigns was based on the results of an evaluation of this homogeneity that will be performed on the material taken from a stockpile.

In the RRT, the following tests were carried out on each selected RAP collected from laboratories: 1- Analysis of RAP particle size on the material before (black curve) and following (white curve) bitumen extraction; 2- fragmentation test; 3- cohesion test; 4- homogeneity test; 5- RAP particles characterization (shape, texture, absorption and specific gravity), and 6- analysis of recovered binder (binder content, penetration, ring-and-ball test, asphalting). In this paper, only the part dealing with fragmentation results is presented and discussed.

To analyze the RAP particle size, grading analyses were performed on a dried material at 30 °C after washing with water. Table 1 shows the main characteristic of RAP materials tested in the RRT, and Fig. 1 presents the grading curves.

Fragmentation testing was conducted on single size aggregates passing through a specific size sieve, and was retained on the next smallest one in standard order. From each source of RAP materials, different fractions of uniform RAP particles

**Table 1** Summary table of the main characteristics of RAP materials

| | LAB-A | | LAB-B | LAB-C | LAB-D | | LAB-E |
|---|---|---|---|---|---|---|---|
| | RAP-A | RAP-B | RAP-C | RAP-D | RAP-E | RAP-F | RAP-G |
| b (%)[a] | 5.2 | 4.4 | 4.1 | 4.5 | 4.8 | 3.8 | – |
| Pen (0.1 mm) | 7 | 7 | 13 | 18 | 11 | 13 | 33 |
| TR&B (°C)[b] | 77 | 70 | 76 | 66 | 70 | 77 | 56 |

[a]b % = bitumen content—% parts by weight of the mixture
[b]TBA = temperature from the ring-and-ball test

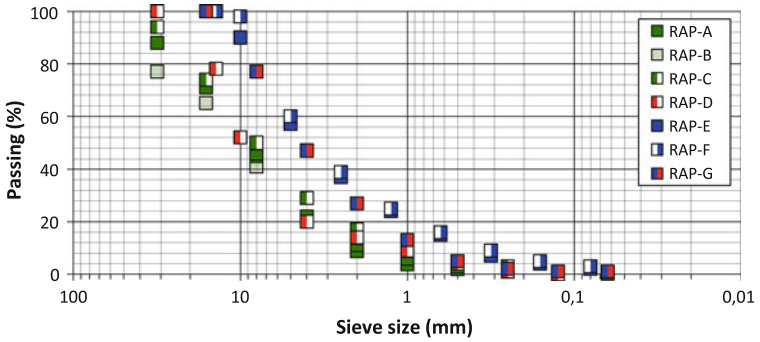


**Fig. 1** Grading curve of RA (*black curve*)

were formed. The RAP material was first dried at 30 °C before each RAP fraction sample was formed. Four fraction groups were considered in this RRT: 20/30, 14/20, 10/14 and 5/10 mm. For each fraction group, all RAP particles were completely retained on the smaller size sieve, but and passed right through the larger size one. For each fraction, we considered that the mean particle size between two consecutive sieves is defined by the following relationship:

$$\text{mean particle size} = \sqrt{\text{size of the sieve “i”} \; x \; \text{size of the sieve “i + 1”}} \quad (1)$$

Based on “Eq. 1”, the mean particle size of fraction groups 20/30, 14/20, 10/14 and 5/10 mm are 24.5, 16.7, 11.8 and 7.1 mm, respectively.

## 4 Testing Procedures

The fragmentation test consisted of an evaluation of the amount of material passing through a control sieve after a fixed series of strokes carried out with a normalized falling mass. In this specific case, the AAHSTO modified Proctor test procedure (ASTM D1557-12 (2012) or AASHTO T180) was adopted to perform a series of

**Fig. 2** Picture of apparatus used by LAB-D to perform fragmentation tests done on a setup based on ASTM D 1557 requirements

**Table 2** Summary of testing procedure used by each laboratory involved in the RRT

| | LAB-A | LAB-B | LAB-C | LAB-D | LAB-E |
|---|---|---|---|---|---|
| Inside mould dia. (mm) | 101.6 | 150.0 | 100.0 | 151.2 | 152.3 |
| Rammer weight (g) | 4535 | 4535 | 4500 | 4535 | 4800 |
| Height of fall (cm) | 45.7 | 45.7 | 45.7 | 45.7 | 45.0 |
| Blows per layer | 56 | 56 | 56 | 56 | 50 |
| Number of layers | 5 | 5 | 5 | 5 | 5 |
| Control sieve (mm) | 1.6 | 1.6 | 1.6 | 1.7 | 1.6 |

tests on different sources of RAP. Figure 2 shows a picture of the apparatus used for the fragmentation testing.

The dynamic fragmentation test measures the particle resistance to fragmentation under a series of shocks induced by dropping a steel mass, called a rammer, on a confined sample placed in a steel cylindrical mould. The material crushed to sizes finer than a control sieve is separated and expressed as a percentage of the original weight taken in the mould. The percent passing through the control sieve PCS (%) is noted. Table 2 presents all details regarding the testing procedure followed by each laboratory participating in the RRT.

The fragmentation tests were performed at 3 different temperatures: 5, 20 and 40 °C. Prior to testing, the sample and testing tools were conditioned for at least 4 h at the testing temperature.

## 5 Results and RAP Classification

Tests were performed at different temperatures on different sources of RAP. Figure 3 shows that the fraction of fine passing the control sieve produced under fragmentation evolves differently according to the testing temperature: the

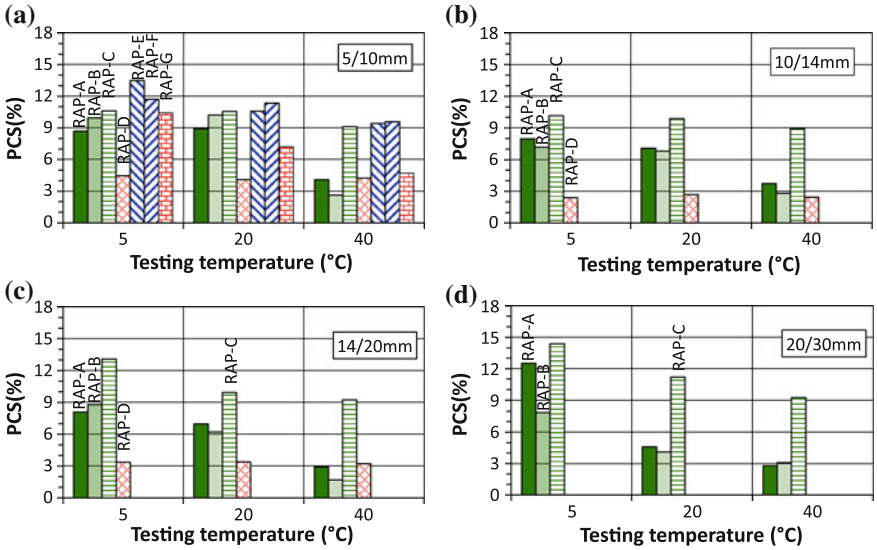


**Fig. 3** Relationship between the percentage passing through the control sieve (PCS%) and the fragmentation testing temperature on different RAP sources: **a** fraction group—5/10 mm, **b** fraction group—10/14 mm, **c** fraction group—14/20 mm, **d** fraction group—20/30 mm

PCS value decreases as the testing temperature increases, for all tested RAP sources. Moreover, with respect to the tested fraction groups, the PCS changes with the testing temperature according to the mean size of particles. For a coarser fraction, the variation of the PCS with the temperature is more pronounced.

RAP particles often consist not of a single "aggregate" particle, but rather, are agglomerates of smaller mineral particles glued together by mastic (Tebaldi[a] et al. 2012, Tebaldi[b] et al. 2012). Of course, mineral particles in the RAP and the RAP bitumen itself will affect fragmentation results. Depending of on the size of a considered fraction group, the RAP particles composition could be very different. At low temperatures, the RAP bitumen becomes brittle, and at high temperatures, it softens. For the latter, RAP bitumen will help dissipate the impact energy under shocks and minimize fine particles production under testing. Moreover, at high temperatures, the bitumen acts as a "glue" and favours fine particles produced at the beginning of the fragmentation test for agglomeration as the strocks go by.

To get an overview of the overall trend of fragmentation results, the results presented in Fig. 3 could be plotted in the same graph, but by considering the mean particle size of tested fraction groups. All the results obtained for all the testing temperatures considered in the RRT program are presented in Fig. 4, where the blank labels are linked to the 5 °C results, the filled labels are matched to the 40 °C results, and the partially filled labels are associated with the 20 °C results.

Without considering the 20/30 mm fraction group, Fig. 4 shows that the PCS values decrease as the mean particle size of RAP particles tested increases.

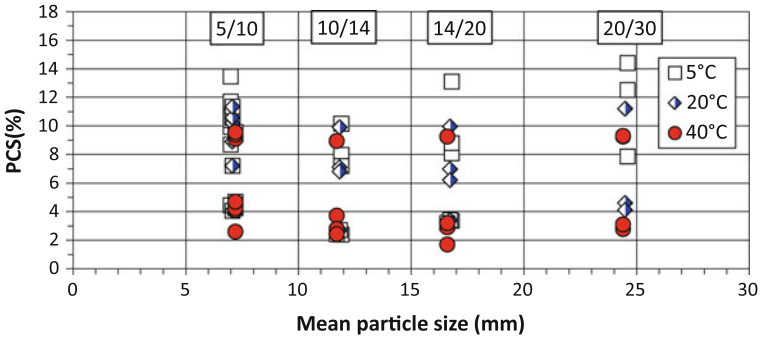


**Fig. 4** Relationship between the PCS% of RAP sources tested and the mean particle size of fraction groups tested at different testing temperatures

## *5.1 Repeatability of Fragmentation Measurement*

RAP properties are different from source-to-source, and could affect the uncertainty of measurements. Some laboratories did 3 repetition tests, and the results could be used to figure out dispersion levels by calculating the coefficient of variation: CV% = (standard deviation /mean value)*100 %.

Figure 5 shows the relationship between the CV values and the mean particle size of the fraction groups tested at different temperatures. Overall, the coefficient of variation is less than 21 %; as well, it changes with the tested particles size: the higher the mean particle size, the greater the dispersion of the results. For the tested fraction group of 5/10 mm, Fig. 5 shows that the CV is at a highly acceptable level—less than 11 %. Furthermore, the results presented in Fig. 5 clearly show that the dispersion of the results is much lower for low temperature (5 °C) measurements compared to those obtained for high temperature (40 °C) measurements. Of course, as indicated in Fig. 3, the fragmentation of RAP particles is more effective at low temperatures and could partly explain this observation.

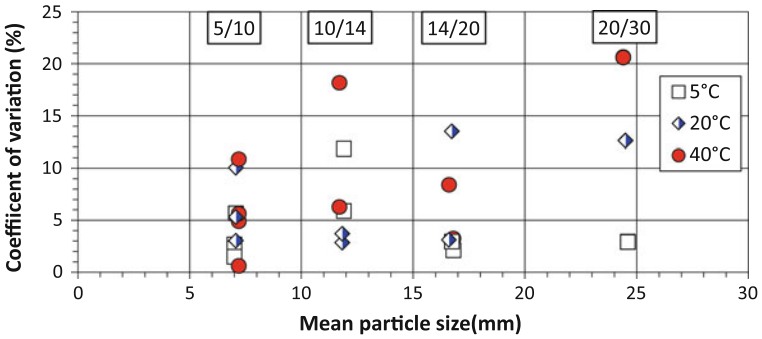


**Fig. 5** Relationship between the coefficient of variation values (CV%) and the mean particle size of fraction group tested at different temperatures

## 5.2 *Fragmentation Test Performed on Virgin Aggregates (VA)*

Fragmentation tests were also performed on two typical virgin aggregates (VA) currently used as aggregate material in road construction. The main characteristics of the tested aggregates are presented in Table 3. The fraction group 5/10 mm was considered. In addition to the measurement of the percentage passing through the control sieve (PCS%), we also checked the percentage passing through the 5 mm sieve. The results are presented in Fig. 6.

Figure 6 shows that the PCS value does not change with respect to the temperature of the test. The behaviour is different between the two tested VAs. The PCS values are more significant for the VA-B than for the VA-A, and follow exactly the same trend as the one associated with the LA values of the aggregates.

According to the NF 18-545 (2011) French standard, the VA-A and the VA-B are classified under categories B and D, respectively, for asphalt road applications.

**Table 3** Main characteristics of tested aggregates

| | | Properties | | | | NF 18-545 standard | |
|---|---|---|---|---|---|---|---|
| Name | Type | $G_b^a$ | Abs(%)[b] | LA(%)[c] | MDE[d] | Foundation and base layer (art. 7) | Surface layer (art. 8) |
| VA-A | Basalt | 2.812 | 0.5 | 12.3 | 11.6 | B | A/B |
| VA-B | Limestone | 2.681 | 1.3 | 30.0 | 15.5 | D | Not classify |

[a]Specific gravity
[b]Water absorption
[c]Los Angeles
[d]MicroDeval in water

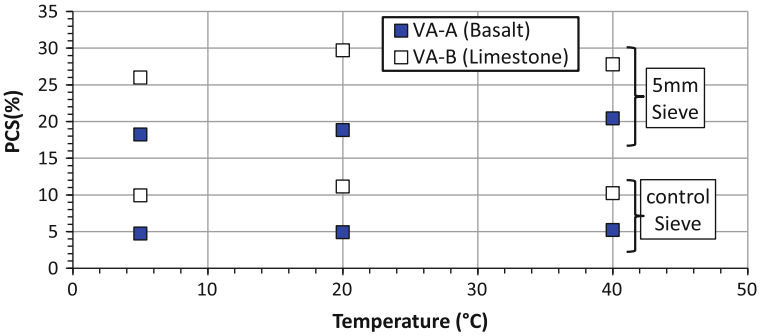


**Fig. 6** Relationship between the percentage passing through the control sieve (PSC%) of fragmentation tests done on the 5/10 mm fraction group of two different sources of virgin aggregates (VA) and the testing temperature measurements

## 5.3 RAP Classification Attempt

One main goal of the RRT campaign was to explore the feasibility of classifying RAP materials based on different performance tests. To define a classification for any material, we need to deal with three different related aspects: (1) the property on which we are to be considered; (2) the appropriate test method which must be referred to, and (3) how to set limits on categories. All these aspects depend on the intended use, and on how the material could change under production and implementation processes, as well as in its lifetime. In the asphalt road industry, it can be stated that RAPs are mainly recycled as: (1) "black rock" in unbounded materials; (2) in cold mix design, and (3) in hot mix asphalt.

Based on the previous statements, it was decided to examine our results with considering different views on the issue: (1) how the size of RAP particles could change under impacts, and (2) how RAP particles could agglomerate in its use.

### 5.3.1 Categorization of RAPs Based on Their Fragmentation Potential

To classify RAPs with respect to their susceptibility to undergo size changes while in use, results of fragmentation tests performed at 5 °C were analysed.

As noted previously, PCS values for tested virgin aggregates were not affected by the temperature at which the test was performed. To classify tested RAP sources based on fragmentation results, it was decided to refer to the categories as defined in the NF EN 12620 European standard (B to E). From virgin aggregates results, PCS values were linked to the Los Angeles (LA) limit values of categories B to E, while assuming a linear relationship. Because only few laboratories performed tests on the four fraction groups, classification was limited to the 5/10 mm fraction group results provided by each laboratory. Table 4 shows the different categories, limits, and the classification of the RAPs tested.

### 5.3.2 Categorization of RAPs Based on Their Agglomerate Potential

In the context of RAP recycling in cold mix applications, the interaction between RAP particles under processing could be affected by the bitumen phase of the RAP. RAP particles containing a softer bitumen could agglomerate more easily

**Table 4** RAP categories and limits with respect to the vulnerability of RAP particles to change size while in use and the corresponding classification of RAPs tested

| Categories | B | C | D | E |
|---|---|---|---|---|
| Limits on $PCS_{5°C\_5/10mm}$% | ≤7 | ≤9 | ≤11 | ≤14 |
| Classification | RAP-D | RAP-A | RAP-B | RAP-E |
| | | | RAP-C | RAP-F |
| | VA-A | | RAP-G | |
| | | | VA-B | |

under processing, and could significantly change the workability and the dynamic of the laying of the cold recycled material. This aspect could be more critical for recycling at elevated temperatures with foam bitumen. Moreover, agglomerate processes could also affect the coating quality of the binder system in cold recycling. To get a quickly idea about the agglomerate potential of a RAP material, the feasibility of referring to the results of fragmentation tests performed at different temperatures was checked.

As pointed out at the beginning of Sect. 5, PCS values change with the temperature at which the fragmentation test was performed. It was decided to look more closely at the results in order to use them for classification. To determine the temperature effect on the fragmentation behaviour, RAP source results for each specific fraction group, were first normalized with respect to the PCS result obtained at 5 °C ($PCS_{STDto5°C}$). It should be noted that the $PCS_{5°C}$ value is typically the highest one in the testing temperature range. A standardized value of 1 means that the temperature does not affect the fragmentation results. For example, Fig. 7a shows the results of the RAP-A material for standardized PCS values ($PCS_{STDto5°C}$) obtained for all tested fraction groups. For a given fraction group, a reduction of the standardized PCS values is observable when the temperature rises. This trend is typically observed for all normalized results of the tested RAP sources. In such cases, the reduction reveals a higher thermal susceptibility of the material. By assuming a linear relationship, it becomes possible to associate this thermal susceptibility with the slope value (s) of the $PCS_{STDto5°C}$–T° relationship. We did that with all results of the tested RAP, and the overall results are presented in Fig. 7b with respect to the mean particle size of the tested fraction groups.

A low value for this slope (s) mean a lower thermal susceptibility of the material. The "s" value could be correlated to the RAP-bitumen content and/or RAP-bitumen properties.

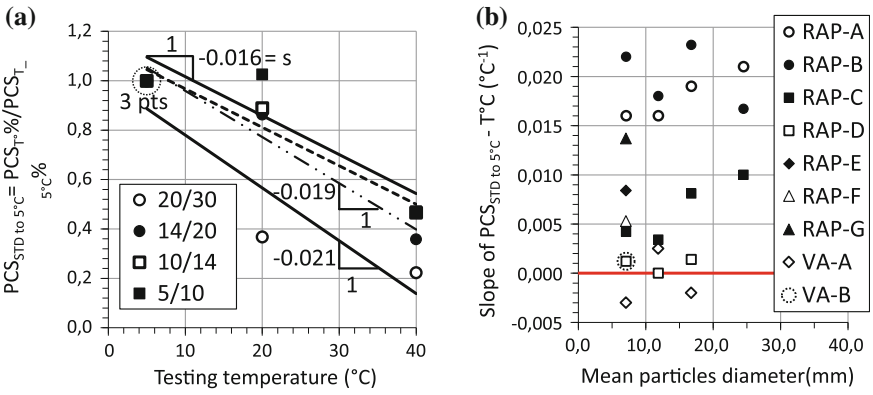


**Fig. 7** Representation of the effect of the testing temperature on the potential RAP material fragmentation: **a** example of relationships between the $PCS_{STDat5°C}$ values and the testing temperature of RAP-A; **b** relationship between the rate of change of $PCS_{STDat5°C}$ with temperature and the mean size of all tested RAP particles

**Table 5** RAP categories and limits on with respect to the vulnerability of RAP particles to change size in its use and the corresponding classification of RAP tested

| Categories | 1 | 2 | 3 | 4 |
|---|---|---|---|---|
| Absolute value of the rate of change of $PCS_{STDto5°C}$ with temperature ($\times 10^3$) ($°C^{-1}$) | ≤5 | ≤10 | ≤18 | ≤25 |
| Classification | RAP-C | RAP-E | RAP-A | RAP-B |
| | RAP-D | RAP-F | RAP-G | |
| | VA-A | | | |
| | VA-B | | | |

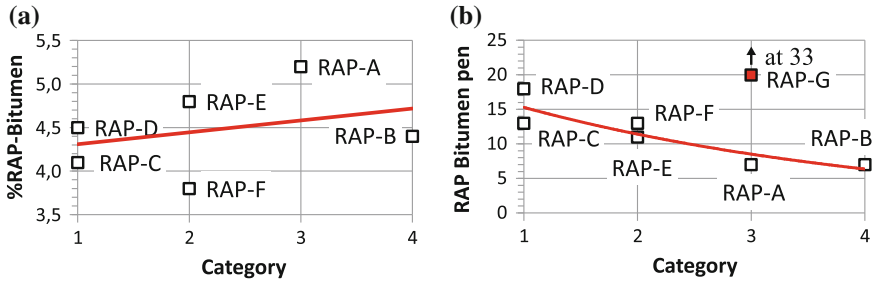


**Fig. 8** Relationship between the RAP categorization and the asphaltic part of the RAP: **a** effect of the dosage of the bitumen on the RAP, and **b** effect of the penetration index (pene) measured on the recovery bitumen of the RAP

Figure 7b clearly shows that the slope is different for each RAP source. Much the same as in Sect. 5.3.1, we defined categories and limits to classify the RAP source based on the "s" value of the $PCS_{STDto5°C}$-Temperature relationship, as presented in Table 5. The corresponding classification of the RAP material tested in this RRT is also reported in Table 5, considering results of the 5/10 fraction group.

The RAP categorization was correlated to the RAP-bitumen content of the tested RAP (Fig. 8a) and with the penetration index (pene) of the recovery RAP-bitumen (Fig. 8b). We may recall that RAP-bitumen characteristics are reported in Table 2. As shown in Fig. 8a, a certain trend is observed, but the correlation is not very significant. Furthermore, because of the penetration value of RAP-G is very high, the correlation presented in Fig. 8b is not very convincing. Nevertheless, if the RAP-G value is take off from the analysis, the correlation in that case becomes quite good, as shown in Fig. 8b (solid line). However, test results are definitely required to draw significant conclusions.

## 6 Conclusion

Based on results of the RRT program, we can conclude on the capability of the fragmentation test to characterize RAP material and to be used to possibly classify them in according to the source. RRT results clearly show that the fragmentation

potential of RAP materials can successfully differentiate by referring to the fragmentation test.

The following main conclusions can be drawn from our tests:

1. Overall, the percentage passing through the control sieve (PCS) decreases as the mean particle size of RAP particle tested increases;
2. By considering all results from the RRT, we obtained a coefficient of variation (CV) less than 21 %. The CV changes with the tested particles size: the higher the mean particle size, the greater the dispersion of the results.

Furthermore, results obtained from series of tests performed at different temperature (5, 20 and 40 °C) on different materials show that:

1. PCS values decrease as the testing temperature increases, for all tested RAP source;
2. The PCS values do not change with respect to the temperature for virgin aggregates;
3. Results dispersion is much lower for low temperature (5 °C) measurements as compared to those obtained for high temperature (40 °C) measurements.

Finally, we can say that one main goal of the RRT campaign was to explore the feasibility to classify RAP material based on fragmentation test. In this paper two categories were tentatively proposed to first classified RAP sources based on their fragmentation potential and, secondly, based on their agglomerate potential.

## References

ASTM D1557-12, 2012, Standard Test Methods for Laboratory Compaction Characteristics of Soil Using Modified Effort (56,000 ft-lbf/ft3 (2,700 kN-m/m3)), ASTM International, West Conshohocken, PA, 2012, www.astm.org

Isola M., 2014, Effect of interstitial volume characteritics on asphalt mixture durability and cracking performance. PhD dissertation at UF.

NF 18-545, 2011, Granulats – Éléments de definition, conformité et codification, Norme AFNOR, 53p.

Tebaldi[a] G, Dave E, Marsac P, Muraya P, Hugener M, Pasetto M et Alt., 2012, Classification of recycled asphalt (RA) material. 2nd International symposium on asphalt pavements & environment, ISAP TC APE, Fortaleza. Brazil.

Tebaldi[b] G, Dave E, Marsac P, Muraya P, Hugener M, Pasetto M et Alt., 2012, Synthesis of Specimen Preparation and Curing Processes for Cold Recycled Asphalt Mixes, 2nd International symposium on asphalt pavements & environment, ISAP TC APE, Fortaleza. Brazil.

Tebaldi G., Dave E.V., Marsac P., Muraya P., Hugener M., Pasetto P., et Alt., 2014, Synthesis of standards and procedures for specimen preparation and in-field evaluation of cold recycled asphalt mixtures, Road Materials and Pavement Design

# Part XI
# Cracking and Damage Characterization of Asphalt Pavements

# Comparison of Laboratory Cracking Test Results with Field Performance of Moderate and High RAP Content Surface Mixtures on the NCAT Test Track

**Randy C. West, Nam H. Tran, Adam J. Taylor and Richard J. Willis**

**Abstract** In 2006, a group of experimental test sections was built on the National Center for Asphalt Technology Test Track to evaluate surface-layer mixtures containing 20 and 45 % Reclaimed Asphalt Pavement (RAP) with variations in the Superpave performance grade of the virgin binder. This paper discusses several laboratory tests that have been proposed as indicators of cracking susceptibility and how the results of these tests conducted on the mixtures used in the test sections compare with the observed cracking performance on the Test Track after five years. The cracking tests performed on the mixtures were the bending beam fatigue test, the Energy Ratio method developed at the University of Florida, the simplified viscoelastic continuum damage method developed at the North Carolina State University, and the Overlay Tester developed at the Texas Transportation Institute. On the track, the test sections performed very well, but exhibited a range of low-severity cracking, mostly near the edges of the wheelpaths. Cores were extracted to confirm that the cracks were limited to the surface layer. The field cracking performance indicates that the performance grade of virgin binder affects cracking resistance. The creep strain rate, measured as part of the Energy Ratio method, and the Overlay Tester results best matched the field performance of the test sections.

**Keywords** Cracking · RAP · Performance · Sustainability

R.C. West (✉) · N.H. Tran · A.J. Taylor · R.J. Willis
National Center for Asphalt Technology at Auburn University, Auburn, USA
e-mail: westran@auburn.edu

N.H. Tran
e-mail: nht0002@auburn.edu

A.J. Taylor
e-mail: tayloa3@auburn.edu

R.J. Willis
e-mail: willi59@auburn.edu



F. Canestrari and M.N. Partl (eds.), *8th RILEM International Symposium on Testing and Characterization of Sustainable and Innovative Bituminous Materials*, RILEM Bookseries 11, DOI 10.1007/978-94-017-7342-3_78

## 1 Background

The use of reclaimed asphalt pavement (RAP) in new asphalt mixtures has been a common practice in the United States of America (USA) for decades. Given the economic and environmental benefits of using RAP in asphalt mixtures, interest continues for using higher RAP contents. Recent surveys indicate that the average amount of RAP used in asphalt mixtures in the USA increased from an estimated 12 % in 2007 to about 20 % in 2012. However, it is important to note that the percentages of RAP permitted and used vary considerably from state to state. Although most state highway agencies have decades of experience with asphalt mixtures containing low to moderate percentages of RAP (i.e., below 25 % by weight of mix), many are reluctant to increase RAP contents due to the general perception that RAP mixtures may be more susceptible to various modes of cracking.

Numerous research studies have been conducted to evaluate higher RAP contents, but very few have assessed mixture performance in the field. The National Center for Asphalt Technology (NCAT) has conducted several field experiments using asphalt mixtures containing moderate and high RAP contents on the NCAT Test Track since 2006. The first Test Track experiment using high RAP content mixes included seven test sections—two surface mixes containing 20 % RAP, four surface mixtures having 45 % RAP, and one (control) surface mix with no RAP. The objectives of the study were to (1) evaluate the constructability and performance of asphalt mixes containing moderate and high RAP contents under accelerated loading, (2) examine the effect of virgin binder grade on moderate and high RAP content mixes, and (3) assess how well laboratory tests results correlate with the performance of RAP mixes in the field.

The information regarding materials, construction and the initial performance evaluation of the test sections was described in a previous paper by West et al. (2009). This paper reports and compares the field performance of the test sections after five years and the results of laboratory cracking tests conducted on the experimental surface mixtures.

## 2 Field Evaluation of Moderate and High RAP Mixtures

In 2006, seven 61-m test sections were milled and inlaid at a thickness of 50-mm with asphalt mixtures designed for this study. The pavement structure beneath the experimental surface layers was quite substantial with approximately 56-cm of asphalt concrete over a 16-cm unbound aggregate base and a stiff subgrade. This strong structure essentially isolated distresses to the surface layer. The mixtures were designed in accordance with Superpave guidelines in AASHTO M 323 for a 10 million ESAL category design except that the number of gyrations was 60. Figure 1 shows the layout of the NCAT Test Track. The mixtures were designed

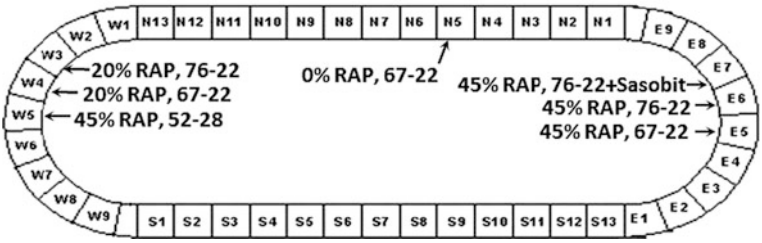


**Fig. 1** Layout of the test sections on NCAT pavement test track

using the same aggregate and RAP stockpiles, but the virgin asphalt binder and the amount of RAP used in each mixture was changed as follows.

- A control mix (no RAP) with an unmodified PG 67-22 binder.
- A 20 % (by weight of total mix) RAP mixture with a PG 67-22 binder.
- A 20 % RAP mixture with an SBS-modified PG 76-22 binder.
- A 45 % RAP mixture with a softer, unmodified PG 52-28 binder.
- A 45 % RAP mixture with a PG 67-22 binder.
- A 45 % RAP mixture with a PG 76-22 binder.
- A 45 % RAP mixture with a PG 76-22 plus 1.5 % Sasobit®.

Table 1 summarizes the quality control (QC) data from the construction of the test sections. The laboratory compacted air void contents for a few of the sections

**Table 1** As built quality control data for the test sections

| Section no. | N5 | W3 | W4 | W5 | E5 | E6 | E7 |
|---|---|---|---|---|---|---|---|
| RAP % | 0 | 20 | 20 | 45 | 45 | 45 | 45 |
| Virgin PG | PG 67-22 | PG 76-22 | PG 67-22 | PG 58-28 | PG 67-22 | PG 76-22 | PG 76-22[S] |
| AC (%) | 5.8 | 5.6 | 5.8 | 4.9 | 5.1 | 5.0 | 4.9 |
| Sieve | % Passing | | | | | | |
| 12.5 mm | 97 | 97 | 97 | 97 | 95 | 97 | 97 |
| 9.5 mm | 85 | 87 | 88 | 86 | 80 | 85 | 84 |
| 4.75 mm | 65 | 65 | 66 | 58 | 53 | 59 | 59 |
| 2.36 mm | 54 | 54 | 54 | 46 | 42 | 47 | 48 |
| 0.60 mm | 31 | 31 | 31 | 28 | 25 | 28 | 28 |
| 0.075 mm | 6.8 | 7.5 | 7.6 | 8.3 | 6.2 | 7.3 | 7.2 |
| Air voids (%) | 2.9 | 1.9 | 2.1 | 1.7 | 3.2 | 3.5 | 3.6 |
| VMA (%) | 15.9 | 14.2 | 14.5 | 12.5 | 13.8 | 13.9 | 13.9 |
| VFA (%) | 81.3 | 86.6 | 85.4 | 86.3 | 76.9 | 74.9 | 74.2 |
| Vbe (%) | 13.0 | 12.3 | 12.4 | 10.8 | 10.6 | 10.4 | 10.3 |
| Density (%) | 94.8 | 92.0 | 93.9 | 95.3 | 94.0 | 95.5 | 96.0 |

[S]1.5 % Sasobit® was added to the virgin asphalt binder at the plant

were around 2 %, and voids filled with asphalt (VFA) were about 10 % above the design range for heavy traffic pavements. These would be considered failing test results in most quality assurance specifications. These results were likely caused by gradation differences of the RAP stockpiles between mix design and production. The RAP fractionating unit was not available to the contractor until a few days before the test sections were produced, so the mix designs were performed with lab-fractionated RAP. Although the QC results caused some concern about the rutting potential of some mixes, the project had a tight schedule and limited quantities of fractionated RAP and PG 58-28 binder, which led to the decision to leave the mixtures in place and evaluate them as produced. It is important to note that there are substantial differences among the mixes with regard to the volume percentage of effective asphalt. Post-construction in-place density results show that each test section was well compacted. Additional details regarding the mixtures and tests on the recovered binders are provided in West et al. (2009).

The test sections were open to traffic in November 2006. Except for the control section, the sections with RAP mixtures were trafficked for 20 million ESALs over a period of five years to complete two typical research cycles. The control section (N5) was removed in 2009 to correct a settlement problem on the north tangent of the Test Track. Weekly field performance measurements were conducted including rutting, roughness, surface texture, and cracking. When a crack was detected, it was manually traced on the pavement and measured to generate crack maps. The crack maps were used to track the progress of cracking in the sections over time.

Table 2 shows the field performance results for the test sections after 20 million ESALs except for the control section. The data for the control section is for 10 million ESALs of traffic after which it was removed from service.

A very minor amount of low severity cracking (<1 mm wide) appeared in a few test sections after four years. The bottom two rows summarize the cracking data; the second to the last row is the total length of cracking for each test section, and the bottom row is the percent of the lane area of cracking for each section. Although the amount of cracking was quite low for the sections, the results appeared to be

**Table 2** Summary of field performance data for the test sections

| Section no. | N5[a] | W3 | W4 | W5 | E5 | E6 | E7 |
|---|---|---|---|---|---|---|---|
| RAP % | 0 | 20 | 20 | 45 | 45 | 45 | 45 |
| Virgin PG | PG 67-22 | PG 76-22 | PG 67-22 | PG 58-28 | PG 67-22 | PG 76-22 | PG 76-22[S] |
| Field performance after 20 million ESALs | | | | | | | |
| Rutting (mm) | 5.3 | 2.6 | 8.1 | 2.2 | 2.0 | 0.5 | 1.7 |
| Cracking (m) | 0 | 10.3 | 0 | 1.1 | 4.3 | 16.4 | 44.4 |
| Cracking (%) | 0 | 2 | 0 | 0 | 1 | 3 | 8 |

[a]Data for this section were obtained at 10 million ESALs after which it was removed

affected by the virgin binder grade and the total volume of effective binder. Cores taken on the cracks in each section verified that all of the cracks were limited to the surface layers. Since the sections had performed extremely well, most were left in place for additional trafficking through 2014. Section E7 was replaced in 2009 for another experiment.

## 3 Laboratory Evaluation of the Experimental Mixtures

Plant-produced mixes sampled during track construction or cores obtained from the test sections were used for the following cracking tests: bending beam fatigue, overlay tester, energy ratio, and simplified visco-elastic continuum damage.

### *3.1 Bending Beam Fatigue Test*

The most prevalent laboratory method for assessing fatigue resistance of asphalt mixes in the USA is the bending beam fatigue (BBF) test developed in the 1960s and later simplified and modified to provide more reliable results (Pronk 1997). The test can be conducted according to two standardized procedures, AASHTO T 321-07 and ASTM D7460-10, which differ most significantly in regard to waveform and analysis of specimen failure points. BBF tests conducted at multiple strain levels can be used to determine the fatigue endurance limit which is utilized in mechanistic-empirical pavement design methodology and has been linked with field performance in limited field studies at the Federal Highway Administration Accelerated Loading Facility (Romero et al. 2005) and the NCAT Test Track (Willis et al. 2010).

Although the BBF is typically used for evaluating base layer mixes, because of its familiarity, it was of interest to use it to evaluate the surface layer mixes in this study. Specimens were compacted in a kneading beam compactor to a target air void level of 5.5 ± 1.0 % and then trimmed to the standard dimensions. The air void target was chosen to represent the field compacted air voids. Before testing, the beams were long-term aged according to AASHTO R 30-08. BBF testing was performed in accordance with AASHTO T 321-07 at 500 με and 20 ± 0.5 °C. Three replicates were tested for each mixture.

#### 3.1.1 Test Results

Table 3 shows the BBF test results for the seven mixtures, including the average number of cycles to failure, the standard deviation (Std. Dev.) for the cycles to failure, the coefficient of variation (COV), the simple rank of the mixture sections

**Table 3** Summary of bending beam fatigue test results for the mixtures

| Section no. | N5 | W3 | W4 | W5 | E5 | E6 | E7 |
|---|---|---|---|---|---|---|---|
| RAP % | 0 | 20 | 20 | 45 | 45 | 45 | 45 |
| Virgin PG | PG 67-22 | PG 76-22 | PG 67-22 | PG 58-28 | PG 67-22 | PG 76-22 | PG 76-22$^{S}$ |
| Bending beam fatigue results, cycles to failure | | | | | | | |
| Average | 245,003 | 200,817 | 181,330 | 52,157 | 49,393 | 42,328 | 27,250 |
| Std. dev. | 94,961 | 41,287 | 35,804 | 7,299 | 18,953 | 14,247 | 18,442 |
| COV (%) | 39 | 21 | 20 | 14 | 38 | 34 | 68 |
| Simple rank | 1 | 2 | 3 | 4 | 5 | 6 | 7 |
| Stat. group | A | A | A | B | B | B | B |

based on the average results, and a statistical grouping of results that were not significantly different at $\alpha = 0.05$ using the Tukey-Kramer test (Montgomery 2013).

The virgin control mix had the best results (highest cycles to failure). As RAP contents increased, the BBF cycles to failure decreased. It is important to note that the decrease in cycles to failure also follows the trend of the volume of effective asphalt for the mixtures. It can be seen that all of the 45 % RAP mixtures were grouped together by the statistical analysis and the 20 % RAP mixtures were grouped with the virgin mix. From this, it can be inferred that the BBF results were not statistically affected by changing the virgin binder grade but were affected by the amount of RAP.

## *3.2 Overlay Test*

The Overlay Test (OT) was developed in the 1970s by the Texas Transportation Institute (TTI) to evaluate reflection cracking of asphalt overlays on concrete pavements. The test was validated with field data from five pavements with reflection cracking in Texas (Chen 2008). The OT also was strongly correlated with fatigue performance of HMA mixtures tested at the FHWA ALF (Zhou and Scullion 2005). In the past decade, equipment to conduct the test has been commercially developed. In 2013, the Texas DOT implemented OT criteria for different mix design types. Several researchers have specifically used the method to assess general cracking resistance of mixes containing recycled materials.

In this study, OT testing was conducted following Texas DOT method 248-F. Specimens were prepared from Superpave gyratory compactor (SGC) samples compacted to 7 ± 1 % air voids. The SGC samples were then trimmed to the standard OT dimensions and glued to the test platens. Triplicate specimens were

**Table 4** Summary of overlay test results for the mixtures

| Section no. | N5 | W3 | W4 | W5 | E5 | E6 | E7 |
|---|---|---|---|---|---|---|---|
| RAP % | 0 | 20 | 20 | 45 | 45 | 45 | 45 |
| Virgin PG | PG 67-22 | PG 76-22 | PG 67-22 | PG 58-28 | PG 67-22 | PG 76-22 | PG 76-22$^{S}$ |
| Overlay tester, 0.635 mm displacement, cycles to failure | | | | | | | |
| Average | 75.7 | 6.0 | 13.3 | 10.3 | 3.3 | 3.3 | 2.7 |
| Std. dev. | 45.6 | 2.6 | 9.0 | 5.5 | 0.6 | 0.6 | 0.6 |
| COV (%) | 60 | 43 | 68 | 53 | 18 | 18 | 22 |
| Simple rank | 1 | 4 | 2 | 3 | 5 | 5 | 7 |
| Stat. group | A | B | B | B | B | B | B |
| Overlay tester, 0.432 mm displacement, cycles to failure | | | | | | | |
| Average | 55.0 | 202.0 | 180.5 | 46.3 | 4.3 | 19.5 | 31.3 |
| Std. dev. | 35.6 | 110.1 | 92.2 | 35.6 | 2.1 | 12.2 | 22.9 |
| COV (%) | 65 | 55 | 52 | 77 | 49 | 63 | 73 |
| Simple rank | 3 | 1 | 2 | 4 | 7 | 6 | 5 |
| Stat. group | B | A | A | B | B | B | B |

tested at 25 °C. A lateral displacement cycle (open-close) was applied to specimens at a rate of one cycle every 10 s. The standard peak displacement per cycle was 0.635-mm. The maximum resistant force of the specimen for each cycle was recorded. Tests continued until the force was reduced by 93 % from the first cycle. During the course of this testing, several mixes failed within the first few cycles, so additional tests were conducted at a displacement of 0.432-mm and using four replicates per mix.

### 3.2.1 Test Results

Table 4 shows OT results. At the standard displacement (0.635 mm), all the mixes failed in less than 100 cycles which is below current TxDOT and New Jersey criteria (Estakhri et al. 2013; Bennert 2012). All 45 % RAP mixes failed within just a few cycles, indicating that the mixtures were intolerant to the very high strains applied in this test. Except for the virgin mix, OT results improved for the tests conducted with the smaller displacement (0.432 mm). However, in this case, the virgin mix was statistically grouped with the 45 % RAP mixes. Given the large variability of the test results, the OT was unable to discriminate mix factors such as the virgin binder grade.

## 3.3 *Energy Ratio*

Top-down cracking has been documented as a common form of distress in asphalt pavements. It is a load-related type of cracking that initiates at the top of an asphalt pavement structure and propagates downward. The Energy Ratio (ER) method was developed at the University of Florida to evaluate the resistance of asphalt mixtures to top-down cracking (Roque et al. 2004). The ER method includes three indirect tensile tests to obtain tensile and fracture properties of an asphalt mixture. Figure 2 illustrates how the strength (St), fracture energy (FE), and dissipated creep strain energy at failure ($DCSE_f$) are determined from the stress-strain plots obtained from the tests.

ER criteria were initially developed and validated based on testing conducted on cores from 22 roadway sections in Florida. In addition, Wang et al. (2007) integrated the top-down cracking model into a mechanistic-empirical flexible pavement design framework and showed its capability to perform a thickness design and predict pavement resistance to top-down cracking. Validation of the design framework has been performed on more than 30 field sections.

For this study, cores were obtained from each of the sections in January 2008 to determine ER. The cores were tested and analyzed by the Florida Department of Transportation following the method described above. The tests were performed at 10 °C. Test specimens were 150-mm in diameter by approximately 38-mm thick.

### 3.3.1 Test Results

Table 5 summarizes Fracture Energy (total area under the stress-strain plot for the tensile strength test) data. These data were available for replicate tests, allowing reporting of variability data and statistical comparisons. The Fracture Energy (FE) results show that the E7 mix was statistically grouped with the virgin mix and mixes with 20 % RAP. The other 45 % RAP mixes were not statistically grouped with the virgin mix, but were grouped with all other mixes. This indicates that this parameter alone is not sensitive enough to discern the effect of key mix

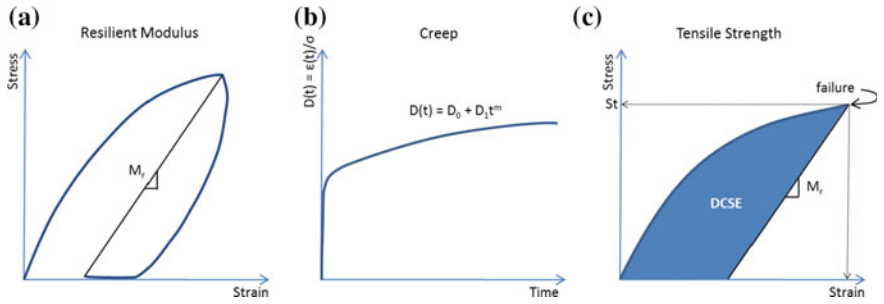


**Fig. 2** Parameters determined from **a** resilient modulus, **b** creep, and **c** strength tests

**Table 5** Summary of fracture energy results for the mixtures

| Section no. | N5 | W3 | W4 | W5 | E5 | E6 | E7 |
|---|---|---|---|---|---|---|---|
| RAP % | 0 | 20 | 20 | 45 | 45 | 45 | 45 |
| Virgin PG | PG 67-22 | PG 76-22 | PG 67-22 | PG 58-28 | PG 67-22 | PG 76-22 | PG 76-22$^S$ |
| Fracture energy (kJ/m$^3$) | | | | | | | |
| Average | 2.08 | 1.30 | 1.25 | 0.60 | 0.55 | 0.93 | 1.35 |
| Std. dev. | 0.28 | 0.71 | 0.58 | 0.18 | 0.06 | 0.45 | 0.42 |
| COV (%) | 13 | 55 | 46 | 30 | 11 | 48 | 31 |
| Simple rank | 1 | 2 | 4 | 6 | 7 | 5 | 2 |
| Stat. group | A | AB | AB | B | B | B | AB |

characteristics. Table 6 shows other parameters determined as part of the ER method. The ER analysis program combines data from multiple specimens, so it was not possible to analyze variability. Creep Strain Rate (CSR) results indicated that the virgin control mix and the 20 % RAP mix with PG 67-22 binder were much more compliant. The two mixes with the highest ER, and therefore expected to perform best with respect to top-down cracking, were mixes from E7 and W3. Three mixes had ER results less than 1.0 which indicates a high potential for top-down cracking.

## *3.4 Simplified Visco-Elastic Continuum Damage Test*

The Simplified Visco-Elastic Continuum Damage (SVECD) test was developed at North Carolina State University (NCSU) over the past two decades. The

**Table 6** Summary of energy ratio test results for the mixtures

| Section no. | N5 | W3 | W4 | W5 | E5 | E6 | E7 |
|---|---|---|---|---|---|---|---|
| RAP % | 0 | 20 | 20 | 45 | 45 | 45 | 45 |
| Virgin PG | PG 67-22 | PG 76-22 | PG 67-22 | PG 58-28 | PG 67-22 | PG 76-22 | PG 76-22$^S$ |
| Dissipated creep strain energy (kJ/m$^3$) | | | | | | | |
| Result | 1.9 | 1.1 | 1.2 | 0.5 | 0.4 | 0.8 | 1.1 |
| Simple rank | 1 | 3T | 2 | 6 | 7 | 5 | 3T |
| Creep strain rate (1/sec E-7) | | | | | | | |
| Result | 10.73 | 5.26 | 12.84 | 6.49 | 4.81 | 4.55 | 2.44 |
| Simple rank | 2 | 4 | 1 | 3 | 5 | 6 | 7 |
| Energy ratio | | | | | | | |
| Result | 1.32 | 1.68 | 0.71 | 0.60 | 0.61 | 1.22 | 2.90 |
| Simple rank | 3 | 2 | 5 | 7 | 6 | 4 | 1 |

development and theory of the method are presented in several publications (Kim et al. 1997; Daniel and Kim 2002; Underwood et al. 2006; Hou et al. 2010). AASHTO TP 107 allows the SVECD test to be conducted in the Asphalt Mixture Performance Tester (AMPT), which is a compact universal testing machine developed to perform a variety of advanced asphalt mixture characterization tests.

To obtain the SVECD fatigue characteristics of an asphalt mixture, two tests are performed. First, the dynamic modulus (E*) of the mixture is determined to quantify the linear viscoelastic (LVE) characteristics of the mix. Second, a controlled crosshead cyclic fatigue test is performed using the SVECD software in AMPT (Hou et al. 2010). In the fatigue test, a specimen is epoxied to two end platens, which are then bolted to the actuator and reaction frame of the AMPT prior to installing on-specimen LVDTs. The fatigue test is performed at 19 °C and a frequency of 10 Hz. Two replicate specimens are tested at two strain levels. These strain levels are selected so that the cycles to failure of the mix at the two strain levels are approximately an order of magnitude apart (i.e. 1,000 cycles to failure for one strain level versus 10,000 cycles to failure for another strain level).

Specimens for SVECD testing were prepared in accordance with AASHTO PP 60-09. Typically, for each mix, three specimens were required for E* and four to six specimens were needed to obtain SVECD fatigue parameters. Fatigue simulations were performed in an EXCEL® spreadsheet using the NCSU ALPHA-Fatigue version 2.1 algorithms with a constant-strain level of 500 με.

### 3.4.1 Test Results

Table 7 shows the predicted fatigue lives from the SVECD testing and analysis. All of the mixtures containing RAP had much lower fatigue lives than the virgin control mix. For the mixtures containing 20 % RAP, the polymer modified binder appeared to provide a substantial improvement. For the mixes containing 45 % RAP, the mix containing the softer virgin binder had the best results.

**Table 7** Predicted fatigue lives (loading cycles) based on SVECD testing and analysis

| Section no. | N5 | W3 | W4 | W5 | E5 | E6 | E7 |
|---|---|---|---|---|---|---|---|
| RAP % | 0 | 20 | 20 | 45 | 45 | 45 | 45 |
| Virgin PG | PG 67-22 | PG 76-22 | PG 67-22 | PG 58-28 | PG 67-22 | PG 76-22 | PG 76-22$^{S}$ |
| Result | 93,570 | 15,176 | 5,217 | 6,207 | 331 | 317 | 375 |
| Simple rank | 1 | 2 | 4 | 3 | 6 | 7 | 5 |

**Table 8** Summary of best fit regressions and coefficients of determination

| Test | Least squares regression equation | $R^2$ |
|---|---|---|
| BBF | Cracking (m) = 313,883(BBF Nf/1000)$^{-2.848}$ | 0.362 |
| OT @ 0.635 mm | Cracking (m) = 6002.4(OT Nf @ 0.635)$^{-4.818}$ | 0.679 |
| OT @ 0.432 mm | Cracking (m) = 170.64(OT Nf @ 0.432)$^{-1.228}$ | 0.209 |
| Fracture energy | Cracking (m) = 1.7147(FE)$^{-0.843}$ | 0.008 |
| Creep stain rate | Cracking (m) = 122,287(CSR)$^{-6.621}$ | 0.848 |
| Energy ratio | Cracking (m) = 17.626(ER)—9.9282 | 0.899 |
| SVECD | Cracking (m) = 2576 (SVECD Nf @ 500 με)$^{-0.981}$ | 0.198 |

## 4 Comparison of Field Performance with Lab Test Results

Relationships between the Test Track cracking performance and the laboratory cracking test results were explored using simple least squares regressions. Table 8 summarizes the best fit regression equations and the coefficients of determination ($R^2$). From this summary, it would appear that the strongest relationship was for Energy Ratio. However, this relationship was the opposite of the expected trend that a higher ER provides more cracking resistance. The CSR had the next highest $R^2$ and the trend indicates that mixtures with higher CSRs were more resistant to cracking. The only other test result that had a good correlation with field performance was the OT using the standard displacement of 0.632-mm.

## 5 Summary of Findings

From the measured field performance and laboratory cracking tests conducted on moderate and high RAP content surface layer mixes at the NCAT Test Track, the following observations are made:

- The 20 and 45 % RAP mixes designed according to Superpave standards have performed very well under very heavy traffic for five years. Only low-severity cracking of the surface layers has been observed to date.
- Using a softer virgin binder for high RAP content mixes appears to improve cracking resistance as evident on the Test Track sections.
- The Bending Beam Fatigue test results had poor precision and therefore were unable to statistically distinguish the effect of the virgin binder grade on cracking resistance. Results were poorly correlated with test track performance data. A lower strain level may have been more appropriate for surface layer characterization.
- The Overlay Test using the standard displacement had very poor precision and was unable to statistically distinguish the effects of virgin binder grade or

between 20 and 45 % RAP mixtures. Reducing the displacement did improve average cycles to failure, but repeatability remained poor. The standard displacement OT results did correlate reasonably well with Test Track cracking performance data. However, the test results for all mixes would be considered poor according to the published OT criteria, contrasting with the good performance documented on the Test Track.

- The only parameter from the Energy Ratio test that correlated well with field performance was Creep Stain Rate. This parameter should be further examined to assess its precision and its potential to be a cracking performance indicator.
- Simplified Viscoelastic Continuum Damage test results did not correlate well with observed surface layer cracking on the Test Track in this study.

## References

Bennert, T., NJDOT High RAP Specification and Implementation - I-295, presentation to the Northeast Asphalt User Producer Group, Philadelphia, 2012.

Chen. D., Field Experiences with RDD and Overlay Tester for Concrete Pavement Rehabilitation, Journal of Transportation Engineering, Vol. 134, No. 1, pp. 24-33, 2008.

Daniel, J.S., and Y.R. Kim, Development of a Simplified Fatigue Test and Analysis Procedure Using a Viscoelastic, Continuum Damage Model, Journal of Association of Asphalt Paving Technologists, 2002.

Estakhri, C., D. Rand, T. Scullion, F. Zhou, L. Walubita, Update on the Texas Overlay Tester, presentation to the Rocky Mountain Asphalt Conference and Equipment Show, 2013.

Hou, T., B. S. Underwood, and Y. Kim, Fatigue Performance Prediction of North Carolina Mixtures Using the Simplified Viscoelastic Continuum Damage Model, Journal of Association of Asphalt Paving Technologists, 2010.

Kim, Y.R., H.J. Lee, and D.N. Little, Fatigue Characterization of Asphalt Concrete Using Viscoelasticity and Continuum Damage Theory, Journal of Association of Asphalt Paving Technologists, 1997, pp. 520-569.

Montgomery, D. Design and Analysis of Experiments, 8th Edition, Wiley, 2013, pp. 752.

Pronk, A.C. Comparison of 2 and 4 Point Fatigue Tests and Healing in 4 Point Dynamic Bending Test Based on the Dissipated Energy Concept, Eighth International Conference on Asphalt Pavements, Seattle, Washington, 1997, pp. 987-994.

Romero, P., K.D. Stuart, and W. Mogawer, Fatigue Response of Asphalt Mixtures Tested by the Federal Highway Administration's Accelerated Loading Facility, Journal of the Association of Asphalt Paving Technologists, Vol. 69, 2005, pp. 212-235.

Roque, R., B. Birgisson, C. Drakos, and B. Dietrich, Development and Field Evaluation of Energy-Based Criteria for Top-Down Cracking Performance of Hot Mix Asphalt, Journal of the Association of Asphalt Paving Technologists, Vol. 73, 2004, pp. 229–260.

Underwood, B.S., Y. R.. Kim, and M. Guddati, Characterization and Performance Prediction of ALF Mixtures Using a Viscoelastoplastic Continuum Damage Model, Journal of Association of Asphalt Paving Technologists, 2006.

Wang, J., B. Birgisson, and R. Roque, Windows-Based Top-Down Cracking Design Tool for Florida Using Energy Ratio Concept, Transportation Research Record No. 2037, 2007, pp. 86–96.

West, R., A. Kvasnak, N. Tran, B. Powell, and P. Turner, Testing of Moderate and High RAP Content Mixes Laboratory and Accelerated Field Performance Testing at the NCAT Test Track, Transportation Research Record No. 2126, 2009, pp. 100-108.

Willis, J.R., D. Timm, A. Taylor, N. Tran, and A. Kvasnak. Correlating Laboratory Fatigue Endurance Limits to Field-Measured Strains, Journal of the Association of Asphalt Paving Technologists, 2010.

Zhou, F. and T. Scullion, Overlay Tester: A Rapid Performance Related Crack Test, FHWA/TX-05/0-4467-2, Final Report, Texas Transportation Institute, 2005.

# Implementation of Laboratory Testing to Predict Low Temperature Cracking Performance of Asphalt Pavements

**Eshan V. Dave, Benjamin Helmer, Chelsea Hanson, Jared Munch and Luke Johanneck**

**Abstract** In cold climate regions, thermal cracking of asphalt pavements is a major pavement distress. Cold climates cause a thermal contraction within the pavement. When combined with the brittle behaviour of asphalt at low temperatures, the thermally induced stresses are relieved by transverse cracks forming in the pavement. This cracking facilitates poor ride quality and premature failure of the pavement. There is currently no asphalt mixture performance test required by majority of Department of Transportations (DOTs) in the United States to address the issue of thermal cracking. Previous research has indicated that fracture energy of asphalt mixtures is a reliable predictor of transverse cracking performance. This mechanistic property of asphalt mixtures can be found using the disk-shaped compact tension (DCT) test. On basis of previous research, a low-temperature cracking performance specification that uses DCT fracture energy has been developed. During 2013 construction season, five construction projects were chosen to implement provisional specifications that use fracture energy as a required mix parameter. The projects encompassed different construction techniques, material compositions and climatic zones. The implementation procedure as well as the results from testing is presented in this paper. The results indicate a shift in the DCT fracture energy values between laboratory produced specimens that were provided

E.V. Dave (✉)
Department of Civil and Environmental Engineering, University of New Hampshire, Durham, USA
e-mail: eshan.dave@unh.edu

B. Helmer · C. Hanson · J. Munch
Department of Civil Engineering, University of Minnesota Duluth, Duluth, USA
e-mail: helme065@d.umn.edu

C. Hanson
e-mail: Chelsea.hanson@state.mn.us

J. Munch
e-mail: munc0010@d.umn.edu

L. Johanneck
Minnesota Department of Transportation, Saint Paul, USA
e-mail: luke.johanneck@state.mn.us



F. Canestrari and M.N. Partl (eds.), *8th RILEM International Symposium on Testing and Characterization of Sustainable and Innovative Bituminous Materials*, RILEM Bookseries 11, DOI 10.1007/978-94-017-7342-3_79

as part of mix design acceptance and those manufactured using plant produced mix. Other findings include reaffirmation of common knowledge that use of higher binder contents and/or improved low temperature binder grades provide mixtures with improved fracture energies.

**Keywords** Thermal cracking · Fracture energy · Cold climate · Performance based specifications · Disk-shaped compact tension test

## 1 Introduction

Low-temperature cracking is the primary pavement distress in climates that experience extreme low temperatures and/or high rates of temperature drop. The discrete cracking of a material, as in the case of low temperature cracking, is a highly complicated phenomenon, and evaluation of the material beyond the linear response range helps close the gap between experimental results and actual field performance. Restrained by the layers below, the top layer of the pavement structure typically relieves these built up tensile forces by forming a transverse crack on the surface. These cracks lead to poor ride quality, along with expediting moisture related issues and potholes forming at the crack location.

The formation and propagation of low-temperature cracking is controlled by both the mechanical properties of asphalt and climatic conditions imposed on the pavement. No nationally adopted criterion is currently required for determining the low-temperature cracking potential of an asphalt mixture. Superpave specifications attempt to mitigate thermal cracking by mandating a specific low temperature grade for the asphalt binder (e.g. PG XX-28 vs. PG XX-34). While this contributes to thermal cracking prevention, specifying a low temperature binder grade does not account for the many variables in an asphalt mixture (aggregate types, gradation, recycled asphalt materials, aging etc.). In addition, not all asphalt binders of same Superpave low temperature grade have equivalent mechanical properties (modified vs. neat, different sources of crude etc.). Research has shown that the fracture behavior of the asphalt mixture and the mechanical properties of the binder are equally important in terms of low-temperature transverse cracking performance (Marasteanu et al. 2007, 2012; Dave et al. 2013). Evidently, several factors impact the low-temperature cracking performance for asphalt pavements. Modifying the asphalt binder in a mixture in itself is not an adequate method of preventing this distress. A viable method of measuring an asphalt mixture's resistance to low-temperature cracking is through performance testing (Dave and Koktan 2011).

The disk-shaped compact tension (DCT) fracture test has been successfully utilized in the past few years for prediction of the low temperature cracking performance of asphalt pavements and overlays (Dave et al. 2008; Cascione et al. 2011; Marasteanu et al. 2012). This project used an integrated approach of laboratory mixture fracture testing, field evaluations, and sophisticated modeling to

develop a low temperature cracking specification for asphalt mixtures and determined that the DCT is the most suitable test available to measure the fracture resistance of asphalt mixtures. The DCT test measures a mechanistic property known as fracture energy ($G_f$). The test specimen geometry is a circular specimen with a single notch loaded in tension at low temperature. Fracture energy can be used to describe the fracture resistance of an asphalt mixture; mixtures with a high $G_f$ have better low temperature performance and are more desirable. The DCT has been shown to discriminate between asphalt mixtures better than other tests, such as the Indirect Tensile Test. A study that evaluated State Department of Transportation (DOT) asphalt mixture specifications, as well as conducted a State of the Practice and State of the Art review on the topics of performance based specifications, recommended the use of the DCT as a suitable performance test for low temperature cracking distress (Dave and Koktan 2011). The repeatability of the DCT test is also superior to other fracture based tests (Marasteanu et al. 2012).

## 1.1 Description of Disk-Shaped Compact Tension (DCT) Test

The DCT test is standardized by ASTM D7313-13. Test specimens for the DCT can come from either 150 mm gyratory compacted pills or field cores. Sample preparation involves sawing across the diameter of the pill to a thickness of 50 mm. The flat face of the sample is then cut, followed by coring the 25 mm holes, cutting the notch and attaching the gage points. Figure 1 shows typical DCT specimen geometry.

Test temperature for the DCT test was initially recommended to be 10 °C warmer than the asphalt binder PGLT required at 98 % reliability as determined by LTPPBind 3.1 software (Marasteanu et al. 2007). For example, at a location requiring PG XX-34 binder, test temperature would be −24 °C. Test temperatures for this study were based on this approach. Further testing has now recommended

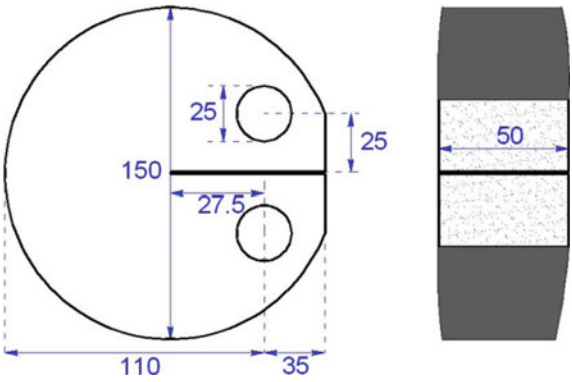


**Fig. 1** DCT specimen geometry (dimensions in mm)

that the test temperature be determined on the 98 % reliability temperature (not the 98 % reliability binder grade). For example, if a location reached 98 % reliability at −31 °C the test temperature would be −21 °C even though the designated PGLT would be XX-34.

The DCT test results are highly dependent on the temperature of the specimen. Test specimens are loaded into a temperature chamber or freezer, and are cooled down to ±1.2 °C of test temperature at a controlled rate. This rate is from room temperature (roughly 20 °C) to desired test temperature over a period of two hours. The test specimen may be loaded into the loading frame after conditioning at the desired temperature for 2 h.

The DCT test is conducted to achieve a constant crack mouth opening displacement (CMOD) rate of 1.0 mm/min. This loading rate is fast enough to essentially minimize any creep behavior of the mixture during the test. Data essential to the calculation of fracture energy are load and CMOD. By plotting load (y axis) against CMOD (x axis), the area under the curve can be determined. This is considered the fracture work. When normalized for specimen thickness and the initial ligament length, this area under the load versus CMOD curve is converted to the fracture energy. The fracture energy of asphalt mixture is defined here as the energy required to create a unit surface fracture of the asphalt mixture. The specimen thickness and initial ligament length are measured prior to DCT testing of the sample.

## *1.2 Overview of the Pilot Implementation Study and Specification*

The goal of the project was to incorporate the low temperature performance specifications recommended from the Low Temperature Cracking Pooled-Fund Study into practice on 3–5 bituminous paving projects. The feasibility of implementing the DCT test as a performance specification in Minnesota was assessed, while noting successes and challenges associated with the implementation.

Material engineers from MnDOT were contacted in order to help identify construction projects that had a significant amount of bituminous paving to be constructed in 2013. The focus was on new construction (over granular base or full depth reclamation), as the performance specifications were based on new construction projects, i.e. no pre-existing distresses were present. However, mill and overlay projects were also considered, as there was not an overabundance of new construction projects to choose from. Additionally, the research staff wanted to assess whether the recommended fracture energy levels for new construction would also be validated on mill and overlay construction projects. The research staff wanted to incorporate the DCT specification on a variety of construction types, binders, and climatic regions.

## 2 Project Selection

After consulting with the agency engineers, and contractors, five construction projects, as seen in Table 1, were selected for the low temperature fracture testing pilot project. These five projects were located across the State of Minnesota, had four different PG binders, and covered several types of construction. The objective of choosing projects with varying climatic conditions was met and can be seen by the project locations in Fig. 2.

The pilot project required the contractor to provide test specimens at the mix design stage. The mix design specimens were then tested for determination of fracture energies using the DCT test to verify that the proposed mix designs met the newly proposed fracture energy requirement. If the specimens did not meet the minimum fracture energy threshold of 400 J/m$^2$, mixture adjustment recommendations were made by the research team, and the mix producer made adjustments to the mix accordingly. Some of the potential modifications were as follows:

- Selecting an asphalt binder that has a better low-temperature grade than the specified grade (PG XX-34 instead of PG XX-28), or while keeping same low-temperature grade, use binder with better high temperature grade (PG 64-XX instead of PG 58-XX).
- Using a modified asphalt binder instead of an unmodified asphalt binder.
  - Previous studies have shown that elastomeric polymers (SBS or Elvaloy) perform slightly better than polyphosphoric acid, mineral filler, and other binder modifiers.
- Using a harder crushed quarry rock instead of limestone or gravel aggregates.
- Increasing the binder content of the mixture.
- Reducing the amount of recycled materials (RAP or shingles).
- Using a smaller nominal aggregate size.

**Table 1** Summary of selected projects

| Trunk highway (TH) | Design AC[1] (%) | PG grade | Agg. size (mm) | Design traffic level ($10^6$ ESALs) | Design air voids (%) | Construction type | Test temp (°C) | RAP (%) |
|---|---|---|---|---|---|---|---|---|
| 10 | 4.6 | 64–28 | 12.5 | 3–10 | 4.0 | Mill and overlay | −24 | 20 |
| 56 | 5.5 | 58–34 | 12.5 | 1–3 | 4.0 | SFDR[2] | −24 | 20 |
| 69 | 5.6 | 58–28 | 12.5 | 1–3 | 4.0 | Mill and overlay | −18 | 30 |
| 310 | 5.2 | 58–34 | 12.5 | 1–3 | 4.0 | FDR[3] | −30 | 20 |
| 371 | 4.8 | 64–34 | 9.5 | 3–10 | 4.0 | New construction | −24 | 20 |

[1]*AC* Asphalt Content
[2]*SFDR* Stabilized full-depth reclamation
[3]*FDR* Full-depth reclamation

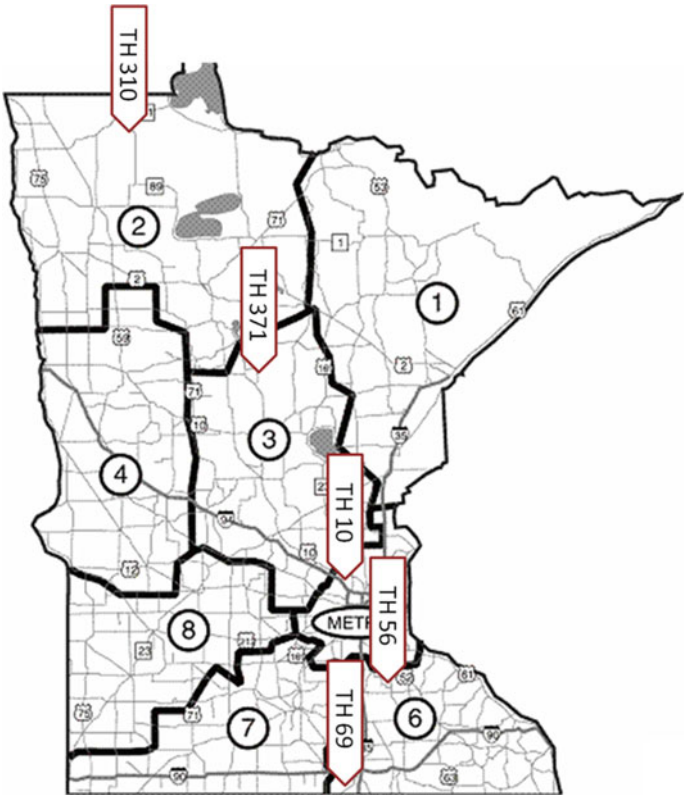


**Fig. 2** Map of project locations across Minnesota

The adjusted mix was also sampled and tested. Any increased costs incurred for materials were compensated by the Minnesota Department of Transportation (MnDOT).

Because this was a pilot study, the intent was to gather information about the mixtures and the effects of the adjustments made, while keeping the influence on construction operations to a minimum. Due to the expeditious nature of bituminous pavement construction, time permitted only one mixture adjustment (if necessary) per project. A flowchart of the mixture testing and adjustment process can be seen in Fig. 3.

Under ideal circumstances, an additional DCT test would be conducted between mix adjustments and paving of the mix. Due to time constraints, this was not possible for this study. It should be noted that production samples were taken from the truck box at the asphalt plant for the majority of the projects.

Mix information for the five projects (mix design, PG grade, aggregate size, traffic level, air voids, construction type, test temperature, and RAP content) can be found in Table 1. A brief overview of construction practices for each project is as follows:

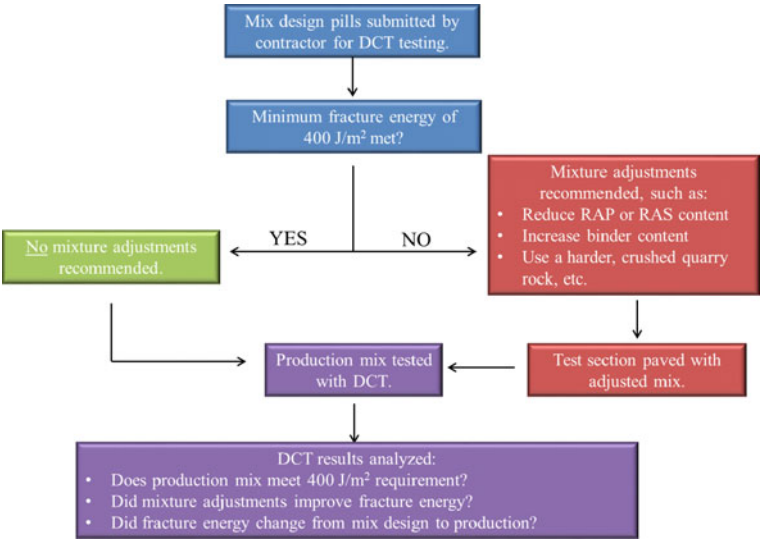


**Fig. 3** Flowchart of mixture testing and adjustment process

- **TH 10**: On this mill and overlay, 7.5 cm of existing pavement was removed by cold-milling, and replaced with 7.5 cm bituminous surfacing.
- **TH 56**: This project was a candidate for SFDR, with 7.5 cm of the existing bituminous pavement was cold-milled and replaced with 7.5 cm of material. The first pass of the reclaimer was at a variable depth of 15–30.5 cm, with the second pass injecting 3.8 % of asphalt emulsion into the top 15 cm of the reclaimed layer.
- **TH 69**: This mill and overlay consisted of the top 5 cm of the existing 10 cm bituminous pavement being milled and replaced by 9 cm of asphalt.
- **TH 310**: This project was a candidate for FDR, with the top 7.5 cm of existing pavement being milled and replaced with 11.5 cm of bituminous surfacing. Inplace pavement was reclaimed at a variable depth of 23–30.5 cm.
- **TH 371**: A majority of the project consisted of a realignment, warranting new construction. The bituminous surfacing consisted of 15 cm of bituminous, with the bottom 10 cm consisting of 12.5 mm aggregate and the top 5 cm having 9.5 mm aggregate.

## 3 Mixture Testing Results and Discussions

The first phase of this study was to conduct the DCT testing on the mix design specimens for the selected sites. As can be seen noted on Table 2, the first set of mix design specimens for TH 310 were made with incorrect binder by the mix producer.

This was found when initial fracture energy results were significantly lower than anticipated. Upon further investigation by the research team, it was discovered that the poor fracture energy was a result of use of old and heavily aged binder. Furthermore, the binder was of the wrong performance grade. Correction of this mistake was made and proper mix design samples were tested. Another unexpected situation occurred with TH 69. Due to circumstances outside the control of the research team, TH 69 samples could not be tested at the mix design stage. Production mix from the early phases of the project was substituted as a "mix design" specimen. Any required adjustments for TH 69 were quickly applied to production mixes.

Three of the mixes failed to meet the minimum required fracture energy of 400 J/m$^2$ at mix design. As a result, the following adjustments were made to the corresponding mixes:

- TH 56: increase virgin asphalt content by 0.1 % (5.5 to 5.6 %)
- TH 69: two adjustments recommended
  1. Decrease amount of RAP from 30 to 20 %
  2. Change binder grade from PG 58-28 to PG 58-34
- TH 310: decrease amount of RAP from 20 to 0 %

A summary of results from mix design testing and corresponding adjustments can be found in Table 2. Note in both Tables 2 and 3: fracture energy values in italic indicate failing results and bold indicate passing, based on the 400 J/m$^2$ threshold.

Table 3 displays the results from testing on production mixes. Unadjusted mixes are defined as a mix that failed the mix design phase ($G_f$ below 400 J/m$^2$) and was sampled before any aforementioned adjustments. This provided the research team with a way to quantify the impact of the adjustments. Upon review of Table 3, the adjustments for each production mix had varying levels of success. Due to the complex nature of asphalt mixtures, a multitude of factors can potentially impact DCT results. The primary conclusion from the applied adjustments is each was effective at increasing the corresponding fracture energy. All adjusted mixes saw an increase in fracture energy from the unadjusted mix.

**Table 2** Summary of results and adjustments at mix design

| Trunk highway (TH) | Test temp (°C) | Avg $G_f$ (J/m$^2$) | Avg peak load (kN) | Is $G_f \geq 400$ J/m$^2$? |
|---|---|---|---|---|
| 10 | −24 | **627** | 3.76 | YES |
| 56 | −24 | *334* | 2.78 | NO |
| 69 | Mix design specimens not available for testing[b] | | | |
| 310 | −30 | *195*[a], *318* | 2.37[a], 3.11 | NO |
| 371 | −24 | **543** | 3.25 | YES |

[a]First set of mix design pills for TH 310 made with incorrect binder
[b]Mixture adjustments for TH 69 made during production

**Table 3** Summary of results at production

| TH | Avg $G_f$ (J/m$^2$) | | Avg peak load (kN) | | Change in $G_f$ from mix design to (adjusted) production mix (J/m$^2$) | Change in $G_f$ from unadjusted to adjusted production mix (J/m$^2$) |
|---|---|---|---|---|---|---|
| | Unadjusted | Adjusted | Unadjusted | Adjusted | | |
| 10 | **444** | | 3.83 | | −183 | N/A |
| 56 | *292* | *310* | 2.92 | 2.89 | −24 | +18 |
| 69 | *324*[a] | **549** | 3.12 | 3.26 | N/A | +225 |
| 310 | *257* | *317* | 3.02 | 3.31 | −1 | +60 |
| 371 | **470** | | 3.49 | | −73 | N/A |

[a]Fracture energy of 324 J/m$^2$ not a result from mix design, but rather production mixture tested before adjustments

Figure 4 summarizes all testing results from this study. The red horizontal line illustrates the 400 J/m$^2$ threshold required as the minimum fracture energy. As can be seen in both Table 3 and Fig. 4, production mixes from four of the five sites exhibited a lower fracture energy than the mix design specimens. TH 69 is excluded, as mix design specimens were unavailable. It is unclear what factors cause this impact. This phenomenon currently being investigated in an ongoing research study.

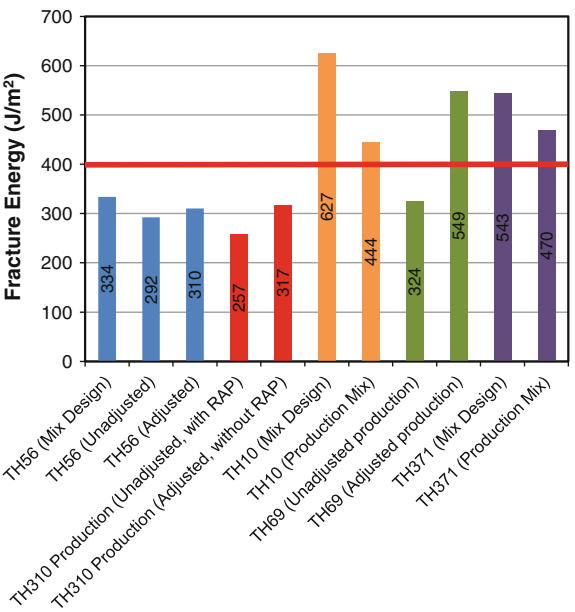


**Fig. 4** Summary of DCT pilot study testing

## 4 Summary

This paper discusses the efforts undertaken to implement a low-temperature cracking performance specification for asphalt mixtures. The specification utilizes DCT fracture energy as a performance criteria. A pilot implementation was undertaken in 2013 by use of performance specification for five construction projects in the State of Minnesota (United States). The implementation required the mix design specimens to be tested as part of mix approval and verification testing conducted on production mix samples. The pilot study helped in identifying some challenges to full scale implementation as well as helped find out certain deviations in DCT fracture energy measurements that can be seen between lab prepared mix design samples and plant produced production mix. On basis of the lessons learned through the work discussed in this paper, the current research efforts are underway in modifying and finalizing the DCT fracture energy performance specifications. A full scale implementation of the specifications for the Minnesota Department of Transportation (MnDOT) is presently scheduled for 2016.

This study also reaffirms traditional viewpoints on asphalt mix design, such as, increasing levels of binder content and/or the use of a "colder" performance grade low temperature binder presumably creates a softer mix, and results in higher fracture energies. Further research on the impact of these individual mix design parameters, along with other relevant parameters (VMA, VFA, PG spread, percent of recycled materials, etc.), on fracture energy is ongoing. Furthermore, the pavement sections constructed during the pilot implementation (with and without adjusted mixes) are continually being observed and their field cracking performance is being documented to study the effects of fracture energies on cracking performance.

## References

Cascione, A.A., R.C. Williams, W.G. Buttlar, S. Ahmed, B. Hill, D.S. Haugen, and S. Gillen. "Laboratory Evaluation of Field Produced Hot Mix Asphalt Containing Post-Consumer Recycled Asphalt Shingles and Fractionated Recycled Asphalt Pavement," *Journal of the Association of Asphalt Paving Technologists*, Vol. 80, pp. 377-418, 2011.

Dave, E.V., A.F. Braham, W.G. Buttlar, G.H. Paulino, and A. Zofka, "Integration of Laboratory Testing, Field Performance Data, and Numerical Simulations for the Study of Low-Temperature Cracking," Proceedings of the 6th RILEM International Conference on Cracking in Pavements, Chicago, USA, Eds. Al-Qadi, Scarpas, and Loizos, CRC Press Taylor and Francis Group, New York, ISBN: 978-0-415-4757-54, pp.369-378, 2008.

Dave, E.V., P. Koktan, "Synthesis of Performance Testing of Asphalt Concrete," Report No. MnDOT 2011-22. Minnesota Department of Transportation, Research Services Section, 395 John Ireland Boulevard, MS 330, St. Paul, Minnesota 55155, 2011.

Dave, E.V., W.G. Buttlar, S.E. Leon, B. Behnia and G.H. Paulino, "IlliTC – Low Temperature Cracking Model for Asphalt Pavements," Road Materials and Pavement Design, Vol. 14 (Sup. 2), pp. 57-78, 2013.

Marasteanu, M., A. Zofka, M. Turos, X. Li, R. Velasquez, X. Li, C. Williams, J. Bausano, W. Buttlar, G. Paulino, A. Braham, E. Dave, J. Ojo, H. Bahia, A. Gallistel, and J. McGraw, "Investigation of Low Temperature Cracking in Asphalt Pavements", National Pooled Fund Study 776, Minnesota Department of Transportation, Research Services MS 330, St. Paul, MN 55155, 2007.

Marasteanu, M., K.H. Moon, E.Z. Teshale, A.C. Falchetto, M. Turos, W. Buttlar, E. Dave, G. Paulino, S. Ahmed, S. Leon, A. Braham, B. Behnia, H. Bahia, H. Tabatabaee, R. Velasquez, A. Arshadi, S. Puchalski, S. Mangiafico, C. Williams, A. Buss, J. Bausano, A. Kvasnak, "Investigation of Low Temperature Cracking in Asphalt Pavements," National Pooled Fund Study -Phase II, Report No. MN/RC 2012-23, Minnesota Department of Transportation, August 2012.

# Fatigue Performance of Stone Mastic Asphalt Designed with the Bailey's Method

**Marco Pasetto and Nicola Baldo**

**Abstract** This paper presents the results of a laboratory analysis and a theoretical study on the fatigue performance of Stone Mastic Asphalt (SMA) mixtures, evaluated by the four-point bending test. The trial was performed on SMA mixes made with Electric Arc Furnace (EAF) steel slags and Coal Bottom Ash, integrated in the aggregate skeleton in partial substitution of natural limestone and filler, respectively. The Bailey's method as well as a conventional trial and error approach, were used in order to design the grading curves of the mixes. The bitumen content evaluation was based on the optimization of the volumetric properties and the moisture resistance of the SMA mixtures, using the gyratory compactor and the indirect tensile test. The purpose was that to compare the fatigue resistance of the mixtures designed by means of Bailey's and the trial and error procedures, considering both the empirical approach, related to a 50 % reduction in the initial stiffness modulus and the dissipated energy analysis, which allows a more rational evaluation of the fatigue performance. Bailey's SMA mixtures presented better fatigue behaviour than the reference mixes designed with the trial and error procedure. Moreover, with respect to the control SMA mixes prepared with natural aggregates, the mixes made with EAF slags and Coal ash showed improved fatigue properties.

**Keywords** Stone mastic asphalt · Steel slags · Coal ash · Bailey method · Fatigue performance

M. Pasetto (✉)
Department of Civil, Environmental and Architectural Engineering, University of Padua, Padua, Italy
e-mail: marco.pasetto@unipd.it

N. Baldo
Chemistry, Physics and Environment Department, University of Udine, Udine, Italy
e-mail: nicola.baldo@uniud.it



F. Canestrari and M.N. Partl (eds.), *8th RILEM International Symposium on Testing and Characterization of Sustainable and Innovative Bituminous Materials*, RILEM Bookseries 11, DOI 10.1007/978-94-017-7342-3_80

# 1 Introduction

In order to properly design the aggregate structure of a bituminous mixture, a trial and error procedure, related to a reference grading envelope, is typically used most of the times in the mix design process. Whenever the aggregates are characterized by a very high particle density, a volumetric procedure should be adopted, as for instance the Bailey's method (Pasetto and Baldo 2014). The performance characterization of the asphalt mixtures designed with the Bailey's method, is very often focused on the compactability and the permanent deformation resistance evaluation, in order to appreciate the contribution of a volumetrically designed aggregate skeleton (Graziani et al. 2012). However, even if the aggregate skeleton gives a structural contribution primarily to the permanent deformation resistance, also the fatigue resistance could benefit by an improvement on the packing properties of the lithic structure, due to the volumetric design.

The paper presents the results of a comparative laboratory testing concerning the fatigue resistance of Stone Mastic Asphalt (SMA) mixes designed by means of a conventional trial and error procedure, as well as a volumetric procedure, namely the Bailey's method. The SMA mixes investigated were partially made with Electric Arc Furnace (EAF) steel slag and coal ash, in order to valorize the environmental sustainability of the designed mixes.

# 2 Materials and Methods

## *2.1 Materials*

EAF slag, coal ash and crushed limestone (CS) were the granular materials used in the laboratory trials here described. The steel slags and the limestone aggregates have been made available in three different grading fractions: 0/5, 5/10 and 10/15 mm. On the conrary, the particle size of the coal ash was that of a typical mineral filler (passing percentage at the 0.075 mm sieve equal to 82 %). The physical-mechanical properties of the aggregates are reported in Table 1.

For all the mixtures studied, a SBS polymer modified bitumen was adopted. The laboratory investigation, outlined a 46 mm/10 penetration (EN 1426), a Ring & Ball softening point of 75 °C (EN 1427) and a Fraass breaking point of −13 °C (EN 12593). The elastic recovery value, certified by the bitumen manufacturer, is higher than 50 % at 25 °C (EN 13398).

The mix design and performance evaluation were focused on four different SMA mixes, two with both recycled and natural aggregates (S/RA, B/RA) and two, used as a control, with limestone only (S/LS, B/LS). Hereinafter, "S" stands for standard, "B" for Bailey, "RA" for recycled and "LS" for limestone. For the control LS mix, a conventional Portland Cement (PC) has been used as a filler, instead of the coal ash.

**Table 1** Aggregate properties

| Physical/mechanical properties | CS 0/5 | CS 5/10 | CS 10/15 | EAF 5/10 | EAF 10/15 | Coal ash |
|---|---|---|---|---|---|---|
| Los Angeles coefficient (%) EN 1097-2 | – | – | 30 | – | 8 | – |
| Equivalent in sand (%) EN 933-8 | 69 | – | – | – | – | – |
| Shape Index (%) EN 933-4 | 7 | 5 | 5 | 11 | 1 | – |
| Flakiness Index (%) EN 933-3 | 6 | 8 | 6 | 9 | 5 | – |
| Loose unit weight (g/cm$^3$) AASHTO T-19 | 1.47 | 1.25 | 1.26 | 1.72 | 1.67 | 0.85 |
| Rodded unit weight (g/cm$^3$) AASHTO T-19 | 1.57 | 1.38 | 1.40 | 1.87 | 1.88 | – |

## 2.2 *Methods*

### 2.2.1 Aggregate Structure Design

The particle size distribution of the mixes S/RA and S/LS has been optimized by means of a conventional trial and error procedure, with reference to the design grading envelope of SITEB (2000).

The aggregate structure of the mixes B/RA and B/LS was instead developed on the basis of the Bailey's method (Vavrik et al. 2002), in order to improve the aggregate interlock and packing effects. For this study, the Bailey's procedure has been implemented in an electronic spreadsheet, on the basis of the equations reported in the Transportation Research Circular No. E-C044 (Vavrik et al. 2002).

The packing characteristics within each of the three portions of the designed mixture are then analyzed by means of three specific ratios, namely the coarse aggregate ratio (CA Ratio), the fine aggregate coarse ratio ($FA_c$ Ratio), and the fine aggregate fine ratio ($FA_f$ Ratio). The CA Ratio is defined by the equation:

$$CA\ Ratio = \frac{\%\,Passing\ Half\ Sieve - \%\,Passing\ PCS}{100\,\% - \%\,Passing\ Half\ Sieve} \tag{1}$$

The primary control sieve (PCS) is defined as the closest sized sieve to the numerical result computed according to the formula:

$$PCS = NMPS \times 0.22 \tag{2}$$

where the nominal maximum particle size (NMPS) is assumed as the sieve larger than the first sieve that retains more than 10 %, as reported by Superpave terminology (Vavrik et al. 2002). The formula for the computation of the $FA_c$ Ratio is given by the equation:

$$FA_c = \frac{\%\,Passing\ SCS}{\%\,Passing\ PCS} \tag{3}$$

where the 0.22 factor already used for the overall mix gradation is applied to the PCS to establish a secondary control sieve (SCS). Lastly, the $FA_f$ Ratio is computed according to the formula:

$$FA_f = \frac{\%\,Passing\ TCS}{\%\,Passing\ SCS} \tag{4}$$

where the tertiary control sieve (TCS) is obtained by multiplying the SCS by the 0.22 factor.

In order to evaluate the level of interlock actually achieved in the design mixes, in relation to the loose unit weight of the coarse aggregates, it is necessary to determine the voids in the coarse aggregate of the mixture ($VCA_{mix}$) after laboratory compaction and the voids in the coarse aggregate in the dry rodded conditions ($VCA_{DRC}$), in accordance to AASHTO T-19. $VCA_{DRC}$ is then computed on the basis of the following equation:

$$VCA_{DRC} = \left[\frac{(G_{CA} \cdot \gamma_w) - \gamma_S}{G_{CA} \cdot \gamma_w}\right] \cdot 100 \tag{5}$$

where $G_{CA}$ is the bulk specific gravity of coarse aggregate portion of the aggregate matrix, $\gamma_w$ is the unit weight of water and $\gamma_s$ is the unit weight of coarse aggregate portion of the aggregate matrix.

The $VCA_{mix}$ is calculated according to the formula:

$$VCA_{MIX} = \left[1 - \frac{(G_{MB} \cdot P_{CA})}{G_{CA}}\right] \cdot 100 \tag{6}$$

where $G_{MB}$ is the bulk specific gravity of the SMA mix, $G_{CA}$ is the bulk specific gravity of coarse aggregate retained at the breakpoint sieve and $P_{CA}$ is the percent coarse aggregate retained at the breakpoint sieve, by weight of total granular mix. According to NCHRP project 9-8, the 4.75 mm sieve represents the breakpoint sieve for 12.5 mm NMPS. $P_{CA}$ is determined with the following formula:

$$P_{CA} = \frac{\%\,Retained\ On\ Break\ Point\ Sieve}{100} \times \left(1 - \frac{\%\,Bitumen\ Content}{100}\right) \tag{7}$$

The stone to stone contact condition, that represents a fundamental requirement for a proper SMA mix design, is achieved if the $VCA_{mix}$ results lower or equal to the $VCA_{DRC}$ (Pasetto and Baldo 2014).

### 2.2.2 Mix Design Principles

According to CIRS-Italian Ministry of Infrastructure Specifications (2001), a mix design method based on the gyratory compaction and the Indirect Tensile Strength (ITS) test at 25 °C, on both dry and wet cylindrical specimens, was adopted in order to optimize the bitumen content, for all the SMA mixes. Regarding the main gyratory test parameters, a speed of 30 revs/min, a pressure of 600 kPa, an angle of rotation of 1.25° and a diameter of the mould of 150 mm, were adopted. For each SMA mix, the Optimum Bitumen Content (OBC) was identified with respect to specific volumetric requisites: a residual air voids content ($V_a$) at 10, 100 and 180 revs, of 8–12 %, 2–4 % and over 2 %, respectively (CIRS 2001). Then, for the optimal mixes, the dry indirect tensile strength at 25 °C and the Tensile Strength Ratio (TSR) were determined and compared with the CIRS acceptance requisites. The TSR was calculated as the ratio between the indirect tensile strength of the samples conditioned by means of 15 days of immersion in a thermostatic bath at 25 °C ($ITS_{wet}$) and unconditioned ($ITS_{dry}$), respectively. The $ITS_{dry}$ and the TSR values of the optimal SMA mixtures should result higher than 0.6 MPa and 75 %, respectively.

### 2.2.3 Fatigue Analysis

The four-point bending fatigue tests were conducted following the general indications given in the Annex D of the European EN 12697-24 Standard, in a regime of stress control, with a wave of sinusoidal loading without rest periods. The fatigue tests were all conducted at a temperature of 20 °C, frequency of 10 Hz, and at three stress levels: 0.9, 1.4 and 1.9 MPa. The stress levels have been identified on the basis of preliminary tests. The beam specimens submitted to the bending tests, with dimensions of 400 mm × 50 mm × 60 mm, were cut from 300 mm × 400 mm × 50 mm slabs, prepared using a laboratory compacting roller in accordance with the EN 12697-33 Standard. The results of the fatigue tests were interpreted with two different approaches. In addition to the classical methodology based on a 50 % reduction of the initial stiffness, an energy approach was also applied (Pronk 1997).

## 3 Results and Discussion

### *3.1 Aggregate Structure Design Results*

The present study have been focused on 12.5 mm nominal maximum particle size (NMPS). Therefore, according to the Bailey's criterion, Half Sieve, Primary Control Sieve (PCS), Secondary Control Sieve (SCS) and Tertiary Control Sieve (TCS) resulted equal to the 6.25 mm, the 2.36 mm, the 0.60 mm and the 0.150 mm

sieve, respectively (Vavrik et al. 2002). To achieve the level of coarse aggregate interlock desired in the SMA mix, the rodded unit weight, which is determined for each specific coarse aggregate, is used as the reference for the chosen unit weight of the coarse aggregate. With regards to different coarse aggregates, the Bailey's Method combines them by volume mathematically, using the corresponding chosen unit weights. The chosen unit weight for the coarse aggregates (namely EAF 10/15 and Limestone 10/15) has been fixed to 125 % of their corresponding rodded unit weight. Table 2 reports the composition of the mixtures; the corresponding grading curves are presented in Fig. 1.

The aggregate ratios, computed according to Eqs. (1, 3 and 4), as well as the recommended ranges for the aggregate ratios in SMA mixtures (Vavrik et al. 2002), have been reported in Table 3. The aggregate ratios requisites, recommended in the Transportation Research Circular No. E-C044 (Vavrik et al. 2002), for SMA mixes

**Table 2** Aggregate type and composition of the mixtures

| Aggregate type | S/RA content [%] | S/LS content [%] | B/RA content [%] | B/LS content [%] |
|---|---|---|---|---|
| EAF slag 5/10 | 20 | 0 | 10.92 | 0 |
| EAF slag 10/15 | 0 | 0 | 8.54 | 0 |
| Coal ash | 10 | 0 | 10.37 | 0 |
| CS 0/5 | 25 | 25 | 20.79 | 22.56 |
| CS 5/10 | 45 | 65 | 49.38 | 60.22 |
| CS 10/15 | 0 | 0 | 0 | 6.89 |
| Synthetic filler PC | 0 | 10 | 0 | 10.33 |

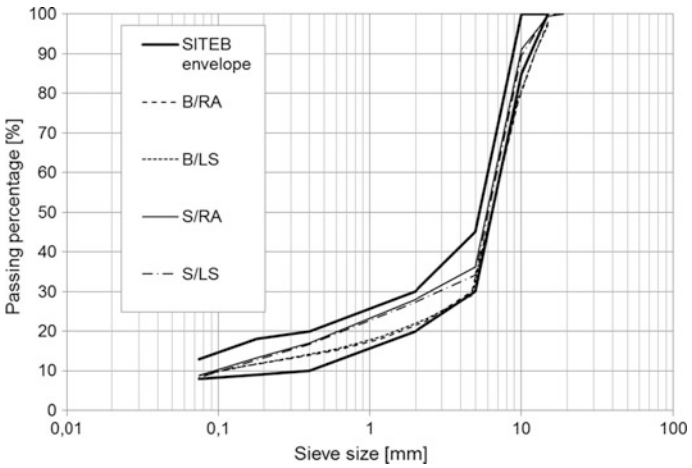


**Fig. 1** Grading curves of the mixes

**Table 3** Aggregate ratios for the design mixes

| Aggregate ratio | B/RA | B/LS | Recommended range |
|---|---|---|---|
| CA Ratio | 0.389 | 0.390 | 0.250–0.400 |
| $FA_c$ Ratio | 0.675 | 0.672 | 0.600–0.850 |
| $FA_f$ Ratio | 0.734 | 0.725 | 0.600–0.850 |

**Table 4** Comparison of VCA results

| Mixes | $VCA_{mix}$ % | $VCA_{DRC}$ % | $VCA_{mix} < VCA_{DRC}$ |
|---|---|---|---|
| S/RA | 36.0 | 45.5 | Yes |
| S/LS | 31.7 | 45.9 | Yes |
| B/RA | 36.58 | 46.84 | Yes |
| B/LS | 32.87 | 46.05 | Yes |

with a 12.5 mm NMPS, were completely satisfied for the B/RA as well as for the B/LS.

However, a partial noncompliance of the Bailey design grading curves with respect to the SITEB reference envelope, is worth mentioning. The discrepancies are related to the passing percentages at the largest sieves (greater than 4.75 mm), so denoting a coarser gradation for the design curves obtained by the Bailey's method.

The results of the voids in the coarse aggregate determination are presented in Table 4; it is possible to observe that the stone to stone contact condition has been verified for all the mixes and therefore a satisfactory level of coarse aggregate interlock should be ensured for each of the designed SMA mixtures.

## *3.2 Mix Design Results*

The results of the mix design procedure are presented in Table 5.

**Table 5** Mix design results

| Property | S/RA | S/LS | B/RA | B/LS | Acceptance requisites |
|---|---|---|---|---|---|
| Va @ 10 revs (%) | 9.13 | 9.08 | 8.79 | 8.22 | 8–12 % |
| Va @ 100 revs (%) | 3.79 | 3.74 | 3.69 | 3.65 | 2–4 % |
| Va @ 180 revs (%) | 3.67 | 3.55 | 3.36 | 3.13 | >2 % |
| VMA (%) | 17.75 | 17.00 | 17.76 | 17.02 | >17 % |
| VFB (%) | 78.66 | 78.00 | 79.23 | 78.56 | 75–85 % |
| Bulk density (g/cm$^3$) | 2.59 | 2.46 | 2.61 | 2.48 | – |
| $ITS_{dry}$ (MPa) | 1.24 | 1.13 | 1.31 | 1.25 | >0.6 MPa |
| $ITS_{wet}$ (MPa) | 1.08 | 0.85 | 1.16 | 0.98 | – |
| TSR (%) | 87 | 75 | 89 | 78 | >75 % |

The Air Voids ($V_a$) requisites prescribed by CIRS mix design procedure, at 10, 100 and 180 revs, were completely fulfilled, for all the SMA mixes, in correspondence of a bitumen content equal to 5.5 % of the weight of the aggregate. For SMA mixtures a percentage of Voids in the Mineral Aggregate (VMA) higher than 17 % and a percentage of Voids Filled with Bitumen (VFB) between 75 and 85 % are needed. According to data in Table 5, all the additional volumetric requisites are verified for the designed mixes. The mechanical requisites, in terms of $ITS_{dry}$ and TSR were also satisfied, for all the designed SMA mixes (Table 5). The SMA mixes designed by the Bailey method (B/RA and B/LS) showed improved ITS values, with respect to the reference asphalt mixtures (S/RA and S/LS), varying from 5 to 18 %, depending on the dry/wet condition. Focusing the attention on the comparison between mixes with and without marginal aggregates, it is possible to observe higher ITS values for the SMA mixes made with EAF steel slag and coal ash. The highest TSR values recorded for the mixes with marginal aggregates, with respect to the corresponding natural SMA mixes, confirm the strong affinity between EAF steel slag and the modified binder, already observed in other investigations (Pasetto and Baldo 2013).

## 3.3 *Fatigue Analysis Results*

### 3.3.1 Fatigue Analysis Based on the Stiffness Reduction Approach

The conventional fatigue curves (FC), elaborated on the basis of the initial value of strain $\varepsilon_0$ and number of cycles $N_f$, at which a 50 % reduction of the initial stiffness is recorded, are presented in Fig. 2. The initial strain was evaluated at the 100th

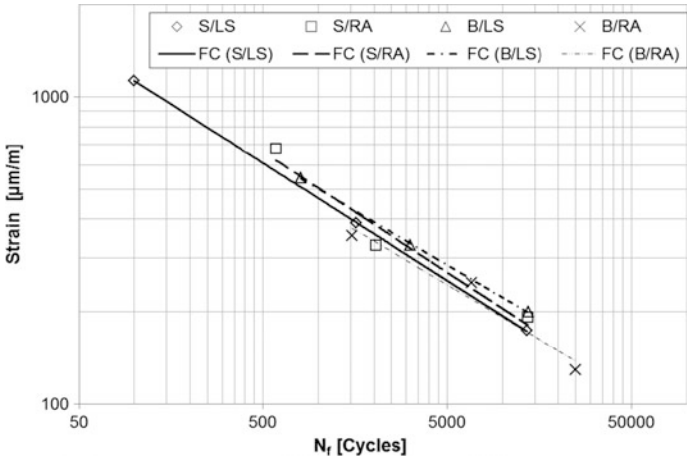


**Fig. 2** Fatigue life $N_f$ versus initial strain

**Table 6** Fatigue curves—regression coefficients ($N_f$ approach)

| Mixture | a (μm/m) | b (–) | ε ($10^6$) (μm/m) | $R^2$ (–) |
|---|---|---|---|---|
| S/RA | 7601.9 | −0.392 | 34 | 0.9594 |
| S/LS | 6571.5 | −0.383 | 33 | 0.9999 |
| B/RA | 5088.0 | −0.356 | 37 | 0.9581 |
| B/LS | 5712.0 | −0.352 | 44 | 0.9997 |

cycle (EN 12697-24, Annex D). The regression analysis of the fatigue data was performed using a power law model of the type:

$$\varepsilon_0 = aN_f^b \tag{8}$$

where a and b are regression coefficients depending on the type of material. Table 6 report the regression coefficients and coefficient of determination $R^2$.

For all the mixtures, the coefficient of determination was higher than 0.9 and therefore the regressions can be considered really effective. With reference to a fatigue resistance of 1,000,000 loading cycles (as indicated in Standard EN 12697–24, Annex D), and using Eq. (8), it was possible to calculate the corresponding tensile strain ε ($10^6$), which was higher for the mixes designed by means the Bailey method; in particular the highest value, 44 μm/m, was obtained for B/LS (Table 6).

### 3.3.2 Fatigue Analysis Based on the Energy Ratio Approach

The energy approach adopted (Pronk 1997) is based on the calculation of the energy ratio $R_n$, defined as the ratio between the cumulative energy dissipated up to the n-th cycle and that dissipated at the n-th cycle, according to Eq. (9):

$$R_n = \frac{\pi \sum_{i=0}^{n} \sigma_i \varepsilon_i sen\phi_i}{\pi \sigma_n \varepsilon_n sen\phi_n} \tag{9}$$

where σ is the stress, ε the strain, ϕ the phase angle, i the generic i-th cycle, n the n-th cycle.

The study of the evolution of the energy ratio during the test allows the number of cycles $N_1$ to be determined in correspondence to which macro-cracks form. Figure 3 presents an example, relative to the S/LS mix, of the determination of $N_1$: the peak value of the curve in the $R_n$-N plane, can be clearly identified.

Figure 4 presents the fatigue curves in terms of $N_1$ and the initial strain value, for the various mixtures. Similarly to what was previously done for the classical fatigue curves, represented as a function of $N_f$, a power function, analogous to Eq. (8), was also used in this case, substituting $N_1$ for $N_f$. Table 7 reports the value of ε ($10^6$) as well as the coefficients of regression and determination; the latter resulted higher than 0.9 for each mix considered, thus the regressions can be evaluated as fully satisfactory. Although the comparative analysis of the ε ($10^6$) values related to the

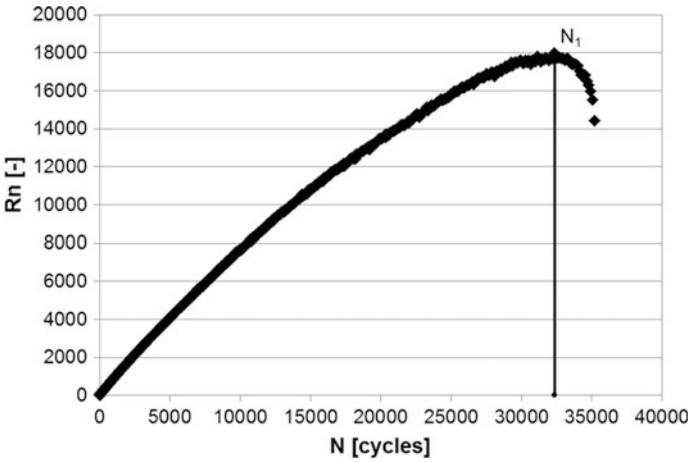


**Fig. 3** Determination of failure $N_1$ for mix S/LS at 0.9 MPa

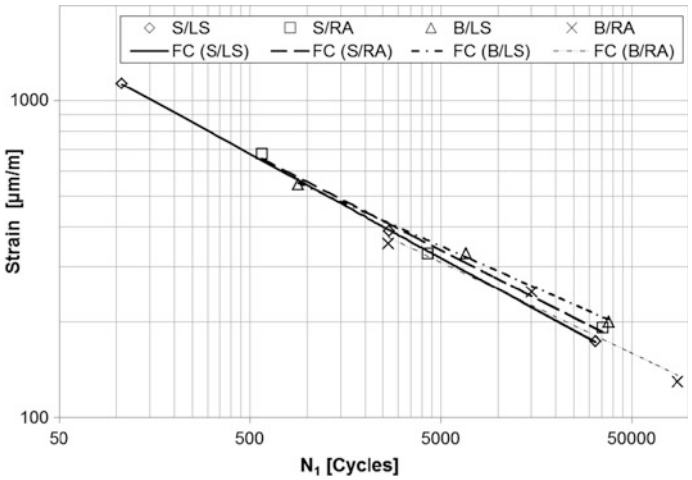


**Fig. 4** Fatigue life $N_1$ versus initial strain

**Table 7** Fatigue curves—regression coefficients ($N_1$ approach)

| Mixture | a (µm/m) | b (–) | ε ($10^6$) (µm/m) | $R^2$ (–) |
|---|---|---|---|---|
| S/RA | 4604.9 | −0.307 | 66 | 0.9903 |
| S/LS | 5237.1 | −0.329 | 56 | 0.9999 |
| B/RA | 3363.1 | −0.266 | 85 | 0.9979 |
| B/LS | 3600.8 | −0.288 | 67 | 0.9732 |

different mixtures, using the conventional as well as the Pronk approach, leads to a similar ranking of the various materials (at least from a qualitative point of view), it can be observed that, in any case, $\varepsilon$ ($10^6$) values determined from $N_1$ are higher than those calculated with reference to $N_f$; therefore, the analysis with the energy approach determines a longest fatigue life of the mixtures. In addition, the trends for the $N_1$ criterion are reversed for the Bailey's mixes, with respect to the $N_f$ method; therefore the highest $\varepsilon$ ($10^6$) value was obtained for B/RA.

## 4 Conclusions

According to the mix design results, the Bailey's skeleton design method led to SMA mixtures characterized by an improved moisture damage resistance, with respect to the trial and error's mixtures. The four point bending fatigue tests, conducted in a regime of stress control, have demonstrated the improved performance of the Bailey's mixtures when compared with those designed with a conventional trial and error procedure. The better performance of the Bailey's mixes is also fully confirmed by means of the Pronk's energy based approach. The improved mechanical response of the Bailey's mixtures can be ascribed to the better packing of the grains, that translates into a more compact structure, with benefits for the mechanical properties of such mixtures.

The effectiveness of the Bailey's method in the increase of fatigue life was also clear for the mixtures made with EAF steel slag and coal ash up to 20 and 10 % on the weight of the aggregates, respectively. However, the use of marginal aggregates provides improved fatigue, as well as moisture resistance, also for the trial and error's mixes.

The results of the fatigue evaluation with the criterion $N_f$ don't show much variation within the mixes designed with the trial and error approach. On the other hand, a difference with the criterion $N_1$ can be noticed.

The comparison between the mixtures conducted with the criteria $N_f$ and $N_1$ led to a similar quality evaluation, but the energy criterion showed increases in fatigue life quantitatively higher than those of the classical approach.

## References

Pronk AC (1997) Comparison of 2 and 4 point fatigue tests and healing in 4 point dynamic test based on the dissipated energy concept. Paper presented at the 8th International Conference on Asphalt Pavement, Seattle, USA, 10-14 August, 1978.

SITEB (2000) Capitolato d'appalto per pavimentazioni stradali con bitume modificato. Roma. [in Italian]

CIRS-Italian Ministry of Infrastructure Specifications (2001) Norme tecniche di tipo prestazionale per capitolati speciali d'appalto. Roma. [in Italian]

Pasetto M, Baldo N (2013) Fatigue Performance of Asphalt Concretes Made with Steel Slags and Modified Bituminous Binders. Int J Pav Res Technol 6(4):294-303. doi: 10.6135/ijprt.org.tw/2013.6(4).294

Pasetto M, Baldo N (2014) Influence of the aggregate skeleton design method on the permanent deformation resistance of stone mastic asphalt. Mater Res Innov 18(S3):S96-S101. doi: DOI: 10.1179/1432891714Z.000000000588

Graziani A, Ferrotti G, Pasquini E, Canestrari F (2012) An application to the European practice of the Bailey Method for HMA aggregate grading design. Procedia - Social and Behavioral Sciences 53:991-1000. doi: 10.1016/j.sbspro.2012.09.948

Vavrik WR, Huber G, Pine WJ, Carpenter SH, Bailey R (2002) Bailey Method for Gradation Selection in HMA Mixture Design. Transportation Research Circular no. E-C044. Transportation Research Board.

# Evaluation of Different Methods for the Estimation of the Bitumen Fatigue Life with DSR Testing

**André Pereira, Rui Micaelo, Luís Quaresma and Maria Teresa Cidade**

**Abstract** Asphalt fatigue cracking is one of the phenomena that contribute most to degradation of road pavements and it may initiate within the bitumen or at the bitumen-aggregate interface. The cohesive cracking resistance can be evaluated with bitumen testing. Commonly, the Dynamic Shear Rheometer (DSR) is used for bitumen testing. This paper presents an evaluation of different methods proposed in literature for the estimation of the bitumen fatigue life. A neat and a polymer modified bitumen (PMB) were tested with time sweep tests (continuous and discontinuous loading) and with incremental load amplitude (linear amplitude sweep test). The results are analysed with the traditional approach ($N_{f,50}$ corresponding to 50 % initial modulus reduction) and other methodologies, namely the Ratio of Dissipated Energy Change (RDEC) and the Viscoelastic Continuum Damage (VECD) approach. The results obtained showed, as expected, that the PMB has a higher resistance to fatigue than the neat bitumen. The test conditions and the method used to evaluate the fatigue resistance lead to significant differences in the estimated bitumen fatigue life. The plateau value (RDEC) shows very good correlation with $N_{f,50}$ obtained from constant strain amplitude tests, regardless of the type of bitumen or test conditions. The fatigue life parameters obtained from the linear amplitude sweep test is very sensitive to the analysis method. Healing during non-loading periods has a large effect on the PMB fatigue life while no effect in the neat bitumen fatigue life for small to intermediate rest periods.

A. Pereira · R. Micaelo (✉) · L. Quaresma
Department of Civil Engineering, Universidade Nova de Lisboa, Caparica, Portugal
e-mail: ruilbm@fct.unl.pt

A. Pereira
e-mail: air.pereira@campus.fct.unl.pt

L. Quaresma
e-mail: lmtq@fct.unl.pt

M.T. Cidade
Department of Materials and CENIMAT/I3 N, Universidade Nova de Lisboa, Caparica, Portugal
e-mail: mtc@fct.unl.pt



F. Canestrari and M.N. Partl (eds.), *8th RILEM International Symposium on Testing and Characterization of Sustainable and Innovative Bituminous Materials*, RILEM Bookseries 11, DOI 10.1007/978-94-017-7342-3_81

**Keywords** Fatigue life · DSR · VECD · Healing

## 1 Introduction

Asphalt fatigue cracking due to repeated traffic loading is one of the phenomena that contribute most to degradation of road pavements. This failure mode is considered in all pavement design guides. The fatigue resistance law, which relates the asphalt fatigue life with the loading conditions, is usually obtained from lab tests and then calibrated to field based on the local road network pavements data. Even that asphalt fatigue tests have been developed and widely used in the last decades, it is known that these tests are time consuming and relatively expensive. On the other hand, fatigue properties of mixtures are strongly related with those of binders and, in this context, fatigue testing of bituminous binders is an important task with considerable research potential (Partl et al. 2013; Botella et al. 2012).

In fact, cracking may initiate within the bitumen (cohesive cracking) or at the bitumen-aggregate interface. The cohesive cracking resistance can be evaluated with bitumen testing and, commonly, the Dynamic Shear Rheometer is used for that purpose. Furthermore, this equipment can also be used to evaluate the so-called self-healing capacity of bitumen. This phenomenon can be defined as the self-recovery capability of bituminous materials under certain loading and/or environmental conditions, especially during rest time, and it can have a significant effect on the fatigue life of those materials (Shen et al. 2010).

An adequate characterization of the bitumen fatigue resistance and healing potential will help with the design and selection of bitumens, which may contribute to the increase of road pavements' service life.

## 2 Estimation of Fatigue Life

There are several methods and failure criteria proposed in literature to evaluate the fatigue resistance of bituminous binders. By carrying out several tests it is possible to obtain a fatigue law of the material by fitting a power-law model, as:

$$N_f = A \cdot X^B \tag{1}$$

where, $X$ represents the cyclic loading amplitude (stress or strain amplitude), $N_f$ is the number of cycles to failure and, $A$ and $B$ are material dependent constants.

Focusing on strain-controlled fatigue tests, traditional fatigue analysis defines failure as the point at which the material's complex modulus value reduces to 50 % of its initial value and the corresponding number of cycles is typically denoted as $N_{f,50}$. Although arbitrary and controversial, this failure criterion has been widely

used by many researchers (Soenen and Eckmann 2000; Lu et al. 2003; Soenen et al. 2004; Shen et al. 2010; Santagata et al. 2013).

An alternative approach is based on the dissipated energy (DE) concept. When sustaining cyclic fatigue loading, the viscoelastic materials, like bitumen, exhibit different paths for the loading and unloading cycle and creates hysteresis loops (Shen et al. 2010). The area inside of the loop is the DE, which can be calculated with:

$$DE_n = \pi \cdot \tau_n \cdot \gamma_n \cdot sin\,\delta_n \tag{2}$$

where, $DE_n$ is the dissipated energy at cycle $n$ and, $\tau_n$, $\gamma_n$ and $\delta_n$ are, respectively, the stress amplitude, the strain amplitude and the phase angle at cycle $n$.

However, not all dissipated energy is responsible for damage propagation. Only the relative amount of energy dissipation coming from each additional load cycle, while excluding the energy dissipated through passive behaviours such as plastic DE, viscoelastic damping and thermal energy, will produce further damage (Shen et al. 2010; Sutharsan 2010; Zhang et al. 2013). Consequently, it was developed the concept of Ratio of Dissipated Energy Change (RDEC), which for a test in controlled strain mode is:

$$RDEC_b = \frac{DE_a - DE_b}{DE_a(b-a)} \tag{3}$$

where, a and b are the initial and final number of cycles of the interval (usually 100 cycles) used for the calculation of RDEC. The RDEC approach has been proved to be a good approach for the characterization of asphalt materials fatigue and healing properties (Sutharsan 2010).

During a fatigue test under a strain-controlled loading mode three different phases of RDEC variation are usually identified. First there is a fast increase of the RDEC value, then a phase with an almost constant value and finally a sharp decrease before the test is terminated. The RDEC value in the second stage is named as the Plateau Value (PV). Shen et al. (2010) found a unique relation between PV and $N_{f,50}$ (power-law model) for the complete set of bitumen type and test conditions. A higher magnitude of the PV indicates higher incremental damage energy and a shorter fatigue life. Thus, the effect of healing (self-recovery capacity under certain loading and/or environmental conditions) can be quantified as the reduction in the PV value due do the application of rest periods in the cyclic load test (Shen and Carpenter 2007; Shen et al. 2010; Sutharsan 2010; Van den bergh 2011).

The main disadvantage of the previously mentioned approaches is that several tests must be performed at various strain amplitude levels. The duration of these tests is undefined before the test and it is known that some binders can take many hours to show enough degradation to accurately assess their fatigue properties. The Linear Amplitude Sweep (LAS) test was proposed to overcome this challenge employing a cyclic loading at systematically increasing loading amplitudes to accelerate damage

and, as such, it can be seen as an accelerated procedure to characterize the fatigue resistance (Johnson 2010). LAS test results are analyzed using the viscoelastic continuum damage (VECD) approach to predict the bitumen fatigue life. The VECD is based on Schapery's theory of work potential to model damage growth (Hintz et al. 2011; Willis et al. 2012). According to this theory, for a viscoelastic material, work is related to damage by:

$$\frac{dD}{dt} = \left(-\frac{\partial W}{\partial D}\right)^{\alpha} \tag{4}$$

where, W is the work performed, D is the damage intensity and α is a material constant that is related to the rate at which damage progresses. The parameter α can be taken as 1 + 1/m or 1/m (there is no consensus in the literature as to which definition should be used). Nevertheless, Johnson (2010) defined α as 1 + 1/m and demonstrated that the slope, m, of a log-log plot of storage modulus (G′) versus angular frequency (w) can be used to calculate α. Thus, the LAS test protocol also includes a frequency sweep test at very low strain amplitude of 0.1 % to obtain the undamaged material properties and to allow the calculation of m and α. The amplitude sweep can be run directly after the low strain frequency sweep as no damage is induced during this stage (Johnson 2010; Hintz et al. 2011).

The work done by Johnson (2010) resulted in the development of AASHTO TP101-12 (MARC 2014). According to this standard, the damage accumulation in the specimen during the strain sweep test can be calculated with:

$$D(t) \cong \sum_{n=1}^{N} \left[\pi \cdot \gamma_0^2 (C_{n-1} - C_n)\right]^{\frac{\alpha}{1+\alpha}} (t_n - t_{n-1})^{\frac{1}{1+\alpha}} \tag{5}$$

where, C(t) is equal to |G*|sin δ at time t divided by the initial "undamaged" value of |G*|sin δ, $\gamma_0$ is the applied strain for a given data point (%), |G*| is the complex shear modulus (MPa),  is the phase angle and $t$ is the test time (sec). The C(t)-D(t) curve can be fitted with a power-law model:

$$C(t) = C_0 - C_1[D(t)]^{C_2} \tag{6}$$

where, $C_0$ is the initial value of C(t) ($C_0$ = 1), and $C_1$ and $C_2$ are curve-fit coefficients.

The parameters A and B of the fatigue law can then be calculated with (MARC 2014):

$$A = \frac{f\left(D_f\right)^{1+(1-C_2)\alpha}}{[1 + (1 - C_2)\alpha](\pi \cdot C_1 \cdot C_2)^{\alpha}} \tag{7}$$

$$B = -2\alpha \tag{8}$$

where, $f$ is the loading frequency (Hz), $D_f$ is the damage accumulation at failure, which is defined as the D(t) value that corresponds to a 35 % reduction in C(t) and calculated with:

$$D_f = \left(\frac{0.35}{C_1}\right)^{1/C_2} \tag{9}$$

# 3 Experimental

## 3.1 Materials

One paving grade bitumen (35/50) and a polymer modified bitumen (PMB 45/80-65) were selected for this study. PMB binder is modified with 2–4 % of SBS polymer using an undisclosed procedure by the supplier. Both binders were tested without considering any aging effect. The conventional properties of bitumens are given in Table 1. The bitumens were rheologically characterized using a Bohlin Gemini HRnano rotational rheometer. For dynamic tests, this equipment is equivalent to a Dynamic Shear Rheometer (DSR). Frequency sweeps were performed in constant strain loading mode at temperatures from 15 to 75 °C and frequencies between 0.1 and 10 Hz. The tests were performed with the 8 mm (2 mm gap) and 25 mm (1 mm gap) plate-plate set-up. The results for the complex modulus (G*) and the phase angle (δ) showed, as expected, higher phase angle values (lower elasticity), at given stiffness level, for the paving grade bitumen in comparison with the PMB.

## 3.2 Fatigue Tests

All fatigue tests were performed under controlled strain conditions, at a frequency of 10 Hz and at a temperature of 15 °C. It was used the parallel plate setup with the 8-mm spindle and a 2-mm gap between the plates. Two types of fatigue tests were performed: time sweep tests at constant strain and linear amplitude sweep tests (LAS).

**Table 1** Conventional properties of bitumens

| Method | Property | Bitumen | |
|---|---|---|---|
| | | 35/50 | PMB 45/80-65 |
| EN 1426 | Penetration (0.1 mm) | 43.0 | 51.0 |
| EN 1427 | Softening point (°C) | 51.0 | 70.4 |

The time sweep tests were performed without rest periods (continuous tests) and with rest periods (intermittent tests) to evaluate the effect of healing on fatigue life. The continuous tests were conducted at three strain levels: 1.2, 1.6 and 2 %. The intermittent tests were carried out at the single strain level of 1.2 % and rest periods of 4 and 8 s were introduced after every 10 s of loading. For the neat bitumen it was also considered a rest period of 16 s. To limit the total testing time, all time sweep tests were carried out until a 50 % reduction of the initial complex modulus was attained. Furthermore, the ratio between loading and rest duration was selected so that the duration of the tests did not exceed 14 h. The time sweep tests results were analyzed considering the traditional failure criterion ($N_{f,50}$) and the RDEC approach.

The LAS tests were performed based on the work done by Johnson (2010) and AASHTO TP 101-12 protocol (MARC 2014). Thus, before the fatigue test it was performed a frequency sweep at the low strain level of 0.1 %, and over a range of frequencies from 0.1 to 30 Hz. Then, it was performed a strain sweep at 10 Hz. The test procedure consists of applying an initial 100 cycles at 0.1 % strain to determine the undamaged linear viscoelastic properties of the bitumens and each subsequent load step consists of 100 cycles at a rate of increase of 1 % applied strain per step for 19 steps, beginning at 1 % and ending at 19 % applied strain. The LAS tests results were analyzed using the VECD approach.

Two repetition tests were performed for repeatability analysis purpose.

## 4 Results and Discussions

### *4.1 Time Sweep Tests*

Figure 1 illustrates the complex modulus during the continuous fatigue tests for both bitumens. As shown, the higher the level of deformation, the shorter the number of cycles until there is a 50 % reduction of the initial complex modulus

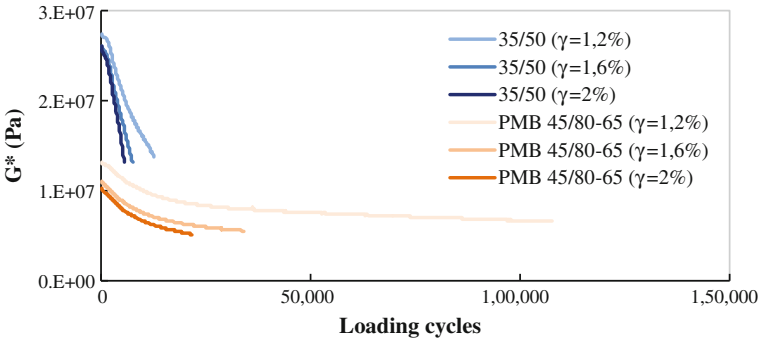


**Fig. 1** G* evolution for the 35/50 bitumen with different strain levels

and therefore, a shorter fatigue life. It is also noticed that for the same temperature (15 °C), the neat bitumen has a higher initial complex modulus and, consequently, for the same strain level, the 35/50 bitumen is subject to higher shear stress.

The PMB shows a reduction of the complex modulus from the beginning of the test while the neat bitumen has a constant value during the first 2,000 cycles. Then, the 35/50 shows a much faster reduction of G* with the loading cycles than the PMB. Figure 2 presents the $N_{f,50}$ results and the fatigue laws fitted to data. As expected, the fatigue life of the neat bitumen is much lower than of the PMB. However, the increase of the strain level has a larger effect on the PMB' fatigue life. For the largest strain levels tested, the initial decrease in complex modulus counts for an important share of the 50 % reduction of the initial complex modulus though it may not be necessarily due to fatigue. Some aspects such as the internal heating or the edge effects due to lower initial stiffness of the PMB may have caused the unexpected reduction of the initial complex modulus. Hence, the traditional failure criterion may not be the most appropriate to evaluate the fatigue resistance of the PMB, especially for higher strain levels.

The effect of rest periods on the fatigue life defined by the traditional failure criterion is presented in Fig. 3.

The effect of rest periods on the fatigue life is much more evident for the PMB than for the 35/50 bitumen. With the introduction of rest periods, the fatigue life of the PMB is significantly longer, showing a sharp increase with the duration of the rest period. Therefore, it can be inferred that the PMB has a larger self-healing capacity. Instead, in the case of the neat bitumen, the rest periods of 4 and 8 s lead to small reduction in the fatigue life, being comparable with the no rest situation. Nevertheless, for a rest period of 16 s there is an increment of the fatigue life and therefore it can be assumed that with sufficiently long rest periods, the neat bitumen also has self-healing capacity.

It should be emphasized that the PMB has a lower initial stiffness than the neat bitumen, meaning lower shear stress for the same strain level. So, the damage accumulated by the PMB tends to be smaller and the self-healing process might have developed more efficiently. The fact of the PMB showing a lower stiffness at

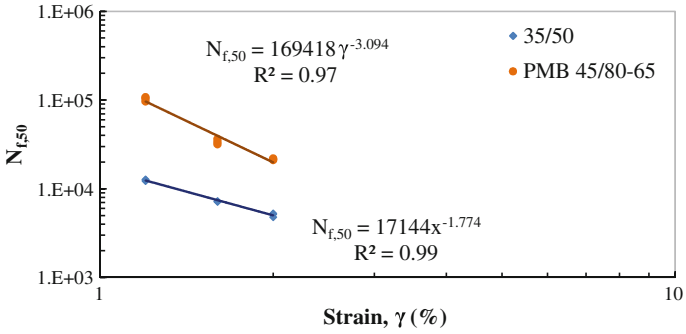


**Fig. 2** Traditional $N_{f,50}$—strain relationship for bitumen's fatigue testing results

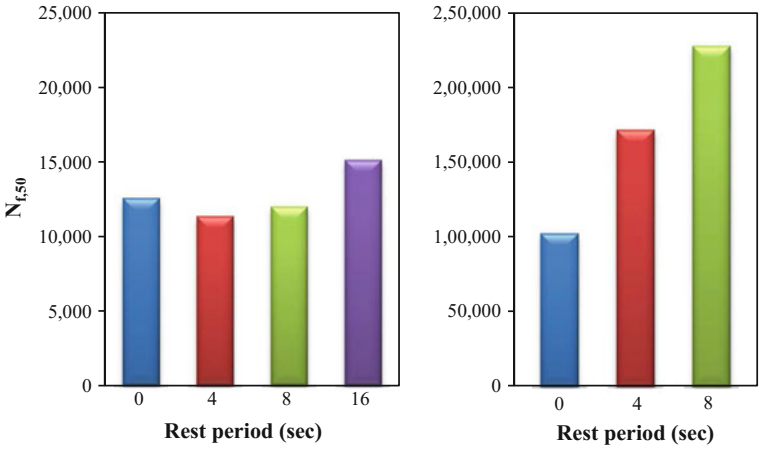


**Fig. 3** Effect of rest periods on fatigue life

15 °C should be seen as an important advantage and that undoubtedly contributes to the fatigue resistance during the test.

To evaluate the fatigue resistance using the concept of RDEC, it was first calculated the dissipated energy in accordance with the Eq. (2). Then, it was calculated the RDEC in accordance with Eq. (3). However, as mentioned by Shen and Carpenter (2007), Shen et al. (2010), due to testing noise, the raw DE data points are not directly useable since it can cause ambiguity for RDEC and PV calculation. Thus, in order to obtain a representative PV from fatigue testing data and minimize the error due do testing data variation, a linear regression was fitted to the DE-LC curve, and the slope of the curve was obtained. In order to ensure that the curve segment used for regression is in the plateau stage where the variation rate of DE is almost constant, the adjustment was done with respect to the following conditions: (i) for the 35/50 bitumen, the adjustment was made from cycle 2000 until the cycle in which there was a 50 % reduction of the initial complex modulus; (ii) for the PMB, the adjustment was made from cycle 15,000 until the cycle in which there was a 50 % reduction of the initial complex modulus. These considerations were applied to all measurements (including repetitions of the same test), regardless of the strain level and the type of test (continuous or intermittent).

Taking into account the linear regressions that were obtained and defining the PV as the RDEC value at the 50 % stiffness reduction failure point ($N_{f,50}$), it was possible to determine the PV for both binders tested and for the different test conditions. The results are plotted versus fatigue life ($N_{f,50}$) in Fig. 4. Each data point represents a specific combination of bitumen and test conditions, with 6 points referring to the 35/50 and 5 points to the PMB.

As shown, no matter the binder type (35/50 or PMB 45/80-65), the strain level (1.2, 1.6 or 2 %), the test type (continuous or intermittent) and the rest period duration (4 s, 8 s or 16 s), all data points follow a unique PV-$N_{f,50}$ line with an

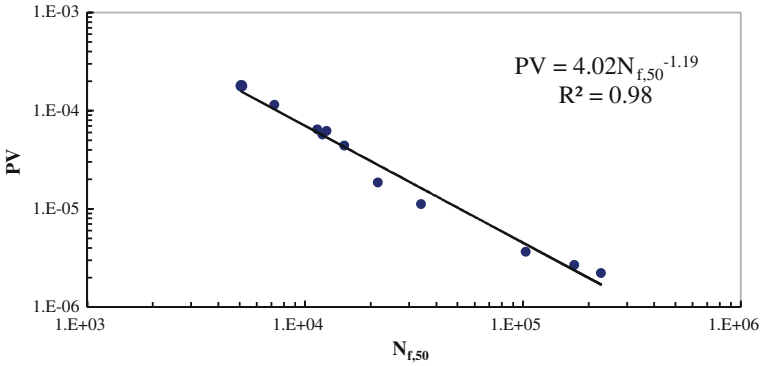


**Fig. 4** PV versus $N_{f,50}$ plot for all tested binders

R-square value of 0.98. This is in accordance with the conclusions of Shen et al. (2010). It is also noted that for higher strain levels, the PV tends to increase. This was expected because for higher strain levels, the variation of dissipated energy between each loading cycle is more pronounced and the fatigue resistance is lower. Furthermore, it is possible to confirm that the rest periods have a beneficial effect, particularly in the case of PMB 45/80-65, since they lead to a significant reduction in PV. For all test conditions that were used, the PMB 45/80-65 presents lower PV values than the 35/50 bitumen.

## *4.2 Linear Amplitude Sweep Tests*

Following the protocol for the LAS test, the test begins with a frequency sweep test for the determination of the undamaged material properties. Due to the ambiguity in literature about the calculation of α, it was determined as 1 + (1/m), according to Johnson (2010), and as 1/m in accordance with a recent draft proposal for AASHTO TP-101-12 (MARC 2014). Table 2 shows the m and α values obtained for the two bitumens.

Figure 5 shows the variation of C(t) with D(t) obtained from the tests with the two different α values. The influence of α is so small that cannot be detected in the figure. The PMB shows a more gradual decrease of the integrity parameter C(t), which means that it is able to accumulate much more damage than the neat bitumen. Table 2 presents the fatigue laws obtained from the LAS test, which were calculated following the procedure described in Sect. 2. The value of A is very sensitive to the value of α, being approximately 15 and 25 times higher with α = 1 + (1/m) for the 35/50 and the PMB, respectively. The differences in B values are justified by the variable B being a single function of α (Eq. 8). For the same α equation there are not significant differences between the bitumens. Figure 6 compares fatigue life predicted by the fatigue laws obtained from the time sweep tests ($N_{f,50}$) and from the

**Table 2** LAS test results

| Bitumen | m | $\alpha = 1 + (1/m)$ | $\alpha = 1/m$ | $C_1$ | $C_2$ | $D_f$ | A | B |
|---|---|---|---|---|---|---|---|---|
| 35/50 | 0.771 | | 1.297 | 0.088 | 0.510 | 15.981 | 6485.5 | −2.593 |
| | | 2.297 | | 0.100 | 0.481 | 13.410 | 102569.5 | −4.593 |
| PMB 45/80-65 | 0.696 | | 1.437 | 0.085 | 0.461 | 21.359 | 26042.0 | −2.875 |
| | | 2.437 | | 0.103 | 0.421 | 18.481 | 613634.8 | −4.875 |

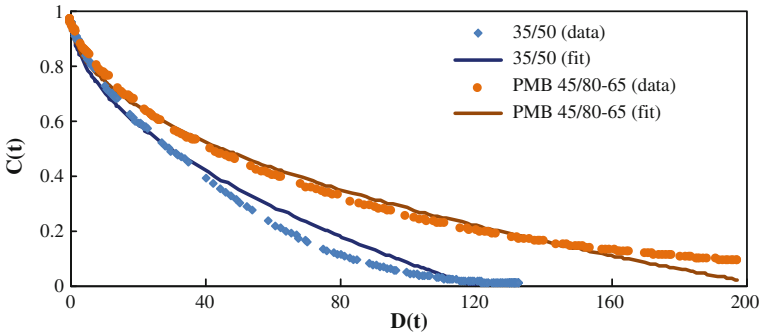


**Fig. 5** Plot of C(t) versus D(t)

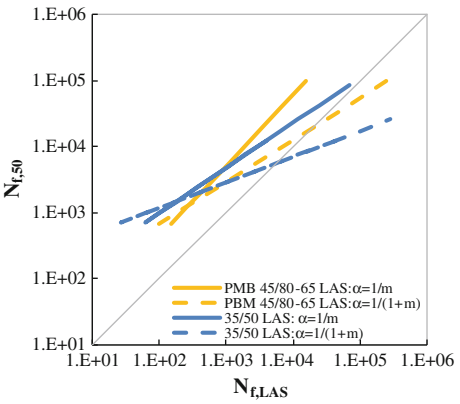


**Fig. 6** Comparison of different fatigue laws' predictions

LAS tests ($N_{f,LAS}$). It is concluded that the two methodologies provide very different laws regardless of α equation selected for LAS. The fatigue laws from the time sweep test determine, in general, longer periods to failure for both bitumens. The A values derived from the time sweep tests are much lower than the ones obtained from the LAS test with α = 1 + (1/m) while when α is 1/m it is significantly higher for the 35/50 and lower for the PMB. Also, the B values obtained

from the time sweep tests are significantly different between bitumens while the ones derived from the LAS are very similar.

Johnson (2010) recommended the value of 35 % in C(t) reduction for the determination of the fatigue life based on the comparison of time sweep and LAS tests. The results obtained in this study show that more tests are needed, with different materials and test conditions, to establish an adequate fatigue failure criteria.

## 5 Conclusions and Recommendations

This paper presents an evaluation of different methods proposed in literature for the estimation of the bitumen fatigue life. A neat bitumen and a polymer (SBS) modified bitumen were tested with continuous and discontinuous loading (time sweep tests) and with incremental load amplitude (linear amplitude sweep tests). The results of time sweep tests were analysed with the traditional approach ($N_{f,50}$–50 % initial modulus reduction) and using the Ratio of Dissipated Energy Change approach. The results of the linear amplitude sweep tests were analysed with the Viscoelastic Continuum Damage approach.

The results obtained showed, as expected, that the PMB has a higher resistance to fatigue than the neat bitumen. However, it was found that the traditional failure criterion can significantly underestimate the true fatigue resistance of the PMB, particularly for higher strain levels. Healing during non-loading periods has a large effect on the PMB fatigue life while no effect in the neat bitumen fatigue life for small to intermediate rest periods. Consequently, it was possible to infer that the PMB shows a higher healing potential, at least for these testing conditions.

By using the concept of RDEC and evaluating the fatigue resistance with the Plateau Value (PV), it was possible to confirm that regardless of the bitumen type, strain level, test type (continuous or intermittent) and rest period duration, all data points follow a unique PV-Nf, 50 line.

The fatigue life obtained from the linear amplitude sweep tests and using the VECD analysis shows that, for the same strain level and for the same definition of α, the PMB always shows a higher fatigue resistance than the neat bitumen. The fatigue law obtained with this method is very sensitive to the value of α considered. However, there are significant differences between the fatigue laws obtained with the two different methodologies. Such differences can be attributed to the fact that the testing procedures are different, the failure criteria being arbitrary and the VECD model formulation and its suitability for bitumen still needs further investigation.

New specifications for the fatigue resistance and self-healing capacity assessment testing, as the AASHTO TP-101-12 (MARC 2014), are valuable improvements to current bituminous materials' performance testing. It is required to continue research both in the methodologies used for the test analysis and in the lab testing.

## References

Botella R, Pérez-Jiménez F, Miró R (2012) Application of a strain sweep test to assess fatigue behavior of asphalt binders. Construction and Building Materials, 36:906-912.

Hintz C, Velasquez R-A, Johnson C-M, Bahia H-U (2011) Modification and Validation of the Linear Amplitude Sweep Test for Binder Fatigue Specification. Transportation Research Record: Journal of the Transportation Research Board, 2207:99-106.

Johnson CM (2010) Estimating Asphalt Binder Fatigue Resistance Using an Accelerated Test Method. PhD Thesis, University of Wisconsin – Madison, Madison, USA.

Lu X, Soenen H, Redelius P (2003) Fatigue and Healing Characteristics of Bitumens Studied Using Dynamic Shear Rheometer, Paper presented at the sixth International RILEM Symposium on Performance Testing and Evaluation of Bituminous Materials, Zurich, Switzerland, 2003.

MARC (2014) Revision of draft proposal for AASHTO TP-101-12 standard proposal. Modified Asphalt Research Center. Available via http://uwmarc.wisc.edu/files/linearamplitudesweep/AASTO%20TP%-20101-UL-LAS-Modified-highlighted-3-11-2013.pdf, (accessed in January, 2014).

Partl M, Bahia H-U, Canestrari F, De la Roche C, Di Benedetto H, Piber H, Sybilski D (2013) Advances in Interlaboratory Testing and Evaluation of Bituminous Materials. State-of-the-Art Report of the RILEM Tecnhical Committee 206-ATB, Vol. 9, Springer.

Santagata E, Baglieri O, Tsantilis L, Dalmazzo D (2013) Evaluation of self healing properties of bituminous binders taking into account steric hardening effects. Construction and Building Materials, 41:60-67.

Shen S, Asce A-M, Chiu H, Huang H (2010) Characterization of Fatigue and Healing in Asphalt Binders. Journal of Materials in Civil Engineering, 22(9):846-852.

Shen S, Carpenter S-H (2007) Dissipated Energy Concepts for HMA Performance: Fatigue and Healing. COE Report Nº 29, Technical Report of Research Supported by the Federal Aviation Administration, Department of Civil and Environmental Engineering, University of Illinois at Urbana-Champaign, Urbana, Illinois, USA.

Soenen H, De La Roche C, Redelius P (2004) Predict mix fatigue tests from binder fatigue properties, measured with a DSR. Paper presented at the third Eurasphalt & Eurobitume Congress, Austria, 2004.

Soenen H, Eckmann B (2000) Fatigue Testing of Bituminous Binders with a Dynamic Shear Rheometer. Paper presented at the second Eurasphalt and Eurobitume Congress, Vol. 1, pp. 827-834, Barcelona, Spain, 2000.

Sutharsan T (2010) Quantification of cohesive healing of asphalt binder based on dissipated energy analysis. MSc Thesis, Washington State University, Washington, D.C., USA.

Van den bergh W (2011) The Effect of Ageing on the Fatigue and Healing Properties of Bituminous Mortars. PhD Thesis, Delft University of Technology, Delft, The Netherlands.

Willis J, Turner P, Julian G, Taylor A, Tran N, Padula F (2012) Effects of changing virgin binder grade and content on rap mixtures properties. NCAT Report Nº 12-03, National Center of Asphalt Technology, Auburn University, Auburn, Alabama, USA.

Zhang J, Sabouri M, Guddati M-N, Kim R (2013) Development of a failure criterion for asphalt mixtures under fatigue loading. Road Materials and Pavement Design, 14(2):1-15.

# Evaluation of Crack Propagation in Asphalt Mixture Through Photoelasticity

**Stephan Büchler, Michael Wistuba and Augusto Cannone Falchetto**

**Abstract** In this paper the possibility of using photoelasticity to visualize and evaluate deformation and crack propagation on the surface of asphalt mixture is investigated. This technique uses a reflection polariscope which also allows to identify strain patterns. Six asphalt mixtures commonly used in Germany for base (AC 22), binder (AC 16) and surface (AC 8) layers were selected for performing monotonic and fatigue tests on notched semi-circular bending specimens, under constant strain rate and cyclic loading, respectively. Deformations were recorded through a digital camera capable of acquiring 30 images per second; for fatigue tests, pictures were taken every two seconds. During monotonic testing, very little deformation on the specimen surface could be visualized as load increased. As peak load was reached, cracking occurred suddenly, suggesting a typical quasi-brittle behavior; nevertheless, crack propagation could be recorded. Fatigue tests showed similar trend, but over a longer time. Cracking appeared at the end of the tests and needed an additional number of load cycles to reach complete failure.

**Keywords** Photoelasticity · Crack propagation · Notched specimen · Visualization

S. Büchler (✉) · M. Wistuba · A. Cannone Falchetto
Department of Architecture, Civil Engineering and Environmental Sciences - Pavement Engineering Centre (ISBS), Technical University of Braunschweig, Beethovenstraße, 51 b, 38106 Braunschweig, Germany
e-mail: s.buechler@tu-bs.de

M. Wistuba
e-mail: m.wistuba@tu-bs.de

A. Cannone Falchetto
e-mail: a.cannone-falchetto@tu-bs.de



F. Canestrari and M.N. Partl (eds.), *8th RILEM International Symposium on Testing and Characterization of Sustainable and Innovative Bituminous Materials*, RILEM Bookseries 11, DOI 10.1007/978-94-017-7342-3_82

## 1 Introduction

The multilayer theory for asphalt structures assumes that cracks appear at the bottom layer due to bending associated to traffic load. Within this theoretical framework and under the funding support of the research project FE 09/0189/2011/ERB "Numerische Simulation der Rissausbreitung in flexiblen Asphaltbefestigungen Infolge von Verkehrslasten, Teil II", a basic model was developed to simulate crack propagation in asphalt specimen by the "Institut für Straßenwesen" of the RWTH Aachen.

In order to verify and validate this newly developed model two testing procedures were implemented. The "Institut für Straßenwesen, Technische Universität Braunschweig (ISBS) and the Professur für Straßenbau des Instituts für Stadtbauwesen und Straßenbau", Technische Universität Dresden (ISSD), proposed two methods based on photoelasticity (ISBS) and on photogrammetry (ISSD) for obtaining an advanced visualization of crack propagation. The results of the photoelasticity technique on crack detection and visualization and propagation are presented in this paper.

## 2 Principles of Photoelasticity

Photoelasticity is not a new measurement technique (Harris and Jessop 1949); however, as this technique wasn't yet applied to asphalt materials, a short introduction to photoelasticity will follow. The main principle of photoelasticity is based on the refraction of light rays passing a transparent material under load; a polariscope is used to visualize stress patterns at the material surface. A polariscope consists of a light source and a transparent sample between two polarizing filters, see Fig. 1.

The polarizer P converts the light to plane polarized light. The light rays pass the unloaded and transparent sample and hits the second polarizing filter A (analyzer). As the analyzer is rotated by 90° with respect to the polarizer, no light can pass through the analyzer and black image is observed. When a sample is loaded, a certain component of the light rays is refracted while the remaining can pass the analyzer and, eventually, a stress pattern consisting of isochromatics can be seen.

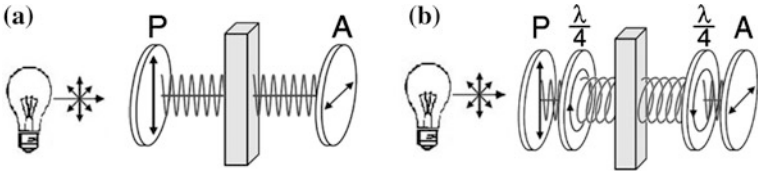


**Fig. 1** Principles of photoelasticity **a** plane polarized light, **b** circular polarized light

Light rays which are randomly refracted by 90° to the polarizer, cannot be seen; black areas will appear. To prevent these areas a quarter wave filter before and after the sample is used to convert the plane polarized light into circular polarized light, see Fig. 1. The difference between plane polarized light and circular polarized light is shown Fig. 2.

As asphalt specimens are not transparent, photoelasticity is not directly applicable. An alternate method has to be used: the reflection method (Fig. 3).

A photoelastic coating is applied on the specimen surface. This coating consists of a transparent sheet of high-elongation material, such as rubber, with a thickness of 3 mm and a modulus of elasticity of 4 MPa. Within this layer the light rays are refracted depending on the specimen deformation. The photoelastic coating is glued to the specimen through a reflecting adhesive which consists of glue with reflecting particles having a small modulus of elasticity equal to 7 MPa; therefore, even small deformations can be transferred to the photoelastic coating and can be visualized by the polariscope.

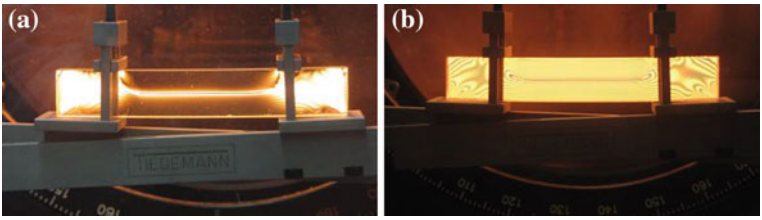


**Fig. 2** View on a sample rayed by monochromatic **a** plane polarized light and **b** circular polarized light

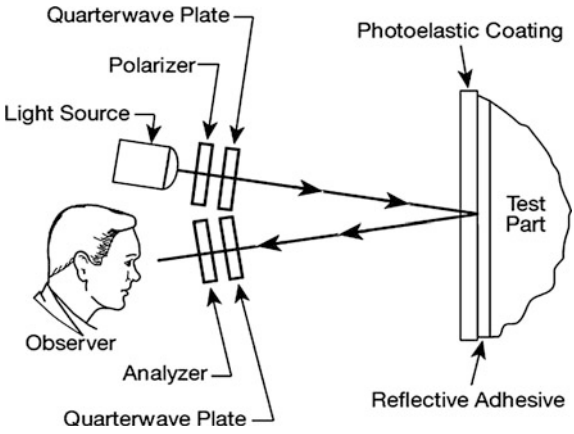


**Fig. 3** Principle of the reflection polariscope (Micro Measurement 2011a, b, c)

# 3 Materials and Test Methods

## 3.1 Materials

Three types of asphalts mixtures commonly used in Germany were selected for the experimental phase: a base layer AC 22 T S, a binder layer AC 16 B S and a surface layer AC 8 DS. Two asphalt binder contents were used for each mix design; hence six different asphalt mixtures were produced, see Table 1.

Specimens were prepared with a roller compactor according to EN 12697-33 (2013) capable of compacting asphalt mixture slabs up to a size of 50 cm × 70 cm. Then specimen with a diameter of 150 mm and a thickness of 60 mm were cored out of the slabs and grinded on the front sides to obtain a smooth surface. Afterwards each core was sawn in the middle and notched (width: 2 mm; depth: 10 mm). After drying each specimen was coated with a transparent layer of photoelastic material.

## 3.2 Monotonic Semi-circular Bending Test

Semi-circular bending (SCB) tests were selected for the experimental phase, based on previous research (Krans et al. 1996; Büchler and Wistuba 2013). SCB tests were performed according to the European specifications (EN 12697-44 2010); a schematic of the test is be presented in Fig. 4.

Specimens were first conditioned at 5 °C for 4 h and tests performed at room temperature of 25 °C. Load was applied in deflection control mode with rate of 5 mm/min. The stress at the tip of the notch was calculated according to EN 12697-44 (2010). Each test was filmed with 30 pictures per second for a maximum duration of 20 s. Single picture-frame were then extracted and used for interpreting the results.

## 3.3 Cyclic Semi-circular Bending Test

Samples and experimental design of the cyclic semi-circular bending tests are similar to the monotonic semi-circular bending procedure. A cyclic sinusoidal load

**Table 1** Binder contents for mix design

| | Lower content (M.-%) | Higher content (M.-%) |
|---|---|---|
| AC 22 T S | 4.1 | 4.6 |
| AC 16 B S | 4.5 | 5.0 |
| AC 8 D S | 6.2 | 6.7 |

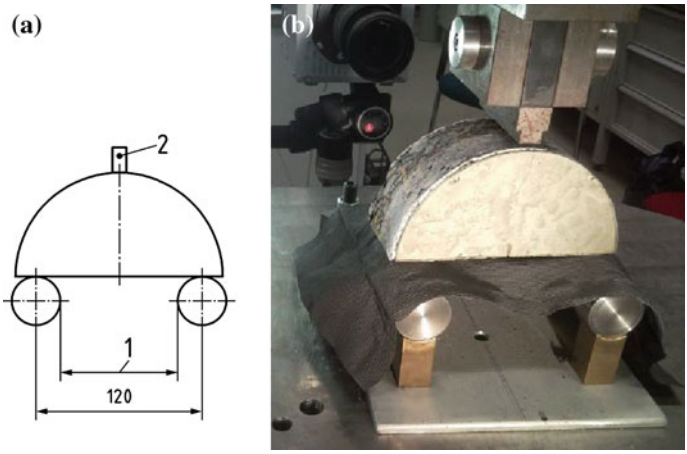


**Fig. 4** **a** Monotonic semi-circular bending test and **b** experimental setup with coated specimen

**Table 2** Applied load as terms of stress at the tip of the notch

| | Binder content 1 (M.-%) | Amplitude 1 (MPa) | Binder content 2 (M.-%) | Amplitude 2 (MPa) |
|---|---|---|---|---|
| AC 22 T S | 4.1 | 2.9 | 4.6 | 3.2 |
| AC 16 B S | 4.5 | 2.2 | 5.0 | 2.2 |
| AC 8 D S | 6.2 | 2.4 | 6.7 | 2.5 |

was applied to the specimen with a frequency of 10 Hz. The amplitude of the applied load was selected based on the maximum load used for the monotonic tests (see Table 2). The minimum stress level was fixed to 0.1 MPa.

The maximum duration of the tests was 28 min; as this duration was beyond the storing capacity of the cameras, picture/frames were recorded only every 2 s.

## 4 Visualization

### *4.1 Monotonic Semi-circular Bending Test*

In Fig. 5 the difference between a homogenous elastic specimen (plexiglass) and an asphalt specimen (AC 8 D S) is shown. For the plexiglass an accumulation of ischromatics can be observed at the three points of the load application, which are connected by an area of a single isochromatic. A clear pattern can be also identified at the tip of the notch, which expand and propagate to the top of the specimen.

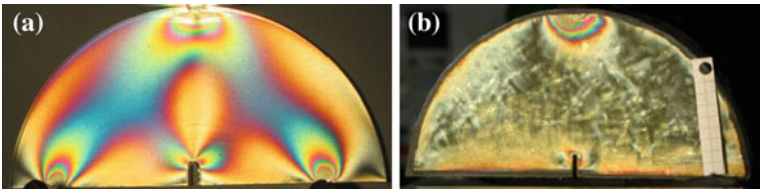


**Fig. 5** **a** Visualized isochromatics in a homogeneous and elastic specimen and **b** nearly no isochromatics on an asphalt specimen AC 8 D S under load

These patterns are confirmed by literature (Ferber 1999; Backes 2009). Only one accumulation of isochromatics could be observed on the asphalt specimen surface under the top loading point.

This effect is caused by the compression of the glue at the top, transmitting its deformation to the refracting coating material. All tested specimen showed nearly no deformation (and therefore stresses) up to the point of crack. Figure 6 shows the development of deformation (and stress) during a test for a AC 8 DS.

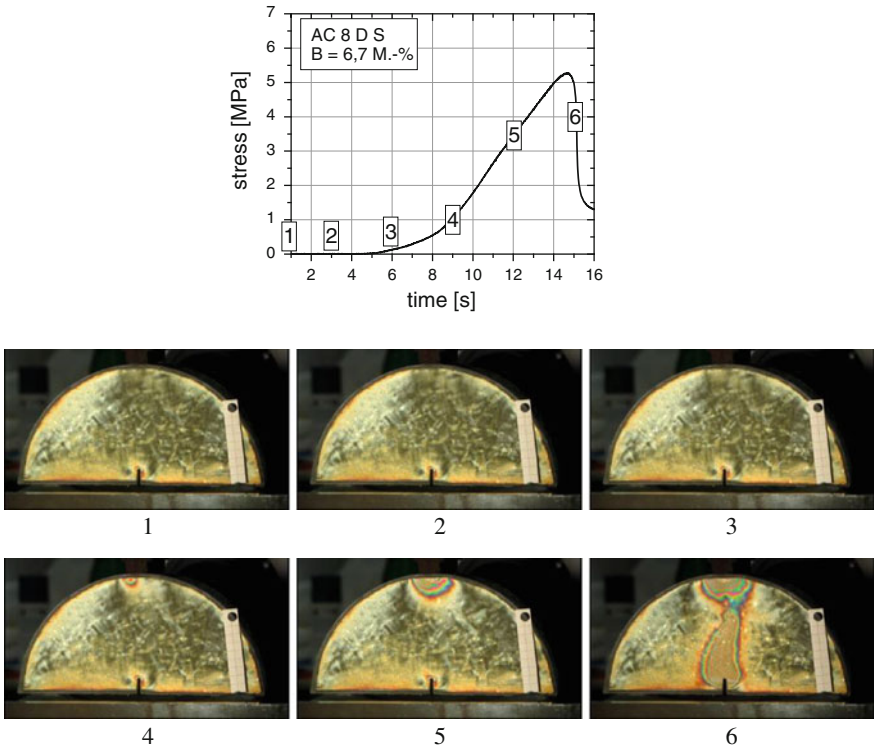


**Fig. 6** Visualization of the deformation evolution during a monotonic bending test (AC 8 D S)

In Fig. 7 the crack propagation is presented; the crack propagates from the tip of the notch and reaches the top of the specimen within half a second.

The propagation of the crack does not follow the ideal line of maximum stress, straight to the top of the specimen (see Fig. 7); the crack is deflected by single grains constituting the aggregate skeleton of the mixture. At failure the crack has reached the top of the specimen which is entirely cracked; however, the photoelastic coating hold the specimen together. Therefore, the exact cracking line cannot be directly observed behind the coating surface, especially when a crack completely extends through the specimen.

Observing the test, the crack seems to appear very fast, a quasibrittle failure happens. By analyzing the series of pictures obtained for each test, the crack propagation is not linear. It will start with a slow movement and increases exponentially.

No statistically significant effects of the asphalt binder content could be observed on the crack initiation and propagation. Asphalt mixtures AC 22 T S and AC 16 B S showed a similar behavior with respect to crack propagation, with small differences associated to the crack path which showed limited deflection from a straight line for

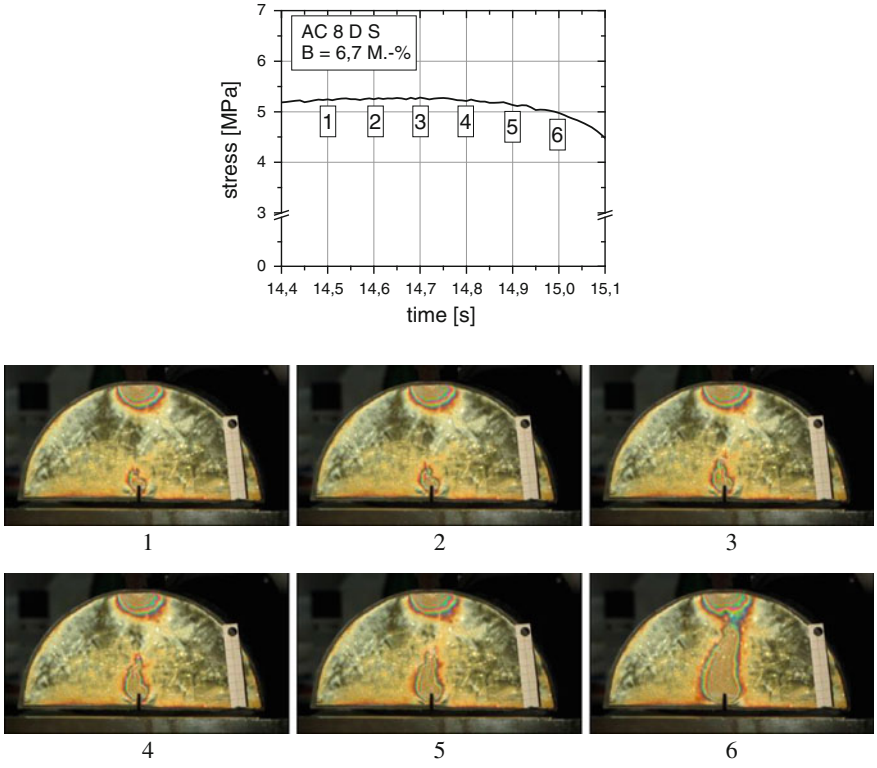


**Fig. 7** Crack propagation in a monotonic bending test (AC 8 D S)

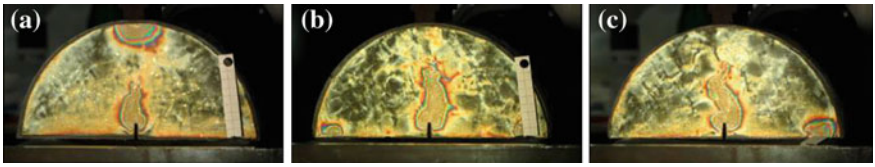


**Fig. 8** Crack line for asphalt mixtures **a** AC 8 D S, **b** AC 16 B S and **c** AC 22 T S

the mixture prepared with larger aggregates. Figure 8 shows the difference during cracking for the three asphalt mixtures investigated.

## *4.2 Cyclic Semi-circular Bending Test*

The visualization of the cyclic tests resulted in pictures are comparable to the monotonic tests. Up to 10 % of the test duration no strain or stress could be observed in the specimen. Then small patterns of isochromatics occurred at the top of the specimen. This patterns of isochromatics increased very slowly until 80–90 % of the test duration. Then cracking occurred at the tip of the notch and propagated slowly (with respect to the monotonic tests) till the top of the specimen. Figure 9 shows an AC 8 D S after 258 load cycles without any significant strain. After 12,900 load cycles the crack is developing and propagates through the specimen, showing a typical pattern observed in three-point bending tests. Finally, after 200 additional load cycles the specimen failed.

While the crack was propagating the isochromatic pattern showed a V-shape above the crack. In the middle of the specimen a strainless zone could be detected. In the monotonic tests (Fig. 5a) this zone could also be identified, but its size is significantly smaller compared to what observed for cyclic loading. The specimens prepared with mixtures having larger aggregates (AC 16 B S and AC 22 T S) showed this patterns only basically. The location of single grains has a large impact on the crack pattern (see Fig. 10). On the other hand, the AC 8 D S mixture showed consistently a V-shape pattern with a strainless zone above the notch or the crack.

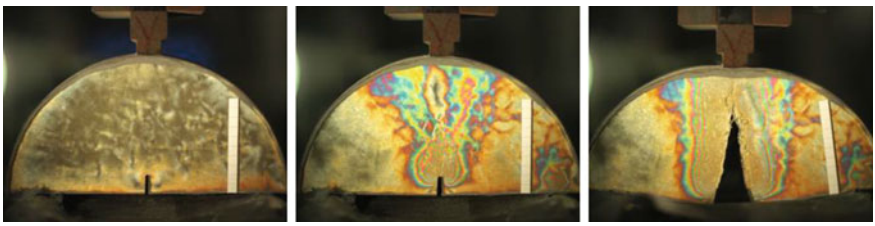

**Fig. 9** Isochromatic patterns in a cyclic semi-circular bending test, after 258 load cycles (*left*), after 12,900 load cyles (*middle*) and after 13,100 load cycles (*right*)

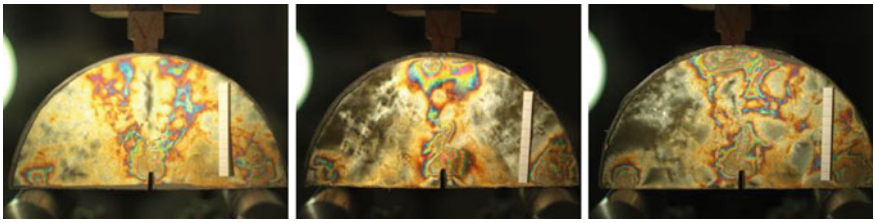

**Fig. 10** Isochromatic patterns in a cyclic semi-circular bending test at ~90 % of the test duration. AC 8 D S (*left*), AC 16 B S (*middle*) and AC 22 T S (*right*)

As the timing of the camera was not exactly fixed on two second (it scatters around approximately 0.2 s), the pictures were taken randomly around the 2 s interval. So at the time a picture was taken, the load could vary from minimum load to maximum load. But there was only little effect to the patterns by this load difference.

## 5 Summary

In this paper the possibility of using photoelasticity to visualize and evaluate deformation and crack propagation of asphalt specimen was investigated. In order to observe strain patterns on the surface of asphalt mixture specimens a reflection polariscope was used. Three asphalt mixtures commonly used in Germany with two different binder contents, were selected to perform monotonic and cyclic (fatigue) semi-circular bending tests on notched specimens. The deformation patterns were recorded through a digital camera capable of acquiring 30 images per second; for fatigue tests, pictures were taken every two seconds.

During monotonic testing, very little deformation on the specimen surface could be visualized as load increased. As peak load was reached, cracking occurred suddenly, suggesting a typical quasibrittle behavior. Fatigue tests showed similar trend, but over a longer time. First strain patterns appear after 10 % of the test duration, but cracking occurred at the end of the tests and needed an additional number of load cycles to reach complete failure.

The technique of photoelasticity, based on the use of a reflection polariscope, showed the possibility to visualize deformation at the surface of asphalt specimen. Cracks can be detected and their propagation can be recorded for further analysis. For future research correlations to homogenous materials and the link to stress calculation models should be investigated.

**Acknowledgments** The authors gratefully acknowledge the funding support of Federal Ministry of Transport, Building and Urban Development under the research grant FE 09/0189/2011/ERB "Numerische Simulation der Rissausbreitung in flexiblen Asphaltbefestigungen Infolge von Verkehrslasten, Teil II".

## References

Backes, D. 2009. Experimentelle Spannungsanalyse - Spannungsoptik. Engineerings Compe-tence Center, Hochschule für Technik und Wirtschaft des Saarlandes, ftp://ecc-s1.htw-saarland.de/Mitarbeiter/backes.

Büchler, S. and Wistuba, M. 2013. Photoelasticity for stress-strain-visualization. Proceedings of the 5th International Conference of the European Asphalt Technology Association (EATA). Braunschweig, Germany.

EN 12697-33. 2013. Bituminous mixtures - Test methods for hot mix asphalt - Part 33: Specimen prepared by roller compactor

EN 12697-44. 2010. Bituminous mixtures – Test methods for hot mix asphalt – Part 44: Crack propagation by semi-circular bending test

Ferber, F. 1999. Numerische und experimentelle Untersuchungen rißbehafteter Strukturen, Ha-bilitationsschrift, Universität Paderborn, Fachbereich Maschinentechnik.

Harris, H.T. and Jessop, F.C. 1949. Photoelasticity principles and methods, Dover Publications.

Krans, R.L., Tolman, F. and Van de Ven, M.F.C. 1996. Semi-circular bending test: a practical crack growth test using asphalt concrete cores. Proceedings of the Third International RILEM Conference on Reflective Cracking in Pavements. Maastricht, The Netherlands.

Micro-Measurements 2011a. Introduction to Stress Analysis by the PhotoStress® Method, Vishay Precision Group, Raleigh, USA, www.vishaypg.com.

Micro-Measurements 2011b. Photostress - A Brief Introduction - Pictorial Examples of PhotoStress-Coated Parts - A Wide Selection of Industrial Case History Applications, Vishay Precision Group, Raleigh, USA, www.vishaypg.com.

Micro-Measurements 2011c. LF/Z-2 Reflection Polariscope Introduction Manual, Vishay Precision Group, Raleigh, USA.

# Author Index





F. Canestrari and M.N. Partl (eds.), *8th RILEM International Symposium on Testing and Characterization of Sustainable and Innovative Bituminous Materials*, RILEM Bookseries 11, DOI 10.1007/978-94-017-7342-3